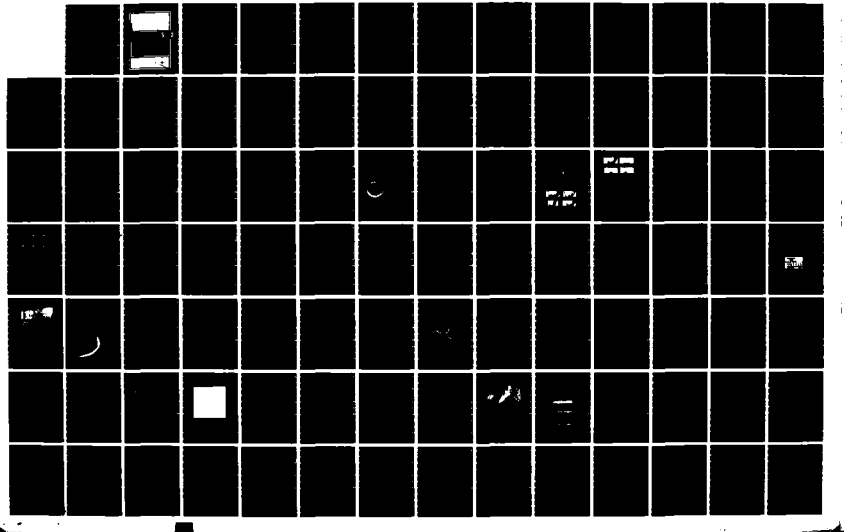
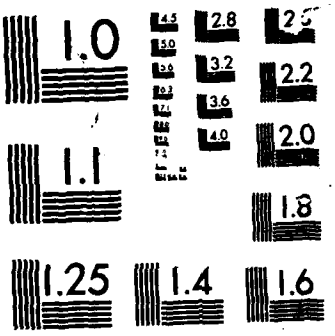
AD-A166 505 CONFERENCE PROCEEDINGS ON PROPAGATION EFFECTS ON MILITARY SYSTEMS IN THE..(U) ADVISORY GROUP FOR AEROSPACE RESEARCH AND DEVELOPMENT NEUILLY.. H SOICER

UNCLASSIFIED NOV 85 AGARD-CP-382 F/G 4/1 NL





MICROCOPY CHART

(2)

AGARD-CP-382

AGARD-CP-382

AGARD

ADVISORY GROUP FOR AEROSPACE RESEARCH & DEVELOPMENT

7 RUE ANCELLE 92200 NEUILLY SUR SEINE FRANCE

AD-A166 585

DTIC
ELECTE
APR 1 4 1986
S D

AGARD CONFERENCE PROCEEDINGS No.382

Propagation Effects on Military Systems in the High Latitude Region

This document has been approved for public release and sale; its distribution is unlimited.

DTIC FILE COPY

NORTH ATLANTIC TREATY ORGANIZATION



DISTRIBUTION AND AVAILABILITY
ON BACK COVER

ERRATUM

Due to a printing error the reference to paper 6.4 was omitted from the list of contents. Pages ix and x should therefore be replaced by this amended version.

	Reference
IONOSPHERIC MODIFICATIONS BY HF HEATERS by M.C.Lee, J.A.Kong, H.C.Carlson and S.P.Kuo	5.2
SESSION VI – INCOHERENT/COHERENT SCATTER	
SESSION CHAIRMAN'S SUMMARY by G.Rose	CS6
EISCAT: A REVIEW OF RECENT SCIENTIFIC WORKS by P.Bauer	6.1
IRREGULAR STRUCTURES IN THE HIGH-LATITUDE F REGION OBSERVED USING THE EISCAT INCOHERENT SCATTER RADAR by J.K.Hargreaves, C.J.Burns and S.C.Kirkwood	6.2
OBSERVATIONS OF THE AURORAL IONOSPHERE USING EISCAT by W.Kofman and C.Lathuillere	6.3
SABRE RADAR OBSERVATIONS IN THE AURORAL IONOSPHERE by T.B.Jones, J.A.Waldock, E.C.Thomas, C.P.Stewart and T.R.Robinson	6.4
SESSION VII – MEASUREMENT TECHNIQUES/MODELS/MORPHOLOGY AND PHYSICS	
SESSION CHAIRMAN'S SUMMARY by E.Thrane	CS7
DANISH AND US GEOPHYSICAL MEASUREMENTS IN GREENLAND AND SURROUNDING AREAS RELATED TO ARCTIC RADIOPROPAGATION by J.Taagholt	7.1
PROGRESS IN MODELLING THE POLAR IONOSPHERE FROM SOLAR AND MAGNETOSPHERE PARAMETERS by B.J.Watkins, S.-I.Akasofu and C.D.Fry	7.2
STATISTICS OF AURORAL RADIO ABSORPTION IN RELATION TO PREDICTION MODELS by J.K.Hargreaves, M.T.Feeney and C.J.Burns	7.3
FORMATION AND DETECTION OF HIGH LATITUDE IONOSPHERIC IRREGULARITIES by M.C.Lee, J.Buchau, H.C.Carlson, Jr.., J.A.Klobuchar and E.J.Weber	7.4
DIRECT IN-SITU MEASUREMENTS OF IRREGULARITIES IN THE MESOSPHERE (85-50 KM) AT 69°N (ANDENES, NORWAY) by H-U.Widdell	7.5
SESSION VIII – LOW FREQUENCY PROPAGATION	
SESSION CHAIRMAN' SUMMARY by J.Taagholt	CS8
CONDUCTIVITY PROFILES OF THE DISTURBED POLAR IONOSPHERE FROM VLF REFLECTION DATA by P.A.Kossey, J.E.Rasmussen, E.C.Field and C.R.Warber	8.1
A STUDY OF VLF PROPAGATION AT HIGH SOUTHERN LATITUDES USING SFERICS by A.Volland, M.Schmolders, G.Proelss and H.Kröninger	8.2
EFFECTS OF THE IONOSPHERE ON ELF SIGNALS DURING POLAR CAP ABSORPTION EVENTS: COMPARISON OF THEORY AND EXPERIMENTS by E.C.Field, C.R.Warber and R.G.Joiner	8.3

Reference

WORLD ATLAS OF GROUND CONDUCTIVITIES WITH PARTICULAR EMPHASIS ON THE HIGH LATITUDE REGION
by K.N.Stokke 8.4

SESSION IX – METEOR BURST/SCATTER

SESSION CHAIRMAN'S SUMMARY
by J.H.Blythe CS9

METEOR SCATTER RADIO COMMUNICATION AT HIGH LATITUDES
by P.S.Cannon, A.H.Dickson and M.H.Armstrong 9.1

CHARACTERISTICS OF HIGH LATITUDE METEOR SCATTER PROPAGATION PARAMETERS OVER THE 45–104 MHz BAND
by J.C.Ostergaard, J.E.Rasmussen, M.J.Sowa, J.M.Quinn and P.A.Kossey 9.2

ROUND TABLE DISCUSSION RTD

LIST OF PARTICIPANTS P

BIBLIOGRAPHY B

AGARD-CP-382

NORTH ATLANTIC TREATY ORGANIZATION

ADVISORY GROUP FOR AEROSPACE RESEARCH AND DEVELOPMENT

(ORGANISATION DU TRAITE DE L'ATLANTIQUE NORD)

AGARD Conference Proceedings No.382

PROPAGATION EFFECTS ON MILITARY SYSTEMS IN THE HIGH LATITUDE REGION

Edited by

H.Soicher
US Army Communications-Electronics Command
Center for Communications Systems
Fort Monmouth, New Jersey 07703
USA

Papers presented at the 36th Symposium of the Electromagnetic Wave Propagation Panel held in Fairbanks, Alaska, USA, 3—7 June, 1985.

THE MISSION OF AGARD

The mission of AGARD is to bring together the leading personalities of the NATO nations in the fields of science and technology relating to aerospace for the following purposes:

- Exchanging of scientific and technical information;
- Continuously stimulating advances in the aerospace sciences relevant to strengthening the common defence posture;
- Improving the co-operation among member nations in aerospace research and development;
- Providing scientific and technical advice and assistance to the Military Committee in the field of aerospace research and development (with particular regard to its military application);
- Rendering scientific and technical assistance, as requested, to other NATO bodies and to member nations in connection with research and development problems in the aerospace field;
- Providing assistance to member nations for the purpose of increasing their scientific and technical potential;
- Recommending effective ways for the member nations to use their research and development capabilities for the common benefit of the NATO community.

The highest authority within AGARD is the National Delegates Board consisting of officially appointed senior representatives from each member nation. The mission of AGARD is carried out through the Panels which are composed of experts appointed by the National Delegates, the Consultant and Exchange Programme and the Aerospace Applications Studies Programme. The results of AGARD work are reported to the member nations and the NATO Authorities through the AGARD series of publications of which this is one.

Participation in AGARD activities is by invitation only and is normally limited to citizens of the NATO nations.

The content of this publication has been reproduced
directly from material supplied by AGARD or the author.

Published November 1985

Copyright © AGARD 1985
All Rights Reserved

ISBN 92-835-0383-X



Printed by Specialised Printing Services Limited
40 Chigwell Lane, Loughton, Essex IG10 3TZ

THEME

With the advent of new systems operating at high latitudes in the field of detection, navigation and communications and with the new experiments at high latitudes ranging from incoherent scatter studies to satellites for studying high latitude irregularity structure, it is of considerable importance to relate the advances in high latitude studies to military systems. The concept of this proposal for a meeting on propagation effects on military systems in the high latitude region is to bring together these two areas.

The behaviour of the propagation environment at high latitudes differs from that at lower latitudes, affecting radiowave propagation across the RF spectrum. The differences are ascribed to the interplanetary and magnetospheric geophysical events which are guided earthward by the geomagnetic field.

The high-latitude ground region is characterized by a rugged terrain and by a tremendous variation in ground electrical characteristics.

The severe climatic conditions include a large daily and seasonal temperature variation, extremes of temperatures, high winds, ice accumulation, precipitation (rain, snow, ice crystals, sleet, hail), surface and elevated temperature inversions which produce large refractive gradients and ducts.

The high latitude ionosphere is affected by two major phenomena: energetic particles from the sun and from the outer magnetosphere penetrate the atmosphere and create ionization at various altitudes; and solar wind induces an electric field perpendicular to the magnetic field which causes ionization drifts and thus contributes to the formation of ionization irregularities. Some of the ionospheric propagation anomalies created include: auroral and polar cap absorption; sporadic E, small scale irregularities (spread F) giving rise to scattering and fading phenomena and causing transionospheric amplitude and phase scintillations; effects of magnetic substorm activity, density troughs, and large sheets of field-aligned ionization.

The Symposium directed its efforts towards propagation problems and solutions for many systems. The topics include satellite communication over polar and auroral latitudes, over-the-horizon radar, low frequency propagation under high latitude conditions, remote sensing of high latitude regions by active and passive EM systems, and HF communications at auroral and polar latitudes. Unique lower atmospheric effects and multipath problems of importance at high latitudes will also be discussed.

With the NATO northern flank nations (in both the European and North-American sectors) situated in the high-latitude region, with NATO air routes across the Atlantic traversing that region, and with surveillance and early-warning systems looking in the direction of the region, the propagation characteristics of the high-latitude region are of critical importance to the mission of the alliance in the areas of communications, navigation and surveillance.

* * *

L'apparition de nouveaux systèmes de détection, de navigation et de communications fonctionnant à des latitudes élevées et les expériences récemment effectuées à ces mêmes latitudes dans des domaines allant de la diffusion non cohérente aux satellites chargés d'étudier la structure irrégulière des latitudes élevées, confèrent une importance extrême à l'établissment d'une liaison entre les progrès des études sur ces latitudes et les systèmes militaires. Le concept de base de cette réunion qui traite des Effets de la Propagation sur les Systèmes Militaires dans la Région des Latitudes Elevées est de rapprocher ces deux domaines. Le comportement du milieu de propagation aux latitudes élevées diffère de celui que l'on peut observer aux faibles latitudes et affecte la propagation des ondes radio à travers le spectre des fréquences radio. Les différences observées sont attribuées aux phénomènes géophysiques interplanétaires et magnétosphériques qui sont guidés vers la terre par le champ géomagnétique.

La zone terrestre située aux latitudes élevées est caractérisée par un terrain accidenté et par une énorme variation des caractéristiques électriques au sol.

Les conditions climatiques y sont rigoureuses: variations considérables des températures quotidiennes et saisonnières, températures extrêmes, vents forts, accumulation de glace, précipitations (pluie, neige, cristaux de glace, grésil, grêle), inversions des températures en surface et en altitude avec production d'importants gradients de réfraction et de conduits.

Aux latitudes élevées, l'ionosphère est affectée par deux phénomènes majeurs: des particules énergétiques issues du soleil et de la magnétosphère externe pénètrent dans l'atmosphère et créent une ionisation à diverses altitudes; le vent solaire crée un champ électrique perpendiculaire au champ magnétique qui entraîne des dérives d'ionisation, contribuant ainsi à la formation d'irrégularités d'ionisation. Parmi les anomalies de propagation ionosphérique ainsi créées, on peut citer: l'absorption par la calotte aurorale et polaire, l'E sporadique, les irrégularités de faible échelle (F diffus) entraînant des phénomènes de diffusion et d'affaiblissement et créant des scintillations d'amplitude et de phase à travers l'ionosphère; les effets des activités des sous-orages magnétiques, les creux de densité et de vastes nappes d'ionisation alignées dans le champ.

Les conférenciers du Symposium ont concentré leurs efforts sur les problèmes de propagation et leurs solutions dans le cas de nombreux systèmes. Les sujets traités comprennent les communications par satellites aux latitudes polaires et

aurorales, le radar au-delà de l'horizon, la propagation basses fréquences dans des conditions de latitude élevée, la détection à distance des régions situées aux latitudes élevées grâce à des systèmes électromagnétiques actifs et passifs, et les communications hautes fréquences aux latitudes aurorales et polaires. Sont également étudiés les effets uniques de la basse atmosphère et les problèmes de multi-trajets, importants aux latitudes élevées. Les pays du front septentrional de l'OTAN (en Europe comme en Amérique du Nord) étant situés dans la région des latitudes élevées, les itinéraires aériens de l'OTAN au-dessus de l'Atlantique traversant cette région et les systèmes de surveillance et d'alerte éloignée étant orientés vers celles-ci, les caractéristiques de propagation dans les zones situées aux latitudes élevées revêtent une importance critique pour la mission de l'Alliance en matière de communications, de navigation et de surveillance.

ELECTROMAGNETIC WAVE PROPAGATION PANEL

Chairman: Dr J.H.Blythe
Marconi Research Centre
Great Baddow
Chelmsford, CM2 8HN
UK

Deputy Chairman: Dr H.Soicher
US Army Communication-
Electronic Command
Center for Communications
Systems
ATTN: AMSEL-COM-RN-1
Fort Monmouth, N.J. 07703
USA

PROGRAMME AND MEETING OFFICIALS

Programme Chairman: Dr Haim Soicher
US Army Communications-Electronics Command
Center for Communications Systems
Fort Monmouth, New Jersey 07703
USA

Dr J.Aarons
Department of Astronomy
Boston University
725 Commonwealth Avenue
Boston, MA 02215

Dr P.S.Cannon
Royal Aircraft Establishment
Radio & Navigation Dept.
Farnborough, Hants GU14 6TD
United Kingdom

Prof. C.Goutelard
Laboratoire d'Etudes de
Transmissions Ionosphériques
9, Avenue de la Division
Leclerc
94230 Cachan
France

Prof. R.D.Hunsucker
Geophysical Institute
University of Alaska
Fairbanks, Alaska 99701

Dr G.Rose
Max Planck Institut für Aeronomie
D-3411 Katlenburg-Lindau
FRG

Mr J.Taagholt
Danish Scientific Liaison for Greenland
10 Oster Volgade
DK 1350 Copenhagen K, Denmark

Dr E.V.Thrane
Norwegian Defence Research
Establishment
Division for Electronics
P.O. Box 25
Kjeller, Norway

Prof. M.Cutolo
Universita di Napoli
Instituto de Fisica
Via Monteoliveto 3
80134 Napoli, Italy



HOST NATION COORDINATOR

Mr V.J.Coyne
Rome Air Development Center/OCS
Griffiss AFB, N.Y. 13441
USA

Accesion For
NTIS CRA&I
DTIC TAB
Unannounced
Justification
By
Distribution /
Availability Codes
Dist | Avail and / or Special
A-1

LOCAL HOST

Prof. R.D.Hunsucker
Geophysical Institute
University of Alaska
Fairbanks, Alaska 99701
USA

PANEL EXECUTIVE

Lt. Colonel Timothy B.Russell

EDITOR'S COMMENTS

These proceedings represent the totality of the AGARD/EPP symposium on "Propagation Effects on Military Systems in the High Latitude Region" held in Fairbanks, Alaska, USA, 3—7 June 1985. It is hoped that these proceedings will constitute the state-of-the-art document on this important subject.

The papers appearing in the proceedings of this symposium have been printed from copies furnished directly by the authors. For the most part, the question-and-answer comments which followed individual presentations, were written by the discussors for inclusion in these proceedings. This procedure gave the discussors the opportunity to rephrase and possibly re-think their comments. The session summaries, which highlight the subject matter presented and discussed during the sessions, were prepared by the session chairman. The editor wishes to thank them for their efforts here and for ably directing the presentation and discussion periods during the symposium.

The general discussion portion of these proceedings was summarized by the session chairman from taped transcriptions. Quite often the coherency of thought is lost in the transcription, and considerable freedom was used in the interpretation of the comments. The editor apologizes for any changes in meaning or style that may have been made in preparing a printable version of the discussions.

The success of the symposium was assured by the collective support afforded by members of the program committee whose names are given elsewhere in these proceedings.

The editor wishes to thank the EPP Chairman for his interest and support in the preparation and execution of the symposium. Further, he wishes to acknowledge the support of the EPP Executive and his staff as well as his own organization in the preparation of these proceedings.

HAIM SOICHER

CONTENTS

	Page
THEME	iii
TECHNICAL PROGRAMME COMMITTEE AND PANEL OFFICERS	v
EDITOR'S COMMENTS by H.Soicher	vi
TECHNICAL EVALUATION REPORT by R.D.Hunsucker	xi
	Reference
WELCOMING ADDRESS by J.G.Roederer	W
SESSION I – OVERVIEW	
SESSION CHAIRMAN'S SUMMARY by H.Soicher	CS1
SOLAR-TERRESTRIAL RELATIONSHIPS IN THE HIGH LATITUDE REGION by S.-I.Akasofu	1.1
MEDIA EFFECTS ON SYSTEMS IN THE HIGH LATITUDE REGION by E.V.Thrane	1.2
SESSION II – TRANSIONOSPHERIC PROPAGATION AND CONSIDERATIONS	
SESSION CHAIRMAN'S SUMMARY by J.Aarons	CS2
RECENT HILAT RESULTS by E.J.Fremouw	2.1
TOTAL ELECTRON CONTENT AND L-BAND AMPLITUDE AND PHASE SCINTILLATION MEASUREMENTS IN THE POLAR CAP IONOSPHERE by J.A.Klobuchar, G.J.Bishop and P.H.Doherty	2.2
VARIABILITY OF TRANSIONOSPHERIC SIGNAL TIME DELAY AT HIGH LATITUDES NEAR SOLAR MINIMUM by H.Soicher	2.3
F LAYER IRREGULARITIES AT PLASMAPAUSE AND AURORAL LATITUDES by J.Aarons	2.4
INFLUENCE OF IONOSPHERIC IRREGULARITY SHAPE AND VELOCITY ON THE DESIGN OF AIRBORNE SATELLITE COMMUNICATIONS SYSTEMS by A.L.Johnson	2.5
PROPAGATION EFFECTS ON SATELLITE-BORNE SYNTHETIC APERTURE RADARS* by C.L.Rino and J.Owen	2.6
HIGH-LATITUDE SCINTILLTIONS USING NNSS SATELLITES by L.Kersley	2.7
SHF/EHF RAY BENDING by D.L.Zimmerman, G.F.Providakes, D.L.Post and S.H.Talbot	2.8

*Abstract only.

	Reference
SESSION III – PROPAGATION ASPECTS OF HF COMMUNICATION	
SESSION CHAIRMAN'S SUMMARY by P.Cannon	CS3
IONOSPHERIC MODELLING AND HF RADIO SYSTEMS AT HIGH LATITUDES by S.Quegan, J.D.Milsom and R.N.Herring	3.1
HIGH LATITUDE SPATIALLY ADAPTIVE PROPAGATION EXPERIMENT by G.S.Sales, R.J.Cormier, R.A.Greenwald and K.B.Baker	3.2
TECHNIQUES FOR IMPROVING THE RELIABILITY OF MOBILE HF COMMUNICATIONS OVER HIGH-ABSORPTION PATHS by M.Darnell	3.3
PROPAGATION CHARACTERISTICS OF MEDIUM FREQUENCY SKYWAVE SIGNALS FROM THE CONTINENTAL US AND CANADA RECEIVED AT FAIRBANKS, ALASKA by R.D.Hunsucker, B.S.Delana and J.C.H.Wang	3.4
OPTIMISATION DES SYSTEMES DE TRANSMISSION NUMERIQUE TRANSAURORAUX EN ONDES DECAMETRIQUES par C.Goutelard, J.Caratori et A.Nehme	3.5
OBSERVATIONS WITH AN IONOSONDE IN NORTHERN GERMANY NEAR THE MID-LATITUDE TROUGH by T.Damboldt	3.6
SESSION IV – HIGH LATITUDE HF PROBING	
SESSION CHAIRMAN'S SUMMARY by C.Goutelard	CS4
IONOSPHERIC FACTORS AFFECTING THE PERFORMANCE OF HF SKY-WAVE SEA-STATE RADARS AT HIGH LATITUDES by P.A.Bradley, A.J.Gibson, J.C.Schlobohm and D.E.Westover	4.1
SPECTRAL CHARACTERISTICS OF HIGH FREQUENCY WAVES BACKSCATTERED BY SMALL SCALE F REGION IRREGULARITIES: EVIDENCE OF STRONG SUB-AURORAL ION FLOW by A.Bourdillon	4.2
SMALL-SCALE IRREGULARITIES IN THE HIGH-LATITUDE F REGION by C.Hanvise, J.P.Villain, C.Beghin and G.Caudal	4.3
ON THE RELATIONSHIP OF F-REGION STRUCTURE IN THE DAYSIDE AURORAL OVAL TO HF BACKSCATTER SIGNATURES ATTRIBUTED TO THE POLAR CUSP by J.D.Kelly, R.T.Tsunoda, J.K.Olesen and P.Stauning	4.4
OBSERVATIONS OF VERY HIGH LATITUDE IONOSPHERIC IRREGULARITIES WITH THE GOOSE BAY HF RADAR by R.A.Greenwald and K.B.Baker	4.5
OBSERVATIONS OF THE MID-LATITUDE IONOSPHERIC TROUGH FROM ANTARCTICA by F.T.Berkey and M.J.Jarvis	4.6
THE VARIABILITY AND PREDICTABILITY OF THE MAIN F-REGION TROUGH DETERMINED USING DIGITAL IONOSPHERIC SOUNDER DATA by A.S.Rodger and J.R.Dudeney	4.7
SESSION V – IONOSPHERIC MODIFICATION	
SESSION CHAIRMAN'S SUMMARY by H.Soicher	CS5
THE INFLUENCE OF IONOSPHERIC HEATING ON THE PROPAGATION OF RADIO WAVES by T.B.Jones and R.Robinson	5.1

Reference

IONOSPHERIC MODIFICATIONS BY HF HEATERS
by M.C.Lee, J.A.Kong, H.C.Carlson and S.P.Kuo 5.2

SESSION VI – INCOHERENT/COHERENT SCATTER

SESSION CHAIRMAN'S SUMMARY
by G.Rose CS6

EISCAT: A REVIEW OF RECENT SCIENTIFIC WORKS
by P.Bauer 6.1

IRREGULAR STRUCTURES IN THE HIGH-LATITUDE F REGION OBSERVED USING THE EISCAT INCOHERENT SCATTER RADAR
by J.K.Hargreaves, C.J.Burns and S.C.Kirkwood 6.2

OBSERVATIONS OF THE AURORAL IONOSPHERE USING EISCAT
by W.Kofman and C.Lathuillere 6.3

SESSION VII – MEASURMENT TECHNIQUES/MODELS/MORPHOLOGY AND PHYSICS

SESSION CHAIRMAN'S SUMMARY
by E.Thrane CS7

DANISH AND US GEOPHYSICAL MEASUREMENTS IN GREENLAND AND SURROUNDING AREAS RELATED TO ARCTIC RADIOPROPAGATION
by J.Taagholt 7.1

PROGRESS IN MODELLING THE POLAR IONOSPHERE FROM SOLAR AND MAGNETOSPHERE PARAMETERS
by B.J.Watkins, S.-I.Akasofu and C.D.Fry 7.2

STATISTICS OF AURORAL RADIO ABSORPTION IN RELATION TO PREDICTION MODELS
by J.K.Hargreaves, M.T.Feeney and C.J.Burns 7.3

FORMATION AND DETECTION OF HIGH LATITUDE IONOSPHERIC IRREGULARITIES
by M.C.Lee, J.Buchau, H.C.Carlson, Jr., J.A.Klobuchar and E.J.Weber 7.4

DIRECT IN-SITU MEASUREMENTS OF IRREGULARITIES IN THE MESOSPHERE (85-50 KM) AT 69°N (ANDENES, NORWAY)
by H-U.Widdell 7.5

SESSION VIII – LOW FREQUENCY PROPAGATION

SESSION CHAIRMAN'S SUMMARY
by J.Taagholt CS8

CONDUCTIVITY PROFILES OF THE DISTURBED POLAR IONOSPHERE FROM VLF REFLECTION DATA
by P.A.Kossey, J.E.Rasmussen, E.C.Field and C.R.Warber 8.1

A STUDY OF VLF PROPAGATION AT HIGH SOUTHERN LATITUDES USING SFERICS
by A.Volland, M.Schmolders, G.Proelss and H.Kröninger 8.2

EFFECTS OF THE IONOSPHERE ON ELF SIGNALS DURING POLAR CAP ABSORPTION EVENTS: COMPARISON OF THEORY AND EXPERIMENTS
by E.C.Field, C.R.Warber and R.G.Joiner 8.3

WORLD ATLAS OF GROUND CONDUCTIVITIES WITH PARTICULAR EMPHASIS ON THE HIGH LATITUDE REGION
by K.N.Stokke 8.4

SESSION IX – METEOR BURST/SCATTER

SESSION CHAIRMAN'S SUMMARY
by J.H.Blythe CS9

	Reference
METEOR SCATTER RADIO COMMUNICATION AT HIGH LATITUDES by P.S.Cannon, A.H.Dickson and M.H.Armstrong	9.1
CHARACTERISTICS OF HIGH LATITUDE METEOR SCATTER PROPAGATION PARAMETERS OVER THE 45—104 MHz BAND by J.C.Ostergaard, J.E.Rasmussen, M.J.Sowa, J.M.Quinn and P.A.Kossey	9.2
ROUND TABLE DISCUSSION	RTD
LIST OF PARTICIPANTS	P
BIBLIOGRAPHY	B

TECHNICAL EVALUATION REPORT

Professor Robert D. Hunsucker, Ph.D.
Geophysical Institute
University of Alaska
Fairbanks, Alaska 99775-0800
USA

Introduction

The 36th Symposium of the AGARD Electromagnetic Wave Propagation Panel (EPP) was held at the University of Alaska in Fairbanks, 3-7 June, 1985, with the title "Propagation effects on military systems in the high latitude region". The chairman of the EPP, Dr. J. H. Blythe was assisted by the Technical Program Committee (Chairman, Dr. H. Soicher), the AGARD panel Executive, Lt. Col. T. B. Russell and the Host Nation coordinator, Professor R. D. Hunsucker in facilitating a stimulating symposium which had both technical breadth and depth. Some 70 scientists, engineers and administrators representing eleven NATO countries and Australia presented 43 papers, took three technical tours, participated in a 1 1/2 hour roundtable discussion and in many informal technical discussions. (See Appendix A for a listing of the specific papers presented and Appendix B for a list of symposium participants.

Theme

The following theme of the symposium taken from the meeting announcement explains cogently how and why the Symposium topic was selected.

"With the advent of new systems operating at high latitudes in the field of detection, navigation and communications and with the new experiments at high latitudes ranging from incoherent scatter studies to satellites for studying high latitude irregularity structure, it is of considerable importance to relate the advances in high latitude studies to military systems. The concept of this proposal for a meeting on propagation effects on military systems in the high latitude region is to bring together these two areas.

The behavior of the propagation environment at high latitudes differs from that at lower latitudes, affecting radiowave propagation across the RF spectrum. The differences are ascribed to rugged terrain, severe climatic conditions, and influences of the interplanetary and magnetospheric geophysical events which are guided earthward by the geomagnetic field.

The high-latitude ground region is characterized by a rugged terrain and a tremendous variation in ground electrical characteristics.

The severe climatic conditions include a large daily and seasonal temperature variation, extremes of temperatures, high winds, ice accumulation, precipitation (rain, snow, ice crystals, sleet, hail), surface and elevated temperature inversions which produce large refractive gradients and ducts.

The high latitude ionosphere is affected by two major phenomena: energetic particles from the sun and from the outer magnetosphere penetrate the atmosphere and create ionization at various altitudes; and the solar wind induces an electric field perpendicular to the magnetic field which causes ionization drifts and thus contributes to the formation of ionization irregularities. Some of the ionospheric propagation anomalies created include: auroral oval absorption and polar cap absorption; sporadic E, small scale irregularities (spread F) giving rise to scattering and fading phenomena and causing trans-ionospheric amplitude and phase scintillations; effects of magnetic substorm activity, density troughs, and large sheets of field-aligned ionization.

The symposium will direct its efforts towards propagation problems and solutions for many systems. These topics include satellite communication over polar and auroral latitudes, over-the-horizon radar, low frequency propagation under high latitude conditions, remote sensing of high latitude regions by active and passive EM systems, and HF communications at auroral and polar latitudes. Unique lower atmospheric effects and multipath problems of importance at high latitudes will also be discussed.

With the NATO northern flank nations (in both the European and North-American sectors) situated in the high-latitude region, with NATO air routes across the Atlantic traversing that region, and with surveillance and early-warning systems looking in the direction of the region, the propagation characteristic of the high-latitude region are of critical importance to the mission of the alliance in the areas of communications, navigation and surveillance."

Purpose and Scope

The purpose of this meeting was to bring together ionospheric physicists, communications and systems engineers, plus managers and users of communications and surveillance systems from the NATO countries to exchange information on the subject of the symposium. Included in the scope of the meeting were: (1) detailed experimental studies of ionospheric irregularities and regular structure, (2) results of ionospheric modification (HF heating) experiments, (3) theoretical studies of ionospheric irregularity formation, (4) a global survey of ground conductivities, (5) results of disturbance modeling studies, and (6) high latitude effects on the following systems: a) HF radio communication, b) Trans-ionospheric communications, c) Satellite synthetic aperture radar (SAR), d) MF radio broadcasting, e) Spatially adative propagation, f) HF digital, g) Skywave HF sea-state radar and h) meteor burst communication.

The actual titles of the symposium sessions were:

I. Overview (2 papers)
II. Transionospheric Propagation and Considerations (9 papers)
III. Propagation Aspects of HF Communications (6 papers)
IV. High Latitude HF Probing (7 papers)
V. Ionospheric Modification (2 papers)
VI. Incoherent/Coherent Scatter (4 papers)
VII. Measurement Techniques/Models/Morphology and Physics (5 papers)
VIII. Low-Frequency Propagation (3 papers)
IX. Meteor Burst/Scatter (2 papers)

Evaluation

This section is an attempt to distil the essence of the following items:

A) The Session chairmen's summaries
B) The TER author's evaluation of salient papers
C) The Round Table discussion
D) The TER author's assessment of the overall technical-scientific situation viz à viz AGARD/NATO

The TER author is responsible for the selection, paraphrasing and editing of information from items A and C and bears sole responsibility for opinions expressed in items B and D.

A. Session Summaries

Session I There were two invited review papers; "Solar-terrestrial relationships in the high latitude region" (#1.1), by Professor S.-I. Akasofu of the University of Alaska, and "Media effects on systems in the high latitude region" (#1.2), by Dr. E. Thrane of NDRE-Kjeller, Norway. Paper 1.1 discussed how the magnetosphere responds to the interplanetary magnetic field (IMF) and to the characteristics of the solar wind. This analysis technique makes it possible to predict the geometry of the auroral oval and the intensity of a geomagnetic storm as a function of time if the IMF and solar wind parameters are known. Thrane reviewed the transmission media effects across the radio spectrum at high latitudes, including high latitude propagation effects on the important signal parameters. He concludes that modern technology makes it possible that communications and sensing systems can adapt to the high latitude propagation conditions, but that accurate modeling of this medium is necessary.

Session II Over the last 20 years, the morphology of high latitude irregularities at high latitudes has been explored. These irregularities can be divided into 1. - polar cap, 2. - auroral, 3. - trough and 4. - plasmapause regions. The scintillation studies have clearly shown that auroral irregularities are a function of geomagnetic index, time of day and solar flux. Polar irregularities morphology is also generally understood. The first measurements of total electron content were reported at this conference, giving more information on the extent of polar irregularities including their form and velocity. More importantly there were attempts to link the irregularity studies to large-scale probing of the ionosphere-magnetosphere interaction. The future holds the possibility of understanding the processes that link the high-latitude ionosphere to the magnetosphere and eventually to the sun. The interaction of these physical studies with propagation measurements will lead to means of forecasting and predicting fading of transionospheric signals and to methods for reducing the effects of F-layer irregularities on transionospheric satellite propagation.

Session III The papers by Darnell, Goutelard and Caratori concerned how improved equipment and system design could overcome the problems associated with high latitude propagation. The papers by Quegan, Milsom and Herring and by Damboldt addressed ionospheric modeling at high latitudes, and at mid-latitudes during disturbed periods. The paper by Cormier, et al., described a new experiment between Thule and Goose Bay to measure azimuth and elevation arrival angles of HF skywave signals and illustrated the variability of the auroral ionosphere.

Hunsucker, et al., compared theoretical predictions with experimental results for medium frequency (MF) skywave signals received at Fairbanks, Alaska, and concluded that these signals were dominated by D-region absorption and that the FCC standard curves should include some variability for auroral latitudes.

Session IV This session was devoted to measurements at high latitudes, five of the papers dealt with oblique backscatter and two described zenithal sounders. The reports presented show that the measurements taken in high latitudinal regions are particularly difficult, notably because of the complexity of the phenomena which develop there. They imply the implementation of complex systems, and the results show the necessity of following up these studies in the years to come.

Session V Intentional modication (or heating) of the ionosphere by high-powered radio waves continues to be a subject involving much experimental and theoretical interest. Ionospheric changes that result from such heating are on a wide range of spatial and temporal scales. Such changes permit detailed investigation of the physical processes occurring through observations of the amplitude, phase and spectral content of radio waves that traverse the heated volume.

Session VI Bauer reviewed recent scientific work using EISCAT. Results of large, medium and small scale studies were discussed, and comparisons between EISCAT and the STARE radar measurements were communicated.

In order to investigate small structures in the high latitude F-region, Hargreaves et al., have used beam scanning of EISCAT. The magnitudes of irregularities observed in four runs between 1982 and 1984 are analyzed with periods shorter than 2 minutes. Field aligned irregularities of scales of more than a few kms can be traced by the EISCAT UHF radar up to heights of about 700 km.

Kofman and Lathuillere used EISCAT to investigate the response of the ionospheric plasma to the energy deposition of particle precipitation during disturbed conditions as compared to undisturbed situations. They obtained results on the change of ion composition in response to electron precipitation and Joule heating, and on the variation of neutral density and temperature depending on the energy input.

Jones et al., presented results obtained from experiments with the SABRE radar. The strongest backscatter between 13-19 UT and 23-03 UT was found associated with the main electrojets, and only weak backscatter occurred around the convection reversals. The aspect angle attentuation can take any value between 0 and 10 dB per degree depending on the absolute intensity measured. The characteristics of the backscatter irregularities are important to estimate the qualty of communications and surveillance systems operating in either HF or VHF frequency bands at these latitudes.

Session VII As suggested by the session title, a variety of subjects were discussed. The first paper by Taagholt gave an overview of geophysical measurements in the Greenland area, emphasizing the importance of this area for Arctic radio propagation and giving examples of the very considerable activity initated by Danish and US agencies.

Modelling of the Arctic propagation medium was addressed in two papers by Watkins and Hargreaves. The two authors had very different approaches: Watkins described a three dimensional ionospheric model based on physical processes governing solar-terrestrial interactions, whereas Hargreaves presented a statistical model for ionospheric absorption based on riometer measurements at arctic stations.

Lee described an interesting study of the physical mechanisms responsible for the generation of high latitude ionospheric irregularities. Progress is being made in this field, which is of great importance for radio systems in high latitudes.

The final paper in the session dealt with phenomena in the mesosphere. Dr. Widdel presented new results from tracking of chaff clouds. These measurements provide new insight into the dynamical processes in the non-ionized air in the lower ionosphere. These processes are of importance for the understanding of the coupling between the ionized and neutral species.

Session VIII Field presented lower ionosphere conductivity profiles which were derived from oblique VHF soundings in North Greenland during a large solar proton event. The results were compared with conductivity data derived from satellite measurements of the proton flux, at various energies. Although the results obtained from the two data sources differ, both methods show a conductivity during a solar proton event, which exceeds the conductivity during undisturbed conditions, by two or more orders of magnitude.

Prolss presented a study which comprises theoretical calculations and measurements of lightning discharges. The maximum spectral energy of the pulses are typically in the 5-9 KHz frequency range. The lightning discharges seem to be the predominant natural source of electromagnetic energy in this frequency range, and the analysis has shown, that it is possible to determine the propagation characteristics of the Earth - Ionosphere waveguide at VLF frequencies, by receiving the signals from this source at a distant location. In addition, it is possible to determine the location of thunderstorm areas.

In a second paper, Field presented a study which concerned unexpected attenuation of ELF signals in the Gulf of Alaska during PCA events. Calculations show that the attenuation might be caused by refraction of the ELF field into the Polar Cap during PCA events.

Stokke discussed ground conductivities with particular emphasis on the high latitude region. The earth's conductivity is a determining factor for low frequency propagation. Typical values of arctic ground conductivity, which can vary by six orders of magnitude for different types of terrain was presented. The importance of including information on the seasonal variation of the earth conductivity in the Arctic areas in the first edition of the CCIR conductivity atlas was discussed. An atlas is planned for publication during the fall 1985.

Session IX This session comprised just two papers. However, in combination they give a rather complete account of the current state of the art. Meteor Burst Communication (MBC) systems were actively studied in the 50's and have been under review ever since, but have never been used significantly in military systems. Recent advances in receiver systems and integrated circuit technology have led to renewed interest, reflected in the two papers, which concentrate on aspects relevant to high latitudes.

The two papers form a valuable complementary pair, showing that data is being gained which would enable system design to be undertaken with confidence in the event of a decision to deploy. This data covers many new aspects which were not addressed in earlier studies, such as the integrity of security in various propagation events, the effect of polarization rotation, and the overall influence of frequency.

B. Comments on Some Salient Papers

The following discussion contains summaries by the TER author of papers in the order they were presented at the symposium which he considered to be of the most importance to the mission of NATO as defined by AGARD.

Welcoming address by Professor Juan Roederer.

Professor Roederer, Vice Chairman of the U.S. Arctic Research Commission and Director of the Geophysical Institute of the University of Alaska, described the developments leading to signing

into U.S. law the formation of the Arctic Research and Policy Act of 1984 which establishes an Arctic Research Commission and an Interagency Arctic Research Policy Committee. It designates the National Science Foundation as the lead agency responsible for implementing arctic research policy. It mandates the formulation of a comprehensive five-year Arctic Research Plan and it requires the preparation of a single, integrated multiagency budget request for arctic research.

In the fields of research of NATO/AGARD interest, some important recommendations and related priorities are being considered.

Concerning defense-related issues, the following research areas are being identified as needing special emphasis:

1. To improve the reliability of prediction of auroral, ionospheric and magnetic disturbances in the Arctic regions.

2. To study the mechanisms responsible for the formation of ionospheric inhomogeneities and their effects on electromagnetic wave propagation.

3. To obtain a long-term data base and to maintain a real-time information flow on the natural electromagnetic and particle radiation background using ground-based, rocket and satellite techniques.

The present AGARD Symposium dealt with a research subject that will be given high priority by the Arctic Research Commission, and which in its applied aspects, is already receiving high priority in the framework of the general Arctic Policy that is being forged by the President.

The new U.S. Arctic Policy decisions should be welcomed not only by the United States scientific community with interests in the Arctic, but also by the residents of the Arctic, by the private sector operating in the Arctic, and by our NATO partners.

Session I - Paper 1.1. Professor S.-I. Akasofu, "Solar-terrestrial relationships in the high latitude Region". Akasofu presented a prediction scheme which has as inputs the solar wind parameters and the vector description of the interplanetary magnetic field, then uses a very sophisticated computer modeling scheme to obtain the geometry of the auroral oval and the intensity of the geomagnetic storm - which are the main parameters of use to model the disturbed high-latitude ionosphere. The paper by Watkins, et al., in Session VIII extends these results to the polar ionosphere.

Session I - Paper 1.2. Dr. Eivand Thrane, "Media effects on systems in the high latitude region", Thrane - gives a good review of the salient media effects.

Session II - Paper 2.2. Dr. J. A. Klobuchar, et al., "Total electron content and L-band amplitude and phase scintillation measurements in the polar cap ionosphere", presented the first measurements of absolute total electron content (TEC) and L-band amplitude and phase scintillations from a polar cap station. The observations showed a 100% increase in TEC above background levels, sometimes lasting for over two hours. Phase scintillations were highest during some of the enhanced TEC periods. These results should be applicable to the design and operation of L-band satellite systems operating in the polar cap.

Paper 2.4. - Dr. Jules Aarons, "F layer irregularities at plasmapause and auroral latitudes" - summarized the morphology of F-layer irregularities in two latitude regions of considerable importance to radio propagation - the plasmapause and auroral latitudes.

Paper 2.8. - Dr. S. Talbot, et al., "EHF/SHF ray bending", showed that ray bending was about 0.1° for 10° elevation angles to about 0.75° for 0° elevation angle under standard atmospheric conditions. This bending was nearly independent of frequency in the SHF/EHF range. These results have implication on tracking and spatial acquisition for satellites at high latitudes.

Session III - Paper 3.2. Dr. S. Quegan, et al., "Ionospheric modelling and HF radio systems at high latitudes" - describes a physically-based numerical model of high latitude ionospheric structure which is at a fairly advanced state of development. When completed, it should provide better HF system performance.

Paper 3.3. - Dr. M. Darnell, "Techniques for improving the reliability of mobile HF communications over high-absorption paths", presented description of a system which uses various forms of diversity processing, relaying, meteor burst and ionospheric scatter modes and modulation and coding schemes to increase the reliability of high latitude HF mobile communication.

Session IV - Paper 4.5 - Dr. R. A. Greenwald, et al., "Observations of very high latitude ionospheric irregularities with the Goose Bay HF radar", provided information on the morphology of F-region irregularities in the latitude range of importance to some OTH radar systems.

Papers 4.6 and 4.7. - Dr. Berkey, et al., and Mr. Rodger, et al., respectively, "Observations of the main ionospheric trough from Antarctica", these papers, taken together describe the variability of the trough, which is a governing factor for HF propagation between midlatitudes and higher latitudes.

Session V - Paper 5.1. - Dr. T. B. Jones, et al., "The influence of ionospheric heating on the propagation of HF waves", an excellent review of how ionospheric modification can markedly affect HF propagation.

Session VI - Paper 6.1. - Dr. P. Bauer, "EISCAT: A review of recent scientific works", results obtained using the EISCAT system in northern Scandinavia, such as - plasma convection and heating in the auroral oval, particle precipitation, etc., are described, The EISCAT radar provides

excellent data describing the ionospheric conditions for NATO northern area HF communications.

Paper 6.4 - Dr. T. B. Jones, et al., "SABRE radar observations in the auroral ionosphere". This VHF radar system provides a comprehensive picture of E-region structure and dynamics in the ionospheric region off the central west coast of Norway.

Session VII. - Paper 7.1 - Dr. Jorgen Taagholt, "Danish and U.S. geophysical measurements in Greenland and surrounding areas related to arctic radio propagation", describes the large array of geophysical instrumentation in and near Greenland which can quite comprehensively describe the ionosphere from 60° to 80° geographic latitute in an area of considerable strategic importance for north Atlantic radio communication.

Paper 7.2. - Dr. B. J. Watkins, "Progress in modelling the polar ionosphere from solar and magnetosphere parameters", as mentioned in the Section I Summary, this paper is complementary to Dr. Akasofu's paper and extends the prediction and modelling scheme to include the polar ionosphere.

Session VIII - Paper 8.1 - Dr. E. C. Field, et al., "Effects of the ionosphere on ELF signals during polar cap absorption events: Comparison of theory and experiments" - gives a 2D computer ray-tracing analysis of conditions in the polar D-region which may have influenced a severe ELF signal loss at a submarine in the Gulf of Alaska. Could be of use in similar communication scenarios.

Paper 8.4. - Dr. K. N. Stokke, "World atlas of ground conductivities with particular emphasis on the high latitude region", described methodology and contents of a forthcoming CCIR Atlas on ground conductivities which should be of help in designing systems and communication links at high latitudes.

Session IV - Papers 9.1 and 9.2 - Dr. P. S. Cannon, et al., and by Dr. J. Ostergard et al., - these complementary papers review meteor burst communication (MBC) and describe some recent results pertaining to design and implementation of the MBC mode, which has considerable utility for some NATO communications requirements.

C. Summary of Round Table Discussion

A lengthier description of the Round Table Discussion held during the last session of this symposium by Professor Hunsucker is included in AGARD-CP-382, so only the highlights will be included in the TER.

Four questions were posed to Symposium participants the day before the Panel Discussion.

1. In the context of the subject of this symposium (Propagation effects on Military Systems in the High Latitude Region), what is the state of our understanding at this time?

2. What answers has this symposium provided?

3. What directions for future research?

4. What operational needs require this understanding?

The four Round Table Discussion panel members' statements are herewith summarized.

Dr. R. A. Greenwald (U.S.) - Discussed the differing points of view of the ionospheric physicists (researchers) and the communications and radar system operators and designers ("users") and concluded that people who are users should give a bit more attention to what is going on in the research community and see how the results and equipment used by researchers might be supported and might lead to improved understanding of their problem.

Dr. Piere Bauer (France) - emphasized the need for good physical characterizations of specific communication channels and pointed out the importance of using incoherent scatter radars and other radio techniques together to help solve the ionospheric research problems. He also stressed the importance of constructing complete, accessible uniformly formatted data bases.

Dr. G. Rose (W. Germany) - reviewed the capabilities of ionospheric modification (heating) techniques to learn the physics of the ionosphere, and indicated some practical communication applications.

Dr. E. Thrane (Norway) - described his experience with present versions of ionospheric propagation prediction schemes and made a plea for improving these prediction programs by utilizing presently existing ionospheric data bases.

Mr. Alan Rodger (U.K.) - stressed the importance of utilizing simple ionosonde data to supplement incoherent scatter data on the ionosphere. He also mentioned the use of coherent backscatter systems added to the other systems to obtain a data base to include ionospheric models. In closing, he stressed the importance of validating northern hemisphere ionospheric models in the Antarctic because the solar and geophysical coordinate system down there is fundamentally different - also he stressed the importance of the midlatitude trough physics for radio propagation studies.

After the panel members presentations, a rather lively audience participation ensued. The gist of most discussions concerned the needs of the users - the common perception being that they are quite often unmet in ionospheric research - and the concerns of the physicists that they needed adequate support and time to produce physically correct models.

The following closing comments were made by the Chairman of the Round Table Discussion.

In addition to the foregoing discussion, some conference participants submitted written responses to the four questions posed at the start. The following points were salient in the written responses:

1. The EPP should continue to study the arctic ionospheric effects on radio systems.

2. The arctic regions have a very strong strategic position in the NATO radio communication system.

3. HF modes may be one of the last means of communication in a conflict.

4. Future meetings should contain at least one classified session to ensure that specific needs are being met.

Conclusions

This 36th Symposium of the AGARD Electromagnetic Wave Propagation Panel (EPP) has reinforced the conviction that the high latitude environment has profound effects upon specific military systems such as OTH radar, HF "analog" and digital communication systems, and EHF/SHF satellite navigational systems. Furthermore, there seems to be a very favorable juxtaposition of advances in ionospheric modeling, radio research techniques, and to a lesser extent, theoretical studies in the mid 1980's which can ameliorate these high latitude effects. To give two examples, recent advances in integrated circuit and receiver technology suggest that Meteor Burst Communication (MBC) systems offer a viable method of achieving secure medium-range point-to-point comunication; while advances in equipment and system design now make operational HF Mobile adaptive networking systems possible.

The table below is an effort to summarize the status of development of elements of the research Triad of "Theory-Experimental Results - Modeling" as a function of some specific military systems. The letters G = Good, F = Fair, and P = Poor express the TER author's opinion.

In the High Latitude Region
Adequacy of:

Specific Radio System	Theory	Experimental Results or Data Base	Model (Simulation)	Comments
HF Digital Comm., HF voice point-to-point HF Mobile	G	G	F	In the next 5 years quite good models should be available
OTH Radar	F	F - G	F	Data available from new techniques is now becoming available
Meteor Burst Comm. (MBC)	G	P - F	?	Holds considerable promise in near future
Satellite Navigation Satellite Surveillance (SAR) Satellite Comm.	F - G	F - G	F	New data are becoming available
MF Broadcasting	G	P	P	New data are becoming available
ELF Comm.	F - G	F	F - G	Improved models are becoming available
Ionospheric Modification	F - G	F - G	F	Considerable information is now available

The need for "interpreters" to communicate the results of theory, experiment and modeling to the "user community" became apparent during this symposium. "Users" need to be cognizant of recent research findings in order to ask the correct questions, and researchers need to be aware of specific user needs in order to "fine tune" some of their research efforts. Vehicles such as the AGARD/EPP Symposia are necessary, but not sufficient in themselves. Individuals must also take positive steps to improve communication between these groups.

Recommendations

1. Continue the AGARD/EPP Symposia and Lecture series.
2. Attempt to identify good "interpreters" between the communities.
3. Increase the awareness of the radio research community of the AGARD/EPP meetings and encourage more scientists to participate.
4. NATO/AGARD should further encourage visits and exchanges between radio researchers and users - even possibly visits to selected communication facilities.
5. Perhaps there should be wider dissemination of AGARD Conference Proceedings and other reports.

APPENDIX A

PROPAGATION EFFECTS ON MILITARY SYSTEMS IN THE HIGH LATITUDE REGION

PROGRAMME

Monday, 3 June 1985

Session I - Overview

Chairman: Dr. H. Soicher (US)

0930 1.1. *Solar Terrestrial Relationships in the High Latitude Region (Invited Review)*
S.-I. Akasofu, University of Alaska, Fairbanks, Alaska, US

1015 1.2. Media Effects on Systems in the High Latitude Region (Invited Review)
E. Thrane, NDRE, Kjeller, NO

1025 Break

Session II - Transionospheric Propagation and Considerations

Chairman: Dr. J. Aarons (US)

1100 2.1. Recent Hilat Results (Invited Review)
E. Fremouw, Physical Dynamics, Inc., Bellevue, WA, US

1130 2.2. Total Electron Content and L-Band Amplitude and Phase Scintillation Measurements of the Polar Cap Ionosphere
J. A. Klobuchar, G. J. Bishop, AFGL Hanscom AFB, MA and D. H. Doherty, Emmanuel College, Boston, MA, US

1200 2.3. Variability of Transionospheric Signal Time Delay at High Latitudes Near Solar Minimum
H. Soicher, U. S. Army CECOM, Fort Monmouth, NJ, US

1230 Lunch

1400 2.4. F-Layer Irregularities at Plasmapause and Auroral Latitudes
J. Aarons, Boston University, Boston, MA, US

1430 2.5. Influence of Polar Irregularity Shape and Velocity on the Design of Airborne Satellite Communications Systems
A. L. Johnson, USAF Avionics Lab, Wright Patterson AFB, OH, US

1500 2.6. Propagation Effects on Satellite-Borne Synthetic Aperture Radars
C. L. Rino and J. Owen, SRI International, Menlo Park, CA, US

1530 Break

1600 2.7. High-Latitude Scintillations using NNSS Satellites
L. Kersley, University College of Wales, Aberystwyth, UK

1630 2.8. EHF/SHF Ray Bending
S. Talbot, RADC Griffiss AFB, New York, D. Providakes, D. Zimmerman and D. Post, MITRE Corporation, Bedford, MA, US

1700 2.9. E.H.F. Propagation Measurements along Satellite-Earth Paths in the Canadian High Arctic
I. Lam and J. I. Strickland, CRC, Ottawa, CA

Tuesday, 4 June 1985

Session III - Propagation Aspects of HF Communications

Chairman: Dr. P. Cannon (UK)

0930 3.2. Ionospheric Modelling and HF Radio Systems at High Latitudes
S. Quegan, J. D. Milsom, and R. N. Herring, GEC Research Labs, Marconi Research Centre, Chelmsford, UK

1000 Break

1030 3.3. *High Latitudes Spatially Adaptive Propagation Experiment*
R. J. Cormier, E. Tichovolsky, RADC, Hanscom AFB, MA and R. Greenwald, Johns Hopkins University, Laurel, MA, US

1100 3.5. Techniques for Improving the Reliability of Mobile HF
M. Darnell, University of York, UK

1200 Lunch

1330 3.6. Propagation Characteristics of Medium Frequency Skywave Signals from the Continental US and Canada Received at Fairbanks, Alaska
R. D. Hunsucker, B. S. Delana, University of Alaska, Fairbanks, AK and J. C. H. Wang, FCC, Washington, D.C. US

1400 3.7. Optimization of HF Digital Radio Systems at High Latitudes
C. Goutelard and J. Caratori, University of Paris-Sud, FR

1430 3.8. Observations with an Ionosonde in Northern Germany near the Mid-Latitude Trough
T. Damboldt, Forschunginsstitut der DBP, Darmstadt, FRG

1500 Break

Session IV - High Latitude HF Probing

Chairman: Prof. C. Goutelard (FR)

1530 4.1. Ionospheric Factors Affecting the Performance of HF Sky-Wave Sea-State-Radars at High Latitudes (Invited Review)
P. A. Bradley and A. J. Gibson, Rutherford Appleton Lab, Chilton, UK

1600 4.2. Spectral Characteristics of High Frequency Waves Backscattered by Small Scale F region Irregularities: Evidence of Strong Sub-Auroral Ion Flow
A. Bourdillon, Laboratoire Exosphere, Paris, FR

1630 4.3. Small-Scale Irregularities in the High-Latitude F-Region
C. Hanuise, J. P. Villain, LSEET/CNRS, Toulon, C. Beghin, LPCE/CNRS, Orleans, and G. Caudal, CNET-CRPE, St. Maur les Fosses, FR

1700 4.4. On the Relationship of F Region Structure in the Dayside Auroral Oval to HF Backscatter Signatures Attributed to the Polar Cusp
J. D. Kelly, R. T. Tsunoda, SRI International, Menlo Park, CA, US, J. K. Oleson and P. Stauning, Danish Meteorological Institute, Copenhagen, DE

Wednesday, 5 June 1985

Session IV - Continued

0830 4.5. Observations of Very High Latitude Ionospheric Irregularities with the Goose Bay HF radar
R. A. Greenwald and K. B. Baker, APL/Johns Hopkins University, Laurel, MD, US

0900 4.6. Observations of the Mid-Latitude Ionospheric Trough from Antarctica
F. T. Berkey, Utah State University, Logan, UT, US and M. Jarvis, British Antarctic Survey, Cambridge, UK

0930 4.7. The Variability and Predictability of the Main F-Region Trough Determined Using Digital Ionospheric Sounder Data
A. S. Rodger, J. R. Dudeney, British Arctic Survey, Cambridge, UK

1000 Break

Session V - Ionospheric Modification

Chairman: Dr. G. Rose (FRG)

1400 5.1. EISCAT: A Review of Recent Scientific Works (Invited Review)
P. Bauer, CNET-RPE, Issy-les-Moulineaux, FR

1445 5.2. Irregular Structures in the High Latitude F-Region Observed Using EISCAT Incoherent Scatter Radar
J. K. Hargreaves, C. J. Burns and S. C. Kirkwood, University of Lancaster, Lancaster, UK

1515 Break

1545 6.3. Observations of the Auroral Ionosphere Using EISCAT
W. Kofman and C. Lathuillere, CEPHAG, Domaine Universitaire, Grenoble, FR

1630 6.4. Sabre Radar Observations in the Auroral Ionosphere
T. B. Jones, J. A. Waldock, E. C. Thomas, C. P. Stewart and T. R. Robinson, University of Leicester, UK

Thursday, 6 June 1985

Session VII - Measurement Techniques/Models/Morphology and Physics

Chairman: Prof. E. THRANE (NO)

0830 7.1. Danish and US Geophysical Measurements in Greenland and Surrounding Areas Related to Arctic Radio Propagation
J. Taagholt, Danish Scientific Liaison Officer for Greenland, Copenhagen, DE

0900 7.2. Progress in Modelling the Polar Ionosphere from Solar and Magnetosphere Parameters
B. J. Watkins, S.-I. Akasofu and C. D. Fry, University of Alaska, Fairbanks, Alaska, UK

0930 7.3. Statistics of Auroral Radio Absorption in Relation to Prediction Models
J. K. Hargreaves, M. T. Feeney and C. J. Burns, University of Lancaster, Lancaster, UK

1000 Break

1100 7.5. Formation and Detection of High Latitude Ionospheric Irregularities
M. C. Lee, MIT, Cambridge, MA, J. A. Klobuchar and H. C. Carlson, AFGL, Hancom AFB, MA, US

1130 7.7. Direct In-Situ Measurements of Turbulent Zones in the Mesosphere (85-50 km) at 69 N (Andenes, Norway)
H. W. Widdell, Max Planck Institut, Lindau, FRG

1200 Lunch

Session VIII - Low Frequency Propagation

Chairman: Mr. J. Taagholt (DE)

1330 8.3. Comparison of D-Region Conductivity Profiles of the Disturbed Polar Ionosphere Calculated from Incident Particle Flux Data and by Inversion of VLF Sounding Data
E. C. Field and C. R. Warber, Pacific Sierra Research Corp., Los Angeles, CA, P. A. Kossey and J. E. Rasmussen, RADC, Hanscom AFB, MA, US

1430 Break

1500 8.4. World Atlas of Ground Conductivities with Particular Emphasis on the High Latitude Region
K. N. Stokke, Norwegian Telecommunications Administration, Oslo, NO

Friday, 7 June 1985

Session IX - Meteor Burst/Scatter

Chairman: Dr. H.J. BLYTHE (UK)

0900 9.1. Meteor Scatter Radio Communications at High Latitudes
P. S. Cannon, A. H. Dickson and M. H. Armstrong, Royal Aircraft Establishment, Farnorough, UK

0930 9.2. Characteristics of High Latitude Meteor Burst Propagation Parameters Over the 40-150 MHz Band
J. Ostergaard, Elektronik Centralen, Copenhagen, DE, J. E. Rasmussen, P. A. Kossey, M. J. Sowa, J. M. Quinn, RADC, Hanscom AFB, MA, US

1015 Break

1045 Round Table Discussion

Chairman: Prof. R. D. Hunsucker (US)

1215 Closing Ceremonies

WELCOMING ADDRESS

Juan G. Roederer
Vice Chairman, U.S. Arctic Research Commission
and
Director, Geophysical Institute
University of Alaska-Fairbanks
Fairbanks, Alaska 99775-0800

It is both a pleasure and an honor to welcome you as the Vice Chairman of the newly established United States Arctic Research Commission, and as the director of the Geophysical Institute of the University of Alaska, Fairbanks.

Your meeting deals with a research subject that will be given high priority by the Arctic Research Commission, and which in its applied aspects, is already receiving high priority in the framework of the general Arctic Policy that is being forged by President Reagan.

Until a few years ago, the U.S. had no coherent arctic research policy. General arctic policy guidelines had been issued by the National Security Council, but were only occasionally referred to by the Departments of State and Defense -- and more or less ignored by other federal agencies. Several attempts to establish a research policy for the Arctic were made during the seventies, but none ever reached the stage of implementation. By and large, the responsibility for planning, implementing, and funding arctic research remained divided between several federal agencies, the State of Alaska, and private groups whose mandates or objectives were often unconnected.

The result of this pluralistic approach to U.S. science in the Arctic was that research was being conducted in piece-meal fashion; individual studies were proposed and supported separately, and their costly logistic requirements were being funded in competition with research carried out under lesser demanding environmental conditions in the rest of the country. Fundamental data-gathering and interpretation of information were the responsibility of public agencies whose missions and budgets did not reflect the priorities of arctic issues. All this, in spite of the fact that the resource development in the United States arctic and subarctic regions and adjacent waters and the deployment of defense systems at high latitude in North America and in the Arctic Ocean had become a vital part of our nation's economy, trade, and security.

Fortunately, the situation has begun to change. A change that should be welcomed not ony by the United States scientific community with interests in the Arctic, but also by the residents of the Arctic, by the private sector operating in the Arctic, by our NATO partners and even also by our neighbor across the Bering Strait, because a better knowledge of the Arctic will be an increased insurance for peace.

Several important developments concerning arctic research policy took place in recent years, involving the National Academy of Sciences, some federal agencies and Alaska Senator Frank Murkowski who in 1982 introduced a bill in Congress that was passed in final form as the Arctic Research and Policy Act of 1984, signed into law by President Reagan in July of that year.

Prior to this, the President had issued a National Security Decision Directive reaffirming earlier statements on general arctic policy, and declaring that this policy will be based on (i) the protection of essential U.S. security interests in the Arctic; (ii) the support of a sound and rational development in the arctic region; (iii) the promotion of scientific research on the Arctic or which can best be done in the Arctic; and (iv) the promotion of international cooperation in the Arctic.

The Arctic Research and Policy Act of 1984 establishes an Arctic Research Commission and an Interagency Arctic Research Policy Committee. It designates the National Science Foundation as the lead agency responsible for implementing arctic research policy. It mandates the formulation of a comprehensive five-year Arctic Research Plan and it requires the preparation of a single, integrated multiagency budget request for arctic research.

Our Commission was appointed by the President in February, 1985. It is advisory in nature, but its mandate, if carried out responsibly, may well lead to a departure from the currently fragmented, in part neglected, in part duplicated, research on arctic problems. We are to develop and recommend an integrated research policy for the Arctic, assist the Interagency Committee in implementing the policy and in developing a 5-year research plan, to be updated biennially, and facilitate the cooperation in research between federal, state, and local agencies, the private sector, and the residents of the Arctic. In addition, federal agencies are directed to consult with the Commission before undertaking major federal actions relating to arctic research, and the Commission must report to Congress on the adherence of the President's annual budget request to the 5-year Arctic Research Plan.

The Polar Research Board of the National Academy of Sciences is helping both the Interagency Committee and the Presidential Commission to identify research needs and

define priorities therefor. The Commission will consider the Academy's recommendations exclusively on the basis of their scientific and technological merit, in independence of individual agencies' views and in independence of cost factors -- without, of course, losing sight of the constraints given by the chronic financial austerity that is here to stay.

In the fields of research of your meeting's particular interest, some important recommendations and related priorities are being considered.

Concerning defense-related issues, the following research areas are being identified as needing special emphasis:

1. To improve the reliability of prediction of auroral, ionospheric and magnetic disturbances in the Arctic regions.

2. To study the mechanisms responsible for the formation of ionospheric inhomogeneities and their effects on electromagnetic wave propagation.

3. To obtain a long-term data base and to maintain a real-time information flow on the natural electromagnetic and particle radiation background using ground-based, rocket and satellite techniques.

Concerning basic research issues, the following problems are being identified for special attention:

1. The study of polar cap phenomena and their relations to magnetospheric tail and boundary processes.

2. The study of solar variability-controlled effects on the neutral atmosphere at high latitude.

3. The study of processes responsible for magnetosphere-ionosphere coupling.

This gives you a glimpse into the immense task that lies before us, for we must focus with equal attention on and give equal time to other scientific areas, as diverse as the social sciences, glaciology, economics, human biology, native culture, arctic engineering and medicine.

Wish us luck -- as I do wish you luck and success in the conference that is to begin.

SUMMARY OF SESSION I

Overview

by

Dr H.Soicher
Session Chairman

This introductory session consisted of two invited reviews. The first dealt with the role of the solar wind and the interplanetary magnetic field (IMF) in controlling high latitude upper atmospheric phenomena, while the second dealt with system radio propagation characteristics in the high latitude transmission media.

Akasofu first discusses how the magnetosphere responds to the three components of the interplanetary magnetic field (IMF) and to the power of the solar wind — magnetosphere dynamo. Through the understanding gained by such analysis it is possible to predict the geometry of the auroral oval and the intensity geomagnetic storm as a function of time, if the time variations of the solar wind speed and the IMF three components could be predicted. He demonstrates a prediction scheme by a computer model study.

Thrane reviews the transmission media effects across the radio frequency (RF) spectrum at high latitudes. General and unique high latitude propagation effects on signal attenuation, refraction/reflection, scatter, polarization changes, diffraction, multipath and ducting are discussed. He concludes that modern technology opens possibilities for communication and remote sensing systems that can adapt to a complex and rapidly changing media, such as the high latitude propagation media, but accurate modelling of the transmission media is necessary for optimal system design.

SOLAR-TERRESTRIAL RELATIONSHIPS IN THE HIGH LATITUDE REGION

S.-I. Akasofu

Geophysical Institute, University of Alaska, Fairbanks, Alaska 99701

1. SUMMARY

In the first part of the paper, we show how the magnetosphere responds to the three components (B_x, B_y, B_z) of the interplanetary magnetic field (IMF) and to the power ε of the solar wind-magnetosphere dynamo. In particular, it is shown that the geometry of the auroral oval and the polar cap depends greatly on the magnitude and signs of the IMF three components. Geomagnetic storms result when the dynamo power ε exceeds $\sim 10^6$ Mwatts. Once such knowledge is available, it is possible to predict the geometry of the auroral oval and the intensity of a geomagnetic storm as a function of time, if one can predict time variations of the solar wind speed and the IMF three components. We demonstrate such a possibility by a computer model study, namely by the first generation numerical forecasting scheme.

2. INTRODUCTION

Geomagnetic storms and auroral activity are caused by a large-scale electrical discharge process surrounding the earth and are known to be one of the most serious hazards to radio communications, navigation and radar systems. The magnetic fields produced by the fluctuating discharge currents can be identified as the geomagnetic storm fields. The aurora is an optical manifestion of the discharge process which is caused by collisions of current-carrying electrons with the polar upper atmospheric atoms and molecules.

During the last several years, we have made major progress in understanding the function of the dynamo which supplies the power for this auroral discharge and the role of the solar wind and the interplanetary magnetic field (IMF) in controlling the dynamo power and high latitude upper atmospheric phenomena, in particular, the three components (B_x, B_y, B_z) of the IMF. Responses of the magnetosphere to the IMF changes may be classified as:

(a) $B_z < 0$
(b) $B_z > 0$, $B_y \sim 0$, $B_x \sim 0$
(c) $B_z > 0$, $B_y \gtrless 0$
(d) $B_z > 0$, $B_x \gtrless 0$

The reasons for this classification are as follows:

(a) When the IMF B_z component becomes negative, the power of the dynamo is large and magnetospheric substorms result. As a result, effects of the IMF $B_z < 0$ are too dominant to see effects of the other components.
(b) When the IMF B_z component has a large positive value (but $B_y \sim 0$, $B_x \sim 0$), the magnetosphere seems to have a unique response to it.
(c) and (d) When the IMF B_z component is positive, effects of the B_y and B_x components can be much more clearly seen than during a period of $B_z < 0$.

It should also be mentioned that the dynamo power ε of the solar wind-magnetosphere dynamo is given by

$$\varepsilon = VB^2 \sin^4 (\theta/2) \ell_o^2 \qquad (1)$$

Where

V = the solar wind speed
B = the magnitude of the IMF
θ = the polar angle of the IMF
ℓ = constant ($\sim 7 R_E$)

In the first part of this paper, we examine in some detail responses of the magnetosphere for the conditions (a), (b), (c) and (d). In the second part of this paper, we study how solar activities cause changes of the three IMF components and the solar wind-magnetosphere dynamo power ε. It is hoped that such a study will eventually lead us to numerical forecasting of magnetospheric disturbances.

2. RESPONSES OF THE MAGNETOSPHERE TO THE IMF

It is instructive to examine effects of the three components of the IMF vectors on the basis of a simple modeling method. We construct first a model of the magnetosphere without the presence of the IMF, using the standard procedure, namely by having an image dipole and the tail current system. The IMF is superimposed by a linear superposition - like a situation in vacuum. We test the qualitative validity of this method by determining the geometry of the open field line region for a set of the observed values of the IMF three components, B_x, B_y and B_z and then comparing the geometry of the open

field line region thus determined with the geometry of the observed oval about one hour after the IMF observation. An example of such tests is shown in Figure 1 (Murphree et al., 1984). In the figure, a dot indicates the foot of a closed field line. That is to say, a field line originating at the location of a dot reaches the conjugate point in the southern hemisphere after crossing the equatorial plane, while a circled dot indicates the foot of an open field line. The field line originating at the location of a circled dot is connected to the IMF field line across the magnetopause. One can see that the open field line region is fairly accurately bounded by the poleward boundary of the observed oval. It is quite obvious that the above test can provide only a qualitative validity of our modeling and the fair agreement of the boundary of the open field line region and the poleward boundary of the oval may be somewhat fortuitous, particularly because we are using a simple (vacuum) superposition method. Nevertheless, such a modeling method may provide some guidance in interpreting complicated upper atmospheric phenomena in the highest latitude region, particularly when the IMF B_z is positive. We shall see in the following that this is indeed the case.

For the purpose of our study, we assume an IMF vector of magnitude of 5nT. Then, we examine changes of the geometry of the open field line region for two situations: (i) the IMF vector lies and rotates in the y-z plane and (ii) the IMF vector lies and rotates in the x-z plane.

(i) Rotation in the y-z plane

The lower right diagram in Figure 2 shows the geometry of the open field line region when the IMF vector is directed southward ($B_x = 0$, $B_y = 0$, $B_x = -5nT$); for details see Akasofu and Covey (1980) and Akasofu and Roederer (1984). The boundary of the open field line region thus obtained is similar to the poleward boundary of the auroral oval which is a little larger than the average one. Effects of the rotation of the IMF vector can clearly be seen by examining successively the lower middle, lower left, upper right, upper middle and upper left diagrams. One of the interesting features revealed by such a study is that the geometry of the open field line region changes only a little with the rotation of the vector so long as the B_z component is negative. In fact, those changes are, perhaps, difficult to identify by observations. The asymmetry of the open field line region with respect to the noon-midnight meridian becomes obvious only when the B_z component becomes zero or positive. For IMF $B_x = 0$, $B_y = 2.5nT$, $B_z = +4.3nT$ (the latitude angle $\theta = 60°$), the main part of the open field line region is confined in the morning sector. Since the IMF B_z component cannot cause the asymmetry with respect to the noon-midnight meridian, the asymmetry must be caused by the IMF B_y component. It should be noted that the simultaneous open field line region in the southern hemisphere is the mirror image of the northern one, so that it is mainly confined in the evening sector for the same IMF three component values. It should also be noted that when the B_y component is negative ($B_x = 0$, $B_y = -2.5nT$, $B_z = +4.3nT$), the whole situation is reversed; the open field line region in the northern hemisphere is mainly confined in the evening sector, while the southern one is confined in the morning sector.

(ii) Rotation in the x-z Plane

Here, we rotate the IMF vector (of magnitude 5nT) by 360° in the x-z plane. In the upper left diagram of Figure 3a, the IMF is pointed northward ($B_x = 0$, $B_y = 0$, $B_z = +5nT$). Then, as the vector is rotated toward the sun ($B_x > 0$) the open field line region has a circular shape and becomes larger; the lower left diagram shows the situation, when the vector is pointing directly toward the sun. Then, as the vector is rotated further and thus has the southward component (IMF $B_z < 0$), the open field line region is very much like the area bounded by the averge auroral oval. As the vector is further rotated, it points away from the sun ($B_x < 0$) and has the southward component (the two lower diagrams in Figure 3b). The open field line region is still similar to the area bounded by the average oval. The upper right diagram shows the situation when the vector points directly away from the sun. As the vector is further rotated and the B_z component becomes positive (the upper left and middle diagrams), the open field line region has a crescent shape.

Therefore, once again, when the IMF B_z component has a negative value, the open field line region has the geometry which is close to that bounded by the average oval. However, the open field line region has a considerably different geometry, when the IMF B_z component has a positive value. Note also when the IMF has ($B_x = -2.5nT$, $B_y = 0$, $B_z = +4.33nT$), the northern open field line region has a crescent shape, while the geometry of the simultaneous southern region is the same as that for ($B_x = 2.5nT$, $B_y = 0$, $B_z = +4.33nT$.

One of the best ways to test the validity of our simple model is to study solar electron events which also have practical importance in protecting astronauts in polar orbiting shuttles. As mentioned earlier, solar energetic electrons are, in general, perhaps the best tracer of magnetic field lines. McDiarmid et al. (1980) examined the area of entry of solar energetic electrons for various IMF orientations. Figure 3c shows schematically the entry area for (a) IMF $B_x = -20nT$, $B_y = -5nT$, $B_z = +30nT$, and (b) IMF $B_x = 4.3$ nT, $B_y = -0.7nT$, $B_z = +9.2nT$. One can see qualitative similarities between the upper left open field line region in Figure 3b and Figure 3c and between the upper left one in Figure 2 (by reversing the sign of the B_y component) and Figure 3c. In fact, such a close agreement with a very crude modeling method is remarkable (Akasofu et al., 1981).

One of the problems in determining the open field line region by the entry of solar energetic electrons is that their flux is high enough to be used only after a major solar flare, so that this method will not be available at all times. Nevertheless, it is important to extend the work made by McDiarmid et al. (1980) in studying the geometry of the open field line region for various IMF orientations. As we shall see later, other methods have great uncertainties.

3. THE IMF AND THE AURORAL AND PRECIPITATING ELECTRON DISTRIBUTION

Effects of the IMF B_z component on the distribution of the aurora were most systematically studied by Lassen and Danielsen (1978). Their figure is reproduced here in Figure 4. One can see clearly that when the IMF B_z component has a large negative value (-6.9nT), (i) the auroral oval is large and (ii) there is no auroral arc inside the area bounded by the enlarged oval; auroral substorms are invarably in progress in such a situation. As the other extreme situation of a large positive B_z value (+7.0nT), there is no clear indication of auroral arcs along an oval-shaped belt. Instead, the highest latitude region is covered by arcs which align approximately along the sun-earth line (or the noon-midnight meridian). For other values of the B_z component, the auroral distribution varies systematically between the above two extreme situations.

Effects of the IMF B_y component during the period of positive values of the B_z component were also examined by Lassen (1979), but are not necessarily very clearly brought out in his study. However, he suggested that for $B_y > 0$, there is an area of auroral absence in the morning sector, while for $B_y < 0$ it is located in the evening sector.

It is instructive to examine the above IMF effects in 'snap shots'. In Figure 5a and 5b, we see a series of the nightside half of the auroral oval, obtained by the DMSP F-6 satellite, on January 10 and 11, 1983. In the first photograph (1359 UT), the auroral oval was very large, and the auroral activity was high and typical; note that the bottom center is approximately the midnight sector, the upper left and upper right corners are approximately the 18 and 06 MLT meridians, respectively. In the second photograph (1537 UT), the oval became smaller and the aurora became less active. However, the major auroral activity is confined in the morning half of the oval, instead of the midnight sector. In the third and fourth photographs, the oval became even smaller (partly due to the geographic effects). Further, the width of the auroral oval in the morning sector became considerably larger than that in the evening sector, making the area bounded by the oval very asymmetric with respect to the noon-midnight meridian; and the center of the area of auroral absence was located in the evening sector. The situation was similar at 1857 UT. The first photograph on January 11 (0653 UT) shows that a major change occurred after the last photograph (1857 UT) had been taken. The auroral oval was absent (or became too faint to be registered). On the other hand, a number of auroral arcs occupied approximately the area bounded by the average oval. In the following photograph (1520 UT), those arcs disappeared, and instead there appeared two bright arcs. Further at 1152 UT, there was a faint glow covering an area which resembles the area bounded by the auroral oval; there were several faint arcs as well.

At about 03-06 UT on January 10, the B_z component was negative and had a large magnitude. The B_y component became less as time progressed and became positive at ~14 UT. However, the B_y component was equally large and negative. The magnitude of the B_z component became less as time progressed and became positive at ~14 UT. However, the B_y component remained negative. It changed the sign at ~06 UT and had a small magnitude. Therefore, the B_y (<0) effect became apparent only after the IMF B_z component became positive, and the center of the area of auroral absence was located in the evening sector. Thus, this series of observations are qualitatively consistent with the results of the statistical studies by Lassen and Danielson (1978) and Lassen (1979). Assuming that the area of auroral absence coincides with the open field line region, the result is consistent with our model study as far as the asymmetry caused by the B_y component.

After 04 UT on January 11, the B_z component was the dominant component. The appearance of a large number of arcs aligned parallel to the noon-midnight meridian and of the oval-shaped faint glow are one of the most interesting features associated with this large magnitude of the positive B_z component. It has long been known that auroral arcs occur in the highest latitude region during the quiet period and that they tend to align parallel to the noon-midnight meridian. Their general characteristics are very similar to those of arcs which appear along the oval, except for the sun-aligned orientation. Therefore, the formation mechanisms for these arcs and oval arcs must be at least very similar and perhaps identical. These arcs have traditionally been called the 'polar cap arcs' and have received much attention during the last two years as spectacular auroral images taken from the Dynamic Explorer have become available (Frank et al., 1982).

4.1 Auroral Electron Precipitation

As a polar orbiting satellite traverses across the polar region along a dawn-dusk orbit, it crosses the auroral oval twice, once in the evening sector and the other in the morning sector. For example, as the satellite advances into higher latitudes from the dusk side, it will see the so-called 'hard precipitation region' and then the 'soft precipitation region' a little higher on the high-latitude side. Then, after crossing the highest latitude region, the satellite crosses first the 'soft precipitation region' and then 'hard precipitation region' in the lower latitude side. For the IMF $B_z \sim 0$, both precipitation regions are located approximately where the oval is located, namely between ~65° and ~75°. However, as the magnitude of the $B_z > 0$ component increases for several hours, there occurs a spectacular change. Figure 6 is such an example (Meng, 1981). The soft precipitation region expands poleward and tends to fill almost

completely the area bounded by the pre-existing soft precipitation region (Meng, 1981; Makita and Meng, 1984; Hardy, 1984). In the lower part of Figure 6, both precipitation zones are marked along the satellite orbit. In this particular example, one can see that the soft precipitation region is present everywhere, except for a small area above invariant latitude ~85°. In Figure 3a, we found that such a situation could occur for $B_x > 0$ and $B_z > 0$. On the other hand, as soon as the IMF B_z component becomes negative, the width of the soft precipitation region becomes drastically reduced. The corresponding changes of the hard precipitation region is relatively very small. Figure 7 shows an example of this change. One can see that the poleward boundary of the soft precipitation zone shifted from 83.6° to 80.8° in the morning sector, while it shifted from 80.3° to 71° in the evening sector.

Makita et al. (1985) examined also overall changes of the precipitation regions for a number of substorms. Figure 8 shows changes of the distribution of the precipitation regions during a substorm which was associated with a southward turning of the IMF vector, resulting in an increase of the dynamo power ε. One can see that as the IMF B_z component turned southward at the libration point (~250 R_E upstream of the solar wind), the distance between the poleward boundaries of the dawn and dusk soft precipitation regions began to expand equatorward about one hour later, namely when the IMF B_z 'signal' arrived at the magnetosphere. An important point to make here is that the expansion had begun well before the AE index began to increase and that the expansion reached the maximum at about the time when the AE index reached the maximum value. Makita et al. (1984) showed that similar changes occur along the noon-midnight meridian as well.

Assuming that the dawn-dusk dimension of the region of no precipitation gives a reasonable measure of the 'diameter' of the open field line region, one can infer that the amount of the open magnetic flux increases and decreases in harmony with the AE index. That is to say, the amount of the open magnetic flux is not reduced to a minimum value at the peak of a substorm, indicating that substorms are not caused by a sudden conversion of magnetic energy stored prior to substorm onset.

4. DEVELOPMENT OF A GEOMAGNETIC STORM FORECASTING SCHEME

As we have seen in the previous two sections, our understanding of the responses of the magnetosphere to the IMF and solar wind changes has significantly been increased during the last several years. Some of these magnetospheric responses are defined as magnetospheric disturbance features, such as magnetospheric (auroral, geomagnetic, ionospheric, etc.) substorms and storms. Thus, it has become possible to predict or forecast quantitatively magnetospheric substorms and storms as a function of time, if the IMF $B_x(t)$, $B_y(t)$, $B_z(t)$ and V(t) can be predicted. It is opportune to initiate a study of a numerical forecasting scheme, departing from the traditional empirical one.

The success of this forecasting will depend on the progress of two major projects.

(A) Prediction of the power ε (t), $B_x(t)$, $B_y(t)$, $B_z(t)$ and V(t) as function of time with a 6 ~ 12-hour lead time after major solar activities, such as solar flares, sudden disappearance of filaments and coronal mass ejections.

(B) Prediction of the following key magnetospheric quantities as a function of the power ε(t) or of the interplanetary magnetic field $B(B_x, B_y, B_z)$.

(i) The cross-polar cap potential $\phi_{pce}(t)$
(ii) The geometry and size of the polar cap
(iii) The geomagnetic indices AE(t) and Dst(t)

Figure 9 shows our forecasting scheme in a form of block diagram which can be divided into two parts, A and B. In this section, we describe the present numerical forecasting scheme by following Figure 9 and present a progress report in this endeavor. A tentative criteria for most systems which utilize the polar ionosphere are:

ε < 105 Mwatt - Normal operation
ε ~ 5×10^5 Mwatt - Require alert
ε ~ 10^6 Mwatt - Prepare for system failure
ε > 5×10^6 Mwatt - System failure

4.1 Prediction of Power ε(t)

The first step of the prediction of geomagnetic storms and thus of the power ε(t) is reduced to the prediction of solar wind quantities V(t), B(t) and θ(t) in equation (1). This section is based on the method developed by Hakamada and Akasofu (1982) and Akasofu et al. (1983). Note that their method is to provide only a first order construction, temporarily and spatially, of flare-generated shocks and their multiple interactions with each other, as well as with the so-called 'interplanetary corotating interaction regions'. Their method does not simulate the other dynamic, thermodynamic properties that can be found only from the MHD solutions. There have already been a number of simulation studies of solar wind disturbances which are based on numerical solutions of the MHD equations (Dryer, 1974; Wu et al., 1977; Wu, 1980; Dryer et al., 1983; Wu et al., 1983; Dryer, 1984; Han et al., 1984; Gislason et al., 1984). However, a full three-dimensional MHD simulation (which is required for our purpose) has not been developed yet. Thus, instead of waiting for the completion of a full three-dimensional MHD simulation, we attempt to obtain V(t), $\underline{B}(t)$ and θ(t) by the method developed by Hakamada and Akasofu (1982).

4.2 The Quiet Time Solar Wind

We have to determine, first of all, the quiet time pattern of the solar wind into which disturbances can be introduced by solar activity. This requires the determination of:

(A) The solar magnetic equator

A number of observations are available to infer the magnetic equator; they are Hα filtergrams, the Kitt Peak magnetograms, the Stanford magnetograms, coronal observations at the Sacramento Peak Observatory, the Kitt Peak He(10830Å) observations. During the declining phase of the sunspot cycle, the magnetic equator can often be approximated by a curve $\chi\sin(\lambda+\lambda_o)$ in the heliographic coordinate systems, where χ denotes the angle between the 'dipole axis' and the rotation axis of the sun and λ denotes heliographic longitude. This situation is thus equivalent to assume that the solar "dipole axis" is inclined by χ with respect to the rotation axis. In the example presented in this paper, the inclination angle χ is taken to be 20°.

(B) Latitudinal Gradient of the Solar Wind Speed

A number of studies have been made to determine the distribution of the solar wind speed V as a function of magnetic latitude using spacecraft and interplanetary scintillation data. These studies have enabled us to infer the latitudinal gradient on the so-called 'source surface', of a sphere of radius 2.5 solar radii. A tentative distribution of the latitudinal distribution is given at the top panel of Figure 10. Note that the speed is minimum along the magnetic equator (corresponding to the curve of V = 300 km/sec) and increases towards higher latitudes in both the northern and southern hemispheres. As the sun rotates, the earth scans the solar wind within the heliographic latitude belt of ±7° (depending on the seasons); for example, in Figure 10, the earth encounters the solar wind from the northern (magnetic) hemisphere during the first two weeks (~one-half of the solar rotation period) and then from the southern (magnetic) hemisphere during the rest of the solar rotation period. The northern wind peaks at the end of the first week and the southern wind peaks at the end of the third week. Therefore, in this situation, the sun has two high speed streams which are separated by 180° in longitude. The determination of the solar magnetic equator (A) and the latitudinal gradient of the solar wind speed (B) can be 'calibrated' on the basis of the 27-day variations of V and B which can be observed by satellites.

(C) Stream-Stream Interaction

Since the two high speed streams interact with the slower streams ahead of them, we determine the stream-stream interaction by the method developed by Hakamada and Akasofu (1982), from which the distance (R) traveled by solar wind particles can be determined as a function of time t. A number of one- and two-dimensional MHD studies on this subject have already been conducted (cf. Dryer and Steinolfson, 1976), so that we can calibrate the method employed here by the MHD solutions. It is in this way that we now have a tentative R-t relationship (Hakamada and Akasofu, 1982).

Figure 11 shows the resulting solar wind magnetic field lines in the ecliptic plane for the solar wind distribution given in the top panel of Figure 10 (except for the superimposed flare-generated disturbances near the sun which will be discussed shortly). Note the familiar spiral pattern of the field lines. Since the sun has two high speed streams in this particular situation, two 'spiral arms' develop as a result of the stream-stream interaction at distances greater than 1.5 au. The spiral arms are often referred to as the 'corotating interaction region (CIR).' During a certain phase of the sunspot cycle, the sun develops four high speed streams and thus four spiral arms; this is the situation in which the solar magnetic equator is given by $\chi\sin(2\lambda+\lambda_o)$.

It is useful to envisage the surface which divides the region of the northern and southern winds. The first panel of Figure 12 (T = 0 HR) shows the geometry of this surface at the onset time of the first flare, viewed from the longitude 240°, latitude 30°. Since the solar magnetic equator is appreciably inclined (~20°) with respect to the rotation axis and since the solar wind speed is finite, this surface appears as a warped plane. Actually, there is an azimuthal current in this plane, and for this reason the surface is often called the 'heliospheric current disk (or sheet).'

Suppose that the solar "dipole moment" is directed northward (as was in 1970-1975). Then, the magnetic field lines from the northern hemisphere spiral <u>out</u> above the solar current sheet and the field lines from the southern hemisphere spiral <u>in</u> below the solar current sheet. Thus, at ~1 a.u. above the current sheet, the IMF <u>B</u> vector makes an angle (the IMF angle PHI) of ~135° with respect to the sun-earth line and ~315° below the current sheet.

4.3 Parameterization of a Solar Flare

In the present modeling scheme, it is assumed that solar activity enhances the solar wind speed from a circular area centered around the solar activity center; it is illustrated in the middle panel of Figure 10. This velocity field is parameterized by six parameters.

(A) Onset time T
(B) Longitude of the center of the circular area (ϕ)
(C) Latitude of the center of the circular area (θ)
(D) Maximum speed V_F (km/sec)
(E) Time variation of the flow expressed by $V(t) = V_F te^{-(t/z)}$; thus, τ is the time variation parameter; as an example of V(t) for τ = 12 hrs, see the bottom panel of Figure 9.
(F) Extent of the circular area by assuming the Gaussian distribution with the standard deviation $\sigma°$.

Thus, altogether, we have the six parameters, T, ϕ, θ, V_F, τ and $\sigma°$ for each solar flare.

4.4 Tracing Solar Disturbances

With the above preparations (4.2) and (4.3), it is now possible to trace solar wind and magnetic field disturbances in interplanetary space after flare onset. Figure 11 shows an example of the propagation of solar wind and magnetic field disturbances in the ecliptic plane, caused by two flares separated by 48 hours from the same active region. The figure shows four 'snapshots' taken 2.0, 2.5, 3.0 and 3.5 days after the first solar flare. The shock wave generated by the first flare is reaching a distance of 1 a.u. on the second day (T = 2.0 day). The propagating shock structure from the second flare became visible on the third day (3.0 day). Note that the direction of the propagation of the second shock wave is appreciably different from that of the first shock wave, because the active region rotated by about 28° between the first and the second flares.

Figure 12 shows a large-scale distortion to the current disk which is caused by the two high-speed flows originating from the two flares. Suppose that if the earth is located above the current sheet prior to the flare. As the current sheet is pushed upward (in this particular case) by the flare-generated flow, the earth will be located below the current sheet after the passage of the shock wave. Thus, the azimuth angle PHI suddenly jumps from ~135° to ~315°. Such a sudden change of the angle PHI by 180° during major storms is of common occurrence.

The present modeling method allows us to detemrine V(t) and B(t) as a function of time at any point in inner interplanetary space. Thus, knowing the accurate location of the earth (specifying the date and UT of a flare), it is possible for us to determine the above two quantities as a function of time. Figure 13 shows the solar wind speed V, the IMF magnitude $|B|$ and the angle PHI variations which result from a flare specified by ϕ = 0°, θ = 0°, V = 800 km/sec, τ = 12 hrs. In this particular case, the shock wave has developed the so-called 'forward' and 'reverse' shocks by the time it reaches the earth, as can be seen in the V(t) profile. The magnetic field magnitude is greatly increased in the region between the forward and reverse shocks.

In this simulated situation, however, the angle θ does not change. In order for the angle θ to change, other changes must take place. Here we consider only a simple situation in which linearly polarized Alfvén waves propagate along the magnetic field lines; for details of the superposition of the Alfvén waves, see Hakamada and Akasofu (1982). As a result, the angle θ varies in time, causing ε to vary as well. In the third panel of Figure 13, the resulting ε is given. The last two panels of Figure 13 will be discussed in the next section.

5. PREDICTION OF THE GEOMAGNETIC STORM QUANTITIES

Once the power $\varepsilon(t)$ can be predicted as a function of time, it is possible to predict the geomagnetic storm quantities as a function of time.

5.1 Cross-Polar Cap Potential $\Phi_{pc}(t)$

The cross-polar cap potential Φ_{pc} drives the convective motion of the ionospheric plasma across the polar cap, which causes various auroral activity. Fortunately, we have now an empirical relationship between Φ_{pc} and the power ε (Reiff et al., 1981). Figure 14 shows their results. Thus, if $\varepsilon(t)$ becomes predictable, it will be possible to predict $\Phi_{pc}(t)$. One of the objectives of our study is to develop a numerical scheme to determine the electron density distribution profile over the entire polar region as a function of time, if $\varepsilon(t)$, $\Phi_{pc}(t)$ and the dawn-dusk dimension of the polar cap can be given. The potential drop Φ_{pc}, together with the size of the auroral oval (see section 3.2), determines the convection speed of the F region plasma. Watkins and Richards (1979) and Sojka et al. (1981) have already made an extensive modeling of the F region electron density profile for given convection patterns.

5.2 Geometry and Size of the Polar Cap

In section 2, we have already studied a numerical scheme by which the geometry and size of the open region in the polar cap can be determined for an arbitrary magnitude and direction of the solar wind magnetic field (Akasofu and Roederer, 1984). Another important quantity for HF radio wave propagation is the equatorward boundary of the diffuse aurora. There have already been several studies which relate it to the IMF B_z and the geomagnetic indices AE and Dst (Hardy et al., 1981; Meng and Akasofu, 1983; Makita et al., 1983). Those empirical relations, together with the numerically predicted B_z, can be used to predict the location of the equatorward boundary of the diffuse aurora as a function of time.

5.3 Geomagnetic Indices AE and Dst

Akasofu (1982) gave an empirical relationship between AE(t) and ϵ(t) and between Dst(t) and ϵ(t). Using the results obtained there, we can determine both AE and Dst as a function of time. In the bottom two panels of Figure 13, we show the AE and Dst indices thus determined. It is in this way that we can numerically predict the geomagnetic storm indices AE(t) and Dst(t) as a function of time.

5.4 Future Projects

At this stage of progress in solar-terrestrial physics, it is easy to argue that the kind of efforts described here is premature. However, it is through such an effort that we can recognize which areas of this discipline require *more effort* in accomplishing the prediction. Our goal is to understand various processes involved in solar-terrestrial physics, so that the prediction of geomagnetic storms would eventually become possible. It is not too early to initiate the efforts described in this paper toward this goal.

At the present time, we are concentrating our efforts in (i) identifying all necessary computer codes which are needed for this particular purpose, (ii) developing missing codes, (iii) assembling all the codes for this particular purpose, and (iv) testing and improving the whole numerical prediction scheme. This project requires 'state of the art' knowledge in every element in the scheme.

At present, the weakest element in the whole scheme is the prediction of the polar angle of the solar wind magnetic field θ(t). Obviously, there must be many causes for the changes of V(t), B(t) and θ(t), other than those mentioned in this paper. In order to improve our knowledge on θ(t), much future effort is needed to examine the relationship between solar activity and the solar wind magnetic fields during disturbed periods. Pudovkin and Chertkov (1976) suggested that θ can be predicted by observing the solar magnetic field in the vicinity of the flares. However, Tang et al. (1984) could not find any obvious relationship between the solar (photospheric) magnetic field distribution and the IMF B_z component. Although this is a disappointing finding, the results suggest the importance of the meridional component of the solar wind near the sun in producing θ. Klein and Burlaga (1982) suggested that "magnetic clouds" are responsible for some of the changes of the IMF B_z component, so that such clouds are another cause of IMF (B_x, B_y, B_z) changes. Their magnetic clouds arise from magnetic field-aligned currents, so that it may be possible to accommodate this feature in our future modeling.

References

1. Akasofu, S.-I., and M. Roederer, Dependence of the polar cap geometry on the IMF, Planet. Space Sci., 32, 11, 1984.
2. Akasofu, S.-I., K. Hakamada, and C. Fry, Solar wind disturbances caused by solar flares: Equatorial plane, Planet. Space Sci., 31, 1435, 1983.
3. Akasofu, S.-I., D.N. Covey, and C.-I. Meng, Dependence of the geometry of the region of open field lines on the interplanetary magnetic field, Planet. Space Sci., 29, 803, 1981.
4. Akasofu, S.-I., and D.N. Covey, Effects of the interplanetary magnetic field on the magnetotail structure: large-scale changes of the plasma sheet during magnetospheric substorms, Planet. Space Sci., 28, 757, 1980.
5. Dryer, M., Interplanetary shock waves generated by solar flares, Space Sci. Rev., 15, 403, 1974.
6. Dryer, M., Interplanetary evolution of solar flare-generated disturbances and their potential for producing magnetic activity, Proc. Internat. Workshop on Solar Physics and Interplanetary Travelling Phenomena, Kunming, China, Science Press, Beijing, 1984.
7. Dryer, M., S.T. Wu, G. Gislason, S.M. Han, Z.K. Smith, J.F. Wang, D.F. Smart, and M.A. Shea, Magnetohydrodynamic modelling of interplanetary disturbances between the sun and the earth, J. Geophys. Res., (submitted), April 1983.
8. Frank, L., J.D. Craven, K.L. Ackerson, R.C. Carovillano, and R.H. Eather, Polar view of earth-global imaging with Dynamics Explorer, EOS, 63, 386, 1982.
9. Gislason, G., M. Dryer, Z.K. Smith, S.T. Wu, and S.M. Han, Interplanetary disturbances produced by a simulated solar flare and equatorially-fluctuating heliospheric current sheet, Astrophys. and Space Sci. (submitted), August 1984.
10. Hakamada, K., and S.-I. Akasofu, Simulation of three-dimensional solar wind disturbances and resulting geomagnetic storms, Space Sci. Rev., 31, 3, 1982.
11. Han, S.M., S. Panitshob, S.T. Wu, and M. Dryer, A numerical simulation of three-dimensional transient ideal magnetohydrodynamic flows, presented at Southern Conference on Theoretical and Applied Mechanics, May 1984.
12. Hardy, D.A., Intense flares of low energy electrons at geomagnetic latitudes above 85°, J. Geophys. Res., 89, 3883, 1984.
13. Lassen, K., On the classification of high latitude auroras, Geophys. Pub., 29, 87, 1979.
14. Lassen, K., and C. Danielson, Quiet time pattern of auroral arcs for different directions of interplanetary magnetic field in the Y-Z plane, J. Geophys. Res., 83, 5277, 1978.
15. Makita, K., and C.-I. Meng, Average electron precipitation patterns and visual aurora characteristics during geomagnetic quiescence, J. Geophys. Res., 89, 2861, 1984.

16. Makita, K., C.-I. Meng, and S.-I. Akasofu, Temporal and spatial variations of the polar cap dimension inferred from the precipitation boundaries, J. Geophys. Res., 90, 2744, 1985.
17. McDiarmid, I.B., J.R. Burrow, and M.D. Wilson, Comparison of magnetic field perturbations and solar electron profiles in the polar cap, J. Geophys. Res., 85, 1163, 1980.
18. Meng, C.-I., Polar cap arcs and the plasma sheet, Geophys. Res. Let., 8, 273, 1981.
19. Murphree, J.S, C.S. Anger, C.-I. Meng, and S.-I. Akasofu, Large-scale auroral distribution and the open field line region, Planet. Space Sci., 32, 105, 1984.
20. Wu, S.T., M. Dryer, and S.M. Han, Non-planar MHD model for solar flare-generated disturbances in the heliospheric equatorial plane, Solar Phys., 84, 395, 1983.
21. Wu, S.T., Theoretical interpretation of traveling interplanetary phenomena and their solar origins, p. 443 in Solar and Interplanetry Dynamics, ed. by M. Dryer and E. Tandberg-Hanssen, D. Reidel Pub. Co., Dordrecht-Holland, 1980.

Acknowledgments: The work reported here was supported in part by grants from the United States Air Force (F19628-82-K-0035 and F19628-81-K-0024) and by a grant from the National Aeronautics and Space Administration (NSG7447).

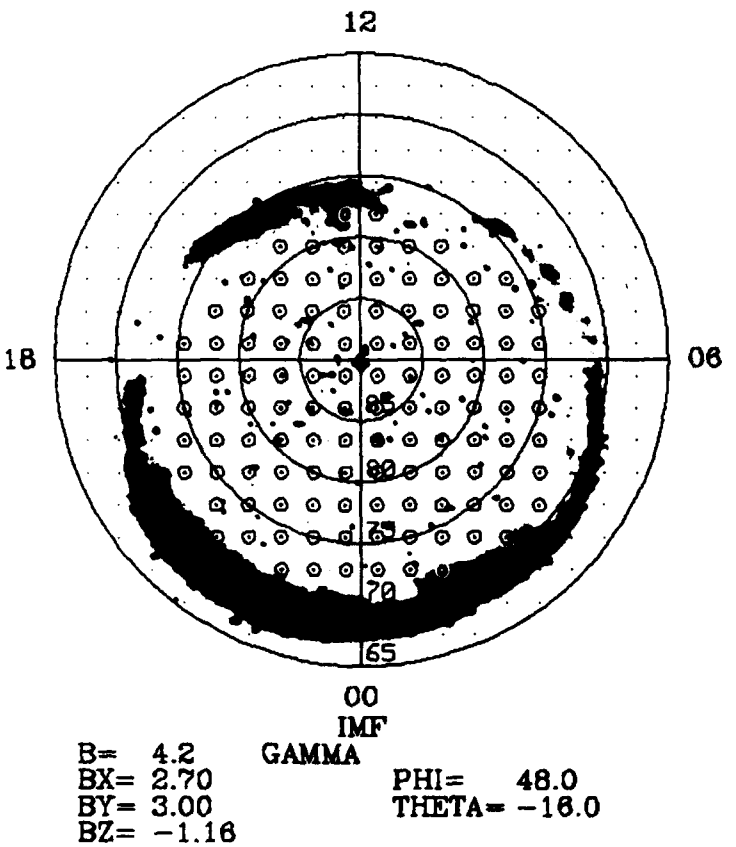


Fig. 1. Test of a magnetospheric model. An observed IMF is superimposed, and the open field line region is determined. The 'simultaneously' observed auroral oval is shown together with the computed open field line region (Murphree et al., Can. J. Phys., 60, 349, 1984).

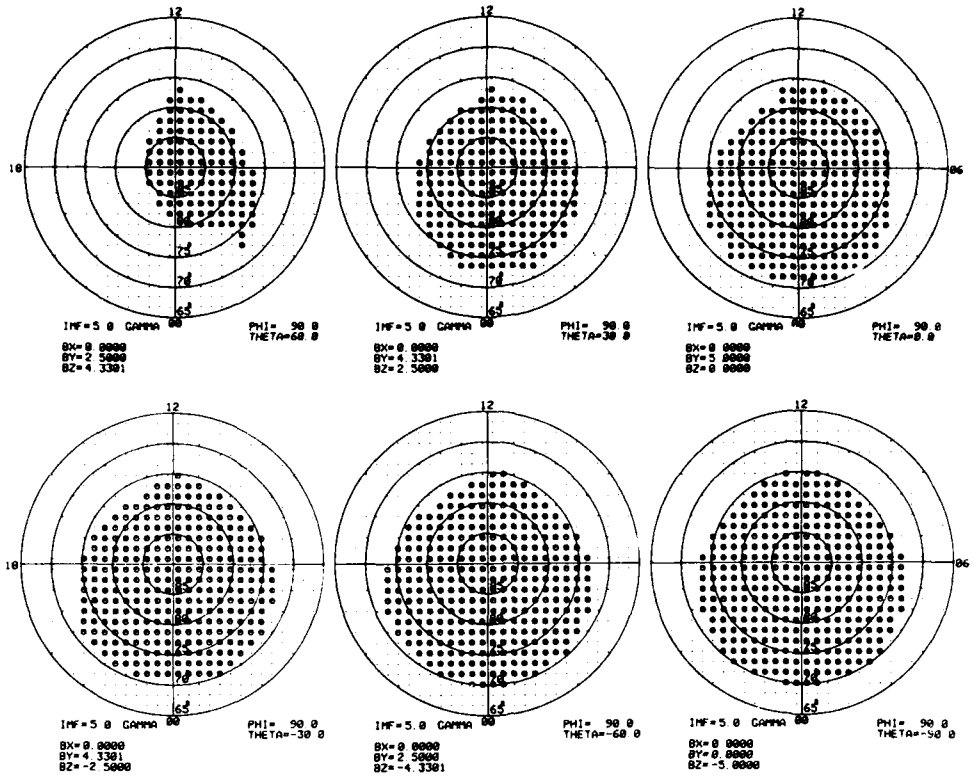


Figure 2. Changes of the geometry of the open field line region as the IMF vector of B = 5nT in the y-z plane rotates (Akasofu and Roederer, Planet. Space Sci., 32, 11, 1984).

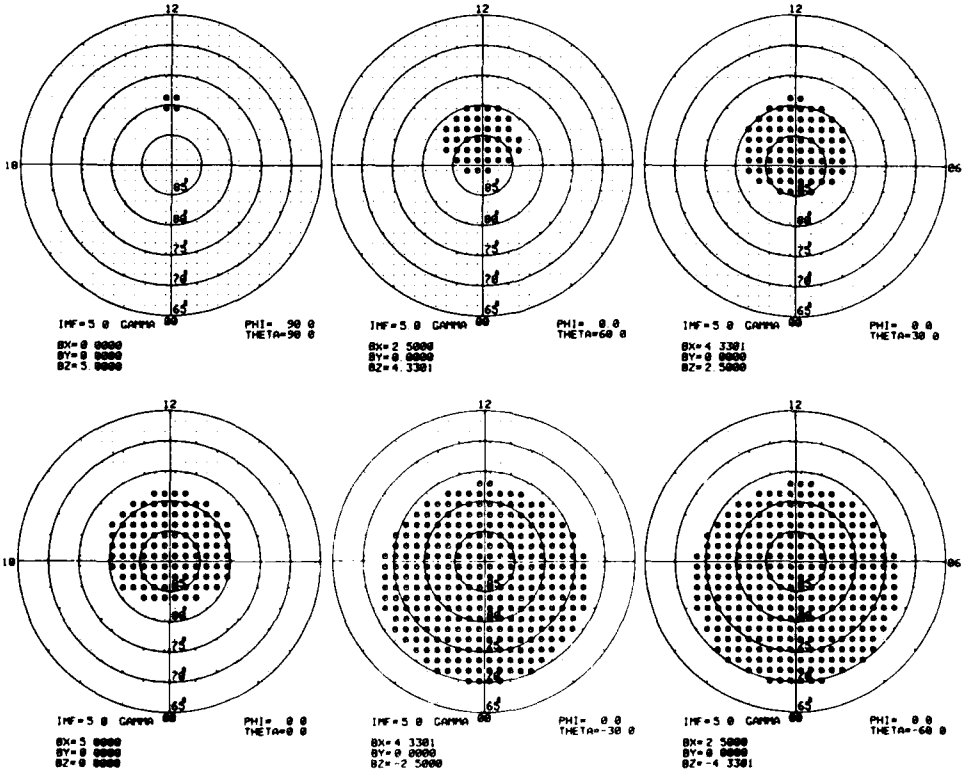


Fig. 3a

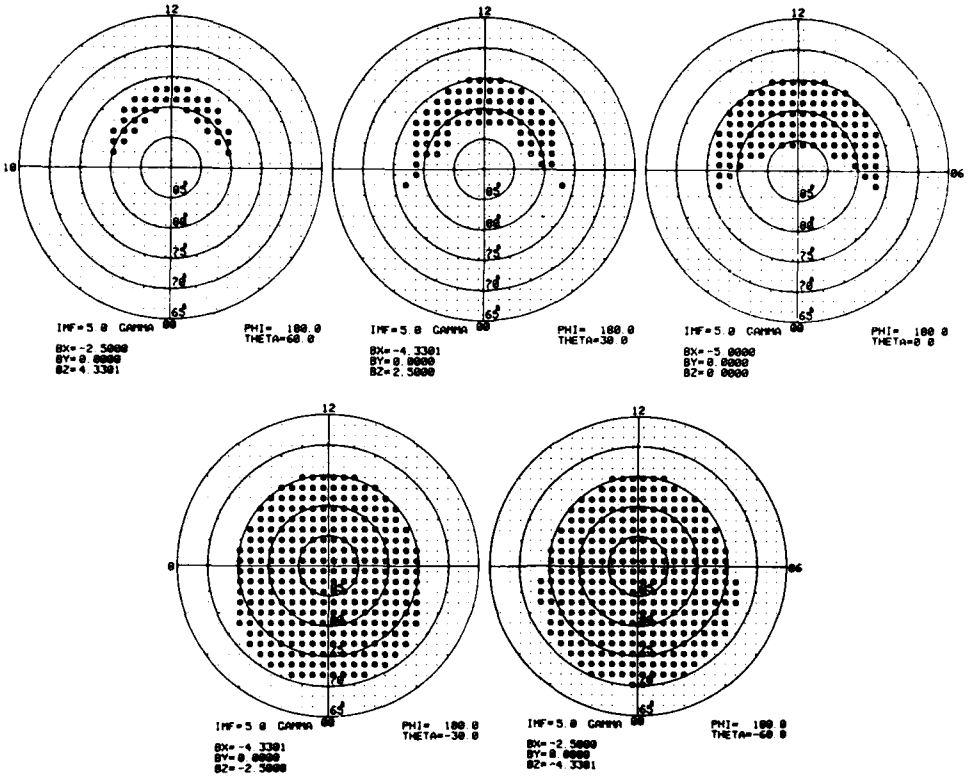


Fig. 3b

Figure 3a and 3b. Changes of the geometry of the open field line region as the IMF vector of B = 5nT is rotated in the x-z plane (Akasofu and Roederer, Planet. Earth Sci., 32, 11, 1984).

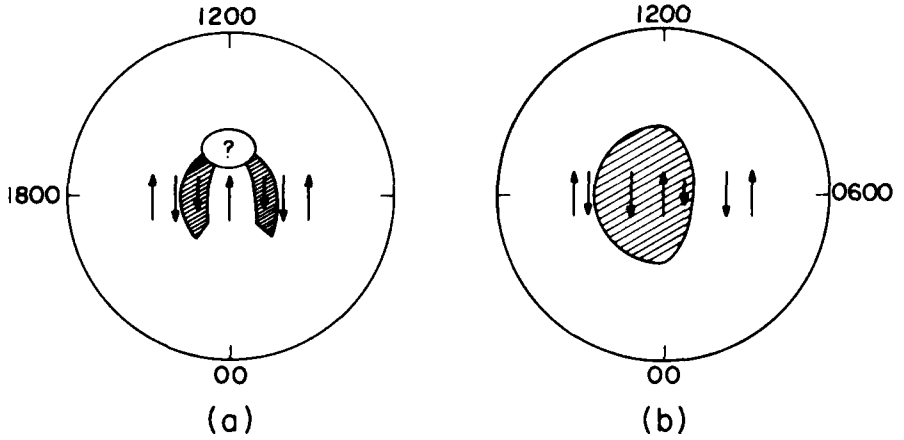


Fig. 3c. Area of the entry of solar energetic electrons for two IMF conditions (a) B_x = -20nT, B_y = -5nT, B_z = +30nT; (b) B_x = 4.3nT, B_y = -0.7nT, B_z = +9.2nT (McDiarmid et al., J. Geophys. Res., 85, 1163, 1980).

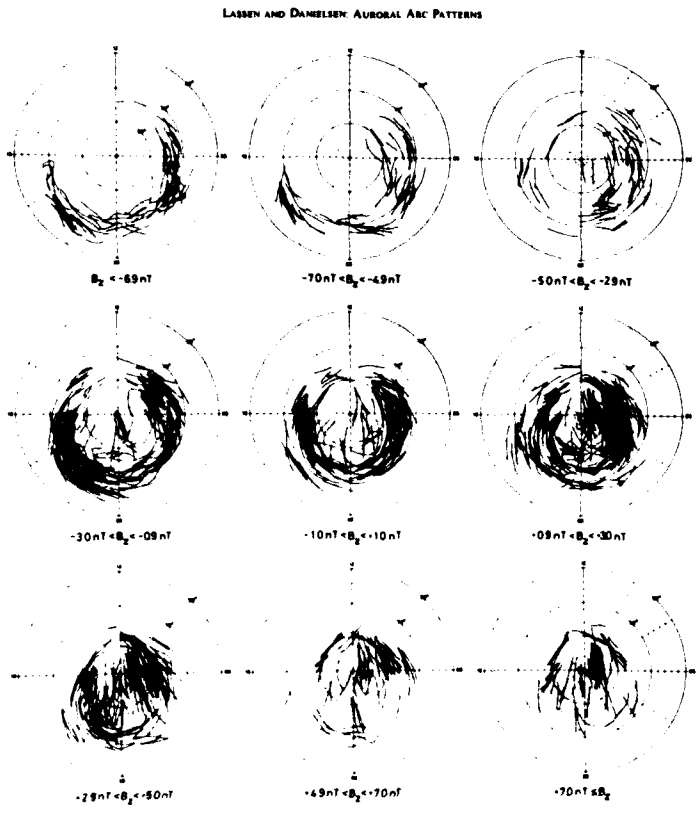
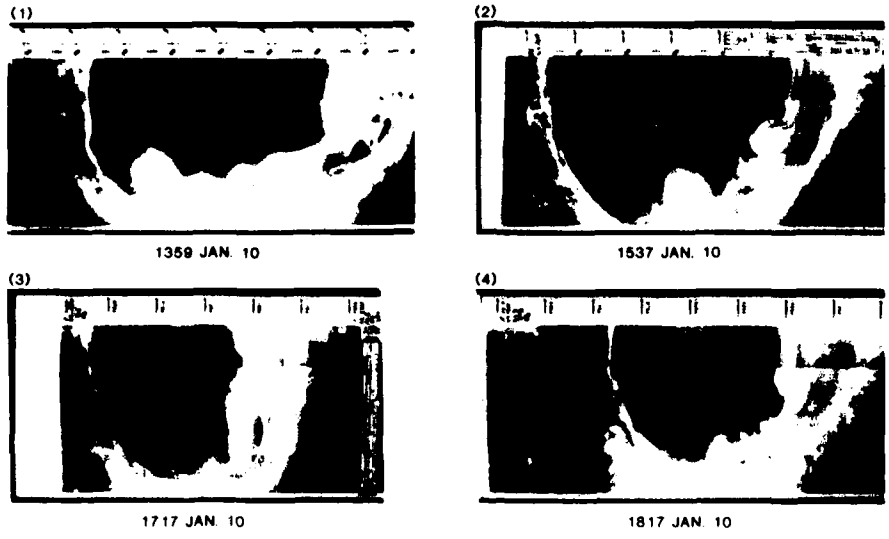


Fig. 4. Distribution of auroral arcs for different values of the IMF B_z component (Lassen and Danielsen, J. Geophys. Res., 83, 5277, 1978).



JAN 10, 1983
(DMSP-F6)

Fig. 5a

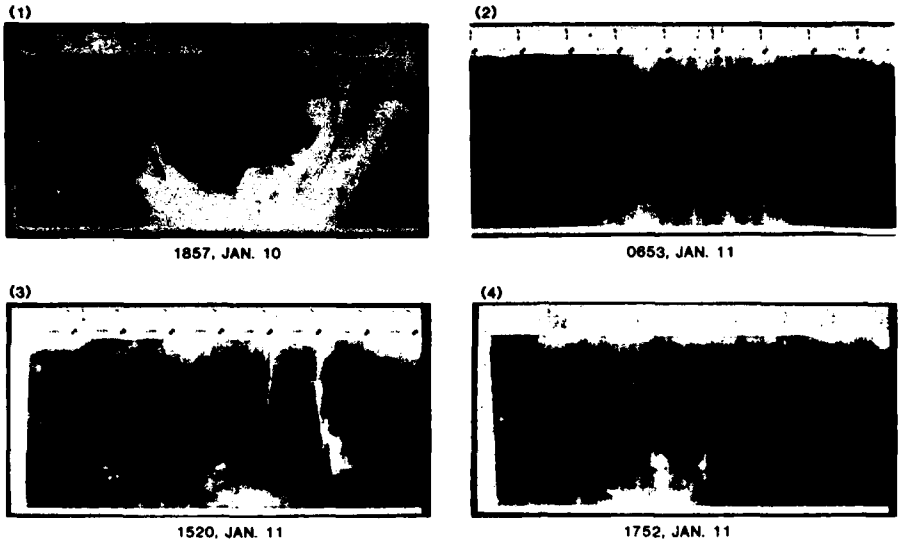


Fig. 5b

Fig. 5a and 5b. DMSP-F6 images of the nightside half on January 10-11, 1983 (Akasofu and Tsurutani, Geophys. Res. Lett., 11, 1086, 1984).

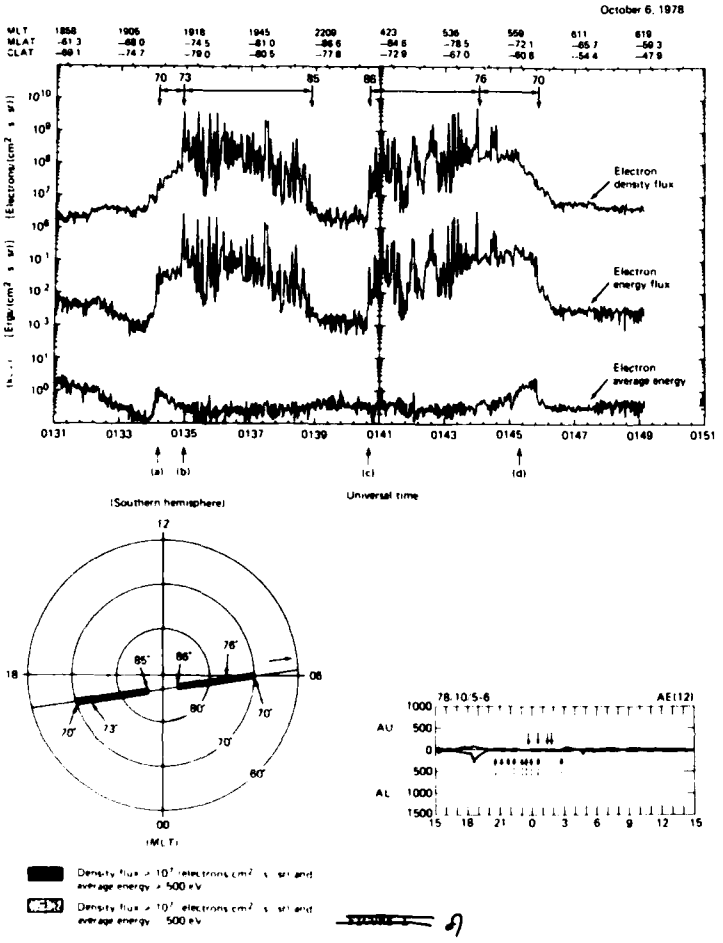


Fig. 6. Dawn-dusk profile of the electron density flux, energy flux and average energy during a very quiet period. The satellite (DMSP) orbit and the AU/AL index are also shown (Meng, J. Geophys. Res., 86, 4067, 1981).

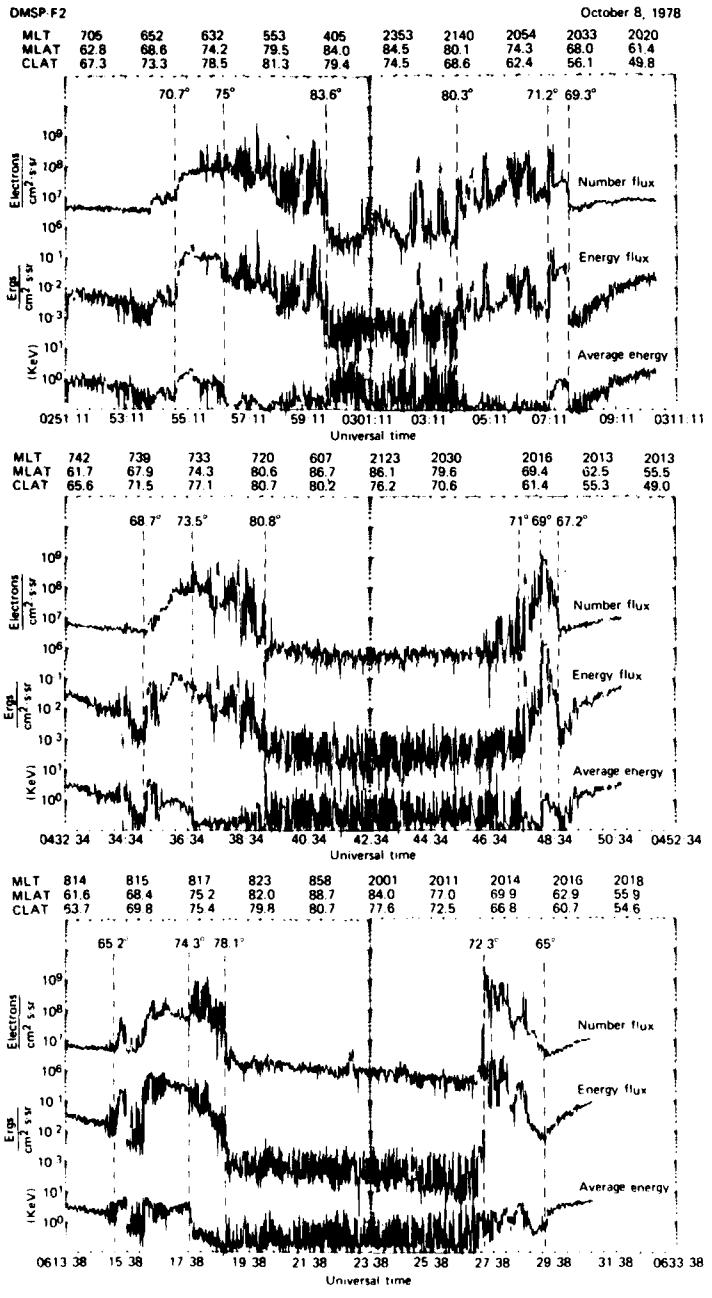


Fig. 7. Three successive profiles of the electron precipitation characteristics (for the format see the caption for Figure 6) (Makita et al., J. Geophys. Res., 90, 2744, 1985).

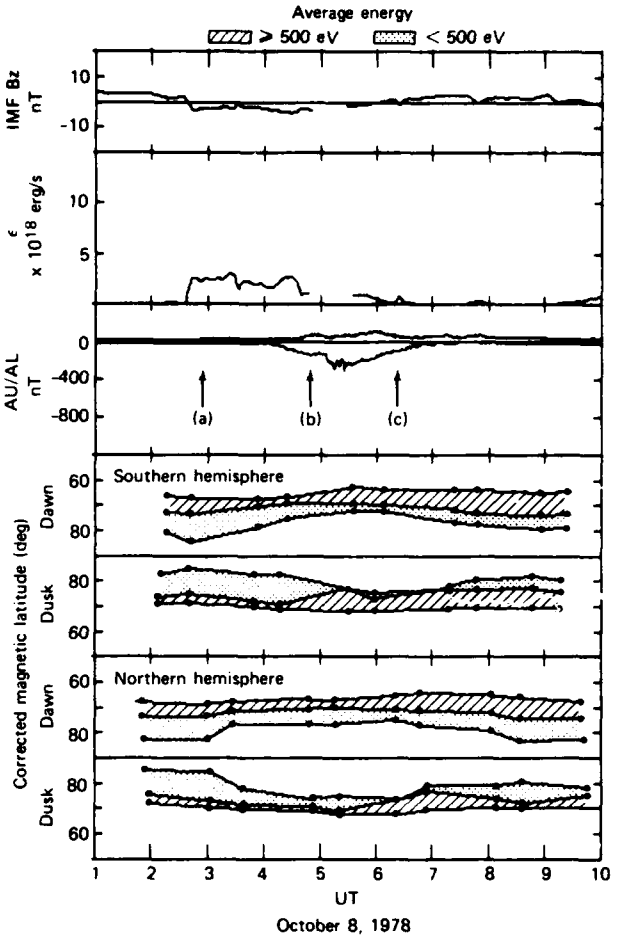


Fig. 8. Changes of the dawn-dusk precipitation profiles in both hemispheres during the early half of October 8, 1978; the soft zone and hard zones are distinguished. The corresponding IMF B_z component, the dynamo power ε and the AU/AL index are shown (Makita et al., J. Geophys. Res., 90, 2744, 1985).

GEOMAGNETIC STORM PREDICTION SCHEME

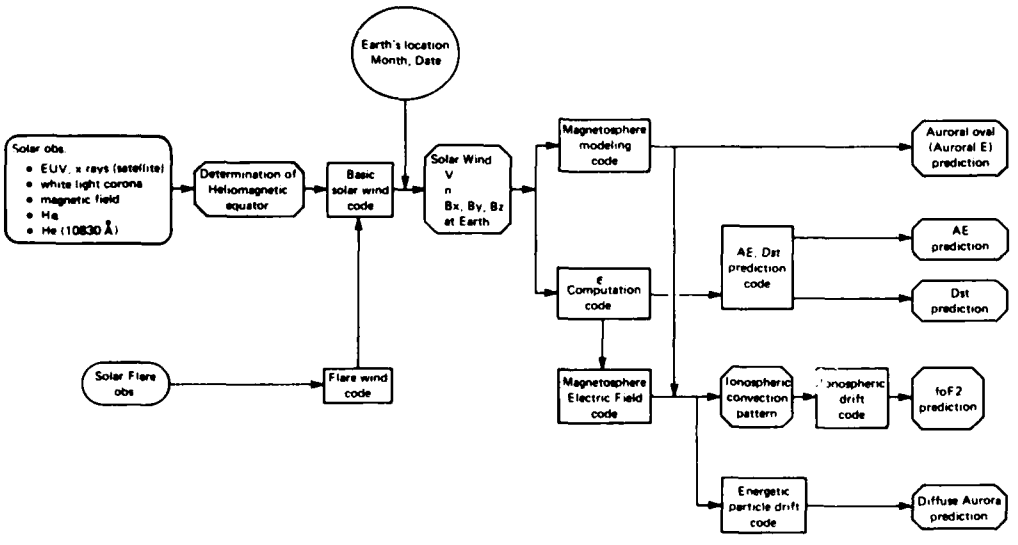


Fig. 9. Geomagnetic storm prediction scheme in a block diagram form which consists of two parts A and B. Part A deals with the prediction scheme for the solar wind-magnetosphere dynamo power $\varepsilon(t)$ on the basis of solar parameters. Part B deals with the prediction scheme for various magnetospheric disturbance parameters for a given $\varepsilon(t)$.

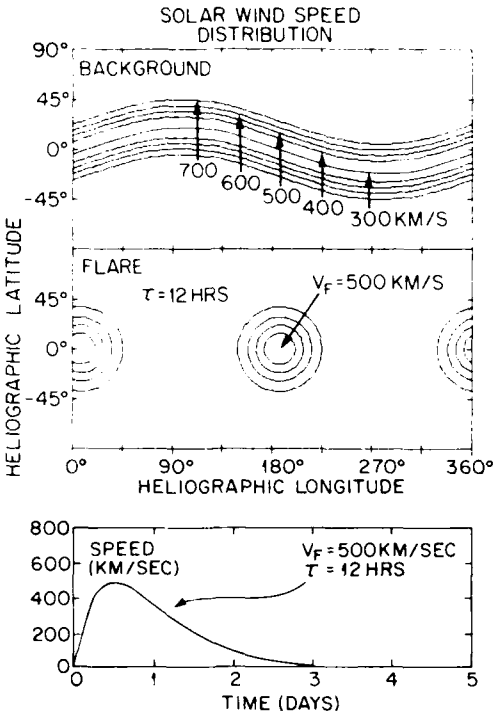


Fig. 10. From the top, the quiet-time solar wind speed distribution on the surface of a spherical sheet of radius of 2.5 solar radii; the high wind speed distribution induced by flare activity at the maximum epoch (ϕ = 180°, θ = 0°, V_F = 500 km/sec, τ = 12 hrs and σ = 30°; the time variations of the high wind speed characterized by τ = 12 hrs and V_F = 500 km/sec.

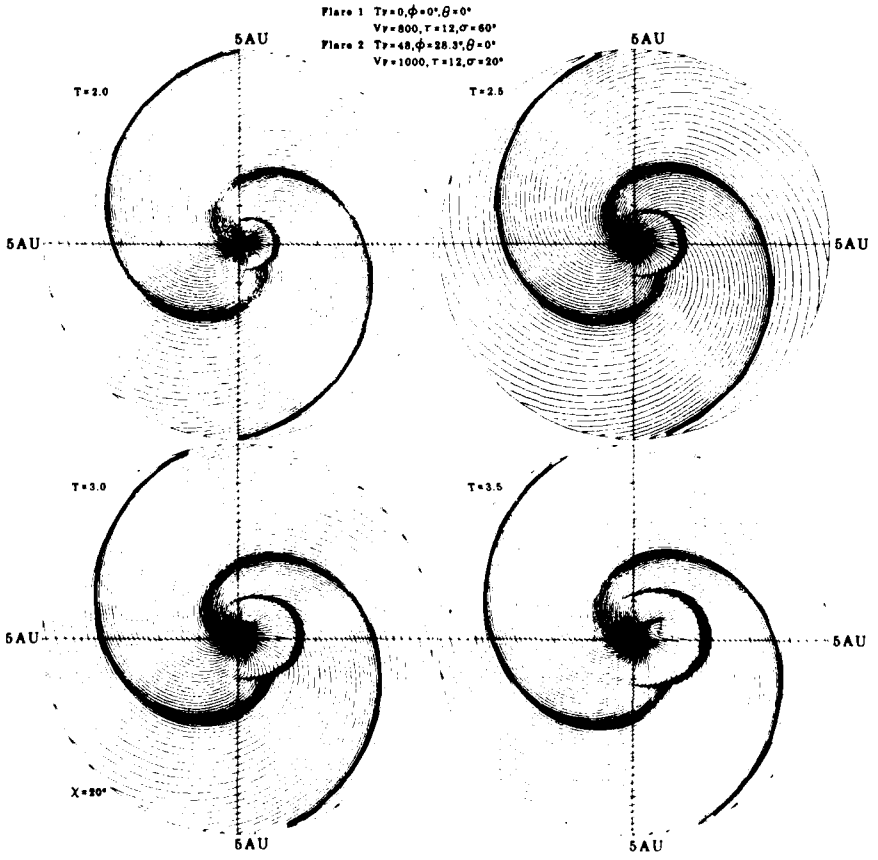


Fig. 11. The propagation of solar wind disturbances in the ecliptic plane (within 5 au) caused by 48 hrs, from the same active region (T = 0, ϕ = 0°, θ = 0°, V_F = 500 km/sec, τ = 12 hrs and σ = 60°; T = 48, ϕ = 28.3°, θ = 0°, V_F = 1000 km/sec, τ = 12 hrs and σ = 20°), 2.0, 2.5, 3.0 and 3.5 days after the onset time of the first flare. The basic pattern of two-spiral arm is produced by the stream-stream interaction of the quiet time solar wind. Note the two flare-induced shock waves caused by the two flares.

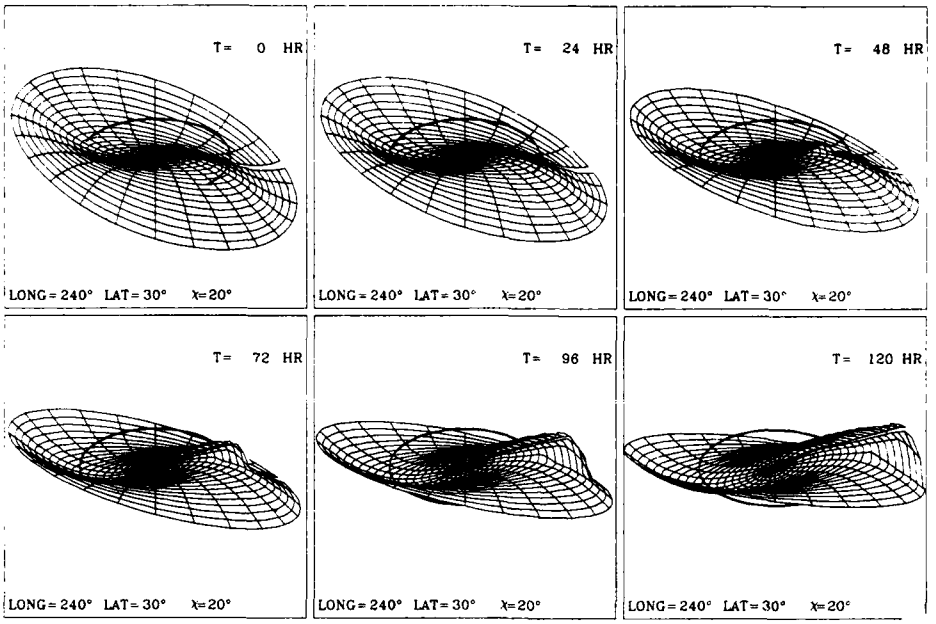


Fig. 12 The distortion of the solar current disk, by a solar flare, viewed from the direction of longitude 240° and latitude +30° at 0, 24, 48, 72, 96 and 120 hrs after the flare; the 'gap' in the current sheet indicates the zero longitude. Note that the solar current disk is rotating as a result of the solar rotation (the quiet-time disk at T = 0). The flare effect is propagating in the direction of longitude 0° and form a large convex distortion on the solar current disk.

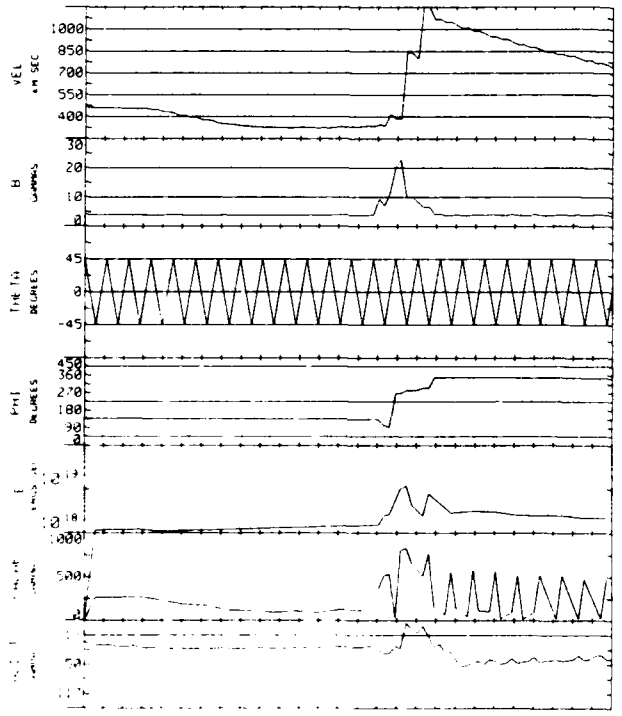


Fig. 13. The predicted solar wind disturbance, V(t), B(t) and the azimuth angle PHI caused by a solar flare parameterized by T = 0, ϕ = 0°, θ = 0°, V = 300 km/sec, τ = 12 hrs.

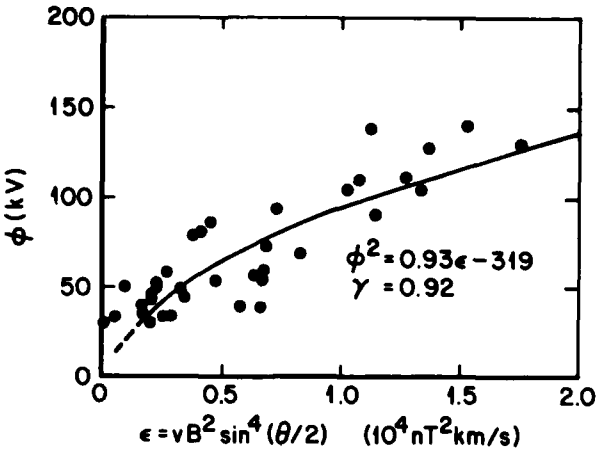


Fig. 14. Empirical relationship between the cross polar cap potential φ(KV) and the solar wind-magnetosphere dynamo power ε (Reiff et al., J. Geophys. Res., 86, 7639, 1981).

DISCUSSION

E.J.Fremouw, US

Do you intend to integrate your predictive code with a magnetospheric convection model and, if so, which model?

Author's Reply

We have been developing our own model, because both changes of the geometry of the open field line region by the IMF (B_x, B_y, B_z) and changes of the cross-polar-cap-potential ϕ_{pc} by ε must be incorporated. This is because the *average* oval is not useful in predicting day-to-day changes of the F2 ionization distribution.

G.W.Prolss, Ge

A significant number of geomagnetic storms are not flare produced but are of the recurrent type. Assuming that this latter type of disturbance has its origin in coronal hole structures/XBP region how do you incorporate this activity in your geomagnetic storm prediction scheme?

Author's Reply

It is our finding that the envelope of the AE index of recurrent geomagnetic storms can be expressed by VB^2 where V and B are the solar wind speed and the IMF magnitude (Hakamada, K. and S.I.Akasofu, Space Sci. Rev. *31*, 3, 1982; Figs. 3.6, 3.7, 3.8). Our scheme can predict both V and B, so that it is possible to predict the general trend of the recurrent storms *quantitatively*. However, it is not possible to predict individual substorms during a recurrent storm.

N.C.Gerson, US

What percentage of time do your theoretical predictions agree with observations, and what percentage of time do they not?

Author's Reply

A geomagnetic storm is quantified by the two geomagnetic indices AE and Dst which depend on how the solar wind speed V, the IMF magnitude B and the two angles (σ, ϕ) of the IMF vary as a function of time. It is then not a matter of "yes" or "no". We are reasonably confident that our scheme will predict V, B and ϕ.

However, at the present time, we are far from satisfactory in predicting σ, but it is a crucial parameter. There has been little study of the σ changes, so that we need a great deal of effort in understanding them.

S.Quegan, UK

Your model predicts equipotentials over the polar cap, i.e. open field lines. Does it extend to predictions of the equipotentials in the closed field line region, i.e. the region where plasma is convecting back sunwards.

Author's Reply

If one assumes that the poleward boundary of the oval is the boundary of the open field line region, our model should be able to predict the convection pattern in the closed field line region. However, at present our model does not include the plasmasphere.

MEDIA EFFECTS ON SYSTEMS IN THE HIGH LATITUDE REGION

by E V Thrane
Norwegian Defence Research Establishment
N-2007 Kjeller, Norway

ABSTRACT

The effects of the transmission medium on radio systems in the high latitude regions are reviewed. First, some general properties of propagation media are discussed, followed by brief descriptions of the effects on radio waves of the earth' surface, the troposphere and the ionosphere in high latitudes. General principles are illustrated by examples from observations and model calculations.

1. INTRODUCTION

The propagation medium which separates transmitter and receiver in a communication system, or a remote sensing system from its target, influences the electromagnetic waves in a number of ways. The medium can be a nuisance, an obstacle which causes deterioration in the quality of the signals, but it can also provide a vehicle for propagation, making communication and probing possible beyond line-of-sight distances. The characteristics of the Earth's surface, the non-ionized atmosphere and the ionosphere all play a role in the propagation of radio waves over a wide frequency range. In high latitude regions the waves propagate in a particularly complex environment which offers difficult problems as well as interesting possibilities for the system engineer. The purpose of the present paper is to review some basic physical principles of how the medium supports and limits transmissions of radio signals, as a background to the mre detailed papers that follow. Detailed discussions of theory are beyond the scope of this paper, instead the media effects will be illustrated with a few relevant examples from experimental investigations and modelling.

2. A SURVEY OF MEDIA EFFECTS IN THE RADIO FREQUENCY SPECTRUM

Electromagnetic waves in the frequency range from Hz to GHz are used for communication, navigation and remote sensing. It is obvious that a system must be tailored not only to the needs of the user, but also to the properties of the propagation medium. The challenge to the system engineer is to design systems that can adapt to changing conditions in the transmission medium in an optimal way. Modern technolgy offers opportunities to improve present system designs, but basic knowledge about the medium is still missing in may areas.

Figure 2.1 summarizes, in a schematic form, the main effects of the medium upon the waves. These include attenuation, time delay, doppler shifts, refraction, reflection, scatter, polarization changes, focussing and defocussing, multipath propagation and ducting. Although these media effects are present all over the world, we shall see that many of them are particularly important in high latitude regions.

2.1 SOME FUNDAMENTAL CONSIDERATIONS

The system engineer needs information on how the transmission medium influences certain basic characteristics of the transmitted signals:

- path loss, which determines the signal-to-noise ratio
- bandwidth, which determines the rate of information transfer
- spatial coherence, which is of importance for space diverity reception
- temporal coherence, which influences fading rates and integration times

It may be useful at this stage briefly to review some fundamental propagation mechanisms.

2.1.1 Refraction and reflection

The medium may be characterized by a complex refractive $n = \mu - i\chi$ where the real part μ determines the refraction or bending of a ray, and the imaginary part χ is a measure of the absorption. In many cases it is possible to describe the propagation by ray tracing based upon a simple application of Snell's law through a stratified medium. The refractive index n is normally a function of the properties of the medium and of the frequency, so that both refraction and absorption are dispersive and may introduce distortion of the signals. It is important to realize that raytracing can in principle only be used when the medium changes slowly along the ray path. Whenever the refractive index changes rapidly with distance so that the changes are significant withing a radio wavelength, ray theory breakes down. In such cases reflection becomes a gradual process along the path of the wave, and sophisticated "full wave" theories must be applied to calculate accurate values of reflection coefficients and absorption. Such may be the case for ducting of VHF and UHF waves in the troposphere and for long waves reflected from the ionosphere. Figure 2.2 illustrates the mechanism.

2.1.2 Scatter and diffraction

Irregular variation in refractive index give rise to scatter as illustrated in Figur 2.3. If the variations in the medium are expressed in terms of the permitivity $\varepsilon(\vec{r})$ (refractive index squared), and if the incident wave field varies slowly compared to the changes in permittivity, it may be shown (see for example Gjessing 1978) that the scattered field is

$$\vec{E}_s = (k^2 \vec{E}/4\pi R) \int_V \epsilon(\vec{r}) \exp(-i\vec{K}\cdot\vec{r})\, d^3\vec{r} \qquad (2.1)$$

Here $\vec{r}$ is a position vector, R the distance from the scattering element to the receiver, and $\vec{K} = \vec{k}_o - \vec{k}_s$ where $\vec{k}_o$ and $\vec{k}_s$ are the wave numbers of the incident and scattered fields respectively. This equation states that the scattered field $\vec{E}_s$ is proportional to the Fourier transform of the spatial veration in refractive index within the scattering volume V. Information about the scattered power P as a function of the scattering angle θ may be obtained by multiplying $\vec{E}_s$ by its complex conjugate. The scattering cross section $\sigma(\theta)$ is defined as the mean power in the scattered wave per unit power density in the incident wave in the scattering volume, per unit solid angle in the direction of $\vec{k}$, per unit scattering volume.

$$\sigma(\theta) = (\pi k^4/2)\, \phi(\vec{K}) \qquad (2.2)$$

Here $\phi(\vec{K})$ is the Fourier transform of the spatial autocorrelation function of the refractive index fluctuations. The situation is illustrated in Figur 2.4 a. The point to note here is that if the function $\phi(\vec{K})$ describing the medium is known, it is in general possible to calculate bandwidth, delay function (pulse distortion) as well as horizontal and vertical correlation distance of the field strength of a signal. It is, of course, also possible to go the other way and to derive information about the structure of the medium from observations of the scattered wave fields. In scattering by tropospheric turbulence the form of $\phi(\vec{K})$ is often assumed to be $\phi(\vec{K}) = K^{-n}$ where $n = 11/3$.

The same principles may be applied to diffraction effects. If the permittivity of the medium is constant within a volume the relation between the field $\vec{E}$ within the scattering volume and the diffracted field is given by:

$$\vec{E}_D = (k^2 \epsilon/4\pi R) \int_V \vec{E}(\vec{r}) \exp(-i\vec{K}\cdot\vec{r})\, d^3\vec{r} \qquad (2.3)$$

The situation is shown in Figure 2.4 b. Again it may be shown that the angular spectrum is the Fourier transform of the autocorrelation function of the spatial variation of the electric field within the scattering volume.

3. PROPAGATION EFFECTS OF THE EARTH'S SURFACE

The earth's surface will absorb, reflect, diffract and scatter radio waves. The effective conductivity of the ground will depend upon vegetation, moisture content of the soil, snow cover etc. Various models, such as the Longley-Rice model (Longley and Rice 1978) have been developed to describe the effects over a wide frequency range. The properties of the ground are important down to a depth which depends upon radio wavelength and conductivity. This skin depth may be expressed as

$$\sigma_s = 1/\sqrt{\pi f \sigma_s \mu_o} \qquad (3.1)$$

Here f is the wave frequency, σ_s the ground conductivity, and μ_o the permeability of free space. The skin depth varies from typically a few centimeters at VHF and UHF to 100 m at VLF. In high latitudes there are special problems associated with snow, ice, permafrost and Arctic tundra which have very low ground conductivities. Figure 3.1 shows measurements of HF backscatter coefficients in the Arctic and illustrates the effects of various types of surface on the scatter of radio waves (Burdick et al 1976). The backscatter sounder has been swept in azimuth.

The values to the right in the top figure represent scatter from the sea, those to the left scatter from islands and broken sea ice. We note that the latter are about 20 dB smaller than the sea scatter coefficients. Of particular interest are the very small values (35 dB below sea values) observed for the 19 MHz wave when it is scattered from the Greenland icecap. The scatter region coincides with the region of maximum icecap thickness. It is also well known that the Greenland and Antarctic icecaps cause significant phase lags for VLF waves in the Omega navigation system (Westerlund et al 1969).

Figure 3.2 shows the effects of low condictivity tundra (0.001 S) on LF waves (Thrane and Andreassen 1985). At a distance of 1000 km from the transmitter the ground wave field is attenuated by 20 dB relative to the field over sea. These calculations were made for a smooth earth surface. In practice rugged and mountainous terrain will cause diffraction effects and make realistic estimates of ground wave field strength very difficult. A case in point is North Norway, where mountainous, low conductivity land is penetrated by fjords. Nevertheless progress is being made in simulation studies using digital terrain mapping.

4. PROPAGATION EFFECTS OF THE TROPOSPHERE

The effects of the troposphere are most important for radio frequencies above the HF band, and they are most pronounced for transmission at low elevation angles. The frequency dependence of the real part of the refractive index is neglible for frequencies below 100 GHz, and the absorption by atmospheric gases

is small, except near the absorption line for water vapour at 22.5 GHz and the absorption line for oxygen at 60 GHz. The refractive index n is very close to unity and is commonly expressed in N units where

$$N = (n-1)\ 10^6 \qquad (4.1)$$

N depends upon atmospheric pressure, temperature and humidity and may be approximated by:

$$N = 77.6\ (P/T) + 3.73\ 10^5\ e/T^2 \qquad (4.2)$$

where the total pressure P and the partial pressure of water vapour e are given in mB and the temperature T in Kelvin. The height variation of N is approximately exponential and may be written

$$N(h) = N_s \exp(-h/H) \qquad (4.3)$$

where the surface value N_s is typically 313 and the scale height H = 7 km. We understand that the low temperatures and dry air in Arctic and Antarctic regions may cause deviations of N from values typical of low and middle altitudes. In general N_s varies geographically from about 400 in humid tropical regions to about 300 in desert climates and in high latitudes (Bean and Dutton 1966).

4.1 PATH LOSS AND FADING

Figure 4.1 (Gjessing 1983) summarizes some factors determining the path loss in troposheric propagation. Within the line-of-sight the power density decreases with distance squared, but interference between a direct wave and waves reflected from the ground may cause oscillations in the field strength pattern. These can be controlled by changing frequency or the height of the antennas.

Beyond line-of-sight diffraction and scatter become important. In general the earth's curvature and terrain obstacles determine the diffraction, whereas troposheric turbulence cause scatter. As pointed out earlier, transmission parameters such as bandwidth and delay spectrum may be calculated if the spectrum of refractive index fluctuations in the medium is known. The intensity of such fluctuations depends upon climatic and weather conditions. Gutteberg (1984) reports on a study of the characterictics of 11.8 GHz signals from the geostationary satellite OTS, received at Spitsbergen (78° N). The signals arrive at the receiver at an elevation angle of 3.2 degrees and have a path length of about 120 km through the Arctic troposhere. Figure 4.2 shows the fading depth for different seasons plotted against monthly mean air temperature at ground level. There seems to be a good correlation, with minimum fading in the stable winter troposhere and maximum in unstable, turbulent summer conditions. A further interesting result of this study is a significant space diversity improvement obtained by using two receivers separated by about 1 km transverse to the beam.

4.2 TROPOSHERIC DUCTING

Abrupt changes with height in the refractive index may occur and are caused by changes in humidity and/or temperature. Such feature may cause trapping or ducting of waves and give rise to complex field strength patterns, as illustrated in Figure 4.3. Shadow zones and zones where waves arriving via different paths interfere may occur. The occurence rate of ground based ducts shows distinct seasonal and geographic changes. Figure 4.4 demonstrates this point and indicates that ground based ducts are frequent in the high latitude continental climate in winter. A typical thickness of a ground based duct is 66 m at Fairbanks, Alaska. Ducts are also frequent in a tropical maritime climate (Bean and Dutton 1966).

5. PROPAGATION EFFECTS OF THE HIGH LATITUDE IONOSPHERE

The high latitude ionosphere is characterized by its complex structure and extreme variability. The study of its effects on radio systems is a vast subject, and here we can do no more than give a few examples of the most important phenomena. Some propagation problems encountered in the HF band have been reviewed by Thrane (1983).

5.1 ABSORPTION

Ionospheric absorption associated with auroral phenomena and solar proton events are of particular importance in the MF and HF bands. The absorption is strongly frequency dependent (Abs. in dB α $1/f^2$). The absorption is caused by enhanced electron densities in the lower ionosphere, and may result in radio blackouts which completely disable radio systems over wide areas and for long time periods. For auroral absorption a typical blackout may cover an area which extends 100 km across the auroral zone and 1000 km along the zone. The disturbance lasts for 1/2 hour to a few hours. A solar proton event may cause a Polar Cap Absorption event (PCA) which in extreme cases can cover the entire polar cap down to 60 degrees latitude and last for 10 days.

It is essential to obtain a good statistical description of the occurence rate of such phenomena. Statistics are available, mainly in the form of riometer absorption measurements of cosmic noise intensity at frequencies near 30 MHz. Figure 5.1 shows the classical picture of the geographical probability distribution of such absorption (Harz et el 1963). For radio systems it is of interest to relate the riometer absorption measurements to absorption at oblique incidence. Table 1 gives rough estimates of the oblique incidence absorption over a 450 km path with a 1 hop reflection from the F-layer. Note that a 1 dB riometer absorption may give absorption of the order of 100 dB for frequencies in the lower HF band.

Frequency MHz	Ratio = Oblique path absorption (dB) / Riometer absorption (dB at 30 MHz
2.5	128
3.5	80
8	22
15	7

Table 1 Approximate relation between oblique incidence and riometer absorption

For modelling of circuits is is also important to relate riometer absorption A_r to the electron density profile in the lower ionosphere, so that both reflecting and absorbing properties may be calculated. Friedrich and Torkar (1981) have constructed model electron density profiles for different degrees of ionospheric distubance as measured with a 27.6 MHz riometer. The model profiles are based upon more than 50 rocket measurements of electron density by means of the Faraday rotation technique. The night-time model is shown in Figure 5.2.

The effects of auroral absorption on circuit reliability are illustrated in Figure 5.3 for a medium distance path within the auroral zone in North Norway (Thrane 1979). Reliability measurements have been made for quiet conditions (A_r < 0.2 dB), for moderately disturbed condition (0.2 dB < A_r 2 dB), and for disturbed conditions (A_r > 2 dB). It is interesting to note that the reliability may actually increase during moderate disturbances. This is because even a weak disturbance will tend to wipe out the interference in the HF band, so that the signal-to-noise ratio may increase, even if the signal strength is decreased.

In all circuit planning in high latitudes one should keep in mind that there is a small chance for large disturbances with devastating effects for systems operating in the MF and HF bands. This simple fact often seems to be forgotten!

5.2 RAY PATHS IN THE HIGH LATITUDE IONOSPHERE

The complex structure of the high latitude ionosphere causes very complex ray paths through the medium. Strong horizontal gradients and field-aligned irregularities give rise to refraction, reflection and scatter, as indicated in Figure 5.4 (Buchau 1972). Note that the horizontal structure in this case cases a "dead zone" in addition to the well known skip zone. Tilts in the ionosphere also cause changes in the angle of arrival of a radio signal and often limits the accuracy of HF direction finding.

The effects of multipath propagation on signal bandwidth are important. Figur 5.5 shows results of HF spread spectrum transmissions with different bandwidths for a case when multipath is important (Skaug 1984). The results indicate that the percentage detection of the signal increases with increasing bandwidth up to a bandwidth of 80 kHz. The reason is simply that this bandwidth allows the resolution of the multipath echoes. For 160 kHz bandwidth the signal is no longer coherently reflected from the ionospheric layer, and the detection percentage is low.

Sporadic E-layers are often associated with auroral disturbances and may give rise to very strong, stable reflections of HF and even VHF waves. Figure 5.6 shows such a layer as measured with the EISCAT radar (*Hall and Kirkwood, private communication*).

It is also worth noting that a disturbance causing a blackout in the HF band may enhance signal strength in the LF and VLF bands. Figure 5.7 shows interference between ground wave and skywave for a 153 kHz wave during a 2 dB riometer absorption event. The skywave dominates over the ground wave for distances beyond 600 km. For the undisturbed case the sky wave is more heavily absorbed and the interference is much less pronounced (Thrane and Andreassen 1985).

The total electron content of the high latitude ionosphere influence the accuracy of space tracking and satellite navigation systems, and it is difficult to model the necessary correction for a rapidly varying medium. Figure 5.8 shows an example of range tracking errors of a 425 MHz radar (in Bedford Massachusetts) tracking the Transit satellite (Tomljanovich and Long 1978).

5.3 THE EFFECTS OF IRREGULARITIES AND SCATTER

Irregularities may profoundly influence propagation of radio waves reflected from, or penetrating the high latitude ionosphere. In the ionospheric D-region the irregularities have a spectral distribution corresponding to turbulence in the non-ionized air, whereas in the E- and F-regions irregularities are produced by electrodynamic processes in the plasma. The autocorrelation function $\phi(\vec{K})$ discussed in Section 2 therefore has a different form below and above about 95 km (Thrane and Grandal 1981). Typical observed spectral slopes are -11/3 below 95 km and 0 above this height. In the F-region the irregularities are field-aligned and cause strongly directional scatter.

Plasma irregularities in the high latitude regions cause scatter and may significantly influence radio propagation. Figure 5.9 shows a coverage diagram for 7 and 10 MHz for a transmitter in South Norway directed towards the north. The position of the auroral zone is indicated, and it is obvious that scatter from irregularities associated with auroral phenomena may be important. VHF radar studies have shown that scatter may also occur far south of the auroral zone (T B Jones private communication). The presence of irregularities is likely to reduce the efficiency of communication systems as well as OTH radars.

Plasma irregularities in the F-region give rise to scintillation in signals from satellites. Again these scintillations are related to the position of the auroral zone as shown in Figure 5.10 (Whitney and Aarons 1976). The intensity of the phase fluctuactions imposed on the signal is illustrated in Figure 5.11 (Aarons and Whitney 1980).

6. CONCLUSION

A brief review has been given of some important transmission medium effects in the radio frequency spectrum at high latitudes. Modern technology opens possibilities for communication and remote sensing systems which can adapt to a complex and rapidly changing medium, but accurate modelling of the transmission medium is necessary for optium system design. Although progress has been made in recent years, a substantial effort is still needed to map and understand the characteristics of the high latitude troposhere, upper atmosphere and ionosphere, as well as the relevant properties of the earth's surface.

REFERENCES

Aarons, J., Whitney, H. E. (1980). Recent Observations of Equatorial and High Latitude Scintillations. AGARD-CP-284, Propagation Effects in Space/Earth Paths, edited by Dr H J Albrecht, paper No 31, AGARD, Paris.

Bean, B. R., Dutton, E. J. (1966). Radio Meteorology, National Bureau of Standards Monograph 92. US Government Printing Office.

Buchau, J. (1972). Instantaneous Versus Averaged Ionosphere. Air Force Surveys in Geophysics No 241. Air Force Systems Command, US Air Force, 1.

Burdick, B. J., Chrisholm, J. H., Nichols, B. E. (1976). Polar Ionosphere Modelling Based on HF Backscatter, Beacon, and Airborne Ionosonde Measurements. AGARD-CP-173, Radio Systems and the Ionosphere, paper No 30, AGARD, Paris.

Friedrich, M., Torkar, K. M. (1981). High latitude plasma densities and their relation to riometer absorption. INW 8109. Technische Univerität Graz, A-8010 Graz, Austria.

Gjessing, D. (1978). Scattering Mechanisms and Channel Characterization in Relation to Broad Band Radio Communication Systems. AGARD-CP-244, Aspects of Electromagnetic Wave Scattering in Radio Communications, edited by A. N. Ince, paper No 1, AGARD, Paris.

Gjessing, D. (1983). Wave Propagation and Remote Sensing. Proc URSI Commision F 1983 Symposium, Louvain, Belgium (ESA SP-194).

Gutteberg, O. (1984). Measurements of Atmospheric Effects on Satellite Links at Very Low Elevation Angle, Norwegian Telecommunications Administration Research Establishment. Report No 18/18.

Harz, T. R., Montbriand, L. E., Vogan, E. L. (1963). Canad J Phys 41, 581.

Longley, A. G., Rice, P. L. (1978). Predictions of Tropospheric Radio Transmission Loss over Irregular Terrain -- a Computer Method, 1968. Department of Commerce, ESSD Research Laboratories Report ERL 79-ITS 67, US Government Printing Office, (1968). Modifications to this computer model were published as an Appendix to Department of Commerce, Office of Telecommunications Report 78-144.

Skaug, R. (1984). Experiment with Spread Spectrum Modulation on an HF Channel. IEE Proceedings, 131, Part F, No 1.

Thrane, E. V. (1979). Results of transmission tests in Norway using high frequency radio waves reflected from the ionosphere. Internal report E-303, Norwegian Defence Research Est, N-2007 Kjeller, Norway.

Thrane, E. V., Grandal, B. (1981). Observations of Fine Scale Structure in the Mesosphere and Lower Thermosphere, Journal of Atmospheric and Terrestrial Physics, 43, No 3, pp 179-189.

Thrane, E. V. (1983). Propagation II. Problems in HF propagation. AGARD-LS-127, Modern HF Communication, paper No 11, AGARD, Paris.

Thrane, E. V., Andreassen, Ø. (1985). Field strength calculations for Vannøy Broadcasting station. FFI/RAPPORT-85/7005, Norwegian Defence Research Est, N-2007 Kjeller, Norway.

Tomljanovich, N. M., Long, R. J. (1978). Satellite-Referenced Ionospheric Propagation Correction for USAF Spacetrack Radars, AGARD-CP-238, Vol 1, Operational Modelling of the Aerospace Propagation Environment, Edited by H. Soicher, paper No 8, AGARD, Paris.

Westerlund, S., Reder, F. H., Abom, C. (1969). Effects of Polar Cap Absorption events on VLF transmissions Planet Space Sci 17, 1329.

Whitney, H. E., Aarons, J. (1976). Amplitude Scintillation Observations and Systems Application. AGARD-CP-173, Radio Systems and the Ionosphere, paper No 2, AGARD, Paris.

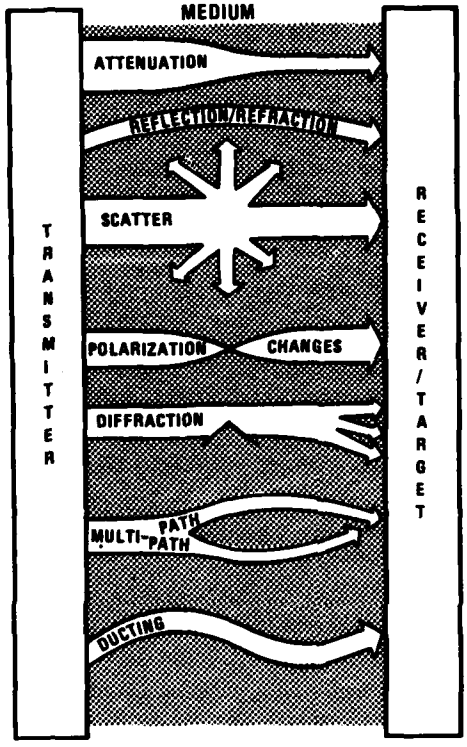


Figure 2.1 Schematic illustration of media propagation effects

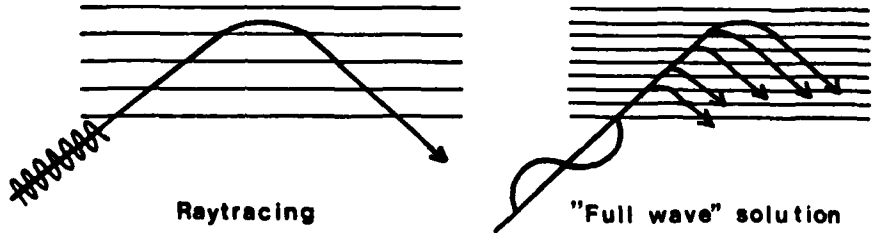


Figure 2.2 Ray tracing techniques break down if the medium changes significantly within a radio wave length.

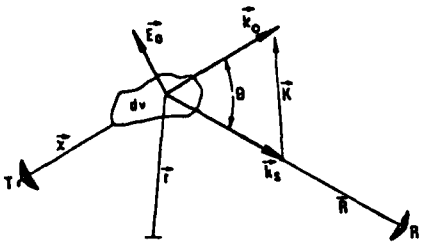


Figure 2.3 Scattering from an elementary scattering element

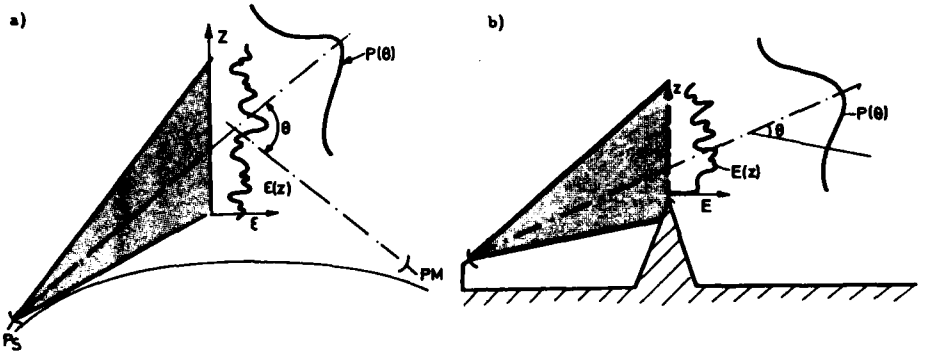


Figure 2.4 a) The scattered field is the Fourier transform of the spatial variations in refractive index
b) The diffracted field is the Fourier transform of the spatial variations in the illuminating field $\vec{E}(z)$ (Gjessing 1978)

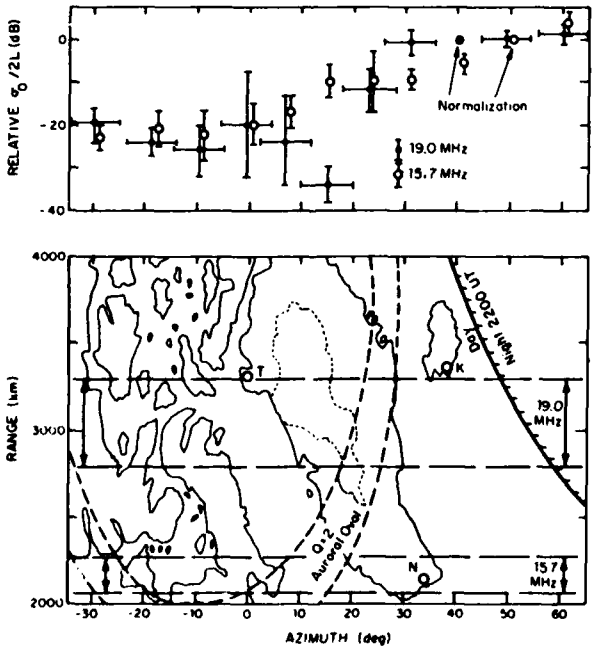


Figure 3.1 Backscatter coefficients for 19.0 MHz and 15.7 MHz for different surface characteristics (Burdick et al 1976)

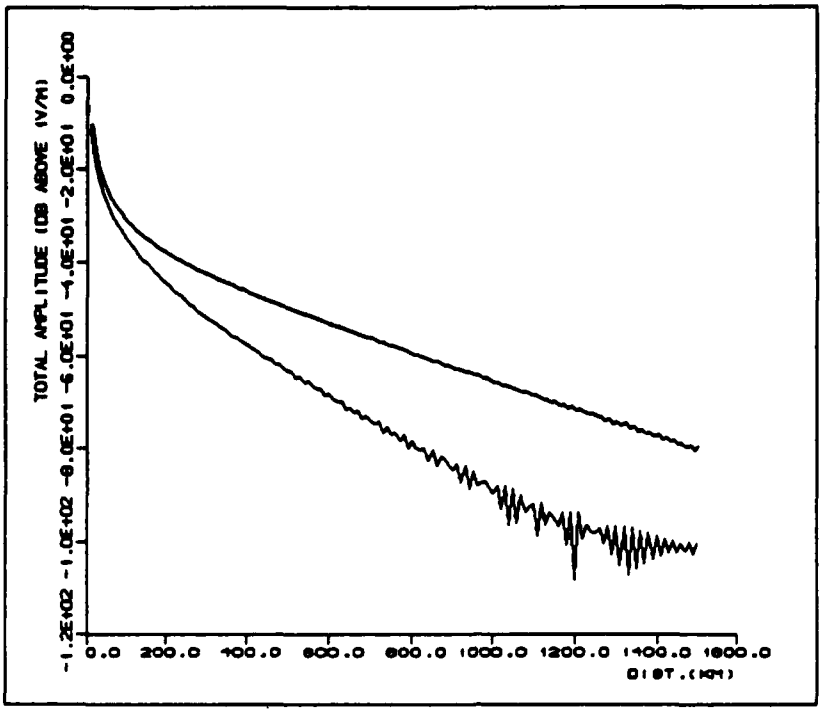


Figure 3.2 Field strength as a function of distance for a 153 kHz radio wave calculated by a "wave hop" method. The ionospheric model represent undisturbed day time in high latitudes (Thrane and Andreassen 1985).
Upper curve: Ground conductivity = 4 S (sea)
Lower curve: Ground conductivity = 0.001 S (tundra)

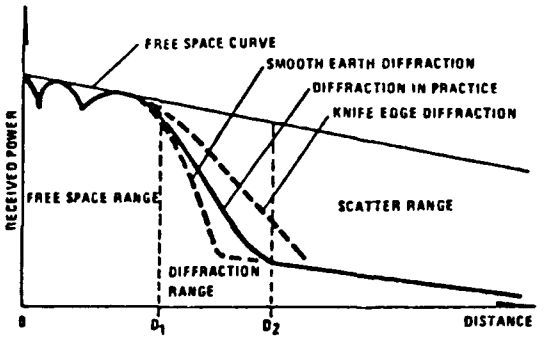


Figure 4.1 Factors determining path loss in troposheric propagation (Gjessing 1983)

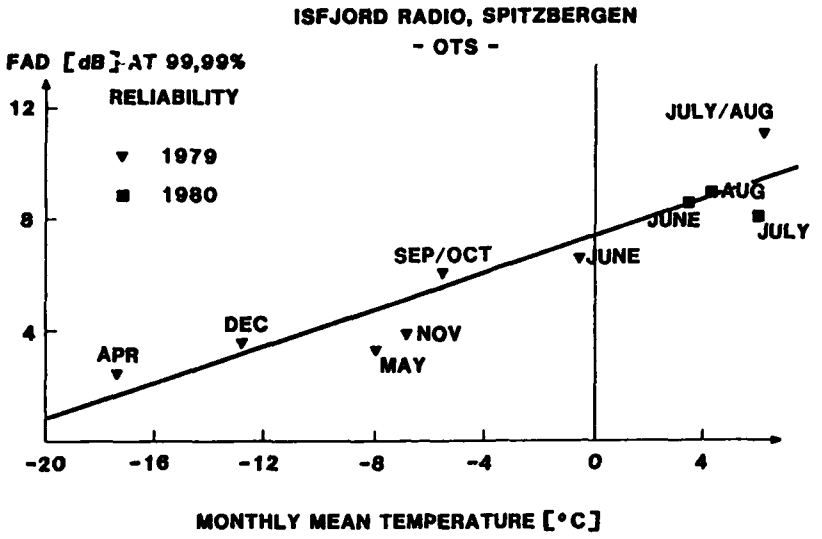


Figure 4.2 The fading level at 99.99 % of time versus monthly mean air temperature at ground level, for a 11.8 GHz transmission from a geostationary satellite (Gutteberg 1984)

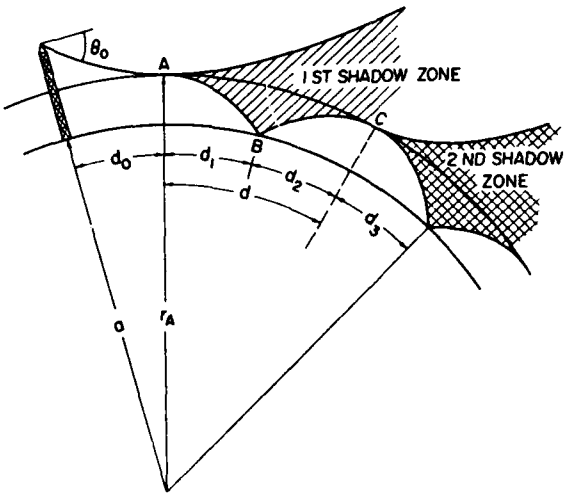


Figure 4.3 Shadow zone occurence of a curved earth with the transmitter above the duct (Bean and Dutton 1966)

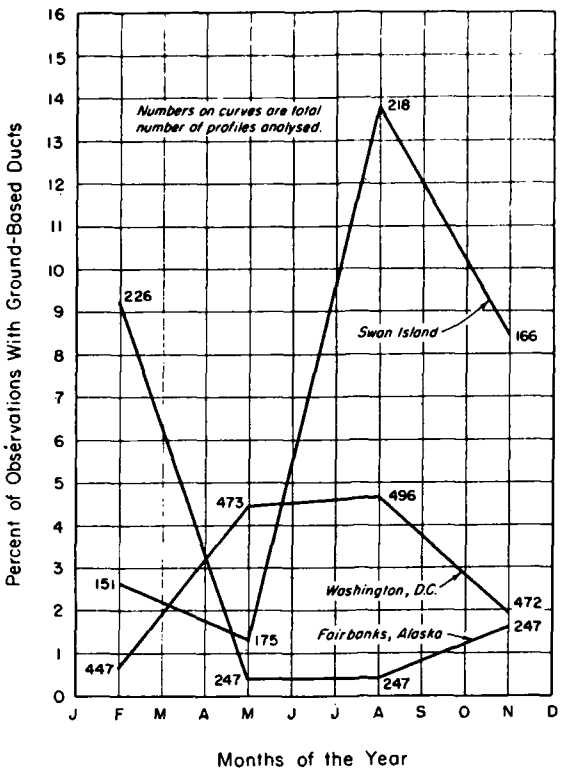


Figure 4.4 Frequency of occurence of ground based ducts (Bean and Dutton 1966)

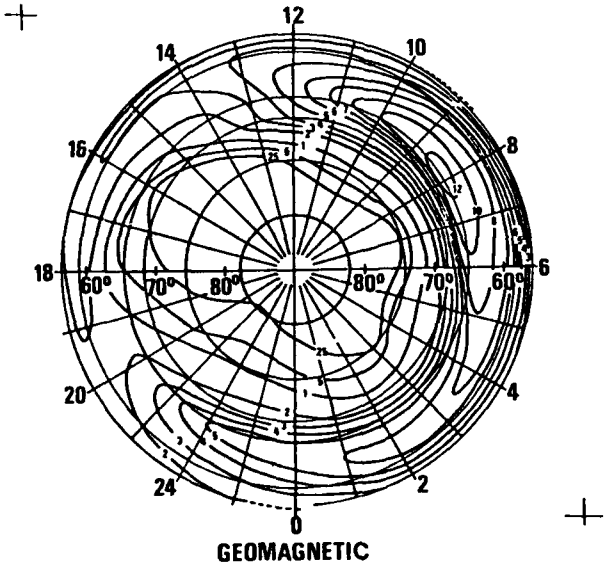


Figure 5.1 Distribution in geomagnetic time of the occurence probability of auroral absorption. The curves give the percentage probability that the 30 MHz riometer absorption exceeds 1 dB (Hartz et al 1963)

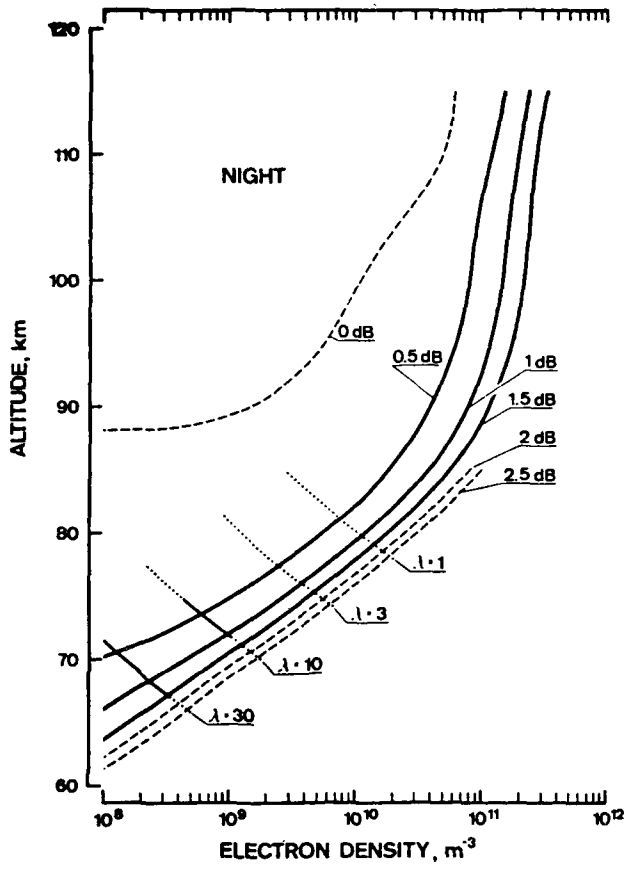


Figure 5.2 Night time model electron density profiles in the auroral zone for different degrees of riometer absorption (Friedrich and Torkar 1981)

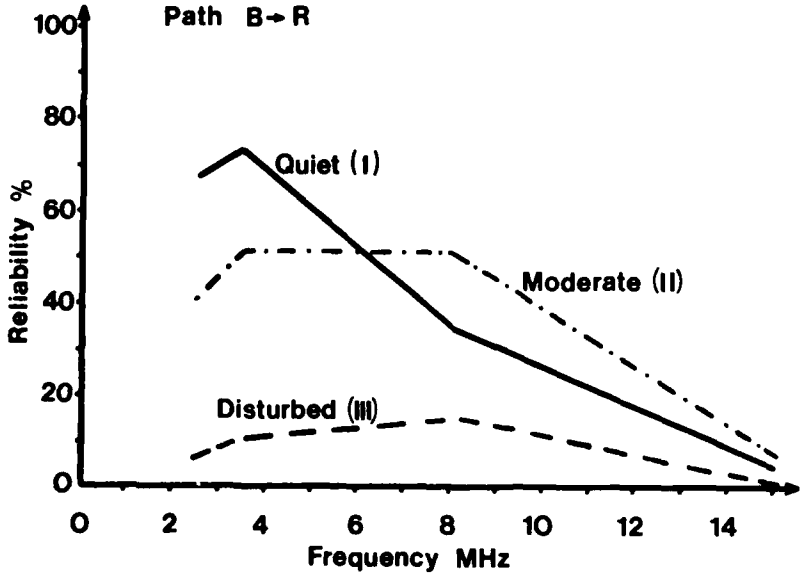


Figure 5.3 Average reliability curves for a 450 km transmission path in the auroral zone, for different degrees of distubance.

I Quiet	A_r (30 MHz) < 0.1 dB
II Moderately disturbed	0.2 < A_r < 2 dB
III Disturbed	A_r > 2 dB

(Thrane 1979)

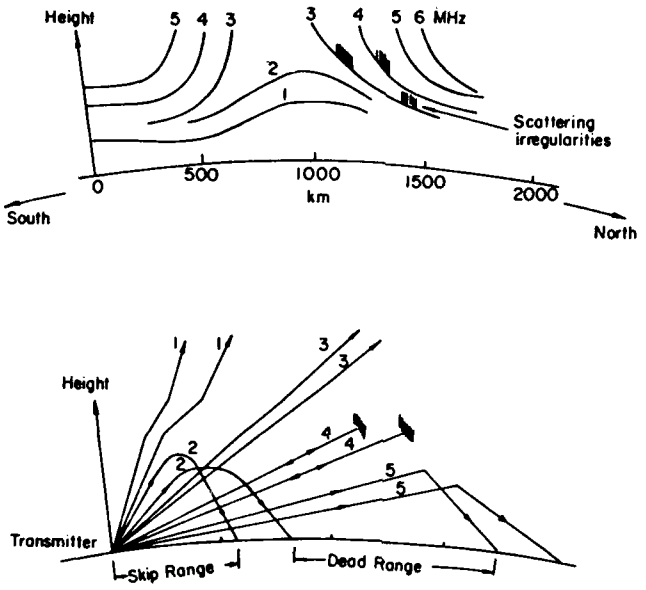
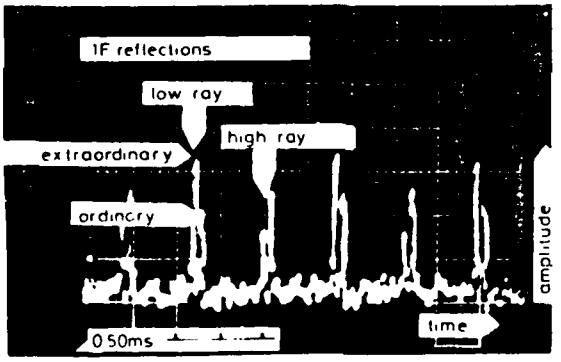
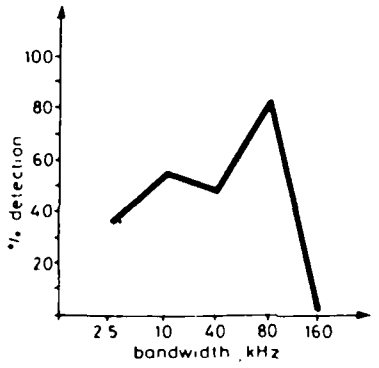


Figure 5.4 HF propagation paths via the ionosphere in high latitude (Buchau 1972)
Top panel : Model distribution of electron concentrations
Bottom panel: Ray paths for signals at constant frequency launched with different elevation angles



Correlator output recording
f = 8.1 MHz, MUF = 8.2 MHz



Comparison of the performance for five different bandwidths
f = 8.1 MHz, MUF = 8.2 MHz

Figure 5.5 Detection probability for a 8.1 MHz spread spectrum signal for five different bandwidths (Skaug 1984).
Top panel : Measured multipath echoes
Bottom panel: Detection percentage of spread spectrum signal

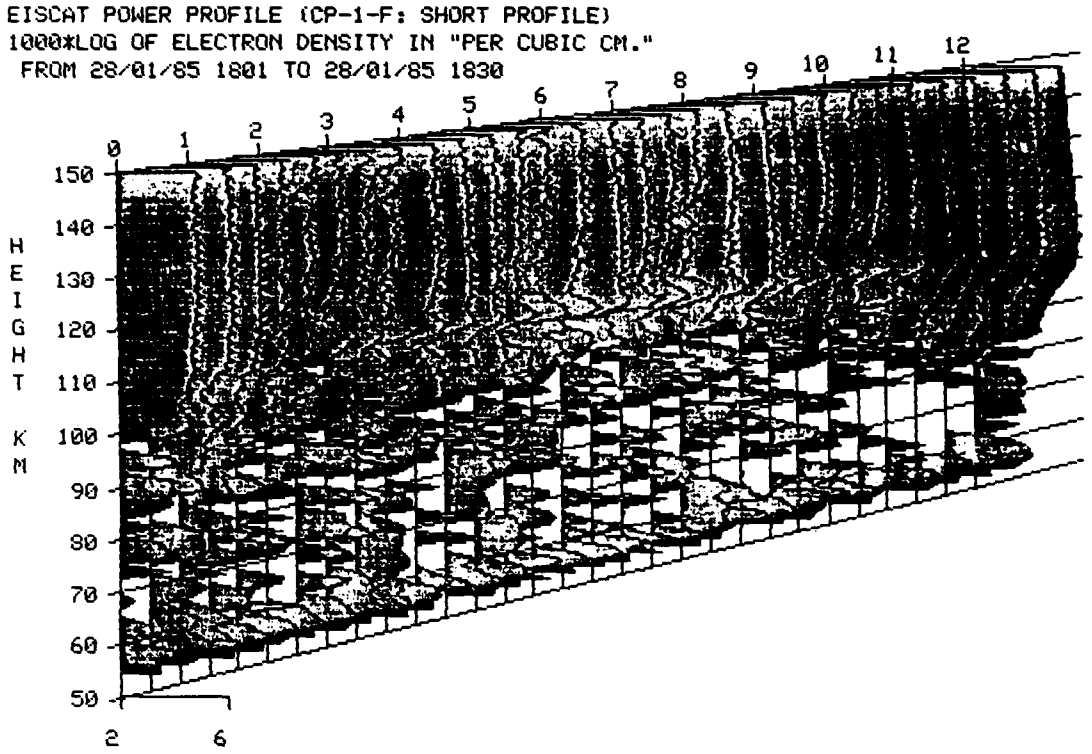


Figure 5.6 EISCAT power profiles showing the presence of sporadic E-layer. The measurements were made as part of the "Common program" and the height resolution of the radar is not optimal. The sporadic E-layer is therefore blurred in height.

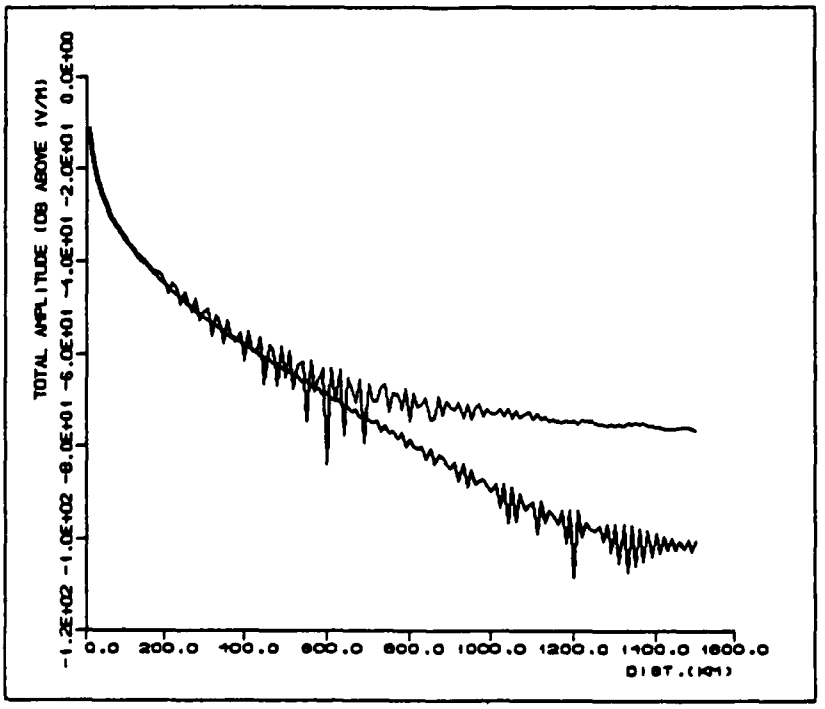


Figure 5.7 The effect of an ionospheric disturbance on a 153 kHz transmission over poorly conducting ground (0.001 S) (Thrane and Andreassen 1985).
Upper curve: Field strength versus distance for disturbed conditions (A_r = 2 dB)
Lower curve: Field strength for undisturbed daytime (A_r = 0 dB)

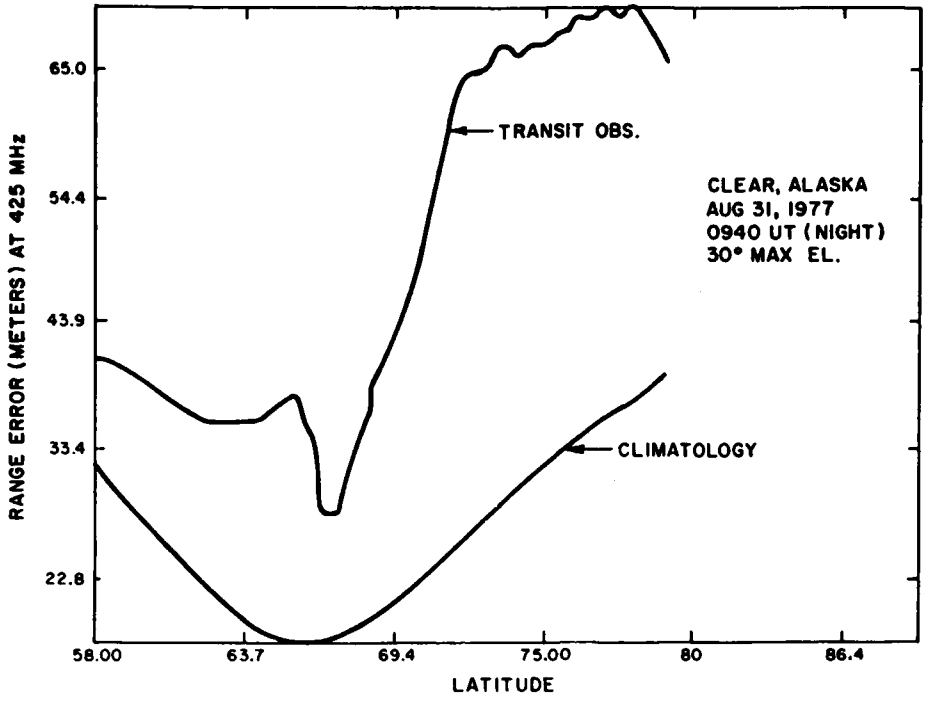


Figure 5.8 Ionospheric range corrections along a TRANSIT path (Tomljanovich and Long 1978)

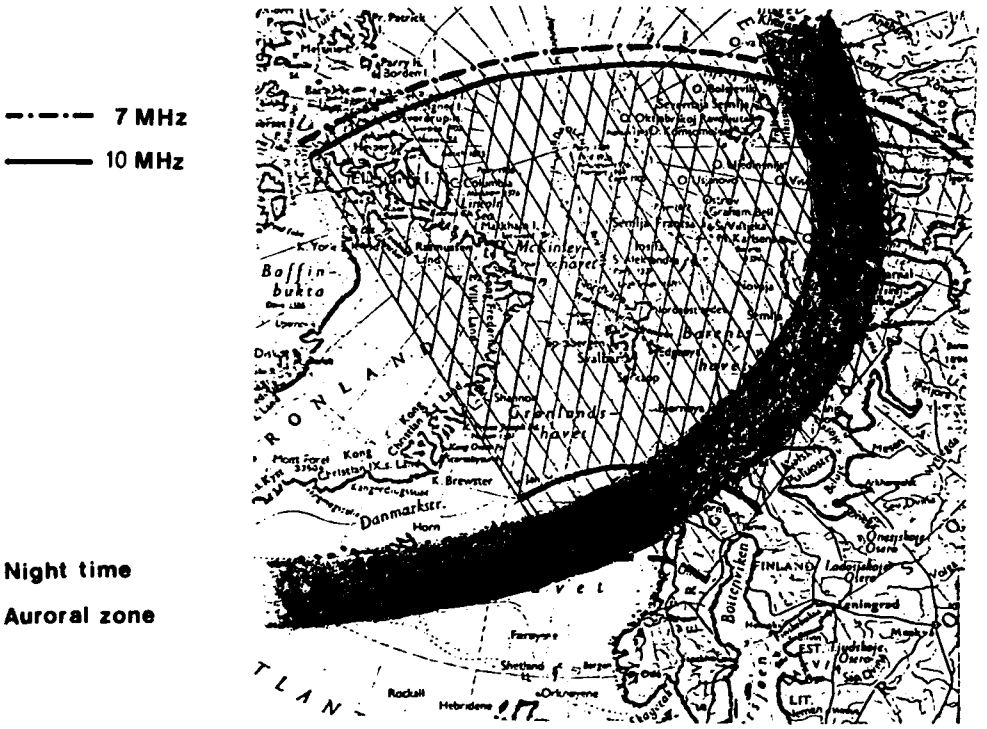


Figure 5.9 Coverage diagram for 7 MHz and 10 MHz waves from a transmitter in South Norway

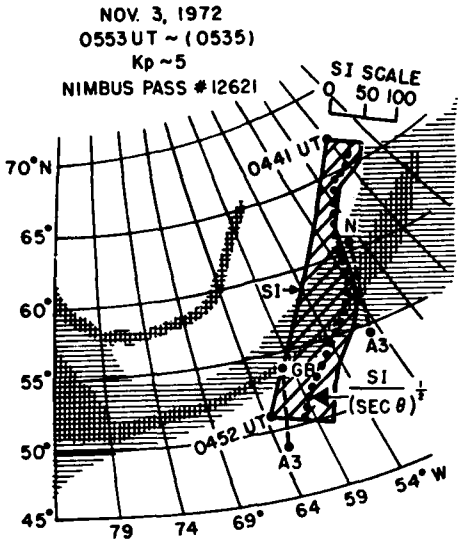


Figure 5.10 Scintillation index for signals from the NIMBUS satellite measured across the auroral zone (Whitney and Aarons 1976)

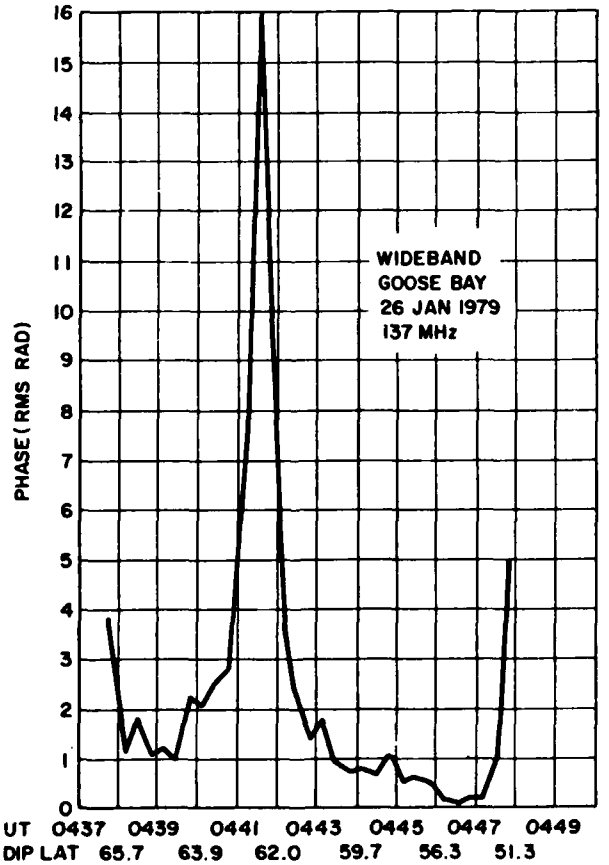


Figure 5.11 Strength of phase scintillations at 137 MHz measured in high latitude (Aarons and Whitney 1980)

DISCUSSION

J.S.Belrose, CA

Concerning your calculations of field strength (ground and skywaves) at 153 KHz I would like to make two comments:

1. The ground conductivities that you have used for arctic tundra are too high, at least for Canadian latitudes. The LF ground conductivity of Arctic land is typically 0.3 mS/m (even lower); and
2. In spite of this difference, I consider that your calculations underestimate the amplitudes of the skywave. At Canadian latitudes over northern and Arctic paths we have concluded that the skywave dominates the ground wave at distances >750 km for a summer day. (When skywave is most strongly absorbed.)

Author's Reply

The conductivity was chosen to correspond to terrain in North Norway. The intensity of the skywave depends, of course, strongly on the model used for the ionosphere. The model I used for daytime was based on rocket measurements during relatively quiet conditions.

SUMMARY OF SESSION II

Transionospheric Propagation and Considerations

by

Dr J.Aarons
Session Chairman

Over the past 20 years the morphology of irregularities over the high latitude region has been explored. Both phase and amplitude scintillations have been studied. It is clear now that the high latitude irregularities can be divided into four major groups. These are the polar cap, the aurora, the trough and the plasmapause region. As determined by scintillation observations auroral irregularities have been clearly shown to be a function of magnetic index, time of day, and solar flux. Polar irregularities have only recently been explored but their morphology is generally understood. Somewhat less is known about lower latitude irregularities; their importance for communications is reduced since these are regions of irregularities with low intensities.

In the AGARD conference more information on the extent of the polar irregularities was indicated with the first measurements of total electron content variations reported. The form and velocity of auroral irregularities were outlined. Plasmapause irregularities were clearly separated from auroral disturbances.

More importantly, however, there were attempts to link the irregularity studies to large scale probing of the ionosphere-magnetosphere interaction. Various techniques are being used including coordinated in-situ satellite observations and incoherent scatter radars.

The future holds the possibility of understanding the processes that link the high latitude ionosphere to the magnetosphere and eventually to the sun. Irregularity generation is being tied to convection patterns at high latitude as well as to precipitation. The interaction of these physical studies with the propagation measurements serving as a data base will lead to means of forecasting and predicting when fading of trans-ionospheric signals will occur and probably to methods of reducing the effects of the F layer ionospheric irregularities on trans-ionospheric satellite propagation.

RECENT HILAT RESULTS

E.J. Fremouw
Northwest Division
Physical Dynamics, Inc.
P.O. Box 3027
Bellevue, WA 98009 USA

Summary

The DNA HiLat Satellite was launched on 27 June 1983 for the purpose of studying the development and dynamics of F-layer irregularities between the plasmapause and the pole. In a circular 800-km orbit at 82 inclination, it carries (1) a coherent radio beacon for measuring complex-signal scintillation and TEC, (2) a three-instrument thermal-plasma experiment consisting of a Langmuire probe (debilitated on launch), a retarding-potential analyzer (RPA), and an ion drift meter; (3) an energetic-electron spectrometer operating between 20 ev and 20 kev, (4) a three-axis fluxgate magnetometer, and (5) an optical package consisting of a vacuum-ultraviolet (vuv) imaging spectrophometer (failed after collecting forty orbits of data) and two visible-wavelength telephotometers. All instruments other than the Langmuire probe and the vuv imager continue to operate reliably. To date, HiLat has returned the following three specific observations of note: first auroral image in full daylight, most intense field-aligned current flowing into the ionosphere, and energy-dispersed electron precipitation impulses with about a one-second periodicity. This paper summarizes these observations and on-going analyses of HiLat's bulk data base.

OBJECTIVES

Performance degradation of a wide variety of C^3I systems due to phase, angle, and intensity scintillations produced in ionospheric irregularities would be exacerbated by enhanced plasma density left after high-altitude nuclear detonations. The Defense Nuclear Agency (DNA) seeks to understand the development of such irregularities by studying them as they occur under conditions of natural disturbance when substantial plasma-density gradients are present. At high latitudes, which we define here as extending from the plasmapause to the poles, the F layer is replete with macroscale gradients and with sources of free energy that can cause the neutral, ion, and electron gases to move along and across those gradients. When directional requirements are met, such conditions are unstable to the growth of irregularities throughout a large range of scales.

Reliable statistical characterization of complex-signal (amplitude and phase) scintillation permits design of mitigation schemes. Besides the strength and radio-frequency dependence of the fluctuations (the latter well-known), their temporal and spatial spectra are of particular interest. In the HiLat program, we seek to understand plasma-density irregularities over a spectral range of scales extending from thousands of km down to tens of meters. The HiLat Satellite is providing *in-situ* measurements of the particles, fields, and currents that lead to high-latitude irregularities, simultaneously with direct radio-beacon observations of the scintillations they produce.

From an operational point of view, points of concern include the observing-geometry dependence of scintillation, which is dictated by the three-dimensional shape of the irregularities. Beyond this, besides questions of nuclear enhancement, a useful capability would be an ability to predict when, where, and under what solar-geophysical conditions disruptive levels of scintillation will occur. This is possible now only in a crude, statistical sense.

The first objective of HiLat is to provide definitive, quantitative information on high-latitude scintillation strength and, more particularly, on the spatial and temporal spectra of the intensity and phase fluctuations of which it is composed. The second is to extend into new locations and local times of day/night the diagnosis of three-dimensional irregularity shape begun with HiLat's single-experiment predecessor, the Wideband Beacon Satellite (Fremouw *et al*, 1978). The third is to provide the additional diagnostic information on background ionospheric processes that cannot be provided by a beacon experiment alone and that is necessary for definitive identification of irregularity development and dynamics.

DESCRIPTION

Table 1 lists the HiLat experiments, their intended purposes and basic characteristics, and the principal experimenters associated with each, and Figure 1 shows the location of the sensors on the satellite. Data are collected by means of real-time transmissions to the four high-latitude receiving stations shown by encircled stars in Figure 2, which are as follows: Tromso, Norway (auroral zone); Sondre Stromfjord, Greenland (polar cusp); Churchill, Manitoba (auroral zone); and Bellevue, WA (plasmapause). A second Canadian station (non-circled star) is planned for Inuvik, Northwest Territories (auroral cusp). The Bellevue receiver, nicknamed Rover, is transportable to other locations for limited-duration observing campaigns.

The experiment payloads normally are operated over the northern quadrisphere of the earth, although they can be turned on for any quarter of the orbit. The satellite is in

TABLE 1. THE HILAT EXPERIMENTS
LEON WITTWER (DNA), PROGRAM MANAGER

PAYLOAD	OBSERVABLES	CHARACTERISTICS	EXPERIMENTERS
BEACON	Scintillation TEC	138, 390, 413, 436 MHz 1239-MHz reference Circular polarization	Carlson et al (AFGL) Forsyth et al (UWO) ¶Fremouw et al (PDNW) *Rino et al (SRI)
PLASMA MONITOR	$\Delta(\text{Log } N_e)$, N_e, T_e N_i, N_{O+}, N_{H+}, T_{H+} $\vec{V}_d \Rightarrow \vec{E}$	Langmuir Probe[§] RPA Resolution to 5 km Ion Drift Meter Resolution to 400 m	Hanson (UTD) Heelis (UTD) *Rich (AFGL)
ELECTRON SPECTROMETER	Electron Flux & Energies	20 ev - 20 kev Zenith, Nadir, 40° Resolution to 400 m	*Hardy (AFGL)
MAGNETOMETER	$\vec{B}$, $\Delta\vec{B} \Rightarrow \vec{J}$	3-axis Fluxgate Quantization 12 nt Resolution 400 m	Bythrow (APL) *Potemra (APL) Zanetti (APL)
AIM PHOTOMETERS[†]	Aurora	3914 & 6300 Å	*Huffman (AFGL) Meng (APL)

[§]Not fully operable

[†]VUV Imager failed on 23 July

UWO = University of Western Ontario

¶HiLat Project Scientist
*Experiment P.I.

DNA = Defense Nuclear Agency
AFGL = Air Force Geophysics Laboratory
UWO = University of Western Ontario
PDNW = Physical Dynamics, Inc., Northwest Division
SRI = SRI International
UTD = University of Texas, Dallas
APL = Applied Physics Lab, The Johns Hopkins University

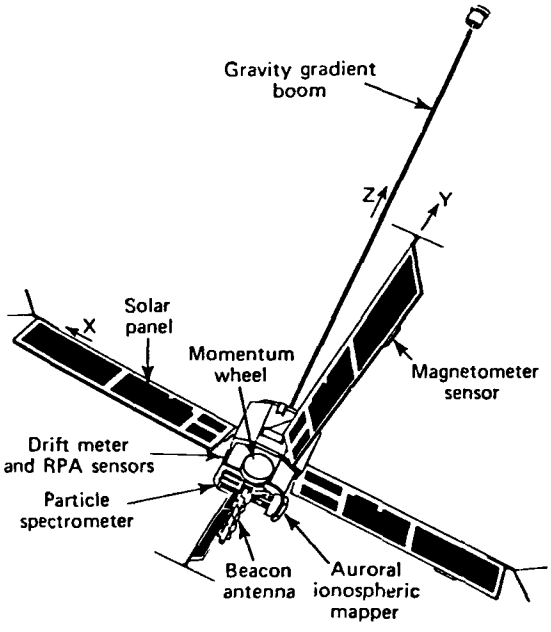


Figure 1. The HiLat Satellite, P83-1. The orbital velocity vector is in the x direction.

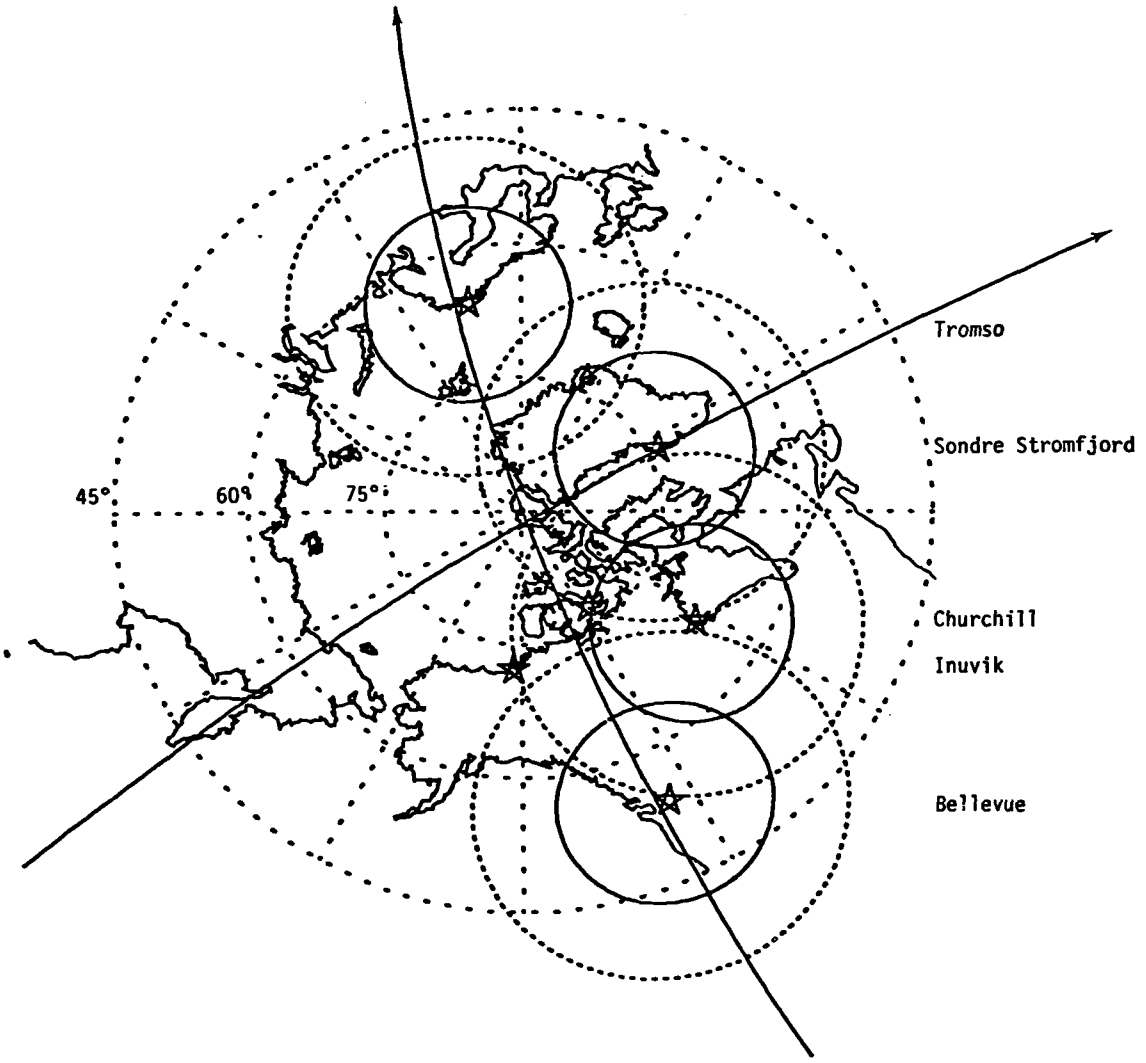


Figure 2. HiLat receiving stations and data coverage for beacon (solid circles) and other (dashed) experiments in offset-magnetic-dipole coordinates. Two representative passes are shown.

an approximately 800-km circular orbit at 82° inclination, and the orbital plane precesses through 24 hours of solar time approximately twice per year. Data collection is planned for three years.

A SAMPLING OF RESULTS TO DATE

Following launch, all experiments operated as designed, with the exception of the Langmuire probe. Later, the high-voltage power supply to the imaging spectrophotometer in the optics package failed after producing several tantalizing images of both the nightside and dayside aurora, including some in full sunlight. This Auroral Ionospheric Mapper (AIM) produced data simultaneously with the electron spectrometer, magnetometer, and plasma probe on approximately forty passes during the engineering-initialization phase of the mission. Unfortunately, the failure occurred prior to activation of the fully equipped HiLat receiving stations for the operational phase of the mission. Consequently, beacon data are not available from the passes that produced AIM images.

Some of the spectacular vuv images produced by AIM during the HiLat initialization phase have been published elsewhere. Pertinent to the present discussion is that appearing as Plate 1 in the paper by Fremouw *et al* (1985a). Figure 3 shows partial data from the *in-situ* instruments recorded during that pass at the ESRANGE Station at Kiruna, Sweden. At about 69570 sec UT, HiLat passed from the diffuse aurora into the discrete-arc oval on the evening side of the earth (~1940 Magnetic Local Time, MLT) near 69° magnetic Eccentric Dipole Latitude (ELAT). Dynamic energy spectra from the three directional energetic-electron sensors (Plate 2 in Fremouw *et al*, 1985) showed strengthening and hardening of both precipitating and upwelling electrons as the discrete-arc oval was reached, which persisted until the satellite passed into the polar rain about 100 sec later. After traversing the polar cap, HiLat encountered the morning-side oval near 75° ELAT at about 70000 sec UT.

The two traverses of the discrete-arc oval are demarked clearly in Figure 3 by elevated fluxes of precipitating electrons (JTOT), multiple current sheets inferred from the magnetometer, and directly by the vuv emission recorded in AIM's nadir pixel. The thermal-ion sensors disclosed rapid shear flows in the auroral-oval plasma, with the horizontal ion velocity closely correlated with the magnetic-field perturbations on the evening side. They also showed elevated plasma density on the evening side, including the region of diffuse aurora, as compared with the early-morning side, and some density enhancement associated with the nightside arcs. Although many topside density enhancements are related to precipitating-electron flux, there is by no means a one-to-one correspondence.

The brightest auroral region was one of generally upward current, presumably carried by the precipitating energetic electrons represented in the top trace in Figure 3. The magnetometer, however, indicated an intricate pattern of currents locally flowing downward and upward, as superimposed on an enlarged auroral image in Plate 3 of Fremouw *et al* (1985). The locally strongest current was one flowing downward near HiLat's first encounter with the auroral form. The high-resolution plots in Figure 4 disclose a complex of electrodynamic phenomena associated with the current, as uncovered and analyzed by Bythrow *et al* (1984).

First, direct application of Ampere's law yields an evaluation of the current itself. Specifically, given the orientation of the magnetometer's x, y, and z sensors, the steep inclination of the field lines, and the satellite velocity (7.44 km/sec in the x direction), one finds from the rate of change of the y-componenet B-field (in nanoteslas/sec) that the field-aligned current was approximately

$$J_z \approx 0.1 \frac{dB_y}{dt} = -90\ \mu a/m^2$$

which is the strongest downward flowing Birkeland current yet observed on any satellite.

The middle two panels disclose a discontinuity in the number flux and energy flux of precipitating electrons about 2 km (1/4 sec) equatorward of the current sheet. Bythrow *et al* (1984) analyzed the electron energy spectra obtained at the foot and at the top of the discontinuity to infer plasma-density profiles and corresponding field-line-integrated Pedersen conductivities. What they found was an x-directed conductivity gradient of 2 mhos/km. Given a minus x-directed (i.e., southward) electric field of 45 mv/m, the conductivity gradient is sufficient to account for the field-aligned current, as follows:

$$J_z = \nabla \cdot \vec{J}_\perp \approx E_x \frac{\partial \Sigma_P}{\partial x} = \left(-45 \frac{mv}{m}\right)\left(2 \frac{\mho}{km}\right) = -90\ \mu a/m^2$$

The background electric field, while observationally consistent with a value of 45 mv/m southward in the region just north of the conductivity discontinuity, could not be measured directly there because of strong plasma-velocity variation encountered in that region, as displayed in the bottom panel of Figure 4. These fine-scale velocity shears represent another phenomenon associated with the field-aligned current. If carried by upwelling electrons, as deduced above, the current corresponded to an electron flux of

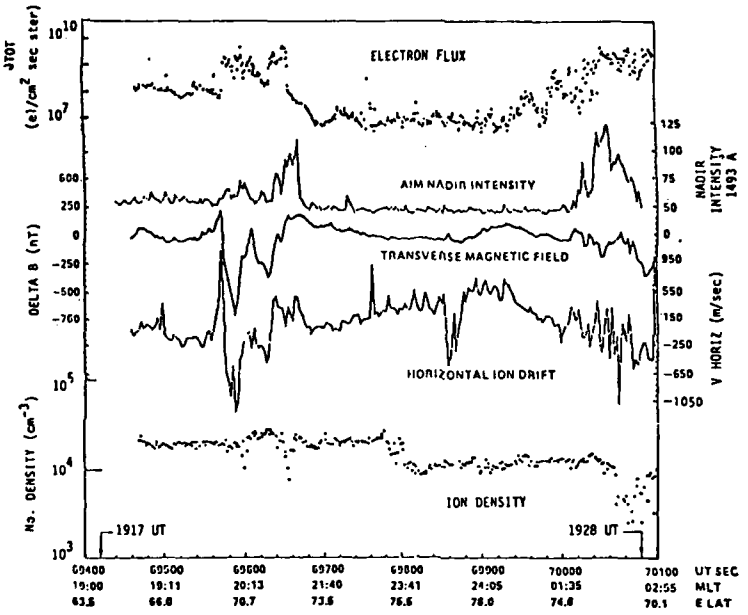


Figure 3. Data from on-board sensors taken during passage over auroral oval and northern polar cap on 23 July 1983.

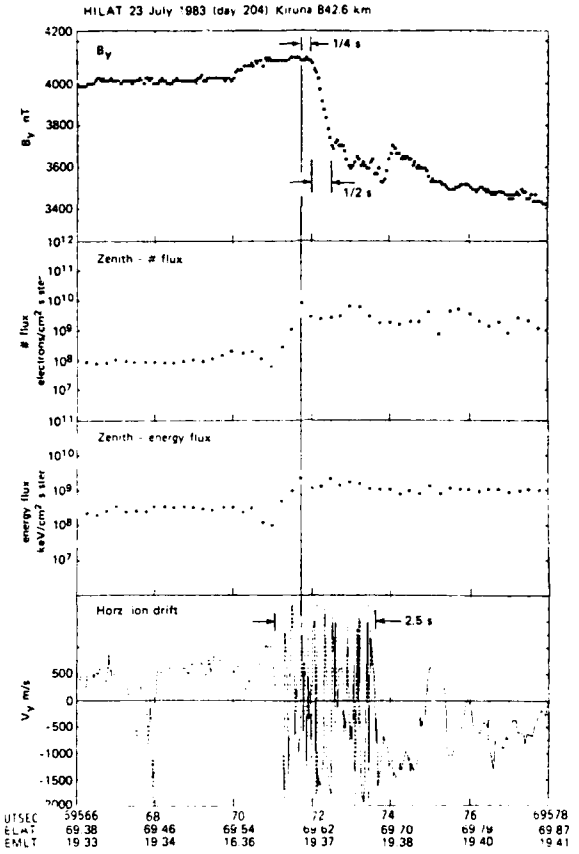


Figure 4. High-resolution data from near the equatorward edge of the evening side auroral oval traversed early in Figure 3. Top: y-axis magnetometer trace. Middle: number and energy flux of precipitating electrons. Bottom: Cross-track plasma drift measured with the ion drift meter. (From Bythrow *et al*, 1984.)

$$\frac{J_z}{e} \approx 6 \times 10^{10} \text{ el/cm}^2 \text{ sec},$$

which is sufficient to drive the 0^+ ion-cyclotron instability. Thus, it is concluded that the electric field fluctuations inferred from the plasma-velocity structures are the signature of the ion-cyclotron instability driven by the observed downward Birkeland current.

Moreover, a thermal-plasma density of about 2×10^4 el/cm^3 was measured at the satellite. If this represents the density of the upwelling electrons constituting the current, then the upward velocity of the electrons is

$$V_e = \frac{J_z}{en_e} \approx \frac{6 \times 10^{10} \text{ el/cm}^2 \text{ sec}}{2 \times 10^4 \text{ el/cm}^3} = 30 \text{ km/sec}.$$

Now, a cross-field gradient length of about 3 km was observed for the precipitating-electron flux from which the Pedersen conductivity was deduced. This combination of plasma-density gradient and drift velocity is ample to trigger the current-convective instability, a member of the family of convective interchange instabilties thought to play a dominant role in the development of scintillation-producing irregularities.

Unfortunately, the foregoing observations were made before the complete HiLat stations, with their beacon receivers, were operating. Since that time, however, numerous scintillation observations have been made, ranging from weak intensity and phase fluctuations at the plasmapause (from Bellevue and on a Rover field trip to AFGL at Hanscom Field) to much stronger scintillations observed in the auroral zone and in the polar cap and cusp. A report on results to date from the dayside cusp will be presented by Livingston *et al* (Proceedings of this symposium).

A typical example of polar scintillation and correlative measurements is displayed in terms of reduced parameters on the standard edited-data summary chart reproduced in Figure 5. From top to bottom, the three data panels respectively contain beacon data, parameters relating to auroral precipitation, and information on the density and drift velocity of the thermal plasma at the satellite. Above and between the panels are various scales relating to the location and time of the observations, plus relevant propagation angles. The former include the magnetic apex latitude of the satellite, the F-layer radiowave penetration point, and the F-layer footprint of the field line through the satellite, as well as magnetic (eccentric dipole) time at the satellite.

The auroral-precipitation data include the log of low-energy electron number flux, the vertical current densities derived from the x and y (horizontal) magnetometer sensors, and the log of the output from the nadir-viewing 6300 A telephotometer (absent in the daytime pass illustrated). The cold-plasma measurements displayed include the ion density from the drift meter and the three component velocities from the drift meter and RPA. (The example shown is from a time prior to automated processing of RPA measurements, so there is no x-velocity trace.)

The panel of beacon data contains measurements of TEC and intensity and phase scintillation. Specifically, VTEC is the vertical equivalent total electron content, VS4V is the VHF S_4 scintillation index converted to an equivalent vertical measurement, and the remaining (solid) curve is a phase-scintillation index. Both the intensity and phase scintillation indices are edited automatically according to criteria chosen to exclude dead channels, interference, and the like.

For phase, the VHF index is scaled from UHF if the former is contaminated and the latter passes all editing tests. The S in VTVS stands for "scaled" to indicate this possibility. The basic parameter, T, is the power spectral density (PSD) at a fluctuation frequency of 1 Hz (Rino, 1979) derived from a single-regime power-law fit through the fast Fourier transform of the phase time series measured over a 30-sec window. This PSD is divided by the secant of the radiowave incidence angle on the F layer to produce an equivalent vertical parameter. Finally, the square root of VTVS is taken to produce a parameter proportional to the electron-density fluctuation rather than its square.

The dominant scintillation feature of the pass shown, which occurs on many passes, is the four-fold increase in $\sqrt{\text{VTVS}}$ near the point of closest alignment of the radio propagation vector with the magnetic field line at the F-layer penetration point (indicated by the minimum in "Briggs-Parkin" angle). While VTVS has been converted to a vertical equivalent parameter, otherwise it has been left unadjusted for geometrical effects. The proximity of the prominent scintillation feature to the magnetic zenith, therefore, is an indication that it probably resulted from geometrical enhancement by anisotropic irregularities.

Moreover, the fact that the feature occurred at the minimum off-field (Briggs-Parkin) angle and not as the line of sight grazed through the local L-shell (minimum off-shell angle = 0) indicates that any anisotropy was field aligned, in contrast to the additional cross-field anisotropy experienced in the night-side auroral oval at latitudes such as that of Poker Flat (Fremouw *et al*, 1977; Rino *et al*, 1978). It is interesting to

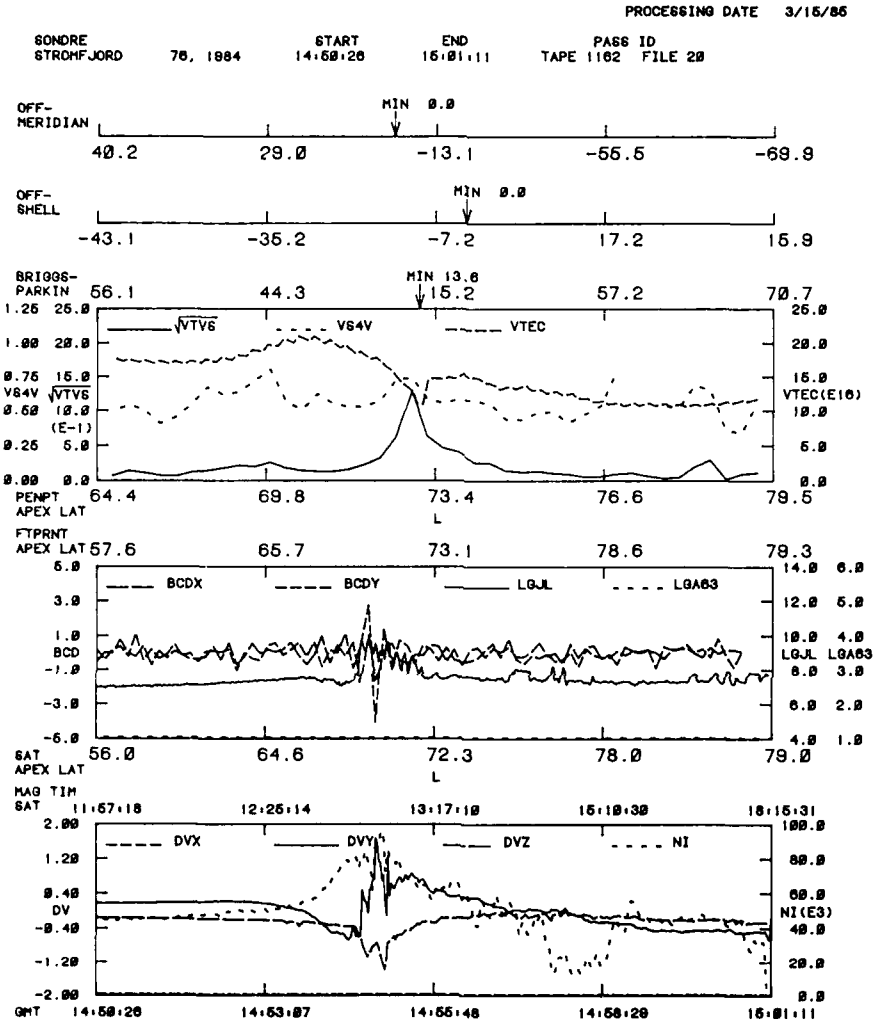


Figure 5. Example of edited and processed high-latitude scintillation and TEC data (top panel) and correlative parameters obtained from HiLat, recorded at Sondre Stromfjord on 16 February 1984.

note, also, that the most prominent TEC feature observed on this pass was an apparent "hole" also co-located with the point of closest approach to the magnetic zenith. Thus, field alignment of large-scale structures (transverse wavelengths greater than 60 km, say) can reveal itself in TEC recordings.

Complete description of irregularity anisotropy in specific instances must await analysis of the interferometer data being collected in HiLat, a rather ambitious data-processing task (Rino and Livinston, 1982). Meanwhile, however, an aggregate description of dominant irregularity configuration can be built up from the bulk data base on phase-scintillation enhancements. A start has been made, as illustrated first for nighttime data from Sondre Stromfjord in Figure 6.

What is shown is a contour plot of $\sqrt{VTVS}$ on a grid of off-shell angle and off-magnetic-meridian angle of the line of sight at the F-layer penetration point. On such a plot, the magnetic zenith lies at the origin. Contours displaying circular symmetry about the origin, then, are the signature of field-aligned irregularities displaying rod-like axial symmetry. Such a feature does appear about the origin in this plot, which contains only about six weeks of nighttime data from Sondre Stromfjord. The equally strong feature appearing near -10° off-meridian angle and -20° to -30° off-shell angle presumably is a region of geophysically enhanced irregularity, which is expected to average out as additional data are accumulated.

In contrast to the circular symmetry of the feature near the origin in Figure 6, the corresponding feature observed at Tromso during the same period, shown in Figure 7, shows a tendency to be elongated along the L-shell direction. If reinforced by additional data as other features average out, such elongation will indicate the presence of cross-field as well as along-field anisotropy (i.e., "sheetlike" irregularities). Thus, a first look at HiLat data from the nightside auroral oval at Tromso appears to be in accord with corresponding Wideband data from Poker Flat and to contrast with nighttime polar data from Sondre Stromfjord. This study is continuing with the addition of accumulating measurements from both stations and from Churchill to the data base.

Once anisotropy factors in the dayside and nightside oval and in the polar cap are assessed, the phase-scintillation spectra can be used directly to infer the height-integrated spatial spectrum of irregularities. This process already has been started by C.L. Rino (private communication), who is performing systematic analysis of multi-regime power-low spectra, such as those observed near the equator (Rino *et al*, 1981) and in auroral-zone data from Wideband (Fremouw *et al*, 1985).

While systematic analysis of the bulk data base accumulating from HiLat continues, and indeed intensifies, individual observations of note continue to be identified. A recent example is discovery by D.A.Hardy (private communication) of periodically repeating energy-dispersion traces in dynamic spectra from the electron spectrometer. The traces, which visually resemble whistlers on such a display, occur in the highest-energy bins of the zenith-directed and oblique electron sensors but not in those of the nadir-directed sensor. Thus, they appear to represent electrons scattered into the loss cone, presumably by wave-particle interaction.

Figure 8 shows high-resolution time-series traces of the counts in five of the energy bins during a brief portion of a morning pass over Tromso. The features of interest are marked with arrows. The temporal/spatial resolution available in the HiLat electron spectrometer permits identification of these features and discloses that they recur periodically with about a one-second repetition period. From their energy-dispersion characteristic, Hardy (private communication) has concluded that the electrons that they represent were scattered into the loss cone in the magnetosphere south of the equator. Continued study of their periodicity and of the time of day and solar-geophysical conditions in which they occur is expected to lead to identification of the type and source of the wave responsible.

CONCLUSION

While HiLat suffered some instrument debilitation early in its mission and experiences modestly troublesome attitude variations from time to time, it is producing a wealth of information on high-latitude irregularities and the plasma and electrodynamic environment in which they arise and evolve. Specific and bulk analysis of the accumulating data base continues, along with comparison of those data with information from incoherent-scatter radars and other sources.

From the foregoing combination of information, the HiLat Science Team is beginning to sort out contributions to irregularity development by particle precipitation, plasma convection, and convective-interchange instabilties. By continuing to pursue these efforts while remaining open to identification of other source mechanisms (eg, E-field structures imposed from outside the ionosphere), we hope to provide definitive descriptions of the evolution of high-latitude F-layer irregularities at a future AGARD meeting.

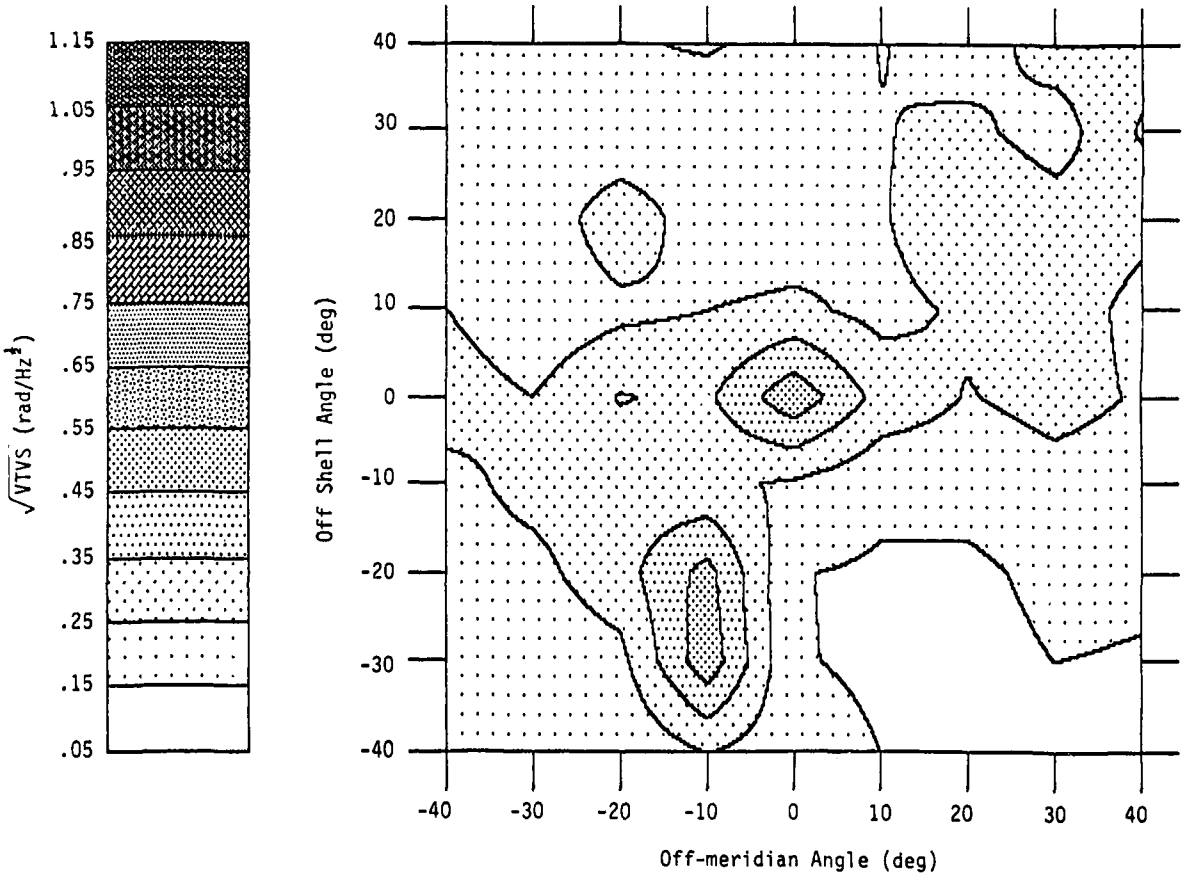


Figure 6. Contour plot of phase scintillation index (gray-scale left) measured at night at Sondre Stromfjord during six weeks in February and March of 1984, suggesting that the dominant anisotropy in the nightside polar cap is field-aligned (i.e., that the dominant configuration of irregularities is rodlike).

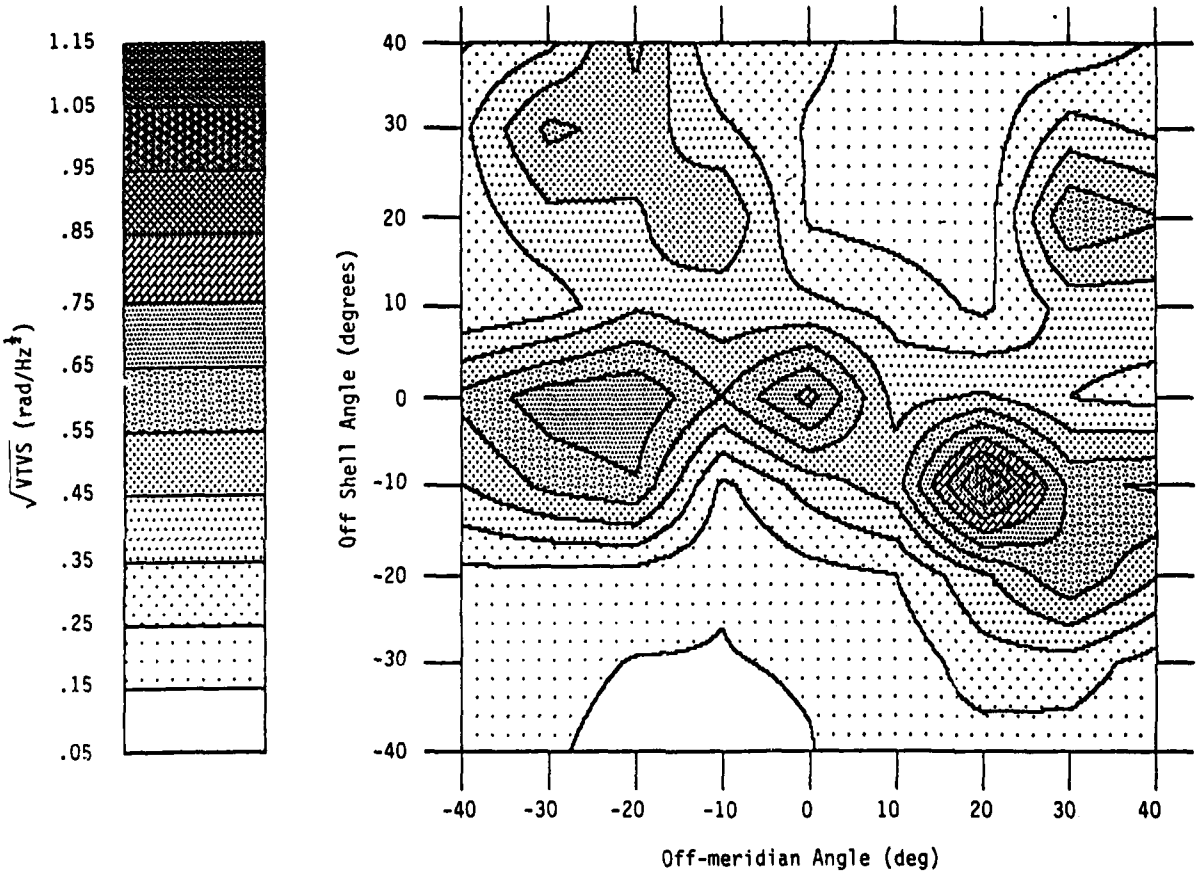


Figure 7. Contour plot of phase-scintillation index (gray-scale left) measured at night at Tromso during the same six weeks that the observations in Figure 6 were made, suggesting the existence of sheetlike irregularities aligned along the L shells.

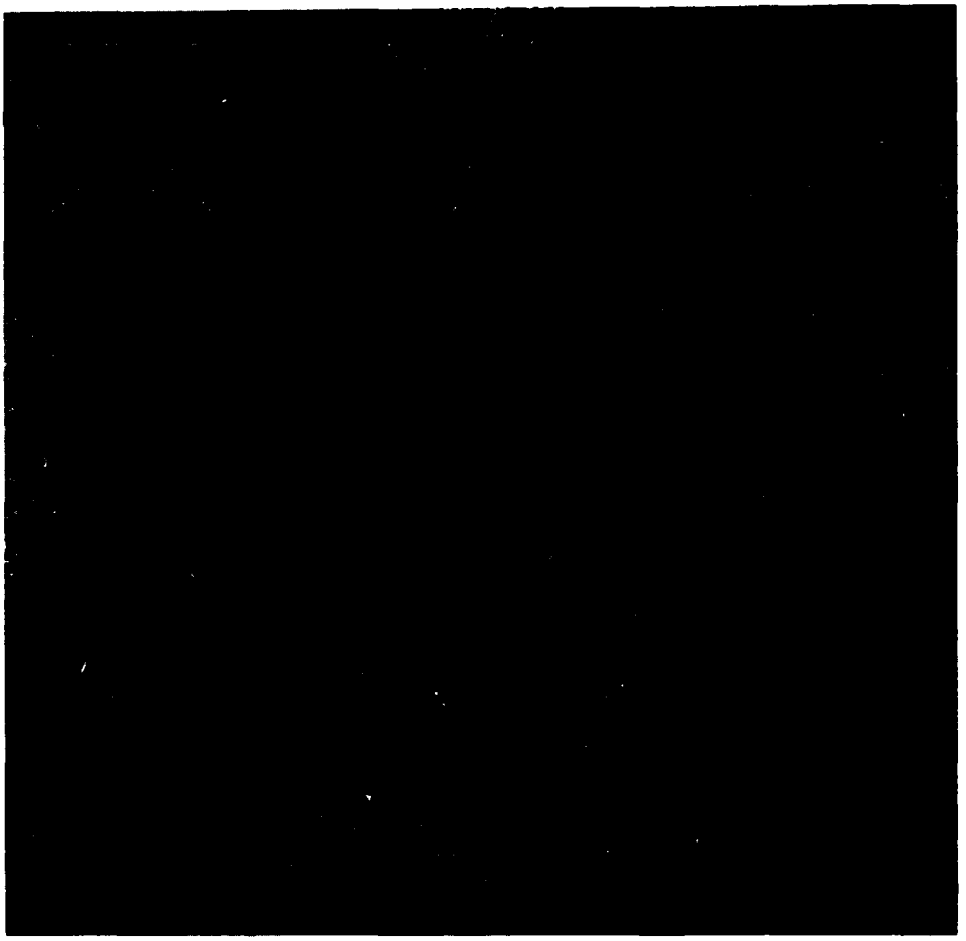


Figure 8. High-resolution time series of precipitating-electron counts in five energy bins during a portion of a pass recorded at Tromso on the morning of 28 December 1983, showing rapidly periodic energy-dispersion signatures. (From D.A. Hardy, private communication.)

REFERENCES

Bythrow, P.F., T.A. Potemra, W.B. Hanson, L.J. Zanetti, C.-I. Meng, R.E. Huffman, F.J. Rich, and D.A. Hardy, "Earthward Directed High-Density Birkeland Currents Observed by HILAT," J. Geophys. Res., 89 (A10), October 1, 1984, 9114-9118.

E.J. Fremouw, H.C. Carlson, T.A. Potemra, P.F. Bythrow, C.L. Rino, J.F. Vickrey, R.L. Livingston, R.E. Huffman, C.-I. Meng, D.A. Hardy, F.J. Rich, R.A. Heelis, W.B. Hanson, and L.A. Wittwer, "The HiLat Satellite Mission," Rad. Sci., 20 (3), 1985a, in press.

Fremouw, E.J., R.L. Leadabrand, R.C. Livingston, M.D. Cousins, C.L. Rino, B.C. Fair, and R.A. Long, "Early Results from the DNA Wideband Satellite Experiment--Complex-Signal Scintillation," Rad. Sci, 13 (1), 1978, 167-187.

Fremouw, E.J., C.L. Rino, R.C. Livingston, and M.C. Cousins, "A Persistent Subauroral Scintillation Enhancement Observed in Alaska," Geophys. Res. Ltrs., 4 (11), 1977, 539.

Fremouw, E.J., J.A. Secan, and J.M. Lansinger, "Spectral Behavior of Phase Scintillation in the Nighttime Auroral Region," Rad. Sci., 20, 1985b, in press.

Rino, C.L., "A Power Law Phase Screen Model for Ionospheric Scintillation: 1. Weak Scatter," Rad. Sci., 14 (6), 1979, 1135.

Rino, C.L. and R.C. Livingston, "On the Analysis and Interpretation of Spaced-Receiver Measurements of Transionospheric Radio Waves," Rad. Sci., 17 (4), 1982, 845-854.

Rino, C.L., R.C. Livingston, and S.J. Matthews, "Evidence for Sheetlike Auroral Ionospheric Irregularities," Geophys. Res. Ltrs., 5 (12), 1978, 1039.

Rino, C.L., R.T. Tsunoda, J. Petriceks, R.C. Livingston, M.C. Kelley, and K.D. Baker, "Simultaneous Rocket-borne Beacon and In-situ Measurements of Equatorial Spread F - Intermediate Wavelength Results," J. Geophys. Res., 86 (A4), 1981, 2411-2420.

TOTAL ELECTRON CONTENT AND L-BAND AMPLITUDE AND PHASE SCINTILLATION MEASUREMENTS IN THE POLAR CAP IONOSPHERE

J.A. Klobuchar and G.J. Bishop
Ionospheric Physics Division
Air Force Geophysics Laboratory
Hanscom AFB, MA 01731

P. H. Doherty
Physics Research Division
Emmanuel College
400 The Fenway
Boston, MA. 02115

SUMMARY

The first measurements of absolute Total Electron Content (TEC) and L-band amplitude and phase scintillation were made from Thule, Greenland, a polar cap station, in early 1984. These measurements were made using signals transmitted from the Global Positioning System (GPS) satellites. The variability of the TEC, especially during the afternoon to pre-midnight hours, is large, with increases in TEC above the background values of greater than 100 percent not uncommon. During one disturbed time quasi-periodic TEC enhancements having periods as short as ten minutes and amplitudes equal to the background TEC were observed for over two hours. The TEC during some of the disturbed periods in the dark Thule ionosphere exceeded mid-latitude daytime values. Amplitude scintillations were small, not exceeding 3 dB peak to peak during the entire observing period, but they were associated with the times of TEC enhancements, with some evidence for stronger scintillation occurring during the negative gradients of the TEC enhancements. Phase scintillations were highest during some of the times of enhanced TEC, and depend critically upon the phase detrend interval used.

INTRODUCTION

Measurements of total electron content (TEC) obtained from high elevation angle satellites have been obtained for the first time from the polar cap station located at Thule, Greenland, 76.5° geographic latitude, 86° invariant latitude. The only previous TEC measurements reported from Thule, ([1]Mendillo and Klobuchar, 1973) were recordings of Faraday rotation obtained from a geostationary satellite viewed at an approximate 5° elevation angle where the ionospheric intersection of the ray path to the satellite was over the auroral zone rather than the polar cap.

It is particularly important to study the behavior of the F region in the polar cap during the winter when solar EUV is minimal, and much of the F region is dominated by transport, rather than by local production. TEC measurements are also important because of ionospheric time delay effects on satellite positioning systems.

In addition to making the first high elevation absolute TEC measurements from Thule, both L-band amplitude and phase scintillation data were also obtained. During an eight day period in January-February, 1984 approximately 120 hours of recordings were obtained during both relatively magnetically quiet and magnetically disturbed conditions. Amplitude scintillation can limit satellite communications ([2]Aarons, et. al.,1982) while phase scintillation, a measure of irregularities of scale size greater than a few hundred meters can seriously affect the imaging from satellite-borne Synthetic Aperature Radars (SARs), ([3]Szuszczewicz, et. al., 1983).

THE MEASUREMENT TECHNIQUE

Dual frequency, L-band, psuedo-random-code modulated signals transmitted from the US Defense Department Global Positioning System (GPS) satellites were used for determining absolute TEC and for the measurements of amplitude and phase scintillation. GPS is an advanced satellite system, ([4]Parkinson and Gilbert, 1983), in which the user determines his range and range-rate from signals transmitted from 4 satellites by comparing his own clock time against those received from the 4 satellites. In this manner the three dimensional user position and velocity are determined. A fourth satellite is required to correct any user clock error. In order to provide simultaneous visibility of at least 4 satellites to a user anywhere on, or near, the earth's surface, a total of 18 satellites will eventually be required.

For our measurements in early 1984 only 5 satellites were available for navigation, affording only a few hours of simultaneous 4 satellite visibility per day. However, due to both the high geographic latitude of Thule, and the high inclination of the GPS satellites, there was at least one of the total of 5 satellites above 20° elevation for over 18 hours per day during our test period, thereby allowing us to make TEC and scintillation observations for over 3/4 of each day during our test period.

The importance of the GPS satellites for ionospheric research lies in the dual, coherently transmitted frequencies designed for the navigation user to correct for the group delay and carrier phase advance effects of the earth's ionosphere which otherwise would degrade both the range and range rate accuracy of the measurements. The signals

from the GPS satellites can be reduced, by the use of an appropriate receiving system, to equivalent coherent carriers at 1.228 and 1.575 GHz with coherent modulation at 10.23 MHz from which both the carrier phase advance and the modulation group delay can be directly measured, ([5]Rino, et. al.,1981). Carrier phase advance can be related to relative TEC , ([6]deMendonca, 1963), as:

$$\delta\phi_c = \frac{1.34 \times 10^{-7}}{f} \quad TEC \qquad \text{(cycles)}$$

where: TEC is in el/m^2 column and f is the carrier frequency in Hertz.

Since ionospheric changes imposed on the phase of a radio frequency wave transmitted from a satellite are more easily measured by comparison against a reference phase at a higher frequency we can write the difference in the ionospheric phase advance at two frequencies, referenced to the lower frequency as:

$$\Delta(\delta\phi) = \frac{40.31}{cf_2} \times \frac{(m^2 - 1)}{m^2} \quad TEC$$

where m = 154/120 for GPS satellites, c = 2.998x10^8 m/sec, f_2 = 1.228 GHz. For the GPS frequencies: TEC = 2.32 x $10^{16}\Delta(\delta\phi_c)$ el/m^2 where $\Delta(\delta\phi_c)$ is in cycles.

Because of the relatively close spacing of the two coherent GPS carriers the measured ionospheric phase at the lower frequency, f_2, minus that at the higher frequency, f_1, is only 39% of the total phase advance at f_2. Nevertheless, this technique has excellent sensitivity of better than 0.1 radians r.m.s. in a 16 Hertz bandwidth using a nearly omnidirectional antenna and automaticallly removes all the contributions to phase changes due to geometric Doppler changes.

The measured differential carrier phase advance from the GPS satellites, $\Delta(\delta\phi_c)$, can be related to the equivalent ionospheric phase advance, $\delta\phi_c(f)$, at any single frequency, f, by:

$$\delta\phi_c(f) = \frac{1.228 \times 10^9}{f} \times 2.546\ \Delta(\delta\phi_c)_{GPS}, \text{ where f is in Hertz.}$$

For ease of comparing our phase scintillation results against those of others we have referenced them to an equivalent single frequency carrier phase advance at a standard frequency of 1 GHz.

The differential carrier phase advance measurement can be used to measure the relative changes in TEC with great accuracy. The background values of TEC, however, generally produce much more than one complete cycle of differential carrier phase advance; thus, some other technique must be used to determine the absolute TEC values.

The GPS satellites also transmit coherently derived modulated signals on each of the two carriers, providing a means for measuring absolute TEC values. The group delay measured between the two, 10.23 MHz equivalent modulation envelopes at the carrier frequencies is related to the equivalent TEC by:

$$TEC = 2.852 \times 10^{16}\delta(\Delta t_m)$$

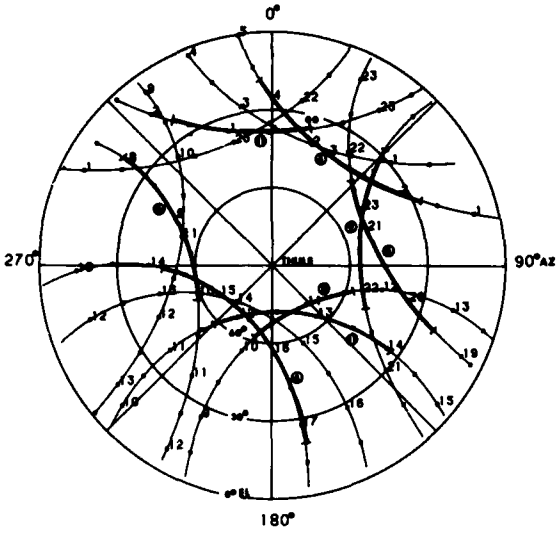
where $\delta(\Delta t_m)$ is the differential group delay measured at the two modulation frequencies in nanoseconds.

In order to obtain an absolute value of TEC, while at the same time retaining the excellent relative accuracy of the phase measurements, it is also necessary to utilize the group delay data to obtain one value of TEC to fix the relative phase advance scale throughout each satellite pass to an absolute one. In practice, several independent values of group delay are fitted on an r.m.s. basis to the continuous relative scale of carrier phase advance.

The carrier phase advance, amplitude scintillation at the two frequencies, and the group delay were all sampled at a 20Hz rate. Group delay was averaged over a one minute interval to obtain smooth absolute values of TEC, and the differential carrier phase data was high pass filtered with various detrend times to illustrate the relative size of the observed phase scintillations remaining after detrending.

THE MEASUREMENTS-IONOSPHERIC REGION PENETRATED

Figure 1 illustrates the geometry of the GPS satellites as a function of elevation and azimuth as viewed from Thule during the middle of our eight day observing period. The satellites are in 12 hour, sidereal synchronous orbits which cross over essentially the same position in the sky approximately 4 minutes earlier each day. The receiving system was capable of receiving only one satellite at a time, thus we generally observed the satellite with the highest elevation angle. Note that in figure 1 only the heavier portion of each satellite's track was received.



THULE
DAY 32 YEAR 84

Fig. 1. Elevation & azimuth of GPS satellites as viewed from Thule, Greenland on February 1, 1984. The heavy portions of each satellite track indicate the times & locations of actual GPS data recording.

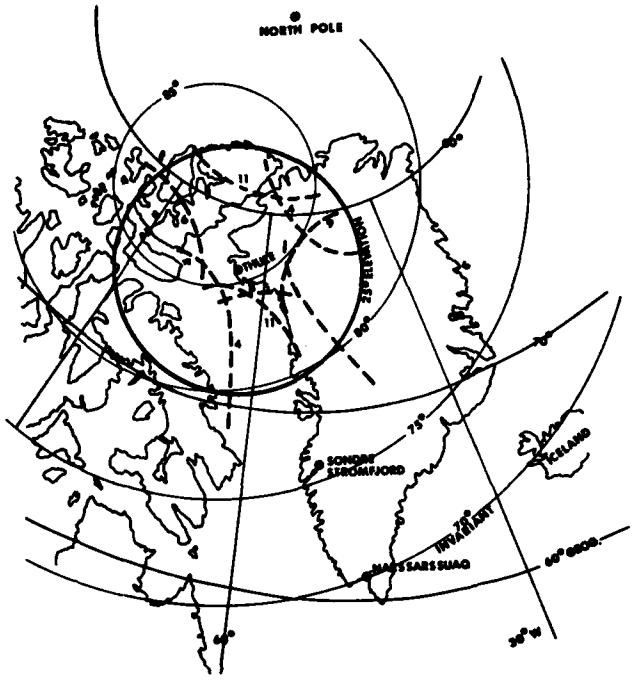


Fig. 2. Locus of 400 km height intersection of ray path to indicated GPS satellites. Invariant latitudes are also shown.

In figure 2 the equivalent ionospheric location of the propagation path to each satellite at an average height of 400 km is shown, along with both the geographic and corrected geomagnetic latitudes. Note that most of the data taken from Thule refer to corrected geomagnetic latitudes above 80°, the only exceptions being when satellites were not visible at higher elevation angles. At those times we followed a satellite down to below 25° elevation. The corrected geomagnetic latitudes through which we measured ionospheric effects from the GPS satellite signals were always above the poleward side of the statistical position of the auroral oval as determined by [7]Feldstein and Starkov, (1967); thus, direct auroral precipitation effects on the TEC should not occur often at the invariant latitudes of our observations. However, Weber (private communication) has frequently observed sub-visual auroras above 80° corrected geomagnetic latitude using an all-sky image intensified optical system. During our eight day observing period several such auroral forms were recorded by Weber above 80° corrected geomatic latitude. The comparison of those results with TEC changes will reported elsewhere.

THE MEASUREMENTS-TEC RESULTS

The diurnal behavior of equivalent vertical TEC for our eight day observation period is shown on the daily overplot curves in figure 3. A clear diurnal variation of TEC can be seen in these daily overplot curves with a maximum in the local afternoon sector and a minimum in the predawn period. Thule at 76.5° N. geographic latitude has a maximum solar elevation angle above the horizon at a height of 150 km, assumed to be near the height of maximum production, of only 9.5° during our observing period. This maximum occurs at 1650 hours U.T. , nearly coincident with the time of our observed diurnal TEC maximum. Thus, even though the sun is indeed very low, there is still some apparent solar production of F region electron density. It is possible that the observed diurnal variation shown in figure 3 is actually a U.T. effect having the same phase as the solar controlled TEC would have. With observations from only one station it is not possible to separate U.T. and local time effects.

Of greater importance than the apparent solar controlled diurnal changes in the polar cap F region is the large day-to-day variability in TEC we observed, mainly during the afternoon (U.T.) and extending until the midnight hours (U.T.). The variability of the TEC during this period, also seen in figure 3, is extremely high on a percentage basis, especially during the period 20-24 hours U.T.

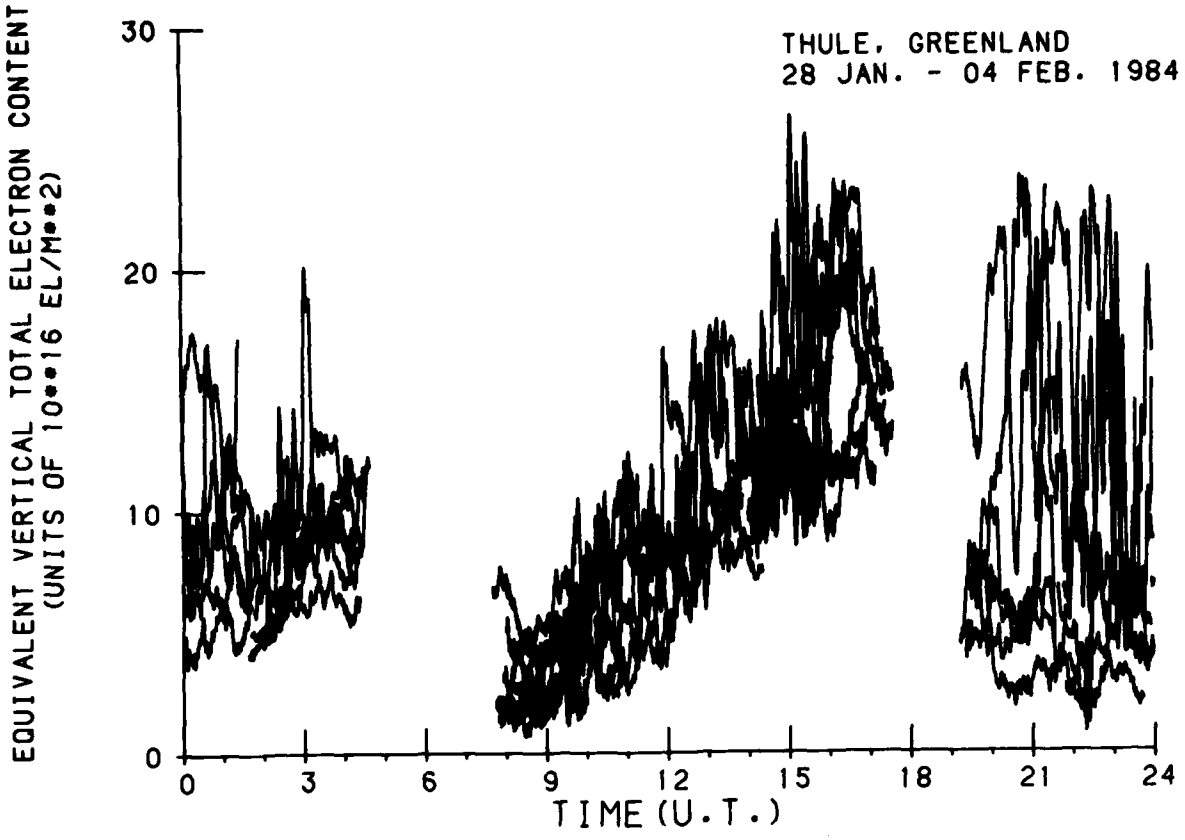


Fig. 3. Diurnal behavior of equivalent vertical TEC vs UT for the period 28 Jan-4 Feb 84.

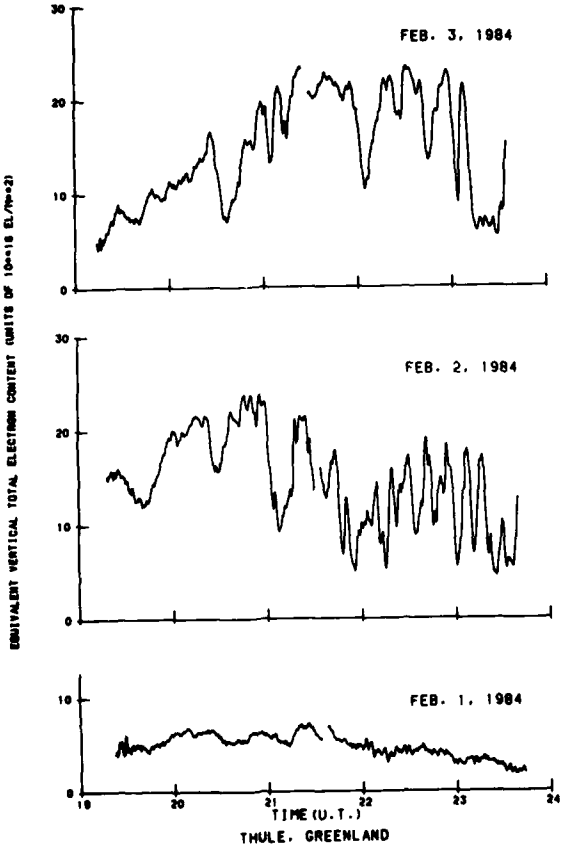


Fig. 4. TEC for the pre-midnight hours of 1-3 February 1984.

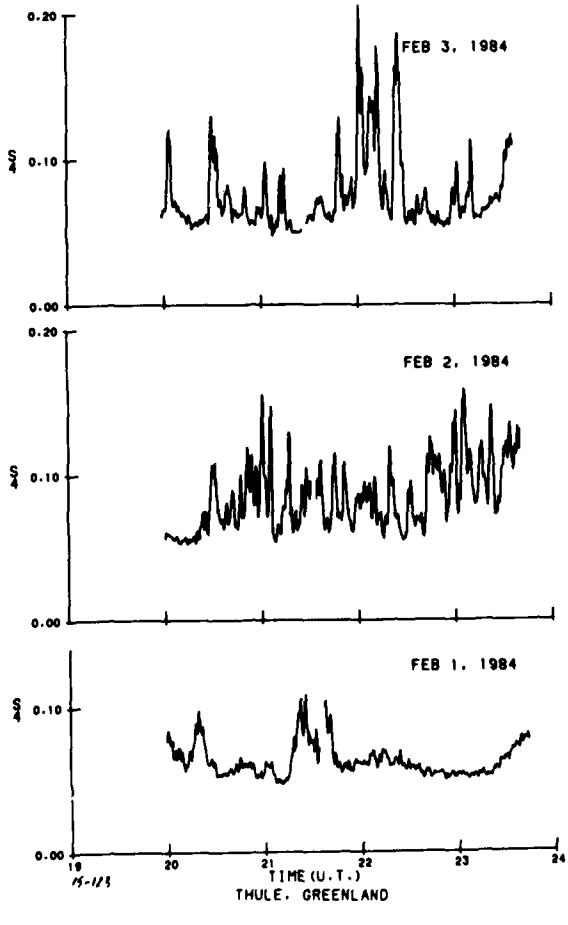


Fig. 5. Example of amplitude scintillation on 1.2 GHz for the prenight hours of 1-3 Feb 84.

Figure 4 shows a particularly dynamic period during the late hours of February 2 and 3 when the equivalent vertical TEC values varied in a quasi-periodic manner for several hours, having periodic components as short as ten minutes, particularly on February 2, and amplitudes of approximately 50% of the mean TEC during the time. For comparison, figure 4 also shows the variation of TEC during the same period of the day on February 1 when the background TEC was very low and quiet. If we assume that the diurnal TEC behavior seen on February 1 is the contribution remaining from direct solar production earlier in the day, and is representative of quiet ionospheric conditions during our eight day observing period, then the large enhancements seen on the evenings of February 2 and 3 represent much greater than a 100% enhancement above the solar controlled TEC.

THE MEASUREMENTS-AMPLITUDE AND PHASE SCINTILLATION

Amplitude scintillation measurements at L-band and higher frequencies have not previously been made in the polar cap. In our 8 days of observations we observed numerous short periods of several minutes duration having significant amplitude scintillation. Figure 5 shows the S_4 amplitude scintillation index on 1.228 GHz for the premidnight U.T. periods of 1-3 February, the same days for which the equivalent vertical TEC was shown in figure 4. The S_4 values for February 1, with the exception of two minor peaks near 2015 and 2120 U.T., represent the contribution of receiver noise in the absence of scintillation. The numerous short term peaks of S_4 seen in figure 5 on 2 and 3 February occurred during the same time of day when large TEC enhancements were seen. In a detailed comparison between the occurrence of amplitude scintillation and the TEC enhancements we found that many of the peaks in S_4 occurred on the negative gradients of the TEC enhancements.

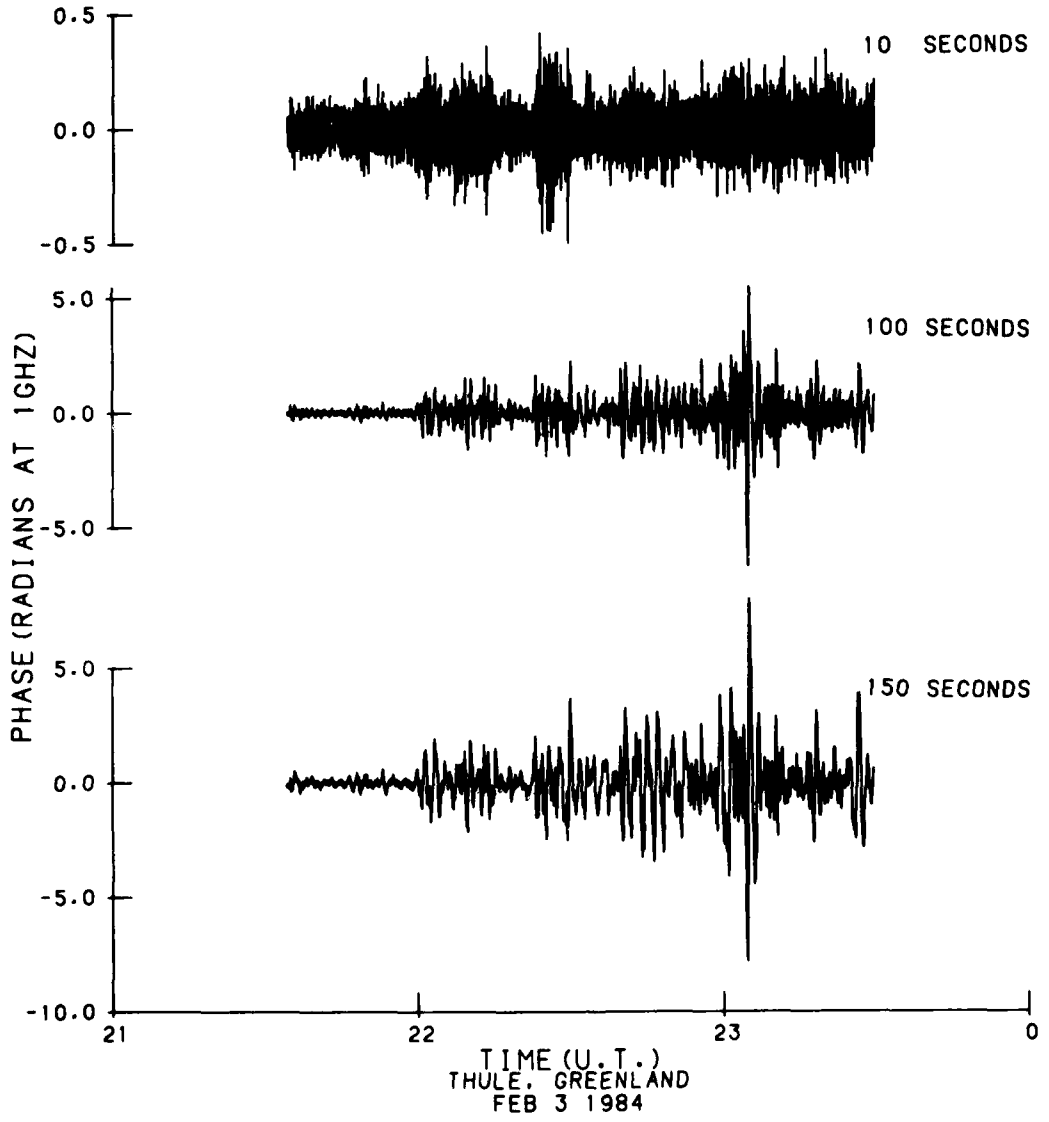


Figure 6. Example of phase scintillation seen on 3 February 1984, for detrend intervals of 150, 100 and 10 seconds.

Phase scintillation effects are shown in the recorded differential carrier phase records shown in figure 6. Three different linear phase detrend intervals were used to construct the phase scintillation residuals illustrated in figure 6. These high pass detrend cutoff times were 10 seconds, 100 seconds and 150 seconds. Note that one of the largest phase deviations seen at the longer two detrend intervals completely disappears when the shortest detrend interval of 10 seconds is used.

With the relatively slow velocity of the GPS satellites through the ionosphere most of the phase excursions from a linear detrend are produced by the movement of irrregular ionization structure through the viewing direction to the satellite. When the shortest detrend interval of ten seconds is used the size of the ionospheric structure responsible for the residual phase observed is similiar to the less than one kilometer size irregularities responsible for amplitude scintillations. The longer detrend intervals, on the other hand, depict the larger scale changes in background TEC which occur with time scales fast enough for them to be called "phase scintillation" by most workers. The use of the dual frequencies on the GPS satellites allows us to record ionospheric phase changes for periods as long as the total satellite viewing time over our station, which is a few hours for most satellites, so that any reasonable length of phase detrending interval can be used depending upon the scale size of the ionospheric structure which one desires to investigate.

DISCUSSION

The diurnal variation of TEC shows a clear minimum during the predawn period and a maximum near local noon. However, the day to day variability in TEC is very large. Because of the rapid time changes seen in the enhancements of TEC which occur throughout the day, but are particularly large in the evening and pre-midnight hours, it is tempting to say that those enhancements are due either to direct auroral precipitation or to motion of plasma into the ray path of the GPS satellite being received at the time. If we assume that the enhancements in TEC add directly to the direct solar produced TEC, which should be small in the winter polar cap ionosphere, we can then consider that the direct solar produced TEC is represented approximately by the minima of the curves shown in figure 3. The enhancements above our assumed level of solar produced ionization then are truly large. For instance, the enhancements in TEC which occur near 21 hours U.T., which range up to 24 x 10^{16} el/m^2 represent at least a several hundred percent increase, or approximately 21 x 10^{16} el/m^2, above the minimum value of TEC for 21 hours. For comparison purposes the dirunal maximum values of equivalent vertical TEC measured at Hamilton, MA (42.6°N.) did not exceed 22 x 10^{16} el/m^2 at any time during this same 8 day period.

[8]Basu, et. al., (1983) using a reasonable value for the flux into the auroral region estimated an order of magnitude time of 700 seconds necessary to increase TEC by 10^{17} el/m^2. We therefore cannot immediately rule out direct production from particle precipitation in all cases, as many of our observed increases in TEC occur over that approximate time interval. However, all-sky images of 6300A emission made by [9]Weber, et. al. (1984) and by [10]Buchau, et. al. (1983) have shown that large scale patches of plasma drift in the anti-sunward direction across the polar cap during magnetically disturbed periods.

If we assume that the ten minute periodic TEC enhancements are not locally produced, but drift through our ray path with a velocity of from 250 to 700 m/sec, typical of the velocities seen by [10]Buchau, et. al., (1983) in the polar cap during disturbed periods, then we obtain scale sizes for these TEC enhancements between 150 to over 400 km. These enhancements are certainly large enough to be seen as individual patches with the resolution of all-sky optical imaging systems. [9]Weber, et. al., (1984) reported on large scale plasma patches of size 800-1000 km in horizontal extent drifting in the anti-sunward direction in the polar cap during a moderately disturbed period.

The phase scintillation illustrated in figure 6, is referenced to a standard frequency of 1 GHz, which we propose should be a standard frequency for researchers to reference their phase scintillation results. When we compare our phase scintillation results obtained in the polar cap with those of [8]Basu, et. al., (1983), taken looking through the southern edge of the auroral region from Goose Bay, Labrador using similiar detrend intervals, we find good agreement. They showed phase fluctuations of a few radians, referenced to 1 GHz, in general agreement with our results.

The periods of enhanced phase scintillation we observed with the longer detrend times did not generally agree with observations of weak amplitude scintillation in individual cases, or with the times of individual TEC enhancements. There was general overall agreement, however, between the overall occurrence of enhanced phase scintillation and observable amplitude scintillation during the periods when the TEC was showing large variability.

CONCLUSIONS

Signals from the GPS satellites have been used to make the first absolute TEC and L-band amplitude and phase scintillation measurements of the polar cap ionosphere. TEC enhancements from the assumed solar controlled TEC background were very large and were likely due to ionization produced elsewhere and convected over the polar cap. Amplitude scintillation generally occurs during periods of TEC enhancements with a preference for scintillation to occur on the negative gradients of the large TEC enhancements. Ionospheric measurements using the dual frequency carrier and modulation transmissions of the GPS satellites can be used to greatly improve our understanding of the physical processes which govern transionospheric propagation in the polar cap ionosphere.

REFERENCES

1. Mendillo, M. and J.A. Klobuchar, "Low elevation angle measurements of total electron content taken from Thule, Greenland", AFCRL-TR-73-0098, No. 257, 1973, AD762481, available from National Technical Information Service (NTIS), 5285 Port Royal Road, Springfield, VA 22151.

2. Aarons, Jules, "Global morphology of ionospheric scintillations", Proceedings of the IEEE, 70, No. 4, 360-378, 1982.

3. Szuszczewicz, E.P., P. Rodriguez, M. Singh and S. Mango, "Ionospheric irregularities and their potential impact on synthetic aperture radars", Radio Sci., 18, No. 5, 765-774, 1983.

4. Parkinson, Bradford W. and Stephen W. Gilbert, "NAVSTAR: Global positioning system - Ten years later", Proceedings of the IEEE, 71, No. 10, 1177-1186, 1983.

5. Rino, C.L., M.D. Cousins and J.A. Klobuchar, "Amplitude and phase scintillation measurements using the Global Positioning system", in Effect of the Ionosphere on Radiowave Systems, J.M. Goodman, editor, U.S. Government Printing Office, Wash. D.C., 1981.

6. de Mendonca, Fernando, "Ionospheric studies with the differential Doppler technique", in Radio Astronomical and Satellite Studies of the Atmosphere, J. Aarons, editor, North Holland Publishing Co. - Amsterdam, 1963.

7. Feldstein, Y.I. and G.V. Starkov, "Dynamics of auroral belt and polar geomagnetic disturbances", Planet. Space Sci., 15, 209-229, 1967.

8. Basu, Sunanda, Eileen MacKenzie, Santimay Basu, H.C. Carlson, D.A. Hardy, F.J. Rich, and R.C. Livingston, "Coordinated measurements of low-energy electron precipitation and scintillations/TEC in the auroral oval", Radio Sci., 18, No. 6, 1151-1165, 1983.

9. Weber, E.J., J. Buchau, J.G. Moore, J.R. Sharber, R.C. Livingston, J.D. Winningham and B.W. Reinisch, "F layer ionization patches in the polar cap", J. Geophys. Res., 89, No. A3, 1683-1694, 1984.

10. Buchau, J., B.W. Reinisch, E.J. Weber, and J.G. Moore, "Structure and dynamics of the winter polar cap F region", Radio Sci., 18, No. 6, 995-1010, 1983.

DISCUSSION

R.A.Greenwald, US

What is the short wavelength resolution of the TEC measurements (small scale size)? Why aren't these measurements of the same structures as the longer wavelength structures measured with the scintillation technique?

Author's Reply

With the combination of both amplitude and phase scintillation we can measure irregularity scale sizes from a few hundred metres to several hundreds of kilometres.

E.J.Fremouw, US

The fact that you observe intensity scintillation predominantly on the trailing edge of the TEC features is just what one would expect from the ExB instability. The fact that it is better correlated with the TEC structure than is phase scintillation is interesting in view of recent NRL suggestions of an outerscale cutoff for ExB in the presence of finite layer thickness. I think this is a point worth pursuing.

Author's Reply

Our initial result is preliminary as it is based upon a very limited data set. We, of course, intend to pursue this work further.

C.L.Rino, US

Dr Fremouw made a comment regarding a long wavelength cutoff of the ExB instability that would restrict growth above 1 km based on NRL theory. The cutoff is well known, but it remains very uncertain what its precise nature or impact is.

Author's Reply

One of the major advantages of using signals from the GPS satellites is that we can make simultaneous measurements of amplitude and phase scintillations using relatively slowly moving satellites, thereby observing irregularities covering a wide range of wavelengths.

A.Rodger, UK

There is obviously a strong diurnal variation in the occurrence of the 300 km scale size irregularities. Is this consistent with a source mechanism in the cusp when Thule is effectively downstream from the cusp?

Author's Reply

We believe the source of the large TEC enhancements is the mid-day midlatitude ionosphere with resulting convection reaching the polar cap in the pre-midnight time sector.

VARIABILITY OF TRANSIONOSPHERIC SIGNAL TIME DELAY AT HIGH LATITUDES NEAR SOLAR MINIMUM

HAIM SOICHER
CENTER FOR COMMUNICATIONS SYSTEMS
US ARMY COMMUNICATIONS-ELECTRONICS COMMAND
FORT MONMOUTH, NEW JERSEY 07703-5000

ABSTRACT

Faraday observations were conducted at Anchorage, Alaska (61.04°N, 149.75°W) utilizing beacon transmissions from a geostationary satellite during the period just following the minimum phase of solar cycle 21.

Average maximum monthly values of total electron content (TEC), which is proportional to transionospheric signal time delay, were below 15×10^{16} el m^{-2}, while individual daily maximum values never exceeded 20×10^{16} el m^{-2}. Seasonal and day-to-day variabilities were observed.

Unique representation of the data has permitted the study of day-to-day variability of TEC. For example, during all seasons the TEC structure appears uniform from day to day during the buildup and decay phases of the local ionosphere. During the maximum and minimum of the diurnal phase, the TEC structure variability is seasonally dependent.

During periods of magnetic sudden commencements, which rarely occurred in the observations period, significant positive phase response of TEC did not materialize.

INTRODUCTION

The transit time of a transionspheric signal from a satellite to a ground observer is

$$t = \int_O^S \frac{ds}{v_g} = \frac{1}{C} \int_O^S n_g ds \qquad (1)$$

where ds is an element of distance along the signal's path, v_g is the group velocity of the signal, n_g is the group refractive index, c is the speed of light, and O and S are the observer and satellite positions, respectively. In the high-frequency approximation, the group refractive index is

$$n_g = 1 + \frac{40.3N}{f2} \qquad (2)$$

where N is the electron density per meter cubed, and f is the operating frequency in hertz. Equation (1) becomes

$$t = \frac{1}{c} \int_0^S ds + \frac{40.3}{cf2} \int_O^S N ds \qquad (3)$$

The first term in (3) represents the transit time of the signal in free space, whereas the second term represents the excess time-delay of the signal along the path. The excess time-delay is directly proportional to the total electron content (TEC) along the signal path and is inversely proportional to the frequency squared.

The Faraday polarization rotation technique has been used to obtain TEC data. A plane polarized wave propagating in the anisotropic ionosphere may be regarded as the vector sum of the ordinary and extraordinary magnetoionic components. Since the two components travel at different phase velocities, the plane of the polarization rotates continuously along the signal's path. The total rotation from a satellite signal source to observer is directly proportional to TEC. Faraday rotation is a terrestrial-magnetic-field dependent phenomenon. Since its magnitude is heavily weighted near the earth, it is considered to provide electron content values at altitudes below ~1500 km. Signal excess time delay at higher altitudes is due to free electrons in the plasmasphere. Plasmaspheric delays have been measured to be ~15% of the ionospheric time delays (Soicher, 1977).

Faraday rotation observations were conducted at Anchorage (61.04°N, 149.75°W), using the signal of a geostationary satellite located at 96°W. The geographic subionspheric point (i.e. the coordinates of the point at which the signal path intersects a mean ionospheric altitude of 420 km) is at 52.5°N, 135.5°W. The ionospheric characteristics observed are considered to be those of which are prevalent at the subionospheric point rather than those at the location of the receiving apparatus. The beacon frequency of the satellite was 136.38 MHz.

The receiving equipment was composed of an electronically rotated polarimeter which compares the left and right circular polarization components of the incident linear polarization on an eight element crossed yagi antenna (Hicks, 1972). The recording of the polarimeter output is done in analog form on a chart recorder. The conversion of polarization rotation to total electron content (TEC) is accomplished by standard procedures, at 15 minute intervals, taking into account the initial polarization transmission at the satellite source and antenna polarization

calibration (Klobuchar, 1966).

The transmission from the satellite is continuous except for an occasional shut off of the satellite for power conservation purposes. Occasional fast polarization fluctuations, generally produced by irregularities in an environment of high ambient ionization (Lee et al, 1982), do not allow polarization tracking and hence cause data gaps.

TEC Structure

The superposed diurnal variation of TEC grouped in monthly intervals for the seasonally representative months of October, December 1976 and April, August 1977, are shown in Figures 1 (a,b,c,d) and 2 (a,b,c,d). The smoothed observed sunspot numbers were 13, 15, 22, 33 respectively, which were near the minimum of sunspot cycle 21 (12) which occurred in March 1976. The TEC values are normalized to the vertical direction, and have the unit of 10^{16} electrons m^{-2} (a TEC unit = 10^{16} electrons m^{-2}). As is well known, the data exhibit diurnal, day-to-day and seasonal variability. Figure 3 (a,b,c,d) shows the variation of the monthly average of TEC (upper curves), and the standard deviation of TEC about the monthly average (lower curves) as a function of time for the four months.

The low solar cycle epoch and the northern geographic location of the subionospheric point are exhibited by the rather low absolute values of the TEC for all reported months. The TEC never exceeded 20 TEC units, and average monthly values of TEC were always below 15 TEC units. As is well known, the data exhibit diurnal day-to-day and seasonal variability,. The seasonal variation is exhibited by the time length of the post-sunset to dawn minimum TEC values indicating no illumination, and by the progressively lower average day values of the Spring (April), Summer (August), Autumn (October) and Winter (December) TEC, respectively.

The low winter values are possibly related to the mid-latitude trough; the differences, however, were quite small (1 to 3 TEC units). This is in contrast to TEC values at midlatitudes (Fort Monmouth, NJ) near solar minimum where summer TEC was higher than winter TEC and both were higher than TEC during the equinoctial periods. No seasonal variability of the day-to-day changes is exhibited by the comparable values of the standard deviation to the average TEC values as a function of time. Such ratios are plotted in Figure 4 (a,b,c,d) for the various months. For the most part, the ratio is below ~25% during the daytime for all reported months. During darkness, the ratio may exceed 25% and often exhibits variable periodic behavior. The daytime observations of the ratio agree with those at other locations and other times (Soicher and Gorman 1980, 1985; Soicher et al 1982, 1984).

A complementary method of assessing the day-to-day variability of TEC is to plot iso-TEC contours as a function of day-of-month and diurnal time. Such plots for the reported months are shown in figures 5 through 8. The values of the intervals of the TEC contours are of the order of the standard deviations, so as to eliminate the appearance of normal day-to-day undulations (e.g. those due to travelling ionospheric disturbances) in these plots.

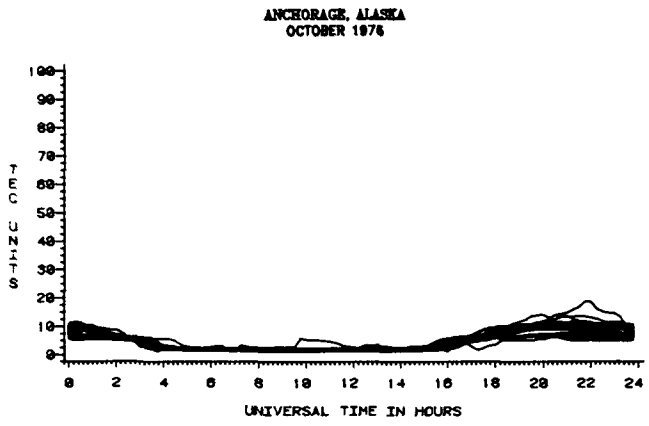
The following day-to-day features may be ascertained form the figures. For the winter data the iso-TEC contours appear to vary little throughout the month during the buildup (17-19UT) and final decay (02-04UT) phases of the diurnal variation. During the maximum phase of the diurnal variation enhanced TEC is normally maintained for a number of consecutive days. Similarly, during the predawn phase depressed TEC values are normally maintained for a number of consecutive days.

The increase in the nighttime TEC on 29 December followed by depressed values on 30 December may be associated with TEC positive phase response to sudden commencement (SC) which occurred on 28 December at 20:36 UT. No such response during daytime is observed, although enhanced values are observed on 30 December.

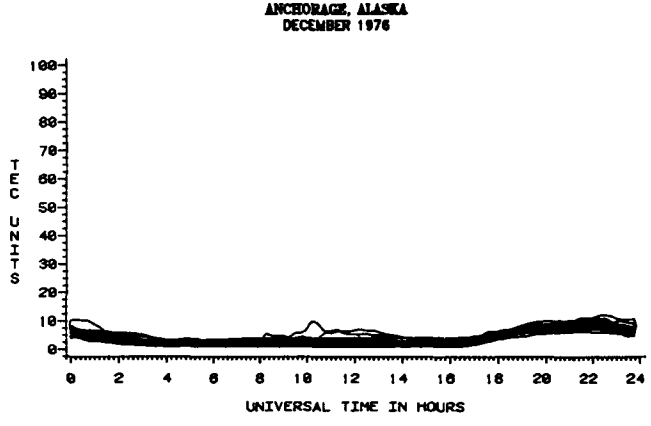
For the spring data the iso-TEC contours appear to vary little throughout the month during the buildup (15-17UT) and final decay (06-08UT) phases of the diurnal variation. During the maximum phase of the diurnal variation enhanced TEC may be maintained for a number of consecutive days. Similarly, during the predawn phase, depressed TEC values are normally maintained for a number of consecutive days. The low TEC values during the predawn period on 20 April may be due to SC at 0106 on the 19 April. The 6-7 April period was magnetically disturbed, and this is exhibited by the variability of content during the maximum phase of the diurnal variation.

During the summer little variation of the iso-TEC contours is observed during the decay and buildup phases of the diurnal variation. TEC enhancements/depressions during the day/night periods normally extend over few consecutive days. One day enhancements/depressions which do occur are not correlated with magnetic sudden commencement.

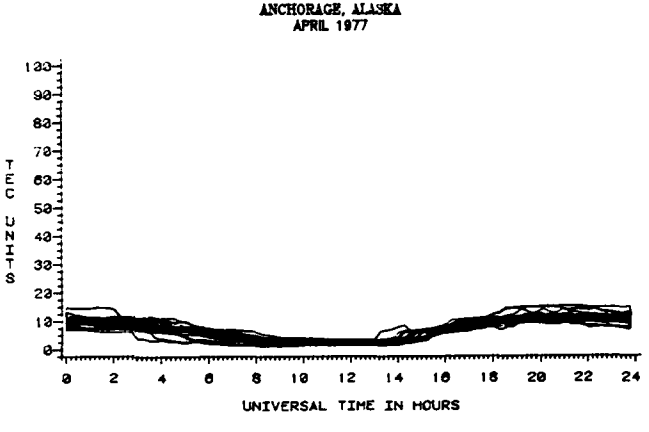
During the Autumn little variation of the iso-TEC contours is observed during final decay and sunrise period of the diurnal variation. Enhancements/depressions of TEC during maximum/minimum phases of the diurnal variation normally occur for a number of consecutive days. One day enhancements/depressions of TEC are not



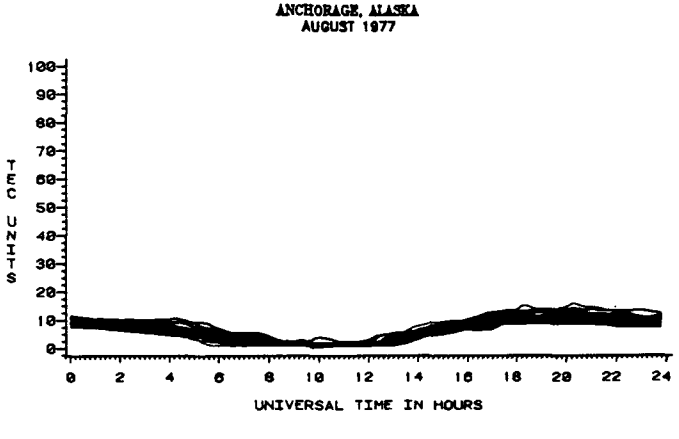
1(a)



1(b)

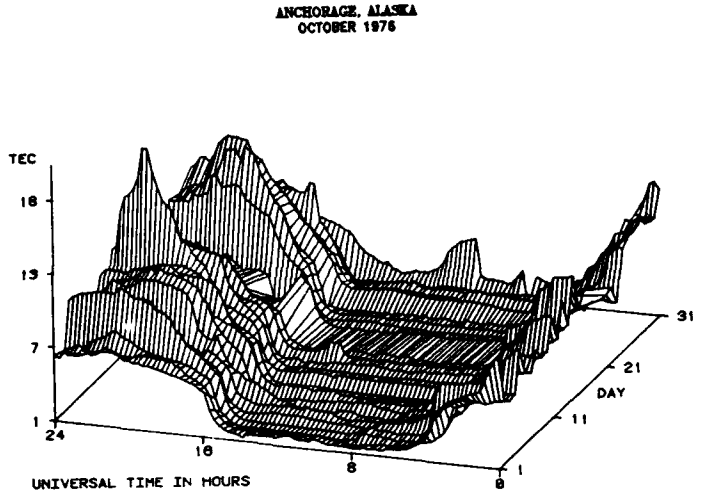


1(c)

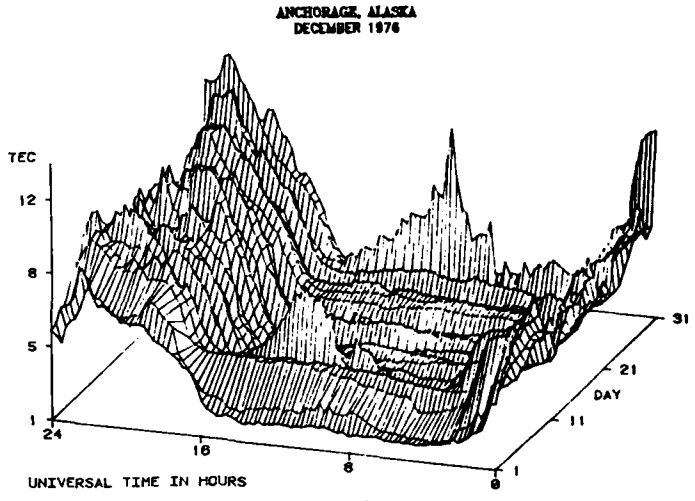


1(d)

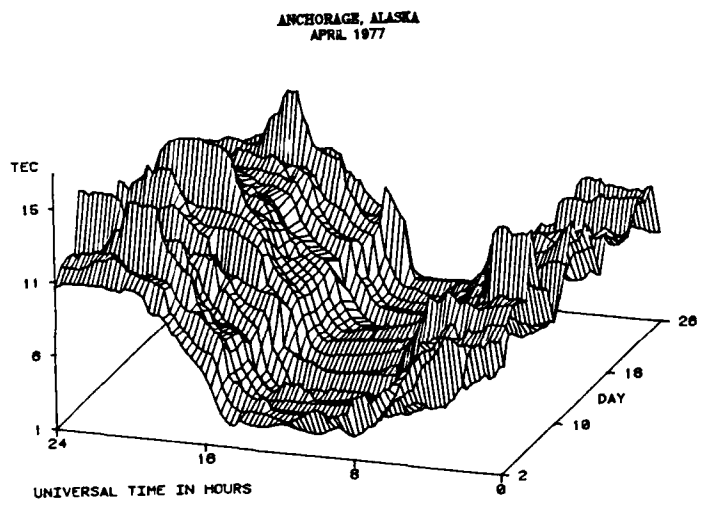
Figure 1



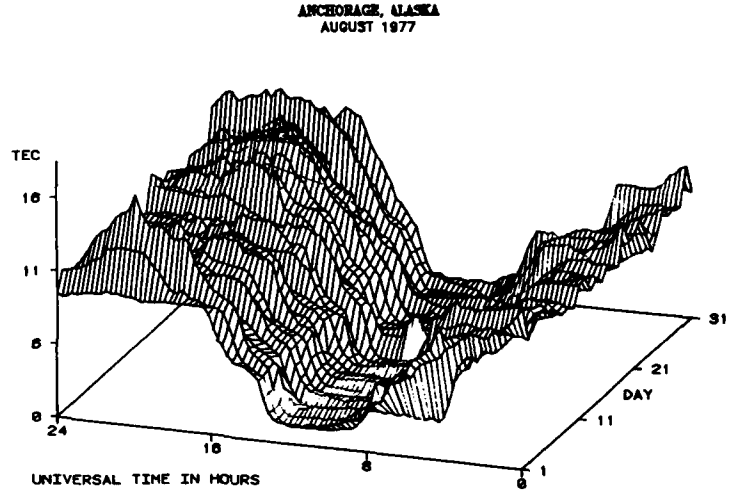
2(a)



2(b)

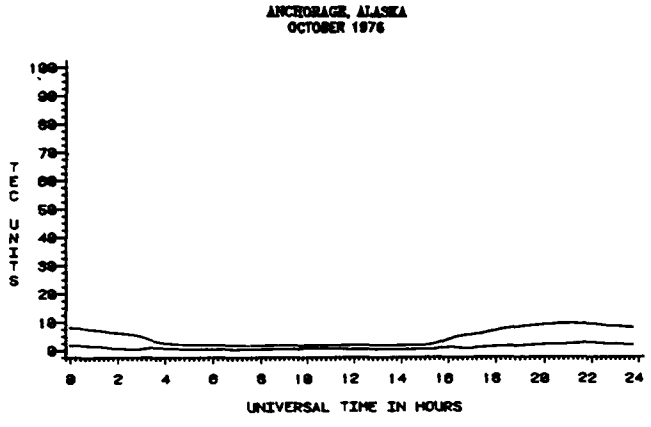


2(c)

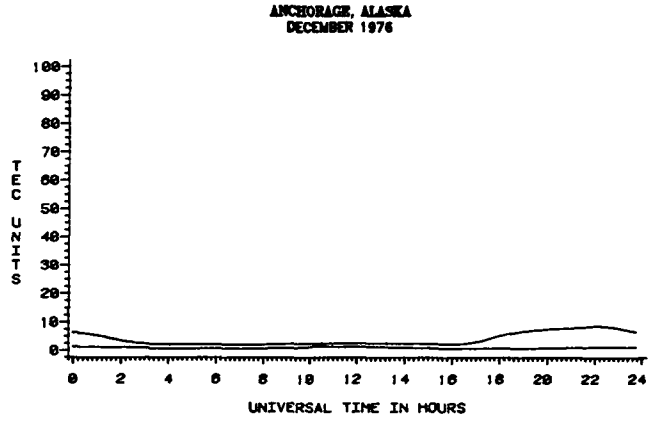


2(d)

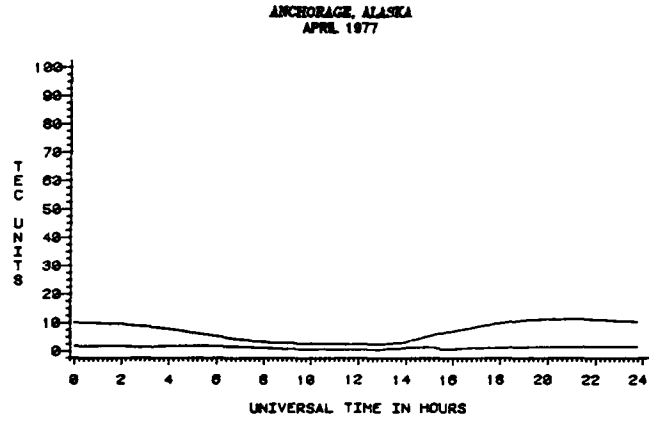
Figure 2



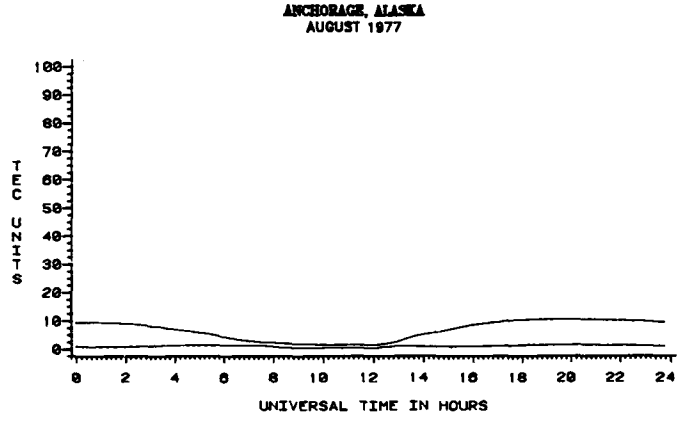
3(a)



3(b)

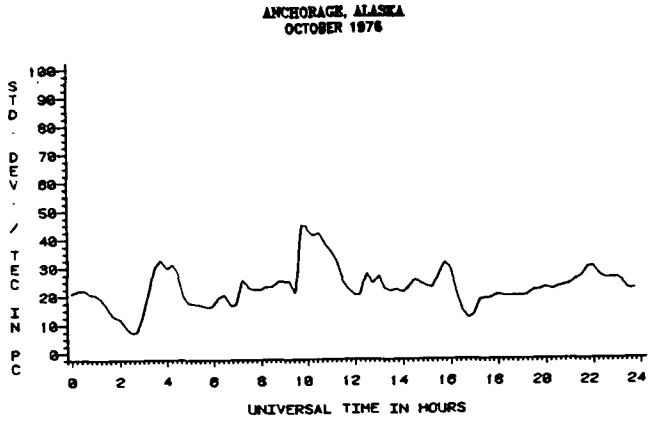


3(c)

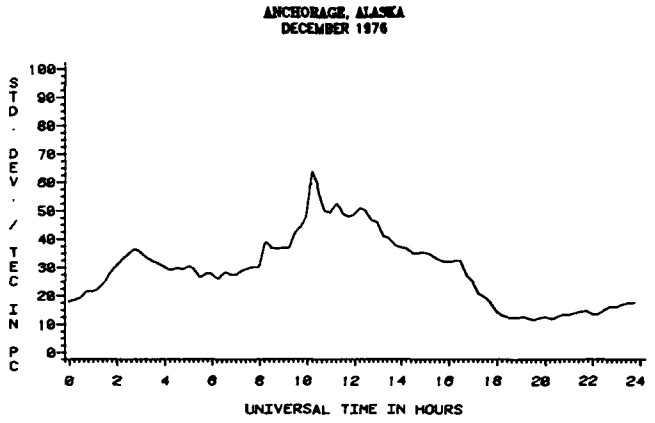


3(d)

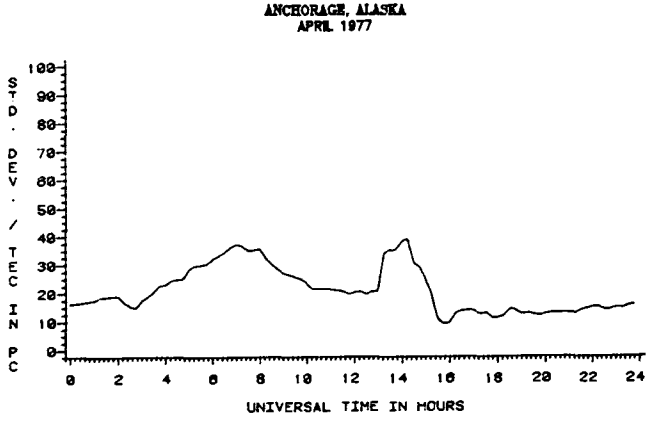
Figure 3



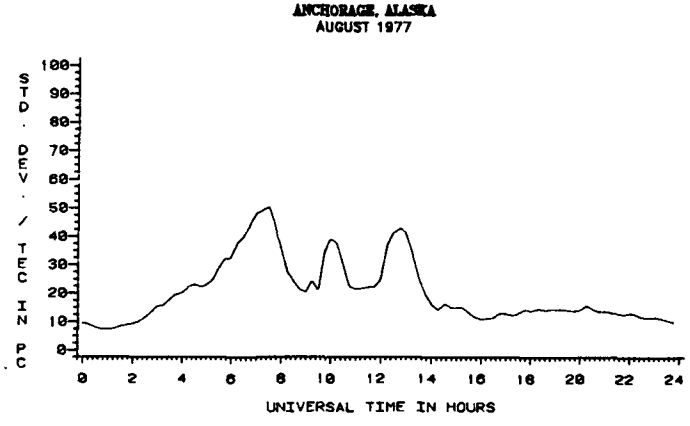
4(a)



4(b)



4(c)



4(d)

Figure 4

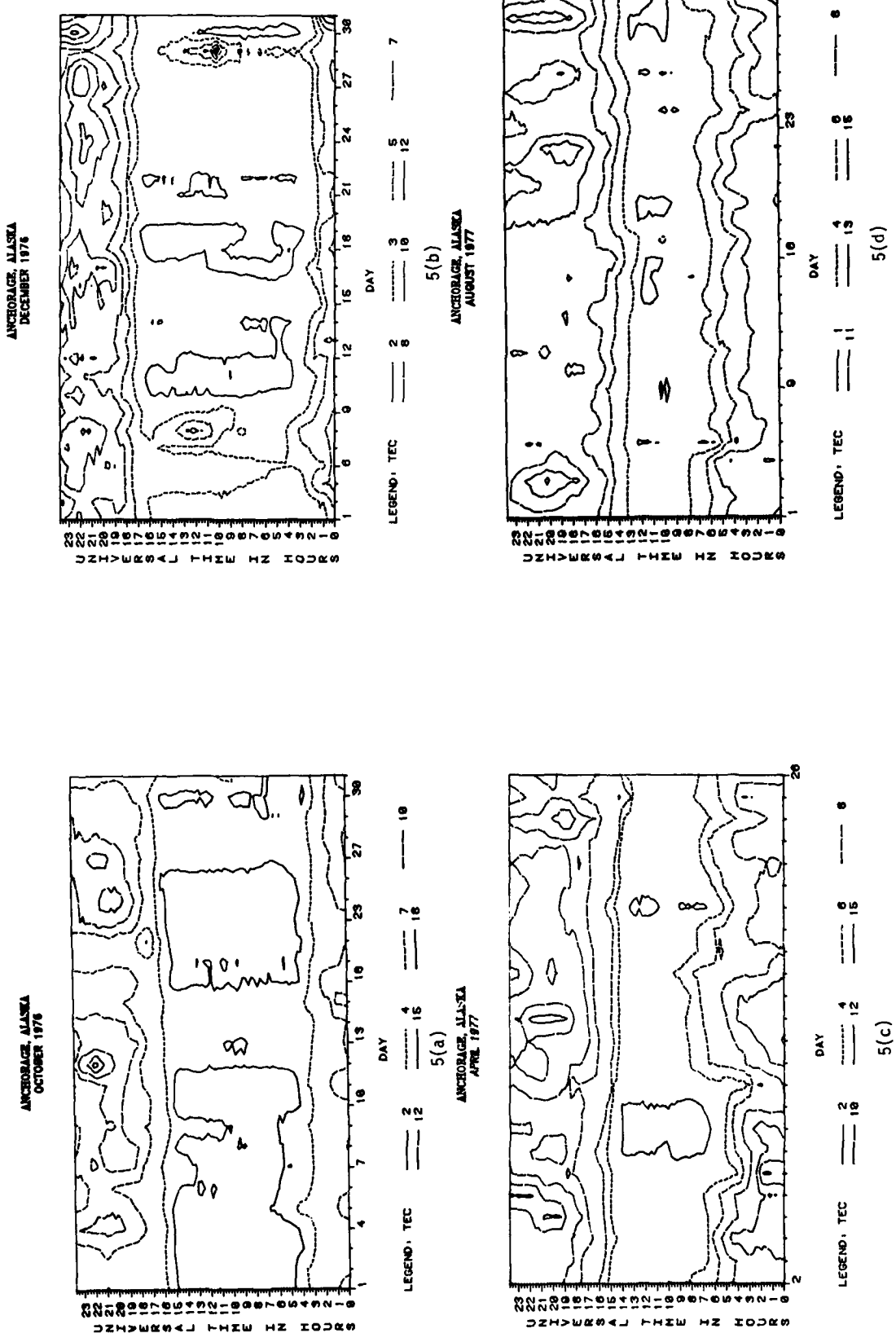

ANCHORAGE, ALASKA
OCTOBER 1976
LEGEND, TEC
2
12
4
16
7
18
10
DAY
5(a)
ANCHORAGE, ALASKA
DECEMBER 1976
LEGEND, TEC
2
8
3
10
5
12
7
DAY
5(b)
ANCHORAGE, ALASKA
APRIL 1977
LEGEND, TEC
2
10
4
12
6
15
8
DAY
5(c)
ANCHORAGE, ALASKA
AUGUST 1977
LEGEND, TEC
1
11
4
13
6
15
8
DAY
5(d)

Figure 5

associated with magnetic activity.

CONCLUSIONS

The behavior of TEC at a high latitude location during a period near the minimum phase of the current solar cycle is presented. Seasonal and day-to-day variabilities are observed.

The seasonal variability is seen in the magnitude of the absolute values of TEC maximizing in the spring minimizing in the winter (possibly due to the mid-latitude trough) and being somewhere in between for the summer and autumn. Although absolute differences of [illegible] are small for the various seasons, these results are in contrast to midlatitude TEC behavior during similar periods. For all seasons the day-to-day behavior of TEC appears uniform during the buildup and decay phases of the diurnal variation, although for the fall period the former is more confined to the sunrise period. TEC enhancements/depressions during maximum/minimum phases of the diurnal variation are maintained for a few consecutive days during all seasons, but single day enhancements/depressions are often observed. TEC enhancements during the nighttime periods in winter may be associated with positive response to sudden commencement. Similarly, TEC depressions on following nights in winter may be associated with storm behavior of TEC. No daytime TEC response, either positive or negative has been observed. During the other months magnetic activity was rather subdued. However, no single day enhancement/depression of TEC appears correlated with magnetic activity.

The ratio of standard deviation to average TEC is a good indicator for day-to-day variability. For the winter and summer periods the ratio, during the day, is normally $\lesssim 25\%$. The nighttime ratio is significantly higher, and it often undulates with variable periods. Since day-to-day variability is a most difficult quantity to predict, the results, which describe day-to-day patterns of behavior, have important implications to prediction improvements.

ACKNOWLEDGEMENTS

The Faraday observations were performed under the guidance of Mr. F.J. Gorman, US Army, Center for Communications Systems, Fort Monmouth, NJ. The analysis of the raw data and basic computations were performed under the guidance of Mr. W. Chaffee, Monmouth College, West Long Branch, New Jersey.

REFERENCES

Hicks, P.A., A low cost, all electronic Faraday rotation polarimeter, paper presented at COSPAR Symposium on the Future Application of Satellite Beacon Measurement, Comm. on Space Research, Graz, Austria, 1972.

Klobuchar, J.A., Polarization of AZ-El mounted antenna viewing celestial objects, IEEE Trans. on Antennas and Propagation, AP-14, 650, 1966.

Lee, M.C., A. DasGupta, J.A. Klobuchar, S. Basu, S. Basu, Depolarization of VHF geostationary satellite signals near the equatorial anomaly, Radio Science, 17, 399-404, 1982.

Soicher, H., Ionospheric and plasmaspheric effects in satellite navigation systems, IEEE Trans. on Antennas and Propagation, AP-25, 5, 705-708, 1977.

Soicher, H., and F.J. Gorman, Variability of total electron content at temperate and high latitudes, proceedings of the COSPAR/URSI Symposium on "Scientific and Engineering uses of Satellite Radio Beacons", Warsaw, Poland, May 19-23, pp 91-98, 1980.

Soicher, H., Z. Houminer, and A. Shuval, Total electron content structure in the Middle East, Radio Science, 17, No. 6, 1623-1631, 1982.

Soicher, H., J.A. Klobuchar, P.H. Doherty, Spatial variability of total electron content in the eastern Mediterranean region, Radio Science, 19, 3, 764, 1984.

Soicher, H., F.J. Gorman, Seasonal and day-to-day variability of total electron content at midlatitudes near solar maximum, Radio Science (in the press) 1985.

FIGURES

1. Superposed diurnal variations of total electron content (TEC) in Anchorage, Alaska for a. October 1976; b. December 1976; c. April 1977; d. August 1977. Ordinate: 1 TEC unit - 10^{16} el m^{-2}; Abscissa: time in UT.

2. Diurnal variation of total electron content (TEC) in Anchorage, Alaska as a function of day of month for: a. October 1976, b. December 1976, c. April 1977, d. August 1977.

3. Monthly average variation of total electron content (TEC) - upper curves, and the

standard deviation of TEC about the monthly average - lower curves, in Anchorage, Alaska for: a. October 1976; b. December 1976; c. April 1977; d. August 1977.

4. The diurnal variation of the ratio (in percent) of the monthly standard deviation of TEC to the average TEC in Anchorage, Alaska for: a. October 1976; b. December 1976; c. April 1977; d. August 1977.

5. Iso-TEC contours as a function of day of month and time in UT at Anchorage, Alaska for October 1976.

6. Same as Figure 5 but for December 1976.

7. Same as Figure 5 but for April 1977.

8. Same as Figure 5 but for August 1977.

F LAYER IRREGULARITIES AT PLASMAPAUSE AND AURORAL LATITUDES

by
Jules Aarons
Department of Astronomy
Boston University
Boston, MA 02215

SUMMARY

Distinctive effects of two irregularity regions, one at plasmapause latitudes and the second in the auroral region, were explored using primarily radio scintillation data. Using scintillation measurements at times numbering seven to nine sensors within a relatively confined area, it is possible to document the morphology of development of irregularities in the plasmapause and in the auroral region over a period of time, a technique difficult with only low altitude satellite scintillation observations. Two cases of "irregularity storms" one in the plasmapause and the second in the auroral oval are reported.

Over several years, various observers have recorded irregularities in the F layer at latitudes which were identified as the plasmapause region. During the stable auroral red arc of March 5/6, 1981, intense irregularities were centered at plasmapause latitudes but levels tapered off in the same longitude sector at auroral latitudes. Reported SAR measurements indicated no visible aurora until areas 4 L shells polewards. Low energy ($\sim$ 8ev) electron precipitation has been reported within the region covered by the SAR arcs. Higher temperatures have also been reported within the SAR arc, perhaps indicating a need to invoke the temperature gradient drift instability as the source for the generation of irregularities. Scintillation of moderate level is not uncommon for the plasmapause region. In March 1981 approximately 60% of the nights had scintillation levels > 6 dB at 137 MHz lasting over one hour.

At auroral latitudes on some nights patches of irregularities several hundred kilometers in longitude will be relatively fixed over several hours. During one magnetic storm scintillation activity maximized along a relatively fixed longitude. For some magnetic storms and sub-storms it is likely that once an irregularity patch is formed, convection patterns may limit it to a narrow longitudinal region.

INTRODUCTION

Using available data from several sources a model of F layer irregularity intensity as shown by scintillation observations was proposed by Aarons (1982) and is illustrated in Figure 1. Two features will be discussed, one in the plasmapause region and the second in the auroral area.

In situ, spread F, and scintillation observations have identified irregularities in the plasmapause region, equatorwards of the trough, with a moderate level of activity. These irregularities have a morphology differing from auroral irregularities. There are periods when high levels of scintillation activity are noted with low levels of magnetic activity (Bramley, 1974). The trough in this picture of midnight scintillation intensity is a region of relatively low scintillation activity while the auroral oval is a region very sensitive to magnetic activity (Aarons and Allen, 1971, Rino and Matthews, 1980) with irregularities spreading equatorwards with increasing magnetic excursions. The auroral oval shows high levels of activity during years of low and high solar activity but is subject to solar flux variations.

The concept of this study is to discuss two aspects of scintillation activity:

(1) Irregularities at plasmapause latitudes. This includes correlation of scintillation with stable auroral red arcs as well as scintillation activity at these latitudes without observable SAR arcs.

(2) Auroral latitude scintillation activity confined at times to a longitudinal sector.

At Goose Bay, Labrador, Hanscom Air Force Base, Mass., and Sagamore Hill, Mass there is an ongoing program by the Air Force Geophysics Laboratory and the Air Weather Service of routinely measuring scintillation and total electron content using available beacon satellites. The satellite transmissions of ATS-5 used in this paper measure total electron content studies by means of Faraday rotation and scintillation. In addition from Goose Bay and Hanscom AFB, observations are made of a beacon satellite transmitting at 250 MHz. The observations are made to the Northeast and Northwest of each station. Angles of elevation are high in the data utilized. Additional measurements include observations at 250 MHz of two FLTSAT satellites from both Hanscom AFB and Goose Bay (each station observing a different FLTSAT satellite) and of MARISAT from Goose Bay. The path intersections with the ionosphere at 350 km are shown in Figure 2. It should be noted that Corrected Geomagnetic Latitude ionospheric intersections of synchronous satellites such as MARISAT and FLTSAT differ considerably in observations from Goose Bay.

A. STABLE AURORAL RED ARCS

Stable auroral red arcs (SAR arcs) occurring in "middle latitudes" have been associated with F layer irregularities by utilizing several measurement techniques. Basu (1974) established that during the post-main phase of several magnetic storms scintillation activity was observed during the appearance of SAR arcs. Without referring to SAR arcs. Clark and Raitt (1976) found with the total ion current probe on ESRO-4 , irregularities extending to almost 40° geomagnetic latitude in a distinct sub-auroral feature peaking near 55° geomagnetic latitude and separated from the high latitude zone. Rodger (1984) found in a study of conjugate ionograms two distinct regions where considerable spread F was observed. One was the region where SAR arcs occur and the second begins at the poleward edge of the mid-latitude trough. His data set consisted of conjugate point measurements of F layer irregularities for an SAR arc reported for October 20-21, 1981 with the signature then extended to other data. Basu (1978) reporting primarily on OGO-6 data, established the existance of small scale irregularities in the region L=2-4; these were observed during moderate geomagnetic activity as well as during very quiet periods.

The use of the DE satellites using multi-energy sensors as well as optical observations has lead to the identification of the low energy electrons of 8 ev as the source for the production of heated SAR arcs rather than either higher energy electrons or ions (Gurgiolo et al., 1982).

We shall attempt to map irregularity levels as recorded by scintillation observations over a region for a dramatic SAR arc i.e. that of March 5-6, 1981. The data of Watanabe and Kim (1982) indicated the arc was unique in that (1) the arc was the most intense observed during the past twelve years at Albany, N.Y. and (2) a visible aurora was not sighted during the observation period. The arc occurred in the aftermath of the magnetic storm of March 4-5. Slater and Kleckner (1981) also recorded the arc with maximum emission at L=2.8. They found the SAR arc with an extremely pronounced separation from the aurora of 4 L shells. The SAR arc extent, as mapped by Slater and Kleckner (1981) is noted in Figure 2.

Magnetograms from the AFGL magnetometer network (D. Knecht, private communication, 1984) are shown in Figure 3 with the magnetic storm clearly observed on the night of March 4-5 and the relatively quiet period following on the night of March 5-6.

The scintillation data used on in this paper differs from that of Basu (1974) in that a large series of ground observations are available intersecting latitudes ranging from 52° CGL to 71° CGL thus encompassing the auroral oval as well as the plasmapause latitudes.

B. MARCH 5-6, 1981 SAR ARC AND RECOVERY PHASE OF MAGNETIC STORM

1. Lower Latitude Observations

Figure 4 contains plots of the optical and radio observations of the night of March 5-6. The 6300 A data was taken from Figure 1 of Watanabe and Kim (1982). The 137 MHz recordings shown in Figure 4 show saturation of fading (and therefore a flat top) but with maximum activity during the peak intensity of the SAR arc; the 250 MHz scintillations from FLTSAT records peak at about the same time as the optical amplitudes. All three parameters shown in Figure 4 maximize during the period 0200-0515 UT. A subsequent decrease is clearly shown in the FLTSAT data. Irregularity intensity and 6300 A emission are correlated in this region.

2. High Latitude Observations

The observations from Goose Bay are plotted in Figure 5; they indicate higher levels of activity before the detection of the SAR arc. From the beacon satellite records taken at Goose Bay, observing at times to the northeast (66° CGL) and at other times to the northwest (69° CGL), it is seen in Figure 5 that peak scintillation activity occurred earlier in the region of these geomagnetic latitudes and had essentially been considerably reduced by 0300 UT, the peak of the SAR arc optical intensity. However the scintillations while reduced were still observable on the 250 MHz records; the 137 MHz records of an intersection of 62° showed moderate to high levels. The indications from the high latitude data set are that irregularities were extant in the auroral region, although at a reduced level from recordings taken during magnetic storms.

We shall not discuss Goose Bay Faraday rotation records of ATS-5 (supplied by J.A. Klobuchar) except to note there are total electron content variations with periods of several minutes which are observed at high latitudes during magnetic disturbances but which were absent during the magnetically quiet period of the SAR arc event.

C. MAGNETIC ACTIVITY AND SCINTILLATIONS OF ATS-5 AT 53° CGL AND 61° CGL IN MARCH 1981

Indications are that plasmapause irregularity generation at L values of 2.8 are frequent during this year of high solar flux. As the DE data indicated (Gurgiolo et al., 1982) the low energy particle flux events similar to those which take place during SAR arcs are not unique. Neither are the strong scintillation events at the latitude of 53° CGL. In order to determine the occurrence pattern of scintillation activity, the Sagamore Hill data set of ATS-5 of March, 1981 was examined. During this month 60% of the nights showed strong scintillation (> 6 dB) at 137 MHz lasting one hour or longer.

In a comparison with the observations of J.S. Kim (personal communication) at the State University of New York at Albany it was found that on three nights in March, 1981 with good seeing there were high scintillation levels with no SAR arc or visible auroral present. High scintillation levels on these nights lasted from three to five hours.

D. MAPPING STUDIES: ACTIVITY DURING THE PERIOD OCTOBER 14-16, 1980

Using a multiplicity of sensors it is possible to plot the extent and level of scintillation activity over a relatively large area (the coverage shown in Figure 2). Putting together scintillation intensities at 250 MHz and suitably reducing the 137 MHz dB excursions according to previous studies (Whitney et al., 1972) allows the plotting of scintillation activity over the region contiguous to the path intersections of Goose Bay, Hanscom AFB, and Sagamore Hill with the satellites. Over a relatively short period of time in October 1980 several patterns of scintillation activity over the auroral and subauroral regions were exhibited. We illustrate intense activity primarily centered along a longitudinal corridor. In addition the reaction of irregularities to a moderate magnetic storm (on October 14-15) could be clearly noted. K indices are indicated in Figure 6.

1. The Night of October 13-14, 1980: Magnetically Quiet Period

The night of October 13-14 was magnetically quiet. At high auroral latitudes there was the usual scintillation activity which takes place even under quiet magnetic conditions. A photograph of Goose Bay records is shown in Figure 7 with the beacon satellite activity high in the northwest (at 69° CGL) and low in the northeast (66° CGL). MARISAT scintillations were moderate (~ 10 dB), middle trace, and the bottom trace (FLTSAT records) showed less than 1 dB of scintillation. The levels of activity are typical of magnetically quiet nights.

For the entire period we have graphed 15 minute scintillation indices (Figure 8) for the Goose Bay data. For the 00-06 UT time period on October 14, FLTSAT indices were low. MARISAT scintillations were high until 0330 UT. Scintillation levels of FLTSAT and MARISAT similar to those of Figure 7 essentially continued through the night.

Similar sets of data were obtained from observations in the Boston area and are used to plot the next series of diagrams.

2. The Night of October 14-15: Magnetic Storm

In contrast to the data for October 13-14, on the next night, October 14-15, with a moderate magnetic storm in progress, FLTSAT scintillations were high while those from MARISAT were low (Figure 10) even before the magnetic storm. The beacon satellite scintillations were high again in this time period near local midnight.

The Hanscom FLTSAT observations showed relatively high activity from 04-08 UT, October 15, indicating activity along this longitudinal sector. (It should be noted that Goose Bay and Hanscom view different FLTSAT satellites both at approximately the same frequency.)

Local Kp of 2 was noted at Goose Bay until the 0300-0600 UT time period, indicating the storm did not reach its maximum activity until after 0300. The local K index was 4 for the next 6 hours. From the point of view of scintillation activity the storm built up gradually and was in its initial phase at 0500 UT on October 15 in the Goose Bay, Labrador area. It is possible to graph scintillation activity before the moderate magnetic storm as well as after. In order to determine instantaneous intensities over a large area we have plotted with varying degrees of shading, the scintillation levels through individual paths from the observing sites.

During limited time periods it is possible to utilize the maximum number of sensors (in this case 9) and to obtain scintillations over the area shown in the maps. It was possible to do so for the time period around 2400 UT within plus or minus one hour. Figure 10 utilizes extrapolation and interpolation of data to obtain a real time map. The data are consistent and show an intensification within a longitudinal sector beginning at 2400 UT and (as will be shown) intensifying later in the night.

The contours of equal irregularity intensity for this night are dramatically skewed towards greater activity in the western portion of the area probed. At 2400 UT the local standard time for Goose Bay was 2000 and for Hanscom 1900. The intense scintillation activity took place in the N-S corridor encompassing Hanscom. This remained through the night as will be shown in later figures.

As the magnetic storm progressed higher levels of scintillation activity could be noted (Figure 11a, 0200 UT, Figure 11b, 0400 UT, and Figure 11c, 0600 UT). Even this moderate magnetic storm showed high levels of scintillation activity.

The pattern for the night of October 14-15 is for scintillation activity to appear in the auroral oval but with an intensive "finger" along a narrow longitude range, in this case encompassing the MARISAT and beacon satellite paths.

3. The Night of October 15-16, 1980: Recovery Phase

The next night, October 15-16, was magnetically quiet with a Goose Bay K index of 2 for the time period studied. Figure 12, a contour map, was developed for 2400 UT. Equal scintillation values are lower than those noted in Figure 11 and contours fall along lines of corrected geomagnetic latitude.

DISCUSSION

1. Plasmapause Latitudes

The data indicate that (1) During the post recovery period, the plasmapause associated SAR arc was accompanied by F layer irregularities at these latitudes with little association with higher latitude irregularities. (2) During other days when SAR arcs are not observed irregularities are noted at plasmapause latitudes; electron precipitation may have existed at the plasmapause latitudes but not of the level to produce SAR arcs.

In a series of papers on observations with the Chatanika radar (such as Muldrew and Vickrey, 1982) it has been found that boundary blobs or regions of increased electron density from 200 km to 600 km in altitude are the source of some irregularities in the auroral region. The blobs as observed from Chatanika, Alaska are in the CGL range from $61° - 71°$. However the latitudes at which irregularities are noted in this series of observations are of the order of $52° - 57°$ CGL. The boundary blobs appear therefore to be associated with the auroral oval and not with plasmapause electron density variations.

The question arises to how the plasmapause irregularities fit into the total picture of F layer irregularities. From Gurgiolo et al. (1982) it is clear that during SAR arcs and during times when SAR arcs were not visible to either ground or satellite observations, 8 ev precipitation regions were noted at plasmapause latitudes.

During SAR arcs, temperature enhancement has been noted (Watanable and Kim,1984). The indications are that the precipitation of low energy electrons leads to temperature enhancements which develop instability processes that in turn produce the irregularities. Watanabe and Kim (1984) show the enhancement of temperatures of the order of $100 - 200°$ K for intense SAR arcs, temperature enhancements which were maintained even when the intensity of the arc decreased. This indicated that the time constant for energy loss is large. Various mechanisms have been suggested. Gradient drift instability can be operative (Hudson and Kelley, 1976). In enhancements of electron gas temperatures of a few hundred degrees Kelvin by high power high frequency transmissions, artificially created field aligned irregularities have been created in the F layer; other instability mechanisms have been invoked (Perkins, 1974). Temperature enhancements which would produce instabilities are also addressed by Lee (1984).

During periods when SAR arcs are not visible, irregularities appear at plasmapause latitudes; it is not clear at this time if temperature enhancements or precipitation is observed during these times although Basu (1978) found that the irregularities recorded by the OGO-6 instruments were not associated with appreciable temperature enhancements.

2. Auroral Oval Scintillations

The irregularity intensity at auroral latitudes increases dramatically during magnetic activity as has been shown by Aarons and Allen (1971) and Rino and Matthews (1980). The magnetic storm irregularities were produced in all likelihood by precipitation as has been shown by Basu et al. (1983). The magnetic storm effects spread equatorwards from the auroral oval as shown by Aarons (1976).

As pointed out by Kelley and Vickrey (1982) the observed irregularities are the result of precipitation and instability processes. However their extended lifetimes mean that long lived regions are convected as has been shown by Weber et al. (1984). In the case of the October 14-15, 1980 magnetic storm the convection appears to be confined to a particular longitude region and therefore to a poleward or equatorward convection. The hypothesis is that in some magnetic storms the convection carries the long lived irregularity patches equatorwards or polewards producing the confined longitudinal region. Many phenomena such as plasma injection during moderate geomagnetic activity (Arnoldy and Moore, 1983) show relatively narrow longitudinal spread. This coupled with convection patterns for the irregularities may explain the confinement of the activity.

REFERENCES

Aarons, J. and R. S. Allen (1971) Scintillation boundary during quiet and disturbed magnetic conditions, J. Geophys. Res. 76, 170-177

Aarons, J. (1976) High latitude irregularities during the magnetic storm of October 31-November 1, 1972, J. Geophys. Res., 81, 4725-4728

Aarons, J.,(1982) Global morphology of ionospheric scintillations, Proc. IEEE 70, 360-378

Arnoldy, R.L. and T.E. Moore (1983) Longitudinal structure of sub- storm injections at synchronous orbit, J. Geophys. Res. 88, A8, 6213-6220

Basu, Sun. (1974) VHF ionospheric scintillations at L=2.8 and formation of stable auroral red arcs by magnetospheric heat conduction, J. Geophys. Res. 79, 3155-3160

Basu, Sun. (1978) OGO-6 observations of small scale irregularity structures associated with sub-trough density gradients J. Geophys. Res. 83, 182

Basu, Sun., E. MacKenzie, S. Basu, H.C. Carlson, D.A. Hardy, F.J. Rich and R.C. Livingston (1983) Coordinated measurements of low energy electron precipitation and scintillations/TEC in the auroral oval, Radio Sci., 18, 1151

Bramley, E.N., (1974) Fluctuations in direction and amplitude of 136 MHz signals from a geostationery satellite, J. Atmos. Terr. Phys. 36, 1503-1513

Clark, D.H., and W.J. Raitt (1976), The global morphology of irregularities in the topside ionosphere, as measured by the total ion current probe on ESRO-4, J. Planet. Sp. Sci. 24, 873-881

Gurgiolo, D., D.W. Slater, J. D. Winningham, J. L. Burch (1982) Observation of a heated elctron population associated with the 6300 A SAR Arc emission Geo. Res. Let. 9, 965-968

Hudson, M.K. and M.C. Kelley (1976) The temperature gradient drift instability at the equatorward edge of the ionospheric plasma trough J. Geophys. Res. 81, 3913

Kelley, M.C., J.F. Vickrey, C.W. Carlson, and R. Torbert (1982) On the origin and spatial extent of high-latitude F region irregularities J. Geophys. Res., 87, 4469-4475

Lee, M.C. (1984) Ohmic dissipation of Pedersen current as the cause of high-latitude F region ionospheric irregularities J. Geophys. Res. 89, 7482-7486

Muldrew, D. B., and J.P. Vickrey (1982) High-latitude F region irregularities observed simultaneously with ISIS 1 and the Chatanika Radar, J. Geophys. Res. 87, 8263-8272

Perkins, F.W. (1974) A theoretical model for short-scale field-aligned plasma density striations Rad. Sc. 9, 1065-1070

Rino, C. L. and S.J. Matthews (1980) On the morphology of auroral zone radio wave scintillation, J. Geophys. Res. 85, 4139

Rodger, A.S. (1984) Spread-F ionospheric irregularities and their relationship to stable auroral red arcs at magnetic mid-latitudes, J. Atmos. and Terr. Phys. 46, 335-342

Slater, D.W. and E. W. Klockner (1981) An extraordinary SAR arc event EOS, 62, 530

Watanable, T. and J.S. Kim (1982) Photometric and interferometric observations of the SAR arc event of March 5/6, 1981, Geophys. Res. Lett.,9, 64-67

Watanabe T. and J.S. Kim (1984) Photometric and interferomatric observations of recent SAR arec events, J. Geomag. Geoelectr. 36, 1-10,

Weber, E.J., J. Buchau, J.G. Moore, J.R. Sharber, R.C. Livingston, J. D. Winningham, and B. W. Reinisch, (1984) F layer ionization patches in the polar cap, J. Geophys. Res. 89, 1683-1694

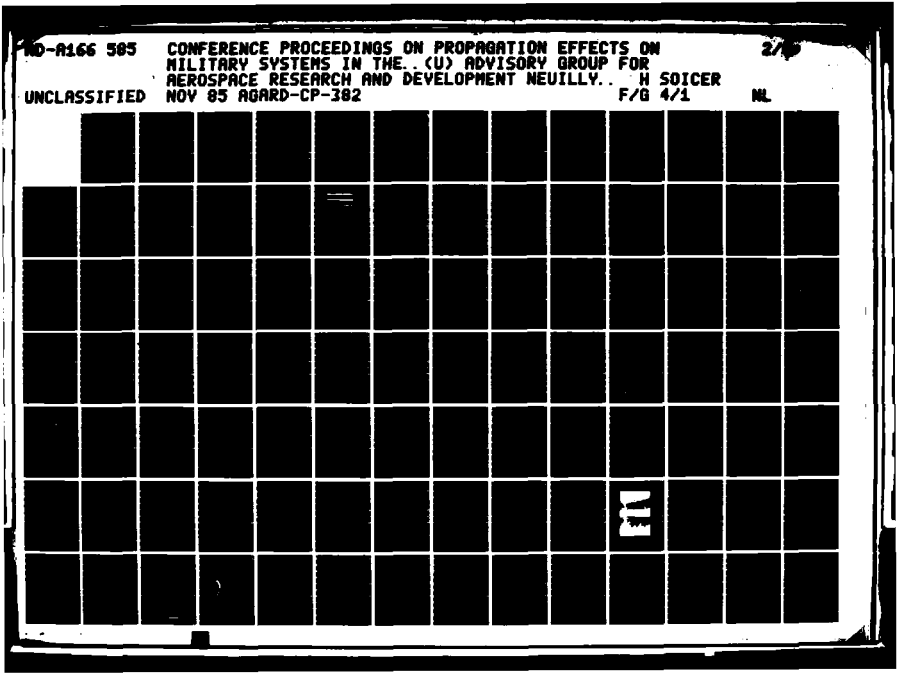
Whitney, H.E., J. Aarons, R.S. Allen and D. R. Seeman (1972) Estimation of the cumulativce amplitude probability distribution function of ionospheric scintillations, Radio Sci., 7, 1095-1104

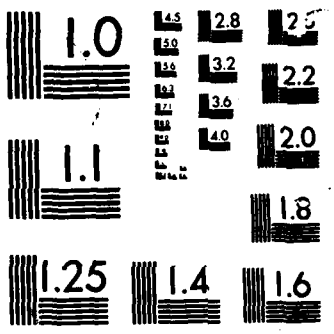
ACKNOWLEDGEMENTS

J.S. Kim of the State University of N.Y. at Albany was kind enough to supply me with the results of his SAR arc observations of March, 1981. J. A. Klobuchar and H. A. Whitney furnished me with the scintillation observations made by the Air Force Geophysics Laboratory and the Air Weather Service. This study was in part supported by the Air Force Geophysics Laboratory.

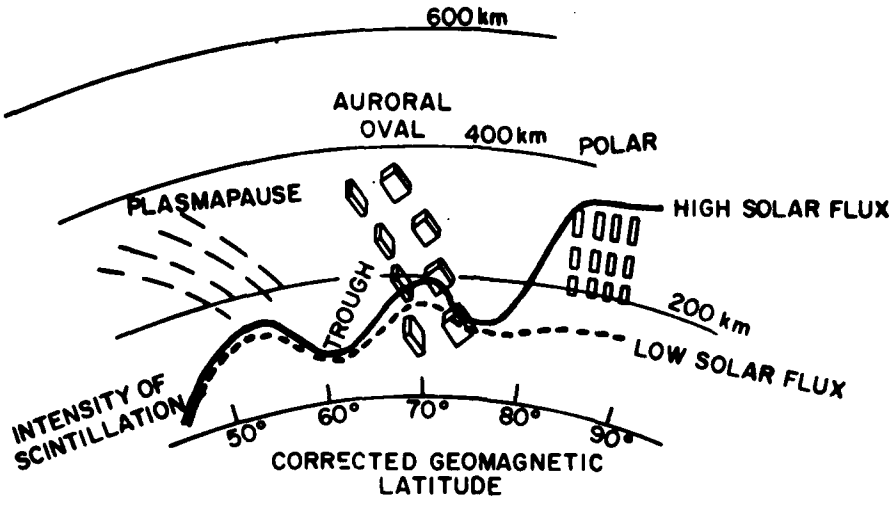
AD-A166 505 CONFERENCE PROCEEDINGS ON PROPAGATION EFFECTS ON MILITARY SYSTEMS IN THE..(U) ADVISORY GROUP FOR AEROSPACE RESEARCH AND DEVELOPMENT NEUILLY.. H SOICER

UNCLASSIFIED NOV 85 AGARD-CP-382 F/G 4/1 NL

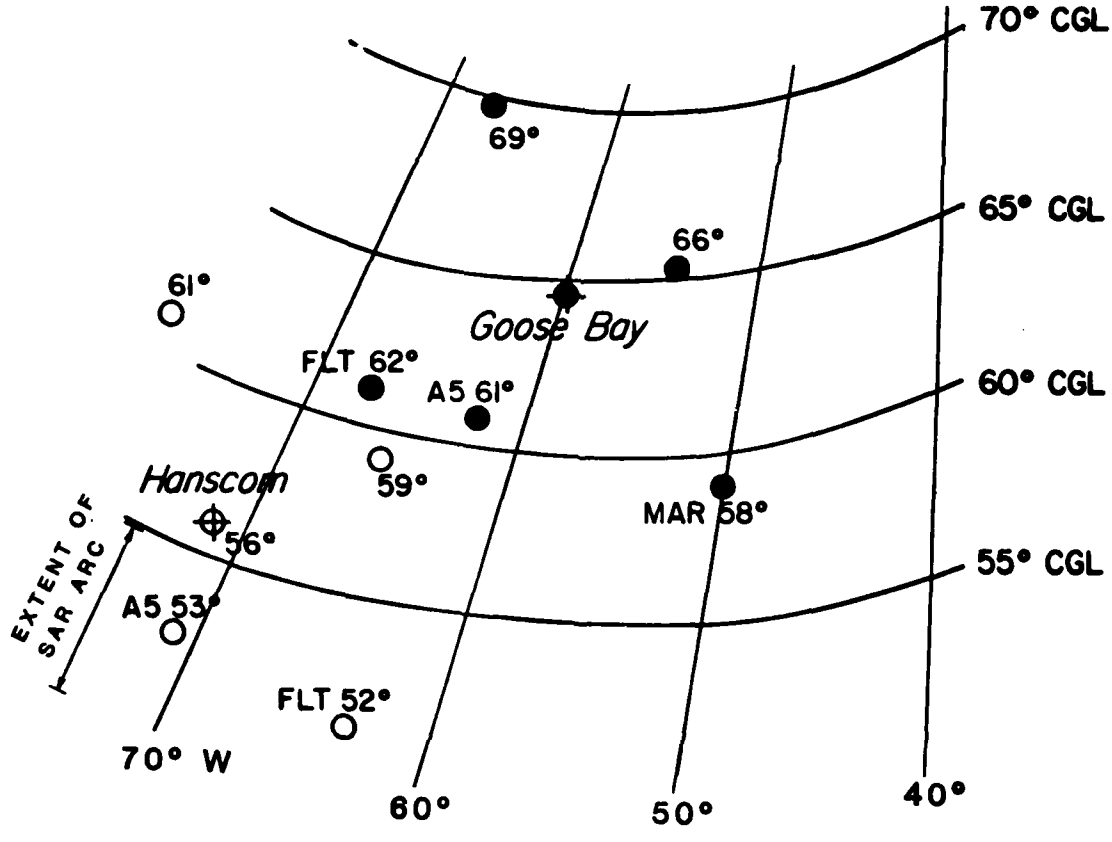




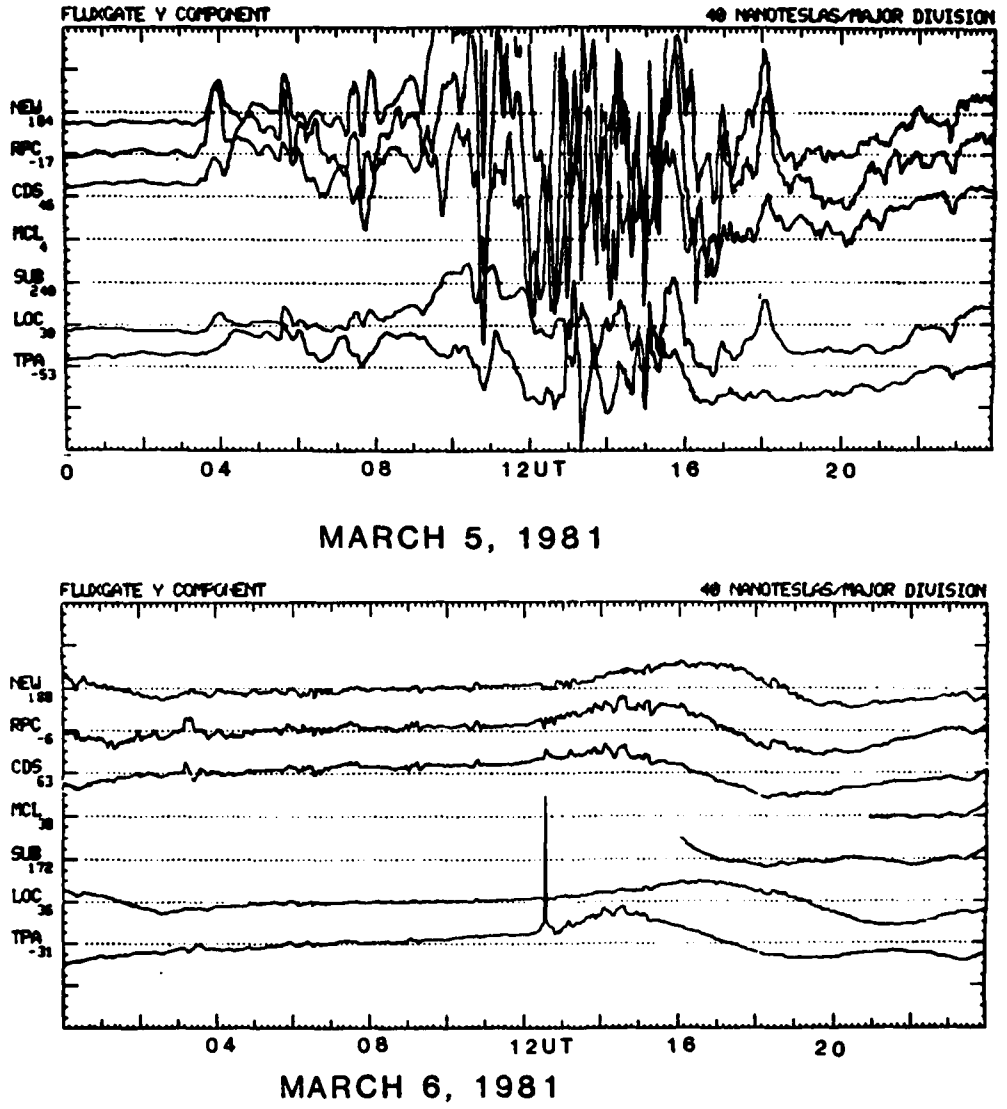
MICROCOPY CHART



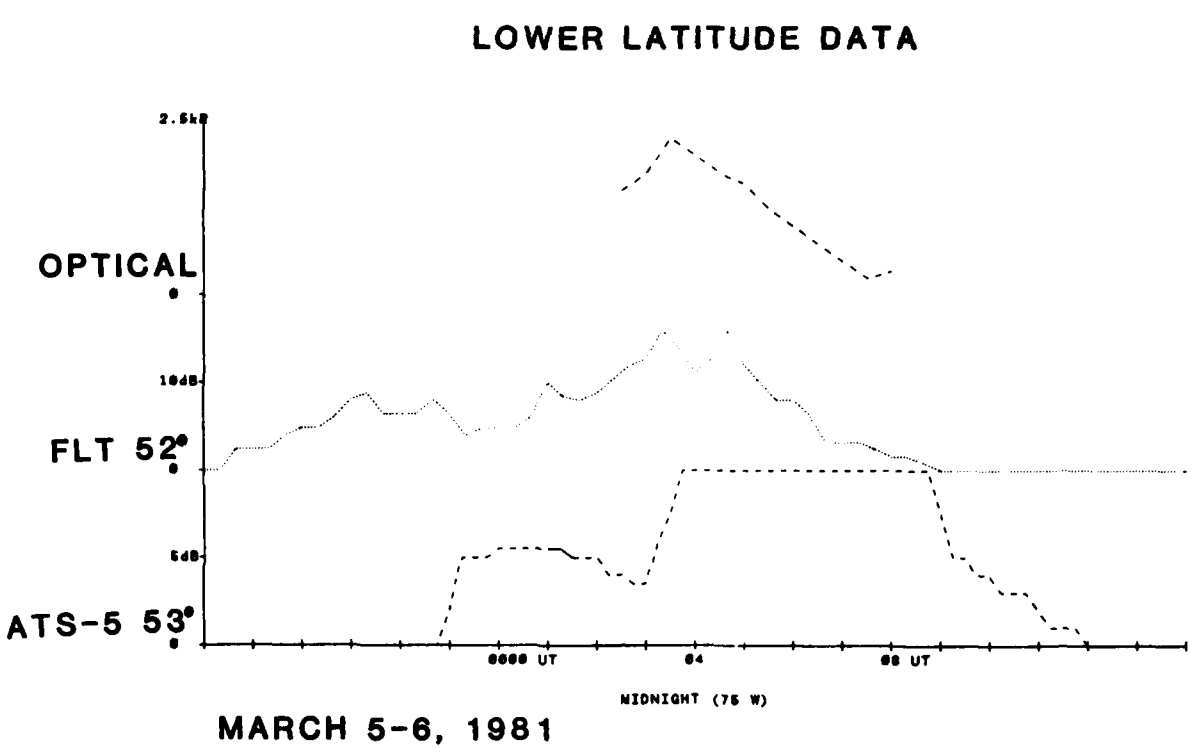
1. A model of scintillation activity proposed for the high latitudes by Aarons (1982). A moderate level of irregularity intensity is noted in the plasmapause region, a lower level in the trough and high levels for the auroral oval. The oval shows great sensitivity to local magnetic effects.



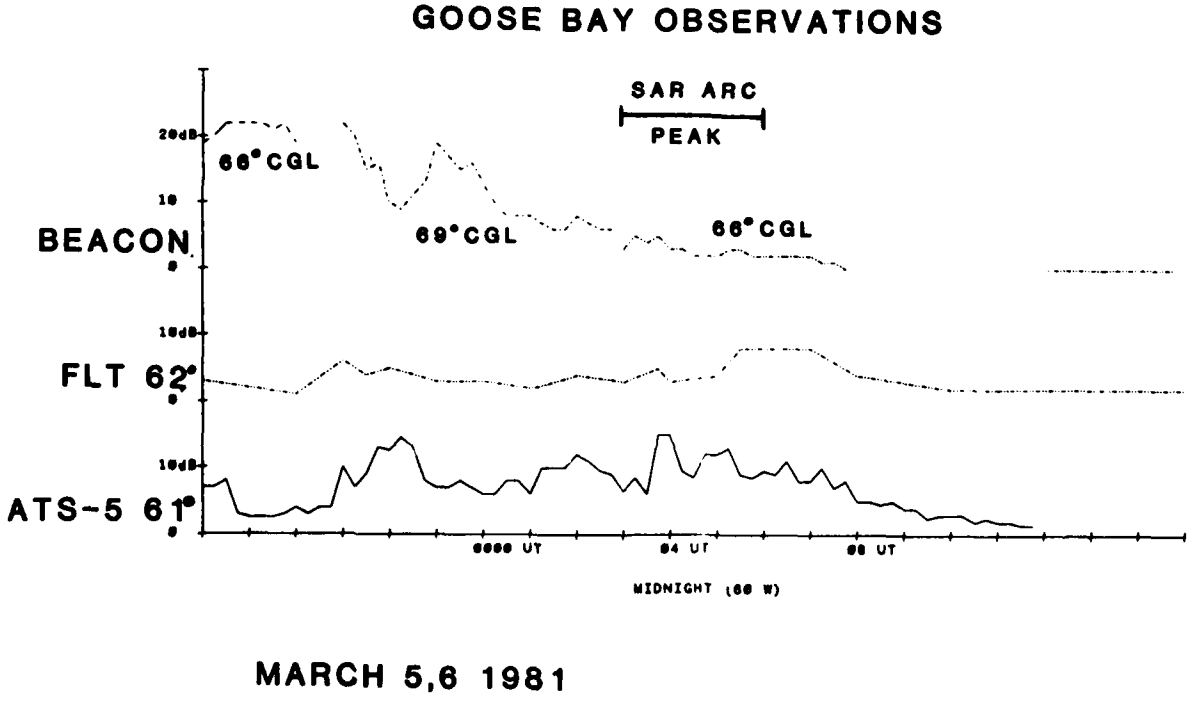
2. A map of sensors operating in the high latitude region near Goose Bay and the Boston area in the period of the study. The extent of the SAR arc of March 5/6, 1981 is also shown from the Slater and Klockner (1981) data. In all likelihood all the longitudes covered by the map were encompassed by the width of the SAR arc area illustrated.



3. Magnetometer records from the AFGL Magnetometer Network for March 5 and for March 6, 1981. (D. Knecht, personal communication, 1984)



4. Plots of low latitude scintillation index, data taken in the Boston area, bottom traces, and intensity of 6300 A (Watanabe and Kim, 1982).

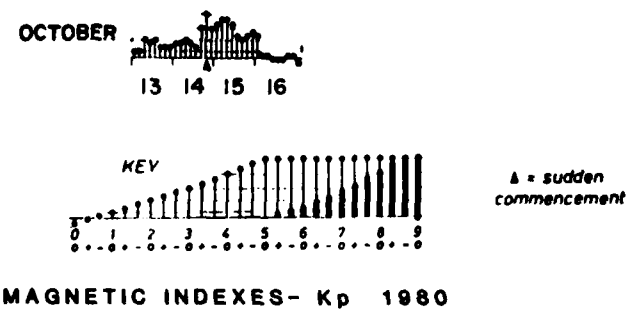


5. Plots of high latitude scintillation data

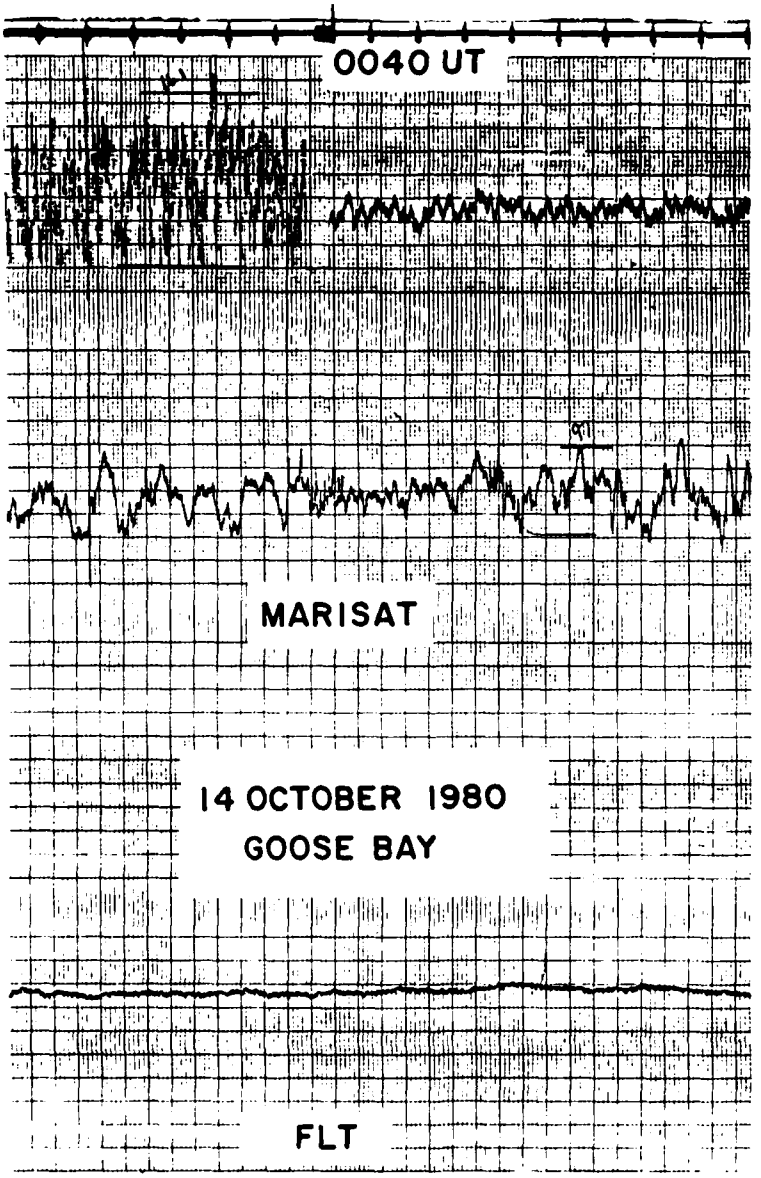
Top: Scintillation in dB of the beacon satellite transmissions at 250 MHz with intersections of 69° to the Northwest of Goose Bay and 66° to the Northeast.

Middle: Scintillation activity of FLTSAT as observed from Goose Bay.

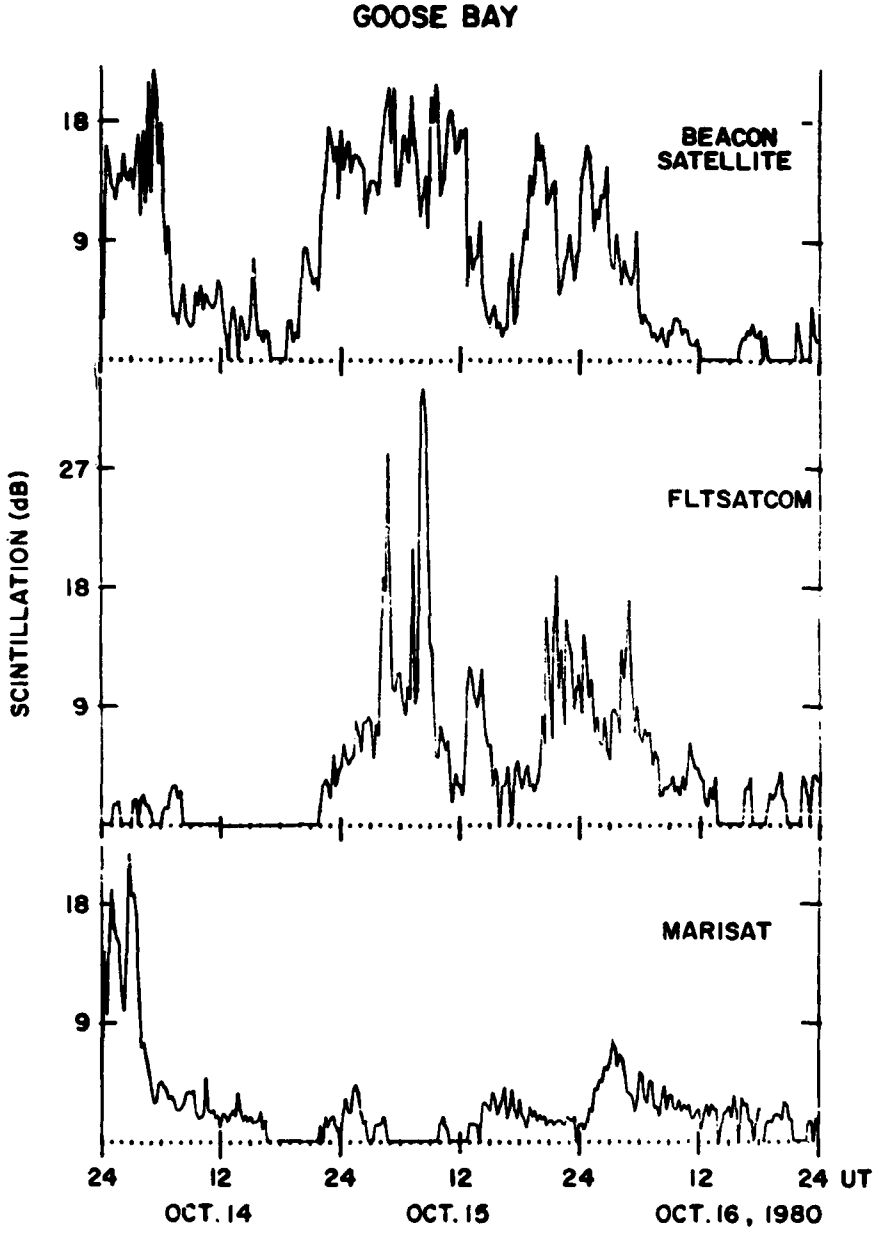
Bottom: Scintillation levels of ATS-5 at 137 MHz. Scintillations showed slow fading characteristics of magnetically quiet nights.



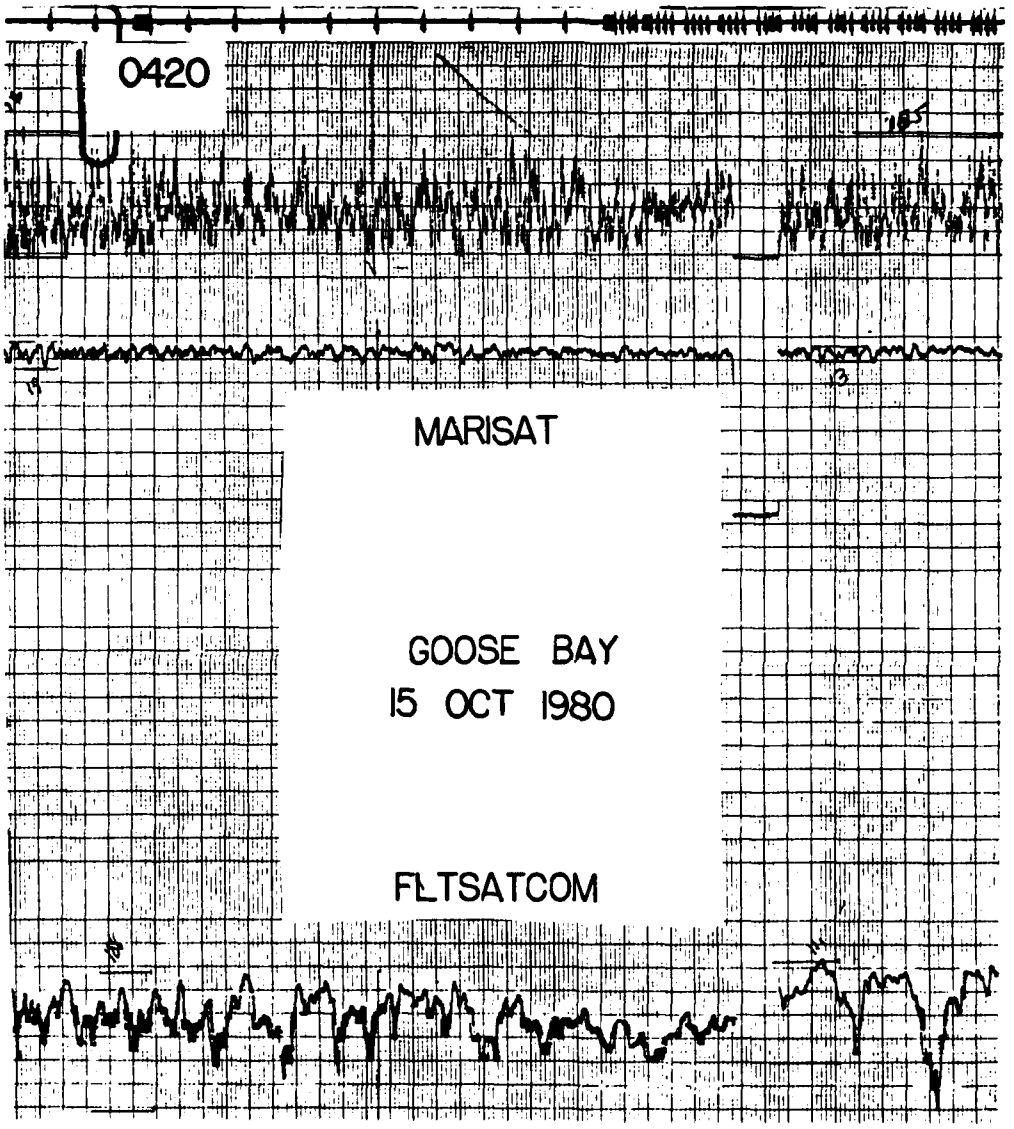
6. Magnetic indices for the October 1980 period analyzed encompassing, the moderate magnetic storm of October 14-15. Sudden commencement started at 2200 UT October 14.



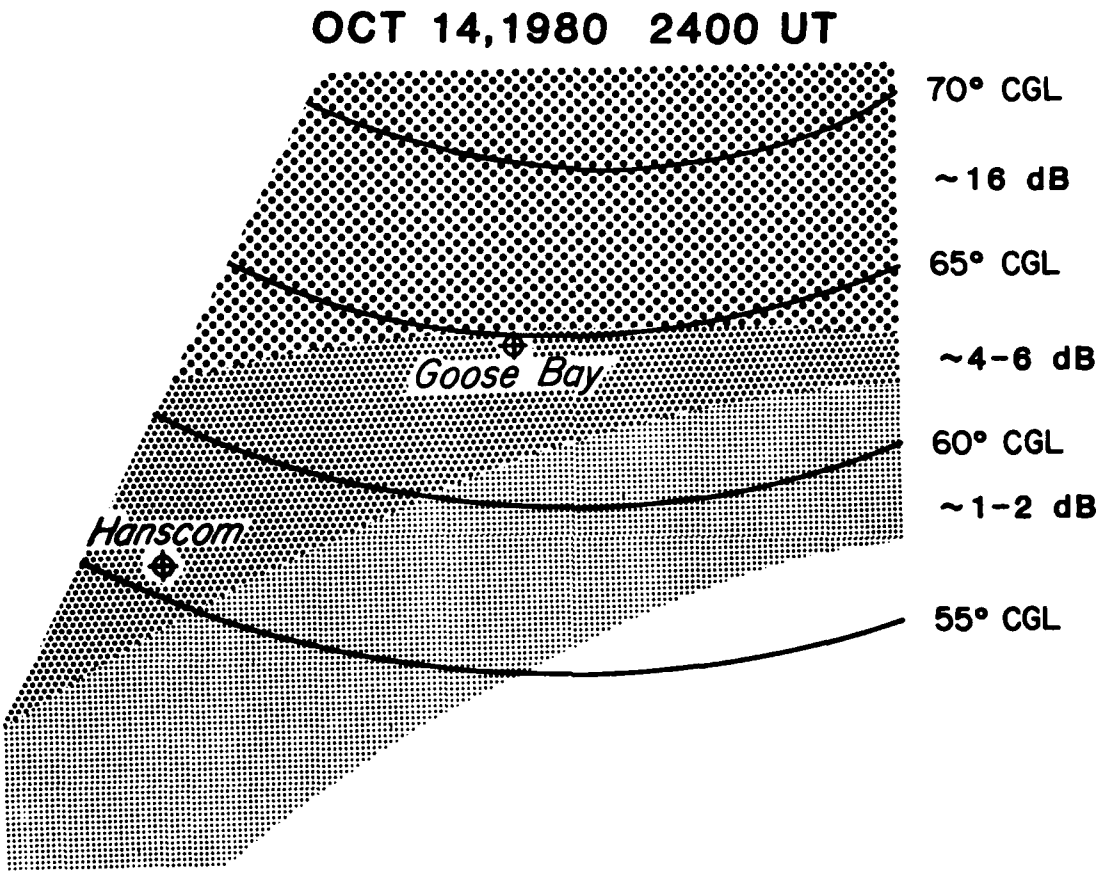
7. Goose Bay records for the time period near 2400 October 13-14. High levels are seen to the Northwest and low levels to the Northeast for the Beacon Satellite. MARISAT levels are high for the night; FLTSAT levels are low. Local Standard Time at Goose Bay is 2000.



8. 15 minute indices in dB are graphed for the Goose Bay data. One can note the high indices thru the night October 13-14 on the MARISAT path and low indices on the FLTSAT path. The reverse is true for the night of October 14-15.



9. October 15 0420: Recordings show high scintillation levels on FLTSAT and very low levels for MARISAT during this period of the development of the magnetic storm. Figure 9 can be contrasted to Figure 7 which had high scintillation activity for MARISAT and low activity for FLTSAT. LST at Goose Bay is 0020.



10. October 14 2400: Increased sensing (using all of the sensors) is available during this period, allowing the construction of scintillation intensities across the areas shown. Scintillation levels in dB at 250 MHz are shown (lower frequencies have been converted).

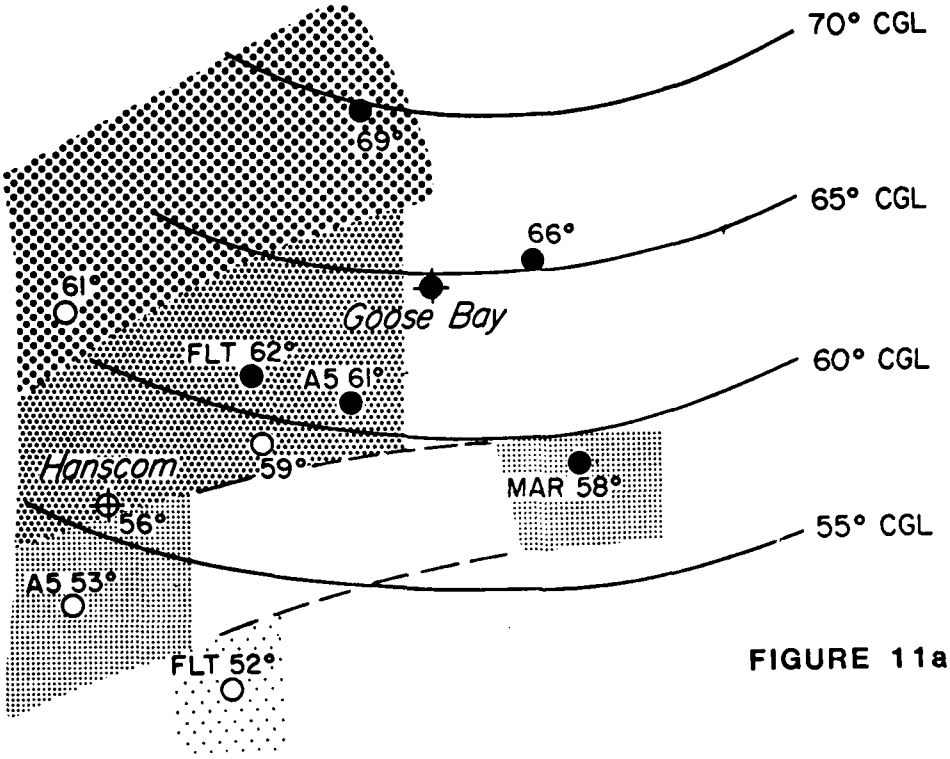


FIGURE 11a

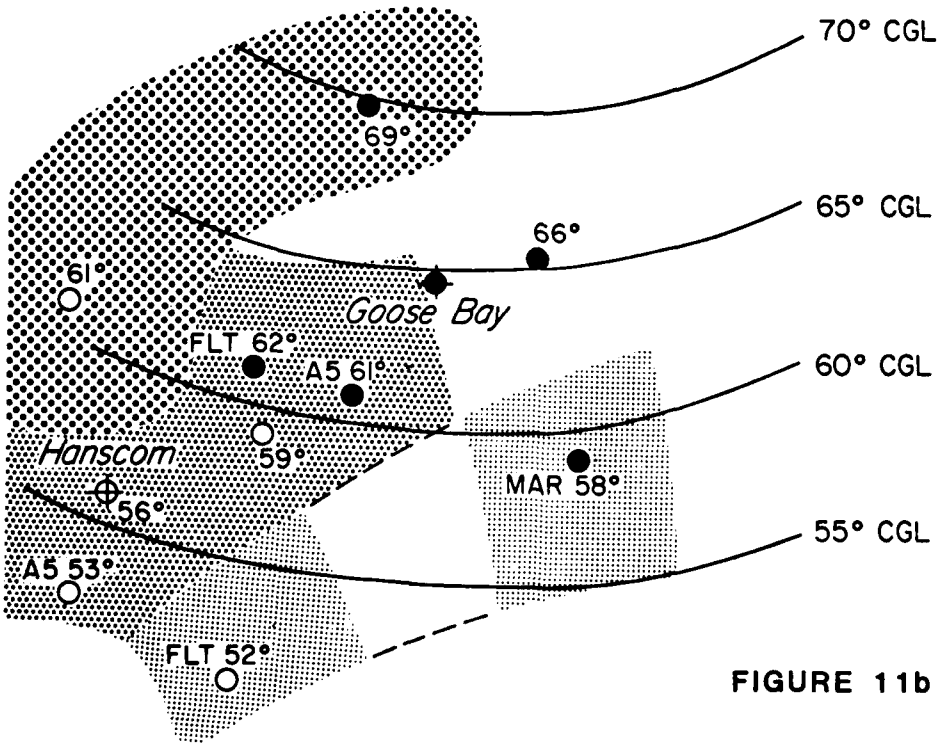


FIGURE 11b

11. In this series of plots various shadings have been used to indicate instantaneous scintillation levels in the area mapped. As the storm develops higher intensities encompass the lower latitudes.

    a. October 15 0200 UT

    b. October 15 0400 UT

    c. October 15 0600 UT

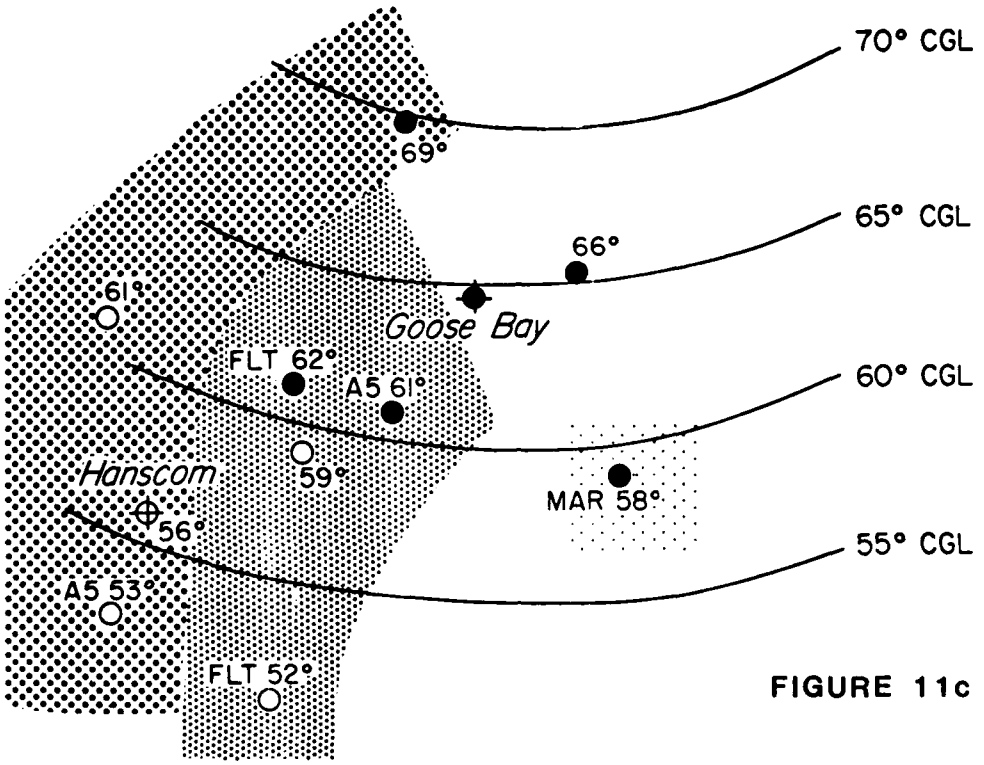
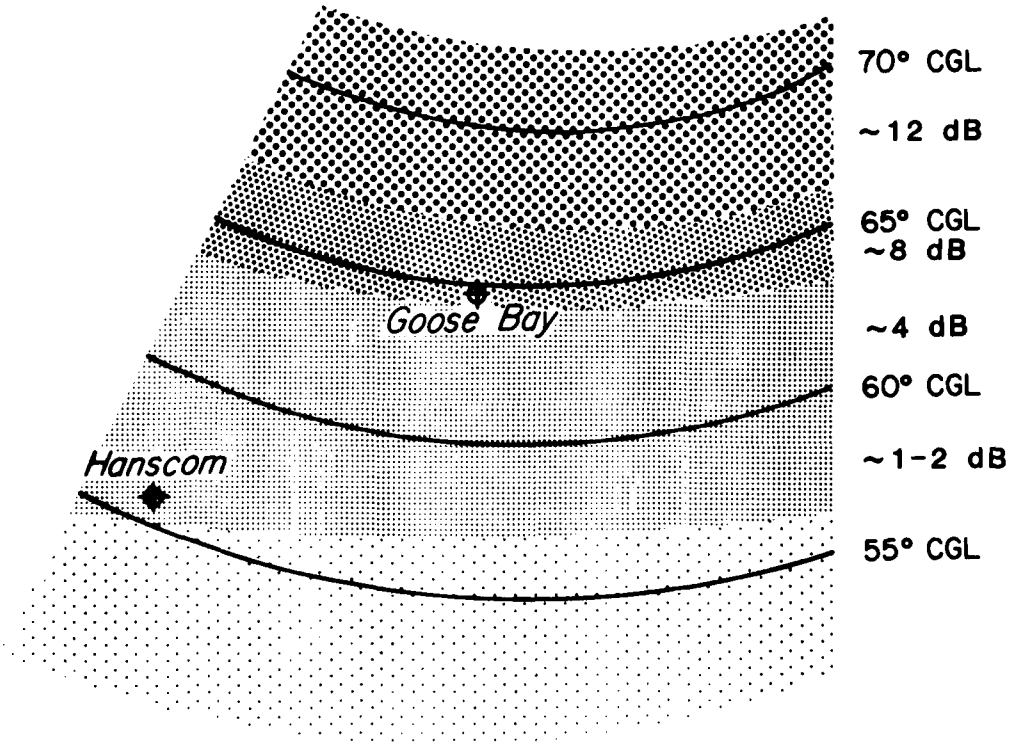


FIGURE 11c



12. October 15 2400 UT: For much of this quiet observation period the scintillation levels are aligned along lines of corrected geomagnetic latitude.

DISCUSSION

N.C.Gerson, US

Would you be willing to extrapolate your results to practical systems? Would not spaced antennas in diversity reception remove many of the scintillation problems affecting a practical system?

Author's Reply

Space and time diversity would definitely improve the scintillation problem — at the loss of some system capability and at the expense of inserting new modulation or receiver equipment into functioning systems.

E.J.Fremouw, US

You mentioned a correlation between plasmapause scintillation and SAR arcs and also that such scintillation does occur with the arcs. Do the arcs occur without scintillation?

Author's Reply

In two examples I have found scintillation absent when SAR arcs were present. However in one case the arc was not present near the intersection of the propagation path to the satellite. In the second case I have been unable to examine the SAR arc data in detail.

E.V.Thrane, NO

Have you done spectral analysis of the scintillations associated with the SAR arcs, and what can be learned from such studies of the generation mechanism for the irregularities?

Author's Reply

Spectral analysis has not been done on these fluctations in signal level. Their relatively long period (compared to auroral scintillations) may help reveal the mechanism involved.

INFLUENCE OF IONOSPHERIC IRREGULARITY SHAPE AND VELOCITY ON THE DESIGN OF AIRBORNE SATELLITE COMMUNICATIONS SYSTEMS

ALLEN L. JOHNSON
AVIONICS LABORATORY (AFWAL/AAAI)
WRIGHT-PATTERSON AFB, OHIO 45406

SUMMARY

Extensive ground and airborne UHF ionospheric scintillation measurements were conducted in the polar region during the peak of the current solar cycle. Using three spaced antennas the speed and direction of the irregularity drift was obtained from cross-correlation plots. Measurement taken during 1980 at Thule, Greenland; Sondrestrom, Greenland, and Goosebay, Labrador showed velocities of up to 1000 meters per second. A diurnal pattern of rapid direction changes provided information on the two cell polar circulation of the irregularities from the noon sector of the auroral oval over the polar cap to the midnight section and back around the oval to the noon section. Airborne ionospheric scintillation fading measurements conducted near Goosebay were compared with simultaneous ground measurements to investigate the ionospheric irregularity shape. Polar ionospheric scintillation fading measurement indicates that special care is required in the design of airborne satellite communications systems intended for polar operation. The fading rate, depth, and duration dictate some form of coding and interleaving to redistribute the burst errors in a random manner so they can be corrected by a forward error correction decoding technique. The paper describes applicable coding techniques, interleaving length, modulation schemes, and message length to provide an airborne satellite communication system protection against polar ionospheric scintillation fading.

INTRODUCTION

Studies on the effects of the polar ionosphere on earth-to-satellite communications have been underway for over 15 years (Aarons, 1970; Aarons et al, 1976). Ground and airborne measurements in Greenland, Canada, and Alaska have studied the influence of solar flux, magnetic index, time-of-day, and season on the occurrence and intensity of ionospheric scintillation fading. These studies have shown the 250 MHz military UHF Band can experience severe ionospheric scintillation with fading amplitudes greater than 25 dB. In the polar region the occurrence of scintillation seems to be most sensitive to solar flux and season, while the auroral region exhibits a strong dependence on time-of-day and magnetic index in addition to solar flux (Aarons et al, 1980-1).

The drift velocities of polar ionospheric irregularity have also been under study for the past decade (Haerendel et al, 1967; Heppner, 1972; Reiff et al, 1978; Evans et al, 1980). Due to the limited number of observation stations in the polar region, few direct measurements of polar ionospheric drift have been reported until recently.

The shape and velocity of the ionospheric irregularities in the polar region will affect the fade rate seen on the ground or by an airborne communications terminal. Overcoming message errors caused by ionospheric scintillation fading requires judicious choice of modulation, coding techniques, and message format.

DRIFT OF POLAR IRREGULARITIES

In the polar region ionospheric irregularity drift is much more complex than the almost linear irregularity drift exhibited in the equatorial region. Polar all-sky photometer 6300 Å images usually showed sun aligned polar arcs of fade-producing irregularities (Johnson et al, 1981). The arcs often drifted from dawn-to-dusk while individual irregularities are moving rapidly in a perpendicular, noon-to-midnight direction.

To evaluate polar irregularity drift an arrangement of three UHF antennas placed in a triangle was used at Thule, Greenland; Sondrestrom, Greenland; and Goosebay, Labrador. By recording the signal amplitude received from a UHF polar satellite, individual irregularity fades were identified at all three antennas at different times, Figure 1.

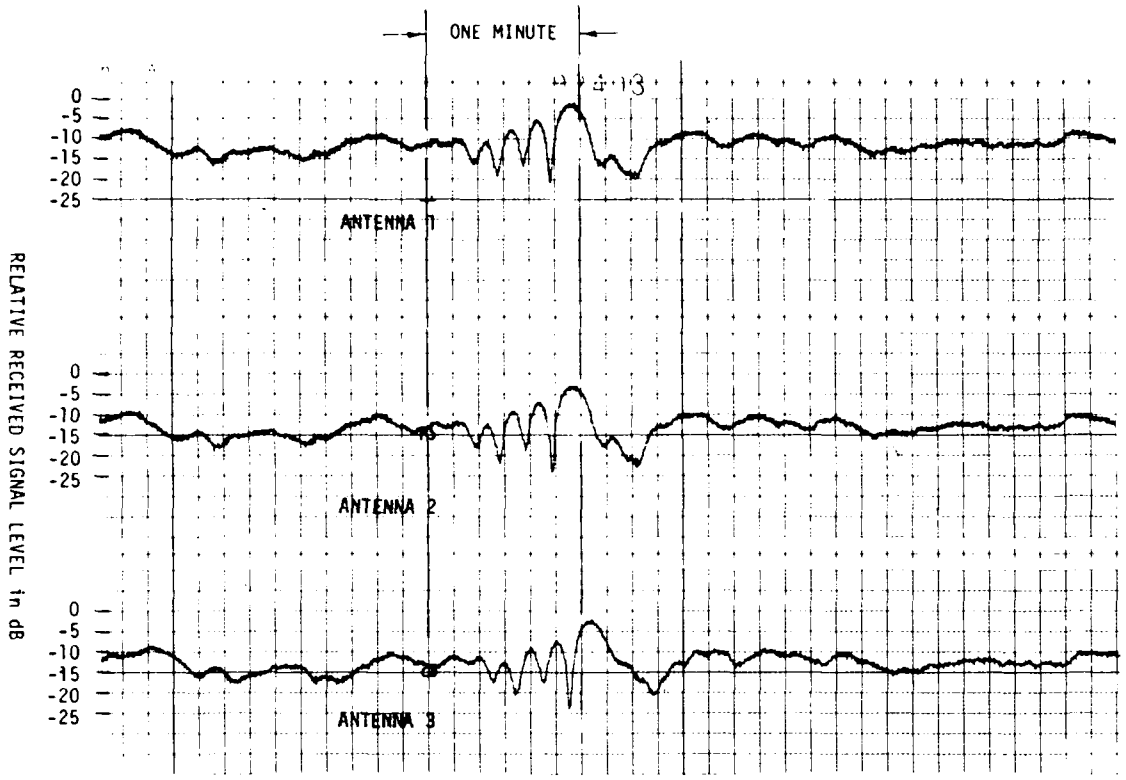


Figure 1 CORRELATION OF IONOSPHERIC SCINTILLATION FADING

By correlating the relative delay in the arrival of a particular fade at each antenna, one could calculate the direction and speed of the irregularities. Correlation of the data from the three antennas showed the pattern of irregularity flow repeated every 24 hours. Velocities from a few meters-per-second up to a thousand meters-per-second were measured. Typically, the data showed strong correlation over distances of 100 meters and time delays of a few seconds. Occasionally during extremely severe fading conditions, poor correlation was exhibited over short distances and times. This suggests most of the time the irregularities are relatively stable as they move through the ionosphere, but there are periods when the ionosphere is extremely dynamic with the irregularity changing shape in a few seconds. A 3-dimensional plot of correlation was made using sixty individual correlation plots taken at one minute intervals, Figure 2. This plot shows consistently strong correlation with no change in delay, indicating a stable irregularity velocity. An abrupt change in drift direction is apparent in Figure 3. The first few curves show a time lag for the arrival of the fade at two selected antennas of plus one-second. A quarter of an hour later the correlation decreased and appeared erratic. Then the correlation again became strong but with a minus three-second time lag. The time lag is seen more clearly in Figure 4. This data indicates a reversal of drift direction occurred in a ten-minute period.

The general movement of ionospheric irregularities on the polar cap is postulated to follow a two-cell model with irregularities flowing from the noon-time auroral oval across the pole to the midnight sector and then rotating back around the auroral oval to the noon sector (Heelis et al, 1976). Heppner, 1977, has postulated a slightly modified two-cell flow to include the disturbance produced by the earth's rotation, Figure 5. Using a technique described by Whalen, 1970, the three antenna measurement drift velocities are plotted on Heppner's polar drift model, Figure 6.

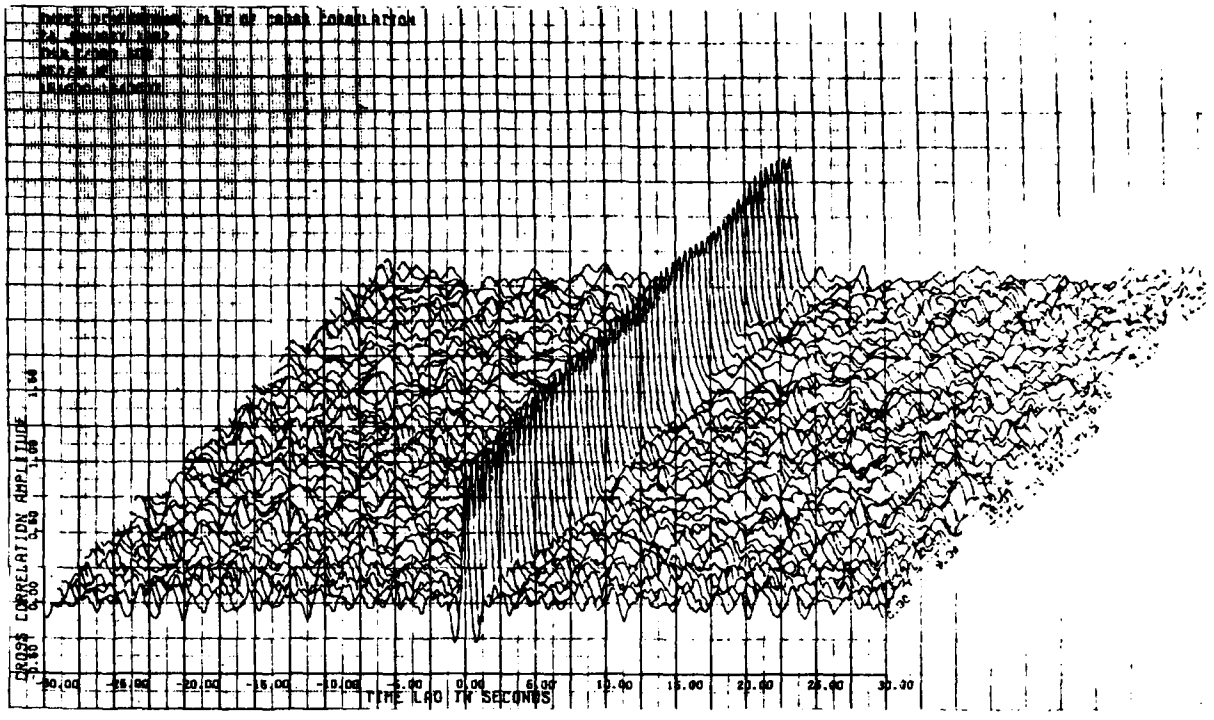


Figure 2 CROSS-CORRELATION OF FADING ON TWO ANTENNAS AT THULE

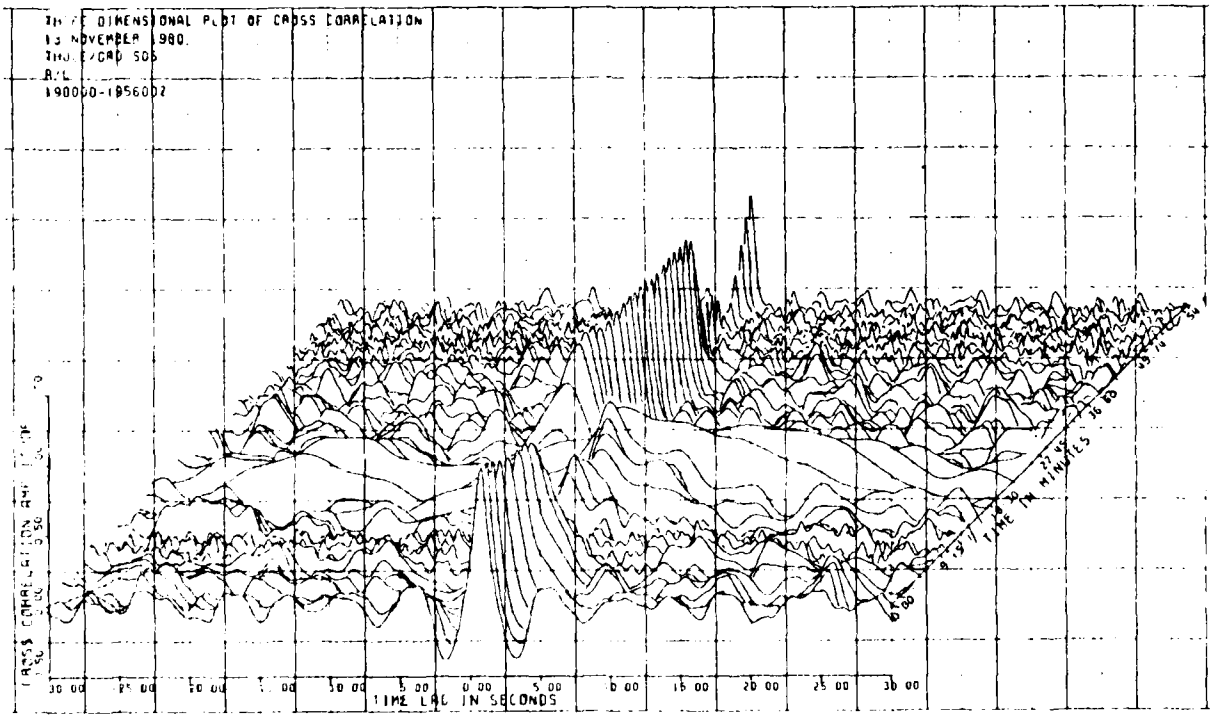


Figure 3 CROSS-CORRELATION OF FADING WITH CHANGE OF DIRECTION OF THE IRREGULARITY DRIFT

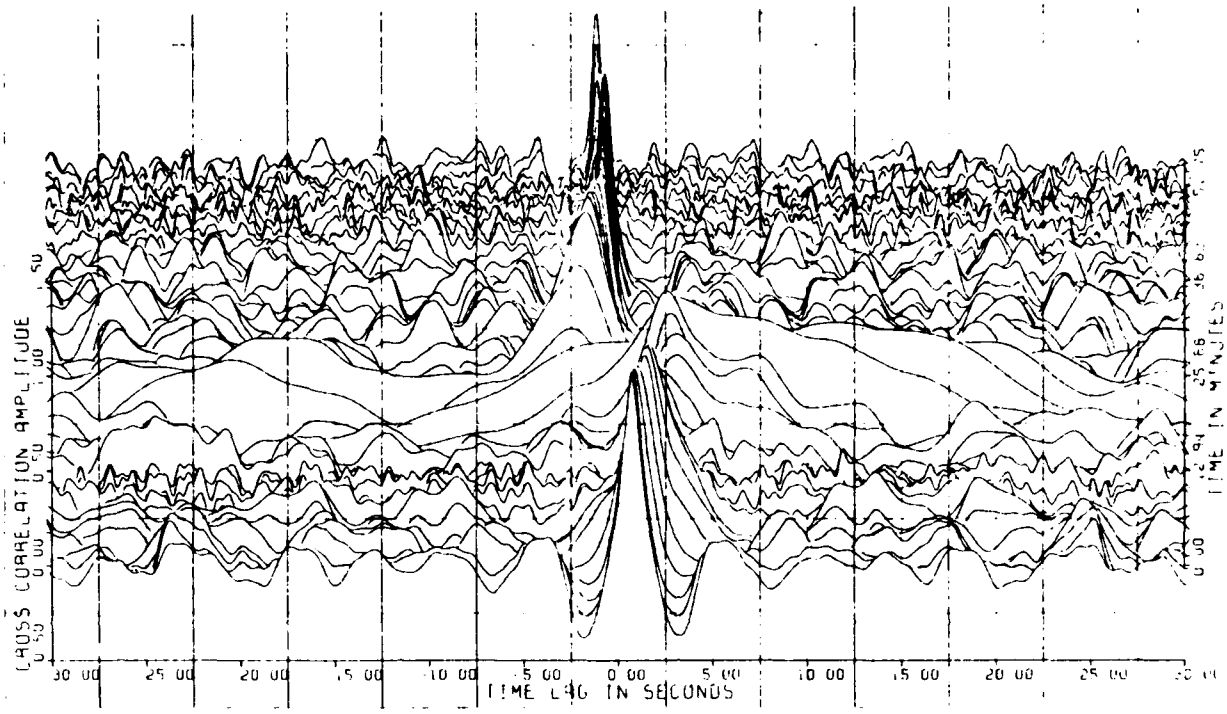


Figure 4 CROSS-CORRELATION OF FADING WITH CHANGE OF DIRECTION OF THE IRREGULARITY DRIFT

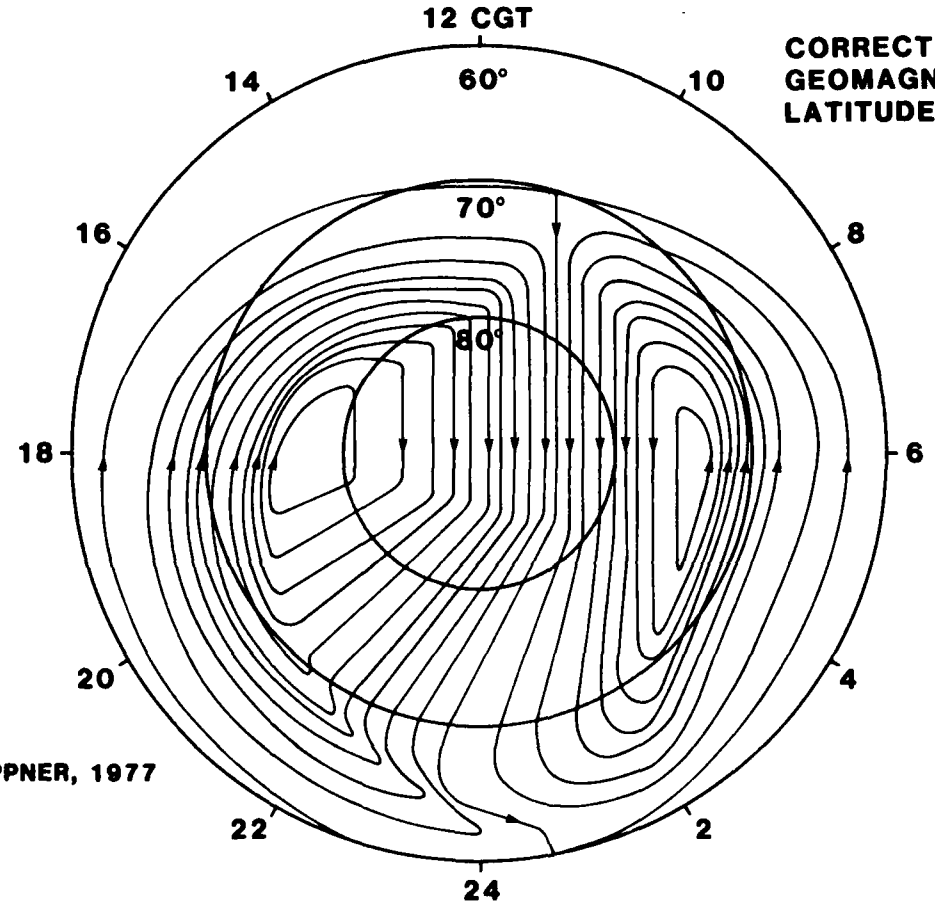


Figure 5 IONOSPHERIC IRREGULARITY CONVECTION PATTERN MODIFIED TO FIT NIGHTSIDE OBSERVATIONS

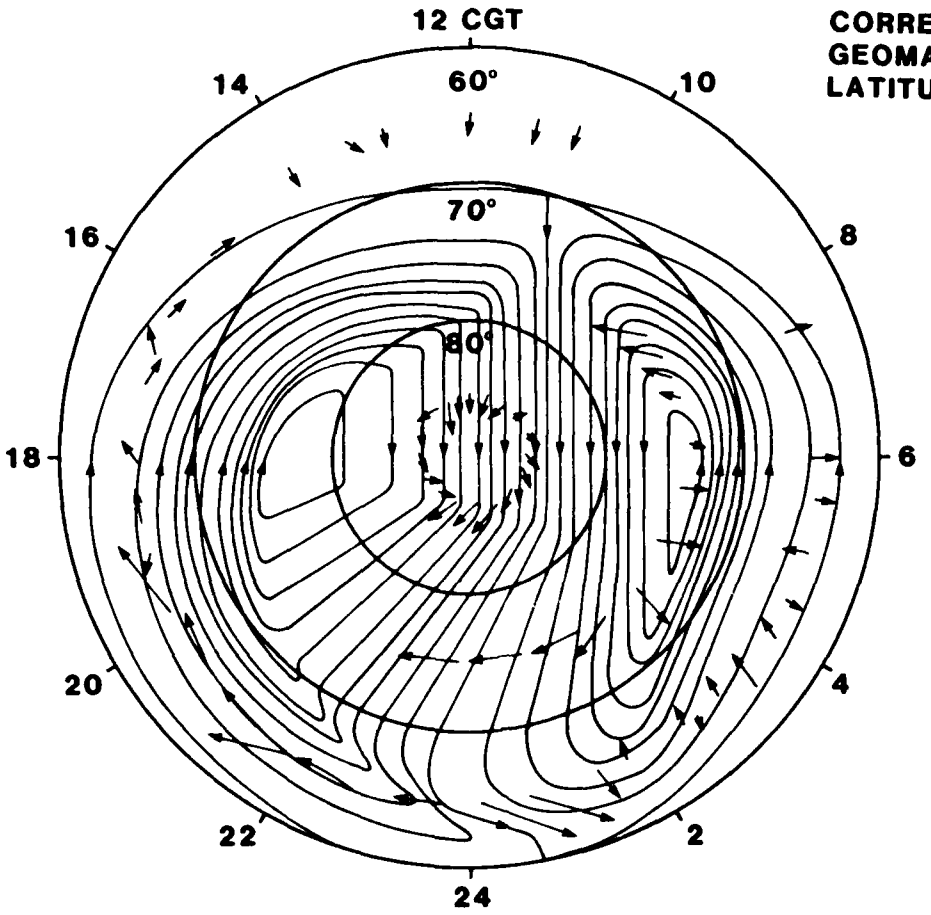


Figure 6 IONOSPHERIC IRREGULARITY CONVECTION PATTERN WITH DRIFT OBSERVATIONS

IRREGULARITY SHAPE

To evaluate the shape of the ionospheric irregularities in the auroral region a combined airborne/ground test was conducted at Goosebay, Labrador. Simultaneous measurements of the fade rate on the ground and in the air provided a direct comparison of the effect of the airborne velocity on the fade rate. These measurements were taken over a two hour period while the aircraft flew eight headings, each 45° apart. The ratios of the ground and airborne ionospheric scintillation fade rates given in Table 1 are plotted in Figure 7 for each of the eight aircraft directions. Assuming the irregularity velocity remained relatively constant during the two-hour measurement period, the velocity was 200 meters-per-second from the north east.

These airborne measurements provide information on irregularity shape. Similar tests done in the equatorial region where the ionospheric irregularities are extremely elongated in the north-south direction provided a ratio of airborne to ground fade-rate versus direction shown by the solid line in Figure 8 (Aarons et al, 1980-2). By synchronizing the aircraft speed with the speed of the ionospheric irregularity it was possible, in the equatorial region, to approximately zero out the fade rate (note fade rate at 270° and 180°). If on the other hand, the auroral irregularities had little or no elongation, the ratio of the fade-rate would be almost independent of aircraft direction, as indicated by the solid line in Figure 9. Comparison of the measured fade-rate ratios with the elongated and circular models suggest that a small degree of elongation does occur in the auroral irregularities in the direction perpendicular to the irregularity velocity.

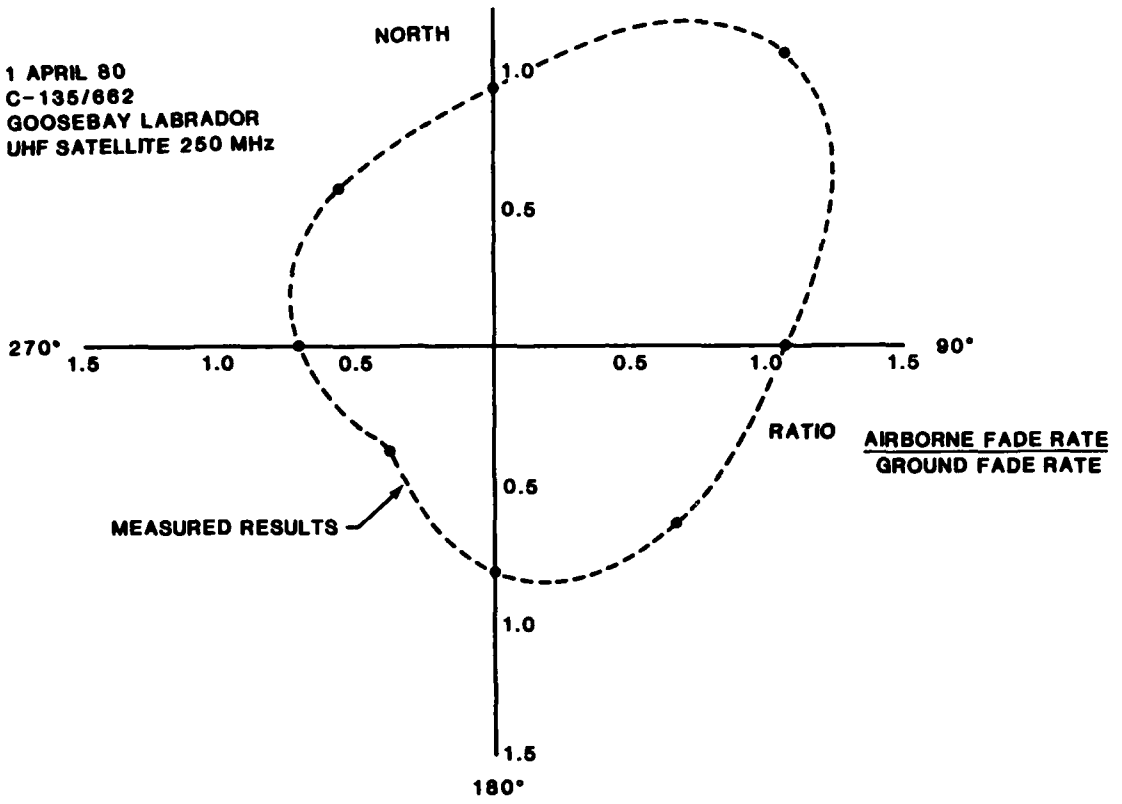


Figure 7 COMPARISON OF AIRBORNE AND GROUND FADE RATE

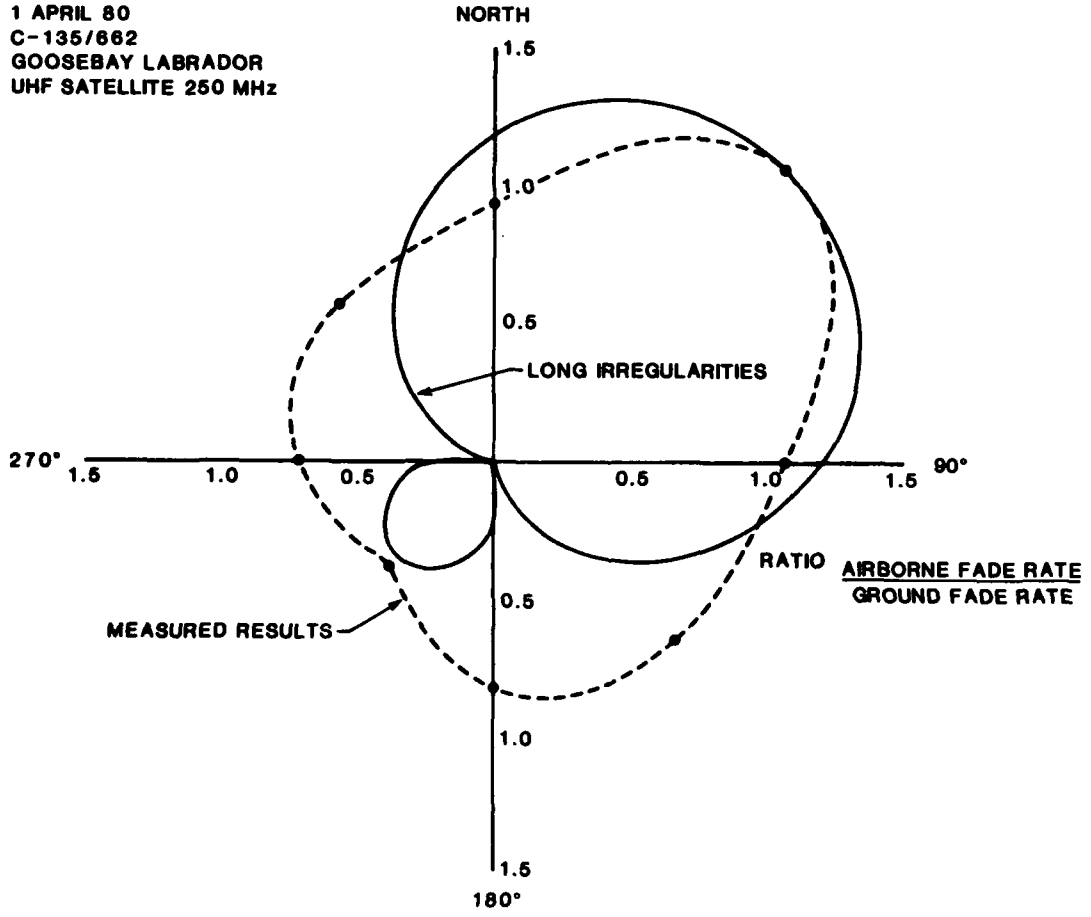


Figure 8 COMPARISON OF AIRBORNE AND GROUND FADE RATE

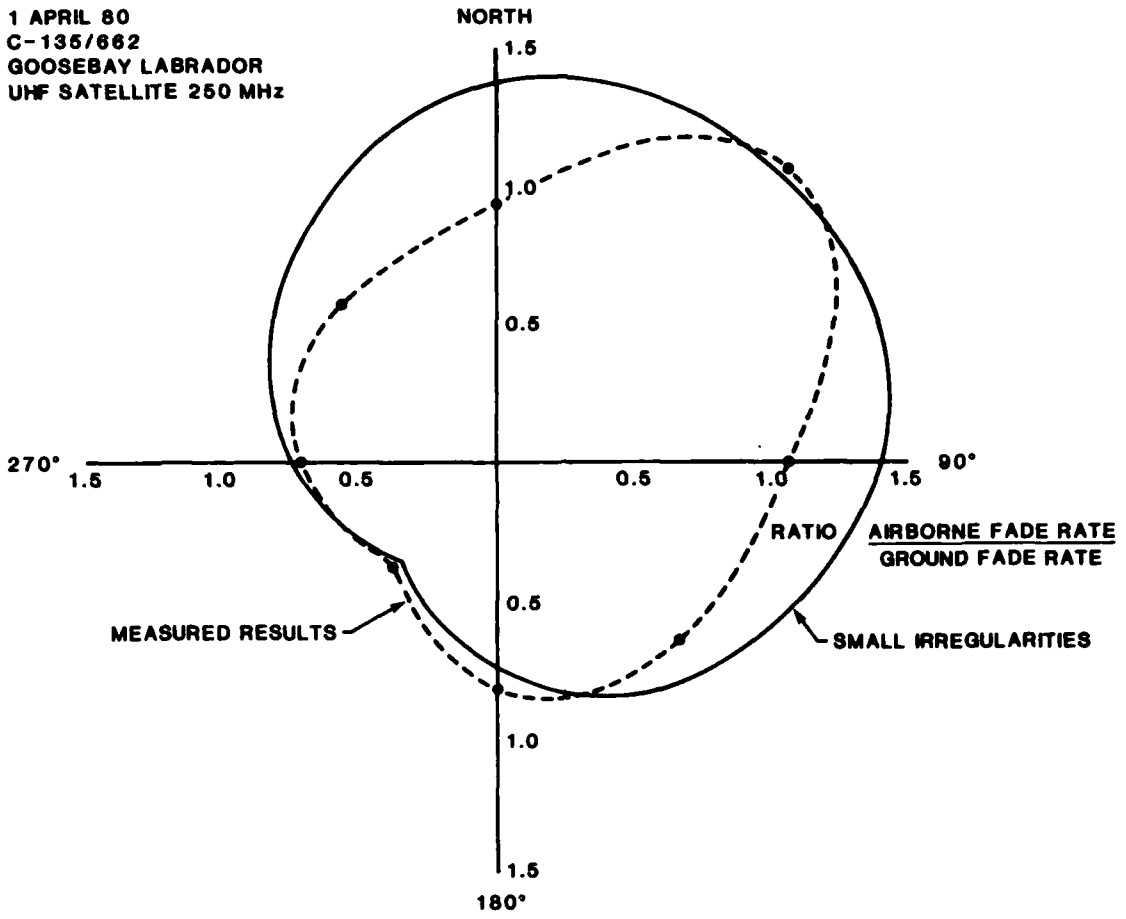


Figure 9 COMPARISON OF AIRBORNE AND GROUND FADE RATE

Table 1 Comparison Of Airborne And Ground Fade Rates

1 April, 1980
Goosebay, Labrador

Time UT	Gnd Fade Rate fades/minute	Abn Fade Rate fades/minute	Ground Speed Knots	Abn Fade Rate Normalized (400 Kts)	Heading Degrees	Fade Ratio Abn/Gnd
1919-1924	137	75	407	74	225°	0.54
1929-1934	85	75	381	79	360°	0.93
1939-1944	67	60	384	63	135°	0.94
1949-1954	60	42	391	43	270°	0.72
2000-2005	64	95	393	97	045°	1.52
2012-2017	70	60	416	58	180°	0.83
2022-2027	76	60	378	64	315°	0.84
2034-2039	60	60	415	63	090°	1.05

CHOICE OF COMMUNICATION PARAMETERS

The design of an airborne satellite communications system to operate in the polar region must consider the shape and velocity of the ionospheric irregularities in order to minimize the detrimental effect of the ionospheric fading. Measurements have shown that an airborne satellite communications system can expect fade rates which vary from several fades-per-second to one fade-per-minute as depicted by Figure 10. However, due to the high irregularity velocities usually experienced in the polar region and the

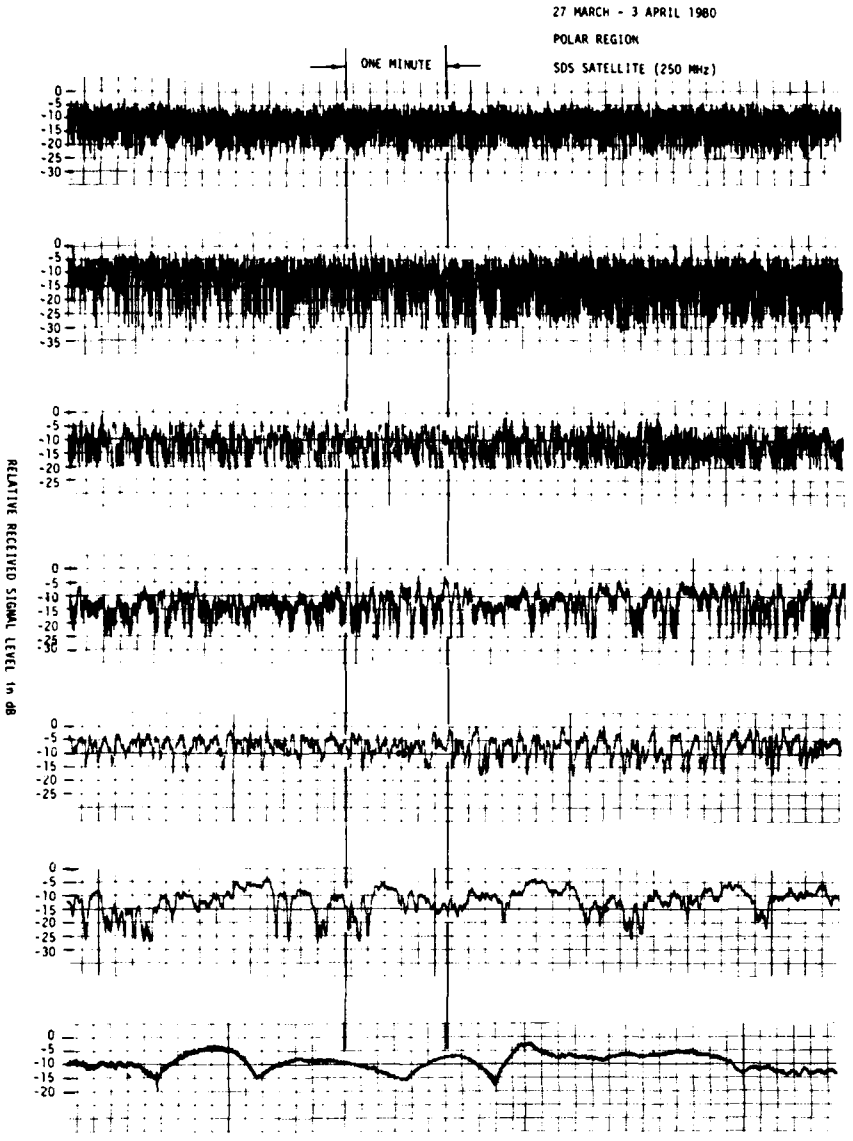


Figure 10 VARIATIONS IN SCINTILLATION FADING RATE

small degree of irregularity elongation, rapid fading is more likely to occur than slow fading. In addition to the amplitude fading, severe phase variations can be expected in the polar region, Figure 11.

The modulation chosen for an airborne satellite communication system must be robust in order to minimize the phase and amplitude effects of polar fading. Calculations have shown that phase modulation, such as BPSK, would experience an irreducible bit-error-rate due to the severe phase variations of the polar fading (Prettie, 1982). By contrast a frequency shift keyed modulation such as binary FSK or 8-Ary FSK is less sensitive to phase variations and exhibits a more robust behavior in the fading environment.

Some type of diversity should be employed in the communications system to alleviate the burst errors caused by ionospheric fading. Fade depth changes very slowly with frequency, making frequency diversity impractical. Antenna diversity, in general, requires antennas spaced hundreds of meters apart to get the necessary improvement. While this may be acceptable for ground stations, it is not practical for an airborne terminal. Time diversity, such as coding and interleaving, appear to provide the most practical solution for improving the performance of an airborne terminal. Most of the time fade duration is a fraction of a second. Interleaving over several seconds can

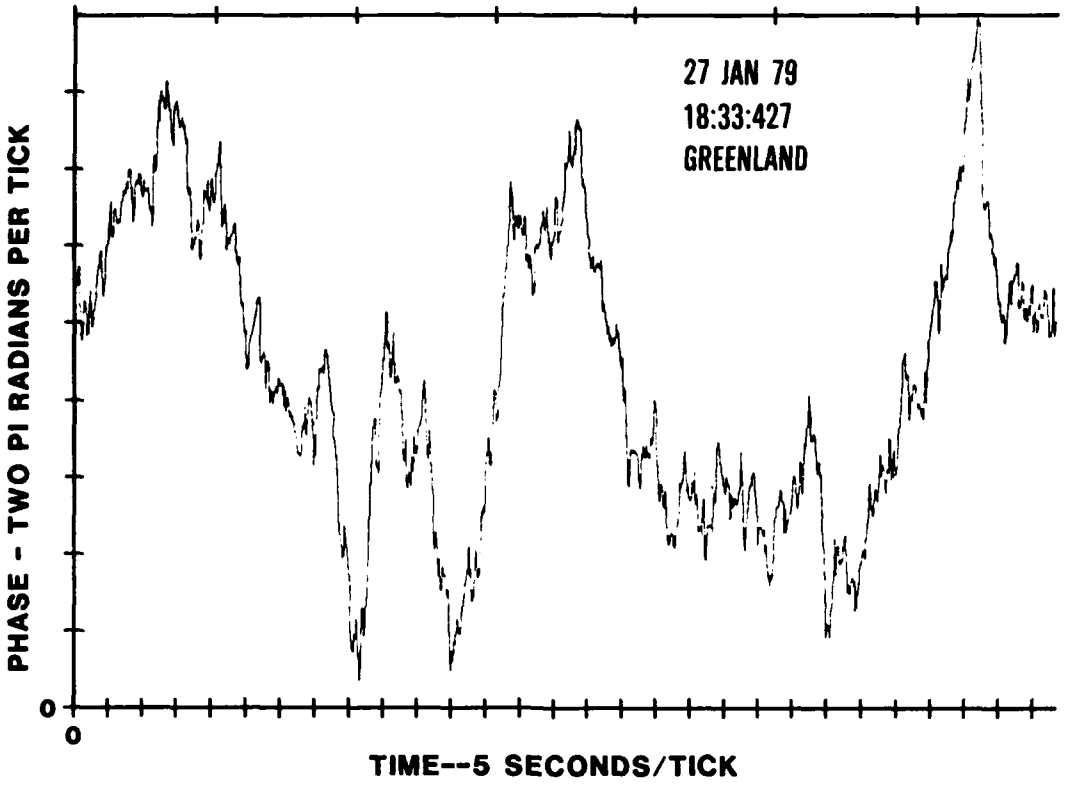


Figure 11 PHASE VARIATIONS INDUCED BY POLAR IONOSPHERIC IRREGULARITIES

successfully convert burst errors caused by the fading into random errors which can be corrected by a forward-error-correction decoder. Tests with 1/3 rate, 1/2 rate and 3/4 rate coding have shown that 1/2 rate or 3/4 rate coding is adequate to significantly improve the error rate during most ionospheric scintillation. The 1/3 rate coding provided only marginally better performance and reduces communications throughput rate. An experimental satellite communications terminal was built using two-tone FSK with four-second interleaving and a 3/4 rate feedback decoder. Error-free message reception improved from 10 percent without coding/interleaving to 90 percent with coding/interleaving during polar ionospheric scintillation fading.

Another parameter available to the communications system designer is message length. When operating through polar ionospheric scintillation, it is desirable to keep the message length short, i.e. a few seconds. Under rapid fading conditions, the coding and interleaving will correct the burst errors and provide error-free messages. Under conditions of extremely slow fading, where the fade may last for several seconds, only one or two of the short messages would be lost per minute and these can be corrected by selective message repeating. Using longer messages might make it impossible to send a complete, error-free message under conditions of slow ionospheric scintillation fading.

CONCLUSION

Fifteen years of measurements in the polar region have shown that ionospheric scintillation fading can occur during all hours of the day and may at times last for several days. However, a satellite communications system which employs a robust modulation (such as FSK), proper coding and interleaving, and short message length can provide a reliable communications link in the polar region between a satellite and mobile terminals.

REFERENCES

1. Aarons, J., (1970), "High-Latitude F-Region Irregularity Structure During the Oct 30 - Nov 4 1968 Magnetic Storm," Radio Science, Vol. 5, No. 6, pp. 959-966, June 1970.

2. Aarons, J., J. Mullen, H. Whitney, E. Martin, K. Bhavnani, and L. Whelan (1976), "A High-Latitude Empirical Model of Scintillation Excursions," AFGL-TR-76-0210, Air Force Geophysics Laboratory, Hanscom AFB, MA, 17 Sept 1976.

3. Aarons, J., E. MacKenzie, K. Bhavnani (1980-1), "High Latitude Analytical Formulas for Scintillation Level," Radio Science, Vol. 15, No. 1, Jan 1980.

4. Aarons, J., J.P. Mullen and H.E. Whitney (1980-2), "The Dynamics of Equatorial Irregularity Patch Formation, Motion and Decay," Journal of Geophys Research, Vol. 85, No. A1, pp. 139, 1 Jan 1980.

5. Aarons, J., J.P. Mullen, H.E. Whitney, A. Johnson, E. Weber (1981), "UHF Scintillation Activities Over Polar Latitudes," Geophys Research Ltrs, Vol. 8, No. 3, March 1981.

6. Evans, J.V., J.M. Holt, W.L. Oliver, and R.H. Ward (1980), "Millstone Hill Incoherent Scatter Observed Observations of Auroral Convection over 60° to 75°," Journal of Geophysics Research, Vol. 85, No. A1, pp. 41, 1 Jan 1980.

7. Haerendel, G.R., R. Lust, and E. Reiger (1967), "Motion of Artificial Ion Cloud in the Upper Atmosphere," Planet Space Science, 15 Jan 1967.

8. Heelis, R.A., W.B. Hanson, J.L. Burch (1976), "Ion Convection Velocity Reversals in the Dayside Cleft," Journal of Geophysics Research, Vol. 81, No. 22, pp. 3803, 1 August 1976.

9. Heppner, J.P. (1972), "The Harang Discontinuity in Auroral Belt Ionospheric Currents," Geoifys Publ 29, 105, 1972.

10. Heppner, J.P. (1977), "Empirical Model of High Latitude Electric Fields," Journal of Geophysics Research, Vol. 82, No. 7, p. 1115, 1 March 1977.

11. Johnson, A., J. Aarons, J. Buchau, J. Mullen, E. Weber, and H. Whitney (1981), "Occurrence of F-Layer Irregularities in the Polar Cap," IES Symposium, Alexandria, VA, 15 April 1981.

12. Prettie, C.W. (1982), "Measurements of Phase Effects Associated with Ionospheric Scintillation," EOS, Vol. 63, No. 18, Abstract SA-41-6, 4 May 1982.

13. Reiff, P.H., J.L. Burch, R.A. Heelis (1978), "Dayside Auroral Arcs and Convection," Geophysics Research Letters, Vol. 5, No. 5, pp. 391, May 1978.

14. Whalen, J. (1970), "Auroral Oval Plotter and Nomograph for Determining Corrected Geomagnetic Local Time, Latitude, and Longitude for High Latitudes in the Northern Hemisphere," AFCRL-TR-70-0422, Hanscom AFB, MA, 27 July 1970.

PROPAGATION EFFECTS ON SATELLITE-BORNE SYNTHETIC APERTURE RADARS

by

Charles L.Rino and Jacqueline Owen
SRI International
333 Ravenswood Avenue
Menlo Park, California
USA

ABSTRACT

Strong amplitude scintillation at frequencies above UHF is rarely observed on high-latitude transionospheric paths; however, satellite-borne, L-band synthetic aperture radars (SARs), such as the SEASAT-A SAR, synthesize apertures approaching 20 km. In previous work (Rino and Gonzalez, 1983, AGARD Oberammergau Symposium) we showed that moderate auroral-zone scintillation degrades the azimuthal SAR point spread function significantly, particularly the sidelobe level. We concluded that this degradation could explain the contrast reduction that had been observed in some auroral zone SAR images.

In more recent work, we have developed a numerical SAR simulator. The simulator can generate and process image segments with full or partial corrections for range walk and quadratic phase-error correction. The simulations also include the effects of coherent target speckle, which is important in assessing SAR image quality. Our results show that moderate auroral-zone scintillation will degrade an image to about the same level as any undisturbed image processed with only partial range-walk compensation. Thus, propagation effects are undoubtedly present in many of the SEASAT-A high-latitude images, but the degradation is comparable to other distortions introduced in the processing itself. Phase error compensation is effective, but amplitude scintillation is also important for larger disturbances.

We shall present these new results and discuss their ramifications for SAR imaging.

DISCUSSION

J.A.Klobuchar, US

Don't write off the high latitude ionospheric effects on SARs so quickly. Our GPS observations of S_4 max $\approx$0.2 are, by no means, a "worst case" condition. Also, Dr Soicher's TEC data from Anchorage shows large phase changes under an active aurora.

Author's Reply

I believe that S_4 indices greater than .2 at L band are very rare occurrences. In any case, at these levels the loss of resolution in a SEASAT-A type system is on the order of a few hundred metres, which can be serious in some cases.

S.Knowles, US

There are presently fairly routine very long baseline observations in the Arctic at Gilmore Creek (near Fairbanks) by NASA. These have showed phase rotations of up to 180° at X-band within a few minutes. This type of phenomenon will affect SAR images.

Author's Reply

This information should be integrated into the appropriate data base — and compared to scintillation measurements.

F.Christophe, FR

Could you comment on the feasibility of "self-coherence" techniques to compensate for those propagation effects?

Author's Reply

Methods of phase compensation based on splitting the aperture into subapertures and cross correlating the subapertures are being studied. I suspect that the improvement in severely degraded images will be limited, however. Other schemes have been proposed but not, to my knowledge, tested.

HIGH-LATITUDE SCINTILLATIONS USING NNSS SATELLITES

L KERSLEY
University College of Wales
Aberystwyth, SY23 3BZ
UK.

SUMMARY

The paper describes an experiment which has been established in Northern Sweden since September 1984 to monitor scintillations using transmissions from NNSS satellites. Designed for long-term nearly-unattended operation, with control and data handling based around a PDP 11/23 minicomputer, the equipment records and processes data from more than 20 NNSS passes per day. Stored on magnetic tape for further study for each 20s segment of received signal after suitable detrending, are S_4-indices for both frequencies, the r.m.s. differential phase fluctuations, the differential phase rotation (differential doppler), together with statistics of signal fading below selected thresholds and durations of individual fades. Determination of satellite position in nearly-real time from the transmitted ephemeris parameters enables estimates of effective ionospheric irregularity height to be made for high-elevation passes by means of the cross correlation of signals received on two separated antennas.

A second mode of operation allows the raw data to be stored for subsequent analysis. This has been used successfully for coordinated special program experiments in conjunction with the EISCAT ionospheric radar facility in the study of the physical processes responsible for the scintillation-producing irregularities.

In the present paper attention is focussed on selected early results of scintillation morphology and the structure of the fading signal. Also presented are the first results from coordinated experiments with EISCAT, where scintillation is shown to be associated with irregularities occurring in a region of strong horizontal gradient in electron density in the ionospheric F-region.

INTRODUCTION

Radio waves traversing the ionosphere undergo spatial modulations in phase due to irregularities present in the medium. The intensity and phase of the resultant signal received at the ground are subject to random fluctuations, known as scintillations. The propagation aspects of radio-wave scintillations including both theoretical and experimental results have been reviewed by Yeh and Liu (1982). In addition, the current knowledge of the morphology of ionospheric scintillations, based on studies of the monitoring of radio beacons aboard satellites over two and a half decades has been reviewed by Aarons (1982). On a global scale there are three zones of intense scintillation activity. One is in the post-sunset equatorial ionosphere, while it is the others, at high latitudes in the vicinity of the auroral ovals, which are of concern here. Studies of scintillation at high latitudes and European sector longitudes were made in the early 1960's. However, the satellite sources then available were at frequencies such that the received scintillations were subject to receiver saturation so that a full statistical description of the fading structure was not possible. With the development of digital signal processing and improved understanding of scintillation mechanisms a further description of the fading signal can now be made. In the high-latitude zone most of the interest in scintillation has been concentrated until recently on observations around the 70°W longitude and in the Alaskan sector. More recently, with the advent of the EISCAT ionospheric radar facility in northern Scandinavia attention has again become focussed on the European high-latitude ionosphere.

This paper describes an experiment to study high-latitude scintillations, which involves the monitoring of transmissions from the Navy Navigation Satellite System (NNSS) satellites at a site in northern Sweden. Early results are presented, obtained from the analysis of some 2000 satellite passes recorded during a three-month period, which illustrate the potential of the experiment both in its application to propagation studies of the basic morphology and signal fading statistics of scintillation and also in increased understanding of the physical mechanisms responsible for the small-scale scintillation-producing ionospheric irregularities themselves.

EXPERIMENT

The experiment aims to study the occurrence of high-latitude scintillations over northern Europe, to obtain information on the effective height of the small-scale ionospheric irregularities responsible for the scintillation, to yield statistics on the fading structure of the signals, and in conjunction with coordinated observations with the EISCAT diagnostic ionospheric radar facility to investigate the conditions responsible for the formation and growth of the scintillation-producing ionospheric irregularities.

The transionospheric signals used are transmissions from the NNSS satellites, a constellation of usually 5 satellites in nearly-circular polar orbits at altitudes around 1000 km. The satellites, whose primary function is for navigation purposes, transmit phase-coherent signals on 150 and 400 MHz, and so can be used to monitor both amplitude and differential phase scintillations.

The receiver system used in the present experiment is based around a receiver originally designed for use with the geostationary ATS-6 satellite. The modifications allow for search and acquisition of the doppler-shifted 400 MHz transmission from an approaching NNSS satellite. Phase-locked-loop tracking of this signal provides a phase reference to enable narrow band reception and tracking of the 150 MHz transmission. Two 150 MHz receivers are used, fed from antennas separated by some 700m in the meridional sub-satellite

track. The outputs from these receivers, in the form of quadrature components, together with the 400 MHz signal amplitude are filtered, using active fourth-order Butterworth low-pass filters with cut-off at 23 Hz, before being interfaced to the analogue to digital converter of a PDP 11/23 minicomputer. The sharp response filter is necessary to eliminate noise from the signals arising from the transmission of ephemeris data as a phase modulation on both carrier frequencies. A sampling rate of 50 Hz is used for the digitization of the data, so that with satellite passes lasting up to 18 min, the resultant volume of data makes on-line processing essential, with only reduced parameters which characterise the scintillation being retained for subsequent analysis. The processor, with 128K bytes of memory and dual-disk drives, has two TU58 magnetic tape cartridge devices for data storage, so that tapes containing reduced data can be forwarded to Aberystwyth for further processing at approximately weekly intervals. A JMR-1 navigation receiver is also interfaced to the computer. This receiver decodes the modulation on the satellite transmissions to provide the ephemeris parameters in digital form for the computer, allowing the satellite position to be calculated for any time. The 150 MHz receivers are fed from discone antennas at the local and remote sites. The preamplifier, filter and r.f. amplifier/mixer for the second receiver are housed at the remote site, with the local oscillator frequency stepped down to about 17 MHz being fed along the 1km cable to be amplified and multiplied at the remote site. The returning i.f. signal at 11.7MHz is also amplified before being brought to the main receiver by means of a second coaxial cable.

The control software allows acquisition of data when the main receiver and the JMR are locked to the 400 MHz signal from the satellite, with special provision being made to handle the early part of the pass before JMR ephemeris data reception is activated on an even two-minute marker on the satellite transmission. Data processing cannot keep pace with the real-time collection of data, and in practice processing can take up to some 30 min after the end of a pass. During processing the software inhibits the collection of additional data from any new pass to which the receivers are locked.

The on-line processing is carried out for 20s samples of data. The quadrature components are first converted to intensity and phase (differential phase for 150 MHz with respect to 400 MHz reduced to a common frequency), and samples with a mean intensity above a defined threshold are analysed. The slow trends are removed by means of a detrending filter. A third-order Butterworth low-pass filter with cut-off at 0.2 Hz is used for this purpose. The trend is eliminated from the data by division in the case of intensity (local and remote 150 MHz and 400 MHz) and by subtraction for the differential phase. The auto- and cross-correlation functions are computed for both sets of data at 150 MHz and the effective height of the irregularities responsible for the scintillation is calculated from the time delays. By restricting attention to a carefully chosen set of overhead passes estimates of irregularity height can be obtained to a reasonable accuracy for the conditions of the anticipated field-aligned irregularity configurations (E.N. Bramley, private communication, 1984).

The scintillations on signal intensity are characterised by an S_4-index defined as the normalised variance of signal intensity, which is calculated for both local and remote signals at 150 MHz and for the 400 MHz signal, while the corresponding index for the phase fluctuations is $\sigma\phi$, the root mean square phase deviation. For scintillation exceeding a predefined S_4 level information on signal fading below certain thresholds and the durations of individual fades is also recorded.

A sample computer print-out of some of the data acquired during a typical satellite pass and stored on tape cassette for subsequent processing is shown in Fig.1.

In mid-September 1984 the equipment was installed at Kiruna in Northern Sweden (67.83N, 20.43E). At the high-latitude site several of the polar-orbitting satellites may be above the horizon simultaneously, however the narrow-band tracking receivers and the control software enable the automatic signal acquisition system to make a random selection of satellite passes without contamination of the data from mutually interfering signals from more than one satellite. In practice, data can be obtained for up to 30 satellite passes per day with an average of 22 passes per day. The average pass duration is 14 minutes, giving 42 data samples each of 20s duration, while a single cassette contains stored data for an average of 126 passes.

RESULTS

(a) Morphology

Some examples of early results obtained from a preliminary analysis of data obtained during the first three months of operation of the experiment in Kiruna are presented here. In keeping with the aims of the experiment the results fall into two categories, those related to applications aspects of transionospheric radio-wave propagation like scintillation morphology and signal-fading structure and those concerned with the study of the ionospheric irregularities including special investigations coordinated with observations using the EISCAT ionospheric radar facility.

Examples of scintillation activity observed on successive satellite passes on the night of 19 September 1984 are shown in Fig.2. Plotted are S_4 for 150 MHz and $\sigma\phi$ values as a function of satellite latitude. The variable nature of the high-latitude irregularity occurrence can be seen from these examples. The first pass shows strong scintillation throughout the entire pass but this is replaced by a more patchy structure in the later observations. A further point to note is the lack of exact mapping between S_4 and $\sigma\phi$, although a few very high values of $\sigma\phi$ in the first figure must be treated with caution. In noting the differences in behaviour between S_4 and $\sigma\phi$ it must be remembered that the main contribution to S_4 arises from irregularities of scale size close to that of the first Fresnel zone for the observations, whereas the effect of larger irregularities with scales essentially determined by the detrending procedure in the processing of the phase data dominates the phase fluctuations which determine the $\sigma\phi$ value.

In a preliminary analysis of the first three months data high elevation north-south satellite passes have been selected and average S_4 values above a threshold of 0.15 computed for the 150 MHz signal for different time ranges throughout the day are presented in Fig.3. These composite results for all levels of geomagnetic activity, plotted as a function of geographic latitude, show broad features which can be

identified with the known behaviour of the auroral oval. However for further geophysical interpretation the data are being organised on the basis of a geomagnetic coordinate system.

(b) Signal-fading structure

Information on the structure of the fading signal during scintillation is available from the data. The probabilities of occurrence of different intensity levels within the fading signal are presented in Fig.4 for four ranges of S_4 covering weak to strong scintillation at 150 MHz. These show good agreement with the theoretical Nakagami-m distribution with $m = (S_4)^{-2}$ in confirmation of the work of Whitney et al. (1972). Corresponding cumulative plots give the percentage of time for which the signal is below a given threshold. However, in addition to amplitude distributions further information is needed to describe fully the signal fluctuations, in particular temporal information relating to the durations of fades. A feature of the present experiment is the information it provides on the durations of individual fades of the 150 MHz signal. The average numbers of fades of given duration within a 20s data window are plotted in Fig.5. Results for different threshold intensities are shown for three different ranges of S_4 corresponding to weak, moderate and strong scintillation. The complex nature of the fade duration structure can be seen from the graphs, although it can be noted that for strong scintillation and deep fading there is some limited support for the exponential model inferred by Crane (1977) from a very restricted set of NNSS observations. However, as signal threshold intensity increases the importance of the longer fades becomes apparent in the distributions. For satellites in low orbit the effective scan rate of the electron density irregularities at F-regions heights at ~ 2km s^{-1} determines the essential magnitude of the fade durations. The scan rate is in turn affected by the height of the irregularities, while the influence of larger-scale irregularities is masked in the intensity data by Fresnel filtering. The results presented here have been obtained from the analysis of some 5000 individual samples of scintillation and so represent averages for all irregularity configurations encountered at high latitudes. Data on fading structure is normally only acquired during moderate or strong scintillation, so that the results for weak scintillation presented here have been obtained from a much more limited set of some 200 data samples.

Cumulative plots giving the fraction of fades below a series of defined threshold levels whose duration exceeds a given value are plotted in Fig.6 for S_4 values corresponding to weak, moderate and strong scintillation.

(c) Irregularity studies

A second aspect of the experiment is the study of the scintillation producing irregularities themselves and the conditions in the ambient ionosphere which give rise to their formation and growth. Information on the background ionisation is available in the routine data in the form of the number of cycles (rotations) of differential phase observed in each 20s data window from which the variation of ionospheric electron content along the pass can be estimated. However, of greater importance is a special mode of operation of the experiment for use with coordinated runs of the European Incoherent Scatter (EISCAT) radar facility. In this mode the raw values of signal intensity and differential phase for an entire pass, digitized at 50 Hz, are stored on the cassette tapes for subsequent analysis. The associated EISCAT special program runs involve a meridional scan of the radar starting in the zenith and stepping by ~ 0.7° elevation every 20s through 54 steps, giving, in principle, an essentially horizontal resolution at F-region heights ~ 3 km for electron density and plasma temperatures with electric field information also being available. A complete program cycle involves one scan to the north and two the south.

An example of this coordinated experiment is that for 17 September 1984 when the ray path from an NNSS satellite to Kiruna intersected the EISCAT ionospheric scan above Tromso at F-region heights. A preliminary analysis of the EISCAT run has produced the fan plot of electron density contours as a function of height and latitude which is presented in Fig.7. The universal times relevant to different parts of the EISCAT scan are shown at the top of the diagram while the track of the intersection of the ray path from the satellite is also drawn, with each 20s segment of the track labelled with the letters A to E. It can be seen that the satellite pass coincided exactly in time with the early part of the radar scan. The electron density plot shows a trough overhead with a region of steep rising gradient to the south, within which are embedded what are probably field-aligned structures with horizontal scales of the order of tens of kilometers. The electron density increases by ~ 5 times in a horizontal distance ~ 100 km. Fig.8 shows the S_4 values as a function of time computed for each 20s data window of the southbound NNSS pass. The S_4 values are low from the north through the trough minimum (A) but rise dramatically in the region of the sharp electron density gradient (B-E) indicating the presence of small-scale (100m - 1km) irregularities. Initial indications suggest that this gradient may be unstable to the $\underline{E} \times \underline{B}$ plasma instability, although further information on the electric field from the EISCAT observations is awaited, and, this, together with the temperature data will provide information on whether the larger scale irregularity structures in the density gradient represent local particle precipitation or plasma convection from elsewhere. Data from a further 15 satellite passes with coordinated EISCAT runs are now being studied.

CONCLUSIONS

An experiment, deployed in Northern Scandinavia, to study radio-wave scintillations has been described. Early results on morphology and signal-fading structure have been presented, together with initial results from a coordinated experiment using the EISCAT ionospheric radar. This shows strong scintillation, indicating the presence of small-scale irregularities, in a region of steep horizontal gradient in electron density containing large field-aligned irregularity features.

Acknowledgements

This work is supported by the Departmental Users' Programme of the Science and Engineering Research Council through the award F/QF/726 and by the United States Air Force, Air Force of Geophysics Laboratory with the grant AFOSR-84-0037.

Grateful thanks are extended to numerous individuals for assistance and advice with aspects of the

development, deployment and data analysis of this project. These include technical and research workers in both Physics and Computer Science Departments at U.C.W, staff at the Rutherford and Appleton Laboratories (and in particular Mr. A. Stevens), the director and staff of Kiruna Geophysical Institute, and members of the project monitoring committee.

REFERENCES

Aarons, J.'Global Morphology of Ionospheric Scintillations' Proc. IEEE, 70, 1982, 360-378.

Crane, R.K. 'Ionospheric Scintillation' Proc. IEEE, 65, 1977, 180-199.

Whitney H.E., Aarons, J., Allen, R.S. and Seeman, D.R., 'Estimates of the cumulative amplitude probability distribution function for ionospheric scintillations' Radio Sci., 7, 1972,1095-110.

Yeh, K.C. and Liu, C.H.'Radio Wave Scintillations in the Ionosphere' Proc. IEEE, 70, 1982, 324-360.

B>

SAT	DAY	A	ECC	INC	RAAN	ARGP	MEAN MOT	GST
20	261.619329	7391.92	0.0176	80.0015	147.8468	60.3470	4917.7813	219.6744
					0.0001	2.0213		

DATE	TIME	S	IL	IR	I4	S4L	S4R	S44	ROTS	RMSP	LONG	LAT	HGT	RHMX	CORT	ETA
840917	220128	20	27	24	24	0.000	0.000	0.000	0.00	0.0	-179.6	87.8	921	0.000	0.000	0.000
840917	220149	10	28	20	25	0.550	0.575	0.126	4.59	70.7	20.9	75.2	154	0.932	-0.005	0.051
840917	220208	8	31	24	25	0.380	0.363	0.100	8.57	26.6	20.4	74.7	160	0.927	-0.018	0.060
840917	220229	8	31	23	29	0.275	0.288	0.076	4.40	21.5	19.8	74.8	186	0.918	-0.025	0.063
840917	220247	8	31	24	29	0.302	0.275	0.083	0.71	20.5	19.2	75.2	223	0.903	-0.023	0.062
840917	220308	8	33	26	29	0.263	0.263	0.083	2.81	16.3	18.7	74.4	220	0.903	-0.044	0.069
840917	220330	8	30	29	31	0.288	0.288	0.072	5.18	24.2	17.2	75.8	317	0.896	-0.020	0.056
840917	220348	0	26	29	33	0.288	0.240	0.069	5.73	14.4	-0.1	84.1	930	0.000	0.000	0.000
840917	220409	0	31	28	35	0.174	0.151	0.083	4.83	18.8	-0.2	82.8	932	0.000	0.000	0.000
840917	220428	0	32	26	33	0.174	0.166	0.069	3.86	13.0	-0.3	81.7	933	0.000	0.000	0.000
840917	220449	0	30	29	32	0.200	0.174	0.076	5.54	15.7	-0.4	80.5	935	0.000	0.000	0.000
840917	220507	0	31	29	32	0.174	0.158	0.076	5.40	24.3	-0.4	79.4	936	0.000	0.000	0.000
840917	220528	0	26	28	33	0.209	0.138	0.066	3.85	14.1	-0.5	78.2	938	0.000	0.000	0.000
840917	220549	0	29	30	36	0.166	0.126	0.063	3.98	14.6	-0.6	77.0	939	0.000	0.000	0.000
840917	220608	0	29	30	38	0.158	0.105	0.105	3.82	11.6	-0.7	75.9	941	0.000	0.000	0.000
840917	220629	0	29	29	36	0.151	0.096	0.072	2.66	12.1	-0.8	74.7	943	0.000	0.000	0.000
840917	220647	0	28	27	37	0.138	0.110	0.072	1.50	8.7	-0.9	73.6	944	0.000	0.000	0.000
840917	220708	0	28	29	39	0.138	0.079	0.038	-0.35	10.6	-1.0	72.4	946	0.000	0.000	0.000
840917	220730	0	25	31	39	0.191	0.076	0.050	-0.14	11.2	-1.0	71.1	948	0.000	0.000	0.000
840917	220748	0	27	31	38	0.174	0.076	0.063	1.02	14.5	-1.1	70.0	949	0.000	0.000	0.000
840917	220809	0	29	31	37	0.200	0.132	0.100	-0.95	15.9	-1.2	68.8	951	0.000	0.000	0.000
840917	220828	0	31	32	34	0.182	0.166	0.105	5.72	29.1	-1.3	67.8	953	0.000	0.000	0.000
840917	220849	8	33	33	33	0.302	0.302	0.132	6.42	33.6	13.0	67.6	273	0.763	-0.186	0.077
840917	220907	8	30	33	33	0.398	0.398	0.132	-5.55	55.0	13.2	67.3	253	0.766	-0.210	0.063
840917	220928	8	30	32	32	0.347	0.363	0.126	-6.17	27.1	12.8	66.9	256	0.715	-0.195	0.075
840917	220949	0	26	30	33	0.302	0.240	0.126	-0.23	18.9	-1.6	63.0	960	0.000	0.000	0.000
840917	221008	8	24	27	34	0.363	0.347	0.145	-3.71	36.0	13.5	66.5	211	0.664	-0.229	0.083
840917	221619	17	0	0	0	0.000	0.000	0.000	0.00	0.0	-3.3	40.5	999	0.000	0.000	0.000

Data written to TPEFIL 76 DDO:
F>

Fig.1. Sample computer print-out of data obtained during a satellite pass

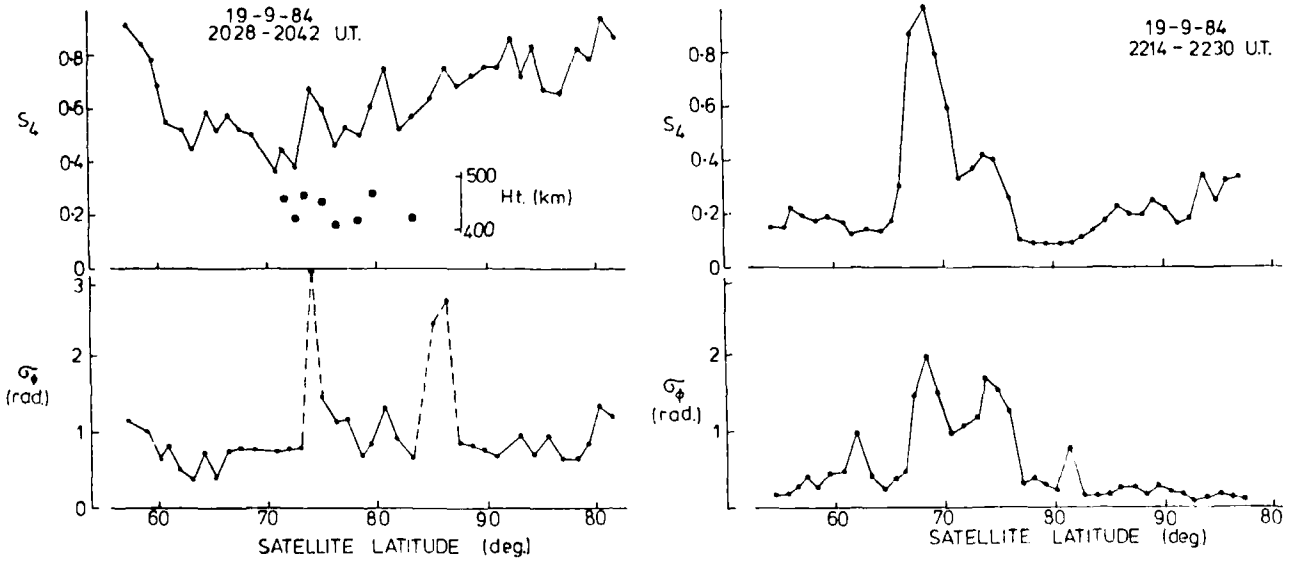


Fig.2. Examples of S_4 on 150MHz and $\sigma\phi$ values as a function of latitude for two successive satellite passes.

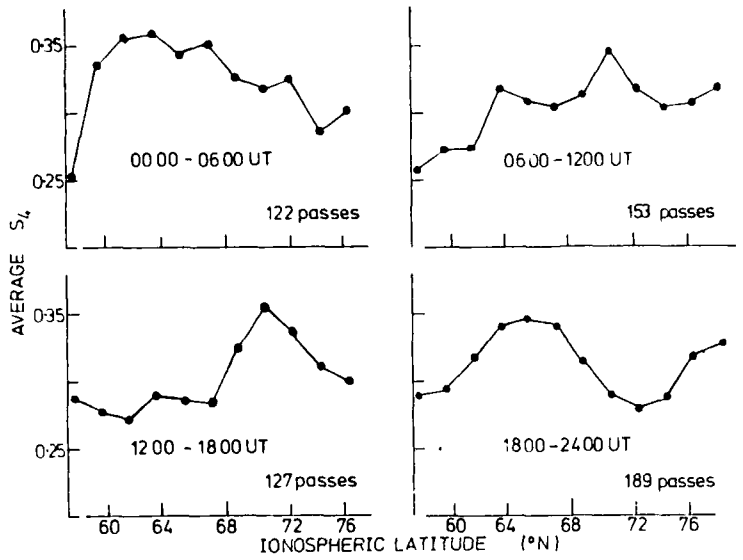


Fig.3. Average S_4 values (above a threshold value of 0.15) plotted as a function of ionospheric latitude for high-elevation passes with data divided into four time groupings throughout the day.

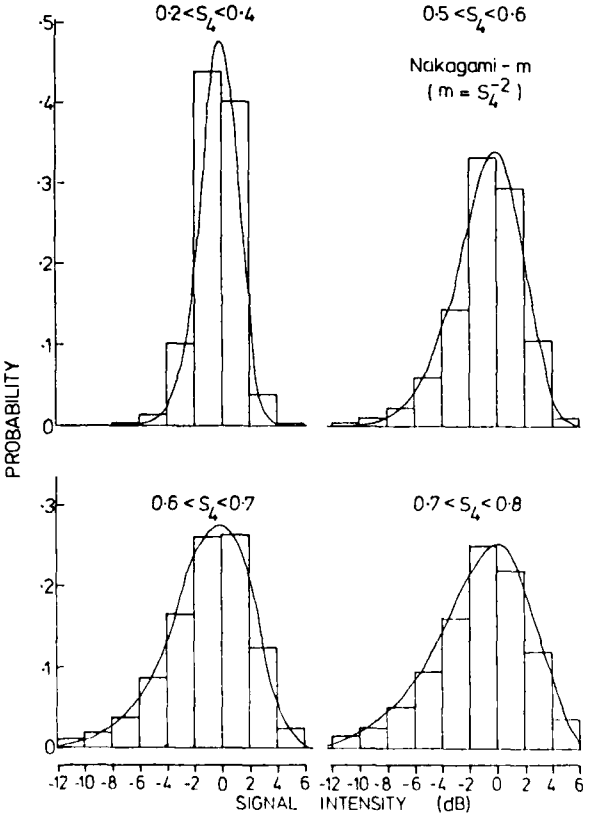


Fig.4 Probability of occurrence of different intensity levels within the fading signal for four different ranges of S_4 covering weak, moderate and strong scintillation. Also shown are the theoretical Nakagami-m distributions with $m = S_4^{-2}$.

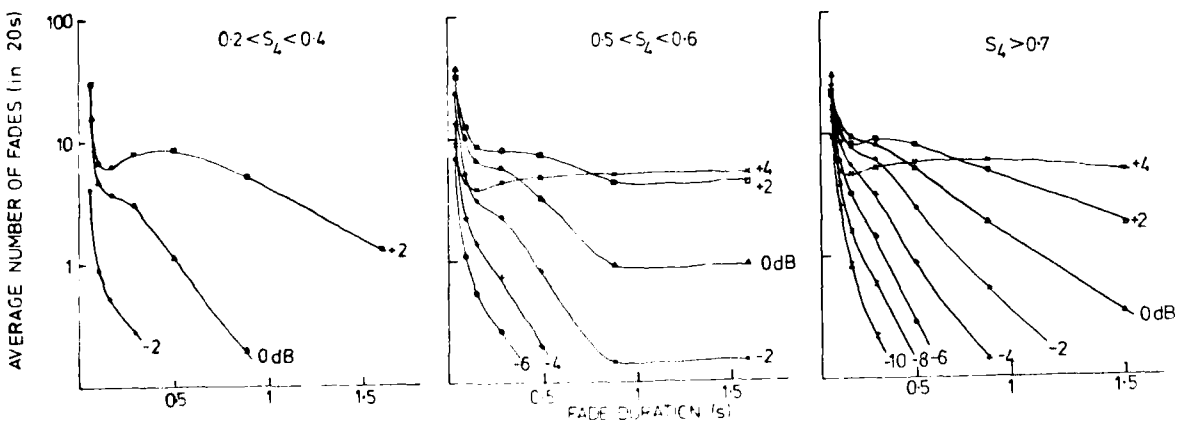


Fig.5 The average number of fades below specified threshold levels plotted as a fun tion of fade duration for three ranges of S_4 covering weak, moderate and strong scintillation.

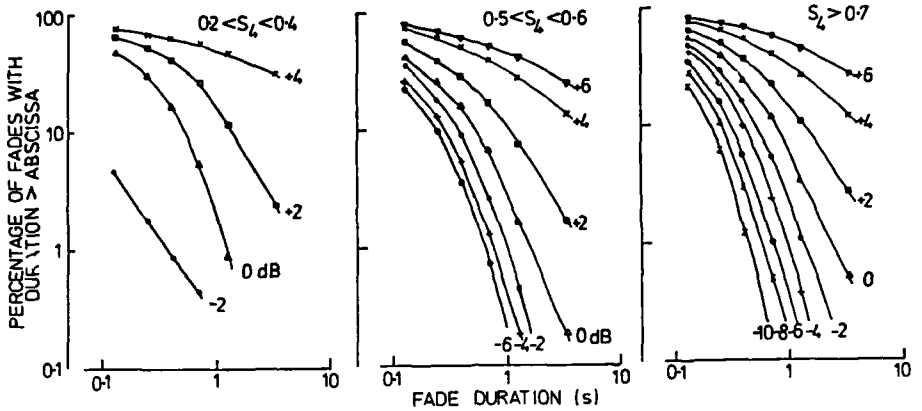


Fig.6. Cumulative plots of the percentage of fades below specified threshold levels with durations greater than a given value for three ranges of S_4 covering weak, moderate and strong scintillation.

Fig.7. Contours of relative electron density plotted as a function of height and latitude obtained from an EISCAT scan on 17 Sept.1984 at the Universal Times shown at the top of the diagram. The locus of the intersection of the ray path from an NNSS satellite to Kiruna is also shown with the times of the end points marked and each 20s segment labelled by a letter A to E

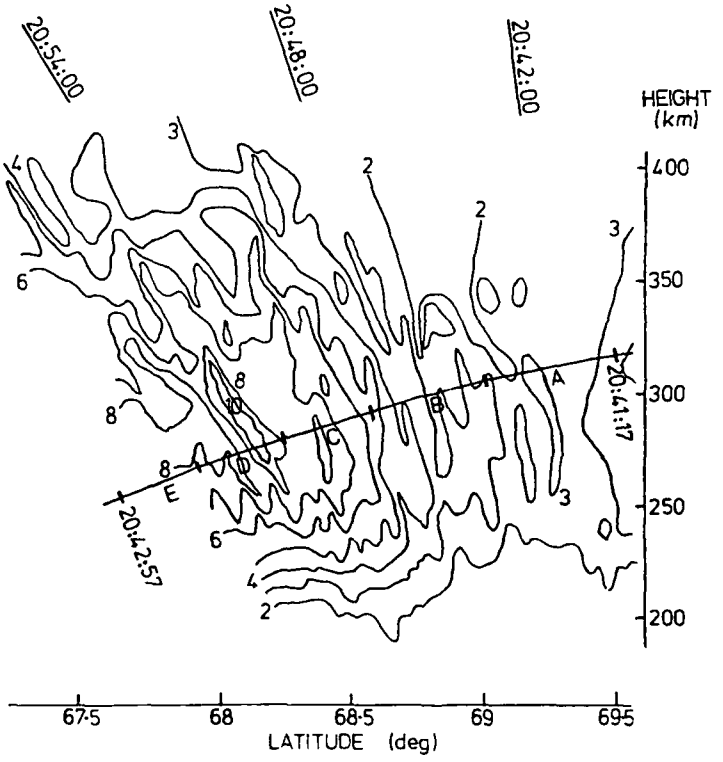
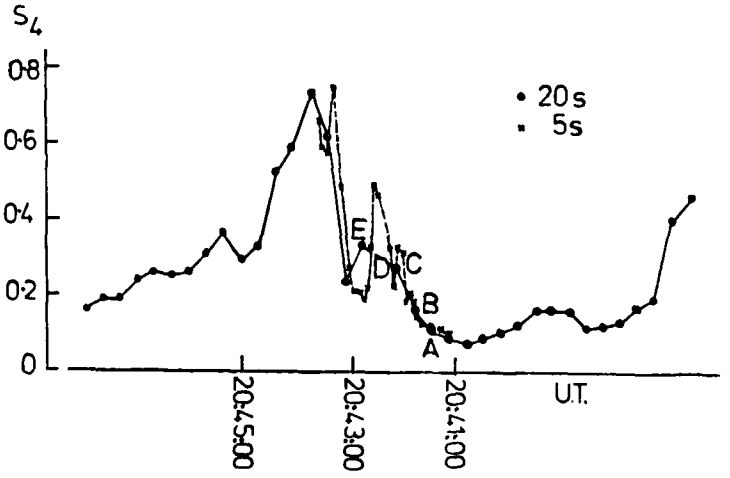


Fig.8. S_4 scintillation indices for an NNSS pass on 17 September 1984 plotted as a function of Universal Time. The values identified by letters correspond to the ray path intersections labelled in Fig.7.



DISCUSSION

A.Rodger, UK

(1) Have you investigated the temperature structure of these plasmaspheric irregularities? (2) Why do you favour electric field driven instabilities rather than Rayleigh-Taylor or temperature gradient drift instabilities; the latter has been suggested by Hudson & Kelly (1976) at the equatorward edge of the mid-latitude trough.

Author's Reply

(1) A first look at the electron temperature data for the part of the EISCAT scan showing the density gradient appears to indicate that there is also a gradient in temperature with lower temperatures towards the equator. There is some evidence to suggest structure in the temperature of a tens of kilometres scale with colder temperatures in the irregularities. This may indicate that the irregularities have convected for some time rather than having been formed locally by precipitation. (2) At this stage of the analysis we can only really speculate on instability mechanisms. However, a temperature driven instability must be considered if the westwards electric field component turns out to be small. A gravitationally driven instability is less likely in this region where the dip angle of the magnetic field is steep.

T.B.Jones, UK

(1) The high latitude ionosphere can be a very dynamic region. Your EISCAT scan took ~20 minutes; do you think the ionosphere would change appreciably during this period? (2) The comparison you presented would benefit from improved spatial and temporal resolution such as provided by the STARE/SABRE auroral radar. Do you intend to examine this type of data?

Author's Reply

(1) The change occurring during the 20 min scan will depend on the convection. In the example shown here the basic gradient does not appear to have changed appreciably betwen the successive scans, suggesting that the main flow is probably essentially normal to the plane of the scan. The scan pattern has been designed to try to get information with adequate signal to noise ratio about structures with scales close to the beamwidth resolution of the system while still covering a large enough sector for there to be a reasonable chance of scintillation occurrence on the satellite signal. This, of necessity, implies compromises in both space and time. (2) Data from an auroral radar looking at the E-layer or field lines within our scan volume would give useful additional information. However, it must be remembered that there is a minimum threshold field for the E-layer instabilities detected by the radar and, of course, the electric field may not always be mapped upwards into the F-layer. As you know, we have started recently to compare your SABRE data with our routine scintillation observations. One of the powerful features of the UHF radars is their abilities to determine regions of shear in the electric field and it will be interesting to look at scintillation occurrence in conjunction with these shears in the field.

SHF/EHF RAY BENDING

D.L. Zimmerman, G.F. Providakes, and D.L. Post
The MITRE Corporation
Bedford, MA 01730

S.H. Talbot
Rome Air Development Center
Griffiss AFB, NY 13441

ABSTRACT

This paper reports on the ray bending expected for narrow-beam satellite links in the atmosphere. Satellite communications terminals in the upper latitudes frequently operate at low elevation angles with high gain antennas. These antennas produce narrow beams that pass through the atmosphere at low terminal-to-satellite elevation angles for communication with geostationary equatorial satellites. The propagation paths experience ray bending caused by earth curvature and a decrease in atmospheric refractivity with altitude. Unless these effects are properly accounted for, acquisition and tracking problems can occur.

Ray bending was found to vary from about 0.1° for 10° elevation angles to about 0.75° for 0° elevation angles under standard atmospheric conditions. Bending was found to be nearly independent of frequency in the SHF/EHF (20 GHz to 50 GHz) region. Warm high-humidity areas tended to produce more bending.

Based on this study, potential problem areas, including tracking and spatial acquisition, are discussed for satellite systems. The authors propose using elliptic reflectors and analytic prediction of ray bending to minimize adverse effects of ray bending.

INTRODUCTION

The future direction of satellite communications is toward higher link frequencies, higher data rates, and wider geographic dispersion of ground stations. The higher link frequencies allow greater antijamming capability. Higher frequencies and larger antennas also allow higher data rate transmission with a lower probability of interception. Some of the consequences of this evolution will be terminals located in regions that require very low antenna elevation angles. The terminals will use high gain antennas, up to 70 dB (35-ft parabolic at 45 GHz), to communicate with equatorial satellites. The narrow beams associated with these high gain systems make them very sensitive to atmospheric propagation disturbances. A potential problem to overcome is initial spatial acquisition of the satellite and continued tracking under narrow beamwidth and low elevation angle conditions. More complications would arise if the atmospheric ray bending were changing with time. Further complications are caused by increased atmospheric attenuation at low elevation angles.

For example, assume that we are trying to spatially acquire a geostationary satellite located over the Atlantic Ocean at 30°W longitude from Umanak, Greenland (52°W longitude, 71°N latitude). The earth coverage contours in figure 1 indicate a 5° elevation angle for this situation. If the antenna is initially open-loop pointed according to the ephemeris data base, the computed elevation angle may turn out to be too low. As shown in figure 2, the Earth's atmosphere has bent the propagation path concave downward.

Atmospheric bending becomes important only when the bending is comparable to or greater than the antenna beamwidth. Figure 3 shows standard atmospheric bending for various elevation angles. For the example above, figure 3 gives a yearly average of 0.2° downward bending for 5° elevation angles. Suppose we have a 15-ft diameter parabolic antenna receiving a 20-GHz downlink. This antenna has a 3-dB beamwidth of 0.2° (0.1° from center to 3-dB point). If we point the antenna at 5° rather than 5.2°, the resulting off-axis reduction in link strength would be 15 dB. Beginning an antenna acquisition step scan from the 5° point and stepping the elevation angle in 0.05° increments, so as to get within 1 dB of maximum strength, would result in a seven-step search before acquisition. These steps are 5.00, 4.95, 5.05, 4.90, 5.10, 4.85, and 5.15. Consequently, up to seven times the nominal acquisition time might be needed. Configurations with higher frequencies, larger antennas, or lower elevation angles would result in even greater acquisition time. One approach to this problem would be to start searching from the anticipated yearly average bending. Figure 4 shows the 3-dB beamwidth for various antenna diameters and operating frequencies. The horizontal line illustrates a typical 5° elevation angle ray bending of 0.2°. It is seen that millimeter wave systems are a concern even for antenna diameters in the 10-foot range.

BACKGROUND

Factors affecting the direction of propagation of electromagnetic radiation through the atmosphere have been studied for years [1,2,3]. Wave redirecting or ray bending can be caused by a number of factors. For Earth terminal-to-satellite links, the gradient of the atmospheric refractive index with altitude is the most significant factor. For standard atmospheric conditions, the refractive index, n, decreases with altitude, as in figure 5. This effect is similar to the ray bending and trapping associated with fiber optics, where the radial gradient of the refractive index is designed and built into the fiber [4].

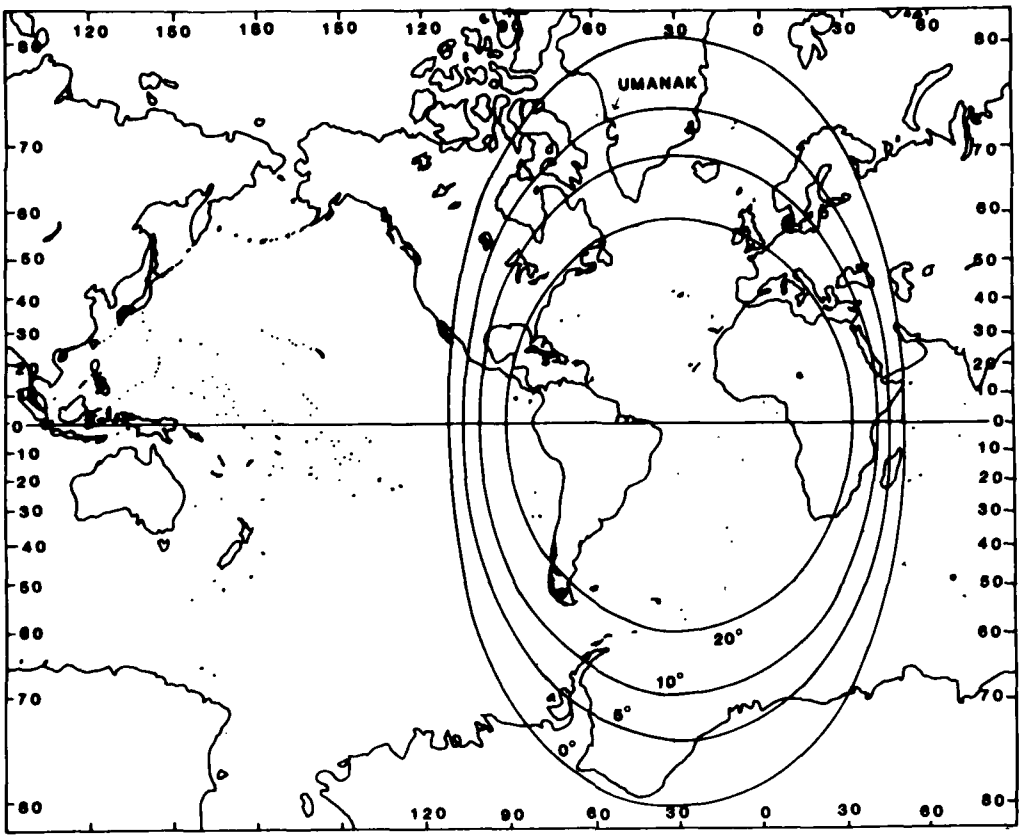


Figure 1. Earth Coverage Contours from Geostationary Satellite at 30°W Longitude for 0°, 5°, 10° and 20° Elevation Angles

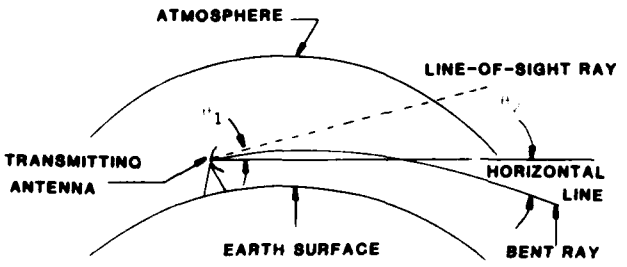


Figure 2. Geometry of Ray Bending

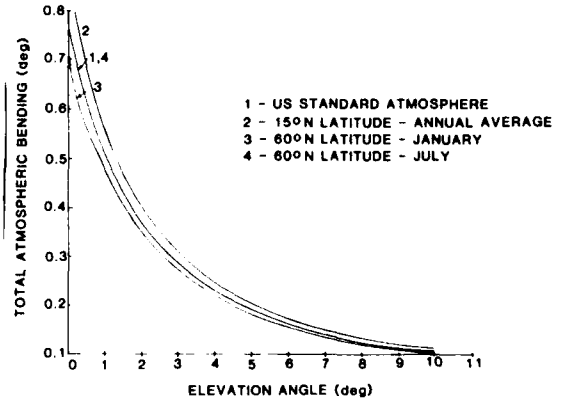


Figure 3. Atmospheric Bending Versus Elevation Angle for Various Climates With 50% Relative Humidity

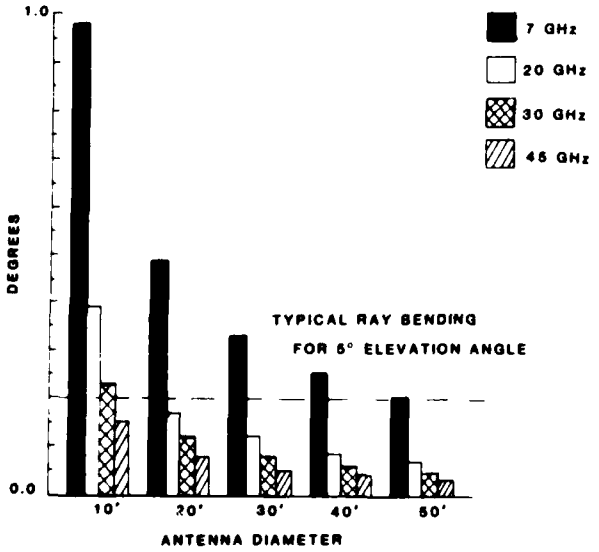


Figure 4. Antenna 3 dB Beamwidth

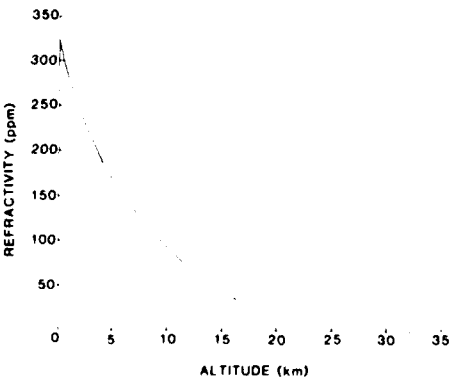


Figure 5. Refractivity Versus Altitude for U.S. Standard Atmosphere

In the case of the atmosphere, a wave transmitted horizontally will be bent toward the Earth by the natural gradient caused by the decreasing air density with altitude. As the Earth terminal-to-satellite elevation angle increases from 0°, the ray propagation path departs from horizontal. In a standard atmosphere, a ray is bent about 0.75° when launched with a 0° elevation angle and only 0.1° when launched with a 10° elevation angle (figure 2).

RAY BENDING ALGORITHM

These issues prompted us to examine the extent of the atmospheric ray bending. The following briefly describes the algorithm used to compute the ray bending. A change in the refractive index of a medium will cause a change in the direction of propagation of an electromagnetic wave. Schulkin [5] has come up with a method of approximating the total bending through the atmosphere by using atmospheric refractivity profiles. The total bending is a summation of incremental bends obtained when the atmosphere is thought of as a multilayered shell, each shell having a given refractivity, N. Schulkin's results are:

$$\tau_n \cong \sum_{k=0}^{n} \frac{2(N_k - N_{k+1})}{(\theta_k + \theta_{k+1})}$$

where

$$\theta_{k+1}(\text{mrad}) \cong \sqrt{\theta_k^2(\text{mrad}) + \frac{2(r_{k+1} - r_k) \times 10^6}{r_k} - 2(N_k - N_{k+1})}$$

τ_n = total bending in milliradians

N_k = refractivity of kth layer in parts per million $(n-1) \times 10^6$

θ_k = angle of ray entering the kth layer (milliradians)

r_k = distance to the kth layer from Earth's center

As the transmitted ray penetrates the second layer of new refractivity, usually smaller in value than the first layer, the ray is bent toward the earth. For elevation angles of 10° or less, this method allows errors of no more than 1.0%.

The atmospheric refractivity is computed by using the Millimeter Wave Propagation (MPM) program developed by Liebe [6] and modified for our application. The MPM program computes the refractivity, dispersion, and attenuation of the atmosphere based on the atomic and molecular spectra of the atmospheric constituents. The pressure and temperature effects on the spectra are included in the analysis. The MPM program includes "standard" atmospheric profiles for tropical, temperate, subarctic, and arctic regions for January and July.

RAY BENDING AND ATTENUATION

Figure 6 shows the amount of ray bending calculated for the arctic and subarctic winter and summer with 100% humidity. Limited bending and attenuation variations occur in arctic regions since cool air cannot hold much water vapor. Using the refractivity contours in Bean and Dutton [3], we can compute the ray bending over a 12-month period for several locations in North America. The contours for Washington, DC, are shown in figure 7. These contours are used in the ray bending algorithm to develop the seasonal changes in ray bending. Figure 8 shows the ray bending for 2-week intervals when a ray is launched at 5° above the horizon. If data were available over time durations of the order of minutes and hours, larger variations from the nominal bending would be experienced. The antenna must be able to track these changes if the bending variation is comparable to or greater than the beamwidth. One possible solution to alleviate this problem is to use an elliptic antenna with a broad vertical and narrow horizontal beamwidth. This antenna would maintain high gain but be less sensitive to elevation bending variations. It would also offer low profile installation advantages.

The MPM program also computes dispersion and attenuation for rays propagating through the atmosphere. Figures 9 and 10 show the computed attenuation along a bent ray for winter and summer at arctic and subarctic latitudes. The plots show the attenuation for 1°, 5°, and 10° elevation angles, for link frequencies of 20 GHz to 50 GHz. The MPM program can compute the atmospheric propagation from 1 GHz to 1000 GHz.

Figures 3 and 6 show that total ray bending is greatest on low elevation links. Also, more bending occurs in regions of high water vapor content. The wetter air has a larger refractivity and results in a larger overall refractivity gradient from the Earth's surface to space.

Ray bending is weakly dependent on frequency since refractivity values vary only slightly with frequency. Figure 11 shows that at most a 0.45 parts per million (ppm)

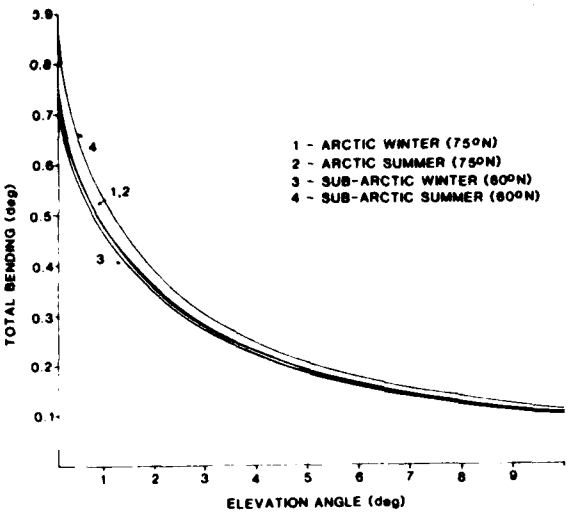


Figure 6. Bending Versus Elevation Angle for High Latitudes (100% Humidity)

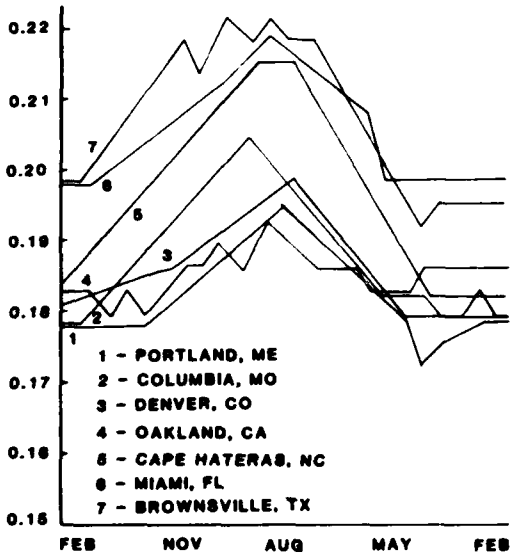


Figure 8. Seasonal Ray Bending for 5° Elevation Angle

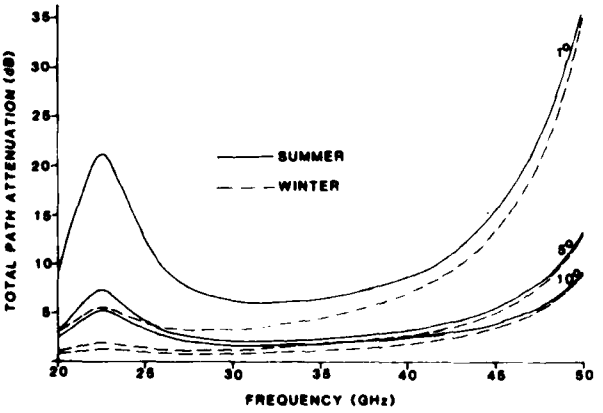


Figure 10. Atmospheric Attenuation at 1°, 5°, and 10° Elevation Angles for Subarctic Summer and Winter (60°N, 100% Humidity)

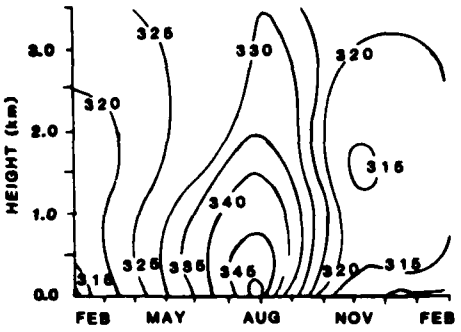


Figure 7. Seasonal Variation of Normalized Refractivity N_o for Washington, DC (ref. 3)

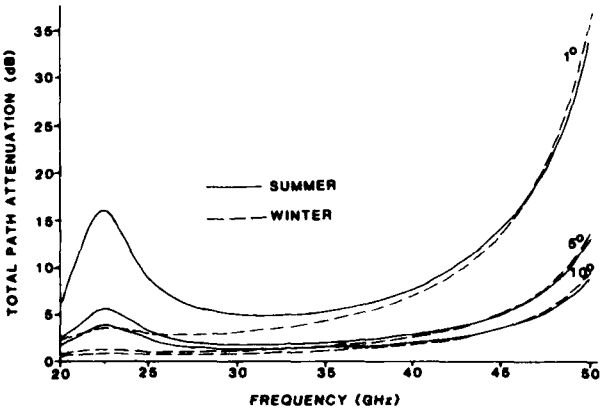


Figure 9. Atmospheric Attenuation at 1°, 5°, and 10° Elevation Angles for Arctic Summer and Winter (75°N, 100% Humidity)

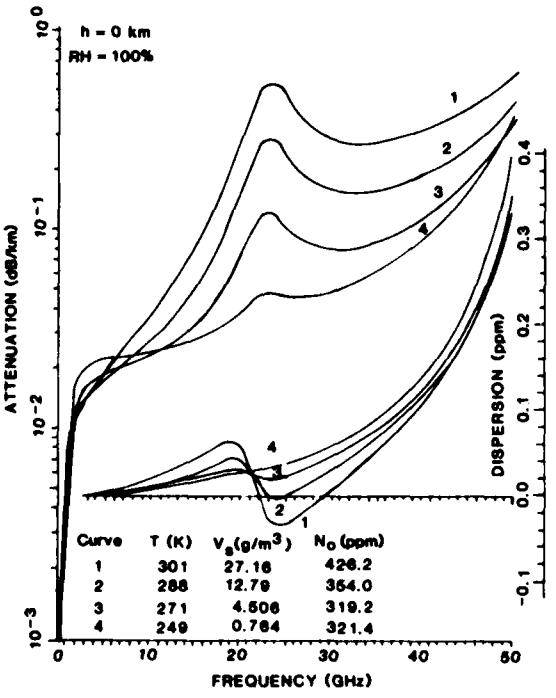


Figure 11. Specific Attenuation and Refractive Dispersion Over Frequency Range 0.5-50 GHz for Saturated Sea-Level Air (1013 mbars Pressure) at Four Temperatures (ref. 6)

change in refractivity occurs from 1 GHz up to 50 GHz. This limits the differential bending to less than 0.1% of the nominal ray bending over this frequency range. A terminal's parabolic reflector can thus support widely varied uplink and downlink frequencies without mispointing caused by differential bending. Figure 11 includes the increased dispersion and attenuation due to water vapor around 22 GHz. Again note that higher temperatures allow more water vapor at a given relative humidity (RH) and therefore more attenuation and dispersion.

Figures 12 and 13 show the strong effect of water vapor at 22 GHz. Even though 50% humidity exists in both cases, the higher yearly average temperatures at 15°N latitude allow a greater mass of atmospheric water vapor than occurs during summer months at 60°N. For a 22 GHz link at a 5° elevation angle, an 8-dB yearly average attenuation occurs at 15°N and 50% humidity. For the high attenuation summer months at 60°N and 50% humidity, the attenuation averages only 4 dB. This difference shows the low path attenuation advantages that may be available to high latitude terminals operating low elevation angle satellite links below 35 GHz.

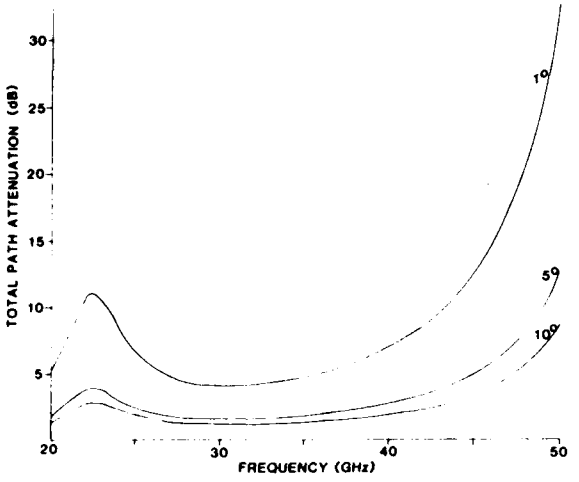


Figure 12. Attenuation Versus Frequency for Subarctic Summer (60°N, 50% Humidity)

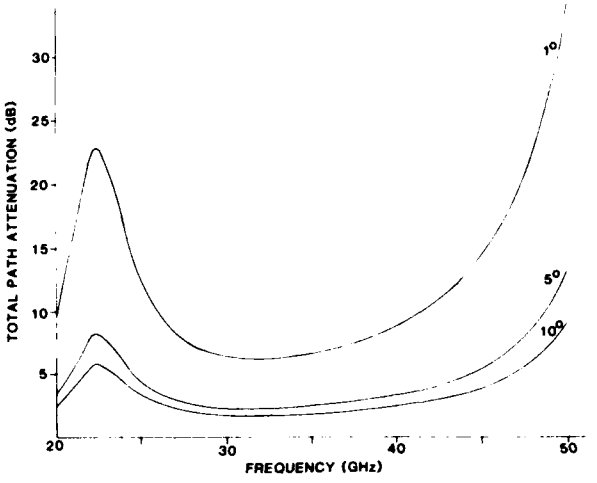


Figure 13. Attenuation Versus Frequency for Yearly Average Tropics (15°N, 50% Humidity)

CONCLUSIONS

Ray bending phenomena occur on different scales. The rays bend up to about 1°, depending on the elevation angle and local refractivity profile. The rays can undergo seasonal bending changes of about ±20% from the nominal bending on a 2-week basis. Shorter time durations will lead to larger variations. Dispersion effects occur on scales of less than 0.1% of nominal bending and, except for very wideband systems, seem negligible. The greatest ray bending seems to be dominated by the local long-term climate. A knowledge of ray bending can greatly reduce signal acquisition times for terminals with small beamwidths and low elevation angles.

Nominal ray bending is predictable (figure 3) and can be used to precorrect initial open loop antenna pointing to reduce acquisition time. Rapid changes in bending may cause acquisition as well as tracking difficulties. Further short-term statistics must be gathered to assess the magnitude of this effect. One solution to this problem is to use an elliptic antenna that has a broader vertical beamwidth less sensitive to bending changes.

The low water vapor content of the upper latitudes offers advantages to low elevation angle communications for geosynchronous satellites below 35 GHz. Higher link availability may also be possible because the rain occurs with less frequency and intensity.

Further research is needed to determine the statistics of short-term ray bending effects due to local and rapidly changing weather conditions. However, at present, we believe that ray bending will not affect satellite link performance significantly if simple and prudent precautions are taken.

ACKNOWLEDGMENT

This work was sponsored by U.S. Air Force Advanced Space Communications Project 1227, Airborne Terminal Technology.

REFERENCES:

1. Smyth, J.B., and Trolese, L.G., "Propagation of Radio Waves in the Lower Atmosphere," Proc IRE, Volume 35, November 1947, pp. 1198-1202.

2. Budden, K.G., Radio Waves in the Ionosphere, Cambridge, England: Cambridge University Press, 1961.

3. Bean, B.R., and Dutton, E.J., Radio Meteorology, New York: Dover Publications, 1968.

4. Verdeyen, J.T., Laser Electronics, Englewood Cliffs, NJ: Prentice-Hall, 1981.

5. Schulkin, M., "Average Radio-Ray Refraction in the Lower Atmosphere," Proc IRE, Volume 40, May 1952, pp. 554-561.

6. Liebe, H.J. "An Atmospheric Millimeter Wave Propogation Model," DTIC AD A139154 (NTIA 83-137), December 1983.

DISCUSSION

N.C.Gerson, US

This paper attempts to examine the influence of tropospheric refractivity gradients on the trajectory of EHF-SHF waves. The computations were based upon the work of Bean and Dutton. However, Bean and Dutton's values have been superseded by a more recent and more comprehensive evaluation of surface refractivities and vertical refractivity gradients as a function of month for many locations over the globe. By using the mean values given by Bean and Dutton, the full extent of the angular deviation of the ray trajectory is considerably subdued. It should be recognized that the more recent results are also based upon radiosonde data. Since the water vapor sensor of the radiosonde is sluggish, and since radiosonde data are sampled at altitudes specified for meteorological interests, even the new results are conservative and show more gradual and subdued vertical refractivity gradients than actually exist. Thus, in any redetermined evaluation of EHF-SHF refraction errors, appropriate caveats indicating the limitations of the results must be indicated. In any event, a recomputation based upon a more extensive data base is warranted.

Author's Reply

I agree that a larger data base is needed to evaluate rapid bending angle changes while a terminal is tracking a satellite to evaluate tracking performance. For initial open loop pointing acquisition, however, more recent data would probably not result in significant reductions in spatial acquisition time. Only an averaged bias angle offset would be practical in terminal applications.

E.H.F. PROPAGATION MEASUREMENTS ALONG SATELLITE-EARTH PATHS IN THE CANADIAN HIGH ARCTIC

I. Lam and J.I. Strickland
Communications Research Centre
Department of Communications
Ottawa Canada

SUMMARY

Experimental observations of the signal received from an EHF satellite beacon were made during June, August and December 1984 from a location in the Canadian arctic north of 80°N. The satellite follows an inclined orbit and as a result is visible for about eleven hours per day. During this period the elevation angle to the satellite varies between zero and approximately 21 degrees. The pointing of the receive antenna towards the satellite was achieved through computer-controlled tracking with a resolution better than 5 % of the antenna beamwidth.

Throughout the experimental period the changes in atmospheric conditions were mainly due to movement of air masses rather than diurnal variations in ground heating. Also, even though fog from the nearby ocean occurred frequently, there were no significant amounts of precipitation during the experiment.

The results of the experiment indicate that signal fading occurs almost entirely at elevation angles less than approximately 5 degrees. Variations in the median signal level are presented as a function of the elevation angle. Also included are cumulative distributions of received signal level computed for various elevation angles.

In general, the experimental results correlate well with the atmospheric conditions. The fading was found to be less severe in the winter than either spring or summer.

INTRODUCTION

Communications via geostationary satellites to locations in the Canadian arctic are generally provided along propagation paths at low elevation angles. Previous studies have shown that the effects of tropospheric fading become increasingly severe as the elevation angle decreases [1,2] and this results in the need for earth stations with large diameter antennas. The studies also suggested that fading is less severe in the winter months and in the more northern locations [1,3].

There are additional problems for locations in the high latitude region beyond approximately 80°N as these locations are inaccessible to any geostationary satellite. Adequate communications coverage to these areas, however, may be provided by using a set of satellites placed in inclined orbits.

To study the characteristics of EHF propagation in the high latitude region a series of observations were made from a location in the Canadian arctic of the signal strength received from an EHF beacon on board the Lincoln Experimental Satellite (LES-8). Some of the experimental results are presented in this paper.

EXPERIMENTAL ARRANGEMENT

The 38 GHz signal source originated from the LES-8 satellite which follows an orbit inclined at 23 degrees and has an orbital period of approximately 24 hours. The receiver was located north of 80°N where the satellite was accessible for 11 hours per day. As observed from the ground the satellite describes a figure eight pattern the upper half of which is visible (Figure 1). The range in azimuth is less than 6 degrees and the elevation varies between zero and 21 degrees. The physical horizon of the receiving antenna was limited to approximately 0.9 degrees by a ridge located at a distance of 3.5 km from the experimental site.

The receiver employed a 0.45 m diameter Cassegrain antenna with a 3 dB beamwidth of 1.2 degrees. The antenna position was controlled by a small computer using look angles previously computed from the satellite orbital elements. By using precision optical encoders a resolution of better than 0.05 degrees was achieved. Thus, variations in the received signal level will be due to propagation effects or errors in pointing the spot-beam antenna of the satellite.

The received signal was monitored by a phase-lock receiver with a loop bandwidth of 1 KHz and the receive margin was better than 30 dB. The signal level was digitally recorded by sampling the receiver AGC voltage at 0.42 s intervals.

OBSERVATIONS

In order to study the propagation characteristics under a variety of atmospheric conditions, three sets of measurements of the received signal level were made over a period of several months.

The first set of measurements was made in early spring from May 27 to June 6 and the second set was made during the summer from August 1 to August 8. The sun was always above the horizon during these periods. The third set of measurements was made during the winter from November 30 to December 7 when the sun was always below the horizon.

A plot of the signal level recorded on December 1 is shown in Figure 2. The vertical scale is normalized so that 0 dB represents the median signal level at an elevation angle of 20 degrees. The results shown in Figure 2 are typical for days when little fading is observed. The signal was acquired as the satellite rose above the horizon and in a few seconds the signal was within several dB of its median level. As the elevation angle increased, the fading amplitude decreased rapidly. At the same time the average signal level increased slowly with the elevation angle due to reduced atmospheric absorption. For elevation angles above 5 degrees a stable signal persisted with virtually no fading. Finally, a decrease in average signal level and increase in fading amplitude were observed as the satellite set. On this day, the weather was clear and calm with an average surface temperature of -30°C.

Since fading was observed typically only at low elevation angles, the signal characteristics during these periods are examined in more detail. Figure 3 shows the signal level observed on December 1 as the satellite rose to an elevation angle of 10 degrees. The peak-to-peak fading amplitude was approximately 10 dB while the satellite was between 1 and 2 degrees but was rapidly reduced to less than 3 dB for elevation angles above 3 degrees. These observations are typical of those observed during December and parts of May.

Low-angle fading was generally more severe during June and August. This is illustrated in Figure 4 which shows the signal level recorded on August 7. Very rapid signal fading with a peak-to-peak amplitude of greater than 25 dB was observed while the satellite elevation was between 1 and 2 degrees. At the same time the increased atmospheric absorption associated with the warmer and more humid August atmosphere resulted in much lower signal medians at low elevation angles compared with the December measurements. Despite the more severe fading at low angles, a relatively steady signal resumed as the satellite rose above approximately 3 degrees. On this day, the atmosphere was clear with only isolated high clouds and the average temperature was approximately 0°C.

RESULTS

The experimental data were processed by grouping into 1 degree increments in elevation angle.

Median Signal Level

The median signal level observed for each range of elevation angle for all data is shown in Figure 5. Each point represents the median level observed during one day. The spread in median level at the higher angles amounts to 3 dB or less but increases to more than 6 dB for angles below 2 degrees.

The dotted line in Figure 5 shows the median level calculated from all the data combined. The median levels calculated separately for each of the three sets of data show very good agreement except for the August data at angles below 2 degrees, where the median level is some 2.5 dB less than the May and December values.

The solid line in Figure 5 shows the effect of atmospheric absorption due to oxygen and water vapour calculated for a surface water vapour density of 5 g m^{-3} and including the effect of regular refraction. The line forms an approximate upper bound on the experimental signal medians. Thus, the distribution of signal levels in the presence of fading is very non-symmetrical about its mean, in agreement with a model of low-angle fading based on focussing and defocussing by curved refractive index discontinuities in the atmosphere [4].

Signal Level Distributions

Cumulative distributions of the received signal level are computed separately for each set of data. The distributions for the May-June and August data are shown in Figures 6 and 7 respectively on Rayleigh coordinates. The distributions for the two sets of data are consistent with each other for angles above 3 degrees.

At lower angles more fading and lower signal medians were observed in August. These characteristics are consistent with the seasonal changes in the arctic atmosphere. During early spring in May and June, the ground was snow covered. The average surface temperature varied between -10 and 0°C and there were occasional snow flurries. The weather was also highly variable, with clear skies changing to heavy fog, caused by the nearby ocean, within thirty minutes. Although the same variability in weather conditions existed in August, the ground was no longer snow covered and the average surface temperature had risen to between zero and 10°C. This allows for a higher water vapour content in the atmosphere and accounts for the lower signal medians. During both periods there were no significant diurnal ground heating effects as the sun never set.

Figure 8 shows the signal level distributions for the December data. Much less fading was observed even for the low elevation angles when compared with the spring and summer data. This is further illustrated in Table 1 which summarizes, for each set of data, the fade depths relative to the median (50 %) levels which are not exceeded for 99 % of the time. This will be referred to as the 99 % fade depth in the following. For the 1-2 degrees range, the 99 % fade depth in winter was 5.6 dB compared with a value of approximately 14.5 dB for both spring and summer. The sun never rose in December and the average surface temperature was approximately -35°C. This period includes days which were clear and calm and those with gusty winds and blowing snow.

TABLE 1. Comparison of the fade depths which are not exceeded for 99 % of the observation time. The fade depths are measured relative to the median levels for the respective ranges in elevation angle.

Measurement Period	99 % Fade Depth (dB)		
	1-2°	2-3°	3-4°
May - June	14.3	8.0	5.1
August	14.5	6.8	3.7
November - December	5.6	3.3	2.2

Figure 9 shows a comparison between the amount of fading observed on the best (December 1) and worst (June 5) days which were selected based on visual inspection of the signal level plots. The respective 99 % fade depths for the best and worst days are 5.8 dB and 17 dB for the 1-2 degrees range. The signal level distribution for the 1-2 degrees range on the worst day corresponds to that of a Rayleigh distribution.

CONCLUSIONS

A comparative study of EHF propagation characteristics was made based on experimental data collected during spring, summer and winter in the Canadian high arctic. Several conclusions may be drawn from the results.

Very little fading was observed when the satellite was above 5 degrees elevation angle. For all elevation angles, the fading was less severe in the winter than in the spring and summer. No precipitation attenuation of the signal was observed.

From a propagation point of view, a communications system operating at EHF for high latitude coverage appears feasible. Based on the data collected, the fade depth relative to the median for 99.99 % of the observation time is less than 6.5 dB for elevation angles exceeding 5 degrees.

ACKNOWLEDGMENTS

The authors wish to acknowledge with thanks the support received from the Lincoln Laboratory in providing part of the receiver and operating the LES-8 satellite, the assistance of personnel in the Canadian Armed Forces and the Atmospheric Environment Service, and the advice and help of colleagues and support staff at the Communications Research Centre, Ottawa.

REFERENCES

[1] K.S. McCormick, R.L. Olsen and L.A. Maynard, "Amplitude fading of satellite communications signals at SHF", NATO/AGARD Conf. Proc., 197, pp.18/1-8, 1972.

[2] R.V. Webber and K.S. McCormick, "Low elevation angle measurements of the ATS-6 beacons at 4 and 30 GHz", Annales des Telecom., vol.35, no.11-12, pp.494-500, Nov-Dec 1980.

[3] J.I. Strickland, R.L. Olsen and H.L. Werstiuk, "Measurements of low angle fading in the Canadian arctic", Annales des Telecom., vol.32, no.11-12, pp.530-535, Nov-Dec 1977.

[4] J.I. Strickland, "Site-diversity measurements of low-angle fading and comparison with a theoretical model", Annales des Telecom., vol.36, no.7-8, pp.457-463, 1981.

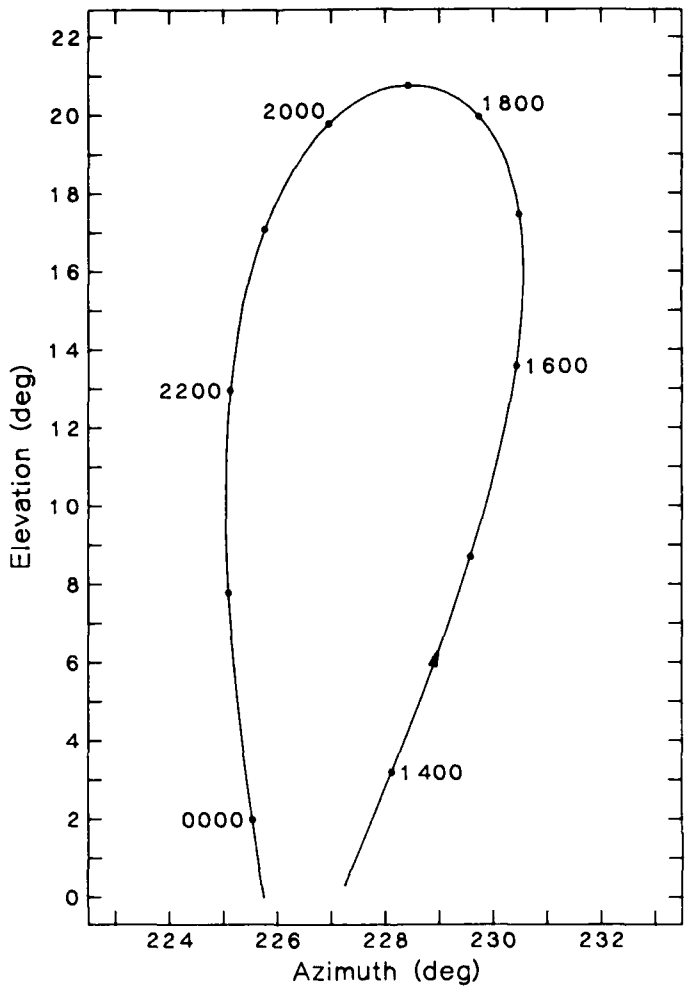


Figure 1. LES-8 satellite look angles on May 30, 1984. The numbers indicate Universal Time.

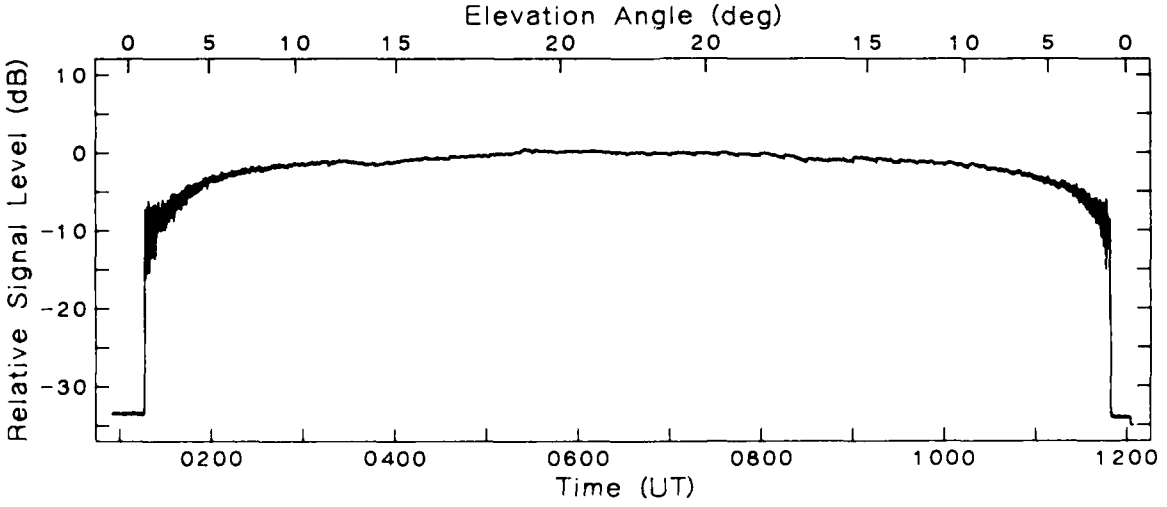


Figure 2. Received signal level on a day when little fading was observed (December 1, 1984).

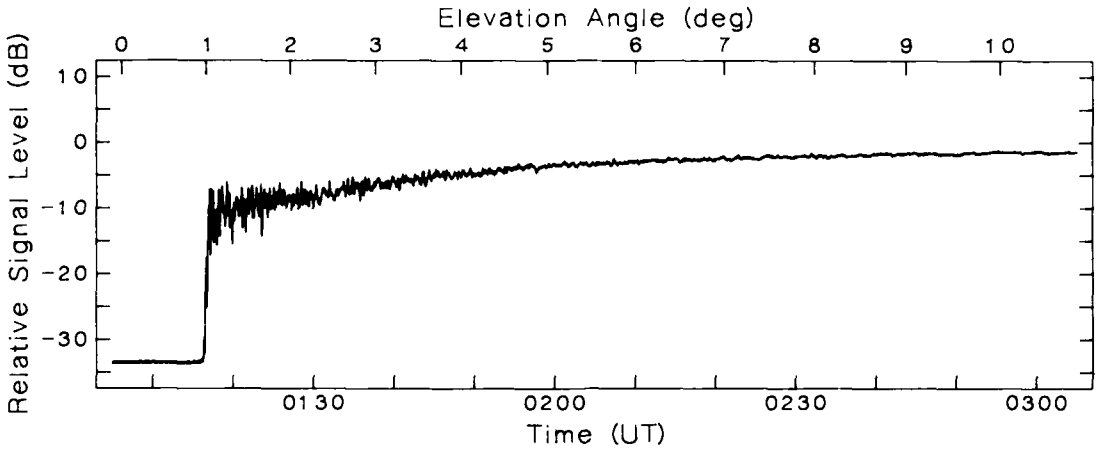


Figure 3. Signal level observed as the satellite rose on December 1, 1984.

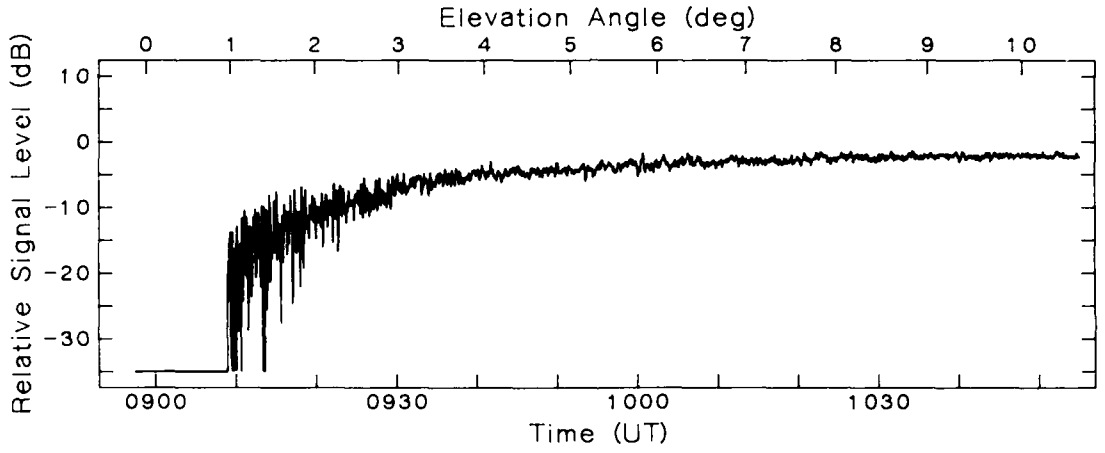


Figure 4. Signal level observed as the satellite rose on August 7, 1984.

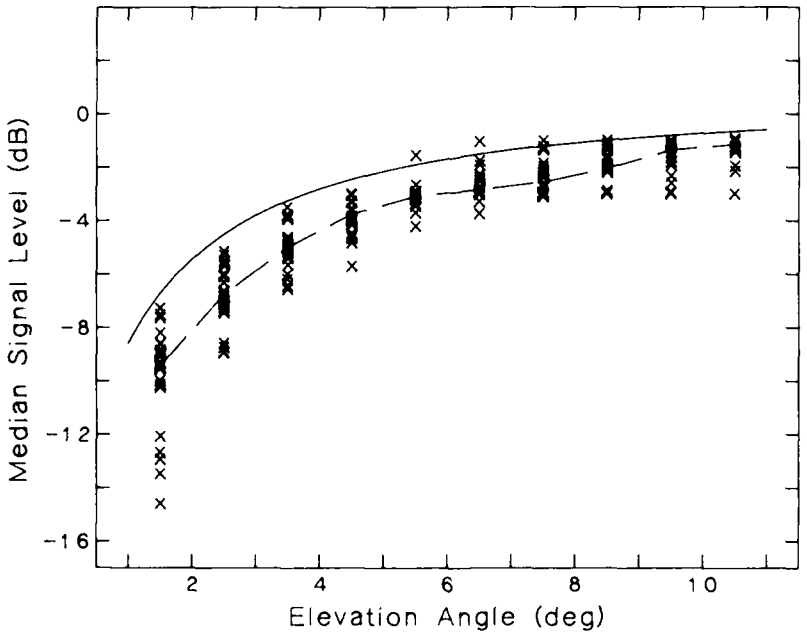


Figure 5. Median signal level versus elevation angle. Each point represents the median level during one day.

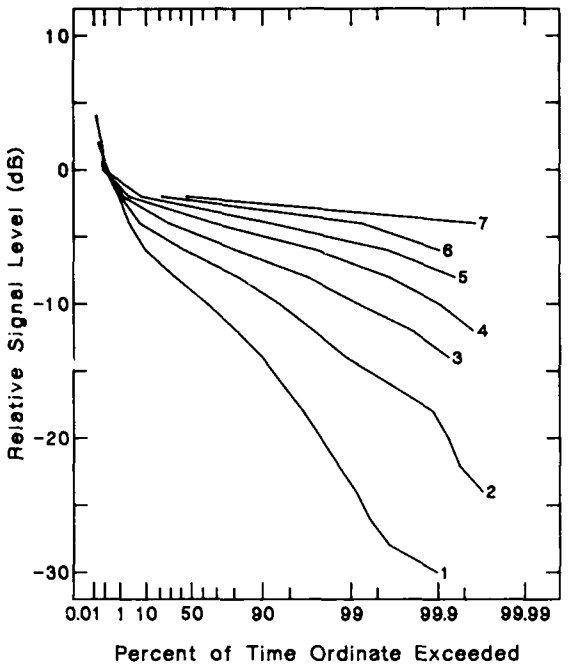


Figure 6. Cumulative signal level distributions for the May-June measurements computed for each 1 degree increment in elevation angle. Subscript 1 indicates elevation angle 1-2 degrees, etc.

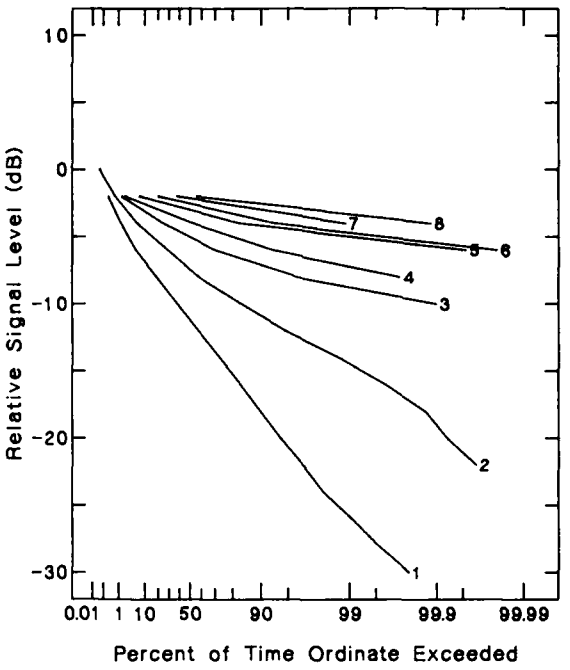


Figure 7. Cumulative signal level distributions for the August measurements computed for each 1 degree increment in elevation angle. Subscript 1 indicates elevation angle 1-2 degrees, etc.

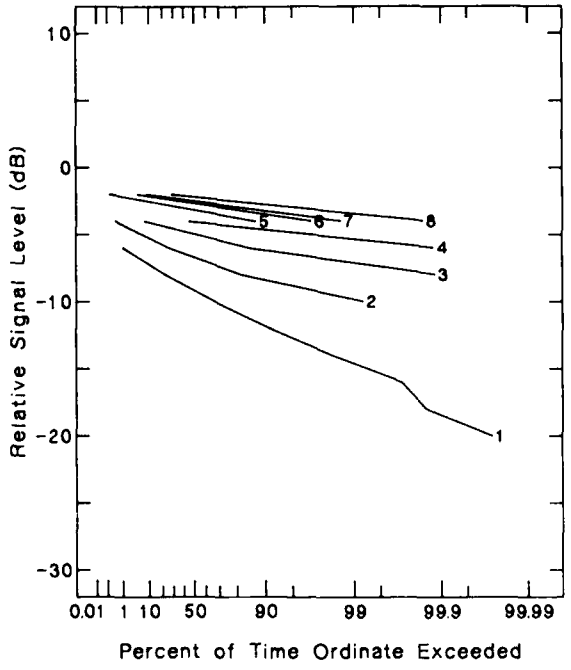


Figure 8. Cumulative signal level distributions for the December measurements computed for each 1 degree increment in elevation angle. Subscript 1 indicates elevation angle 1-2 degrees, etc.

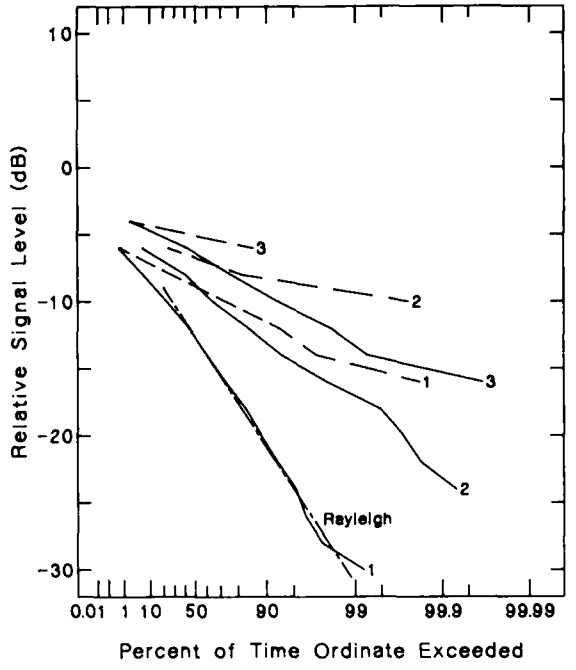


Figure 9. Comparison of the signal level distributions for the best (broken line) and worst (solid line) days. Subscript 1 indicates elevation angle 1-2 degrees, etc.

DISCUSSION

N.C.Gerson, US

The results show a large scatter in signal strengths, for summer, when the angle to the satellite is below an elevation angle of 5°. I would like to suggest that this result is caused by superrefractive conditions in the troposphere which permit multipath conditions to exist.

J.Borgholthaus, US

(1) Was a radiosonde employed to determine refractivity profile? (2) Why wasn't multipath considered as a mechanism for the low angle fading?

Author's Reply

(1) No, refractivity profiles are not available. (2) Atmospheric multipath is certainly one possible cause of the low-angle fading observed. However, fading could also have resulted from a focussing or defocussing effect due to a non-linear refractivity profile.

V.J.Coyne, US

(1) Since you do not believe conditions are appropriate for reflections from the snow as a source of multipath fading — what mechanism do you propose? (2) If the multipath is due to refractive discontinuities — what are the scales and intensities involved?

Author's Reply

(1) As I mentioned earlier, both atmospheric multipath and signal focussing and defocussing are possible mechanisms. (2) Since refractivity profile data is not available, it is not easy to give a good estimate of the values of these parameters. Reference [4] does give a good discussion of low-angle fading due to a defocussing effect with relevant ray-tracing results.

SUMMARY OF SESSION III

Propagation Aspects of HF Communication

by

Dr P.Cannon
Session Chairman

The six papers in this session covered a wide range of subjects applicable to a better understanding and better design of HF communications systems.

The papers by Darnell, and Goutelard and Caratori concerned themselves with how improved equipment and system design could overcome the problems associated with high latitude propagation. In particular, Darnell discussed the structure of a networked system designed to overcome the low availability often associated with mobile operation at high latitudes. Goutelard presented data, collected over sub-auroral, auroral and transauroral links, which was displayed in terms of 3-dimensional plots of power, frequency and time. He showed how these plots could be applied to modems designed to operate in these disturbed regions.

The papers by Quegan, Milsom and Herring, and Damboldt addressed ionospheric modelling and its success, or otherwise, at high latitudes and also at middle latitudes during disturbed periods. Quegan described the requirements for a high latitude model and substantiated his view that a theoretical model based upon an understanding of the physics, rather than a statistical model, is feasible. He also stated his belief that more work is needed to obtain a better understanding of ionospheric irregularities and their modelling, since these are extremely important for HF radar planning.

Damboldt compared median characteristics of the F2 region with measurements taken at a specific location in northern Germany. He showed that the average experimental values agreed well with the predicted values, but that the spread of values is high, especially at times of high geomagnetic activity. During the period of reported observations disturbed conditions occurred one night in two.

The paper by Cormier, Tichovolsky and Greenwald described a new experiment set up between Thule and Goose Bay in order to measure azimuthal and elevation arrival angles of HF skywave signals. The experimental technique graphically demonstrated the variability of the auroral ionosphere. Results which show the apparent movement of the transmitter due to ionospheric perturbations from the quiet state, were discussed.

Hunsucker, Delana and Wang also compared theoretical predictions with experimental results. This paper, however, described comparison of experimental HF field strength measurements against FCC predicted field strengths. The paper concluded that in auroral Alaska the received signal strength is dominated by D-region absorption and that, in future, FCC standard curves include some variability for auroral latitudes.

IONOSPHERIC MODELLING AND HF RADIO SYSTEMS AT HIGH LATITUDES

S. Quegan, J.D. Milsom and R.N. Herring

GEC Research Laboratories,
Marconi Research Centre,
Great Baddow,
Chelmsford.
Essex, CM2 8HN, U.K.

SUMMARY

Successful planning of HF radio systems to operate at high latitudes requires some means of predicting ionospheric morphology, both as regards ambient electron density and ionospheric irregularities causing backscatter. Because of the presence of several physical processes, and the sparsity of data, reliable statistical models are not easily constructed. However, increasing knowledge of the processes operating, and the availability of powerful computers, makes the construction of physically-based numerical models of ionospheric structure a viable proposition. This paper describes such a model at a fairly advanced stage of development, and gives examples of calculated electron densities. The ingredients and shortcomings of the model will be described, together with the steps to be taken to account for ionospheric irregularities, and to allow us to predict HF system performance using ray-tracing.

1. INTRODUCTION

An essential element in the successful planning of high frequency (HF) radio systems, which exploit the sky-wave mode of propagation, is a description of the ambient ionospheric electron density. At low and mid-latitudes statistically based models have been developed over many years and are an integral part of many long term prediction programs. As we move polewards, however, the ionosphere becomes less regular and predictable, and reliable statistical models are not easily formulated. Certain large-scale structures are normally observed, e.g. the mid-latitude trough, the auroral oval and the central polar cap, but they show large scale variations as a function of local time, universal time, season, and geomagnetic activity.

Despite these modelling difficulties it is highly desirable to have some predictive/forecasting capability at higher latitudes. Important features of the ionosphere such as the trough are absent from the commonly used ionospheric maps. It is therefore extremely difficult to estimate the behaviour of radio systems which rely on ionospheric support from these areas. Robust communication systems which employ low speed digital modulation may usually be able to cope on high-latitude circuits. However, there is a noticeable trend towards more sophisticated signalling waveforms such as frequency-hop and direct sequence spread spectrum. The performance of these wideband systems at high latitudes is difficult to estimate at the present time. Communications engineers require advice on the group time delay structure of sky-wave channels, active elevation angles and the effect of small scale ionospheric irregularities. Radar engineers who are investigating the use of over-the-horizon-radars (OTHR) need additional information about possible bearing errors. These are some of the reasons for our interest in this subject.

2. IONOSPHERIC PROCESSES AT HIGH AND LOW LATITUDES

The difference between the low and high-latitude ambient ionosphere can be attributed to four causes:-

(1) an electric field, $\bar{E}_m$, of magnetospheric origin, which dominates plasma electrodynamics at high latitudes, but is negligible at low latitudes;

(2) the presence of intense particle precipitation in regions surrounding the magnetic poles;

(3) the different character of ionosphere/magnetosphere flows at low and high latitudes;

(4) the separation of the geographic and geomagnetic poles, giving rise to universal time (UT) effects which are only significant at high latitudes.

All four causes are interrelated, and can be understood qualitatively as consequence of the single process of magnetospheric convection. Such an overall magnetospheric view is not initially necessary to explore their effects on the ionosphere.

The magnetospheric electric field, $\bar{E}_m$, is always present at high latitudes, but shows considerable variation in magnitude and morphology. In its most frequently-observed form, it drives a two-celled convection pattern of plasma with anti-sunward flow within the polar cap and return flow at lower latitudes (figure 1). The size and orientation of the cells is time-dependent and correlated with solar wind parameters. This electric field is the major cause of the complexity of the high-latitude ionosphere, since even a steady-state field causes plasma to follow a great variety of trajectories.

The electric field also affects other important determinants of ionospheric behaviour, due to the dynamic coupling between the ion and neutral species. Ion drag dominates neutral gas dynamics at ionospheric heights at high latitudes, leading to very large thermospheric winds. These have important consequences for the formation of the mid-latitude trough and the key ionospheric parameters NmF2 and hmF2. Collisional heating alters the crucial reaction rates of O^+ with O_2 and N_2, affecting the time-scales of ionospheric decay. Current systems in the lower ionosphere cause Joule heating, and provide a source of plasma instabilities leading to irregularities in the electron density.

Particle precipitation is continually present in belts (the auroral zones) surrounding the magnetic poles. The dayside and nightside precipitation regions have different characteristics, the dayside region (the 'cleft' or 'cusp') typically involving particles of lower energy than on the nightside. There is rapid variation in the intensity and location of precipitation. Precipitating particles provide a source of ionization and ionospheric hearing, though this latter effect is of less consequence than the Joule heating caused by the intense electric fields observed in the auroral zones.

Flows between the ionosphere and magnetosphere provide a slow-acting but important influence on F-region behaviour. At high latitudes there is a continuous outflow of plasma into the magnetosphere (the polar wind) which affects the dayside F-region only slightly, but is a significant factor on the nightside, particularly as regards trough formation and depth. At low to mid-latitudes, a diurnal ebb and flow of plasma between the ionosphere and magnetosphere occurs. This stabilises the behaviour of NmF2, depressing dayside values and sustaining nightside values.

The separation of the geographic and geomagnetic poles adds a further complication to high-latitude ionospheric behaviour. Solar illumination is under geographic control, while $\bar{E}_m$ and particle precipitation are under geo-magnetic control. The rotation of the magnetic pole around the geographic pole causes the convection pattern to show significant universal time (UT) variation when viewed from the geographic frame. Figure 2 illustrates how complex plasma trajectories may be (in the geographic frame) as a result of the combined co-rotation and magnetospheric electric fields, when UT effects are taken into account. This diurnal dependence of convection causes plasma densitites and dynamics to exhibit UT variations, on top of variations due to changes in $\bar{E}_m$ and particle precipitation boundaries. This UT dependence has been modelled and experimentally verified (Sojka et al, 1982). The ensuing complexity, coupled with the lack of extensive data coverage, explains the difficulties of developing useful empirical models of the high latitude ionosphere.

3. IONOSPHERIC MODELS

3.1 Empirical Models

Empirical models of the low and mid-latitude ionosphere have been developed over many years. Ionospheric maps of this type are presently recommended for use by the CCIR for long-term sky-wave system planning. Due to the smoothing of data which occurs in the preparation of the CCIR maps some important features of the high-latitude ionosphere are badly represented. The absence of such features affects the usefulness of propagation predictions in an unknown way. Such features have been shown to be important for propagation studies by, e.g. Lockwood (1980), who demonstrated that HF propagation in the sub-auroral ionosphere is significantly affected by the dynamics of the mid-latitude trough.

In recent years imporvements have been made in the quality of empirical ionospheric models at high-latitudes. Within UK the best high latitude empirical model is the over-smoothed CCIR representation.

3.2 Theoretical Models

Parallel with the systematisation of observations has been a growing theoretical understanding of the processes determining ionospheric phenomena.

The incorporation of the physical processes into a mathematical model of the ionosphere is achieved through the Navier-Stokes equations, as they apply to a dilute plasma. An important consequence of the momentum equation is that the dynamics of the plasma can be separated into two decoupled components, one perpendicular and one parallel to the magnetic field. Motion perpendicular to the magnetic field (Hall drift) is driven by electric fields, and has the property that plasma sharing a field-line at one time continues to share a field-line as time progresses. One therefore has the concept of tubes of plasma drifting under the influence of electric fields. Motion along the field-lines is driven by diffusion under the influence of gravity, pressure gradients, collisions and electrostatic forces.

The modelling procedure involves following the behaviour of individual tubes of plasma as they make discrete time-steps along the trajectories determined by the electric field. Figure 3 depicts a model convection pattern based on ion drift measurements by the Atmosphere Explorer satellites (Spiro et al, 1978). Other models in current use are based on the work of Heppner (1977) (e.g. Figure 1) and latterly, data from the Dynamics Explorer satellites. Figure 4 depicts the tubes of plasma travelling along convection paths. At each step it is necessary to supply a description of the neutral atmosphere, including its velocity. We must also supply a description of photochemical production and loss, effects due to particle precipitation, ionosphere/magnetosphere flows and a temperature profile. Neutral atmosphere dynamics are closely coupled to the ion dynamics (Fuller-Rowell et al, 1984), but full coupling of a neutral atmosphere and ionosphere model is probably too time-consuming for routine modelling of the ionosphere. The ionosphere is also not too sensitive to changes in the neutral gas dynamics, and relatively crude models give realistic results. Models for particle precipitation must be based at present on crude time average estimates. Polar wind flows have been measured by Isis-2 (Hoffman and Dodson. 1980) and also by Dynamics Explorer. However, the recent observations of the importance of outflowing O^+ at disturbed times (e.g. Klumpar et al, 1984) should be taken into account. Temperature profiles can be calculated assuming known energy inputs, though at present empirical profiles are used in the work described here.

At each step, the coupled continuity and momentum equations are solved along the magnetic field line, to produce the time-dependent behaviour of the electron density along a convection path. The global structure of the ionosphere is then constructed by following the behaviour of many such tubes of plasma, to produce a dense set of point descriptions of the ionosphere, and interpolation between points.

The behaviour of an individual tube of plasma along a convection path (path 6 of Figure 3) is illustrated in Figure 5 (after Quegan et al, 1982). Figure 6 shows a cut across the 0200/1400 LT meridians for a large set of convection paths. The mid-latitude trough and auroral belt show up clearly in the nightside results, with a much narrower auroral spike on the dayside. Topside results are of no direct relevance to propagation modelling, but show the occurrence of the light-ion trough on both day and night sides. It should be noted that the results displayed in Figures 5 and 6 are calculated with UT effects being excluded. It is clear that a set of meridional cuts such as that displayed in figure 6 will allow interpolation to any desired grid, to be used in propagation modelling.

4. IONOSPHERIC IRREGULARITIES

Small scale ionospheric irregularities should be regarded as a permanent feature at high-latitudes. The irregularities have an elongated shape due to the anisotropy of the plasma conductivity, caused by the earth's magnetic field. These structures may be pictured as elongated cyclinders aligned with the magnetic field direction. Rino et al (1983) have also established the existence of sheet-like irregularities associated with the auroral electrojets. Irregularities exist over a wide range of heights within the F-region but are also present within a few kilometres of the E-region peak.

There are various theories regarding the mechanisms by which the E and F-region auroral zone irregularities arise. These include direct production of particle precipitation, plasma instabilities and turbulent mixing by electrostatic fields (Fejer and Kelley, 1979). The relationships between large and small-scale irregularities have been discussed by Kelly et al (1982) and Vickrey and Kelley (1982), who also show that plasma convection will distribute irregularities throughout the polar cap. However, many questions remain unanswered (Rino et al, 1983), and it is at present not possible to construct a demonstrably consistent picture of plasma dynamics and plasma irregularities at high latitudes. In the mean time progress has been made, most notably by T. J. Elkins (1979), who suggests that the temporal and spatial characteristics of the irregularities can be deduced from the observations of sporadic-E and spread-F which are made by vertical incidence ionospheric sounders.

Some means of modelling the effect of these features on radio systems is a definite requirement. In particular the influence of auroral "clutter" on HF radar systems can be particularly damaging.

5. AURORAL CLUTTER IN RADAR SYSTEMS

In this section the need for an improved model of the background ionosphere and the embedded irregularities is emphasised with regard to a particular class of radio system, the HF radar.

Although the volumetric backscattering cross-section of auroral clutter is small by microwave radar standards, the volume of the resolution cell for HF systems tends to be very large. Consequently a system may find it difficult to discriminate between target and clutter on the grounds of signal strength alone. Often it is possible to resolve target and clutter by Doppler analysis, but in the case of auroral clutter drift velocities are spread over a wide range so as to obscure even fast aircraft.

Three conditions must be satisfied if auroral clutter is to be observed:

i) A part of the ionosphere containing irregularities must be illuminated by the radar.

ii) The ray direction must be orthogonal, or near orthogonal, to the Earth's magnetic field in the region of the ionospheric irregularities.

iii) The volumetric backscattering cross-section of the irregularity region must be sufficiently high.

Given suitable raytracing methods and a good ionospheric model searches for condition (ii) can be performed, (see Figure 7). Quite apart from any clutter amplitude calculation,this raytracing exercise would be useful,for it tends to be the orthogonality condition which determines the spatial distribution of clutter.

Until more auroral clutter amplitude data is gathered and interpreted the most satisfactory method of estimating the morphology is probably to use the sporadic-E and Spread-F statistics but to scale the occurrence probability in terms of a volumetric scattering cross-section in the style of Elkins, (1979). In due course more data will become available from well calibrated radars, and empirical auroral clutter models will follow. Progress on our physical understanding of the production of irregularities, and their relation to overall plasma dynamics, can also be expected. A long-term aim would be a consistent model where the irregularity structure was a consequence of the magnetospheric processes determining the ambient ionospheric morphology.

An estimate of the vector velocity of ionospheric irregular may be deduced from the high-latitude plasma convection pattern which plays such an important role in the theoretical modelling technique (Kelley et al, 1982). Additional information on the spectral spreading is available separately from the work of Greenwald (1981).

6. RAYTRACING THROUGH IMPROVED IONOSPHERIC MODELS

For middle-latitude sky-wave paths it has proved possible to make optimum working frequency predictions using simple raytracing procedures. In many cases simple transformations are used sc that oblique path performance can be inferred from vertical incidence critical frequencies.

The complexity of the high-latitude ionosphere demands that a more rigorous approach be adopted in the prediction method. For HF radar system planning it will be necessary to use three dimensional raytracing programs so that the troublesome clutter geometries and off great-circle propagation can be identified. These raytracing procedures are now well established and can be readily applied to a general ionospheric structure.

7. CONCLUSIONS

Within the last decade substantial advances have been made in our under standing of processes in the high-latitude ionosphere. The development of a theoretical model is feasible and would have immediate applications in HF sky-wave calculations. A better quantitative description of high-latitude ionospheric irregularities is needed for HF prediction work and in particular for HF radar system planning.

REFERENCES

Elkins T. J. 'Radio Auroral Effects at HF', Boston College, (1979)

Fejer B. G., and Kelley, M. C., 'Ionospheric Irregularities' Rev. Geophys. Space. 18, 401, (1980).

Fuller-Rowell T. J., Rees, D., Quegan, S., Bailey, G. J., and Moffett, R. J. 'The Effect of Realistic Conductivities on the High-Latitude Neutral Thermospheric Circulation', Planet. Space Sci. 32, NO. 4, 469 (1984).

Greenwald, R. A., 'Doppler Spectral Characteristics of High Latitude Ionospheric Irregularities; Effects on HF Radars', RADC-TR-81-93, (1981)

Heppner, J. P., 'Empirical Models of High-Latitude Electric Fields', J. Geophys. Res. 82, 1114, (1977).

Hoffman, J. H., and Dodson, W. H., 'Light Ion Concentrations and Fluxes in the Polar Regions During Magnetically Quiet Times', J. Geophys. Res. 85, 626, (1980)

Kelley, J. C., Vickrey, J. F., Carlson, C. W., and Torbet, R. 'On the Origin and Spatial Extent of High-Latitude F-Region Irregularities', J. Geophys. Res. 87, 4469, (1982)

Klumpar, D. M., Peterson, W. K., and Shelley, E. G., 'Direct Evidence for Two-Stage (Bimodel) Acceleration of Ionospheric Ions', J. Geophys. Res., 89, 10770, (1984)

Lockwood, M. 'The Bottomside Mid-Latitude Ionospheric Trough', J. Atmos. Terr. Phys., 42, 605, (1980).

Quegan, S., Bailey, G. J., Moffett, R. J., Heelis, R. A., Fuller-Rowell, T. J., Rees, D., and Spiro, R. W., 'A Theoretical Study of the Distribution of Ionization in the High-Latitude ionosphere and the plasmasphere: first results on the mid-latitude trough and the light-ion trough', J. Atmos. Terr. Phys. 44, 619, (1982).

Rion, C. L., Livingston, R. C., Tsunoda, R. T., Robinson, R. M., Vickrey, J. F., Senior, C., Cousins, M. D., Owen, J. and Klobuchar, J. A., 'Recent studies of the structure and morphology of auroral zone F-region irregularities', Radio Sci. 18, 1167, (1983).

Sojka, J. J., Raitt, W. J., Schunk, R. W., Rich, F. J., and Sagalyn, R. C., Observations of the diurnal dependence of the high-latitude F-region ion density by DMSP Satellites', J. Geophys. Res, 87, 1711, (1982).

Spiro, R. W., Heelis, R. A., and Hanson, W. B., 'Ion Convection and the formation of the mid-latitude F-region ionization trough', J. geophys. Res. 83, 4255, (1978).

Vickrey, J. F., and Kelley, M. C., 'The Effects of a conducting E Layer on classical F-region cross-field plasma diffusion', J. geophys. Res. 87, 4461, (1982).

Villain, J. P., Greenwald, R. A., and Vickrey, J. F., 'HF ray tracing at high latitudes using measured meridional electron density distributions', Radio Sci. 19, No. 1, 359 (1984).

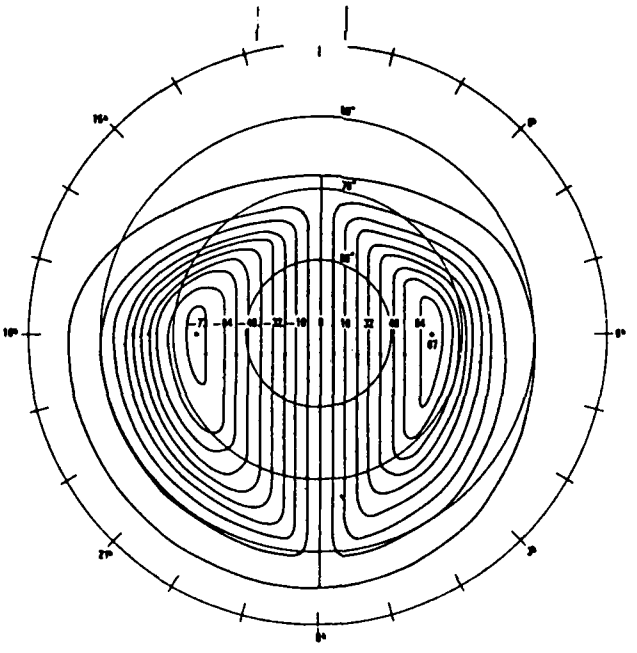


Figure 1. Two-celled model convection pattern driven by $\underline{E} \times \underline{B}$ forces (after Heppner, 1977)

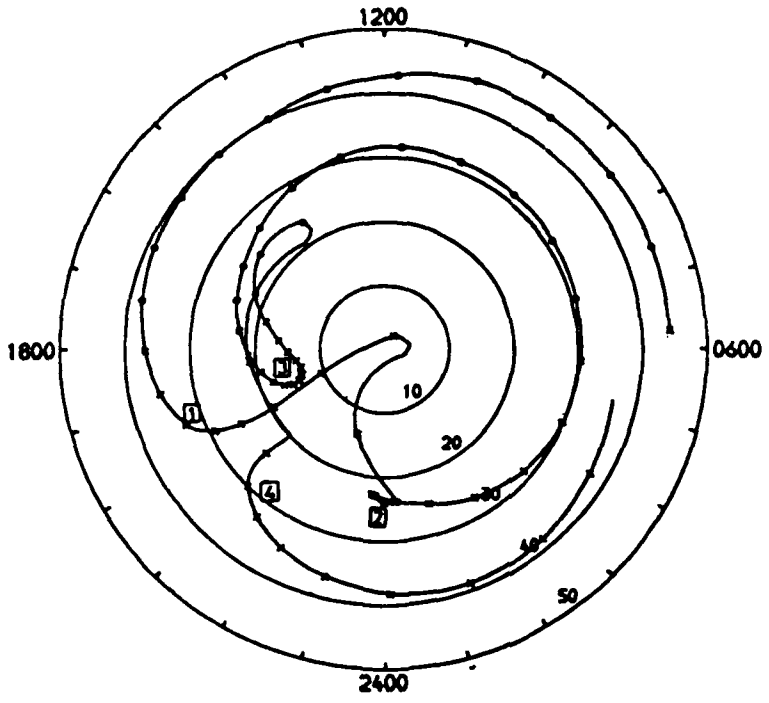


Figure 2. A plasma convection path in the geographic coordinate frame.

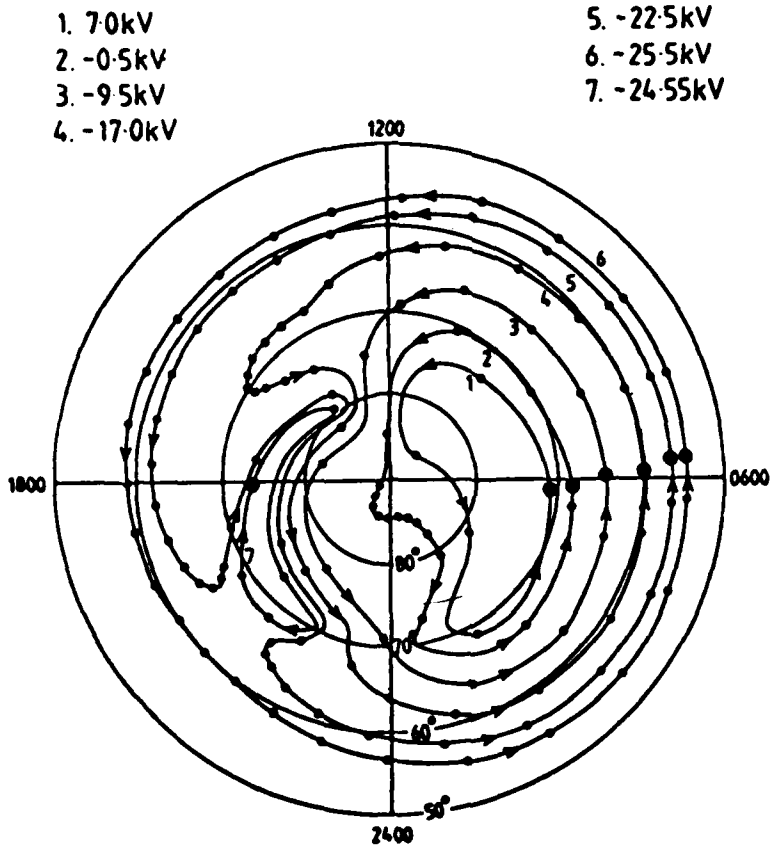


Figure 3. Example convection paths in a fixed Sun-Earth frame (UT effects neglected) (after Quegan et al, 1982). Dots on the paths indicate one hour of travel time.

PLASMA 'TUBES' USED IN THEORETICAL MODELS

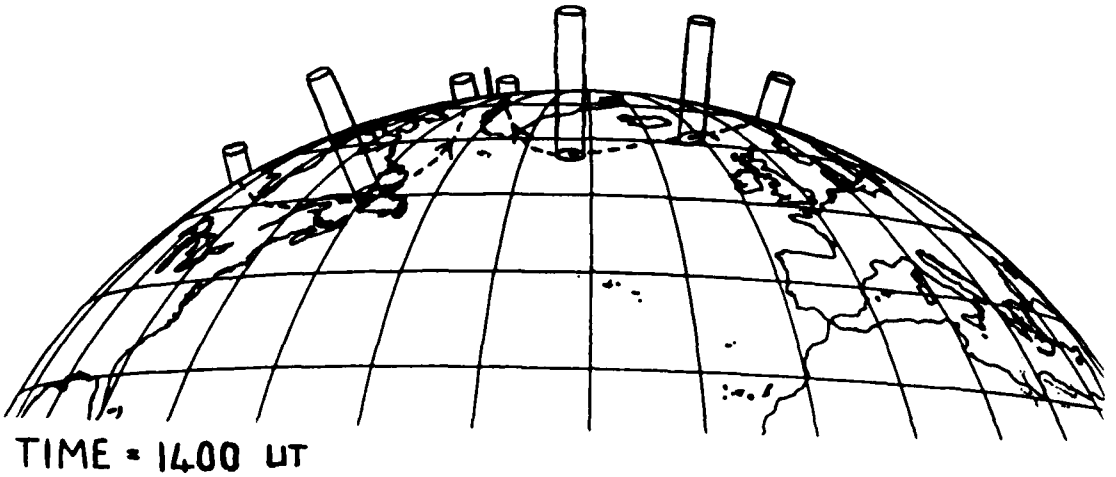


Figure 4. Illustration of the convection of tubes of plasma along trajectories determined by E x B forces.

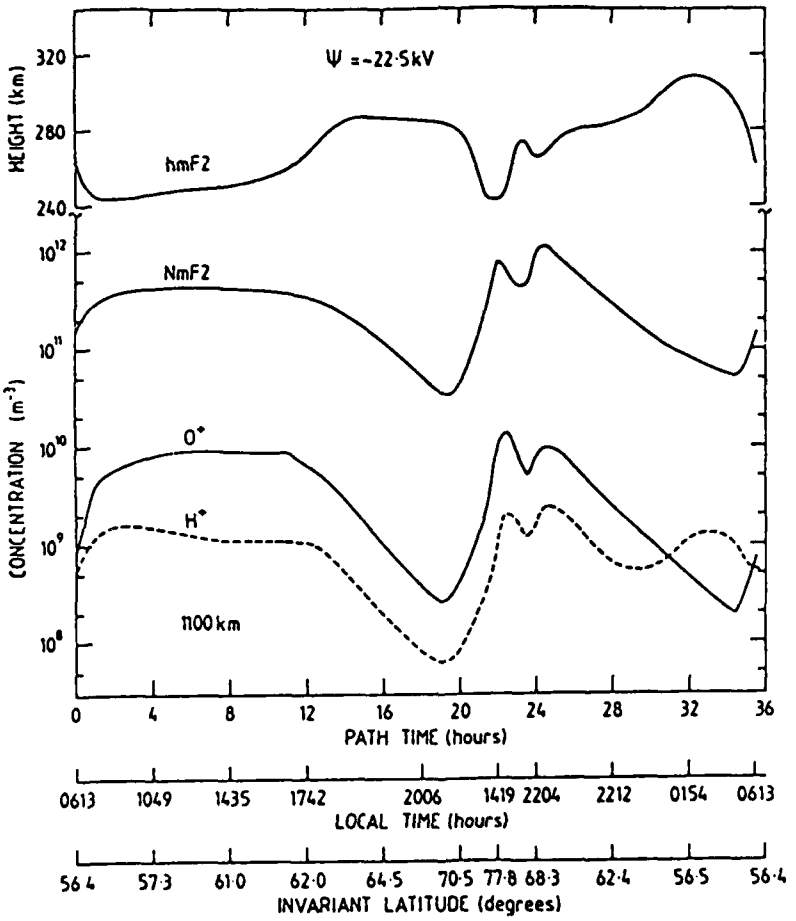


Figure 5 . Calculated variations with time (along the path) of hmF2, NmF2 and the O^+ and H^+ concentrations at 1100 km for a high-latitude tube of plasma convecting along the -22.5 kV equipotential (path 5 in Figure 3) after steady state in a day-to-day sense has been reached. The lower two scales show local time and invariant latitude (after Quegan et al 1982).

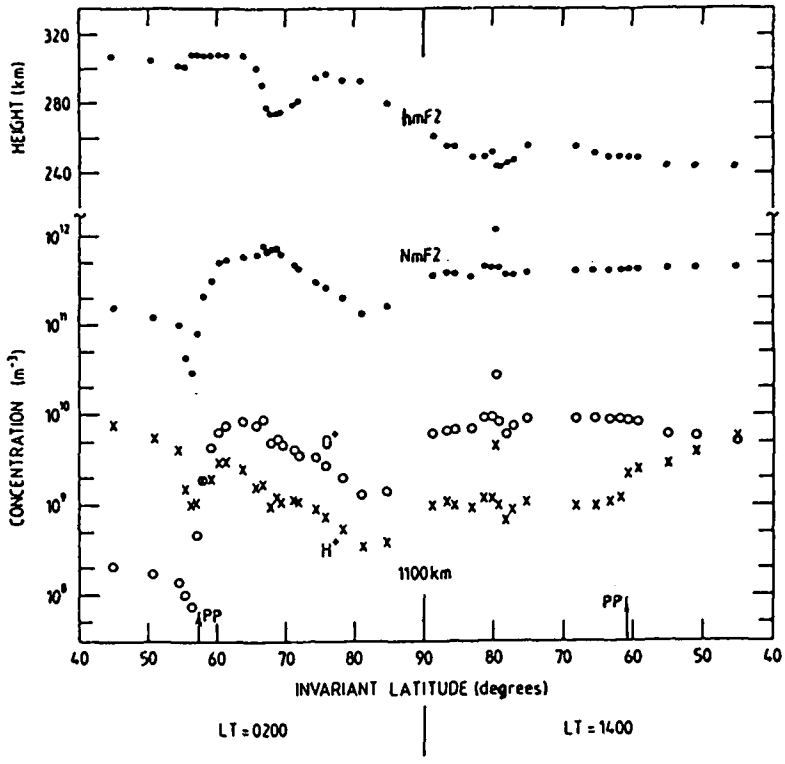


Figure 6 Calculated variations with invariant latitude of hmF2, NmF2 and the O^+ and H^+ concentrations at 1100 km along the 0200-1400 LT meridian (after Quegan et al 1982).

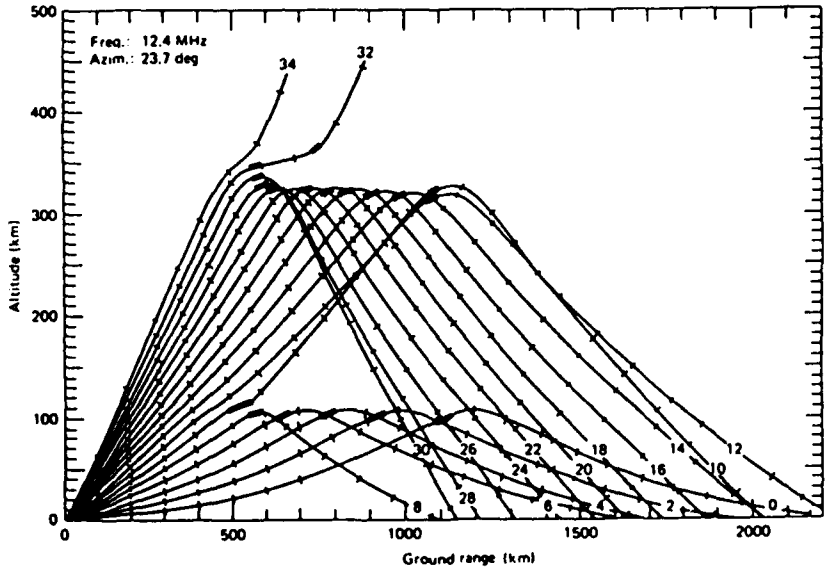


Figure 7. Ray tracing in a geomagnetic meridian plane for a HF radar located at Anchorage, Alaska, with elevation angle rays from 0° to 34°, in 2° steps, indicated by the number at the end of the ray. The tick marks on the rays correspond to a group path of 100 km. The rectangles on the rays indicate that the ray is within 1° of normal to the earth's magnetic field (after Villian et al, 1984).

HIGH LATITUDE SPATIALLY ADAPTIVE PROPAGATION EXPERIMENT

by

Gary S. Sales* and Raymond J. Cormier
Rome Air Development Center
Electromagnetic Sciences Division
Hanscom AFB, MA 01731, USA

and

Raymond A. Greenwald and Kile B. Baker
Applied Physics Laboratory
Johns Hopkins University
Laurel, MD 20702, USA

SUMMARY

A special HF phased array was used to obtain high latitude HF propagation data. The antenna located at Goose Bay, Labrador, Canada, received HF transmission (8-20 MHz) from Thule, Greenland. The receiving antenna at Goose Bay consisted of two parallel linear arrays each with 16 horizontal log-periodic antennas. This system was used to measure both the azimuth and elevation angle of arrival of the propagated radio wave. Comparisons are made with model calculations and the received modes are analyzed to determine the presence of ionospheric tilts.

INTRODUCTION

Advancing technology in HF communications offers the potential for developing adaptive receiving antenna systems permitting effective communication in an environment shared by other users of the radio spectrum, friendly or otherwise. However, there is very little information available today concerning the fluctuations in the arrival angle of the HF radio wave over an arctic path, where ionospheric disturbances and irregularities are prevalent.

For this reason a CW coded HF sounding system over a path from Thule, Greenland, to Goose Bay, Labrador, a distance of about 2600 km, was established. Figure 1 shows the geographical configuration of this almost north to south path and its relation to the auroral oval. This system operated in a sounding mode and a Doppler spectral mode. The sounding operation, where the frequency is stepped from 8 to 20 MHz in 10 kHz steps, is designed to characterize the propagation modes that are present at any particular time. This identification is used to aid in the analysis of the vertical arrival angle data. The oblique ionogram takes 60 seconds to step through the 1200 frequencies and has a range resolution of 200 μs (60 km).

The spectral mode is a more complicated mode since the system must operate totally automatically and step through eight preselected frequencies in the 8 to 20 MHz band to insure a successful selection in terms of which frequencies are propagating at the particular time. For each of the eight frequencies, the system steps through eight predetermined azimuthal beam positions and repeats this cycle 32 times so that there are 32 complex samples for each frequency for each beam position. This cycle for each frequency takes 6.375 seconds and is repeated four times in ten minutes with an 80 second spacing. Figure 2 shows the schedule of measurements, typically performed one day per week. Every three hours the system begins its 30 minute operation in both the sounder mode and the spectral mode. The two sets of measurements take about ten minutes and are repeated twice in the one-half hour. The cycle then begins again in three hours and this continues to be repeated to complete a 24 hour period.

The antenna configuration at the receiver site at Goose Bay is shown in Figure 3. It consists of 32 horizontal log periodic antenna elements arranged in two broadside linear arrays of 16 elements each. The spacing of the elements is 16 m and the two linear arrays are separated by 100 m in the direction towards Thule. A phased array network establishes 16 azimuthal receive beams with a 4 degree spacing, symmetrically located about the direction towards Thule. The eight beams used for these experiments are shaded in Figure 3; the direction to Thule lies between beam numbers 4 and 5.

By analyzing the amplitude variations of the received signal as it appears in adjacent beams, it is possible to determine the apparent azimuthal direction of arrival of the Thule signal to within approximately one-half the beam spacing of 4 degrees. For this study emphasis has been placed on the vertical angle of arrival and its variations. Using an interferometric technique for the elevation measurements, the received digital output of the two linear arrays are recorded for spectral processing and phase delay analysis at the laboratory.

The observed phase delay between spectral components on the two arrays can be interpreted in terms of a vertical arrival angle, though with some ambiguity. This is

*Now with the University of Lowell, Center for Atmospheric Research, Lowell, MA 01854.

shown in Figure 4 where for two frequencies, 10 and 20 MHz, the phase delay vs. elevation angle has been plotted. As can be seen, the ambiguity begins at elevation angles greater than 27 degrees. As will be shown later from model calculations, the expected elevation angles for one hop and two hop propagation modes lie below 27 degrees and the inherent ambiguity causes no problem.

For each sounding frequency the 32 data points for each azimuthal beam position are Fourier transformed for each of the two linear arrays. Once the peak spectral component is identified in terms of range and Doppler, the phase difference is calculated for these components on the two arrays. Then the elevation angle E is given by:

$$E = \arccos\left[\frac{\Delta\phi}{2\pi}\frac{\lambda}{D}\right]$$

where $\Delta\phi$ is the measured phase difference
λ is the wavelength
and D is the array spacing = 100 m.

ANALYSIS

For this preliminary report, data samples for the 17 March 1985 at 1403 UT have been analyzed. The Thule to Goose Bay path lies some four hours west of Greenwich and this period represents a daytime measurement.

An example of the received spectrum for the two arrays at 8.41 MHz is shown in Figure 5 for all the receiver beam positions. The solid curve is for the forward face of the two linear arrays and the dotted curve for the rearward face. In this particular case the strongest signals arrive in beam 5 and because at these low frequencies the natural beam width is approximately 13 degrees the signal overlaps onto adjacent beam positions. These spectra represent a rather benign ionospheric condition with little Doppler shift on either array. Only the magnitude of the spectrum is shown in Figure 5, though the phase information is available for use in the elevation angle analysis.

Figure 6 shows the time variation of the elevation angle for 8.41 MHz at several range gates, spaced by 60 km. It is clear that ranges 7 and 13 lie at the edge of the received signal and should not be considered. The signal itself is spread over several range bins from 8 through 11. All of these range gates result in a similar elevation variation averaging 26 degrees with small fluctuations. Figure 7 shows the measured elevation angle at four frequencies. While the 8.4 MHz curve averages approximately 26° elevation, the three higher frequencies are in the 14° to 16° range. This will be explained below when the mode analysis is discussed.

For the mode analysis the IONCAP program developed by the Institute of Telecommunication Sciences was run for the specified experimental conditions at low sunspot number. Figure 8 shows the synthesized oblique ionogram for the path from Thule to Goose Bay at 14 UT. The numbers printed on the curves identify the elevation angle for each mode at each frequency. The 1F2 mode has an average elevation angle of 7 degrees while the 2F2 mode averages around 21 degrees. The Maximum Usable Frequency (MUF) for each mode is obtained from this median prediction program: the MUF(1F2) is about 14 MHz while MUF(2F2) = 8.5 MHz and there is no frequency overlap between the one hop and two hop modes, typical of daytime propagation. To the extent that this simulation represents the real world, it is reasonable to expect the 8.4 MHz signal to be a two hop mode while the higher three frequencies to be one hop modes. The elevation angles for these two modes have also been indicated on Figure 7. In both cases, one hop and two hop, the observed elevation angles are greater than predicted by IONCAP. This can result from either an F2 layer which was higher than assumed by the model or by a tilted ionosphere. Both conditions are possible, though with this limited data it is difficult to separate these two effects. The IONCAP program assumes a horizontal stratified ionosphere, that is, no tilts are assumed in the ray tracing even when the local ionosphere has a horizontal gradient.

Using simple geometry for a curved earth, it is possible to analyze these results in terms of a locally tilted ionosphere. Assuming a reflection height of 300 km and no horizontal gradients, the expected arrival angle is 8 degrees, very close to the IONCAP value for the one hop mode. If the measured arrival angle is 16 degrees then a tilted structure can be assumed and it is possible to calculate the required tilt angle. This simple analysis yields a tilt angle of approximately 3 degrees and a displacement of the reflection point of about 400 km from the midpoint of the path towards the receiver. These calculated numbers do not change very much if a reflection height of 400 km is assumed and these results indicate a likely tilt angle of 2° to 3° in the polar ionosphere. This is a relatively small and realistic tilt that is likely to exist in that ionosphere.

CONCLUSIONS

This technique provides a measure of the fluctuations in arrival angle of an HF signal, both in azimuth and elevation and will produce the data base necessary to develop algorithms for adaptive antenna control in the arctic environment.

ACKNOWLEDGEMENT

The authors wish to recognize Mr. D. Mark Haines and Mr. Bertus Weijers who did the detail design of the software for signal transmission and the instrumentation for the Thule, Greenland site. We appreciate the cooperation of the Air Force Geophysics Laboratory and their contractor, Canadian Marconi, who support this experiment at the AFGL Goose Bay Ionospheric Observatory. Special thanks to Mr. J. Waaramaa of AFGL who provided the supervision necessary to have the Goose Bay antenna array erected.

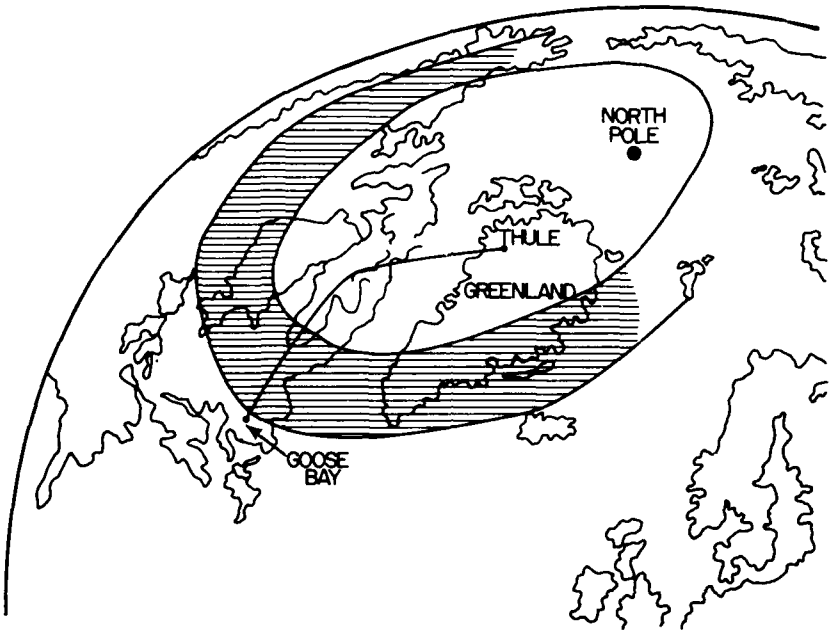


Figure 1. Communication Path, Thule - Goose Bay

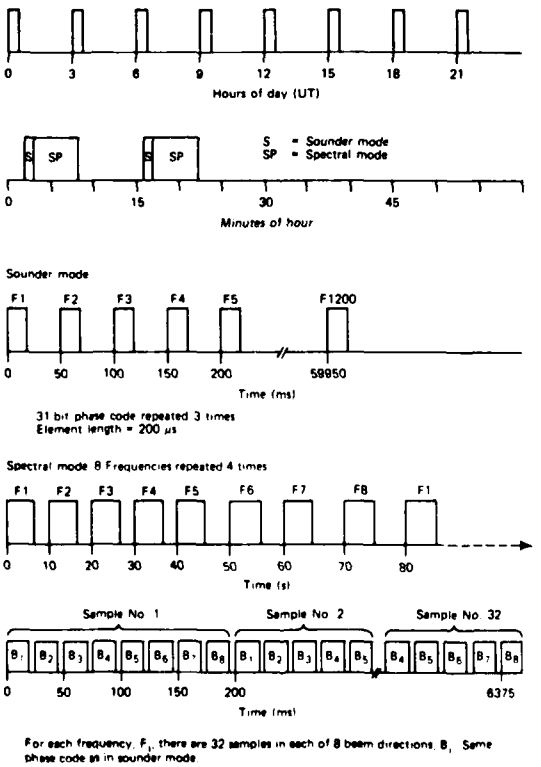


Figure 2. Experiment Test Plan

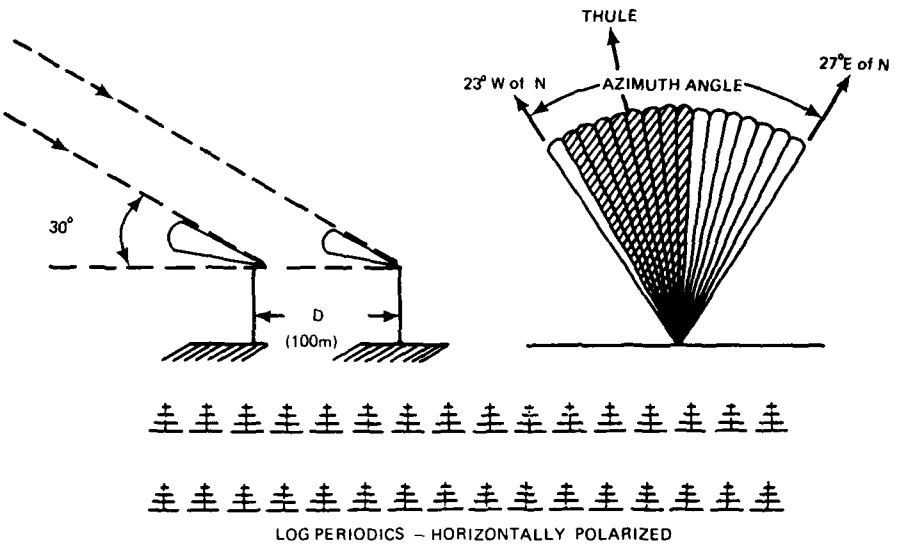


Figure 3. Antenna array - Goose Bay

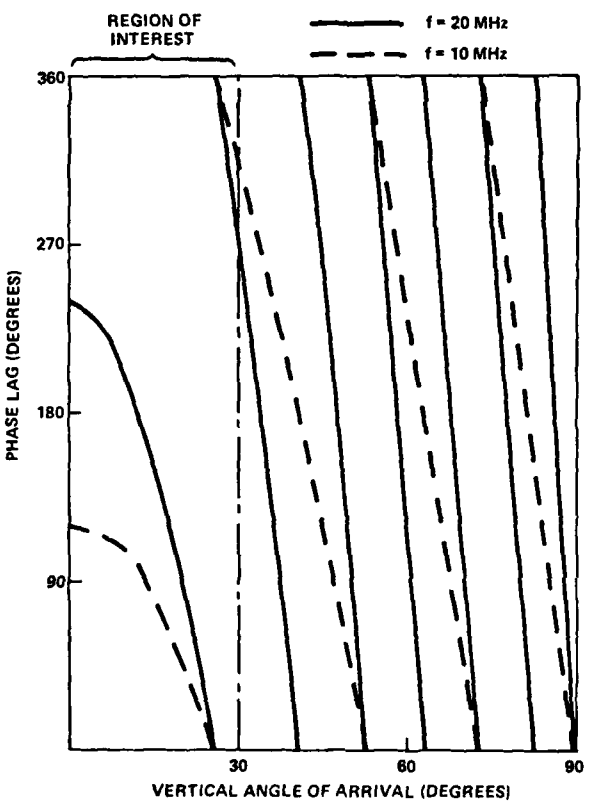


Figure 4 Vertical Angle of Arrival versus Phase Lag

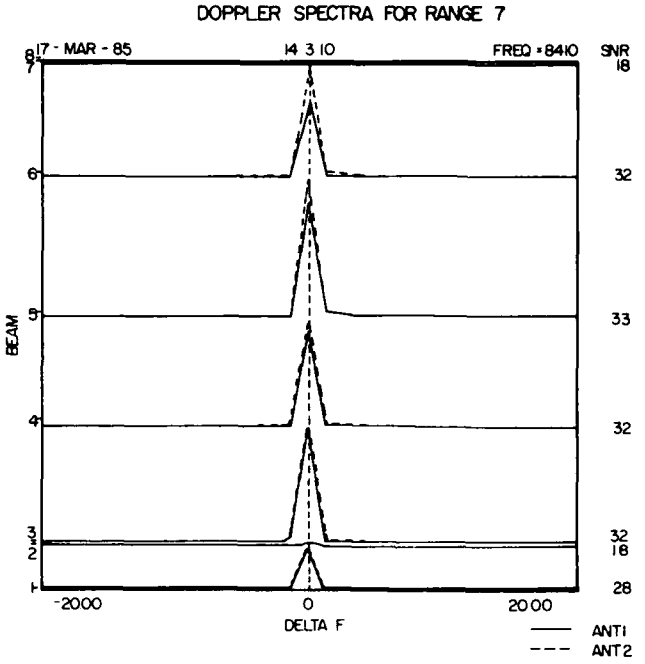


Figure 5. Example of Doppler Spectra

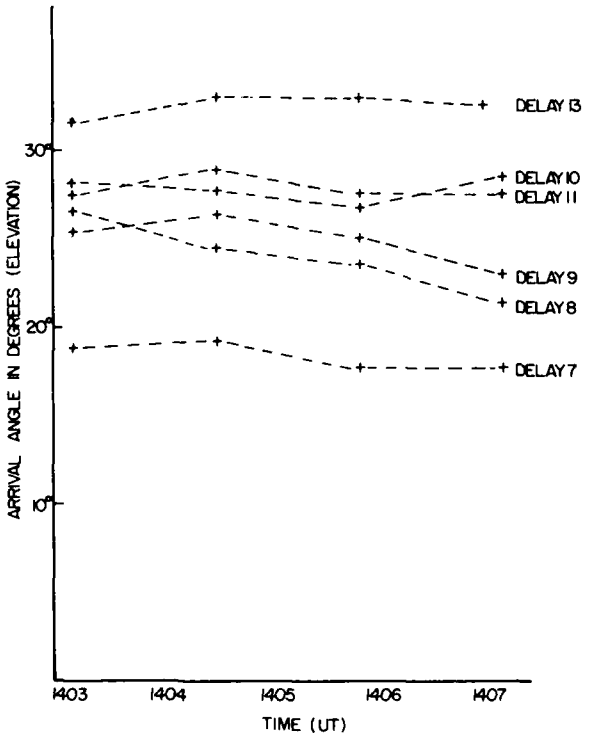


Figure 6. Time Variation of Arrival Angle for 8.410 MHZ at 1403 UT Beam 5

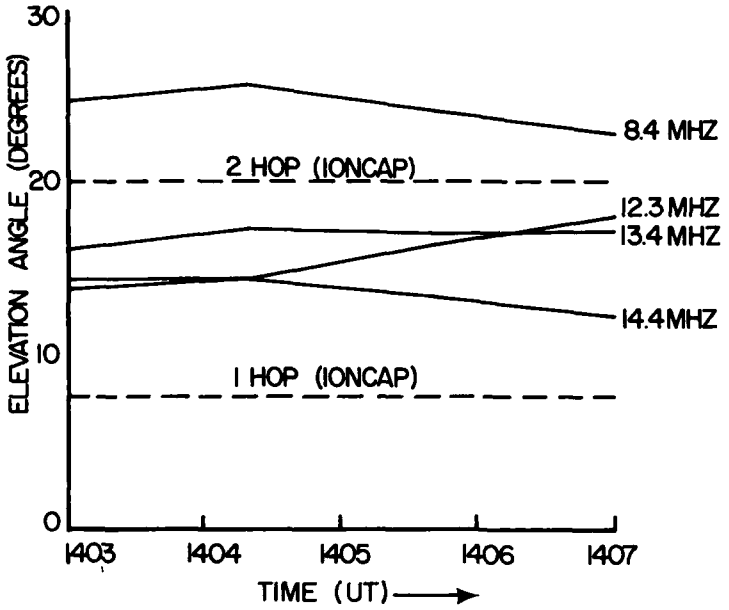


Figure 7. Measured Elevation Angle of Arrival-17 Mar 1985

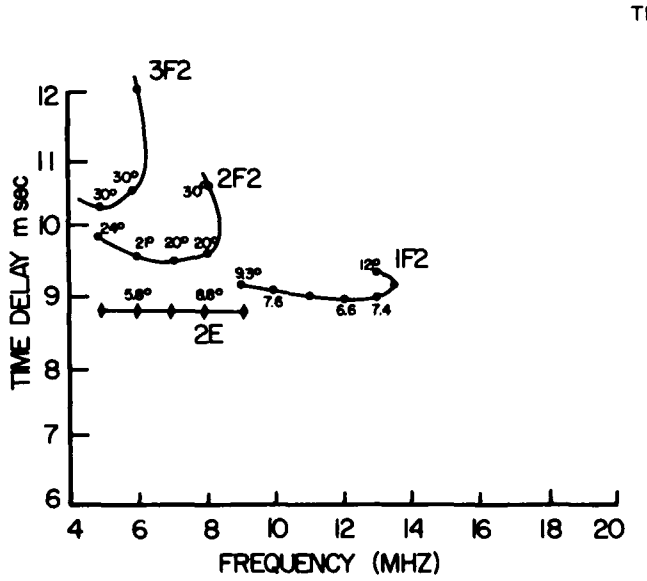


Figure 8. Synthesized Oblique Ionograms using IONCAP

DISCUSSION

J.Belrose, CA

What is the height of your log periodic antennas?

Author's Reply

50 feet.

J.Belrose, CA

In which case the response of your antenna systems for signals arriving at low angles above the horizon is poor. At 14 MHz the main vertical lobe would be directed at about 32°, at 8 MHz this angle is greater than 40°. For improved low angle operation you should have employed vertically polarized log periodic antennas.

Author's Reply

Although I am not certain of the exact peak elevation angles for these antennas you are correct in stating that the low angle performance will be down from the peak but only around 8 to 10 dB. It is not clear at this point whether this reduced response would affect the detection of the 1 hop signals given that what we suppose is a 2 hop signal is some 30 dB above noise. We are continuing to look into this question.

T.B.Jones, UK

A major problem in this type of observation is the non-linearity of the incoming wave front. Have you compared your measurements with the extensive work undertaken at CRC Canada, presented at previous AGARD conferences?

Author's Reply

Non-linear wavefronts result when several signals propagating to the radar from different directions are combined. This question correctly recognizes that the determination of a meaningful arrival angle assumes a linear wavefront. The requirement is to separate the arriving signals into their angular components before attempting to determine the arrival angle. Two types of processing are considered for this purpose. For the present experiment, which uses a deterministic beam former, we used Doppler frequency processing to resolve the several propagating components that make up the irregular wavefront. This approach assumes that each angular component has a distinguishable Doppler frequency. If this is not the case, then an error will be made in determining the arrival angle. An alternate approach is to use an antenna array with sufficient angular resolution to separate the various propagating components.

TECHNIQUES FOR IMPROVING THE RELIABILITY OF MOBILE HF COMMUNICATIONS OVER HIGH-ABSORPTION PATHS

by

M.Darnell
Dept. of Electronics
University of York
Heslington
York YO1 5DD, UK

SUMMARY

The paper is concerned primarily with system design aspects of the mobile HF communications problem in high-latitude regions. It attempts to identify the various techniques available for enhanced reliability of reception under high-absorption conditions and to indicate how these can be coalesced into an improved HF system design.

The basic problem associated with excess absorption is that received signal-to-noise ratios (SNR's) are lower than those which might be expected for say mid-latitude paths. Thus, the paper considers specific methods by which the value of the SNR required at the receiver can be reduced, either directly or effectively. Techniques discussed include:

(a) the use of various forms of diversity processing, emphasising the value of path/geographical diversity combining;

(b) relaying out of the disturbed region with a view to avoiding the perturbed ionosphere and operating the transmitting antenna system more efficiently at a high frequency;

(c) the use of meteor-burst and ionospheric scatter communication to complement normal HF communication;

(d) the use of modulation and coding schemes requiring a relatively low SNR at the receiver.

(v) system control procedures.

1. INTRODUCTION

This paper considers methods by which the reliability of HF communication systems incorporating mobile terminals can be improved in high-latitude regions. The major propagation mechanisms which can influence HF communications in these zones are (Thrane, 1983):

(a) polar cap absorption (PCA) events due to the influx of high energy protons and alpha particles penetrating to the lower ionosphere: such events may persist for several days, causing severe attenuation of skywave signals and an effective communication "blackout" over a wide geographical area;

(b) auroral absorption, caused by high energy electrons penetrating the ionospheric D-region: this source of signal attenuation typically persists for a few hours only and affects a more restricted geographical area than does a PCA;

(c) irregular behaviour of sporadic E-layer, spread F-layer and auroral oval propagation modes, giving rise to abnormal and variable multipath time spreads;

(d) abnormal doppler shifts and phase instability of received signals due to the variable nature of the high-latitude ionosphere, manifesting itself in the form of very rapid signal fading;

(e) large variability of maximum usable frequencies (MUF's) from very low to abnormally high values: the former may result in spectral congestion and hence high levels of co-channel interference, whilst the latter may allow HF type propagation to take place in an extended frequency range above 30 MHz.

Clearly, the propagation environment in polar regions is relatively unstable and unpredictable, thus limiting the effectiveness of off-line propagation analysis programs.

The emphasis in this paper is on HF systems involving mobile terminals such as ships and aircraft. In addition to the natural difficulties arising from the propagation medium, mobile terminals have certain other fundamental weaknesses when contrasted with fixed, or land-based, HF stations; these include:

(a) comparatively low transmitter powers, limited by the generation capacity of the mobile platform;

(b) simple, narrowband, and relatively inefficient transmitting antennas, with minimal directivity;

(c) electromagnetic compatibility (EMC) problems due to the HF communications equipment being co-sited with other electromagnetic systems such as radars and communications transmitters in other frequency bands;

(d) a propagation path which, in addition to the sources of variability mentioned previously, is also affected by the constantly changing position of the mobile.

Land-based (fixed) stations, on the other hand, can use high powers and efficient and directive antennas, coupled with electrically quiet receiving locations. It is also relatively straightforward to provide interconnections between fixed sites to give a capability for networking.

In military applications, mobile terminals may represent a particularly vital element in the operational strategy: as a consequence there may be additional requirements placed on the mobile to function in such a way that the probability of its transmissions being decoded, intercepted, located or jammed is minimised.

Mobile terminals operating at high-latitudes can thus be considered as a class of "disadvantaged" users of the HF spectrum, who may nevertheless be required to communicate reliability and securely over a wide geographical region, possibly via an ionosphere exhibiting severe irregularities.

It will be shown in Section 2 that the design of many mobile HF systems takes only limited account of the problems listed above. The later sections of this paper are used to develop a design philosophy which will allow more reliable operation. This design exploits the strengths of fixed terminals and minimises the effects of any problems associated with mobile terminals, at the same time placing as few constraints as possible upon mobile operational flexibility. In essence, the complexity of the design resides in the fixed terminals of the system, with the mobile equipment being kept simple. Extensive use is made of diversity processing to reduce the required average signal-to-noise ratio (SNR).

2. EXISTING HF COMMUNICATION SYSTEMS INCORPORATING MOBILE TERMINALS

In a generalised HF communication system incorporating both fixed and mobile terminals, there may be a requirement for any of the following:

(a) fixed terminal-to-fixed terminal communication;

(b) fixed terminal-to-mobile terminal communication;

(c) mobile terminal-to-fixed terminal communication;

(d) mobile terminal-to-mobile terminal communication;

The manner in which each of the links above is currently implemented will now be outlined briefly.

2.1 Fixed Terminal-to-Fixed Terminal

Because relatively high transmitter powers and directive antennas can be installed at fixed sites, the engineering of a fixed terminal-to-fixed terminal link can normally be accomplished to give a reasonable communications reliability - at least for simple forms of traffic, eg low-speed telegraphy data and analogue speech. However, digital data, or digital speech, at say 2.4 kbits/s will present a greater problem, and circuit reliabilities for this form of traffic will be relatively low.

If a fixed link operates with a defined frequency complement on a regular schedule, there will be a significant frequency "airing" effect which will tend to deter other users of the spectrum from encroaching upon those frequencies, thus minimising the levels of co-channel interference.

2.2 Fixed Terminal-to-Mobile Terminal

Fixed terminal-to-mobile terminal communication is frequently implemented via a broadcast-type system; this again allows high transmitter powers and directive antennas to be used at a fixed site in order to radiate signals simultaneously to multiple mobile terminals, possibly situated anywhere within a wide geographical region.

A basic broadcast system operates on the principle of long-term frequency selection diversity; Figure 1 illustrates the principle. It is seen that at any time of day, the same traffic signal will be radiated on a number of distinct frequencies or components, with the assumption being that at least one of the components will propagate effectively to any given mobile. The frequencies must therefore be chosen to provide a compromise coverage over the complete mobile operational area for both day and night conditions.

Typically, each component will comprise multiple sub-channels arranged within a nominal channel bandwidth, as shown in Figure 2. The sub-channels correspond to

traffic signals originating from various message sources; a given mobile will only extract those sub-channels of interest to it from the multiple sub-channel raster. If all sub-channels are not assigned, it is possible to transmit the same information on more than one sub-channel to provide in-band frequency diversity. In Figure 2, the ith sub-channel is employed for engineering order wire (EOW), or system control, purposes.

The system thus has the potential for frequency diversity at two levels: a given mobile selects the best component in terms of received SNR and, within that component, may also be able to apply in-band frequency diversity combining.

It is also possible for the same broadcast traffic to be radiated simultaneously from different fixed sites, giving path diversity in addition to frequency diversity.

2.3 Mobile Terminal-to-Fixed Terminal

The mobile terminal-to-fixed terminal situation is, in many respects, the complement of that discussed in Section 2.2. Two basic options exist as indicated in Figure 3: the first where the mobile must access a single fixed terminal; the second where a number of alternative fixed terminal accesses are available. For the situation shown in Figure 3(a), there may also be occasions when a bi-directional, full duplex link must be engineered between the two terminals. This can be difficult to maintain because of changes in mobile antenna characteristics as it changes position and orientation, coupled with the need for co-ordinated frequency changes.

In Figure 3(b), the mobile has a choice of fixed terminals with which to communicate. If the fixed terminals are widely separated, there will be a high probability that both propagation and co-channel interference effects will be largely decorrelated at the various locations. Thus, it can be expected that at least one of the fixed terminals will be able to receive the mobile traffic in a reasonably optimum manner over the complete ranges of time and position; this traffic can then be passed to the desired recipient by HF or non-HF communications links from the fixed terminals.

2.4 Mobile Terminal-to-Mobile Terminal

Figure 4 shows the two basic methods by which a mobile terminal can communicate with another mobile terminal. In Figure 4(a), the mobiles communicate directly via skywave or surface wave HF propagation. In the latter case, vertically-polarised antennas mounted on ships allow links to be established over distances up to a few hundreds of kilometres. Skywave links over comparable ranges necessitate high-angle propagation via horizontally-polarised antennas, which may be difficult to mount on ships. Both terminals suffer from the fundamental limitations listed in Section 1, and thus direct mobile links are difficult to operate reliably over a wide range of distances.

Figure 4(b) illustrates an alternative arrangement in which traffic is routed from one mobile to another via a fixed "relay" terminal. In this case, the advantages of the fixed station can be exploited in its relay role and communication between mobiles can be maintained over a wider range of distances with greater reliability - at the expense of more sophisticated control procedures.

HF links of various types are normally controlled by using data obtained from off-line propagation analysis programs, eg (Bradley, 1975). More recently, various forms of real-time channel evaluation (RTCE) are being used to aid frequency selection and system control (Darnell, 1978).

3. THE VALUE OF DIVERSITY PROCESSING IN HF COMMUNICATIONS

It has long been recognised that diversity processing of various types can be applied with advantage to HF communications. The most widely-used types are:

(a) spaced receiving antenna diversity;

(b) diversity obtained from receiving antennas of different polarisations;

(c) frequency diversity, either within a given assigned channel or over different assigned channels;

(d) time diversity, in which the same signal is repeated at different time offsets;

(e) diversity arising from the availability of independent multipath components.

All forms of diversity combining require there to be available two or more independently-derived received versions of the wanted signal. Under these circumstances, fades or interference affecting one version may be decorrelated with similar mechanisms affecting the other version(s), thus allowing a better overall signal estimate to be derived by using information from all versions (Stein & Jones, 1967).

Figure 5 shows the reduction in received SNR admissible, under Gaussian White Noise (GWN) and Rayleigh fading conditions, when 2nd and 4th-order selection diversity combining is used rather than non-diversity reception. It is seen that for

dual-diversity combining, an SNR reduction of about 10dB can be expected for an error probability of 1 in a 1000 - equivalent to a ten-fold increase in transmitter power, or the difference between an omnidirectional and a highly directional receiving antenna (Darnell, 1985).

In Section 2.3, a network of widely-separated fixed terminals for the reception of mobile transmissions was described. This concept will now be extended to that of a "geographical diversity" system in which data from a number of spaced receiving stations can be combined in a systematic manner to provide an improved estimate of a desired mobile transmission. The value of such path diversity in improving communication availability been demonstrated experimentally (Rogers & Turner, 1985).

Figure 6 is a schematic diagram of a geographical diversity network involving multiple fixed terminals interconnected by means to be described in Section 4. The basis of operation of the network is that transmissions emanating from a given mobile terminal will be received at the fixed terminals via propagation paths which will normally be skywave, but may also be surface wave; these paths can be considered as independent if the separation of the fixed terminals is chosen appropriately. Similarly, interfering transmissions will also be received via independent paths. Thus, taking the network as a whole there will be a high probability that the signal and interference conditions on those links which are propagating between mobile and fixed terminals will be uncorrelated. This situation lends itself to some form of diversity combining in which all received versions of the mobile signal are brought together at a central control and processing site to allow an improved signal estimate to be made. There are several possible combination algorithms which could be considered, eg:

(a) selection of the path giving the greatest SNR at any time, ie selection diversity combining;

(b) alternative classical forms of diversity combining such as maximal ratio (Stein & Jones, 1967);

(c) operation on the demodulated and shaped versions of the propagating received signals by say majority voting;

(d) more elaborate combining techniques applied to demodulated and shaped signals, taking account of soft-decision data associated with the received data symbols.

The most important considerations associated with the establishment of a geographical diversity network will be reviewed in the following three sections.

4. GEOGRAPHICAL DIVERSITY NETWORK: INTERCONNECTION CONSIDERATIONS

The fixed terminal interconnections shown in Figure 6 are clearly vital to the operation of the system; they need therefore to be robust and reliable. The following media may be considered for interconnection purposes:

(a) HF skywave and surface-wave point-to-point links;

(b) meteor-burst links;

(c) ionospheric or tropospheric scatter links;

(d) satellite links;

(e) some form of common-user telephone/telecommunication system, eg such as those implemented by PTT's.

Links of types (a), (b) and (c) are essentially "stand-alone", point-to-point interconnections, whilst (d) and (e) require the availability of separate communications systems, possibly controlled and operated by independent organisations. Hence, from the viewpoint of survivability in the face of physical or electromagnetic attack, (a), (b) and (c) are to be preferred. The most promising candidates will now be discussed in greater depth.

4.1 HF Interconnection

In a geographical diversity network of the form proposed, fixed receiving terminals may be separated by distances from say a few hundreds of kilometres to several thousands of kilometres. Interconnection via HF links will thus involve skywave, and possibly surface-wave, paths exhibiting a wide variety of propagation characteristics. There is a need for data transfer between terminals to be effected with high integrity and resistance to disruption. This will require links with sophisticated and possibly embedded RTCE (Dawson & Darnell, 1985), together with adaptive error control (Hellen, 1985). Inevitably, the data rates which can be sustained reliably will be relatively low.

4.2 Meteor-Burst Interconnection

Meteor-burst links (Bartholomé & Vogt, 1968) make use of the short-duration ionised trails, caused by the passage of micrometeorites through the lower ionosphere, in order to reflect radio wave energy. Such links are naturally

intermittent, although the statistics of meteor trail occurrence are relatively predictable. It has been demonstrated experimentally that average data rates of a few hundreds of bits/s can be sustained over a complete 24-hour period, which would normally be sufficient for the role envisaged here. The diurnal and seasonal variability of meteor-burst links is less than for the corresponding HF skywave links; they are also less susceptible to excess absorption effects following severe ionospheric disturbances.

The most effective frequency range for meteor-burst operation is from about 25 to 100 MHz which allows compact, efficient and directive antennas to be used.

4.3 Ionospheric or Tropospheric Scatter Interconnection

Ionospheric scatter propagation makes use of radio wave energy scattered by the lower ionsphere (Bartholomé & Vogt, 1965). Tropospheric scatter propagation employs scattered energy emanating from the troposphere (Yeh, 1960). Since the troposphere is at a much lower altitude than the lower ionosphere, the ranges achievable by tropospheric scatter are substantially less. In both cases, the scatter loss is high which necessitates the use of high transmitter powers and directive antennas to illuminate the "scattering volume" efficiently.

Propagation via these scattering mechanisms is relatively reliable, although significant fading may occur.

4.4 Satellite Interconnection

Inexpensive and reliable satellite links are becoming available, although there may be coverage limitations at high latitudes. In a military context, the HF system should operate as an independent entity under threat conditions which might involve the satellite being jammed. For this reason, such links are not considered suitable for interconnection purposes, although they may be useful in benign operating environments.

4.5 Common-User System Interconnection

Possibly the cheapest interconnection medium is a PTT-type of network in which all fixed HF terminals and control sites are subscribers. Again, this has the disadvantage that it can be disrupted by physical or electromagnetic attack. However, the diversity of propagation media and routes makes it inherently more robust than a satellite system alone.

Practically, a combination of interconnection media would appear to offer the best prospect for reliable operation over the whole range of operational conditions. Transmission systems covering say the range from 2 to 60MHz, having relatively high radiated powers (a few kW) and directive antennas, could form the primary basis for interconnection; they could operate in HF skywave, HF surface-wave, meteor-burst or ionospheric scatter modes, as available and appropriate. Also, a parallel interconnection could be established via a PTT network.

Obviously, some delay will be introduced into the reception of mobile terminal signals by the need to transfer data around the network. This delay will tend to increase as the number of mobile terminals accessing the network simultaneously increases. The longer the delay which can be tolerated, the greater is the potential for accurate reception. In general, it can be expected that the fixed terminal interconnections will be able to sustain a higher average data rate than that which will be associated with the mobile-to-fixed terminal transmissions. The effect of delays can be minimised by the signal design and network control strategies to be discussed in the following sections.

5. GEOGRAPHICAL DIVERSITY NETWORK: SIGNAL DESIGN CONSIDERATIONS

From the discussion in Section 1, it is seen that the high-latitude ionosphere can be subject to severe natural disturbances giving rise to excess multipath delay, signal fading, low signal levels and possibly abnormal doppler spreads or extreme phase instability. Under these circumstances, it is necessary to use robust transmission formats which are resilient to such perturbations.

It has been shown experimentally that the information transfer capacity of an HF skywave channel varies continuously with time due to propagation and interference effects (Darnell, 1977) and can only be considered constant over relatively short intervals of time. For this reason, a "window" model of HF propagation was developed (Darnell, 1983). This indicates that the natural mode of operation for HF skywave transmission is one in which the data is block-formatted, eg via an automatic repeat request (ARQ)-type system (Van Duuren, 1951).

5.1 Mobile Signal Formats

Normally, it will be necessary for a geographical diversity network to handle signals originating from several distinct mobiles. A block transmission format would be convenient since it would allow simple time and frequency multiplexing to take place, with only one mobile using a particular frequency at a specific time. To allow this, accurate time and frequency standards would have to be available at all

terminals in the system, but this can now be accomplished relatively simply and economically.

The major requirements for a robust mobile transmission can be summarised as follows:

(a) that its time of occurrence and frequency of propagation are accurately controlled;

(b) that the SNR required at the receiver for a specified error rate is minimised;

(c) that no elaborate synchronisation techniques are necessary;

(d) that long multipath delays can be tolerated;

(e) that high levels of phase instability can be tolerated;

(f) that moderate doppler frequency offsets can be tolerated;

(g) an ability to operate in any of a limited number of modes which can become progressively more robust as propagation conditions deteriorate;

(h) that signals should be digital to enable data to be protected by encryption.

A possible signal format on which the mobile transmission could be based is basic wide-shift FSK, in which detection is accomplished by a Law assessor arrangement (Alnatt et al, 1957) giving the effect of dual, in-band diversity under frequency-selective fading conditions. Simple block error control codes could be applied to the data blocks, with more powerful (more redundant) coding being used as path conditions worsened. In extreme cases, the mobile would simply repeat its message many times to allow signal averaging to be employed at the receivers. Under white noise conditions, signal averaging improves the effective SNR by a factor proportional to the square root of the averaging time (Hewlett-Packard J, 1968).

Under poor SNR conditions, a trade-off must be made between SNR and transmission time; ie as the SNR reduces, the user must allow more time for the transmission of a given message if it is to be received with a specified level of fidelity. In effect, variable redundancy error control is required (Hellen, 1985).

In circumstances where frequency offsets are negligible and short-term phase stability reasonable, systems of the PICCOLO type (Bayley & Ralphs, 1972) or reduced multiple FSK systems, eg (Chapman, 1985), would provide robust communication.

In general, transmissions should be designed so that soft-decision data, or confidence information, can be extracted readily at the receiver.

5.2 Interconnection Signal Formats

Most of the comments made above in the context of mobile signals also apply to signals transferred over the interconnection links between fixed terminals.

Labelled data blocks relating to the signals from specific mobiles would be a convenient vehicle for passing data between the fixed nodes and the control/processing site.

In principle, the design and operation of reliable point-to-point links is a simpler problem than is the design of a mobile-to-fixed link because more efficient antennas and higher transmitter powers are available. Again, an ARQ mode of operation would seem to be appropriate (Dawson & Darnell, 1985), since this would be well-matched to the characteristics of the interconnection media proposed, ie HF skywave, meteor-burst or ionospheric scatter.

6. GEOGRAPHICAL DIVERSITY NETWORK: SYSTEM CONTROL CONSIDERATIONS

From the previous section, one of the potential problems which can be identified is that the maximum capacity required for the interconnection links is considerably greater than for the mobile-to-fixed links. This arises because the interconnection links may be carrying simultaneously information relating to:

(a) a number of distinct mobile transmissions;

(b) system control data for the network.

These will now be discussed in greater depth, together with other considerations affecting the control of the network.

6.1 Data describing Mobile Transmissions

One mode of operation for a geographical diversity system is where the various versions of the mobile signal received at the different fixed terminals are demodulated and reconstituted at those terminals, with the reconstituted data being forwarded to the site where combination is to be carried out. A further retirement

to this process could be the transmission of soft-decision data, relating to each of the detected data elements, to the combination site. Alternatively, the complete analogue baseband signal from each fixed receiving terminal could be forwarded to the combination site. In the latter two cases, the information carried by the interconnecting links would be considerably increased in comparison with that contained in the original signal transmitted by the mobile. However, since the mobile transmissions would normally be of short duration, this data expansion would be acceptable of some decoding delay is admissible.

6.2 System Control Data

It will also be necessary for system control data to be transferred on a regular basis between fixed terminals, simply to maintain the integrity of the network. This system control data would relate to frequency selection options, available data rates, changes in coding levels, etc. It is envisaged that, in a ARQ-based system, the capacity overhead associated with this data would be relatively small.

6.3 Frequency Management

Frequency management of a geographical diversity system would logically be carried out at two levels:

(a) on a link-by-link basis;

(b) on a network basis.

In the former case, each of the interconnection links would have its own embedded RTCE and protocols (Dawson & Darnell, 1985) operating over the frequency range of from 2 to about 60 MHz. The propagating mechansism giving the greatest predicted SNR would typically be selected.

At the network level, there is a need for a more sophisticated RTCE procedure which attempts to assess the general propagation state of the region in which the fixed and mobile terminals are situated. This could be accomplished by either a vertical-incidence ionosonde placed at the eastern edge of the region, or by oblique-incidence sounding carried out between the fixed terminals of the network. Measurements of this type would indicate the onset of ionospheric disturbances and possibly their approximate geographical extent.

An additional function of the overall frequency management would be to ascertain the extent to which frequencies could be shared or re-used by different fixed terminal interconnection links.

6.4 Other Control Functions

In military operations, the control of the communications system must, in part, be directed towards maintaining the security of the mobile traffic. Thus, the mobile would, for example, be assigned frequencies which would have the minimum probability of being intercepted or disrupted in the prevailing propagation conditions. Also, the mobile would exercise radiated power control (RPC) in response to control data sent to it by the fixed network.

The system control procedures would also seek to make maximum use of relatively local and transient propagation phenomena as they became available. There would also be a need to reconfigure the fixed terminal interconnections in order to avoid localised ionospheric disturbances. In this context, Figures 7 and 8 illustrate the benefit to be gained from the use of a geographical diversity network. Figure 7 shows a situation in which an ionospheric disturbance affects the skywave path between the mobile (M) and a fixed terminal (F1); the skywave path to fixed terminal (F2), at a greater distance from M, avoids the disturbed region completely, as does the interconnecting path between F1 and F2. Figure 8 is a more complex situation where the region of disturbance affects both the mobile-to-fixed terminal (F1) path and interconnections from F1 to F3, and from F1 to F4. In this case, the interconnecting links must be re-routed as shown to maintain network connectivity.

Clearly, similar re-configuration procedures could be employed to offset attempts to disrupt mobile transmissions reaching specific fixed terminals.

7. GEOGRAPHICAL DIVERSITY NETWORK: SYSTEM DESIGN CONSIDERATIONS

An attempt will now be made to coalesce many of the concepts outlined in the previous sections of this paper into an overall system design to provide improved HF communications reliability and survivability, particularly in high-latitude regions.

Figure 9 illustrates a possible format for such a system in which mobile-to-fixed transmissions are received by a geographical diversity network, whilst fixed-to-mobile transmission is carried by single broadcast system sited at a convenient location.

System control and signal generation and combination are carried out at a specified control and processing site. Interconnections are implemented by 2 to 60 MHz ionospheric links, or via a PTT network, as appropriate. Broadcast traffic for

all mobiles in the operational area is transmitted using a multiple sub-channel format from which each mobile can extract the data addressed to it. The EOW sub-channel of the broadcast is used to request repeats of mobile data blocks received in corrupted form, and also to disseminate frequency management data to all mobiles who may wish to access the system.

Data transfer between the HF system and message originators and recipients can be effected via a PTT network or possibly via other dedicated HF or non-HF links.

Figure 10 shows an alternative system format where the centralised broadcast system of Figure 9 is replaced by a distributed network of lower power transmitters, possibly co-sited with the fixed receiving terminals. Thus in principle, for any specified mobile position, a broadcast transmitter site having maximum probability of successfully propagating to that mobile can be selected - as illustrated in Figure 10.

8. CONCLUDING REMARKS

This paper has identified the problems associated with mobile HF communications in high-latitude regions. Outline solutions to these problems have been proposed based upon a network of geographically-dispersed and interconnected receiving terminals.

Interconnection options have been considered for:

(a) a "stand alone" network;

(b) a network which makes use of communication media other than HF for interconnection.

A distributed network of the type illustrated in Figures 9 and 10 poses additional control problems. However, the increase in operational flexibility and robustness potentially available from such a system would appear to merit further research. In particular, the ability to reconfigure in the face of ionospheric disturbances, or physical or electromagnetic attack, would be most valuable.

Several areas for further investigation can be readily identified, ie:

(a) the problems of frequency management on a network basis, coupled with the development of appropriate RTCE procedures;

(b) the development of optimum signal formats and coding algorithms for the complete range of path conditions likely to be encountered;

(c) the development of say 2 to 60 MHz interconnection links capable of exploiting a variety of modes of propagation;

(d) techniques for disseminating control information to all points of the network.

It should be stressed finally that a system design of this nature would be capable of handling relatively resricted data rates, eg low-speed telegraphy. Data rates compatible with secure speech transmission (1.2 to 2.4 kbits/s) could not be sustained by such a system.

9. REFERENCES

1. Thrane, E. V., 1983: "Problems in HF propagation", AGARD Lecture Series No. 127 on "Modern HF Communications".

2. Bradley, P. A., 1975: "Long-term HF-propagation predictions for radio circuit planning", Radio & Electronic Engineer, Vol. 45.

3. Darnell, M., 1978: "Channel evaluation techniques for dispersive communications paths", in "Communication systems & random process theory", ed. J. K. Skwirzynski, Sijthoff & Noordhoff, the Netherlands.

4. Stein, S. & Jones, J. J., 1967: "Modern Communication principles", McGraw-Hill.

5. Darnell, M., 1985: "Problems of Mobile HF communication and techniques for performance improvement", to be published in Special Issue of Proc. IEE (Part F) concerned with "Mobile Radio".

6. Rogers, D. C. & Turner, B. J., 1985: "Connectivity improvement through path and frequency diversity", IEE Internatonal Conf. on "HF Communication Systems and Techniques", Conf. Publication No. 245.

7. Dawson, J. F. & Darnell, M., 1985: "An HF system design with embedded channel evaluation", as (6).

8. Hellen, P., 1985: "The provision of computer quality data transmission on HF", as (6).

9. Bartholomé, P. J. & Vogt, I. M., 1968: "COMET - a new meteor-burst system incorporating ARQ and diversity reception", IEEE Trans., Vol. COM-16, No. 2.

10. Bartholomé, P. J. & Vogt, I. M., 1965: "Ionoscatter communications: new design concepts and experimental results", SHAPE Technical Centre Report TR-83.

11. Yeh, L. P., 1960: "Simple methods for designing troposcatter circuits", IRE Trans., Vol. CS-8(3).

12. Darnell, M., 1977: "Medium-speed data transmission over HF channels", Proc. IERE International Conf. on "Digital processing of signals in communications", Loughborough.

13. Darnell, M., 1983: "HF system design principles", as (1).

14. Van Duuren, H. C. A., 1951: "Typendruktelegraphie over radiooverbindigen (TOR)", Tijdscr. Nederlands Radiogenoot, Vol. 16(2).

15. Alnatt, J. W., Jones, E. D. J. & Law, H. B., 1957: "Frequency diversity in the reception of selectively fading binary frequency - modulated signals", Proc. IEE, Vol. 104 (Part B).

16. Hewlett-Packard Journal, 1968: Special issue on signal averaging, April.

17. Bayley, D. & Ralphs, J.D., 1972: "PICCOLO 32-tone telegraph system in diplomatic communication", Proc. IEE, Vol.119(9).

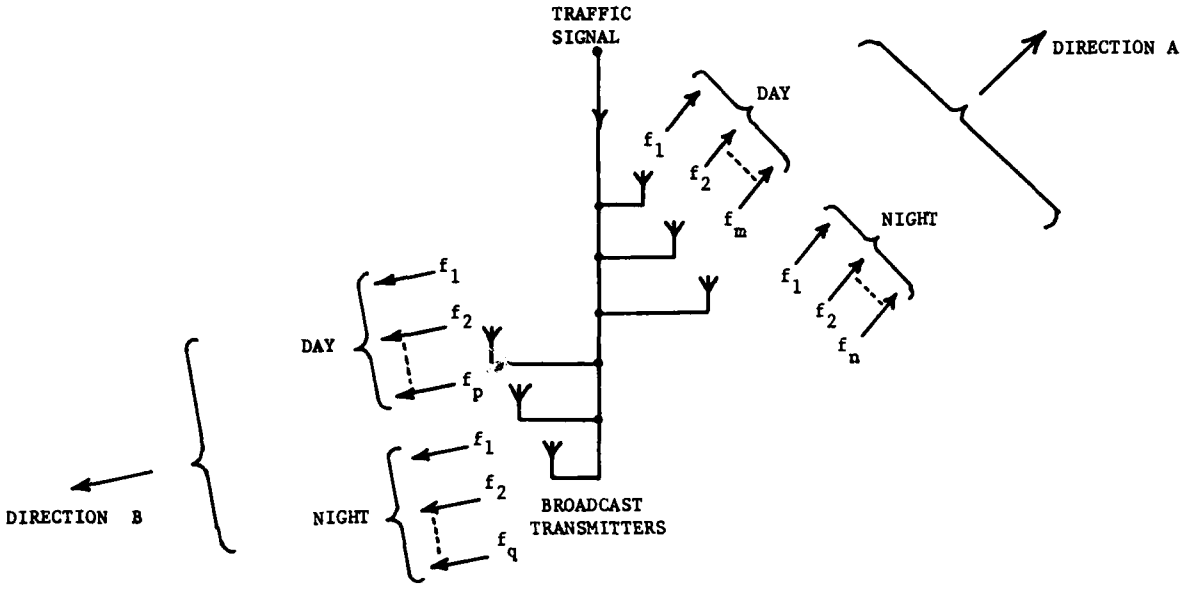


Figure 1 Fixed-to-Mobile Broadcast System

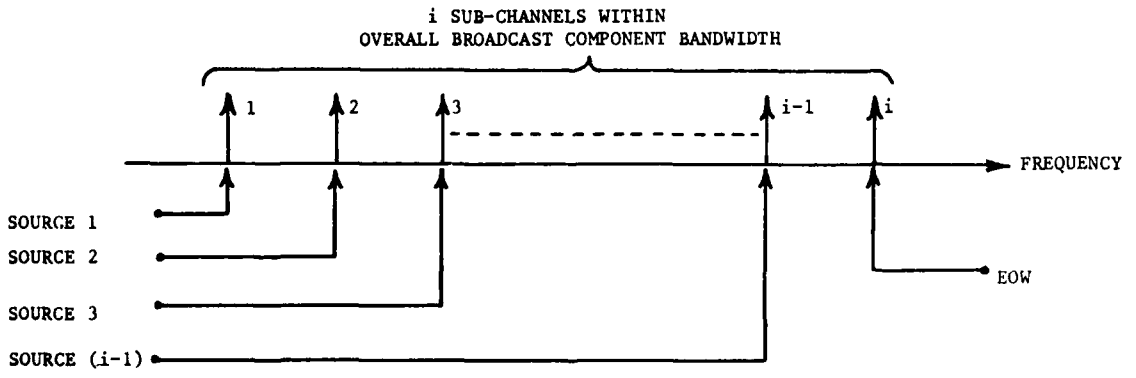


Figure 2 Broadcast Sub-Channel Raster

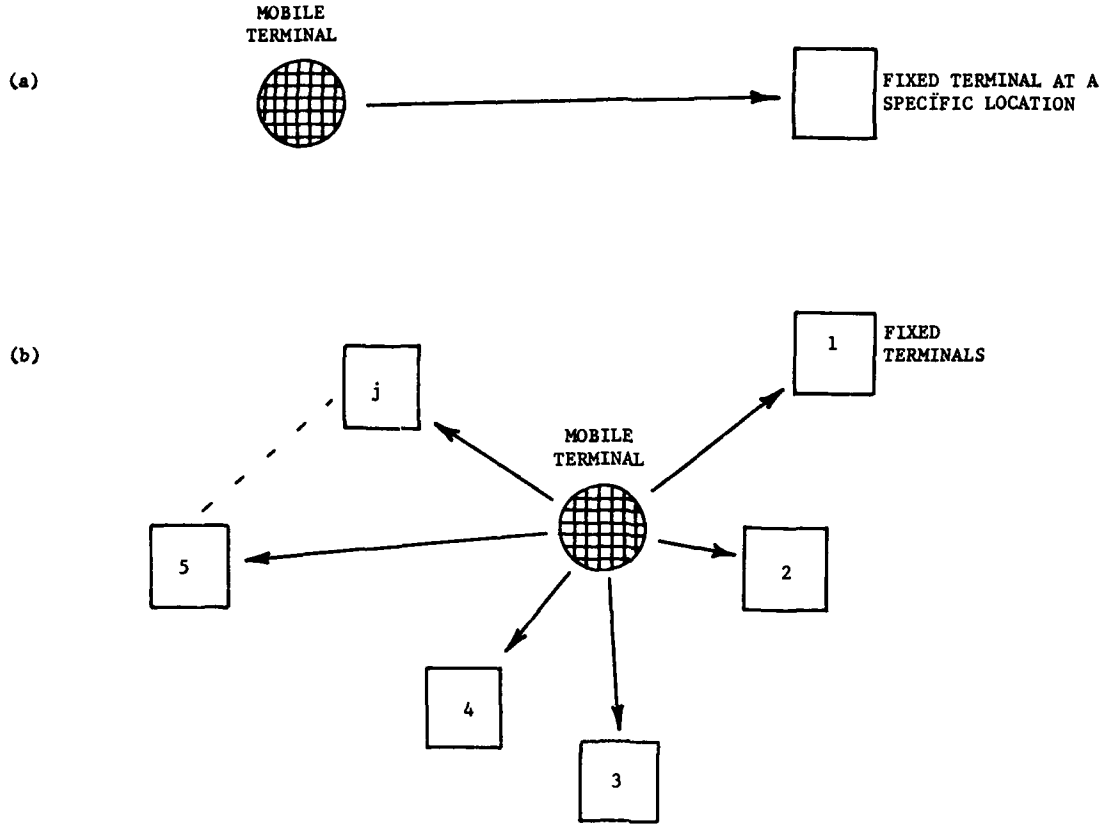


Figure 3 Options for Mobile Terminal-to-Fixed Terminal Communication

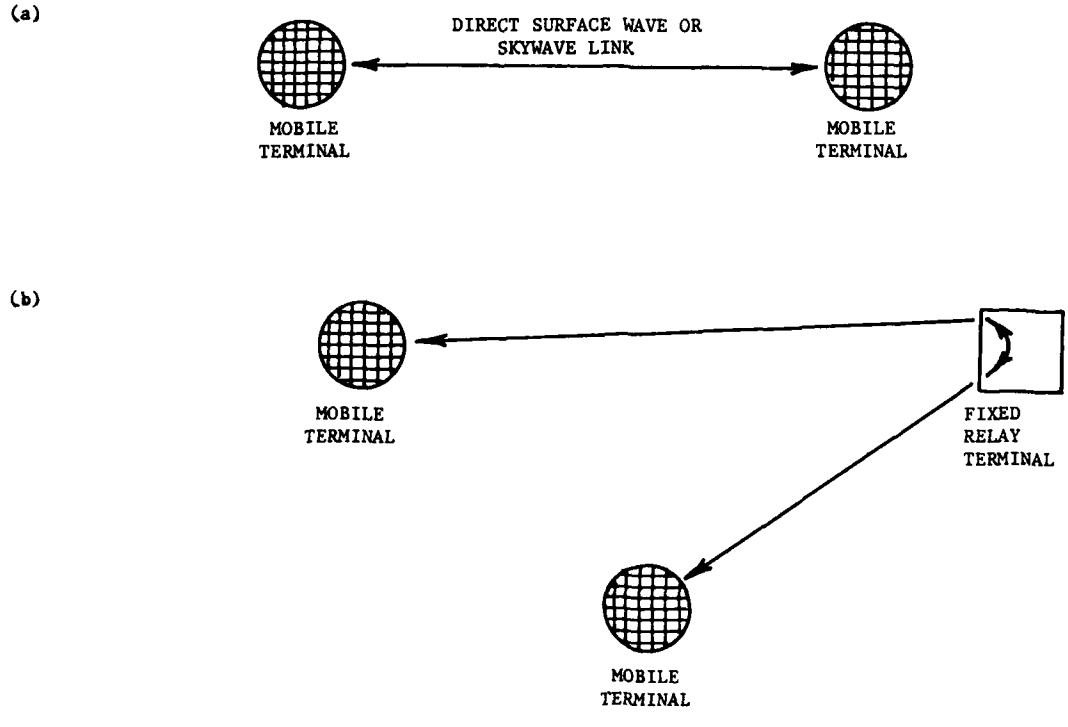


Figure 4 Options for Mobile Terminal-to-Mobile Terminal Communication

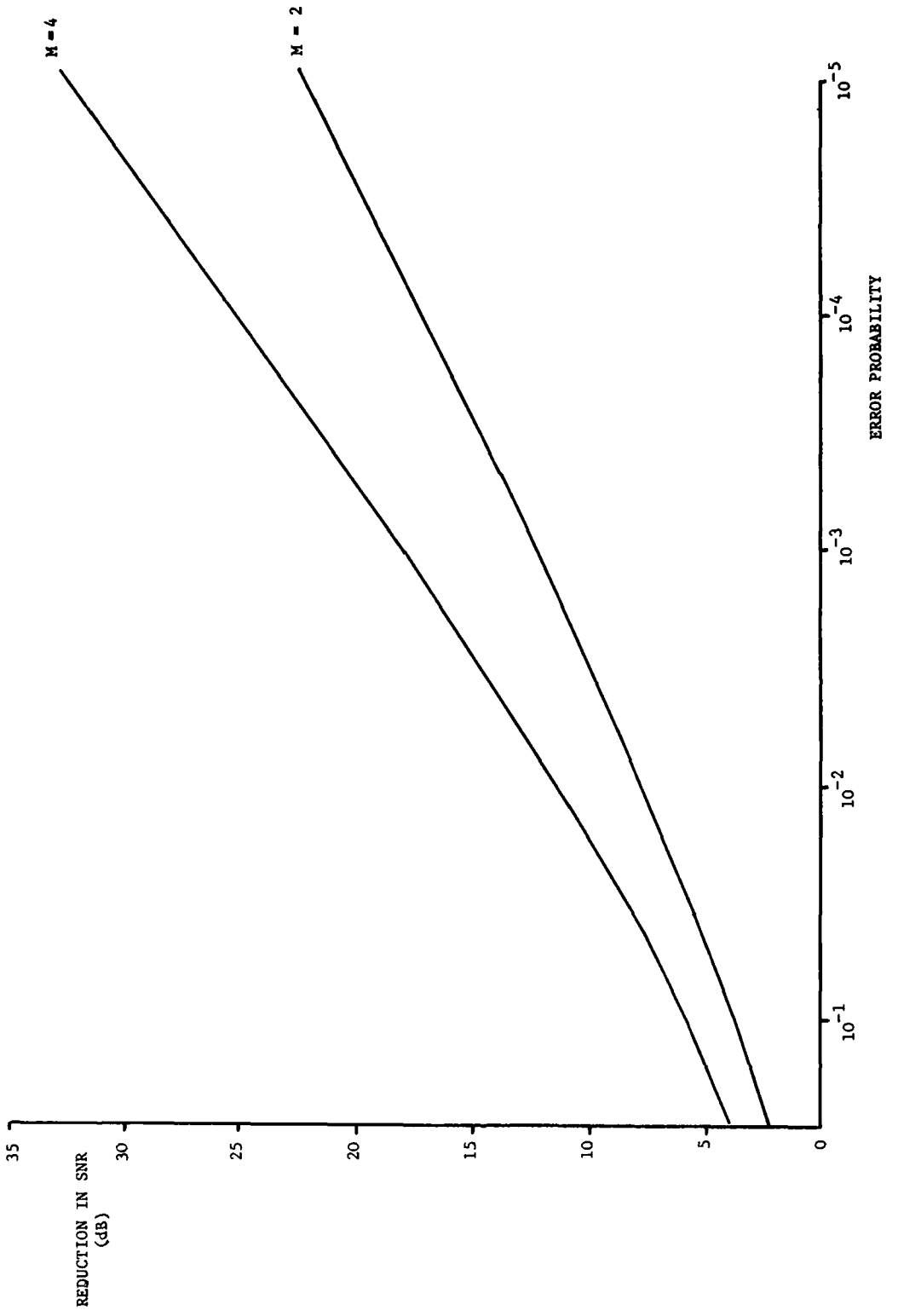


Figure 5 Effect of 2nd- and 4th-Order Diversity Combining on SNR required at Receiver

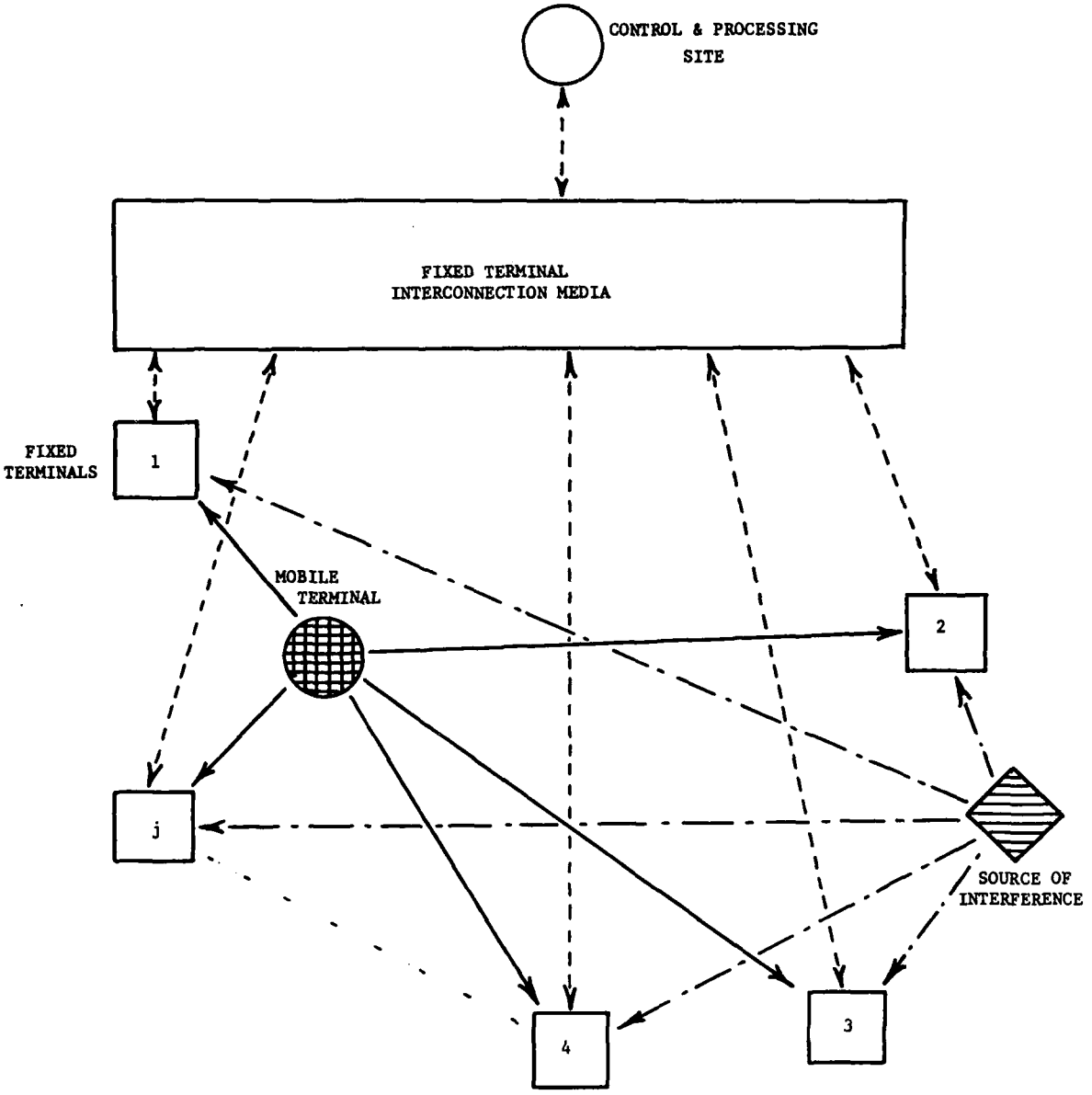


Figure 6 Schematic Diagram of a Geographical Diversity System

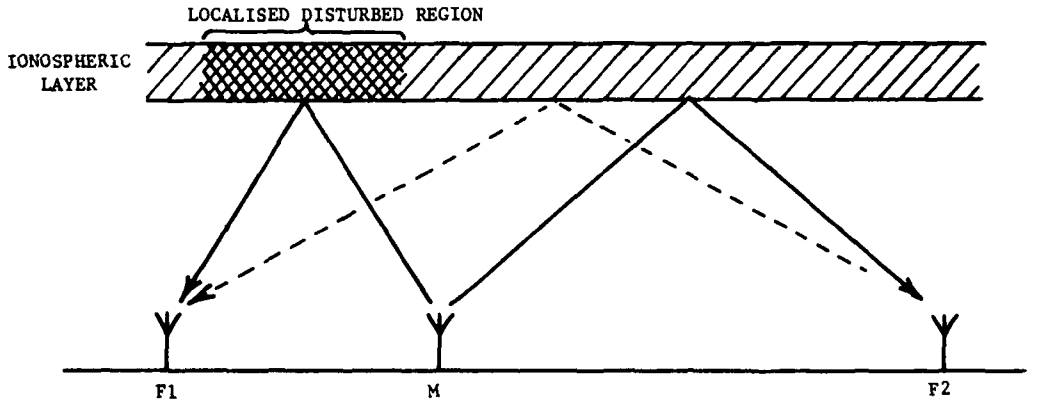


Figure 7 Avoidance of a Region of Localised Ionospheric Disturbance

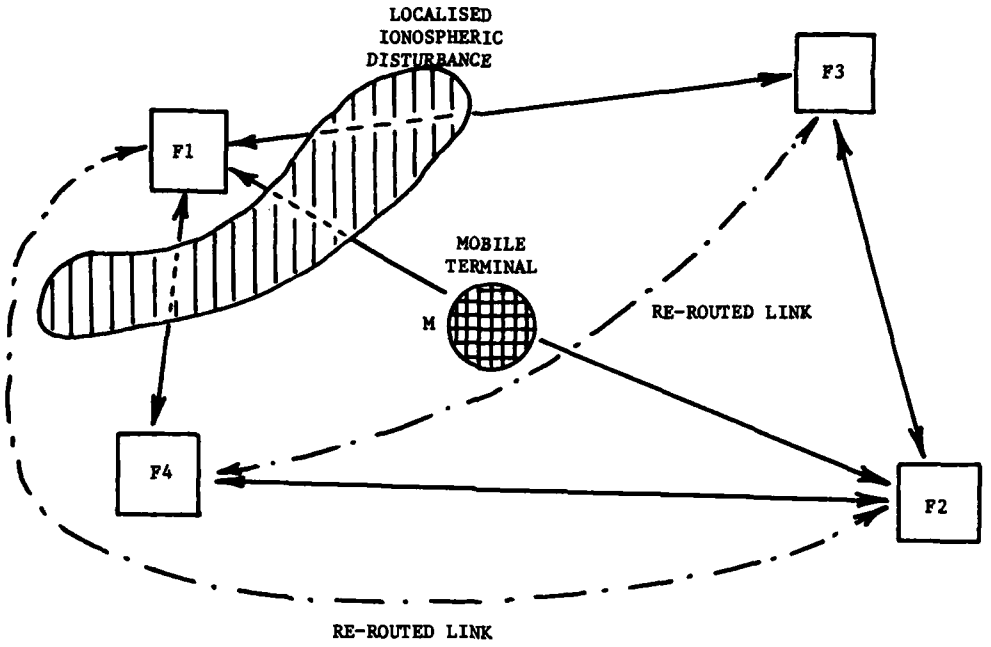


Figure 8 Reconfiguration of Geographical Diversity Network

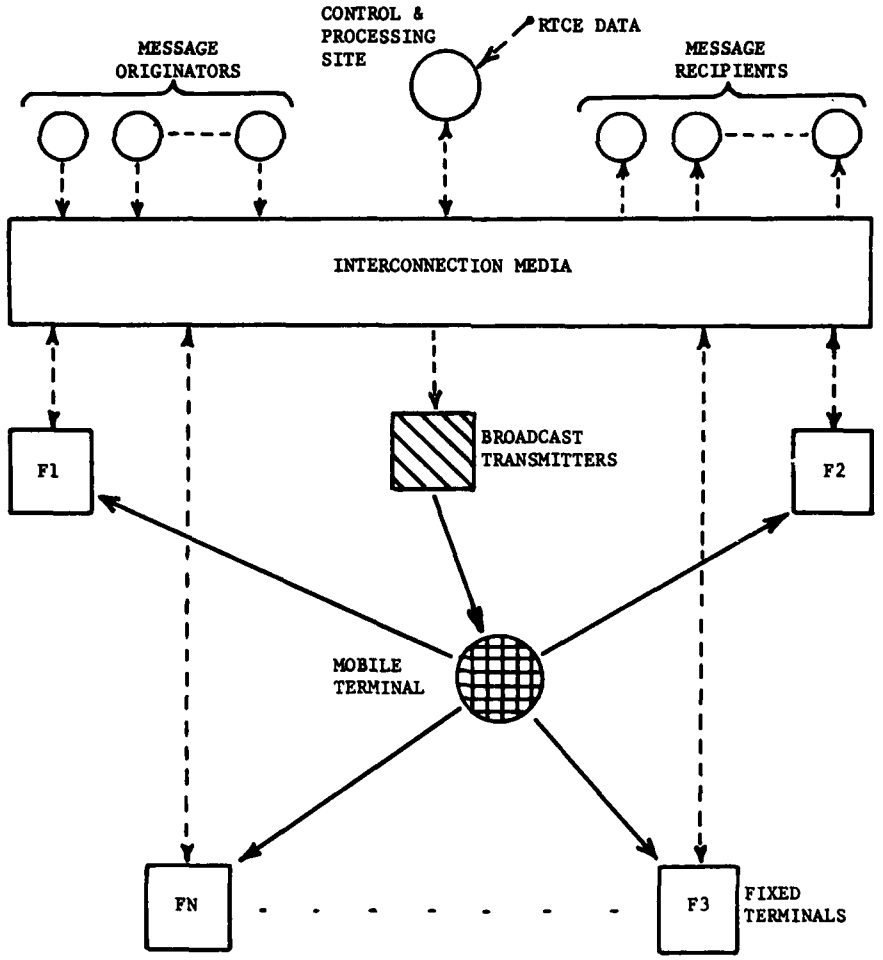


Figure 9 Communications System Format I: Centralised Broadcast

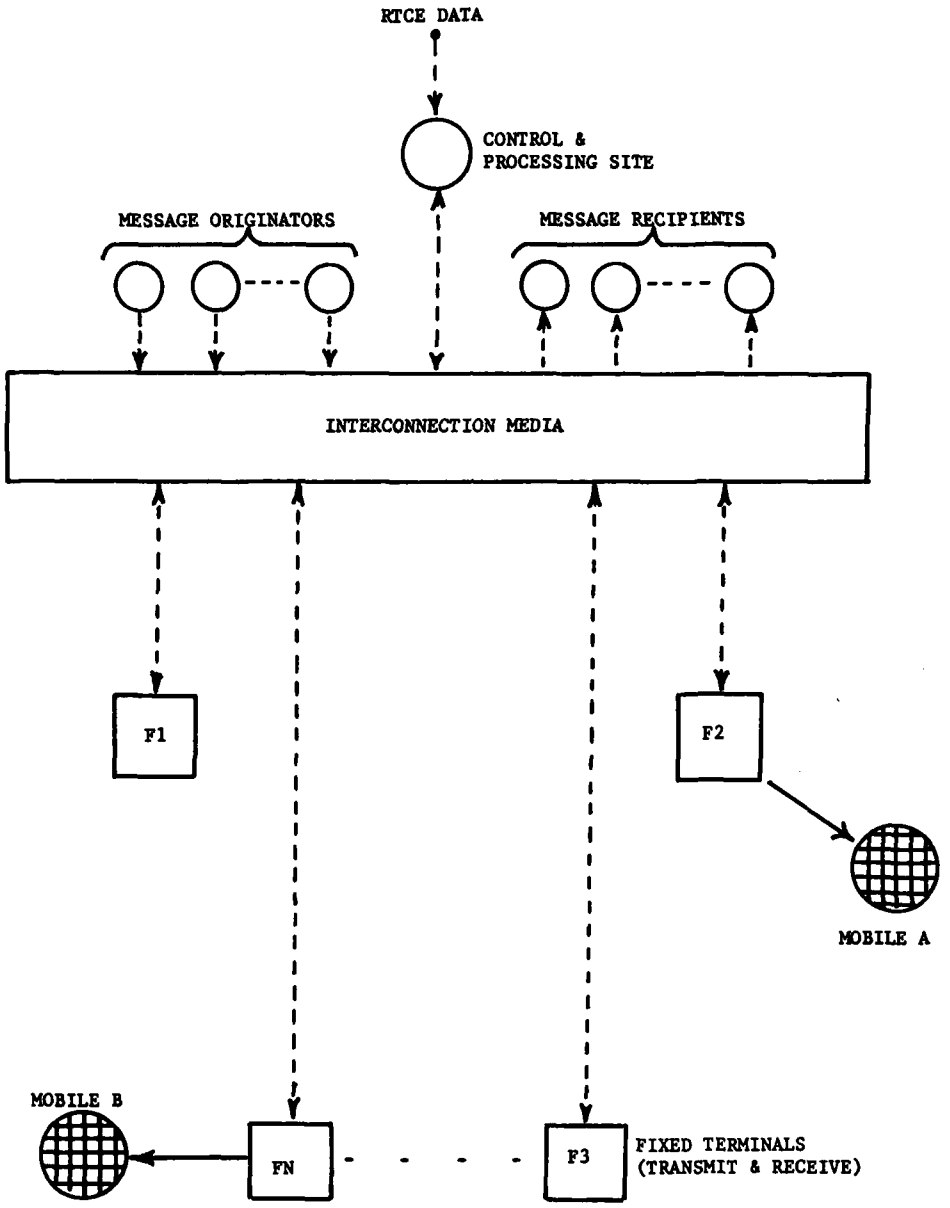


Figure 10 Communications System Format II: Distributed Broadcast

DISCUSSION

C.Goutelard, FR

Vous parlez de transfert de l'information en blocs courts. L'apparition des erreurs et leur distribution dépend non seulement de la liaison (bilan de liaison, bruit local...) mais aussi du modem.

Au congrès AGARD de juin 1984 nous avions présenté un système de correction d'erreur sur un modem auto-adaptatif et nous avions trouvé que pour gagner un facteur 100 sur le Taux d'erreurs il fallait utiliser des blocs de 7000 bits d'information.

Pouvez-vous préciser ce que vous entendez par blocs courts? Avez-vous des ordres de grandeur des longeurs utilisables?

Author's Reply

It is not possible to specify a single block length which will be applicable to all HF skywave paths and all modulation schemes. Rather, the transmission system must be configured to work in a basic block mode, with the actual length of the block being determined on-line as a result of channel evaluation (RTCE) measurements, modulation type and data rate in use.

P.S.Cannon, UK

COMMENT: In designing a geophysical diversity system for operation at high latitude it is important to know the necessary spacing of stations. The work of John Hargreaves, which gives the probability of riometer absorption at one location given a riometer absorption of a certain magnitude at another location, would be extremely useful in this regard.

PROPAGATION CHARACTERISTICS OF MEDIUM FREQUENCY SKYWAVE SIGNALS FROM THE CONTINENTAL U.S. AND CANADA RECEIVED AT FAIRBANKS, ALASKA

Robert D. Hunsucker and Brett S. Delana
Geophysical Institute
University of Alaska
Fairbanks, Alaska 99775-0800

John C. H. Wang
Office of Science and Technology
Federal Communications Commission
Washington, D.C. 20554

SUMMARY

Since September 1981, an F.C.C.-sponsored medium-frequency (MF) skywave monitoring program has been in continuous operation at the Geophysical Institute of the University of Alaska. The receiver frequency is automatically stepped through 16 channels every five minutes by the system programmer. Recordings are continuously made of ten or more standard broadcast stations on digital tape cassettes, which are then transferred on a weekly basis to form a data base on a VAX 11/780-785 computer. A noise source has also been provided for system calibration. Three antennas have been utilized during the program to date, a 32-meter top-loaded vertical with ground screen being the primary antenna. Measurements of the electrical characteristics and computer modeling of the antenna systems have been made, and selected results are presented, as well as daily, seasonal and sunspot variation effects on measured MF skywave signal strengths. The summer/winter and magnetic activity effects are profound on medium and long-distance paths to Fairbanks. Present plans are to continue this monitoring program until Fall 1987 - at least half of a sunspot cycle.

I. INTRODUCTION

Because of Alaska's particular location in respect to the contiguous United States, its rugged terrain with inhomogeneous ground electrical characteristics and its aurorally-disturbed ionosphere, sky-wave radio propagation between Alaska and the continental U.S. abounds with anomalies. This is especially true in the medium-frequency (MF) portion of the radio spectrum (300 to 3000 KHz) where the U.S. standard broadcasting service operates.

Assignment of broadcast band channels in the high latitude areas (e.g. Alaska) has, until now, been based on Part 73 of the Rules and Regulations of the Federal Communications Commission (FCC) which, among other things, contains MF skywave field strength curves. The data used to establish these curves were acquired essentially at midlatitudes, hence these curves do not fully represent propagation conditions in the high latitude areas. The FCC and the operators of Alaskan broadcasting stations have recognized this problem for some time and the result has been the implementation of a research program at the Geophysical Institute of the University of Alaska-Fairbanks to provide new MF skywave data over the appropriate paths. The study started at the Geophysical Institute May 15, 1981, and we hope to continue it through 1987 in order to describe MF skywave behavior over one-half of a sunspot cycle.

One effect of the previously mentioned propagation anomalies is to make it extremely difficult to predict MF skywave field strengths on Alaska-to-contiguous U.S. propagation paths. For instance, one can utilize the various formulas listed by Pokempner (1) and Wang (2) and the skywave propagation prediction programs such as those analyzed by Sailors et al. (3) with reasonable success to predict MF skywave signal strength and/or signal-to-noise ratio (S/N) on paths within the contiguous states, but <u>not</u> very successfully on propagation paths to and from Alaska.

The purpose of the MF skywave propagation investigation then, is to continue the program of medium frequency (MF) skywave signal strength measurements at Fairbanks, Alaska, of selected standard broadcast stations located in the U.S., Canada and Alaska. The end result of this program is to provide the FCC with sufficient median signal strength values throughout the standard broadcast band to quantitatively describe the diurnal, seasonal, sunspot cycle, and geophysical disturbance variations of MF skywave signals on these high latitude propagation paths. Thus, future standard broadcast band frequency allocations can be made on a realistic non-interference basis. Work done to date on this MF skywave research program has been reported by Hunsucker and Delana (4), Hagn (5), Hunsucker, et al. (6), and Hunsucker and Delana (7).

II. DESCRIPTION OF THE MONITORING PROGRAM

A. Location and Characteristics of the Field Site

Table 1 shows some characteristics of the Ace Lake Field Site

B. Description of Equipment

The equipment and antennas used in this experimental program are located at the Ace Lake Field Site approximately 4 km due west of the Geophysical Institute. The system is built around a commercial general purpose receiver modified for analog AGC output. The receiver frequency is automatically stepped through 16 channels every five minutes by the system programmer. Digital tape cassette recordings of signal amplitude are continuously made on ten or more standard broadcast stations. These data are then transferred on a regular basis to standard format computer tape for analysis on a VAX 11/780-785 computer. A noise source is also recorded continuously for regular system calibration.

C. Antennas

Three antennas have been utilized during the program to date: 1) a 187 meter longwire, 2) a 12 meter vertical monopole with ground screen, and 3) a 32 meter top-loaded vertical with ground screen. In an effort to quantitatively describe our antenna systems, extensive impedance and VSWR measurements and computer modeling efforts have been made on the antennas.

Figure 1 shows the 32 meter top loaded vertical antenna (TLVA) and Figure 2 is a drawing of the end-fed-longwire (EFLW) antenna model used for computer pattern modeling. An example of the "NEC" plot of the vertical radiation pattern of the EFLW antenna for f = 1.030 MHz and 0° azimuth is shown in Figure 3. The vertical and horizonal radiation patterns of the top-loaded-vertical antenna (TLVA) were modeled using a "method-of-moments" computer code called "MININEC" (8), (9), (10). This computer code is a less sophisticated (and much less expensive) version of the Numerical Electromagnetic Code (NEC) (4), (5). These antenna patterns may be considered to be a first approximation of the actual TLVA patterns, and are shown in Figures 4 and 5 in the vertical and horizonal planes, respectively. These figures indicate that both the vertical and horizontal patterns are quite uniform for the range of elevation and azimuth angles characteristic of skywave signals being monitored at Fairbanks.

These MININEC results are quite encouraging in their uniformity for the TLVA patterns and should make quantitative path signal strength calculations possible for all stations monitored.

We plan to use the full NEC program to model the TLVA patterns, as well as to attempt some airborne measurements of the pattern before the end of this project.

III. RESULTS

Figures 6 and 7 are plots of receiver AGC voltage for various MF skywave transmissions monitored at Fairbanks. The location and frequency of each standard broadcast station are listed on the borders of the figures and universal time is plotted along the abscissa (Alaska standard, 150° west meridian time or U.T. - 10 hrs). The AGC voltage scale is included at the lower left corner and the calibration curve for converting receiver AGC to r.f. signal strength at the receiver input is given in Figure 8. The diurnal behavior of the MF skywave signals is shown for a magnetically quiet winter day for high sunspot number. For example, signals from KFAX and KGO (San Francisco) are received from ~ 06 - 16 UT or 2000 - 0600 AST in Figure 6.

For a disturbed day the diurnal behavior changes considerably, as illustrated in Figure 7 when the only MF skywave signals received in Fairbanks were from Kotzebue and McGrath, Alaska. All signal propagation from the contiguous U.S. disappeared.

The next four figures illustrate the seasonal behavior of the monitored MF skywave signals. Figure 9 is a fifty-one day median plot of all signals received for winter 1981 for high sunspot number and illustrates the consistent propagation during night of the signals from the western and northwestern regions of the contiguous U.S. to Alaska. A rather dramatic contrast is shown in Figure 10 for summer 1982, when the only measurable signal strengths occurred for a few hours per night from Spokane, Washington; Anchorage, Alaska; and San Francisco, California.

The equinoctial period behavior is displayed in Figures 11 and 12 for Spring 1982 and Fall 1983 respectively, showing transitional signal strengths between summer and winter.

Sunspot Cycle Effects

Figure 13 shows a plot of solar cycle 21 with the interval of MF skywave monitoring indicated by a bar at the bottom. From mid-winter 1981 to mid-winter 1984 the relative sunspot number (RI) decreased from 147 to 18 and the 10.7 cm solar flux (SF) decreased from 208 to 76. This represents a decrease in RI by ~ a factor of 8 and in SF by ~ 3, which should have significant effects on MF skywave propagation.

IV. DISCUSSION

Propagation Path Geometry

Figure 14 illustrates the uniqueness of the Faibanks MF skywave monitoring station as a high latitude site, Hunsucker (12). The figure depicts great-circle paths from most of the standard AM stations monitored at Fairbanks on an azimuthal equidistant map projection. The stipled sections depict the location of auroral ovals for midwinter near magnetic midnight (1200 UT or 0200 AST - Alaska Standard Time). The lightly stipled auroral oval section shows the location of the oval for disturbed magnetic conditions (planetary K-index, Kp = 5.0), and the darker oval (further north) depicts the oval for quiet conditions (Kp = 1.0). Only the portion of the oval affecting the paths is shown. The single letters denote standard broadcast band transmitters as:

N = Nome, Alaska	E = Edmonton, Alberta, Canada
M = McGrath, Alaska	C = Casper, Wyoming
A = Anchorage, Alaska	P = Philadelphia, Pennsylvania
S = Seattle, Washington	V = Vladivostok, USSR

As may be seen, during very quiet magnetic conditions (Kp = 1.0) only the Philadelphia to Fairbanks path is directly affected - with the Chicago to Fairbanks path marginally affected. During disturbed conditions (Kp = 5.0) all paths are aurorally disturbed (San Francisco the least). Most of the time 1.0 < Kp < 5.0, and most of the paths will be affected near 1200 UT.

This qualitative discussion helps to better understand the specific disturbance behavior of each path. For instance, one would expect aurorally disturbed behavior of the short paths from Kotzebue, McGrath and Anchorage ~ 50% of the nights of the year, since their ionospheric reflection points will be in the auroral oval, on an average, 50% of the nights. Consequently, auroral D-region and sporadic-E ionization (10) will govern these propagation modes.

On the other hand, the San Francisco to Fairbanks path appears to have an ionospheric reflection point in the auroral oval only during quite disturbed conditions (Kp = 5.0), but most probably will have one reflection point in the region of low electron density, the "main ionospheric trough" (13), (14). Specific descriptions of MF skywave signal strength variation for the conditions described above will be given in following sections.

At least a qualitative idea of the sunspot cycle effect may be gained by comparing specific paths in winter 1981 with the same paths in winter 1984.

Four paths can be compared, with transmission characteristics as shown in Table 2.

Also remembering that D-region absorption $\approx (\frac{1}{f^2})$, KSKO at 870 KHz with its reflection point almost always in the auroral oval should show higher signal strengths in 1984 over 1981 compared to KGA at 1510 KHz with its ionospheric reflection point usually lying outside the auroral oval. We are further assuming that MF skywave propagation is more profoundly affected by sunspot cycle changes in D-region absorption than by changes in ionization of the E and F layers.

With this background information in mind we can make the comparison shown in Table 3.

The values in Table 4 seem to support the hypothesis that MF skywave signals propagating at high latitudes are dominated by D-layer absorption, and that these absorption effects are considerably less severe during sun spot minimum periods than near sunspot maximum. These results, of course, only strictly apply to the given MF stations monitored in Fairbanks during midwinter.

CONCLUSIONS

Analysis of data obtained from the medium-frequency skywave monitoring program carried out at Fairbanks, Alaska, from 1981-1985 yields the folllowing conclusions.

- The recording and data analysis system continues to perform very reliably with total data loss of only 3.3% in 1984.
- The top-loaded-vertical-antenna (TLVA) has performed very well, displaying stable electrical characteristics through the severe climatic conditions characteristic of this continental sub-arctic environment.
- A simplified "method-of-moments" antenna pattern modeling program called "MININEC" was utilized to obtain azimuth and elevation patterns for the TLVA for 1.1 MHz. The modeling effort shows that the azimuth and elevation patterns are very uniform at this frequency.
- An auroral overlay was plotted on an azimuthal equidistant map projection centered on Fairbanks which reveals the qualitative explanation of the general behavior of various MF skywave paths.
- The daily and seasonal behavior of signal strength on most paths does not markedly differ from 1983 to 1984 except during midsummer. KFAX San Francisco shows five to six hours per day of usable signal in 1984 compared to about three hours of barely detectable signal in 1983 (sunspot cycle effect).
- More specific sunspot cycle effects on four selected paths illustrate the dominance of D-layer absorption on MF skywave high latitude propagation through a solar cycle. From 1981 midwinter to 1984 midwinter, the signals from Kotzebue, Alaska increased in duration by 35%, while the Spokane, Washington signal showed no significant change. Stations which propagated signals to Fairbanks in 1981-82, but not in 1984 include Detroit, Albuquerque, Santa Monica, Eugene, Louisville, and Vladivostok.

There are still several "unknowns"

1. What is the actual skywave mode structure (how many and what kind of ionosphere reflection modes).
2. What are the actual antenna patterns in elevation and azimuth.
3. Polarization effects (Elliptical, predominantly vertical or horizontal)?

Acknowledgements

We gratefully acknowledge the advice and encouragement of Mr. Augie Hiebert, Chairman of Northern Television, Inc., Dr. Charles M. Northrip, Director, Alaska Public Broadcasting Commission, Mr. Henry Hove, also of the APBC, and Mr. John C. H. Wang, Office of Science and Technology, Federal Communications Commission. We also express our gratitude to Geophysical Institute staff members Stanley Schwafel for valuable assistance on maintenance and operation of the system, Rick Guritz and Celia Rohwer for software development and ongoing assistance, to Kay Driscoll for continued cooperation in making her property available for use as a field site for this project, and to Patricia Jones for typing and editorial assistance. Funding for this effort has been provided by FCC Contract Number FCC-0375 and by Grants from the APBC.

Table 1
Pertinent Parameters of the Ace Lake Field Site

Location =	64°52'	North geographic latitude
	147°56'	West geographic latitude
	64°45'	North geomagnetic latitude
	103°01'	West geomagnetic latitude
	64°40'	Invariant latitude
Dip =	76°54'	
L =	5.46	
h =	600 ft. MSL	

Geographic Azimuth	Radio Horizon
90°	0°
135°	1.5°
180°	2.2°
225°	1.6°
270°	3.2°

*Tundra underlain with permafrost	Conductivity, σ in mhos/meter (siemens)	Permittivity (ε)
(a) surface	~ 0.018 to 0.036	~ 25-42
(b) two feet below surface	~ 0.025 to 0.098	~ 33-788

*Acquired in August 1982 by Open-wire-line (OWL) technique from 500 Khz to 12,000 KHz by G. Hagn. (5)

Table 2
Comparison of transmission characteristics on four paths

Call Letters	Location	Frequency (kHz)	Power Output (kw)	Path Length and Remarks
KSKO	McGrath Alaska	870	--	Short north-south auroral path
KTWO	Casper Wyoming	1030	50	D=3553 km, long path. One ionospheric reflection point in auroral oval during moderately disturbed conditions.
KFAX	San Francisco California	1100	50	D=3464 km, long path. One ionospheric reflection point in auroral oval during disturbed conditions.
KGA	Spokane Washington	1510	50	D=2640 km. Similar to KTWO path.

Table 3
Comparison of signal strength changes on four paths from 1981 to 1984

Station	1981 (RI = 147) Signal Present % *	1981 (RI = 147) Signal Maximum (μv)	1984 (RI = 18) Signal Present % *	1984 (RI = 18) Signal Maximum (μv)	Signal Increase 1981-1984 Signal Present % *	Signal Increase 1981-1984 Signal Maximum (μv)
KSKO	53%	7 μv	87%	20 μv	35%	13 μv
KTWO	30	8	41	8	11	0
KFAX	62	9	75	13	13	4
KGA	50	7	50	7	0	0

*Percentage of operating period when signal was present.
All signal levels referred to receiver input.

REFERENCES

(1) Pokempner, Margo, Comparison of available methods for predicting medium frequency skywave field strengths, (1980), NTIA Report 80-42, pp. 26-28 and Appendix C.

(2) Wang, John, C. H. A., Interference and sharing at medium frequencies: Skywave propagation considerations, AGARD Conf., Proceedings on Propagation Aspects of Frequency Sharing, Interference and System Diversity, (1983), pp. 9-1 to 9-6.

(3) Sailors, D. B., W. K. Moison and R. P. Brown, Accuracy of high frequency maximum usable frequency (MUF) predictions,(1981), NOSC Tech. Report 695, Naval Ocean Systems Center, San Diego, CA.

(4) Hunsucker, R. D. and B. S. Delana, High-latitude field-strength measurements of standard broadcast band transmissions, (1983), Report for the period 15 May 1981-14, November 1982, to Office of Science and Technology, Federal Communications Commission under Contract No. FCC-0375, Washington, D.C. 20554.

(5) Hagn, G. H., Calibration of the University of Alaska 615-ft. end-fed longwire antenna, (1983), Report to the Geophysical Institute, University of Alaska under Purchase Order No. 44735, Fairbanks, Alaska 99701.

(6) Hunsucker, R. D., B. S. Delana and P. L. Brooks, High-latitude field-strength measurements of standard broadcast and skywave transmissions, (1983), Report for the period 15 November 1982-31, December 1983, to Office of Science and Technology, Federal Communications Commission under Contract No. FC-0375, Washington, D.C. 20554.

(7) Hunsucker, R. D. and B. S. Delana, Medium frequency skywave propagation characteristics of signals received at Fairbanks, Alaska, (1984), Presented at URSI National Radio Science Meeting, 11-13 January 1984, University of Colorado, Boulder, Colorado.

(8) Julian, A. J., J. C. Logan and J. W. Rockway. MININEC: A mini-numerical electomagnetics code, (1982), Technical Document 516, Naval Ocean Systems Center, San Diego, California 92152.

(9) Miller, E. K. and G. J. Burke, Personal computer applications in electromagnetics, IEEE Antennas & Propagation Society Newsletter, (1983), 25 (4), 5-9.

(10) Campbell, D. V., Personal computer applications of MIKNINEC, IEEE, Antennas and Propagation Society Newsletter, (1984), 5-9.

(11) Burke, G. J. and A. J. Poggio, Numerical Electromagnetics Code (NEC)--Method of Moments, (1981), Technical Document 116, Naval Ocean Systems Center, San Diego, Calfornia 92152.

(12) Hunsucker, R. D. and H. F. Bates, Survey of polar and auroral region effects on HF propagation, Radio Science, 4(4), (1969), 347-365.

(13) Muldrew, D. B., Alouette-ISIS radio wave studies of the cleft, the auroral zone, and the main trough and of their associated irregularities, Radio Science, 18 (6), (1983), 1140-1150.

(14) Dudeney, J. R., A. S. Rodger and M. J. Jarvis, Radio studies of the main F region trough in Antarctica, Radio Science, 18 (6) (1983), 927-936.

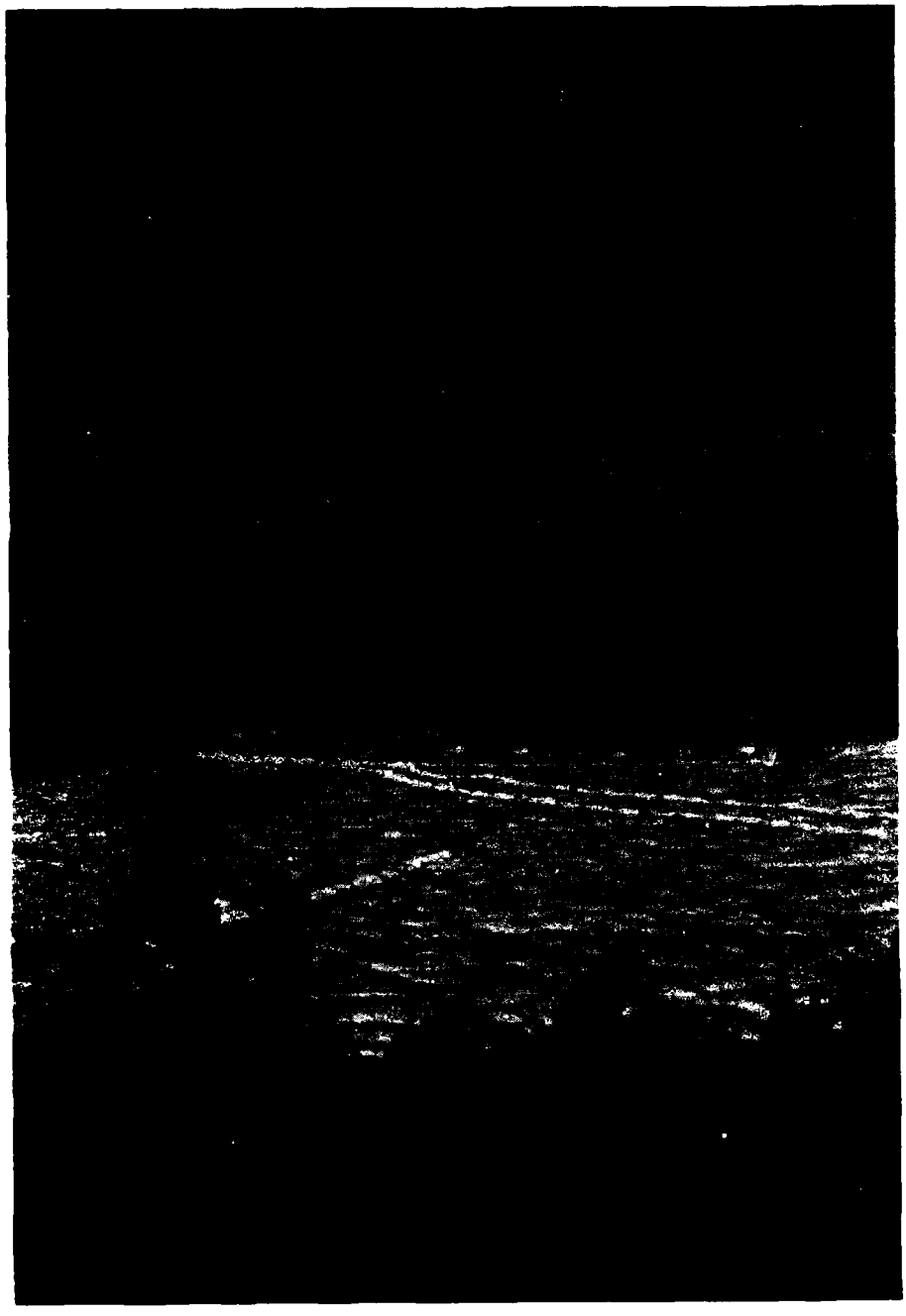
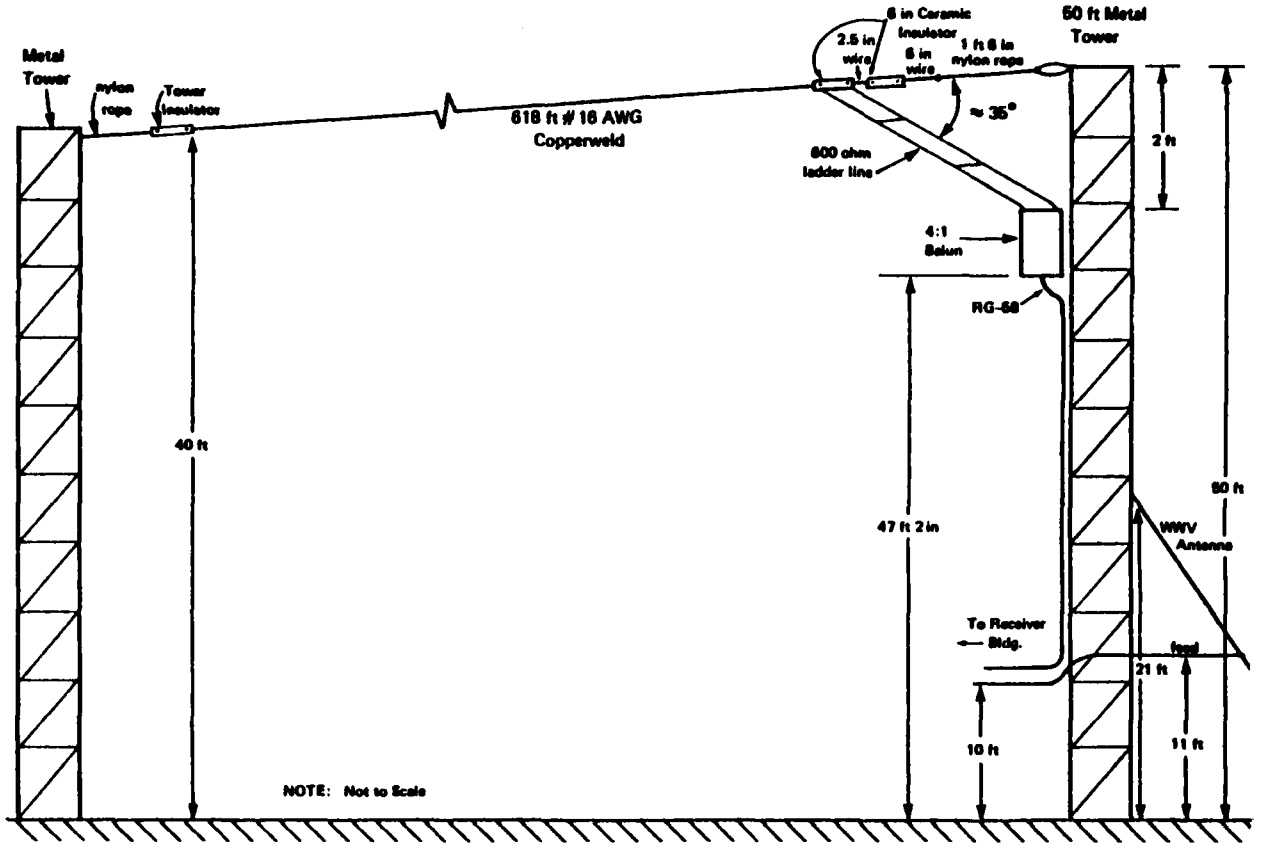


Figure 1. Thirty-two meter top-loaded vertical antenna (TLVA) located at Ace Lake field site near Fairbanks, Alaska. The "top hat" consists of four 22 meter wires at an angle of 45° with the tower. The TLVA is fed at the base through a 16.5 μHy inductor, and the ground screen consists of thirty equally-spaced 100 meter radial copper wires.

Figure 2

Sketch of end-fed longwire antenna



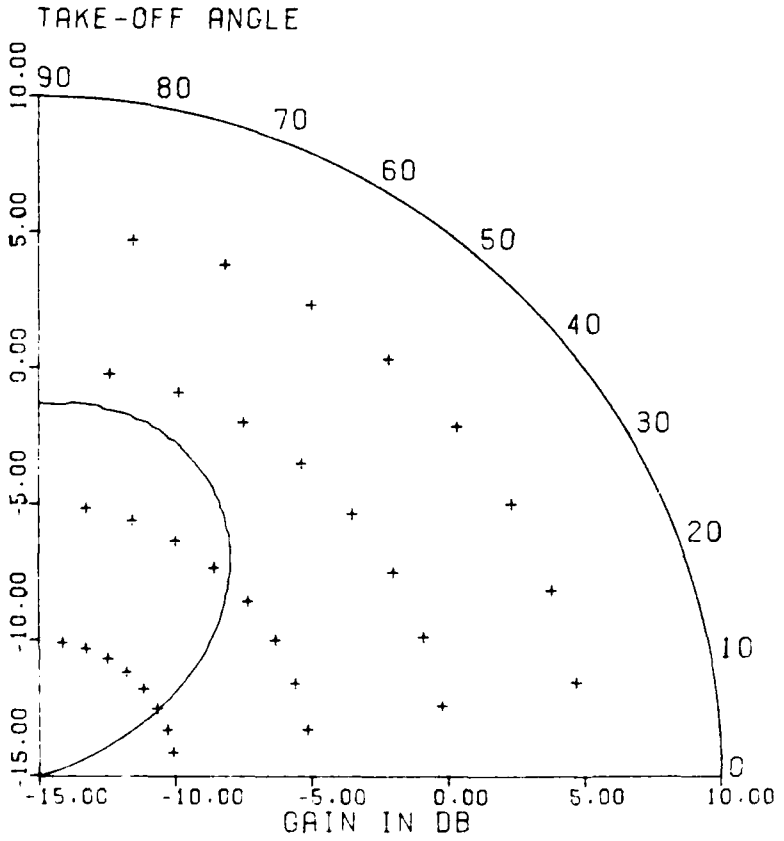


Figure 3. Example of Numerical Electromagnetic Code (NEC) plot of the vertical radiation pattern of the end-fed longwire antenna (EFLW) for f = 1.030 MHz and 0° azimuth.

Figure 4

CALCULATED VERTICAL RADIATION PATTERN FOR TLVA AT AN AZIMUTH OF 140° (San Francisco - Fairbanks Path, D = 3354km, Az = 138.5°)

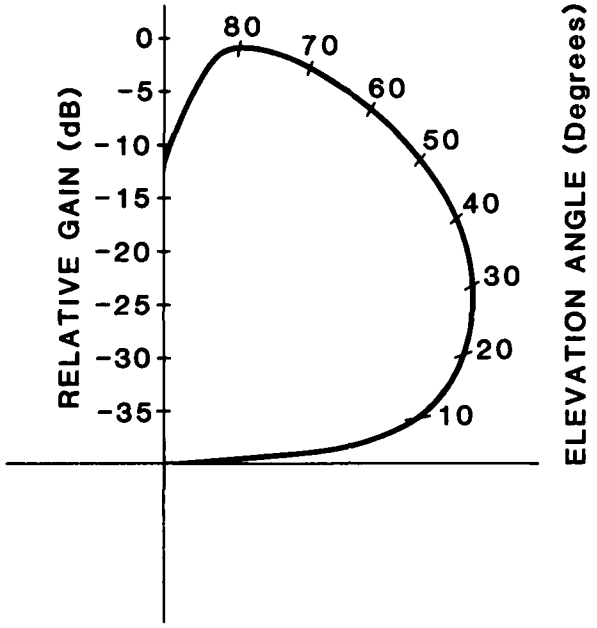
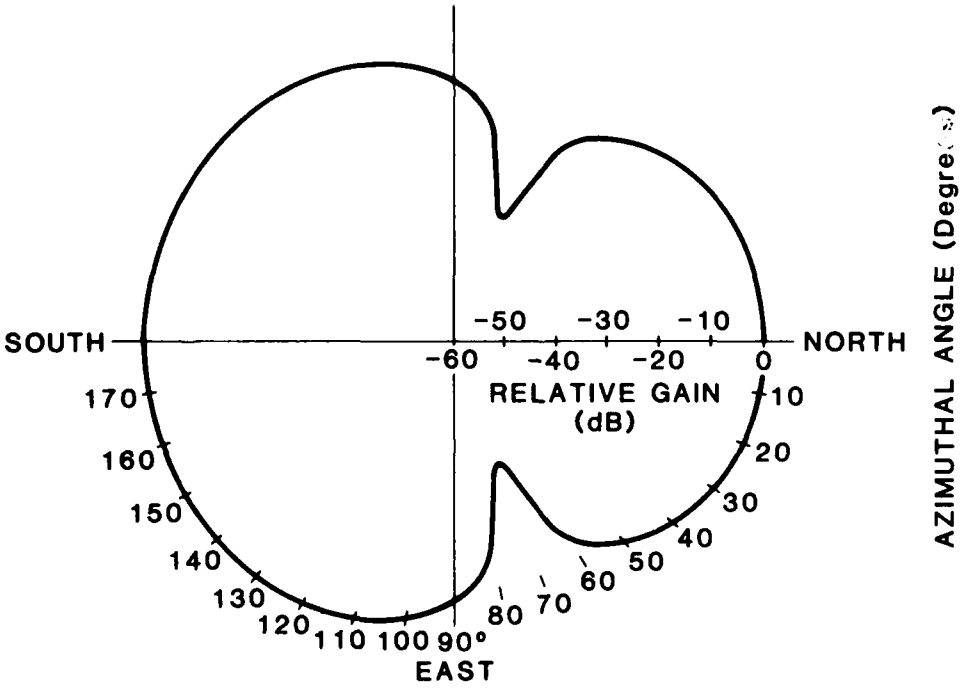


Figure 5

CALCULATED AZIMUTHAL RADIATION PATTERN FOR TLVA AT AN ELEVATION ANGLE OF 20° (San Francisco - Fairbanks Path)



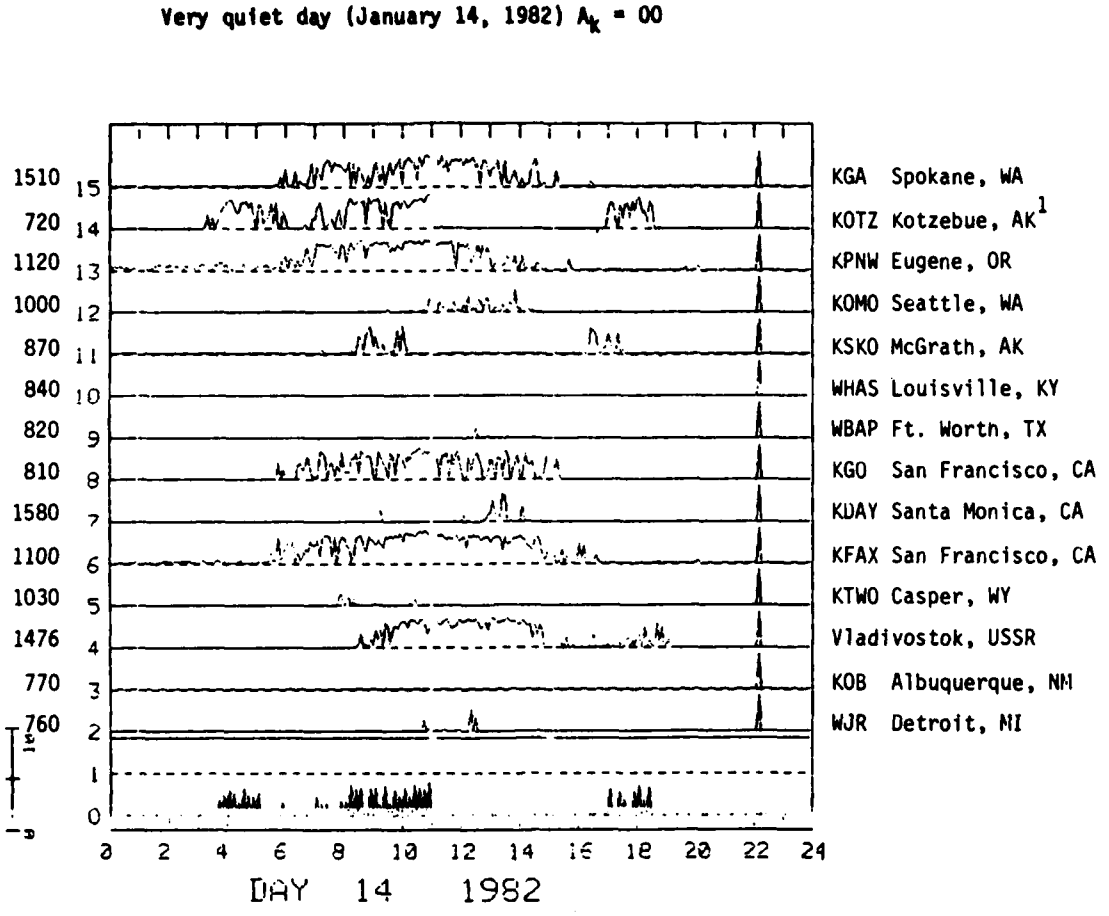


Figure 6. Diurnal signal strength behavior. Plot of receiver AGC voltage for standard broadcast stations listed at right received at Fairbanks during quiet midwinter period. Scale at lower left is receiver AGC in volts. Time on abscissa is Universal time (Alaska Standard Time = UT -10 hours). Frequencies in KHz listed on left border.

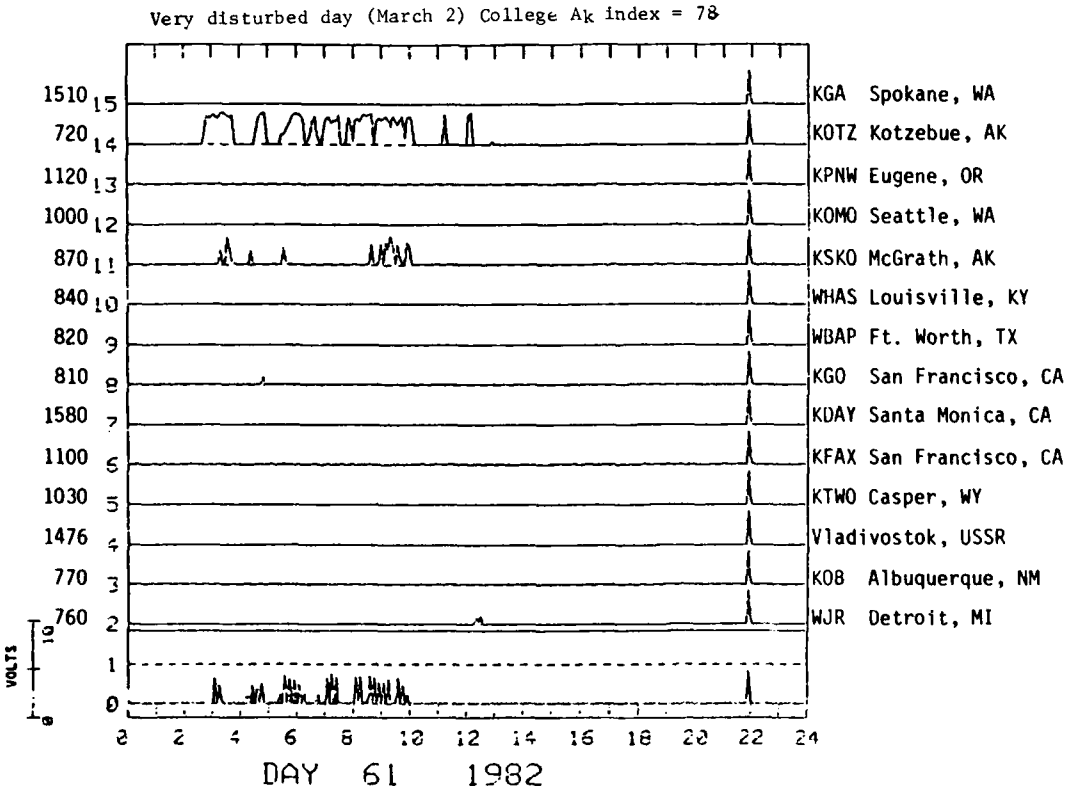
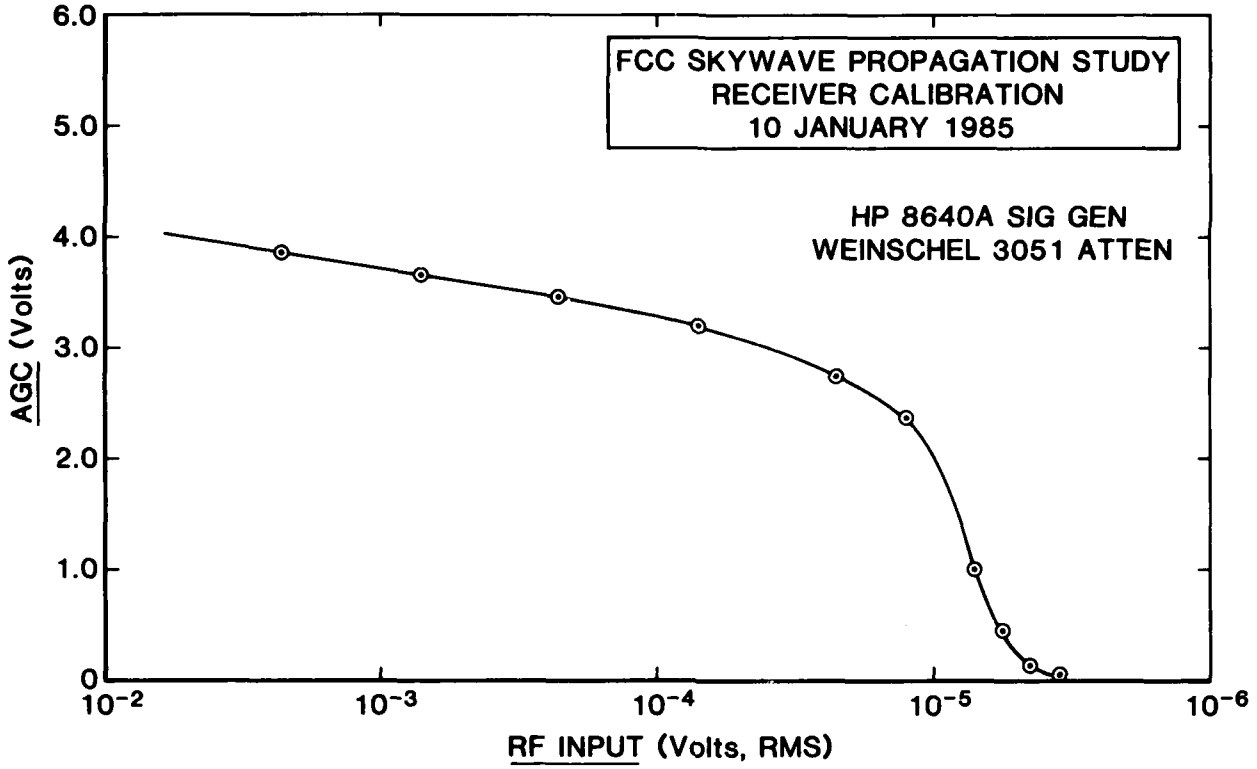
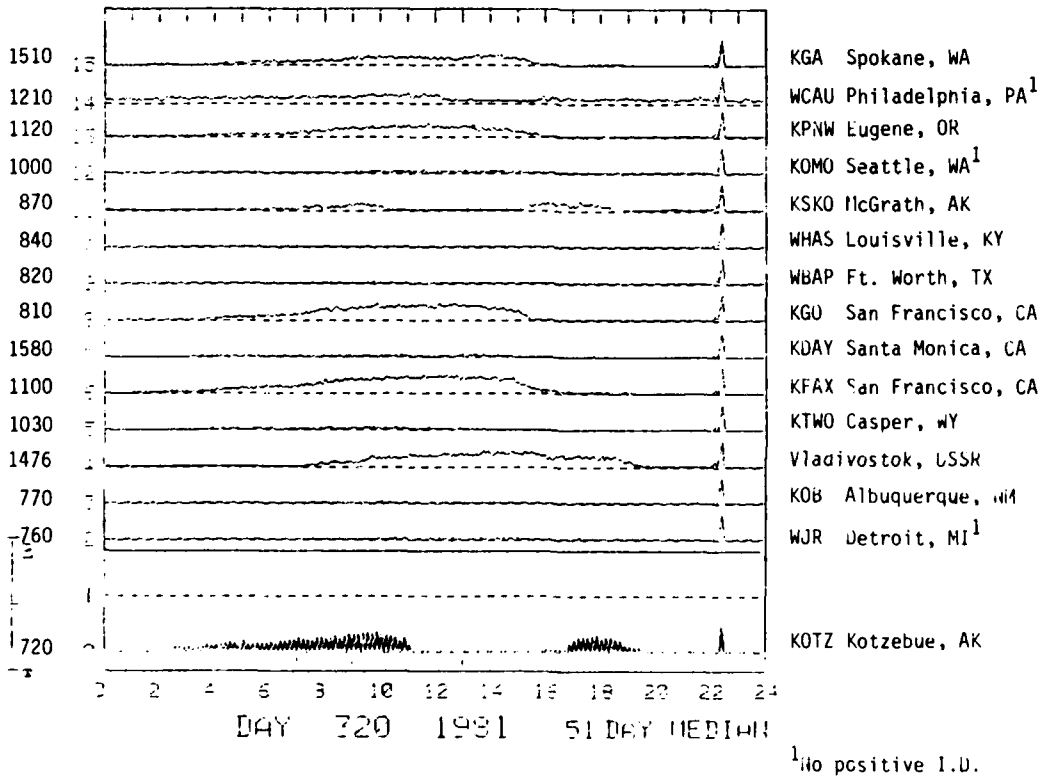


Figure 7. Plot similar to that in Figure 6, except for very magnetically disturbed day during Spring Equinox.

Figure 8



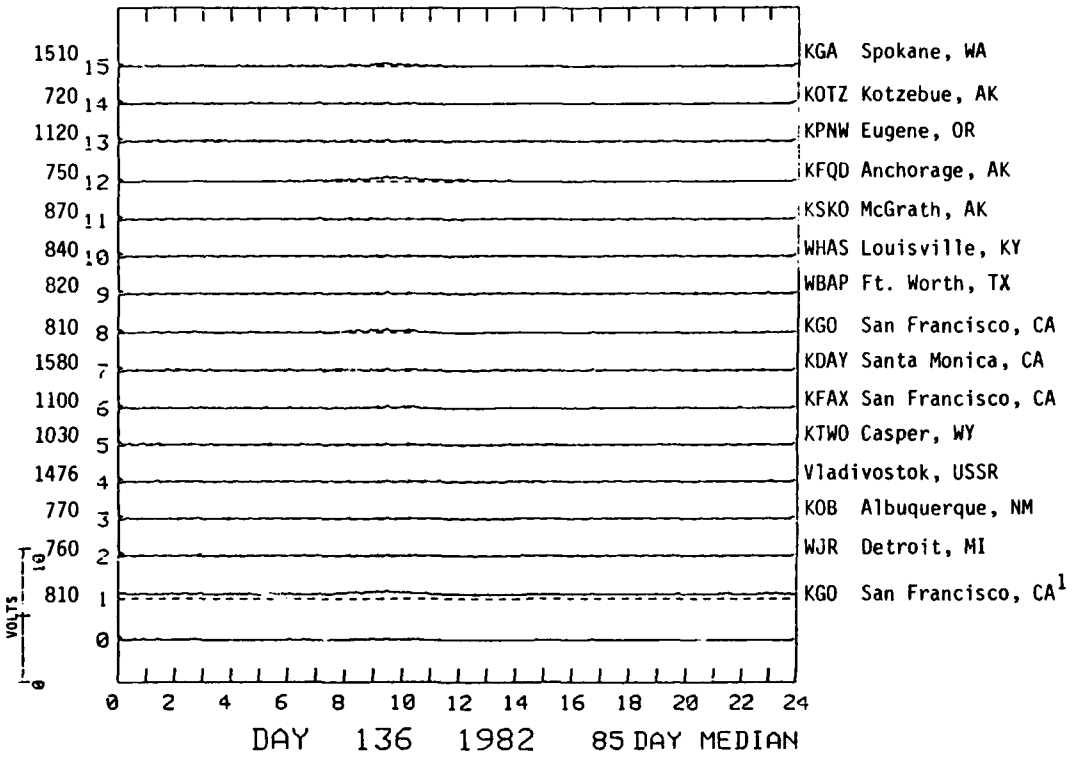
51-day median for period 15 November 1981 to 5 January 1982



[1]No positive I.D.

Figure 9. Seasonal signal behavior - Midwinter 1981-82.

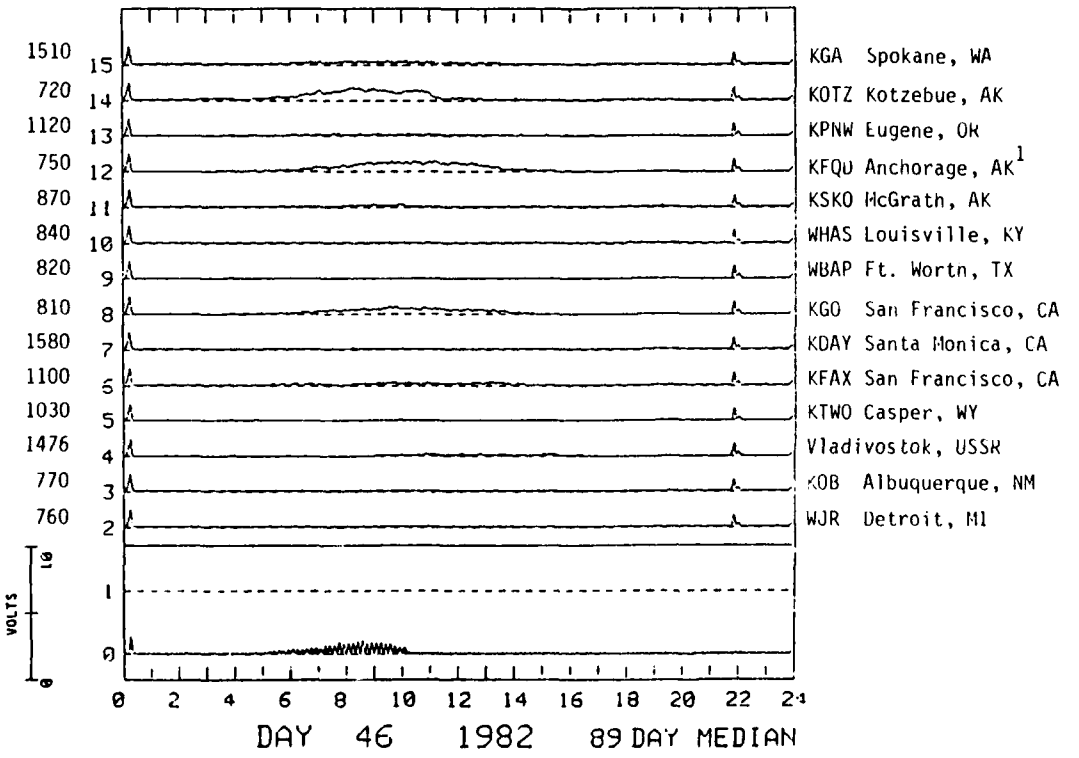
Median data for the quarter 15 May to 15 August, 1982.
Only 85 days were used because of antenna experimentation
toward end of quarter.



[1]KGO San Francisco on monopole.

Figure 10. Seasonal signal behavior - Summer 1982.

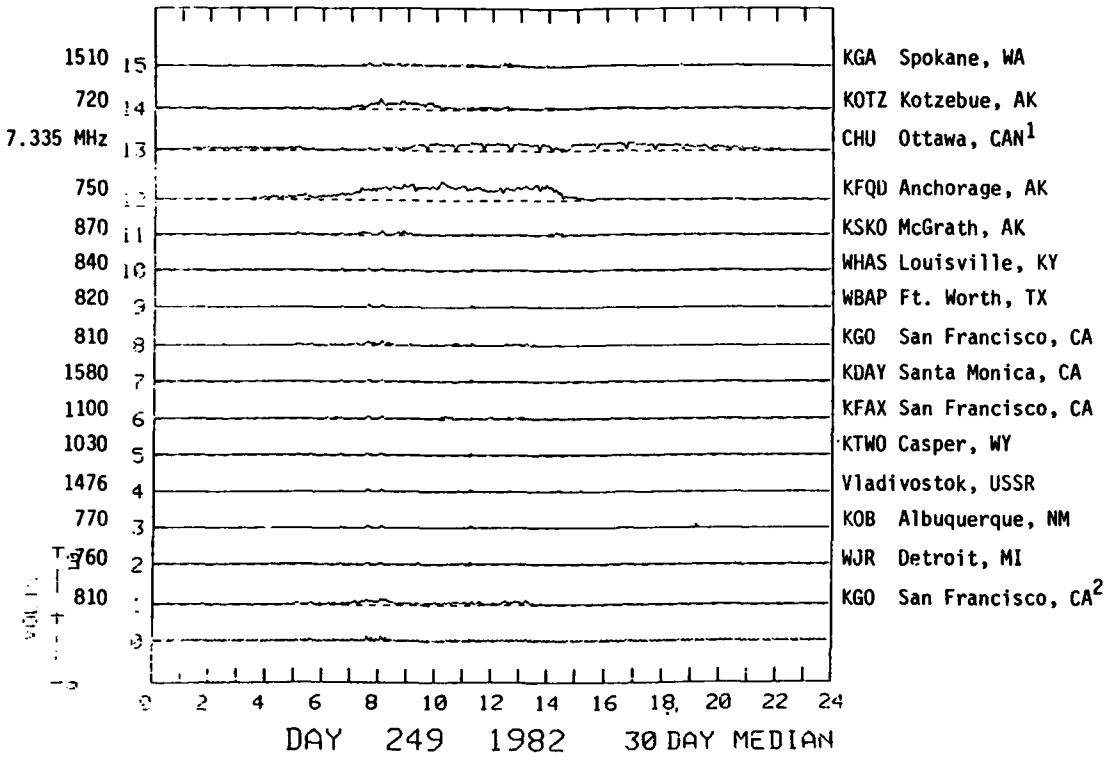
Median MF skywave for quarter 15 February to
15 May, 1982



[1]KOMO Seattle deleted, KFQD Anchorage added, 29 March 1982.

Figure 11. Seasonal signal behavior - Spring Equinox, 1982.

Thirty-day median, 15 days on either side of September 21.



[1]KPNW Eugene deleted, CHU Ottawa added, October 2, 1983.

[2]Monopole.

Figure 12. Seasonal signal behavior - Fall 1982.

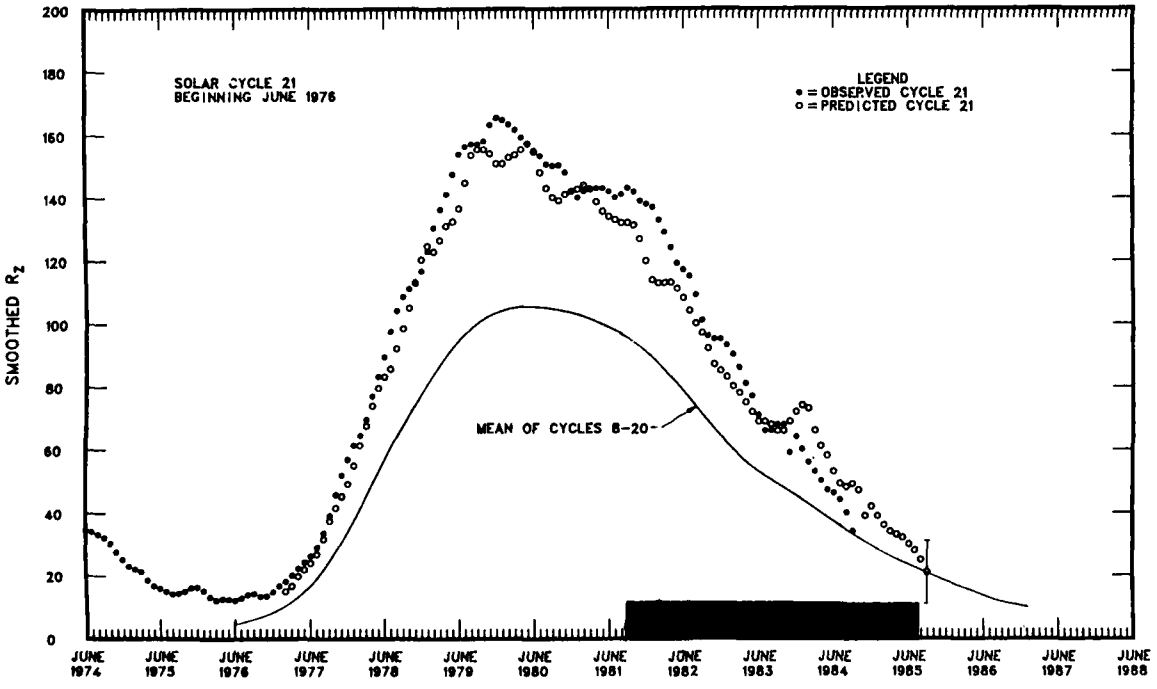


Figure 13. Observed and one-year-ahead predicted smoothed sunspot numbers.

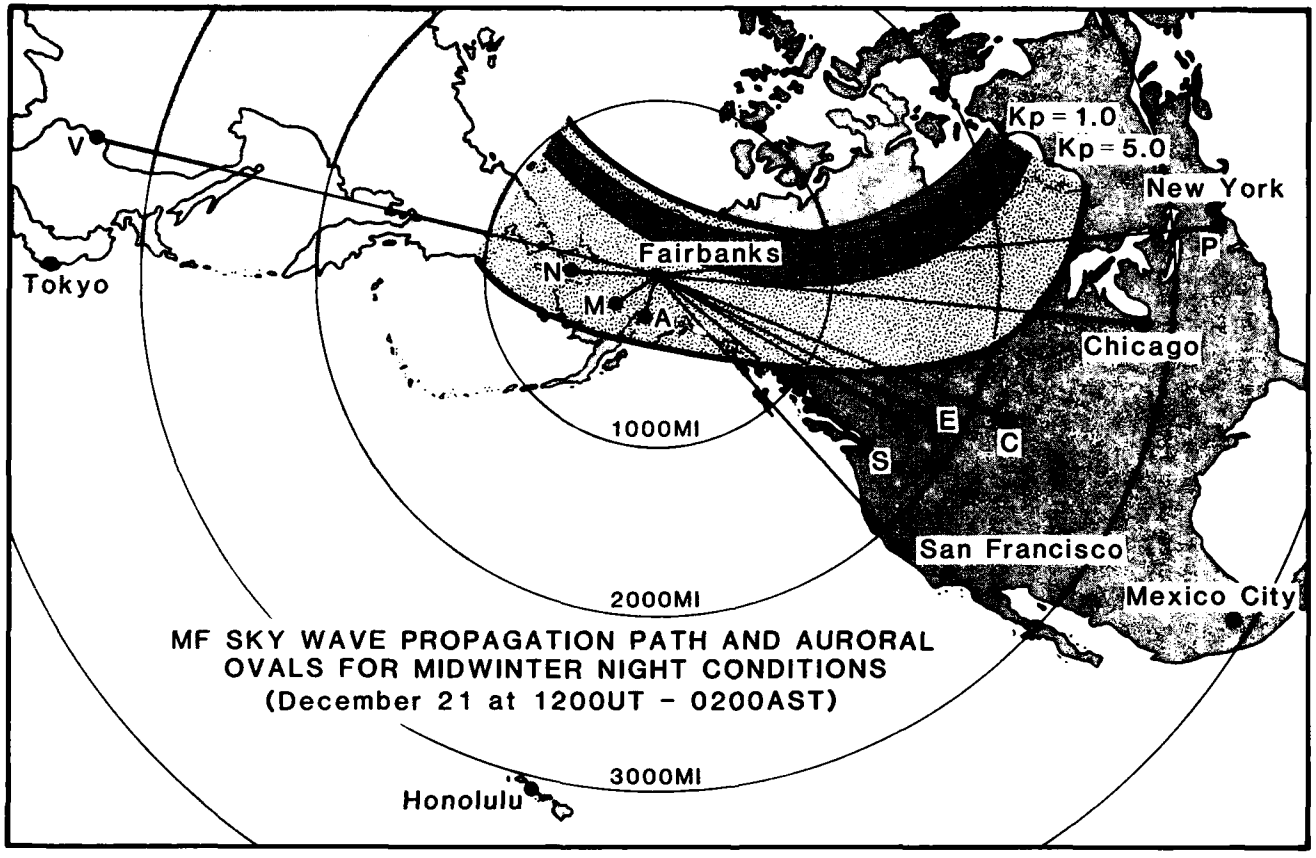

Kp = 1.0
Kp = 5.0
New York
V
Tokyo
Fairbanks
N
M
A
P
Chicago
E
C
S
1000MI
San Francisco
Mexico City
2000MI
MF SKY WAVE PROPAGATION PATH AND AURORAL
OVALS FOR MIDWINTER NIGHT CONDITIONS
(December 21 at 1200UT - 0200AST)
3000MI
Honolulu

Figure 14

DISCUSSION

J.S.Belrose, CA

I would like to make two comments on your paper: (1) the microcomputer version of the Numerical Electromagnetic Code (NEC), MININEC, assumes a perfectly conducting ground, and it is therefore inappropriate to employ MININEC for your application. However, NEC 3 contains the Sommerfeld-Norton groundwave, and as such it can be used to calculate the pattern of vertical monopoles over a finite radial ground system. (2) MF propagation over high latitude paths is, as you have pointed out, quite variable. In fact, for auroral zone paths the variability is so great that in my view median values of field strengths have little physical meaning. The data should be sorted into two blocks: quiet and disturbed, or perhaps more meaningfully nights of high field strengths and slow fading rates, and nights of rapid fading and low field strengths. These two blocks or three blocks of data should be studied separately, to determine: frequency of occurrence of quiet nights at different epochs of the solar cycle and season; statistical variability of disturbed days and dependence or non-dependence on magnetic activity. A dominating factor affecting MF field strengths is "after geomagnetic storm effects". Two to four days after certain geomagnetic storms, nighttime field strengths can be abnormally low for a day or two, up to a week after certain large storms. During years of high magnetic activity low MF field strengths at auroral latitudes may be dominantly due to overlapping "after geomagnetic storm effects".

Author's Reply

In regard to question 1, you are correct about "MININEC". We only used this program for a *first estimate* of our new antenna pattern. As soon as we obtain version 3 of the NEC program, we will model the vertical antenna with it. Concerning question 2, we have emphasized in reports to our sponsor, the importance of the short term variations of MF signal strength and are continuing our investigation of the short term fading and of utilizing other geophysical parameters to characterize MF signal behaviour. We have also noticed the "after-geomagnetic-storm effects" on signals received at Fairbanks.

OPTIMISATION DES SYSTEMS DE TRANSMISSION NUMERIQUE TRANSAURORAUX EN ONDES DECAMETRIQUES

OPTIMIZATION OF H.F. DIGITAL RADIO SYSTEMS AT HIGH LATITUDES

C. GOUTELARD - J. CARATORI - A. NEHME

Université PARIS-SUD - Laboratoire d'Etude des Transmissions Ionosphériques

9, avenue de la division Leclerc - 94230 CACHAN

RESUME

La traversée des zones de haute latitude est inévitable dans certaines configurations de liaisons par ondes décamétriques, notamment pour des liaisons à longue distance.

Aux latitudes élevées, des phénomènes particuliers apparaissent : absorption polaire et aurorale, couches E sporadique et F diffus, perturbations alignées sur le champ magnétique... qui modifient de manière spécifique les caractéristiques des liaisons longues distances.

A partir d'observations expérimentales sur des liaisons traversant les zones de haute latitude, on a établi un modèle de canal de transmission. Ce modèle tient compte des perturbations observées ainsi que de l'influence de la longueur de la liaison et de sa position par rapport au pôle magnétique.

A partir de ce modèle on a examiné les classes de signaux utilisables pour les systèmes de transmission numérique dans le cadre des diverses techniques : transmission série ou parallèle, systèmes autoadaptatifs, systèmes de transmission codée.

ABSTRACT

High latitudes are inevitably encountered in telecommunications, especially in long distance transmissions.

At high latitudes the following phenomena appear : auroral and polar absorptions, spread F, perturbations aligned with the magnetic field, sporadic E... which make long distance transmission characteristics special.

We were able to establish a channel model from experimental observations of transmissions travelling through high latitudinal regions. The parameters of the model must include the perturbations found at high latitudes, the lengh of the transmission, and its position relative to the magnetic pole and the auroral zone.

From these models, which point out the spectral modifications of the signal, the fading , the duration of coherence, we determined the classes of signals which can be needed for H.F. digital telecommunications with the aim of diverse techniques : serial or parallel transmissions, autoadaptative systems, coded transmission systems.

I. - INTRODUCTION -

Les zones de hautes latitudes sont inévitables pour un certain nombre de liaisons en ondes décamétriques, soit parce que l'une des extrémités est située au voisinage des pôles, soit parce que l'arc mineur du grand cercle de la liaison traverse cette région.

Les phénomènes particuliers qui apparaissent dans les régions de hautes latitudes et leurs conséquences sur la propagation ont été répertoriés [1] [2] et classés. On distingue habituellement :

- L'absorption au niveau de la calotte polaire (Polar Cap Absorption) causée par la précipitation de protons de très haute énergie jusqu'à la base de l'ionosphère et qui entraine des affaiblissements très importants pouvant interrompre toute communication pendant des durées pouvant atteindre plusieurs jours.

- L'absorption aurorale causée par des électrons précipités jusque dans la région D et qui accroissent l'absorption pendant des durées de plusieurs heures. Elle s'accompagne également de modifications de la région E pouvant entraîner une modification de la MUF (Fréquence maximum utilisable) des liaisons.

- Des phénomènes particuliers, spécifiques des régions E et F aurorales, et qui entraînent l'apparition des couches E sporadiques, des couches de F diffus et de perturbations qui introduisent des gradients d'ionisation horizontaux importants.

Ces phénomènes se traduisent par des variations importantes et rapides des caractéristiques du canal de transmission qu'il est difficile de prévoir [4] . Les effets principaux sont :

- L'augmentation de l'absorption pendant les périodes perturbées qui diminue au point de réception le rapport signal/bruit et qui impose de prévoir des systèmes permettant de conserver une énergie suffisante par bit d'information.

- L'étalement de la réponse impulsionnelle du canal causée par l'apparition des trajets multiples et qui entraîne dans certains modems une réduction du débit d'information.

- L'apparition d'un phénomène doppler important causé par les variations du milieu et qui se traduit par des élargissements des spectres [5] ou l'apparition de raies distinctes. On constate alors des fluctuations importantes du signal, notamment dans les systèmes à spectre étroit.

- Une grande variabilité de la plage de fréquence utilisable, soit par une modification de la MUF soit par une modification de la LUF. Une adaptation au canal peut être envisagée par une évaluation en temps réel (Real Time Channel Evaluation) [6] .

Les techniques utilisables pour compenser les effets de ces phénomènes peuvent être classés en deux catégories :

- La première englobe tous les aspects liés à l'utilisation des techniques de diversité appliquées :
  * aux antennes (Diversité d'espace ou de polarisation),
  * dans le domaine temporel (Entrelacement redondance et répétition des messages),
  * dans le domaine fréquentiel (Diversité de fréquence).

- La seconde est liée aux techniques de modulation, de codage et de traitement du signal.

L'exposé qui suit est consacré aux solutions possibles adoptables dans l'exploitation des systèmes destinés à assurer des liaisons à travers la zone aurorale.
Une première partie est consacrée à l'étude des problèmes de propagation à partir de liaisons tests traversant la zone aurorale ou l'évitant.

La seconde partie est consacrée à l'étude des caractéristiques du canal de transmission.
La dernière partie examine les incidences de ces caractéristiques sur les systèmes de transmission numérique.

II. - ANALYSE DE LA PROPAGATION -

II.1. Liaisons expérimentales étudiées

Les propagations ont été étudiées en utilisant des émissions de caractéristiques connues que l'on a reçues avec une station expérimentale (station STUDIO : Système de Traitement Universel de Diagnostics Ionosphériques) localisée à une quarantaine de kilomètres au sud de Paris.

Les liaisons qui ont été utilisées sont indiquées sur la figure 1 et leurs caractéristiques sont résumées sur le tableau 1.

TABLEAU 1

LIAISON	COORDONNEES GEOGRAPHIQUES	FREQUENCES (MHz)	DISTANCE AZIMUT	TYPE DE LIAISON	TYPE DE MODULATION
FORT COLLINS USA (WWV)	40° 41' N 105° 02' W	2,5 5 10 15 20	7780 km 309° 38'	Transaurorale	Code du CCIR par impulsion double
OTTAWA Canada (CHU)	45° 18' N 75° 45' W	3,330 7,335 14,670	5656 km 297° 31'	Subaurorale	Code du CCIR par impulsion double
REDWOOD-CITY USA	37° 33' N 122° 14' W	11,715	8954 km 318° 39'	Transaurorale	Radiodiffusion
MOSCOU URSS (RWM)	55° 45' N 37° 33' E	4,996 9,996 14,996	2465 km 58° 55'	Subaurorale	Code du CCIR par impulsion double
NOVOSIBIRSK URSS (RTA)	55° 04' N 82° 58' E	10 15	5234 km 50° 26'	Subaurorale	Code du CCIR par impulsion double
IRKOUTSK URSS (RID)	52° 23' N 104° 27' E	5,004 10,004 15,004	6559 km 48° 08'	Subaurorale	Code du CCIR par impulsion double

II.2. Dispositif expérimental

Dans la configuration utilisée la station STUDIO a été organisée conformément au diagramme fonctionnel représenté sur la figure 2. L'expérimentation utilise :

- Un système d'aériens large bande composé de 32 antennes dont le lobe, orientable tout azimut, a une ouverture de 15 degrés à 15MHz.
- D'un récepteur dont la dynamique est 120dB.
- D'un analyseur de spectre numérique.
- D'un enregistreur magnétique.
- D'un miniordinateur pilotant la station et commandant :
    * l'orientation du lobe d'antenne ,
    * la fréquence du récepteur et son gain,
    * les paramètres d'analyse du signal reçu,
    * l'enregistrement des résultats.

Un standard de fréquence assure une précision relative de 5.10^{-10} au système.

On a effectué les mesures des spectres des signaux qui contiennent un maximum d'information. Les résolutions utilisables sont inférieures à 0,01Hz mais on s'est en général limité à 0,1Hz compte tenu des variations temporelles du canal.
Le système de mesure a été organisé de façon à pouvoir mesurer simultanément les caractéristiques de 4 liaisons.

II.3. Etude des liaisons expérimentales

Les liaisons expérimentales choisies ont permis d'étudier de façon comparative les différents types de trajets différenciés par leur configuration géographique et/ou par leur fréquence d'émission.
On a ainsi défini quatre types d'étude :

(a) Etude de l'influence des longueurs de liaisons à fréquence constante pour des trajectoires subaurorales. Le cas type est constitué par les liaisons Irkoutsk-Paris (6559 km) et Moscou-Paris (2465 km).

(b) Etude de l'influence de la zone aurorale par comparaison d'une liaison transaurorale avec une liaison subaurorale de longueur et de fréquence voisines. Le cas typique est constitué par les liaisons : Ottawa-Paris (5656 km, 14,670MHz, subaurorale) et Fort Collins-Paris (7780 km, 15MHz, transaurorale).

(c) Etude de l'influence de la fréquence d'émission pour les liaisons transaurorales en utilisant un même point d'émission à deux fréquences différentes. Le cas typique est constitué par la liaison Fort Collins-Paris (7780 km) pour les deux fréquences 15 et 10MHz.

(d) Etude de l'influence de la géométrie des liaisons transaurorales par le choix de deux stations d'émission de fréquences voisines. Le cas typique est constitué par les liaisons Fort Collins-Paris (10MHz, 7780 km) et Redwood-Paris (11,715MHz, 8954 km).

Les résultats obtenus ont montré que si des évènements apparaissaient de façon corrélative sur l'une et l'autre des liaisons, les caractéristiques du canal n'étaient pas corrélées entre elles comme dans le cas (c).

II.3.1. Trajectoire subaurorale. Influence de la longueur de la liaison.

L'influence de la longueur de la liaison est illustrée par le cas typique présenté sur la figure 3, pour les liaisons :
Irkoutsk - Paris (6559 km, 15,004MHz)
Moscou - Paris (2465 km, 14,996MHz).

Les figures 3a et 3b représentent les spectres obtenus en fonction du temps de 14h23 à 21h10 TU (GMT). Pour plus de clarté, il n'a été représenté qu'un échantillonnage du spectre en fonction du temps, à raison de 1 spectre toutes les 6 minutes.
Ces enregistrements font apparaître les périodes d'émission d'une onde entretenue et les périodes d'émission des signaux horaires dont la fréquence de la modulation est de 1 hertz. Malgré la différence des longueurs des liaisons on note la bonne corrélation qui existe entre les spectres.
Cette corrélation apparaît sur la figure 3c qui représente les diagrammes des fréquences doppler de la liaison Moscou-Paris portées en abscisse et Irkoutsk-Paris portées en ordonnée. Ces diagrammes sont obtenus en sélectionnant d'abord dans chaque spectre les composantes d'amplitudes supérieures à un seuil fixe - ici 50% de l'amplitude maximale - pour deux spectres simultanés. Soient $\{Fi\}$ et $\{Fj\}$ les ensembles des fréquences de ces composantes respectivement sur chaque liaison.
Les points portés P ont pour coordonnées :

$$P(x_p = Fi,\ y_p = Fj) \qquad \forall\ i,\ j$$

Il est évident que si la corrélation est parfaite $\{Fi\} = \{Fj\}$ et la figure admet la première bissectrice comme axe de symétrie.
Chacun des diagrammes de la figure 3c est tracé pour une période de 2h40'. On peut constater la bonne corrélation des spectres qui s'explique par le fait que la propagation est essentiellement assurée par les rayons bas pour lesquels, en période calme, la dispersion doppler demeure faible [7] .

II.3.2. Comparaison de liaisons voisines transaurorale et subaurorale.

Les effets auroraux sont mis en évidence en comparant les résultats de liaisons voisines, l'une transaurorale, l'autre subaurorale.
Les résultats présentés concernent les liaisons :
Ottawa - Paris (5656 km, 14,670MHz) subaurorale
Fort Collins - Paris (7780 km, 15MHz) transaurorale.

En période calme on note une bonne corrélation des spectres mesurés comme le montre la figure 4 qui représente les résultats obtenus pour la même période que ceux représentés sur la figure 3.
En période agitée deux types de situation se présentent.
La première se traduit par l'apparition d'une composante supplémentaire dans le spectre du signal de la liaison transaurorale. Le cas typique est celui représenté sur la figure 5 qui montre un enregistrement effectué de 4h38 à 12h40, l'activité magnétique étant ce jour perturbée à très perturbée, un orage magnétique étant apparu à 0h00 et un PCA étant présent de 2h00 à 18h00.
La représentation des spectres de la figure 5a a été effectuée avec un échantillonnage de 1 spectre toutes les 3 minutes.
La décorrélation des spectres des deux liaisons est flagrante. La composante supplémentaire présente dans le spectre de la liaison Fort Collins-Paris traduit l'apparition d'un trajet dû à des irrégularités de la zone aurorale. Ce type d'effet a été observé par différents auteurs qui ont mis en évidence un étalement de la réponse impulsionnelle dû à des propagations hors du grand cercle et des décalages doppler importants [8] [9] .
La seconde situation se traduit par un étalement du spectre dû à des phénomènes de diffusion dont la figure 6 rend compte. L'étalement du spectre devient très important sur la liaison transaurorale alors qu'il demeure beaucoup plus limité sur la liaison subaurorale. L'étalement du spectre qui est un phénomène connu dans les liaisons transaurorales [5] est causé par des effets de diffusion accompagnant souvent des perturbations magnétiques. L'évènement représenté sur la figure 6 correspond à un jour magnétiquement perturbé où deux orages magnétiques (1h30-7h30) et (15h00-18h00) ont été observés.

II.3.3. Influence de la fréquence d'émission.

Une bonne corrélation est généralement observée entre deux liaisons transaurorales dont les extrémités sont identiques mais dont les fréquences de trafic sont différentes.
Les figures 7 et 8 montrent deux cas typiques observés sur les liaisons Fort Collins-Paris à 10 et 15MHz.
Chaque période d'observation correspond à une activité magnétique perturbée.
On peut noter l'excellente corrélation dans l'apparition des phénomènes qui se manifestent de façon semblable sans être identiques pour chaque fréquence.
Le cas de la figure 7 montre une bonne corrélation de l'ensemble des phénomènes bien qu'il apparaisse une double trace à 10MHz due vraisemblablement à une double réflexion sur la perturbation.
Le cas de la figure 8 montre une corrélation dans l'apparition des phénomènes mais les fréquences doppler sont différentes et sensiblement dans le rapport des fréquences d'émission. Le trajet supplémentaire paraît ici également causé par une perturbation de la zone aurorale.

III. - CONSEQUENCES SUR LA FONCTION DE TRANSFERT DU CANAL -

On a classé les conditions de propagation rencontrées en trois catégories :

- Les périodes calmes que nous appellerons classe N, où le spectre des signaux obtenus est comparable à celui des liaisons subaurorales (cas de la figure 4).
- Les périodes perturbées avec apparition d'un ou plusieurs trajets supplémentaires que nous appellerons classe P1 et dont des cas typiques sont donnés sur les figures 5, 7 et 8.
- Les périodes perturbées où un phénomène de diffusion produit un élargissement du spectre et que nous appellerons classe P2. Cette classe correspond au cas de la figure 6.

On peut noter que ces phénomènes apparaissent pendant des périodes longues, souvent de plusieurs heures et sont donc susceptibles de perturber les liaisons numériques de façon importante et durable.
L'évaluation de leurs effets a été effectuée en calculant le champ total reçu et en estimant la fonction de transfert du canal.

III.1. Estimation du champ reçu.

Les signaux étudiés ont été enregistrés dans leur représentation fréquentielle de Fourier. On a donc pu simplement, par le calcul de la transformée de Fourier inverse, retrouver leur représentation temporelle.
Cette étude a été faite pour chaque liaison sur la fréquence porteuse du signal d'émission.
La figure 9 montre les résultats obtenus sur les cas typiques. On constate que :

* en période calme, classe N, le champ total est comparable pour les liaisons transaurorales et subaurorales (Ottawa 14,670MHz - Fort Collins 15MHz - Figure 9a).
* En période agitée où des trajets supplémentaires apparaissent, classe P1, on voit se produire (figure 9b) des fluctuations quasi périodiques très rapides de l'intensité du champ causées par l'effet doppler important dont est affecté le trajet supplémentaire.
* En période agitée, classe P2, le champ résultant subit des fluctuations très rapides dans lequel l'aspect quasi périodique observé pour la classe P1 a tendance à disparaître.

Ces résultats montrent qu'en période perturbée les fluctuations du champ sont importantes et rapides.
Les lois de fluctuation sont identiques à celles observées pour les liaisons subaurorales et peuvent être décrites par les lois de distribution classiques : Rice, Rayleigh ou Nakagami, selon la complexité des modes de propagation.

III.2. Estimation de la fonction de transfert.

La fonction de transfert du canal ionosphérique dans la bande des ondes décamétriques est localement représentable par l'introduction des différents trajets. Elle peut s'écrire pour sous la forme :

$$F(\omega, t) = \sum_{i=1}^{N} a_i \, e^{j[\Omega i t - \omega t_{pi} + \Psi_i(\omega)]}$$

où

i est l'indice repérant le ième trajet parmi les N existants.

Ωi est la pulsation doppler pour ω voisin de ωo

t_{pi} le temps de groupe du ième trajet pour ω voisin de ωo

$\Psi_i(\omega)$ un angle de phase dépendant de la fréquence et qui s'exprime par $\Psi_i(\omega) = \frac{\omega^2}{2}\left(\frac{dtpi}{d\omega}\right)_{\omega=\omega_o} + \Psi_o$ où Ψo est constant.

La fonction de transfert dépend du temps puisque le canal n'est pas stationnaire.

Les variations des champs reçus portées sur la figure 9 représentent, à une constante près, $//F(\omega o, t)//$ où ωo est la pulsation de l'onde porteuse étudiée. Ces enregistrements donnent donc une représentation de la fonction de transfert sur l'axe ωo.
Sa représentation complète peut en être déduite par la connaissance des temps de groupe tpi et de leurs dérivées $\frac{dtpi}{d\omega}$ qui traduisent l'effet de dispersivité du milieu. Ces paramètres sont directement mesurés dans les sondages obliques bistatiques. Ils peuvent être déterminés avec une bonne précision à partir des paramètres ionosphériques pour les modes de propagation normaux. Par contre, ils sont plus difficiles à déterminer pour les modes de propagation anormaux où les valeurs observées varient dans des proportions très importantes en fonction de la géométrie de la liaison et des perturbations.
Pour obtenir une estimation statistique de la fonction de transfert, on a calculé pour les modes de propagation normaux les valeurs de tpi et $\frac{dtpi}{d\omega}$ à partir des cartes de prévision et on a étudié les variations de la fonction de transfert en fonction des paramètres tpi et $\frac{dtpi}{d\omega}$ attribuables aux modes de propagation anormaux.
Les résultats sont illustrés par les graphes de la figure 10 où les parties noires représentent les zones où

$$//F(\omega, t)//^2 \geqslant \overline{F^2(\omega, t)} / 2$$

et les parties claires celles où

$$//F(\omega, t)//^2 < \overline{F^2(\omega, t)} / 2$$

$\overline{F^2(\omega, t)}$ dénote la valeur quadratique moyenne établie sur l'espace temps fréquence. La figure 10a donne un exemple de $//F(\omega, t)//^2$ et la figure 10b la partie de $//F(\omega, t)//^2 < \overline{F^2(\omega, t)} / 2$.
En période calme (figure 10c), on retrouve les résultats des liaisons subaurorales. Dans ce cas, les zones où la fonction de transfert s'affaiblit (zones claires), mettent en évidence une variation lente du canal qui peut être considéré comme localement stationnaire pour des temps de cohérence de l'ordre de quelques secondes.

En période perturbée, de classe P1 (figure 10d), on note une configuration complexe mais quasi périodique des variations de la fonction de transfert. Les zones d'affaiblissement varient avec des pseudo périodes très courtes causées par l'effet doppler important du trajet supplémentaire mais aussi avec des pseudo périodes composites résultant de l'ensemble des trajets. Le temps de cohérence est alors réduit à quelques dizaines de millisecondes.

Dans le cas de la classe P 4 des périodes perturbées, la configuration que l'on obtient (figure 10e) perd une grande part de son allure périodique à cause de l'existence du grand nombre de trajets créés par la diffusion. Il est important de noter que dans la bande d'analyse de 3KHz on voit apparaître un "fading plat", c'est-à-dire qu'à un instant donné l'affaiblissement atteint la totalité de la fonction.

IV. - CONTRAINTES IMPOSEES PAR LES PROPAGATIONS AURORALES DANS LE CHOIX DES SIGNAUX -

La propagation dans la zone aurorale fait apparaître les points caractéristiques suivants :

- Existence de trajets supplémentaires qui provoquent un double étalement de la réponse impulsionnelle dans les domaines temporel et fréquentiel.
- Apparition de phénomènes de diffusion créant un étalement de la réponse impulsionnelle dans le domaine fréquentiel.
- Variabilité soudaine des caractéristiques du canal lors de l'apparition des perturbations.

Le choix des signaux utilisables dans les modems numériques doit prendre en compte l'ensemble de ces phénomènes représentés par la fonction de transfert $F(\omega , t)$.
On utilise, en général, pour ces transmissions une bande B limitée à 3KHz. On classe les modems en deux grandes catégories :

- Les modems parallèles qui sont constitués d'une ou d'un ensemble de voies à bandes étroites. Le débit de chaque voie est faible.
- Les modems série qui utilisent pour chaque symbole transmis toute la bande allouée. Dans cette catégorie se classent les modems autoadaptatifs.

L'occupation de la bande par ces deux classes de modems est représentée sur la figure 11a.
Les zones d'affaiblissement caractéristiques sont également schématisées sur la figure 11b où apparaissent :

* des zones traversant lentement la bande pour les trajets normaux,
* des zones traversant rapidement la bande lorsqu'il y a perturbation.

Le problème des transmissions numériques se pose en terme de probabilité d'erreur directement liée à l'énergie fournie par bit d'information, et à la répartition de ces erreurs dans les messages transmis.
Si on prend comme hypothèse de base des systèmes opérant dans la bande 0-3KHz avec un spectre émis optimum, c'est-à-dire uniforme dans la bande, un symbole occupe une surface moyenne S_0 déterminée par sa durée d'émission T_0 et l'étendue B_0 de son spectre. Si le symbole est à 2^N moments il transporte N Shannon (ou bit) d'information.
Pour les modems série et parallèle les surfaces S_0 sont représentées par l'aire unitaire portée sur la figure 11a : dans le premier cas B_0 est faible mais T_0 grand et dans le second les ordres de grandeur sont inversés.
Ces surfaces S_0 représentent à une constante près $\propto$ inversement proportionnelle à N, l'énergie émise par bit d'information. L'énergie reçue est donc de la forme :

$$E = S_0 \int_{\omega \in [0,B_0]} \int_{t \in [0,T_0]} //F(\omega , t)//^2 \, d\omega \, d t$$

Si S_0 est logée dans une zone d'affaiblissement il y a diminution de l'énergie et risque d'erreur. Le choix optimum consiste à répartir les aires unitaires de façon à éviter des fluctuations trop importantes de l'énergie par bit d'information reçu et le groupement des erreurs.
Si on appelle

S la surface des zones d'affaiblissement pendant une durée T

S'_0 la surface commune à S_0 et aux zones d'affaiblissement,

le choix optimum conduit :

- A utiliser en permanence la totalité de la bande B.
- A réaliser l'équiprobabilité d'erreur des symboles, ce qui se traduit par la relation :

$$\frac{S}{BT} = \frac{S'_0}{S_0}$$

La solution optimale consiste à déterminer, en tenant compte des caractéristiques du canal schématisé sur la figure 11b, les formes possibles des aires élémentaires qui assurent l'équiprobabilité des erreurs. Cette équiprobabilité s'obtient d'autant plus facilement que S_0, donc la quantité d'information par symbole, est grande.

Lorsque N = 1, S_o a ses dimensions les plus faibles, et on est alors conduit à prendre soit T_o soit B_o très grand.
La première solution conduit à utiliser un nombre important de sous porteuses.
La seconde solution n'est viable que si on s'autorise un dépassement de la bande B_o. On aboutit alors aux techniques d'étalement de spectre.
En fait, on peut utiliser toute forme de surface S_o qui respecte l'équiprobabilité. A titre d'exemple, la figure 12 montre la possibilité d'une modulation linéaire de fréquence qui est une solution intermédiaire entre les deux précédentes et qui permet de réduire le temps T_o de l'une et l'étendue du spectre de l'autre. La valeur de T_o et la pente de la modulation peuvent être optimisées à partir des prévisions de propagation normales.

S_o étant proportionnel à N, on conçoit l'intérêt d'augmenter le nombre de moments pour obtenir une meilleure répartition des probabilités d'erreurs. Une solution consiste à utiliser un signal de modulation à 2^N moments mais cette technique est rapidement limitée. Une autre solution consiste à utiliser les techniques de codage pour lesquelles N peut être notablement plus élevé en y associant les techniques d'entrelacement. La répartition de la surface S_o revêt alors l'aspect schématisé sur la figure 13, donnant une bonne équirépartition des erreurs.
L'apparition de fading doublement périodique (cas 3 de la figure 5) conduit alors à utiliser un double entrelacement. Cette technique associée à des codes performants [10] a donné de bons résultats. Dans le cas des liaisons transaurorales, les périodicités du fading conduisent à utiliser une technique d'entrelacement irrégulière qui évite un regroupement des erreurs [11] .

V. - CONCLUSION -

On a tenté dans ce bref exposé, à partir d'expérimentations sur le canal ionosphérique utilisé en liaisons transaurorales et subaurorales, de définir les caractéristiques essentielles à prendre en compte pour le choix des signaux utilisables dans les modems.

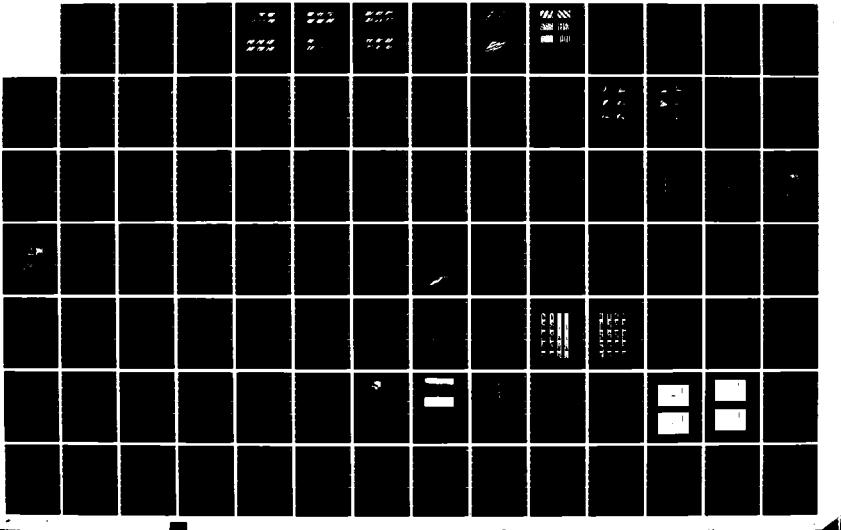
Les caractéristiques du milieu sont rapidement variables et se traduisent par une altération importante de la fonction de transfert.

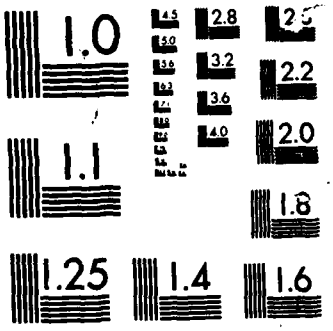
L'optimisation du choix des signaux conduit à positionner une surface élémentaire qui doit statistiquement recouvrir des zones d'absorption.

Les caractéristiques de ces surfaces conduisent à la définition de signaux statistiquement robustes.

AD-A166 585 CONFERENCE PROCEEDINGS ON PROPAGATION EFFECTS ON MILITARY SYSTEMS IN THE..(U) ADVISORY GROUP FOR AEROSPACE RESEARCH AND DEVELOPMENT NEUILLY.. H SOICER

UNCLASSIFIED NOV 85 AGARD-CP-382 F/G 4/1 NL





MICROCOP CHART

BIBLIOGRAPHIE

1 E.V. THRANE. Problems in HF propagation.
AGARD LECTURE SERIES N° 127 : Modern HF communications.

2 K. DAVIES. Ionospheric radio propagation. N.B.S. - Monograph 80 - 1965

3 E.K. SMITH. Word wide occurrence of sporadic E.
NBSCira Boulder 1957.

4 V. AGY. Perspective on the prediction of Auroral Absorption.
AGARD CONFERENCE N° 263. Special Topics in HF propagation.

5 R.D. HUNSUCKER, H.F. BATES. Survey of polar and auroral region effects on HF propagation.
RADIO SCIENCES 4, 347-365.

6 M. DARNELL. Real channel time evaluation.
AGARD LECTURE SERIES N° 127 : Modern HF communications.

7 B.W. REINISCH, K. BIBL. Multipath and doppler observation during transatlantic digital HF propagation experiments.
AGARD CONFERENCE N° 363. Propagation influences on digital transmission systems : Problems and solutions.

8 T.B. JONES, P.L. HAYHURST. An ionosphere mode detection system for HF communication application.
AGARD CONFERENCE N° 363. Propagation influences on digital transmission systems : Problems and solutions.

9 R.W. JENKINS, E.L. HAGG, L.E. MONTBRIAND. Direction and doppler characteristics of medium and long path HF signals within the night-time subauroral region.
AGARD CONFERENCE N° 263. Special Topics HF propagation.

10 F. CHAVAND, C. GOUTELARD, S. HARARI. Codage correcteur d'erreurs pour modem autoadaptatif. Résultats théoriques et expérimentaux.
AGARD CONFERENCE N° 363.

11 C. GOUTELARD. Optimisation de l'entrelacement des codes dans les canaux à évanouissement sélectif.
Revue du Traitement du Signal - Vol. 1 N° 2.1. Numéro spécial 1984.

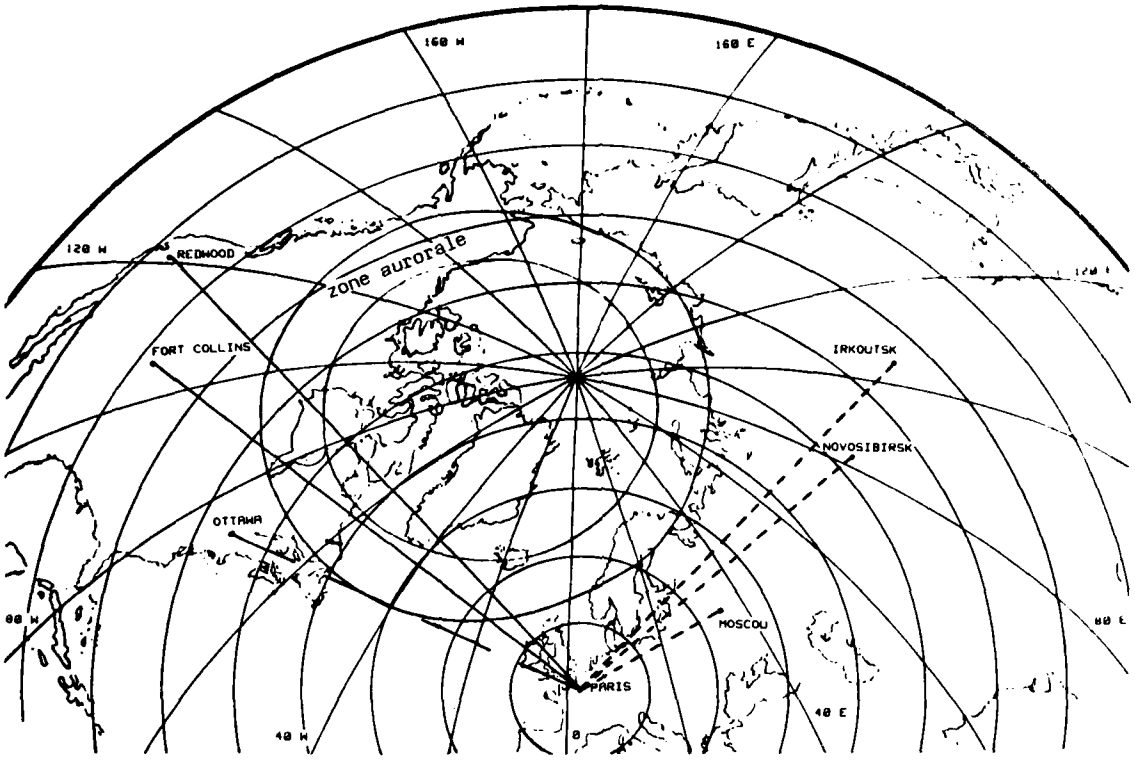


Figure 1 : Liaisons expérimentales étudiées.
Experimental links studied.

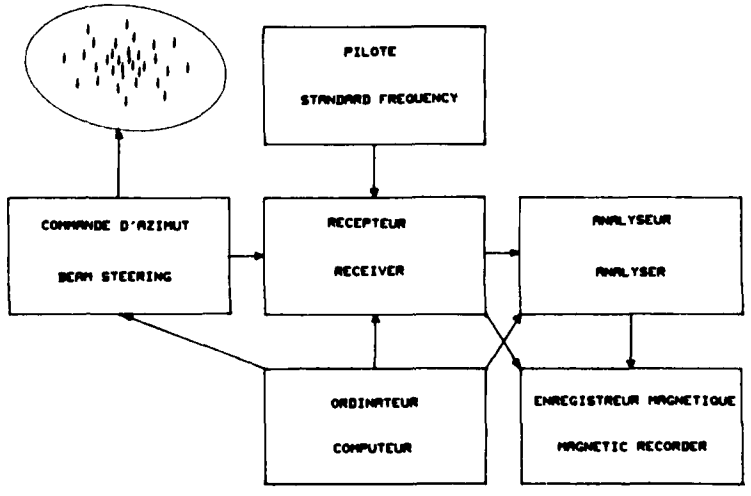


Figure 2 : Configuration du système de réception.
Reception system structure.

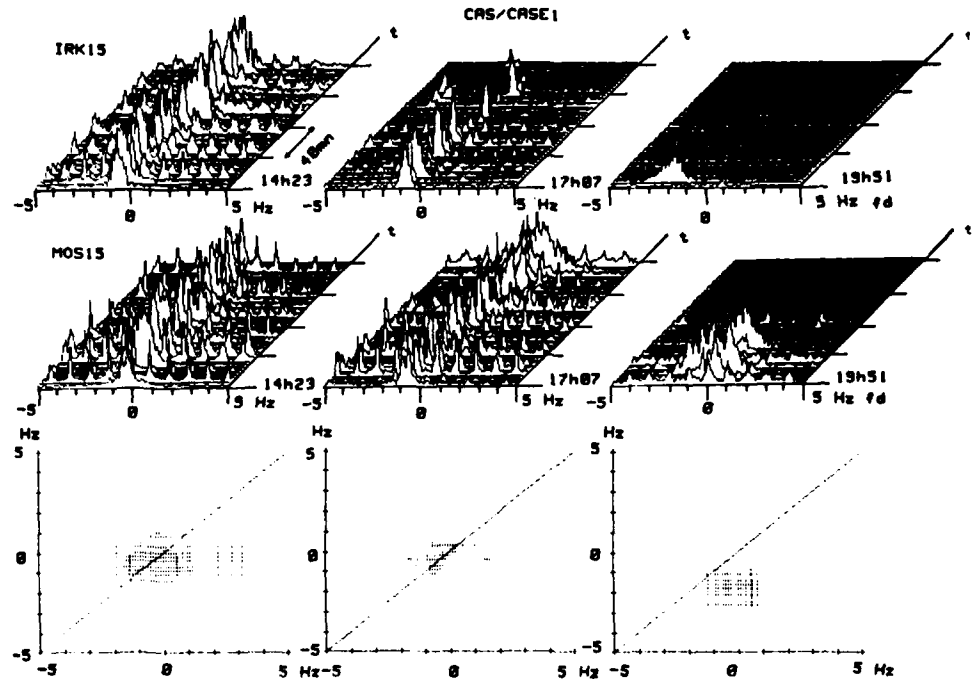


Figure 3 - cas 1 : Liaisons subaurorales MOSCOU 14,996MHz et IRKOUTSK 15,000MHz. 14h23 - 22h30 TU.
Subauroral links MOSCOVA 14,996MHz and IRKOUTSK 15,000MHz. 14h23 - 22h30 UT.

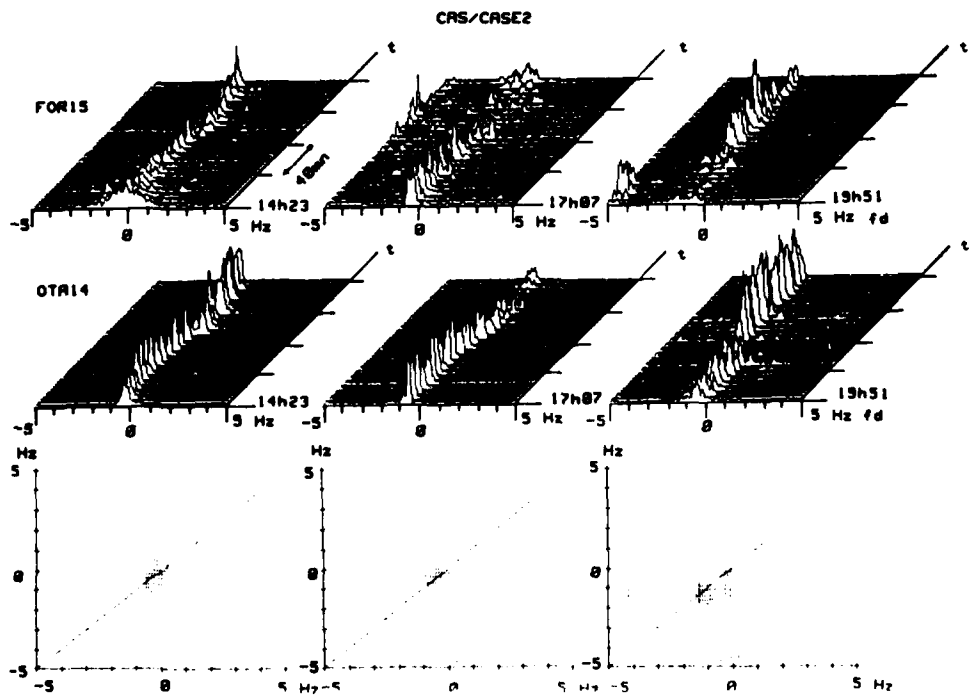


Figure 4 - cas 2 : Liaison subaurorale OTTAWA 14,670MHz et transaurorale FORT COLLINS 15,000MHz. 14h20 - 22h30 TU. Période calme PN.
Subauroral link OTTAWA 14,670MHz and transauroral FORT COLLINS 15,000MHz. 14h20 - 22h30 UT. Quiet period PN.

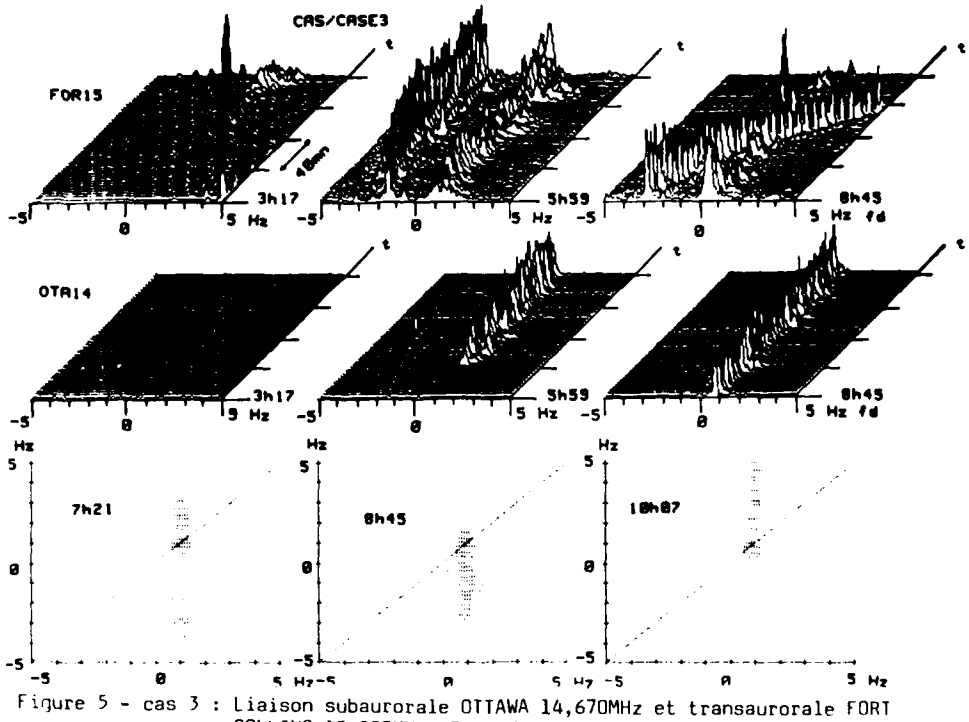


Figure 5 - cas 3 : Liaison subaurorale OTTAWA 14,670MHz et transaurorale FORT COLLINS 15,000MHz. Période perturbée P1. 3h17 - 11h30 TU.
Subauroral link OTTAWA 14,670MHz and transauroral FORT COLLINS 15,000MHz. Disturbed period P1. 3h17 - 11h30 UT.

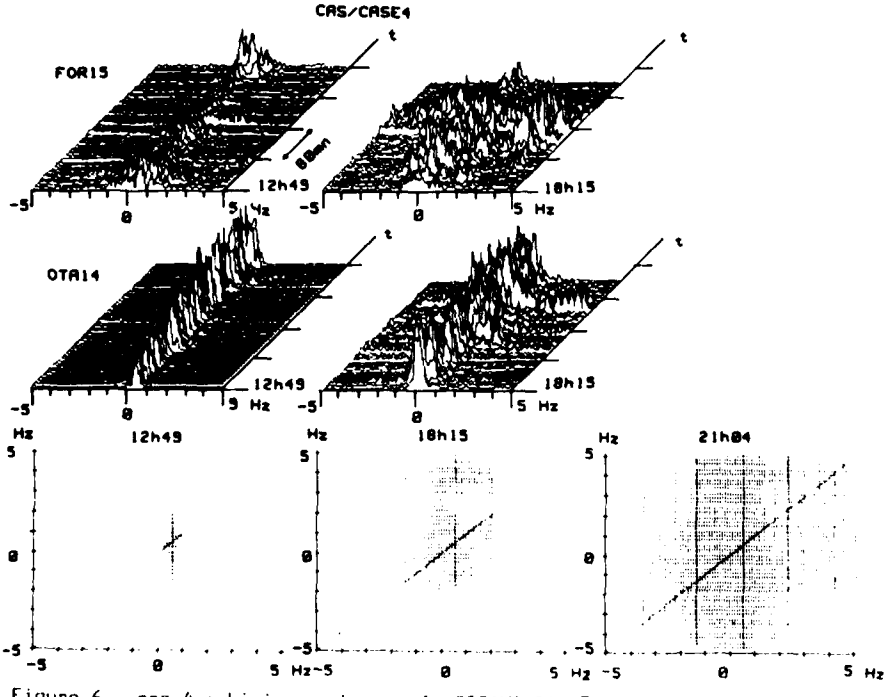


Figure 6 - cas 4 : Liaison subaurorale OTTAWA 14,670MHz et transaurorale FORT COLLINS 15,000MHz. Période perturbée P2. 12h49 - 21h04 TU.
Subauroral link OTTAWA 14,670MHz and transauroral FORT COLLINS 15,000MHz. Disturbed period P2. 12h49 - 21h04 UT.

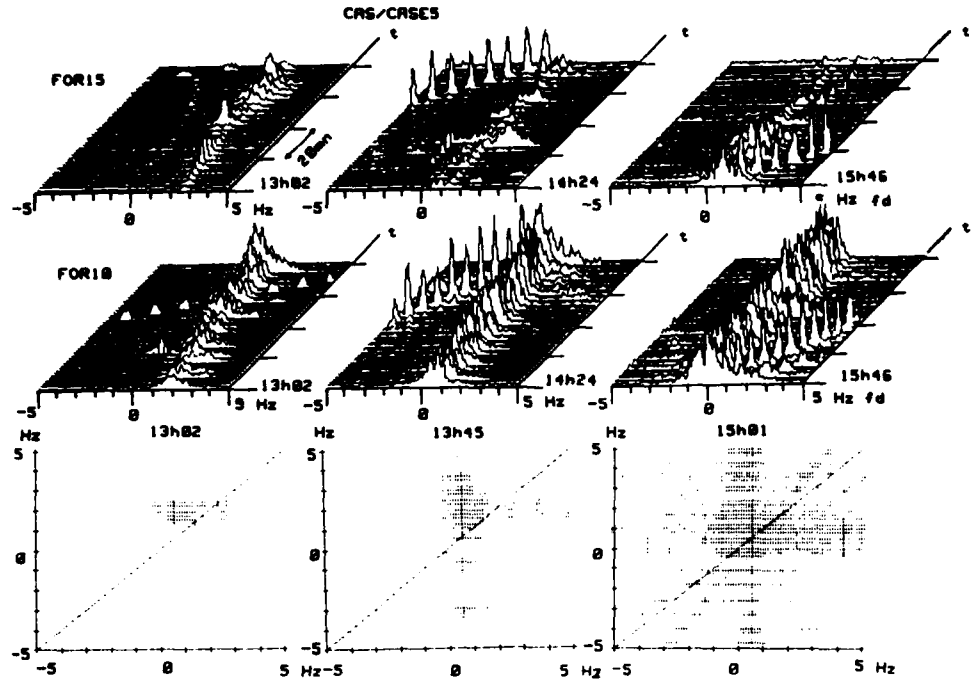


Figure 7 - cas 5 : Liaison transaurorale FORT COLLINS 10,000MHz et 15,000MHz.
13h02 - 17h09 TU.
Transauroral link FORT COLLINS 10,000MHz and 15,000MHz.
13h02 - 17h09 UT.

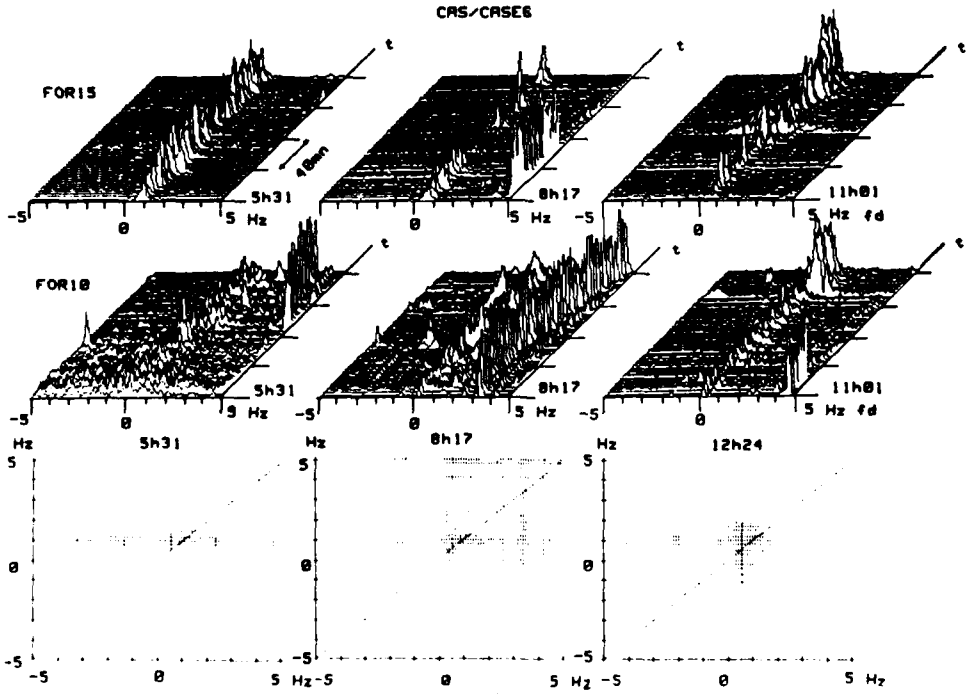


Figure 8 - cas 6 : Liaison transaurorale FORT COLLINS 10,000MHz et 15,000MHz.
4h09 - 12h34 TU.
Transauroral link FORT COLLINS 10,000MHz and 15,000MHz.
4h09 - 12h34 UT.

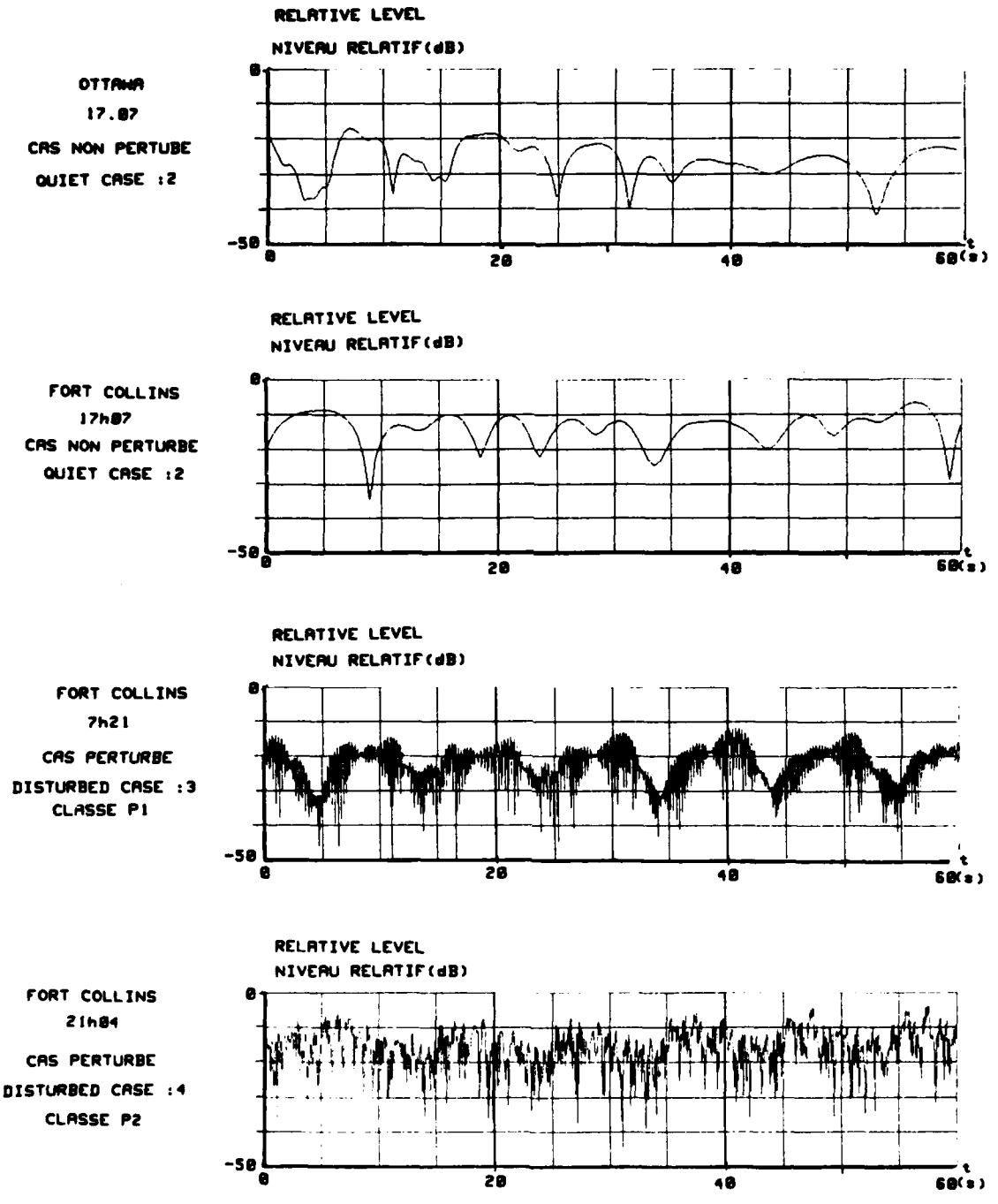


Figure 9

Variations relatives du champ dans les cas de canal calme et perturbé.
Relative variations of signal strength in cases of quiet and disturbed channels.

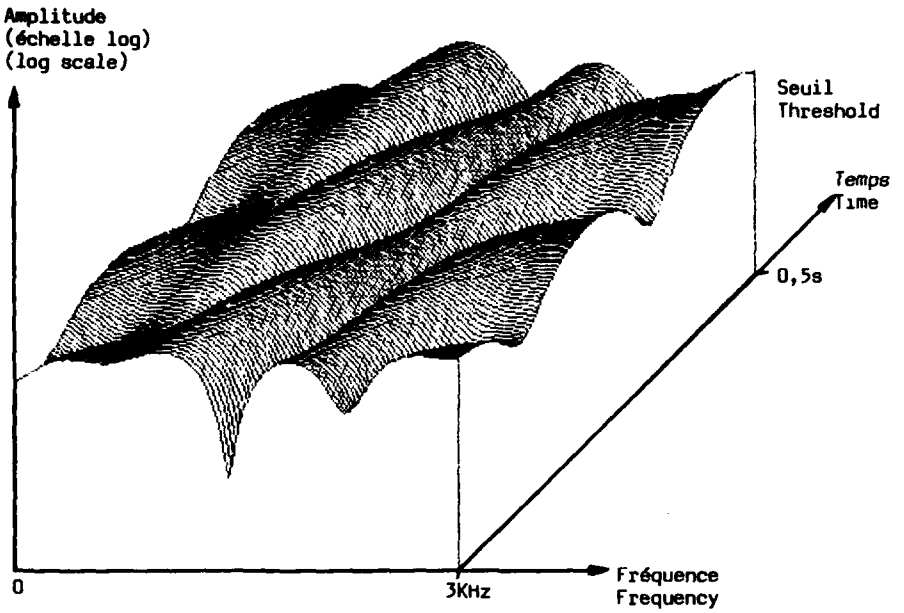


Figure 10a : Fonction de transfert.
Transfer function.

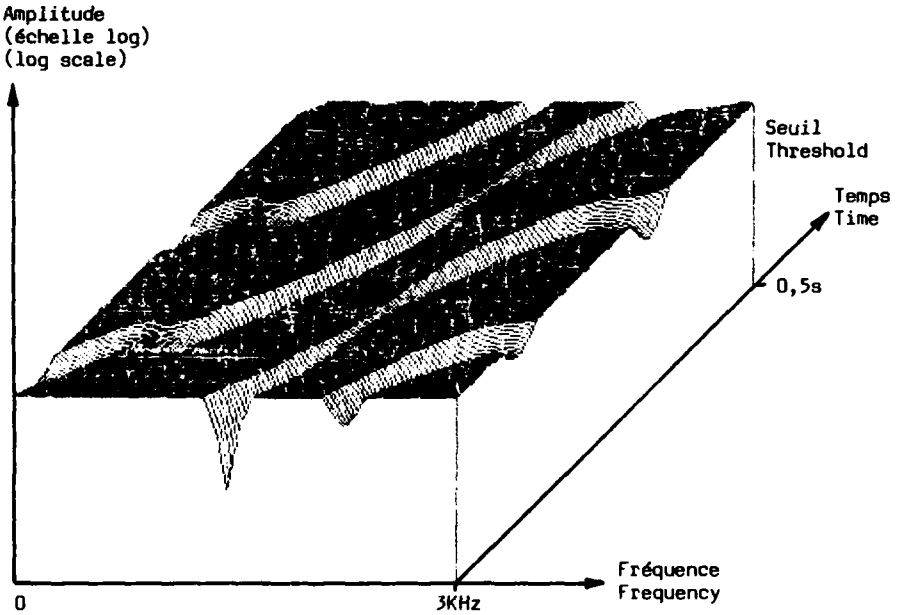


Figure 10b : Moitié inférieure de la fonction de transfert.
Lower half of the transfer function.

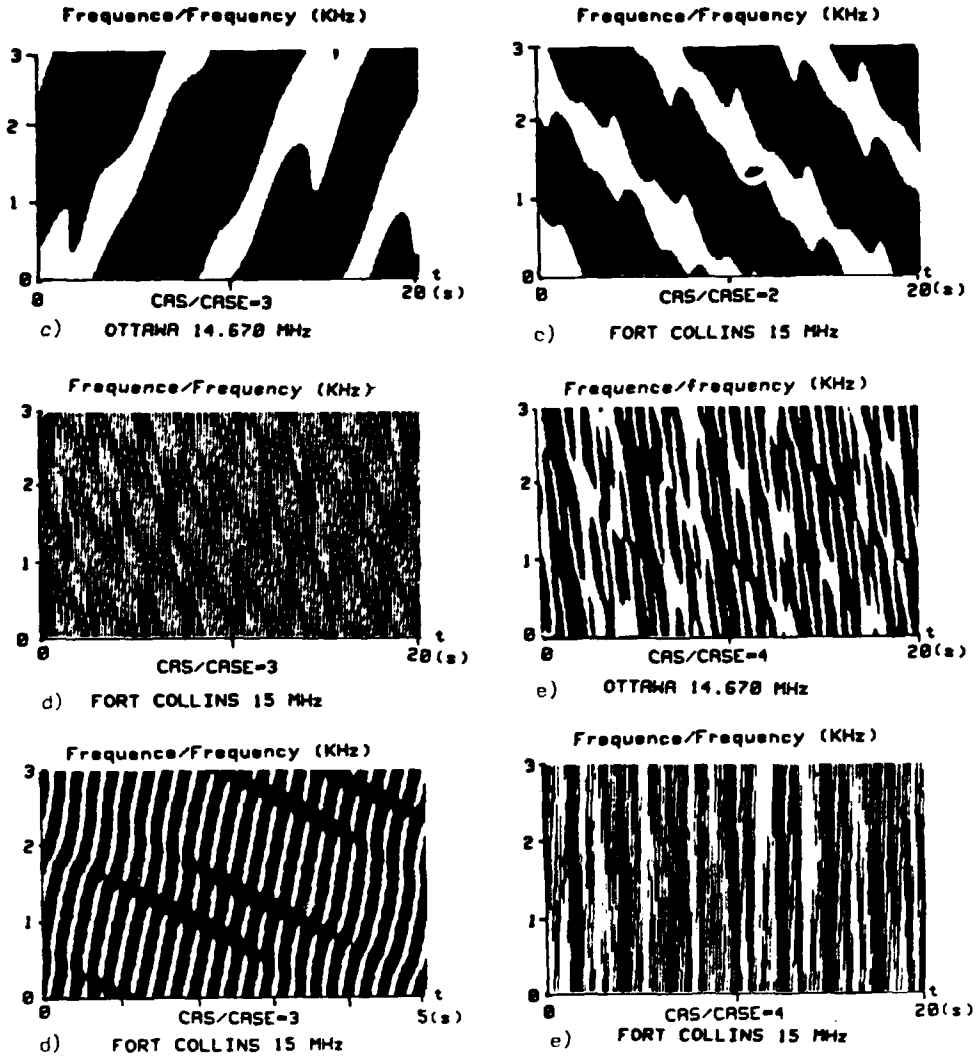


Figure 10 : Altération des fonctions de transfert dans les cas de canal calme et perturbé.
Changes in transfer functions in cases of quiet and disturbed channel.

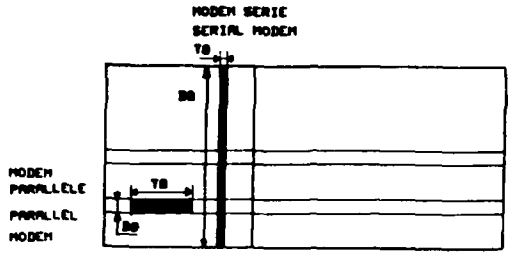


FIGURE 11a

Répartition de l'information dans le domaine temps fréquence pour les modems série et parallèle.
Time frequency domain distribution of information for serial and parallel modems.

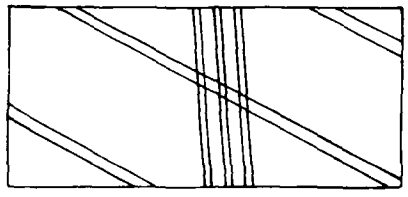


FIGURE 11b

Schématisation des zones d'affaiblissement dans le domaine temps fréquence.
Pattern of attenuation areas in the time frequency domain.

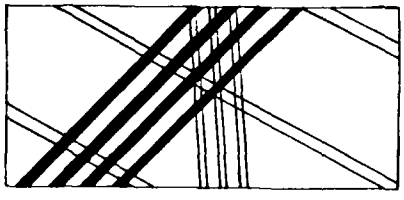


FIGURE 12

Modem à modulation linéaire de fréquence.
Linear frequency modulation modem.

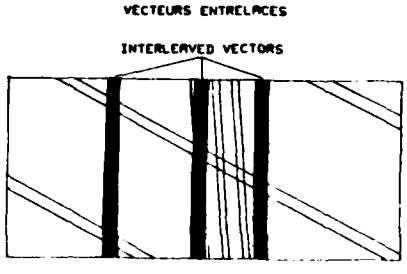


FIGURE 13

Modem à codage et entrelacement.
Encoding and interleaving modem.

OBSERVATIONS WITH AN IONOSONDE IN NORTHERN GERMANY NEAR THE MID-LATITUDE TROUGH

Thomas Damboldt
Forschungsinstitut der Deutschen Bundespost
Postfach 5000
D-6100 Darmstadt

SUMMARY

A near-vertical incidence ionosonde was installed more than two years ago near Hamburg, in order to improve HF propagation predictions and frequency management. HF propagation in the North-Sea and Baltic-Sea areas - close to the auroral zone, near the mid-latitude trough - is highly variable. This manifests itself also on the ionograms. Many of them show peculiarities normally not seen farther south. This paper compares the day-to-day variation of measured ionospheric characteristics with those obtained by the CCIR method (Report 340). In addition statistics of ionospherically disturbed days in the years 1983 and 1984 are given and compared with measurements of the variations of the geomagnetic field at the near-by observatory Wingst.

Although the ionosonde is used mainly as a tool for up-to-date HF propagation predictions, the collected data can be of considerable use also for the design of new HF radio systems in the area under consideration.

1. INTRODUCTION

Hourly measurements of the ionospheric parameters foF2, M3000, foEs and fmin have been made by the Research Institute of the Deutsche Bundespost with an ionosonde near Hamburg since January 1983. At present the ionograms are printed in the form of virtual height plots in real time, and the evaluation of the characteristic values is done manually according to the "Ionogram Interpretation Handbook" (1). The data are primarily used for short-term HF propagation predictions. They are also distributed through the URSIgram service.

Most ionograms show clearly the expected traces (Fig. 1). Apparently, the high interference level in the European HF environment does not affect the quality of the ionograms (2).

The transmitter antenna used is a wideband horizontal fan dipole, the receiver employs a short active dipole. The wide antenna beams and the location are the cause of a great number of disturbed ionograms (Fig. 2) (3).

2. COMPARISON OF OBSERVATIONS WITH DATA FROM CCIR REPORT 340

CCIR Report 340 (4) contains monthly hourly medians of the ionospheric characteristics in the form of maps and numerical values as a function of geographic location, time of day, season and sunspot number. These values are used as the basis in most HF propagation prediction methods.

A comparison of the 576 (=24x24) monthly hourly predicted medians of the critical frequency foF2 and the observations yielded an average difference of only -0.09 MHz with an RMS difference of 0.52 MHz.

A comparison of the 16387 measured hourly foF2-values and the predicted monthly median values showed an average difference of -0.08 MHz with an RMS difference of 0.95 MHz (136 hourly values departed more than +/- 2.75 MHz from the predicted monthly medians, see Fig. 3).

Both comparisons prove the high degree of accuracy of the "CCIR Atlas" in Europe, although the spread of the data is large.

3. INFLUENCE OF MAGNETIC ACTIVITY ON foF2

As mentioned above, the difference between all measured and predicted foF2-values is -0.08 MHz for the hourly values of the two years period. If only those hours were compared, during which the average K-value (measured at the near-by geomagnetic observatory Wingst) was lower than 5 in the preceding 18 hours, the average difference becomes -0.07 MHz; when only K-values lower than 4 were compared it becomes +0.01 MHz and +0.17 MHz for K-values lower than 3. This means that (in the past two years of low solar activity) the CCIR Atlas fits the observations of our ionosonde best for days of rather low magnetic activity ($K<4$). For very quiet days ($K<3$) the CCIR Atlas estimates of the hourly foF2-values are too low.

Looking at magnetically disturbed days, we find that for days with $K>4$ (average K-value for the preceding 18 hours at Wingst) the average difference between the hourly measured

and predicted foF2-values is -0.72 MHz with an an RMS difference of 0.94 MHz (Fig. 4), for days with K>5 the average difference becomes -1.42 MHz, with an RMS difference of 1.09 MHz (Fig. 5) and for very disturbed days with K>6 the difference between measured and predicted foF2-values becomes -3.05 MHz, with an RMS difference of 1.43 MHz (Fig. 6). This means, that the predicted values may be up to about 3 MHz higher than the measured ones. Table I shows the average differences between measured and predicted foF2-values for different levels of magnetic activity.

4. INFLUENCE OF MAGNETIC ACTIVITY ON THE OCCURRENCE OF SCATTER ECHOES

The hourly measurements carried out over a two year period yielded 17544 ionograms (365 x 24 + 366 x 24). On 535 ionograms no traces could be identified because only scatter echoes occurred. Of the remaining ionograms, 3246 showed more or less pronounced traces together with spread-F or backscatter echoes at frequencies above foF2. There is a pronounced dependence of magnetic activity on the occurrence of scatter echoes. Fig. 7 shows the frequency of occurrence of scatter as a function of magnetic activity. Fig. 8 shows the magnetic activity dependence of ionograms where determination of the ionospheric characteristics was impossible because of too high absorption, too low critical frequency (below 1.6 MHz) or scatter echoes (see Fig. 2). The percentage occurrence of scatter echoes as a function of magnetic activity is delineated in Fig. 9.

Fig. 10 shows the diurnal variation of scatter occurrence during the two years. Scatter echoes were observed mainly at night. A closer look at the numbers reveals that at 3501 hours out of a total of 8772 night-hours (i.e. on 40 percent of all night-hours) backscatter echoes occurred. If only the 6 hours around midnight are considered, 2279 of 4386 hours (52 %) showed scatter echoes.

5. CONCLUSION

The objective of this paper was to compare the observed and predicted median characteristics of the ionospheric F2-region at a specific location. The agreement of measurements with predictions is very good, although the spread of the differences between measured and predicted values is large. It should be pointed out, however, that at the location of our ionosonde (between the mid-latitude ionosphere and the high-latitude ionosphere) the F2-layer at night during magnetically disturbed times has a depleted electron content (low critical frequencies) and exhibits strong backscatter echoes. This in turn leads to severe limitations for all types of HF systems.

In the two years of medium and low solar activity (sunspot number between 10 and 100) these "disturbed" conditions were observed on 20 percent of all hours, or 40 percent of the night-hours or 52 % of the 6 hours around midnight. This means that essentially in every other night the ionosphere in this region of the world would not support HF systems requiring low signal distortion.

6. REFERENCES

(1) Piggott, W.R. and K. Rawer: URSI Handbook of ionogram interpretation and reduction, Report UAG-23A, 1978

(2) Damboldt, Th.: Der Chirpsounder als Ionosonde, Kleinheubacher Berichte, Vol 27, pp. 525-528, 1983

(3) Eyfrig, R.: Über die Auswertung komplizierter Chirpsounder-Ionogramme, Kleinheubacher Berichte, Vol 27, pp. 529-534, 1983

(4) CCIR, Report 340, CCIR Atlas of ionospheric characteristics, UIT, Geneva, 1982

	12h	15h	18h
K<9	-0.08/0.95	-0.08/0.95	-0.08/0.95
K<5	-0.06/0.93	-0.06/0.93	-0.07/0.93
K<4	0.01/0.92	0.01/0.91	0.01/0.91
K<3	0.12/0.90	0.15/0.89	0.17/0.88
K>6	-2.35/1.67	-2.71/1.47	-3.05/1.43
K>5	-1.12/0.96	-1.26/1.02	-1.42/1.09
K>4	-0.60/0.91	-0.67/0.93	-0.72/0.94
K>3	-0.31/0.94	-0.34/0.94	-0.37/0.93

Table I Average differences and RMS differences between measured and predicted foF2-values for different levels of magnetic activity (expressed as average K-index for the 12, 15 and 18 preceding hours).

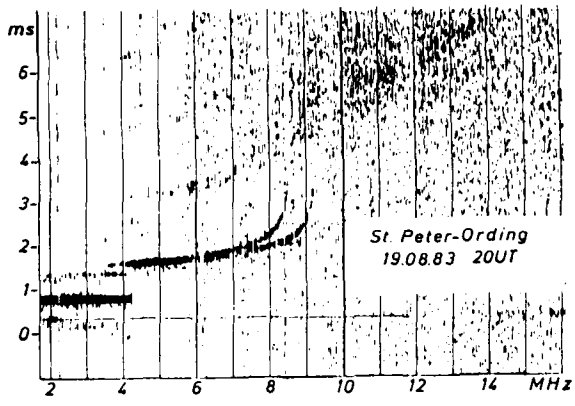


Fig. 1 Typical daytime ionogram at St. Peter-Ording, showing groundwave at about 0.3 ms, E-layer at about 0.7 ms (the trace at about 1.4 ms is a phantom), and F-layer at about 1.8 ms. Note 2 F backscatter up to 14 MHz.

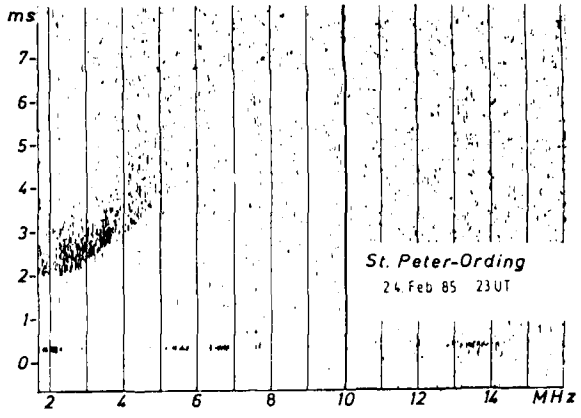


Fig. 2 Typical ionogram showing only backscatter echoes.

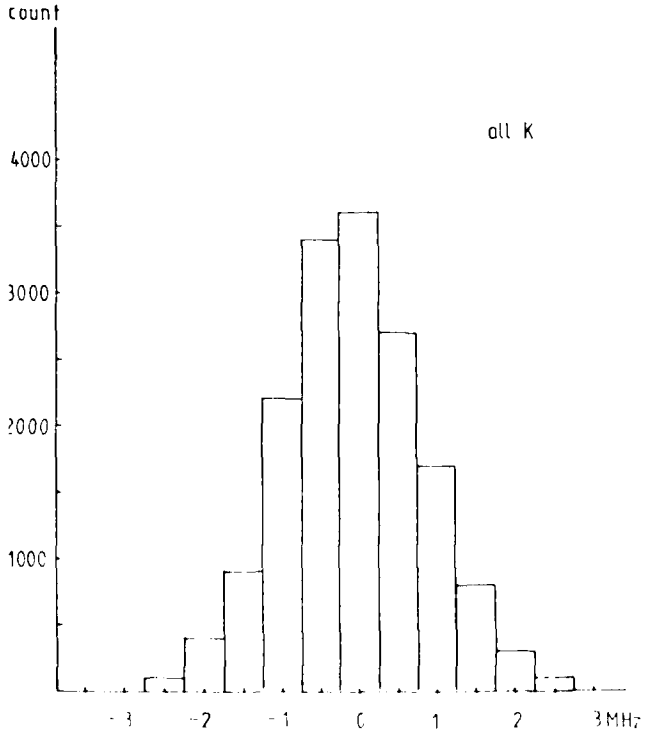


Fig. 3 Histogram showing differences between measured and predicted hourly foF2-values. Total count: 16387, average difference: -0.08 MHz, RMS difference: 0.95 MHz

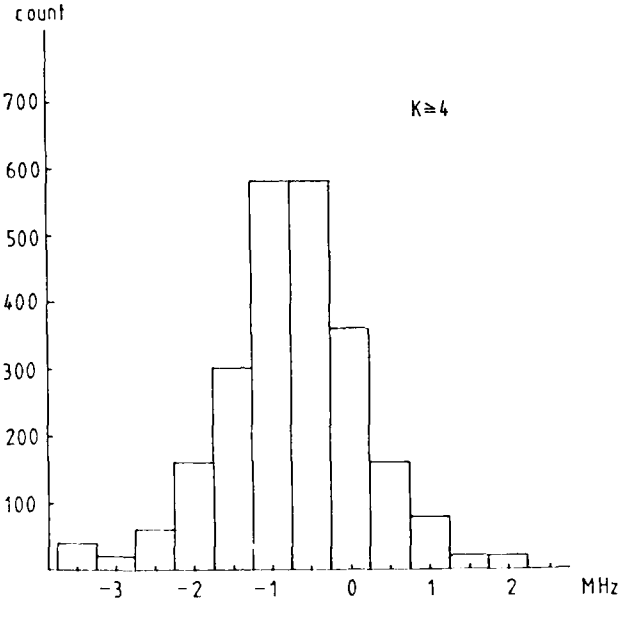


Fig. 4 Histogram showing differences between measured and predicted hourly foF2-values when the average K-value of the preceding 18 hours was greater or equal than 4. Count: 2368, average difference: -0.72 MHz, RMS difference: 0.94 MHz.

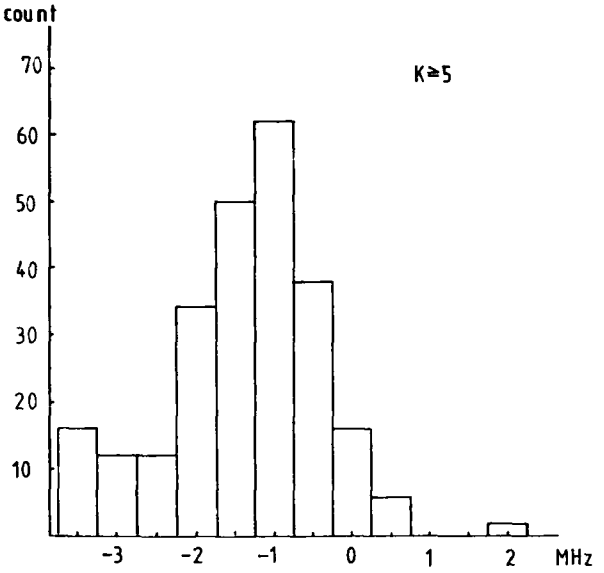


Fig. 5 Histogram showing differences between measured and predicted hourly foF2-values when the average K-value of the preceding 18 hours was greater or equal than 5. Count: 241, average difference: -1.42 MHz, RMS difference: 1.09 MHz.

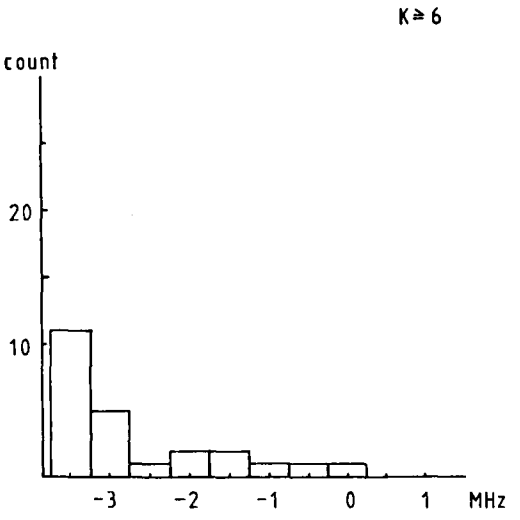


Fig. 6 Histogram showing differences between measured and predicted hourly foF2-values when the average K-value of the preceding 18 hours was greater or equal than 6. Count: 24, average difference: -3.05 MHz, RMS difference: 1.43 MHz.

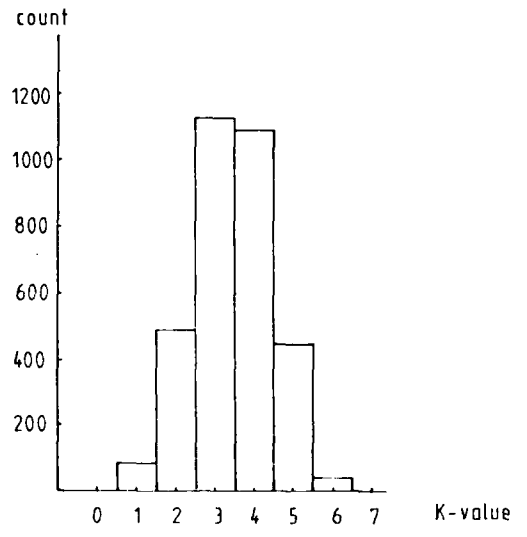


Fig. 7 Frequency of occurrence of backscatter echoes (F-traces still detectable) as a function of magnetic activity (average K-value for the preceding 18 hours). Count: 3246.

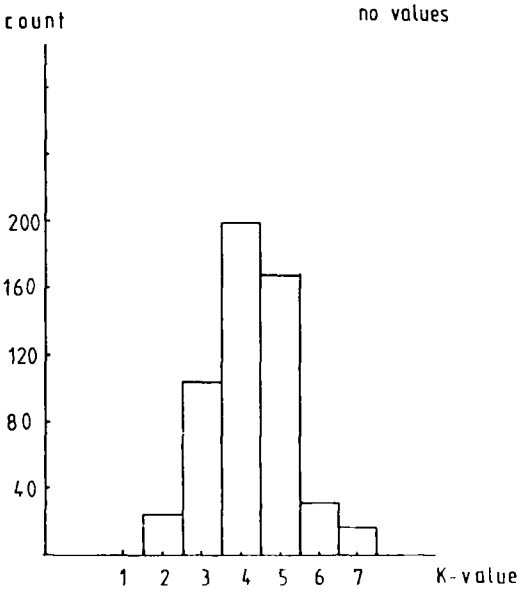


Fig. 8 Magnetic activity dependence of ionograms where determination of ionospheric characteristics was impossible because of too high absorption, too low critical frequency (below 1.6 MHz) or only scatter echoes. Count 535.

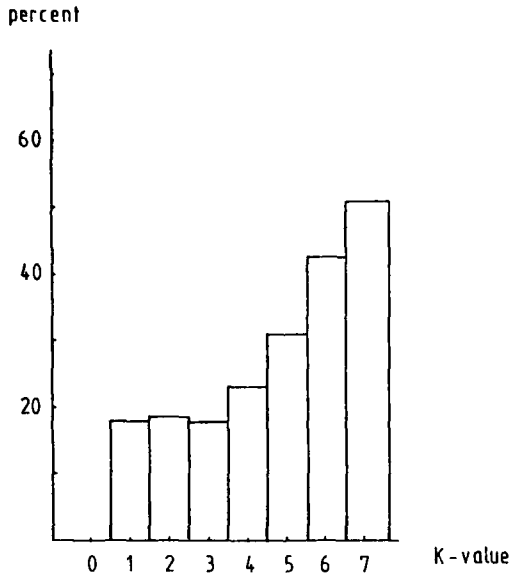


Fig. 9 Percentage occurrence of backscatter echoes as a function of magnetic activity.

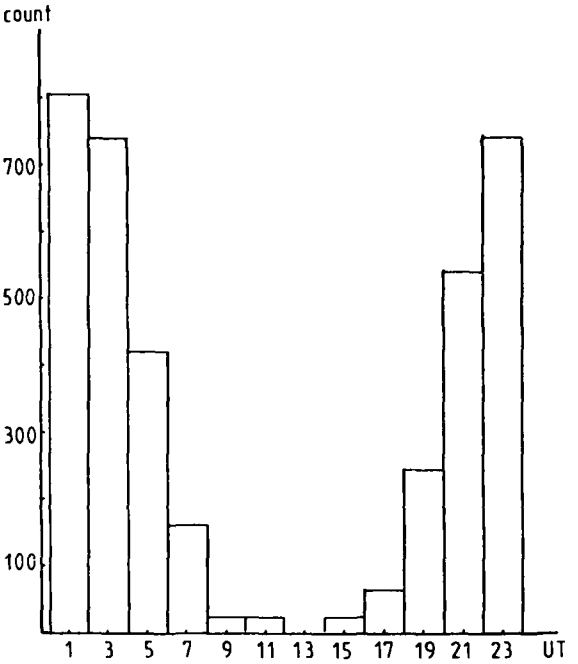


Fig. 10 Diurnal variation of backscatter occurrence.

DISCUSSION

E.Thrane, NO

Were you able to observe Travelling Ionospheric Disturbances?

Author's Reply

Although our ionosonde can make up to 12 ionograms per hour, we operate it only once per hour and therefore we have not looked for TID's.

J.Aarons, US

It is doubtful that the spread F occurring when Kp is 0, 1, 2, 3 is associated with the trough for a latitude of 55° corrected geomagnetic latitude. It is more likely associated with plasmapause latitude irregularities.

Author's Reply

Figure 7 showed that about 50% of the ionograms with spread F were observed during magnetically quiet conditions ($K \leq 3$). I agree that those cases are not associated with the trough at the geomagnetic location in question. Unfortunately, however, we did not yet have the time to study the various reasons for the occurrence of spread F in detail.

SUMMARY OF SESSION IV

High Latitude HF Probing

by

Prof. C.Goutelard
Session Chairman

Session IV of this meeting was devoted to measurements in high latitudes. Seven communications were presented: five of them were based on measuring techniques by backscatter and two studies were done by means of zenithal sounders.

Bradley's account was aimed at a study of ground range measured by backscatter in high latitudinal regions. He carries out a classification of obtained configurations and establishes a statistic of their occurrence which can serve as a basis for future works.

Bourdillon's report, presented by G.Sales, deals with the study of disturbances aligned on the magnetic field using two backscatter sounders enabling the measurement of the perpendicular components of the speed of irregularities. An interpretation of the results was done using a theoretical model.

Hanuise reported on an experiment at high and very high latitudes in the Europe zone with the help of coordinated measurements from satellite, incoherent scatter radar, and backscatter sounder. The comparison of the results obtained with the different systems shows a good agreement between the measures, but the discussion pointed out the difficulty of interpretations.

Kelly's report was devoted to the analysis of backscatter and ionosonde signatures and their interpretation from main ionospheric parameters measured by an incoherent scatter sound. A correlation was established between certain types of signatures and convection plasma patterns which develop in the polar zone.

Greenwald presented an experiment on the ionosphere at high latitudes by mean of a backscatter sounding system. A detailed description of the system, which presents original characteristics, was given and the results presented. These results, accompanied by bistatic oblique sounding measurements show the spatial and temporal variations of irregularities, whose occurrences are related to disturbances of the magnetospheric — ionospheric system.

The report presented by Berkey shows observations carried out by means of a coherent digital sounder in the Antarctic. Simultaneous measurements were done in the zone of auroral depression and an examination of the results was done during calm and disturbed periods. The complexity of the results is pointed out and their interpretation, made easier for the use of sophisticated material, shows the influences of fundamental phenomena on the signatures.

Rodger presented a study of the zone of auroral depression and its predictability from results of digital sounders in the Antarctic. A detailed study of the morphology of this region was done and the causes of its variations examined. The important points necessary to examine in order to improve the precision of forecasts were established.

The reports presented show that the measurements taken in high latitudinal regions are particularly difficult, notably because of the complexity of the phenomena which develop there. They imply the implementation of complex systems and the results show the necessity of following up these studies in the years to come.

IONOSPHERIC FACTORS AFFECTING THE PERFORMANCE OF HF SKY-WAVE SEA-STATE RADARS AT HIGH LATITUDES

P A Bradley and A J Gibson
(Rutherford Appleton Laboratory, Chilton, Didcot, Oxon, OX11 0QX, UK)

J C Schlobohm and D E Westover
(SRI International, 333 Ravenswood Avenue, Menlo Park, California 94025, USA)

1. INTRODUCTION

Sky-wave radars provide a means of ocean surveillance beyond line of sight and beyond the ranges achievable with a ground-wave radar. However, the ionosphere introduces a number of important propagation limitations. Firstly, it is necessary to provide illumination of the areas of interest, which may place restrictions on radar siting and periods of operation. Then, backscattered signals must have sufficient amplitude to provide adequate discrimination above the naturally occurring and interference backgrounds. A radar measures time-of-flight and such information needs transforming to equivalent ground range in terms of the prevailing ionospheric path. Finally, ionospheric motions create Doppler shifts and spreads of the returned signals which prevent spectral resolution of Bragg scattered components.

The high-latitude ionosphere is characterised by features which exhibit marked spatial and temporal variability. This paper examines the principal effects which can arise by presenting data from a number of sources. Specific problems are discussed and possible ways of alleviating some of these considered.

2. ILLUMINATION

For a given ocean area of interest, illumination may be provided over a band of frequencies between the maximum usable frequency (MUF) and the lowest usable frequency (LUF). Typically MUF's associated with reflection from the regular F-layer are lower than at middle latitudes because of the reduced solar ionising radiation, particularly in the Winter night. On the other hand, energetic electrons incident at E and F-region heights create additional ionisation at auroral latitudes. These can give rise to increased MUF's but with considerable day-to-day variability, making difficult performance prediction and frequency management.

Existing readily available reference ionospheric data derived from vertical sounding information, such as the CCIR numerical maps of ionospheric characteristics (*CCIR, 1982a*), are based on a mapping procedure which fails to represent important high-latitude features such as the auroral oval and night-time trough. Other mapping efforts within recent years (Rush et al, 1984) in which vertical-incidence data are combined with results derived from thermospheric wind theory, show potential for improved accuracy in these regards. Whereas such data are needed for planning, there is no doubt that for post-mortem investigations it is preferable to prepare models with spatial ionisation changes derived as far as possible from all relevant sensor information pertinent to the epoch of interest. Figure 1 shows a map of foF2 from one such model (Rush et al. 1982) derived specifically for radar performance assessment. In this model the trough of ionisation evident in the example around 60° geographic latitude is assumed to have a poleward boundary coinciding with the equatorward boundary of the oval and an equatorward boundary and depth which vary on a daily basis. The position of the oval is given as a function of magnetic activity (Whalen, 1970). Other models, like that of Rush et al. (1982) which can be used for radar performance determination and which include features that are set for each day as a function of planetary magnetic activity index Kp or local magnetic K index, are those of Vondrak et al. (1978) and of Elkins (1979, 1980). The importance of the trough has been investigated through ray-tracing studies by Lockwood (1981). Besides the reduction of MUF he shows not surprisingly that focusing by the convex and concave reflecting surfaces occurs at certain hours, with defocusing at other times.

Other important features of high latitude ionisation are the marked auroral E-region which represents an enhancement over the solar-controlled E-layer, particularly at night-time. foE and the locations of the boundaries of this layer are given as a function of magnetic activity index. The auroral E-region has greater thickness than the normal E-layer and at certain times its electron densities can exceed those in the F-region. For some paths it will have a dominant effect on the MUF.

Also associated with auroral precipitation at E-region heights is the development of a band of irregularities closely following the position of the auroral oval. A representation of auroral Es taken from Elkins (1970) based on vertical-incidence observations and analyses of Besprozvannaya and Shchuka (1972) shows a somewhat similar morphology. Figure 2 gives the percentage of time that the maximum frequency of sporadic-E reflection exceeds 3 MHz. Auroral Es occurrence exhibits a marked midnight maximum, and other maxima at 04 and 19 hours magnetic local time at lower latitudes where it is responsible for diffuse direct-scattered radar returns. There is a pronounced minimum around 65° corrected geomagnetic latitude. The phenomenon is independent of sunspot number, but shows a strong dependence on Kp.

Small-scale irregularities in the high-latitude F-region are a very common phenomenon regularly observed at night with vertical-incidence sounders. Their occurrence probability increases with geomagnetic latitude. At auroral latitudes there is a maximum around 02-04 magnetic local time (Fig. 3). Spread-F is most common in Winter and least frequent in the Summer. Its incidence increases with magnetic activity, particularly in the equinoxes. The equatorward boundary moves to lower latitudes with increasing geomagnetic activity.

The importance of each of the above phenomena to ocean illumination clearly depends on radar frequency, path geographical position and epoch. Weak auroral irregularities are likely to have little effect, but as these become more pronounced they can give rise to direct backscatter. If the scattering

is only partial, they may provide the means of raypath reflection to illuminate a more distant ground scatterer. At other times they may serve as a screen. Auroral spread-F irregularities are elongated along the direction of the local magnetic field and scattering efficiencies are aspect sensitive. HF radar results of Baggaley (1970) give reductions in scattering efficiencies of 10dB per degree off-perpendicularity, although other workers have deduced reductions of only 3-4dB per degree.

Möller (1974) has investigated the movements of high-latitude irregularities using an HF radar located in W. Germany. He finds direct returns from two belts of F-region irregularities, one associated with the equatorwards edge of the auroral oval present at all local times with minimum latitude at midnight, and the second belt seen only at night appearing northwards of the ionisation trough and moving equatorwards towards sunrise.

Other information recently available has been taken using a radar located in S. England. This has a nominal antenna beamwidth of 5° at 15 MHz and can be steered over the range 35°W to 35°E of N. Figures 4 and 5 show sample widesweep backscatter ionograms of the 5-30 MHz frequency band. Records may be categorised as regular (R) arising mainly in the daytime from ground-backscatter supported by single and two-hop F2-mode propagation (Fig. 4a), multiple (M) with ground backscatter supported by F2 and E/F1 mode propagation in the Summer daytime (Fig. 4b), or auroral (A) mainly at night. The auroral records display a variety of form. (Figs. 4d-f and 5a-f).

With the onset of evening, irregularities develop within the F2-layer and these can give rise to ghosted ground-backscatter returns in advance of the main trace (Fig. 4c) (Croft, 1968). In the example of Fig. 4(d) direct auroral returns are also seen between frequencies of 13 and 26 MHz over radar ranges of 1100-1300km. The auroral trace is approximately horizontal, but with some retardation at the lower frequencies. Figures 4(e) and (f) show other examples of a full F2 ground-backscatter trace at the same time as direct auroral returns are observed. In Fig. 4(e) there are two groups of echoes, consistent with the data of Möller. The record of Fig. 4(f) clearly shows geometrical cut-off of the auroral trace at frequencies around 12-17 MHz depending on range.

The auroral trace has a sharp approximately horizontal leading edge at 1000km range (Fig. 5a) and at 1150km range (Fig. 5b) with some retardation at the lower frequencies. The spread diminishes with increase of frequency but echoes are still observed at 20 MHz when the UK-measured foF2 is only 4 MHz. There is some evidence in the record of Fig. 5(b) of ground-backscatter returns at a radar range of 2000km at frequencies of 5-6 MHz; ground backscatter might have been seen at shorter ranges were the sounder to have operated below 5 MHz.

At times the auroral trace is quite thin, extending over only say 200km at the lower frequencies (Fig. 5d), whereas more often it is much fatter (Fig. 5e). Some records like those of Figs. 4(d)-(f) indicate the F2-trace at all ranges; in others it is observed only at shorter ranges than the direct backscattered trace. The origin of some traces of the form of Fig. 5(c) has yet to be identified, but is believed to involve an auroral element.

With synoptic sample measurements at all hours, Table 1 shows for the different four-hour time periods and seasons the numbers of ionograms categorised as regular(R), multiple(M) and auroral(A). The predominance of A records in the night-time ie. 18-08 hours by Winter and 20-04 hours in the Summer, is evident. For all times combined, a breakdown of the numbers of the different types of auroral traces is given in Table 2. Nearly 30% of the time auroral traces are diffuse or weak with F2-mode ground-backscatter or Es direct backscatter at shorter ranges (Fig. 5f).

Sequences of continuous successive widesweep ionograms for a N pointing antenna show that generally ionogram features do not change significantly over periods of less than an hour. The variation over a whole single night is often small, but there can be marked differences in range and form from one night to the next. Consecutive data recorded for different azimuths show that often the spatial extent of auroral returns is large, with no major differences over the band of angles that can be covered. For a selection of ionograms of the different types but all with a flat leading edge, Fig. 6 gives the variation throughout the night hours of the minimum range of the auroral echo. Values lie between 600-1500km, with no clear dependence on time or local magnetic K index.

Figure 5(f) for a bearing of 30°W indicates flat traces at ranges of 1750 and 1800km which can be interpreted as arising from two separate ionospheric modes with ground scatter from the Iceland coastline. Such occurrences are quite common for this azimuth, showing that in these cases the auroral irregularities are partially reflecting for frequencies considerably greater than the regular F-region MUF.

TABLE 1

NUMBERS OF WIDE-SWEEP IONOGRAMS DESIGNATED REGULAR (R), MULTIPLE (M) AND AURORAL (A)

	UT	00-04	04-08	08-12	12-16	16-20	20-24
Summer (Jun, Jul, Aug)	R	0	35	37	34	28	4
	M	0	11	46	40	40	0
	A	72	34	0	0	14	80
Autumn (Sept, Oct)	R	0	22	46	33	13	0
	M	0	4	18	14	2	0
	A	74	45	0	5	29	48
Winter (Nov, Dec, Jan)	R	0	4	68	53	0	0
	M	0	0	16	12	0	0
	A	89	77	13	13	82	86

TABLE 2

NUMBERS OF WIDE-SWEEP AURORAL IONOGRAMS WITH DIFFERENT TYPE CATEGORISATION - ALL HOURS AND MONTHS COMBINED

TYPE	DESCRIPTION	NUMBER
A1	Flat fat auroral only	54
A2	Flat thin auroral only	20
A3	Flat auroral + F2 trace	169
A4	Flat auroral + F2 trace below auroral only	65
A5	Upwards sloping auroral + F2 trace	32
A6	Wedge shaped trace	26
A7	Auroral + wedge shaped trace	55
A8	Diffuse auroral, some F2 trace below	116
A9	Diffuse auroral, Es trace below	224

3. ADEQUATE AMPLITUDE

Ignoring those instances noted above where for the particular raypath geometry in relation to the irregularity locations it is possible to obtain ground illumination at frequencies in excess of 20 MHz, more commonly ionospheric support requires lower frequencies than at lower latitudes. This leads to problems of wider antenna beamwidths, greater amounts of ionospheric absorption and often greater atmospheric noise background intensities, all contributing to lower signal/noise ratios.

Auroral particles penetrating to the D and E-regions give rise to additional ionisation which leads to extra absorption. This so-called auroral absorption has a morphology closely allied to the morphology of the auroral oval. Foppiano and Bradley (1983) have produced a model of auroral absorption showing that this has two diurnal maxima around midnight and 08 hours, consistent with the morphology of the 'splash' and 'drizzle' particle precipitation model (Fig. 7) postulated by Hartz and Brice (1967). The band of auroral absorption moves equatorward and intensifies when magnetic activity is increased.

Careful attention has to be paid to polarisation effects on high-latitude paths, particularly for propagation along the magnetic meridian. A detailed study of the phenomenon has been presented by Moorat (1968) and values of polarisation-coupling loss for paths under different conditions are quoted by Bradley (1968). Generally, the ordinary wave has a polarisation ellipse with major axis oriented along the direction of the projection of the magnetic field onto the wavefront plane (approximately vertical) and the extraordinary wave polarisation ellipse is normal to this direction (horizontal). With elevation angles of 10-20°, raypaths in the lower ionosphere tend to be nearly transverse to the field, so that these ellipses are highly elongated. Figure 8 shows that horizontally-polarised backscattered signals (or those radiated by a repeater with a horizontal antenna) can suffer large polarisation-coupling losses.

Direct auroral returns lead to the phenomenon of auroral clutter, showing a morphology related to the incidence of auroral irregularities in both the E and F-regions. Backscatter clutter power depends on the volume of auroral scatterers illuminated by the radar, and the volumetric scattering cross-section, which in turn is a function of the magnetic aspect angle. One such model of pseudo-volumetric scattering cross-sections is presented by Elkins (1980), based on standardisation in terms of equivalent point-target cross-sections derived from measured radar results. He finds that this cross-section parameter differs for the E and F-regions, and includes both a frequency and a Kp dependence. Auroral clutter shows a wide range of Doppler spreads, sometimes extending over tens of Hertz depending on the motions of the auroral irregularities. In all cases, the normal Bragg-scattered returns from ocean spectra with shifts at HF of only a few tenths of a Hertz are never avoided.

Reference atmospheric noise data based on past measurements are presented by the CCIR (1982b). These measurements were made with a short vertical whip antenna and no azimuthal dependence of the noise is assumed. Recent data collected by Gibson et al. (1985), in which atmospheric noise and interference in the fixed and broadcast service bands were measured with directional antennas pointing in different directions, confirm the validity of the assumption. This result is at first surprising, but arises because even with antennas of modest gain for noise incident from a range of azimuths the contribution to the total received power from the sidelobes exceeds that from within the main beam. Remembering that even with a northwards pointing radar, many interfering signals are propagated across the pole, it seems reasonable to conclude to a first order that HF background intensities are comparable to those found at middle latitudes.

Figure 9 shows for the UK radar, which was operated at a series of fixed frequencies for the collection of amplitude and Doppler spectral information, those frequencies giving greatest ground-backscattered signal-to-noise ratio. For a series of radar ranges the dependence on season and time of day is illustrated. Generally, optimum frequencies are between 7-15 MHz, being greater by day than night. However, attention is drawn to the marked day-to-day variability at a given time. This suggests long-term predictions are of only limited value for frequency management.

4. RANGING

The ranging accuracy needed depends on the application. For many purposes with say a range resolution cell size of 75km it is of doubtful necessity to even know the propagation mode, a single mean algorithm relating ground and slant range being quite adequate. When however greater ranging accuracy is sought, either recourse must be made to ray tracing through model ionospheres or to use of some ranging calibration feature.

There have been many efforts at developing ionospheric models for use with ray tracing in order to simulate radar ranges. Some of these approaches have proved useful at middle latitudes, but experience difficulties when applied to the high-latitude ionosphere, both because of the paucity of real-time ionospheric data and the marked spatial gradients which arise. Hatfield (1970) and Dubroff et al. (1979) have attempted to simulate an ionosphere composed of parabolic segments matching backscatter data. Milsom (1985) has shown how the model ionosphere of Bradley and Dudeney (1973) may be used with effect for radar raypath simulations. Thomason et al. (1979) described a model based on long-term numerical maps of the ionosphere, but incorporating sophisticated ray tracing. Rush and Miller (1973) have developed a three-dimensional model ionosphere suitable for ray tracing in the presence of gradients. Incorporation of daily measured ionospheric parameters into a prediction model is discussed by Miller and Gibbs (1975). The updating of monthly median predicted values by measured parameters is considered by Edwards et al. (1975). A particular problem is the correlation distance over which measured data remain pertinent. At high latitudes this is certainly less than the 500km in the N-S direction found for middle latitudes.

Mention is made of the existence of returns that can be attributed to scattering from a land/sea interface. Alternatively, repeater data are useful for ranging purposes as well as for transmission-loss assessment. Figure 10 notes the fractions of occasions that a repeater located at Iceland could be detected. Seasonal and diurnal differences are consistent with changes in absorption and auroral activity following the onset of night-time. Studies are planned to assess ground ranges from the measured radar range to the repeater, using simultaneous vertical incidence ionograms taken at the radar site and collected at South Uist, approximately a third the distance to the repeater. Comparison with the known repeater position will serve to indicate the ranging accuracy improvement achieved with an uprange ionosonde.

5. SPECTRAL DISTORTION

The spectral distortion created by the ionosphere has been considered at length by Georges et al. (1981) and by Jones et al. (1983). There is a fundamental limitation to the improvement in spectral quality that can be achieved with different forms of coherent and incoherent spectral integration, depending on the ionospheric motions present. This work for high latitudes will form the basis of further studies. Here attention is restricted to sample spectra presented in Fig. 11 for times close to those at which the widesweep ionograms of Fig. 5 were taken. These relate to a coherent integration time of 2.5s providing a Doppler resolution of 0.4 Hz so that the two first-order Bragg peaks are not separated; however in this way in order to investigate propagation effects it was possible to take measurements at a large series of frequencies and azimuths within a single hour. The Doppler range covered is ±6.25 Hz.

Figure 11(a) shows the spectra for successive ranges of 75km extent at a frequency of 10.5 MHz corresponding to the widesweep ionogram of Fig. 5(b). The spectra associated with the sharp leading edge of the backscatter return at a range of 1200km and other spectra over the next 375km are all seen to be relatively sharp. On the other hand (Fig. 11(b), for the ionogram of Fig. 5(d)) the backscatter leading edge spectrum at 5.0 MHz is broad. This feature is confirmed in the data of Fig. 12 where histograms of spectral widths near the leading edge for these two ionograms, as derived from data for a range of frequencies, are contrasted. For the wedge-shaped ionogram of Fig. 5(c) the spectra at 11.0 MHz (Fig. 11(c)) are also broad, despite the sharp leading edge.

Spectra are shown in Figs. 11(d) and (e) for frequencies of 11.1 MHz and 19.7 MHz, corresponding to the diffuse auroral returns of Fig. 5(f). At 11.1 MHz associated with the diffuse aurora the spectra are broad, but there are narrow spectral peaks at 1725 and 1800km range related to backscatter from the Iceland coastline. For 19.7 MHz at ranges of 1200-1600km the diffuse aurora gives rise to spectra consisting of narrow peaks superimposed on a broad background. Clearly there are a variety of spectral forms and spectral width is not an unambiguous criterion for judging propagation mechanism.

6. CONCLUSIONS

There are shown to be a number of physical factors which make ocean surveillance more difficult than at middle latitudes. Nonetheless the rewards of using an HF radar to collect data over restricted ranges and times are considerable. The technique also has merit as an ionospheric probing tool, both for synoptic and aeronomic studies.

7. REFERENCES

BAGGALEY, W.J., 1970, "Backscatter observations of F-region field aligned irregularities during the IQSY", J. Geophys. Res. 75, 152-158.

BESPROZVANNAYA, A.S., and SHCHUKA, T.I., 1972, "Sporadic ionization of the ionospheric E-region at high latitudes as a function of magnetic activity", Geomag. and Aeron. 12, 401-404.

BRADLEY, P.A., 1968, "Wave polarisation and its influence on the power available from a radio signal propagated through the ionosphere - Part II", Proc. IEE, 115(6), 777-781.

BRADLEY, P.A., and DUDENEY, J.R., 1973, "A simple model of the vertical distribution of electron concentration in the ionosphere", J. Atmos. Terr. Phys., 35, 2131-2146.

CCIR, 1982a, "CCIR atlas of ionospheric characteristics", Report 340, International Telecommunication Union, Geneva.

CCIR, 1982b, "Characteristics and applications of atmospheric radio noise data", Report 322-2, International Telecommunication Union, Geneva.

CROFT, T.A., 1968, "The influence of ionospheric irregularities on sweep-frequency backscatter", J. Atmos. Terr. Phys., 30, 1051-1063.

DuBROFF, R.E., RAO, N.N. and YEH, K.C., 1979, "Backscatter inversion in spherically asymmetric ionosphere", Radio Sci., 14(5), 837-841.

EDWARDS, W.R., RUSH, C.M. and MILLER, D.M., 1975", Studies on the development of an automated objective ionospheric mapping technique", Air Force Surveys in Geophysics, No. 302, Air Force Cambridge Research Laboratories, Mass. 01731.

ELKINS, T.J., 1979, "Recent advances in HF propagation simulation" in "Special Topics in HF propagation" Ed V.J. Coyne, AGARD Conf. Proc. CP-263.

ELKINS, T.J., 1980, "A model for high frequency radar auroral clutter", Rome Air Development Center Report TR-80-122, Griffiss Air Force Base, New York 13441.

FOPPIANO, A.J. and BRADLEY, P.A., 1983, "Prediction of auroral absorption of high-frequency waves at oblique incidence", Telecomm. J., 50(10), 547-560.

GEORGES, T.M., MARESCA, J.W., CARLSON, C.T., RILEY, J.P., JONES, R.M. and WESTOVER, D.E., 1981, "Recovering ocean waveheight from HF radar sea echoes distorted by imperfect ionospheric reflection, NOAA Tech. Mem. ERL WPL-73, Wave Propagation Lab., Boulder, Colorado 80203.

GIBSON, A.J., BRADLEY, P.A. and SCHLOBOHM J.C., 1985, "HF spectrum occupancy measurements in Southern England", Third International Conference on "HF Communication Systems and Techniques", IEE Conf. Publication 245, pp71-75.

HARTZ, T.R. and BRICE, N.M., 1967, "The general pattern of auroral particle precipitation", Planet. Space Sci., 15, 301-329.

HATFIELD, V.E., 1970, "Derivation of ionospheric parameters from backscatter data" in "Ionospheric forecasting" Ed V. Agy, AGARD Conf. Proc. CP-49.

JONES, R.M., RILEY, J.P. and GEORGES, T.M., 1983, "Measured ionospheric Doppler spreading of HF ground-backscatter", NOAA Tech. Mem., ERL WPL-109, Wave Propagation Lab., Boulder, Colorado 80203.

LOCKWOOD, M., 1981, "A simple model of the effects of the mid-latitude total ion trough in the bottomside F-layer on HF radiowave propagation", Radio Sci., 16(3), 385-391.

MILLER, D.C and GIBBS, J., 1975, "Ionospheric analysis and ionospheric modelling", Scientific Report 2, AFCRL-TR-75-0549, Air Force Cambridge Research Laboratories, Mass. 01731.

MILSOM, J.D., 1985, "Exact raypath calculations in a modified Bradley/ Dudeney model ionosphere", Proc. IEE, Part H, 132 (1), 33-38.

MÖLLER, H.G., 1974, "Backscatter results from Lindau-II. The movement of curtains of intense irregularities in the polar F-layer", J. Atmos. Terr. Phys., 36, 1487-1501.

MOORAT, A.J.G., 1968, "Wave polarisation and its influence on the power available from a radio signal propagated through the ionosphere - Part I", Proc. IEE, 115(6), 771-776.

RUSH, C.M. and MILLER, D., 1973, "A three-dimensional ionospheric model using observed ionospheric parameters", Environmental Resch. Paper 455, Air Force Cambridge Research Laboratories, Mass. 01731.

RUSH, C.M., ROSICH, R.K., BROOKS, C.B., LEISE, D.L. and POKEMPNER, M., 1982, "A simplified model of the high latitude ionosphere for telecommunications applications", NTIA Report 82-94, Institute for Telecommunication Sciences, Boulder, Colorado 80203.

RUSH, C.M., POKEMPNER, M., ANDERSON, D.N., PERRY, J., STEWART, F.G. and REASONER, R., 1984, "Maps of foF2 derived from observations and theoretical data", Radio Sci., 19(4) 1083-1097.

THOMASON, J, SKAGGS, G and LLOYD, J., 1979, "A global ionospheric model", NRL Report 8321, Naval Research Laboratory, Washington DC.

VONDRAK, R.R., SMITH, G., HATFIELD, V.E., TSUNODA, R.T., FRANK, V.R., and PERRAULT, P.D., 1978, "Chatanika model of the high-latitude ionosphere for application to HF propagation prediction", Rome Air Development Center Report TR-78-7, Griffiss Air Force Base, New York 13441.

WHALEN, J.A., 1970, "Auroral oval plotter and nomograph for determining corrected geomagnetic local time, latitude and longitude for high latitudes in the northern hemisphere", Environmental Resch. Paper 327, AFCRL-70-0422, Air Force Cambridge Research Laboratories, Mass. 01731.

ACKNOWLEDGMENTS

The authors gratefully acknowledge the contributions to data analyses by Mrs R Blake and Mrs A Vernon.

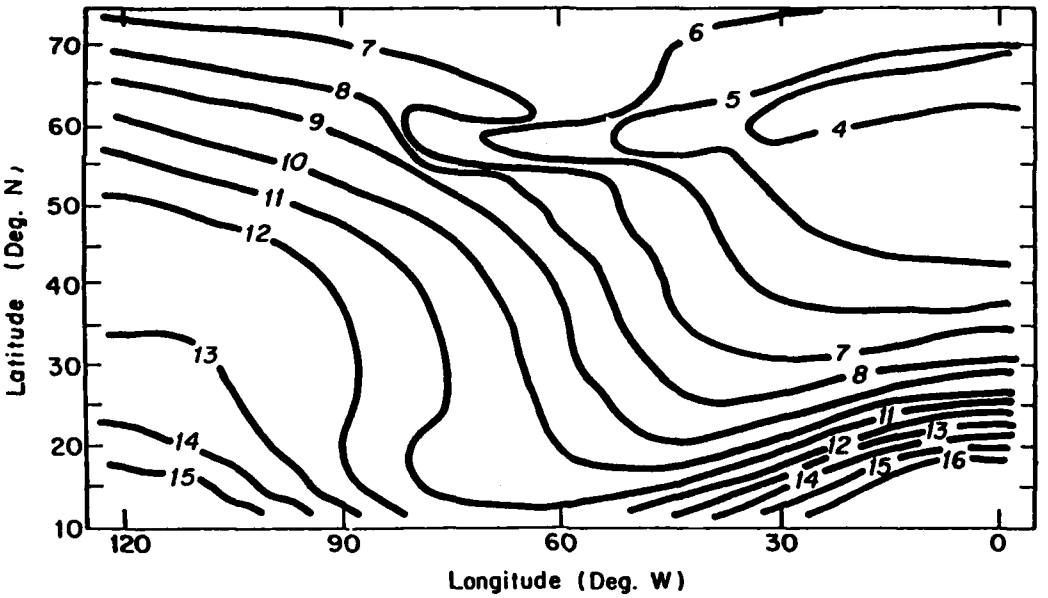


Figure 1 foF2 for 20 January 1981 at 2300 UT given by Rush et al. (1982).

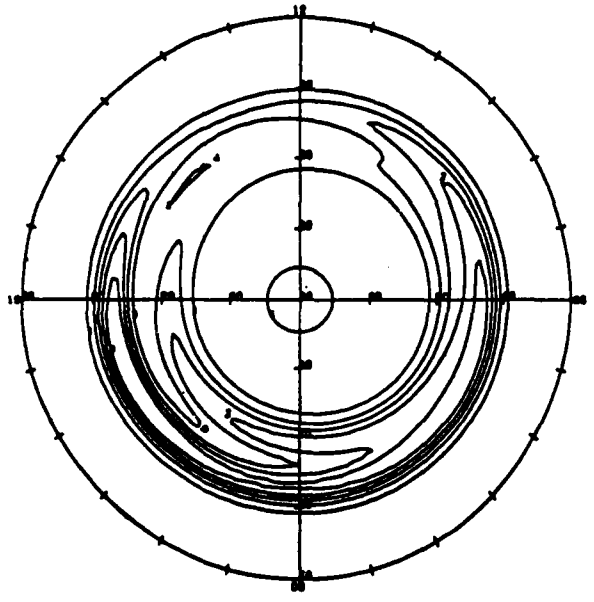


Figure 2

Probability of foEs>3MHz as a function of corrected geomagnetic latitude and local time for 12 h UT in June with Kp = 4 (from Elkins, 1980). Contours in increments of 0.2.

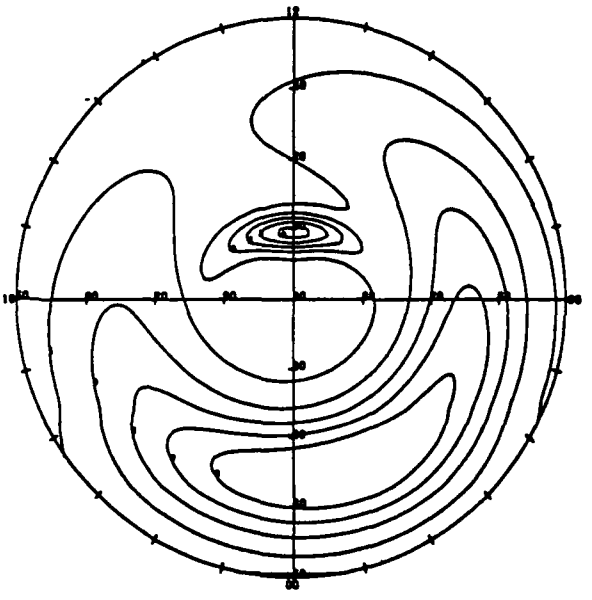


Figure 3

Probability of F-region irregularity occurrence as a function of corrected geomagnetic latitude and local time for 12h UT in June with Kp = 4 (from Elkins, 1980). Contours in increments of 0.2.

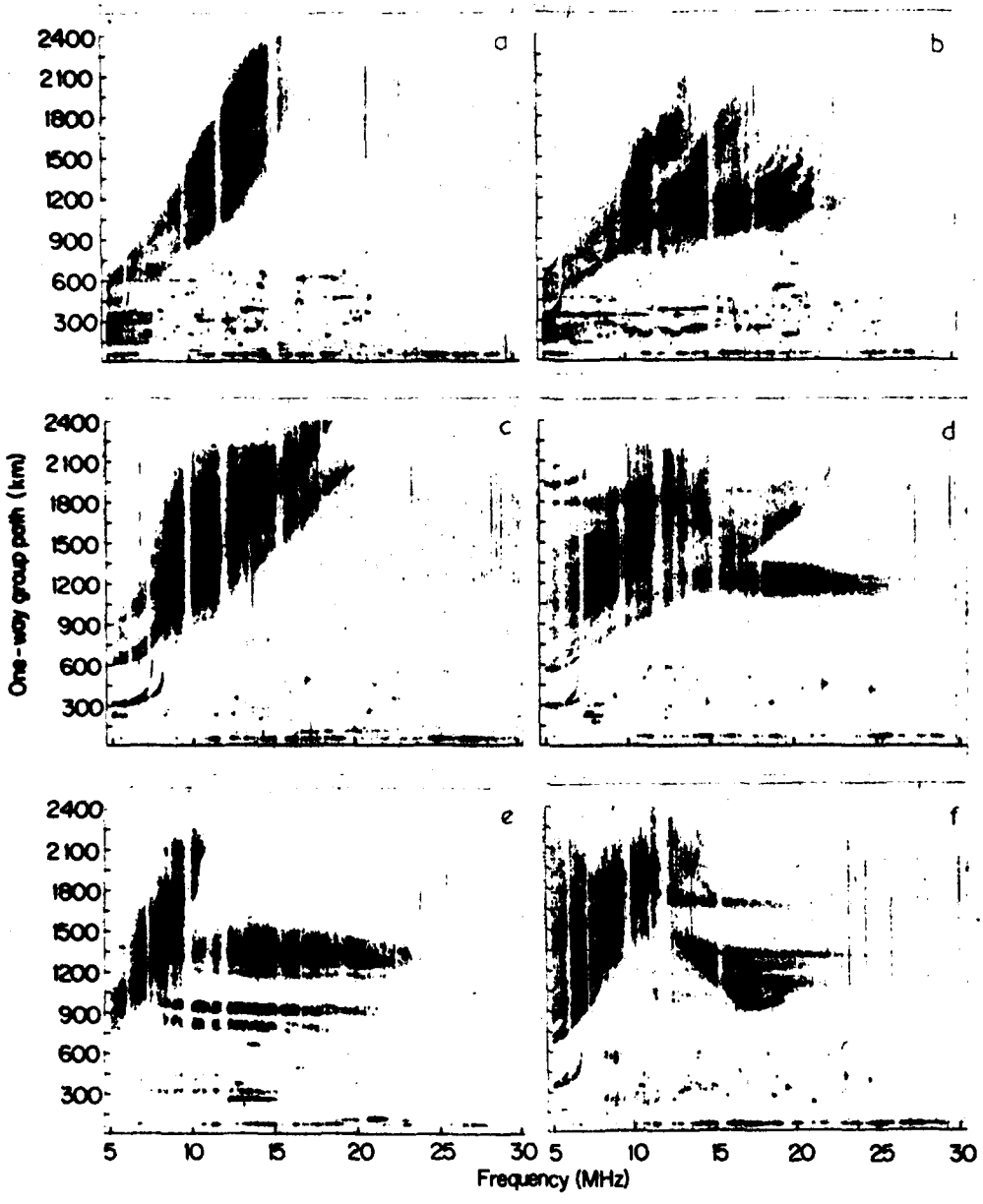


Figure 4 Sample widesweep backscatter ionograms taken in S. England:

(a) Regular F2-mode supported ground backscatter
-N beam, 13 June 1984, 1511 UT

(b) Multiple F2 and E/F1 mode supported ground backscatter
-N beam, 7 June 1984, 1002 UT.

(c) Ghosted leading edge attributed to F-region irregularities
-N beam, 13 June 1984, 1907 UT.

(d) Direct auroral returns giving flat trace
-N beam, 20 September 1984, 1832 UT.

(e) Auroral return with banded structure
-N beam, 25 October 1984, 1758 UT.

(f) Auroral trace with geometrical cut-off
-N beam, 8 June 1984, 2230 UT.

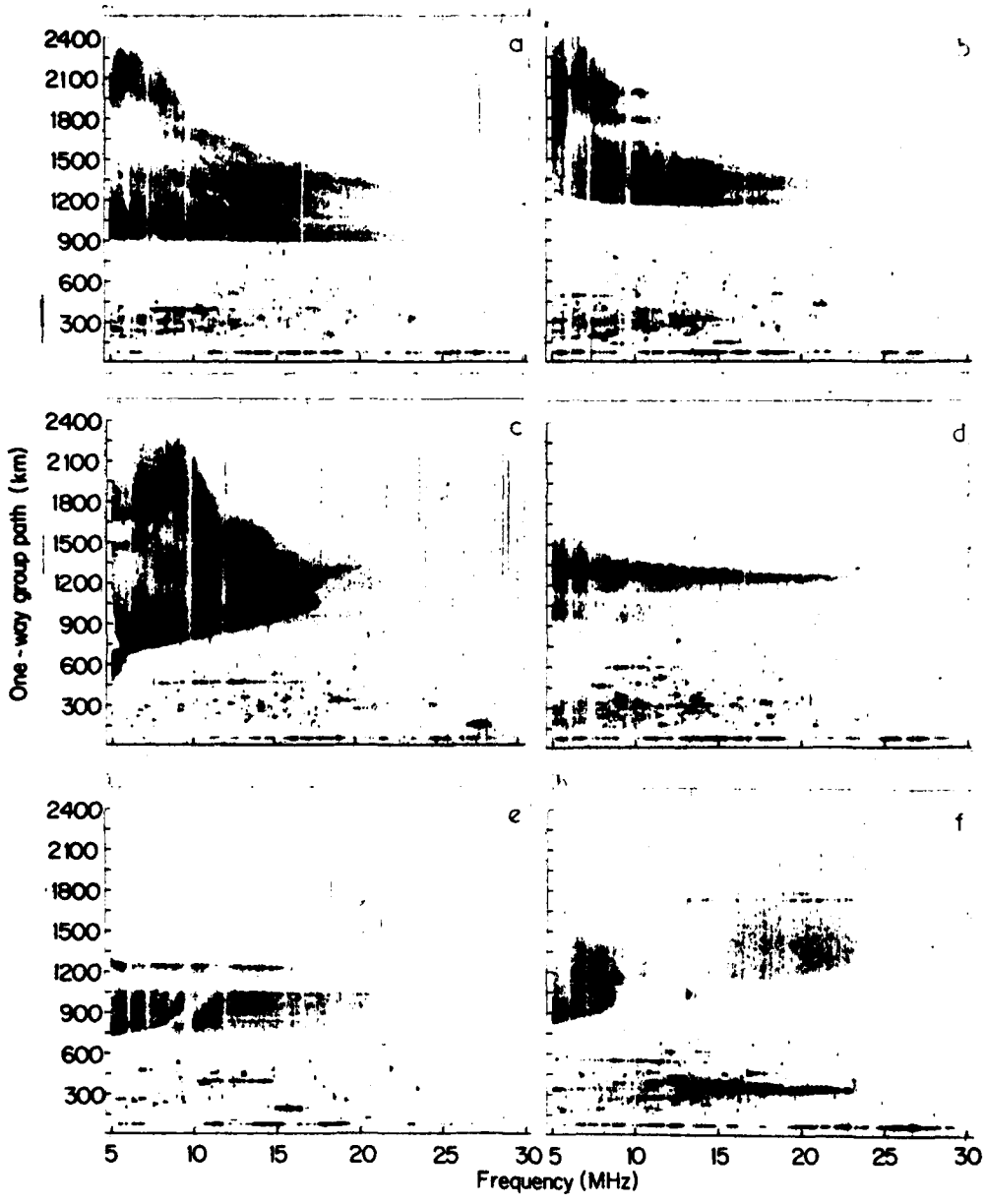


Figure 5 Sample widesweep backscatter ionograms taken in S. England:

(a) Sharp leading edge with no lower-frequency retardation
-N beam, 9 October 1984, 0111 UT.

(b) Sharp leading edge with retardation at lower frequencies
-N beam, 18 September 1984, 2306 UT.

(c) Wedge-shaped trace
-N beam, 20 June 1984, 0013 UT.

(d) Thin auroral trace
-N beam, 30 September 1984, 2359 UT.

(e) Fat auroral trace
-N beam, 25 October 1984, 2047 UT.

(f) Diffuse auroral trace with Es below
-30°W beam, 24 October 1984, 0135 UT.

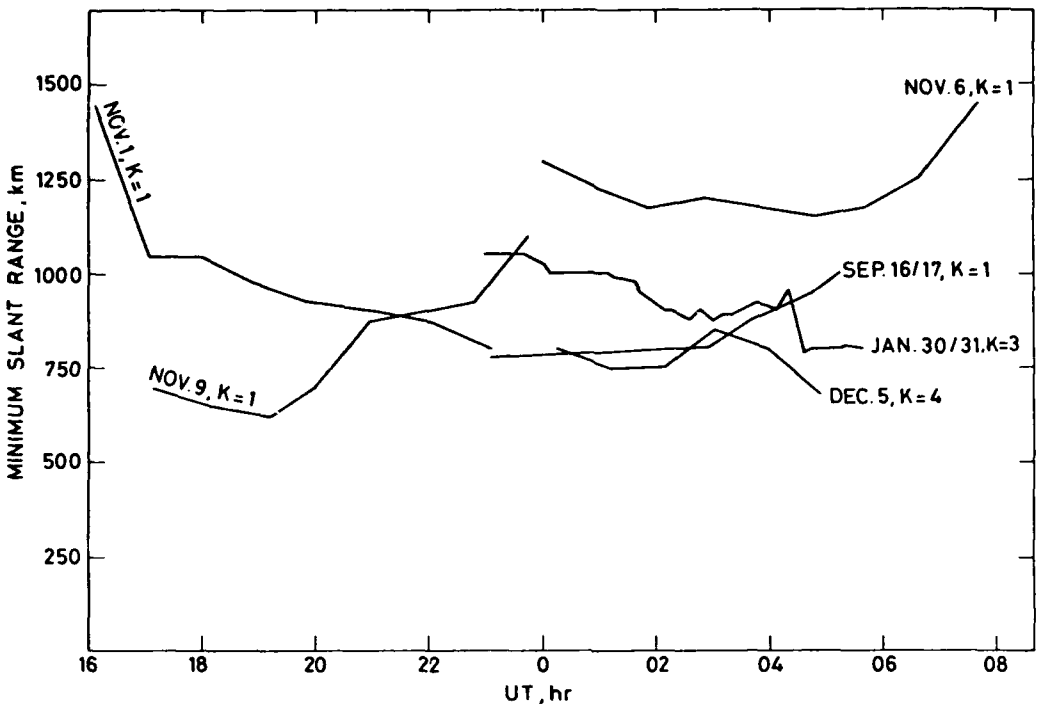


Figure 6 Minimum slant range of direct backscattered returns from the ionosphere. Sample data for different nights labelled with the corresponding values of local K for 00-03 UT.

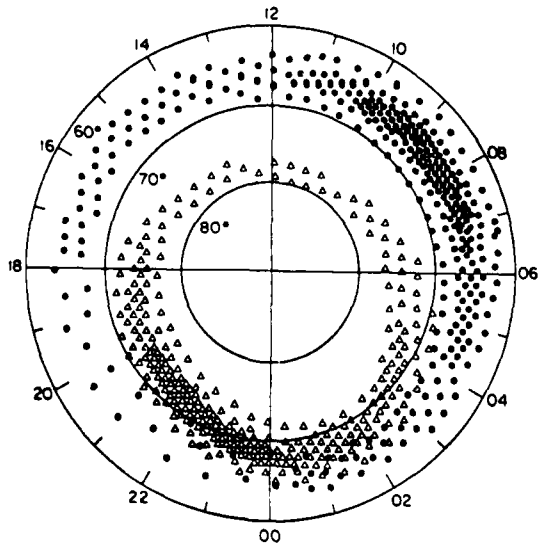


Figure 7

Zones of precipitating particles expressed in corrected geomagnetic latitude and geomagnetic local time (adapted from Hartz and Brice, 1967). Dots relate to the so called 'drizzle' precipitation and triangles to the 'splash' precipitation.

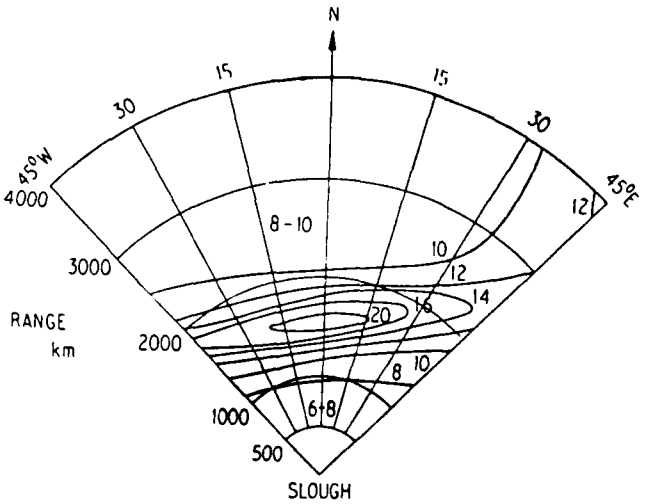


Figure 8 Polarisation-coupling loss in decibels for the ordinary wave between horizontally polarised transmitting and receiving antennas at 10 MHz (from Bradley, 1968).

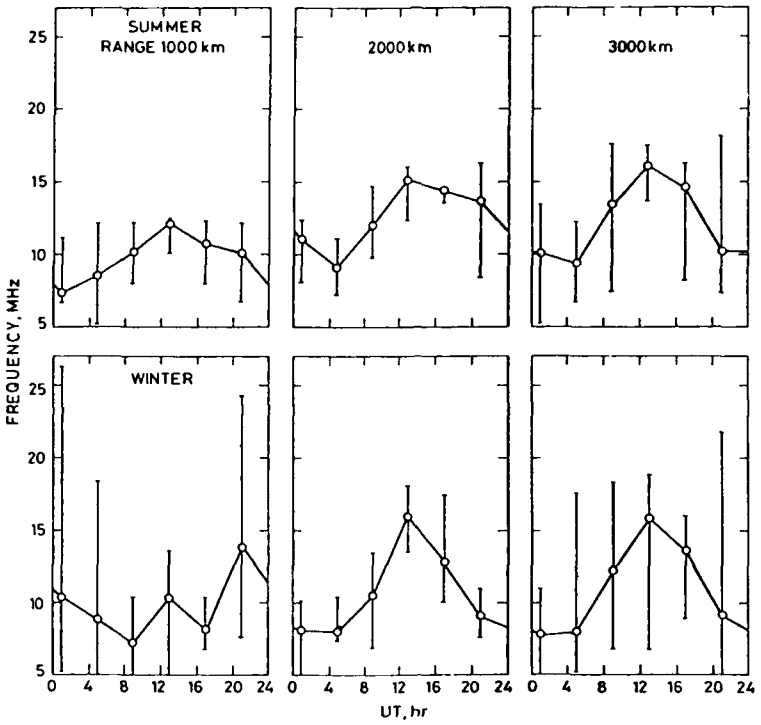


Figure 9 Frequencies giving greatest signal/noise ratio in Summer and Winter for ranges of 1000, 2000, and 3000 Km and 30°W beam-open circles indicate seasonal median values and vertical lines show decile extremes.

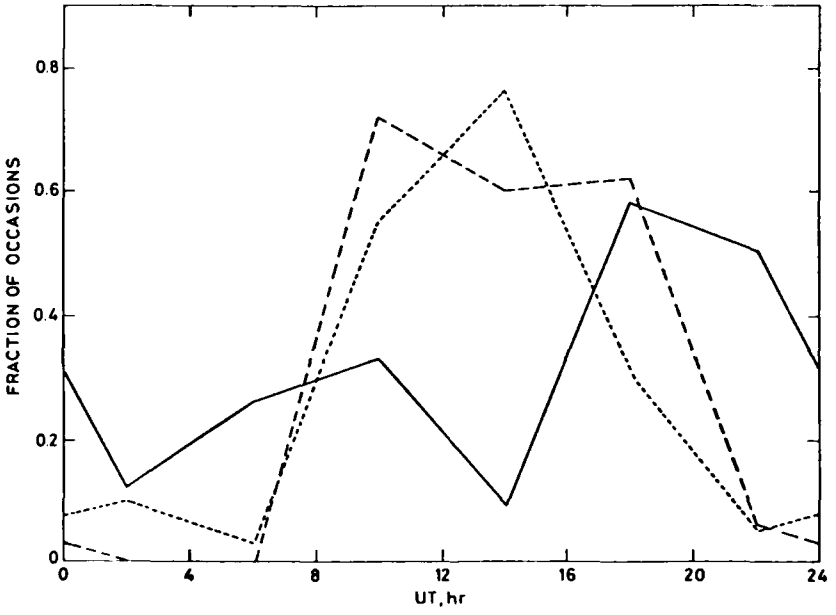


Figure 10 Fraction of occasions that Iceland repeater signals were received _____ Summer
_ _ _ _ _ Autumn
..... Winter

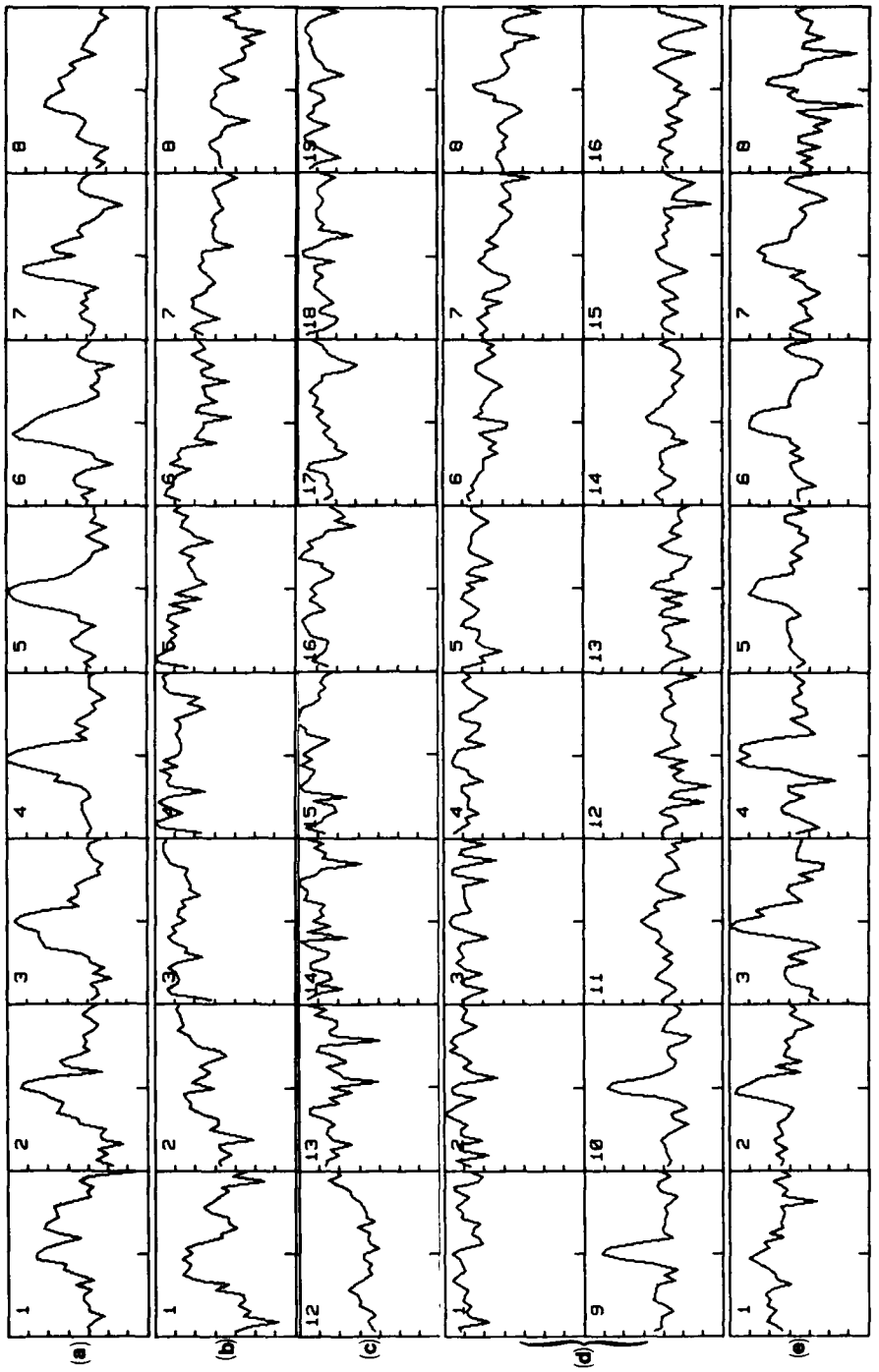


Figure 11 Sample spectra showing broad and narrow features:

(a) 18 September 1984, 2331 UT, N beam, 10.5 MHz, ranges 1125-1650 Km
(b) 30 September 1984, 2327 UT, N beam, 5.0 MHz ranges 1125-1650 Km
(c) 20 June 1984, 0043 UT, N beam, 11.0 MHz, ranges 750-1250 Km
(d) 24 October 1984, 0154 UT, 30°W beam, 11.1 MHz, ranges 1125-2250 Km
(e) 24 October 1984, 0158 UT, 30°W beam, 19.7 MHz, ranges 1125-1650 Km

amplitude scale: 10 dB per division; frequency scale: ± 6.25 Hz.

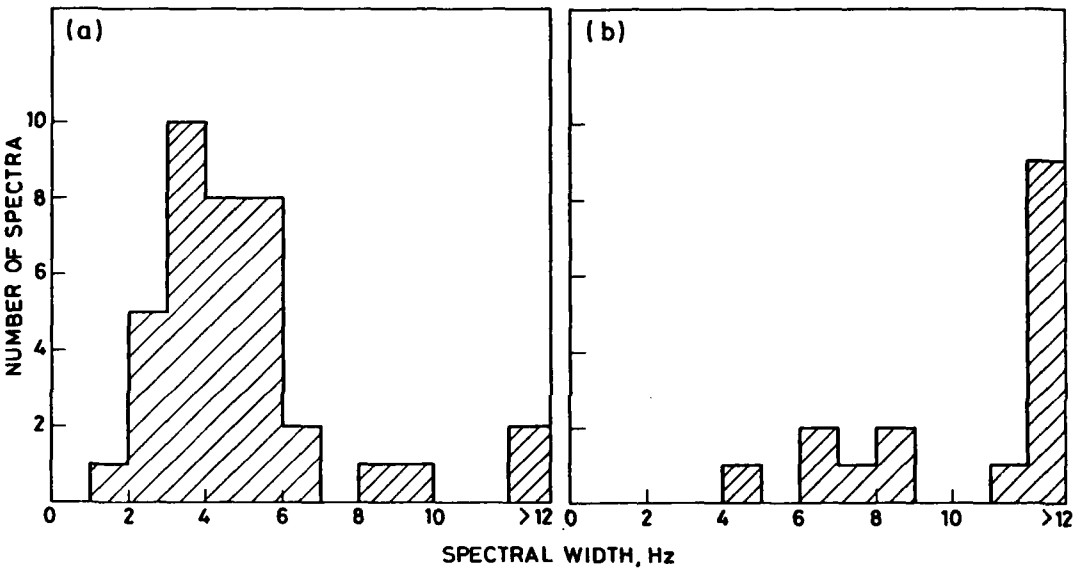


Figure 12 Number of leading edge spectra at different frequencies between 5-20 MHz with spectral widths 25 dB below the peak in 1 Hz bands as indicated:

(a) 18 September 1984, 2325-2335 UT.

(b) 30 September 1984, 2325-2335 UT.

DISCUSSION

R.Greenwald, US

Do you feel that you can explain the ionospheric structure associated with your more complex ionograms from the ionogram information alone? Wouldn't it be an improvement if you also had angle of arrival information?

Author's Reply

To date, we have devoted only limited effort to resolving propagation mechanisms. Useful clues came from examining the diurnal and seasonal morphologies and in making comparisons with conventional propagation predictions. Clearly the availability of other data collected simultaneously, such as up-range vertical incidence ionograms and magnetic activity indices are of great value; present studies are using this information. We are also making comparison with SABRE results. We would certainly welcome having elevation-angle measurements, but the complexity and cost of these, coupled with their achievable accuracy, need to be carefully considered.

T.B.Jones, UK

Comment on statement by Dr R.Greenwald. Measuring the vertical angle of arrival does not necessarily lead to good mode resolution. On oblique paths the angular separation of the modes is often only one or two degrees and is, therefore, very difficult to resolve.

T.A.Croft, US

To some extent our inability to identify the nature of the causes of bizarre backscatter records is due to research and funding conventions and is not due to technical limitations. Most of the computer technology needed to simulate such forms was fully developed 21 years ago. Most of the work that has ever been done was done at that time. What is needed now is a "production line" which starts with a sequence of ionospheric models (i.e. Ne distributions) and yields, for each model, an image of the backscatter record that each model would cause. My main point is that the *technology* and *computer programs* have existed a long time but our systems of research and funding do not result in such activity.

All backscatter form explanations known to me have come from such an approach. The researcher has not set out to explain a particular feature, but rather has formed or modified an Ne model without anticipating the form of the result. Such work has been rewarding when previously puzzling features showed up in the simulated backscatter; once that occurred the phenomenological explanations have always been forthcoming from computation elements.

This "unexplained backscatter" problem is not due to the lack of a technical means for finding explanations. A wide-ranging atlas of simulated backscatter would be of great value. The only creative aspect of making such an atlas is the selection of models; the rest of the task is tedious, and similar to bookkeeping in character.

Spectral characteristics of high frequency waves backscattered by small scale F region irregularities : Evidence of strong sub-auroral ion flow

by
A. Bourdillon
Laboratoire de Physique de l'Exosphère
4 Place Jussieu
75230 Paris Cédex 05
France

Abstract

The spectra of H.F waves backscattered at night by small scale (10-20 m) sub-auroral F region irregularities often exhibit large doppler shifts and widths in the local time sector 2000-2400. After local midnight the doppler shifts and the widths of the spectra decrease rapidly. We present examples of experimental data, obtained with the two coherent backscatter radars of the EDIA experiment, showing the spectral characteristics just mentionned. From the doppler shift measured at the two sites we deduced the perpendicular velocity of the irregularities, which can reach values as high as 2000 m/s. These observations are interpreted using results of theoretical models which predict strong sub-auroral ion flow in the trough region

Introduction

Irregularities with scales ranging from hundred of kilometers down to tens of meters are a common feature of the high latitude ionosphere. Large scale ($\lambda > 10$ km) and intermediate scale structures ($0.1 < \lambda < 10$ km) have mainly been studied by satellite measurements [Dyson et al., 1974; Clark and Raitt, 1976; Phelps and Sagalyn, 1976], scintillations measurements [Aarons et al, 1969 ; Aarons and Allen, 1971; Aarons, 1973; Basu, 1978; Rino and Matthews, 1980; Fremouw and Lansinger, 1981; Livingston et al., 1982] and incoherent scatter radars [Vickrey et al., 1980; Kelley et al., 1982]. The density gradients associated with intermediate scale structures can be unstable to small scale irregularities ($\lambda \sim 10$ m) which are detected by HF backscatter radars when the incident wave vector is directed normal to the geomagnetic field. Bates (1960) reported early observations of direct backscatter from the F-region and Bates and Albee (1970) described the aspect sensitivity of the echoes.

Recently, several experiments using HF coherent radars have been set up to study small scale irregularities in the high latitude ionosphere [Hanuise et al., 1981; Baker et al., 1983; Greenwald et al. 1983; Greenwald et al., 1985]. Bourdillon et al. (1982) reported first results of a bistatic system (EDIA* experiment) which consists of two coherent radars located in middle latitudes, an experiment mainly concerned with the study of sub-auroral F region irregularities. In the pre-midnight sector the spectra of HF waves backscattered by sub-auroral irregularities often exhibit large doppler shifts and widths in regions of a few degrees in latitudinal extent. The systematic azimuthal dependence of the observed doppler shifts suggests a cosine type projection of the velocity of the irregularities along the radar line of sight. A bistatic system thus allows the measurement of the perpendicular velocity of the irregularities.

At least, three components contribute to the doppler shift measured by an HF radar : (a) the motion of the background plasma, (b) the phase velocity of the irregularities with respect to the ambiant plasma, (c) the doppler shift induced by the temporal variations of the electron density along the radio ray path.

Usually, at high latitudes, contribution (a) greatly dominates over contributions (b) and (c) . One can then expect a good agreement between the velocity of F region irregularities and the convection velocity of the plasma. In the polar cap Baker et al. (1983) found an average flow pattern of F-region irregularities consistent with standard convection models.

---

* EDIA is the french acronym for Etude Doppler des Irrégularités Alignées.

In the sub-auroral F-region we observed irregularities with relatively high westward velocities. We expect this westward irregularity flow to be closely linked with the sub-auroral ion flow enhancement (the so-called SAID) detected on board satellites [Smiddy et al., 1977; Maynard et al., 1978; Spiro et al., 1979; Rich et al., 1980; Maynard et al., 1980]. In one case, reported by Smiddy et al. (1977), the poleward electric field at 1500 km was 245 mV/m, which corresponds to a westward drift velocity of 9,8 km/s. Satellite observations of such strong events are unfrequent. Our radar measurements show that westward velocities of 1500-2000 m/s are common phenomena, in the sub-auroral ionosphere, during substorms. In the present paper we discuss the characteristics of the spectra of HF waves backscattered by sub-auroral F-region irregularities and we present one example of a relatively strong westward flow observed in the pre-midnight sector on December 16, 1982.

Experimental set up

The EDIA system consists of two pulsed wideband coherent backscatter radars located in southern France. The first radar is located near Valensole (44°N, 6°E) and the second near Bordeaux (45°N, 1°W) At Bordeaux the beam of the antenna is oriented in a fixed direction (6°E). At Valensole a linear phased array can be steered in a sector of ± 48° centered on the direction of the geographic north. The angular separation between the beams near azimuth 0° is 3° which is roughly the 3 dB beamwidth at a frequency of 15 Mhz. During the EDIA experiments seven beams only were used in the sector 0 to 18° West. Geographical coverage of the two radars is depicted in figure 1 and characteristics of the antennas can be found in table I.

Data presentation

Figures 2 and 3 give examples of spectra recorded on Dec 14, 1983, respectively at Valensole and Bordeaux. At Valensole 24 range gates separated by 75 km were spectrally analysed (FFT algorithm with 64 complex points). Each spectrum is the average of 15 spectra. In this mode the transmitted pulse length was 500 μs, corresponding to a radial resolution of 75 km. Acquisition and calculation time for one azimuth is about 50 seconds. Every 5 minutes the Valensole's radar performed a fast azimuthal scan, with a transmitted pulse length of 100 μs, to measure the backscattered power with a 20 km radial resolution. The integration time used was 0,4 second. To take into account the longer calculation time at Bordeaux, because of the reduced computing facilities at this site, one cycle of analysis was completed every 15 minutes. At Bordeaux 15 range gates separated by 75 km were spectrally analysed (fig.3) and each spectrum is the average of 4 spectra. The data plotted in figures 2 and 3 were recorded between 2215 and 2230 UT. For comparison purpose, figure 4 shows the spectra recorded two hours later (0015-0030 UT) at Valensole. An increase of the doppler shifts and widths is observed in figure 2 from gate n°1 (group path GP = 1000 km) to gate n°8 (GP = 1525 km). Beyond gate n°8 the doppler shifts and widths of the spectra decrease somewhat. Several spectra are structured with two ore more peaks. A typical example of a double peaked spectrum is observed in gate n°12 in azimuth 18°W. In this case it is clear that the double peak is due to the spatial variations of the doppler shift within the resolution cell. Such a structure could probably be resolved using narrower antenna beams and shorter transmitted pulses.

An important point evidenced by figure 2 is that the positive doppler shifts oberved in azimuth 0° decrease and become more and more negative in the westernmost azimuths. The variations of the doppler shifts with azimuth are in agreement with the positive shifts usually observed at the same time at Bordeaux in azimuth 6°E (Fig.3). On noisy spectra the peaks centered at zero doppler shift are of instrumental origin and they must be discarded. Similar variations of the doppler shifts, but of weaker amplitudes, were observed at Valensole two hours later (Fig.4).

The backscattered power recorded in azimuth 15°W on Dec 12-13 and 14-15, 1983 is plotted respectively in figures 5 and 6. These plots demonstrate the variability of the backscattering regions observed at one day interval. During the night Dec 13-14, 1983 scattering regions were also detected but with a very low signal-to-noise ratio and they are not presented here.

The mean doppler shifts and widths, computed in each of the resolution cells, are plotted in figures 7a and 7b, respectively in azimuths 0° and 15°W. In the pre-midnight sector one finds again the negative doppler shifts in azimuth 15°W and the positive doppler shifts in azimuth 0°. Figures 7a and 7b

also show the correlation between the width (lower panel) and the doppler shift (upper panel) of the spectra. The computation of the mean doppler shifts and widths works well for high signal-to-noise ratio and without interfering signals so it is mainly used as a quick look on the data. To construct a velocity map with the maximum number of points, a visual inspection of the spectra is needed, which is a rather tedious task. A velocity map obtained by combining the doppler shifts measured at Valensole and Bordeaux on Dec 16-17, 1982 is presented in figure 8. The velocity maps of the previously presented data are not yet available but the map in figure 8 shows the general characteristics of the irregularity flow in the sub-auroral F region. In constructing this map the components of the velocity were projected in a geomagnetic coordinate system and strict perpendicularity between the incident wave vector and the geomagnetic field was assumed. We are then only concerned with the perpendicular component of the flow. To reduce the effects of spatial variations of the velocity, the doppler shifts measured at Valensole and Bordeaux were only combined when the local time difference of the center of the corresponding range cells was smaller than 10 minutes. A strong westward flow ($V \gtrsim$ 2000 m/s) is observed near 60° (geographic latitude) between 2230-2330 LT. It decreases rapidly after local midnight to form a southeastward flow near 02 LT with a westward return flow at lower latitudes. Figure 9 shows the westward component of the velocity for five values of the geographic latitude (the experimental values were interpolated using a cubic spline). The upper panel shows the H component of the magnetic field recorded at Tromsö for the same period. The increase of the westward velocity is clearly correlated with the onset of a substorm.

Discussion

As described above the EDIA radar data indicate that the westward velocity of small scale sub-auroral F region irregularities can reach values as large as 2000 m/s. Considering the geometrical configuration of the experiment such high velocities involve aliasing of the spectra when the azimuth of observation moves somewhat aside of the direction of the geomagnetic north. This is schematically depicted in figure 10-a. Part of the broadening of the spectra can be attributed to the finite antenna beamwidth (Fig 10-b). The experimental values of the spectral width can be larger or smaller than the theoretical width deduced from geometrical considerations alone. In the former situation it is expected that turbulence within the scattering volume widens the spectra. The latter situation can probably be attributed to an inhomogeneous cross-section in the scattering volume. We sometimes detected strong scattering regions with no characteristic peaks appearing in the spectra. These events are most likely linked with very strong velocities producing broad spectra which look like white noise spectra because of the aliasing effect. To measure the very strong velocities it would be more suitable to transmit a multipulse sequence [Greenwald, et al., 1983] rather than the single pulse we used until now. At time of strong doppler shifts the operator can change the pulse repetition frequency but the ambiguity in range can then become another problem.

The event reported here presents the following characteristics :

- a strong westward flow in the pre-midnight sector. The corresponding northward electric field value would be about 90 mV/m.
- an intensification of the velocity associated with substorm activity.
- the event is restricted to a narrow latitudinal region.
- the duration of the event is somewhat less than 2 hours.

These characteristics are in agreement with localized westward plasma flow velocities in the sub-auroral ionosphere as reported for instance by Rich et al. (1980). Baker et al. (1983) consider that theory of the measurements performed by coherent radars is "still in need of refinement". Our results seem to be in favor of the possibility to use HF radars to study the convection velocity of the plasma. More theoretical and experimental efforts are nevertheless necessary to get a clear understanding of this point.

Southwood and Wolf (1978) provided a simple model to explain the formation of large sub-auroral electric fields. In their model a northward electric field is generated when ring current ions penetrate to a lower L shell than the plasma sheet electrons. The magnitude of the field is inversely related to the separation of the two boundaries. Large sub-auroral electric fields also appeared in computer simulations [Harel et al., 1981]. However, experimental measurements of high electric field inside the plasmasphere contradict the simple model of Southwood and Wolf (1978) and the simulations of Harel et

al. (1981) [Maynard et al., 1980]. Using a semi-analytical model, Senior and Blanc (1983) were able to explain the large sub-auroral electric field intensities. In particular they found a meridional electric field amplitude somewhat less than 100 mV/m for a 3 degrees displacement between proton and electron boundaries, which is in good agreement with the event we reported here.

Conclusion

We presented data showing the doppler shifting and broadening of the spectra of HF waves backscattered by sub-auroral F region irregularities.

By combining the doppler shifts measured at two distant sites we were able to construct a map of the perpendicular velocity of the irregularities. This map shows a strong westward flow ($V \gtrsim 2000$ m/s) in the pre-midnight sector during substorm activity.

We interpret this event to be the signature of a SAID (large sub-auroral ion drifts).

References

Aarons, J., A descriptive model of F layer high-latitude irregularities as shown by scintillation observations, J. Geophys. Res., 78, 7441, 1973.

Aarons, J., and R.S. Allen, Scintillation boundary during quiet and disturbed magnetic conditions, J. Geophys. Res., 76, 170, 1971.

Aarons, J., J.P. Mullen, and H.E. Whitney, The scintillation boundary, J. Geophys. Res. 74, 884, 1969.

Baker, K.B., R.A. Greenwald, and R.T. Tsunoda, Very high latitude F region irregularities observed by HF radar backscatter, Geophys. Res. Lett., 10, 904, 1983.

Basu, S., Ogo 6 observations of small-scale irregularity structure associated with subtrough density gradients, J. Geophys. Res., 83, 182, 1978.

Bates, H.F., Direct HF backscatter from the F region, J. Geophys. Res., 65, 1993, 1960.

Bates, H.F., and P.R. Albee, Aspect sensitivity of F layer HF backscatter echoes, J. Geopys. Res., 75, 165, 1970.

Bourdillon, A., M. Nicollet, and J. Parent, Velocity characteristics of F region irregularities at sub-auroral latitudes, Geophys. Res. Lett., 9, 696, 1982.

Clark, D.H., and W.J. Raitt, The global morphology of irregularities in the topside ionosphere as measured by the total ion current probe on ESRO-4, Planet. Space Sci., 24, 873, 1976.

Dyson, P.L., J.P. Mc Clure, and W.B. Hanson, In situ measurements of the spectral characteristics of F region ionospheric irregularities, J. Geophys. Res., 79, 1497, 1974.

Fremouw, E.J., and J.M. Lansinger, Dominant configurations of scintillation - producing irregularities in the auroral zone, J. Geophys. Res., 86, 10087, 1981.

Greenwald, R.A., K.B. Baker, R.A. Hutchins, and C. Hanuise, An HF phased-array radar for studying small scale structure in the high-latitude ionosphere, Radio Sci., 20, 63, 1985.

Greenwald, R.A., K.B. Baker, and J.-P. Villain, Initial studies of small-scale F region irregularities at very high latitudes, Radio Sci., 18, 1122, 1983.

Hanuise, C., J.-P. Villain, and M. Crochet, Spectral studies of F region irregularities in the auroral zone, Geophys. Res. Lett., 8, 1083, 1981.

Harel, M., R.A. Wolf, R.W. Spiro, P.H. Reiff, C.-K. Chen, W.J. Burke, F.J. Rich, and M. Smiddy, Quantitative simulation of a magnetospheric substorm, 2. Comparisons with observations, J. Geophys. Res., 86, 2242, 1981.

Kelley, M.C., J.F. Vickrey, C.W. Carlson, and R. Torbert, On the origin and spatial extent of high-latitude F region irregularities, J. Geophys. Res., 87, 4469, 1982.

Livingston, R.C., C.L. Rino, J. Owen, and R.T. Tsunoda, The anisotropy of high latitude nightime F region irregularities, J. Geophys. Res., 87, 10519, 1982.

Maynard, N.C., On large poleward-directed electric fields at sub-auroral latitudes, Geophys. Res. Lett., 5, 617, 1978.

Maynard, N.C., T.L. Aggson, and J.P. Heppner, Magnetospheric observation of large sub-auroral electric fields, Geophys. Res. Lett., 7, 881, 1980.

Phelps, A.D.R., and R.C. Sagalyn, Plasma density irregularities in the high-latitude topside ionosphere, J. Geophys. Res., 81, 515, 1976.

Rich, F.J., W.J. Burke, M.C. Kelley, and M. Smiddy, Observations of field- aligned currents in association with strong convection electric field at subauroral latitudes, J. Geophys. Res., 85, 2335, 1980.

Rino, C.L., and S.J. Matthews, On the morphology of auroral-zone radiowave scintillation, J. Geophys. Res., 85, 4139, 1979.

Senior, C., and M. Blanc, On the control of magnetospheric convection by the spatial distribution of ionospheric conductivities, 89, 261, 1984.

Smiddy, M., M.C. Kelley, W. Burke, F. Rich, R. Sagalyn, B. Shuman, R. Hays, and S. Lai, Intense poleward-directed electric fields near the ionospheric projection of the plasmapause, Geophys. Res. Lett., 4, 543, 1977.

Southwood, D.J., and R.A. Wolf, An assessment of the role of precipitation in magnetospheric convection, J. Geophys. Res., 83, 5227, 1978.

Spiro, R.W., R.A. Heelis, and W.B. Hanson, Rapid subauroral ion drifts observed by Atmospheric Explorer C, Geophys. Res. Lett., 6, 657, 1979.

Vickrey, J.F., C.L. Rino, and T.A. Potemra, Chatanika/TRIAD observations of unstable ionization enhancements in the auroral F region, Geophys. Res. Lett., 7, 789, 1980.

Acknowledgments. We wish to acknowledge the hospitality of the CEA-CESTA authorities. This work was partially supported by CNRS (UA 706).

Table I : Antenna system of the EDIA experiment

Valensole

Transmitting antenna :

Array of 16 broadband elements spaced 8 m apart.
Beamwidth : 6° at 20 Mhz
Azimuthal coverage : ± 53° (13 positions)
VSWR 2 : 1 from 8 to 30 Mhz
Side lobe level : - 13,5 dB
Front to back ratio : ∿ 20 dB
Peak transmitted power : 100 Kw

Receiving antenna :

Broadside Array of 32 whip pairs spaced 11,50 m apart.
Beamwidth : 2° at 20 Mhz
Azimuthal coverage ± 48° (33 positions)
Side lobe level : - 21 dB
Front to back ratio : 10 to 20 dB

Bordeaux

Transmitting - Receiving antenna :

Array of 32 broadband elements spaced 9,5 m apart.
Beamwidth : 2,4° at 20 Mhz
Main lobe bearing : 6° East
VSWR 2 : 1 from 8 to 30 Mhz
Side lobe level : - 13,5 dB
Front to back ratio ∿ 20 dB
Peak transmitted power : 30 Kw

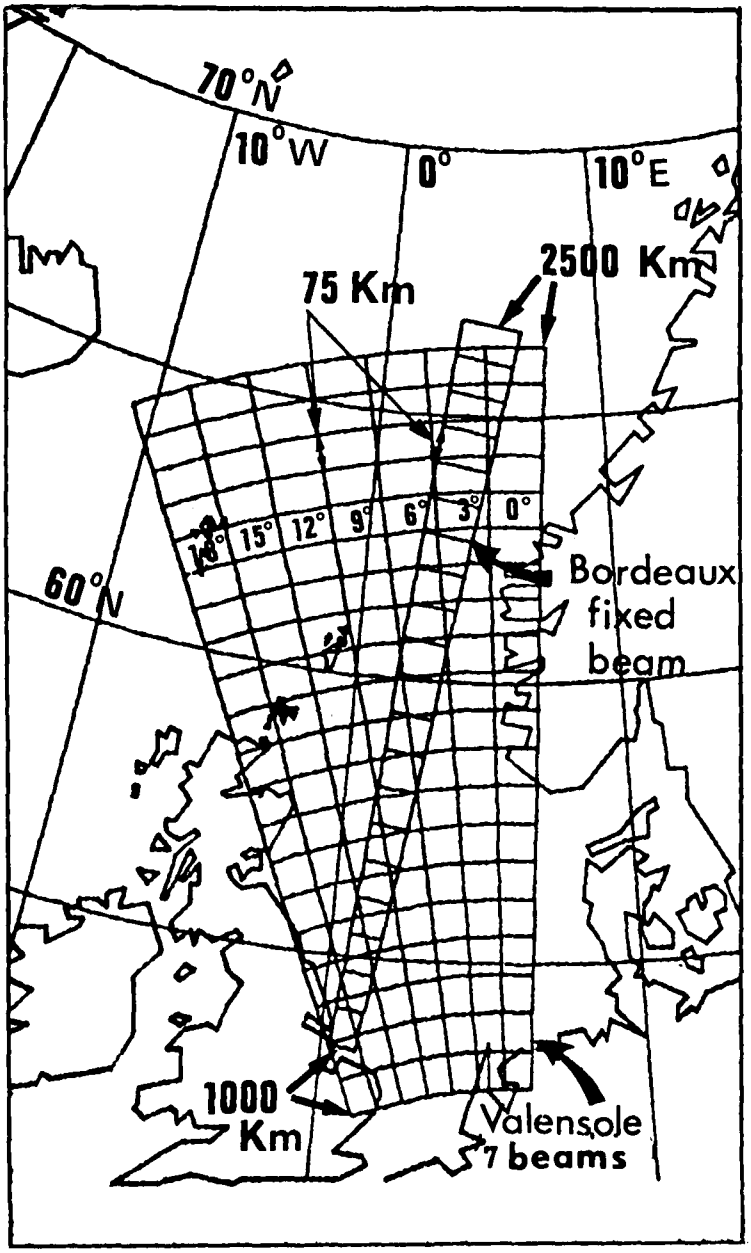


Figure 1. Intercept zone of the beams of Valensole and Bordeaux. The seven beams used at Valensole are indicated. The resolution cells are drawn for a 3 dB beamwidth at a frequency of 15 Mhz and for a transmitted pulse length of 500 μs.

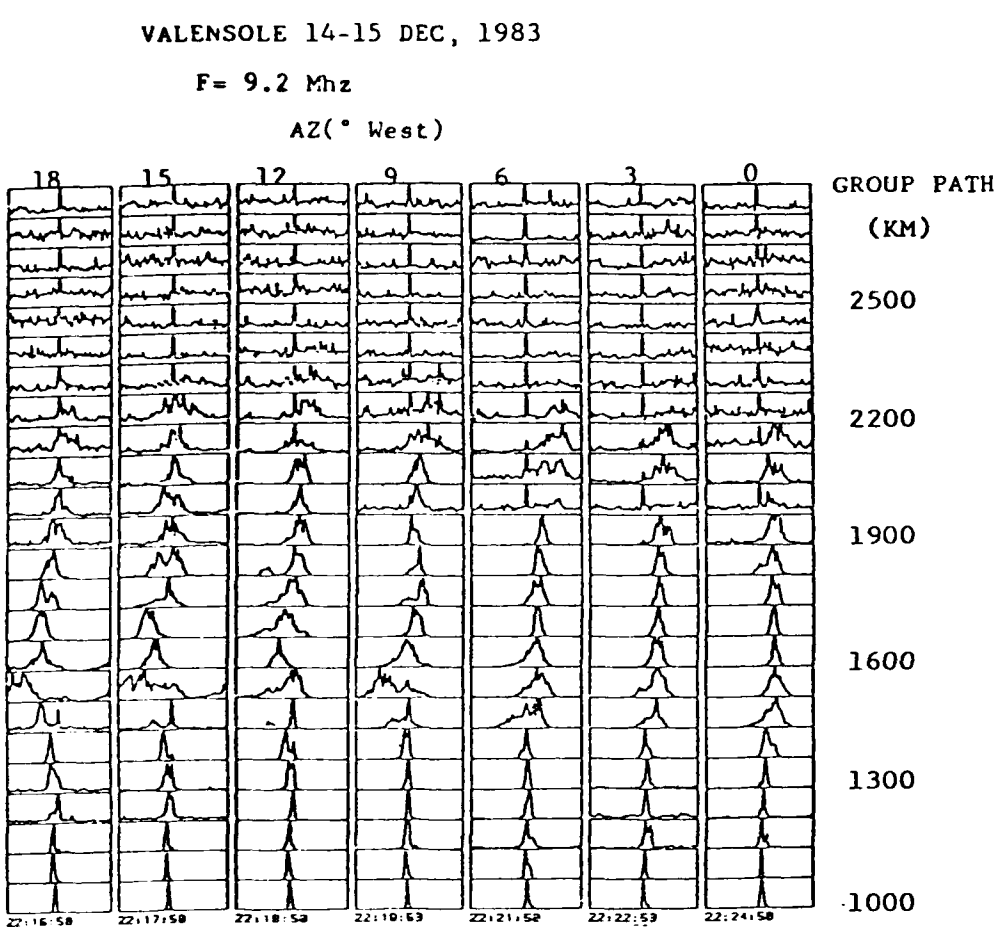


Figure 2. Normalized doppler spectra recorded between 2215-2230 UT on DEC 14-15, 1983 at Valensole. The frequency scale corresponds to $\pm$ 407 m/s. Each spectrum is an average of 15 spectra computed on 64 complex points. The azimuth of the antenna beam varies from 0° (rightmost column) to 18° west (leftmost column).

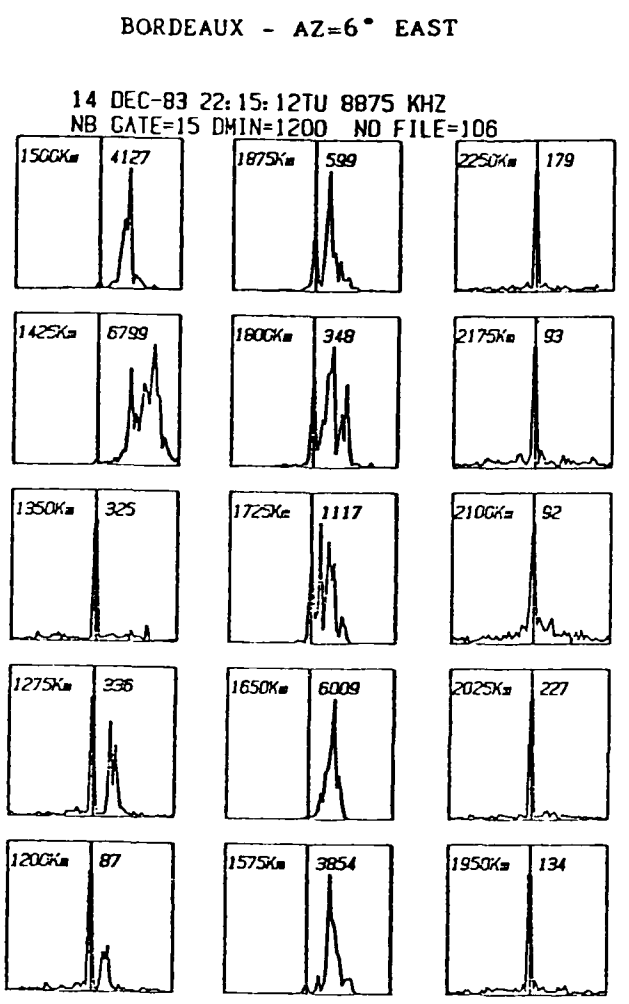


Figure 3. Normalized doppler spectra recorded between 2215-2230 UT on DEC 14-15, 1983 at Bordeaux in the azimuth 6°East. The frequency scale corresponds to $\pm$ 422 m/s. Each spectrum is an average of 4 spectra. Group path (Km) and power are indicated in each panel.

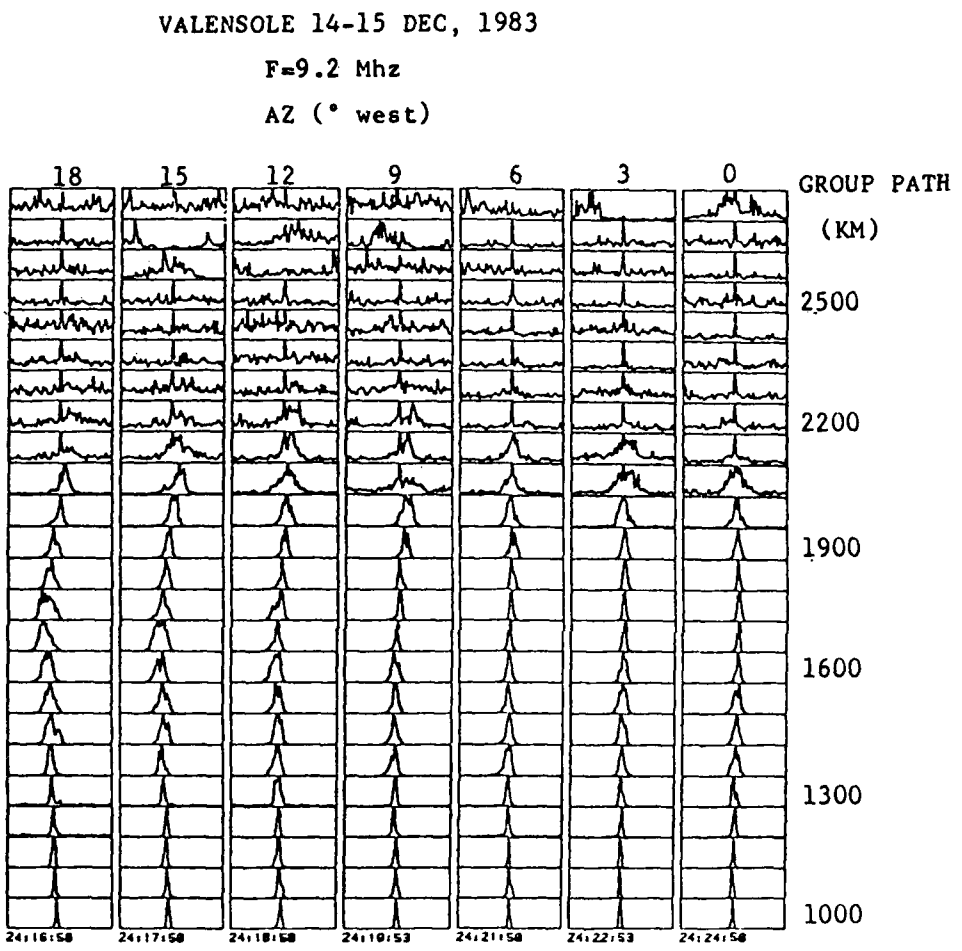


Figure 4. Normalized doppler spectra recorded between 0015-0030 UT on DEC 14-15, 1983 at Valensole. The frequency scale corresponds to $\pm$ 407 m/s. Each spectrum is an average of 15 spectra computed on 64 complex points. The azimuth of the antenna beam varies from 0° (rightmost column) to 18° West (leftmost column).

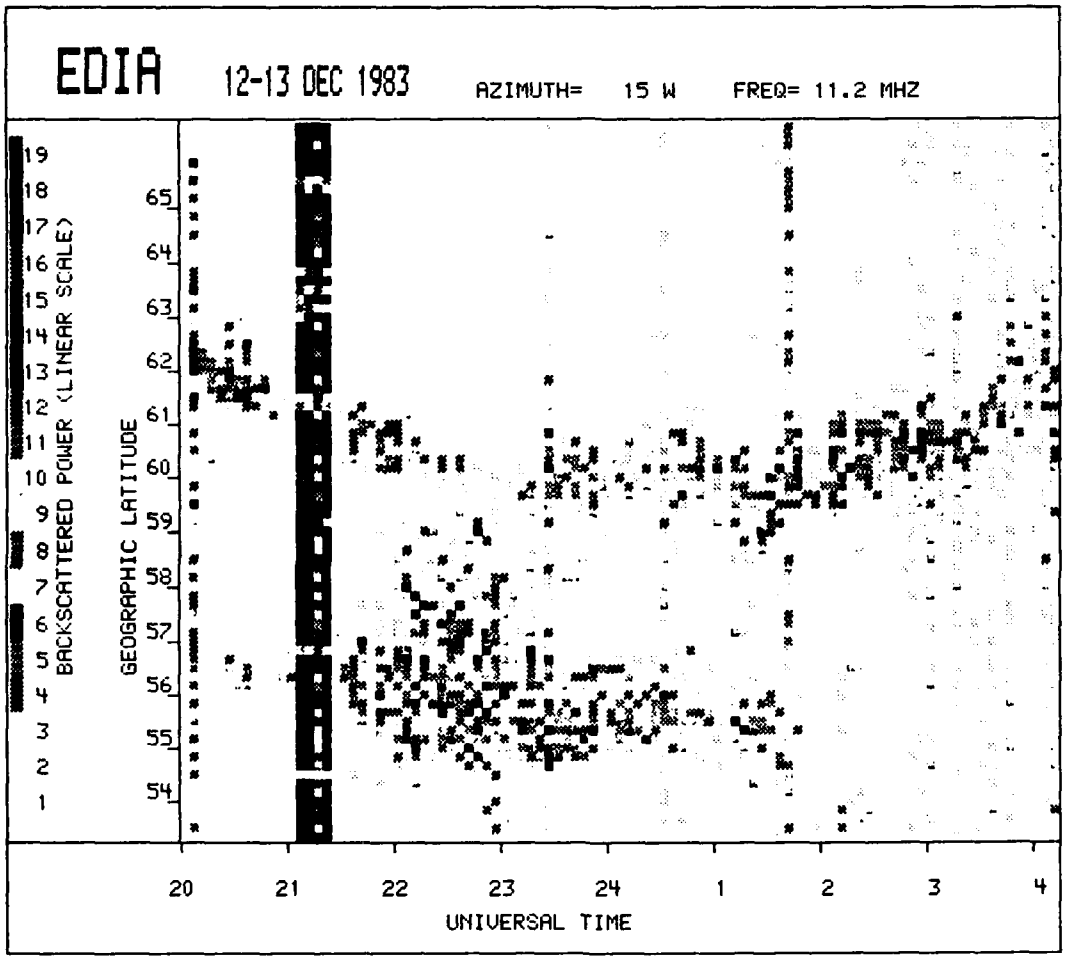


Figure 5. Plot of the backscattered power measured at Valensole on DEC 12-13, 1983 in azimuth 15° West.

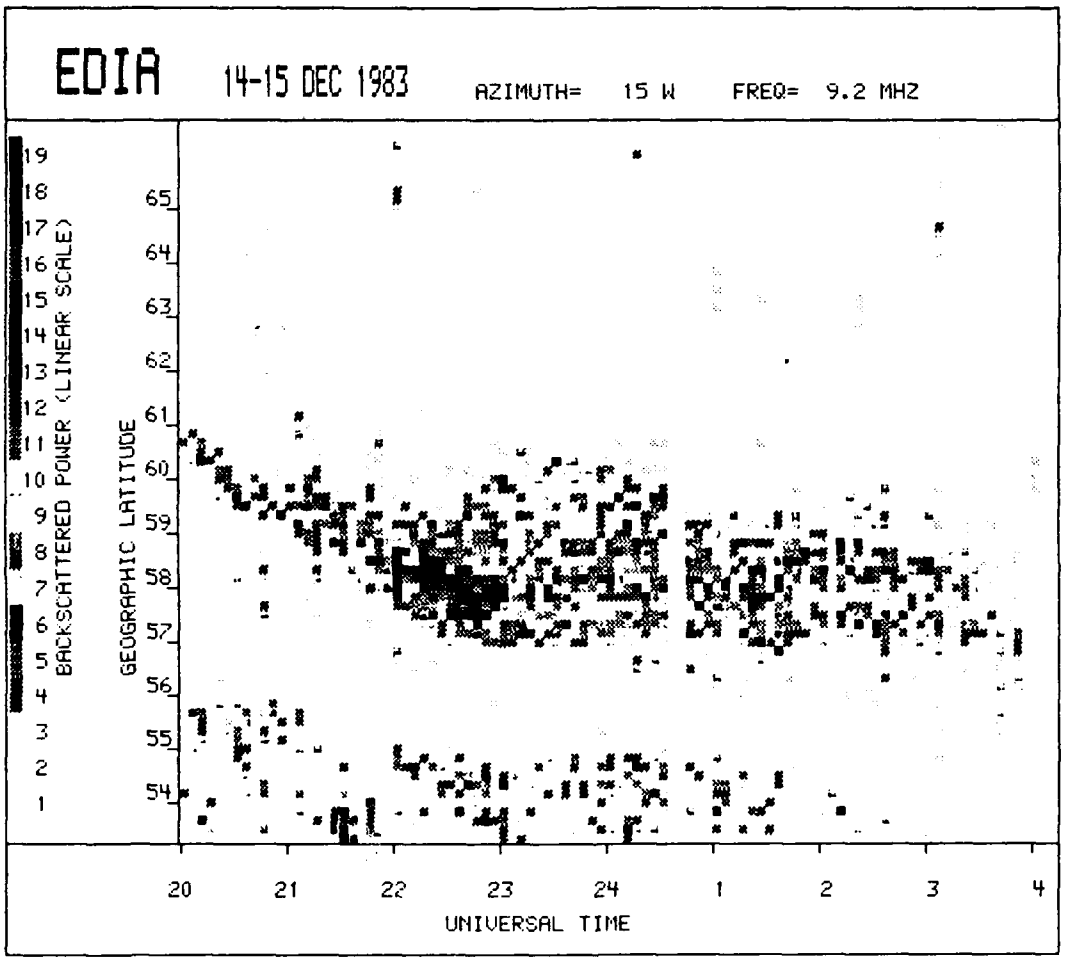


Figure 6. Plot of the backscattered power measured at Valensole on DEC 14-15, 1983, in azimuth 15° West.

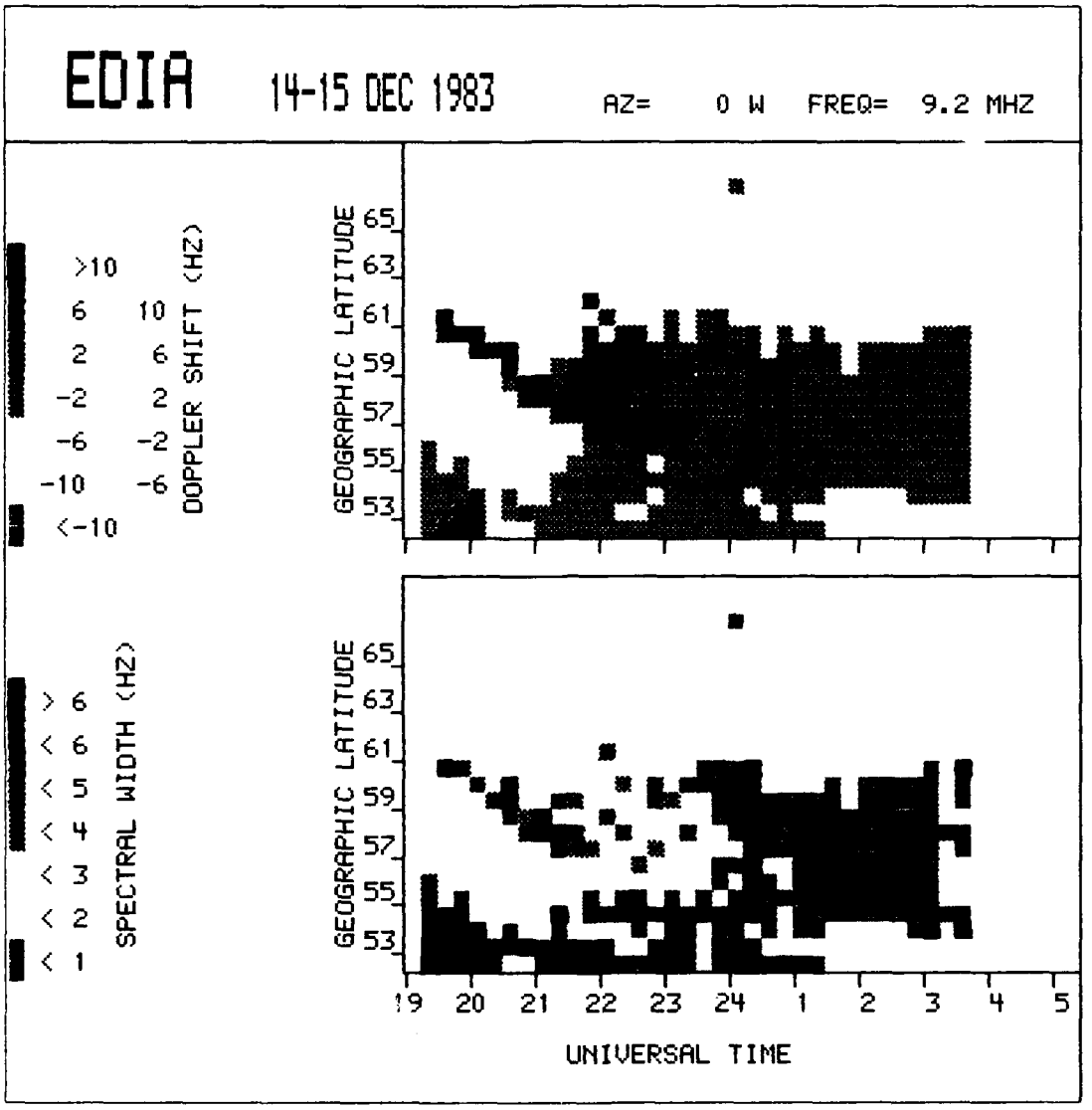


Figure 7a. Doppler shifts (upper panel) and widths (lower panel) of the spectra of sub-auroral F region irregularities for DEC 14-15, 1983 in azimuth 0°. The doppler shifts are mainly positive. The widths of the spectra do not vary significantly with azimuth but they correlate with the magnitude of the doppler shifts.

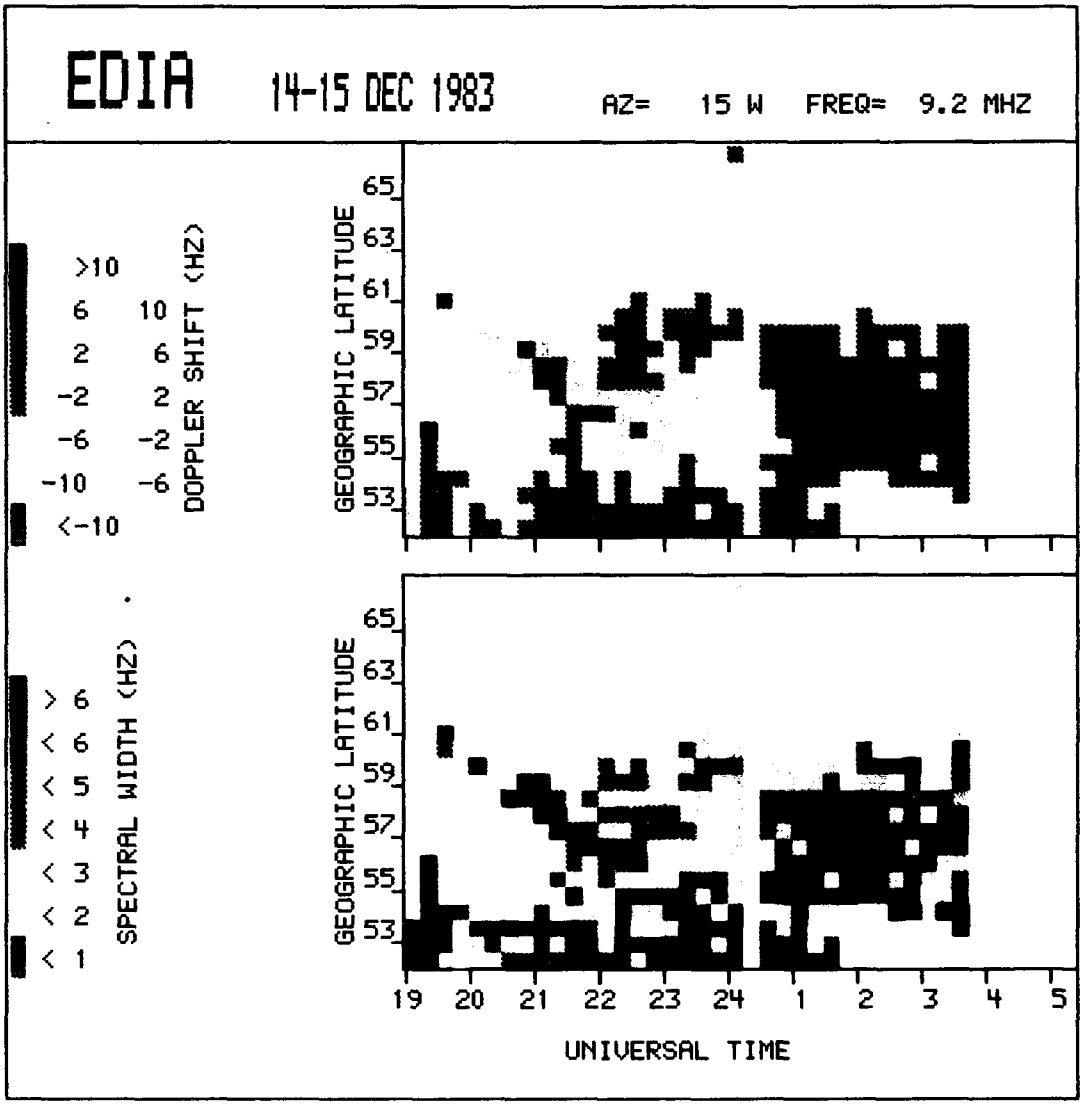


Figure 7b. Doppler shifts (upper panel) and widths (lower panel) of the spectra of sub-auroral F region irregularities for DEC 14-15, 1983 in azimuth 15° West. The doppler shifts are mainly negative.

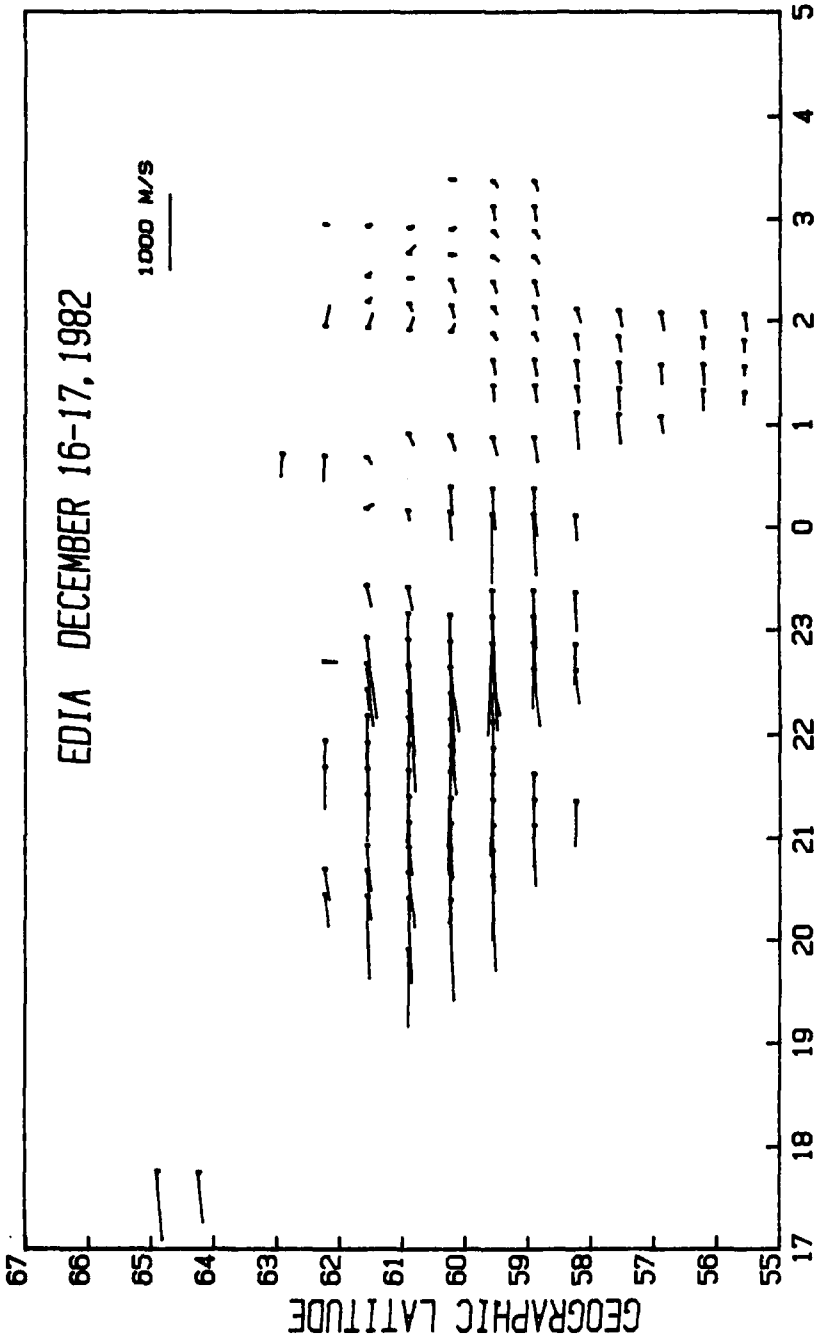
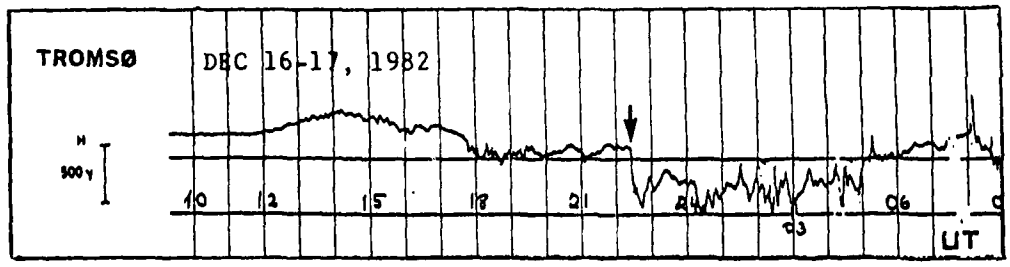


Figure 8. Map of the velocity of F region irregularities, constructed by combining the doppler shifts measured at Valensole and Bordeaux on DEC 16-17, 1982. Westward (southward) velocity is plotted toward the left (bottom) of the figure.



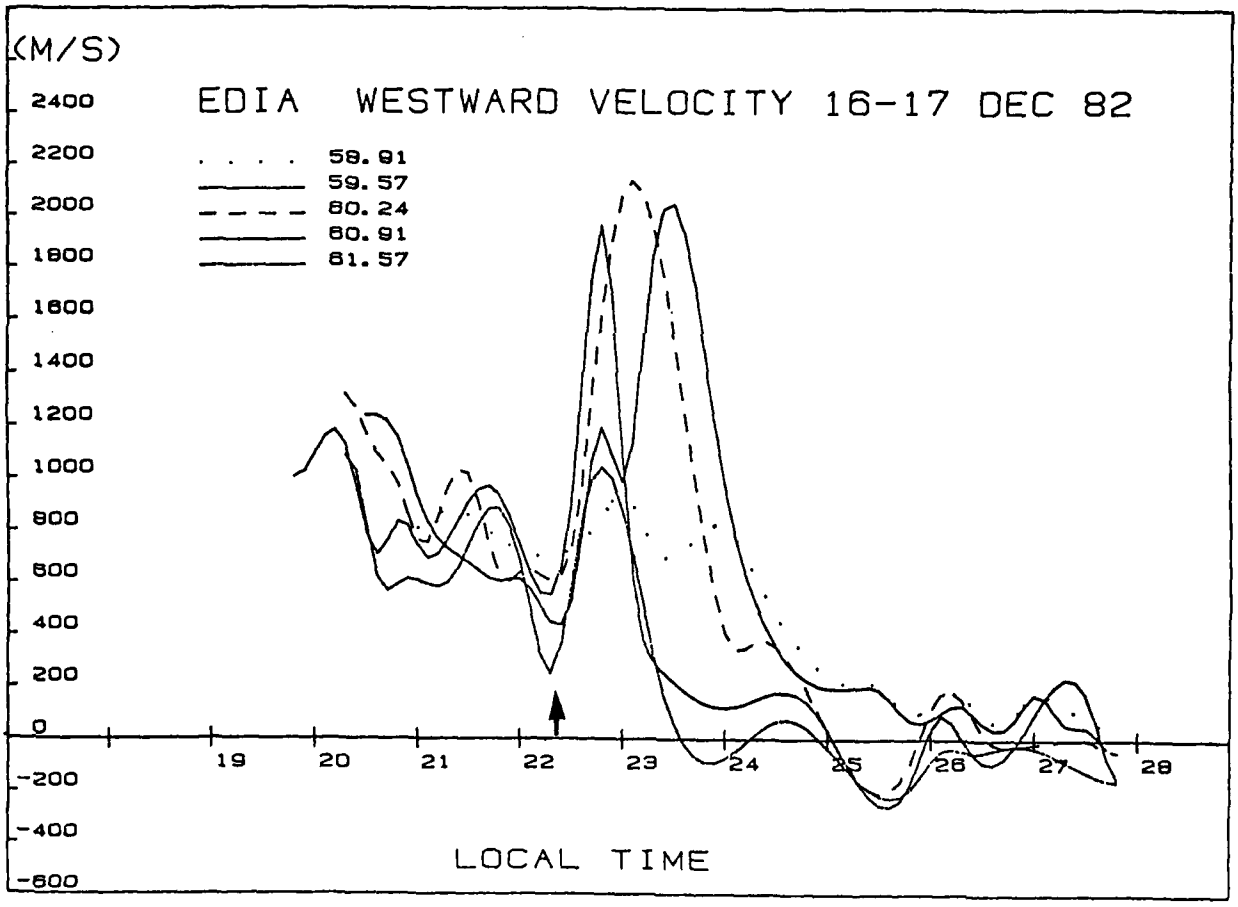


Figure 9. Westward component of the velocity of F region irregularities (lower panel) versus local time (LT≃UT+10 min). The H component of the magnetic field at Tromsö (upper panel) shows onset of a substorm at 2225 UT which correlates with an increase of the westward velocity.

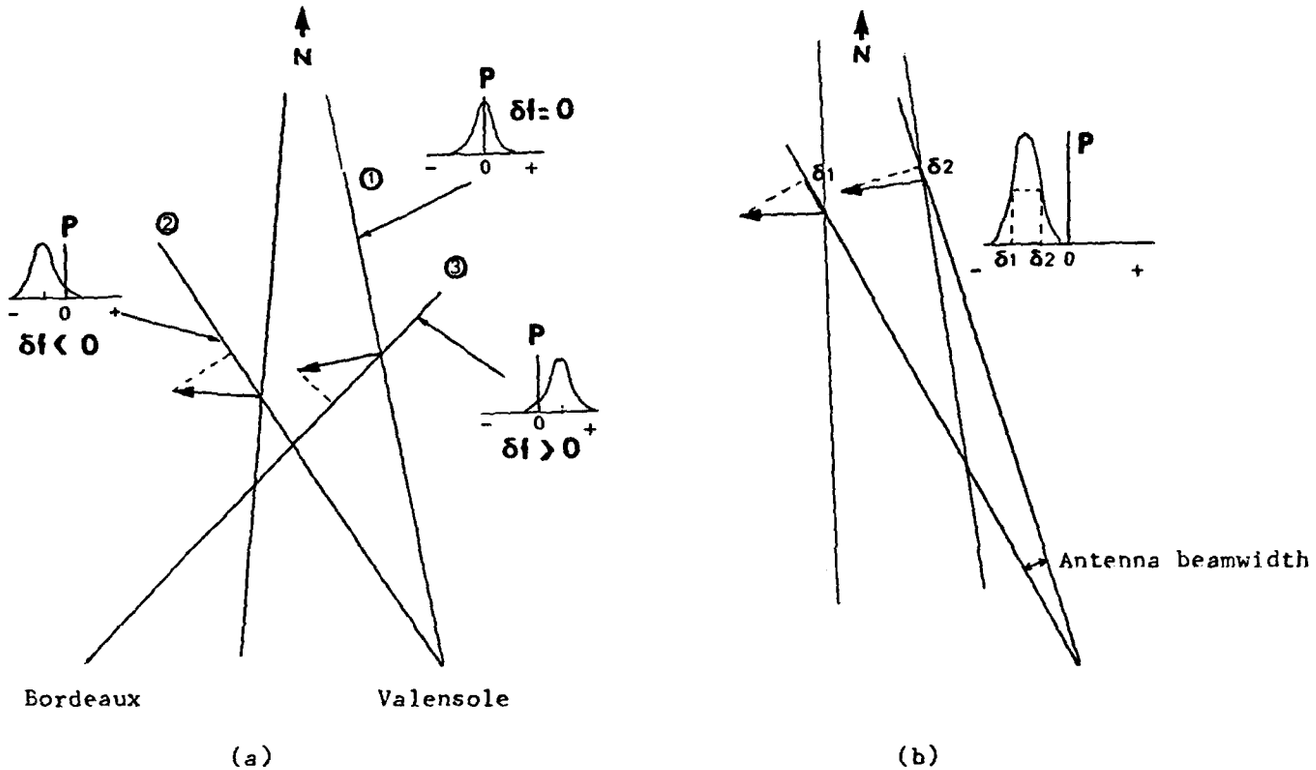


Figure 10. (a) Variations of the doppler shift with azimuth for a westward velocity. (1) Az=0°: zero doppler shift - (2) Westward azimuth: negative doppler shift - (3) Eastward azimuth: positive doppler shift.

(b) Broadening of the spectrum due to finite antenna beamwidth.

DISCUSSION

J.S.Belrose, CA

In describing the geometry of the experiment the authors have made mention of the aspect sensitivity of F-region backscatter. While the ray path does not have to exactly be orthogonal to the earth's field, in our experience the backscatter is confined to region about ±10° off orthogonality.

Author's Reply

Refraction effects at HF permit the ray to achieve orthogonality over a wide range of azimuths including, in the extreme, propagation towards the south. Where backscatter is actually achieved depends not only on orthogonality but also on the existence of irregularities at these locations. This will certainly limit where backscatter is observed and will depend on site location.

B.Reinisch, US

Your last figure showed an increase in plasma velocity from 800 to 1800 m/s at the onset of a magnetic substorm. Did the measurements show a simultaneous change in the direction of the velocity vector?

Author's Reply

There appears to be a small but distinct change in direction of the flow at the time of the increased velocity.

J.Aarons, US

The particular region where the irregularities appear on the radar is a function of the refraction as well as the region where the irregularities exist. That is probably why the Canadian results (where the transmissions are launched at a high latitude) differ from those launched at a lower latitude (Valensole).

Author's Reply

This comment agrees with my answer to the question by J.Belrose.

R.Greenwald, US

The drift velocity observations in December (last viewgraph) are consistent with the general high latitude convection pattern under disturbed conditions. The large enhanced westward velocity may be associated with a further expansion associated with the substorm onset. It may be possible to confirm this hypothesis by looking for enhancements in the eastward electrojet (westward flow) by checking magnetograms from lower latitudes.

Author's Reply

Regions of strong westward velocity are likely linked to a low E-region conductivity. The net effect on magnetograms is then probably weak.

SMALL-SCALE IRREGULARITIES IN THE HIGH-LATITUDE F REGION

C. HANUISE and J.P. VILLAIN
Laboratoire de Sondages Electromagnétiques de l'Environnement Terrestre
CNRS/Université de Toulon, 83100 Toulon,France

C. BEGHIN
Laboratoire de Physique et Chimie de l'Environnement
45045 Orléans la Source, France

G. CAUDAL
Centre de Recherche Physique de l'Environnement
94100 St Maur des Fossés, France

SUMMARY

We report coordinated observations performed at high and very high latitudes in the european sector with the ISOPROBE experiment on board the AUREOL 3 satellite, the EISCAT incoherent scatter radar and the SAFARI HF coherent radar system. The latitudinal profiles of electron density measured by the incoherent scatter radar are used to determine the influence of the propagation of the HF radio wave on the detectability of the irregularities. The presence of HF backscatter echoes is also related to the spectral power of the density variations deduced from in-situ measurements. The physical processes leading to the formation of the fluctuations are studied at several wavelengths from in-situ and radar data. The phase velocity vector constructed from the radial velocities measured by two HF radars are compared to the plasma drift measured with the EISCAT facility under various geophysical conditions. The excellent agreement between the estimates confirms, as predicted theoretically, that the F-region small-scale irregularities are drifting with the bulk plasma. Their motion can therefore be used to derive the two-dimensional flow pattern of plasma convection in the auroral and polar ionosphere.

INTRODUCTION

The last decade has seen a tremendous development of the ionospheric research at high latitudes, related to the primary importance of the auroral and polar regions to understand the global solar wind/magnetosphere/ionosphere system. A large number of new ground-based and in-situ instruments has been successfully put into operation during the period, among them the incoherent scatter radars located in Alaska, Scandinavia and Greenland, and numerous polar-orbiting satellites. Another technique useful in this scope, owing to its most recent improvements, is the HF backscatter from small-scale irregularities located in the F region.

The existence of field-aligned density fluctuations in the high-latitude F region has been known since the late fifties from ground-based observations (Bates, 1959; Weaver, 1965; Hower et al., 1966). Subsequent studies were developed with both in-situ probes and ground-based radars. Observations performed with satellites confirmed the presence of structures ranging from tens of kilometers down to tens of meters (Dyson, 1969; Mc Clure and Hanson, 1973; Sagalyn et al., 1974), while concurrent radar investigations helped to determine the characteristics of the fluctuations at the smaller wavelengths (Bates and Albee, 1970; Baggaley, 1970; Basu et al., 1974; Oksman et al., 1979). These have been relatively few due to the limitations of the HF radars, like the imprecision on the ray path, the poor spatial resolution, or the lack of velocity measurements. It is only in the last few years that new phase-coherent HF radars have been specifically constructed to observe the high-latitude F region irregularities (Hanuise et al., 1981; Greenwald et al., 1983; Hanuise, 1983). Their spatial resolution is much improved over the older systems through the use of large antenna arrays, while sophisticated computer equipment allows to derive the Doppler spectra and associated velocities from the backscattered echoes.

In spite of the numerous observations already mentionned, few papers report on coordinated experiments performed with ground-based and in-situ instruments (Kelley et al., 1980), especially for the short wavelength part of the fluctuation spectrum. Such joint investigations are yet necessary to answer the unresolved questions concerning both the generation of the irregularities and the relation between their motion and the plasma drift. We therefore initiated a study combining the data from three instruments operating in the european sector: the EISCAT incoherent scatter radar, measuring the electron density and plasma drift velocity along a meridian scan, the SAFARI (Scandinavian And French Auroral Radar Investigations) HF coherent backscatter radar, detecting small-scale F-region irregularities, and the Interferometer Self Oscillating Probe (ISOPROBE) on board the AUREOL 3 satellite, measuring the electron density along its trajectory. The aim of our paper is to present the results of these coordinated observations. In a first part, we describe the three instruments, together with the geophysical and experimental conditions encountered during the campaigns. Then, we present and compare the results obtained from each experiment and derive some physical parameters, such as, for example, the minimum fluctuation level required to detect radar echoes. Finally, we draw a coherent picture for the generation and the motion of the irregularities in the light of the theories existing for the high-latitude F region.

DESCRIPTION OF THE EXPERIMENT

The coordinated observations presented hereafter have been performed during three campaigns organized respectively in February 1982, December 1982 and December 1983 with the EISCAT incoherent scatter radar, the SAFARI HF backscatter radar and the AUREOL 3 satellite. The data were not all gathered simultaneously with the three instruments, because of various operational problems. For example, the EISCAT radar did not operate in February and December 1982 as a consequence of its technical difficulties, while the ISOPROBE experiment could not be used significantly during the December 1983 campaign because of inadequate orbit configuration. We have therefore concentrated our study on the processes of irregularity formation during the earlier period, and on the comparison between the motion of these irregularities and the bulk plasma drift during the later one.

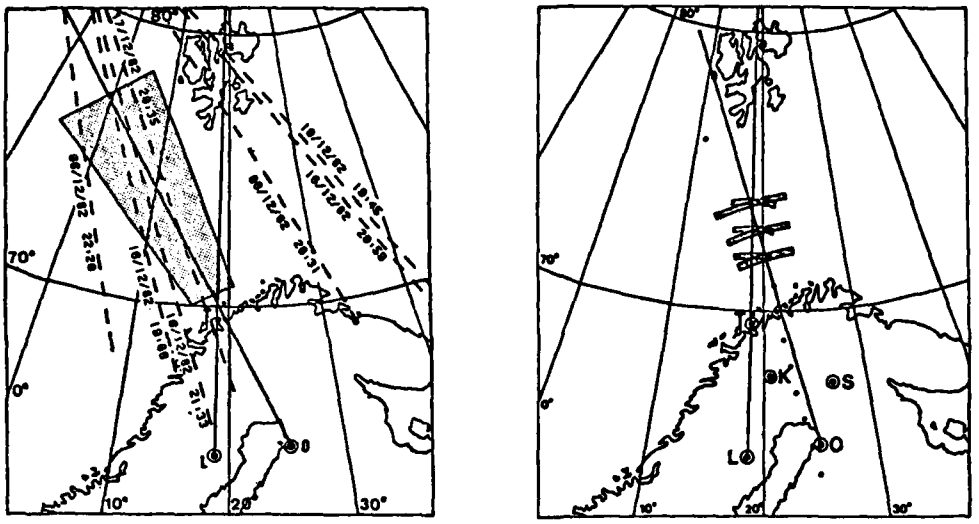


Fig. 1. Geographical configuration, projected onto the horizontal plane over northern Scandinavia, of the SAFARI/ISOPROBE (Fig. 1a), and of the SAFARI/EISCAT (Fig. 1b) experiments. The hatched areas correspond respectively to the beamwidth for the Oulu radar in Fig. 1a and to the radar cells at different distances along the beams in Fig. 1b. The dashed lines are projections on the ground of the satellite orbits, and the dots are the locations of the EISCAT plasma drift measurements in the course of a meridian scan.

The geographical location of the three instruments and the configuration of the experiment are presented in the two panels of Fig. 1. The directions of the two SAFARI radar beams are drawn in a geographic reference frame. In Fig. 1a are also indicated the area in which F-region radar echoes are usually observed from Oulu, together with the horizontal projections of the orbits during which joint data were obtained in December 1982 (Villain et al., 1985a). Four nights of coordinated observations were performed, on December 8, 10, 16 and 17, but only one of the two SAFARI radars, in Oulu, was operating during the first two nights. Fig. 1b shows the configuration of the joint EISCAT-SAFARI experiment performed on 10 December 1983. EISCAT operated in a meridian scan mode with 13 positions for plasma drift measurements, which are plotted as full dots. The two HF radar beams intersected at the northern edge of the scan, where three among the EISCAT positions could be used for comparative studies. The associated HF radar cells are plotted on the figure as shadded areas.

Each of the instruments has already been described in the literature. We shall therefore limit ourselves to a short summary of their typical characteristics during the joint campaigns. The two SAFARI HF coherent radars (Hanuise et al., 1981), located respectively at Lycksele, Sweden, and Oulu, Finland, were transmitting pulses 100 μs long (corresponding to a spatial resolution of 15 km along the beam) at a frequency of 14.4 MHz. They were therefore sensitive to irregularities of 10.4 m wavelength. The pulse rate frequency could be varied by steps from 20 Hz to 1000 Hz. It was changed along similar patterns in both stations in a way to avoid any range or frequency aliasing in the Doppler spectra. The two antenna systems were not identical and their beamwidths were therefore different. The Lycksele array was made of 8 Yagi antennas spaced by 12.5 m, giving a half power width of the order of 10 degrees. In Oulu, the array consisted in only 4 similar Yagi antennas installed 15 m apart, giving a half-power width of approximately 16 degrees. The associated azimuthal resolutions were respectively 170 km and 280 km at a range of 1000 km, which is typical for the observation of F-region irregularities. In Lycksele, the radar beam was fixed towards geographic north, while, in Oulu, its direction could be changed by means of a coaxial phase shifter. At the intersection of the two beams, the phase velocity vector could be computed from the two radial components measured by each radar.

The EISCAT facility (e.g. Baron, 1984) had been programmed to operate in a scanning mode along a magnetic meridian. For each of the positions, the electron density was sampled every 27 km along the Tromsö line of sight. The remote stations at Kiruna and Sodankylä were intersecting the beam at a constant altitude of 325 km to measure the ion drift velocity at that altitude. The integration time on each position was comprised between 60 s and 90 s. The pulse length of 360 μs was equivalent to a spatial resolution of 54 km, which could be sensibly reduced through the use of an autocorrelation function. The beam width was 0.6 degree at 3 dB or, correspondingly, the azimuthal resolution was 10 km at a range of 1000 km. The scattering volume probed by EISCAT at each point of its scan was therefore much smaller than the corresponding cell of the HF radar.

The ISOPROBE experiment (Beghin et al., 1982), carried by the AUREOL 3 satellite launched in September 1981, makes use of the mutual impedance probing technique originally proposed by Storey et al. (1969) to measure the characteristics of thermal electrons. Two identical, but oppositely directed, mutual impedance probes are used to excite the natural frequencies and thermal waves in the surrounding plasma. They measure the upper-hybrid frequency with a precision of the order of 1.5 KHz and a spatial resolution of the order of 10 m. Irregularities with wavelengths of the same order of magnitude are then detected by ISOPROBE and the HF radars. Power spectra are computed for successive segments corresponding to 1.2 s of data, or 10 km along the satellite trajectory. After removing from each section the variations with scale sizes of the order of the record length, the resonance frequency is converted into electron density. The data are then transformed into a zero mean time series of values of relative fluctuations $\Delta n_e/n_e$, where n_e is deduced from the trend line, and spectral powers are computed by a Fast Fourier Transform (FFT) technique.

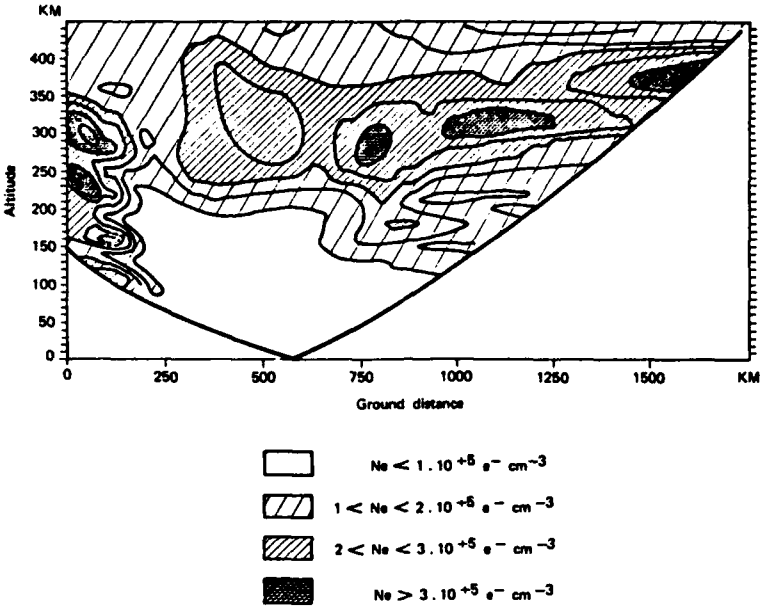


Fig. 2. Projection, on the initial azimuth of the radar beam, of the two-dimensional altitude-latitude map of electron density obtained during an EISCAT meridian scan. The zero location represents the radar station. This particular map has been obtained on 12/10/1983 between 18:00 and 18:30 UT.

GEOGRAPHICAL LOCALIZATION OF THE IRREGULARITIES

The location of the ionospheric volume probed by the satellite or the EISCAT facility is directly known from the geographical position of these instruments, but the problem becomes much more complex in the case of the HF backscatter. Indeed, it is well known (e.g. Hanuise, 1983) that the irregularities present in the high-latitude F region are field-aligned, and can be detected by a ground-based backscatter radar only when its wave vector is nearly perpendicular to the earth's magnetic field. In the auroral and polar ionosphere, the magnetic field is almost vertical, and this geometry cannot be achieved with a line of sight propagation from the transmitter. On the contrary, the rays need to be bent under the effect of the ionospheric refraction, and this condition limits the usable radar frequencies to those below about 20 MHz. The benefit of using an HF radar is nevertheless balanced to some extent by the increased difficulty in determining the exact location of the echoes, especially in the high-latitude ionosphere where vertical, latitudinal and also longitudinal gradients are present in the electron density, and unpredictable.

When electron density data are available from an incoherent scatter facility, one can partly overcome the above limitation by computing the paths of wave propagation in the real ionosphere (Villain et al., 1984). For our study, the two-dimensional maps of latitude-altitude profiles of the density measured by EISCAT during the meridian scans (e.g. Fig. 2) have been used for the ray tracing. The result will be strictly exact only if no spatial or temporal variations occur during the scan, which is

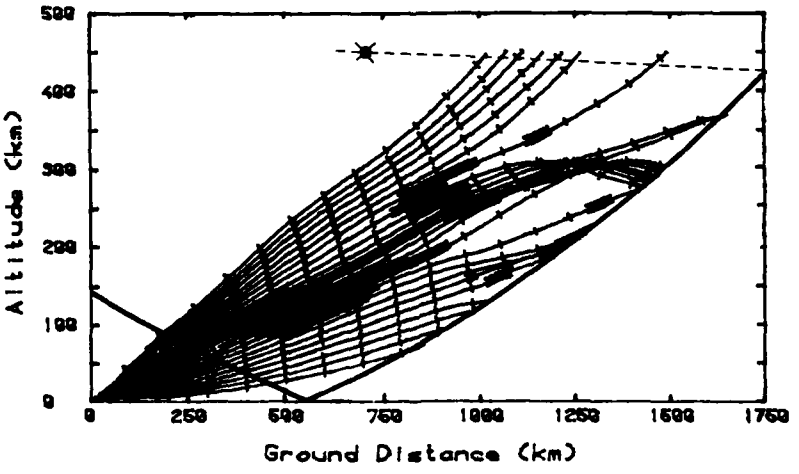


Fig. 3. Ray tracing calculated with the electron density map of Fig. 2. On the ray paths, the dark segments correspond to the region where the electromagnetic wave is within 1 degree of perpendicularity with the earth's magnetic field. The earth is considered as flat, so that staight line propagation appears curved. The angles appear to be distorted because of different scales on the two axes. A typical orbit of the AUREOL 3 satellite is also shown.

certainly not the case at high latitudes for a 30 min. period. Nevertheless, the pattern derived from the ray tracing gives an overall view of the conditions of propagation encountered during a scan. Moreover, it reduces the uncertainty on the echo location, as most of the refraction needed to achieve the perpendicularity condition occurs in the last part of the ray path in the F region. At any point in the scan, we use electron density and backscatter data that are obtained simultaneously. The precision of the ray tracing at this point is therefore much better than the precision which could be expected while considering the ray tracing as a whole.

Fig. 3 presents the propagation derived from the electron density map of Fig. 2 for the HF radar at Oulu, together with an example of AUREOL 3 trajectory. The darker segments indicate that the wave vector is within 1 degree of normal to the earth's magnetic field. Tick marks are plotted on each ray every 100 km in group path. The first group of perpendicularity, between 300 km and 750 km in range, corresponds to E-region altitudes and should be ignored. One observes that the perpendicularity condition is almost continuously satisfied in the F region for group distances ranging from 860 km up to 1400 km. During the first ten minutes of the scan, the Oulu radar observed the presence of backscatter from 900-950 km for the nearest echo up to 1300-1500 km. Thus, a good agreement is found between the distances where the perpendicularity condition, as calculated from EISCAT data, is satisfied, and the distances where radar backscatter is really observed. For the comparative studies, the HF signal is simply analyzed at a distance obtained by the intersection of the magnetic field lines of interest with the rays that are normal to it.

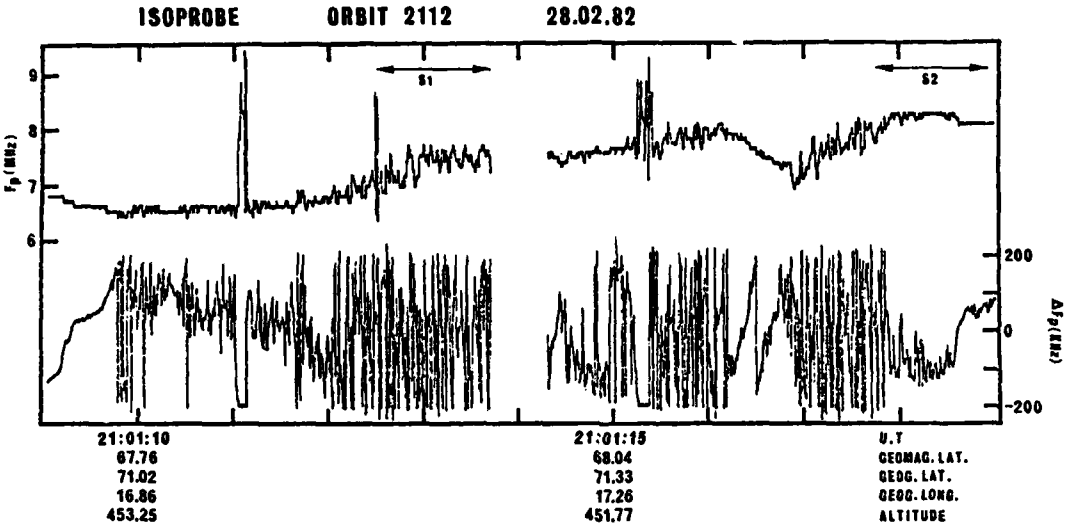


Fig. 4. Electron density data measured by ISOPROBE on 02/28/1982. The upper panel shows the plasma frequency and the lower panel its fluctuations (opposite sign) in a band of 400 KHz around the local mean value quantified by steps of 400 KHz. Note the correlation between the sign of the density gradient and the amplitude of the fluctuations.

ISOPROBE/SAFARI OBSERVATIONS

Coordinated observations between the SAFARI radar and ISOPROBE have been successfully performed during four nights in December 1982, on the occasion of seven passes of the satellite. Four among them, at 20:30 UT on 12/8, at 19:45 UT and 21:33 UT on 12/10, and at 20:59 UT on 12/16, have been analyzed in detail. The three others, showing no electron density variations in the raw data, have been missed out of the study. As a complement, we have also used other data, gathered by the satellite while none of the radars were operating. For example, typical patterns of in-situ data were obtained on 28 February 1982, especially during one orbit at 20:58 UT.

The small number of joint observations is a consequence of the coincidence needed between the orbit parameters and the requirements of the ISOPROBE experiment to perform measurements with a high sensitivity and temporal resolution. Thus, all the observations were performed between 19:00 UT and 22:30 UT, i.e. near local magnetic midnight in the Scandinavian sector. Besides, their altitude varied mostly between 400 km and 450 km, only one of the passes reaching altitudes up to 540 km. Finally, the magnetic activity was very intense for the whole set of data, the Kp index being above 4 and up to 6+.

Fig. 4 shows a typical example of the raw electron density data derived from 10 s of ISOPROBE observations. The variations of the plasma frequency, Fp, which can be easily converted into electron density, are plotted on the upper panel. The lower panel shows the same data, as coming out of the discriminator channel, in a range of 400 KHz around a temporal mean value, which jumps by steps of 400 KHz. Note that this signal represents the density fluctuations in opposite phase. The spikes occuring on the two curves are of instrumental origin and should be neglected. While comparing the two plots, one notices that a clear relationship exists between the presence of the density fluctuations and the sign of the density gradient. When the density decreases, as for example before 21:01:10 UT or between 21:01:16 UT and 21:01:17 UT, the fluctuations are absent from the lower panel. On the contrary, weak variations are present when the gradient is slightly positive, as from 21:01:10 UT to 21:01:12 UT, but the strongest fluctuations appear on the sharpest positive gradients, as from 21:01:12 UT to 21:01:14 UT or from 21:01:17 UT to 21:01:18 UT.

This association between the level of fluctuation and the density gradient led Cerisier et al. (1985) to suggest that the irregularities are generated by the gradient-drift instability (Reid, 1968), eventually extended to include the destabilizing effects of field-aligned currents (Ossakow and Chaturvedi, 1979). From the linear theory, the instability occurs when the convection velocity is parallel to the density gradient. If the velocity and the gradient are antiparallel to each other, the medium remains stable. The electric field, as measured on board the satellite by the VLF experiment

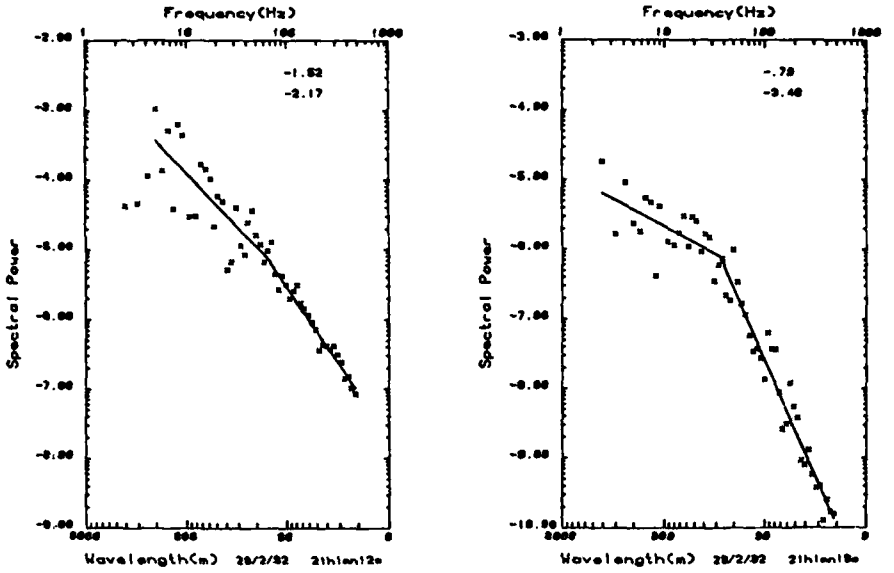


Fig. 5. Power spectra computed from 1.2 s of ISOPROBE data on 02/28/1982, corresponding respectively to positive (Fig. 5a) and negative (Fig. 5b) density gradients. The level of fluctuation is three orders of magnitude larger in the first case, while the spectrum is steeper at small wavelengths in absence of large fluctuations. A break in the spectrum occurs at a few hundred meters in both cases.

(Berthelier et al., 1982), indicates, for this example, that the convection velocity had a component positively directed along the orbit. In agreement with the observations, the linear theory therefore predicts that positive gradients will be unstable to the ExB instability.

The power spectra of the density fluctuations have been computed for two typical samples choosen from Fig. 4. In the process, we transform the frequency spectrum measured in situ by the probe into a wavelength spectrum, simply obtained by dividing the satellite velocity by the frequency. We shall assume that the irregularities are spatial rather than temporal when sampled by the satellite, and, also, that the plasma velocity and the phase velocity of the fluctuations are much less than the probe velocity (e.g. Kelley and Mozer, 1972). The larger scale size for which the spectrum is physically significant is approximately 2 km, since larger wavelengths could be affected by spurious power related to the detrending process. For clarity of the spectra, the power plotted at smaller wavelengths is an average over a number of points calculated in such a way as to keep equidistance between the plotted points for the scale used.

The two power spectra are plotted in Fig. 5 with logarithmic scales on both axes. Each of them has been computed from 1.2 s of data and corresponds to one of the periods indicated as S1 and S2 in the raw data (Fig. 4). The first spectrum (Fig. 5a) has been computed on a positive gradient associated with strong fluctuations, while the other one (Fig. 5b) corresponds to a region of mainly negative or nul gradient with few irregularities present. One firstly notices the variation in spectral power between the

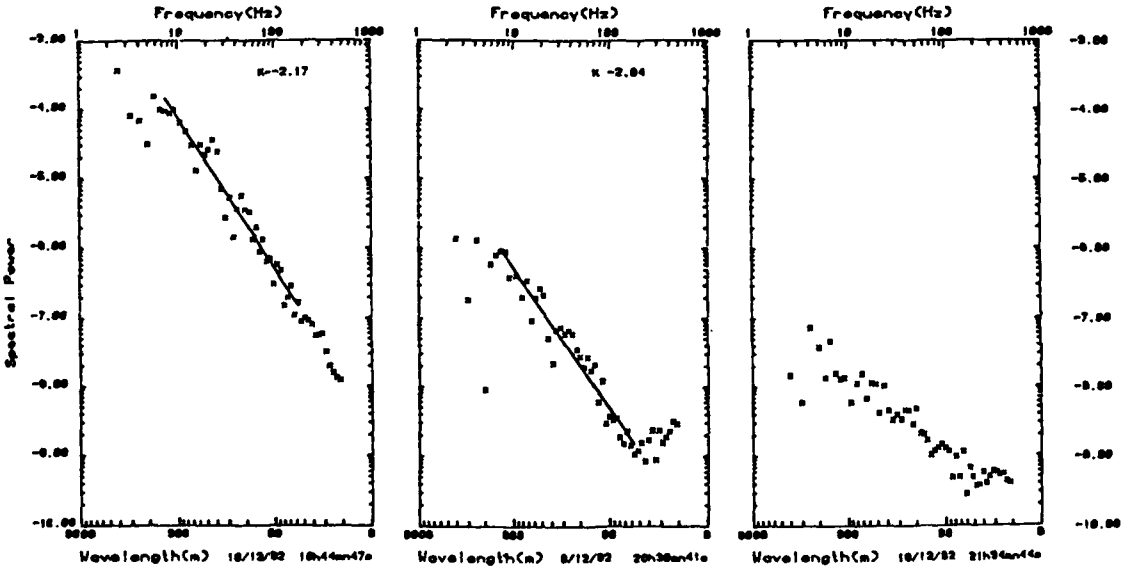


Fig. 6. Variation of the spectral shape with the amplitude of the fluctuations. On 12/10/1982 (Fig. 6a), strong fluctuations were present and the spectral index was -2.17. On 12/08/1982 (Fig. 6b), irregularities have a smaller amplitude. The increase at short wavelengths is an experimental artifact. When the amplitude is very small (Fig. 6c), the spectrum is contaminated by telemetry noise.

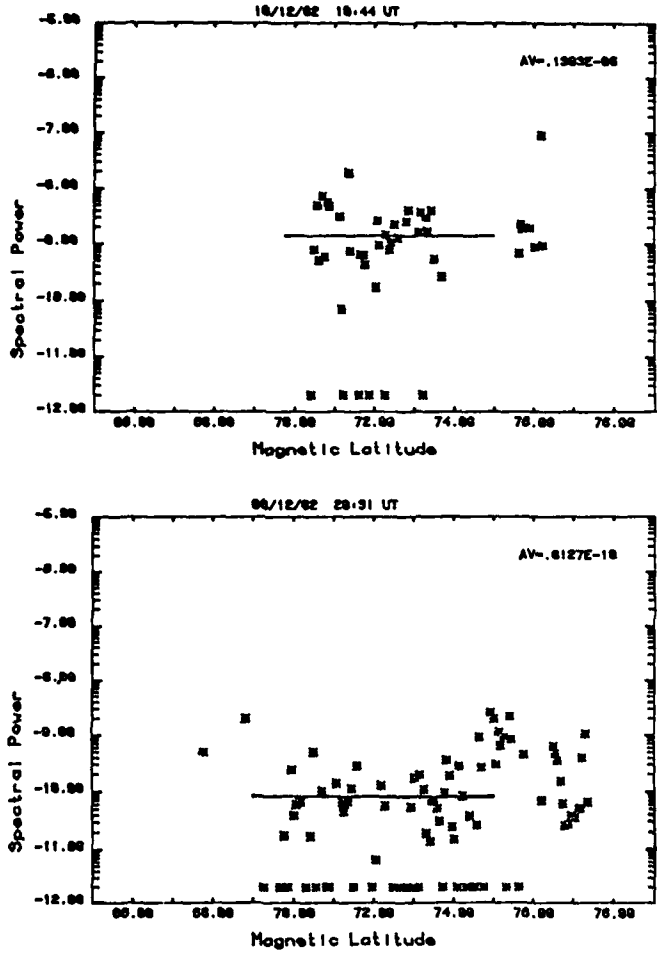


Fig. 7. Spectral power, extrapolated at a wavelength of 10 m, observed along the satellite trajectory for orbits 5874 (Fig. 7a) and 5848 (Fig. 7b). The straight line represents the strip of latitudes over which the spectral power is averaged. Note the ratio of 17 between the fluctuations detected in presence or absence of HF radar echoes. The eliminated data samples are plotted at the bottom of the figure (see text).

two figures. When irregularities are fully developed, the power is three order of magnitude larger at shorter wavelengths, or higher frequencies, and is still about two orders of magnitude larger at longer wavelengths. When we compute the spectral index, we obtain the best fit if we consider two straight lines in the logarithmic scales used in the plot. A break occurs in the spectrum at a wavelength of a few hundred meters, 120 m for S1 and 350 m for S2. It is more obvious in Fig. 5b, as the spectral indices are steeper at shorter wavelengths and shallower at longer wavelengths compared to the spectrum in Fig. 5a. These characteristics are yet not a constant feature in the spectra, but are mostly seen, on about 10% of the cases, when the level of fluctuation is high. This existence of a spectral knee was mentionned in earlier studies (Phelps and Sagalyn, 1976; Kelley and Kintner, 1978), but it occured at longer wavelengths than observed with ISOPROBE.

Other examples of typical spectra, which do not exhibit the spectral knee, are shown in Fig. 6. They correspond to data obtained during the SAFARI-ISOPROBE coordinated observations. Fig. 6a is associated with large disturbances in the electron density profile. The spectrum exhibits a very regular shape from wavelengths of 1 km down to 16 m. The spectral index, calculated between 1 km and 40 m, is equal to 2.17 and is typical of the values between 2.0 and 3.0 found for the well defined spectra. When the level of fluctuation is less important, the slope is more complex. In Fig. 6b, the power is at least two orders of magnitude less than measured in Fig. 6a, but also exhibits an increase at the higher frequencies. This increase is not related to a physical phenomenon, but comes from noise and response of the telemetry system and affects essentially frequencies higher than 200 Hz (i.e. wavelengths below 40 m). The level of this threshold is of the order of a few 10^{-5} $Hz^{-\frac{1}{2}}$ for RMS values of $\Delta n_e/n_e$. When the fluctuation level is extremely small, as in Fig. 6c, the spectral power comes mainly from the telemetry noise. In the most important part of the spectral domain, it is at least four orders of magnitude smaller than in Fig. 6a. Under these conditions, the index computed from these spectra (1.1 for Fig. 6c) is purely artificial and has no physical meaning.

The spectra described in Fig. 6 are among those obtained while small-scale irregularities were detected with SAFARI. It is then possible to compare the irregularity amplitude, derived from the radar observations, with the spectral power measured in-situ at the same wavelength. Though ISOPROBE is not sensitive to the 10-m wavelength fluctuations observed by the radar, it seems reasonable to extrapolate the spectral power calculated for slightly longer wavelengths, namely 16 m to 40 m, down to 10 m with a slope computed from the whole spectrum. The result will, indeed, depend on the value of the slope. For example, a change of 1.0 in the spectral index leads to a change of a factor of 4 in the spectral power

deduced from 40 m down to 16 m. It is therefore necessary to eliminate the data which could introduce spurious effects. Thus, we have deleted wavelengths below 40 m in computing the spectral slope. We have also retained a mere quantitative information when the index was below 1.9, as such a small value could be due to the presence of noise at the higher frequencies.

The spectral power extrapolated to 10 m is plotted in Fig. 7 as a function of magnetic latitude for two orbits of the satellite. Its average value for the strip of latitudes (69° - 75°) in which radar echoes are most likely observed is also indicated. The data eliminated as discussed above are shown at the bottom of the plot, but are not taken into account in the derivation of the average power. The first pass (Fig. 7a) occured while radar echoes were simultaneously detected. The average power was $1.4\ 10^{-9}\ Hz^{-1}$, with a dispersion in a range of two orders of magnitude. In Fig. 7b, the average power is only $0.8\ 10^{-10}\ Hz^{-1}$, and no radar echoes were observed at the same time. One should moreover notice that, in this case, the computed average is a maximum, as many points were deleted from the computation.

The average power measured at the radar wavelength, exhibits a variation of a factor of 5 or more (17 in our example) between the periods when radar echoes were present or absent. The amplitude of an echo is proportional to the backscattering cross-section, which is itself proportional to $n_e^2(\Delta n_e/n_e)^2$ (Booker, 1956). Introducing the absolute electron density measured by ISOPROBE and the aforementionned ratio of 5, we find a variation of at least 10 in the backscatter factor. This should correspond to a difference of 10 dB in the signal to noise ratio. As a matter of fact, the radar also measured a value next to 10 dB or greater when fluctuations were simultaneously present in-situ.

EISCAT/SAFARI OBSERVATIONS

The EISCAT/SAFARI coordinated observations were performed in December 1983. Simultaneous data were obtained on 12/10, between 18:00 UT and 20:30 UT. A synoptic view of the geophysical conditions prevailing at that time, as measured by EISCAT, is presented in Fig. 8. The ion drift is plotted in invariant latitude-MLT coordinates, and the larger dots indicate the vectors for which the comparison has been carried out. The dotted line clearly separates two regions of reversed plasma flow, and is recognized as the Harang discontinuity. The distinction between the regions of reversed flow is not so clear at the northern latitudes, where the comparison will be made, but is true on the average. A very dynamic plasma flow is observed on the poleward side of the discontinuity. During this period, the magnetic activity was disturbed, with the Kp index in the range 4 to 5. These observations of the Harang discontinuity are in agreement with previous results (Nielsen and Greenwald, 1979), which found the plasma flow to be more irregular on its poleward side, and to include large swirls with spatial scales of hundreds of kilometers.

The details of the comparison between the velocity of F-region small-scale irregularities, detected by SAFARI, and the ion-drift velocity, measured by EISCAT, have been given in a paper by Villain et al. (1985b). We shall therefore present only the main conclusions of the joint study. The two velocities have been compared in six points obtained in the course of two meridian scans. The range at which the HF backscatter has to be compared to the EISCAT data is determined from the ray tracing presented in a previous paragraph. The SAFARI data have been analyzed in two steps. Firstly, the number of averages was such that the integration time was, as best as possible, equal to the EISCAT integration time. Other analyses were also carried out with shorter integrations, so as to detect any temporal variation in the velocity. Eventual spatial variations were determined by sampling the signal not only at the group delay calculated from the ray tracing, but also in an area of about 120 km along the ray path. Moreover, the shape of the Doppler spectra is also indicative of the degree of homogeneity for the velocity inside the scattering volume. A narrow and well defined peak corresponds to an homogeneous velocity field, while a complicated spectrum is certainly related to variations inside the scattering volume. Considering the

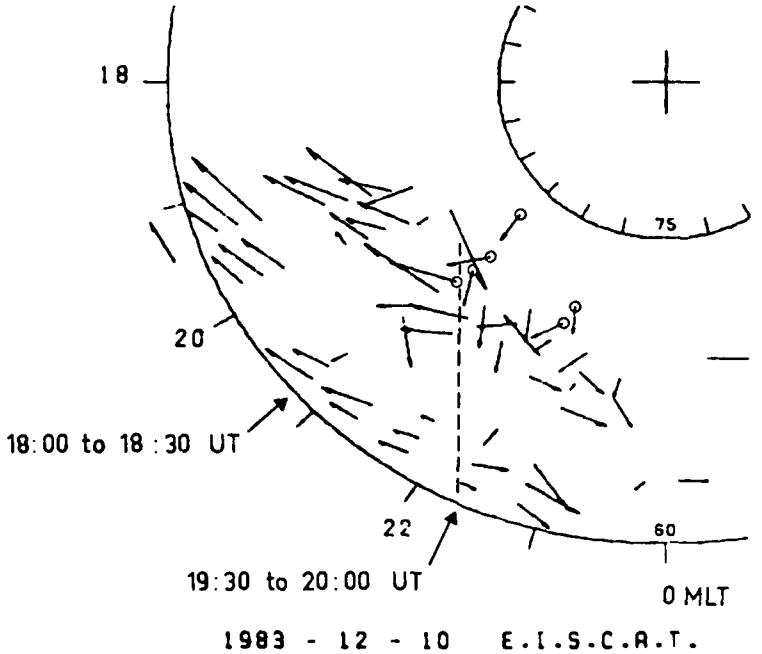


Fig. 8. EISCAT ion drift vectors in invariant latitude- MLT coordinates. The dots indicate the vectors for which the comparison with SAFARI has been made. The dashed line corresponds to the position of the Harang discontinuity as deduced from the data.

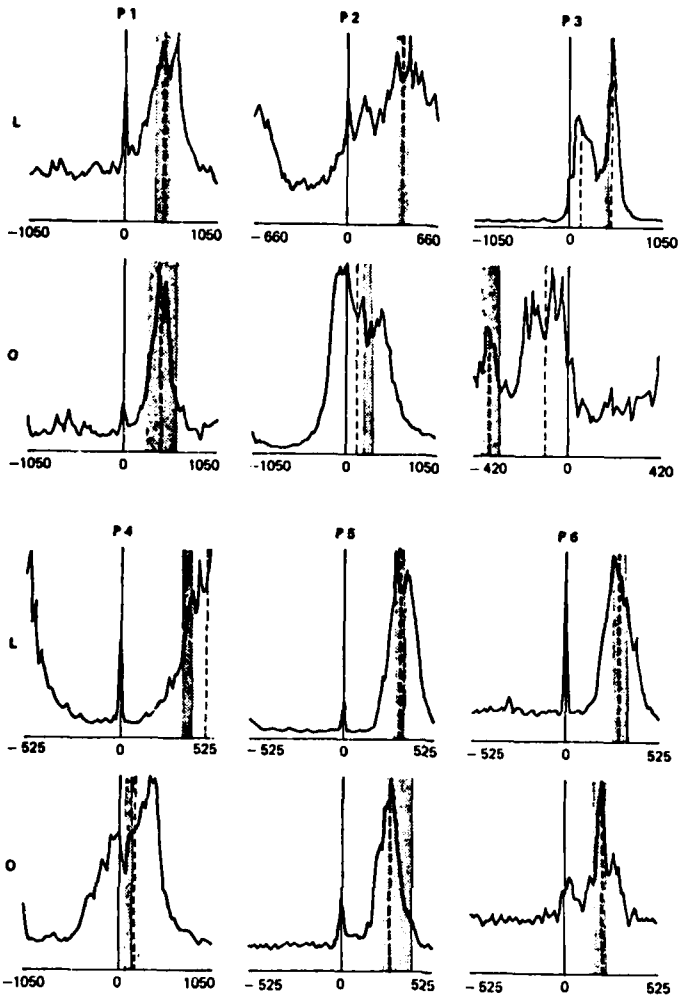


Fig. 9. Summary of the SAFARI Doppler spectra for the six points of comparison with EISCAT. The grey area corresponds to the projection of the EISCAT ion drift velocity vector on the lines of sight of the SAFARI radars. Its width corresponds to the error bars on the EISCAT measurements.

azimuthal width of a radar cell, which is up to 300 km, such conditions are likely to occur, especially near the Harang discontinuity.

As a matter of fact, the Doppler spectra observed during the experiment fall into three categories according to their morphological behaviours. The first category is made up from spectra that exhibit a regular shape and small width, and do not show any spatial or temporal variations during the period of integration. The second category includes the spectra exhibiting temporal variations in the course of the EISCAT integration period. They are usually well defined, but their mean Doppler velocity changes continuously. Finally, the most complex spectra are observed when spatial and temporal variations are simultaneously present during one EISCAT integration. The points located near the Harang discontinuity, and thus in the region of splitting of the plasma flow, fall into this category.

Except for the points being part of the first set, the comparison between the EISCAT and SAFARI data is not straightforward. Therefore, we have first projected the drift velocities measured by EISCAT onto the directions of the SAFARI beams. These values, with their error bars superimposed on each spectrum as a darker band, are plotted together with the SAFARI spectra in Fig. 9. For each point, the Lycksele spectrum is presented at the top and the Oulu spectrum at the bottom. The mean phase velocity is shown as a dashed line on the spectrum. In the case of P3, a mean phase velocity is deduced from each peak, since the two spectral features are well separated. When the spectra exhibit single, well defined peaks with a regular shape, as for P1, P5 and P6, the mean phase velocity fits perfectly to the EISCAT data. For P2 and P4, where spatial and temporal variations are evident, the dark band of EISCAT values lies within the spectra, but the mean phase velocity does not fall exactly into the same range. Finally, P3 presents an interresting configuration, where the EISCAT data fits well with only one of the two peaks present in each spectrum. If we suppose that two independent convection cells were present in the backscattering region, we can conclude that the smaller volume probed by EISCAT lies completely within one of the cells.

The direct comparison between the ion drift velocity and the phase velocity deduced from the SAFARI Doppler spectra is shown in Fig. 10 for the full set of data. Let us review each of these points.

P1 - The scattering volumes of the two instruments did not exactly overlap. In spite of this, both direction and magnitude of the ion drift and phase velocity agree with each other.

P2 - It has not been possible to distinguish among the spatial structures and temporal variations present in the Doppler spectra. We have therefore only drawn the average value of the phase velocity. None of the two peaks present in the Oulu data (Fig. 9) fits the EISCAT data. The two sets of data are probably not affected in the same manner by the variations, explaining the observed discrepancy in the velocity vector.

P3 - The presence of two convection cells within the scattering region is well established from the SAFARI data in Fig. 9. We have therefore combined the peaks in agreement with the EISCAT

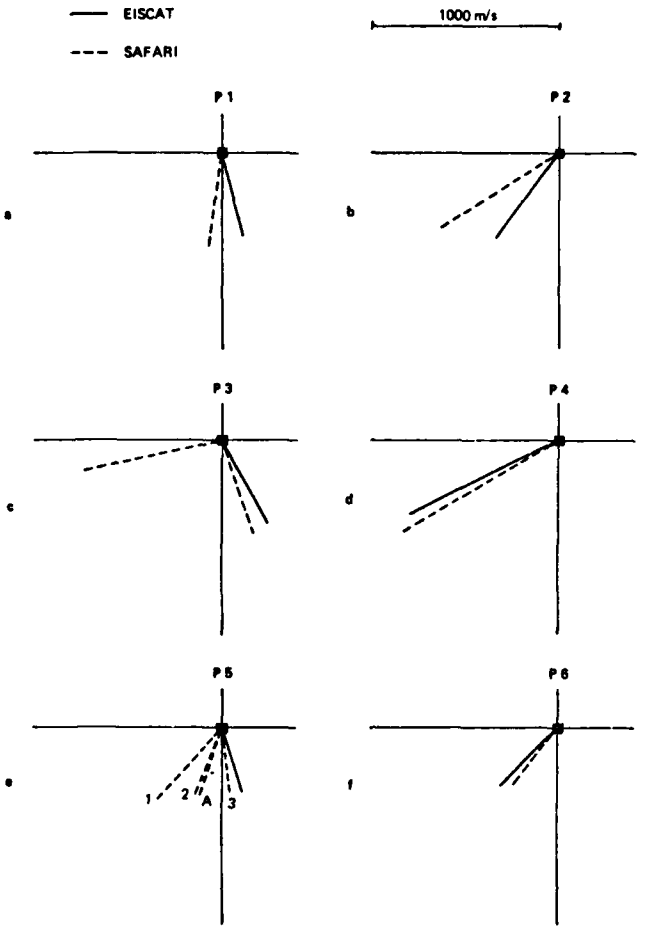


Fig. 10. Comparison of the EISCAT ion drift velocity and irregularity phase velocity deduced from the SAFARI Doppler spectra (see text).

data and built a second vector with the remaining peaks. The agreement is excellent with the EISCAT value for the vector which corresponds to the same ionospheric volume, located on the eastward side of the SAFARI cell. Near the Harang discontinuity, this volume will therefore observe preferentially the eastward convection, as verified experimentally. The same remark is also true for P2.

P4 - The agreement is excellent in spite of some temporal variations in the SAFARI data. Note that these are mostly seen in the Oulu data, and that the EISCAT volume lies exactly in the center of the Oulu radar cell.

P5 - The four vectors show the change in the velocity in the course of the EISCAT integration. It rotates 50 degree towards the east, the last value being in agreement with the EISCAT measurement. P5 corresponds to the same geographical location as P2, and the same remark applies.

P6 - The agreement is excellent between both velocity vectors.

DISCUSSION

The power spectra derived from the ISOPROBE data fit a power law with a spectral index comprised between 2.0 and 3.0, for an average value of 2.3. In a few cases, a spectral knee at a wavelength of a few hundred meters is also present. These characteristics are quite similar to those mentionned in previous works. Most, if not all, of them reported a power law with an index in the neighborhood of 2.0. For example, the Ogo 6 retarding potential analyser found a value near 1.9 over the range 70 m to 7 km (Dyson et al., 1974). ISIS 1 measured positive ion irregularities between 200 m and 100 km. The average value of the spectral index in the auroral zone and polar cap were respectively 2.0 and 2.05 (Phelps and Sagalyn, 1976). The ISOPROBE results are in agreement with those, even if the slopes are sometimes steeper. This might be related to its better spatial resolution (10 km for one spectrum), compared to the distances between 60 km and 100 km over which the spectra were computed with the other instruments.

Several sources have been suggested to explain the production of the F-region irregularities in the high-latitude ionosphere. They include particle precipitations, generation by electrostatic turbulence and generation by plasma instabilities. Gravity waves should also be considered as a possible seeding mechanism, as observed at the equator (e.g. Kelley et al., 1981; Anderson et al., 1982). In addition, the convection may act to distribute the irregular plasma throughout the high-latitude ionosphere (e.g. Kelley et al., 1982). The present understanding is that the larger scale irregularities are originally produced by precipitations (e.g. Vickrey et al., 1980; Kelley et al., 1980), and that plasma instabilities thereafter act to destabilize the shorter wavelengths. Among these, the relative geometries of electric and magnetic fields make the gradient-drift instability (Reid, 1968), or the current-convective instability in presence of field-aligned currents (Ossakow and Chaturvedi, 1979), a

good candidate. It has been shown, both theoretically (Chaturvedi and Ossakow, 1979) and numerically (Keskinen et al., 1980), that non-linear saturation occurs through the generation of linearly damped harmonics, and that the plasma becomes two-dimensionaly unstable with an irregularity flow determined by the plasma motion. Other mechanisms have also been proposed, which may operate in specific conditions. They include instability due to electrostatic electron velocity shears in short-scale structures of field-aligned currents (Keskinen and Huba, 1983), temperature gradient-drift instability (Hudson and Kelley, 1976), ion-cyclotron instability (D'Angelo and Motley, 1962), and velocity shear instability transverse to the magnetic field (Kintner and D'Angelo, 1977).

The various observations presented in this paper will help to progress in the understanding of the mechanisms operating in the high-latitude F-region. The correlation, shown in Fig. 4, between the level of fluctuations and the electron density gradient suggests that the gradient-drift instability operates on the edges of the large-scale irregularities to destabilize the smaller wavelengths. The spectral index obtained numerically for the same instability (Keskinen and Ossakow, 1983) is of the order of 2.5, and is nearly identical to the average in-situ value measured by ISOPROBE. Of course, the theory is not strictly valid down to the wavelengths detected by the HF radar, which are close to the ion gyroradius, but the physical picture of the process remains similar. The small percentage of spectra exhibiting a break in their slope might have to be considered separately. In this case, the variation is approximated by two power laws, with a shallower (steeper) slope at longer (shorter) wavelengths. The existence of a break in the spectrum has already been mentionned in previous works (Phelps and Sagalyn, 1976; Kelley and Kintner, 1978), but, in both cases, the knee occured at longer wavelengths, of the order of several kilometers. For most spectra, the two indices are in good agreement with the predictions of the theory for inertial turbulence in a two-dimensional magnetized plasma, namely 5/3 and 3 (Kraichnan, 1967). The break could also be related to the limit between unstable and damped modes of the gradient-drift instability. Computing the limit from the linear theory in the case of classical diffusion, one finds a value of several tens of meters, slightly lower than observed experimentally. The lack of knowledge in the diffusion mechanisms and coefficients is nevertheless sufficient to eventually reconcile the computation with the data.

All the aforementionned processes, investigated for the generation of the irregularities, predict theoretically a very low phase velocity, mainly because both ions and electrons are collisionless in the F region. The fluctuations detected by the radar should therefore follow the bulk plasma motion under the influence of the convection electric field. This prediction was verified experimentally, for velocities up to 900 m/s, during the joint SAFARI/EISCAT observations. The discrepancies noted during the comparison could be easily explained in terms of spatial variations within the HF radar cells, which had a large latitudinal extent. The effect could be reduced with a better azimuthal resolution of the antenna array. A new system of dual HF coherent radars, featuring improved performances over the SAFARI system, is currently developed by french and american groups in northeastern Canada (Greenwald et al., 1985). It will be able to study the ionosphere at very high latitudes in a region including the Sondre Stromfjord incoherent scatter radar. It will, among others, draw two-dimensional maps of the convection over an area as large as 1000x1000 km^2 with a spatial resolution of 60 km by 30 km at a range of 1000 km and a typical temporal resolution of 80 s. In future years, this instrument will be a primary support of a large number of space-borne and ground-based instruments.

REFERENCES

ANDERSON, D.N., A.D. RICHMOND, B.B. BALSLEY, R.G. ROBLE, M.A. BIONDI and D.P. SIPLER, In-situ generated gravity waves as a possible seeding mechanism for equatorial Spread-F, Geophys. Res. Lett., 9, 789-792, 1982.

BAGGALEY, W.J., Backscatter observations of F-region field-aligned irregularities during the IQSY, J. Geophys. Res., 75, 152-158, 1970.

BARON, M., The EISCAT facility, J. Atmos. Terr. Phys., 46, 469-472, 1984.

BASU, S., R.L. VESPRINI and J. AARONS, F-layer irregularities as determined by backscatter studies at 19 MHz over half a solar cycle, Radio Sci., 9, 355-371, 1974.

BATES, H.F., The height of F-layer irregularities in the artic ionosphere, J. Geophys. Res., 64, 1257-1265, 1959.

BATES, H.F., and P.R. ALBEE, Aspect sensitivity of F-layer HF backscatter echoes, J. Geophys. Res., 75, 165-170, 1970.

BEGHIN, C., J.F. KARCZEWSKI, B. POIRIER, R. DEBRIE, and N. MASSEWITCH, The ARCAD-3 ISOPROBE experiment for high time resolution thermal plasma measurements, Ann. Geophys., 38, 615-629, 1982.

BERTHELIER, J.J., F. LEFEUVRE, N.M. MOGILEVSKY, O.A. MOLCHANOV, Y.I. GALPERIN, J.F. KARCZEWSKI, R. NEY, G. GOGLY, C. GUERIN, M. LEVEQUE, J.M. MOREAU and F.X. SENE, Measurements of the VLF electric and magnetic components of waves and DC electric field on board the AUREOL-3 satellite: the TBF-ONCH experiment, Ann. Geophys., 38, 643-667, 1982.

BOOKER, H.G., A theory of scattering by non-isotropic irregularities with application to radar reflections from the aurora, J. Atmos. Terr. Phys., 8, 204-208, 1956.

CERISIER, J.C., J.J. BERTHELIER, and C. BEGHIN, Unstable density gradients in the high-latitude ionosphere, in Results of the ARCAD 3 project and the recent programmes in magnetospheric and ionospheric physics, Ed. CNES, Publ. CEPADUES, Toulouse, 509-516, 1985.

CHATURVEDI, P.K., and S.L. OSSAKOW, Nonlinear stabilization of the current convective instability in the diffuse aurora, Geophys. Res. Lett., 6, 957-959, 1979.

D'ANGELO, N., and R.W. MOTLEY, Electrostatic oscillations near the ion-cyclotron frequency, Phys. Fluids, 5, 633-634, 1962.

DYSON, P.L., Direct measurements of the size and amplitude of irregularities in the topside ionosphere, J. Geophys. Res., 74, 6291-6303, 1969.

DYSON, P.L., J.P. Mc CLURE, and W.B. HANSON, In-situ measurements of the spectral characteristics of F-region ionospheric irregularities, J. Geophys. Res., 79, 1497-1502, 1974.

GREENWALD, R.A., K.B. BAKER and J.P. VILLAIN, Initial studies of small-scale F-region irregularities at very high latitudes, Radio Sci., 18, 1122-1132, 1983.

GREENWALD, R.A., K.B. BAKER, R.A. HUTCHINS and C. HANUISE, An HF phased-array radar for studying small-scale structure in the high-latitude ionosphere, Radio Sci., 20, 63-79, 1985.

HANUISE, C., High-latitude ionospheric irregularities: A review of recent radar results, Radio Sci., 18, 1093-1121, 1983.

HANUISE, C., J.P. VILLAIN and M. CROCHET, Spectral studies of F-region irregularities in the auroral zone, Geophys. Res. Lett., 8, 1083-1086, 1981.

HOWER, G.L., D.M. RANZ and C.L. ALLISON, Comparison of HF radar echoes and high-latitude Spread F measurements, J. Geophys. Res., 71, 3215-3221, 1966.

HUDSON, M.K., and M.C. KELLEY, The temperature gradient-drift instability at the equatorward edge of the ionospheric plasma trough, J. Geophys. Res., 81, 3913-3918, 1976.

KELLEY, M.C., and P.M. KINTNER, Evidence for two-dimensional inertial turbulence in a cosmic scale low β plasma, Astrophys. J., 220, 339-345, 1978.

KELLEY, M.C., and F.S. MOZER, A satellite survey of vector electric fields in the ionosphere at frequencies of 10 to 500 Hertz -1- Isotropic, high-latitude electrostatic emissions, J. Geophys. Res., 77, 4158-4173, 1972.

KELLEY, M.C., K.D. BAKER, J.C. ULRICK, C.L. RINO, and M.J. BARON, Simultaneous rocket probe, scintillation and incoherent scatter radar observations of irregularities in the auroral zone ionosphere, Radio Sci., 15, 491-505, 1980.

KELLEY, M.C., M.F. LARSEN, C. LA HOZ, and J.P. Mc CLURE, Gravity wave initiation of equatorial Spread F: A case study, J. Geophys. Res., 86, 9087-9100, 1981.

KELLEY, M.C., J.F. VICKREY, C.W. CARLSON, and R. TORBERT, On the origin and spatial extent of high-latitude F-region irregularities, J. Geophys. Res., 87, 4469-4475, 1982.

KESKINEN, M.J., and J.D. HUBA, Generation of lower hybrid waves by inhomogeneous electron streams, J. Geophys. Res., 88, 3109-3115, 1983.

KESKINEN, M.J., and S.L. OSSAKOW, Nonlinear evolution of convecting plasma enhancements in the auroral ionosphere, 2, small-scale irregularities, J. Geophys. Res., 88, 474-482, 1983.

KESKINEN, M.J., S.L. OSSAKOW, and B.E. Mc DONALD, Nonlinear evolution of diffuse auroral F-region ionospheric irregularities, Geophys. Res. Lett., 7, 573-576, 1980.

KINTNER, P.M., and N. D'ANGELO, A transverse Kelvin-Helmotz instability in a magnetized plasma, J. Geophys. Res., 82, 1628-1630, 1977.

KRAICHNAN, R.H., Inertial ranges in two-dimensional turbulence, Phys. Fluids, 10, 1417-1423, 1967.

Mc CLURE, J.P., and W.B. HANSON, A catalog of F-region irregularity behavior based on Ogo 6 retarding potential analyzer data, J. Geophys. Res., 78, 7431-7440, 1973.

NIELSEN, E., and R.A. GREENWALD, Electron flow and visual aurora in the Harang discontinuity, J. Geophys. Res., 84, 4189-4200, 1979.

OKSMAN, J., H.G. MOLLER, and R.A. GREENWALD, Comparison between strong HF backscatter and VHF radar aurora, Radio Sci., 14, 1121-1133, 1979.

OSSAKOW, S.L., and P.K. CHATURVEDI, Current-convective instability in the diffuse aurora, Geophys. Res. Lett., 6, 332-334, 1979.

PHELPS, A.D., and R.C. SAGALYN, Plasma density irregularities in the high-latitude topside ionosphere, J. Geophys. Res., 81, 515-523, 1976.

REID, G.C., The formation of small-scale irregularities in the ionosphere, J. Geophys. Res., 73, 1627-1640, 1968.

SAGALYN, R.C., M. SMIDDY, and M. AHMED, High-latitude irregularities in the topside ionosphere based on Isis 1 thermal probe, J. Geophys. Res., 79, 4252-4261, 1974.

STOREY, L.R.O., M.P. AUBRY, and P. MEYER, A quadrupole probe for the study of ionospheric plasma resonances, Plasma waves in space and laboratory, 1, 302-332, Edinburgh University Press, 1969.

VICKREY, J.F., C.L. RINO, and T.A. POTEMRA, Chatanika/Triad observations of unstable ionization enhancements in the auroral F-region, Geophys. Res. Lett., 7, 789-792, 1980.

VILLAIN, J.P., R.A. GREENWALD, and J.F. VICKREY, HF ray tracing at high latitudes using measured meridional electron density distributions, Radio Sci., 19, 359-374, 1984.

VILLAIN, J.P., C. BEGHIN, and C. HANUISE, ARCAD 3-SAFARI coordinated study of auroral and polar F-region ionospheric irregularities, in Results of the ARCAD 3 project and the recent programmes in magnetospheric and ionospheric physics, Ed. CNES, Publ. CEPADUES, Toulouse, 841-853, 1985a.

VILLAIN, J.P., G. CAUDAL, and C. HANUISE, A SAFARI-EISCAT comparison between the velocity of F-region small-scale irregularities and the ion-drift, J. Geophys. Res., in press, 1985b.

ACKNOWLEDGEMENTS

We are grateful to the staff of the Lycksele Ionospheric Observatory and to Prof. J. Oksman of the Oulu university for their help in the installation and operation of the SAFARI radar. We also acknowledge the efforts of the staffs of the european incoherent scatter radar EISCAT and of the AUREOL 3 satellite. This research has been supported by INAG and CNRS through ATP EISCAT/ANIRA.

ON THE RELATIONSHIP OF F-REGION STRUCTURE IN THE DAYSIDE AURORAL OVAL TO HF BACKSCATTER SIGNATURES ATTRIBUTED TO THE POLAR CUSP

by
J. D. Kelly, R. T. Tsunoda
Radio Physics Laboratory
SRI INTERNATIONAL
Menlo Park, California
94025 USA
J. K. Olesen and P. Stauning
Division of Geophysics
DANISH METEOROLOGICAL INSTITUTE
Copenhagen, Denmark

SUMMARY

Ionosonde measurements in the vicinity of the dayside auroral oval are characterized by complex signal returns. These are thought to be associated with the structure of the electron density in the F-region attributed to processes associated with the polar cusp.

This paper describes the results of a comparison of simultaneous, incoherent-scatter radar measurements and ionosonde measurements of the dayside auroral-zone ionization. This experiment takes advantage of the unique geometry of the Sondrestrom radar operated by SRI International at Søndre Strømfjord, Greenland, and the ionosondes operated by the Danish Meteorological Institute at Gødhavn and Søndre Strømfjord, Greenland. The radar was operated while the antenna scanned in the magnetic meridian. The locations of the ionosondes are in that meridian. The radar data greatly assist in the interpretation of the complex ionograms.

The F-region structure in electron density is closely associated with specific features in the plasma convection patterns. In this study, we examined the F-region structure associated with the plasma convection reversal (polar-cap boundary) in the postnoon sector and its ionogram signature.

The ionograms are characterized by oblique echoes when the convection reversal is either poleward or equatorward of the ionosonde. The radar data indicate that the gradient in the electron density enhancement is similar on the poleward and equatorward edges, and that the enhancement is extended along the convection reversal for many hours. When the reversal is in the vicinity of overhead of the ionosonde, the ionograms are characterized by intense sporadic-E layers.

These signatures are similar to those assumed to be produced by the polar cusp in other studies.[1,2] However, in this case, the F-region structure responsible for oblique and sporadic returns seen on the ionograms is associated with soft-particle precipitation associated with the plasma convection reversal or polar-cap boundary.

1. INTRODUCTION

The dayside auroral-zone ionosphere has been examined for many years using ionosondes. The ionograms are frequently characterized by complex signal returns producing unique signal traces such as oblique echoes and sporadic layers. The ionization structure causing these returns has been thought to be a result of cusp particle precipitation.[1,2] Høeg and Ungstrup[3] have used ray tracing-procedures to synthesize ionograms using a model ionosphere with an enhanced F region similar to expected enhancements owing to cusp particle precipitation. These simple models produce ionograms similar to those observed at high latitudes. With the establishment of the incoherent-scatter radar at Søndre Strømfjord, Greenland,[4] we are able to examine the dayside auroral zone ionosphere in much more detail and consequently assist with interpretation of ionograms using actual ionization profiles. We find that the electron-density structure is closely related to the plasma convection pattern. Specifically, we frequently observe F-region density enhancements in the postnoon sector corresponding to the shear reversal in plasma convection.[5] In this paper, we compare the radar data during such an event with ionogram data taken at Gødhavn and Søndre Strømfjord.

2. OBSERVATIONS

The incoherent-scatter radar at Søndre Strømfjord can measure backscattered signal power and spectral variations. From the backscattered signal power we can deduce the electron density. The spectral width provides the plasma temperature, and the Doppler shift gives the ion velocity. In addition, the radar uses a fully steerable antenna and can scan in latitude. For this experiment, the latitudes examined are from 70° to 80° invariant latitude.

An example of radar data showing the plasma convection deduced from the ion velocity over a 24-hour period is shown in clock-dial format in Figure 1. The pattern is generally a two-celled convection pattern. Of particular interest is the well-defined shear reversal in the flow in the postnoon sector. These velocity shear regions are commonly associated with enhanced electron densities. An example of such a buildup is shown in Figure 2. (This example was chosen because the electron density was strongly enhanced. It does not correspond to the data set presented in Figure 1.) The electron density is represented by iso-valued contours that are plotted as a function of altitude and distance north of the radar.

The lower panel shows the electric field components responsible for the $\vec{E} \times \vec{B}$ drift. The reversal in the north-south component of the electric field coincides with the density enhancement shown in the upper panel.[5] The electron-density enhancement is predominantly in the F region and occurs just equatorward of the reversal of the north-south component of the electric field. In addition to the F-region feature, an enhancement produced by harder precipitation can be seen down to about 130-km altitude.

The event chosen for this comparative study of ionogram signatures to electron-density distribution is 18 May 1983. On this day, the radar measured the convection pattern and electron density as a function of magnetic latitude and time. These data are shown in Figure 3. The upper panel displays the convection pattern. Quite noticeable is the east-west shear reversal in the post-noon sector. (A curve has been drawn to assist the reader.) The lower panel shows the electron density at 250-km altitude. The convection reversal boundary is reproduced on the lower panel. It can be seen that just equatorward of the shear reversal is an enhancement in the electron density. This relationship is identical to that presented in Figure 2 and also by Robinson et al.[5]

We have examined data from the NOAA-7 satellite during this period. The satellite pass that occurred near 1400 local time (LT) traversed this enhancement and observed upward field-aligned currents.

The ionosonde data are from two west-coast stations in Greenland--Gødhavn and Søndre Strømfjord. These two stations lie nearly in the magnetic meridian through the incoherent-scatter radar and are separated by approximately 250 km (as shown in Figure 4). The ionosonde data show complex returns. To help interpret these ionograms, we include figures from Høeg and Ungstrup.[3] Oblique echoes, as shown in Figure 5 (i.e., decreasing virtual height with increasing frequency), are thought to be the result of reflections from ionization structures that exist in the vicinity of the dayside oval.

The ionograms, measured from Gødhavn and corresponding to the time of the radar data, are shown in Figures 6 and 7. Oblique echoes similar to those in Figure 5 can be seen early in the period (e.g., 1259 LT, 1314 LT, and the like). The echoes become more complex with sporadic layers being observed by 1500 LT. Oblique echoes are again visible by 1700 LT.

Early in the ionogram sequence, near 1300 LT, the radar data indicate an enhancement in the electron density about 300 km north of Søndre Strømfjord, as shown in Figure 8. This enhancement is just north of the Gødhavn ionosonde. Oblique echoes were observed during this time. Oblique echoes were thought tc result from reflections from electron-density enhancements located equatorward of the ionosonde.

The radar data at 1515 LT are shown in Figure 9. The F-region electron-density enhancement is essentially overhead of Gødhavn and the ionosonde observation of sporadic E is apparent. Near 1520 LT, the enhancement shown in Figure 10, is clearly equatorward of the Gødhavn ionosonde, and oblique echoes are again observed.

3. DISCUSSION

In order to summarize these results and draw conclusions, we have plotted the radar data and ionosonde data together, shown in Figure 11. The data are shown versus time and invariant latitude. The location of the Gødhavn ionosonde is shown at 77° invariant, and the Sondrestrom radar at 74° invariant. Along each of these baselines is shown the f_0F_2 scaled from the ionograms from Gødhavn and Sondrestrom. Below each of these baselines is indicated the nature of the ionograms--either as oblique (O) or as sporadic E (E). Finally, the convection reversal boundary, as measured by the incoherent-scatter radar, is shown versus latitude and time. We see that when the reversal boundary is overhead at Gødhavn, the f_0F_2 is maximum--the same is also true at Sondrestrom.

The Søndre Strømfjord ionograms show more spread returns and are indicated by two dots joined by a line in the f_0F_2 data. When the reversal is clearly poleward of the ionosonde stations, as in the period from 1300 to 1500 LT, the echoes are generally oblique. When the reversal is near overhead, sporadic E is apparent. When the reversal moves equatorward, the echoes again become oblique.

In this paper, we showed simultaneous incoherent-scatter radar data and data taken from two ionosonde stations in Greenland. The data indicate that echoes that are thought to be related to the polar cusp, i.e., oblique and sporadic-E echoes, can be accounted for by structure produced along the convection reversal boundary characteristic of the polar-cap boundary where particle precipitation is expected.

REFERENCES

1. G. S. Stiles, E. W. Hones, Jr., J. D. Winningham, R. P. Lepping, and B. S. Delana, "Ionosonde Observations of the Northern Magnetospheric Cleft During December 1974 and January 1975," J. Geophys. Res., Vol. 82, No. 1, 1977, pp. 67-73.

2. P. L. Dyson and J. D. Winningham, "Top Side Ionospheric Spread F and Particle Precipitation in the Day Side Magnetospheric Clefts," J. Geophys. Res., Vol. 79, No. 24, 1974, pp. 5219-5230.

3. P. Høeg and E. Ungstrup, "Interpretation of Ionograms in the Vicinity of the Dayside Auroral Oval by Ray Tracing," Radio Science, Vol. 18, No. 5, 1983, pp. 725-737.

4. J. D. Kelly, "Sondrestrom Radar--Initial Results," Geophys. Res. Letts., Vol. 10, No. 11, 1983, pp. 1112-1115.

5. R. M. Robinson, D. S. Evans, T. A. Potemra, and J. D. Kelly, "Radar and Satellite Measurements of an F-Region Ionization Enhancement in the Post-Noon Sector," Geophys. Res. Letts., Vol. 11, No. 9, 1984, pp. 899-902.

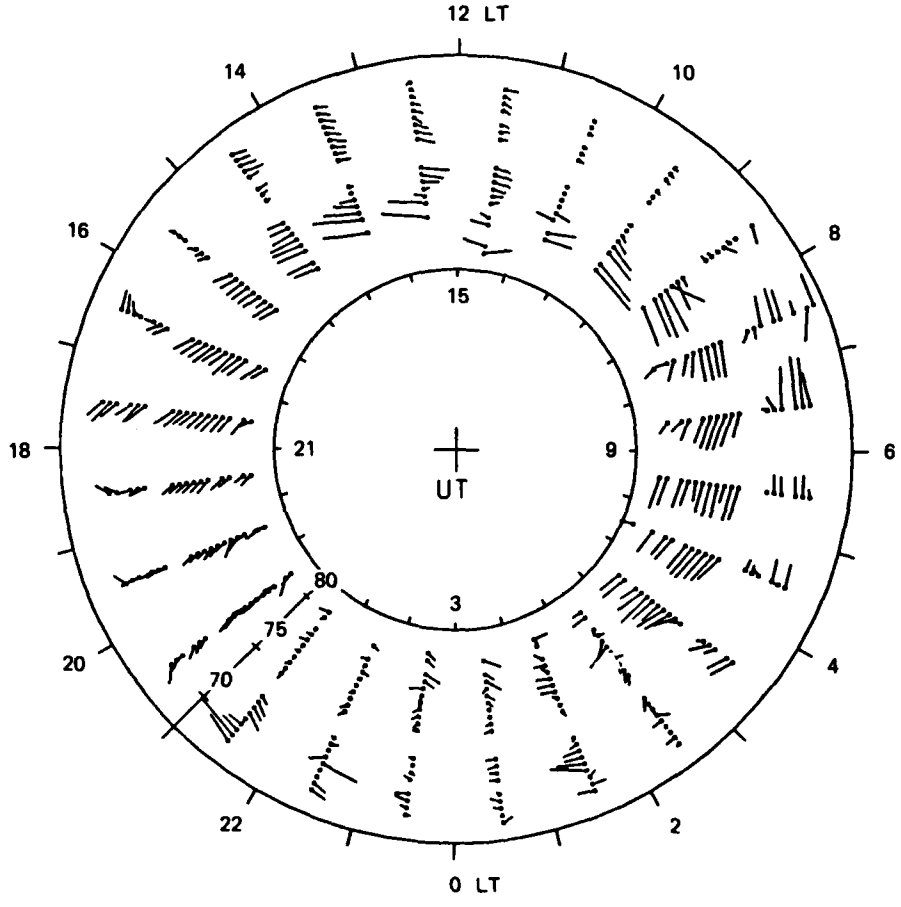


FIGURE 1 CLOCK-DIAL PLOT OF PLASMA CONVECTION PATTERN BETWEEN 68° TO 80° INVARIANT LATITUDE MEASURED BY THE SONDRESTROM RADAR

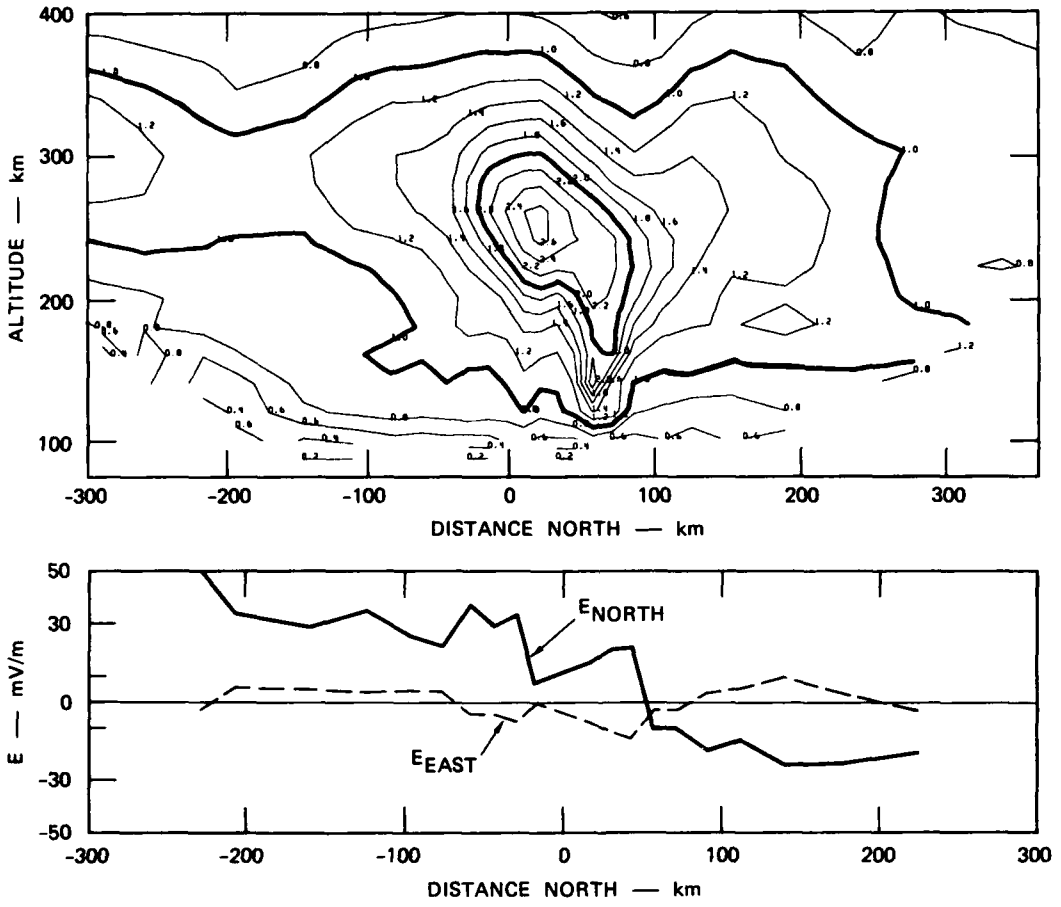


FIGURE 2 EXAMPLE OF RADAR MEASUREMENTS DURING A MERIDIAN SCAN AT ABOUT 15 MLT. The upper panel indicates the enhancement in electron density associated with the convection reversal that is denoted by the zero crossing of E_N in the lower panel.

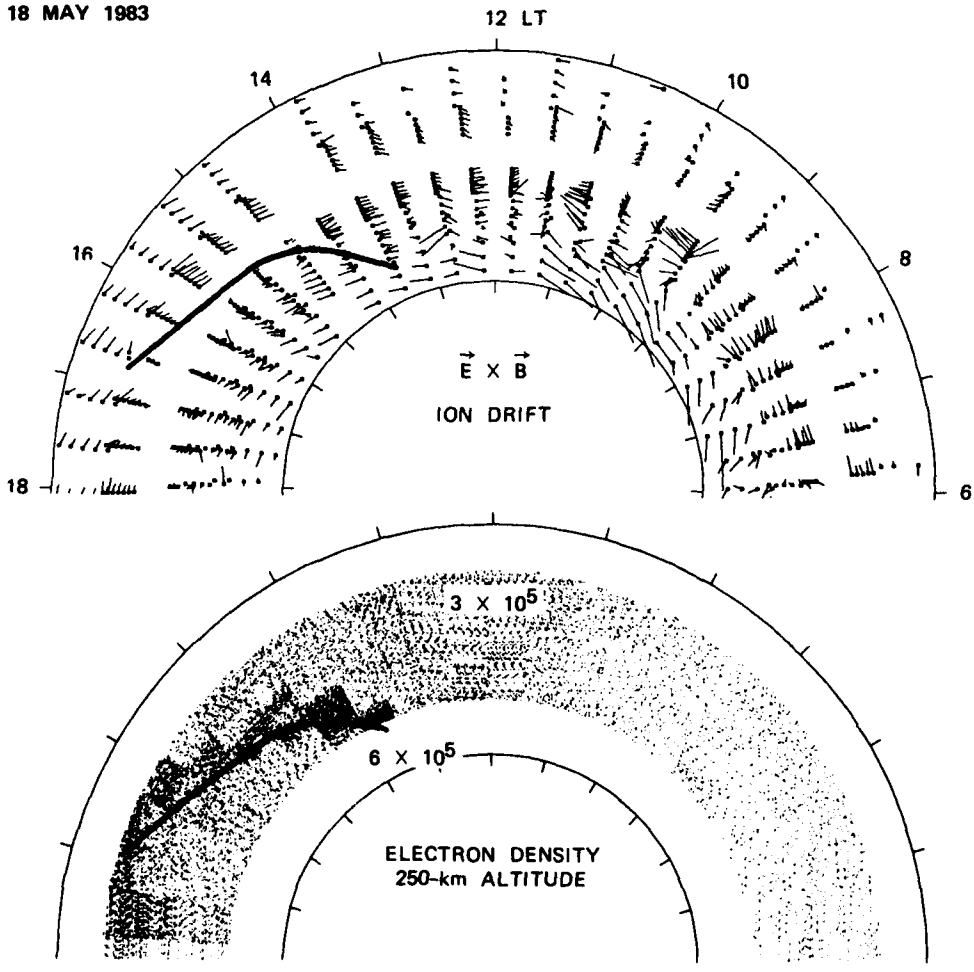


FIGURE 3 RADAR MEASUREMENT OF CONVECTION PATTERN AND ELECTRON DENSITY AT 250 km ON 18 MAY 1983. The density enhancement occurs just equatorward of the convection reversal boundary.

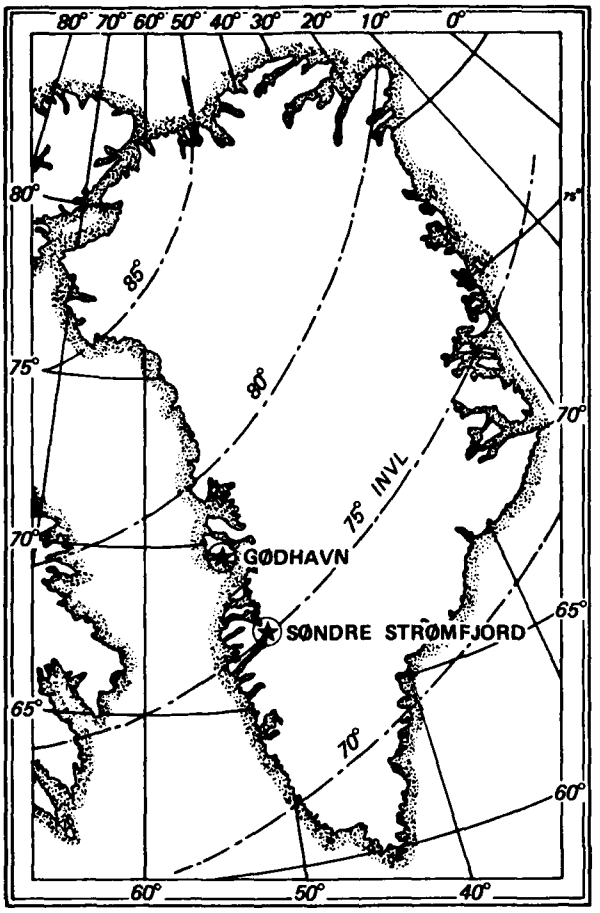


FIGURE 4 MAP OF GREENLAND SHOWING LOCATIONS OF SØNDRE STRØMFJORD AND GØDHAVN. Also shown is the invariant latitude.

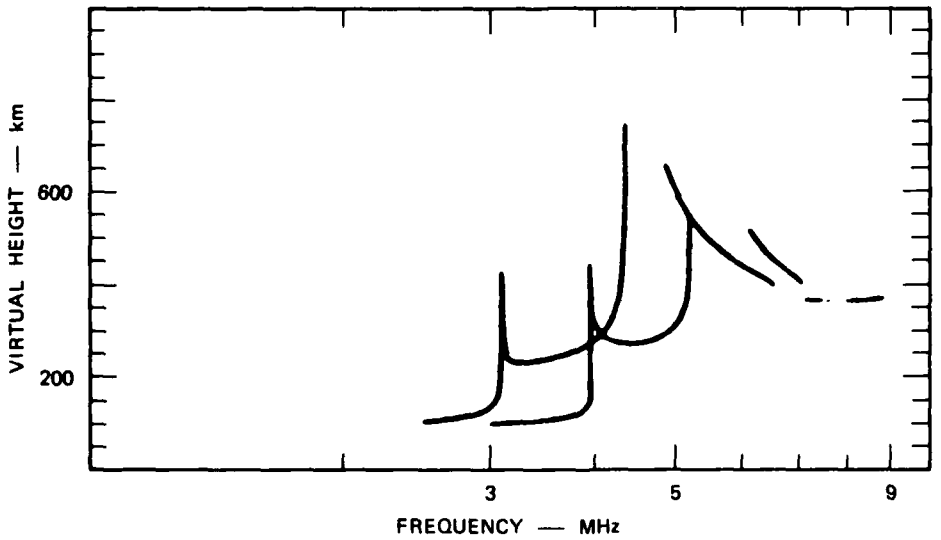


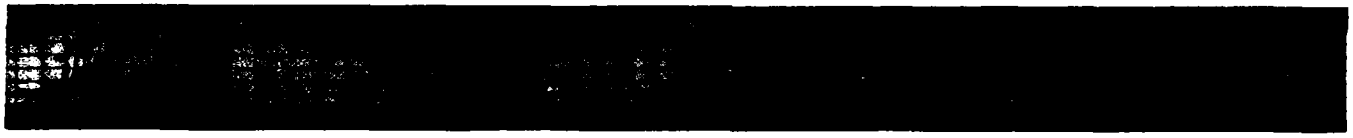
FIGURE 5 SYNTHESIZED IONOGRAM FROM HØEG AND UNGSTRUP [1983] SHOWING OBLIQUE TRACES (decreasing virtual height, increasing frequency)



1158 = LOCAL SUMMER TIME | 1159 | 1214 | 1229 | 1244



1255 | 1258 | 1259 | 1314 | 1329



1344 | 1355 | 1358 | 1359 | 1414



1429 | 1444 | 1455 | 1458 | 1459

FIGURE 6 GØDHAVN IONOGRAMS FOR 18 MAY 1983—LOCAL SUMMER TIME 1158 THROUGH 1459

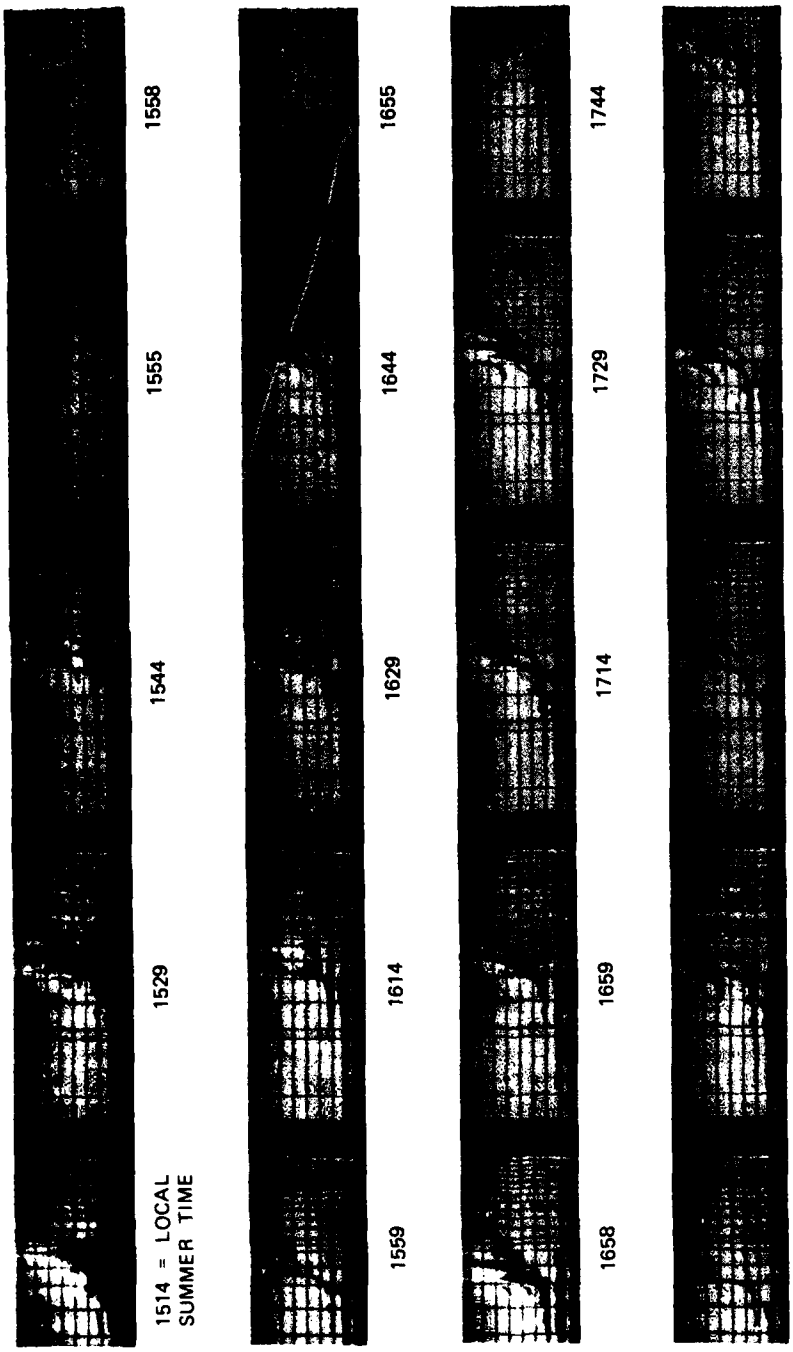


FIGURE 7 GØDHAVN IONOGRAMS FOR 18 MAY 1983—LOCAL SUMMER TIME 1514 THROUGH 1829

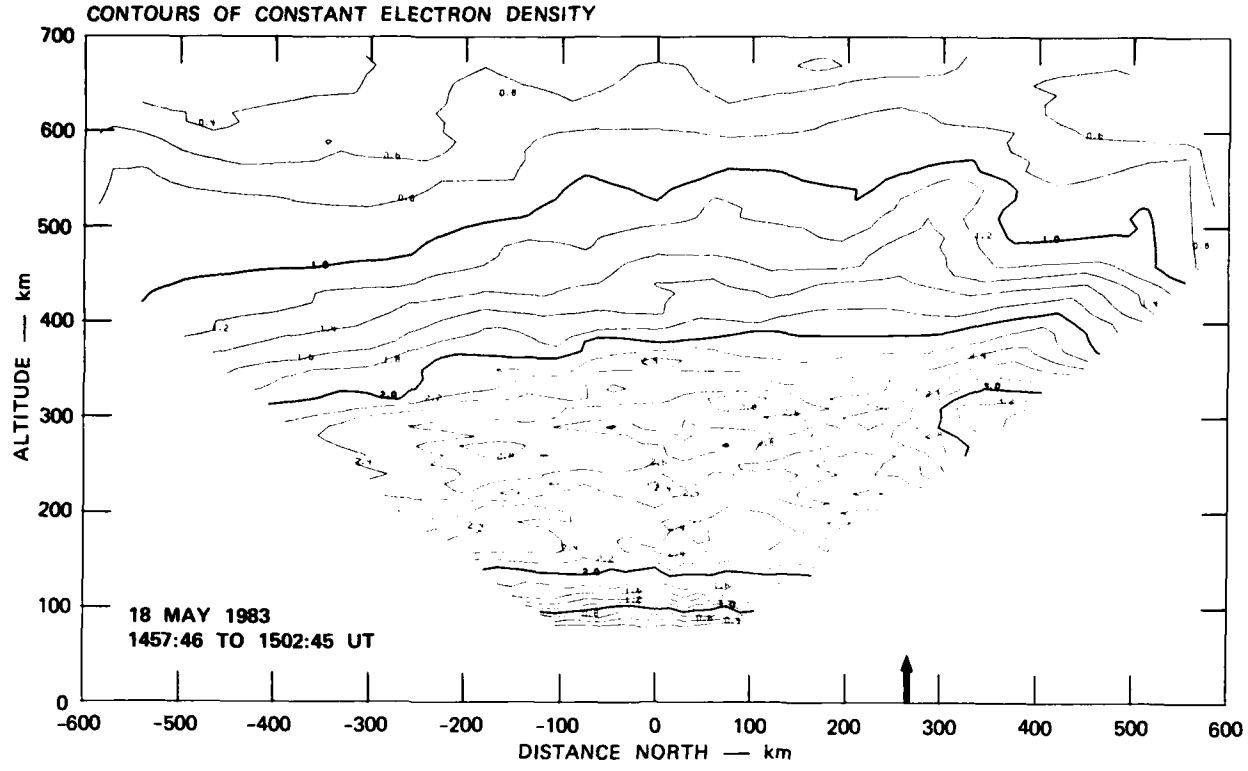


FIGURE 8 RADAR MEASUREMENTS OF ELECTRON-DENSITY CONTOURS. Note F-region enhancement north of Gødhavn. The arrow indicates Gødhavn's location.

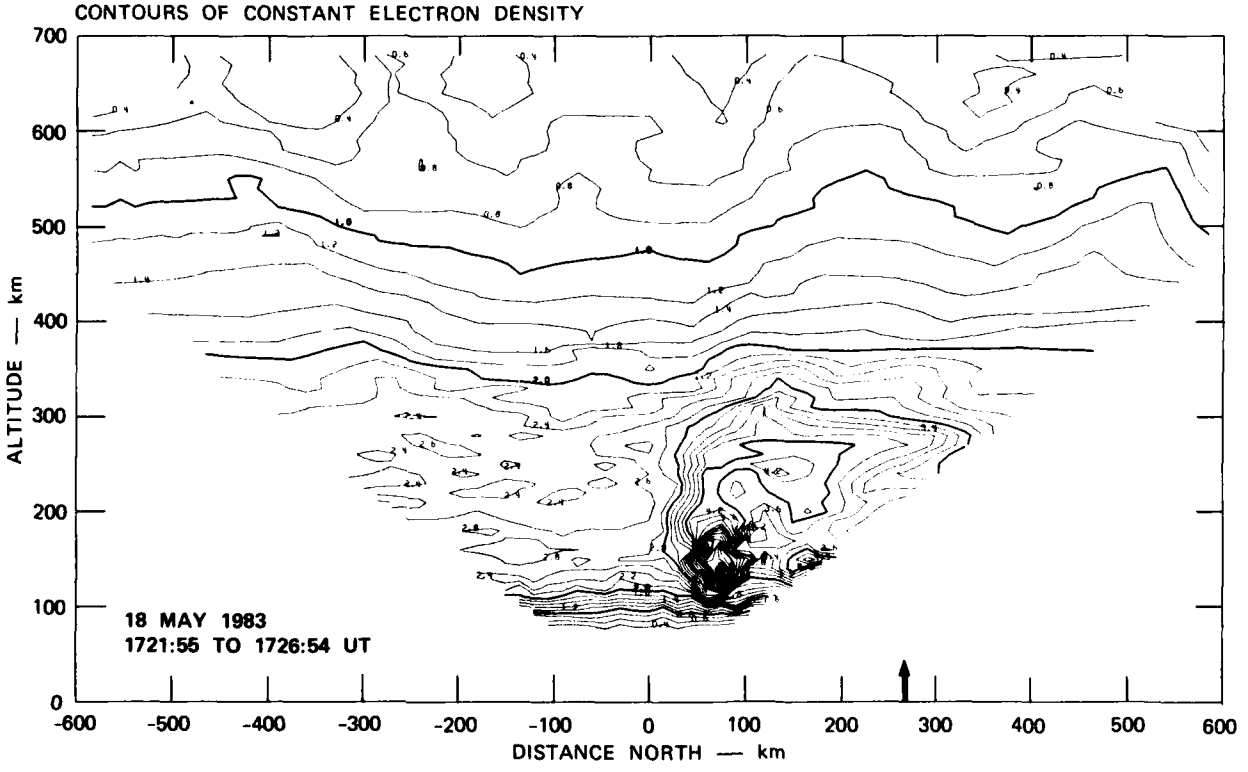


FIGURE 9 RADAR MEASUREMENTS OF ELECTRON-DENSITY CONTOURS. Note F-region density enhancement over Gødhavn. The arrow indicates Gødhavn's location.

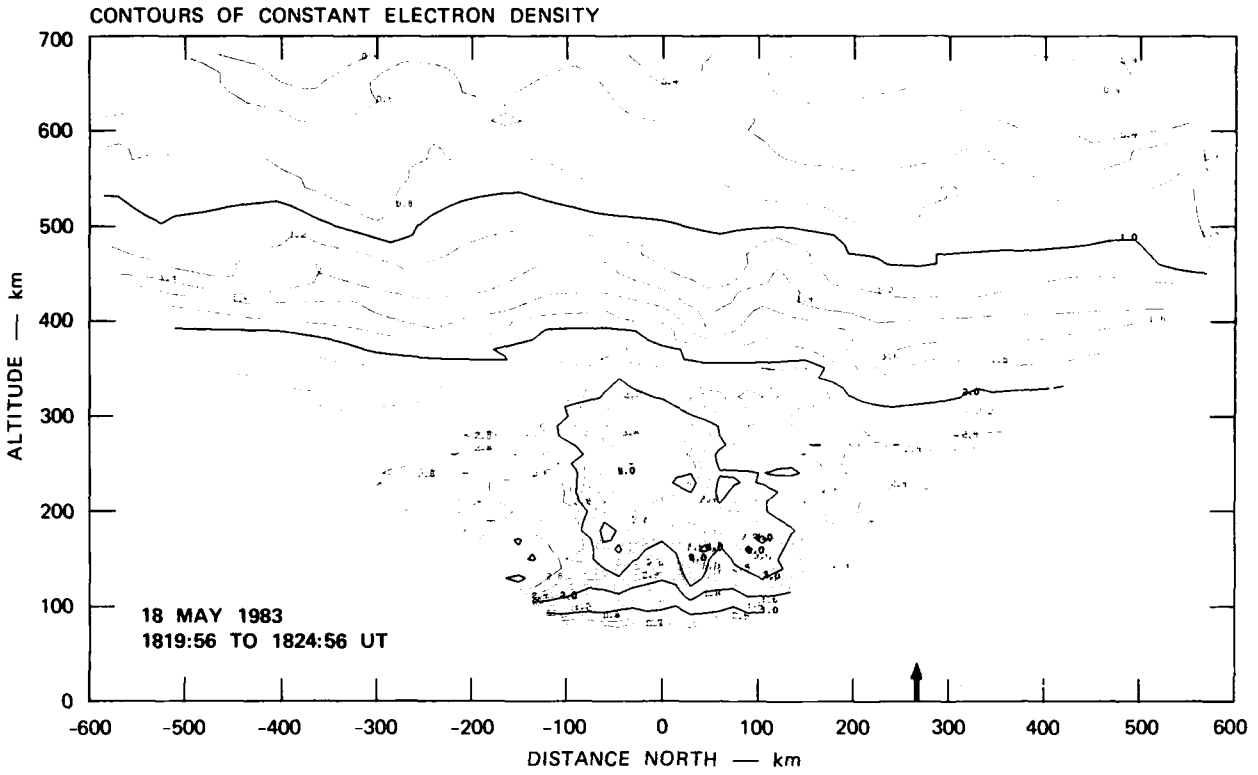


FIGURE 10 RADAR MEASUREMENTS OF ELECTRON-DENSITY CONTOURS. Note F-region density enhancement is south of Gødhavn. The arrow indicates Gødhavn's location.

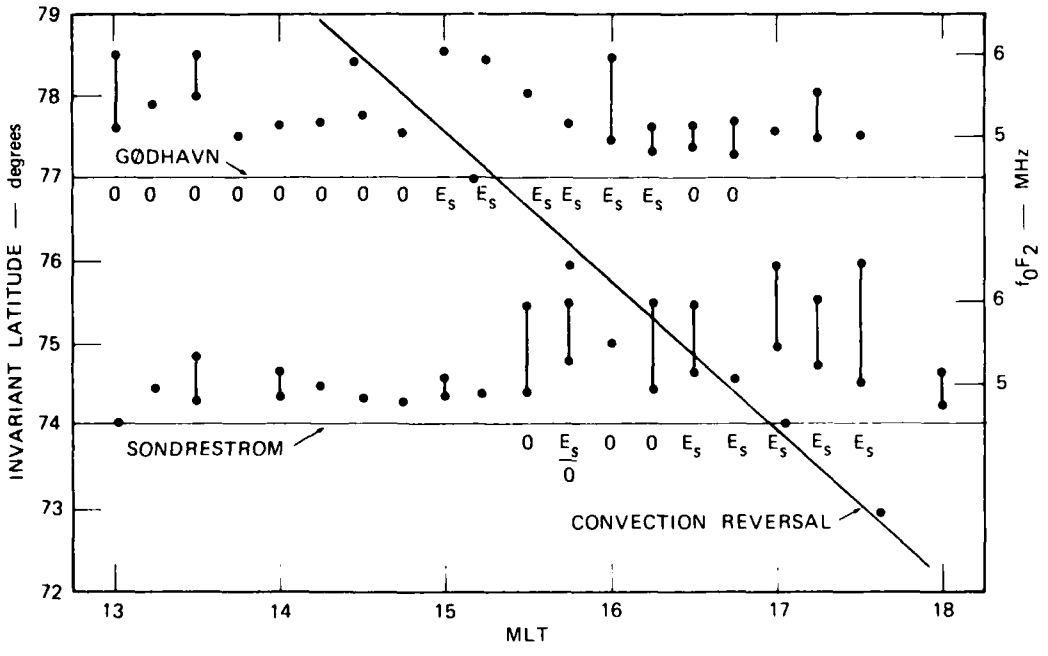


FIGURE 11 SUMMARY OF IONOSONDE AND RADAR DATA. Shown along the baselines for both Gødhavn (77 invariant) and Sondrestrom (74 invariant) is both f_0F_2 values and a symbol describing the ionograms (O = Oblique, E = Sporadic E). Also shown is the location of the convection reversal boundary as a function of invariant and MLT.

OBSERVATIONS OF VERY HIGH LATITUDE IONOSPHERIC IRREGULARITIES WITH THE GOOSE BAY HF RADAR

by

R. A. Greenwald and K. B. Baker
The Johns Hopkins University
Applied Physics Laboratory
Laurel, MD 20707
USA

ABSTRACT

The Goose Bay HF radar is a sophisticated instrument capable of providing detailed information on very high latitude E and F region ionospheric electron density irregularities which act as a source of clutter on OTH radar systems. Through the use of two parallel phased array antennas, this instrument is able to image the location of these irregularities within a three-dimensional volume covering much of northeastern Canada and Greenland. It is also capable of following the temporal variability of these irregularities as well as determining unambiguously the Doppler shift and broadening of radar signals scattered by them. In this paper we present initial results with a single phased array antenna which represent typical examples of the spatial intensity distribution of these irregularities at different local times. We also present examples of Doppler spectra of the irregularities at different local times. Data of this type are of appreciable value in ascertaining the techniques that must be utilized to improve clutter mitigation on high latitude radar systems.

INTRODUCTION

The high latitude ionosphere has always been and undoubtedly will continue to remain a challenging arena for the successful operation of HF radiowave systems. This region, which is directly affected by disturbances on the sun and the many coupling processes that exist between the solar wind and the Earth's magnetosphere and ionosphere, is readily perturbed by energetic particle precipitation in the form of the Auroras Borealis and Australis, as well as by ionospheric and magnetospheric plasma instability processes. As a consequence, the high latitude ionosphere undergoes structuring at both long and short scale sizes. Large scale structuring causes short wave (HF) propagation paths to be radically different from the paths that are predicted by commonly used ionospheric models (e.g., Croft, 1968). Small scale structure scatters radiowave signals and, under appropriate conditions, can act as a severe source of clutter on radar systems. The problem is particularly severe at HF frequencies where ionospheric refraction plays a significant role in propagation and often causes signals from a radar to propagate perpendicular to the Earth's magnetic field in regions where small scale structure is present. This aspect condition results in enormous enhancements of the scattering cross section of the irregularities and intense clutter on radar systems.

The Goose Bay radar has been specifically designed to obtain an improved understanding of the morphology of high latitude E and F region ionospheric irregularities and to understand the mechanisms by which they are produced. Particular attention was given to designing an experiment that would be capable of yielding information on (i) the spatial distribution of the irregularities, (ii) their short term variability as well as their longer term variability with local time and season, and (iii) the Doppler spectral characteristics of the irregularities and their dependence on differing geophysical conditions.

The radar as initially designed included only a single phased array antenna which provided azimuthal resolution of 2.5°-6° depending on the frequency of operation. More recently, through the support of Rome Air Development Center and the Defense Nuclear Agency, a second similar array has been added. Together, they form an interferometer which is capable of determining the vertical angle-of-arrival of the returning signals to an accuracy of approximately 1°. This capability, which is not yet completely implemented, is of considerable value as it enables one to determine the effects of large scale ionospheric structure and nonvertical ionospheric density gradients on a radar's targeting capability. It also will enable one to determine the vertical extent of the ionospheric volume from which clutter is being received. This is an important capability as HF antenna systems in general have poor resolving capabilities in the vertical plane.

Another unique feature of the Goose Bay radar is the multipulse sounding sequence that is used. This sequence enables one to determine unambiguously the Doppler spectral characteristics of the backscattered signals as a function of range even if the irregularity structures are extended over the full field-of-view of the radar and they have Doppler velocities approaching 2000 m/s.

In the following, we present a complete description of the Goose Bay radar along with examples of some of the results that have been obtained to date. These examples include two-dimensional maps of backscattered power levels in the afternoon and evening local time sectors as well as representative examples of Doppler spectral observations in the noon, afternoon, and evening local time sectors. Other examples of this type of data, including two-dimensional maps of the mean Doppler velocity distribution have been reported elsewhere (Greenwald et al.,1985; Greenwald,1985).

DESCRIPTION OF THE GOOSE BAY RADAR

The Johns Hopkins University Applied Physics Laboratory (JHU/APL) HF radar is located in Canada at Goose Bay, Labrador. This site is located in the auroral zone at 65° geomagnetic latitude (53.4° geographic). The field-of-view of the radar extends northward from the site and covers a large geographical region including portions of northeastern Canada and Greenland. Typically, the measurements extend over an azimuth sector of 54° which is centered 2° to the east of geographic north, and over a range interval of 300 to 2400 km. The viewing area is divided into 16 viewing directions, each having an angular separation of 3.3°. Figure 1 illustrates a plan view of the Goose Bay radar field-of-view. Also shown in the figure are the fields-of-view of a similar French HF radar presently being constructed at Schefferville, Quebec, the Sondre Stromfjord incoherent scatter radar, and the Millstone Hill incoherent scatter radar. The fields-of-view of the latter two radars are represented by the circle and the arc segment, respectively. Eventually, the two HF radars will be used in a coordinated fashion to obtain an improved understanding of the drift motions associated with small scale ionospheric structure.

A schematic diagram of the Goose Bay radar is shown in Figure 2. Most of the equipment including the on-line microcomputer, receiver, and frequency synthesizer is in a building located 274 m from the center of the antenna array. At the center of the array, there is a second small shed which houses the phasing matrix, beam select electronics, and the power supplies for the rf amplifiers and transmit/receive (TR) switches. Finally, at the base of each antenna in the original phased array there is a small utility box containing broadband solid state rf amplifiers and TR switches. At the present time, each of the power amplifiers is capable of 125 W peak pulse power, thereby yielding a total output power of 2 kW from the array and an effective peak radiated power of 200 kW (this specification includes the effect of antenna gain). In the future, we are planning to increase the peak radiated power of each amplifier to 2 kW.

The most important part of the Goose Bay radar is the electronically steered phased array antenna. The original array consisted of 16 log periodic antennas used for both transmission and reception in the frequency band from 8 to 20 MHz. Each of these antennas is 12 m in length and has a maximum element length of 15 m (the elements for the lowest frequencies are inductively loaded to achieve resonance). The antennas are situated on top of 15.2 m towers which are also spaced 15.2 m apart. In the Fall of 1984, a second array of 16 antennas was constructed 100 m to the north of the original array and parallel to it. The second array will only be used for reception, and, through the use of interferometric techniques, it will provide information on the vertical angle of arrival of the returning signals.

Figure 3 is a photograph showing a portion of the antenna system. In the foreground, are three of the antennas of the original array and the shed which houses the phasing matrix. One can also see the utility boxes which house the power amplifiers. They are located on the right-hand side of each tower at the approximate height of the shed. In the background of the figure, one can see 7 antennas of the new array.

Signals to and from each of the antenna arrays pass through the broadband phasing matrix shown schematically in Figure 4. The principal elements of the phasing matrix are the eight branching networks noted as "phasing trees." On transmit, signals enter a tree from the receiver side and pass through a network of power dividers and delay lines that ultimately produce progressive time delays at the 16 outputs of the matrix. On receive, signals enter the tree from the antenna side and are reciprocally combined into a composite signal. Consequently, signals that are incident on the antenna array from the direction in which the array is phased undergo constructive interference within the matrix. Signals from other directions interfere destructively. Since the delay lines produce constant time delays, the direction of a particular antenna beam is independent of frequency. However, as the length of the array is fixed, the width of each particular antenna lobe is frequency dependent.

Each phasing tree produces one set of progressive time delays across the array. The 4-way switches are used to select one of the phasing trees, and the double-pole double-throw switches are used to determine whether the selected beam is directed to the right or left of the array normal. Through the use of diode switches, the beam can be steered quite rapidly (~20 microseconds) into any of the 16 beam directions within the true azimuth sector extending from 337° to 27°.

Figure 5 illustrates examples of the theoretical two-way azimuthal patterns of the eight beams directed to the right of the array normal. An additional eight beams are directed to the left of the array normal; however they have been omitted to avoid confusion. Below 16 MHz, the patterns do not exhibit any significant grating sidelobes and other sidelobes are 27 dB below each main lobe. Above 16 MHz, grating sidelobes appear for the outermost beams. For example, the power appearing at -44° in the 18 MHz plot is due to a grating sidelobe of Beam 16. The power at -47.3° is due to a grating sidelobe of Beam 15, etc. To date, these sidelobes have not intoduced any apparent ambiguities in interpreting the data.

Either of the arrays has a broad vertical pattern with an average half-power beamwidth of approximately 30°. The peak of the vertical pattern varies from 15° at 20 MHz to 35° at 8 MHz. With this broad vertical coverage, it is virtually impossible to obtain any information on the height of the irregularity layer or on the propagation mode between the radar and the scattering volume. However, by using the two arrays independently, one can determine the phase difference in the backscattered signal arriving at each of them. As shown in Figure 6, this phase difference may be related to the vertical angle-of-arrival of the returning signal. One can see that there is no ambiguity in the determination of the angle-of-arrival over the first 35° in elevation angle. This is the range of arrival angles that one would expect for the backscattered signals, and it has been used to determine the separation of the two arrays. Given the accuracy that one may achieve in determining the phase difference between the signals arriving at the two arrays, it is estimated that one can expect to achieve an accuracy of 1° or better in the determination of the angle-of-arrival.

The other unique feature of the Goose Bay radar is its use of the burst 7-pulse transmission pattern shown in Figure 7. The backscattered signals from this transmission are sampled by the on-line microcomputer and analyzed to yield, in real time, 17-lag complex autocorrelation functions of the backscattered signals. These autocorrelation functions are averaged over an integration period and stored on magnetic tape. At the Applied Physics Laboratory, they are Fourier transformed into Doppler spectra for subsequent analysis.

The multipulse pattern is used to avoid the ambiguity that often results in the spectral analysis of ionospheric irregularities. Since the irregularities are often observed over an extended range interval, it is desirable to pulse the radar at a relatively low repetition frequency in order to obtain an accurate determination of the irregularity range. In contrast, signals backscattered from ionospheric irregularities at high latitudes often exhibit appreciable Doppler shifts and Doppler broadening. In order to analyze these signals properly, high pulse repetition frequencies are required. This dichotomy of analysis requirements has been a continual frustration to radiophysicists. In the Goose Bay system, the problem is avoided through the use of the multipulse pattern. As can be seen from Figure 7, the pattern yields all lags of a 17-lag autocorrelation function (0-17t0). Ideally, if all of the lags of the autocorrelation function were to occur only once, there would be no ambiguity as to the range of the scattering volume, even if the scatterers were to extend over the entire length of the sequence. However, lags t0, 2t0, and 3t0 all occur twice, and lag 13t0 occurs three times. Fortunately, the time separation between the two occurrences of lags t0, 2t0, and 3t0 is so large (~39 milliseconds under typical operating conditions) that it is impossible to obtain simultaneous backscatter from two distinct scattering regions for the two repetitions of the pattern. The 13t0 lag is a problem, but as there is normally little correlation remaining at the larger lags, it has relatively little effect on the total autocorrelation function or on the Doppler spectrum that is derived from it.

Another problem with the multipulse pattern is that it is entirely possible that a transmitter pulse will occur at a delay for which the backscattered signals from earlier pulses are to be sampled. This problem is particularly severe for certain range delays, and it can result in autocorrelation functions that have a number of "bad" lags. Fortunately, the problem is entirely deterministic. One can use the good lags of the autocorrelation function to obtain an improved estimate of the bad lags. An example of the improvement that can be obtained is shown in Figure 8. The upper portion of this figure displays an autocorrelation function that is badly disturbed by the presence of transmitter pulses (it should be noted that most ranges do not have this problem). The lower portion of the figure shows the same autocorrelation function after the bad lags have been corrected. Bad lags due to foreign transmitters and the ionospheric sounder at the site may be removed in a similar fashion. The Doppler spectra are calculated from the corrected autocorrelation functions.

JUSTIFICATION FOR BROADBAND HF OPERATION

Small scale ionospheric irregularities have been observed in the E and F regions of the high, middle, and low latitude ionospheres where they are produced by a variety of mechanisms (e.g., Fejer and Kelley, 1980). In virtually all cases, these structures share a common attribute which is their tendency to be elongated in the direction of the Earth's magnetic field. The physical reason for this elongation is that the magnetic force confines the transport of electrons transverse to the field whereas it has no influence on their motion in the direction of the field. Consequently, the small scale structures assume an elongat-

ed shape. If we imagine for the moment that these structures may be represented as a collection of magnetic field aligned needles, then it is clear that they will present the greatest cross section to a backscatter radar if they are viewed from a direction that is perpendicular to their axes. At middle and low latitudes, it is possible to achieve such a viewing condition with a radar of any frequency, whereas at high latitudes the near vertical magnetic field lines and the curvature of the Earth combine to present a situation for which it is impossible to achieve this condition.

The geometry that one faces at high latitudes is shown schematically in Figure 9. Signals from a VHF or higher frequency radars are incident obliquely on irregularity structures in both the E and F regions. Some of the incident energy is scattered by their regularities; however, the scattered signals propagate off into space. In contrast, signals from an HF transmitter are refracted toward the horizontal as they enter the E and F layers. In this manner, they may pass through regions where the wave propagation vector is nearly perpendicular to the local magnetic field. Given that the regions also contain ionospheric irregularities capable of scattering the radar signals, then some of the incident energy will be returned to the radar where it can be observed. In principle, there may be as many as four regions where the perpendicularity condition is fulfilled; these occur at the tops and bottoms of the E and F layers, respectively.

One of the difficulties associated with HF radar studies is that, during the course of the day, there is a continual variation of the electron density profiles in both the E and F regions. At high latitudes, the problem is futher complicated by the nonpredictive occurrence of energetic particle precipitation which introduces additional variability to the electron density profiles. Thus, it is difficult to select optimal frequencies for the operation of the radar and to understand completely the propagation modes between radar and target. The choice of a broadband radar operating between 8 and 20 MHz has enabled us to achieve the perpendicularity condition under many conditions. The use of the sophisticated Goose Bay antenna arrays will hopefully enable one to understand the propagation modes.

SENSITIVITY OF THE GOOSE BAY RADAR

Recently, Walker et al. (1985a) have presented an analysis of the sensitivities of several radar systems, including the Goose Bay radar, to ionospheric irregularities. In their analysis, which assumed a power law dependence of the form k^{-n}, $n > 2$, for the wave number spectrum of the irregularities, they found that the signal-to-noise ratio (SNR) observed by the radar could be expressed as

$$\mathrm{SNR} = r_e^2 \langle \Delta N^2 \rangle f_2(\theta_1) \frac{l_p W_g{}^2 P_t}{\Delta\theta_B^2 r'^2} \frac{\lambda_0^{2-n} \lambda_{ref}{}^{5/2}}{K T_{ref} B} \frac{\pi^{1/2}(n/2-1)}{(2k)^{n-1/2}}$$

where

- r_e is the classical electron radius,
- $\langle \Delta N^2 \rangle$ is the mean square fluctuation of electron density,
- f_2 is a function of order unity related to the refraction and focusing of the beam,
- l_p is the pulse length,
- W is the width of the antenna array,
- g is the radiation pattern of the array,
- P_t is the transmitted power,
- $\Delta\theta_B$ is the beamwidth,
- r' is the virtual range,
- λ_0 is the outer scale length,
- λ_{ref} is the reference wavelength, 15 m,
- K is Boltzmann's constant,
- T_{ref} is the sky temperature at the reference wavelength,
- B is the receiver bandwidth, and
- k is the irregularity wavenumber.

One example of the authors' results showing the dependence of SNR on the root mean square fluctuation level of the irregularities is given in Figure 10. This result, which assumes that the irregularities are situated at the maximum of the vertical pattern of radar antenna, indicates that for fluctuation levels of 10^{-4}, the expected signal-to-noise level is on the order of 30 dB. In practice, the backscattered signals occur at elevation angles that are well below the antenna pattern maximum and the expected SNR values are 10-15 dB lower. Nevertheless, these calculations indicate that even modest fluctuations levels in the ionosphere may lead to significant radar backscatter.

In addition to obtaining a theoretical prediction of the sensitivity of the radar to ionospheric irregularities, it is of interest to present a crude statistic of the probability of observing backscatter with

the Goose Bay radar. Keeping in mind that the 1984-1985 time frame was approaching solar minimum conditions, we have taken a random sample of 85 hours of radar observation spread over all local times and over all four seasons. The following table categorizes these observations into whether backscatter (both ground and ionospheric) was or was not observed during each of the hours. Note that the six-hour period about local midnight has been separated from the remaining observations since there appears to be a significantly higher probability of observing backscatter during this local time sector.

Table I. Probability of Observing HF Backscatter

Time Sector	No Backscatter	Backscatter	Total	% Backscatter
Midnight	5	22	27	81
All others	28	30	58	52
All times	33	52	85	61

One can see from Table I that the Goose Bay radar is capable of obtaining backscatter for an appreciable percentage of the total time. While some of these signals are actually due to ground backscatter via a one-hop ionospheric path, other statistics that we do not show here indicate that ground backscatter contributes to less than half of our backscatter observations. Moreover, on many occasions, as we show in the next section, one obtains backscatter power images exhibiting superimposed ground and ionospheric backscatter.

OBSERVATIONS WITH THE GOOSE BAY RADAR

We now present examples of the data that have been obtained with the Goose Bay radar. In Figure 11, one sees an example of an image of the backscattered power as it is observed in the afternoon local time sector at 1920 UT (~1600 magnetic local time (MLT)). The backscatter is projected onto a map of northeastern Canada and Greenland under the assumption that it is located at an altitude of 300 km. One sees that the scattering region stretches across the radar field-of-view, that it has a latitudinal extent of several hundred kilometers, and that it exhibits SNRs of 12-18 dB. In this example, the total power due to ground scatter and to ionospheric scatter has been plotted. Figure 12 shows the same time period with the contribution due to ground backscatter removed. As one can see, there is very little difference between the two figures, leading one to the conclusion that ground backscatter played a relatively minor role in this example. One should not conclude on the basis of this example that ground backscatter always plays a minor role in the afternoon local time sector. The complexity of the backscatter map that one observes is dependent on propagation conditions which are in turn dependent on the frequency of operation and on the level of disturbance of the ionosphere.

In contrast to the previous two figures, Figures 13 and 14 represent examples of power maps of total backscatter and ionospheric backscatter during a period in which a considerable portion of the total backscattered power was due to ground backscatter. The data were obtained in the evening local time sector at 2340:55 UT (~2015 MLT). For this example, the scattering regions extend both across the field-of-view and over a considerable range in latitude. Some of the more intense arc-like scattering regions are due to ionospheric backscatter, whereas others appear to be due to ground backscatter. Clearly, the propagation conditions for this example were considerably more complex than those that existed for the afternoon data. It is our hope that the information provided by our second antenna array will eventually lead to an improved understanding of the propagation modes contributing to an image of this type.

After the raw autocorrelation functions have been corrected for bad lags, ground backscatter, and disturbance signals, they are Fourier transformed into Doppler velocity spectra. As an example of the spectral variations that are typically observed, Figure 15 represents some of the Doppler spectra that were obtained in conjunction with the power map of Figure 12. Due to the relatively short minimum lag of the multipulse pattern used and the relatively low frequency of operation (10.7 MHz), the Doppler spectra are unaliased out to a Doppler velocity of 2340 m/s. Although this may appear to be an extremely large aliasing velocity, it is not beyond the range of plasma drift velocities that have been measured at high latitudes (e.g., de la Beaujardiere and Heelis, 1984; Jorgensen et al., 1984). In the examples shown, all of the spectra have relatively narrow Doppler widths, with the spectra obtained to the east of a magnetic azimuth of 35° exhibiting positive Doppler shifts and those to the west exhibiting negative Doppler shifts. These characteristics are quite similar to those reported by Greenwald et al. (1985) for another example of afternoon HF backscatter. The spectral variations are consistent with a bulk irregularity motion directed slightly to the north of geographic west (-55 magnetic azimuth). The largest Doppler velocities

are observed on the eastern azimuths where the speeds approach 700 m/s. It should be noted that these values are relatively modest in comparison to other velocities observed with this radar (e.g., Hanuise et al., 1985; Baker et al., 1985).

A second example of Doppler spectra is shown in Figure 16. These data were obtained 30 April 1985 at 0311 UT (~midnight MLT). During this local time sector, one would expect to observe irregularities flowing out of the polar cap toward lower latitudes. The expected motion is entirely consistent with the positive Doppler displacements that are observed on all of the azimuths shown. In fact, positive Doppler values were obtained on all azimuths for which scatter was observed. Another interesting feature of this example is the appearance of significantly broader spectra at the highest latitudes. Doppler widths approaching 1200 m/s are observed in several examples.

As a final example of Doppler spectra observed with the Goose Bay radar, Figure 17 exhibits data that are observed near local noon in the vicinity of the dayside cusp/cleft. These data were obtained at 1642 UT (~1315 MLT) on 28 November 1983. Because this region is magnetically connected to the boundary of the Earth's magnetosphere, it is subject to particularly strong disturbances due to the interaction between the solar wind and the Earth's magnetic field. Spectra are presented for a large number of azimuths. The solid curves represent drift paths and are drawn to be roughly consistent with the observed Doppler variations. Each spectrum has been individually normalized to the amplitude of its largest Fourier component. Thus, only those spectra exhibiting a peak correspond to ranges from which there is significant backscattered power. While many of the spectra in the figure have widths ranging from 400-800 m/s, there are also a number of spectra exhibiting widths in excess of 1200 m/s. The latter group of spectra tend to occur at the highest latitudes and on the lowest beam numbers. The spectra on Beam 2 have been reproduced in the lower left-hand corner of the figure in order to more clearly display this spectral variation. For the local time of this measurement, the region most closely identified with the broad spectra would be the polar cusp.

SUMMARY

The preceding examples represent just a few of the many results that have been obtained to date with the JHU/APL Goose Bay HF radar. Recent publications include studies of irregularity formation and dynamics in the vicinity of the cusp/cleft (Baker et al., 1985; Walker et al., 1985b) and studies of irregularity drift motion derived from the radar Doppler data (Hanuise et al., 1985). In addition, several studies seeking to relate E and F region irregularity drifts with ionospheric plasma drifts are currently in progress.

The radar is capable of yielding unaliased autocorrelation functions and Doppler spectra of the backscattered signals from ionospheric irregularities. In the near future, it should also be capable of providing information on the approximate height and thickness of the scattering volumes. The angle-of-arrival information will also be of value in determining the relevant propagation modes in effect at any particular time. As the capabilities of the radar are quite unique for high latitude HF radar systems, the new information that will result from the Goose Bay measurements should be of value in the design of future radar systems.

REFERENCES

Baker, K.B., R.A. Greenwald, A.D.M. Walker, P.F. Bythrow, T.A. Potemra, D.A. Hardy, F.J. Rich, and C.L. Rino (1985), A case study of plasma processes in the dayside cleft, J. Geophys Res., in press.

Croft, T.A. (Guest Editor) (1968), Special issue on ray tracing, Radio Sci., 3, 1-119.

de la Beaujardiere, O. and R.A. Heelis (1984), Velocity spike at the poleward edge of the auroral zone, J. Geophys. Res., 89, 1627-1634.

Fejer, B.G. and M.C. Kelley (1980), Ionospheric irregularities, Rev. Geophys. Space Phys., 18, 401-454.

Greenwald, R.A. (1985), High frequency radiowave probing of the high latitude ionosphere, Johns Hopkins APL Tech. Dig., 6, 38-50.

Greenwald, R.A., K.B. Baker, R.A. Hutchins, and C. Hanuise (1985), An HF phased-array radar for studying small scale structure in the high latitude ionosphere, Radio Sci., 20, 63-79.

Hanuise, C., R.A. Greenwald, and K.B. Baker (1985), Drift motions of very high latitude F-region irregularities: azimuthal doppler analysis, J. Geophys. Res., in press.

Jorgensen, T.S., E. Friis-Christensen, V.B. Wickwar, J.D. Kelly, C.R. Clauer, and P.M. Banks (1984), On the reversal from "sunward" to "antisunward" plasma convection in the dayside high latitude ionosphere, Geophys. Res. Letts., 11, 887-890.

Walker, A.D.M., R.A. Greenwald, and K.B. Baker (1985), Determination of the fluctuation level of ionospheric irregularities from radar backscatter measurements, submitted to Radio Sci.

Walker, A.D.M., R.A. Greenwald, and K.B. Baker (1985), HF radar observations of pulsations near the magnetospheric cusp, submitted to J. Geophys. Res.

ACKNOWLEDGMENTS

The JHU/APL Goose Bay HF radar has been developed through support from the National Science Foundation and the Air Force Office of Scientific Research under NSF Grant ATM-8216571 and through support from Rome Air Development Center and the Defense Nuclear Agency under Contract N00024-83-C-5301 of the Naval Sea Systems Command. Support for this work was provided by the above grant and contract. We also wish to thank the Air Force Geophysics Laboratory for the use of the site and J. Kelsey and his coworkers of Canada Marconi for their support in the daily operation of the radar.

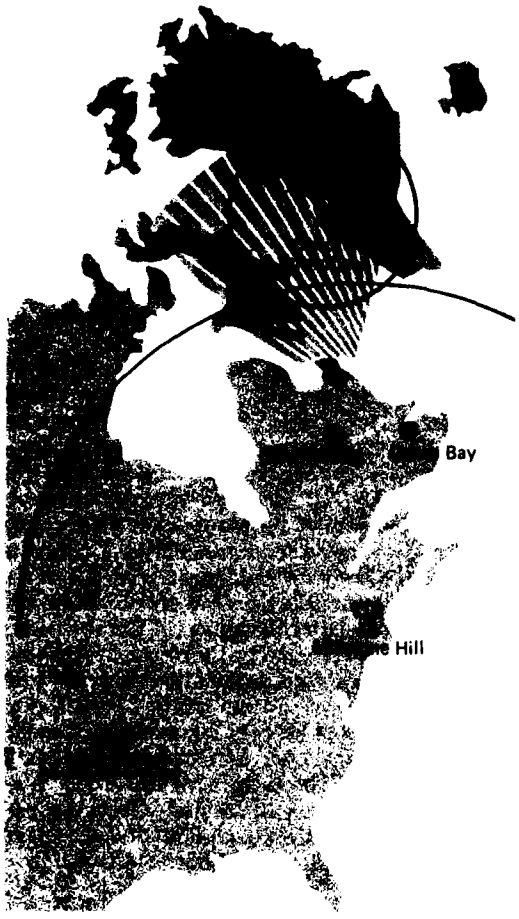


Figure 1 Field-of-view of the JHU/APL HF radar at Goose Bay, Labrador. The radar may be pointed into any of 16 possible viewing directions. Also shown on the figure are the nominal fields-of-view of the Sondre Stromfjord and Millstone Hill incoherent scatter radars and the field-of-view of a French HF radar presently being constructed at Schefferville, Quebec.

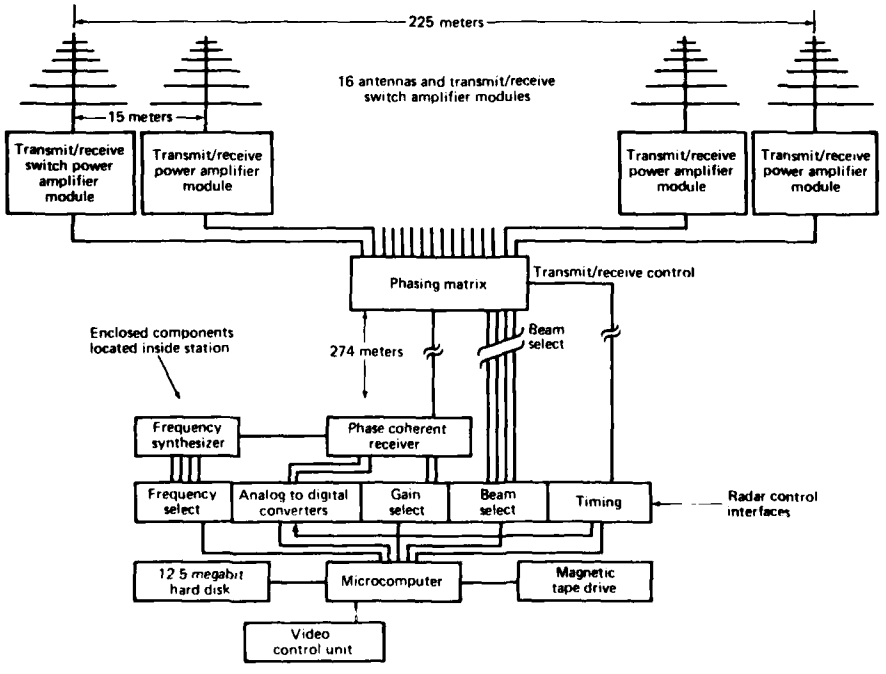


Figure 2 Schematic diagram of Goose Bay radar prior to installation of second antenna array. See text for details.



Figure 3 Photograph of Goose Bay antenna array showing 3 antennas of original array in foreground and 7 antennas of receive-only array in background. Also shown is the shed which houses the phasing matrix and power supplies.

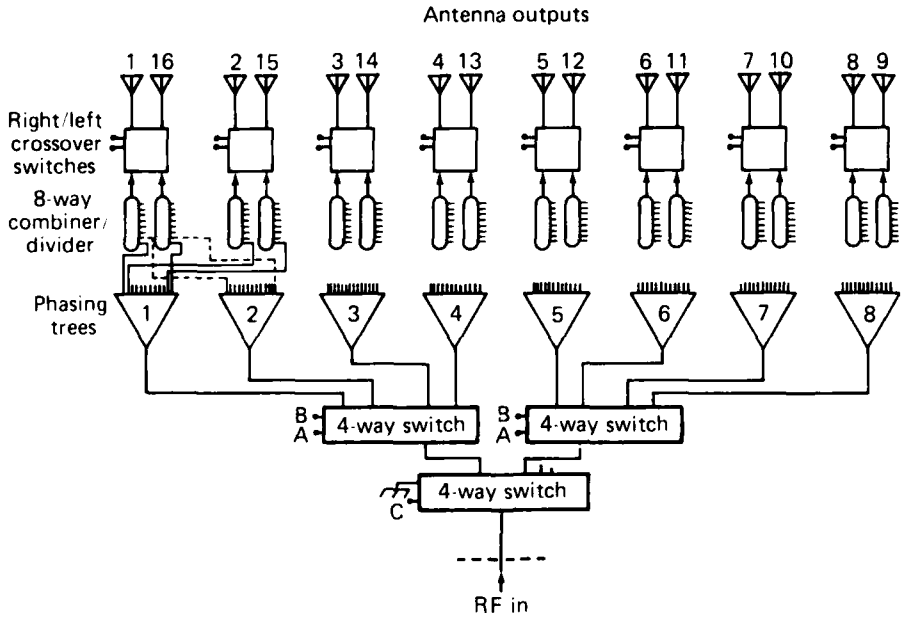


Figure 4 Schematic diagram of phasing matrix. The "phasing trees" establish the progressive phase lag between antennas, the 4-way switches select the phasing tree, and the crossover switches determine whether the beam is directed to the right or left of the array normal.

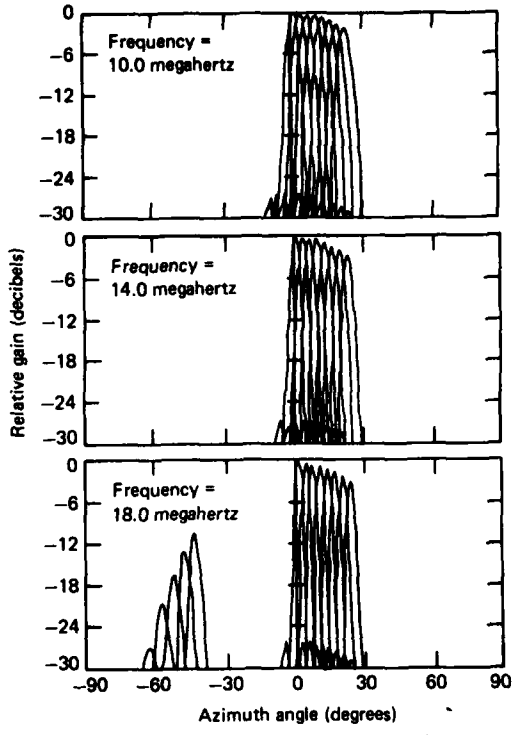


Figure 5 Theoretical two-way azimuthal patterns for the eight lobes to the right of the array normal for several frequencies. Lobes at negative angles for the 18 MHz case are grating sidelobes of the rightmost lobes. A mirror image of these patterns exists to the left of the array normal.

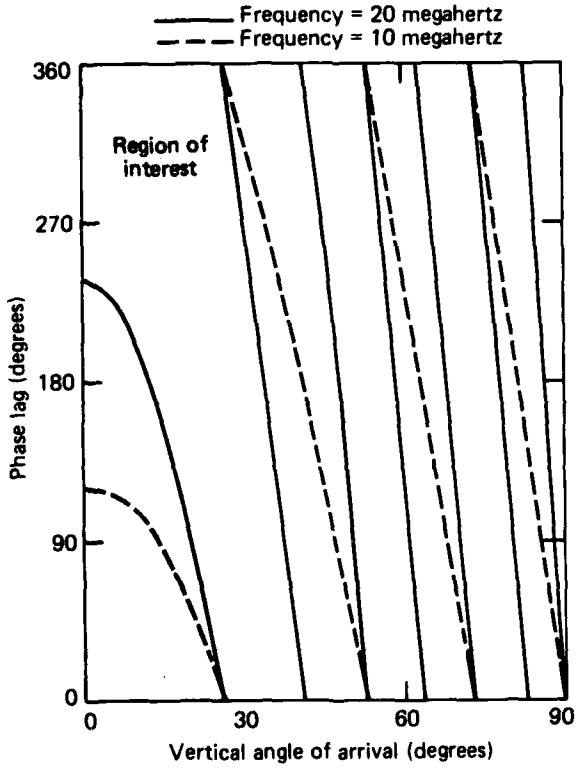


Figure 6 Plot of phase lag versus vertical angle-of-arrival for signals incident on two antenna arrays separated by 100 m along the direction of propagation. Curves are given for frequencies of 10 and 20 MHz.

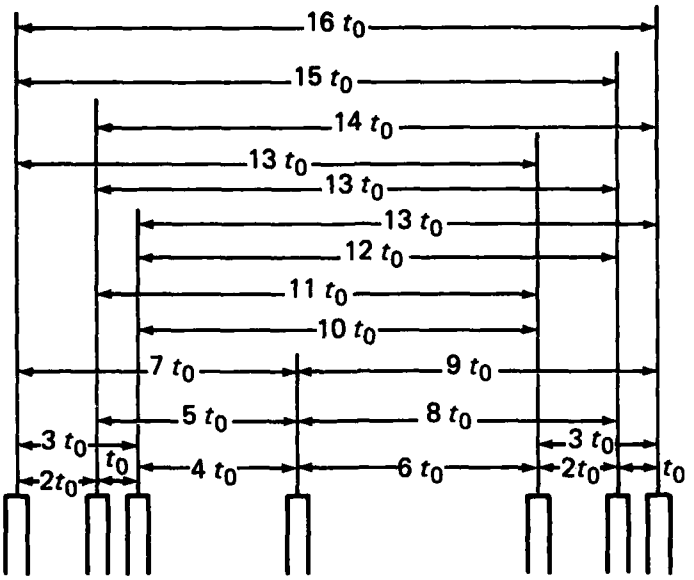


Figure 7 Seven-pulse transmission sequence used for the determination of 17-lag autocorrelation functions of the backscattered signals. From the autocorrelation functions, one can derive Doppler spectra by Fourier transformation.

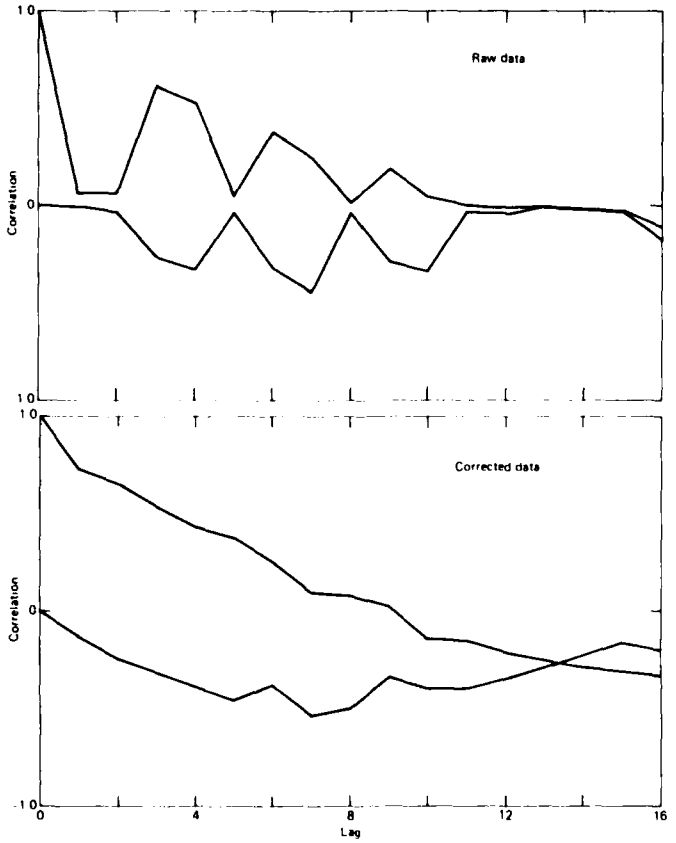


Figure 8 Upper: Example of autocorrelation function of backscattered signal from a range that is seriously disturbed by sample gates occurring during transmitter pulses (see text). Lower: Example of same autocorrelation function after the bad lags have been corrected.

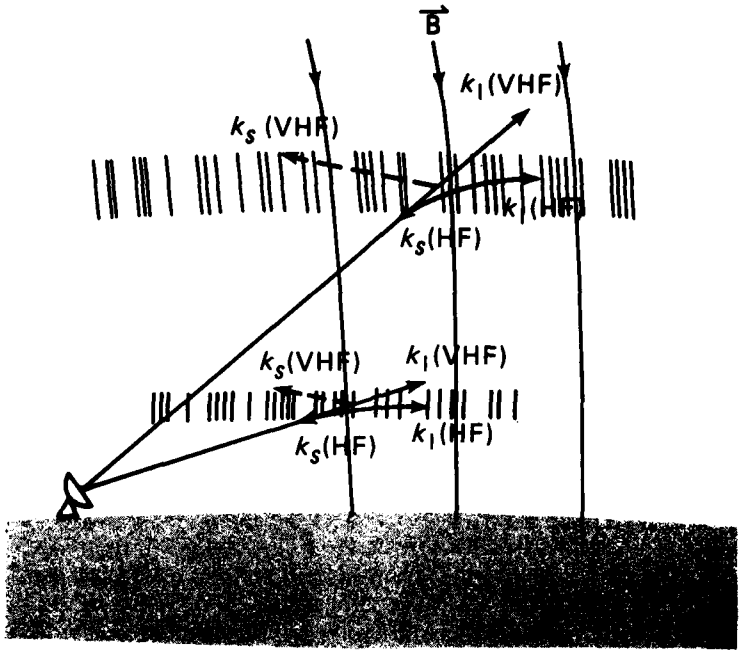


Figure 9 Illustration of the manner in which VHF and higher frequency radar signals are scattered into space by very high latitude E- and F-region electron density irregularities. At HF the signals are refracted toward the horizontal as they enter these two ionospheric layers. If they are propagating normal to the magnetic field when they encounter a region of irregularities, the scattered signals will return to the radar.

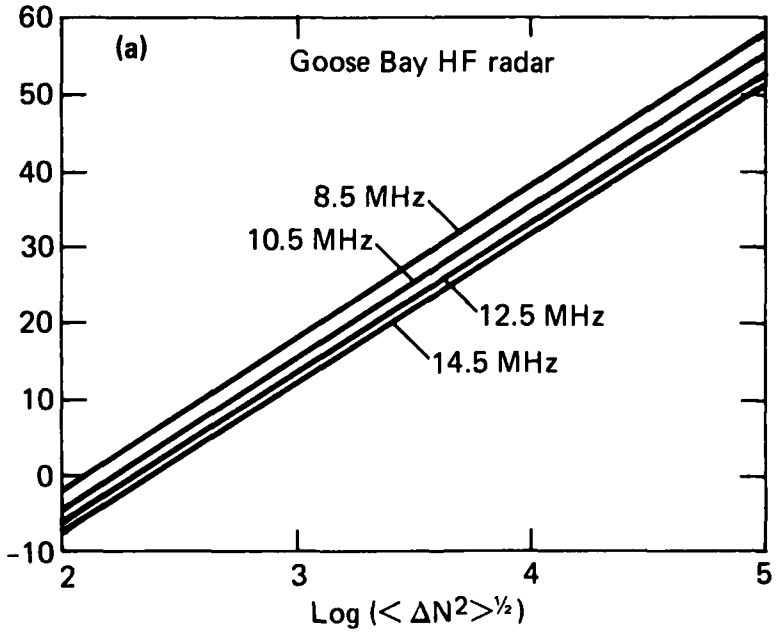


Figure 10 Sensitivity of the Goose Bay radar to ionospheric electron density fluctuations in the range from 10^2-10^5 cm $^{-3}$.

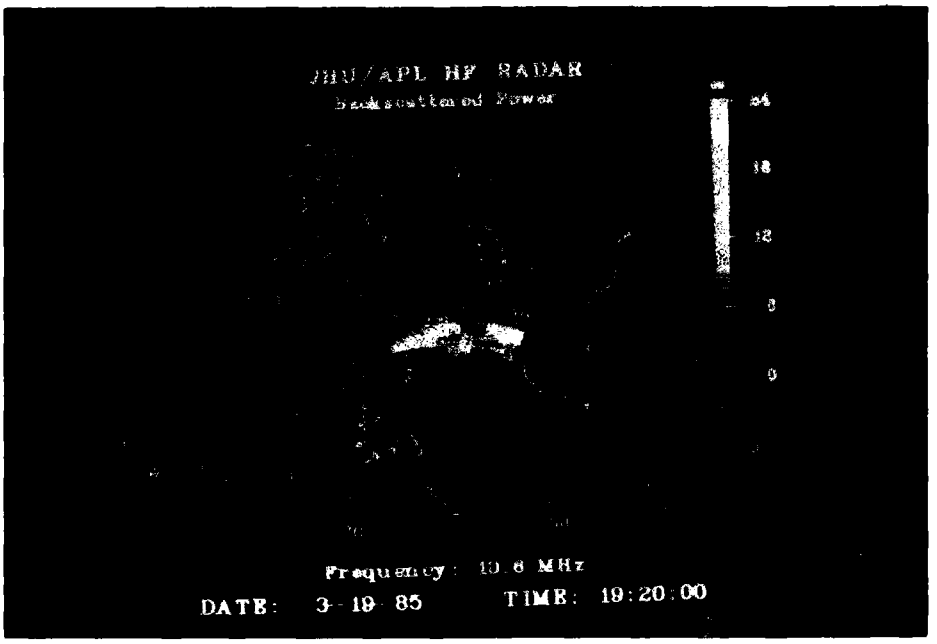


Figure 11 Backscatter power image obtained with the Goose Bay radar at 1920:00 UT (~1600 MLT) on 19 March 1985.

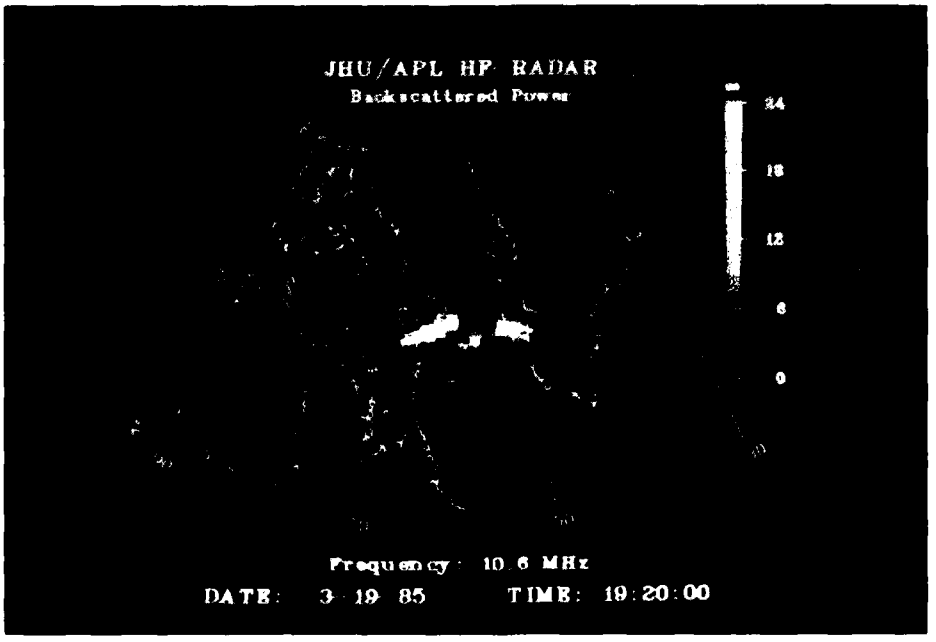


Figure 12 Same backscatter power image as Figure 11 except that contributions due to ground backscatter have been removed.

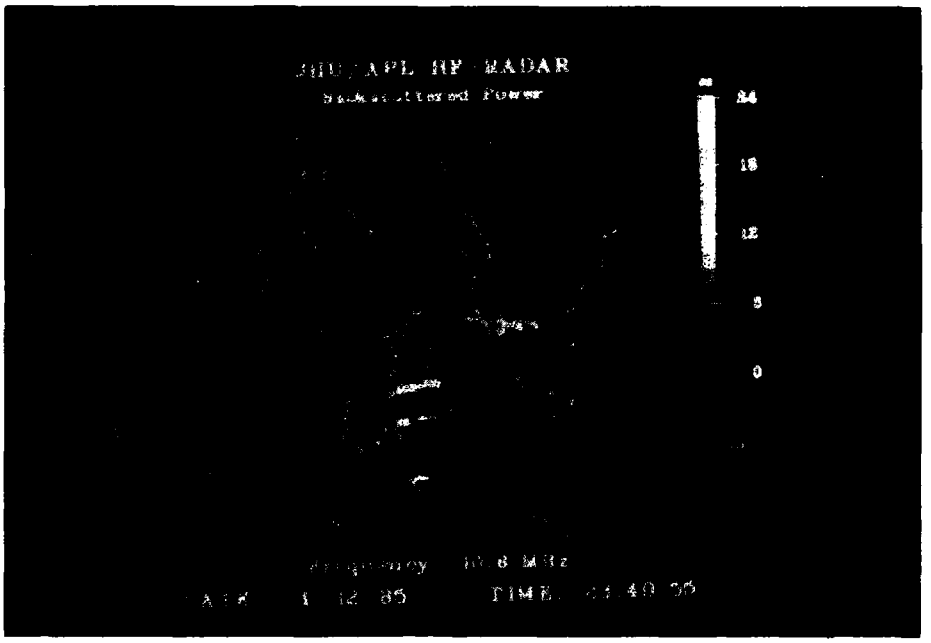


Figure 13 Backscatter power image obtained with the Goose Bay radar at 2340:55 UT (~2015 MLT) on 12 April 1985.

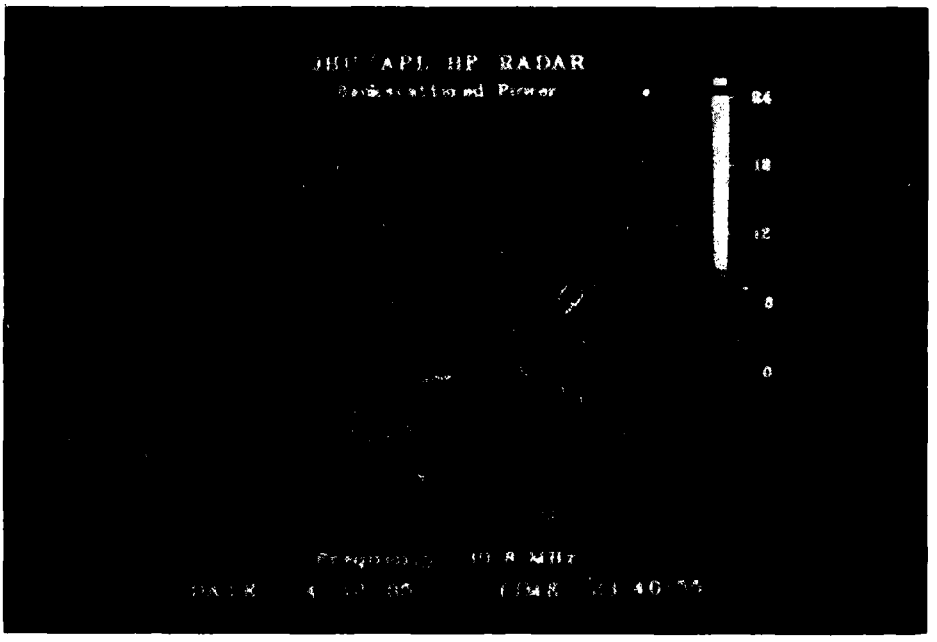


Figure 14 Same backscatter power image as Figure 13 except that contributions due to ground backscatter have been removed.

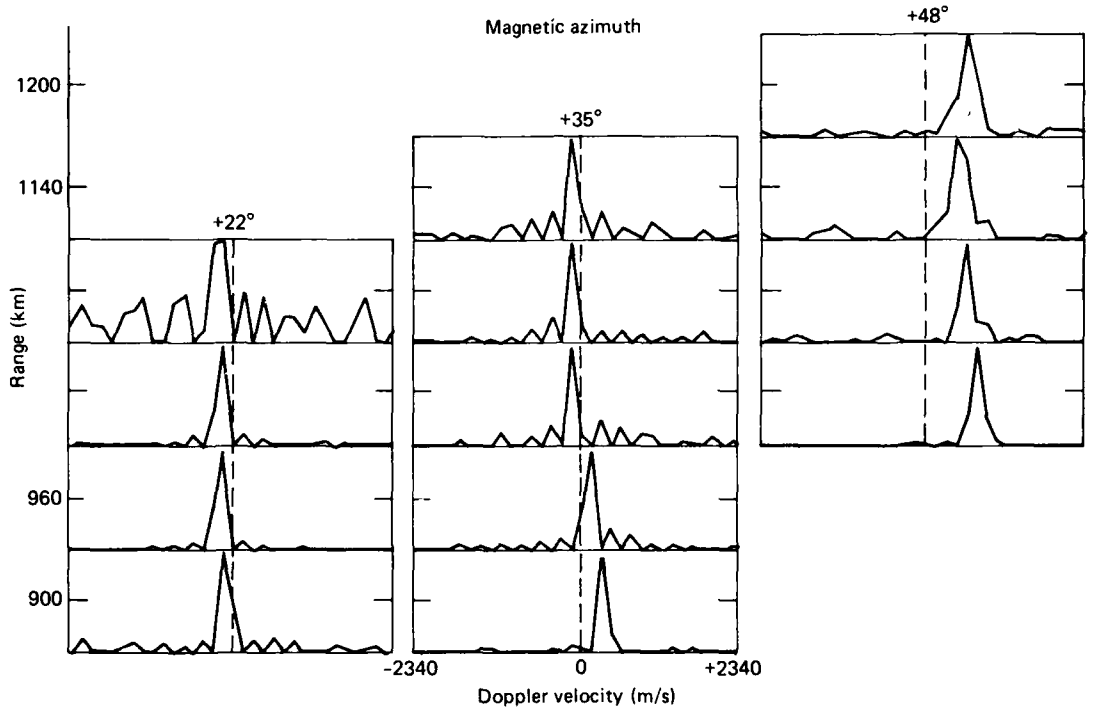


Figure 15 Examples of Doppler spectra associated with the backscatter power image of Figure 11. Each spectrum is plotted linearly in power and normalized to the power in the largest spectral component. The magnetic azimuth of 35° is directed 3° to the east of magnetic north. Note that the spectra are relatively narrow and vary in a manner that is consistent with a westward irregularity drift.

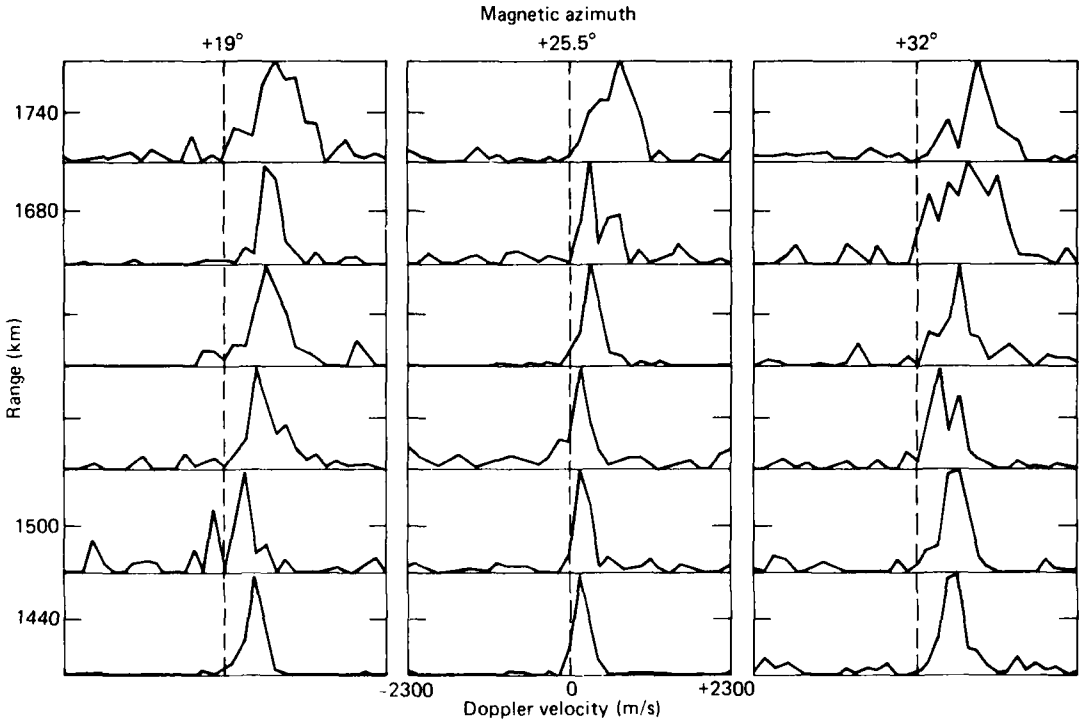


Figure 16 Examples of Doppler spectra that were obtained at 0311 UT (~magnetic midnight) on 30 April 1985 at a frequency of 10.7 MHz. Note that the spectra are appreciably broader than those in Figure 15 and that they have Doppler shifts consistent with irregularity flow out of the polar cap.

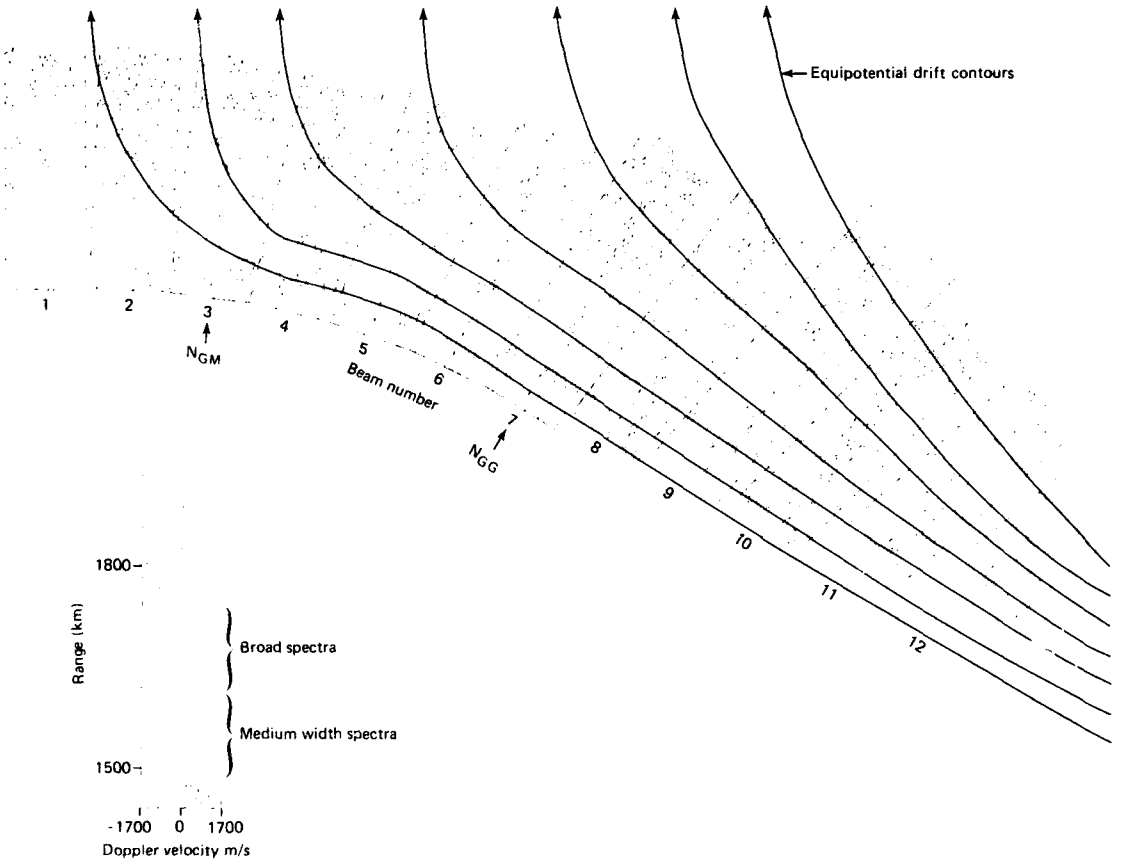


Figure 17 Examples of Doppler spectra obtained at 1642:05 UT (~1300 MLT) on 28 November 1983 at 14.5 MHz. The solid curves represent irregularity drift paths that are consistent with the spectral observations. Note that a number of spectra have widths in excess of 1200 m/s.

DISCUSSION

G.Prolss, GE

Are any correlations observed between the E-field magnitude derived from ion-drift measurements and the backscatter amplitude? And, if yes, do they shed light on possible excitation mechanisms for the observed irregularities (plasma instabilities)?

Author's Reply

For E-region irregularities correlations have been observed between derived plasma drift velocity and irregularity strength. This is consistent with their nature as plasma streaming instabilities. In the F-region, much less is known about the nature of the small scale structure and the correlation studies have not yet been made. It has been observed on one occasion that strongest backscatter is observed when one looks perpendicular to the drift direction.

N.C.Gerson, US

Because of the dynamic nature of the polar ionosphere there must be occasions when other than the midnight sector, sudden, marked changes occur. Have any been observed?

Author's Reply

I am sure that there are many examples within our data base where sudden ($<$80S) variations can be observed in the radar backscatter and Doppler images. I feel that most of these variations will be limited to a portion of the field of view rather than the field of view as a whole. Very large scale variations tend to occur on time scales of several minutes or longer.

J.Belrose, CA

I would like to comment on the difference in the geometry and the nature of the auroral backscatter that we have studied at Ottawa, compared with your experiments. In our experiments we employed a large sampled aperture receiving array (SARA) at Ottawa, and a USAF HF transmitter at Rome, NY. We used vertical monopoles with elevated feed for receive, and a rhombic for transmit. Our HF backscatter came from a region fairly *restricted* in longitude, centered on magnetic north, from a region within the Feldstein auroral oval for the particular magnetic activity at the time of the observation (i.e. at corrected geomagnetic latitudes, CGL $\leq$70°). Observations that fell outside the region where the ray path was greater than about ±10° off normality were considered to be due to the side lobe response of our antenna system. This problem was very carefully studied by my colleague, L.E.Montbriand. The geometry of your experiments, and the frequencies that you have used result in backscatter being observed well north of the auroral oval, at CGL ~75°. I must say however, I am puzzled by the apparent longitudinal extent of the backscatter that you see. Concerning time variability of backscatter, this is short, seconds or less.

Author's Reply

I find your comment to be quite interesting and it indicates to me that the Goose Bay radar is apparently operating quite successfully. Let me begin by noting that the Feldstein oval is located at much higher latitudes on the dayside than it is at night. In particular, near noon it is co-located with the polar cusp/cleft. Moreover, the poleward boundary of the Feldstein oval is closely related to the boundary between sunward and antisunward convection. In the afternoon and morning local time sectors most of our observations exhibit Doppler variations that are consistent with sunward convection, indicating that the irregularities are located equatorward of the convection reversal boundary and presumably equatorward of the poleward boundary of the Feldstein oval. Thus, I would say that during these periods much of what we observed is in the high latitude auroral zone. Also, during these periods much of the backscatter that we observe extends across our field of view for distances of 800—1200 km. On the extreme beams of our array the scatter can be weaker or unobservable. We relate this to reduced antenna sensitivity and to a greater difficulty in obtaining sufficient refraction to achieve good aspect angle sensitivity.

I should also note that during the afternoon and morning periods one can observe regions of backscatter that do not extend across the field of view. Also, in the nighttime sector, where I presume you made many of your measurements, the scattering regions tend to be more localized. I showed an example of more patchy regions of backscatter in my presentation. Presumably this higher degree of patchiness is due to the increased latitudinal and longitudinal ionization structure in the nighttime sector.

With regard to your comment on temporal variability. If one concentrates on a localized region, there can be appreciable variation on time scales of a few seconds. However, if one ignores the embedded fine structure the larger scale features that I showed in my presentation can be roughly constant, for periods ranging from several minutes to several hours.

Observations of the mid-latitude ionospheric trough from Antarctica

by

F. T. Berkey
Center for Atmospheric and Space Sciences
Utah State University
Logan, Utah 84322

and

M. J. Jarvis
British Antarctic Survey
NERC, Madingley Road
Cambridge, CB3 0ET
United Kingdom

ABSTRACT

Measurements of the ionosphere using two identical digitally controlled high frequency radar systems have been conducted in the Antarctic from Halley and Siple Stations. These stations are uniquely sited, both having essentially identical coordinates of geographic and geomagnetic latitude. Furthermore, due to the large offset of the geographic and magnetic poles in Antarctica, the difference in magnetic local time is less than half the separation in local solar time. In this study, the locations of the minimum and poleward edge of the trough have been found for magnetically quiet intervals and mapped into invariant latitude. Simultaneous measurements of the trough location from Siple and Halley have been compared using magnetic, local and universal time coordinates. For geomagnetically quiet conditions, this analysis suggests that the invariant latitude of the poleward edge has a Universal Time dependence prior to local midnight.

The presence of the ionospheric trough introduces a further degree of complexity to the subauroral ionosphere which, in turn, complicates automatic realtime processing of digital ionograms. Several examples of a technique termed elevation angle filtering are presented and the effect of the presence of the ionospheric trough on this process is examined.

1. INTRODUCTION

A unique feature of the sub-auroral ionosphere is a region of anomalously low electron density at F-region heights. This region, which is commonly referred to as the main or mid-latitude trough, was first discovered during the mid-1960's in measurements made aboard polar orbiting satellites (1,2,3,4). This same feature was subsequently identified in data obtained by ground-based techniques, such as the total electron content measurement and ionospheric sounding (5,6). Recently, a comprehensive review of the observational and modelling results pertaining to the mid-latitude trough has been presented by Moffett and Quegan (7) and the reader is urged to consult this work for detailed references to a large body of earlier work.

The following list was compiled by Moffett and Quegan and summarizes those aspects of the mid-latitude trough about which there is general agreement:

1. The mid-latitude trough is primarily a nightside phenomenon extending in a band from the dusk sector to the dawn sector. It is most frequently observed when the solar zenith angle exceeds 90°. Troughs of the mid-latitude type have also been observed in the noon sector.
2. The trough is most regularly observed during winter and equinox; in summer it is only observed near local midnight.
3. The poleward edge of the trough, usually seen as a sharp increase in electron concentration, lies just equatorward of the boundary of diffuse auroral precipitation. The poleward edge is usually steeper than the equatorward edge.
4. The latitude of the trough decreases through the night. At quiet times there may be a movement back toward higher latitudes in the dawn sector.
5. During periods of increased mangetic activity the trough moves to lower latitudes.
6. The occurrence of the trough and the validity of the previous points do not depend markedly on solar cycle variations.

Moffett and Quegan also point out that there are certain aspects of the trough about which there is no general agreement, such as its width or depth and the local time at which the minimum density occurs. Questions of this nature will be examined in this paper.

The Antarctic region is unique because of the large displacement of the South magnetic pole from the geographic pole (8, 9, 10). This displacement causes differences of as much as 25° between the dip and invariant coordinate systems in certain sectors of the Antarctic. To quote from Dudeney and Piggott (10), "the Antarctic offers unique opportunities for resolving complex magnetospheric-ionospheric interactions in which both classes of mechanisms are involved and separating these from phenomena determined by geographically controlled processes."

Aeronomical research has been carried out in Antarctica by many of the Treaty nations since the International Geophysical Year (11). Recently, two identical HF Radar systems were installed in the Antarctic, one at Siple Station (by Utah State University) and the other at Halley (by the British Antarctic Survey). The HF Radar at Halley (referred to as an Advanced Ionospheric Sounder) has been operating continuously since 1981, whereas the Siple radar was operated during 1982 and 1983 and will be reactivated during 1986 and 1987 (Siple Station was closed in 1984 and 1985). Siple Station was established in 1971 (and manned in 1973) by Stanford University primarily in order to stimulate wave-particle interactions in the magnetosphere using VLF waves (12). The station was established at the approximate magnetic conjugate of Roberval, Quebec in the Northern Hemisphere. Fortuitously, Siple was sited at essentially the same latitude in both the geographic and invariant coordinate systems as the British Antarctic Survey base at Halley. No other station pair in either hemisphere is comparably situated. Siple Station (75.94°S, 84.25°W L=4.2) is situated in Ellsworth Land, while Halley (75.52°S, 26.62°W L=4.2) is located on the Brunt Ice Shelf, on the eastern flank of the Weddell Sea. In solar time, Siple and Halley are separated by approximately four hours, but the separation in magnetic time is much smaller, of the order of 1.5 hours. A map of Antarctica upon which invariant magnetic time coordinates have been superposed is presented in Figure 1. As will be shown in the following discussion, the measurements from each station can be ordered and compared in different time frames.

This paper will focus on the results of the analysis of several periods of radar data acquired at Halley and Siple Station during the austral winter of 1982. Analysis has concentrated on three magnetically quiet intervals when both radar systems were operational. These periods are: 22-23 May, 3-4 July and 14-15 August 1982.

2. EXPERIMENTAL DETAILS

The NOAA HF Radar is a digitally controlled high-frequency radar designed and constructed by the Space Environment Laboratory of the National Oceanic and Atmospheric Administration (13). The radar measures the time of flight, phase, and amplitude of transmitted radiowaves reflected from the ionosphere over the frequency range between 100 kHz and 30 MHz. Echoes are measured simultaneously using pairs of dipole antennas aligned in the north-south or east-west planes. Each pair of antennas is connected to a separate phase coherent receiver channel, the outputs of which are combined by the computer to form an interferometer. The spatial location and polarization of each echo can be derived from the interferometer measurements. These parameters are computed knowing the radar wavelength and the phase difference of the echo wavefront incident on each dipole antenna of a given pair. Hence, the excess path length to one antenna that the echo wavefront must traverse if the wavefront is not normally incident on the array, can be determined. The displacement of the echo from the zenith, in each plane of the receiving array, is found from the ratio of the echo range to the antenna separation, multiplied by the excess path length. The azimuth and elevation angles of the echo are found by simple trigonometry and the polarization by the relative phase in the two planes.

All of the functions of the radar are controlled by the computer, which can also be programmed to follow a detailed operating schedule. A typical operating schedule combines both the swept frequency (ionosonde) and fixed frequency sounding modes. In the fixed frequency mode, up to 10 individual frequencies can be sampled, although in practice no more than three or four frequencies are selected. This mode of operation can be used to track various features of the ionosphere if the operator has selected appropriate frequencies. A combination of the two modes can be used to obtain nearly continuous ionospheric measurements. Such measurements were made during the 14-15 August interval when a common operating schedule was programmed at both stations. A realtime display allows the operator to monitor the current sounding; the operating parameters of the radar can be interactively changed so as to optimize data quality.

While identical radar systems were installed at both stations, different types of transmitting antennas are used and the length and spacing of the dipole receiving antennas differs. Since these differences have an effect on the relative sensitivity of the two systems, they are worthy of note. At Siple Station, the transmitting antenna consists of a traveling-wave dipole (14) 670 meters in length while a vertex-down log-periodic antenna, having a maximum element length of 34 meters, is used at Halley. The dipole receiving antennas used at Siple are 29.3 meters in length, configured in a square the sides of which are 100 meters. At Halley the receiving antennae are 5 meters in length and are separated by 30 meters. The net effect of the different transmitting and receiving antenna configurations is that the radar system at Siple attains a somewhat greater

sensitivity at frequencies below about 2 MHz. At these frequencies, the difference in received signal strength is estimated to be of the order of 10 dB. Another noteworthy difference between the two stations is the distance to electrical ground; Halley is situated on the Brunt Ice Shelf where the distance to ground is approximately 170 meters. Siple Station's location in Ellsworth Land is farther inland where the ice thickness is approximately two kilometers. Since ice is a very good attenuator at radio frequencies (15), Siple is located above an efficient absorbing layer and thus second hop echoes (signals reflected twice from the ionosphere with an intermediate ground reflection) are far less frequently observed at Siple than at Halley.

3. OBSERVATIONS

The three intervals used in this investigation occurred during the three magnetically quietest periods of the entire 1982 austral winter. The K_p values for the preceding day and the day used in the analysis are shown in Table I. Magnetometer, riometer and VLF data from both stations have been examined and were found to be representative of quiet conditions. The VLF records show persistent multi-path whistlers with no indication of knee whistlers, which would imply that the plasmapuase was located considerably poleward of L≈4.

In order to illustrate the ionospheric signatures typically associated with the occurrence of the mid-latitude trough, an ionogram recorded at Siple Station at 0630 UT on 15 August 1982 is shown in Figure 2. The two distinct features present in the F-region are a highly spread region between 1.1 and 7 MHz and a region of significantly lower critical frequency which extends from 1.0 to 1.25 MHz. The latter signature is identified as the minimum of the mid-latitude trough. The region, characterized by extensive range spreading, is generally considered to represent the poleward or (less frequently) the equatorial edge of the trough and is generally separated by one or two degrees of latitude from the trough minimum (see Figure 3). Frequently, the poleward edge of the trough can be detected at large ranges either at the onset or end of a trough sequence. The F-region signature at these times is similiar to that modelled by Hoeg and Ungstrup (16) which they have termed an oblique reflection trace.

An example which illustrates the capability of the radar to track the location of the trough is shown in Figure 4. In this diagram, the center column contains fixed frequency data which show (starting from the top) the north-south and east-west echo displacement, the echo range, echo amplitude and radial doppler velocity, as a function of time. Note that no averaging has been done and each point has been derived from an individual echo. The trough minimum was tracked until 0116 UT at which time the plasma density decreased below the probing frequency (2.1 MHz) and the trough minimum echo was replaced by the poleward edge as the dominant echoing region. The two columns of ionograms show the gradual decrease of critical frequency and hence plasma density near the trough minimum and a corresponding increase of density within the poleward edge. At the time of the transition between echoing regimes, the trough minimum was located about 100 km north (i.e. equatorward) of Siple while the poleward edge was approximately 180 km south.

Angle-of-arrival measurements are also obtained for swept-frequency soundings and, for this study, each individual ionogram was subjected to an analysis technique which computes the echo location and corrects the data for angle-of-arrival aliasing. This technique, developed by the BAS, is discussed in detail by Dudeney and Jarvis (17). The echo location was then converted into invariant latitude for an altitude of 250 km using the IGRF magnetic field model for epoch 1980. Here, the derived echo location is an average value obtained from a large number of echoes. Several examples of the ionograms used in the analysis are shown in Figures 5 - 8. Each figure contains four ionograms, one from Halley and three from Siple. The two ionograms on the top row have been recorded at the same Universal Time (UT); Halley ionograms (on the left in each Figure) are annotated in local meridian time while the Siple ionograms are in UT. The bottom row contains Siple ionograms at times which correspond to the same magnetic local time (MLT) and the same solar time (bottom right) as the Halley ionogram. In local solar time (LT), Siple and Halley are separated by 3 hours 50 minutes but in magnetic time coordinates, the separation is much less (approximately 1.5 hours). The small arrows at the bottom of each ionogram denote the start and end frequencies of the sweep.

The Halley ionogram shown in Figure 5 illustrates an example of the oblique reflection trace (16) frequently seen in both Halley and Siple data. Usually, as in this example, only part of the trace appears. In this case, the flat trace between 3 and 8 MHz at a range exceeding 600 km was present for more than two hours. The trough minimum echoes are often quite complex, exhibiting both spread and multiple reflections (see Figure 6 at 0400 UT). At Siple echoes were recorded from 225 kHz on both 22-23 May and 4-5 July. These echoes are generally quite weak and therefore cannot be used to obtain angle-of-arrival information.

In Figure 9, the location of the trough minimum and poleward edge have been plotted in UT (top panel), MLT (center panel) and LT (lower panel) over a 15 hour interval on 22-23 May 1982. These data show that the trough minimum remained nearly constant in latitude throughout most of the night near L≈4. In contrast, the poleward edge moved approximately 7° equatorward (from 70°S to 63°S)

over the same time period. At Halley the radar was operated in a mode which doubled the normal sounding range to 1500 km and on this date the poleward edge was first observed at a range of about 1200 km. The Siple radar was operated using the normal sounding format. A weak magnetic disturbance (≈30nT displacement in the Siple H-component), which occurred between 01 and 04 UT on May 23 did not have any significant effect on the latitude of either the poleward edge or the trough minimum as observed from either station. When the same data are plotted in MLT and LT, the derived locations of the poleward edge from the two data sets are less coincident than they are when organized in UT.

Measurements from 3-4 July and 14-15 August were analyzed in the same manner and a summary diagram is presented in Figure 10. As shown in the bottom panel of Figure 10, the results obtained from Siple for the location of the trough minimum and poleward edge are remarkably consistent for each of the three days. The trough minimum was generally equatorward of Siple and confined in a range between 59.4°S and 61.8°S invariant latitude. Except in the early evening hours, the poleward edge was approximately 2° south of Siple and varied between 62.6°S and 64°S latitude. The results of the analysis using Halley data are somewhat less ordered as displayed in the top panel of Figure 10. Both the trough minimum and the poleward edge had a much larger dispersion in latitude, with the minimum being observed over a range of 6.5°. The dispersion in the Halley data is largely due to the trough location on 14-15 August being farther equatorward.

An average location for both the trough minimum and the poleward edge was derived for each of the three days of observations and plotted in UT, MLT and LT (Figure 11). When the data from both stations are plotted together in the local time frame (lower panel), there is reasonable agreement in invariant latitude after local midnight, but no correspondence before that time. In the UT frame (top panel) there is a close correspondence in the shape of the curves with the locations derived from Halley being generally lower in latitude. Finally, when the data are compared in a local magnetic time frame (center panel), there is a closer agreement after 2200 MLT than before.

These data, which extend over 15 hours of MLT, show that the average separation between the minimum and the poleward edge of the trough is approximately 275 km after 21 hours MLT. Before that time, the separation is considerably larger, ranging from 500 to 750 km. Assuming that the minimum is nearly equi-distant from both the poleward and equatorial edges of the trough, then the width of the trough varies from 1500 km in the early evening to 550 km in the midnight and morning sectors. The latter value is consistent with trough widths derived from satellite measurements.

4. DISCUSSION AND CONCLUSIONS

Modelling studies of the high-latitude ionosphere have shown that the mid-latitude trough is formed as a result of several competing physical processes (18, 19, 20). Which of these various processes plays a dominant role cannot be determined without having experimental observations as a guide. Simultaneous observations at a large number of longitudes is obviously ideal but, of course, not practical in either the Northern or Southern Hemispheres. Siple and Halley are located at high geographic latitude so that there are long periods without solar ionization during mid-winter, and are situated in longitude such that the trough can exist overhead for many hours. Halley, in particular, should see the trough longer than Siple since it is located nearly diametrically opposite the invariant pole. By the same argument, the depth of the trough should be greater at Halley.

The results obtained from Siple and Halley observations during three geomagnetically quiet intervals during the austral winter of 1982 have been summarized in Figure 12. The dashed line represents the average latitude of the trough minimum and poleward edge observed from Halley; the three solid lines show the latitudinal variation of these features at the same UT (diamond), the same LT (circle) and the same MLT (square) as measured from Siple. Presuming that the poleward edge is, in fact, ionization associated with the auroral oval, then the observed equatorward motion of the region is consistent with the rotation of the station with respect to the oval. A poleward retreat in the morning sector is not expected (and **not** observed) since the auroral ionization will corotate at approximately the same latitude, slowly decaying with time. Also included in this diagram are the locations of the poleward edge and trough minimum calculated from the empirical formulas of Halcrow and Nisbet (21) and Spiro (22). These curves have been derived using K_p=1 in the formulation. It is clear that neither empirical relationship exactly fits the observations, although the Halcrow and Nesbit curve has a reasonable agreement before local midnight. The inclusion of a dependency on UT or longitude is clearly necessary if these formulae are to be used for predicting trough location.

For quiet times, the results obtained here suggest that the poleward edge has a UT dependence, although it is not clear that the same dependency holds for the trough minimum. A UT dependency of the trough is a prediction of the modelling studies and a UT effect in F-region densities has been found in a number of previous experimental studies (23, 24, 25, 26). In the Southern Hemisphere, an 06 UT maximum in f_0F_2 was first reported by Knecht (24). Further analysis by Sato and Rourke (25) showed statistically that the increase in f_0F_2 occurred most frequently between 04 and 09 UT.

Recently, incoherent scatter radar measurements at three widely separated longitudes in the Northern Hemisphere have shown a pronounced UT effect in F-region electron densities (26). In the latter results, the largest density occurred in the 18-20 UT sector with a minimum occurring at 04 UT.

While longitudinal differences in electron density appeared in the data examined in this study, no definite trend could be recognized. On each of the three days used in the analysis, times when either the trough minimum or poleward edge densities were noticeably smaller at one of the two stations, could be found. This null result may arise from the relatively small longitudinal separation of the two stations or the small data sample. In fact, trough data may not be suitable for studying longitudinal effects because ray-tracing simulations (27,28,29) have shown that the local geometry of the trough can affect the penetration frequency at the trough minimum.

Appendix A: Elevation angle filtering of digital ionograms in the presence of Spread-F

In certain military applications of digital HF radars, it is required that the radar system be capable of automatically providing an ionogram which can be utilized to determine the vertical distribution of electron density. Algorithms which derive the electron density profile using ionograms have been the subject of considerable investigation (30, 31, 32, 33). These algorithms have been developed to the point that, using a suitably fast processor, the electron density profile can be derived from an ionogram in near realtime. However, one requirement of the true-height analysis technique is that a relatively "clean" ionogram be used as input. Ionograms which exhibit spread-F are not suitable for true-height analysis without some means of reducing the range or frequency spread inherent in the ionogram. Digital data, in which the direction-of-arrival, amplitude and doppler shift are derived, can be subjected to variety of techniques in order to reduce spread. A somewhat different approach to this problem for digitial ionograms acquired by the Digisonde (34) has been discussed by Reinisch and Xueqin (35).

Digital data from the NOAA HF Radar were used in attempting to find a technique which could automatically be applied to all spread F data. The very simple technique of filtering in elevation angle was found to be quite effective in producing a relatively clean trace in the presence of spread-F. Several examples of this technique are included here to illustrate its effectiveness. The data used in these examples were obtained at auroral and sub-auroral locations in both the Northern and Southern Hemispheres.

The number distributions of echoes as a function of elevation angle shown in Figure A-1 were derived from ionograms acquired during quiet, spread and trough conditions. Each distribution has been compiled from several ionograms and is representative of the various conditions. Under quiet conditions, the distribution exhibited a maximum near 86° with a half-maximum width of approximately 5° (Figure A-1(a)). Under ionospheric conditions when the F-region exhibits spread, echoes tend to occur at smaller elevation angles and the width of the half maximum increased. As shown in Figure A-1(b), the distribution maximized near 82°and the half-maximum width was about 12°. Several occurrences of the mid-latitude ionospheric trough were examined using data from both Siple Station and Halley. The very broad (25°) distribution shown in Figure A-1(c) having a maximum near an elevation angle of 79° is indicative of the ionospheric complexity which can occur when the trough is present.

Figures A-2, A-3 and A-4 illustrate the effect of an elevation angle filter on data acquired during severe spread-F. In each sequence, the first ionogram is unfiltered (i.e. all echoes with elevation angles greater than 30°) and following ionograms show the results of applying filters with increasing elevation angle discrimination. At 80° a relatively clean ionogram is obtained; however, an even cleaner ionogram can be obtained if a polarization filter is applied to the data. In the last of each set of examples, only echoes satisfying the criteria for ordinary or extra-ordinary mode polarization have been passed by the filter.

Figures A-5 and A-6 illustrate two instances when the mid-latitude ionospheric trough was overhead of the observing station. These data are from two of the days used in the preceding trough analysis. The data show that, in the presence of the trough, the overhead ionosphere will be represented by the feature closest to the station. For example, in Figure A-5 from Halley Bay, the poleward wall of the trough was closer to the station than the trough minimum and when an 80° filter was applied, the trough minimum signature essentially disappeared. In the example taken from the Siple Station data (Figure A-6), virtually the opposite situation was observed. That is to say, the trough minimum was closer to the transmitter than was the poleward edge and was the dominant feature at large elevation angles.

In the presence of the trough, echoes returned from the trough minimum and the poleward edge of the trough will be the predominant features on an ionogram. Whichever of these features is in closest proximity to the observing station will be selected as the most overhead ionosphere by the

elevation angle filtering technique. In most cases, the chosen feature will not explicitly represent the ionosphere overhead of the observing station. It should also be noted that the trough minimum frequently has densities less than 1.24×10^4 cm^{-3} and will not be seen by ionosondes which do not sweep below 1 MHz.

REFERENCES

1. Muldrew, D.B., F-layer ionization troughs deduced from Alouette data, J. geophys. Res., **70**, 2635, 1965.
2. Sharp, G.W., Mid-latitude trough in the night ionosphere, J. geophys. Res., **70**, 1345, 1966.
3. Thomas, J.O. and A.Y. Sayer, Electron density at the Alouette orbit, J. geophys. Res., **69**, 4561, 1964.
4. Calvert, W., Steep horizontal electron density gradients in the topside F-layer, J. geophys. Res., **71**, 3665, 1966.
5. Stanley, G.M., Ground-based studies of the F region in the vicinity of the mid-latitude trough, J. geophys. Res., **71**, 5067, 1966.
6. Bowman, G.G., Ionization troughs below the F~2-layer maximum, Planet. Space Sci., **17**, 777, 1969.
7. Moffett, R. and S. Quegan, The mid-latitude trough in the electron concentration of the ionospheric F-layer: a review of obs rvations and modelling, J. atmos. terr. Phys., **45**, 315, 1983.
8. King, J.W., D. Eccles and H. Kohl, The behaviour of the Antarctic ionosphere, J. atmos. terr. Phys., **33**, 1067, 1971.
9. Eccles, D., Enhancements of the electron concentration in the F2-layer at magnetic noon, J. atmos. terr. Phys., **35**, 1309, 1973.
10. Dudeney, J.R. and W.R. Piggott, Antarctic Ionospheric Research, in **Upper Atmospheric Research in Antarctica** (Edited by L.J. Lanzerotti and C.G. Park), AGU, Washington, D.C., p.200, 1978.
11. Penndorf, R., Antarctic Research and Data Analysis, Sci. Report 28, Part A, National Science Foundation, Washington, D.C., 1968.
12. Helliwell, R.A. and J.P. Katsufrakis, VLF wave injection into the magnetosphere from Siple Station, Antarctica, J. geophys. Res., **79**, 2511, 1974.
13. Grubb, R.N., The NOAA SEL HF Radar, NOAA Tech. Memo. ERL SEL 55, Boulder, Colorado, 1979.
14. Altshuler, E.E., The traveling-wave linear antenna, IRE Trans. ant. prop., **AP-9**, 324, 1961.
15. Biggs, A.W., Wave Propagation over snow and ice, SCAR Symposium on Antarctic Telecommunications, SCAR, Cambridge, p.160, 1972.
16. Hoeg, P. and E. Ungstrup, Interpretation of ionograms in the vicinity of the dayside auroral oval by ray tracing, Radio Sci., **18**, 725, 1983.
17. Dudeney, J.R. and M.J. Jarvis, A simple graphical method for de-aliasing digital ionosonde echolocation data, Radio Sci., in press 1985.
18. Sojka, J.J., W.J. Raitt and R.W. Schunk, A theoretical study of the high-latitude winter F-region at solar minimum for low magnetic activity, J. geophys. Res., **86**, 609, 1981.
19. Sojka, J.J., W.J. Raitt and R.W. Schunk, Theoretical predictions for ion composition in the high-latitude winter F region for solar minimum and low magnetic activity, J. geophys. Res., **86**, 2206, 1981.
20. Sojka, J.J., W.J. Raitt, R.W. Schunk, F.J. Rich and R.C. Sagalyn, Observations of the diurnal dependence of the high latitude F region density by DMSP satellites, J. geophys. Res., **87**, 1711, 1982.
21. Halcrow, B.W. and J.S. Nisbet, A model of F_2 peak electron densities in the main trough region of the ionosphere, Radio Sci., **12**, 815, 1977.
22. Spiro, R.W., A study of plasma flow in the mid-latitude ionization trough, Ph.D. dissertation, Univ. of Texas, Dallas, 1978.
23. Duncan, R.A., Universal Time control of the Arctic and Antarctic F-region, J. geophys. Res., **67**, 1823, 1962.
24. Knecht, R.W., Observations of the ionosphere over the South Geographic Pole, J. geophys. Res., **64**, 1243, 1959.
25. Sato, T. and G.F. Rourke, F-region enhancements in the Antarctic, J. geophys. Res., **69**, 4591, 1964.
26. de la Beaujardiere, O., V.B. Wickwar, G. Caudal, J.M Holt, J.D. Craven, L.A. Frank, L.H. Brace, D.S. Evans, J.D. Winningham and R.A. Hellis, Universal Time dependence of nighttime F-region densities at high latitudes, J. geophys. Res., **90**, 4319, 1985.
27. Helms, W.J. and A.D. Thompson, Ray-tracing simulation of ionization effects upon radio waves, Radio Sci., **8**, 1125, 1973.

28. Nygren, T., Simulation of vertical incidence ionograms by ray tracing method in the presence of replacement and ionospheric trough, J. atmos. terr. Phys., **39**, 733-739, 1977.
29. Nygren, T., A synthesised trough ionogram, J. atmos. terr. Phys., **40**, 1089-1092, 1978.
30. Wright, J.W. and G.H. Smith, Review of current methods for obtaining electron density profiles from ionograms, Radio Sci., **2**(10), 1119, 1967.
31. Kelso, J.M., in **Radio Wave Propagation in the Ionosphere**, McGraw-Hill, p. 356, 1964.
32. Titheridge, J.E., Increased accuracy with simple means of ionogram analysis, J. atmos. terr. Phys., **41**, 243, 1979.
33. Titheridge, J.E., Ionogram analysis: least squares fitting of a Chapman-layer peak, Radio Sci., **20**, 247, 1985.
34. Bibl, K. and B.W. Reinisch, The universal digital ionosonde, Radio Sci., **13**, 519-530, 1978.
35. Reinisch, B.W. and H. Xueqin, Automatic calculation of electron density profiles from digital ionograms 3. Processing of bottomside ionograms, Radio Sci., **18**, 477-492, 1983.
36. Dudeney, J.R., A.S. Rodger and M.J. Jarvis, Radio studies of the main F region trough in Antarctica, Radio Sci., **18**, 927, 1983.

Acknowledgments : The Siple data were recorded by S. J. Walter, who wintered at Siple Station in 1982 and the Halley observations were carried out by K. H. Wright and R. J. Halliwell. At Utah State University this research has been supported by the National Science Foundation by Grants **DPP 81-00220** and **DPP 83-08044**. The facilities at Halley were provided by the British Antarctic Survey.

FIGURE CAPTIONS

Figure 1. A map of Antarctica upon which invariant latitude and time coordinates have been superposed. The location of the auroral oval at 1530 UT is also indicated. The stations referenced on the map are: Siple (SI), Halley (HB), SANAE (SA), Syowa (SY), Palmer (PA), South Pole (SP), McMurdo (MM) and Vostok (VO) [Figure courtesy of C.G. MacClennan].

Figure 2. An ionogram recorded at Siple Station on August 15, 1982 showing typical signatures of the minimum and poleward edge of the mid-latitude trough. Echo polarization is denoted by the slant of the symbol where a left slanting bar denotes the extra-ordinary mode, a right slanting bar the ordinary mode and a vertical bar unknown polarization. The small arrows at the bottom of an ionogram indicate the beginning and end of the frequency sweep.

Figure 3. A schematic representation of the main ionospheric trough as it frequently appears near Halley, showing the principal echoing regions [after Dudeney et al. (36)].

Figure 4. Ionograms and fixed frequency sounding data which show the transition at 2.1 MHz of echo location from the trough minimum to the poleward edge of the trough. The center panel is a time series of measurements of echo location, range, amplitude and doppler velocity between 00 and 02 UT on August 15, 1982. The two vertical columns show ionograms recorded over the same interval. The transition in echo location is illustrated in the top two time series plots of north-south and east-west echo location shown in the center panel.

Figure 5. These data were recorded at Halley and Siple Stations on May 23, 1982. The Siple ionograms reproduced here show data at the same UT (top right) as the Halley ionogram, the equivalent MLT (bottom left) and the corresponding LT (bottom right). On the Halley ionograms, time is given in local meridian time while UT is used on the Siple data.

Figure 6. Same as Figure 5 for 0400 UT on May 23, 1982.

Figure 7. Same as Figure 5 for 0215 UT on July 4, 1982.

Figure 8. Same as Figure 5 for 0900 UT on July 4, 1982.

Figure 9. The location as a function of time of the minimum and poleward edge of the trough derived from ionograms recorded at Halley (open circles and + signs) and Siple (filled circles and x symbols). The top panel displays the location in Universal Time, the center panel in MLT, and the bottom panel in LT. These data show the trough location for an occurrence on 22-23 May 1982.

Figure 10. Same as Figure 9 for all three days used in the analysis. The top panel shows Halley data plotted in LT coordinates while the bottom panel displays Siple data plotted as a function of UT.

Figure 11. Same as Figure 9 where all three days have been averaged to single curve. Halley data are shown as dashed lines while solid curves are used to represent the Siple data. The notations TM and PE denote trough minimum and poleward edge, respectively.

Figure 12. A summary diagram wherein all of the curves shown in Figure 12 have been replotted. The average echo location for Halley (HB) is shown as a dashed curve while a solid line is used to represent the Siple (SI) data. The Siple curves are displaced according to the time coordinate in which they have been plotted. The basic unit of time is three hours and the time of midnight in UT, LT and MLT is indicated using a diamond, a circle and a square. Using empirical formulae given by Halcrow and Nesbit (21) and Spiro (22) for a K_p of 1, the predicted locations of the poleward edge and trough minimum are also indicated on the diagram.

Figure A-1 The number distribution of echoes as a function of elevation angle for three different ionospheric conditions. Panel (a) was derived from ionograms obtained during undisturbed ionospheric conditions, panel (b) from ionograms in which spread-F was present and panel (c) during an occurrence of the mid-latitude trough.

Figure A-2 A series on ionograms which illustrate the effect of elevation angle filtering in reducing spread-F. In panel (a) an unfiltered ionogram is presented; panels (b), (c) and (d) show the results obtained by applying filters of 70°, 75° and 80° respectively. In panel (e) an additional polarization filter has been applied and only the purely O and X-modes have been plotted. These data were recorded at Cleary, Alaska at 1635 UT on October 26, 1980.

Figure A-3 Same as Figure A-2 for data recorded at Cleary, Alaska at 0355 UT on October 26, 1980.

Figure A-4 Same as Figure A-2 for data recorded at Siple Station at 0606 UT on March 27, 1982.

Figure A-5 Same as Figure A-2 for data recorded at Halley at 0100 UT on August 15, 1982.

Figure A-6 Same as Figure A-2 for data recorded at Siple Station at 0400 UT on May 23, 1982. No polarization filtering is shown for these data.

UT INTERVAL

1982	00-03	03-06	06-09	09-12	12-15	15-18	18-21	21-24	ΣKp
22 MAY	1	1-	1	1+	1	1-	0+	1	7+
23 MAY	2-	1	0+	0	0+	1-	1-	0	4+
3 JULY	2+	2	1+	2-	1+	2-	1	0+	12
4 JULY	1	1	0+	1-	0+	0+	0	1	4
14 AUG	2+	2-	1+	1+	1+	2+	2+	2-	14+
15 AUG	2-	1-	0	0+	1-	1-	1-	2-	6+

TABLE I

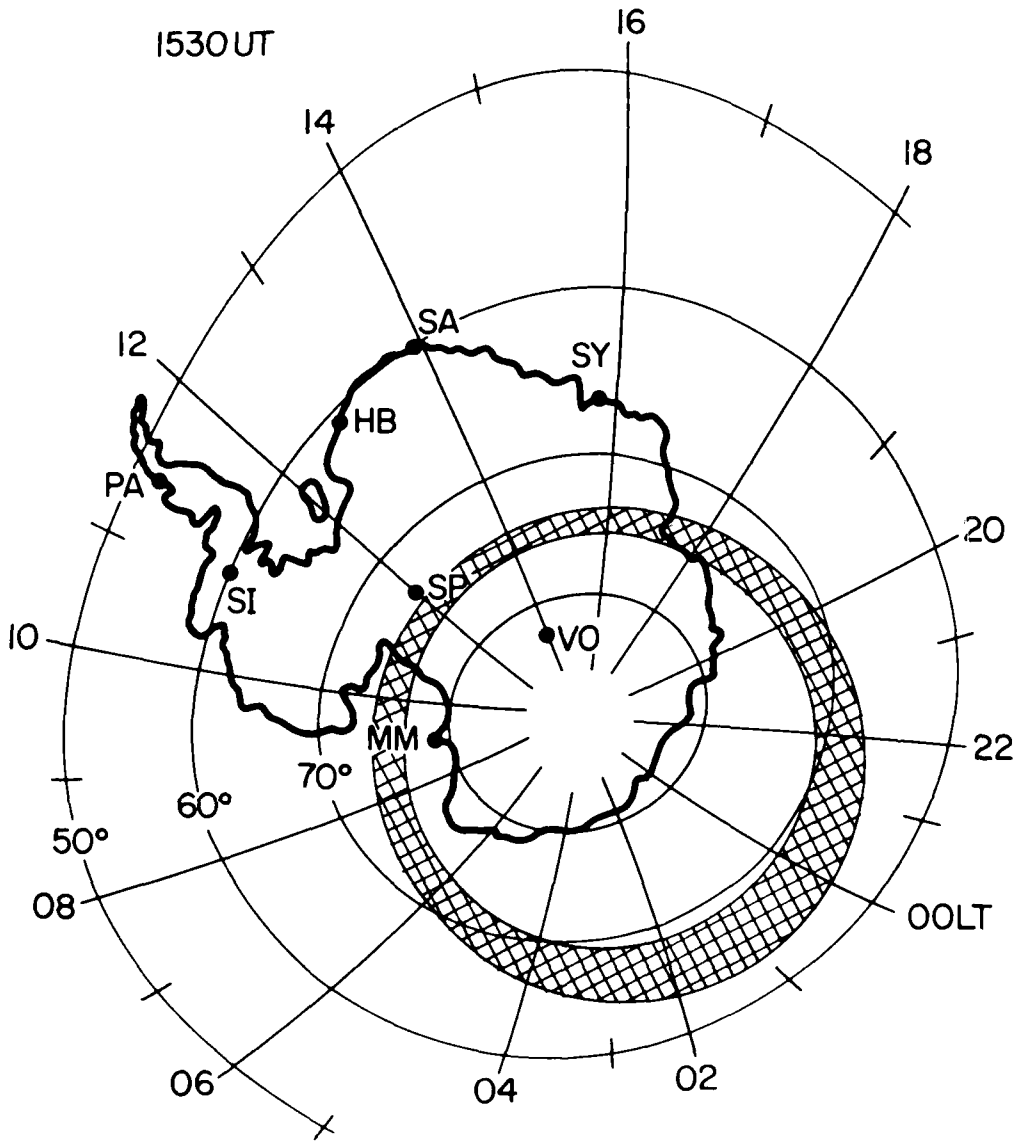


Figure 1.

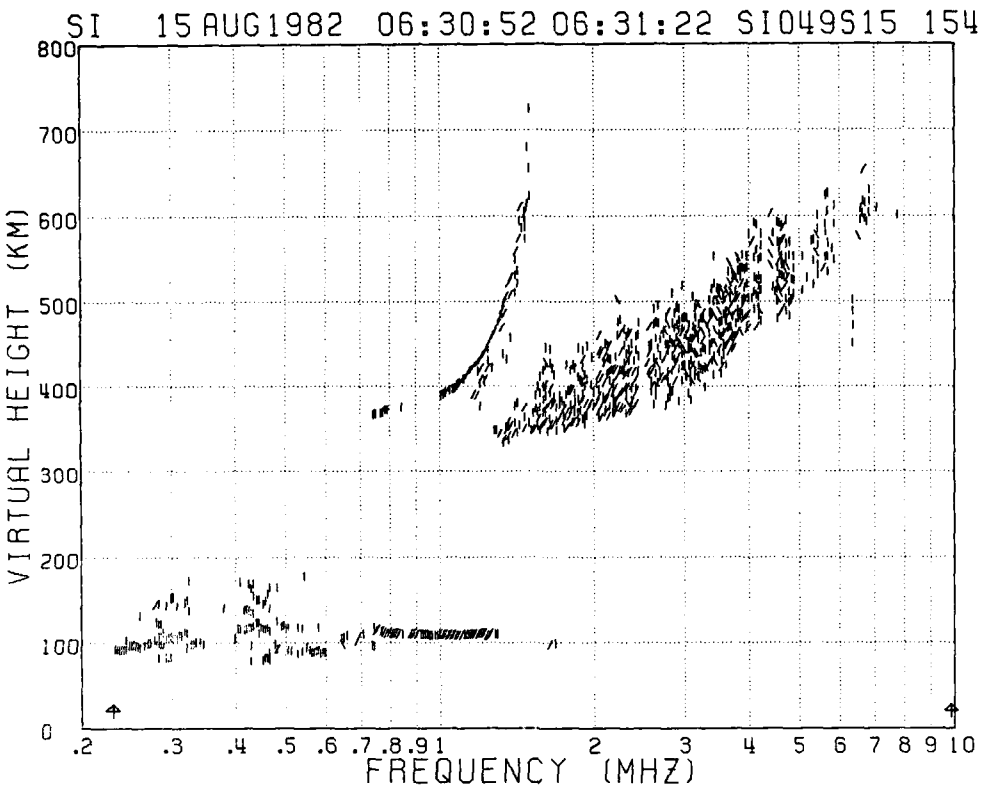


Figure 2.

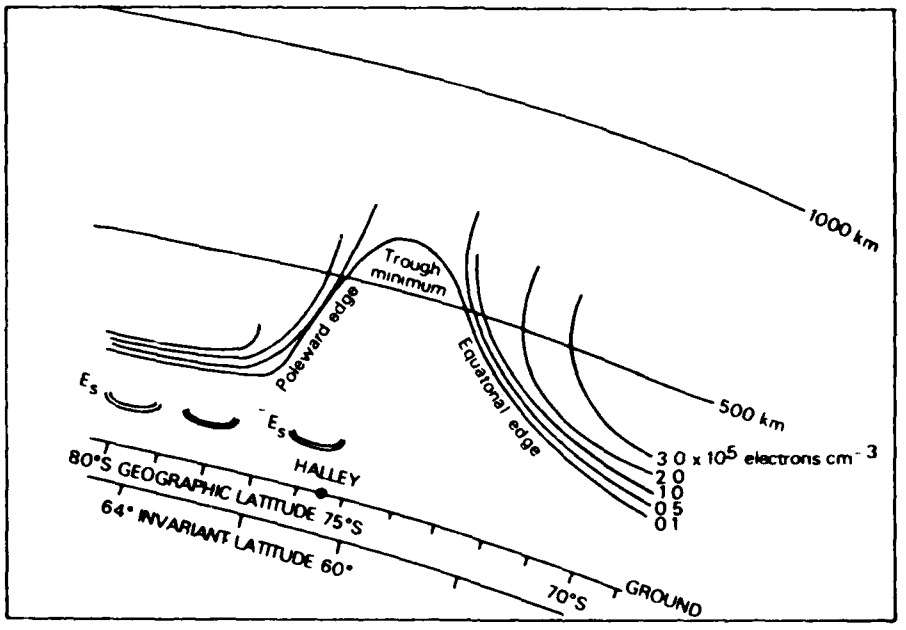


Figure 3.

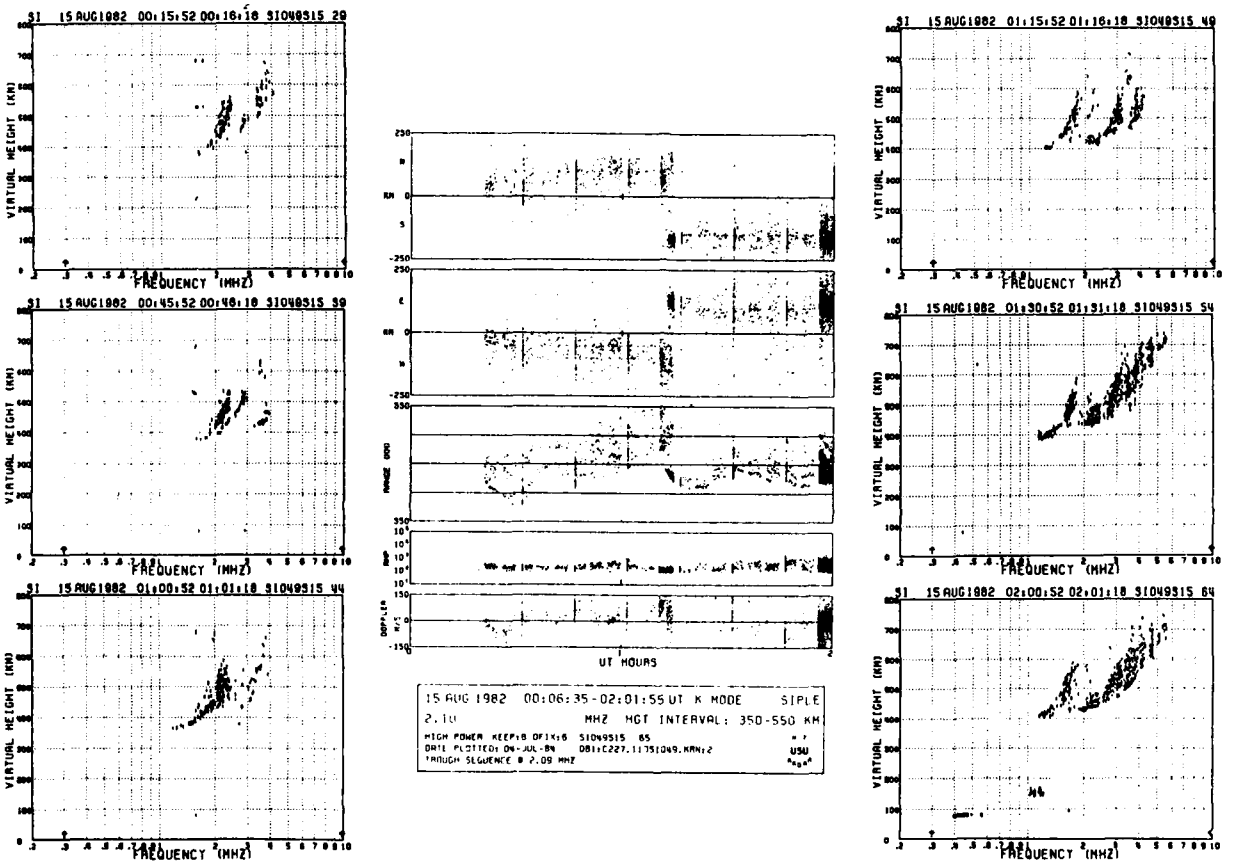

VIRTUAL HEIGHT (KM)
FREQUENCY (MHZ)
UT HOURS
15 AUG 1982 00:06:35-02:01:55 UT K MODE SIPLE
2.10 MHZ HGT INTERVAL: 350-550 KM

Figure 4.

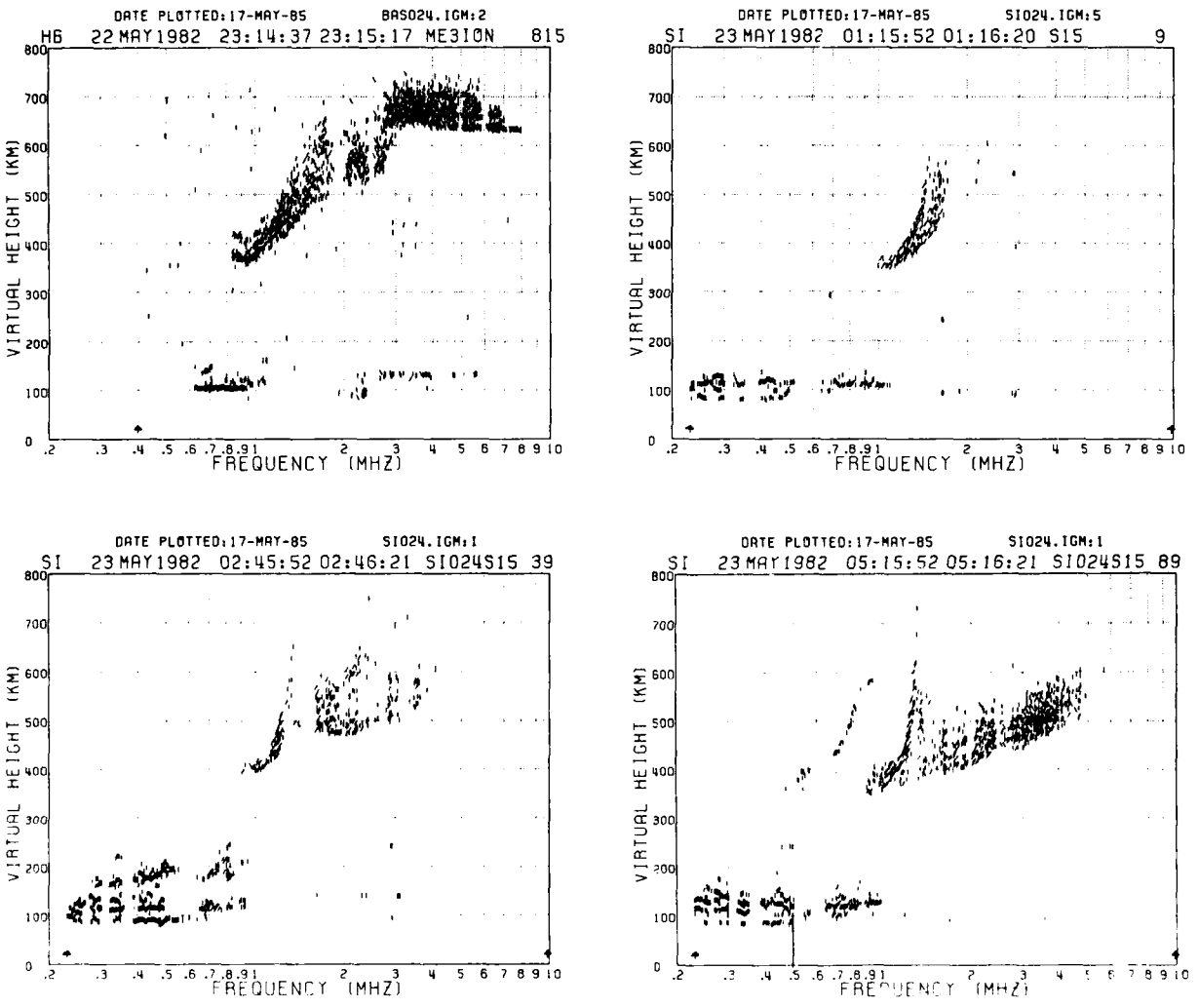
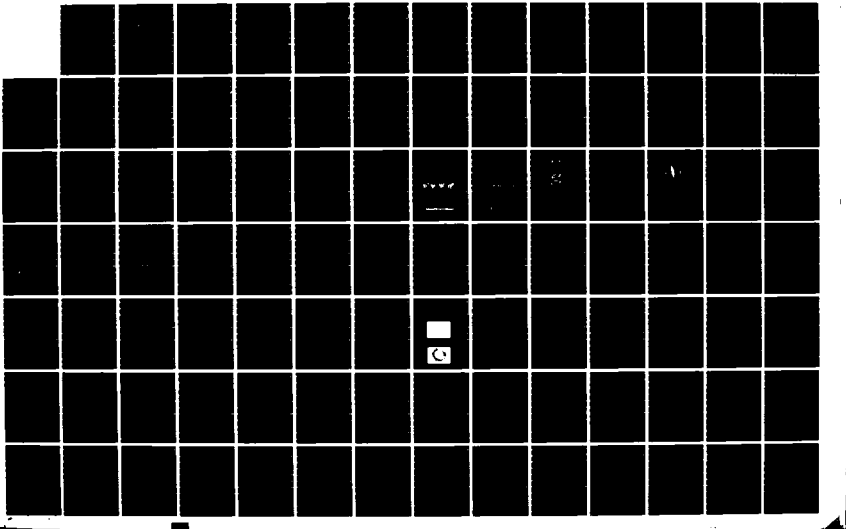
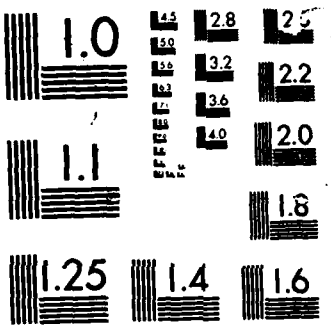

DATE PLOTTED:17-MAY-85 BAS024.IGM:2
H6 22 MAY 1982 23:14:37 23:15:17 ME310N 815
DATE PLOTTED:17-MAY-85 SI024.IGM:5
SI 23 MAY 1982 01:15:52 01:16:20 S15 9
DATE PLOTTED:17-MAY-85 SI024.IGM:1
SI 23 MAY 1982 02:45:52 02:46:21 SI024S15 39
DATE PLOTTED:17-MAY-85 SI024.IGM:1
SI 23 MAY 1982 05:15:52 05:16:21 SI024S15 89
VIRTUAL HEIGHT (KM)
FREQUENCY (MHZ)

Figure 5.

AD-A166 585 CONFERENCE PROCEEDINGS ON PROPAGATION EFFECTS ON MILITARY SYSTEMS IN THE..(U) ADVISORY GROUP FOR AEROSPACE RESEARCH AND DEVELOPMENT NEUILLY.. H SOICER

UNCLASSIFIED NOV 85 AGARD-CP-382 F/G 4/1 NL





MICROCOPY CHART

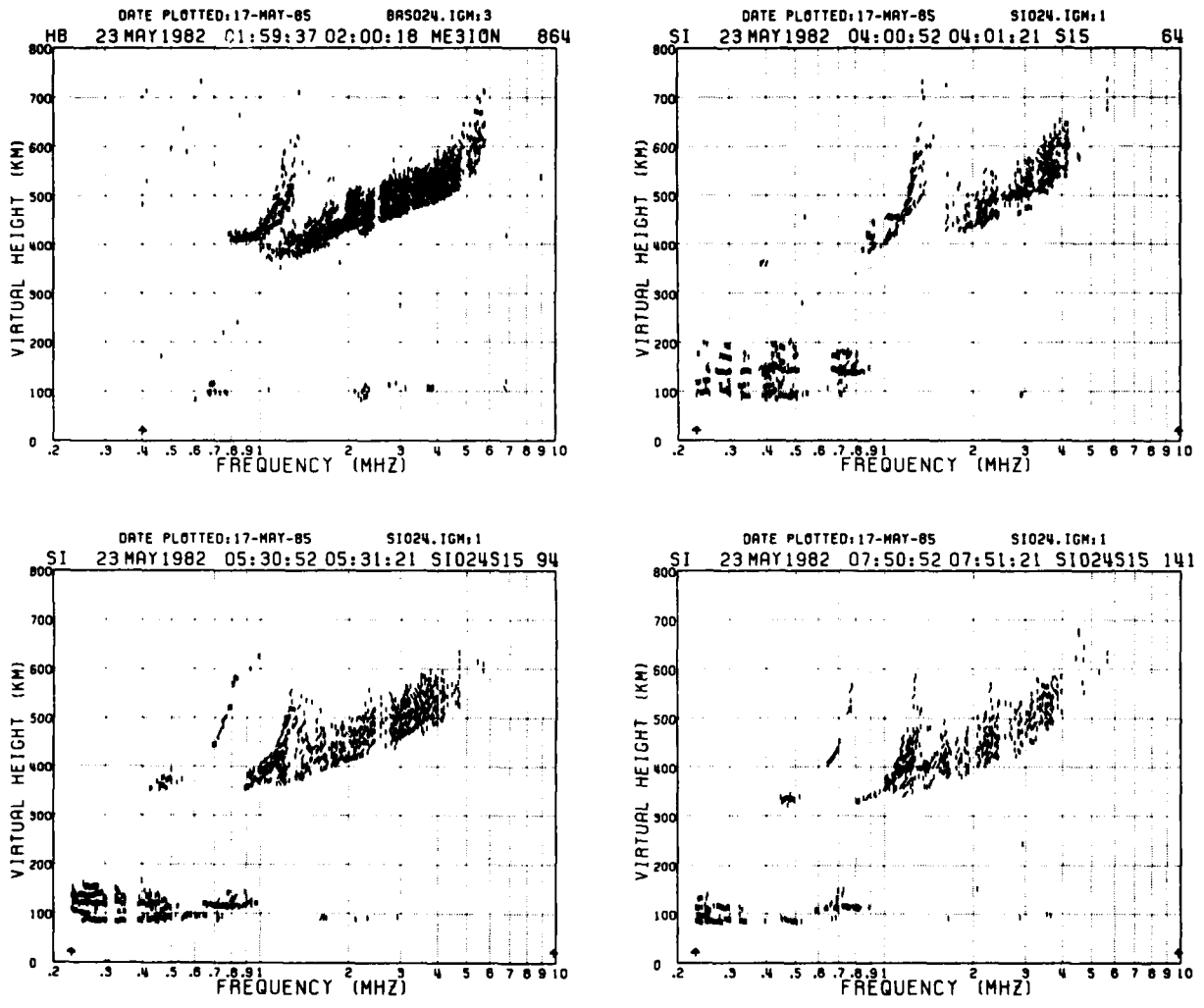

DATE PLOTTED:17-MAY-85 BAS024.IGM:3
HB 23 MAY 1982 01:59:37 02:00:18 ME310N 864
DATE PLOTTED:17-MAY-85 SI024.IGM:1
SI 23 MAY 1982 04:00:52 04:01:21 S15 64
DATE PLOTTED:17-MAY-85 SI024.IGM:1
SI 23 MAY 1982 05:30:52 05:31:21 SI024S15 94
DATE PLOTTED:17-MAY-85 SI024.IGM:1
SI 23 MAY 1982 07:50:52 07:51:21 SI024S15 141
VIRTUAL HEIGHT (KM)
FREQUENCY (MHZ)

Figure 6.

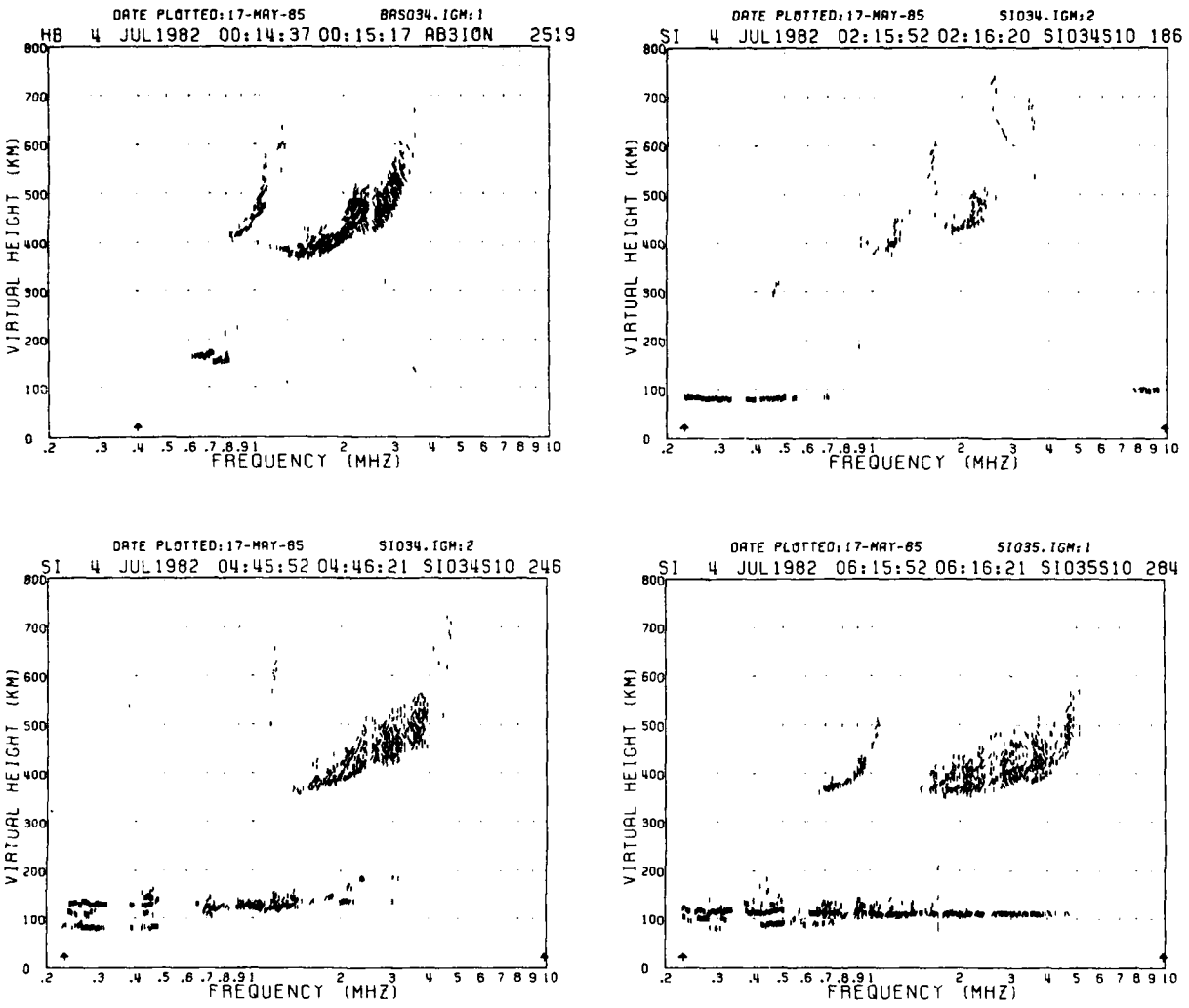

DATE PLOTTED:17-MAY-85 BAS034.IGM;1
HB 4 JUL1982 00:14:37 00:15:17 AB31ON 2519
DATE PLOTTED:17-MAY-85 SI034.IGM;2
SI 4 JUL1982 02:15:52 02:16:20 SI034S10 186
DATE PLOTTED:17-MAY-85 SI034.IGM;2
SI 4 JUL1982 04:45:52 04:46:21 SI034S10 246
DATE PLOTTED:17-MAY-85 SI035.IGM;1
SI 4 JUL1982 06:15:52 06:16:21 SI035S10 284
VIRTUAL HEIGHT (KM)
FREQUENCY (MHZ)

Figure 7.

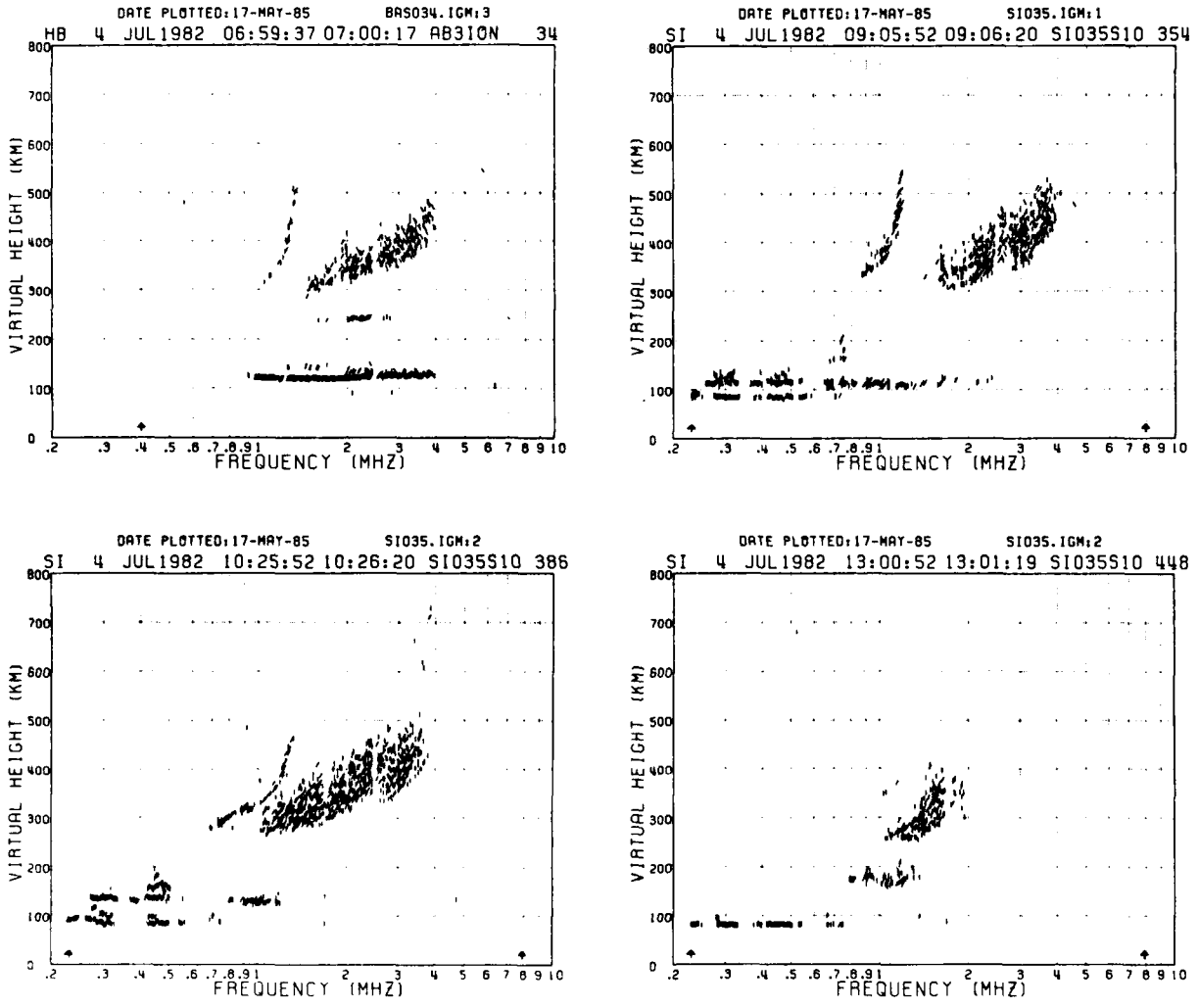

DATE PLOTTED:17-MAY-85 BAS034.IGM:3
HB 4 JUL1982 06:59:37 07:00:17 AB310N 34
DATE PLOTTED:17-MAY-85 SI035.IGM:1
SI 4 JUL1982 09:05:52 09:06:20 SI035S10 354
DATE PLOTTED:17-MAY-85 SI035.IGM:2
SI 4 JUL1982 10:25:52 10:26:20 SI035S10 386
DATE PLOTTED:17-MAY-85 SI035.IGM:2
SI 4 JUL1982 13:00:52 13:01:19 SI035S10 448
VIRTUAL HEIGHT (KM)
FREQUENCY (MHZ)

Figure 8.

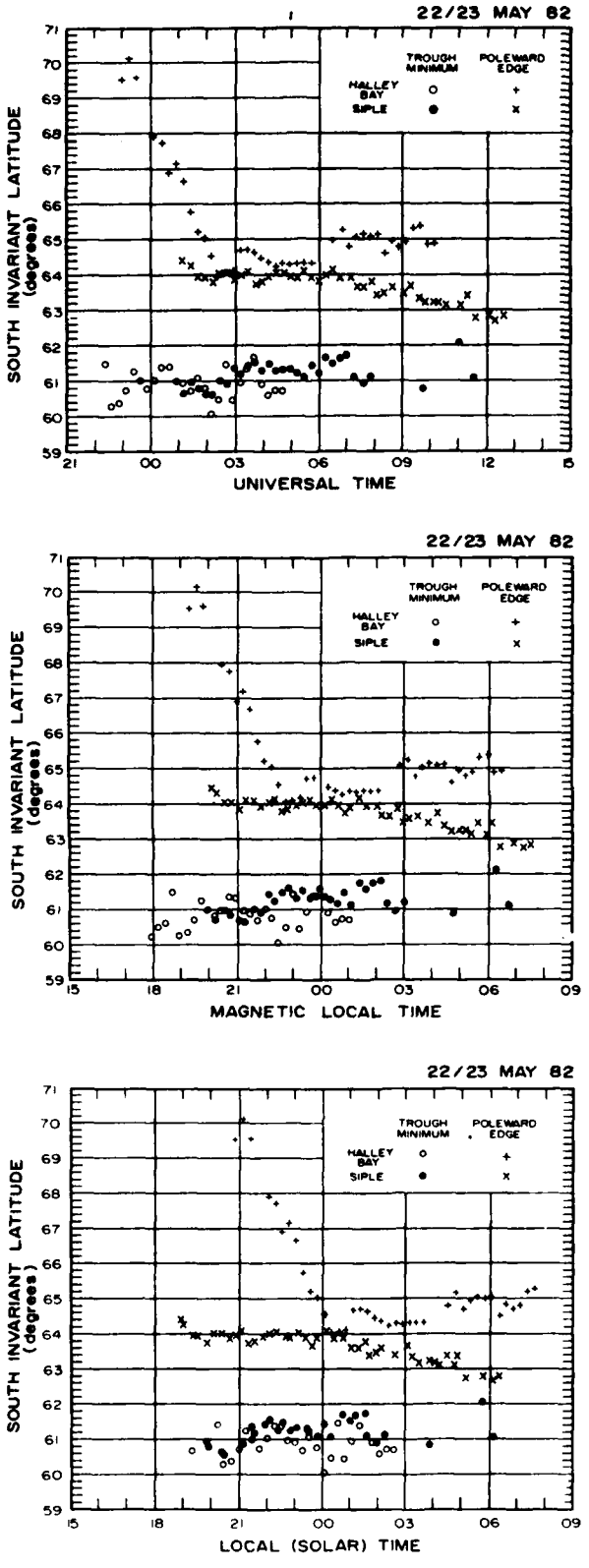
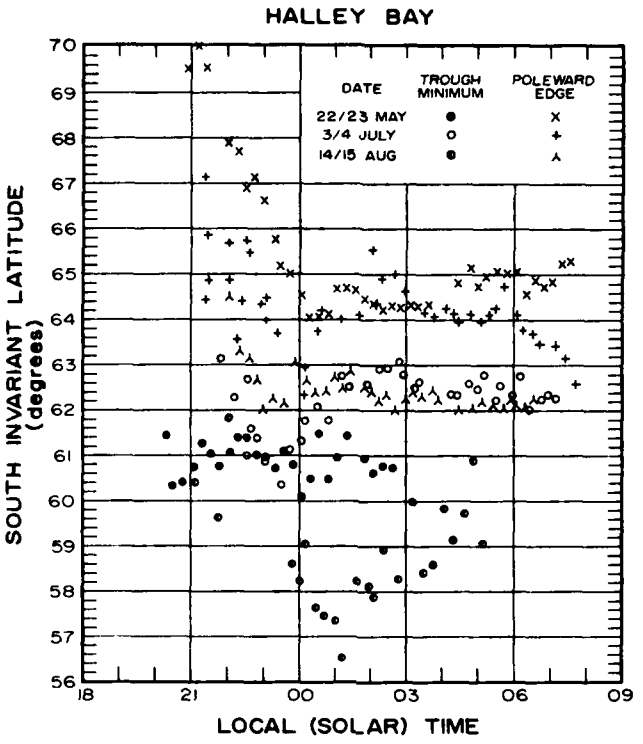

22/23 MAY 82
TROUGH MINIMUM
POLEWARD EDGE
HALLEY BAY
SIPLE
SOUTH INVARIANT LATITUDE (degrees)
UNIVERSAL TIME
22/23 MAY 82
MAGNETIC LOCAL TIME
22/23 MAY 82
LOCAL (SOLAR) TIME

Figure 9.


HALLEY BAY
DATE
TROUGH MINIMUM
POLEWARD EDGE
22/23 MAY
3/4 JULY
14/15 AUG
SOUTH INVARIANT LATITUDE (degrees)
70
69
68
67
66
65
64
63
62
61
60
59
58
57
56
18
21
00
03
06
09
LOCAL (SOLAR) TIME

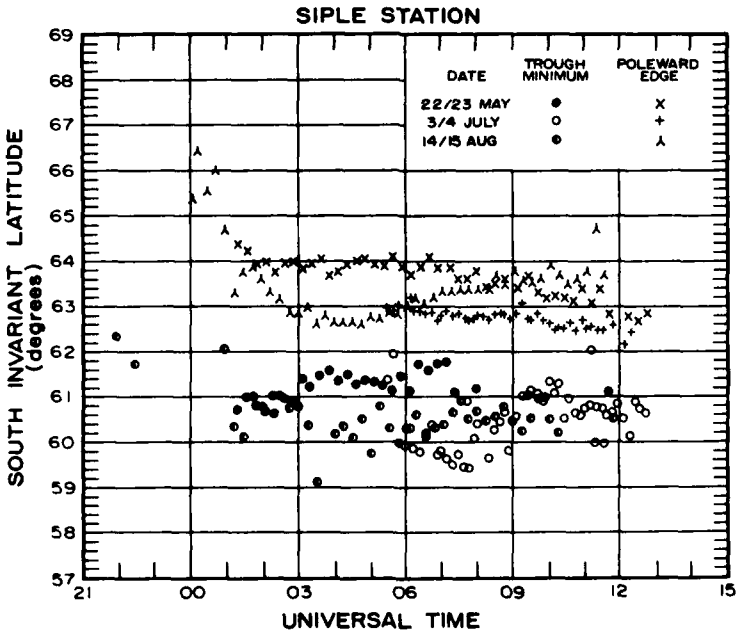

SIPLE STATION
DATE
TROUGH MINIMUM
POLEWARD EDGE
22/23 MAY
3/4 JULY
14/15 AUG
SOUTH INVARIANT LATITUDE (degrees)
69
68
67
66
65
64
63
62
61
60
59
58
57
21
00
03
06
09
12
15
UNIVERSAL TIME

Figure 10.

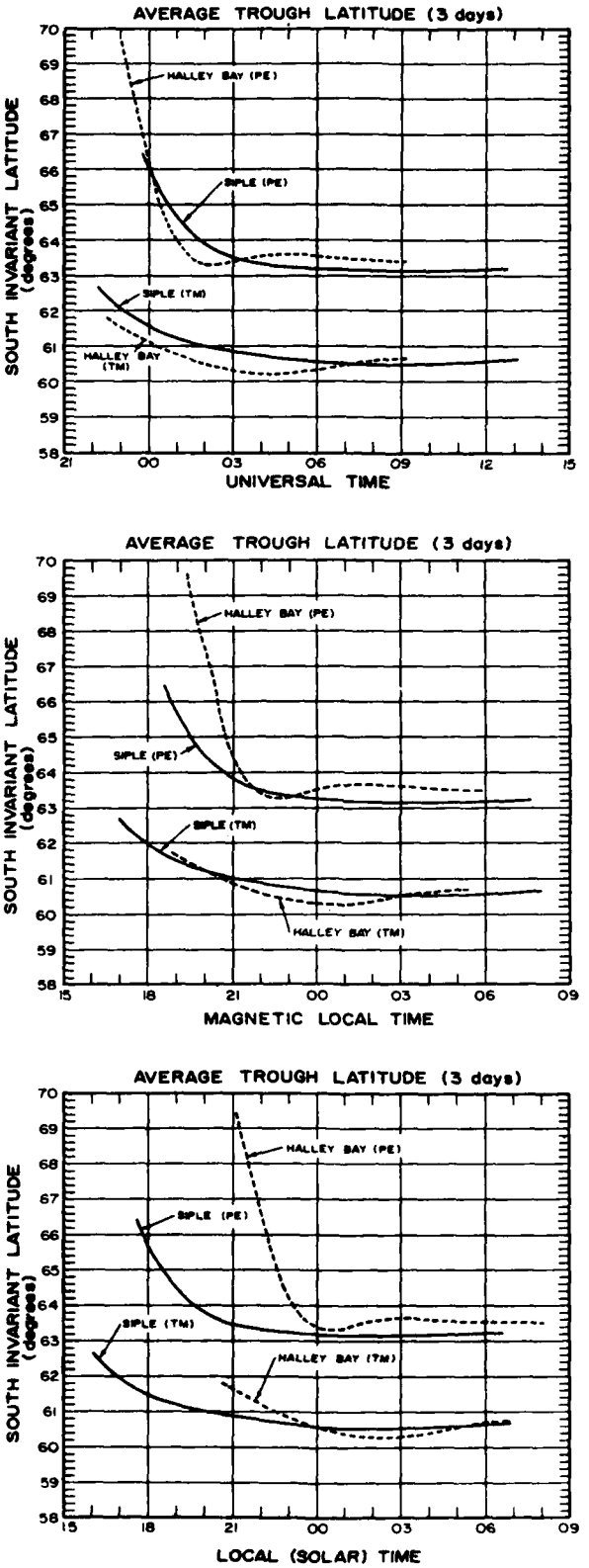

AVERAGE TROUGH LATITUDE (3 days)
SOUTH INVARIANT LATITUDE (degrees)
HALLEY BAY (PE)
SIPLE (PE)
SIPLE (TM)
HALLEY BAY (TM)
UNIVERSAL TIME
AVERAGE TROUGH LATITUDE (3 days)
SOUTH INVARIANT LATITUDE (degrees)
HALLEY BAY (PE)
SIPLE (PE)
SIPLE (TM)
HALLEY BAY (TM)
MAGNETIC LOCAL TIME
AVERAGE TROUGH LATITUDE (3 days)
SOUTH INVARIANT LATITUDE (degrees)
HALLEY BAY (PE)
SIPLE (PE)
SIPLE (TM)
HALLEY BAY (TM)
LOCAL (SOLAR) TIME

Figure 11.

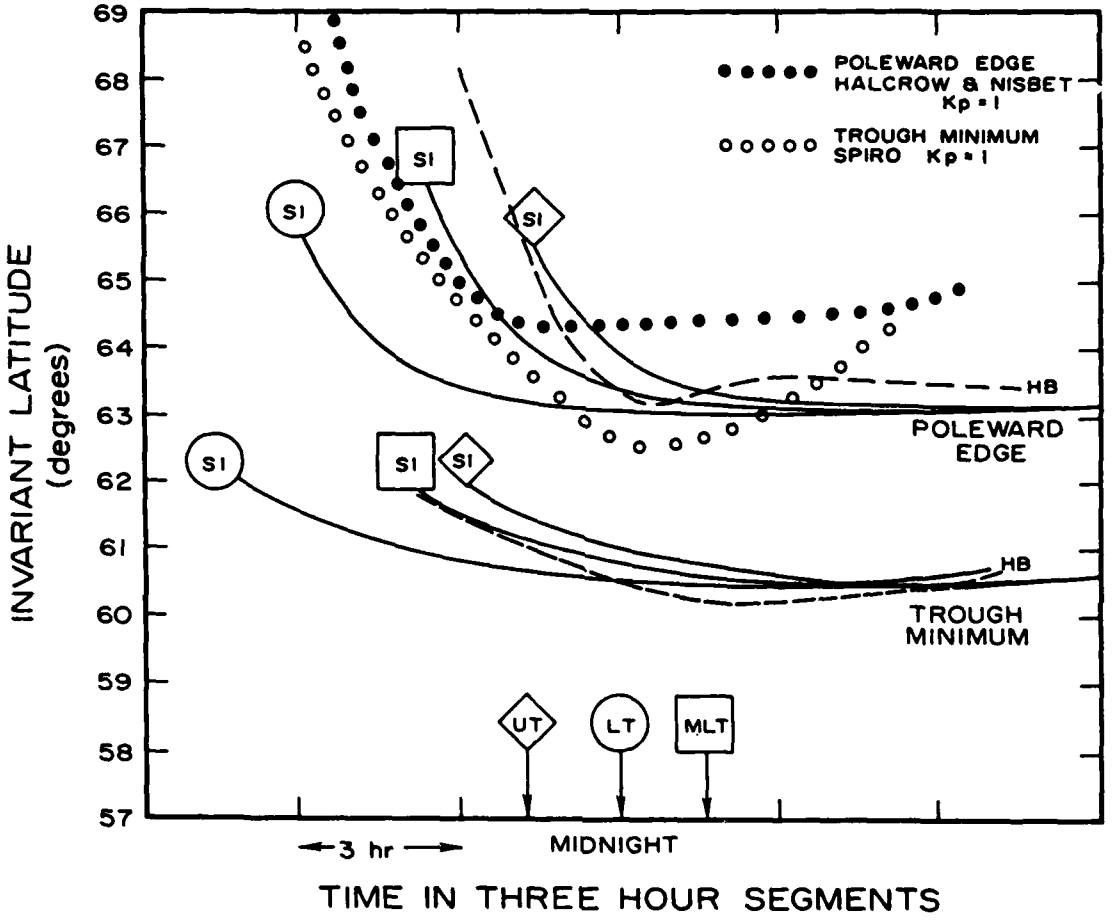

INVARIANT LATITUDE (degrees)
69
68
67
66
65
64
63
62
61
60
59
58
57
POLEWARD EDGE HALCROW & NISBET Kp = I
TROUGH MINIMUM SPIRO Kp = I
SI
SI
SI
SI
SI
SI
HB
POLEWARD EDGE
HB
TROUGH MINIMUM
UT
LT
MLT
3 hr
MIDNIGHT
TIME IN THREE HOUR SEGMENTS

Figure 12.

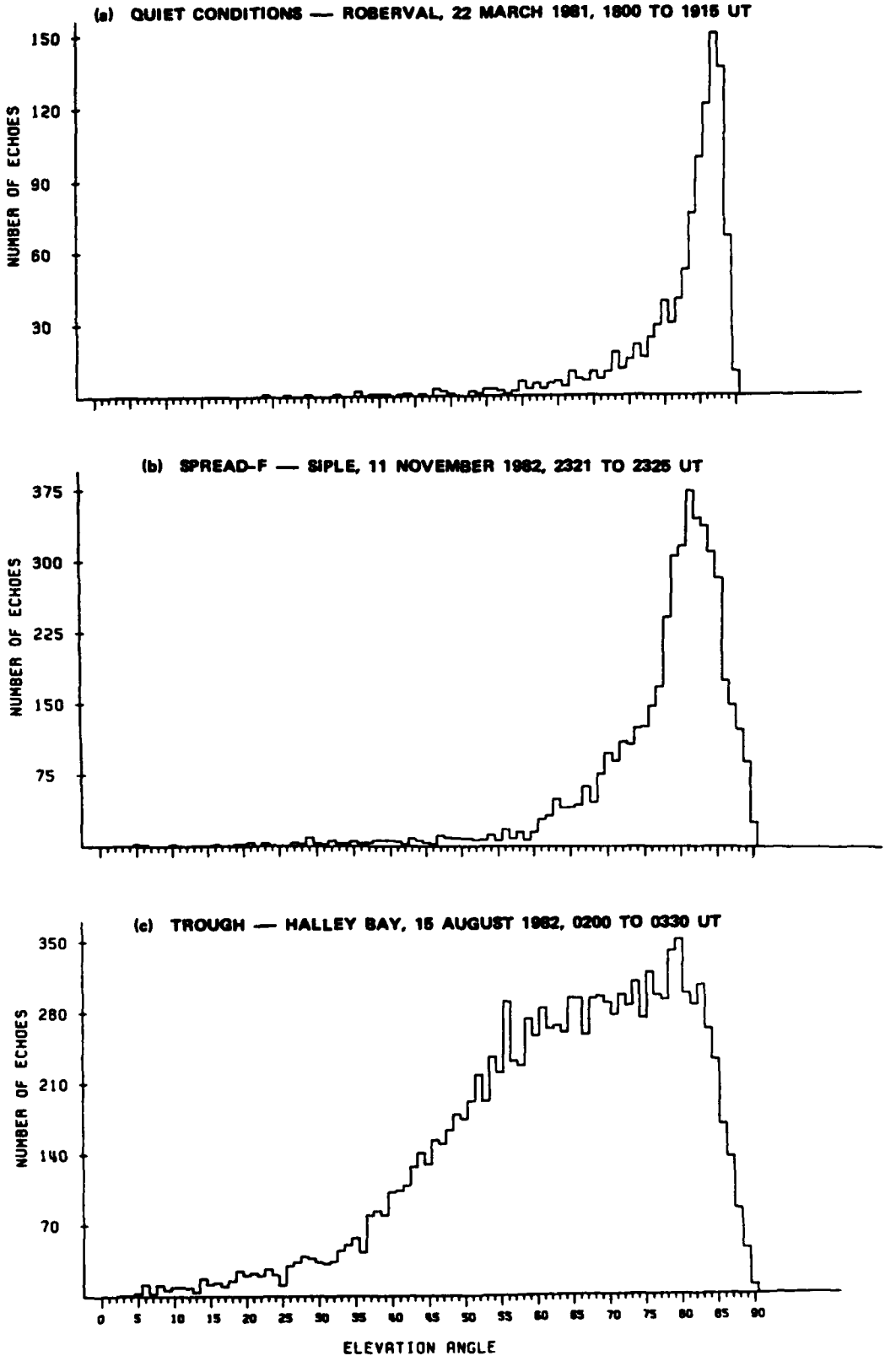
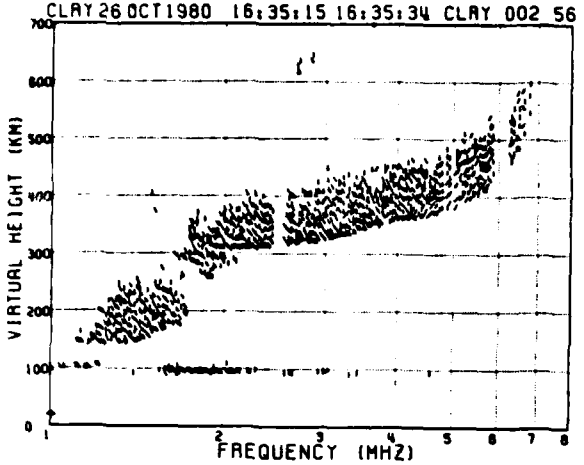
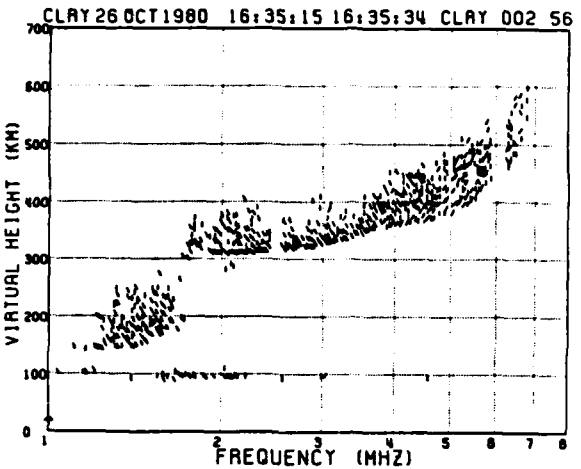

(a) QUIET CONDITIONS — ROBERVAL, 22 MARCH 1981, 1800 TO 1915 UT
NUMBER OF ECHOES
150
120
90
60
30
(b) SPREAD-F — SIPLE, 11 NOVEMBER 1982, 2321 TO 2325 UT
NUMBER OF ECHOES
375
300
225
150
75
(c) TROUGH — HALLEY BAY, 15 AUGUST 1982, 0200 TO 0330 UT
NUMBER OF ECHOES
350
280
210
140
70
0 5 10 15 20 25 30 35 40 45 50 55 60 65 70 75 80 85 90
ELEVATION ANGLE

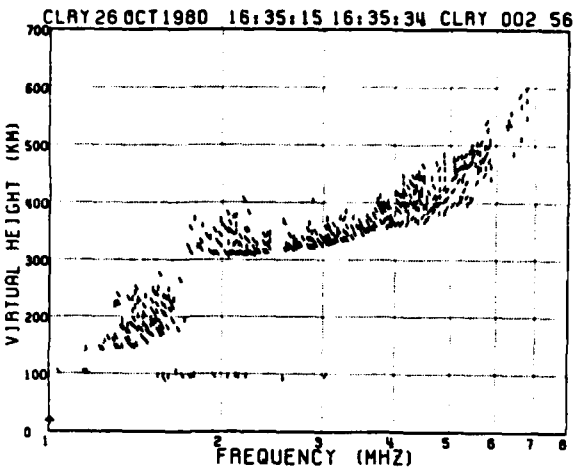
Figure A-1



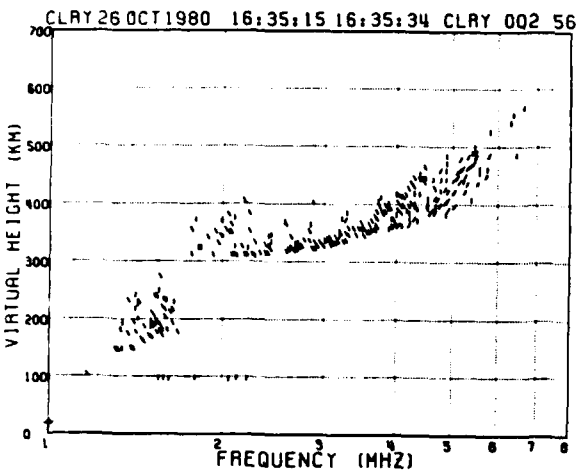
(a) UNFILTERED IONOGRAMS



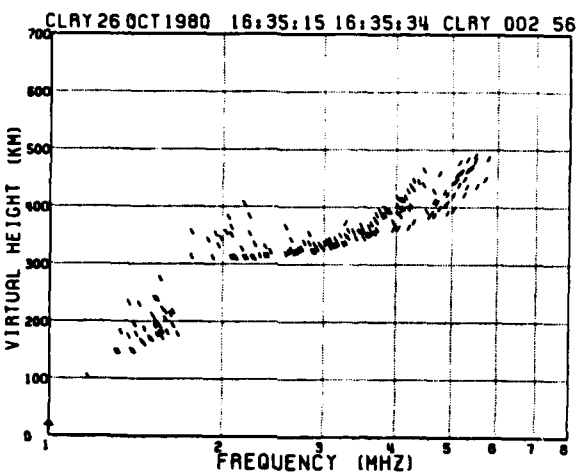
(b) EFFECT OF 70° ELEVATION FILTER



(c) EFFECT OF 75° ELEVATION FILTER

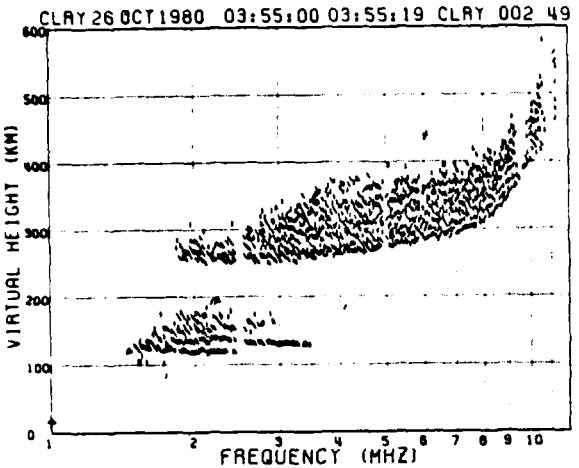


(d) EFFECT OF 80° ELEVATION FILTER (ALL ECHOES)

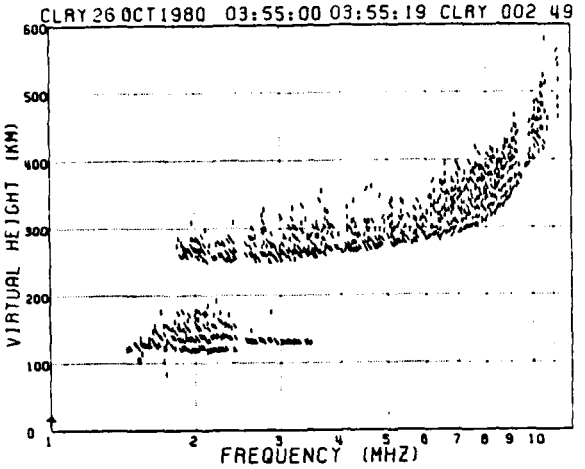


(e) EFFECT OF 80° ELEVATION FILTER (o- AND x-ECHOES ONLY)

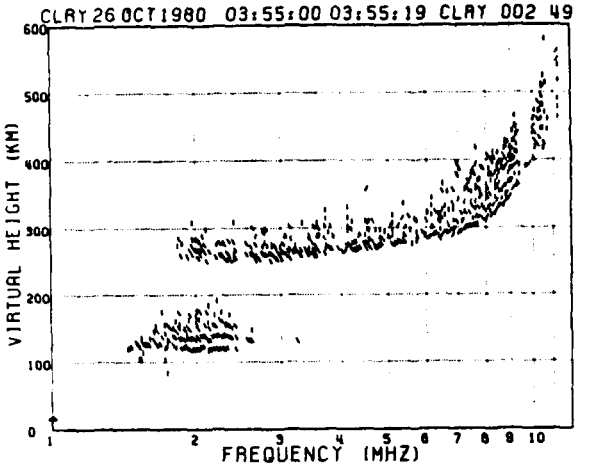
Figure A-2



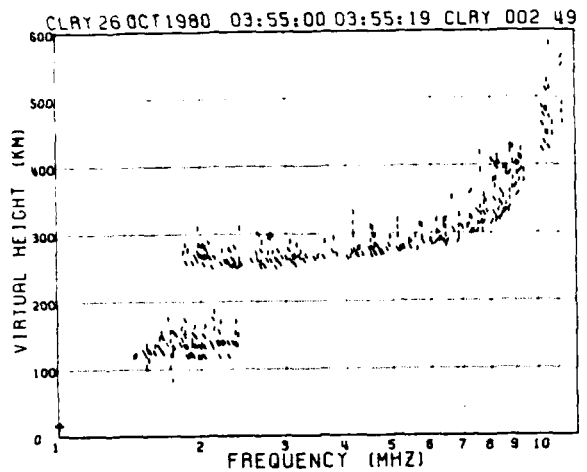
(a) UNFILTERED IONOGRAMS



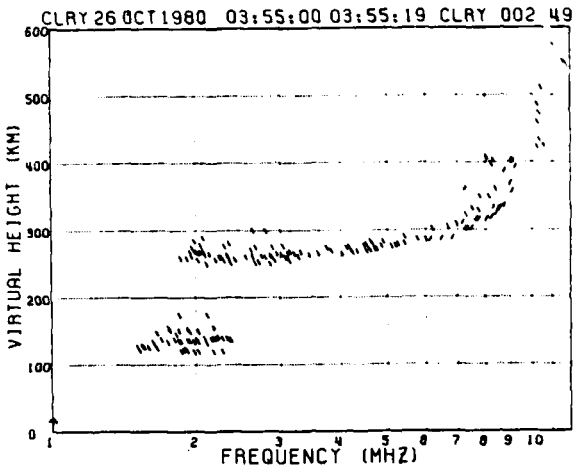
(b) EFFECT OF 70° ELEVATION FILTER



(c) EFFECT OF 75° ELEVATION FILTER

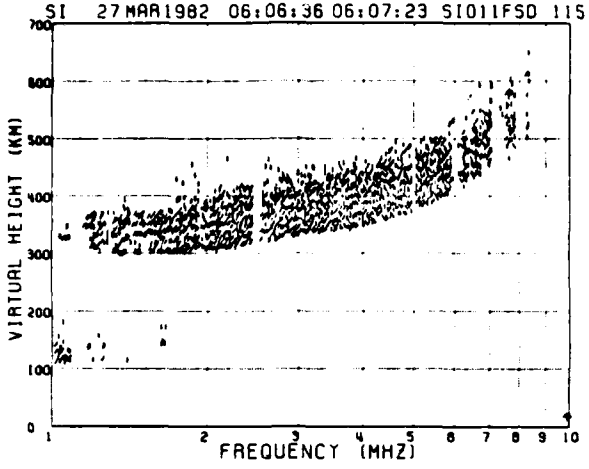


(d) EFFECT OF 80° ELEVATION FILTER (ALL ECHOES)

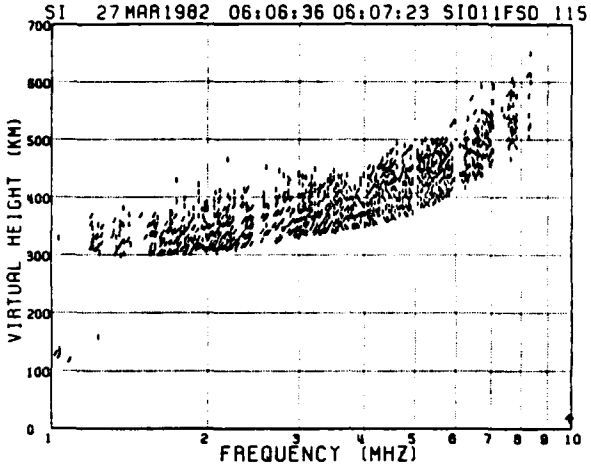


(e) EFFECT OF 80° ELEVATION FILTER (o- AND x-ECHOES ONLY)

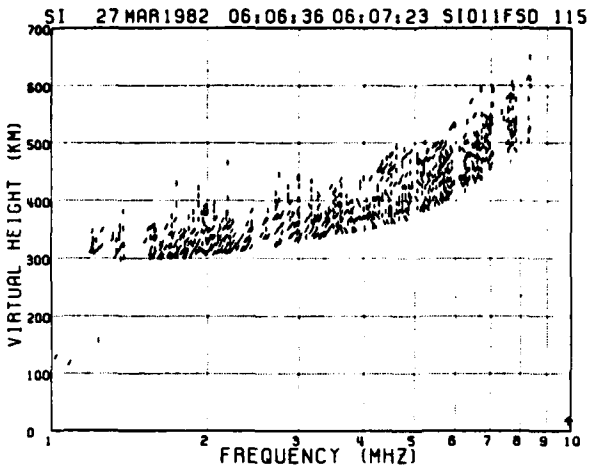
Figure A-3



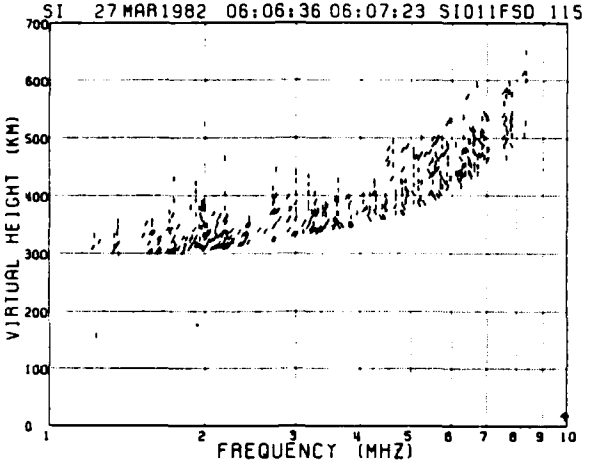
(a) UNFILTERED IONOGRAMS



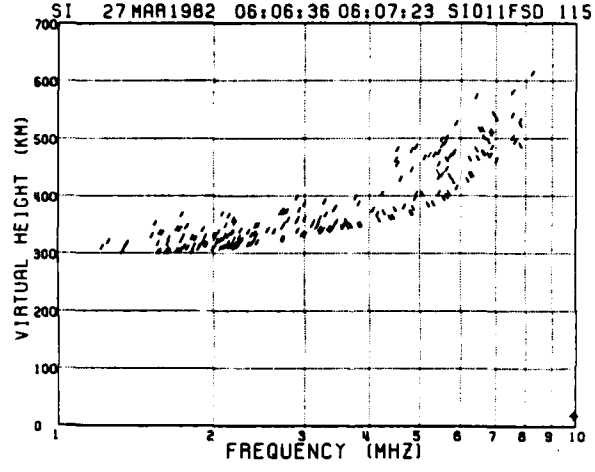
(b) EFFECT OF 70° ELEVATION FILTER



(c) EFFECT OF 75° ELEVATION FILTER

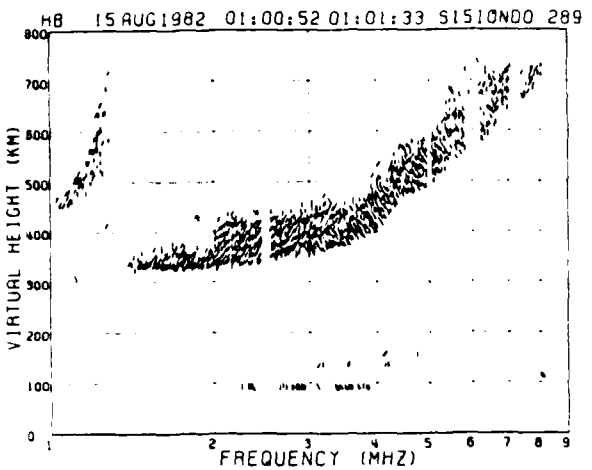


(d) EFFECT OF 80° ELEVATION FILTER (ALL ECHOES)

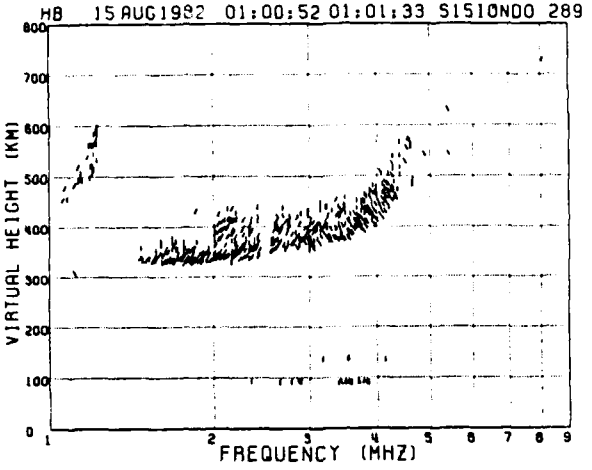


(e) EFFECT OF 80° ELEVATION FILTER (o- AND x-ECHOES ONLY)

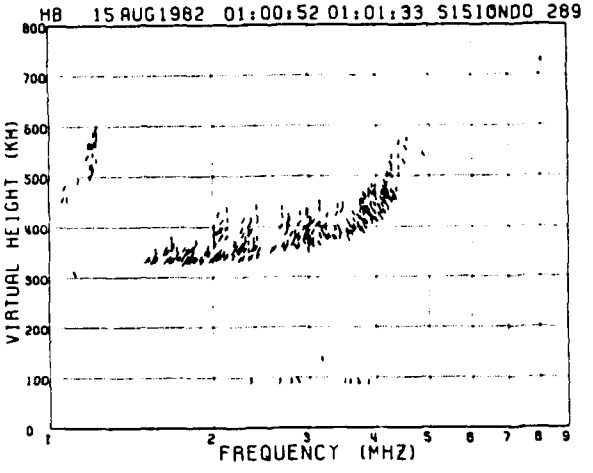
Figure A-4



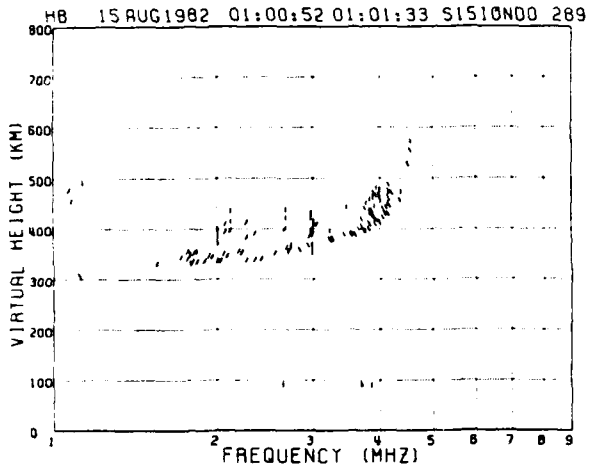
(a) UNFILTERED IONOGRAMS



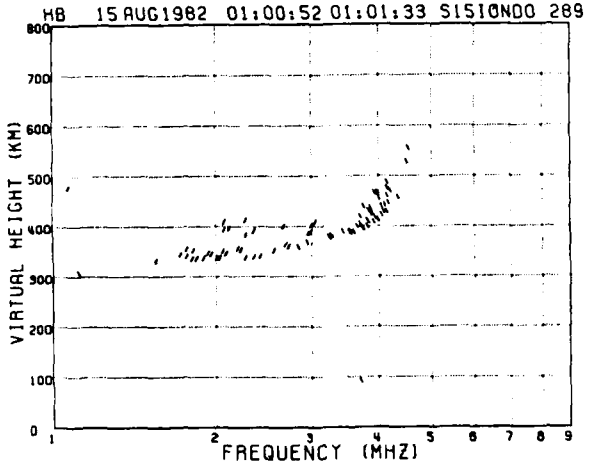
(b) EFFECT OF 70° ELEVATION FILTER



(c) EFFECT OF 75° ELEVATION FILTER



(d) EFFECT OF 80° ELEVATION FILTER (ALL ECHOES)



(e) EFFECT OF 80° ELEVATION FILTER (o- AND x-ECHOES ONLY)

Figure A-5

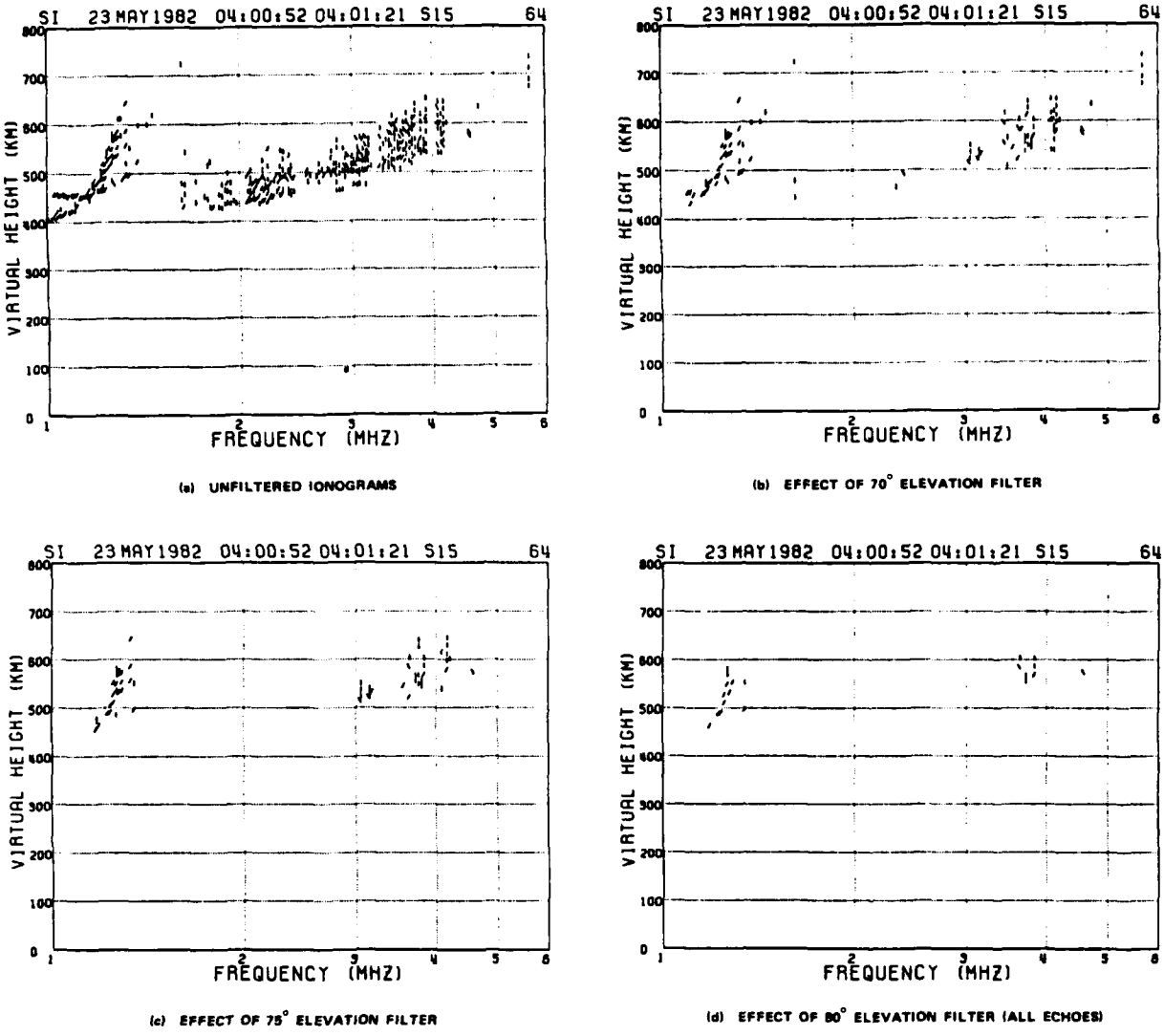


Figure A-6

DISCUSSION

N.C.Gerson, US

Have you considered examining the trough simultaneously in the northern and southern hemispheres, i.e., from both Siple and Ruberval?

Author's Reply

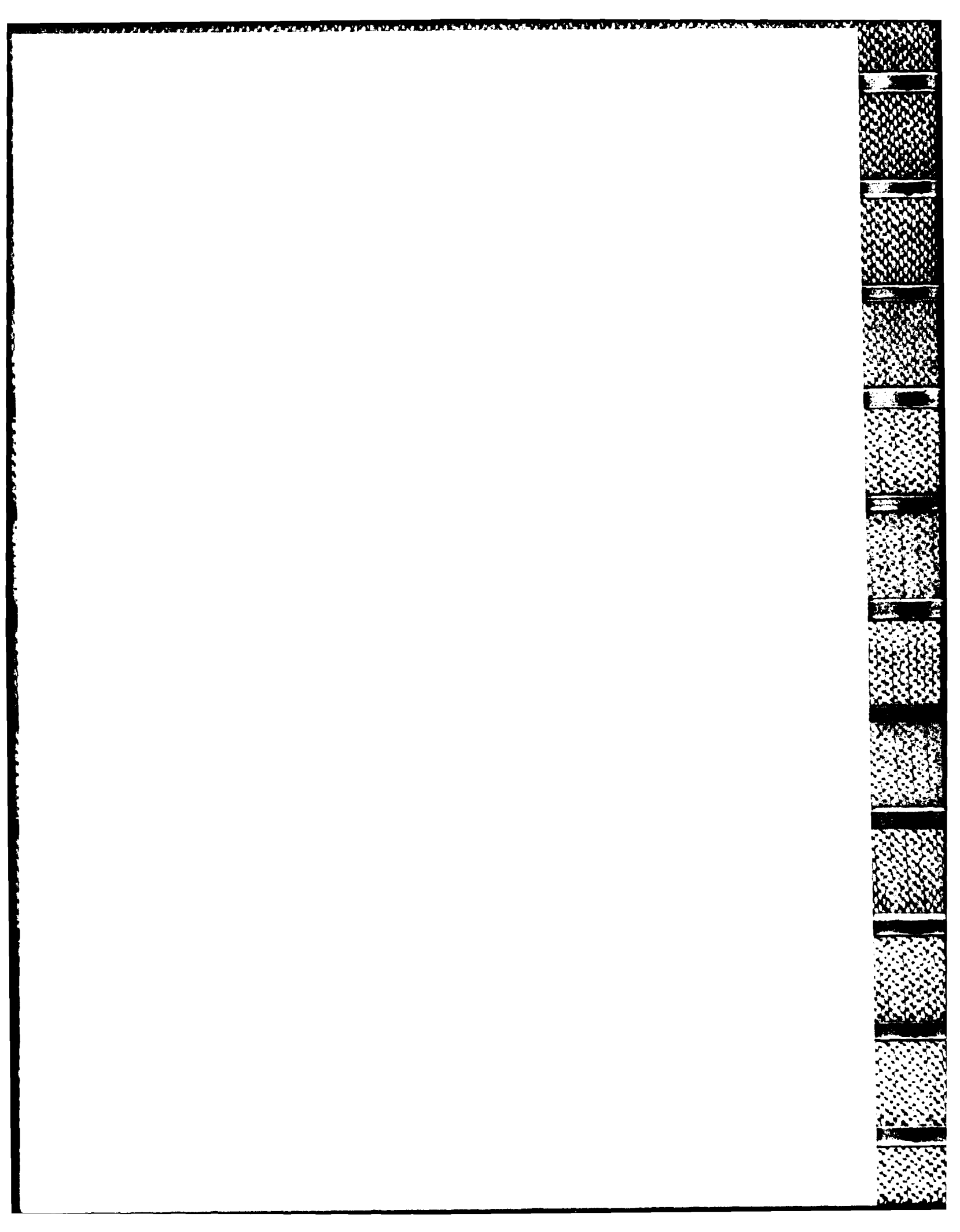
When Siple station is reactivated (December 1985), a number of experimental campaigns will be conducted using both stations. These campaigns will study conjugate trough occurrences as well as other phenomena. Siple station will be operated during 1986 and 1987; the future of the station beyond that date uncertain.

S.Quegan, UK

Siple & Halley are separated by ~1½ hrs in MLT. Have you tried to correlate observations from these 2 stations with this delay taken into account?

Author's Reply

The correlation of parameters such as hmF2 and foF2 has not been carried out. The only detriment to doing such a correlation is the density of measurements, which probably is insufficient. In this study, the measurements were made at 10—15 minute intervals.



THE VARIABILITY AND PREDICTABILITY OF THE MAIN F-REGION TROUGH DETERMINED USING DIGITAL IONOSPHERIC SOUNDER DATA

By
Alan S. Rodger and John R. Dudeney
British Antarctic Survey
Natural Environment Research Council
Madingley Road
Cambridge, CB3 OET
United Kingdom

ABSTRACT

The main F-region (or mid-latitude) electron density trough occurs near $\Lambda = 60°$ and is associated with significant meridional gradients in electron concentration. Despite many satellite studies of the trough, the causes of the variability of its shape as a function of time, geomagnetic and solar activity is still poorly understood. This is illustrated by the large discrepancies between the various empirical formulae that have been developed to estimate the trough latitude for specified geomagnetic conditions. These problems arise partly because satellite data cannot be used to differentiate adequately between spatial and temporal variations. There have been very few detailed ground-based studies of the trough. This is rather surprising considering that it can have a major influence on radio propagation at all frequencies on trans-Atlantic and trans-polar circuits. However, with the deployment of a sophisticated, digital, ionospheric sounder with direction-finding capabilities at Halley, Antarctica (76°S, 27°W; $\Lambda = 61°$) in 1981, a new and powerful research tool for trough studies has become available. The observations from this equipment have significantly improved our understanding of several features of trough morphology and in particular the causes of some of the variability. The four aspects of this variability that are discussed here are the orientation of the poleward edge of the trough with respect to Halley; the variation of the maximum plasma frequency of the poleward edge; the signature of the Harang discontinuity in the poleward edge and the latitudinal movement of the poleward edge as a function of time and geomagnetic activity. A framework is described for incorporating these aspects of trough morphology into a realistic model for predicting the location and maximum plasma density of the poleward edge as a function of time and the prevailing geomagnetic conditions. Such a model should be of significant benefit to those involved with radio communications at high latitudes.

1. INTRODUCTION

The mid-latitude electron density trough or main F-region trough is a major feature of the night-side ionosphere at sub-auroral latitudes. The trough can be considered to consist of three main regions:
- an equatorward edge where the processes of the plasma transport and recombination are the same as those expected at magnetic mid-latitudes,
- a trough minimum where the plasma densities are anomalously low,
- a poleward edge where the maximum plasma density increases significantly, typically by more than an order of magnitude compared with the trough minimum. These features combine to create a large and dynamic structure, which can have very significant effects on radio wave propagation over sub-auroral and trans-polar communications circuits. The mid-latitude trough forms in a region where the co-rotation and convection electric fields are approximately equal in magnitude but opposite in direction in the pre-midnight sector. Modelling studies (1, 2, 3, 4, 5, 6) have shown that this combination of electric fields can give rise to a large region in which plasma is effectively stagnating in fixed sun-earth co-ordinates. If this region is not illuminated by the sun and if there is no production by particle precipitation, then normal recombination processes cause an electron density trough to be formed.

Several other processes that could also contribute to the trough's formation have been suggested. For example, the trough is a region where a large poleward-directed electric field that leads to an increase in the plasma recombination rate is frequently observed. This, in turn, could assist in the formation of the trough (7). Auroral zone heating may cause air rich in molecular nitrogen to be transported to the trough region where an increase in the normal F-region recombination rate would result. Also, the outflow of plasma along magnetic field lines that thread the trough may cause a plasma depletion (8), though it is now considered to be of minor importance for trough formation. The relative importance of all these processes has not yet been fully established under a range of geomagnetic conditions and further modelling work would be desirable.

The mid-latitude trough can be identified readily, both in satellite data and with ground-based sensors such as incoherent scatter radars and ionosondes, and thus it has been studied for over two decades. Much of the early work concentrated upon determining the latitude of the trough as a function of time and geomagnetic activity as well as its location with respect to other ionospheric and magnetospheric features such as the equatorward edge of the diffuse aurora and the plamsapause (See reviews 9, 10). As a

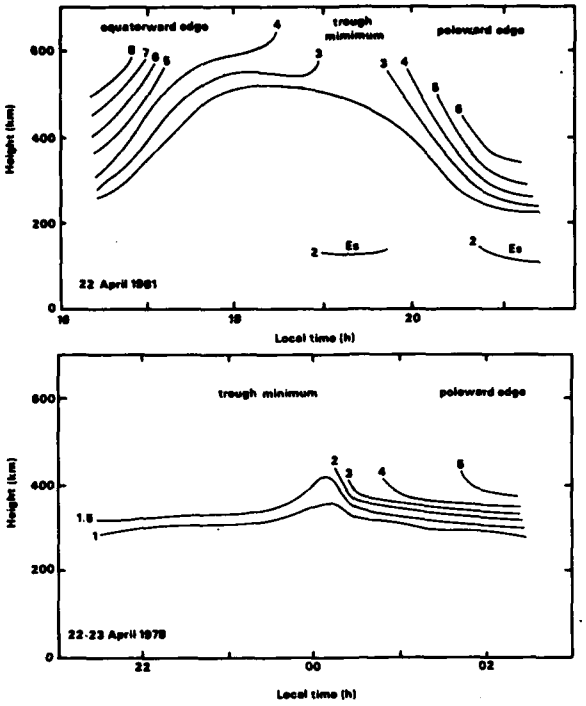


Fig. 1. Iso-ionic contours for two occasions when the mid-latitude trough passed over Halley, Antarctica. The component parts of the trough, the equatorward edge, trough minimum and poleward edge of the trough are labelled. The numbers associated with the contours indicate plasma frequency in MHz. Upper panel after Dudeney et al., (16) and the lower panel from Rodger and Pinnock, (15).

result of these studies, two basic factors regarding trough phenology have been agreed: that the trough moves to lower magnetic latitudes through the night under steady geomagnetic conditions and that, at any given time, the latitude at which the trough occurs is lower the greater the level of geomagnetic activity. However, there are many factors for which there is not a general concensus or that have been inadequately studied to date. For example, there have been observations that variously suggest that the deepest troughs are observed at dawn, at dusk or near midnight. Most studies of the trough have considered the trough under steady geomagnetic conditions and assumed that the magnetospheric convection electric field was constant both in magnitude and direction; observations show clearly that this is not the case (11, 12).

It is this variability of features of the trough and, in particular, of the poleward edge that will be discussed in some detail in this paper, using observations from the Advanced Ionospheric Sounder (AIS) deployed at Halley, Antarctica (76°S, 27°W) (13). As an illustration of this variability, two latitudinal cross-sections of the trough are shown in Fig. 1, one for disturbed geomagnetic conditions and the other for a relatively quiet night. The way that these sections were determined is described in detail by Dudeney et al. (14) and by Rodger and Pinnock (15) from where they have been slightly redrawn. The three component parts of the trough as described above are indicated for the two examples and reveal that marked differences can occur. There are four aspects of the variability of the poleward edge that will be discussed in some detail:
- the orientation of the poleward edge with respect to the observing station, Halley,
- the variation of the maximum plasma frequency of the poleward edge,
- the signature of the Harang discontinuity in the poleward edge,
- the latitudinal movement of the poleward edge as a function of time.

Where appropriate, reference to work using the AIS data that has already been published is made (14, 16, 17). A realistic approach is adopted towards incorporating this information into a predictive model for estimating the location and plasma density of the poleward edge of the trough under a prescribed set of geophysical conditions.

2. OBSERVATIONAL METHODS

The Advanced Ionospheric Sounder was deployed at Halley, Antarctica ($\Lambda = 61°$) in 1981. The AIS consists of a powerful hf pulse transmitter, two sensitive receivers and sufficient computing power both to control all the sounding parameters and to pre-process the data. With its spaced receiving antenna array, it is possible to record the complete vector description of each ionospheric echo (18, 19, 20). Thus, the range, azimuth and elevation of echoing regions can be determined unambiguously (21, 22).

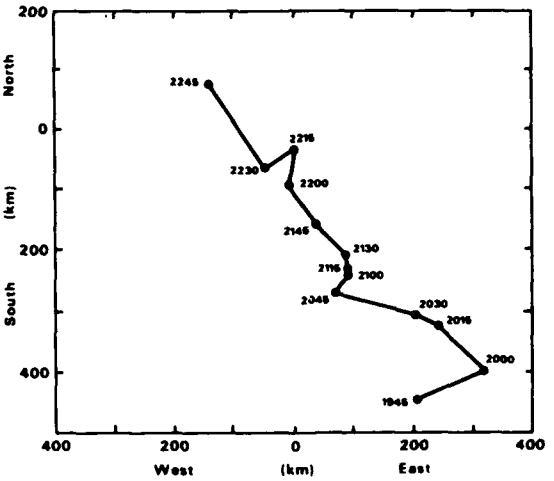


Fig. 2. The location of the poleward edge of the trough for 15 June 1982 in geographic co-ordinates as a function of local time.

The poleward edge of the trough forms a large latitudinal gradient in electron density. If this is suitably orientated, it can be a good reflector of obliquely propagated radio waves from a ground-based sounder over a wide range of frequencies. Thus, the trough can be observed at a considerable distance from an observing station (up to 8 degrees) and its change of location with time can be determined. An example for the 15 June 1982 is shown in Fig. 2. The poleward edge is first located about 450 km to the south-east of Halley at 1945 LT and over the course of the next three hours moves in a north-westerly direction, passing overhead about 2230 LT. Each data point on Fig. 2 is the mean echo location of many individual echoes normally taken over a small range of frequency spread-F (23) on the poleward edge traces when the data are presented as ionograms, hence there is some scatter in the positioning of an echoing region, typically of the order of ± 50 km. This direction-finding capability has been used extensively in this paper. A more comprehensive description of the technique is given by Dudeney et al., (14). A summary of the assumptions that are made and an assessment of their possible effects is discussed by Rodger and Pinnock (24).

3. DATA ANALYSIS

The AIS data-set from Halley used for this paper consists of 37 nights observations during the austral winters of 1982 and 1983. All nights on which the trough and the poleward edge could be readily identified in July 1983 were used (21 nights). On the remaining 11 nights of this month, geomagnetic field was either sufficiently disturbed to cause loss of data through blackout (25), or activity was so low that the trough did not come within the observing range of the AIS. Added to these data were 16 nights taken through June and July 1982 to provide as wide a range of geomagnetic conditions as possible. Thus, the data sets presented in the next sections are representative of Kp in the range 0 - 5.

For each night analysed various summary plots were made, from which it is relatively easy to identify the trough minimum and the poleward edge. Examples of these summaries are given in Fig. 3. Fig. 3a shows the variation in height of all ionospheric echoes received when ionograms were made at 15 minute intervals through the night. From 1800 LT the virtual height of the F-region rises steadily. This rate of rise is greater than that normally observed after sunset at magnetic mid-latitudes and is the typical signature of the trough minimum moving over Halley. The corresponding variation of frequencies reflected from the F-region, defined as being above 250 km, (Fig. 3b) indicates a reduction of the daytime ionisation through recombination between 1800 and 1830 LT, then a stable level until 2030 LT, when the poleward edge of the trough is first observed. Its presence can be confirmed by studying the individual ionograms but, with practice, this becomes unnecessary. Examples of the sequence of ionograms observed as a trough passes over an observatory are given in references 14, 26, 27 and 28. For the next four hours echoes from the trough minimum (those below 1.8 MHz) and those from the poleward edge (echoes above 2.0 MHz) can both be seen. As the poleward edge approaches, its plasma frequency is seen to increase steadily. For this night the poleward edge moved equatorward till about 2230 LT at about 70 m/s. Once the poleward edge passed over Halley, the AIS could no longer be used for studying its equatorward motion. The latitudinal movements are consistent with the decrease in virtual height of the poleward edge (Fig. 3a) followed by a relatively steady height from 2300 LT of about 380 km.

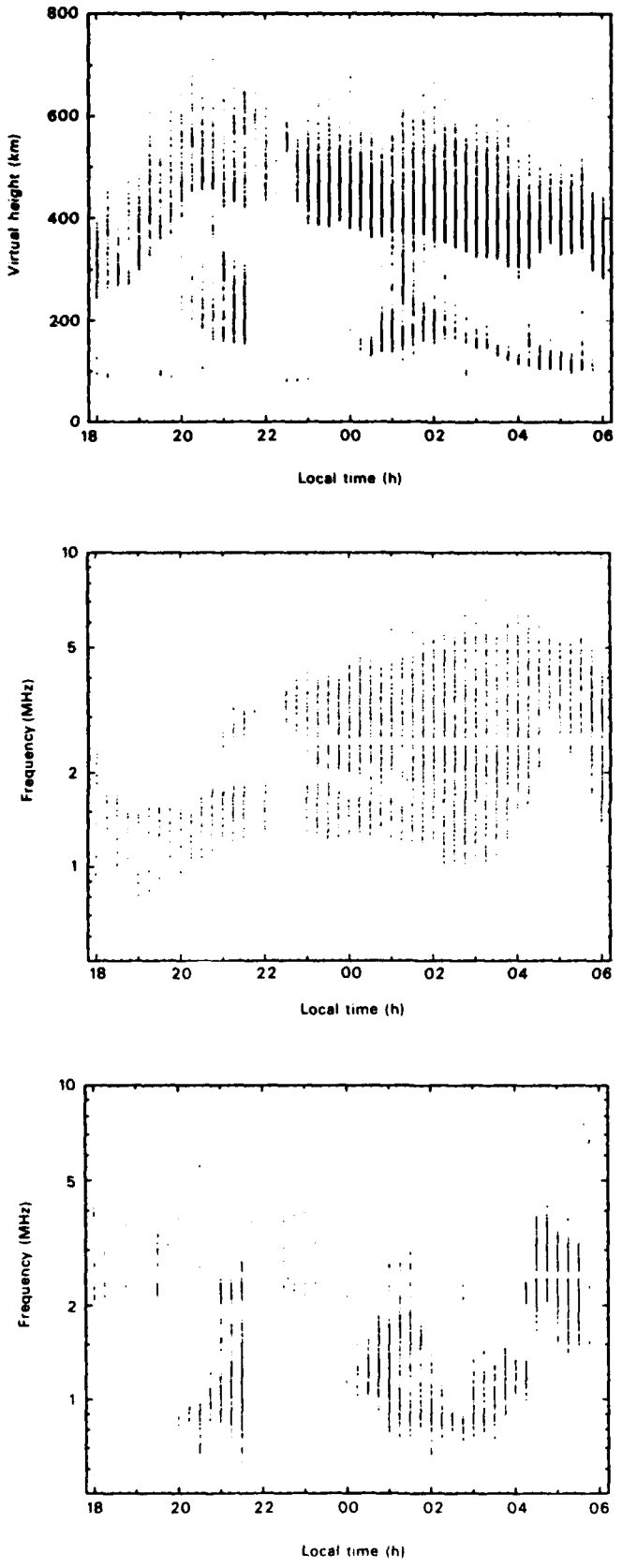


Fig. 3. (a) The virtual height of all o-mode echoes recorded by the AIS between 1800 LT on 21 June and 0600 LT on 22 June 1982. (b) The variations in the frequencies at which o-mode echoes are reflected from the F-region on the same night. (c) Same as 3 (b) but for E-region, o-mode echoes.

The corresponding variations in the frequencies of echoes returned from the E-region, defined as being below 200 km, for the same night are shown in Fig. 3c. For about 90 minutes from 2000 LT, there is some precipitation into the E-region but the fluxes must be relatively low as the maximum plasma frequency remains below 3 MHz under the poleward edge. Direction-of-arrival information shows that the sporadic E at this time is at considerable obliquity. Once the poleward edge is overhead there is a steady drizzle of precipitation into the E-region but again the fluxes must be small as the plasma frequency does not exceed 2 MHz until 0400 LT, when a small substorm occurred. Also, the spectrum of precipitating particles must be relatively soft (< 20 keV) as there is no significant variation in absorption till the substorm occurs. This event could be regarded as typical for relatively quiet geomagnetic conditions, Kp ~ 2.

After identifying each of the features of the trough, the location of the poleward edge was determined and a plot similar to Fig. 2 was produced for each night. From these data the equatorward motion of the poleward edge as a function of time and magnetic activity is clearly demonstrated.

4. THE ORIENTATION OF THE POLEWARD EDGE

Several empirical equations have been used to give the invariant latitude of some features of the trough as a function of time and geomagnetic activity. Two of these (29, 30) include terms that are linear with time but the equation given by Spiro (31) has a polynomial term for time and that due to Halcrow and Nisbet (32) a complex exponential. All these empirical equations were derived using satellite data. In this section, the form of the time term will be discussed using ground-based data from the AIS.

All the data points giving the location of the poleward edge for the 37 nights under study were separated into two-hour local time windows, e.g. 1800-1959, 2000-2159, etc. This was done irrespective of the day or the prevailing geomagnetic conditions. An example of the scatter plot for 0000-0159 LT is shown in Fig. 4a. This again illustrates the general tendency for the data to lie in a plane slightly skewed with respect to the geographic meridian. The line of best fit through the data is also drawn on Fig. 4a. Similar lines of best fit can be found for the other two-hour time bins and each of these is shown in Fig. 4b. It is apparent that the mean angle at which the trough is observed rotates slowly with time. This is not consistent with there being a linear term in the empirical equation describing the variation of the location of the trough with time. The perpendicular to these lines of best fit gives the orientation of the poleward edge with respect to the station. If these angles are mapped up into the equatorial plane, then there is remarkably good agreement between them and the tear-drop model of the plasmapause (33). Although the tear-drop model of the plasmapause may not represent the magnetospheric electric field very well and more representative models now exist, such good agreement between the poleward edge and this simple model could be a great practical advantage for radio communications predictions. The present work provides the largest and most accurate data set available to date, though previous analyses have shown similar results (14, 15, 17).

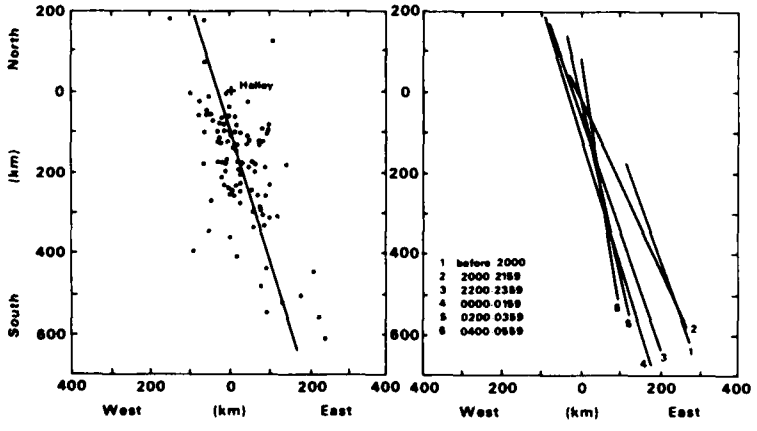


Fig. 4. (a) The geographic location of the poleward edge of the trough with respect to Halley for any of the 37 nights under study for which there were data in the period 0000-0159 LT. together with the line of best fit. (b) Lines of best fit for all the two hour time bins from 1800 to 0559 LT, produced in a similar manner to 4(a).

5. THE MAXIMUM PLASMA FREQUENCY OF THE POLEWARD EDGE

For each of the 37 nights analysed the highest and median maximum plasma frequencies of the poleward edge of the trough were found. These data are plotted in Fig. 5a and b respectively. Each of the data sets shows that there is a pronounced positive correlation between Kp and the plasma frequency of the poleward edge, though there is some scatter in the data. The linear regression line (y upon x) is also drawn on each figure; the gradient and intercept of these lines and the correlation coefficient are given in Table 1. Both correlation coefficients are such that the results are signficiant at the 99% level.

TABLE 1

	Sample size	Slope (MHz/Kp)	Intercept (MHz)	Correlation Coefficient
Highest plasma frequency	37	0.695	3.991	0.567
Median plasma frequency	37	0.313	2.576	0.509

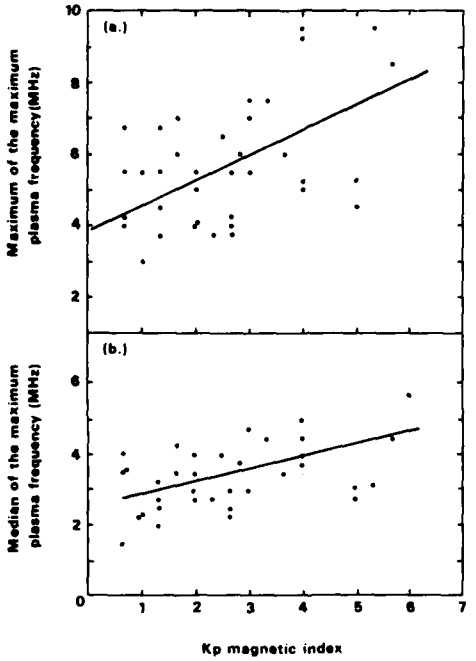


Fig. 5. The variation in (a) the highest and (b) the median maximum plasma density of the poleward edge of the trough as a function of geomagnetic activity. The linear regression lines y upon x are shown also.

The slope of the "maximum" line (for the maximum plasma density) is approximately twice that for the "median", indicating that the former is much more strongly controlled by geomagnetic activity. Since the data sets are from around mid-winter in the Antarctic, there can be no local contribution due to solar photo-ionisation that forms the poleward edge. There is no correlation between either the highest or the median maximum plasma frequency and the time at which it occurred.

6. THE MERIDIONAL MOVEMENT OF THE POLEWARD EDGE

With the direction-finding capability of the AIS, it is possible to determine the equatorward motion of the trough as a function of time. This has been done for the entire data set described in section 2 and is shown in Fig. 6. The data have been separated according to the geomagnetic activity index, Kp. In all of the examples the poleward edge of the trough is seen to move equatorward with time as would be expected from previous observations (see section 1) irrespective of the level of geomagnetic activity. There are a few examples where the poleward edge then moves polewards but these are relatively rare (~ 5% of occasions). Spiro (31), using Atmospheric Explorer satellite data, and Halcrow and Nisbet (32) using Alouette, found that the trough drifted back to higher invariant latitudes after 0330 MLT sufficiently often to dominate the statistics for relatively quiet geomagnetic conditions. Thus, this is a feature of their empirical formulae. Our data are in disagreement with the satellite data over this point.

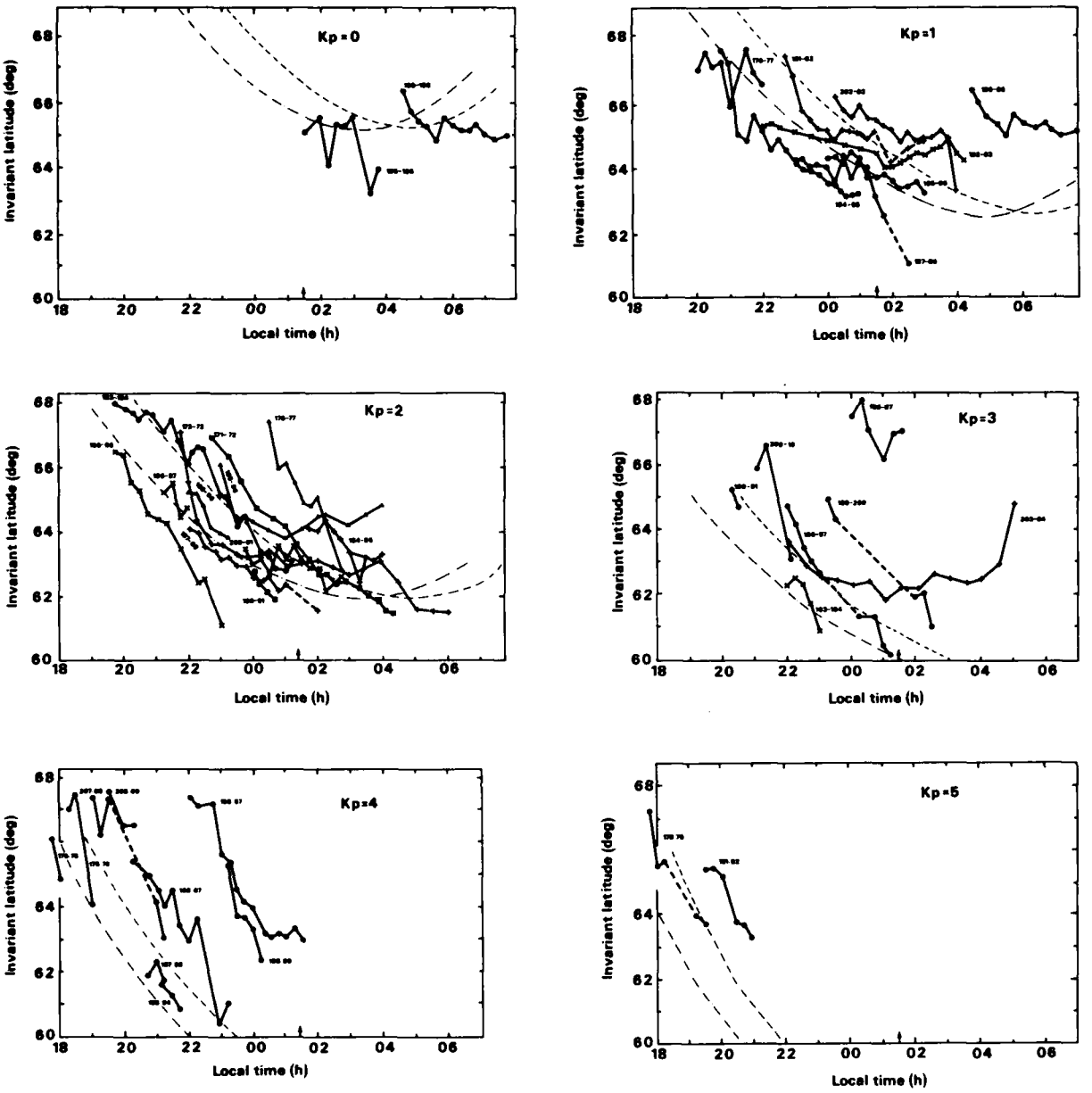


Fig. 6. The variation in the invariant latitude on the poleward edge of the trough as a function of local time separately for each level of geomagnetic activity in the range Kp = 0 - 5. The dot-dash line is the empirical formula for the trough location given by Spiro (31) and plotted in local time. The broken line is Spiro's equation plotted in magnetic local time.

The time at which the poleward edge is observed is in general progressively earlier as Kp increases, again consistent with previous observations. Also, the poleward edge on average moves more rapidly equatorward during periods of increased geomagnetic activity (15, 34).

The most striking feature of these data is the variability, at any given level of geomagnetic activity, in the time that the poleward edge might be observed overhead at a fixed latitude. As an illustration of this important point, the time at which the trough was observed at $\Lambda = 66°$ when Kp = 1 ranged from about 2100-0500 LT; at the same latitude, when Kp = 2, the spread was between 2000 and 0100 LT. The number of samples from other levels of geomagnetic activity are not as high but clearly show considerable variability also.

There has been some discussion about whether the Spiro empirical equation giving trough location should be expressed in local time, LT, or magnetic local time, MLT (14). At Halley, MLT = LT - $1^1/_2$ h. Spiro's equation has been drawn on Fig. 6 as a dot-dash line for LT and as a broken line for MLT. These lines have been moved 1° poleward to make an allowance for the fact that Spiro's equation referred to the trough minimum whilst the data set here is determined using the poleward edge. An analysis of polar

orbiting satellite data measuring electron concentration would suggest that the 1°Λ is reasonable (e.g. 35). It could be suggested that the equation in MLT might give slightly better agreement for all levels of Kp, except at Kp = 1 when LT appears more appropriate and at Kp = 0 when there is insufficient data to draw a firm conclusion. However, there is considerable scatter in the data.

A similar comparison was carried out using the Halcrow and Nisbet (32) equation appropriate for the poleward edge. Overall the match to the data was not quite as good as that for the Spiro equation in either timeframe. However, it should be noted that the basis of the Halcrow and Nisbet result is a northern hemisphere data set.

It can be concluded that Kp is an inadequate index of geomagnetic activity for estimating the latitude of the poleward edge of the trough. Further discussion of this is given in section 8.

7. THE SIGNATURE OF THE HARANG DISCONTINUITY

The Harang discontinuity marks the separatrix of the two convection cells on the night-side of the auroral oval. In principle, there may be a marked difference in the poleward edge of the trough about this time as the plasma that forms it in the morning and evening cells may have different origins and time histories. Also, the shape of the iso-ionic contours of the poleward edge in the vicinity of the Harang discontinuity has not been described in detail before. Therefore both these points are discussed in this section. The method used to identify the Harang discontinuity was that described by Rodger et al., (36) using the local magnetograms from Halley. The following conclusions can be drawn from this analysis:-

1. There was no consistent variation in the maximum plasma frequency about the Harang discontinuity.

2. The rate at which the poleward edge of the trough moves equatorward is the same for the evening and morning cells in the vicinity of the Harang discontinuity.

3. On 9 occasions, there appeared to be a consistent signature in the virtual height of the F-region, which occurred about the same time as the Harang discontinuity. The virtual height was seen to fall steadily prior to the passage of the discontinuity and then to rise significantly typically by ~ 50 km. The reduction was probably associated with the equatorward motion of the poleward edge with time. The subsequent rise could not be explained as a horizontal movement and is a real increase in the height of the F-layer. There appear to be no particular similarities in the geophysical conditions under which the nine examples occurred.

4. On three occasions the poleward edge was seen to the south-east immediately before the passage of the Harang discontinuity then the echoing region moved rapidly westwards to almost due south of Halley where it remained through the rest of the period of observation. It is not clear whether this westward movement of the echoing region is really a Harang discontinuity effect or just a slightly more irregular motion of the echoing region to the south of Halley, which is observed through the night anyway (see section 3).

5. Also, on nine occasions, the passage of the Harang discontinuity was marked by a rapid increase in the maximum plasma frequency of the E-region, indicating that either the flux of precipitating particles had increased or their spectrum had changed. The relationship of the poleward edge of the trough to sporadic E has been discussed elsewhere (37, 38).

This preliminary analysis indicates that there are no outstanding and repetitive features that would be first order terms in any practical model of the poleward edge.

8. DISCUSSION

Four aspects of the poleward edge of the trough, which have an impact upon the production of an empirical formula describing its location and maximum plasma density as a function of time, have been investigated in some detail using data from the Advanced Ionospheric Sounder at Halley. The study of the orientation of the poleward edge with respect to Halley has indicated that a linear term for time in an empirical formula is inappropriate and that a non-linear term should be used. The form of the time term should be very similar to that describing the location of the plasmapause in the simple tear-drop model (33) that is quoted below from Rycroft (39).

$$\frac{91.5}{L(t)} - \frac{91.5}{L(00)} = E \sin \emptyset \; L(t)$$

In this equation, L(t) is the L-shell of the plasmapause at time t, ($\Lambda = \cos^{-1} L^{-1/2}$), L (00) is the L-shell at midnight and $\emptyset$ is the angle from the noon-midnight line (15° equivalent to one hour).

The form of this equation is simpler than the non-linear time term in the Halcrow and Nisbet or the Spiro empirical equations, but it suffers from the limitations that it is based upon an idealistic description of the constant dawn-dusk convection electric field E (in kV Re^{-1}). However, despite this restriction, it appears that such a formulation may be of great value if incorporated into a predictive model for the location of the poleward edge of the trough.

Significant longitude structure can occur in the poleward edge probably as the result of substorm activity. Exactly how such features of the trough (17, 40) could be accounted for in any empirical formula giving the location of the trough is not clear, but a term containing a description of auroral activity over the previous few hours (e.g. the auroral electrojet index AE) would be a possibility.

Two equations describing the variations in the highest and median maximum plasma frequencies of the poleward edge as a function of gemagnetic activity, as indicated by the Kp index, have been determined, although Kp is rather a poor index for these studies (see section 6). Fig. 5 shows that there is a significant geomagnetic control over these maximum plasma frequencies and, in principle, these equations could be included in any empirical formula for the poleward edge plasma densities, though repetition of this work with a more suitable geomagnetic index would be worthwhile. Also, the data set used to formulate the equations was somewhat limited in that it was only representative of winter conditions at very high geographic latitude. Further analyses should be done using similar data from other sub-auroral stations, and the present study should be extended to determine the seasonal and solar cycle variations of the maximum plasma frequency of the poleward edge.

Studies of the poleward edge of the trough in the vicinty of the Harang discontinuity show that there are no important effects that would need to be included in an empirical model (section 7). The most important effect of the Harang discontinuity appear in the E-region where the vertical distribution of ionisation changes significantly about magnetic midnight (38).

The analysis of the equatorward motion of the poleward edge showed that the results from Halley were in general agreement with the well-known facts about the trough (see section 1). However, there is considerable variability of the time at which the poleward edge is seen from one occasion to the next under similar geomagnetic conditions. Much of this variability is attributable to the fact that the geomagnetic index, Kp, is a rather poor index for this type of analysis. The two principal factors that determine the location of the poleward edge are the location of the equatorward edge of the particle precipitation boundaries and the equatorward limit of the flux tubes that have convected across the polar cap. The relative contribution of the two processes as a function of magnetic time have been discussed by Rodger and Brace (17). Both of these processes are very strongly influenced by the magnitude and direction of the Interplanetary Magnetic Field (IMF). For example, the ratio of the sizes of the morning and evening convection cells is very dependent upon the magnitude and direction of the y-component of the IMF, By (11). The equatorward limit of precipitation is mainly controlled by the magnitude of the z-component of the IMF, Bz (41, 42, 43). Therefore, it would be more realistic for any model of the location of the poleward edge to contain terms involving Bz and By. Also, Cowley (44) has pointed out that there should be detectable effects on the convection pattern resulting from the influence of the x-component of the IMF, Bx, and therefore a term involving this component may also be necessary.

Recent evidence suggests that the twin cell convection pattern is maintained for some hours after Bz has turned northward. It is not clear where the trough might form, if indeed it forms at all under these circumstances. However, because the magnetosphere is acting as an integrator of solar wind conditions, some account of these for a few hours preceding the time of observation of the trough may be needed to model its location empirically as a function of time.

Thus, the important factors involved in the location of the poleward edge of the trough and its maximum plasma density which should be incorporated into empirical modelling are:

1. A description of the present IMF (Bx, By, Bz)

2. A temporal variation similar to that of the tear-drop model of the plasmapause.

3. A term describing substorm activity over the past few hours (AE?)

4. A term incorporating the IMF variations over the previous few hours.

At present, the solar-terrestrial community is very poorly placed to have the IMF data in near-real time since the ISEE-3 spacecraft was removed from its halo orbit. However, work should be pursued along these lines so that those interested in radio communications at high latitudes are in a position to capitalize fully when suitable spacecraft data become available again.

9. CONCLUSIONS

1. Data from the Advanced Ionospheric Sounder at Halley, Antarctica have been used to make a detailed study of many features of the poleward edge of the trough. The well-established features of the trough phenology are clearly visible in these digital data, namely that the poleward edge moves to lower invariant latitudes through the night under steady geomagnetic conditions and that the time at which it is seen at Halley is progressively earlier as geomagnetic activity increases.

2. It is found that, on average, the orientation of the poleward edge of the trough with respect to Halley changes steadily through the night in a manner consistent with the tear-drop model of the plasmapause.

3. A very striking feature of the data analysed is the considerable variability in the time at which the poleward edge is observed and in its maximum plasma density under similar geomagnetic conditions. There has been some investigation of the causes of this variability and the use of Kp has been found to be a major source of problems in this work. Also, some of the variability can be attributed to changes in the interplanetary magnetic field and further studies of IMF field effects on the poleward edge are required.

4. It has been further shown that there are no major changes in the properties of the poleward edge in the vicinty of the Harang discontinuity. However, the rise of the F-layer at times later than the Harang discontinuity, which occurs quite frequently, remains to be explained.

5. There is strong geomagnetic control of the maximum plasma density of the poleward edge of the trough.

6. The present empirical formulae used to describe the location of the trough as a function of time and geomagnetic activity (Kp) are rather poor. A list of the important points that need to be considered for a more accurate means of predicting where the poleward edge will occur, and what its maximum plasma density will be, has been proposed.

10. ACKNOWLEDGEMENTS

The authors wish to acknowledge the assistance provided by Miss Sue Linten who carried out much of the basic data analysis used in this paper. Thanks are also due to Mr K. Wright for preparing some of the figures and Miss S.M. Norris for typing the manuscript.

11. REFERENCES

1. KNUDSEN W C, J. geophys. Res. 79, 1046, 1974.
2. SPIRO R W, R A HEELIS and W B HANSON, J. geophys. Res., 83, 4255, 1978.
3. SOJKA J J, W J RAITT and R W SCHUNK, J. geophys. Res., 86, 2206, 1981.
4. SOJKA J J, W J RAITT and R W SCHUNK, J. geophys. Res., 86, 6908, 1981.
5. SOJKA J J, W J RAITT and R W SCHUNK, J. geophys. Res., 87, 187, 1982.
6. QUEGAN S., G J BAILEY, R J MOFFETT, R A HEELIS, T J FULLER-ROWELL, D REES and R W SPIRO, J. atmos. terr. Phys., 44, 619, 1982.
7. SCHUNK R W, W J RAITT and P M BANKS, J. geophys. Res., 80, 3121, 1975.
8. NISHIDA A, J. geophys. Res., 71, 5669, 1966.
9. WRENN G and W J RAITT, Annls. geophys., 31, 17, 1975.
10. MOFFETT R J and S QUEGAN, J. atmos. terr. Phys., 45, 315, 1983.
11. HEELIS R A, Rev. geophys. space Phys., 20, 567, 1982.
12. CLAUER C R, P M BANKS, A Q SMITH, T S JORGENSEN, E FRIIS-CHRISTENSEN, V B WICKWAR, J D KELLY and J DOUPNIK, Geophys. Res. Letts., 1, 891, 1984.
13. DUDENEY J R, New Sci., 91, 714, 1981.
14. DUDENEY J R, A S RODGER and M J JARVIS, Radio Sci., 18, 927, 1983.
15. RODGER A S and M PINNOCK, In Exploration of the polar upper atmosphere (Edited by C S DEEHR and J A HOLTET) Reidel, Dordrecht, Holland, p. 463, 1980.
16. DUDENEY J R, M J JARVIS, R I KRESSMAN, M PINNOCK, A S RODGER and K H WRIGHT, Nature, 295, 307, 1982.
17. RODGER A S and L H BRACE, submitted to J. atmos. terr. Phys., 1985.
18. GRUBB R N, NOAA Tech. Memo. ERL SEL 55, Boulder, Colorado, 1979.
19. WRIGHT J W, NOAA ERL SEL Preprint 206, Boulder, Colorado, 1975.
20. WRIGHT J W and M L V PITTEWAY, Radio Sci., 14, 827, 1979.
21. DUDENEY J R and M J JARVIS, submitted to Radio Sci., 1985.
22. JARVIS M J and DUDENEY J R, submitted to Radio Sci., 1985.
23. PIGGOTT W R and K RAWER, URSI Handbook of Ionogram interpretation and reduction. Rep. UAG-23A, World Data Center-A, Boulder, Colorado, 1978.
24. RODGER A S and M PINNOCK, J. atmos. terr. Phys., 44, 985, 1982.
25. RODGER A S, D H BOTELER and J R DUDENEY, J. atmos. terr. Phys., 43, 1243, 1981.
26. BELLCHAMBERS W H, L W BARCLAY and W R PIGGOTT, The Royal Society IGY Expedition, Halley Bay, 1955-1959, Vol. 2 p 179, Royal Society, London.

27. PIGGOTT W R, High Latitude Supplement to the URSI handbook of ionogram interpretation and reduction. Rep. UAG-50, World Data Center - A, Boulder Colorado, USA, 1975.
28. IONOSPHERIC NETWORK ADVISORY GROUP BULLETIN 42, Edited by A S Rodger, published by the World Data Center-A, Boulder, Colorado, USA, 1984.
29. RYCROFT M J and S J BURNELL, J. Geophys. Res., 75, 5600, 1970.
30. KOHNLEIN W and W J RAITT, Planet. Space Sci., 25, 600, 1977.
31. SPIRO R W, PhD Thesis, Univ. Texas at Dallas, Richardson, USA, 1978.
32. HALCROW B W and J S NISBET, Radio Sci., 12, 815, 1977.
33. KAVANAGH L D, L W FREEMAN Jnr. and A J CHEN, J. geophys. Res., 73, 5511, 1968.
34. BOWMAN G G, Planet. Space Sci., 17, 777, 1969.
35. TULUNAY Y K and J SAYERS, J. atmos. terr. Phys., 33, 1737, 1971.
36. RODGER A S, S W H COWLEY, M J BROWN, M PINNOCK and D A SIMMONS, Planet. Space Sci., 32, 1021, 1984.
37. RODGER A S, C MORRELL and J R DUDENEY, Radio Sci., 18, 937, 1983.
38. MORRELL C, Brit. Ant. Survey Bull., 63, 1, 1984.
39. RYCROFT M J, In Correlated interplanetary and magnetospheric observations. Edited by D E PAGE, D REIDEL Publishing Company, Dordrecht, Holland, p 317, 1974.
40. JARVIS M J and F T BERKEY, EOS, 65, 1025, 1984.
41. KIVELSON M G, Rev. geophys. Space Phys., 14, 189, 1976.
42. COWLEY S W H, Rev. geophys. Space Phys., 20, 531, 1982.
43. MAKITA K, C -I MENG and S -I AKASOFU, J. geophys. Res., 88, 7969, 1983.
44. COWLEY S W H, Planet. Space Sci., 29, 809, 1981.

DISCUSSION

T.A.Croft, US

In past solar wind research, I perceived a tendency for study of the magnetic field and its correlation, but a comparative lack of similar interest in density of the wind. Yet, at times, the density may be so low that the "Wind" is a near-vacuum and this fact is not apparent in magnetic field measurements.

Since onslaughts of dense solar wind plasma clearly affect Earth strongly, it must also be true that intervals when the density is lower than average (7/cc) must be marked by ineffectiveness in modifying Earth's environment. As a result, I would suggest a search for correlations with solar wind density in addition to the magnetic field investigations you have outlined.

Author's Reply

The most significant effects of the solar wind density on the observed plasma densities in the poleward edge of the trough are probably as a result of precipitation in the vicinity of the polar cusp. There is evidence that the magnitude of this precipitation is dependent upon the solar wind density as well as the magnitude and direction of the Bz component of the interplanetary magnetic field. The plasma in the cusp will convect across the polar cap and eventually should be observed in the poleward edge of the trough, although there will be some recombination of this high density plasma in the 1—2 hours which it takes to transit from the cusp to the poleward edge. There has been evidence of high density patches of ionization convecting across the polar cap provided by Weber et al 1984 (Journal of Geophysical Research).

A possible experiment to test the important of this cusp as a source of plasma for the poleward edge of the trough would be to cross correlate the temporal variations of the maximum plasma density of the ionosphere observed in the cusp or the polar cap with similar data from a station observing the poleward edge of the trough.

N.C.Gerson, US

From your observing site, the refractivity gradients of the trough display a longitudinal "tilt" whose magnitude and direction vary throughout the 24 period under this condition. The apparent reflection point of each probing HF ray may be located at a significant displacement from its true reflection point. To what extent would your results be changed by correcting for this error?

Author's Reply

There has been no significant consideration of the magnitude of this potential source of error. Ray-tracing studies by Villian et al, (Radio Science, 1984) through "realistic" distribution of electron density as determined by meridional scans of the Chatanika incoherent scatter radar suggest that as long as propagation of the radio wave is not significantly out of the plane of the magnetic meridian, then the lateral deviation of the radio wave is small. The direction of arrival information used in this paper varies from being in the magnetic meridian to ~25° to the east of it. Thus, I suggest that the magnitude of the effect you describe is small, although I agree that it should be investigated quantitatively.

SUMMARY OF SESSION V

Ionospheric Modification

by

Dr H.Soicher
Technical Program Chairman

Intentional modification (or heating) of the ionosphere by high-powered radio waves continues to be a subject involving much experimental and theoretical interest. Ionospheric changes that result from such heating are on a wide range of spatial and temporal scales. Such changes permit detailed investigation of the physical processes occurring through observations of the amplitude, phase and spectral content of radio waves that traverse the heated volume.

Jones and Robinson, in a review paper, highlight the propagation disturbances which can be produced when the ionosphere is modified by a high-power HF heating wave. Effects of modified ionospheric volume on systems whose frequencies range from ULF to UHF are discussed. While certain heating phenomena may have detrimental effect on radio systems, others may provide new operational channels not normally available in the natural ionosphere.

Lee et al discuss three HF heater wave-induced phenomena: simultaneous excitation of ionspheric irregularities and geomagnetic fluctuations; the enhanced plasma lines associated with electron acceleration by plasma turbulence; and, the conditions for occurrence of artificial spread F.

THE INFLUENCE OF IONOSPHERIC HEATING ON THE PROPAGATION OF RADIO WAVES

T B Jones and T Robinson

University of Leicester, Leicester, UK

Abstract

The ionospheric plasma can be modified on a wide range of spatial and temporal scales by the action of high power radio waves (heaters). As a result the amplitude, phase and spectral content of radio waves which traverse the heated volume can be altered markedly. This paper reviews various heating effects which can affect radio systems whose frequencies range from ULF to UHF. While certain heating phenomena may have a detrimental effect on radio systems, others may provide new operational channels not normally available in the natural ionosphere.

1 INTRODUCTION

The ability of high power radio waves to 'modify' the ionosphere has been recognised since the discovery of the Luxembourg Effect in 1933 (Tellegen, 1933). In the early 1970's it was realised that modification (Heating) with very high power waves could produce a wide range of plasma instabilities in addition to the collision frequency changes associated with the Luxembourg Effect. High power Heating facilities were constructed at Boulder, Arecibo, Tromsø and in the Soviet Union to investigate these important and sometimes unexpected plasma phenomena.

In addition to the plasma physics interest of these experiments it was quickly demonstrated that considerable changes were produced in the characteristics of other radio waves propagating through the modified (heated) ionosphere. Thus the importance of heating in influencing radio system performance was established.

This paper discusses some of the effects produced by HF heating on radio wave propagation in the frequency range ULF to UHF.

2 HEATING FACILITIES

A typical heating installation consists of a transmitter capable of delivering about 2 MW of RF power in range 2 to 10 MHz. The transmitter feeds a large antenna array which normally forms a beam directed vertically into the ionosphere. Provision is made for radiating either O, X or linear polarization. The antenna gain will typically be about 20 db corresponding to an effective radiated power (ERP) of $\sim$ 200 MW. The power density F (μWm^{-2}) in the beam at a range R (km) is related to the ERP (MW) by

$$F = 82.6 \times ERP/R$$

Thus an ERP of 200 MW represents power fluxes of 150 μWm^{-2} and 65 μWm^{-2} at E (110 km) and F (250 km) region heights respectively. The heating transmitter can be modulated or can radiate a CW signal. Details of known heating facilities are given in Table 1.

Many of the experimental results contained in this review have been obtained at the heating facility located at Ramfjord, near Tromsø, Northern Norway, since this has been an active centre for heating research during the last few years. Two of the authors (P S and H K), have been directly involved in the design and construction of this facility.

3 ABSORPTION

The collisional absorption of the heater wave energy in the D-region produces a rapid increase in electron temperature which causes a subsequent increase in the electron collision frequency and hence the absorption co-efficient. These changes will influence the propagation of waves passing through the region, particularly at frequencies in the HF band and below. This type of heater induced D-region absorption effect is illustrated in Figure 1(a) for results obtained with a partial reflection radar during heating at Tromsø. The time constants for these processes are very short $\sim$ 0.2 m sec (Gurevich, 1978), thus when an amplitude modulation is applied to the heater wave, this can be transferred by the absorption process to low power HF waves passing through the D-region to be reflected in the higher levels of the ionosphere (Ginzburg and Gurevich, 1960). It is this process that was observed in the early Luxembourg Effect experiments and which for many years was thought to be the only consequence of ionospheric modification. However, during heating experiments in the early 1970's, new phenomena came to light. For example, during D-region cross modulation experiments in which two heater frequencies were employed, Jones (1973) demonstrated that enhanced effects occurred when the heater frequencies differed by the gyrofrequency (see Figure 1(b)).

Other experiments also demonstrated that marked F-region disturbances occurred when very high power waves were propagated through this region. Some of these disturbances, unlike

those in the D-region, were associated with interaction between EM and electrostatic waves and the generation of plasma instabilities. As a consequence of this, field aligned irregularities were produced ranging in scale size from a few metres to a few kilometres. Various mechanisms are thought to be responsible for the production of the different irregularity scale sizes. A simplified schematic diagram illustrating the processes by which small scale irregularities are produced is presented in Figure 2. These irregularities can modify the propagation characteristics of waves traversing the heated volume in many different ways. One of the most significant effects is the production of anomalous (or wide band) absorption. For this attenuation, energy is absorbed from HF waves propagating in the modified volume by the wave conversion mechanism, a completely different process to the normal deviative absorption. For quiet background ionosphere conditions, the anomalous absorption is independent of heater power provided a threshold of $\sim$ 5 MW is exceeded. Figure 3 illustrates the effect of Anomalous Absorption on the 3.78 MHz signal transmitted from a site some 50 km north of the heater and received some 50 km to the south of the heater (operating on 3.515 MHz). This slightly oblique path ensures that the diagnostic wave is not influenced by D-region effects and that it only interacts with the heated ionosphere at F-region heights (Jones et al, 1982). The measured absorption is about 15 db which is consistent with recent theoretical predictions (Jones et al, 1984).

The Anomalous Absorption process can impose a modulation from the heater wave on to the low power diagnostic propagating through the heated volume (Jones et al, 1983). Figure 4 illustrates how a 2 Hz modulation applied to the heater wave has been transferred to the diagnostic signal during 'O' mode heating. It should be noted that both upper and lower side bands are present in the received signal and are of approximately equal amplitudes.

Most absorption experiments have been conducted at vertical or steep incidence. However, oblique incidence studies have been conducted in the Soviet Union (Bochkarev et al, 1982). Absorption effects are noted on an oblique diagnostic signal propagating along a path nearly the same as that of the heated signal as indicated in Figure 5.

The amplitude of a radio wave is greatly influenced during its propagation through the modified D and F regions. The physical process giving rise to the attenuation are different in the two layers but both produce and decrease in signal amplitude.

4 FADING;SCINTILLATION AND SPREAD F

The larger scale ($\sim$ 1 km) irregularities created in the F-region during the heating process can also influence the propagation of radio waves. In the case of HF diagnostic waves reflected from the heated volume,an increase in the fading rate occurs. This is due to the enhanced 'roughness' of the reflecting surface due to the presence of the striations. Multiple reflections can take place allowing a cone of rays to propagate between the transmitter and receiver compared with the normal specularly reflected path. Interference between the waves contained in the cone produces the observed fading. The heater induced fading rate is found to depend on the state of the ambient ionosphere since in disturbed conditions it becomes difficult to separate the induced fading from the naturally occurring background. Examples of the heater induced fading are presented in Figure 6 (Wright, 1973).

The presence of naturally occurring kilometre scale irregularities produces scintillation effects on radio waves of frequencies high enough to penetrate the ionosphere. These effects have been noted on frequencies up to $\sim$ 10 GHz and are generally accounted for in terms of the ionosphere acting as a phase diffracting screen placed between transmitter (satellite) and the receiver (ground). If the heater enhances the kilometre scale irregularities it modifies the phase diffracting screen so as to increase the scintillation rates (Rufenach, 1973; Basu et al, 1980). Examples of enhanced scintillation rates observed after heater turn on are reproduced in Figure 7. These induced fluctuations in phase and amplitude are likely to affect satellite communication systems especially when low signal to noise ratios are encountered.

The presence of the induced kilometre scale irregularities can sometimes be detected as a 'spread F' signature on vertical incidence ionograms recorded close to the heater. The induced spread F was a common feature of the Boulder heating experiments and an example recorded on the ionosonde located at Erie close to the heater at Plattville is reproduced in Figure 8 (Utlaut and Violette, 1974). A feature of the heating experiments at Tromsø has been the absence of induced spread F. This feature has not been observed on ionosondes close to the heating facility at Ramfjord although a careful search has been made. There is some evidence however of the multiple reflections from HF Doppler recordings which indicate the presence of many Doppler shifted components following heater turn on as indicated in Figure 9. The failure to observe the strong spread F features so common at Boulder has been ascribed to the difference in dip angle between the two locations. At Tromsø the Dip angle is 78° and so the vertical ionosonde views the field aligned situations 'end on', thus presenting a relatively small reflecting area which would account for the absence of the spread signal on the ionograms. Recent VHF scintillation measurement at Tromsø (Frey et al, 1984) have now confirmed the occurrence of heater induced irregularities with scale sizes $\gtrsim$ 1 km.

5 SCATTERING

The heater generated striations of the plasma which cause anomalous absorption are in general field aligned and have a regular spacial structure. A wide variety of scale sizes

can occur ranging from a few metres to tens of kilometres. A radio wave can thus be scattered from the heated volume provided the Bragg criteria, that the scatterers have a spacing equal to half the radio wave length, is satisfied. For maximum scatter intensity the incident ray must be orthogonal to the magnetic field direction. (The attenuation increases by some 6 db per degree away from orthogonality.) Scattering from heater induced striations has been reported for a wide range of frequencies ranging from 3 MHz to 0.5 GHz (Minkoff et al, 1974; Fialer, 1974).

A typical example of HF backscatter is presented in Figure 10 (Hedberg et al, 1983). The HF radar was located at Lycksele some 600 km south of the heater at Tromsø. Backscatter returns were obtained at 14 MHz during 'O' mode heating but were not present during 'X' mode heating. This confirms that plasma wave induced striations are responsible for the backscatter since these are only formed during 'O' mode heating. E-region scattering at VHF frequencies has also been observed from the Tromsø heater. Typical examples of this effect observed with the STARE system are presented in Figure 11. This indicates that even at VHF frequencies the heater volume can provide a scattering centre embedded in the ambient ionosphere. The large dip angle (78°) eliminates the possibility of field aligned VHF and UHF backscatter from the F-region at Tromsø. However, F-region field aligned scatter at 435 MHz (Figure 12) has been obtained at Boulder where the dip angle is 68°.

Many of the scattering experiments have been concerned with direct backscatter with collocated transmitter and receiver. In most practical applications oblique forward scatter is of more interest than direct backscatter. Several modelling studies have been undertaken of the areas that could be illuminated by forward scatter from a heated volume of known location. The results of one such study are reproduced in Figure 13. This illustrates the modelled scattering reception loci in the Mediterranean region. The communications and heating transmitters were respectively located in Spain and Italy for this study (Stathacopoulos and Barry, 1974). Experimental studies of the region illuminated by the scattering process were conducted at Boulder and an example of the results obtained is reproduced in Figure 14. In these experiments TV transmitters operating at $\sim$ 61.2 MHz were employed as the signal sources and the signals were detected over a wide area as indicated in the Figure (Frank, 1974).

There are many possible applications in communications and surveillance for forward scatter systems utilizing the heater induced scattering volume. It is beyond the scope of this review to discuss these in detail but it is likely that their performance will to some extent depend on the heater location since the magnetic dip angle determines the orientation of the scattering irregularities. Since maximum backscatter intensities are obtained along directions which are orthogonal to the irregularities then geometrical considerations will determine the extent and location of the region on the ground or at satellite heights, in which scattered signals can be received.

6 REFRACTION AND REFLECTION EFFECTS

In addition to the small and medium scale plasma irregularities created during heating, large bulk changes are also produced. These changes occur mainly due to the increase in electron temperature. Below 200 km photochemical effects dominate and the temperature dependence of the recombination rate leads to an enhancement of electron density. Above 300 km transport processes dominated and heater enhanced electron diffusion produces density depletions (Figure 15).

These large scale disturbances change the refractive index of the ionosphere and the position of the isoionic contours. Thus both the refraction and reflection of waves are influenced by the heated volume.

The reflection height changes have been investigated by measuring the phase of an HF wave reflected from the heated volume. A characteristic phase advance is noted at heater turn on and a corresponding phase retardation after the heater is switched off. Figure 16 illustrates the phase changes measured on a 3.78 MHz signal propagated at steep incidence through the heated volume at Tromsø. The time constant of the phase change is about 50 seconds compared with a few tenths of a second for that of the plasma striations. These large scale changes will influence the reflection heights and ray paths of signals propagating through the disturbed volume.

A study of the changes induced on a diagnostic signal propagated at oblique incidence along a similar path to a high power heating wave has been undertaken by Bochkarev et al, 1982. In addition to amplitude changes, both the azimuthal and elevation angles of arrival were changed by the heating processes, as illustrated in Figure 17. It should be noted that the diagnostic and heater frequencies were separated by only a few 100 KHz. Nevertheless, well defined heating effects were produced on the obliquely propagated signals from an obliquely propagated heating wave.

The creation of a region of enhanced electron density will produce enhanced refraction and will act as a diverging lens. Conversely a depletion in electron density will increase the refractive index and a converging lens will result.

This latter process is important for the self-focussing instability (Perkins and Valeo, 1974), which leads to locally enhanced heater power densities and electron temperatures.

The ability to form regions in which rays will converge or diverge has important practical applications. For example, it might be beneficial to concentrate (focus) rays at a particular point in or above the ionosphere. Figure 18 illustrates a theoretical model

describing the development of a self-focussing duct in the isoionic contours by the action of a powerful radio wave (Bernhardt and Duncan, 1982). Alternatively, it might be an advantage to increase the divergence of the rays,so that they may enter the F-region duct and so propagate to great disturbances with little attenuation.

Height and conductivity changes are also produced in the D-region and these can influence the terrestrial propagation of low and very low frequency waves. Complex amplitude changes recorded on low frequency signals reflected in the vicinity of the Boulder heater are reproduced in Figure 19. Similar results have been obtained at Tromsø (Barr et al, 1984). It should be noted that disturbances are produced only when the modified region forms a significant part of the propagation path. The propagation of VLF waves to great distances is therefore unlikely to be affected since the modified ionosphere will comprise only a small section of the path. If the heater is located close to the transmitter or receiver, modification effects might be produced on long distance paths but no detailed study of these has yet been undertaken.

7 RADIO EMISSIONS DUE TO HEATING

(a) LOW FREQUENCY WAVES

It has already been noted that below 200 km the temperature dependence of chemical recombination rates result in electron density (N_e) modification due to heating. In the D-region, electron collision frequencies (ν) can also be strongly modified. Changes in the ionospheric conductivity which result from these processes are given by

$$\Delta\sigma = \frac{\delta\sigma}{\delta\nu}\,\Delta\nu + \frac{\delta\sigma}{\delta N_e}\,\Delta N_e$$

The conductivity σ will then be modulated and will affect the electrojet currents flowing through the heated regions. This time varying current will radiate at the frequency of the modulation applied to the heating wave. Stubbe et al (1982) have shown that radiation can occur over a wide range of frequencies from ULF to VLF.

Examples of heater induced emissions produced at Tromsø for a range of modulation frequencies are reproduced in Figure 20. The radiation field strength falls rapidly above 7 KHz but below this frequency the signal strength remains strong,with peaks at 2, 4 and 6 KHz caused by multiple reflections between the ground and the ionosphere.

The induced VLF emissions can propagate to great distances with little attenuation in the spherical wave guide formed by the earth as one wall and the ionosphere as the other. Signals propagating in this mode have been detected at distances of up to 1,200 km from the heater (Barr et al, 1984). A VLF source located in the ionosphere will also radiate energy into the upper ionosphere and magnetosphere. In the magnetosphere these waves will propagate in ducted modes following the geomagnetic field lines. They will reach distances from the earth in the equatorial plane of several earth radii before returning to the ground at the conjugate point in the opposite hemisphere from where they were launched. The possibility therefore exists at these frequencies for communication with satellites and with sites in the conjugate hemisphere.

The generation of ULF and ELF (1-100 Hz) waves has also been demonstrated at Tromsø. The radiation efficiency is similar to that measured in the VLF band but the emissions are now found to be linearly polarized. Waves of these frequencies have a large penetration depth in the earth's surface and they could have applications for sub-surface communications.

At still lower frequencies, in the ULF range, the radiation efficiency increases markedly and is some three orders of magnitude greater than in the VLF band (see Figure 20). The signal strength is found to increase with decreasing frequency as indicated in Figure 20. These frequencies are below those normally used for practical applications but their high radiation efficiencies may enable them to be employed for some specialized applications.

(b) HIGH FREQUENCY WAVES

Radio wave emissions have also been detected from the heated volume in the HF band. These emissions occupy a frequency band some ± 100 KHz around the heating frequency (Thidé et al, 1982, Stubbe et al, 1984(a)). The spectrum of these secondary electromagnetic waves is highly structured and several maxima are present as indicated in Figure 21. The predominant peak appears approximately 10 KHz below the heating frequency.

When heating is performed on two frequencies simultaneously,not only are the features described above generated around each of the heater frequencies, but a new signal is produced at a frequency corresponding to the arithmetic mean of the two heater frequencies.

No applications have yet been proposed for these emission processes but they are important in our understanding of the instabilities (produced by the heater) which generate them.

It is well known that strong electromagnetic emissions at optical wave lengths are excited during heating (Weinstock, 1974). However, it has also been speculated that electromagnetic emissions in the microwave band may also be excited. The mechanism by which this might occur involves the excitation of Rydberg atoms which can exist in the rarified conditions in the upper atmosphere (Ustinov et al, 1979).

8 SELF MODIFICATION

This review has been mainly concerned with the effects produced by the heating wave on signals propagating through the modified volume. It is of interest to examine the influence of the ionospheric modifications on the heater wave itself, particularly since some modification effects are produced at relatively low powers. Kopka et al (1982) have examined the signal strengths of the heater signal reflected from the ionosphere and received some 50 km south of the heater location at Ramfjord. The variation in received signal strength as the heater power is increased from a low value to 260 MW and then decreased, is reproduced in Figure 22. At first the received signal strength increases with radiated heater power but at about ½ full power, self-absorption becomes apparent and the reflected power increases less rapidly than the transmitted power. Above about ½ full power, the received signal decreases as the transmitted signal increases. A constant signal level is then reached which is independent of the radiated power.

As the radiated power is decreased from its maximum value the received signal level remains constant and remains so until the radiated power has fallen to about ½ of full power. A further decrease in radiated power produces a decrease in the received signal power.

It is evident that self-absorption occurs at fairly low radiated power but at about ½ full power a second instability threshhold is exceeded which gives rise to an absorption mechanism which limits any further increase in reflected power. Once this "super self absorption" mechanism is operative it can remain so until the heating power is eventually reduced to about ½ max value, at which point the instability threshhold is no longer exceeded.

Also apparent from Figure 22 is the absorption asymmetry between the increasing and decreasing parts of the power cycle. This 'Hysteresis' effect (Jones et al, 1983) is a consequence of the non-linear nature of the power threshholds for the plasma instability which causes field aligned irregularities.

Recent observations with improved time resolution also indicate that the heater wave suffers very strong ($\sim$ 20 db) self-induced anomalous absorption within the first second after switch on (see Figure 23). This effect occurs even at relatively low powers ($\sim$ ERP = 10 MW). At somewhat higher powers ($\geq$ 40 MW), self-induced fading enhancements also occur (Figure 23).

These results have very important consequences in evaluating the propagation characteristics of very high power waves.

9 CONCLUSIONS

This review highlights the propagation disturbances which can be produced when the ionosphere is modified by a high power HF heating wave. Some of these effects can directly influence the performance of radio communications, navigation and surveillance systems. Others are at present only of academic interest but they may well form the basis of new types of radio systems.

No attempt has been made to include a comprehensive treatment of the plasma physics of the heating processes since these have been dealt with in detail elsewhere.

Acknowledgements

The authors are indebted to the Max Planck Institute for Aeronomy, Lindau, West Germany and the University of Tromsø, Norway for making the Ramfjord heating facility available.

REFERENCES

Barr, R, M T Rietveld, H Kopka and P Stubbe, (1984) Nature 309, 534.

Basu, S, S Basu, A L Johnson, J A Klobuchar and C M Rush, (1980) Geophys Res Lett 7, 609.

Bernhardt, P A and L M Duncan, (1982) J Atmos Terr Phys 44, 1061.

Bochkarev, G S, V A Eremenko, L A Lobachevsky, B E Ljannoy, V V Migulin and Yu N Cherkashin, (1982) J Atmos Terr Phys 44, 1137.

Fialer, P A, (1974) Radio Sci 9, 923.

Frank, V R, (1974) Radio Sci 9, 971.

Frey, A and W E Gordon, (1982) J Atmos Terr Phys 44, 1101.

Frey, A, P Stubbe and H Kopka, (1984) Geophys Res Lett 11, 523.

Ginzburg, V L and A V Gurevich, (1960) Sov Phys Uspekhi 3, 115.

Gurevich, A V, (1978) Non-linear Phenomena in the Ionosphere, Springer, New York.

Hedberg, A, H Derblom, B Thidé, H Kopka and P Stubbe, (1983) Radio Sci 18, 840.

Jones, T B, K Davies and B Wieder, (1972) Nature 238, 33.

Jones, T B, (1973) AGARD Conf Proc 138, 32-1 - 32-5.

Jones, T B, T Robinson, H Kopka and P Stubbe, (1982) J Geophys Res 87, 1557.

Jones, T B, T Robinson, P Stubbe and H Kopka, (1983) IEE Antennae and Propagation Conf Proc Pub No 219, 304.

Jones, T B, T Robinson, P Stubbe and H Kopka, (1983) Radio Sci 18, 835.

Jones, T B, T Robinson, P Stubbe and H Kopka, (1984) J Atmos Terr Phys 46, 147.

Kopka, H, P Stubbe, T B Jones and T Robinson, (1982) Nature 295, 680.

Minkoff, J, P Kugelmann and I Weissman, (1974) Radio Sci 9, 941.

Perkins, F W and E J Valeo, (1974) Phys Rev Lett 32, 1234.

Rufenach, C L, (1973) J Geophys Res 78, 5611.

Stathacopoulos, A D and G H Barry, (1974) Radio Sci 9, 1021.

Stubbe, P et al, (1982) J Atmos Terr Phys 44, 1025.

Stubbe, P et al, (1984) J Atmos Terr Phys - to be published.

Stubbe, P, H Kopka, B Thidé and A Hedberg, (1984a), J Geophys Res 89, 7523.

Tellegen, B D H, (1933) Nature 131, 840.

Thidé, B, H Kopka and P Stubbe, (1982) Phys Rev Lett 49, 1561.

Ustinov, N D, E S Nektarov and V V Sychev, (1979) Sov J Quantum Electron 9, 816.

Utlaut, W F and E J Violette, (1974) Radio Sci 9, 895.

Weinstock, J, (1974) Radio Sci 9, 1085.

Wright, J W, (1973) J Geophys Res 78, 5622.

Table 1 Heating facility parameters

Location	Frequency (MHz)	ERP (MW)
Arecibo	3 - 11	256
Platteville	5 - 10	200
Moscow	4 - 5	80
Gorky	5 - 6	10
	4 - 6	16
	5 - 10	400
Murmansk	3.3	10
Tromsø	2.8-8.0	360

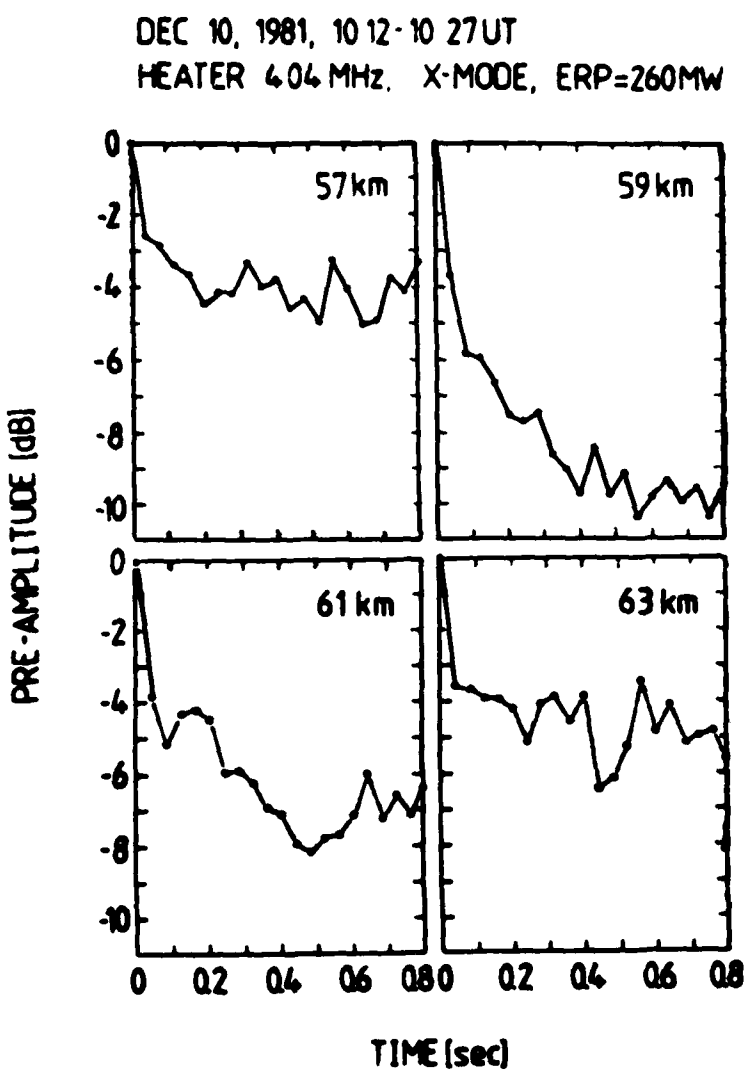


Figure 1(a) D-region absorption of partial reflection radar at Tromsø (Stubbe et al, 1982)

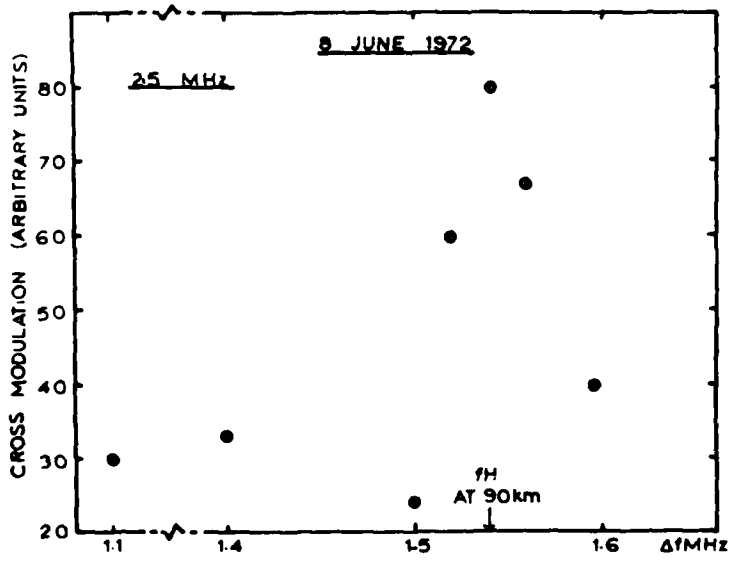


Figure 1(b) Cross-modulation depth on a 2.5 MHz diagnostic as a function of frequency difference between two heaters, 5.4, 5.4 + Δf MHz (Jones, 1973)

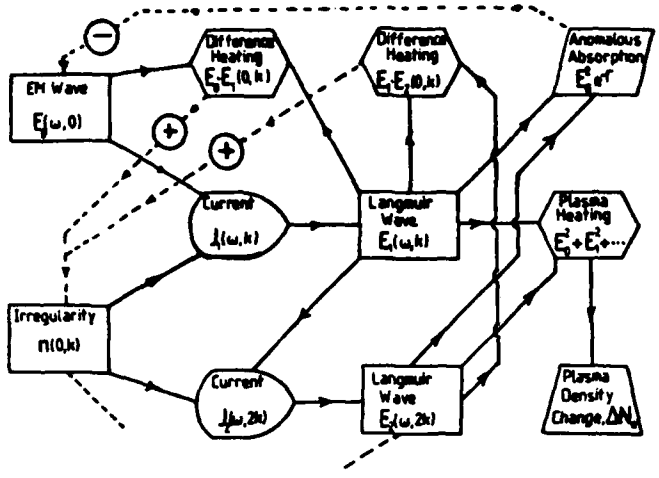


Figure 2 Schematic of small scale irregularity generation mechanisms

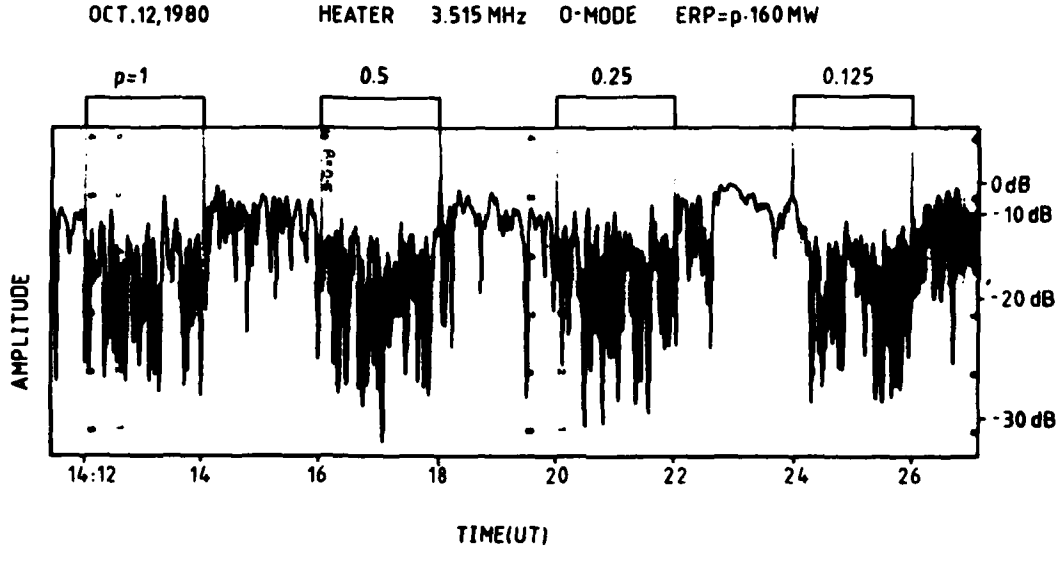


Figure 3 Anomalous absorption of 3.78 MHz diagnostic propagated over a steep incidence path for various heater powers, at Tromsø (Jones et al, 1982)

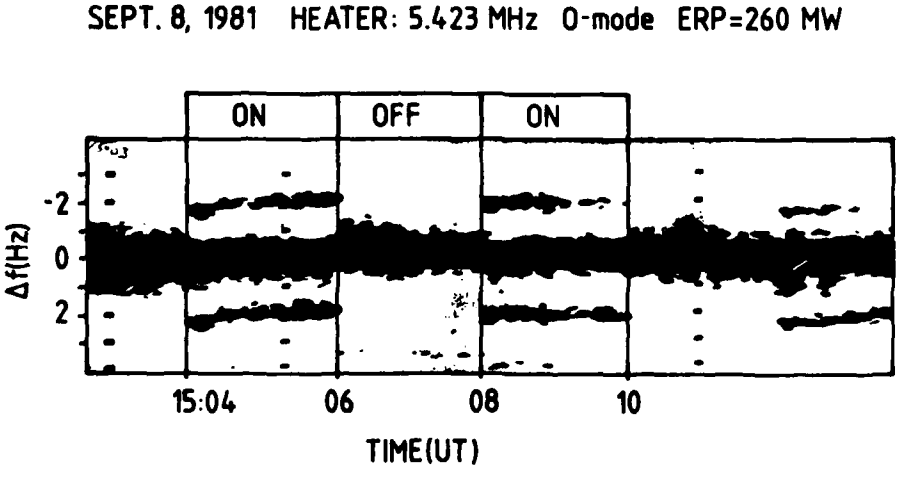


Figure 4 Spectrum of 5.7 MHz diagnostic signal exhibiting cross-modulation sidebands during modulated (2 Hz) heating at Tromsø (Jones et al, 1983)

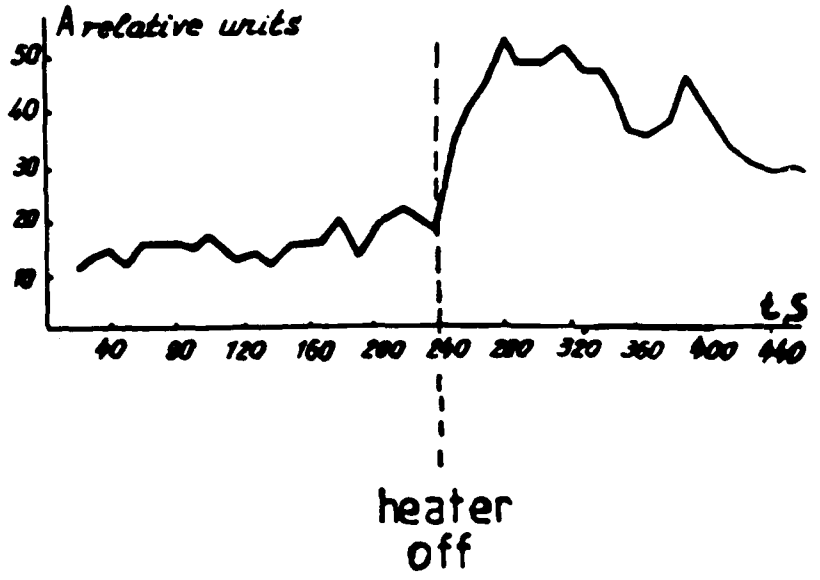


Figure 5 Anomalous absorption over an oblique path (Bochkarov et al, 1982)

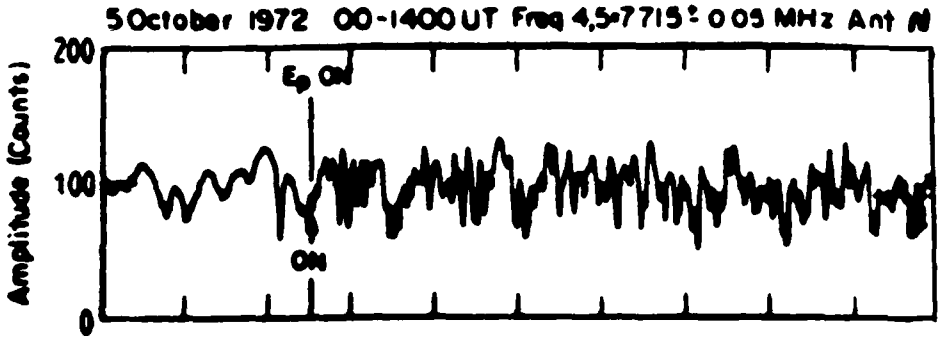


Figure 6 Heater induced fading measured at 7.7 MHz vertical incident. Heating at 5.95 MHz (Wright, 1973)

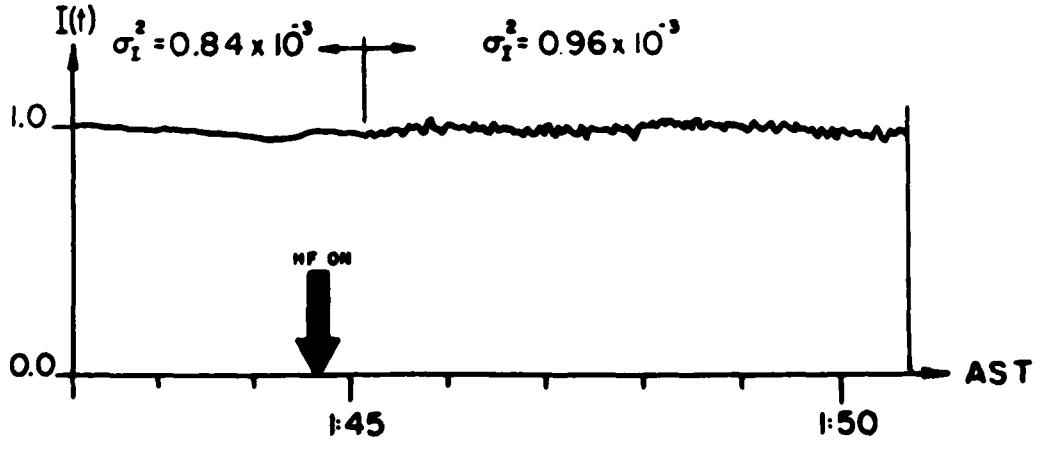


Figure 7 Heater induced scintillations at 1400 MHz (Frey and Gordon, 1982)

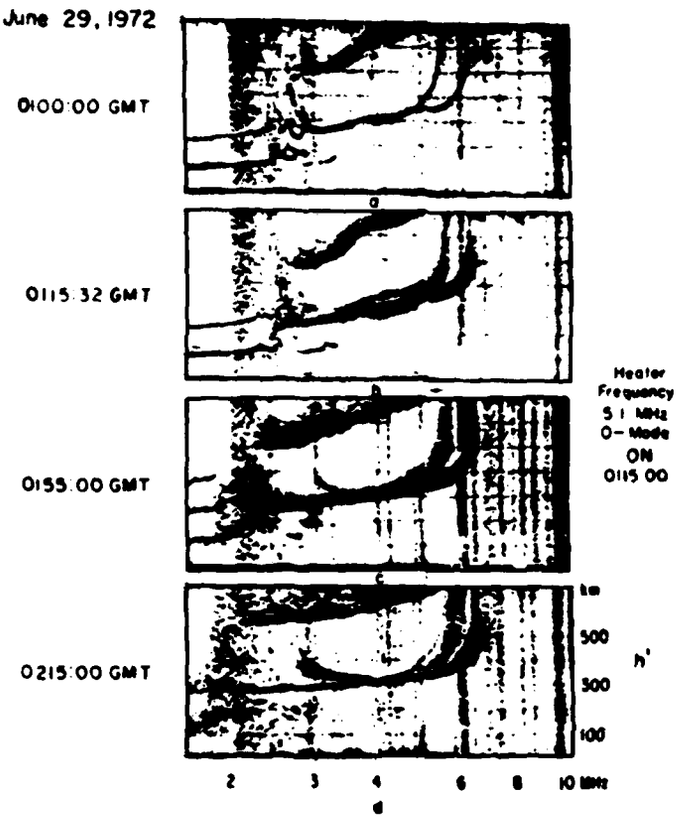


Figure 8 Ionograms exhibiting heater induced spread F (Utlaut and Violette, 1974)

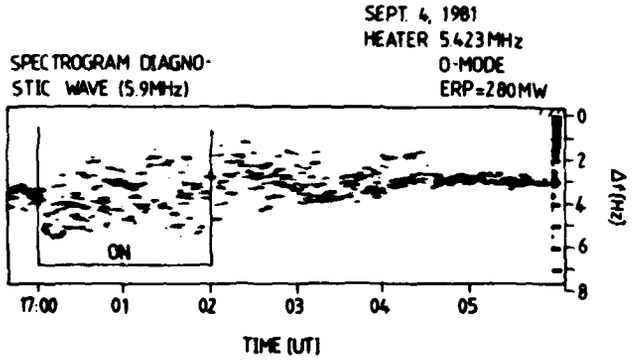


Figure 9 Spread Doppler record during heating at Tromsø (Stubbe et al, 1982)

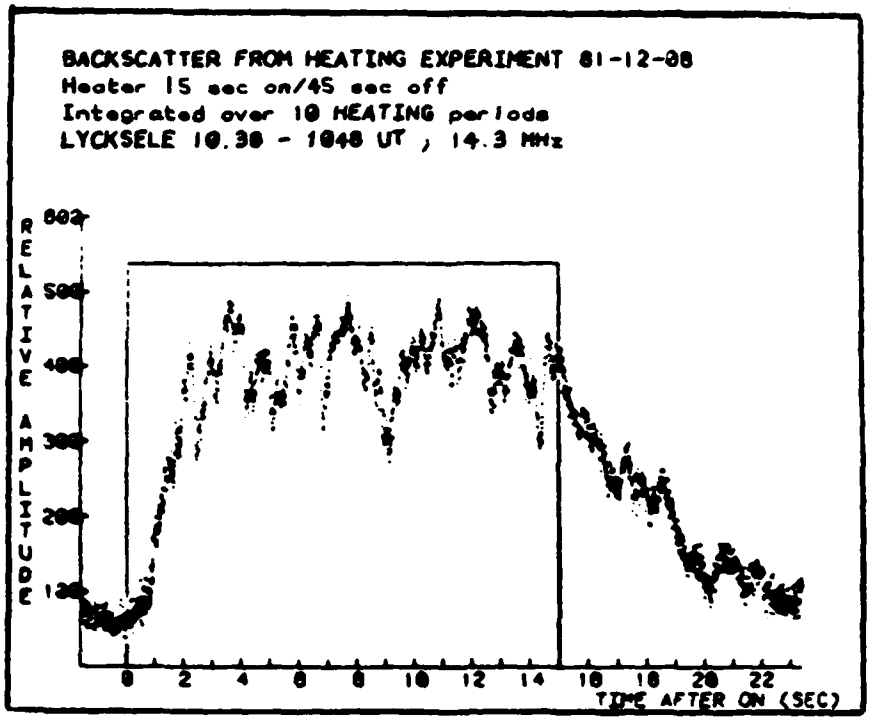


Figure 10 Growth and decay of HF backscatter echo during heating at Tromsø - 600 km path (Hedberg et al, 1983)

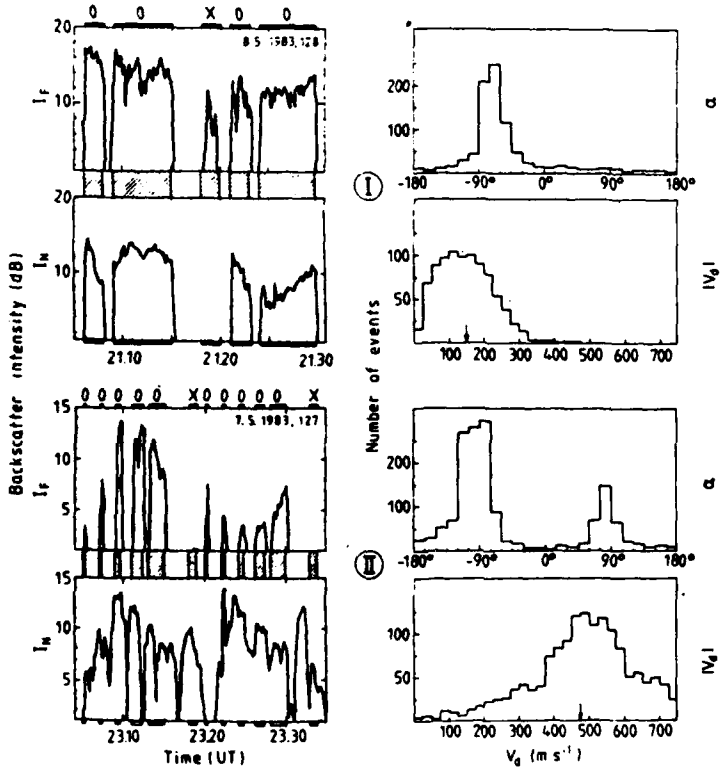


Figure 11 Heater induced VHF (145 MHz) backscatter from the E-region - STARE data. Left panels: Backscatter intensity vs. time in relative units for the Finnish (F) and Norwegian (N) STARE radar. The heater-on times are indicated by hatched areas. O and X refer to the heating mode. The heater operated at 3.324 MHz with ERP = 130 MW (8 May 1983, upper two figures) and at 4.04 MHz with ERP = 200 Mw (7 May 1983, lower two figures). Right panels: Histograms for the direction (clockwise from south) and magnitude of electron drift velocity relating to all analysed type I (upper two figures) and type II data (lower two figures) (Stubbe et al, 1984)

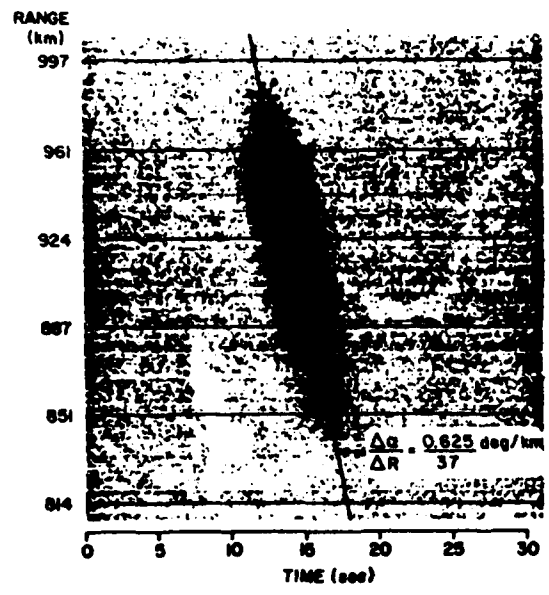


Figure 12 UHF field aligned backscatter (elevation scan) at 435 MHz from Boulder (Minkoff et al, 1974)

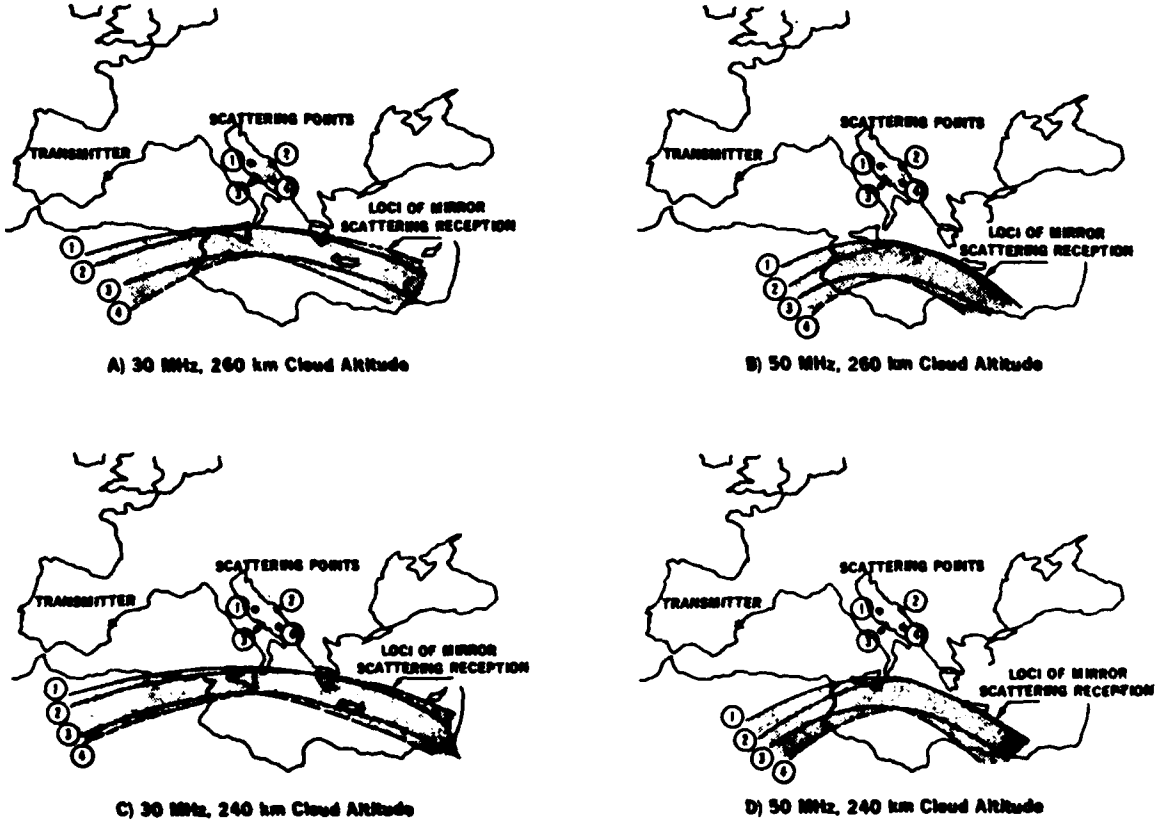


Figure 13 Model predictions for forward scatter communications system over Southern Europe (Stathacopoulos and Barry, 1974)

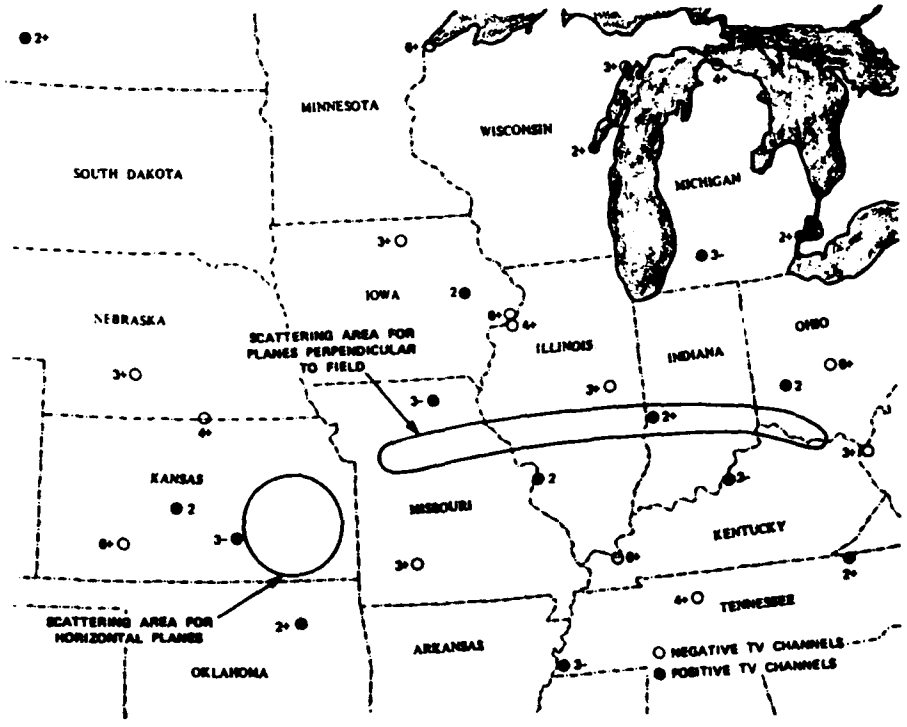


Figure 14 US coverage of forward scatter TV. Dark circles indicate where scattered signals were received, open circles indicate no scatter received (Frank, 1974)

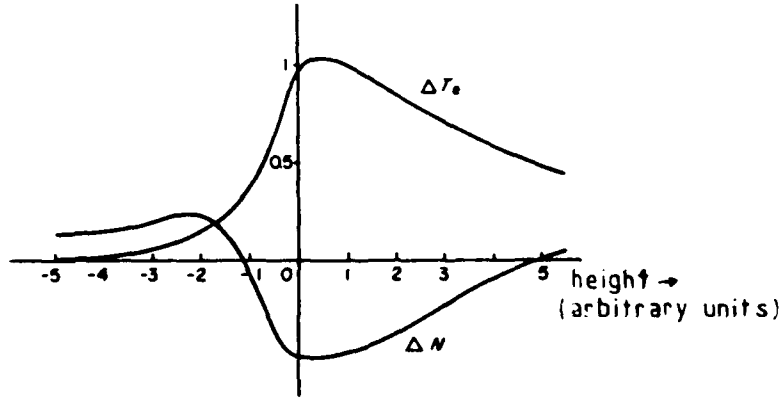


Figure 15 Height variation of heater induced electron density (ΔN_e) and temperature variations (ΔT_e) after Gurevich (1978). The origin corresponds to a heater reflection height in the upper F-region.

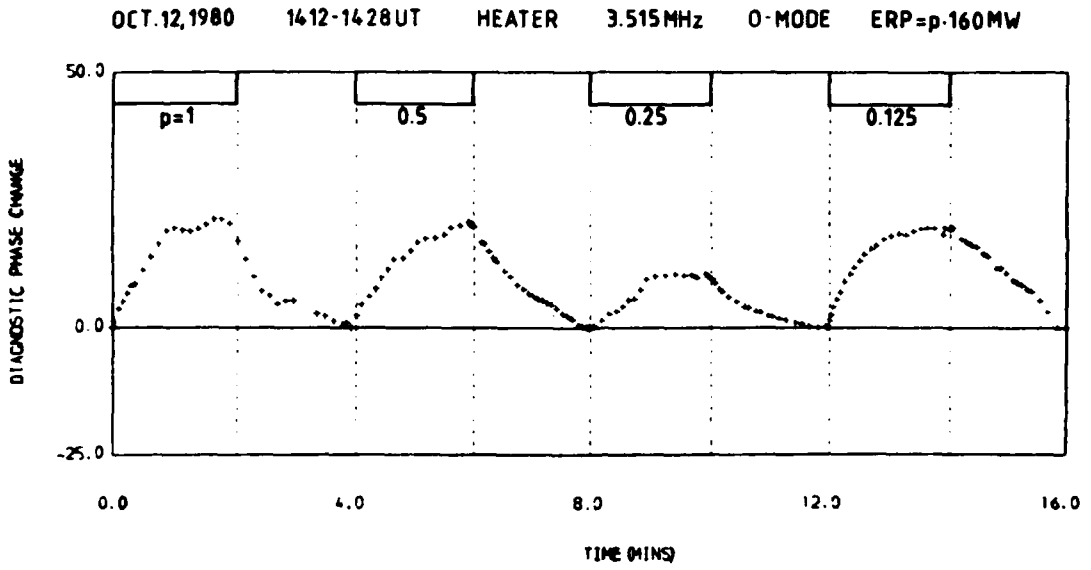


Figure 16 Heater induced phase changes in a 3.78 diagnostic signal reflected from the lower F-region, Tromsø 100 km path (Jones et al, 1982)

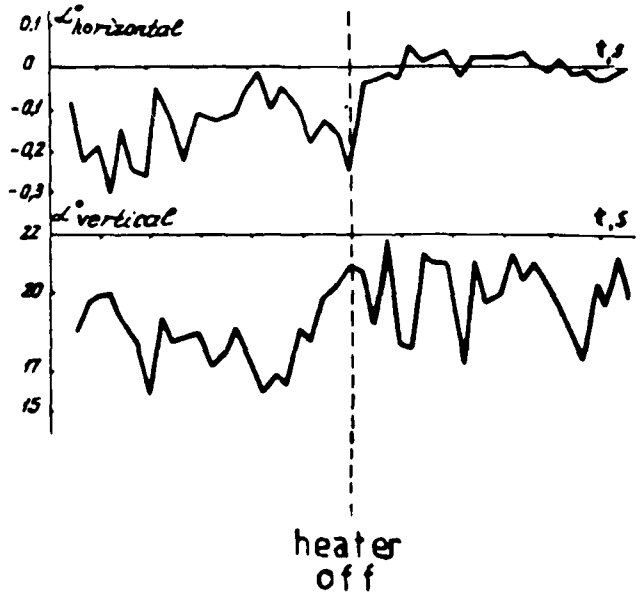


Figure 17 Heater induced changes in angles of arrival (azimuth and elevation) on an oblique propagation path (Bochkarov et al, 1982)

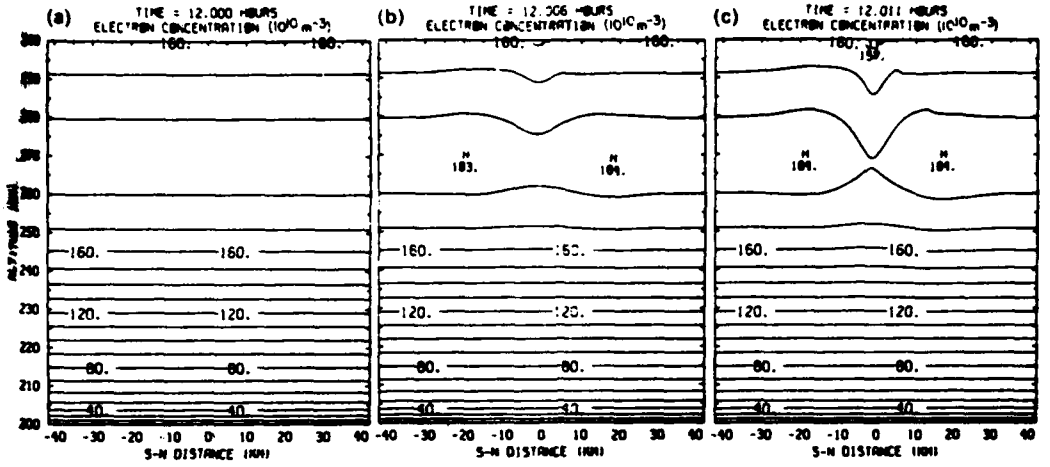


Figure 18 Theoretical model of the development of a self-focussing duct in isoionic contours by the action of a powerful radio wave (Bernhardt and Duncan, 1984)

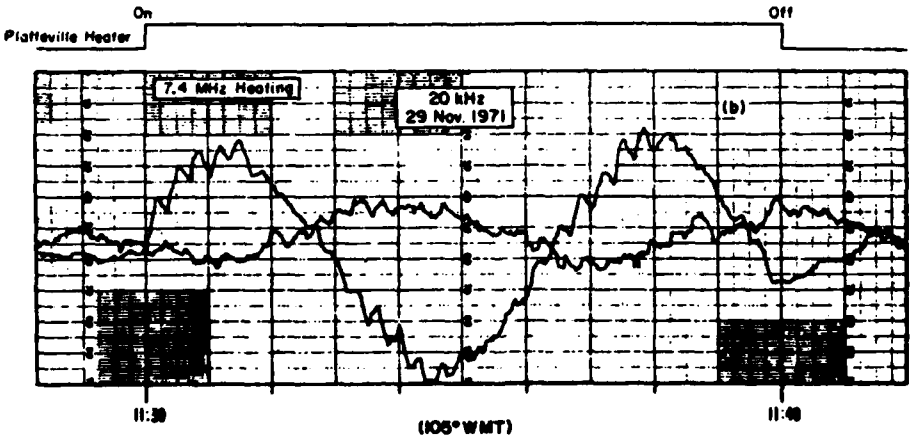


Figure 19 Complex amplitude changes induced in a 20 KHz VLF signal propagated over a steep incidence path, 7.4 MHz heating Boulder (Jones et al, 1972)

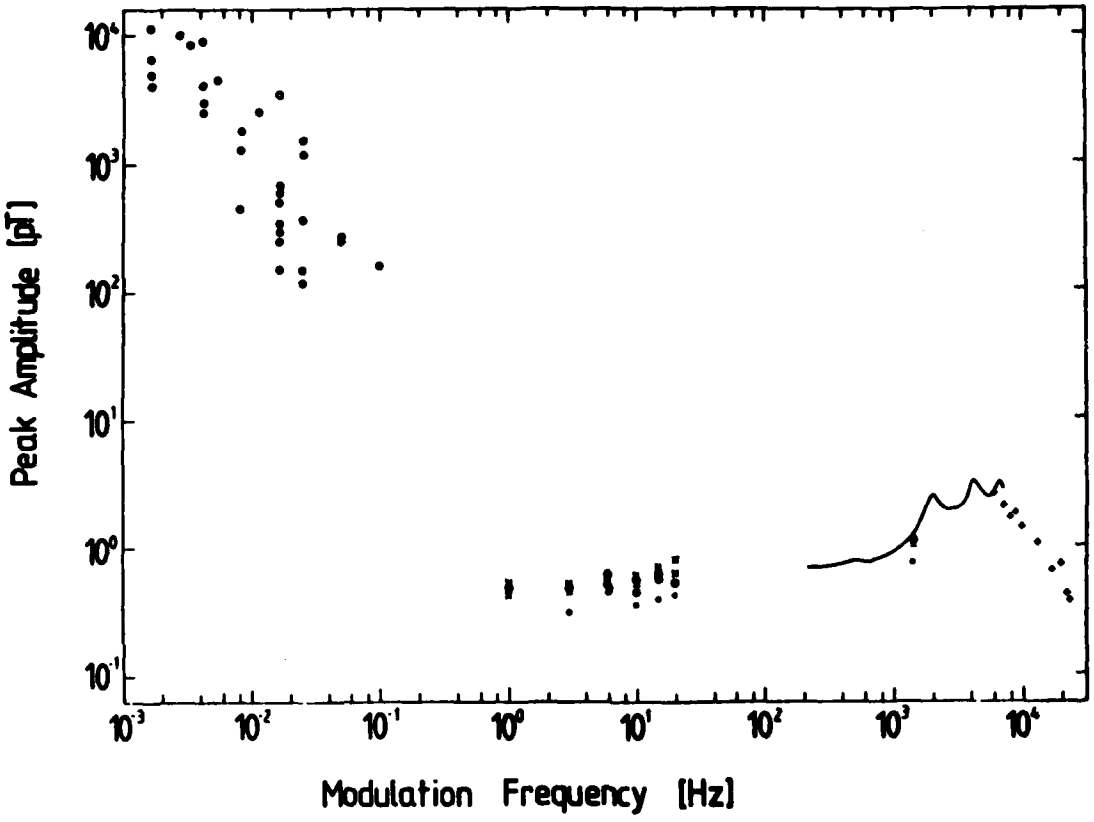


Figure 20 Relative amplitudes of low frequency emissions from modulated auroral electrojet, Tromsø (Stubbe et al, 1984)

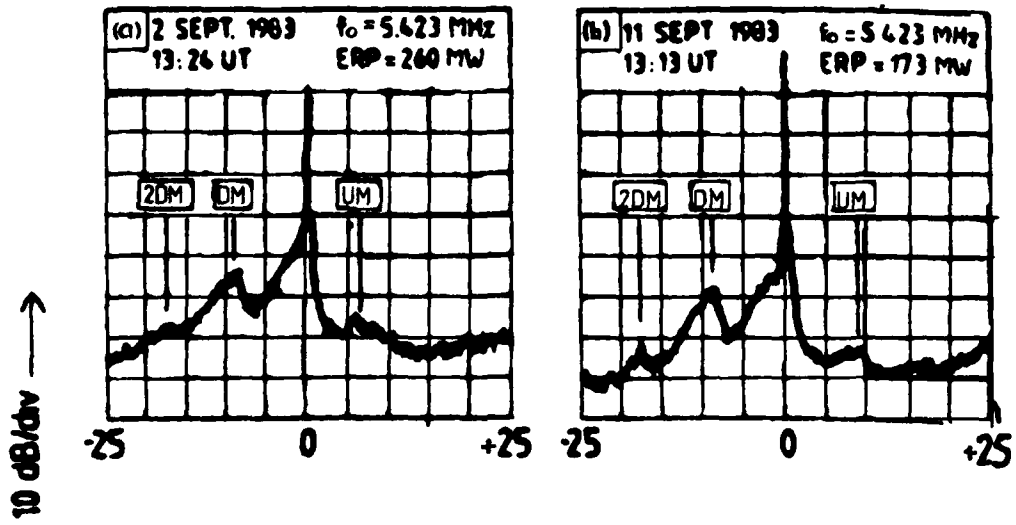


Figure 21 HF stimulated emission spectra measured at Tromsø (Stubbe et al, 1984(a))

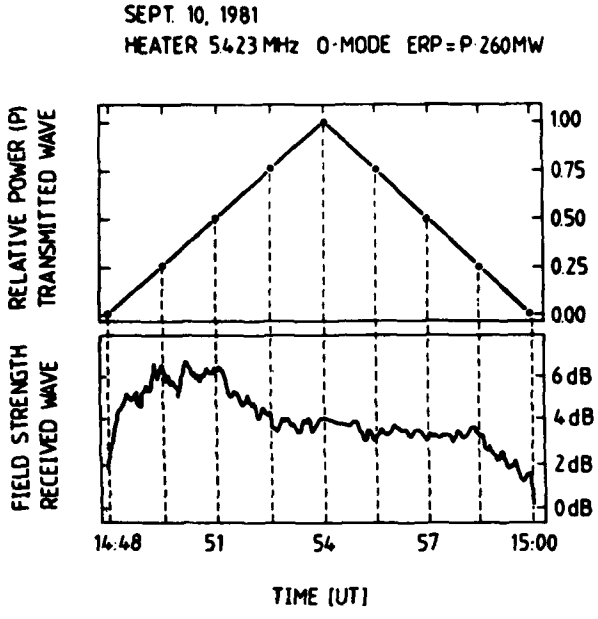
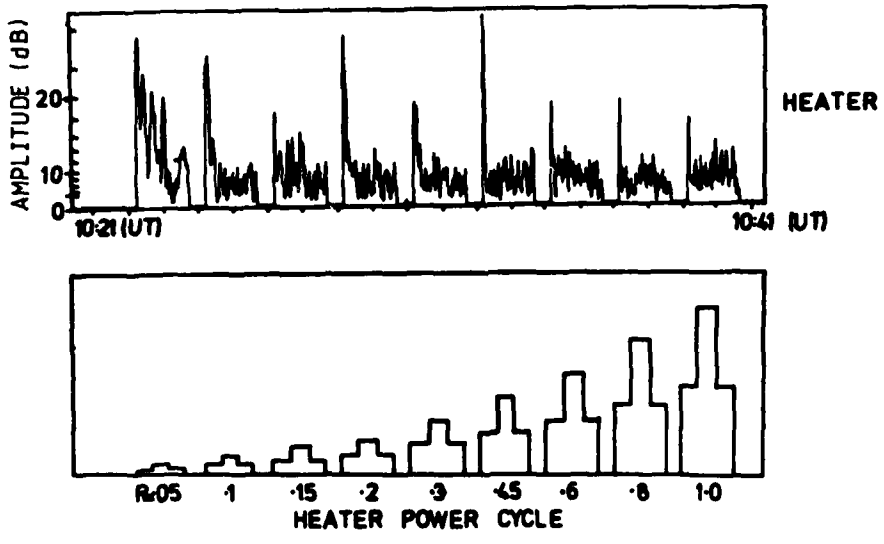


Figure 22 Amplitude of reflected heater signal as a function of transmitted power (increasing and decreasing) from Kopka et al, 1982



Signal amplitude of heater (4.913 MHz) and diagnostic (5.208 MHz) signals from 10:22 (UT) to 10:42 (UT), September 1983.

Figure 23 Amplitude of reflected Tromsø heater signal as a function of time, illustrating self induced anomalous absorption $\simeq$ 1 s after switch on even at the lowest heater powers ($\sim$ 10 MW). Also indicated is the onset of enhanced fading at somewhat higher powers ($\sim$ 40 MW).

DISCUSSION

E.J.Fremouw, US

Your explanation of the absence of heating induced Spread F at Tromso suggests that natural Spread F should show an off-magnetic-zenith dependence opposite to that of scintillation. I don't know of any evidence of such a dependence, although it might be difficult to observe because of inadequate angular resolution. Could you elaborate on your explanation and any evidence to support it?

Author's Reply

The AFGL group measured the occurrence of spread F with their flying ionosonde during the Boulder heating experiments. They observed spread F when at great distances from the heater but this disappeared when they reached a position corresponding to the field line direction through the heated volume. Their results and explanation are similar to that presented in my review, i.e. that the reflection cross section of the field aligned irregularities is smallest when viewed along this field line direction.

E.V.Thrane, NO

Self modulation has been recognized as a problem for high power broadcasting transmitters. Nearly all the heating effects you mentioned will produce self modulation. Have you thought about how these different effects will distort a signal with a typical bandwidth of a broadcasting transmitter?

Author's Reply

Yes, effects can certainly be produced by broadcast transmitters; however, since the signals are propagated at oblique incidence the power densities in the ionosphere are appreciably smaller than those achieved for vertical incidence heating. The heating induced effects observed for oblique heating (broadcasting) are therefore smaller than those measured at vertical incidence.

J.S.Belrose, CA

I have several comments and questions: (1) concerning your steep incidence HF propagation experiments across the Tromso heater, have you drawn the path geometry to scale, or traced raypaths with respect tothe heated volume? I am surprised that you can measure F-region attenuation effects uncontaminated by absorption effects due to the heated D-region below your reflection height in the F-region. (2) In regard to the recent observations that you showed showing signal strength of the heater-reflected wave vs time after onset of heater transmission, and your remarks that OTH radars may not realize the strong reflected-wave expected for the power transmitted; I caution you, do not be so sure, unless you have done the calculations. The oblique OTH radar signal is reflected far from the height where the wave frequency and plasma frequency are equal. (3) In experiments conducted at Ottawa we employed a 2.66 MHz heater, having an estimated ERP of 80 MW. A 0.8 MW transmitter and a 40 dipole antenna array covering 12 acres of ground were employed. The transmitter was our partial reflection transmitter modified for long pulse = about 10 MS. Hence we could not examine convectional heating effects. We looked for the plasma line instability, which we believed would have a short time constant. We made observations at night, when the 2.66 MHz waves were reflected from the F-region. The 470 MHz probe (a 1 kw CW transmitter employing 32 14 dBi yagis) was located at the foot of the field line that passed through the heated region. We looked for backscatter at receive frequencies 470 MHz ±heater frequency. We observed nothing. While the sensitivity of our probe was a far cry from that of the Arecibo radar, Jules Fejer had estimated (I am recalling from memory) that the backscatter for our geometry would be 50 dB stronger than at Arecibo, where the probe transmission path is perpendicular to the field line. Now my question: Have plasma line instabilities been studied employing the Tromso heater?

Author's Reply

(1) We have indeed undertaken ray tracing for the path which indicates that we are well clear of the modified D-region. We have also carried out heating on frequencies much lower than our diagnostic signals i.e. the heating height is well below our sampling height in the F-region. We find a complete absence of heating effects in this case. If we were sensitive to D-region heating we should have seen it in this case. (2) I agree with your comment in that the power densities achieved for oblique heating will be much smaller than those achieved at vertical incidence with the same transmitter. You are also correct in that maximum effects are produced when the heater wave frequency is equal to the local plasma freqency. On the other hand the Soviet work clearly shows that modification effects are observed for oblique incidence heating; their diagnostic signal was however propagated along an almost identical path to the heater. (3) Tor Haagfors and Harry Kohl have indeed observed plasma line emissions with EISCAT (930 MHz) during heating at Tromso. The unusual feature of these emissions is that they observed a marked increase (at least an order of magnitude) in the ion level cross section during heating. The increase is also short lived and lasts for 1 sec after heater turn on.

G.Sales, US

Rome Air Development Center has attempted an oblique heating experiment in the US using transmitters in Rome, NY. A 200 KW transmitter and rhombic antenna were used to disturb the ionosphere some 1400 km away towards the southwest. At the midpoint, a vertical ionosonde was located to detect changes in the overhead ionosphere. After approximately 10 days of phase and amplitude measurements, the data was analyzed to detect the 10 minute heating

cycle. The results were negative and theoretical analysis indicated we were some 6 to 8 dB below what would be required. A future experiment using 4—200 KW transmitters in Alaska is planned.

Author's Reply

We will look forward to having the results of this interesting experiment.

IONOSPHERIC MODIFICATIONS BY HF HEATERS

M. C. Lee and J. A. Kong
Research Laboratory of Electronics and
Department of Electrical Engineering and Computer Science
Massachusetts Institute of Technology
Cambridge, Massachusetts 02139, U. S. A.

H. C. Carlson
Ionospheric Physics Division
Air Force Geophysics Laboratory
Hanscon Air Force Base, Massachusetts 01731, U. S. A.

S. P. Kuo
Polytechnic Institute of New York
Long Island Center, Farmingdale, New York 11735, U. S. A

ABSTRACT

Among the many fascinating HF heater wave-induced phenomena, we single out for discussion the simultaneous excitation of ionospheric density irregularities and earth's magnetic field fluctuations, the electron acceleration by Langmuir turbulence, and the conditions for the occurrence of artificial spread F. The earth's magnetic field perturbations observed at Tromso are possibly produced by the thermal filamentation instability of radio waves that can also excite large scale ionospheric irregularities simultaneously. The diffusion effect of Langmuir wave fields on the background electron distribution is evaluated as the process of generating energetic electrons (> 10 ev) deduced in the measurements of enhanced plasma lines at Arecibo and detected in the in-situ particle measurements at Tromso. Artificial spread F echos are found to be caused by HF wave-induced ionospheric irregularities whose polarization vectors lie within the meridian plane. The phenomenon of artificial spread F can be satisfactorily interpreted to result from the difference in the reflection heights of the returned rays in the presence of these irregularities with scale lengths greater than 100 meters.

1. INTRODUCTION

The ionosphere can be significantly perturbed by HF heater waves, such as the perturbations in plasma density, in plasma temperature, and in the earth's magnetic field (see, e.g., Carlson and Duncan, 1977; Gurevich, 1978; Fejer, 1979; Stubbe et al., 1982; Lee and Kuo, 1983 a). The modification of ionospheric density and temperature were predicted before the planning of ionospheric HF heating experiments at Boulder, Colorado in late sixties (Farley, 1963). But the earth's magnetic field perturbations caused by HF heaters were not appreciated until quite recently in experiments performed at Tromso, Norway with the EISCAT heating facilities. Active research has been conducted both experimentally and theoretically in the USA , the Europe, the USSR etc. to study the nonlinear plasma physics in wave-particle interactions and to explore the potential applications in, for instance, telecommunications, with this relatively new technique.

Among many fascinating HF heater wave-induced phenomena, we single out for discussion the simultaneous excitation of ionospheric irregularities and geomagnetic fluctuations, the enhanced plasma lines associated with electron acceleration by plasma turbulence, and the peculiar occurrence frequencies of artificial spread F (ASF) at different locations. The studies of heater wave-induced ionospheric irregularities have attracted much attention not only for the academic interest but also for the possible establishment of artificial VHF-VHF communication paths in the presence of these plasma density striations Various mechanisms have been suggested as the causes that generally involve plasma instabilities being excited from thermal or nonthermal levels of ionospheric density fluctuations. For instance, Langmuir waves excited parametrically by the decay instability have been considered by Perkins (1974), Lee and Fejer (1978), and Kuo et al. (1983) as the source of producing ionospheric irregularities. It is also possible for HF heater waves to excite directly ionospheric irregularities together with electrostatic sidebands (e.g., Gureuich, 1978 and references therein; Das and Fejer, 1979; Lee and Kuo, 1983b). Explosive instabilities that require pre-existing ionospheric irregularities were discussed by, e.g., Vaskov and Gurevich (1977) and Inhester et al. (1982). In Section 2 we review the thermal filamentation instability of radio waves that can simultaneously perturb ionospheric density and earth's magnetic field. This instability was proposed by Kuo and Lee (1983) as the mechanism of HF heater wave-produced geomagnetic field perturbation in Tromso experiments (Stubbe and Kopka, 1981; Stubbe et al., 1982). In fact, this instability can be excited in the ionosphere by heater waves with a broad frequency range as low as in the MF band (Lee and Kuo, 1984 a) and as high as in the SHF band (Lee and Kuo, 1984 b).

Plasma line enhancement first detected in ionospheric heating experiments at Arecibo, Puerto Rico have been considered to be the indirect evidence of the excitation of parametric decay instability by the ordinary HF heater waves near their reflection heights (Carlson et al , 1972) A broad distribution of enhanced plasma lines in height indicates the generation of energetic electron fluxes with energies exceeding 10 electron volts (Carlson et al , 1982), whose existence was confirmed by the in-situ particle measurements performed recently by the Scandinavian group with a rocket (Grandel et al., 1983). The electron acceleration that produces suprathermal electrons of the order of a few electron volts for airglow enhancement was suggested as either a trapping process (e.g., Fejer and Graham, 1974) or a diffusion process (e.g., Weinstock, 1974; Nicholson, 1977) in the saturation spectrum of Langmuir waves created by the parametric decay instability. We also investigate in Section 3 the diffusion effect of Langmuir wave fields on the background electron distribution Both the quasi-linear and nonlinear processes of wave-particle interactions are analyzed in a velocity diffusion equation Our analysis shows that quasi-linear diffusion may be effective enough to produce energetic electron flux (·10ev) reported by Carlson et al (1982) However, the very energetic electron flux (>25ev) measured by Grandel et al (1983) can only be generated by the diffusion process through nonlinear Landau damping of Langmuir wave pairs propagation in opposite directions.

The problem finally discussed in Section 4 is the detection of HF heater wave-induced ionospheric irregularities by ionosondes (Kuo and Lee, 1984; Kuo et al., 1985). This work was intended for understanding the puzzlement that the artificial spread F's (ASF) were constantly seen in the Boulder experiments (Utlaut, 1973), but they were a rare phenomenon at Arecibo (Showen and Kim, 1978), and they have never been observed in the Tromso experiments (Stubbe et al., 1982). The ASF is generally believed to be caused by large-scale, field-aligned ionospheric irregularities whose excitation by HF heaters was evidenced by the radio star scintillations at Tromso (Frey et al., 1984) and by the scanning radar incoherent backscatter process at Arecibo (Duncan and Behnke, 1978). These facts indicate the limitation of ionosondes as a tool to diagnose ionospheric irregularities. We show that the reflection heights of radio rays vary drastically and, consequently, yield strong spread F echoes in ionograms in the presence of irregularities whose wave vectors lie in the magnetic meridian planes. By contrast, the reflection heights are not affected by those whose wave vectors are perpendicular to the meridian planes. A brief summary of the three afore-mentioned phenomena is finally presented in Section 5 together with a conclusion.

2. SIMULTANEOUS PERTURBATIONS IN IONOSPHERIC DENSITY AND GEOMAGNETIC FIELD

The thermal filamentation instability of HF heater waves can produce in the ionosphere an electromagnetic sideband and zero frequency modes with wave vectors perpendicular to the propagation direction of heater waves. Magnetic field-aligned nonoscillatory modes associated with magnetostatic and ionospheric density fluctuations are formed along the heater wave paths. This instability arises from a nonlinear thermal effect whose physics is elucidated in Figure 1.

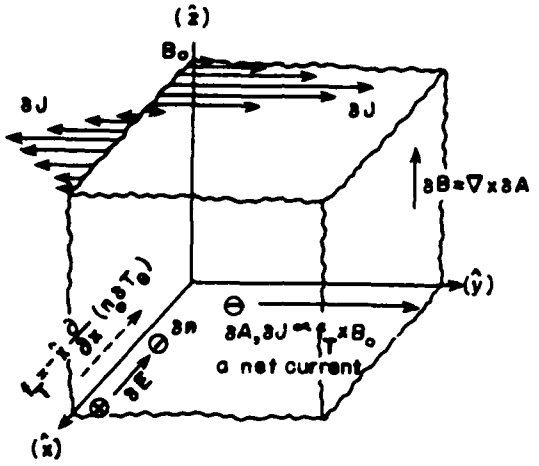


Figure 1. The physical process of a nonlinear thermal effect that causes the excitation of nonoscillatory modes associated with magnetostatic and ionospheric density fluctuations along the HF heater wave path.

Under the incident and sideband fields, electrons but not ions experience a thermal pressure force $[\vec{f}_T = -\hat{x}(\partial/\partial x)(N_0 \delta T_e)]$ across the earth's magnetic field ($B_0 = \hat{z} B_0$), where δT_e, N_0 and B_0 are the electron temperature perturbation, the unperturbed plasma density, and the background earth's magnetic field intensity, respectively. This nonlinear force denoted by a dotted arrow in Figure 1 can be built up only in the electron gas, because high frequency wave fields cause efficient electron heating rather than ion heating. Electron density fluctuations (δN), that are induced consequently by this non-oscillatory force, gives rise to a self-consistent field ($\delta \vec{E} = \hat{x} \delta E$) associated with the excitation of the purely growing modes (i.e., ionospheric irregularities and geomagnetic fluctuations). While the net force acting on electrons is ($\vec{f}_T - eN_0 \delta \vec{E}$), that on singly-charged ions is $eN_0 \delta \vec{E}$. These wave-induced forces combined with the orthogonal earth's magnetic field result in cross-field drift motions of electrons and ions at the velocities of $(\delta \vec{E} - \vec{f}_T / eN_0) \times \vec{B}_0 / B_0^2$ and $(\delta \vec{E} \times \vec{B}_0 / B_0^2)$, respectively. The relative motion between electrons and ions causes a net current, $-\vec{f}_T \times \vec{B}_0 / B_0^2$, flowing along the y axis. This wave-induced current (and vector potential, $\delta \vec{A}$) varies sinusoidally along the x axis. Therefore, it can be visualized as a combination of many sheet-like currents on the y-z plane with a thickness of half the scale length, flowing in opposite directions alternately. Or, equivalently, pairs of dipole current form within the HF wave-heated ionospheric region. The geomagnetic fluctuations ($\delta \vec{B}$), that result from the radio wave-induced current, point to the same direction as the earth's magnetic field's ($\vec{B}_0$) because of $\nabla \times \delta \vec{A} = \delta \vec{B} = \hat{z} \delta B$.

The positive feedback loop of the thermal filamentation instability is outlined in Figure 2. In brief, electron temperature perturbation (δT_e) caused by radio wave heating produces a cross-field thermal pressure force ($\vec{f}_T$) as the key nonlinearity of the instability. This nonlinear force induces geomagnetic fluctuations ($\delta \vec{B}$) and ionospheric irregularities (δN) that, subsequently, cause non-uniform electron heating and, then, perturb the electron temperature in turn. One can expect from the above delineated physical picture that $\delta N \propto \delta B$ because both of them are induced in proportion by $\vec{f}_T$. Such a relation has been, indeed, found in the detailed formulation of our theory with the following form:

$$\frac{\delta N}{N_0} \sim \left\{ 1 + \frac{\nu_e}{\gamma} \left(\frac{2\pi c}{\lambda_\perp \omega_{pe}} \right)^2 \left[1 + \frac{\Omega_e \Omega_i}{\nu_e \nu_i} \left(\frac{\lambda_\perp}{\lambda_\parallel} \right)^2 \right] \right\} \left(\frac{\delta B}{B_0} \right) \tag{1}$$

where the parameters, $\nu_e(\nu_i)$, $\Omega_e(\Omega_i)$, ω_{pe}, c, γ, $\lambda_\perp(\lambda_\parallel)$, and $N_0(B_0)$ have their conventional meanings of effective electron (ion)

collision frequency, electron (ion) gyrofrequency, electron plasma frequency, the speed of light in vacuum, the growth rate of the instability, the perpendicular (parallel) scale length of the instability and the background ionospheric density (earth's magnetic field strength), respectively. The parallel scale length is infinite for ideal field-aligned modes. In reality, a finite parallel scale length is introduced by inhomogeneity effects associated with either the background ionospheric density or the finite cross-section of the radio wave beam. The inhomogeneity effects can be reasonably ignored in the experimental conditions for HF ionospheric heating experiments at Tromso, Norway. This is because the instability becomes effective in the ionosphere for modes with scale lengths less than the scale sizes of the background ionospheric density gradients and the linear dimensions of radio wave beam cross-sections by, at least, two orders of magnitude. Nevertheless, the inhomogeneity effect imposed by the narrow microwave beam cannot be neglected in the case of Solar Power Satellite.

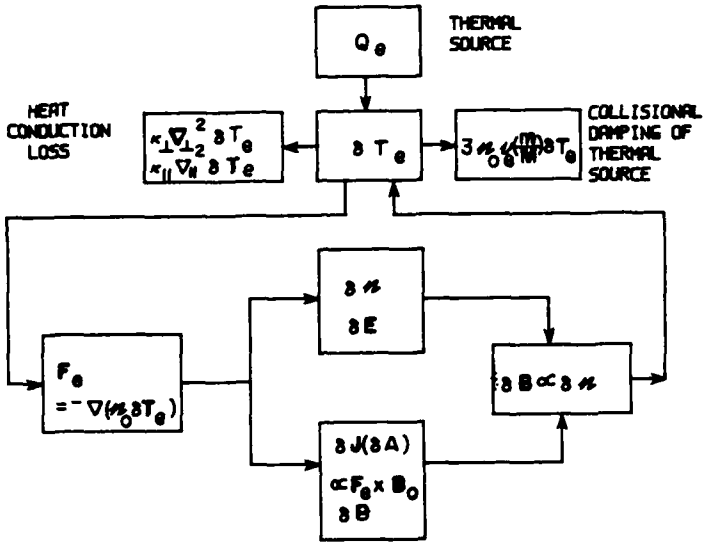


Figure 2. The positive feedback loop of the thermal filamentation instability

It should be pointed out that the radio wave-produced geomagnetic fluctuations do not occur in the "MHD equilibrium" condition. This fact can be seen from Equation (1), that requires $\delta B/B_0 \sim 0$ when $\gamma = 0$ corresponding to the "MHD equilibrium" ionospheric condition either before the onset or after the saturation of the thermal filamentation instability. During the linear stage of the instability (i.e; the growth rate, γ, is a non-zero constant), significant geomagnetic fluctuations can be generated together with ionospheric irregularities by powerful radio waves via the thermal filamentation instability. It is seen from Equation (1) that the fractional density perturbation, $\delta N/N_0$, is proportional linearly to the fractional geomagnetic perturbation, $\delta B/B_0$, with a ratio greater than unity. If this ratio is close to unity, $\delta B/B_0$ comparable to $\delta N/N_0$ can be excited. Otherwise, the geomagnetic field perturbation is negligibly small in comparison with the ionospheric density perturbation.

For highly field-aligned modes, Equation (1) is reduced to the following form

$$\frac{\delta N}{N_0} \simeq \left\{1 + \frac{\nu_e}{\gamma}\left(\frac{2\pi c}{\lambda_\perp \omega_{pe}}\right)^2\right\}\left(\frac{\delta B}{B_0}\right) \tag{2}$$

where the growth rate (γ) increases generally with scale length ($\lambda_\perp$). It is then clear from Equation (2) that smaller ratios of $\delta N/N_0$ to $\delta B/B_0$ are associated with larger scale modes. In other words, significant geomagnetic field fluctuations are excited primarily through large scale thermal filamentation instability. In HF ionospheric heating experiments, large scales are generally referred to a few hundreds and larger.

For the excitation of "large-scale, highly field-aligned" modes, the threshold heater wave fields are found to be inversely proportional to the scale lengths of the instability, i.e., $\epsilon_{th} \propto \lambda_\perp^{-1}$, indicating the favorable generation of large-scale modes. The threshold field is, however, independent of the electron collision frequency (ν_e). The reason is that both the generation rate and the damping rate of the thermal source for the instability are proportional to ν_e. More specifically, electron collisions with ions or neutrals convert the radio wave energy into the thermal source of the instability; meanwhile, the induced electron temperature perturbations are also determined by the collisional loss of heater wave-generated heat. It should be stressed that electron collisions do not weaken the purely growing modes associated with the magnetostatic and ionospheric density fluctuations, because electrons and ions move together in the wave-vector direction of these nonoscillatory modes.

By contrast, the growth rates of the instability are found to be generally proportional to ν_e. This is because large cross-field mobility of charged particles is conducive to the establishment of collective oscillations, namely, the field-aligned purely growing fluid modes. The cross-field mobility relies on electron collisions that, therefore, enhance the instability. Because of $\gamma \propto \nu_e$, the relationship between δN and δB given in Equation (2) turns out not to be a function of ν_e. The electron-ion (or-neutral) collisions play the following roles in the excitation of the thermal filamentation instability: (1) to convert the radio wave energy into the driving heat source of the instability, (2) to reduce the electron temperature perturbations induced

by the heat source; this is also the principal process of energy loss in determining the threshold level of large-scale, highly field-aligned instability, and (3) to facilitate cross-field mobility of charged particles for establishing the collective oscillations (i.e., the field-aligned purely growing modes) and, as a consequence, the growth rate of the instability is generally proportional linearly to the electron collision frequency.

Earth's magnetic field fluctuations of the order of 10 nT had been excited at Tromso, Norway by HF heaters operated in either O (ordinary)-mode or X (extraordinary)-mode (P. Stubbe, personal Communication, 1983), though only results in connection with X mode heating were published in the literature (Stubbe and Kopka, 1981; Stubbe et al., 1982). Our analysis shows that these geomagnetic fluctuations can be produced by either X-mode (Kuo and Lee, 1983) or O-mode (Lee and Kuo, 1983a) heater waves within a few minutes under the experimental conditions at Tromso. This predicted growth time is consistent with the observations that geomagnetic perturbations increased regularly with the operation time of HF heaters in the range from 10 to 360 seconds (Stubbe et al., 1982). The generation of large scale ionospheric irregularities by HF heaters has been investigated by, for example, Fejer (1973), Cragin and Fejer (1974), Perkins and Valeo (1974), Goldman (1974), Cragin et al. (1977), Perkins and Goldman (1981) etc. via various plasma instabilities. The distinctive feature of our theory of thermal filamentation instability as compared with others is that this instability can generate not only large scale ionospheric irregularities but also geomagnetic field fluctuations at the same time. The detection of hundreds meter-scale irregularities by UHF-scintillation technique was recently performed by Frey et al.(1984) in Tromso heating experiments. Frey et al. examined three candidate mechanisms including Perkins and Valeo (1974), Cragin et al. (1977), and ours (Kuo and Lee, 1983). They reported that the thresholds of our thermal filamentation instability were consistent with their measured ones; whereas, those of the other two instabilities were higher by, at least, a factor of 100.

Another interpretation of magnetic fluctuations is that they are caused by perturbations in the auroral electrojet flowing in the ionosphere caused by perturbations in the ionosphere conductivity (Fejer and Krenzien, 1982 and references therein). One would expect from this mechanism that increased magnetic field fluctuations are associated with more intense electrojet current for future experimental verification. The source(s) of magnetic fluctuations can be unambiguously identified by in-situ measurements performed by rockets or spacecraft in the modified ionosphere. While the auroral electrojet as a line source is located at an altitude of about 100 kilometers above the earth's crest, the radio wave-induced DC current appears in a higher and broader heated ionospheric region below the reflection height of the incident heater wave. A unique feature of thermal filamentation instability is that the simultaneously excited magnetic and density fluctuations have identical characteristic scale lengths and growth rates. Moreover, the strengths of those two types of flucutations are interrelated specifically by Equation (1) or (2). The in-situ measurements would provide an excellent diagnosis of the heated ionosphere to test the theories in these aspects.

3. ELECTRON ACCELERATION BY LANGMUIR WAVE TURBULENCE

In the following analysis, Langmuir waves excited parametrically in the ionosphere by HF ordinary (O-mode) heater waves are considered to be the source of generating energetic electrons (>10ev), whose existence was first deduced from the measurements of enhanced plasma lines (Carlson and Ducan, 1977; Carlson et al., 1982) and confirmed later in the in-situ particle measurements (Grandal et al., 1983). The diffusion effect of the Langmuir wave field on the electron distribution is investigated in the derivation of a velocity distribution equation for electron plasmas that are embedded in a uniform magnetic field in the presence of a broad spectrum of Langmuir waves.

Our analysis begins with the collisionless kinetic equation

$$\left\{\frac{\partial}{\partial t} + \vec{v}\cdot\frac{\partial}{\partial \vec{r}} - \frac{e}{m}\left[\vec{E}(\vec{r},t) + \frac{1}{c}\vec{v}\times\hat{z}B_0\right]\cdot\frac{\partial}{\partial \vec{v}}\right\} f(\vec{v},\vec{r},t) = 0 \tag{3}$$

where $f(\vec{v},\vec{r},t)$ is the electron distribution function as a function of velocity ($\vec{v}$), position ($\vec{r}$), and time (t); the earth's magnetic field ($\vec{B}_0$) is taken to be the z axis of a rectangular coordinate system;

$$\vec{E}(\vec{r},t) = -i\sum_k \vec{k}\phi_k \exp[i(\vec{k}\cdot\vec{r} - \omega_k t)] + c.c.$$

is the total electric field of the excited Langmuir waves, where ω_k and $\vec{k}$ are the Langmuir wave frequency and wave vector, respectively. The distribution function, f, can be generally expressed as the sum of four parts (Dupree, 1966):

$$f = < f > + f^{(1)} + \tilde{f} + f_m = < f > + f_1 + f_m \tag{4}$$

where $< f >$ is the average distribution function; $f^{(1)}$ is the phase coherent response to the electric field, $\vec{E}(\vec{r},t)$; $\tilde{f}$ corresponds to the phase incoherent portion due to the nonlinear wave-wave interaction; f_m represents all other effects that are neglected here; the fluctuating portion of the distribution function, $f_1 = f^{(1)} + \tilde{f}$, can be Fourier-expanded as $\sum_k f_k \exp[i(\vec{k}\cdot\vec{r} - \omega_k t)]$.

Along the unperturbed trajectory defined by

$$\frac{d}{dt}\vec{r} = \vec{v} \quad \text{and} \quad \frac{d}{dt}\vec{v} = -\left(\frac{eB_0}{mc}\right)\vec{v}\times\hat{z}, \tag{5}$$

the equations for the average part ($< f >$) and the fluctuating part (f_1) of the distribution function can be obtained as follows after substituting (4) into (3):

$$\frac{d}{dt} < f > = i\frac{e}{m}\frac{\partial}{\partial \vec{v}}\cdot\sum_k \vec{k}\phi_k^* f_k + c.c. \tag{6}$$

$$\frac{d}{dt} f_k \exp[i(\vec{k}\cdot\vec{r} - \omega_k t)] = -i\frac{e}{m}\exp[i(\vec{k}\cdot\vec{r} - \omega_k t)] \left\{\phi_k \vec{k}\cdot\frac{\partial}{\partial \vec{v}} < f > + \sum_{k'\neq k}\left[\phi_{k'}\vec{k}'\cdot\frac{\partial}{\partial \vec{v}} f_{k-k'} - \phi_{k'}^*\vec{k}'\cdot\frac{\partial}{\partial \vec{v}} f_{k+k'}\right] + \sum_{k'=k}\left[\phi_{k-k'}(\vec{k}-\vec{k}')\cdot\frac{\partial}{\partial \vec{v}} f_{k'} + \phi_{k-k'}(\vec{k}+\vec{k}')\cdot\frac{\partial}{\partial \vec{v}} f_{k'}^*\right]\right\} \tag{7}$$

where $f_{k-k'}(\phi_{k-k'})$ and $f_{k+k'}(\phi_{k+k'})$ represent the phasors of the fluctuating distribution function (electric potential) bearing space-time variations of the $\exp\{i[(\vec{k}-\vec{k}')\cdot\vec{r}-(\omega_k-\omega_{k'})t]\}$ and the $\exp\{i[(\vec{k}+\vec{k}')\cdot\vec{r}-(\omega_k+\omega_{k'})t]\}$ types, respectively. On the RHS of (7), while the first and the second terms in the braces stem from the phase coherent responses to the electric field ($\vec{E}(\vec{r},t)$), the third term is contributed from the nonlinear wave-wave interactions. Since in the diffusion process under consideration, only wave-particle interaction is relevant, the wave-wave interaction term will be dropped in the following analysis of electron acceleration. Integrating (7) along the unperturbed trajectory defined by (5) and substituting the resultant form of f_k into (6), we can readily obtain the diffusion equation in a rather complicated form. This equation can be much simplified by the following approximations which can be reasonably made in the ionospheric heating experiments. The theoretical work (e.g., Fejer and Kuo, 1973; Perkins et al., 1974) shows that the saturation spectrum of Langmuir waves is excited by the parametric decay instability in a narrow cone with an azimuthal symmetry with respect to the earth's magnetic field. It is thus reasonable to assume that $< f >$ is also azimuthally symmetric in the velocity space around the geomagnetic field. Further, the Langmuir wave spectrum is noted to peak along the magnetic field. We may expect the background electron distribution to have the modification primarily in the direction of earth's magnetic field. In the present study, only electron acceleration along the magnetic field is considered to be significant for simplicity. We, therefore, assume that the transverse component of the distribution function maintains Maxwellian and, consequently, $< f >= h(v_\perp)g(v_z,t)$, where $h(v_\perp) = (m/2\pi T_\perp)\exp(-mv_\perp^2/2T_\perp)$.

With these assumptions in hand, the diffusion equation after the integration of $< f >$ over $V_\perp$ leads to a modified Forkker-Planck equation for $g(v_z,t)$, namely,

$$\frac{\partial}{\partial t}g = \frac{\partial}{\partial v_z}\left(D\frac{\partial}{\partial v_z} - A\right)g + \frac{\partial^2}{\partial v_z^2}\left(D_1\frac{\partial}{\partial v_z} - A_1\right)g \tag{8}$$

The diffusion coefficient (D), the friction coefficient (A), and the two coefficients (D_1 and A_1) associated with the higher order terms are defined, respectively, by

$$D = D^L + D_+^{NL} + D^{NL}, \qquad A = A^L + A_+^{NL} + A_-^{NL}$$
$$D_1 = D_{1+} + D_{1-}, \qquad A_1 = A_{1+} + A_{1-}$$

where

$$\begin{pmatrix} D^L \\ A^L \end{pmatrix} = 2\pi\left(\frac{e}{m}\right)^2 \sum_{k,r}\begin{pmatrix} 1 \\ \frac{m}{T}\frac{r\Omega}{k_z} \end{pmatrix} k_z^2|\phi_k|^2 \Lambda_r(\alpha)\delta(\omega - k_z v_z - \ell\Omega) \tag{9}$$

$$\begin{pmatrix} D_+^{NL} \\ A_+^{NL} \\ D_{1+} \\ A_{1+} \end{pmatrix} = 2\pi\left(\frac{e}{m}\right)^4 \sum_{k\,k'\neq k} |\phi_k|^2|\phi_{k'}|^2 \sum_{r,q} \frac{k_z(k_z \pm k_z')}{(\omega - k_z v_z - \ell\Omega)^2} \begin{pmatrix} a_{r,q}^{\pm} \\ \frac{m}{T_\perp}\frac{(\ell \pm q)\Omega}{k_z \pm k_z'} a_{r,q}^{\pm} \\ b_{r,q}^{\pm} \\ \frac{m}{T_\perp}\frac{(\ell \pm q)\Omega}{k_z \pm k_z'} b_{r,q}^{\pm} \end{pmatrix}$$
$$\delta[\omega \pm \omega' - (k_z \pm k_z')v_z - (\ell \pm q)\Omega] \tag{10}$$

and where

$$a_{r,q}^{\pm} = 2\pi\int_0^\infty dv_\perp v_\perp h(v_\perp)\left\{\frac{k_z k_z'}{\omega - k_z v_z}\frac{J_r(\beta)J_q(\beta')}{v_z - \ell\Omega} + \frac{k_\perp k_\perp'}{2}\left[\frac{J_{r-1}(\beta)J_{q\pm1}(\beta')}{\omega - k_z v_z - (\ell-1)\Omega} + \frac{J_{r+1}(\beta)J_{q\mp1}(\beta')}{\omega - k_z v_z - (\ell+1)\Omega}\right]\right\}^2 \tag{11}$$

$$b_{r,q}^{\pm} = 2\pi\int_0^\infty dv_\perp v_\perp h(v_\perp)k_z' J_r(\beta)J_q(\beta')\left\{\frac{k_z k_z'}{\omega - k_z v_z}\frac{J_r(\beta)J_q(\beta')}{v_z - \ell\Omega} + \frac{k_\perp k_\perp'}{2}\left[\frac{J_{r-1}(\beta)J_{q\pm1}(\beta')}{\omega - k_z v_z - (\ell-1)\Omega} + \frac{J_{r+1}(\beta)J_{q\mp1}(\beta')}{\omega - k_z v_z - (\ell+1)\Omega}\right]\right\}^2 \tag{12}$$

In (9), $\alpha = k_\perp^2 T_\perp/m\Omega^2$ and $\Lambda_n(\alpha) = I_n(\alpha)\exp(-\alpha)$, where I_n is the modified Bessel function of order n. The modified Fokker-Planck equation, (8), contains all the information about the quasi-linear and the lowest-order nonlinear diffusion processes of Langmuir waves on electrons in a magnetized plasma. The quasi-linear and the nonlinear diffusion processes are evidenced by the delta function in (9) and by the two delta functions in (10), respectively. It is shown in (10) that the coefficients with the subscript "+" (i.e., D_+^{NL}, A_+^{NL}, D_{1+}, and A_{1+}) and with the subscript "-" (i.e., D^{NL}, A^{NL}, D_{1-}, and A_{1-}) represent the nonlinear interaction processes between electrons and the beat products, $\exp[\pm i(\omega \pm \omega')t]$ of the two Langmuir waves, $\exp(-i\omega t)$ and $\exp(\pm i\omega' t)$. For the evaluation of the coefficients given in (9) and (10), the idealized model used in Nicholson (1977) for the Langmuir wave spectrum is adopted here:

$$|\phi_k|^2 = \begin{cases} \dfrac{3.4(\nu_e/\omega_{ri})P^2 n_{ri}T_e}{(1-P^{-1/2})k_m^4}\delta(k-k_m) & \text{for both } 0 < \theta < \theta_{ri} \\ & \text{and } \pi - \theta_{ri} < \theta < \pi \\ 0 & \text{for } \theta_{ri} < \theta < \pi - \theta_{ri} \end{cases} \tag{13}$$

where θ is the angle between the Langmuir wave vector ($\vec{k}$) and the earth's magnetic field ($\vec{B}_{ri}$); k_m corresponds to the Langmuir waves with peak intensities; θ_{ri} defined by $\cos^{-1}(P^{-1/2})$ is the maximum θ of the Langmuir waves, where P is the squared ratio of the local electromagnetic pump field to the threshold field for the parametric decay instability. The other parameters in (13), N_{ri}, T_e, ν_e, ω_{ri}, have their conventional meanings as the local electron density, the electron temperature measured in unit of electron volts, the electron-ion collision frequency, and the incident electromagnetic pump wave frequency, respectively.

For achieving the electron acceleration from the bulk region to the tail region, the diffusion coefficients must remain non-vanishing values through a wide range in the velocity space. The conditions can be derived from the delta functions in (9), (10), and (13) that can be rewritten as follows:

$$\delta(k - k_m)\delta(\omega - k_z v_z - \ell\Omega) = |k_m v_z|^{-1}\delta(k - k_m)\delta(\cos\theta - \cos\theta_1) \tag{14a}$$

$$\delta(k - k_m)\delta[\omega - \omega' - (k_z - k_z')v_z - (\ell - q)\Omega]$$
$$= |k_m v_z|^{-1}\delta(k - k_m)\delta[\cos\theta - (\cos\theta_2 + \cos\theta')] \tag{14b}$$

$$\delta(k - k_m)\delta|\omega + \omega' - (k_z + k_z')v_z - (\ell + q)\Omega|$$
$$= |k_m v_z|^{-1}\delta|\cos\theta - (\cos\theta_3 + \cos\theta')| \tag{14c}$$

where

$$\cos\theta = k_z/k_m, \quad \cos\theta' = k_z'/k_m, \quad \cos\theta_1 = (\omega_m - \ell\Omega)/k_m v_z,$$
$$\cos\theta_2 = -(\ell - q)\omega/k_m v_z, \quad \text{and} \quad \cos\theta_3 = |2\omega_m - (\ell + q)\Omega|/k_m v_z \tag{15}$$

The dispersion relation of Langmuir waves can be well represented by $\omega \sim \omega' \sim \omega_m = \omega_{pe}(1 + 3k_m^2/2k_d^2)$ showing propagation in a weakly magnetized plasma at small angles with respect to the earth's magnetic field, where k_m, k_d, and ω_{pe} are respectively, the wave number of Langmuir waves with peak intensity, the Debye wave number, and the local electron plasma frequency.

Since θ_0 is the maximum propagation angle of Langmuir waves, we deduce that

$$\cos\theta_0 \le |\cos\theta_1|, |\cos\theta' + \cos\theta_2|, |\cos\theta_3 - \cos\theta'| \le 1 \tag{16}$$

from the delta functions on the RHS's of (14a), (14b), and (14c). With the aid of (15), the inequalities in (16) yield the following three ranges of v_z

$$(1) \qquad |\omega_m - \ell\Omega|/k_m \le |v_z| \le |\omega_m - \ell\Omega|/k_m\cos\theta_0 \tag{17a}$$
$$(2)\text{-}(A) \qquad \Omega/2k_m \le |v_z| \le |\ell - q|\Omega/2k_m\cos\theta_0 \quad \text{and}$$
$$\text{-}(B) \qquad |v_z| \ge |\ell - q|\Omega/k_m(1 - \cos\theta_0) \tag{17b}$$
$$(3)\text{-}(A) \qquad |2\omega_m - (\ell + q)\Omega|/2k_m \le v_z \le |2\omega_m - (\ell + q)\Omega|/2k_m\cos\theta_0 \quad \text{and}$$
$$\text{-}(B) \qquad |v_z| \ge |2\omega_m - (\ell + q)\Omega|/k_m(1 - \cos\theta_0) \tag{17c}$$

that assure the non-zeros of (1) D^L and A^L, (2) D_-^{NL}, A_-^{NL}, D_{1-} and A_{1-}, and (3) D_+^{NL}, A_+^{NL}, D_{1+} and A_{1+}, respectively. The two sub-ranges, (2)-(A) and (2)-(B), overlap as $\cos\theta_0 \le 1/3$, namely, $P \ge 9$ because θ_0 is defined by $\cos^{-1}(P^{-1/2})$ where P is the squared ratio of the local electromagnetic pump field to the threshold field for the parametric decay instability. The other two sub-ranges, (3)-(A) and (3)-(B), also overlap as $\cos\theta_0 \le 1/3$. While (2)-(A) and (3)-(B) are determined for Langmuir wave pairs propagating in opposite directions along the geomagnetic field, (2)-(B) and (3)-(A) are found for those propagating in the same direction along the geomagnetic field. Substituting (13) and (14a) into (9) and integrating it over k yield

$$\begin{pmatrix} D^L \\ A^L \end{pmatrix} = 4\pi^2\left(\frac{e}{m}\right)^2 \frac{3.4(\nu_e/\omega_0)P^2 n_0 T_e}{(1 - P^{-1/2})} \sum_{\ell=-\infty}^{\infty} \left(\begin{matrix} 1 \\ \frac{m}{T_e}\frac{\ell\Omega}{k_m\cos\theta_1} \end{matrix}\right) \frac{\cos^2\theta_1 \Lambda_\ell(\alpha_m)}{|k_m v_z|}$$
$$\times |H(|v_z| - |\omega_m - \ell\Omega|/k_m) - H(|v_z| - |\omega_m - \ell\Omega|/k_m\cos\theta_0)| \tag{18}$$

where $\alpha_m = (k_m^2 T_e/m\Omega^2)\sin^2\theta_1$ and $H(x)$ is the Heaviside step function. The sufficient condition for the continuous acceleration of electrons requires that the ranges of v_z be overlapped for either large negative $\ell < (\omega_m/\Omega) - (1 - \cos\theta_0)^{-1}$ or large positive $\ell > (\omega_m/\Omega) + (1 - \cos\theta_0)^{-1}$ as found from (17a). In other words, overlap of quasi-linear diffusion regions can occur in a wide range of v_z with the aid of cyclotron harmonic shift.

However, it is noted from (18) that $A^L/D^L \sim -(m/T_e)|\ell|\Omega/(\omega_m + |\ell|\Omega)v_z$ for a large value of $k_m v_z$ (i.e., a large positive or negative ℓ). If only the quasi-linear diffusion effect is considered, namely, if we only retain the terms associated with D^L and A^L in (8):

$$\frac{\partial}{\partial t}g = \frac{\partial}{\partial v_z}\left(D^L\frac{\partial}{\partial v_z} - A^L\right)g, \tag{19}$$

the steady state solution of (19) obtained by taking $(\partial/\partial t)g = 0$ has the Maxwellian form of

$$g(v_z, t \to \infty) \propto \exp\{-(m/2T_e)|\ell|\Omega/(\omega_m + |\ell|\Omega)|v_z^2\}$$

in each cyclotron shifted region. The effective temperature of this modified distribution function is

$$(\omega_m + |\ell|\Omega)T_e/|\ell|\Omega$$

that approximately equals the unperturbed electron temperature, T_e, for a large $|\ell|$ (i.e., a large $k_m v_z$). This result shows that the quasi-linear diffusion itself cannot produce very energetic electron fluxes (with $v_z > \omega_m/k_m \sim 20$ ev) because it is impeded by the friction force. This force, represented by A^L, is related to a finite Larmor radius (FLR) effect resulting from the coupling of electron parallel motion with transverse motion in the presence of Langmuir wave fields.

We next examine for other possible electron acceleration mechanisms the nonlinear wave-particle interaction terms neglected in (19), namely, $(D_-^{NL}, A_-^{NL}, D_{1-}, A_{1-})$ and $(D_+^{NL}, A_+^{NL}, D_{1+}, A_{1+})$, that correspond to the cases of Langmuir wave pairs propagating along the same and the opposite directions, respectively. Since $A^{NL}/D^{NL} \sim (m/T_e)v_z \sim A_{1-}/D_{1-}$ in the large parallel velocity (v_z) region, the diffusion of electrons is also impeded by frictions and no energetic electron flux can be produced by the process of nonlinear wave-particle interactions when the two Langmuir wave propagate in the same direction along the geomagnetic field. By contrast, it is found from (10) that in the region $v_z > 2\omega_m/(1 - \cos\theta_0)k_m$,

$$D_+^{NL} \sim (2\pi)^3\left(\frac{e}{m}\right)^4\left[\frac{3.4(\nu_e/\omega_0)P^2 N_0 T_e}{(1 - P^{-1/2})}\right]^2\left(\frac{4\omega_m}{k_m^4 v_z^6}\right)\left(1 - \cos\theta_0 - 2\frac{\omega_m}{k_m v_z}\right)$$
$$D_{1+} \sim v_z D_+^{NL}$$

and

$$A_+^{NL} \sim A_{1+} \sim 0 \text{ (negligibly small)} \tag{20}$$

The frictions are not able to prevent electrons from being accelerated in this case when electrons interact with the beat product (at the frequency sum) of two Langmuir waves that propagate in the opposite directions.

We note that the diffusion coefficients in this case have the largest values in comparison with those in the other two cases. Hence, in the calculation of the steady state distribution function (i.e., $g(v_z, t \to \infty)$) for $v_z > 2\omega_m/(1-\cos\theta_0)k_m$, only the coefficients given in (20) need to be retained in (8). The result is

$$g(v_z, t \to \infty) = g(v_{z1})[1 - F(v_z, v_{z1})/F(v_{z2}, v_{z1})] \tag{21}$$

where $F(x, v_{z1} = (1/5)(x - v_{z1})^5 + (5/4)v_{z1}(x - v_{z1}^4 + (10/3)v_{z1}^2(x - v_{z1})^3 + 5v_{z1}^3(x - v_{z1})^2 + 5v_{z1}^4(x - v_{z1})$ for $v_t < v_{z1} < v_z < v_{z2}$ where $v_t = 2\omega_m/k_m(1-\cos\theta_0)$. Since (21) holds for any $v_{z2} > v_z$ and $g(v_{z2}) \to 0$ as $v_{z2} \to \infty$, it is thus concluded that $g(v_z) \simeq g(v_{z1}) \simeq g(v_t)$ for $v_z > v_t$, predicting the formation of a flat electron distribution (i.e., a plateau) in the tail region. This prediction agrees qualitatively with the observatins reported in Carlson et al. (1982).

The level of the plateau depends upon the value of $g(v_t)$. It is seen in (17c) that regions (3)-(A) and (3)-(B) become to overlap when $P \geq 9$ and that region (3)-(A) coincides with the quasi-linear diffusion region defined by (17a) for the case of $\ell = q = 0$. In fact, the plateau starts to be formed by the quasi-linear diffusion process in the suprathermal region defined by (17a) for $\ell = 0$. This suprathermal plateau can be further extended to the very energetic region defined by (3)-(B) in (17c) through the nonlinear diffusion process of electrons that interact with the frequency sum beats of Langmuir wave pairs propagating in opposite directions along the geomagnetic field. Therefore, $g(v_t)$ has the value of the distribution function in the suprathermal plateau, that is, $g(v_t) \lesssim g(5v_{th}) \sim n_0 \exp(-12.5)/(2\pi)^{1/2}v_{th}$, where $v_{th}(= (T_e/m)^{1/2})$ is the thermal electron velocity. The energetic electron flux between the velocity interval, (v_{z1}, v_{z2}), is then given by

$$\Phi \leq n_0 \exp(-12.5)(v_{z2}^2 - v_{z1}^2)/(2\pi)^{1/2}2v_{th} \tag{22}$$

Under the typical ionospheric F condition: $n_0 = 4.5 \times 10^5 \text{cm}^3$, $v_{th} \sim 1.3 \times 10^7$ cm/sec, the calculated Φ from (22) is $4.35 \times 10^8 \text{cm}^{-2}\text{sec}^{-1}$ for $v_{z1} = 1.3 \times 10^8$ cm/sec and $v_{z2} = 1.8 \times 10^8$ cm/sec corresponding to electron energies of 10 ev and 20 ev, respectively.

This theoretical energetic electron flux is greater than the experimentally deduced result, $(2-4) \times 10^7 \text{cm}^{-2}\text{sec}^{-1}$(Carlson et al., 1982), by one order of magnitude. The discrepancy is considered to be reasonable because the calculation of (22) is based upon the assumption that the layer of Langmuir waves is thick enough to allow the formation of electron distribution plateau. We expect that the theoretical value in this ideal case should be greater than the experimental measurements. In conclusion, our analysis shows that the quasi-linear diffusion may be effective enough to produce energetic electron flux with energies exceeding 10 ev reported in Carlson et al. (1982). However, the very energetic electron flux (> 25 ev) measured by Grandal et al. (1983) can only be generated by the nonlinear diffusion process of electrons that interact with the Langmuir wave pairs propagating in directions opposite to each other along the magnetic field. The proposed mechanism can indeed produce the observed energetic electron flux in HF ionospheric heating experiments.

4. APPEARANCE OF ARTIFICIAL SPREAD F

The detection of artificial spread F irregularities by ionosondes is discussed in this section with intention to understand the puzzling occurence frequency of artificial spread F at different locations. Artificial spread F is generally believed to be caused by the excitation of large scale (~a few hundreds of meters to kilometers), field-aligned ionospheric irregularities. However, we note that a lack of artificial spread F does not necessarily imply the absence of HF heater wave-induced ionospheric irregularities in the following outstanding cases. The radio star scintillations (Frey et al., 1984) and the scanning radar incoherent backscatter process (Duncan and Behnke, 1978) indicate that large scale ionospheric irregularities had been excited by HF heaters at Tromso and Arecibo while no spread F echoes were recorded at either place. Based on the work of Kuo and Lee (1984) and Kuo et al. (1985), the following anlyses show that spread F echoes are caused by ionospheric irregularities whose wave vectors are situated within the meridian plane.

We interpret that spread F echoes result from the drastic variation of reflection heights of vertically transmitted radio waves in the presence of ionospheric irregularities. This problem can be understood from analyzing the trajectory of rays described by the following Hamiltonian equations of motion

$$d\vec{r}/dt = \partial\omega/d\vec{k} \tag{23a}$$

$$d\vec{k}/dt = -\nabla\omega \tag{23b}$$

where ω and $\vec{k}$ are the wave frequency and wave vector of transmitted radio waves from the ionosonde; $\vec{r}$ and t have their conventional meanings of displacement and time, respectively. If $\omega^2 \gg \Omega_e^2$ is assumed, the dispersion relation of radio waves in the ionosphere is simply represented by

$$\omega^2 = \omega_{pe}^2 + k^2c^2 \tag{24}$$

where ω_{pe} and c are electron plasma frequency and the speed of light in vacuum.

The unperturbed ionospheric density is modelled by $N_0(x) = N_0(1 + x/L)$ for a horizontally stratified ionosphere having a scale length L, where x is the vertical coordinate and N_0 is the electron density at the reference plane $x = 0$ located at an altitude of H above the earth crest (see Figure 3). Field-aligned ionospheric irregularities can, in general, have two independent polarization directions. One lies in the meridian plane, the electron density fluctuations then have the form of $\delta N_1 \sin k_1(x\cos\theta_0 + z\sin\theta_0)$, where k_1 is the average wave number of the irregularities, θ_0 is the local magnetic dip angle, and z is the horizontal coordinate as shown in Figure 3. The other one is oriented perpendicularly to the meridian plane, the electron density fluctuations can be modelled as $\delta N_2 \sin(k_2 y + \phi)$, where k_2 is the average wave number of this type of irregularities, y is the coordinate perpendicular to the meridian plane, and ϕ is an arbitrary phase angle.

In the presence of ionospheric irregularities the electron density distribution, $n(x, y, z)$, includes the unperturbed and the fluctuating components. The electron plasma frequency, ω_{pe}, then has the following expression

$$\omega_{pe}/\omega_{pe0} = 1 + x/L + (\delta N_1/N_0)\sin k_1(x\cos\theta_0 + z\sin\theta_0) + (\delta N_2/N_0)\sin(k_2 y + \phi) \tag{25}$$

where ω_{pe0} is the electron plasma frequency at the reference plane, $x = 0$. Consequently, the trajectory of rays in the Cartesian

system of coordinate is governed by the following six scalar equations

$$\frac{d}{dt}x = \frac{k_x c^2}{\omega} \tag{26a}$$

$$\frac{d}{dt}y = \frac{k_y c^2}{\omega} \tag{26b}$$

$$\frac{d}{dt}z = \frac{k_z c^2}{\omega} \tag{26c}$$

$$\frac{d}{dt}k_x = -\frac{\omega_{pe_0}^2}{2\omega L}\left[1 + \left(\frac{\delta N_1}{N_0}\right)(k_1 L\cos\theta_0)\cos k_1(x\cos\theta_0 + z\sin\theta_0)\right] \tag{27a}$$

$$\frac{d}{dt}k_y = -\frac{\omega_{pe_0}^2}{2\omega}\left(\frac{\delta N_2}{N_0}\right)k_2\cos(k_2 y + \phi) \tag{27b}$$

$$\frac{d}{dt}k_z = -\tan\theta_0\left(\frac{\omega_{pe_0}^2}{2\omega L}\right)\left(\frac{\delta N_1}{N_0}\right)(k_1 L\cos\theta_0)\cos k_1(x\cos\theta_0 + z\sin\theta_0) \tag{27c}$$

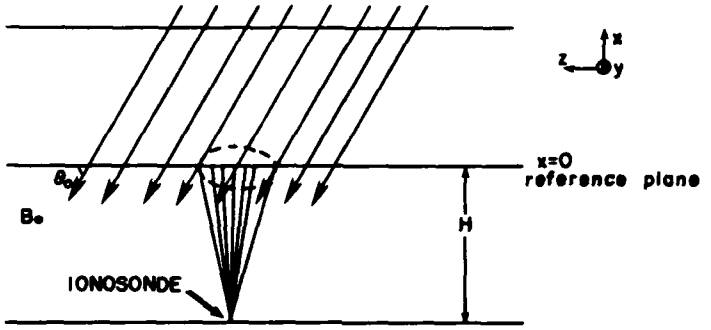


Figure 3. Configuration of the coordinate system

Equations (26b) and (27b) form one set of coupled equations, and equations (26a), (26c), (27a), and (27c) form the other one.

Four invariants of ray trajectory have been found, they are

$$\left(\frac{\delta N_2}{N_0}\right)\sin(k_2 y + \phi) + \left(\frac{k_y^2 c^2}{\omega_{pe_0}^2}\right) = \tau_1 \tag{28}$$

$$k_x - k_z\cot\theta_0 + \left(\frac{\omega_{pe_0}^2}{2\omega L}\right)t = \tau_2 \tag{29}$$

$$x + \left(\frac{\tan 2\theta_0}{2}\right)z + \left(\frac{\delta N_1}{N_0}\right)L\left(\frac{\cos^2\theta_0}{\cos 2\theta_0}\right)\sin k_1(x\cos\theta_0 + z\sin\theta_0) + \left(\frac{c^2 L}{\omega_{pe_0}^2}\right)k_x(k_x + k_z\tan 2\theta_0) = \tau_3 \tag{30}$$

$$\left(\frac{\tan 2\theta_0}{2}\right)z + \left(\frac{\delta N_1}{N_0}\right)L\left(\frac{\sin^2\theta_0}{\cos 2\theta}\right)\sin k_1(x\cos\theta_0 + z\sin\theta_0) - \left(\frac{c^2 L}{\omega_{pe_0}^2}\right)k_z(k_z - k_x\tan 2\theta_0) = \tau_4 \tag{31}$$

where τ_1, τ_2, τ_3, and τ_4 are four constants in time. With the aid of these four invariant relations, the temporal evolution of any one of x, z, k_x, and k_z, and either one of y and k_y can be determined by the corresponding equations of ray trajectory, namely, (26-a,b,c) and (27-a,b,c).

The elapsed time for each ray travelling from the reference height to the reflection height can, in principle, be calculated by integrating (27-a) from $k_x = k_{x_0}$ to $k_x = 0$ with the prescribed initial conditions: $x(t = 0) = 0$, $z(t = 0) = z_0$, and $k_z(t = 0) = k_{z_0}$ and with the aid of the invariant relations, (29), (30), and (31). It is clear from (27-a) that k_x is only affected by ionospheric irregularities (referred to as type A irregularities) whose polarization lies within the meridian plane. Those (referred to as type B irregularities) whose polarization is oriented perpendicularly to the meridian plane do not cause the variation of reflection heights of radio waves. Types A and B irregularities can be excited by the filamentation instability of X-mode and O-modes HF heater waves, respectively (Kuo and Schmidt, 1983).

If the ionosonde-transmitted beam is modelled by many rays having different initial locations on the reference plane, the spread F echoes can be interpreted to be caused by the difference in the reflection heights of the returned signals. The virtual height spread in the ionogram is thus proportional to the maximum difference, Δx_{max}, of these reflection heights. The quantitative analysis of our spread F echo model show that (1) Δx_{max} increases monotonically with the irregularity intensity, (2) with a fixed irregularity intesity, Δx_{max} increases with latitudes and then decreases monotonically to zero at $\theta_0 = 90°$, (3)

significant spread F (i.e., large Δx_{max}) can be observed over a wide range of latitude including Arecibo ($\theta_0 = 50°$), Boulder ($\theta_0 = 68°$), and even Tromso ($\theta_0 = 78°$) as long as type A irregularities exist, and (4) spread F occurs with $\lambda_\perp > 100$ meters, where $\lambda_\perp$ is the scale length of type A ionospheric irregularities. These results indicate that the appearance of the spread F should not depend upon the locations of ionosondes. We conclude that HF heater wave-induced spread F's are caused by type A irregularities with scale lengths greater than 100 meters.

Based upon our model of spread F echoes, we can explain the different occurrence frequency of artificial spread F's noticed at Arecibo, Boulder, and Tromso as follows. The HF heater wave transmitted from Tromso, Norway is either a left (X-mode) or right (O-mode) hand circularly polarized wave propagating along the geomagnetic field. Large-scale irregularities would be excited by the filamentation instability preferentially in the direction perpendicular to the meridian plane for symmetric high frequency sidebands (Kuo and Schmidt, 1983). This, together with the effect of large geomagnetic dip angle ($\theta_0 = 78°$), may explain why artificial spread F's have never been observed at Tromso since the EISCAT heating facilities were operated a few years ago. The HF heater at Arecibo is often operated in O-mode. During the O-mode ionospheric heating, no spread F or change of reflection heights can be seen (L. M. Duncan, private communication, 1984). This can be understood now with the proposed model of spread F echoes, namely, spread F cannot be induced by type B irregularities produced by O-mode heater waves. Finally, we discuss the reason why artificial spread F had been constantly observed at Boulder, Colorado. It is most possibly because the O-mode and X-mode heater waves transmitted from the Boulder facilities cannot be separated as easily as those from the Arecibo or the Tromso facilities. This speculation is based upon the fact that short-scaled (meter-scaled and less) irregularities can still be excited by X-mode heater waves at Boulder though not expected (Fialer, 1974). According to existing theories (see, e.g., Gurevich, 1978; Fejer, 1979; Lee and Kuo, 1983a), only O-mode waves are able to generate short scale ionospheric irregularities.

5. SUMMARY AND CONCLUSIONS

Three outstanding ionospheric phenomena caused by HF heaters have been discussed in this paper. The earth's magnetic field perturbations observed at Tromso (Stubbe and Kopka, 1981; Stubbe et al., 1982) are possibly produced by the thermal filamentation instability of radio waves that can also excite large scale ionospheric irregularities simultaneously. The irregularity strength and geomagnetic fluctuations are found to be in proportion. A standing wave pattern is created in the HF heater-modified ionosphere because zero-frequency modes are associated with the excitation of geomagnetic fluctuations and ionospheric irregularities. Langmuir wave turbulence that is generated by the parametric decay instability of O-mode HF heater waves can be responsible for electron energization in ionospheric heating experiments. The diffusion effect of Langmuir wave fields on the background electron distribution is evaluated as the process of generating energetic electrons deduced in the measurements of enhanced plasma lines at Arecibo (Carlson et al., 1982) and detected in the in-site particle measurements at Tromso (Grandal et al., 1983). Both quasi-linear and nonlinear processes of wave-particle interactons are analyzed in a modified Fokker-Planck equation. Our analysis shows that quasi-linear diffusion may be effective enough to produce energetic electron flux (> 10 ev), reported by Carlson et al. (1982). However, the very energetic electrons (> 25 ev) measured by Grandal et al. (1983) can only be generated by the diffusion process through nonlinear wave-particle interactions with Langmuir wave pairs propagating in opposite directions. A flat electron distribution in the tail region that is deduced from the enhanced plasma line measurements can be formed by the proposed mechanism. Artificial spread F echoes are found to be caused by HF wave-induced irregularities (type A irregularities) whose polarization vectors lie within the meridian plane. The phenomenon of spread F can be satisfactorily interpreted to result from the difference in the reflection heights of the returned rays in the presence of type A irregularities with scale lengths greater than 100 meters.

ACKNOWLEDGEMENTS.

The work at the Massachusetts Institute of Technology was supported by the NASA grant NAG 5-270 and in part by the previous AFGL contract F19628-83-K-0024, that at the Polytechnic Institute of New York was supported jointly in part by the NSF grant ATM-8315322 and in part by the AFOSR grant no. AFOSR-83-001 and -85-0133.

REFERENCES

Carlson, H. C., W. E. Gordon, and R. L. Shower, High frequency induced enhancements of the incoherent scatter spectrum at Arecibo, **J. Geophys. Res.**, 77, 1242, 1972.

Carlson, H. C., and L. M. Duncan, HF excited instabilities in space plasmas, **Radio Sci.**, 12, 1001, 1977.

Carlson, H. C., V. B. Wickwar, and G. P. Mantas, Observation of fluxes of suprathermal electron accelerated by HF excited instabilities, **J. Atmos. Terr. Phys.**, 44, 1089, 1982.

Cragin, B. L., and J. A. Fejer, Generation of large-scale field-aligned irregularities in ionospheric modifiaction experiments, **Radio Sci.**, 9, 1071, 1974.

Cragin, B. L., J. A. Fejer, and E. Leer, Generation of artificial spread F by a collisionally coupled purely growing parametric instability, **Radio Sci.**, 12, 273, 1973.

Das, A. C., and J. A. Fejer, Resonance instability of small-scale field-aligned irregularities, **J. Geophys. Res.**, 84, 6701, 1979.

Duncan, L. M., and R. A. Behnke, Observations of self-focusing electromagnetic waves in the ionosphere, **Phys. Res. Lett.**, 41, 998, 1978.

Farley, D. T., Jr., Artificial heating of the electrons in the F region of the ionosphere, **J. Geophys. Res.**, 68, 401, 1963.

Fejer, J. A., Generation of large-scale field-aligned density irregularities in ionospheric heating experiments, **AGARD Conf. Proc.**, 138, 13, 1973.

Fejer, J. A., Ionospheric modification and parametric instabilities, **Rev. Geophys. Space Phys.**, 17, 135, 1979

Fejer, J. A.,and K. N. Graham, Electron acceleration by parametrically excited Langmuir waves, **Radio Sci.**, 9, 1081, 1974.

Fejer, J. A., and Y. Y. Kuo, Structure in the nonlinear saturation spectrum of parametric instabilities, **Phys. Fluids**, 16, 1490, 1973.

Fejer, J. A. and E. Krenzien, Theroy of generation of ULF pulsation by ionospheric modification experiments, **J. Atmos. Terr. Phys.**, 44, 1075, 1982.

Fialer, P. A., Field-aligned scattering from a heated region of the ionosphere—observations at HF and VHF, **Radio Sci.**, 9, 923, 1974.

Frey, A., P. Stubbe, and H. Kopka, First experimental evidence of HF produced electron density irregularities in the polar ionosphere; diagnosed by UHF radio star scintillations, **Geophys. Res Lett.**, 11, 523, 1984.

Goldman, M. V., Field-aligned instability due to stimulated scattering of intense radio waves from diffusion quasi-modes, **Radio Sci.**, 9, 1077, 1974.

Grandal, B. et al., Preliminary results from the HERO project, in situ measurements of ionospheric modifications using sounding rockets, **Proceedings of International Symposiums on Active Experiments in Space**, ESA SP-195, pp. 75-80, 1983.

Gurevich, A., Nonlinear phenomena in the ionosphere, in **Physics and Chemistry in Space**, Vol. 10, Springer-Verlag, New York, 1978.

Inhester, B., A. C. Das, and J. A. Fejer, Generation of small-scale field-aligned irregularities in ionospheric heating experiments, **J. Geophys. Res.**, 86, 9101, 1981.

Kuo, S. P., and M. C. Lee, Earth magnetic field fluctuations produced by filamentation instabilities of electromagnetic heater waves, **Geophys. Res. Lett.**, 10, 979, 1983.

Kuo, S. P., and G. Schmidt, Filamentation instability in magneto plasmas, **Phys. Fluids**, 26, 2529, 1983.

Kuo, S. P., and M. C. Lee, On the spread F echoes from the ionospheric heated region, **Proceedings of Ionospheric Effects Symposium** (May 1-3, 1984, Alexandria, Virginia) 5b-3, 1984.

Kuo, S. P., B. R. Cheo and M. C. Lee, The role of parametric decay instability in generating ionospheric irregularities, **J. Geopys. Res.**, 88, 417, 1983.

Kuo, S. P., M. C. Lee, S. C. Kuo, A theoretical model of artificial spread F, **Radio Science** (in press), 1985.

Lee, M. C., and J. A. Fejer, Theory of short-scale field-aligned density striations due to ionospheric heating, **Radio Sci.**, 13, 893, 1978.

Lee, M. C., and S. P. Kuo, Ionospheric irregularities and geomagnetic fluctuations due to ionospheric heating, **Proceedings of Internatioal Symposium on Active Experiments in Space**, European Space Agency, SP-195, pp. 81-89, 1983a.

Lee, M. C., and S. P. Kuo, Excitation of upper hybrid waves by a thermal parametric instability, **J. Plasma Phys.**, 30, 463, 1983b.

Lee, M. C., and S. P. Kuo, Excitation of magnetostatic fluctuations by filamentation of whistlers, **J. Geophys. Res.**, 89, 2289, 1984a.

Lee, M. C., and S. P. Kuo, Earth's magnetic field perturbations as the possible environmental impact of the conceptualized Solar Power Satellite, **J. Geophys. Res.**, 89, 11043, 1984b.

Nicholson, D. R., Magnetic field effects on electrons during ionospheric modification, **J. Geophys. Res.**, 82, 1839, 1977.

Perkins, F. W., A theoretical model for short-scale field-aligned plasma density striations, **Radio Sci.**, 9, 1065, 1974.

Perkins, F. W., and E. J. Valeo, Thermal self-focusing of electromagnetic waves in plasmas, **Phys. Rev. Lett.**, 32, 1234, 1974.

Perkins, F. W., and M. V. Goldman, Self-focusing of radio waves in an underdense ionosphere, **J. Geophys. Res.**, 86, 600, 1981.

Perkins, F. W., C. Oberman, and E. J. Valeo, Parametric instabilities and ionospheric modification, **J. Geophys. Res.**, 79, 1478, 1974.

Shower, R. L., and D. M. Kim, Time variations of HF-induced plasma waves, **J. Geophys. Res.**, 83, 623, 1978.

Stubbe, P., and H. Kopka, Generation of P_i 5 pulsations by polar electrojet modulation: first experimental evidence, **J. Geophys. Res.**, 86, 1606, 1981.

Stubbe, P., et al., Ionospheric modification experiments in northern Scandinavia, **J. Atmos. Terr. Phys.**, 44, 1025, 1982.

Utlaut, W. F., A survey of ionospheric modification effects produced by high-power HF radio waves, **AGARD Conf. Proc.**, 138, 3, 1973.

Vaskov, V. V., and A. V. Gurevich, Resonance instability of small-scale plasma perturbations, **Sov. Phys. JETP Engl. Transl.**, 46, 487, 1977.

Weinstock, J., Enhanced airglow, electron acceleration, and parametric instabilities, **Radio Sci.**, 9, 1085, 1974.

SUMMARY OF SESSION VI

Incoherent/Coherent Scatter

by

Dr G.Rose
Session Chairman

Four papers were presented during Session VI.

Bauer reviews recent scientific work using EISCAT. Results of large, medium and small scale studies are discussed, and comparisons between EISCAT and the STARE radar measurements are communicated.

In order to investigate small structures in the high latitude F-region Hargreaves et al have used beam scanning of EISCAT. In their paper, the magnitude of irregularities observed in four runs between 1982 and 1984 are analysed with periods shorter than 2 minutes. Field aligned irregularities of scales of more than a few kms can be traced by the EISCAT UHF radar up to heights of about 700 km. The interesting results of the measurements are presented and discussed.

Kofman and Lathuillere used EISCAT to investigate the response of the ionospheric plasma to the energy deposition of particle precipitation during disturbed conditions as compared to undisturbed situations. They obtained interesting results, amongst others, on the change of ion composition in response to electron precipitation and Joule heating, and on the variation of neutral density and temperature depending on the energy input.

Jones et al present interesting results obtained from experiments with the SABRE radar. Both, geophysical phenomena of the high latitude ionosphere, and the plasma physics of meter scale irregularities have been investigated. The strongest backscatter between 13—19 UT and 23—03 UT was found associated with the main electrojets and only weak backscatter occurred around the convection reversals. An interesting finding was that the aspect angle attenuation can take any value between 0 and 10 dB per degree depending on the absolute intensity measured. It must be stressed that the characteristics of the backscatter irregularities are important to estimate the quality of communications and surveillance systems operating in either HF or VHF frequency bands at these latitudes.

EISCAT : A REVIEW OF RECENT SCIENTIFIC WORKS

P. Bauer
CNET/CNRS
38-40 rue du Général Leclerc
92131 Issy-les-Moulineaux
France

SUMMARY

The EISCAT UHF system located in Northern Scandinavia is in operation since August 1981. In the general frame of observations of the solar wind, magnetosphere and ionosphere interactions, EISCAT has been involved in large, medium and small scales studies. Without being exhaustive this paper deals with each of these scales namely :

- plasma convection and heating in the auroral oval,
- auroral arcs and particle precipitations,
- anisotropic ion velocity distributions, collision and composition effects on incoherent scatter spectra.

INTRODUCTION

The EISCAT Scientific Association was set up in 1975 by research organizations from Finland, France, West Germany, Norway, Sweden and United Kingdom with the purpose of building in Northern Scandinavia two incoherent scatter systems (UHF and VHF) aiming at the study of the auroral ionosphere. The UHF system operates since 1981 [1] and has provided the EISCAT community with a wealth of data. Several of the highlights of the EISCAT scientific return are presented in this paper.

I. THE EISCAT FACILITY

EISCAT stands for European Incoherent SCATter.

The EISCAT facility consists in two radar systems (UHF and VHF) illustrated in figure 1. The UHF system operates since 1981 and includes a transmitter (2 MW peak power) located in Tromsö (Norway) associated with a fully steerable 32 m diameter antenna functioning as a monostatic radar; two identical receiving antennas at kiruna (Sweden) and Sodankyla (Finland) give a tristatic configuration to the system and allow for full velocity vector measurements. The VHF systems should start operating in 1985 and consists in monostatic radar (5 MW peak power) located in Tromsö. The VHF antenna is a 40 x 120 m parabolic cylinder rotating along its horizontal axis. While the UHF system is unique for velocity vector measurements, the VHF system will provide a considerable coverage both in altitude and in latitude.

The basic parameters obtained with these systems are:

- the ion velocity vector $\vec{V}_i$,
- the electron concentration N_e,
- the electron and ion temperatures, T_e and T_i,
- the mean ion mass $< m_i >$,
- the plasma frequency f_{pe}.

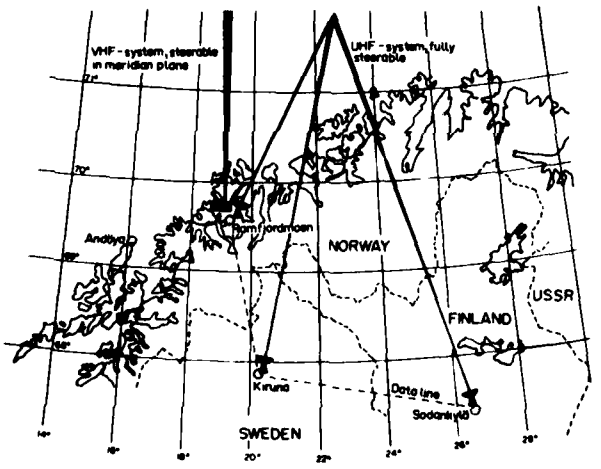


Fig. 1. Map of northern Scandinavia showing the EISCAT locations and Geometry. [1]

II. AURORAL PLASMA CONVECTION

Access to the full ion vector velocity $\vec{V}_i$ is one of the major interests of the EISCAT-UHF system. From it, in the F region of the ionosphere, can be directly derived the auroral convection electric field $\vec{E}$ since the following classical relationship holds:

(1) $\vec{V}_i \wedge \vec{B} = \vec{E}$

(where $\vec{B}$ is the magnetic field vector) which expresses that the Lorentz force balances the Coulomb force for the F_2 region ionospheric plasma.

Eq. (1) can be rewritten as

(2) $\vec{V}_{i\perp} = \frac{\vec{E} \wedge \vec{B}}{B^2}$

II.1

One thus gets an unambiguous determination of $\vec{E}$; Yet such a determination is somewhat limited in horizontal coverage and in time resolution. It is therefore tempting to extend the observations through others means and among them the STARE [2] bistatic coherent radar is an excellent candidate since EISCAT is approximately located in the center of its field of view.

The interpretation of the STARE doppler measurements is, however, not as straightforward as those of the incoherent scatter radar. It was consequently important to conduct a comparison study which was performed by Nielsen and Schlegel [3]. Figure 2 gives the outcome of this comparison for both the amplitudes and the directions.

It appears clearly that while the agreement in direction is always excellent, the agreement of the magnitudes is good for velocities up to about 700 ms^{-1}, for larger amplitudes the STARE estimates are systematically lower than those of EISCAT indicating a "saturation effect".

The interpretation of the STARE data being based upon the simple fluid approximation of the equations governing the two-stream and gradient drift instabilities, the above comparison points to the limit of the approximation for large velocities and to the need of properly accounting for the energy dissipation of plasma waves through heating of the electron gas.

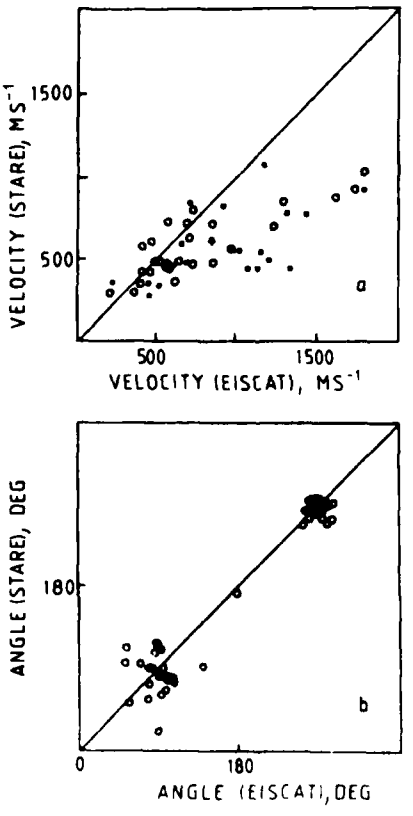


Fig. 2. Comparison of the EISCAT electron drift velocity measurements with the electron drift velocity estimate derived from the STARE Doppler velocity observations. Panel (a) displays amplitudes, and panel (b) displays the directions. [3]

II.2 Case studies

Plasma flows studies above EISCAT have been performed for specific events on several occasions: e.g. by Farmer et al. [4], Lockwood et al. [5], Van Eyken et al. [6].

Lockwood et al. [5] give an account of plasma convection motions observed on November 25, 1982. Above EISCAT while the Tromsö transmitter beam was operated in a fixed mode along the Tromsö field line (CPO mode). Two substorms occur during the period of observation as identified in figure 3 from magnetograms recorded at Soroya (SOR), Alta (ALT), Muonio (MUO) and Sodankyla (SOD). The substorms are triggered respectively at 1710 UT and 2149 UT.

The first one is identified with a Westward Travelling Surge. Figure 4 shows the behavior of the EISCAT field perpendicular velocities (polar plot) with 5 and 20 minutes post integrations. Large westward flows are observed in the afternoon sector from the time (1300 UT) at which data from all three sites became available. In spite of a data gap at the onset of the first substorm, it is clear that the substorm induces a southward swing of the plasma. Such a southward turning during a substorm was also reported by Horwitz et al. [7] and Foster et al. [8]. The flow afterwards returns to westward and the dawn-dusk cell separatrix is observed at about 2120 UT. The second substorm also induces a swing to southward flow and an increase in flow speed. After 00 UT the flows is predominantly eastward and irregular.

In both substorms the F region electron concentrations are depleted while the E region area are enhanced.

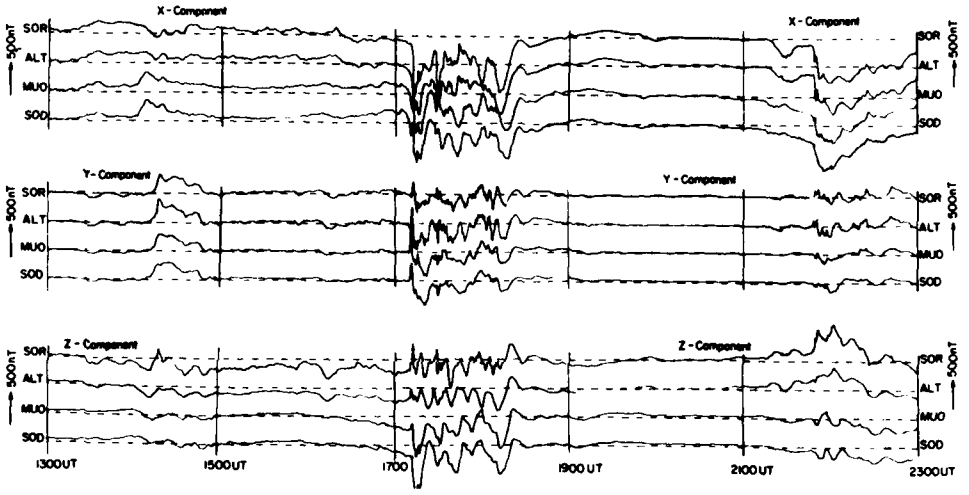


Fig. 3. Magnetograms from SOROYA (SOR), ALTA (ALT), MUONIO (MUO), SODANKYLA (SOD) on 25 November 1982. [5]

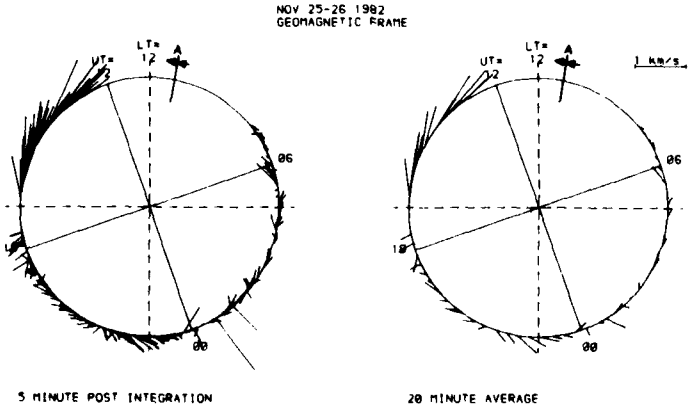


Fig. 4. Polar plot of field-perpendicular velocities. Each vector is plotted pointing away from the circular locus of the intersection scattering volume. A scale for the vectors is given in the top right and A denotes the start and end time of the 24 h observation run. [5]

Van Eyken et al. [6] have demonstrated the EISCAT capability in observing plasma convection at high invariant latitudes (70° - 77°). For large horizontal distances the classical tristatic determination of velocity vectors become inoperative because of the smallness of the viewing angles from the different EISCAT sites. Assuming a reasonable stationarity of the flow pattern in time and space, a beam swinging technique is used consisting in moving at a low elevation angle (19.5°) the Tromsö transmitter beam between two directions 20° apart so as to reconstruct velocity vectors in the plane of observation. Simplifying assumptions lead them to the determination of the ion velocity vector components perpendicular to the magnetic field. The convection pattern thus obtained on November 27, 1982 is exhibited on figure 5. From the start of the experiment up to 1430 UT the usual sunward convection is observed up to approximately 74° invariant latitude where it reverses indicating the location of the polar cap boundary. Between 1430 UT and 1440 UT a large northward flow develops, which from the point of view of Van Eyken et al. [6] might be the ionospheric signature of a time dependent reconnection at the magnetopause called "Flux Transfer Event" (Russell and Elphic [9]). After 1440 UT the sunward convection is restored but the polar cap boundary is no longer easily located.

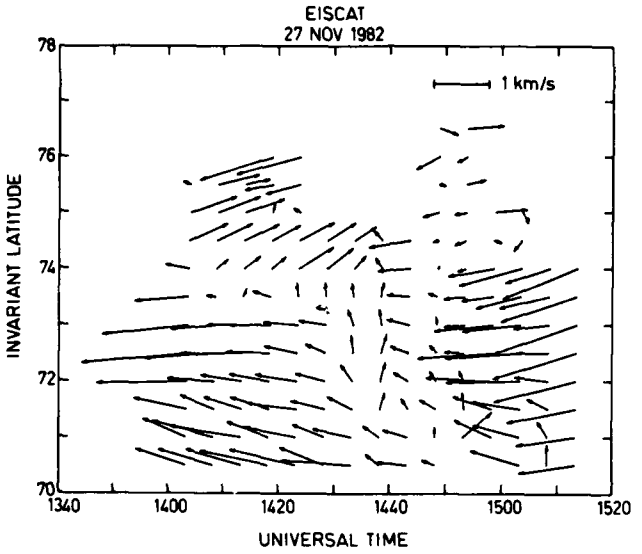


Fig. 5. Plasma drift velocities normal to the geomagnetic field on 27 November 1982, obtained by combining data from equivalent L values at azimuths 315° and 335°. [6]

II.3 Global scale auroral studies

Simultaneous observations from three radars (Millstone Hill radar, Chatanika radar, EISCAT) at locations about equally spaced along the auroral zone have been performed between 1981 and 1982 in the frameword of the MITHRAS program [10]. The data discussed in a paper by Caudal et al. [11] concern observations made during a period of large magnetic activity on November 18, 1981. This paper also includes data from Saint-Santin at midlatitudes.

Figure 6 exhibits the North South electric fields measured by the four incoherent scatter systems. They are plotted versus Universal Time. However the magnetic local time (MLT) is also indicated for each of the auroral zone radar.

The first interesting feature is an apparent correlation between the fields observed at Chatanika and at Tromsö. A closer analysis shows that this is simply due to the fact that Chatanika leaves the auroral zone on the morning side while Tromsö enters the region of cell reversal (coinciding with the Harang discontinuity). The most significant feature is that for this magnetically active period the convection pattern is remarkably stable with strong Northward afternoon electric field, a very early and extended reversal of the field (up to 5 hours at Tromsö) coinciding with the Harang discontinuity (figure 7). It should be noted also that the field strength for similar MLT is twice as large at Tromsö than at Chatanika. At last (figure 6) it is interesting to note that unusually large electric fields are observed at midlatitudes.

The same data set (November 18-19, 1981) as well as data gathered on December 15-16, 1981, were used in a study conducted by de la Beaujardière et al. [12]. In addition to incoherent scatter data satellite data was available from ISEE 1 and 3, NOAA 6 and 7, DE 1 and DE 2. One interesting feature revealed by the data is the considerable differences in electron concentrations measured at 500 km around 00 MLT at the different sites. The concentrations observed at EISCAT are about two times larger than those of Millstone Hill (figure 8). According to the authors, this illustrates the fact that the magnetic field tubes being convected in few hours from the dayside of the auroral oval to the nightside the electron concentration of the F_2 region depends upon the replenishment occurring on the dayside. The differences observed are due to the relative locations of the terminator with the conjugate dayside regions: while the EISCAT conjugate dayside region is well illuminated, the Chatanika conjugate region is hardly illuminated and the Millstone Hill one stays in the shadow. These varying situations are linked to the relative locations of the geographic and geomagnetic poles.

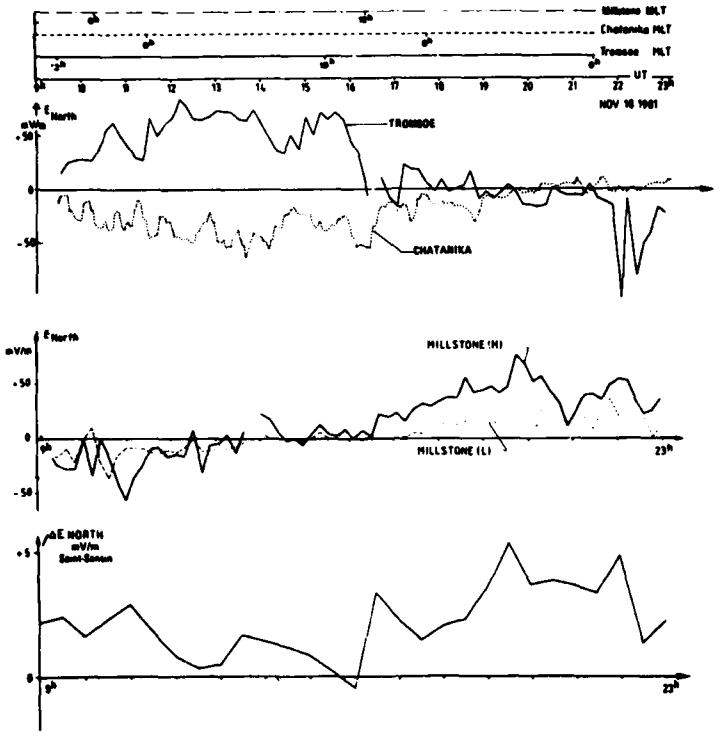


Fig. 6. Comparison of the northward electric field components, plotted versus universal time, for the period when the EISCAT, Chatanika and Millstone Hill radars were operating together. Above the figure, the corresponding magnetic local times at the 3 auroral radars are also indicated. Top : Tromsö (full line) and Chatanika (dotted line) electric fields. Middle : Millstone Hill electric fields at 66.3° and 61° invariant latitude, marked (H) and (L) respectively. Bottom : difference between the northward electric field measured at Saint-Santin and the quiet model electric field for mid-latitude. Note that the vertical scale length for this bottom curve is different from that of the top and middle curves. [11]

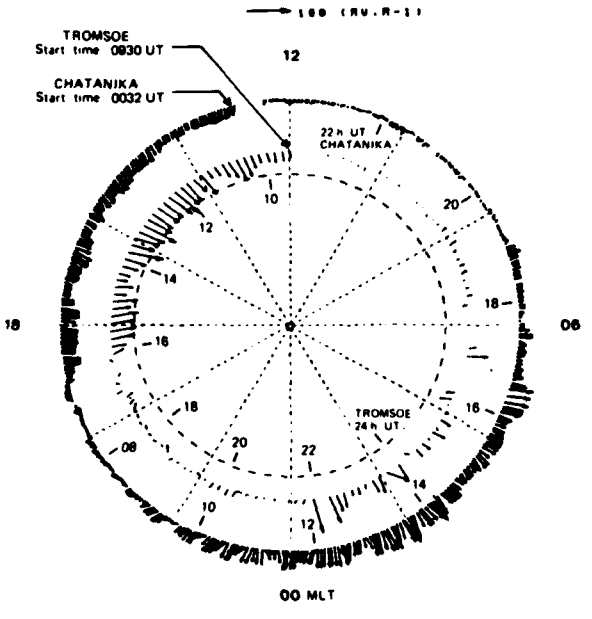


Fig. 7. Comparison of the electric field vectors obtained with the EISCAT radar and the Chatanika radar, versus magnetic local time. Inside each set of vectors, for the overlapping period, the universal time of the measurement is also indicated. The radial distance of the two sets of vectors has been taken arbitrarily. The Tromsö and Chatanika invariant latitudes are respectively 66.3° and 65.1°. [11]

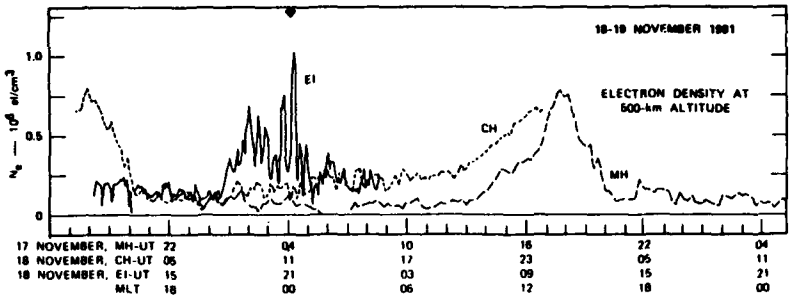


Fig. 8. Electron density at 500-km altitude measured from Millstone, Chatanika, and EISCAT as a function of MLT. The bottom scales indicate the corresponding UT at each site (17-19 November 1981). [12]

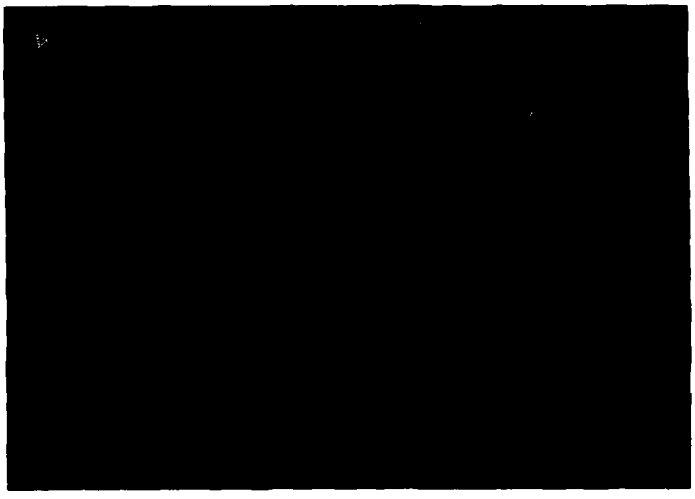


Fig. 9. 16-17 June 1982. Ion convection velocities at 325 km in a polar MLT/Invariant latitude coordinates. Inner and outer circles correspond respectively to 72.5 and 60° invariant latitude. [13]

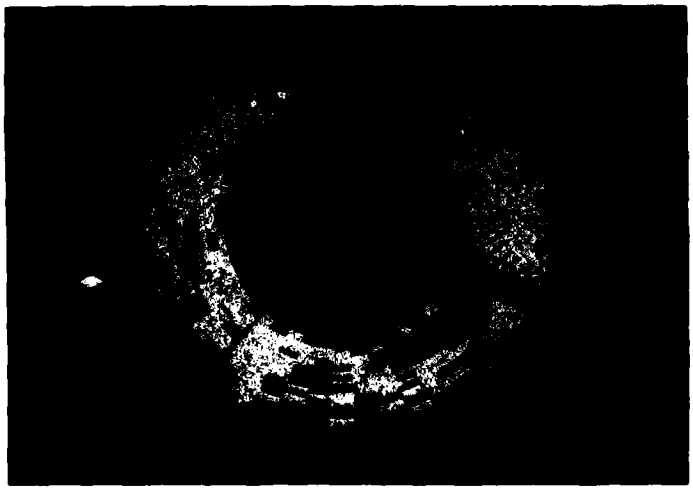


Fig. 10. 16-17 June 1982. Ion temperature at 325 km in a polar diagram in MLT/Invariant latitude coordinates. Inner and outer circles correspond respectively to 72.5° and 60° invariant latitude. [13]

II.4 Large scale ionosphere-magnetosphere interactions

The dynamical coupling of the auroral F region ionosphere and thermosphere has been investigated by Alcaydé et al. [13] and by Rees et al. [14].

Alcaydé et al. [13] for two summer days (June 2-3, 1982 and June 16-17, 1982) show that while strong convection drifts are observed in the afternoon and in the early morning (figure 9), the thermosphere responds to them very differently. Indeed in the early afternoon the drag exerted by the ionosphere on the thermosphere is quite efficient in moving the thermosphere. As a result no definite frictional heating of the ionosphere can be detected (figure 10). On the contrary during the early morning period a strong heating develops (figure 10) which is partly due to the reduction of the ion drag (due to the smaller nighttime electron concentration) as suggested by Baron and Wand [15] and partly due to the counter effect of the Coriolis force associated with the southern winds driven by the global thermosphere circulation. These features corroborate the observations of the McCormac and R. W. Smith [16] using optical interferometric techniques.

Direct comparisons of EISCAT plasma flow measurements and Fabry-Perot Interferometer observations have been made by Rees et al. [14]. Figure 11 exhibits the Fabry-Perot meridional wind compared with the EISCAT derived meridional wind. The agreement is globably satisfactory.

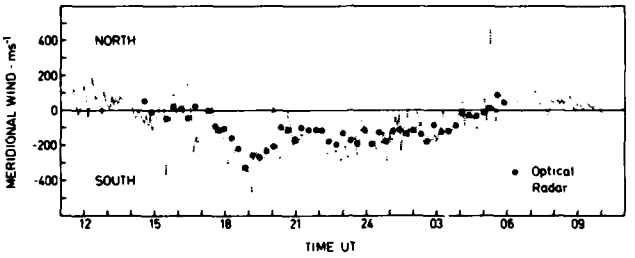


Fig. 11. Meridional thermospheric neutral wind as measured by EISCAT (lines) and the optical Fabry-Perot interferometer (dots) at Kiruna. [14]

III. MEDIUM SCALE STUDIES

III.1 Localisation of the footpoint of the GEOS 2 magnetic field line

Schlegel et al. [17] by combining GEOS 2 satellite high energy particle data and EISCAT E region electron concentration data have been able to clearly identify the footprint of the magnetic field line going through GEOS 2. Indeed the radar being used in a scanning mode in the north south vertical plane allows to locate regions of increased ionization in the E and F_1 layers resulting from particle precipitations observed on the GEOS spacecraft. The region of "apparent precipitation center" is according to the authors closely located to the foot of the GEOS field line.

III.2 Energy spectra of electrons precipitating above the EISCAT area

Perraut et al. [18]using data obtained on June 2, 1982 with the EISCAT radar pointed along the Tromsö magnetic field line, together with conjugate measurements of the ARCAD-3 satellite, have been able to infer electron energy spectra in the range 1 to 10 keV using a technique developed by Vondrak and Baron [19]. The technique consists in inverting vertical profiles of ionization so as to yield as a function of altitude the source of ionization due to particle precipitations; from this, assuming a model of lower thermosphere one can estimate the energy spectra of the precipitating electrons.

Figure 12 gives a comparison of the energy spectra measured on board ARCAD 3 and those determined at EISCAT around the time of conjugacy of EISCAT and ARCAD 3. The agreement is quite good in the range of few hundred eV up to few 10^4 eV.

The method thus qualified allows to differentiate auroral forms: diffuse aurora or intense localized structures.

III.3 Gravity wave observations have been reported by Bertin et al. [20] and Crowley et al. [21]. In the latter paper, use of an HF doppler radar together with EISCAT was also made. Cross spectral analysis of the data allows the vertical variation of the neutral temperature and horizontal wind in the thermosphere to be estimated.

IV. MICROSCOPIC SCALE

IV.1 Ion temperature anisotropies

The tristatic configuration of EISCAT allows to determine the plasma temperatures for different observing directions of the same volume. This particularity was used by Perraut et al. [22] and Perraut et al. [23] so as to investigate possible ion temperature asymmetries between magnetic field aligned ($T_{i//}$) and magnetic field perpendicular directions ($T_{i\perp}$). It was indeed found on November 1982 that for instances of very large convection drifts, the Tromsö temperature estimate (along the field line) was systematically smaller than the one of Kiruna (17° from the field line) itself smaller than the one of Sodankyla (27° from the field line) at an altitude of 312 km (figure 13). From it an anisotropy factor of about 1.5 ($T_{i\perp}/T_{i//}$) can be deduced for a 50 mV/m electric field strength. This demonstrates the anisotropy in ion velocity distributions, predicted theoretically by St-Maurice and Schunk [24], which develops when ions are simultaneously accelerated with respect to the neutrals by perpendicular electric fields and decelerated through collisions with the neutrals.

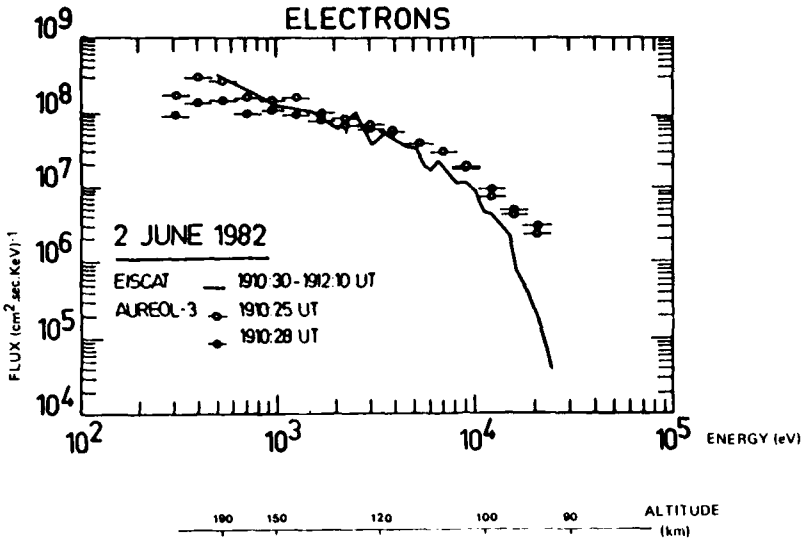


Fig. 12. Energy spectra of precipitated electrons measured by ARCAD 3 at two different time intervals (full and open circles) compared to the spectra computed from the electron density profile simultaneously measured by EISCAT. [18]

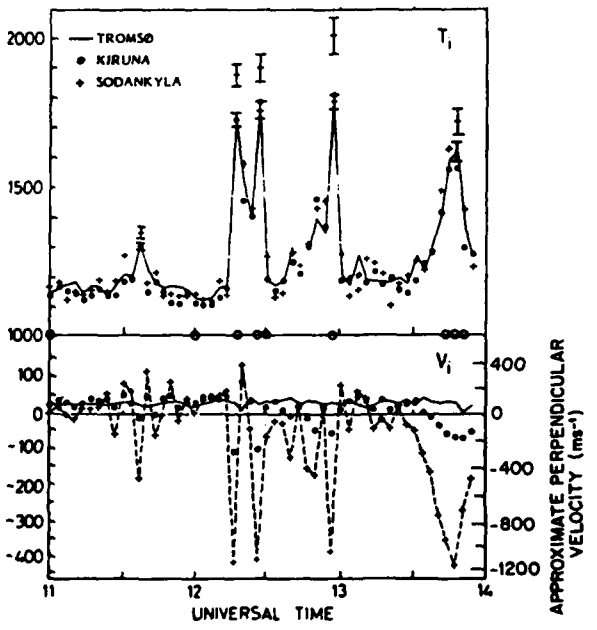


Fig. 13. Ion temperatures and ion velocities as measured at the three EISCAT sites. Note the temperature enhancements coincident with the velocity spikes. During these events the temperature measured at Sodankyla is higher than those measured at the other stations. [22]

IV.2 Extension of incoherent scatter observation to the D region

During the Cold Artic Mesopause Project (CAMP) EISCAT recorded the first D region ion line spectra (Kofman et al. [25]). In addition to temperature and neutral wind measurements the incoherent scatter spectra allow for a determination of the negative ion concentration. Indeed, as shown by Mattews [26] and Fukuyama and Kofman [27] the width of the incoherent scatter spectra ion the D region is very sensitive to the negative ion concentration to electron concentration ratio. This effect is illustrated in figure 14 which at 77 km exhibits rapid changes of the spectra widths over a 30 minutes interval. The larger widths correspond to large negative ion concentrations.

IV.3 F region heating during an intense aurora

Maehlum et al. [28] have reported F region electron heatings correlated to increases of the E region electron concentration. They suggest that the F region heating may be due to current driven instabilities generated during intense precipitation of auroral electrons.

IV.4 Artificial enhancement of plasma lines

The combination of the Max-Planck-Gesellschaft heating experiment installed in Tromsö and EISCAT has allowed (Hagfors et al. [29]) to observe heater enhanced plasma lines. While the spectra (figure 15) observed contain details which can qualitatively be explained, the striking feature is that after an initial overshoot the enhanced fluctuations disappear in contrast with previous observations made at Arecibo, with however a very different configuration of the beam with respect to the magnetic field.

IV.5 Ion composition measurements

Ion composition measurements have been obtained in the F region by Lathuillière et al. [30] who have shown how important they were for obtaining the correct temperature measurements around 200 km.

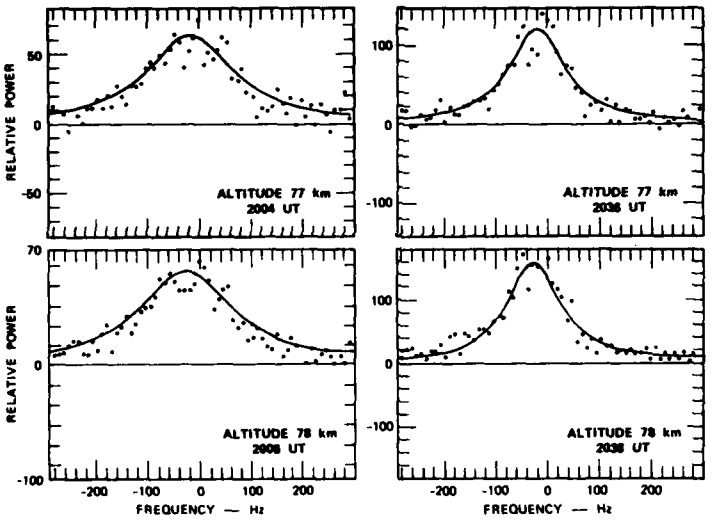


Fig. 14. Sample spectra measured in the monostatis mode with 2 min postintegration time. The altitude corresponds to the centre of the sampling range gate (Tromsö on 28.07.82). [25]

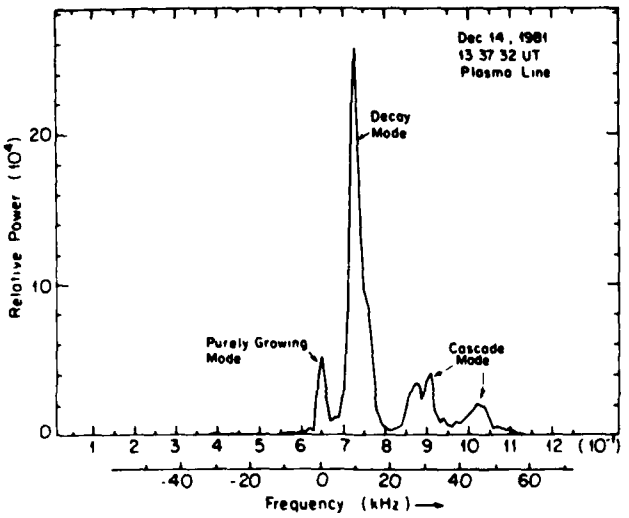


Fig. 15. Typical observed power spectrum encompassing the heater turn-on time, for the height gate containing the maximum signal. [29]

CONCLUSION

The EISCAT results reported here correspond essentially to an initial observing phase. While several original results have already been obtained, most of the matter presented here concerns either the intercomparison of data with other techniques or the trial of new observing schemes. Clearly, EISCAT appears as a remarkable tool which should, in conjunction with other ground based or space instruments, provide a definite quantitative understanding of the auroral processes at large, medium and microscopic scales.

ACKNOWLEDGEMENTS

The author acknowledges the efforts of the Director and staff of the European Incoherent Scatter Radar EISCAT, which is supported by the Suomen Akatemia (Finland), the Centre National de la Recherche Scientifique (France), the Max-Planck-Gesellschaft (West Germany), the Norges Almenvitenskaplige Forskningsråd (Norway), the Naturveterskapliga Forskningsrådet (Sweden) and the Science and Engineering Research Council (United Kingdom).

REFERENCES

1 M.J. Baron, The EISCAT facility, J. Atmos. Terr. Phys., 46, 469-472, 1984.
2 R.A. Greenwald, W. Weiss and E. Nielsen, STARE : A new radar auroral backscatter experiment in northern Scandinavia, Radio Science, 13, 1021-1039, 1978.
3 E. Nielsen and K. Schlegel, A first comparison of STARE and EISCAT electron drift velocity measurements, J. Geophys. Res., 88, 5745-5750, 1983.
4 A.D. Farmer, M. Lockwood, R.B. Horne, B.J.I. Bromage and K.S.C. Freeman, Field-perpendicular and field-aligned plasma flows observed by EISCAT during a prolonged period of northward IMF, J. Atmos. Terr. Phys., 46, 473-488, 1984.
5 M. Lockwood, A.D. Farmer, H.J. Opgenoorth and S.R. Crothers, EISCAT observations of plasma convection and the high-latitude, winter F-region during substorm activity, J. Atmos. Terr. Phys., 46, 489-499, 1984.
6 A.P. Van Eyken, H. Rishbeth, D.M. Willis and S.W.H. Cowley, Initial EISCAT observations of plasma convection at invariant latitudes 70°-77°, J. Atmos. Terr. Phys., 46, 635-641, 1984.
7 J.L. Horwitz, J.P. Doupnik and P.M. Banks, Chatanika radar observations of the latitudinal distributions of auroral zone electric fields, conductivities, and currents, J. Geophys. Res., 83, 1463-1481, 1978.
8 J.C. Foster, J.R. Doupnik and G.S. Stiles, Large scale patterns of auroral ionospheric convection observed with the Chatanika radar, J. Geophys. Res., 86, 11357-11371, 1981.
9 C.T. Russell and R.C. Elphic, ISEE observations of flux transfer events at the dayside magnetopause, Geophys. Res. Lett., 6, 33-36, 1979.
10 O. de la Beaujardière, V.B. Wickwar, M.J. Baron, J. Holt, R.M. Wand, W.L. Oliver, P. Bauer, M. Blanc, C. Senior, D. Alcaydé, G. Caudal, J. Foster, E. Nielsen and R. Heelis, MITHRAS : A brief description, Radio Sci., 19, 665-673, 1984.
11 G. Caudal, O. de la Beaujardière, D. Alcaydé, J. Holt and G. Lejeune, Simultaneous measurements of the electrodynamics parameters in the auroral ionosphere by the EISCAT, Chatanika and Millstone Hill radars, Annales Geophysicae, 2, 369-376, 1984.
12 O. de la Beaujardière, J.D. Craven, G. Caudal, J. Holt, L.A. Frank, V.B. Wickwar, L. Brace, D. Evans and J.D. Winningham, Universal time dependence of nightime F-region densities at high latitudes, Accepted for publication in J. Geophys. Res., 1985.
13 D. Alcaydé, P. Bauer and J. Fontanari, Dynamical coupling of the auroral F-region ionosphere and thermosphere : case studies, J. Atmos. Terr. Phys., 46, 625-633, 1984.
14 D. Rees, N. Lloyd, P.J. Charleton, M. Carlson, J. Murdin and I. Häggström, Comparison of plasma flow and thermospheric circulation over northern Scandinavia using EISCAT and a Fabry-Perot interferometer, J. Atmos. Terr. Phys., 46, 545-564, 1984.
15 M.J. Baron and R.H. Wand, F-region ion temperature enhancements resulting from Joule heating, J. Geophys. Res., 88, 4114-4118, 1983.
16 F.G. McCormac and R.W. Smith, The influence of the interplanetary magnetic field Y component on ion and neutral motions in the polar thermosphere, Geophys. Res. Lett., 11, 935-938, 1984.
17 K. Schlegel, G. Kremser and A. Korth, Data comparison of EISCAT and the energetic particle instrument on GEOS 2, J. Atmos. Terr. Phys., 46, 509-515, 1984.
18 S. Perraut, D. Fontaine, N. Cornilleau-Wehrlin, J.M. Bosqued, D. Alcaydé, R.A. Kovrazhkin, A. Korth, G. Kremser, W. Kofman, Energy spectra of electrons precipitating above the EISCAT area. Comparison with ARCAD measurements. Results of the ARCAD 3 project and of the recent programmes, in magnetospheric physics, CNES, CEPADUES Editions, 819-830, 1985.
19 R.R. Vondrak and M.J. Baron, Radar measurements of the latitudinal variation of auroral ionization, Radio Sci., 11, 939-946, 1976.
20 F. Bertin, W. Kofman and G. Lejeune, Observations of gravity waves in the auroral zone, Radio Sci., 18, 1059-1065, 1983.
21 G. Crowley, T.B. Jones, T.R. Robinson, N.M. Wade and O. Holt, Determination of the vertical neutral temperature and wind profiles using EISCAT and HF Doppler radar, J. Atmos. Terr. Phys., 46, 501-507, 1984.
22 S. Perraut, N. Bjorna, A. Brekke, M. Baron, W. Kofman, C. Lathuillière and G. Lejeune, Experimental evidence of non-isotropic temperature distributions of ions observed by EISCAT in the auroral F-region, Geophys. Res. Lett., 11, 519-522, 1984.
23 S. Perraut, A. Brekke, M. Baron and D. Hubert, EISCAT measurements of ion temperatures which indicate non-isotropic ion velocity distributions, J. Atmos. Terr. Phys., 46, 531-543, 1984.
24 J.P. St-Maurice and R.W. Schunk, Ion velocity distributions in the high-latitude ionosphere, Rev. Geophys. Space Phys., 17, 99-134, 1979.
25 W. Kofman, F. Bertin, J. Röttger, A. Cremieu and P.J.S. Williams, The EISCAT mesospheric measurements during the CAMP campaign, J. Atmos. Terr. Phys., 46, 565-575, 1984.
26 J.D. Mathews, The effect of negative ions on collision-dominated Thomson scattering, J. Geophys. Res., 83, 505-512, 1978.
27 K. Fukuyama and W. Kofman, Incoherent scattering of an electromagnetic wave in the mesosphere : A theoretical consideration, J. Geomag. Geoelectr., Kyoto 32, 67-81, 1980.
28 B.N. Maehlum, T. Hansen, A. Brekke, O. Holt and K. Folkestad, Preliminary results from a study of the F-region heating during an intense aurora observed by EISCAT, J. Atmos. Terr. Phys., 46, 619-623, 1984.
29 T. Hagfors, W. Korman, H. Kopka, P. Stubbe and T. Aijanen, Observations of enhanced plasma lines by EISCAT during heating experiments, Radio Sci., 18, 861-866, 1983.
30 C. Lathuillière, G. Lejeune and W. Kofman, Direct measurements of ion composition with EISCAT in the high latitude F_1 region, Radio Sci., 18, 887-893, 1983.

DISCUSSION

R.A.Greenwald, US

Recent results by Nielson and Schegel indicated that E-region irregularities heat the electrons causing an increase in the acoustic velocity. Thus, as the electric field increases and drives the irregularities more strongly, there are increases in the acoustic velocity and no true saturation of the irregularity Doppler velocity; albeit at a given E-field strength, there appears to be a saturation of measured irregularity Doppler velocity within a cone of angles about the drift direction. Nielson and Schegel obtained an empirical calibration curve for this effect and have been able to obtain good agreement with the EISCAT E-field and plasma drift measurement over a wide range of electric field values.

IRREGULAR STRUCTURES IN THE HIGH-LATITUDE F-REGION OBSERVED USING THE EISCAT INCOHERENT SCATTER RADAR

J.K. Hargreaves, C.J. Burns and S.C. Kirkwood*
Department of Environmental Science
University of Lancaster
Bailrigg, Lancaster LA1 4YQ
England

SUMMARY

An EISCAT experiment using beam scanning has been devised to investigate small structures in the F-region at high latitudes. The paper considers the magnitude of irregularities as observed in four runs between late 1982 and early 1984. For periodicities shorter than 2 mins. the standard deviation of the electron density as a percentage of the mean electron density increases with altitude and can be as large as 30% at altitudes above 600 km. The irregularities studied have periods between about 2 mins. and 30 sec., which corresponds to spatial periods in the range 15-60 km if the drift speed is 500 m/s.

1. INTRODUCTION

As an approach to studying irregular and relatively small-scale structures in the auroral F-region, a program has been developed to scan the beam of the EISCAT UHF radar over a small region of the ionosphere, the region being scanned several times in the course of a run lasting about 90 minutes. The experiment is sensitive to irregularities several kilometres across and more since the UHF beam covers some 3 km at range 300 km, and the radar sensitivity for typical electron densities in the F-region enables variations of a few percent in the electron density to be detected in a time less than 10 s near the F-region maximum. First analysis of the data (Hargreaves et al., In press) has shown that it is possible from the experiment to determine the presence of irregular structure to above 750 km in some cases, and to estimate its magnitude, to observe how the degree of irregularity varies from time to time during a run, to observe periodicities in the structure, and to estimate the velocities of individual field-aligned structures.

When possible, runs have been timed to coincide with other observational opportunities such as passes of the HILAT satellite which measures a wide variety of properties including electron density, temperature and plasma drift velocity (HILAT Science Team, 1983).

The data can be treated in various ways to study different properties of the ionospheric irregularities. The present paper discusses their magnitudes as observed in four runs between late 1982 and early 1984.

2. BEAM-SCANNING EXPERIMENT

The concept of the experiment is illustrated in Fig. 1. In its latest form all scans of the beam are referred to the local geomagnetic field direction; the beam describes a cross having arms 64 km long at 300 km range, oriented north, south, east and west. Since the local magnetic field is inclined 13.5 deg. to the vertical at the transmitter site (Ramfjord, 69.6 deg. N, 19.2 deg. E), the 64 km scan means that at its northern most extreme the beam is just short of the zenith. The beam steps along by 2 km at a time (at the 300 km level) and the returned signal is recorded for 4 s at each step. Another 4 s is allowed for the beam to move between steps, but data are taken continuously giving an effective beam speed of 250 m/s at 300 km range with no data gaps. The range resolution is 37.5 km and in the main experiment ranges from 184 km to at least 600 km are recorded. (E-region measurements at greater range resolution have been included in the more recent runs.)

The normal order of scans is

St, S-N, N-S, S-N, N-S, St, E-W, W-E, E-W, W-E, St,

giving 11 sections. A sweep from south to north, for example, takes 512 s, and stationary periods (St) where the beam is pointed along the magnetic field for 512 s are included in the sequence. One complete run takes about 90 min. For detailed studies each section would be delayed separately, but to assess the slower variations it is also useful to display the whole run since all data refer (at 300 km range) to points within 64 km of the field direction.

---

* Now at EISCAT Scientific Association, Tromsø, Norway.

Table 1 summarises the runs made to date and the state of data reduction.

3. SAMPLE RESULTS

Figure 2 illustrates typical observations in a convenient format. Electron density is plotted as ordinate and is placed on the diagram so that the mean value is at the level of the range mark. The abscissa shows time in seconds. Figure 2a is from a period with strong irregularities, whereas in Figure 2b the irregularities are much weaker. Since the beam was pointed along the geomagnetic field at these times it may be seen that the irregularities, as would be expected, are essentially field aligned.

There is plainly a considerable difference in irregularity intensity between these two examples although the observations are both from the same run. These examples also show a significant variation with range. The irregularity magnitude is obviously smaller at the lower altitudes; at the greatest ranges the measurements become increasingly noisy, though true irregularities are certainly present in the random noise.

4. IRREGULARITY MAGNITUDE AND ITS HEIGHT VARIATION

The runs of November 29-30 1982, December 5-6 1983 and February 10 1984 are comparable in that they were made in the late evening in winter using essentially the same observing program. A HILAT pass occurred during the run of December 1983.

Taking the standard deviation of the electron density as a percentage of the mean electron density during the scan gives values ranging between 3% and 62% at 184 km (the shortest range), and between 15% and 91% at 597 km. After filtering to remove periods greater than 2 min. the standard deviation ranges are 2-19% at 184 km and 12-66% at 597 km. Power spectra confirm visual impressions that the variations at lower altitudes represent real structures, whereas those at the highest levels are mainly random errors due to experiment noise. The spectra shown in Fig. 3a, which were derived from the electron density values of Fig. 2a, show marked periodicities of 152 s and 65 s which are each coherent over a range of heights. Such features are not seen at the greatest heights.

To compensate for the experiment noise, values of the variance during the quieter sections may be averaged and subtracted, height for height, from the variance during the more disturbed sections of the run. Assuming that the experiment noise did not change with the intensity of the irregularities this procedure enables us to quantify the height variation of the irregularity magnitude. (Should there have been some irregularities during the quiet periods - as there well may have been - the procedure gives a *least value* for the variance due to irregularities, and still measures the *change from quiet to disturbed conditions*).

The level of experiment noise depends on the parameters of the radar and on the electron density as a function of range. During the runs of 1982 November 29-30 the electron density profile (Fig. 4) changed relatively little and thus the experiment noise should have been almost constant throughout at any given range. There is no apparent association between the shape of the electron density profile and the intensity of irregularities. In Fig. 4, which shows the profiles during the 6 sections of the runs when the beam was stationary, irregularities were weak during sections 3 and 5, but strong during the other sections.

Fig. 5 shows the vertical structure of the irregularity magnitude as derived by the above procedure, the data having been filtered to remove periodicities longer than about 2 minutes. In absolute terms the standard deviation is largest in the topside ionosphere somewhat above the F-layer maximum. In relative terms, expressed as a percentage of the mean electron density, it increases indefinitely with altitude up to at least 750 km. In deriving these values the variance subtracted exceeded that remaining for heights above about 600 km.

A similar procedure has been applied to the run of 1983 December 5-6, and a similar result was obtained (Fig. 6a). The relative standard deviation varies from 4% at 184 km to 28% at 671 km. (For the reasons given above this will be an underestimate rather than an overestimate.) It is interesting that the shape of the F-region changed markedly during this run (Fig. 7a) but this change was not accompanied by any obvious change in the magnitude of the irregularities. The experiment noise increased at the greater heights as the electron concentration decayed, as would be expected; for this reason the last few sections, when the decay was most rapid, were not included in the analysis leading to Fig. 7a.

In the run of 1984 February 10 (Kp = 5) every section showed irregularities and there was no quiet period against which to compare. Subtracting the smallest variances, from wherever they occurred, from sections 1-4, which appeared to be most active, leads to the results of Fig. 6b. Again the electron density profile changed greatly towards the end of the run (Fig. 7b).

5. CHARACTERISTIC PERIODS AND SPATIAL WAVELENGTHS

The run of February 1984 proceeded without significant breaks, and these data are particularly suitable, therefore, for spectral analysis. Figure 8 shows the power spectral density as a function of range, taken over the whole run for the filtered data. The high-pass filter used (a simple moving-point average) transmitted half power at frequency 8.16×10^{-3} Hz, period 122.5 s; this frequency is marked on Fig. 8. It is seen that most of the power is in periodicities longer than about 30 s, and that the power measured at periodicities below 24 s is mainly noise. Although we have tried to emphasise the shorter periods in this study of the magnitude of the irregularities, there is considerably more power at longer periods.

Assuming that the observed time variations arise because of spatial structures drifting through the beam, a knowledge of the drift speed would enable us to convert the time spectrum to a spatial spectrum. The lower scale of Figure 8 shows the distance scale on the assumption of 500 m/s drift speed.

6. CONCLUSIONS

1. Field-aligned irregularities on scales exceeding a few kilometres can be detected by the EISCAT UHF radar to heights of around 700 km.

2. In four night-time, winter runs studied, the magnitude of the irregularities comes to a maximum at or somewhat above the F-region electron density peak; including only periodicities shorter than 2 minutes, their relative magnitude increases with height, being typically 5-10% of the mean electron density at heights near 200 km, and 15-30% near 650 km.

3. Although the irregularity intensity varies greatly over periods of tens of minutes, there is no apparent relationship between intensity of irregularities and shape of the mean electron density profile.

4. The irregularities quantified by this analysis are in a frequency band 8×10^{-3} to 4×10^{-2} Hz (periods 122 s to 25 s), the lower limit being set by the filter used. Irregularities are not observed above the higher limit. If a drift speed of 500 m/s is assumed this frequency band corresponds to spatial wavelengths of 15-60 km.

REFERENCES

HILAT Science Team
The HILAT Program - EOS 64, 163 (1983).

J.K. Hargreaves, C.J. Burns and S.C. Kirkwood
EISCAT studies of F-region irregularities using beam scanning. Radio Science(InPress)

ACKNOWLEDGEMENTS

The experiments were run at EISCAT during U.K. Campaigns and thanks are due to the EISCAT Group at the Rutherford Appleton Laboratory of the Science and Engineering Research Council for their support. The project has been funded by the Air Force Office of Scientific Research under grants 81-0049, 83-0054 and 83-0371.

Table 1

Summary of EISCAT runs of SP 103

Date	Time(UT)	Kp	Program	Comments
1981 Dec 17	1500-1700	2-	±50 km scans	System performing poorly. No irregularities seen. Analysed in detail and shown that variations no larger than system noise.
1982 June 3	1100-1300	2+, 2	±50 km scans	Daytime. No irregularities seen. No analysis planned.
1982 Nov 29-30	2115-0035 (2 runs)	5-, 4	±64 km scans	Irregularities present. Analysed for magnitudes, spectra and velocities
1983 Dec 5-6	2310-0050	4-, 3+	±64 km scans E region	HILAT pass at 2333 UT. Irregularities analysed for magnitudes and spectra.
1984 Feb 9	2100-2300	3-	Searching mode	Tapes at RAL, not yet accessed. Electron densities low.
1984 Feb 10	2100-2300	5	±64 km scans E region	Irregularities present. Analysed for magnitudes and spectra.
1984 Dec 15	0820-1100 (2 runs)	3/4*	"	Tapes at RAL, not yet accessed. HILAT pass at 0927 UT.
1984 Dec 15-16	2300-0150 (2 runs)	5/4*	"	Tapes at RAL, not yet accessed. HILAT pass at 0026 UT.

* Preliminary values

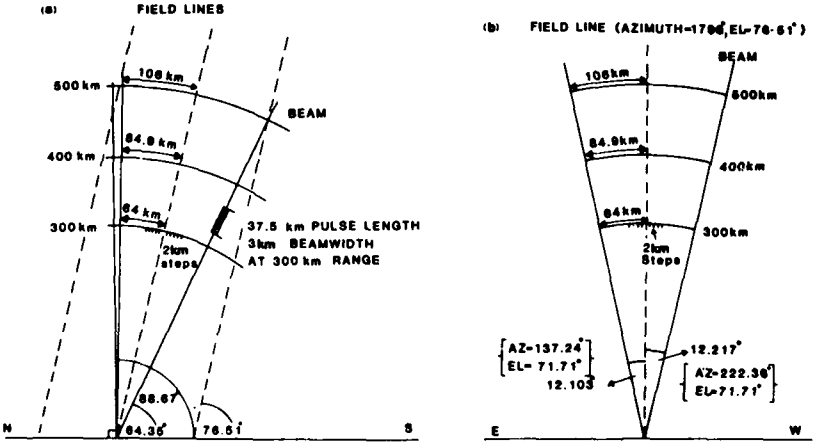


Fig. 1. Scans of the UHF radar beam. Each scan is made up of 64 steps and takes 512 seconds:
(a) Elevation (N-S) ; (b) Azimuth (E-W).

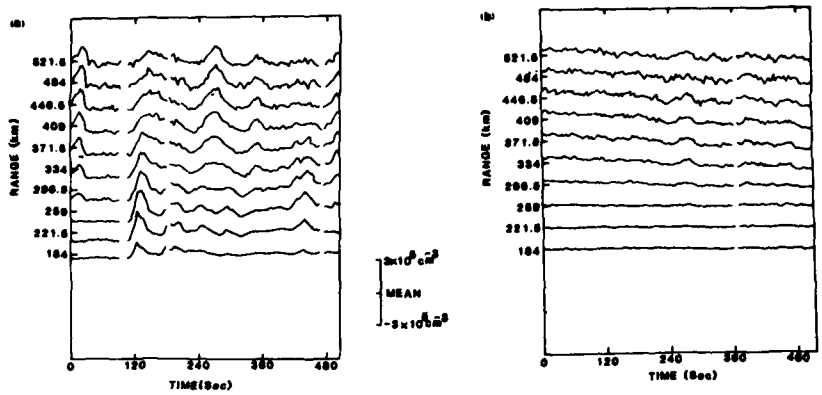


Fig. 2. Examples of electron density variations seen with the beam stationary, 1982 November 29:
(a) 2115-2123 UT, showing strong irregularities;
(b) 2242-2251 UT, showing weak irregularities.

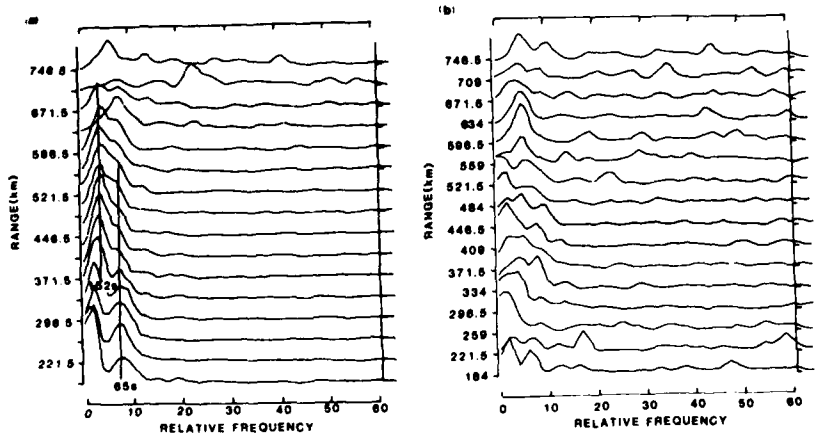


Fig. 3. Normalised power spectra for the observations shown in Figure 2, mean and linear trend having been removed:
(a) 2115-2123 UT, showing periodicities of 152 s and 65 s;
(b) 2242-2251 UT, showing mainly noise.
The frequency unit is 1.98 x 10^{-3} Hz.

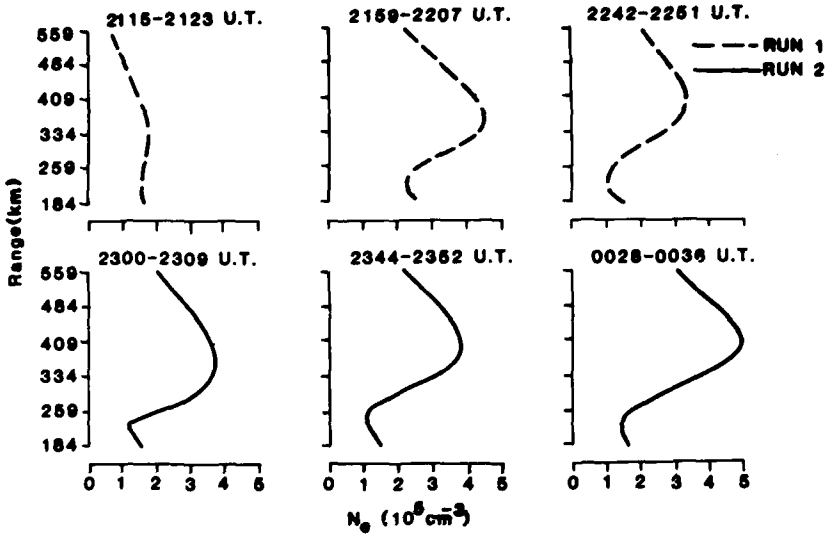


Fig. 4. Mean electron density profiles on 1982 November 29-30, stationary beam.

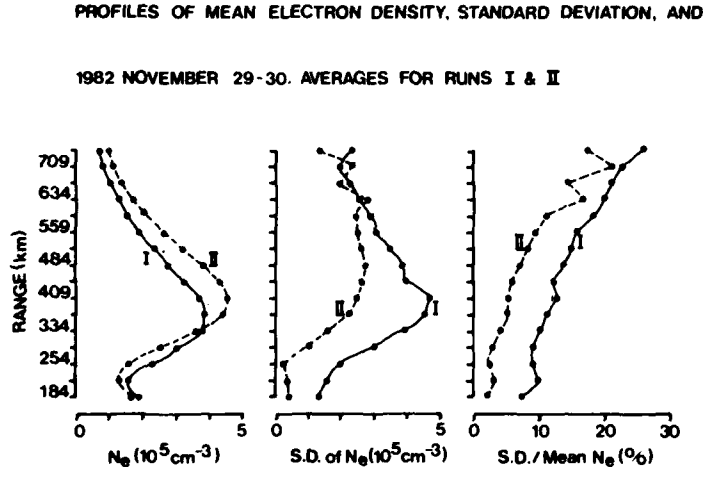


Fig. 5. Vertical structure of irregularity magnitude, 1982 November 29-30, after correction for experiment noise.

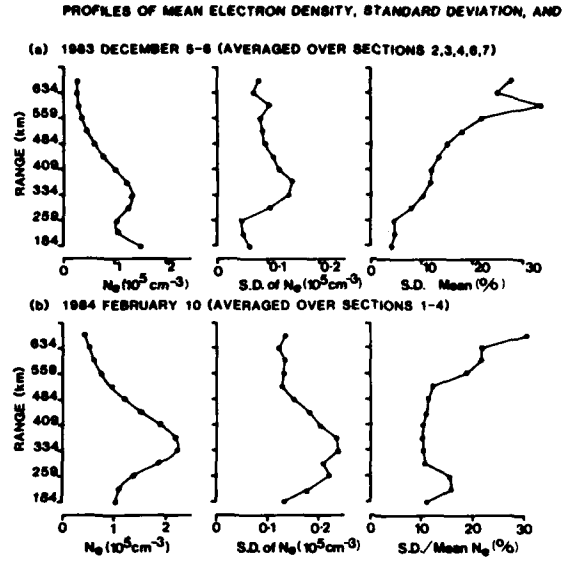


Fig. 6. Vertical structure of irregularity magnitude:
(a) 1983 December 5-6;
(b) 1984 February 10.

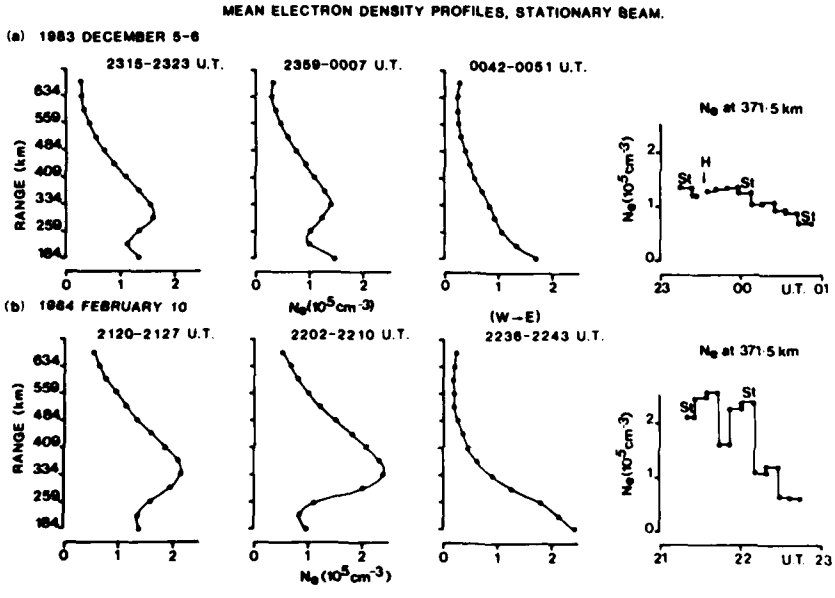


Fig. 7. Mean electron density profiles and variation of electron density at 371.5 km range:
(a) 1983 December 5-6;
(b) 1984 February 10.

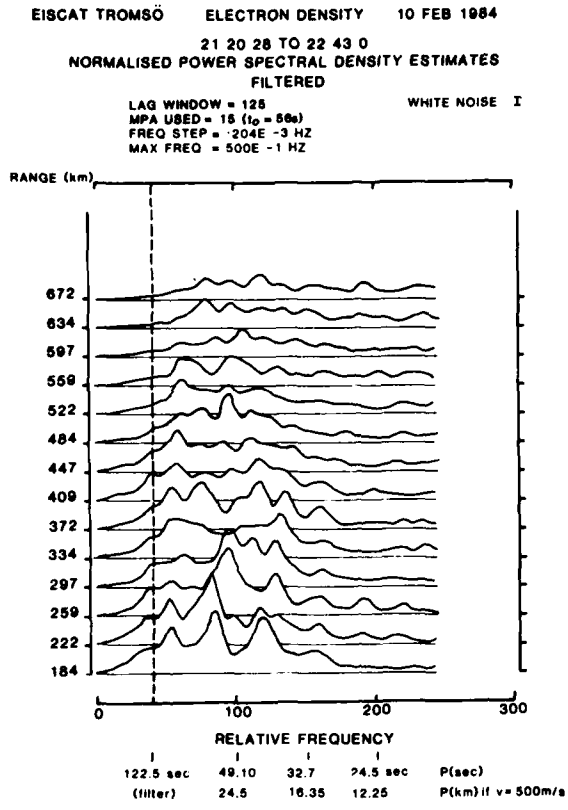


Fig. 8. Normalised power spectra over the whole of the run on 1984 February 10. The frequency unit is 2.04 x 10^{-4}Hz, and a high-pass filter (8.16 x 10^{-3}Hz) was applied.

DISCUSSION

A.Rodger, UK

Have you investigated the ion and electron temperature within the irregularities and compared these with corresponding temperatures of the ambient plasma?

Author's Reply

Lack of time has prevented this being investigated, but it would certainly be interesting to do so as something that might shed light on the origin and age of the irregularities observed.

OBSERVATIONS OF THE AURORAL IONOSPHERE USING EISCAT

W. KOFMAN, Ch. LATHUILLERE

LA346 - CEPHAG - B.P.46 - 38402 ST-MARTIN-d'HERES

ABSTRACT

In the auroral zone, in addition to solar energy input to the atmosphere, energy is deposited on occasion by particle precipitations and electric fields. These energy inputs often very large, modify the circulation and composition of neutral atmosphere and ionosphere. EISCAT facility gives the possibility to study the ionosphere and atmosphere in the auroral zone. We describe the auroral ionosphere during quiet and disturbed periods.

We show the behaviour of the ionospheric plasma : -increase of ionization, electron and ion temperatures, -change in the ion composition in response to electron precipitation and Joule heating. We calculate the total energy deposited locally in the E layer and the energy imput to ambient electrons in the F layer. We show that the precipitated electron flux is composed of both high and low energy electrons. Finally, we show the variation of the neutral density and temperature depending on the energy input.

INTRODUCTION

A basse et moyenne latitude la principale source d'énergie de la thermosphère est constituée par l'absorption des rayonnements EUV et UV solaires ; dans les régions aurorales l'énergie déposée par les particules énergétiques et par les champs électriques, sous forme de chauffage Joule, est souvent plus importante : quelques dizaines de mWm^{-2} (rappelons que $1mWm^{-2} = 1erg\ cm^{-2}s^{-1}$), bien que très variable dans l'espace et le temps comme le montrent les diverses observations effectuées par le radar de Chatanika (Vickrey et al 1982, Banks 1977, Wickwar et al 1975, Ponthieu 1982).

Ces études qui déduisent les taux de chauffage Joule et particulaire à partir des données de diffusion incohérente se basent sur des études théoriques qui d'une part calculent le transfert d'énergie entre ions et neutres en fonction des champs électriques et des conductivités ionosphériques (Rees et Walker 1968, Cole 1962, 1975), d'autre part estiment la fraction de l'énergie incidente des faisceaux d'électrons énergétiques qui est converti en énergie thermique : 50 à 60% (Rees 1975, Banks 1977, Singh et Gerard 1982, Rees et al 1983). Parallélement à l'évaluation des quantités d'énergies déposées dans l'atmosphère aurorale, un effort important est actuellement réalisé pour préciser qualitativement et surtout quantitativement les modifications de l'ionosphère et de l'atmosphère neutre associées à ces dépôts d'énergie. Des models numériques à 3 dimensions de l'ionosphère (Schunk et Raitt 1980, Sojka et al 1981 a b, Schunk et Sojka 1982) et de la thermosphère (Dickinson et al 1981, Fuller Rowell et D. Rees 1980) permettent d'évaluer de manière indépendante la réponse de l'ionosphère (région F) et de la thermosphère (altitudes supérieures à 120 km) aux apports d'énergie auroraux. L'effet du chauffage auroral sur la basse thermosphère (altitudes comprises entre 70 et 350 km) a été examiné très récemment par Roble et Kasting (1984) à l'aide d'un modèle à 2 dimensions.

Malheureusement ces modèles ne traitent pas encore de manière self consistante, le couplage entre ionosphère et atmosphère neutre et la comparaison avec les résultats expérimentaux reste difficile : voir par exemple l'article de Prölss (1980) qui synthétise les résultats obtenus par satéllite concernant les variations de l'atmosphère neutre et de l'ionosphère associées aux orages magnétiques, et les compare avec les différents modèles existants.

Dans notre étude, expérimentale et locale, nous montrons que la même technique de diffusion incohérente permet d'étudier les variations de l'ionosphère (densité électronique, mais aussi températures électronique et ionique) et les variations de la basse thermosphère (températures et densités neutres) associées aux apports d'énergie Joule et particulaire. Pour cela nous utilisons les données du Sondeur Européen Eiscat dont les techniques "single pulse" et "multipulse" sont tout d'abord décrites. Des exemples de dépôts d'énergie Joule et particulaire sont ensuite présentés puis des corrélations entre ces dépôts d'énergie et la composition ionique entre 150 et 350 km d'altitude d'une part, la température et la densité neutre entre 90 et 120 km d'altitude d'autre part sont alors discutées.

TECHNIQUE DE MESURES ET ANALYSES DES DONNEES

Les mesures que nous montrons utilisent en général les possibilités tristatiques d'EISCAT dans le but de déterminer le champ électrique en plus de tous les autres paramètres. L'antenne de Tromsö est dirigée parallélement au champ magnétique, les lobes des antennes de Kiruna et de Sodankyla découpent le lobe de l'antenne de Tromsö à 110 km et 312 km d'altitude. Le shéma d'impulsions est composé de deux ou trois modes différents (CP0 ou CP1). Le mode "multipulse" est construit à partir de 5 impulsions de 15 μsec ce qui correspond à 2.25 km de résolution en altitude. Les données de multipulse sont analysées avec un temps d'intégration de 2 à 4 min. Ce mode est utilisé dans la détermination de paramètres ionosphériques de la région E.

Les paramètres de la région F sont déterminés avec le mode "single pulse", qui donne une résolution en altitude de 54 km avec un pas de 27 km. Le mode "puissance" permet la mesure de la densité électronique de 90 à 350 km avec un pas de 1.5 km (résolution en altitude de 9 km). Les données sont normalement analysées avec le programme développé par G. Lejeune (1979) dans lequel on peut choisir différentes stratégies d'analyse. Les données du mode "multipulse" sont analysées au dessous de 108 km en recherchant la densité électronique (Ne), la température de plasma (température électronique (Te) = température ionique (T_i)), la fréquence de collisions ion-neutre (ν_{in}) et la vitesse des ions (V_i). Au dessus de 108 km les données sont traitées en déterminant N_e, T_e, T_i. Les mesures du mode "single pulse" sont analysées avec un nouveau modèle de composition (Kofman et Lathuillere 1985, Lathuillere et Brekke 1985) et on détermine N_e, T_e, T_i et V_i. Pour certaines données, en plus des paramètres courants nous déterminons les compositions ioniques (p) entre 130 et 350 km d'altitude. Cette analyse n'est pas toujours possible, elle dépend de la qualité des données.

VARIATIONS DE L'IONOSPHERE ET DE LA THERMOSPHERE

Nous avons discuté dans l'introduction les différents mécanismes responsables des dépôts d'énergie dans l'atmosphère aurorale ; champs électriques et précipitations de particules. Nous avons analysé ces processus et leur influence sur l'ionosphère sur des exemples choisis.

a) Chauffage Joule

La figure 1 montre les paramètres ionosphériques en fonction du temps, mesurés par les trois stations d'EISCAT à 312 km. La journée du 30 Novembre est magnétiquement non perturbée entre 1100 et 1400 TU. La densité électronique décroit lentement, ceci étant due au couché de soleil. Une brusque variation de la vitesse ionique mesurée à Sodankyla, qui est le plus sensible au mouvement Est-Ouest du plasma, est visible. Une augmentation brutale du champ électrique indiquée sur la figure par l'augmentation de la vitesse ionique au dessus de 100m/sec à Sodankyla (équivalent à 15 mV/m) est corrélée avec l'augmentation rapide de la température ionique. C'est le chauffage Joule qui est très efficace pendant cet événement. Les différences qui ont été observées dans la température ionique, vue par les trois stations sont expliquées par l'anisotropie de la distribution des ions (Perraut et al 1984). Pendant la période de la convection intensifiée, la température ionique a augmenté en moyenne de l'ordre de 600K.

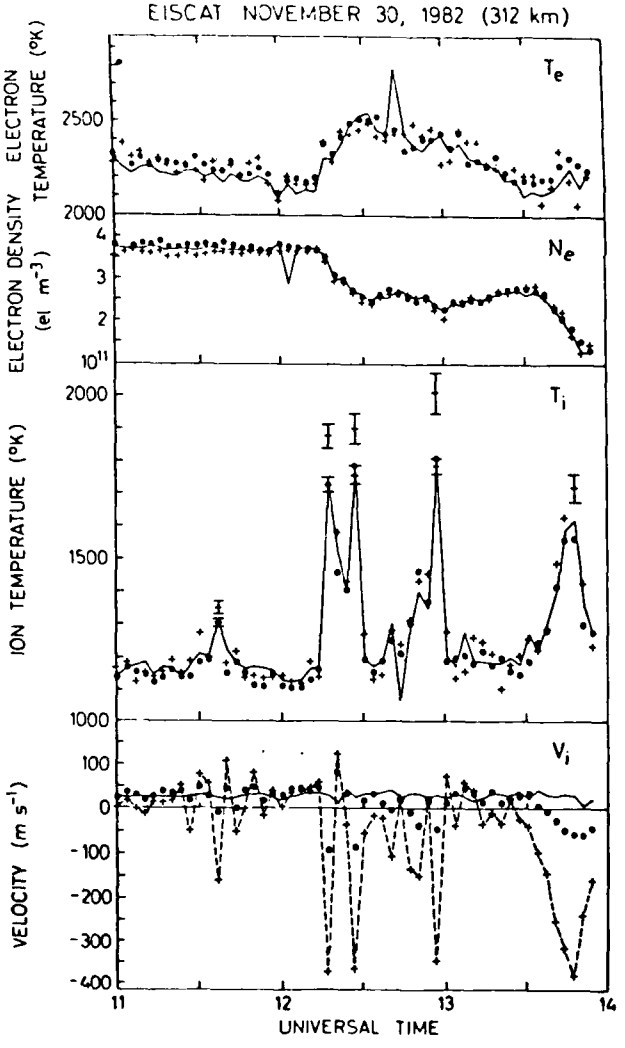


Figure 1 : N_e, T_e, T_i, v_i mesurés à Kiruna, Sodankyla et Tromsö le 30/11/1982. La vitesse perpendiculaire est approximativement égale à celle mesurée à Sodankyla.

Nous montrons les profils de N_e, T_e, T_i, p (figure 2) avant la période du chauffage Joule et pendant cette période. Les légères différences entre les paramètres montrées sur les figures 1 et 2 sont dues à l'analyse qui a été faite pour la figure 1 avec le modèle de composition alors que dans le cas de la figure 2 la composition a été déterminée simultanément avec les autres paramètres. Nous pouvons distinguer deux effets majeurs ; le changement de la composition ionique dans la région F et la diminution de la densité électronique corrélée avec l'augmentation de la température électronique. Le premier effet a été étudié par Kelly et Vickwar (1981) et Lathuillere et Brekke (1985).

L'augmentation de T_i a pour effet le changement du taux de la réaction chimique qui fait diminuer le pourcentage d'ions légers au dessus de 180 km. ($O^+ + N_2 \longrightarrow NO^+ + N \Rightarrow NO^+ + e \longrightarrow N + O$).
Cet effet est visible sur les deux profils de la composition ionique. La température électronique augmente de 500 K ceci étant due en partie au fait qu'à énergie d'entrée dans la haute ionosphère constante (énergie solaire) la diminution de N_e conduit à l'augmentation de T_e.

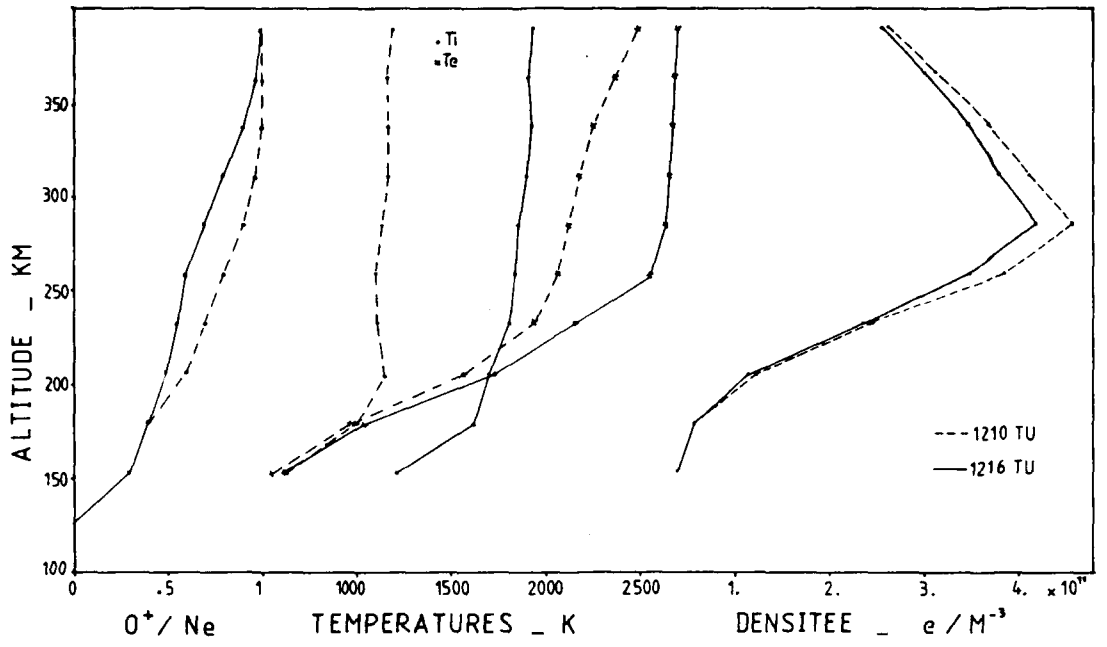


Figure 2 : N_e, T_e, T_i, p mesurés avant et pendant la période du chauffage Joule le 30 Novembre 1982

Cet effet donnerait une augmentation de 200 K. Pour expliquer l'augmentation de 500 K, nous pouvons penser à la présence de précipitations douces qui seraient en concurrence avec l'effet Joule, en ionisant et chauffant les électrons. En effet, Schunk et al (1975) montrent que pour un champ électrique de 50 mV/m (du même ordre de grandeur que dans notre exemple), on obtient une diminution de la densité électronique au maximum de la région F d'un facteur 2.8 c'est-à-dire une diminution beaucoup plus importante que celle que l'on observe.

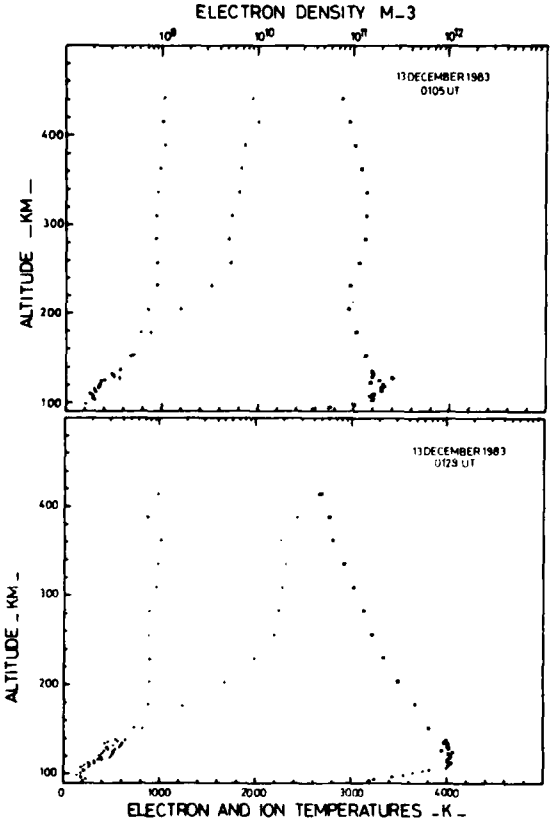


Figure 3 : N_e, T_e, T_i mesurés avant et pendant la période de précipitations le 12/12/83.

b) Chauffage particulaire

Les données du 12 Décembre 1983 montrent la réponse de l'atmosphère aux précipitations ayant un large spectre d'énergie. Les électrons précipités se thermalisent en déposant leur énergie dans l'ionosphère et l'atmosphère. Le résultat de cette action est l'augmentation de l'ionisation et le chauffage des électrons et des neutres. Sur la figure 3 nous montrons les profils des paramètres mesurés pendant deux périodes distinctes : la première période correspond à un flux précipité d'une très faible intensité, et la deuxième à une intensification des précipitations. Pendant la première période la température du plasma (T_e=T_i) est 200 K à 100 km et 600 K à 140 km. Les températures dans la région F sont 1000 K(T_i) et 1800 K(T_e) à 300 km. La densité électronique est faible, de l'ordre de 2.10^{11} el/m^3 aux maximums des régions E et F. A 0130 TU a lieu une injection de particules dans l'atmosphère. La densité électronique augmente d'une manière importante (5 à 10 fois) dans la basse ionosphère (jusqu'à 300 km). La température ionique reste pratiquement inchangée, ce qui indique l'absence d'effet Joule (champ électrique < 10 mV/m). Par contre l'augmentation de T_e est très importante (50 K à 120 km et 600 K à 300 km).

La figure 4 montre l'énergie cédée par les particules précipitées dans la région E. L'énergie qui a été déposée par ces particules atteint 50 mW/m^2 et l'énergie cédée aux électrons thermiques dans la région F atteint 6.10^{-2} mW/m^2 (Kofman et Wickwar 1984). Ce dépôt d'énergie représente une perturbation considérable de l'ionosphère et de l'atmosphère.

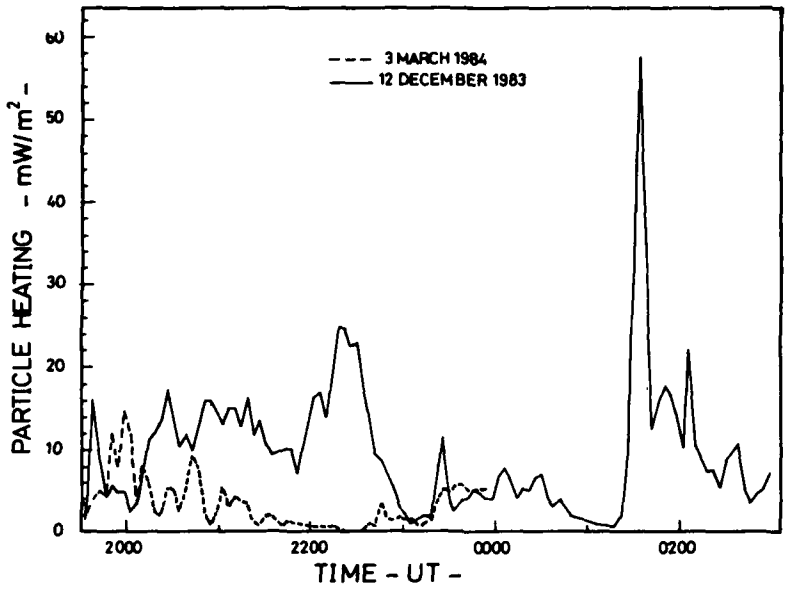


Figure 4 : Chauffage particulaire calculé par $\int \sigma_{en} Ne^2$ dh mesuré le 12/12/83 et le 3/03/84.

L'effet des précipitations d'électrons sur la composition dépend de leur énergie. Pour les électrons d'énergie moyenne grande ($>$ 400 eV), déposant leur énergie essentiellement dans la région E, l'effet consiste dans la diminution de O^+ pour les altitudes entre 140 et 300 km. Ceci signifie que l'altitude de la région de transition entre O^+ et NO^+ augmente. Ceci ressemble aux changements dus à l'effet Joule. Les raisons peuvent être multiples, mais nous pensons que le changement de l'atmosphère neutre dû au chauffage en est responsable. La figure 5 Montre une augmentation de l'altitude de transition par rapport au modèle pour le 12 Décembre 1983. Nous avons moyenné les résultats de mesures sur toute la nuit. L'énergie déposée par les électrons était très élevée pendant toute la nuit (figure 4) ce qui résulte dans le réchauffement de l'atmosphère neutre.

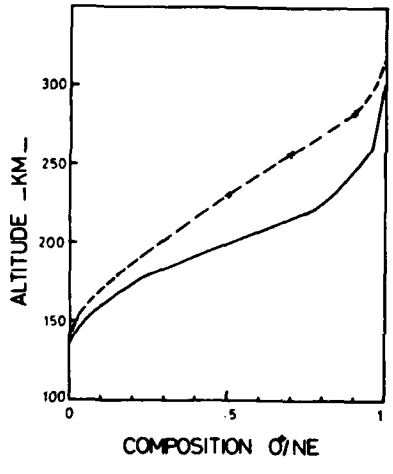


Figure 5 : Modèle de composition ionique utilisé normalement dans l'analyse (ligne continue) et les mesures du 12/12/83.

Sur la figure 6 nous montrons la variation de la région de transition pour une autre journée. On peut voir une bonne corrélation entre l'augmentation de la région de transition et le chauffage particulaire (Lathuillere et Brekke 1985).

Les particules d'énergie faible ($<$ 400 eV) se déposent essentiellement dans la région F. Leur influence sur la composition est directe car le temps de vie des ions O^+ créés est long dans cette région ce qui induit une augmentation du pourcentage de ces ions.

La figure 7 montre le pourcentage des ions O^+ en fonction du temps universel, comparé aux densités électroniques mesurées sur plusieurs altitudes le 9 Mai 1982. On peut voir une bonne corrélation entre l'augmentation de la densité et de l'abondance des ions O^+.

Le dernier effet des dépôts d'énergie que nous voulons montrer est le changement de la fréquence de collision ion-neutre. Sur la figure 4, nous montrons le chauffage particulaire du 12 Décembre 1983 et du 3 Mars 1984. On peut voir que la quantité d'énergie déposée pendant la nuit du mois de décembre est beaucoup plus importante qu'au mois de Mars.

Sur la figure 8, nous montrons la fréquence de collision ion-neutre (densité neutre) mesurée pendant ces deux nuits. On peut voir que la pente de la densité neutre du 12 Décembre est supérieure à celle du 3 Mars, ce qui est corrélé avec l'augmentation de la température neutre mesurée. Etant donné que l'ensoleillement au mois de Mars est plus important, on pourrait s'attendre à l'effet inverse. Ceci montre clairement l'influence du chauffage particulaire sur l'atmosphère neutre locale.

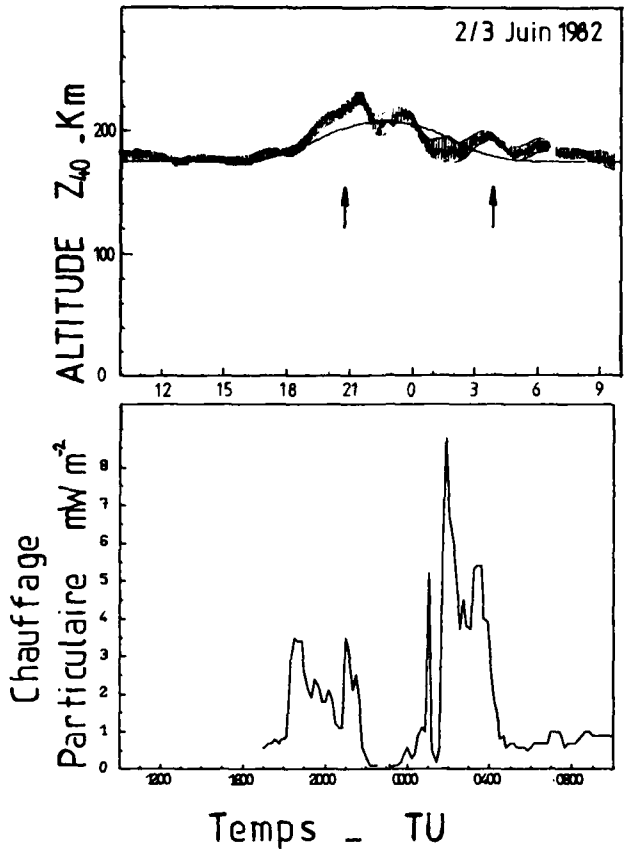


Figure 6 : Altitude de la transition entre 40% O^+ et 60% NO^+ (la surface hachurée représente l'erreur de mesure) comparée au chauffage particulaire le 2-3 Juin 1982.

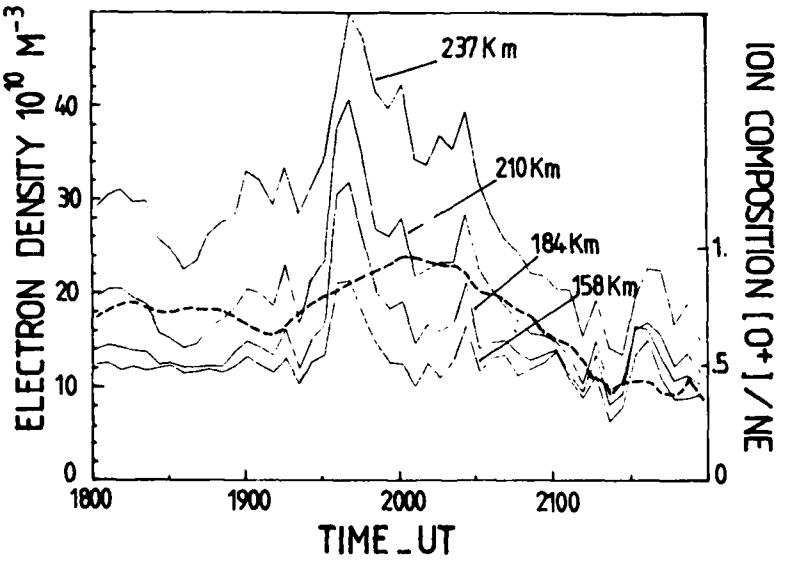


Figure 7 : La densité électronique à 158, 189, 210 et 237 km d'altitude comparée aux variations de la composition à 184 km d'altitude (ligne pointillée) le 9 Mai 1982.

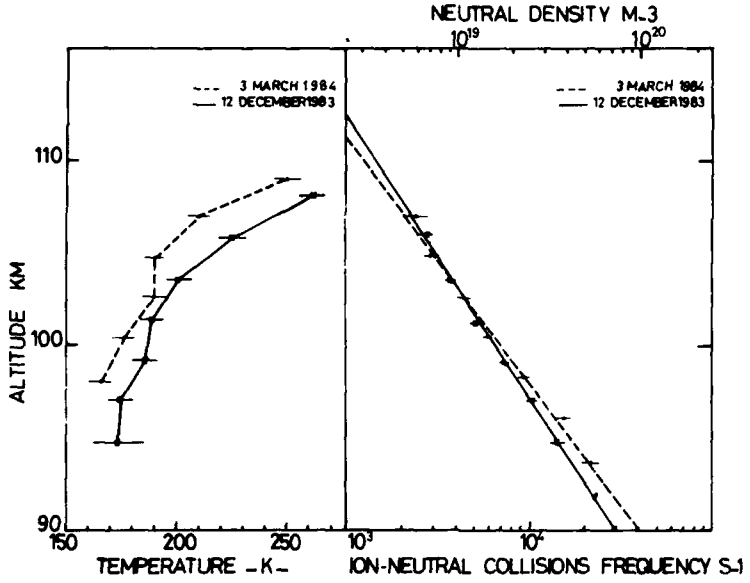


Figure 8 : La densité et la température des neutres mesurées le 12 Décembre 1983 et le 3 Mars 1984

CONCLUSION

Dans les exemples précédents nous avons montré les effets locaux des chauffages Joule et particulaire sur l'atmosphère neutre et ionisée ; les réactions sont en effet différentes selon la nature et l'altitude du dépôt d'énergie.

L'observation simultanée de l'ionosphère et de l'atmosphère neutre n'a été possible que dans le cas du 12 Décembre 1983 mais la généralisation des mesures "multipulse" dès fin 1983, devrait nous fournir d'autres occasions d'étude du couplage de la basse thermosphère et de l'ionosphère aurorale. Pour ces études, nous avons jusqu'à maintenant choisi de travailler avec un mode de fonctionnement où l'antenne de Tromsö reste fixe le long du champ magnétique terrestre, ceci pour deux raisons : -premièrement la difficulté de l'obtention des paramètres de composition p et de fréquences de collisions in, qui impose un temps d'intégration suffisamment long, -deuxièmement, la grande variation temporelle des dépôts d'énergie qui impose une bonne résolution temporelle. Pourtant il semble indispensable d'obtenir une description latitudinale des dépôts d'énergie si l'on veut faire une comparaison correcte avec les modèles numériques ; ceci sera possible avec une meilleure utilisation multifréquences du système UHF et simultanément l'utilisation du système VHF. De plus les mesures optiques permettant d'obtenir les températures et vents neutres en région E, et les mesures satellite de spectres d'électrons précipités, sont des compléments indispensables à une telle étude.

BIBLIOGRAPHIE

-BANKS P.M. : "Observations of Joule and particle heating in the auroral zone". Atmos. Terr. Phys., 39, 179-193, 1977.

-DICKINSON R.E., E.C. RIDLEY and R.G. ROBLE :"A three dimensional general circulation model of the thermosphere". J. Geophys. Res. 86, 1499, 1981.

-FULLER-ROWELL T.J. and D. REES : "A three dimensional time dependent global model of the thermosphere. J. Atmos. Sci., 37, 2545, 1980.

-COLE K.D. : "Joule Heating of the Upper atmosphere". Aust. J. Phys. 15, 223, 1962.

-COLE K.D. : "Energy deposition in the thermosphere caused by the solar wind". J. Atmos. Terr. Phys. 37, 939, 1975.

-KOFMAN W. and Ch. LATHUILLERE :"EISCAT Multipulse technique and its conbribution to auroral ionosphere ans thermosphere description". J. Geophys. Res., 1985 (sous presse).

-KOFMAN W. and V.B. WICKWAR :"Very High ELectron Temperatures in the Daytime F region at Sondrestrom". Geophys. Res. Lett. 11, 919-922, 1984.

-KELLY J. and V.B. WICKWAR :"Radar measurements of high-latitude ion composition between 140 and 300 km altitude". J.Geophys. Res. 86, 7617-7626, 1981.

-LATHUILLERE Ch. and A. BREKKE : "Ion compositions in the auroral ionosphere as observed by EISCAT". Ann. Geophys. 1985 (sous presse).

-LEJEUNE G. :"A program library for incoherent scatter calculation". Tech. Note 79/18, EISCAT 1979."

-PERRAUT S., N. BJORNA, A. BREKKE, M. BARON, W. KOFMAN, C. LATHUILLERE, G. LEJEUNE :" Experimented evidence of non-isotropic temperature distributions of ions observed by EISCAT in the auroral F-region". Geophys. Res. Lett, 11, 519-522, 1984.

-PONTHIEU J.J. :"Les sources d'énergie de la thermosphere en région aurorale : une étude par diffusion incohérente". Thèse Paris VI. 1981.

-PROLSS G.W. :"Magnetic storm associated perturbations of the upper atmosphere : Recent results obtained by satellite-borne Gas Analyzers". Rev. Geophys. Space Phys. 18, 183-202, 1980.

-REES M.H. :"Magnetospheric substorm energy dissipation in the atmosphere". Planet. Space Sci. 23, 1585, 1975.

-REES M.H. AND J.C.G. WALKER :"Ion and electron heating by auroral electric fields". Ann. Geophys. 24, 193, 1968.

-REES M.H., B.A. EMERY, R.G. ROBLE and K. STAMNES :"Neutral and ion gas heating by auroral electrons precipitations". J. Geophys. Res. 88, 6289, 1983.

-ROBLE R.G. and J.F. KASTING :"The Zonally Averaged Circulation, temperature and compositional structure of the lower thermosphere and variations with geomagnetic activity". J. Geophys. Res. 89, 1711-1724, 1984.

-SCHUNK R.W. and W.J. RAITT : "Atomic nitrogen and oxygen ions in the daytime high-latitude F-region". J. Geophys. Res. 85, 1255-1272, 1980.

-SCHUNK R.W. and J.J. SOJKA : "Ion temperature variations in the daytime high-latitude F-region". J. Geophys. Res. 87, A7, 5119, 1982.

-SCHUNK R.W., W.J. RAITT and P.M. BANKS :"Effect of electric fields on the daytime high-latitude E and F regions". J. Geophys. Res. 80, 3121-3130, 1975.

-SINGH V. and J.G. GERARD :"The thermospheric heating efficiency under electron precipitation conditions". Planet. Space Sci. 30, 1083-1089, 1982.

-SOJKA J.J., W.J. RAITT and R.W. SCHUNK :"A Theoritical Study of the high-Latitude winter F region at solar minimum for low magnetic activity". J. Geophys. Res. 86, 609-621, 1981 a.

-SOJKA J.J., W.J. RAITT and R.W. SCHUNK :"Theoretical predictions for ion composition in the high-latitude winter F-region for solar minimum and low magnetic activity". J. Geophys. Res. 88, 2206-2216, 1981 b.

-VICKREY J.F, R. VONDRAK, S.J. MATTHEWS :"Energy deposition by precipitating particles and Joule dissipation in the auroral ionosphere". J. Geophys. Res. 87, 5184-5196, 1982.

-WICKWAR V.B, M.J. BARON, R.D. SEARS :"Auroral energy input from energetic electrons and Joule heating at Chatanika". J. Geophys. Res. 80, 4364-4367, 1975.

DISCUSSION

N.C.Gerson, US

It should be recognized that large depositions of energy into the 80—150 km altitude region occur by (A) Joule heating and (B) particle injection. This energy input ultimately is transferred to the neutral atmosphere which is then heated. Heating then causes (A) thermal winds and (B) atmospheric expansion. In essence the energy deposited regenerates into the kinetic energy of motion. The winds in this altitude region must, of course, be subject to Coriolis and other forces. (At higher altitudes the magnetic field ($V \times B$) forces become more dominant.) The atmospheric expansion would produce a decrease in electron density. Have these horizontal winds, arising from Joule heating and particle injection been observed?

Author's Reply

In this experiment we measure ion velocity along field lines at 300 km; we do not measure neutral velocity. We probably do have strong winds.

E.V.Thrane, NO

You have shown changes in the neutral temperature due to auroral disturbances. Have you considered the possibility of detecting waves in the neutral air due to strong heating by particles and currents?

Author's Reply

Not for the data which I showed here, but I think that it is possible to do.

SABRE RADAR OBSERVATIONS IN THE AURORAL IONOSPHERE

T B Jones, J A Waldock, E C Thomas, C P Stewart and T R Robinson

Department of Physics
Leicester University, University Road, Leicester, LE1 7RH

Abstract

SABRE (Sweden And Britain Radar aurora Experiment) has been in full operation since March 1982 and over 15000 hours of single station backscatter amplitude data and 1500 hours of two-station electric field data have now been collected. These data have been used to investigate both geophysical phenomena of the high latitude ionosphere and the plasma physics of the metre scale scattering irregularities. The former include geomagnetic micropulsations, plasma convection, strong shear flows associated with the convection reversals and possible measurements of the polar cap flows during disturbed conditions. The latter include the statistics of occurrence of the plasma irregularities responsible for the backscatter and investigation of the dependence of the backscatter amplitude on the angle between the radar wave vector and the magnetic field (aspect angle). The strongest backscatter is invariably associated with the main electrojets between 13-19 and 23-03 UT, and only weak backscatter is found near the convection reversals. The aspect angle attenuation rate can take any value between 0 and 10 dB per degree depending on the absolute intensity measured. Average convection patterns are presented which reveal a well-defined 2 cell structure under all geomagnetic conditions. As magnetic activity increases however, the evening discontinuity moves towards earlier local times, the flow speed increases and the morning convection cell expands relative to the evening cell.

The position and intensity of the backscattering irregularities is important in assessing the performance of communications and surveillance systems operating in both the HF and VHF frequency bands at these latitudes.

1 INTRODUCTION

Auroral backscatter of VHF and UHF radio waves, or radar aurora, is produced by non-thermal electron density irregularities which can be generated in the auroral ionospheric E-layer by the two-stream (e.g. Farley, 1963) and the gradient-drift (e.g. Rogister and d'Angelo, 1970) plasma instabilities. If the relative electron-ion drift velocity is less than the ion acoustic speed, only the gradient drift mechanism can drive the plasma into an unstable state, however if the relative electron-ion velocity is greater than the ion acoustic speed the plasma is also unstable to the two-stream process (e.g. Fejer and Kelley, 1980). In either case, linear theory predicts that in the ion rest frame the most unstable irregularities will propagate with a velocity approximately equal to that of the electrons. Once these primary irregularities are produced, nonlinear processes will result in secondary waves propagating in all directions in the plane perpendicular to the magnetic field (Sudan et al., 1973), convecting with the velocity of the primary irregularities (Greenwald and Ecklund, 1975).

The current generation of bi-static auroral radars include the Scandinavian Twin-Auroral Radar Experiment (STARE, Greenwald et al., 1978), the Sweden And Britain Radar aurora Experiment (SABRE, Nielsen et al., 1983) and the Bistatic Auroral Radar System (BARS, McNamara et al., 1983). These radar systems are capable of measuring the backscatter intensity and Doppler velocity of E-region plasma irregularities from two directions over a large area, with high spatial and temporal resolution. The SABRE system came into operation during 1981 although full bi-static operation was not achieved until April 1982. The location and field of view of the SABRE system are illustrated in Figure 1. The two radars are located at Wick in Scotland and at Uppsala in Sweden, and are operated by Leicester University, UK, and by the Max-Planck Institut fur Aeronomie, Lindau, FRG, respectively. The common viewing area extends from approximately 0 to 10° E, and from 64° to 68° N geographic, a total area of approximately 400,000 km^2.

Each radar employs a relatively broad beam transmitting antenna and a narrow beam receiving antenna. A 50 kW peak pulsed power transmitter feeds the transmitting antenna, which comprises two vertical stacks of four eight-element Yagi antennas resulting in a forward gain of 23 dB giving an ERP in excess of 1 MW. The 25° half power beamwidth of the antenna 'illuminates' the whole of the observing volume. The receiving array consists of 64 eight element Yagi antennas arranged in 16 vertical stacks, and has a gain of 28 dB and collecting area of 360 m^2. Signals from the antennas on each vertical stack are combined and amplified by a low-noise pre-amplifier, with 30 dB gain, located on the mast supporting the stack.

The output of the pre-amplifiers is connected to a 16 port Butler matrix, which is a passive phasing network providing the necessary combinations of phase shifts to form 16 antenna lobes in the horizontal plane. Each lobe has a half power beamwidth of 3.2° and the lobe separation is 3.6°. This arrangement allows the radar to look in 16 different directions simultaneously although since the outer beams suffer from poor sidelobe isolation only the eight central beams are employed. The backscatter power and Doppler

velocity are measured at 50 ranges within each of these eight beams simultaneously, every 20 seconds. The data are stored on magnetic tape, and in the case of the Wick system, are automatically transmitted to Leicester overnight via a telephone link. Further technical details of the radar system may be found in Greenwald et al., 1978.

In this study, we report results of a statistical analysis of approximately 15000 hours of backscatter data from the radar at Wick. We also report results of a statistical study of the plasma convection pattern in the auroral E-region, using approximately 1500 hours of two station measurements. An example of shear flows possibly associated with the polar cap boundary are also presented.

2 AURORAL BACKSCATTER

Several factors govern the amplitude of the auroral backscatter and their relative importance has been the subject of some considerable investigation (e.g. Haldoupis et al., 1982; Uspensky et al., 1983; Starkov et al., 1983; Haldoupis and Nielsen, 1984). Comparisons of radar backscatter and ground magnetometer measurements indicate that to within the spatial resolution of the data, radar auroral irregularities are co-located with the auroral electrojet currents (e.g. Greenwald et al, 1975). It appeared that from a knowledge of the amplitude and mean Doppler shift of backscatter from the auroral irregularities, the location, direction and intensity of these currents could be determined. Recent studies, however, indicate that many factors are involved in determining the characteristics of the radar returns. For backscatter in a plane perpendicular to the magnetic field, the received power is given by the radar equation (Farley et al., 1981)

$$P_r = g_r(P_t n_t n_r \sigma c \tau \lambda_r G_r G_t)/(4(4\pi)^3 R^3)$$

where $P_r(P_t)$ is the received (transmitted) power, n is the loss in the antennas and transmission lines, G is the antenna gain, g is the receiver gain, c is the speed of light, τ is the pulse length, λ_r is the radar wavelength, R is the slant range and σ is the absolute radar cross section. Most of the terms in this equation are constant for a given radar; those that vary, such as the receiver gain and the range, are automatically corrected for in the radar software. The residual variations present in the signal strength are therefore due to variations in the backscatter cross section, given by

$$\sigma \sim N^2 <(\Delta N/N)^2> F(\phi,\theta)$$

where N is the mean electron density in the scattering region, $<(\Delta N/N)^2>$ is the mean square of the (small scale) relative electron density fluctuations with wavevectors $2\underline{k}$, where $\underline{k}$ is the radar wave vector and $F(\phi,\theta)$ is a function of the radar aspect angle ϕ and the flow angle θ. Since the auroral irregularities are field-aligned, radar backscatter maximizes when ϕ, the angle between the radar propagation vector and the magnetic field (i.e. the aspect angle), is 90°. As the aspect angle deviates from the orthogonal position, attenuations of between 2 and 10 dB/degree, with an average value of approximately 7.5 dB/degree, have been reported (Leadabrand et al., 1967; McDiarmid, 1972; Ecklund et al., 1975; Uspensky et al., 1983). Experimental evidence (e.g. McDiarmid, 1972; Koehler et al., 1985) indicates that 50 MHz radars are less subject to aspect sensitivity than those operating at higher frequencies, such as SABRE and STARE (~140 MHz). This is possibly because the plasma cross section is several orders of magnitude greater at the lower frequencies. The backscatter intensity also depends on the flow angle θ between the radar propagation vector and the electron drift direction (e.g. Andre, 1983). Little variation of amplitude with flow angle is observed for low electron drift speeds, in accordance with theoretical predictions for gradient-drift driven waves, but for flow speeds greater than the ion acoustic speed stronger backscatter is observed when the electron flow is parallel (or anti-parallel) to the radar wave vector.

3 THE SABRE DATA SET

A standard data block for one radar station consists of intensity and Doppler velocity data from each of 400 locations (8 beams, 50 ranges). At 1600 bpi, approximately 3 days of data can then be stored on a 2400-foot tape. For the purposes of statistical analysis two forms of average have been employed. The first retains only data within a 'strip' 3 degrees wide in longitude, spanning the complete latitude range in 29 steps of 0.2 degrees, and averaging over 15 minutes in time. The second retains data averaged over a central 'cell' approximately 100 km x 100 km in dimension, with an integration time of 1 minute. By this means it is possible to store a summary of the whole data set on a fraction of one magnetic tape. This procedure has been followed for both SABRE radars and the resultant tapes have then been 'merged' to provide a convenient summary of the derived convection velocities. These statistics tapes have, in addition, provided an invaluable 'quick-look' facility, enabling the data available for a given interval to be displayed in a matter of a few minutes.

4 BACKSCATTER STATISTICS

The relative frequency (in percent) of backscatter with a S/N ratio greater than 3 dB as a function of local time is illustrated in Figures 2 and 3, for different levels of magnetic activity (Kp indices from Solar Geophysical Data, NOAA, Boulder). A strong

diurnal variation exists, with backscatter occurring predominantly during the local times when strong electrojet currents are usually present in the auroral E-region. As magnetic activity increases the frequency of occurrence of backscatter increases, but during the local time of the morning reversal this only becomes significant under the most active conditions.

These results are summarized in Figure 4 where the average backscatter signal intensity is plotted as a function of Kp. The lower panel indicates the number of 15 minute data blocks available for each Kp value. There is an obvious trend towards higher intensities at higher levels of magnetic activity, even though there are far fewer points for high Kp. There is an apparent threshold for production of 1m irregularities at around Kp=2-. There is no evidence for a saturation effect at high values of Kp; the rate of increase of backscatter intensity with Kp is approximately constant above Kp=2.

Contours of backscatter intensity as a function of geomagnetic latitude and local time, averaged over all conditions, are illustrated in Figure 5. Strongest backscatter occurs between 13:00-19:00 UT and 22.00-04:00 UT, with a peak at around 16:00 UT. Virtually no backscatter is observed during the morning sector, when the average position of the auroral oval is furthest from the SABRE field of view. The morning convection reversal, or cusp, is normally located at invariant latitudes of between 72-75° (e.g. Meng, 1983) and only penetrates equatorwards to the latitudes observed by the SABRE under the most active conditions. A significant reduction in the mean backscatter amplitude is also observed within the Harang discontinuity.

Since the centre of the auroral electrojet current system is usually situated polewards of the SABRE viewing area, an attenuation of the mean backscatter intensity with decreasing latitude would be expected. This is certainly the case equatorwards of approximately 65°N, however, an attenuation is also evident polewards of this latitude. The data are pre-corrected for range and instrumental effects, therefore this phenomenon must be caused by either aspect angle or flow angle variations.

To highlight the aspect angle dependence of the backscatter amplitudes, the data can be corrected for flow angle variations in the following way. For each local time/latitude interval of Figure 5, the corresponding flow velocity was obtained from the mean flow statistics (e.g. Figure 10) and the flow angle θ calculated. Linear theory predicts that within a 'cone' of aperture Ψ relative to the electron drift direction, where

$$\Psi = \cos^{-1}(C_s/|V_e|),$$

the plasma is unstable to the two-stream instability. For flow angles $\theta < \Psi$ the backscatter intensity is attenuated at a rate of between 0.3 and 0.6 dB per degree away from the direction of the electron drift (Haldoupis and Nielsen, 1984). Accordingly, a figure of 0.45 dB per degree has been used in the present analysis. For flow angles $\theta > \Psi$, and for all flow angles when $|V_e| < C_s$, it is assumed that to a first approximation no variation of backscatter intensity with θ exists. This is consistent with theoretical predictions for waves produced by the gradient drift mechanism (e.g. Andre, 1983). The three possible cases to be dealt with are illustrated schematically in Figure 6. By using the above scheme, together with a value of 350 ms^{-1} for the ion-acoustic speed C_s, the data presented in Figure 5 have been corrected for flow angle dependence and any residual variations are purely due to aspect angle losses.

Figure 7 illustrates the deviation of the aspect angle from 90° for Wick, calculated from the IGRF 1980 field model, for the geographic locations used in the statistical analysis. Within the longitude interval chosen, the aspect angle varies between 0.25 and 1.75 degrees, although elsewhere within the viewing area of the Wick radar, it reaches over 4 degrees. It should be emphasised, therefore, that the results to follow refer to a limited range of aspect angles near perfect perpendicularity.

It is immediately evident from Figure 5 that the backscatter amplitude exhibits a maximum at 65°N, where the radar wave vector is most nearly perpendicular to the magnetic field (Figure 7). In an attempt to estimate the mean aspect angle attenuation observed by SABRE, the data in Figures 5 and 7 were combined as follows. For each 15 minute latitudinal strip of average intensities used in Figure 5 the backscatter amplitude was plotted against aspect angle. The relationship between these quantities was in each case almost linear, and could therefore be accurately represented by a least-square straight line, the gradient of which provides an estimate of the aspect angle loss in dB per degree. The result of this procedure has been plotted in Figure 8, illustrating the aspect angle loss as a function of local time.

A feature of Figure 8 is the variation of the apparent attenuation with time. For a radar at 50 MHz, results of a similar anlysis by Koehler et al. (1985) exhibit a much smaller variation, although the data cover a shorter period (30 hours distributed over approximately three weeks). For the present data set, comparison with Figure 5 suggests that the measured aspect angle loss is strongly dependent on the peak backscattered intensity at that time. This may be expected, since when the backscatter amplitude is low throughout the whole latitude range, such as during the morning hours, it would be impossible to measure a large aspect angle loss. During the afternoon sector, however, the intensities are much larger and the likelihood of measuring a greater amplitude difference between the centre and the edge of the viewing area is increased. To confirm this correlation, the aspect angle loss measured at each time has been plotted against the maximum intensity observed at that time in Figure 9. To obtain a larger spread of peak

amplitudes, this figure is a composite of the results from three separate analyses, for low, medium and high values of Kp. It is evident that the average value of the observed aspect angle attenuation varies between 0 and 10 dB/degree, and is closely governed by the absolute amplitude of the backscatter signal strength. This result may explain the large discrepancies between previously reported values of the aspect angle attenuation, since these studies did not include a sufficiently broad range of geophysical conditions. This conclusion has also been reached by Koehler et al. (1985) who comment that aspect angle sensitivity can be very variable and sometimes non-existent for 50 MHz echoes. The present observations at 140 MHz are in agreement with this result and suggest that it is not possible to determine a unique aspect angle attenuation rate for backscatter from 1m plasma irregularities in the auroral E-region.

5 MEAN PLASMA CONVECTION PATTERNS

The most important factor governing the morphology and properties of the Earth's magnetosphere and its plasma populations is the convection of flux tubes and associated plasma driven by the solar wind. The magnetospheric electric fields associated with this convective flow map along approximately equipotential field lines driving a two-cell pattern of plasma circulation at high latitudes in the ionosphere (e.g. Heppner, 1977; Foster et al., 1981; Heelis, 1982). The main features of this convection pattern are (1) the strong flow near dawn and dusk corresponding to the westward and eastward electrojet currents respectively and (2) the reversals near magnetic noon and midnight. The morning discontinuity is located in the region of the magnetospheric cleft, where the geomagnetic field line configuration allows magnetosheath particles to penetrate directly to ionospheric altitudes. This is therefore an extremely dynamic region and an example of the flow pattern measured by SABRE in the vicinity of the morning reversal has recently been reported (Waldock et al., 1984). Observation and theory suggest that the relative shape and size of the convection cells vary considerably both with magnetic activity and with the orientation of the interplanetary magnetic field (IMF) (Scourfield and Nielsen, 1981; Zi and Nielsen, 1982; Heelis, 1982). In particular, several days of STARE observations indicate that as magnetic activity increases the electric field magnitude increases and the average location of the field maximum moves equatorwards. In addition, the morning cell expands and the whole convection cell rotates towards earlier local times (Zi and Nielsen, 1982).

The causes of magnetospheric convection have been discussed in terms of two main theories, one in which closed magnetospheric flux tubes are transported from the dayside to the nightside in a boundary layer around the flanks of the magnetosphere by a 'viscous-like' process on the magnetopause (Axford and Hines, 1961), and the other in which open flux tubes are transported over the poles of the Earth after reconnection with the IMF at the dayside magnetopause (Dungey, 1961). It has also been suggested that these processes may coexist, with the 'viscous' process contributing a small but sometimes significant 10-30 kV to the typical cross-magnetosphere potential of between 40 and 100 kV (Cowley, 1982).

Averaged measurements of the plasma convection pattern have been previously reported, based on incoherent scatter radar observations (Foster et al., 1981; Oliver et al., 1983; Foster, 1983). A unique advantage of so-called 'coherent' radar systems, such as STARE and SABRE, is their high spatial and temporal resolution, typically 20 km x 20 km and 20s compared to several hundreds of km and 30 minutes for incoherent scatter radars. Furthermore, SABRE and STARE can operate unattended for extended periods and hence a much larger data set can be collected. There are, however, several disadvantages with the SABRE/STARE technique. Firstly, plasma irregularities must be present within the scattering volume to produce backscatter. Thus, no measurements are possible during 'quiet' times, when the electric field is below the threshold of about 15-20 mV/m necessary to excite the appropriate instabilities. Secondly, the inference of the electron drift velocity from the measured irregularity drift involves assumptions which may not be applicable under all conditions and are currently the subject of further investigation (Nielsen and Schlegel, 1983). Comparison with results from the European Incoherent SCATter facility (EISCAT) indicates that STARE (and hence SABRE) progressively underestimate the higher drift speeds (above about 600 m/sec), although the flow directions are accurate (Nielsen and Schlegel, 1983).

Figure 10 illustrates the plasma convection pattern observed by SABRE, averaged over all conditions. The data are presented as a function of geomagnetic latitude and universal time (MLT = UT + 1.5 hrs approximately) averaged over three degrees of longitude. The magnitude and direction of the convection flow are represented by the length and direction of the vector plotted at each grid point, with north towards the top of the figure. The main features of the convection pattern are readily identified from this figure. Strong electrojets are present involving sunward convection in the dawn and dusk sectors, and the morning and evening discontinuities are evident, located at around 09:00 UT and 21:00 UT respectively. These data reveal that the two-cell structure is, on average, an ever-present feature of high latitude convection, and are entirely in agreement with previous F-region incoherent scatter measurements (e.g Oliver et al., 1983).

To investigate the variation of the plasma convection pattern with magnetic activity, the average convection velocities at 64°N were grouped according to Kp and universal time. The results of this analysis are plotted in the same format as Figure 10, but with the ordinate representing Kp instead of latitude (Figure 11). Gaps in the data are either due to an absence of backscatter (for low Kp) or to non-occurrence of those

values of Kp. The most striking feature of this figure is the shift to earlier local times of the Harang discontinuity with increasing activity, from about 21:30 UT at Kp=2 to about 19:00 UT at Kp=6. This is consistent with the STARE results, but is in contradiction to the F-region convection measurements from the Millstone Hill incoherent scatter facility (Oliver et al., 1983). At the highest values of Kp, the flows become irregular. This is to be expected, particularly since only a few days of data are available for inclusion in the averaging process. The flows in the vicinity of the morning reversal are weak under all but the most active conditions. It is therefore difficult to assess the variation in the relative size of the two convection cells with Kp, however it does appear that the afternoon cell shrinks and the morning cell expands as Kp increases. It should be emphasized that interpretation of data from one radar location is difficult. It is uncertain, for example, whether the shift of the Harang discontinuity to earlier times with increasing activity results from a bulk rotation of the whole convection pattern, a displacement of the pattern with respect to the pole or to enhanced asymmetry of the morning and evening cells. A number of radar facilities now exist around the northern hemisphere and collaborative efforts to simultaneously measure the plasma convection pattern should be made to resolve this ambiguity. Future work should also resolve whether the apparent rotation of the convection cells with increasing Kp is a repeatable function of strong magnetosphere-IMF coupling or a transient effect associated with enhanced ionospheric currents and conductivity during substorms.

6 SHEAR FLOWS

Many examples of strong shear flows have been observed by the SABRE. These often occur under magnetically disturbed conditions and correspond to regions in which there exists non-zero divergence of the horizontal currents, and hence significant field-aligned currents. It is often difficult to relate features of the flow pattern observed by SABRE to specific events or phenomena taking place in the magnetosphere, however a notable exception took place on 4 September 1984 during a large magnetic field reconnection event on the dayside magnetopause. Magnetic field data from the AMPTE (Active Magnetosphere Particle Tracer Explorer) UKS (United Kingdom Sub-satellite) spacecraft between 13:45 and 14:45 UT are illustrated in Figure 12. During this interval the spacecraft was inbound near the equatorial magnetopause. The IMF had turned southwards at 13:50 UT and remained so until 14:42 UT when strong reconnection began to occur. During this interval two flux-transfer-events (FTE's) occurred, at 14:14 and 14:32 UT (e.g. Russell and Elphic, 1979). The reconnection lasted for more than an hour, during which time the magnetopause 'followed' the spacecraft inwards. Particle measurements (not shown) indicate that this was due to a greatly enhanced solar wind pressure. Figure 13 illustrates the SABRE flow velocities for this interval. Near the time at which reconnection began on the magnetopause the flow in the ionosphere turned sharply southwards, with a sudden recovery of the ambient westward flow (characteristic of the normal afternoon eastward electrojet) at 15:17 UT. Figure 13 illustrates the ionospheric flow velocities as a function of both latitude and longitude averaged over 20s. During the period of southward flow perturbation (e.g. at 15:14 UT) a strong latitudinal shear in the horizontal drift speed is observed. Reconnection taking place on the afternoon magnetopause (in the Northern hemisphere) would result in field line contraction, and hence plasma flow, in a North-easterly direction. Even combined with the ambient magnetosheath flow (which is in a direction away from the sub-solar point) it is unlikely that this could result directly in a southward flow perturbation when mapped down to ionospheric altitudes. More likely the reconnection taking place on the dayside is widespread, and has resulted in the removal of dayside high latitude open field lines without any corresponding replacement (via convection) from the nightside. The effect of this would be to move all plasma and electrojet boundaries equatorwards (e.g. Meng, 1983) and the flow pattern seen by SABRE could therefore be due to flows observed at the polar cap boundary, where the westward afternoon convection flow meets the anti-sunward polar cap flow. If so, this is the first direct evidence of the occurrence of these flows at latitudes as low as 63°N geomagnetic.

7 SUMMARY

Results of more than two years of observations of E-region auroral backscatter and plasma convection from the SABRE have been presented. Backscatter from 1m wavelength plasma irregularities (radar aurora) occurs most frequently during the afternoon (13:00 - 19:00 UT) and the morning (23:00 - 03:00 UT) sectors. Backscatter is weak near the Harang discontinuity, and is only present in the vicinity of the morning reversal under extremely active conditions (Kp > 6). The aspect angle dependence of backscatter amplitude is, on average, between 0 and 10 dB/degree; the value at any given time is governed by the absolute backscatter amplitude observed.

The average convection pattern measured by SABRE exhibits a well defined two cell structure under all conditions. The Harang discontinuity exhibits a strong local time dependence on magnetic activity, moving to earlier times as Kp increases. The morning convection cell also appears to expand relative to the evening cell with increasing magnetic activity.

Measurements made jointly by SABRE and AMPTE during a strong reconnection event suggest that it may be possible under extreme circumstances for the polar cap to penetrate to latitudes of 62-65°N geomagnetic during the afternoon sector.

These results are of significance to all radio systems operating at high latitudes. The time and spatial variations of the auroral zone scattering regions are of particular relevance to HF and VHF communications and surveillance systems operating at these high latitudes.

Acknowledgements

SABRE is operated jointly by Leicester University, U.K., and by the Max Planck Institut fur Aeronomie, F.R.G., in cooperation with the Uppsala Ionospheric Observatory, Sweden. The authors wish to thank Dr D J Southwood and colleagues at Imperial College London for supplying the AMPTE UKS data.

REFERENCES

Andre, D, The dependence of the relative backscatter cross section of 1m density fluctuations in the auroral electrojet on the angle between electron drift and radar wave vector, J Geophys Res, 88(10), 8043-8049, 1983.

Axford, W I and C O Hines, A unifying theory of high latitude geophysical phenomena and geomagnetic storms, Can J Phys, 39, 1433, 1961.

Cowley, S W H, The causes of magnetospheric convection in the Earth's magnetosphere: a review of developments during the IMS, Rev Geophys Space Phys, 20(3), 531-565, 1982.

Dungey, J W, Interplanetary field and the auroral zones, Phys Rev Lett, 6, 47, 1961.

Ecklund, W L, B B Balsey and R A Greenwald, Crossed beam measurements of the diffuse radar aurora, J Geophys Res, 86, 1805-1809, 1975.

Farley, D T, A plasma instability resulting in field-aligned irregularities in the ionosphere, J Geophys Res, 68, 6083-6097, 1963.

Farley, D T, H M Ierkic and B G Fejer, The absolute scattering cross section at 50 MHz of equatorial electrojet irregularities, J Geophys Res, 86, 1569, 1981.

Fejer, B G and M C Kelley, Ionospheric irregularities, Rev Geophys Space Phys, 18, 401, 1980.

Foster, J C, J R Doupnik and G S Stiles, Large scale patterns of auroral ionospheric convection observed with the Chatanika radar, J Geophys Res, 86, 11357-11371, 1981.

Foster, J C, An empirical electric field model derived from Chatanika radar data, J Geophys Res, 88(2), 981-987, 1983.

Greenwald, R A, W L Ecklund and B B Balsey, Radar observations of auroral electrojet currents, J Geophys Res, 80, 3635, 1975.

Greenwald, R A and W L Ecklund, A new look at radar auroral motions, J Geophys Res, 80(9), 3642-3648, 1975.

Greenwald, R A, W Weiss, E Nielsen and N R Thomson, STARE: A new radar auroral backscatter experiment in northern Scandinavia, Radio Sci, 13, 1021, 1978.

Haldoupis, C I, E Nielsen and C K Goertz, Experimental evidence on the dependence of 140 MHz radar auroral backscatter characteristics on ionospheric conductivity, J Geophys Res, 87, 7666, 1982.

Haldoupis, C I and E Nielsen, Results on relative scattering cross-section of 140 MHz auroral backscatter, J Geophys Res, 89(4), 2305-2312, 1984.

Heelis, R A, The polar ionosphere, Rev Geophys Space Phys, 20(3), 567-576, 1982.

Heppner, J P, Empirical models of high latitude electric fields, J Geophys Res, 82, 1115, 1977.

Koehler, J A, G J Sofko and V Mehta, A statistical study of magnetic aspect effects associated with VHF auroral backscatter, accepted by Radio Science, 1985.

Leadabrand, R L, A G Larson and J C Hodges, Preliminary results on the wavelength dependence and aspect sensitivity of radar auroral echoes between 50 and 3000 MHz, J Geophys Res, 72, 3877, 1967.

McDiarmid, D R, On the aspect sensitivity of radio aurora, Can J Phys, 50, 2557, 1972.

Meng, C I, Case studies of the storm time variation of the polar cusp, J Geophys Res, 88(1), 137-149, 1983.

McNamara, A G, D R McDiarmid, G J Sofko, J A Koehler, P A Forsyth and D R Moorcroft, BARS - A dual bistatic auroral radar system for the study of electric fields in the Canadian sector of the auroral zone, Adv Space Res, 2(7), 145-148, 1983.

Nielsen, E, W Guttler, E C Thomas, C P Stewart, T B Jones and A Hedberg, A new radar auroral backscatter experiment, Nature, 304, 712-714, 1983.

Nielsen, E and K Schlegel, a first comparison of STARE and EISCAT electron drift velocity measurements, J Geophys Res, 88, 5745, 1983.

Oliver, W L, J M Holt, R H Wand and J V Evans, Millstone Hill incoherent scatter observations of auroral convection over $60^\circ<\Lambda<75^\circ$. 3: average patterns versus Kp, J Geophys Res, 88(7), 5505-5516, 1983.

Rogister, A and N d'Angelo, Type II irregularities in the equatorial electrojet, J Geophys Res, 75, 3879-3887, 1970.

Russell, C T and R C Elphic, ISEE observations of flux transfer events at the dayside magnetopause, Geophys Res Lett, 11, 131-134, 1979.

Scourfield, M W J and E Nielsen, Evening (Harang) and morning discontinuities in ionospheric electron drifts and their dependence on the interpanetary magnetic field, J Geophys Res, 86(2), 681-686, 1981.

Starkov, G V, J Oksman, M V Uspensky and A V Kustov, On the dependence of radar aurora amplitude on ionospheric electron density, J Geophys, 52, 49-52, 1983.

Sudan, R N, J Akinrimisi and D T Farley, Generation of small scale irregularities in the equatorial electrojet, J Geophys Res, 78, 240-248, 1973.

Uspensky, M V, R J Pellinen, W Baumjohann, G V Starkov, E Nielsen, G Sofko and K U Kaila, Spatial variations of ionospheric conductivity and radar auroral amplitude in the eastward electrojet region during pre-substorm conditions, J Geophys, 52, 40-48, 1983.

Waldock, J A, T B Jones and E Nielsen, SABRE observation of the morning sector convection reversal, Planet Space Sci, 32(7), 837-843, 1984.

Zi, M and E Nielsen, Spatial variations of electric fields in the high latitude ionosphere, J Geophys Res, 87(7), 5202-5206, 1982.

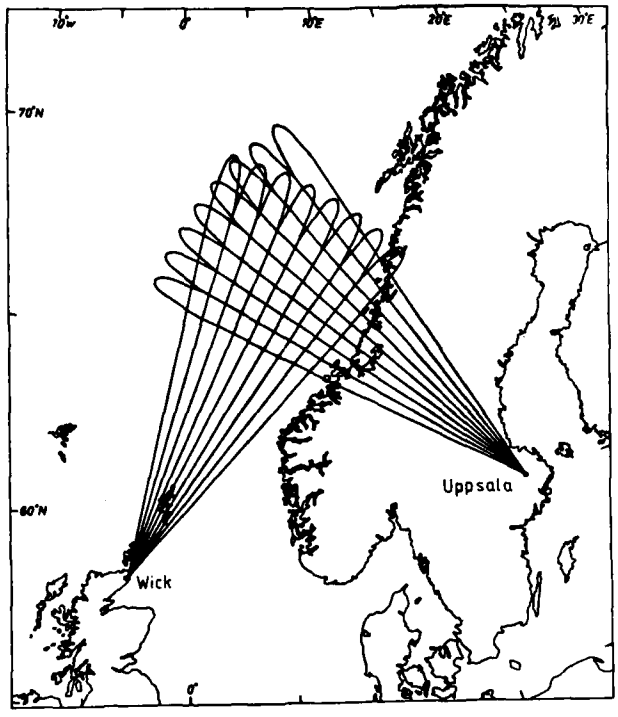


Figure 1 Illustrating the location and field of view of the SABRE radars at Wick in Scotland, and at Uppsala in Sweden.

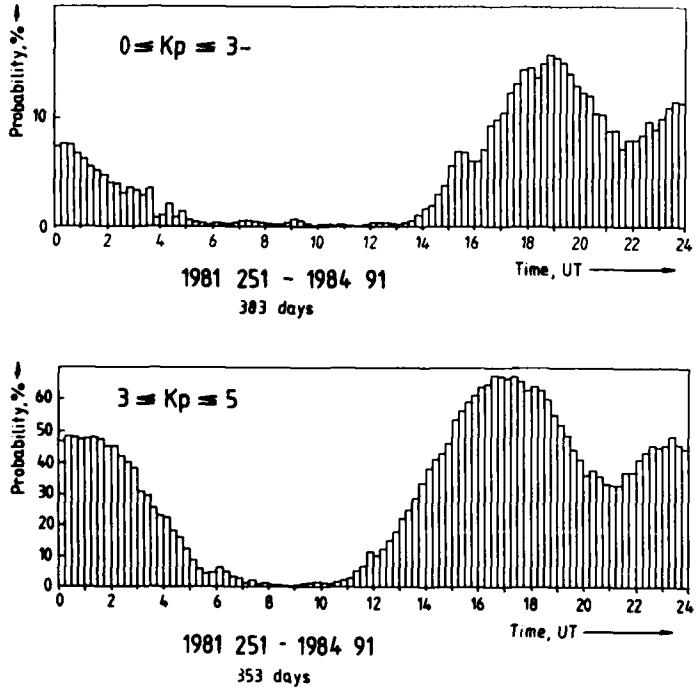


Figure 2 Illustrating the frequency of occurrence of radar auroral backscatter greater than 3 dB, as a function of universal time. The upper and lower panels present the results for low (Kp < 3) and medium (3 < Kp < 5) levels of magnetic activity respectively.

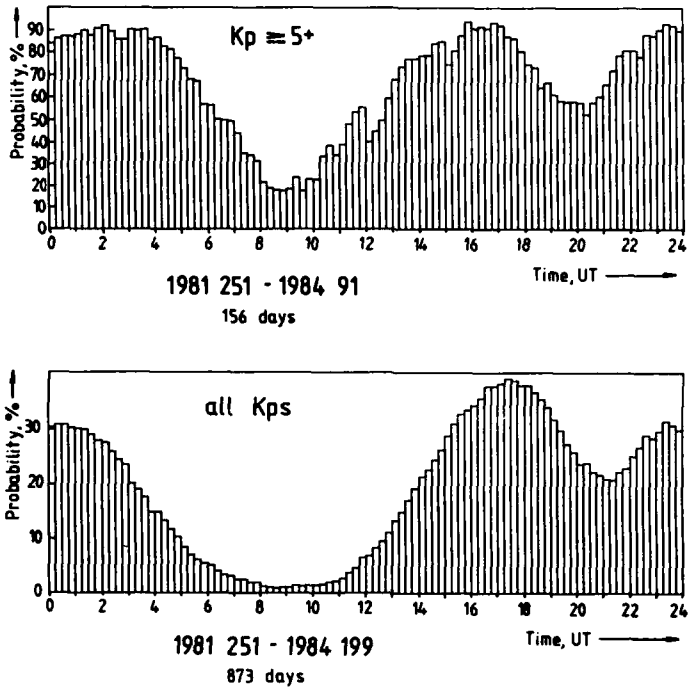


Figure 3 As for Figure 2. The upper and lower panels present the results for high magnetic activity (Kp > 5) and for all conditions, respectively.

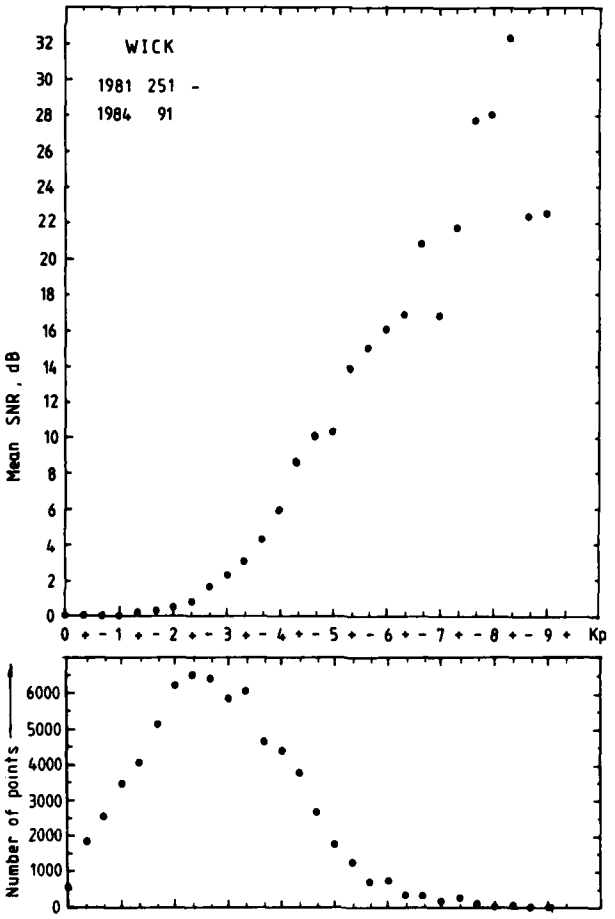


Figure 4 Illustrating the average backscatter as a function of Kp. The lower panel indicates the number of data values within each Kp interval.

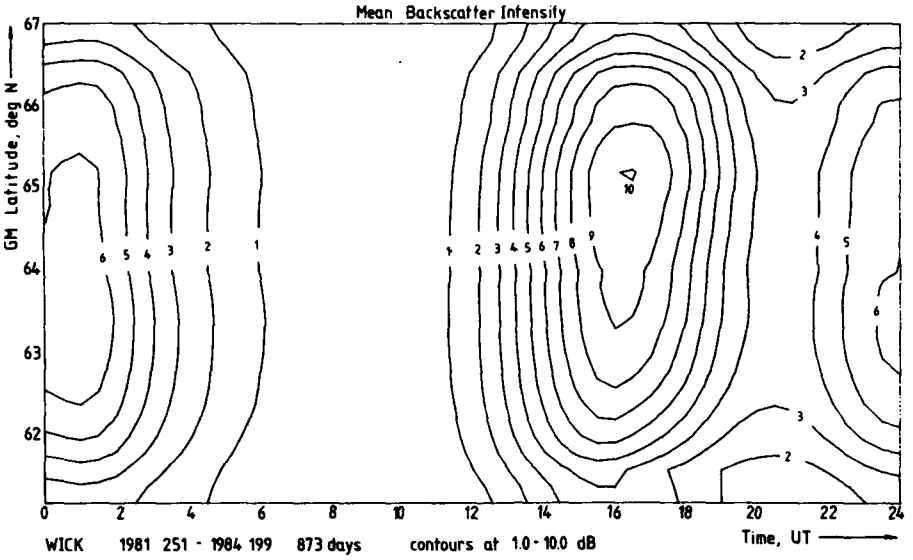


Figure 5 Contours of backscatter intensity as a function of UT and geomagnetic latitude, averaged over geomagnetic longitudes 99-103 degrees east. These data are averaged over all magnetic conditions.

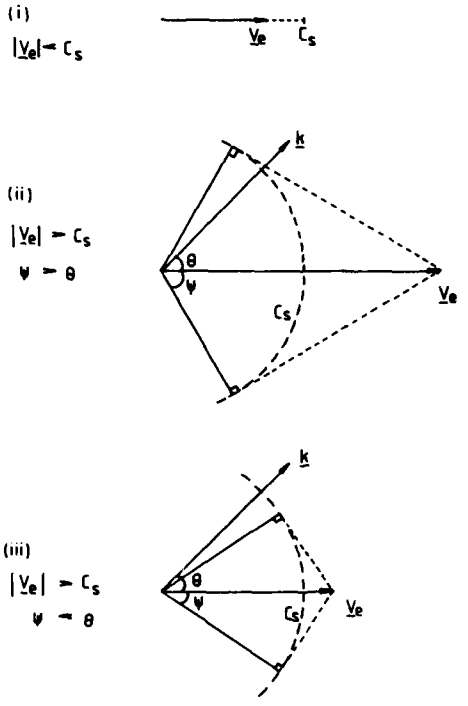


Figure 6 Schematic illustration of the method of flow angle correction for the backscatter data. There are three situations:

(i) if $|V_e| < C_s$, then it is assumed that there is no variation of backscatter intensity with flow angle (θ);

(ii) if $|V_e| > C_s$ and $\theta < \Psi$ [$= \cos^{-1}(C_s/|V_e|)$] then it is assumed that a linear dependence of backscatter intensity with θ exists, $A_{corr} = A + m\theta$, A=amplitude, m=0.45 dB/degree;

(iii) if $|V_e| > C_s$ and $\theta > \Psi$, then $A_{corr} = A + m\Psi$.

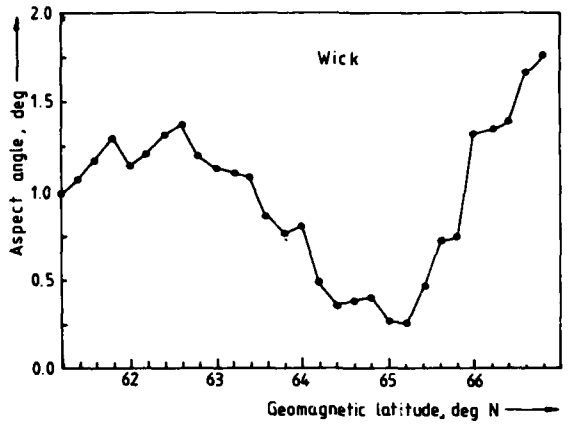


Figure 7 Aspect angle variation with geomagnetic latitude for the locations within the field of view of the Wick radar used in the statistical results presented in Figure 5. The angle indicated is measured in degrees off perpendicular from the magnetic field.

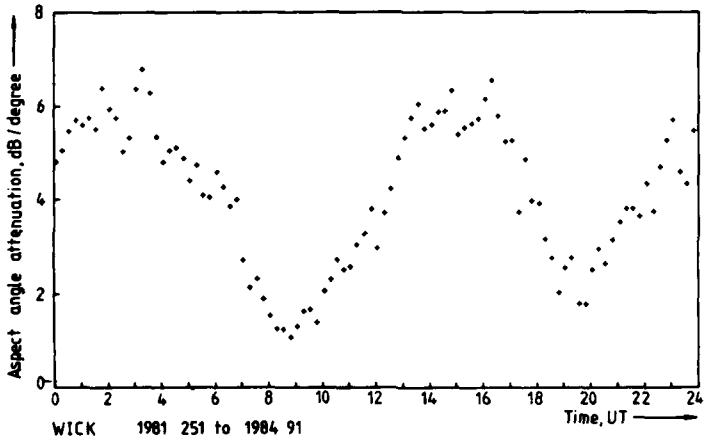


Figure 8 Aspect angle attenuation as a function of universal time, calculated from Figures 5 and 6.

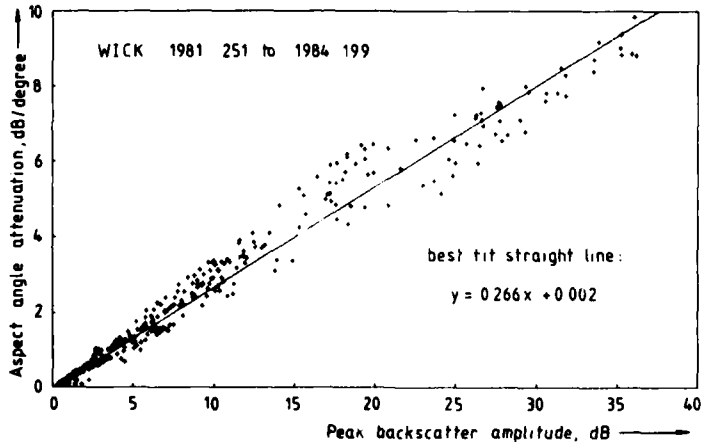


Figure 9 Aspect angle attenuation as a function of peak backscatter amplitude. See text for details.

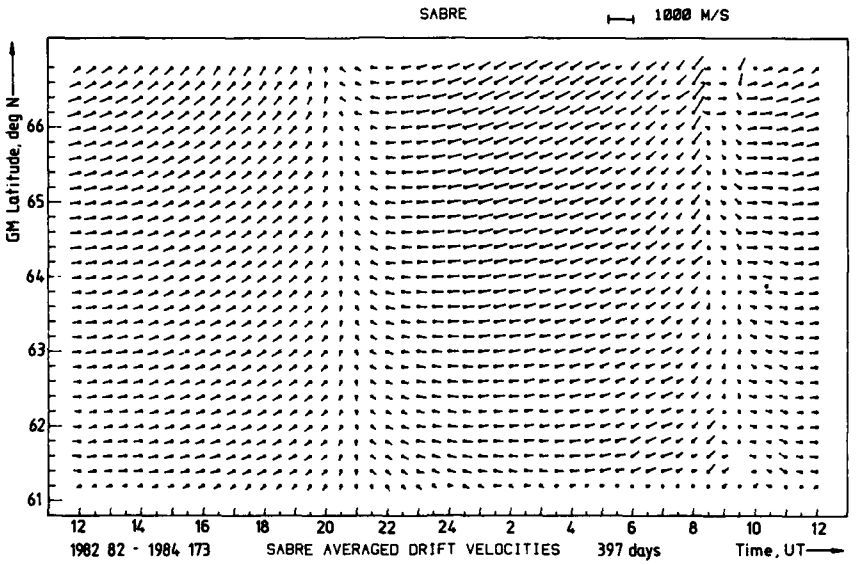


Figure 10 Illustrating the average convection pattern measured by SABRE, averaged over all magnetic conditions.

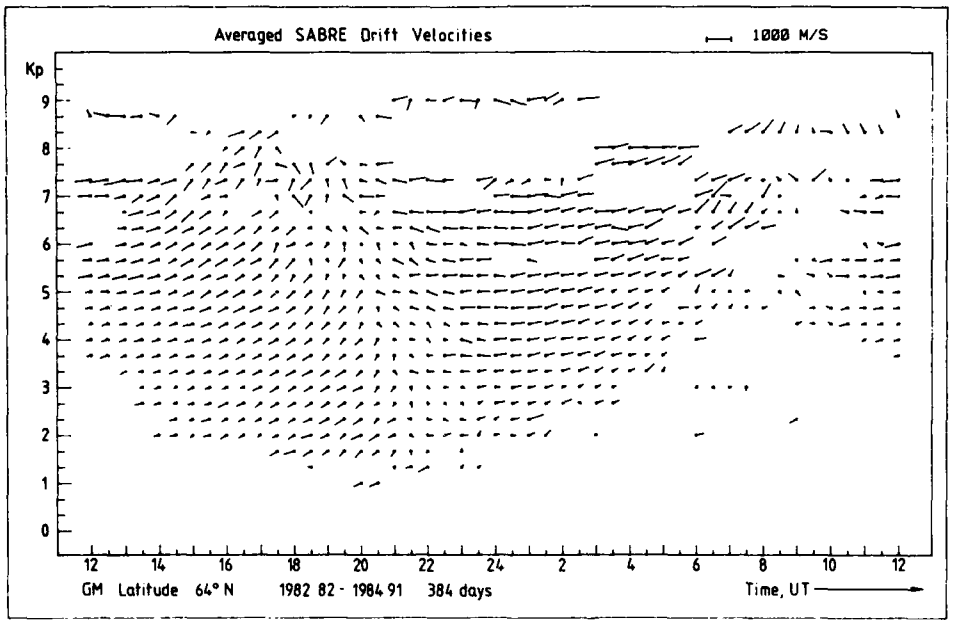


Figure 11 Average convection flow velocities measured by SABRE, presented as a function of universal time and Kp, for the geomagnetic latitude 64°N.

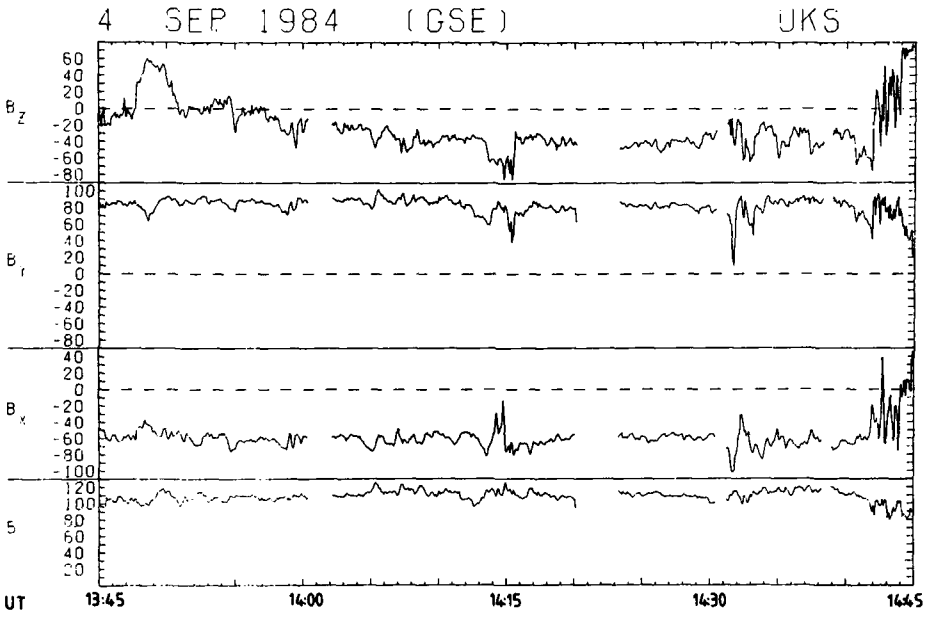


Figure 12 Illustrating the magnetic field data recorded by the AMPTE UKS spacecraft on 4 September 1984 between 13:45 and 14:45 UT. The data are plotted in GSE coordinates, in which the Z component is northwards (out of the ecliptic), the X component is directed sunwards, and the Y component is directed towards dusk (Courtesy of Dr D J Southwood)

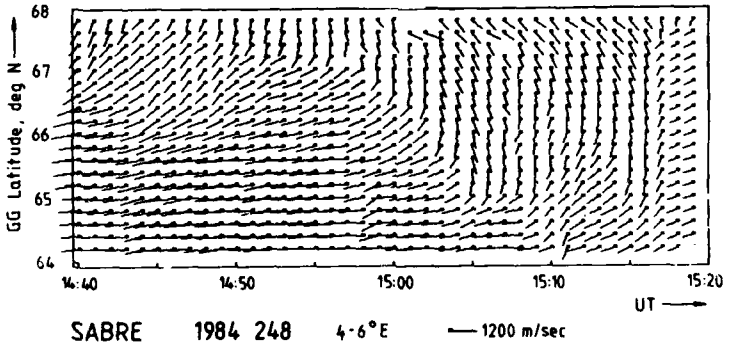
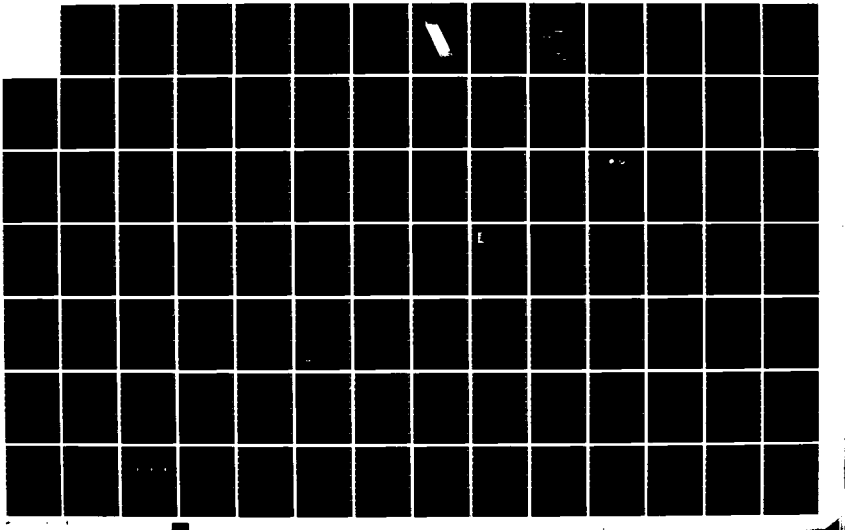
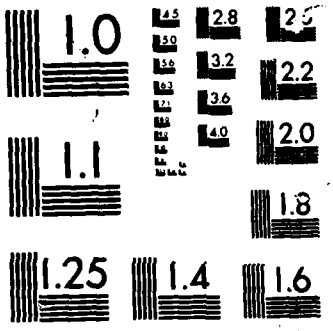


Figure 13 Illustrating the SABRE data for this period as a function of latitude. These data are averaged over 2 degrees of longitude.

AD-A166 585 CONFERENCE PROCEEDINGS ON PROPAGATION EFFECTS ON MILITARY SYSTEMS IN THE..(U) ADVISORY GROUP FOR AEROSPACE RESEARCH AND DEVELOPMENT NEUILLY.. H SOICER

UNCLASSIFIED NOV 85 AGARD-CP-382 F/G 4/1 NL





MICROCOPY CHART

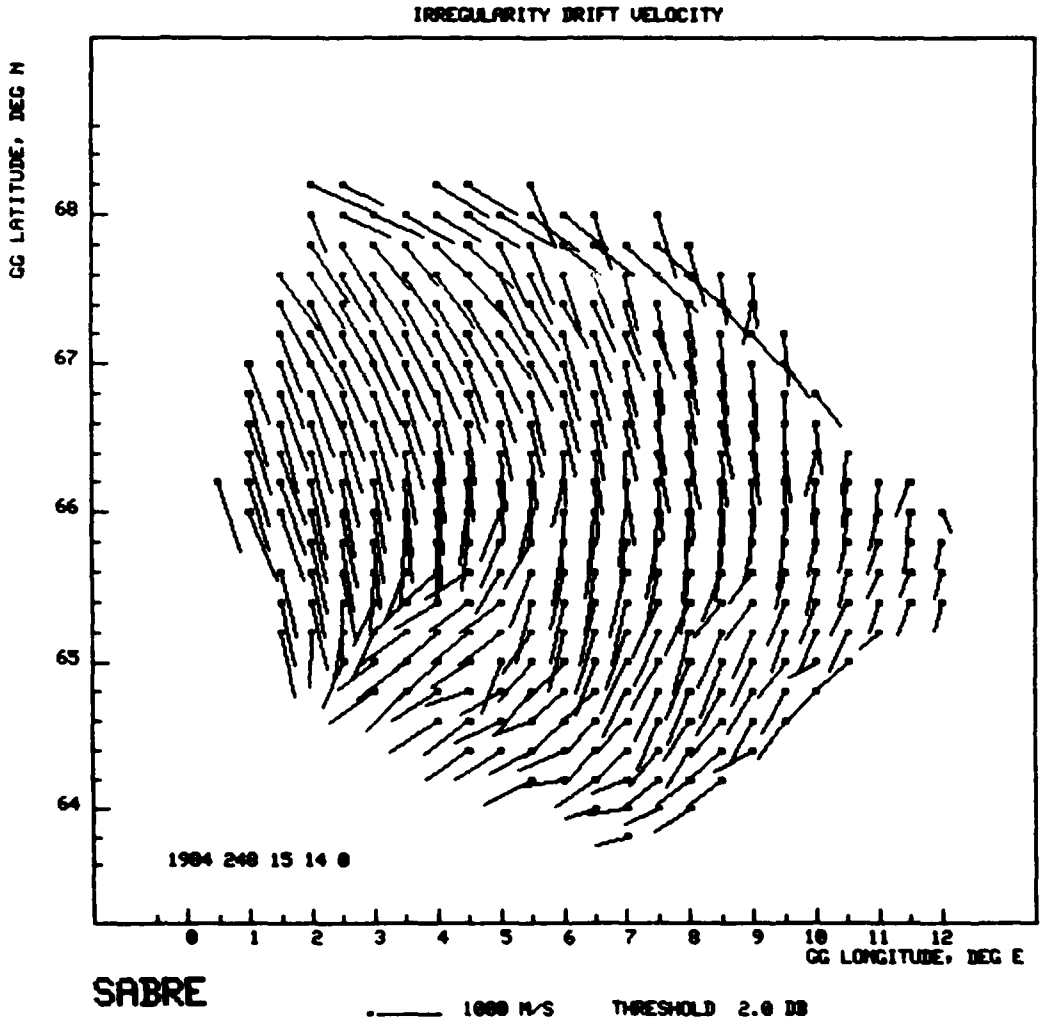


Figure 14 SABRE drift velocity measurements for the 20s interval ending at 15:14 UT on 4 September 1984.

DISCUSSION

R.Greenwald, US

I find it difficult to accept your result that the irregularity aspect angle sensititvity is dependent on the strength of the backscattered signal. This implies that weakly-excited irregularities are less aspect sensitive than strongly excited irregularities which is opposite from what one would expect from theory.

I believe that your results demonstrate very well that these irregularities can extend to what are commonly thought of as plasmapause latitudes. Do you have any comments on this point?

Author's Reply

Our results seem to confirm that the aspect angle sensitivity is indeed dependent on backscatter amplitude. The results presented in the paper have been corrected for flow angle variations and the validity of the technique adopted for the correction could be questioned, although it is the same as used by several other authors. As emphasized in the presentation a large aspect angle dependence (say 10 dB/degree) is impossible during times of low backscatter amplitude since such a large factor would completely attenuate all signals not exactly satisfying the exact orthogonality criteria. We have not examined our results on a day-to-day basis and we intend to do this in future. Our average values clearly demonstrate an increase in aspect angle attenuation with the backscatter amplitude. We have as yet not investigated the theory of the processes responsible for this. The SABRE radar frequently shows saturation in the closest range gate (~420 km) which suggests that the backscattering region could be present at latitudes well to the south of our stations.

N.C.Gerson, US

Are we rediscovering the fact that the communicators discovered 30—40 years ago? They found so much outage and disturbance on radio paths from eastern north America to western Europe that they sought corrective action: circuits for HF were established from eastern US south to Brazil, west to Africa and north to Europe.

Author's Reply

We are certainly seeing the same phenomena as was reported years ago, particularly by amateurs using the 2 metre band. However with modern radars we are able to accurately locate the position of the scatterers and to determine their drift-velocity. We are also able to measure the Doppler velocity of the ion/acoustic waves creating the irregularities and hence to determine the electric flow vector and hence the electric field in the E-region.

G.Sales, US

Addressing the question of the high correlation between backscatter power and aspect sensitivity. I believe we are looking at two different phenomena. The weak backscatter and low aspect sensitivity are primarily a daytime effect while the strong backscatter/high aspect sensitivity occurs at nighttime.

Author's Reply

I agree with this comment. We have not tried to differentiate between day and night time data. However, all the points appear to lie on the straight line plot of figure 9.

A.Rodger, UK

(1) From your SABRE data, could you give an indication of the size of the ionospheric projection of the flux transfer event? (2) It appears from your figure 5, that the maximum backscatter intensity occurs at slightly different latitudes in the morning and evening convection cells indicting that the height of the scattering regions is different. Is this difference in latitude consistent with the differences in the height of the eastward and westward electrojets?

Author's Reply

(1) The size of the disturbance is greater than our field of view. We have not yet examined the STARE data to see if this radar also observed the same event. (2) The occurrence of the maximum in backscatter intensity at slightly different latitudes does not necessarily result from the small difference in heights of the Eastward and Westward electrojet flows. This could be a contributory factor but I doubt that it could account for the magnitude of the effects we observe.

SUMMARY OF SESSION VII

Measurement Techniques/Models/Morphology and Physics

by

Dr E.Thrane
Session Chairman

A total of five presentations were given in this session.

As suggested by the session title a variety of subjects were discussed. The first paper by Taagholt gave an overview of geophysical measurements in the Greenland area, emphasizing the importance of this area for Arctic radio propagation and giving examples of the very considerable activity initiated by Danish and US agencies.

Modelling of the Arctic propagation medium was addressed in two papers by Watkins and Hargreaves. The two authors had very different approaches: Watkins described a three dimensional ionospheric model based on physical processes governing solar-terrestrial interactions, whereas Hargreaves presented a statistical model for ionospheric absorption based on riometer measurements at Arctic stations. Both papers stimulated active discussions on the merits and limitations of the methods.

Lee described an interesting study of the physical mechanisms responsible for the generation of high latitude ionospheric irregularities. Progress is being made in this field, which is of great importance for radio systems in high latitudes.

The final paper in the session dealt with phenomena in the mesosphere. Dr Widdel presented new results from tracking of chaff clouds. These measurements provide new insight into the dynamical processes in the non-ionized air in the lower ionosphere. These processes are of importance for the understanding of the coupling between the ionized and neutral species.

Danish and US Geophysical Measurements in Greenland and Surrounding Areas Related to Arctic Radiopropagation

Jørgen Taagholt
Danish Scientific Liaison Officer for
Greenland, Universitetskomplekset,
Øster Voldgade 10, 1350 Copenhagen K.

SUMMARY

Greenland and its surrounding waters cover a stratetic, important area, in which the radio propagation conditions are influenced by a variety of geophysical phenomena.

During World War II,the US established ionospheric measurements in Greenland and later, the Ionosphere Laboratory of the Technical University of Denmark took over and increased the activity which today count a number of geophysical observatories, ranging from the auroral zone to the geomagnetic pole, just north of Thule.

The geophysical measuring program includes 4 ionospheric vertical sounders, which are operated in cooperation with NOAA, HF oblique backscatter equipment, 23 riometers at 18 different locations, 14 magnetometers, 9 auroral all sky cameraes, from which most of the data are stored in digital form ready for distribution to operational or scientific users. Such geophysical data are among other data used in radiopropagation forecast, and some results of investigations of forecast and practical operation statistics are presented in this paper.

Additional to the routine geophysical measurements, special research installations so as the Incoherent Scatter Radar Facilities at Søndre Strømfjord, the rocket launch facilities at Thule AB and Søndre Strømfjord are used for special investigations. Besides the geophysical program, a serie of radio propagation experiments have been conducted by US and/or Denmark during the past decades, including VLF propagation experiments, HF oblique soundings, UHF propagation experiments, investigations of UHF SHF satellite communication under low and very low horizontal angels. Experiences from operational satellite communication systems in Greenland are presented. Since 1983, Denmark has been involved in investigations related to communication and position determination of distress signals via the SARSAT-COSPAS system. Such investigations are performed primarily to investigate search and rescue procedures but in addition the experience gained will provide a valuable background for future applications in relation to traffic surveillance in the Greenland region.

INTRODUCTION

This paper is based upon information gathered during my more than 25 years involvement in arctic ionospheric studies and maybe mainly based upon my near 20 years involvement in US scientific research in Greenland in my capacity of Danish Scientific Liaison Officer for Greenland. The presentation includes some historical background, information about the extensive Danish net and ground based geophysical measurements in the Arctic and try to touch some of the projects conducted since World War II under influence of the still changing demand for use of radiosystem in communication, navigation and detection but additionally as tools for retrival of information on different geophysical phenomena such as meteorological or oceanographical parameters.

Radiosystems and propagation of radio waves are depending on several geophysical parameters, such as ground conductivity, man made and natural electromagnetic noise, atmospheric conditions including water vapor, rain, snow, dust, ionospheric -atenuation, -reflection, -refraction or -scientillation.

For planning and management of operational radiosystems, there is a need for information and understanding of the variability and frequency depending of these parameters. Further such dependencies can be used in the search for information on these parameters. Thus the vertical sounders are used to give information about the electron density profile, the riometer about relative ionospheric opacity and the Faraday rotation measurements about total electron content etc. etc.

HISTORICAL BACKGROUND FOR THE RESEARCH IN GREENLAND

The idea of starting radio propagation investigations in Greenland was first conceived by the active and foresighted Danish professor P. O. Pedersen who in his book "The Propagation of Radio Waves Along the Surface of the Earth and in the Atmosphere" (1927) - presented the theory of the physical properties of the ionosphere based upon a knowledge of the propagation of radio waves at different frequencies.

During the Second Polar Year 1932-33 professor Pedersen wanted to build an ionosphere station in Godhavn but it was not until 1951 that this wish was fulfilled by his assistant and later successor, professor Jørgen Rybner. The year before, the National Bureau of Standards of The U.S. Department of Commerce had established an ionosphere station at the American Military Base, Bluie West One, in southern Greenland and in 1957 when

the U.S. Armed Forces left what is now called Narsarsuaq, professor Rybner also undertook the responsibility for this station in his capacity as Chairman of the Danish National Committee of the International Radio Union (URSI). Since then, Denmark as well as US has been very actively involved in ionosphere and radio propagation experiments in Greenland.

It was soon realized that operation of the Greenlandic stations would only be feasible if there was an active group in Copenhagen to analyze the ionosphere data obtained and to train the station personnel before leaving for Greenland. To fill this need professor Rybner founded a laboratory at the Technical University based upon financial support from local URSI funds. At the same time rapid technological development made it possible to perform measurements in the ionosphere using instruments launched with rockets or from satellites. Due to the resources at the new laboratory, professor Rybner in 1961 was able to accept a Norwegian proposal for a joint campaign with rocket launching from Andøya in Lofoten, Norway, in co-operation with the National Areonautics and space Administration (NASA). This project later formed the basis for a Greenlandic ionosphere rocket program.

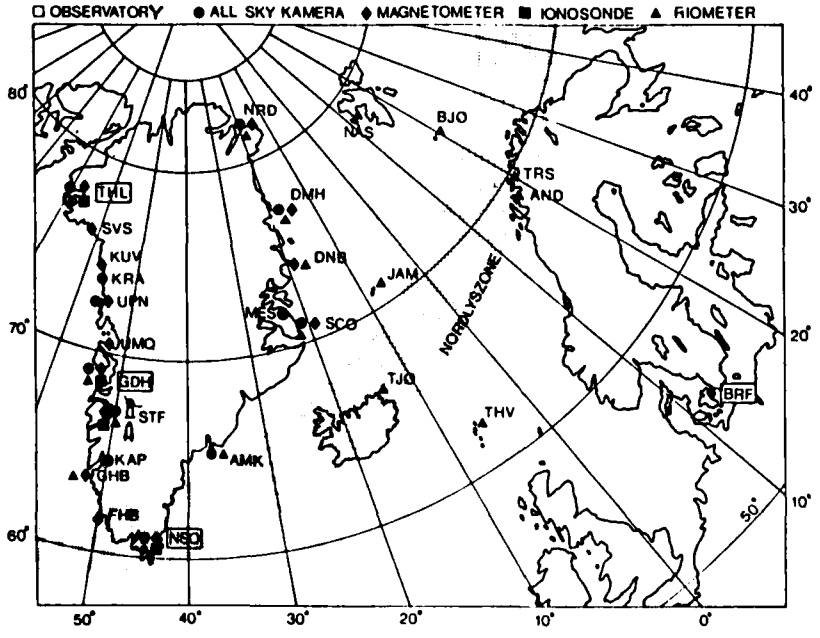
Because of this and other developments in connection with the Danish "Space Research" program supported so far under the Danish URSI Committee, the laboratory was officially established on April 1, 1962 under the Technical University of Denmark.

Recordings of natural generated VLF noise had been made at Godhavn and Narsarsuaq for some years when, in 1964, a "VLF-station" was established at the Danish site Thule/Qanaq, approximately 80 miles north of Thule Air Base. Financial support was given by the U.S. National Science Foundation (NSF) and locally by the U.S. Army Research Support Group (USARSG). When in 1966 the American scientific camp situated approximately 16 miles east of Thule AB was closed down, the U.S. ionosphere station there was transferred to the Danish station at Thule. An ionosonde was made available from the U.S.A. and a 150 sq.m. building was moved from the camp to the station by helicopter. The U.S. National Government took over the financial responsibility.

In 1967 Denmark conducted the first Danish rocket-experiment from Thule Air Base supported by U.S. Air Weather Service as an extension of the U.S. meteorological rocket program. In this program the meteorological rocket payload has been modified in Denmark to include sensors for measurement of proton flux and the proton energy distribution in the range from 200 Rev to 20 MeV which include the major part of particles responsible for Polar Cap Absorbtion Event (PCA) events. In 1971 Denmark built op its own rocket launch facilities at Søndre Strømfjord. Assisted by the Danish Armed Forces 2 Nike-Apache with barium release experiments were launched in August 1971. To support further rocket campaigns a Danish Ionosphere Station was established at Søndre Strømfjord in 1973. Mainly operated in connection with balloon or rocket campaigns and in 1983 the US ISR International - with support from National Science Foundation - established an Incoherent Scatter Radio facility at Søndre Strømfjord.

The Danish Geophycical Observatories, now operated by the Danish Meteorological Institute under the Ministery for Transport, Communication and Public Works, are responsible for a rather extensive program as shown in the map below.

DANISH OBSERVATORIES OR STATIONS 1984 Fig. 1

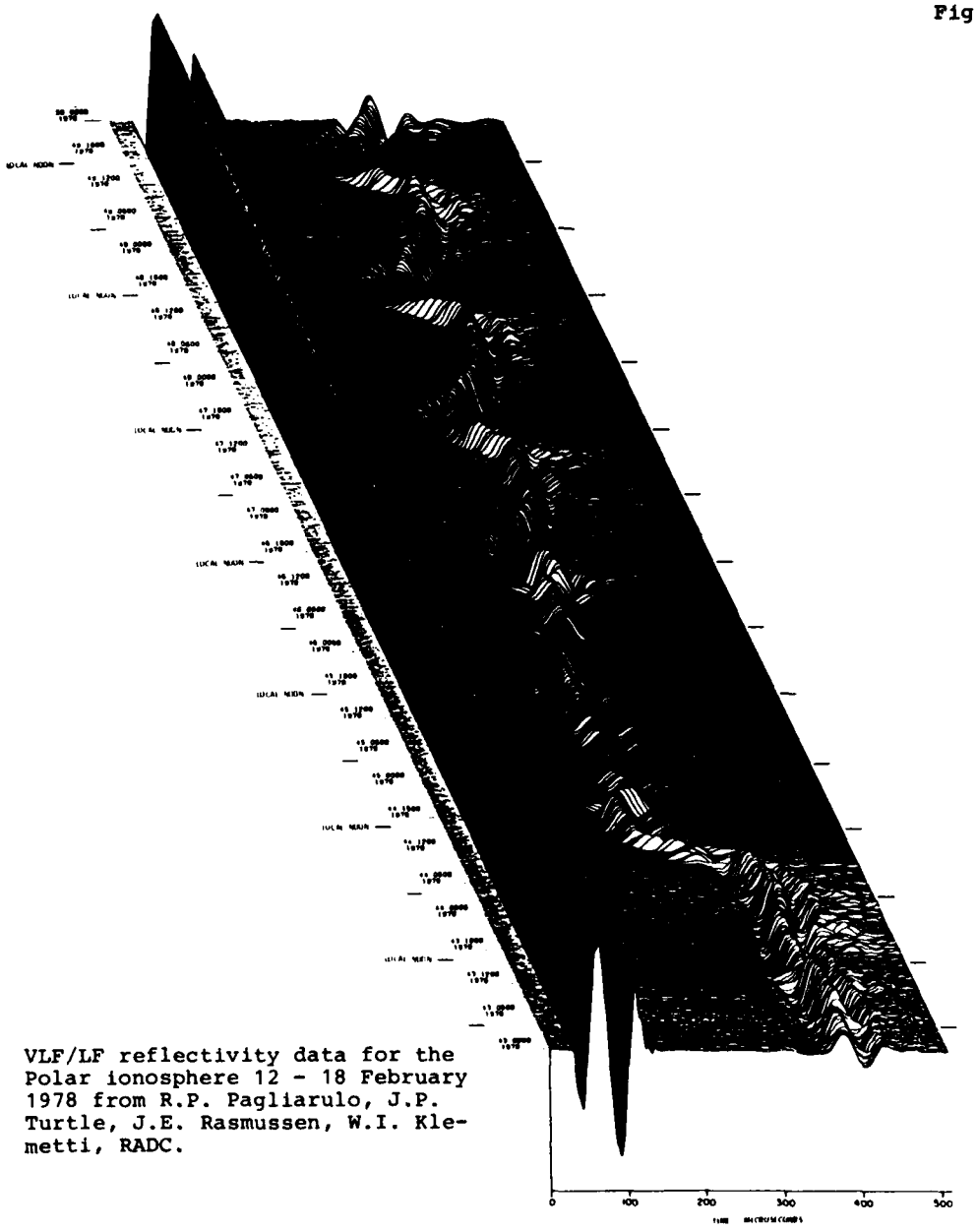


VLF-PROGRAMMES

In addition to the Danish VLF program mainly conducted in the 60ties (Stockflet Jørgensen 1968a - 1968b) US scientific institutes today conduct especially in the Thule district - several VLF propagation experiments, partly based upon receival of signals from fixed VLF transmitters, partly based upon VLF soundings.

At present US Rome Air Develop Center conduct a VLF/LF ionosounder programme for determination of the caracteristics of the lower ionosphere. The transmitter is located at Thule AB, radiating vertically polarized signals from a 130 meter vertical antenna. The receiver and the data acquisition system is located at the Danish Geophysical observatory at Qanaq. Results from the experiment which show the diurnal variation of the reflection height of the lower ionosphere is presented in Fig. 2. The period shown includes a short Polar Cap Absorbtion Event, which occurred in February 1978.

Fig. 2



VLF/LF reflectivity data for the Polar ionosphere 12 - 18 February 1978 from R.P. Pagliarulo, J.P. Turtle, J.E. Rasmussen, W.I. Klemetti, RADC.

Ionospheric Effects Branch of the US NRC conduct studies of VLF propagation in the earth ionosphere waveguide, with special interest in studying the profound effect of the Greenland Ice Cap on VLF propagation. Danish groups have been involved in investigations related o operational use in Greenlandic areas of the worldwide VLF navigation system OMEGA, which today also forms the basis for the Danish aerological routine balloon programme, in which the windprofile is determined automatically by transfer of the OMEGA signal from an OMEGA receiver in the balloon instrumentation to the ground station.

Ground conditions are also of importance related to LF propagation used presently in the Loran-C navigation systems, but more data concerning surface conductivity in arctic areas (tundra, areas of permafrost, open or frozen sea) and the seasonal variation are required.

But today, just before introduction of the advanced NAVSTAR satellite navigation system, maybe too limited efforts are directed towards further investigations with respect to other navigation systems such as OMEGA and LORAN.

VERTICAL SOUNDINGS

Vertical soundings are conducted at Narsarsuaq, Søndre Strømfjord, Godhavn and Qanaq/ Thule. Ionograms are scaled and every day hourly values are transmitted to forecastcenters at Boulder, Colorado and Offut. Ionospheric data from a solar cyclus at Narsarsuaq and Godhavn covering a 15 year period (Olesen and Taagholt 1968) show the well-known feature that although the photoionization in the F-region should be rather limited during the polar night, fairly high electron densities are seen during the winter months. In recent years the data handling at the stations are conducted by means of a microprocessor giving an ideal basis for much more detailed daily transfers of geophysical data via geostationary satellite data collection system, and additionally by end of the month form the basis for monthly summaries as shown in Fig. 3 ideal for statistic analysis.

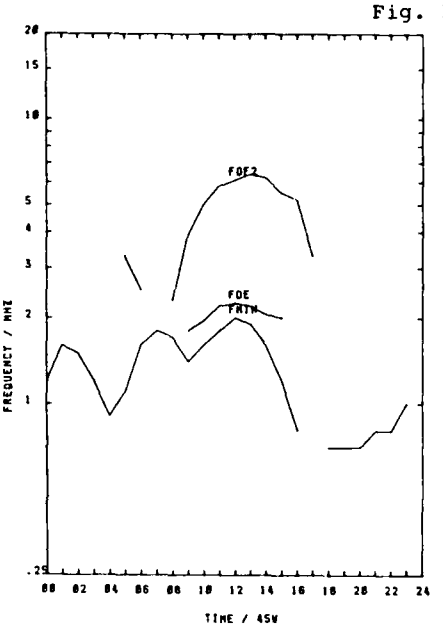
Fig. 3

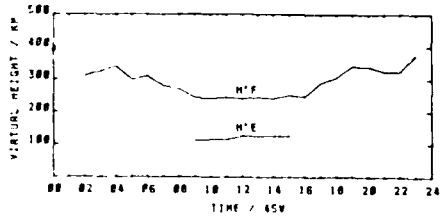
FEBRUARY 1984 — IONOSPHERIC DATA — STATION NARSARSUAQ

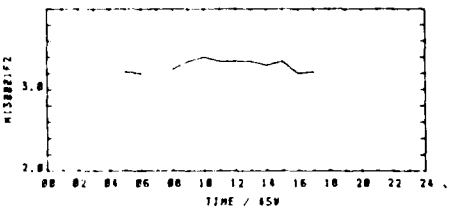
VALUES OF FOF2 — CHARACTERISTIC CODE NO 00 — UNITS (0.1 MHZ) — 45° WEST TIME

DAY\HR	0	1	2	3	4	5	6	7	8	9	10	11
1	A	A	A	A	B	A	B	B	B	B	C	C
2	A	F	F	F	F	018 F	016 F	B	033 F	044 F	059UR	044UR
3	A	F	A	A	F	A	A	A	030 F	039	043	044 F
4	C	C	C	C	C	C	C	C	C	C	F	F
5	F	F	A	A	A	A	A	C	C	C	C	F
6	C	C	C	C	C	C	C	C	C	C	073	C
7	F	A	A	A	A	A	A	A	B	056 F	065	F
8	A	F	C	C	C	C	C	C	C	053	054 F	C
9	C	C	C	C	C	C	C	C	C	052 F	072	C
10	C	C	C	C	C	C	C	C	C	C	C	069 F
11	A	A	A	A	A	A	A	A	B	042UR	047	049 F
12	A	A	A	A	A	A	A	B 024 F	040 F	052	056	056 F
13	F	A	F	A	A	A	A	A	B	039 F	049 F	B
14	A	A	A	A	A	A	B	A	032 F	B	B	B
15	F	F	A	A	A	A	A	A	B	B	B	054 F
16	A	F	A	A	034 F	030 F	023 F	028 F	B	B	056UR	062 F
17	A	F	F	B	A	F	F	025 F	044 F	B	062 F	062
18	A	F	A	A	F	A	A	B	B	060 F	064 F	076
19	F	F	A	A	F	F	026 F	029 F	049 F	057 F	074	072 F
20	A	F	F	035 F	030 F	A	F	F	046 F	062 F	068	072 F
21	F	A	F	A	A	A	A	F	046 F	C	C	C
22	A	F	F	A	F	A	F	F	B 057	075 M	087 F	090
23	A	A	F	A	A	A	A	039 F	048 F	059	063	070
24	A	F	A	A	F	A	F	033 F	043 F	050	058	061
25	A	F	040 F	030 F	028 F	025 F	028 F	A	052 F	055 F	059 F	060
26	C	C	C	C	C	C	C	C	C	C	062	C
27	C	C	C	C	C	C	C	C	C	C	C	C
28	F	A	A	A	A	A	B	B 047	055		057	057
29	028 F	F	F	F	F	F	042 F	046 F	060 F	064 F	068 F	069 F
MED							026	029	046	055	060	063
CNT	1	1	2	3	3	5	7	14	17	20	18	

DAY\HR	12	13	14	15	16	17	18	19	20	21	22	23
1	057	055	060 F	055 F	046 F	F	F	F	A	A	A	A
2	070	072 F	074 F	F	F	F	F	B	A	F	A	A
3	F	043	040 F	C	C	C	C	C	C	C	C	C
4	F	B	F	F	F	C	C	C	C	C	C	C
5	C	C	C	056	055	056 F	F	C	C	C	C	C
6	074 F	071 F	073 F	072 F	A	F	F	F	A	A	F	F
7	073	072 F	069 F	070 F	068 F	067	F	F	A	A	F	A
8	C	C	C	C	C	C	C	C	C	C	C	C
9	C	C	C	068	057 F	C	C	C	C	C	C	C
10	077 F	079 F	F	F	F	F	F	F	F	F	F	F
11	053	050 F	050 F	049 F	039 F	F	F	F	A	F	F	A
12	065	065	071	075	070	052 F	F	A	A	F	F	A
13	044 F	051 F	F	045UF	A	A	A	A	F	A	A	A
14	048 F	050 F	B	044 F	041	A	A	A	042UF	A	A	F
15	054 F	044 F	044	047 F	044 F	063 F	044 F	F	F	A	A	A
16	046	050	068	072	055 F	042 F	023 F	F	F	A	F	A
17	067	071	077	081	075	044	F	F	F	F	F	F
18	083	082	080 F	070 F	F	F	F	F	F	036 F	F	F
19	089	093	089	066 F	056 F	F	F	036UF	F	F	F	F
20	082 F	088	089	089	088	F	F	F	B	F	A	A
21	065 F	078	C	065 F	061	048	F	B	A	A	F	A
22	091	093	095	074	052 F	F	F	A	A	F	A	A
23	079	082 F	079 F	070 F	064 F	F	F	A	F	F	A	A
24	058	065	065	072	050 F	044 F	F	F	A	F	A	A
25	C	C	C	C	C	C	F	C	C	C	C	C
26	071	086	066 F	F	F	F	F	C	F	F	F	F
27	056 F	B	056 F	053 F	038 F	042 F	F	F	A	F	F	F
28	065	066	069 F	066	063	063 H	056 F	051 F	046 F	043 F	033 F	028 F
29	073 F	080	065 F	061	066	065	059	049 F	040 F	F	F	036 F
MED	067	071	069	068	057	056	044					
CNT	23	23	20	22	19	11	5	2	3	2	1	2







NARSARSUAQ GREENLAND
MONTHLY MEDIANS: JANUARY 1984

Monthly ionosphere data from Narsarsuaq, January 1984.

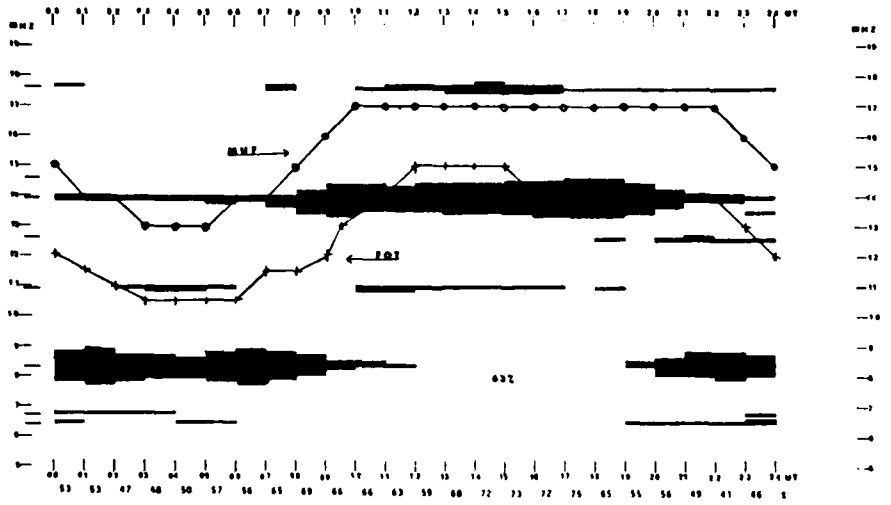
In a joint Danish/US co-operation this year the first digital sounder vil replace the old C4 sounder at Qanaq. The digisounder provides facilities for real time transfers of the ionograms which again open possibilities for a central scaling of the ionograms excluding the effect of individual interpretation.

Just a few decades ago, HF signals formed the basis for near all Arctic communication, and data from the arctic vertical sounders together with other geophysical and solar data were used at the radio propagation forecast centers where the duty is to serve

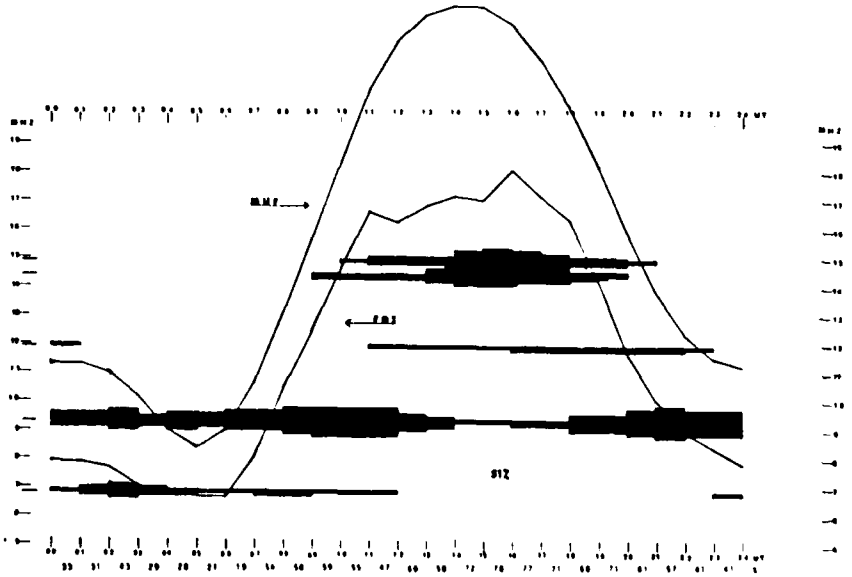
the military and public HF communication network.

As part of the US-Danish co-operation, the Danish geophysical observatories have daily transmitted hourly values of ionospheric parameters to Boulder and Offutt, and the US forecast centers support Danish communication paths with HF forecasts. Based upon our evaluation of this service J. Taagholt et al 1974 presented an investigation on the actual HF radio propagation Greenland-Denmark, seen in relation to the HF propagation predictions. The investigation shows that this path is very sensitive to ionospheric conditions because it intersects the annual zone. During ionospheric absorbtion the communication might be improved due to decrease in interferences, but increasing absorbtions may be so high that radio communication is impossible (black out). Fig. 4 shows the condition during two weeks in spring and summer 1973 respectively. The regularity (commercial time) for the path was about 65% during summer and only 50% during spring. Corresponding periods during sunspot max. years show regularities up to 85-90%. The main reason seems to be the compressed MUF (Maximum Usable Frequency) - LUF (Lowest Usuable Frequency) gab during sunspot min. years causing serious interference problems. Now just 10 years later such regularities seems very historical. The public communication is today based upon an advanced satellite communication system.

Fig. 4.
Comparison of predictions and actual performance of the Reersø - Godthaab HF circuit.



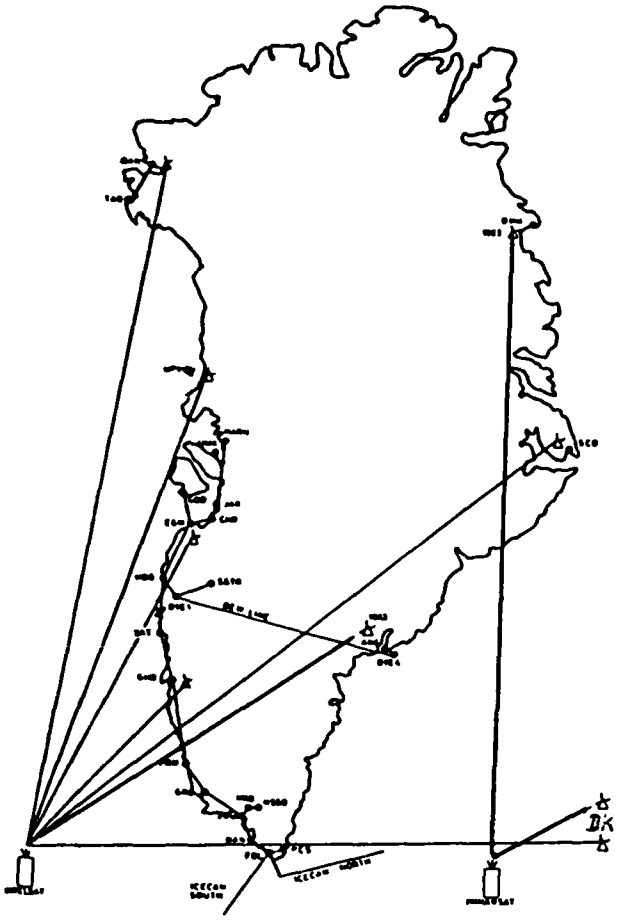
a) Summer period.
The absence of day/night phenomena is clearly seen.



b) Spring period.
Day/night variation clearly seen.

The first operational satellite communication from Greenland was established in 1977 for transmission of meteorological data via the NIMBUS Random Acces Message System. Since then satellite communication has been extensively used in Greenland even over relatively short distances due to the sparce population as described by Johnson and Taagholt 1984, and as seen in Fig. 5 which shows the public Danish satellite communication-net in Green-

land. Additionally the US Armed Forces are using domestic North American geostationary satellites for their communication to Søndre Strømfjord and Thule AB. Further Meteorological data are rutinely transferred via the ARGOS satellite systems or via the European geostationary meteorological satellite METEOSAT. This communication forms the basis for the on-going Danish US studies of ionospheric irregularity impact on high arctic satellite communication.





UGO Stations with ARGOS communication.

FIGURE 5. SATELLITE LINKS FOR TELEPHONE RELAY FROM GREENLAND TO DENMARK

COSMIC NOISE ABSORBTION MEASUREMENTS

The Danish Ionosphere Laboratory has built up an extensive arctic riometer network as shown in Fig. 1. The riometer designed by P. Stauning consists of a sensitive, calibrated receiver with a frequency sweep around the riometer frequence and includes a minimum-value-detector for exclusion of non-cosmic noise of terrestrial origin. To increase the dynamic range, most of the riometer stations are equipped with riometers operating near 20,30 and 40 MHz.

Fig. 6. illustrates an absorbtion event from September 22, 1973 observed by the Danish arctic riometer network prepared by Stauning.

MAGNETOMETER

Particle precipitation from space, mainly with solar origin, observed with the riometer, are under influence of the earth geomagnetic field. Geomagnetic recordings are accordingly important for the understanding of disturbed ionospheric condition. Denmark operates an extensive network of geomagnetic observation stations, either with absolute measurements based upon the classical La Cour magnetometer or relative measurements using fluxgatemagnetometers.

Some riometer and magnetometer data are transferred from Narsarsuaq in near real time data burst via the US geostationary satellite GOES to Boulder.

Various types of geophysical disturbancies such as geomagnetic storm and substorm activities are known to be accompagnied by enhanched electric fields in the polar and auroral region causing strong electric current in the ionosphere.

The geomagnetic pertubations caused by ionospheric currents observed by different observations are combined in the auroral electrojet index.

ROCKET AND SATELLITE EXPERIMENTS

Geophysical disturbances are subject for several US and Danish investigations. Such event studies are frequently based not only on ground based observations but additionally on observations from satellites or rockets or born sensors.

23 scientific sounding rockets have been launched from Søndre Strømfjord since 1971, most often as a Danish/US co-operation but also together with experiments from research institutes from other countries. The scientific aims include observation of ionized and neutral winds, magnetic and electric fields, electron and proton precipitation, studies of polar cusp and auroral oval phenomena, such as polar cap turbulence, polar cusp phenomena, auroral electrodymanics, auroral electrojet turbulence, polar ionosphere irregularities and ionosphere-neutral atmosphere coubling.

Søndre Strømfjord is uniquely situated for interrelated scientific studies of the auroral oval, polar cusp and polar cap regions.

Due to the uniqueness of Søndre Strømfjord with its location relative to the geomagnetic pole and associated auroral and cusp phenomena, an extensive net of ground based scientific instrumentations are available for this campaign. These includes the US Incoherent Scatter Radar Facilities at Søndre Strømfjord, the Danish chain of geophysical observatories in Greenland, Cornell University's portable VHF radar located at Narsarsuaq, Fabry-Perot F-region chain at Calgary, Canada, Ann Arbor, USA, Kiruna, Sweden, Thule, Greenland, APL HF backscatter radars at Goose Bay and La Grande, Canada and the US ground station for the satellite HILAT, located near launch area at Søndre Strømfjord.

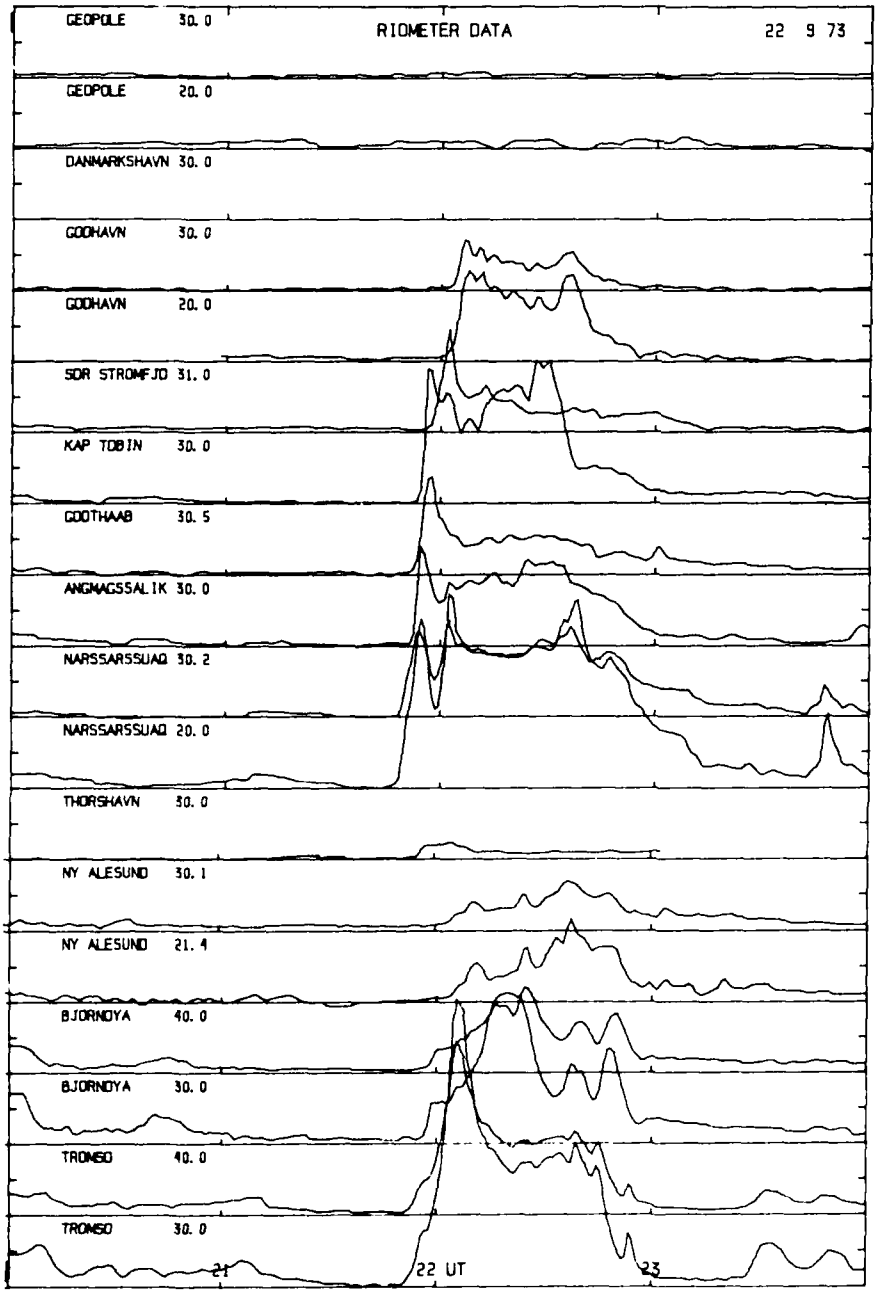


Fig. 6.

Electric fields measurements conducted in an international rocket campaign in 1974/75 with several chemical release experiments launched for example from Søndre Strømfjord are described in Journal of Geophysica Research 1980 and studies especially concerning neutral winds have been conducted in cooperation between the US Cornell University and the Danish Meteorological Institute as described in A Decade of Joint Upper Atmospheric Research 1975-1985.

The first satellite was launched in 1957 and since then more than 2.000 satellites have been launched. During the first decade the satellite served purely scientific purpose. To an increasingly operational role in relation to communication, navigation and detection. Several US and some Danish satellite experiments deal with Arctic upper air phenomena, and satellite data are received at several locations in Greenland, and for the US satellite HILAT the main ground station is located at Søndre Strømfjord. This satellite provides detailed information in the dynamic condition in ionosphere and magnetosphere.

BALLOON EXPERIMENTS

By means of satellites or rockets only transitory recordings can be made at rather fixed paths. In order to study the time variations in the particle radiation, US and Danish scientists have conducted several campaigns in Greenland with measurements based upon balloon borne sensors frequently as from other Arctic locations. As exampel can be mentioned studies of the longitudional extension of electron precipitation during magnetospheric substorms, as described by Anker Jensen et al 1972 and studies of electric DC fields as described by Mozer 1972 and studies of pulsations in electron precipitation as described by Barcus et al 1985.

INCOHERENT SCATTER RADAR

The installation of the US Incoherent Scatter Radar facilities at Søndre Strømfjord during 1983 has placed Greenland in focus with respect to upper air studies. So far some 28 research institutes from different parts of the world have made use of the facilities, and some of the results obtained so far have been published in Geophysical Research Letters 1984.

FUTURE DEVELOPMENT

Greenland and the Arctic region will as described by Bach & Taagholt 1982 play a still more important role, partly due to the increased strategic importance of these geographic regions but also because utilization of non-living arctic resources, metals and particularly oil and natural gas is vital for the industrial world.

The activity pattern in the Arctic regions has changed accordingly. Former small remote communities are now local industrial centers, and areas without manned activity are arctic operation centers as originally proposed by Canada.

Danish control tasks in Greenland and surrounding waters are at present maintained by several institutions and councils, both civilian and military. As the future pattern of activities expands, partly because of national and partly because of foreign activities, the possibility of establishing a Danish/Greenland operations centre under the aegis of defence, ought - for rational as well as for economic reasons - to be contemplated, a centre which would coordinate control of fisheries, air-sea rescue service, ice-reconnaissance, weather services and pollution control. At the same time the centre would collect and distribute on all information relevant to the communication and navigation services, including the system for monitoring of ship movements, all meteorological, oceanographical and environmental conditions etc.

We observe today, that the Post and Telegraph Services direct all their efforts towards the development of advanced telecommunication networks and only defence agencies, prospecting companies and scientific expeditions deal with improvement of old existing technics.

Some examples might have interest:

ARCTIC ADAPTIVE HF FREQUENCY MANAGEMENT

In northern Greenland, Denmark has gathered some experiences with adaptive frequency management for a medium sized HF radio system supporting summer field activity of the Danish Geodaetic Institute and the Greenland Geological Survey during recent years in the northernmost Greenland. The radio system supported approximately 15 field parties and 4 aircrafts. Additional communication when needed was established to Thule AB, Station Nord, Danmarkshavn and Mestersvig airport.

A mobile ionosounder developed in Copenhagen has been used for the frequency management experiment. It is a pulse type sounder with a pulse power of 2.5 kW, and with all signals internally represented as digital signals, facilitating on-line digital signals processing.

The ionosounder was placed in the centre of the expeditions work-area, and the ionograms obtained reflected a mean of the ionospheric conditions in a circular area with an approximate radius of 300-400 km. This means that paths up to 300-800 km for which the ionospheric reflection takes place within the area seen by the ionosounder can be evalu-

ated. For undisturbed conditions, the well-known methods using the critical frequencies for the E, F1 and F2 layers together with the graphical aids published by CCIR were used to identify the optimum communication frequency for the desired range.

The use of the ionograms to select proper frequencies for the single sideband telephony did improve the radio network operation considerably, and the network stayed operative throughout most of the PCA events.

During PCA events path attenuations up to 179 dB were measured, and experiences show that the atmospheric noise level, which normally sets the lower limit for the dynamic range of a communication system, decreased to a level below the receiver front-end noise level. Much effort was spent to remove man made noise in the aircrafts and at the base camp to ensure that the dynamic range of received signals were not limited by other factors than those given by the geophysical environment.

During the development of a PCA event the ionograms were used to identify the frequency range where the D-layer absorbtion is small enough to enable reflections from the ordinary F-layer trace. When this range is narrow the selection of a proper operation frequency must account both for the high f-min and the effect of MUF failure caused by a too high frequency.

Likewise during the recovery from a PCA event the regular ionospheric layers are often not available to support communications. The only traces seen on the ionograms are thick Es layers with the high values for both f-min and fo. The ionospheric conditions varies very rapidly, and the only possible way to choose the optium operating frequency at any time is the use of a real time ionospheric monitor such as the ionosounder. The adaptive frequency management experiment in North Greenland has proved, that frequency management based on ionosounding in connection with communication equipment especially adapted to the geophysical conditions experienced in the polar cap area, can markedly enhance the availability of a HF communication system during periods of disturbed ionospheric conditions.

METEOR BURST COMMUNICATION

At SHAPE Technical Center studies were conducted approximately 20 years ago with respect to utilization of the sporadic ionization in the upper atmosphere caused by meteorites. The study was completed and the conclusion was that radiosignals at 50-100 MHz could be reflected via ionozation caused by meteorits and that such communication seems to offer an excellent propagation method during disturbed ionospheric conditions when appropriate technical development with respect to digital communication have made it possible to handle the data-transmission for a link,only temporarily open for short fractions of a second.

Today the datahandeling is facilitated by the advanced digital technology using microprocessors etc., which has increased the interest in meteor burst communication.

A US Rome Air Development Center program conducted in co-operation with Danish scientists with the aim to study the surviability, reliability and jamming vulnerability of meteor burst communications at high-latitudes as a function of frequency and disturbance severity has been initiated in 1983 and is still further developed.

Today the test bed consists of a communication link from Søndre Strømfjord to Thule AB and an additional propagation path is planned for the near future in order to include transmissions through the auroral zone.

Meteor burst communication seems to offer an ideal solution for stabel communication to and from remote arctic locations where only a limited channel capacity is needed. The system is independant on external units such as line of sight ground stations or satellites, and offers a high security against jamming and simoultanous auscultation.

DATA TRANSMISSION VIA SATELLITES

Application of the ARGOS communication system in Arctic regions has been described by Taagholt & Jensen 1983 based upon experiences gathered from the operation of the net of unmanned geophysical observatories - UGO stations - shown at fig. 5. These stations have since 1978 been equipped with ARGOS transmitters built in Denmark for transfer of meteorological data in the RAMS system operating at about 400 MHz. Some of the stations are additionally equipped for real transmission via the European geostationary satellite METEOSAT using its data collection system.

The Danish experiences indicate, that other geophysical data including data from magnetometer, riometer and vertical sounder, could easily be transferred in near real time from the geophysical observatories to operationel user centrals via the data collection system in GOES/METEOSAT and accordingly improve the services conducted by the space disturbances forecast centers.

Joint US and Danish investigations of UHF scintillation activities over the Arctic have been presented by Aarons et al 1981 and several US investigations in Greenland deal with test of satellite communication systems including measurements of ionospheric

scintillation and communication link parameters especially with respect to investigations of the influence of solar activity, magnetic activity, seasonal and daiurnal variation as presented by Johnson et al 1981.

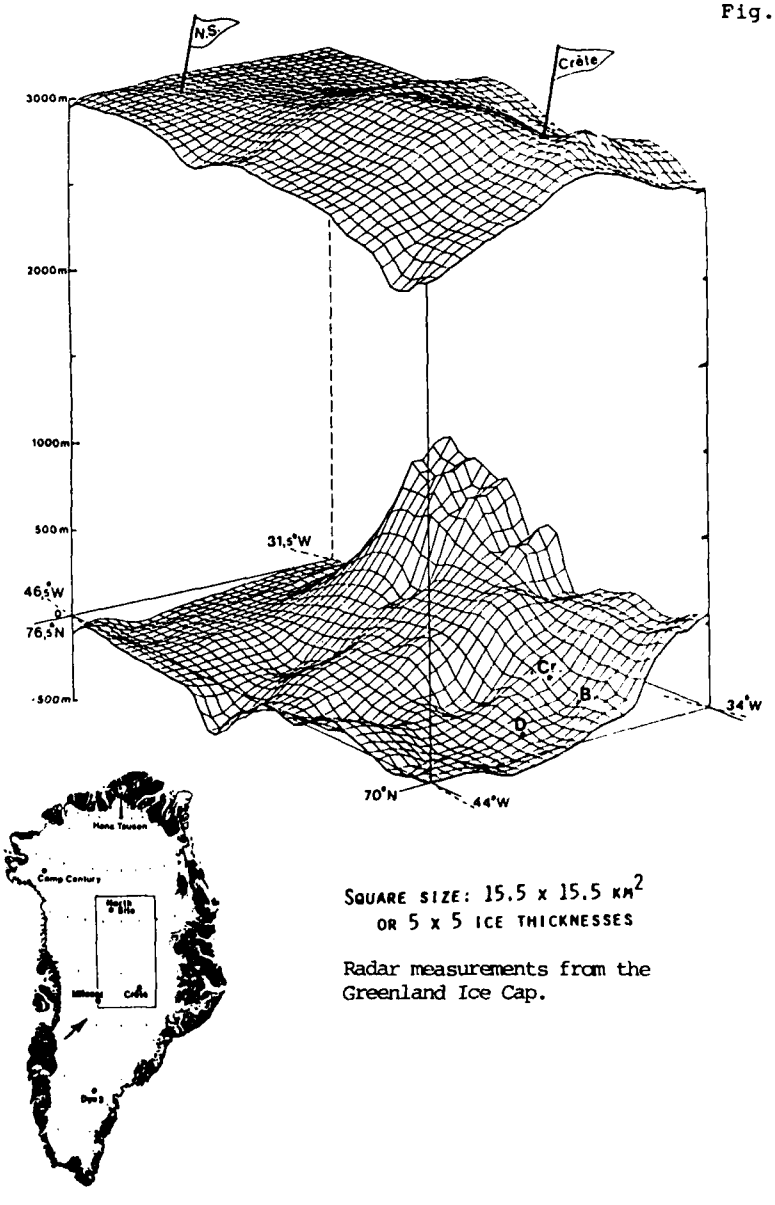
Based upon the experiences gathered through the Danish UGO program Taagholt 1984 has conducted a study of the application of the SARSAT/COSPAS system in Greenlandic areas for retransmission and position determination of distress signals. Initial tests in Greenland indicate that SARSAT Doppler measurements accuracy is not severely degraded by ionospheric scintillations. Studies are additional performed with respect to environmental impact on the emergency transmitter: Antenna icing, high waves, heavv snowstorms and transmitter and antenna placed below deep snow.

Navy officers have to remember that small battery operated transmitters just as the ELT, but operating at an ARGOS frequency, hidden onboard their ships can give the enemy all information about movement of their ship.

ELECTROMAGNETIC DETECTIONS

Electromagnetic remote sensing for Arctic Sea surveillance, Taagholt 1982 has been used for many years and at the Electromagnetic Institute at the Technical University of Denmark several systems have been developed with special emphasis to Arctic applications. Special knowledge about radio propagation is needed in relation to the development of the Danish Ice Radar described by Gudmandsen 1983. With a 60 MHz airborne radar it has been possible to map the topography of the bedrocks below the Greenland Ice Cap as shown at Fig. 7.

Fig. 7.



SQUARE SIZE: 15.5 x 15.5 KM^2
OR 5 x 5 ICE THICKNESSES

Radar measurements from the Greenland Ice Cap.

Similar tests have been conducted with respect to measurements of the thickness of the Polar sea ice, a very difficult task. Side looking radar and synthetic aperture radar for sea, ice and polar ice applications are tested in cooperation with the Danish Armed Forces in Greenland and such data are compared with radiometer data observed from same platform with reference to determination of the observed object, new or old sea-ice, ice flow or ship etc. Remote Sensing will in future play an increasing role with respect to Arctic Surveillance and environmental inspections.

ATMOSPHERIC MICROWAVE ATTENUATION

Satellite transmission of TV signals, digital telephone and high speed datatransmission employ increasingly higher radio frequencies in order to satisfy the still growing demand for such services, related to the proposed Arctic Operation Centers. At frequencies above 10 GHz attenuations of radio signals by clouds, snow and rain have to be taken into account. For the design of future Arctic satellite communication systems it is of great importance to collect accurate statistics of the magnitude and the variation of this attenuation, especially for the Arctic region where the horizontal angles normally will be rather low, which means a long propagation path through the problematic propagation on media.

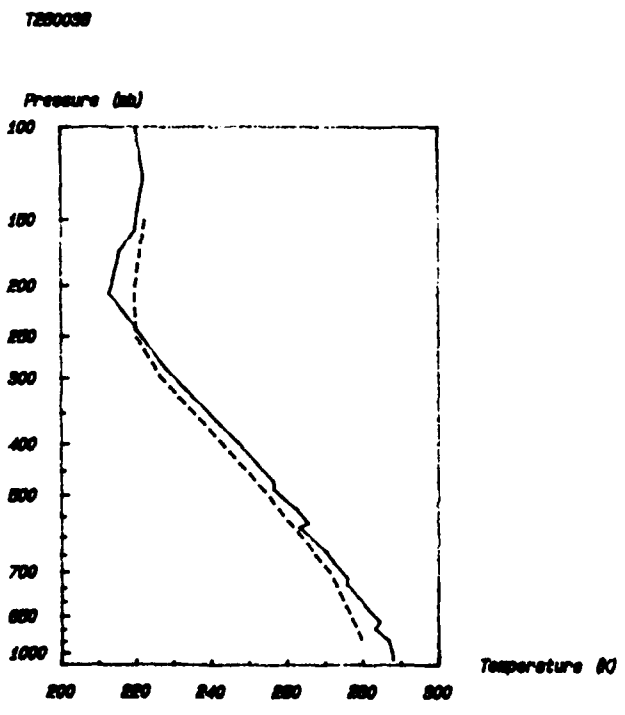
For the frequency range - 10 to 30 GHz - knowledge about the electromagnetic noise plays a vital role. The noise at this frequency are normally of physical nature, because any body generate electromagnetic noise depending on its temperature.

Accordingly much more information must be gathered by means of radiometers about the natural noise, partly to be used in geophysical remote sensing investigations of the earth surface partly needed for design of modern digital transmission systems.

Danish Groups are very actively involved in Arctic remote sensing technics, but the problems call for further international cooperation.

CALCULATION OF ATMOSPHERIC TEMPERATURE FROM SATELLITE DATA

Some of the US meteorological satellites (TIROS & NOAA) have a sensor package named Tiros Operational Vertical Sounder, TOVS, which includes radiometer channels in the infrared and visible part of the spectrum, microwave radiometers operation in the 50 - 57 MHz range, and a stratosphere sounding unit with three radiometer channels round 15 um wawe length, for retrieval of atmospheric parameters, preliminary atmosphere temperature from ground level up to 10 mb level, water vapor content and total ozone content. The Electromagnetic Institute at the Technical University of Denmark has conducted a calculation of the atmosphere temperature profile and the calculation is based upon the data from the Danish Meteorological aerological balloon program in Greenland. The preliminary results, as seen in fig. 8, indicate that in cloudfree areas, temperature can be retrived so far with an RMS error, in the range of 2 - 5°K depending on the pressure level. These results seems not to meet the requirements related to numerical meteorological models, and accordingly improvement is needed.



With this rather sporadic information about US and Danish activities related to Arctic communication navigation and detection systems performed in Greenland I have in no way given a qualified general picture but mainly touched experiments or activities in which I have been more or less personally involved.

The general development trend for the Arctic region cause a demand for still more investigations related to propagation of radiowaves in Arctic regions and such a demand can also in future best be met with in a close international cooperation.

REFERENCES

"A Decade of Joint Upper Atmospheric Research 1975-1985" - Danish Meteorological Institute and Cornell University, School of Electrical Engineering, April 1985.

Bach, H.C. and Taagholt J., "Greenland and the Arctic Regio - Resources and Security policy". The Information Service of the Danish Defence, October 1982, pp.79.

Barcus et al "Observations of Bremsstralung from Solar Electrons in the Earth's Atmosphere". Journal Atm.Terr.Physics. In press.

"Geophysical Research Letters 1984: The Polar Ionosphere - Early Results from Sondre Stromfjord". GRL Vol. 11 No. 9, September 1984, pp 881-942.

Gudmandsen, P. "Application of Microwave Remote Sensing to Studies of Sea Ice", Phil. Trans. Royal Society Lonson, A 309, pp 433-455, 1983.

Jensen, A.P. et al "On the Longitudinale Extension of Electron Precipitation during Magnetospheric Substorms". Zeitschrift für Geophysik, August 1972, pp 851-862.

Johnson, A. et al "Occurrence of F Layer Irregularities in the Polar Cap", Ionospheric Effects Symposium, Alexandria, VA, April, 1981.

Johnson, A. and Taagholt, J. "Ionosphere Effects on C^3I Satellite Communication Systems in Greenland". Presented at the IES Symposium, Alexandria, VA, USA, May 1984.

Journal of Geophysical Research 1980: "Winter 1974/75 - International Rocket Campaign for the Investigation of the Dayside Auroral Oval. JGR Volume 85, June 1980, pp.2891-2940.

Mozer, F.S. "Magnetosperic Electric Field Properties Deduced from Simultaneous Balloon Flights". Journal of Geophysical Research, Vol.76, No.7., March 1, 1971,pp 1697-1712

Olesen, J.K. and Taagholt, J. "Ionosphere Data 1951-1966 Narssarssuaq and Godhavn, Greenland", Ionosphere Laboratory, Technical University of Denmark, January 1968, p.59.

Pedersen, P.O. "The Propagation of Radio Waves along the Surface of the Earth and in the Atmosphere", Danmarks Naturvidenskabelige Samfund - sold by G.E.C. Gad, Copenhagen 1927.

Stockflet Jørgensen, T. "Interpretation of Auroral Hiss Measured on UGO 2 and the Byrd Station in Terms of Incoherent Cerenkov Radiation. Journal of Geophysical Research. Vol 73 No. 3, February 1968, pp. 1055-1069.

Stockflet Jørgensen, T. "On the Naturally Occurring Electromagnetic Noise Called Auroral Hiss". Danish Meteorological Institute, Geophysical Papers R-7, September 1968, p.49.

Taagholt, J. et al "Provisional Investigations of the actual HF Radio Propagation Greenland-Denmark seen in relation to the HF Propagation Prediction". Kleinherbacher Berichte 1973 Band 17. Fernmeldedetechnischen Zentralamt, Darmstadt 1974, pp. 395-401.

Taagholt, J. "Arctic Sea Inspection Technology". The Arctic Hydroagraphic Environment and the Fate of Pollutants. Macmillan, London, U.K. 1982, pp. 393-399.

Taagholt, J. and Jensen, F. "Application of the ARGOS System in Arctic Regions". ARGOS Users Conference, London, UK, September 1983.

Taagholt, J. "SARSAT-COSPAS Experiment", Military-Technical Symposium on Modern Position Location and Navigation, Engineering Society, Copenhagen, Denmark, February 1984.

Aarons, J. et al "UHF Scintillation Activity over Polar Latitudes", Geophysical Research Letters, Vol. 8, No.3, March 1981, pp-277-80.

PROGRESS IN MODELLING THE POLAR IONOSPHERE FROM SOLAR AND MAGNETOSPHERE PARAMETERS

B. J. Watkins, S.-I. Akasofu and C. D. Fry

Geophysical Institute, University of Alaska, Fairbanks, Alaska 99775-0800

1. SUMMARY

Solar and magnetospheric parameters have been used as inputs to a three dimensional ionospheric model covering the polar cap and auroral zone latitudes for heights 120-500 km. The development of this model is reported. Using solar and magnetosphere parameters, the solar radiation and convective electric field structure are defined. Solutions to the momentum and continuity equations for ionization densities are obtained vertically along magnetic field lines as they move under the influence of convective electric fields. This paper also discusses the critical measurements that are needed to use such a model to predict ionospheric conditions at polar regions.

2. INTRODUCTION

This paper presents progress in the development of an ionosphere model with inputs from solar and magnetosphere parameters. Our goal is to predict the real ionosphere as closely as possible.

The model is now applicable to heights 120-500 km and latitudes 50-90 degrees, however this may be extended in future.

While the focus of this paper is on the ionosphere, it is part of a larger geomagnetic storm prediction scheme being developed at the Geophysical Institute. It uses solar observations to compute solar wind parameters velocity, density and magnetic field. These parameters are then used in a magnetosphere model to calculate the size and position of the polar cap and the total polar cap potential. The Figure 1 illustrates the general procedure used. The solar wind code has been developed by Fry (1985). An example of some calculated polar cap configurations for particular interplanetary magnetic field values are shown in Figure 2. Thus, the first inputs for the ionospheric code are, date and time, interplanetary magnetic field, and solar wind velocity. These inputs are shown in Figure 1. The "magnetosphere modeling code" indicated in Figure 1 has been presented by Akasofu and Roederer (1984) and Akasofu et al. (1984) and is used as the second step in generating the magnetosphere electric fields for the ionospheric calculations. In this paper we will discuss how this magnetosphere model is used, the calculation of the electric field from the ε parameter, the electric field model used, and the ionospheric code. The other parameters that may be calculated and are shown in Figure 1 (e.g. auroral oval prediction, AE prediction, etc.) will not be discussed.

We wish to emphasize that this is a first-generation effort to simulate the ionosphere from solar data. It is therefore by no means complete, and is a summary of our progress to date. Several other attempts to model the polar ionosphere have adopted a statistical approach (e.g. Secan and Tassione, 1984). By contrast our effort is based, as far as possible, on the actual large-scale dynamics of the polar plasma motions, and the major physical and chemical processes operating in the ionosphere. Therefore we expect that this approach will eventually prove superior.

Our basic methods are similar to that published earlier by Watkins (1978) and Sojka et al. (1979, 1981). These earlier modelling efforts were focussed primarily on use of models to study ionospheric structures resulting from differing geophysical conditons and the results did not necessarily apply to any specific real situation. The new aspect of this work is the development of a computer code that may be linked to solar, solar wind or magnetosphere parameters for prediction purposes.

3. MODEL INPUT PARAMETERS

In this section, we would like to briefly present the main model inputs used and illustrate how they are used in the model. Their function is to determine the ionospheric convection pattern which is the most critical, and least understood variable in terms of our experimental knowledge of the relevant processes. Other lesser important inputs such as solar-produced ionization and auroral inputs are less important and their methods of calculations have been discussed in several general texts, e.g. Banks and Kockarts (1973).

3.1 Determination of Ionospheric Convection Pattern

Our determination of an ionospheric convection pattern over the polar region follows from several steps. First the interplanetary magnetic field (IMF) is used as an input to a magnetosphere model (Akasofu and Roederer, 1984) which gives the location and size of the polar cap. For our purposes we define the polar cap as the region of open magnetic field lines. The Figure 2 illustrates some possible polar cap configurations for various IMF values. After running this magnetosphere model we determine a best-fit circle to the polar cap. This circle is used as the basis of the electric field model that is derived from two semicircles of charge, positive on the dawn, and negative on the dusk side. The resultant electrostatic potential pattern typically looks like that in Figure 3.

The total cross polar cap potential is determined from the ε parameter that is in turn derived from solar wind observations. The ε parameter is given by

$$\varepsilon = vB^2 \sin^4 (\theta/2) \ell_o^2 \quad (1)$$

where v is the solar wind speed, B is the IMF magnitude, θ is the polar angle of the IMF vector, and ℓ_o is a constant of about 7 earth radii. Reiff et al. (1981) have determined an empirical relationship between ε and the total cross polar cap potential ϕ to be,

$$\phi^2 = 0.93\ \varepsilon - 319 \quad (2)$$

Thus, we are using ε and the IMF (B_i, B_ym B_z components) as our model inputs to generate an electric field pattern using the above relations and the magnetosphere model.

The actual motions of the ionospheric plasma is given by the ExB relation since we are dealing with the collisionless region of the ionosphere. It is important to note that we are solving the problem in the non-rotating magnetosphere frame of reference, magnetic local time and geomagnetic latitude. In this frame there is a tendency for the plasma to corotate around the pole. If this corotation effect is added to the ExB motions, the plasma paths look like those shown in Figure 4. To illustrate the different velocities of plasma at different locations, we have plotted line segments that represent distances travelled in three hours.

4. IONOSPHERE CALCULATIONS

It is assumed that O^+ is the only ion present, then the continuity and momentum equations for O^+ ions are solved vertically along magnetic field lines. The upper boundary condition is an outward O^+ flux of 10^8 cm^{-2} sec^{-1}. A lower boundary condition of chemical equilibrium is chosen. We are able to take into account the effects of neutral gas motions, however at this time we have neglected this by assuming ion and neutral velocities are identical. We will attempt to remove this limitation in future. The recombination time at F-region altitudes is long ($\sim$ 1 1/2 hours) and since horizontal ion velocities are several hundred meters per second, calculation of the ionization density at a given location depends on the past history of the plasma. Our approach is to specify the universal time for the desired results, then to determine from the convection pattern, locations where the plasma originated several hours previously. Then, using an estimate of the vertical ionization profile at the point of origin, we solve the continuity and momentum equations at 5 minute intervals along each plasma path. This finally results in a three-dimensional array of ionization density values. Some sample results are shown in Figures 5 and 6 where we have contoured the peak density. Density values about 2×10^5 cm^{-3} occur on the dayside (top of figures) and lowest nighttime densities are about 1×10^4 cm^{-3}.

Our model so far uses solar ionization as the only source, and chemical recombination as the only loss process for ionization. We have neglected auroral ionization, this is an important source that we will include in figure. The method to calculate the solar ionization production at a given location is through a transformation to the geographic frame, calculation of the solar zenith angle then the solar ionization profile. We are now using a solar production rate appropriate for solar minimum conditions.

5. LIMITATIONS OF MODEL

There are several limitations that will be addressed in future. Briefly, these are listed below.

5.1 Auroral Ionization

This will be included in future and may be estimated from solar conditions or from selected observations.

5.2 Neutral Wind Effects

The neutral wind motions in the auroral zone and polar cap have been observed to approximate the ion motions by Killeen et al. (1985). Through ion-drag, the ions tend to control the neutral gas motions. However, the relatively long time constant (few hours) for momentum exchange frequently results in large differences in ion and neutral velocities. Since the magnetic field lines are in general tilted off vertical, the neutral wind may therefore act to move ionization up or down field lines depending on the wind directions. If ionization is moved upwards where the recombination time is longer, ionization densities will tend to be larger. An illustration of possible effects was shown by Watkins and Richards (1979).

Inclusion of the neutral gas motions in a self-consistent manner is planned for the future.

5.3 Time Dependence

Although the model is time dependent in the sense that we can solve for any time of day or day of year, this is an equilibrium solution, for that particular time. To extend the model to solve for time varying effects, for example as the IMF is changing, would require storage of many convection patterns that apply to the varying conditions. This will require some extensions to our code and substantially more computing time.

6. THE NEED FOR LARGE SCALE E-FIELD OBSERVATIONS

Our model uses a relatively simple representation of the magnetosphere electric fields that is probably unrealistic at times. Unfortunately there are no satellites available now with E-field data for comparison. It would be preferable to use direct observations for the model input or to at least provide some comparisons with actual data. Unfortunately, these large-scale E-fields are probably the most critical factor in the model and are the largest potential source of error. If a satellite with an E-field detector, and/or incoherent-scatter radar(s) could provide real-time E-field data at a few locations, this ionosphere model, when further developed, would be able to provide polar maps of F-region ionization densities.

7. CONCLUSION

In conclusion we have presented our progress to date in modeling the polar cap and auroral zone ionosphere from solar and magnetosphere inputs. With further development we expect to use the model for predicting the three-dimensional time dependent ionosphere. The model is applicable for F-region altitudes and therefore should be useful for HF propagation predictions at high latitudes.

References

1. Akasofu, S.-I., and M. Roederer, Dependence of the polar cap geometry on the IMF, Planet. Space Sci., 32, 111, 1984.
2. Akasofu, S.-I., R. Williams, and M. Roederer, Effects of the passage of an IMF discontinuity on the polar cap geometry and the formation of a polar cap arc, Planet space Sci., 32, 119, 1984.
3. Banks, P. M., and G. Kocharts, Aeronomy, Academic Press, 1973.
4. Fry, C. D., Ph.D. Thesis, University of Alaska, 1985.
5. Killeen, T. L., R. A. Heelis, P. B. Hays, N. W. Spencer, and W. B. Hanson, Neutral motions in the polar thermosphere for northward interplanetary magnetic field, J. Geophys. Res., 12, 159, 1985.
6. Secan, J. A., and Tascione, The 4-D ionospheric objective analysis model, Proceedings of Symposium on the Effect of the Ionosphere on C^3I Systems, May 1984.
7. Sojka, J. J., W. J. Raitt, and R. W. Schunk, Effect of displaced geomagnetic and geographic poles on the high-latitude plasma convection and ionospheric depletions, J. Geophys. Res., 84, 5943, 1979.
8. Watkins, B. J., and P. G. Richards, A theoretical investigation of the role of neutral winds and particle precipitation in the formation of the auroral F-region ionosphere, J. Atmos. Terres. Phys., 41, 179, 1979.

Acknowledgment: This work has been suported by the Air Force Geophysics Lab.

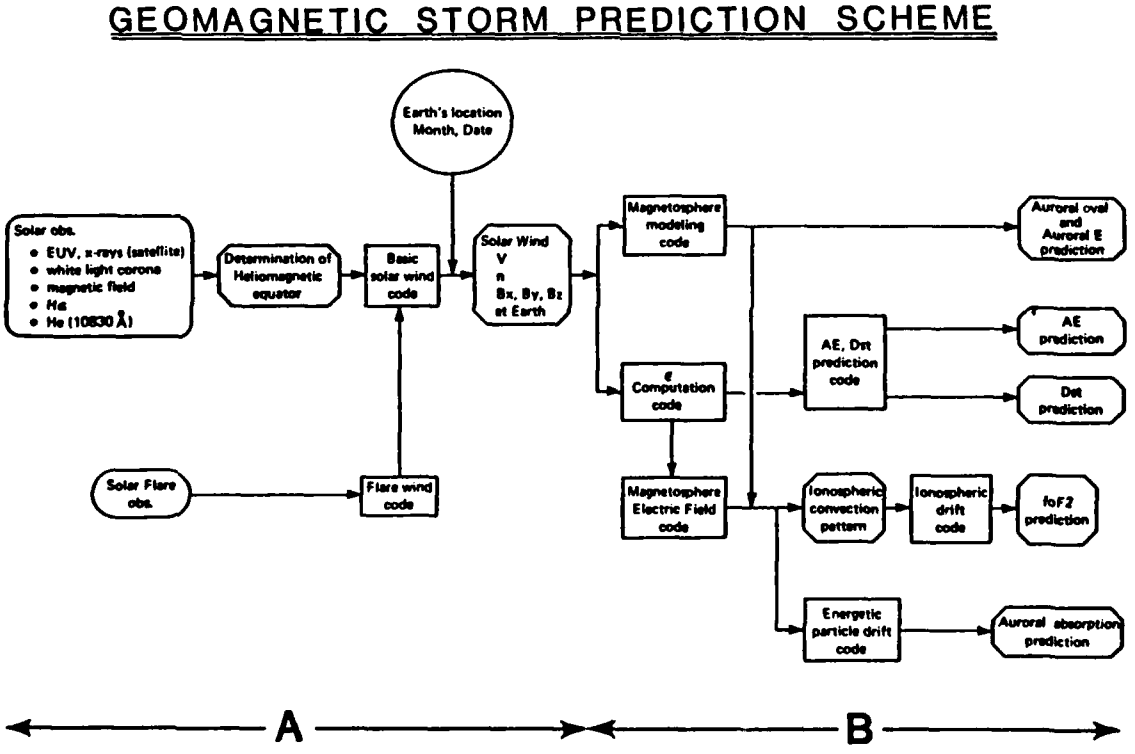


Fig. 1.

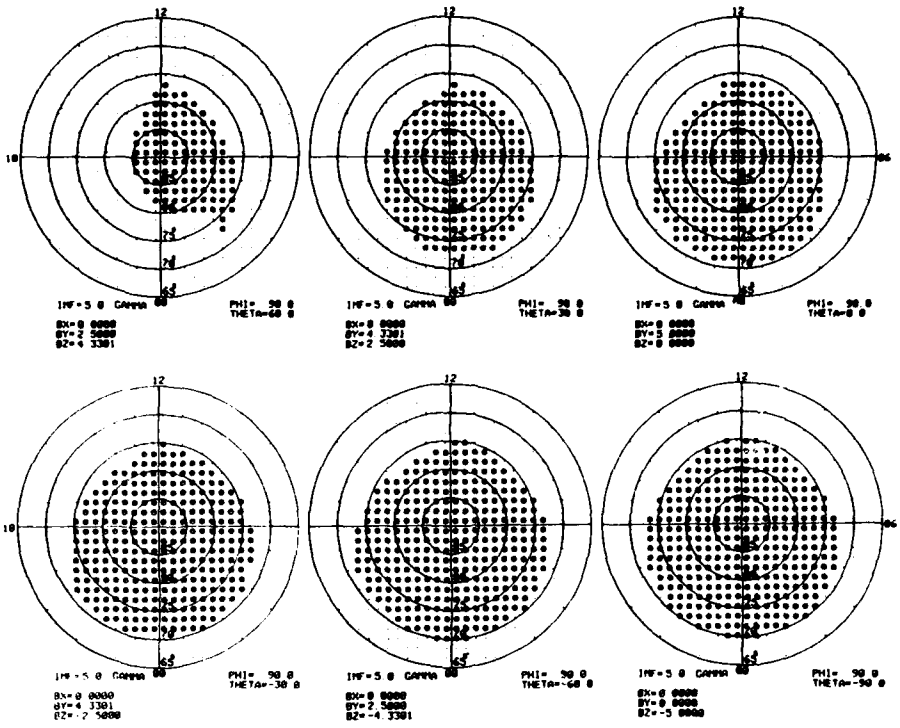


Fig. 2. The geometry of the open field line region for different orientations of the IMF vector in invariant latitude-MLT coordinates. (Akasofu and Roederer, 1984).

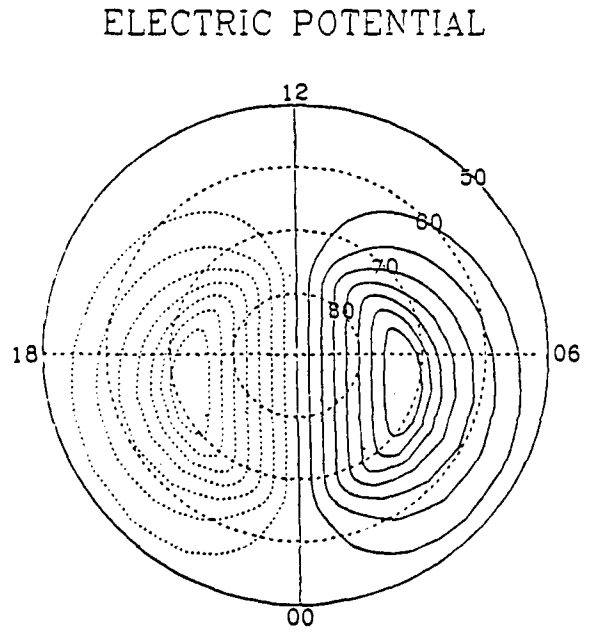


Fig. 3. Contours of electric potential. coordinates are 50-90 degrees invariant latitude and 0-24 hours MLT.

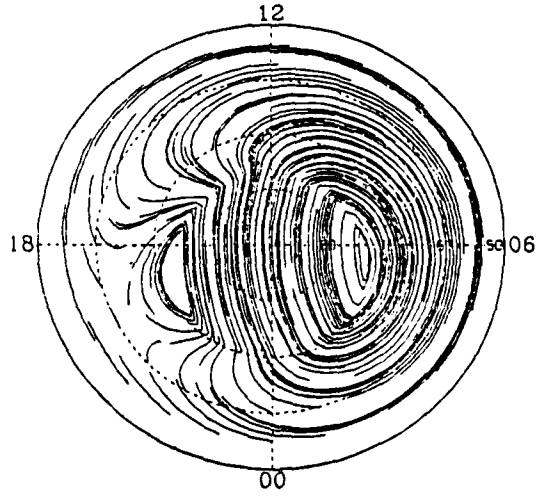


Fig. 4. Contours of electric potential the same as Fig. 3 except that corotation has been added. The line segments represent paths traced by plasma in a 3 hour duration.

DISCUSSION

G.Prolss, GE

Considering that your model is primarily for practical application (prediction purposes) and considering further that many of the input parameters needed for the model are not well known (e.g. neutral winds, composition, convection patterns, etc.) I wonder whether it might not be better to use a more empirical approach by constructing an empirical model of the polar ionosphere?

Author's Reply

At this stage of our model development, a more empirical approach may be better at predicting the real ionosphere. However, this is our first effort. The major limitations will be addressed in our future work. We believe a numerical approach that incorporates the basic physics is worth pursuing. We agree that some inputs are not well known at this time, but future refinements incorporating very new experimental information will help. A major input variable that is not well known, yet very critical, is the large-scale electric field morphology; incoherent scatter radar data are beginning to help with this problem.

T.A.Croft, US

In your work you have three distinct problems: (1) a need for input data from diverse sources; (2) a need for programming modifications; (3) a need for improved knowledge of physics with which to improve the code. From work done so far, can you identify unresolved physics questions that have a significant impact on the accuracy of prediction methods like yours?

Author's Reply

We agree that the input data problem needs to be addressed, especially electric fields. This is our major problem. Programming them is a minor concern. With regard to the physics, we believe the basic physics is understood quite well enough for our purposes, i.e. to predict the major F-region structure. Several papers quoted have been directed to the relevant processes. When we get to the stage of comparison of our model with data, we may choose to include more physics, for example NO+ as well as O+, but at this time the uncertainties in inputs are more important.

B.Reinisch, US

The physical model of the polar ionosphere that you develop is certainly urgently needed. During the last year we measured F-region drifts in the polar cap (Thule) with a spaced antenna Doppler drift system during brief campaigns, and we, indeed, observed the antisunward plasma flow and its diurnal variations. In cooperation with AFGL and DMI we will install a Digisonde at Qanag (Thule) this summer and one of the objectives is to routinely measure the plasma flow. Do you believe that you can use these data as input to your model, or that you can use them for comparison?

Author's Reply

There is certainly a lack of large-scale E-field and/or plasma drift data. Your data would be useful, but should be performed in cooperation with radar experiments at other locations so that the large scale picture can be seen. It is also important to have the IMF data, because the IMF controls the convection pattern.

S.Quegan, UK

QUESTION: At the lower limits of your figures, you are definitely in a region of closed field lines and well into the plasmapause. Under these conditions, the assumption of polar wind outflow is certanly not true... What is the range of validity of your model? COMMENTS: (1) At these trough latitudes, the neutral wind is of critical importance in maintaining the ionosphere, and (2) the degree of penetration of the convection electric field into the plasmapause is poorly known, but is very important for trough dynamics. Realistic modelling requires this information.

Author's Reply

Our model is not applicable to the plasmasphere because of the interchange of ionization between the ionosphere and plasmasphere. The polar wind outflow assumption is valid on closed field lines if those field lines were recently open (because of previous trajectories over polar cap). The lower latitude limit is dependent on the size of the polar cap; for the figures shown, the outflow assumption is valid down to at least 55 degrees on the nightside where the trough is located. We will be including neutral winds in future. Electric fields in the plasmasphere would indeed be a concern, if we extend our model to plasmasphere latitudes.

STATISTICS OF AURORAL RADIO ABSORPTION IN RELATION TO PREDICTION MODELS

J.K. Hargreaves, M.T. Feeney* and C.J. Burns
Department of Environmental Science
University of Lancaster
Bailrigg
Lancaster, LA1 4YQ
England

SUMMARY

The prediction of HF propagation conditions at high latitude requires a knowledge of the statistics of radio absorption in the auroral ionosphere, a highly variable phenomenon depending on local time, magnetic latitude, season and solar activity. Data from riometer stations may be compiled to provide statistics on the auroral radio absorption, and the present paper takes data from Iceland and Scandinavia to consider, in relation to a prediction model, questions such as the probability distribution and variations with latitude, solar and geomagnetic activity, and longitude. Difficulties concerning the smallest absorption values are pointed out.

1. INTRODUCTION

An important factor in predicting HF radio propagation conditions at high latitudes is the amount of absorption in the ionospheric D region; a highly variable quantity since it results principally from energetic particle precipitation whose intensity and distribution are themselves determined, though not in any precisely defined manner, by the level of geophysical disturbance resulting from magnetospheric behaviour energised and somehow triggered by the solar wind. HF radio absorption is thus one practical and undesirable consequence at the end of a long, and somewhat uncertain, chain of events which we may seek to understand but whose ultimate driving force certainly lies beyond our control.

In these circumstances, and particularly when the absorption morphology, as here, is highly structured in both space and time, the most practical approach to prediction is a statistical one which collects past data and attempts to sort and organise the data set in terms of known parameters - time of day, latitude, season, solar or magnetic activity levels, and so on.

The problem of making statistical predictions of the auroral radio absorption has been tackled by a number of workers, notably Agy (1972), Herman and Vargas-Villa (1972), Foppiano (1975), Vondrak et al. (1978), Masi (1980), and Foppiano and Bradley (1984, In press). The data have been taken from riometers which measure the absorption at a radio frequency usually between 20 and 50 MHz by continously monitoring the received intensity of the cosmic radio noise. Strictly, the riometer does not provide what the problem requires since an HF circuit will generally operate at a lower frequency and the signal will pass through the D region much more obliquely. The advantages of basing the data set on riometers are that many data are available which *should be* comparable between different stations operated by different people, and that what purports to be absorption measurements are likely to be just that without significant contamination from other effects. Such data, however, need to be experimentally compared with the performance of HF circuits - and this is more difficult to achieve than the compilation of riometer data.

2. THE FOPPIANO AND BRADLEY MODELS

The problem of statistical predictions breaks into two parts. First is the question of the statistical distribution itself: the probability that various chosen levels of absorption will be exceeded under known conditions of the parameters time-of-day, latitude, etc. This distribution then has to be described by some convenient representation which, hopefully, does not include too many independent parameters. The second part then concerns how these describing parameters themselves depend on the parameters such as time-of-day and latitude.

The papers of Foppiano and Bradley (1984, In press) have addressed these questions. Regarding the statistical distribution, they concluded that it could be described by a log-normal relation of the form

---

* Now at Electrical Engineering Dept., University of Liverpool.

$$f(y) = \frac{1}{\sigma\sqrt{2\pi}} \exp\left[-\frac{(y - y_o)^2}{2\sigma^2}\right] dy$$

where $y = \log(A)$, A being the absorption; y_o is the mean values of y, and σ its standard deviation. One of the describing parameters of the distribution is conveniently taken as Q(1), the probability that 1 dB will be exceeded. In a log-normal distribution,

$$Q(A) = \frac{1}{\sqrt{2\pi}} \int_x^\infty \exp\left[-\frac{x^2}{2}\right] dx = \frac{1}{2}\left[1 - P_x\right]$$

where $x = (y - y_o)/\sigma$ and P_x is the "normal probability integral". Q(1) has become a standard quantity since 1 dB is a level that is readily determined without much error, and is also a level which should produce marked absorption effects (about 20 dB) in a typical HF circuit. The other parameter of the log-normal distribution is really a matter for choice; it can be based on another absorption level such as Q(3) or it can refer to the slope of the distribution which is linear on log-probability paper.

Foppiano and Bradley (In press) consider that Q(1) is formed as the sum of two terms, one peaking in the night sector and the other in the day. Each of these terms is then constructed as the product of several other terms, representing respectively the influence of magnetic latitude, magnetic longitude, local time, season, and sunspot number. Specific relations are given for each term and thus a complete model for Q(1) was developed.

The present paper describes data studies made independently of the foregoing analyses, though with foreknowledge of them, and should be considered as a verification (or otherwise) based on independent data from the European sector.

3. LOG-NORMAL DISTRIBUTION

Hourly absorption values from 30 MHz riometers at Fagurhólsmýri (63.53°N, 16.65°W, L = 5.6) and Siglufjördur (66.15°N, 18.92°W, L = 6.9), both in Iceland, and at Abisko (68.21°N, 18.50°E, L = 5.6) in Sweden were assembled over periods of one month and divided into four, 6-hour periods of the day: 00-05 UT, 06-11 UT, 12-17 UT, and 18-23 UT. Figure 1 shows the data for the winter periods (taken together) for Abisko, plotted on log-probability paper. The threshold marks the level below which the absorption values are not considered accurate. At the higher values, exceeding about 3 dB, there are relatively fewer values. In the middle range of absorption values, the log-normal appears to be a good fit to the data. (We will refer again to the threshold and remark on the small absorption values in Section 6.) When monthly absorption probabilities are plotted in the manner of Figure 1, they also indicate a reasonable fit to the log-normal distribution in the middle range.

Values of Q(1), Q(3), the slope B and the width σ, and A_m the median value have been determined for the 3 stations for each month from Nov 1976 to July 1978, with selection by time of day as above. If we describe the distributions by the pair of values A_m and σ, the conclusion is reached that A_m varies strongly with the monthly mean magnetic activity index $\bar{A}_p$ whereas σ is approximately constant. The best-fit relations for Abisko are given in Table 1. The variation of A_m with $\bar{A}_p$ is strongest in the morning hours.

4. LATITUDE VARIATIONS

The latitude distribution of Q(1) has been studied using hourly absorption values from 6 riometer stations in Finland over the years 1972-1983 (Ranta, 1972-83). The stations are located as in Table 2. For this part of the study the probabilities were assembled over a month at a time but there was no division by time of day.

The Foppiano and Bradley model (In press), following previous studies, adopts a Gaussian form for the latitude variation of Q(1):

$$Q(1) = Q_o \exp\left[-\frac{(\lambda - \lambda_o)^2}{2s^2}\right]$$

The only justification for such a form is if it fits the data, and this appears to be the case, at least for stations not too far from the maximum. The Gaussian is also convenient, being described by only 3 parameters: the maximum value of Q(1), here called Q_o; the magnetic latitude of the maximum, λ_o; and the width of the curve, s. We also adopt this form as the best available for the purpose.

Figure 2 gives examples showing the Gaussian curves fitted for 4 different levels of $\bar{A}_p$. It appears that the Finnish riometer chain barely extends to the statistical

absorption maximum and therefore Q(1) values for latitudes poleward of Kevo are pure extrapolation, not verified in the present analysis. The derived values of λ_o and Q_o might also be questioned, but in fact the λ_o values agree with those from the model (See Table 3), and the obvious levelling of Q(1) at the higher latitude stations gives some confidence in the derived Q_o values. The measure of agreement between observed and model values of Q_o (and of Q(1) for individual stations) depends on the year in question - this point is taken up in Section 5.

The Q(1) values have also been separated by hour of the day and then assembled over the whole period of the data, though retaining the division into 4 $\bar{A}_p$ levels. Gaussian curves were fitted for every hour and then contour maps prepared from these fitted Gaussians. Two stages of smoothing are thereby involved. Figure 3 shows the map for $\bar{A}_p$ = 15-20, which is similar to previous presentations of auroral absorption against latitude and time (Holt et al., 1961 ; Hartz et al., 1963; Driatsky, 1966; Hargreaves and Cowley, 1967). The minimum at 1800-2000 LT shows clearly; this is obviously a well defined feature of the distribution which occurs at all longitudes. The full set of contour maps also shows clearly the intensification and equatorward movement of the daytime maximum with increasing geomagnetic activity. Contours poleward of the maximum in Figure 3 are an extrapolation of the Gaussian curves, and have not been verified in the present study.

5. VARIATIONS WITH SOLAR CYCLE AND MAGNETIC ACTIVITY INDEX

The Foppiano and Bradley model takes account of the sunspot number so as to embody the expectation of more aurora when the sun is more active, with the result that Q(1) values for sunspot maximum are predicted at more than twice those for sunspot minimum. Figure 4 plots daily Q(1) values for Kevo, month by month from 1972 to 1983. Whereas the predictions react to the sunspot number, this is not seen in the data over the long term. The predictions are thus too low in quiet-sun years but nearer the observed average during the years of high sunspot number. At the low latitude end of the chain the sunspot maximum predictions are too large. The physical problem here comes down to the fact that auroral precipitation depends on the solar wind rather than on sunspots directly, and a better way of taking changing solar activity into account may be to use a magnetic activity index (such as A_p) which is also governed by solar wind behaviour and of which predictions are available.

6. UNCERTAINTY IN THE QUIET-DAY CURVE AND THE LONGITUDE EFFECT

A longitude term is included in the model which predicts that Q(1) should vary by a factor of 5 around a longitude circle, and by a factor of 1.7 between Fagurhólsmýri and Abisko, the latter having the greater value. In fact the observed values of Q(1) for these two stations, which are at the same magnetic latitude, are almost the same - See Table 4. Ivalo is only 7° east of Abisko but, according to the model, should have Q(1) 27% greater. In fact the observations (Table 4) indicate a value 47% greater.

The monthly Q(1) values at all three stations are well correlated with each other, as may be seen from Figure 5 and Table 4, but a bias could be introduced through the determination of the quiet-day curves. The data were in fact analysed by two different groups, Fagurólsmýri and Abisko at Lancaster, and Ivalo at Sodankylä. Since it is difficult to conceive of a geophysical mechanism that would cause the absorption to change by 47% over only 7° of longitude, one should ask whether different data handling procedures could cause the differences in the present study, and, by implication, in the model.

Figure 6 takes two log-normal distributions in which Q(1) is respectively 2% and 10%, and with the same typical slope. The solid lines therefore represent two possible absorption distributions assuming that the log-normal form holds. The dashed lines show what happens to these distributions if errors of 0.3 dB are added or subtracted, as if the quiet-day curve were raised or lowered by those amounts. It is seen that in each case the value of Q(1) is changed by nearly a factor of 2. While an error of 0.3 dB may seem rather high (unless the data were of unusually poor quality due to exceptional interference or some equipment problem) smaller uncertainties such as 0.1 or 0.2 dB are indeed possible. In the present case the difference between Ivalo and Abisko could be explained, and thus the present study provides no positive evidence supporting a longitude variation of Q(1) in the Iceland - Finland sector. Whether the factor of 5 predicted in total by the Foppiano model could be explained in this way is another matter, but there could be a contribution to it, particularly since the strong longitudinal gradient predicted for the European sector is caused mainly by the data from one group of stations. Ideally, when data from different stations are to be compared, identically the same reduction procedures should be applied to all. That this may not be possible for stations far separated in longitude makes the determination of longitude effects all the more uncertain.

An "error" in the quiet-day curve has greatest relative effect on the smallest absorption values, producing curvature of the log-normal plot (as in Figure 6). A tendency to curve in the direction of the lines marked "-0.3 dB" is observed in some distributions. On the other hand, the log-normal distribution may not apply at small values. It appears to encounter a theoretical difficulty in that it predicts zero probability of there being zero absorption, and it is questionable whether this is realistic on geophysical grounds. Given the sporadic nature of auroral absorption as a substorm phenomenon, one would surely expect considerable periods during

geomagnetically quiet conditions without energetic precipitation and without auroral radio absorption. For both of these reasons the validity of the log-normal distribution should not be assumed below the range where it has been tested; this does not, of course, prevent its use over the middle range of absorption values where it appears to be rather satisfactory.

7. CONCLUSIONS

1. The probability distribution of auroral radio absorption as measured using riometers follows a log-normal law over a middle range of values between a few decibels and a few tenths of a decibel (at 30 MHz). The law has not been verified for very small nor very large absorption values.

2. If log-normal distributions fitted to data from near the maximum of the absorption zone in the Iceland - Europe sector are described by the median absorption A_m and the standard deviation σ, it is found that A_m varies markedly with the magnetic activity index A_p whereas σ shows no such variation.

3. The latitude distribution of Q(1), the probability of 1 dB being exceeded, can be described by a Gaussian curve between magnetic latitudes 56^0-66^0 (L values 3.3 -6.0). The latitude of the maximum and the width are both in agreement with the Foppiano and Bradley model. Marked changes with A_p are seen.

4. Sunspot number is not a helpful predictor of the magnitude of the absorption; a term based on a magnetic activity index would be more accurate.

5. The longitude effect indicated by previous data is not confirmed. Part of the effect could be due to the use of different data reduction procedures at different observatories.

REFERENCES

V. Agy
AGARD Conference Proceedings No. 97. NATO (1972).

V.M. Driatsky
Study of the space and time distribution of auroral absorption according to observations of the riometer network in the Arctic.
Geomagnetism and Aeronomy 6, 828 (1966).

A.J. Foppiano
A new method for predicting the auroral absorption of HF sky waves.
CCIR Interim Working Party 6/1, Docs. 3 and 10, International Telecommunication Union (1975).

A.J. Foppiano and P.A. Bradley
Day-to-day variability of riometer absorption.
J. Atmos. Terr. Phys. 46, 689 (1984).

A.J. Foppiano and P.A. Bradley
Morphology of background auroral absorption.
J. Atmos. Terr. Phys. (In press).

J.K. Hargreaves and F.C. Cowley
Studies of auroral radio absorption events at three magnetic latitudes. 1. Occurrence and statistical properties of the events.
Planet. Space Sci. 15, 1571 (1967).

T.R. Hartz, L.E. Montbriand and E.L. Vogan
A study of auroral absorption at 30 Mc/S.
Can. J. Phys. 41, 581 (1963).

J.R. Herman and R. Vargas-Villa
Investigation of auroral ionospheric and propagation phenomena related to the Polar Fox II experiment.
Analytical Systems Corporation. Report ASCR-72-62 (1972).

O. Holt, B. Landmark and F. Lied
Analysis of riometer observations obtained during polar radio blackouts.
J. Atmos. Terr. Phys. 23, 229 (1961).

J.L. Masi
Radar studies from Point Barrow, Alaska.
Ph.D. thesis, University of London, England (1980).

H. Ranta
Ionospheric Absorption Data from Finland.
Monthly data reports from Geophysical Observatory, Sodankylä (1972-83).

R.R. Vondrak , G. Smith, V.E. Hatfield, R.T. Tsunoda, V.R. Frank and P.D. Perreault
Chatanika model of the high-latitude ionosphere for application to HF propagation prediction.
Rome Air Development Center Technical Report RADC-TR-78-7 (1978).

ACKNOWLEDGEMENTS

This work has received support from the Royal Aircraft Establishment, Farnborough, and from the Departmental Users' Radio Propagation Programme of the Science and Engineering Research Council in which connections discussions with Dr. P.S. Cannon, L.W. Barclay, P.A. Bradley and Dr. B. Burgess are acknowledged. We appreciate the assistance of Dr. Th. Saemundsson of the University of Iceland with the observations in Iceland (operators S. Kristinsson and O. Jónsson). The work of N.-Å. Andersson at Abisko is appreciated, as is the cooperation of Dr. H. Ranta of Sodankylä in providing data reports and comments.

Table 1 : Equations for A_m and σ

U.T. range (inclusive)	Relation for A_m(dB) in terms of $\bar{A}_p$
00-05	$A_m = 0.0139\ \bar{A}_p - 0.0515 \pm 0.038$
06-11	$A_m = 0.0106\ \bar{A}_p + 0.0096 \pm 0.064$
12-17	$A_m = 0.0051\ \bar{A}_p + 0.0224 \pm 0.034$
18-23	$A_m = 0.0077\ \bar{A}_p + 0.0095 \pm 0.033$

$\sigma = 0.566$

Table 2 : Riometers in Finland

Station	Geographic position		L value
	^{0}N	^{0}E	
Kevo	69.75	27.02	6.0
Ivalo	68.60	27.42	5.5
Sodankylä	67.42	26.40	5.1
Rovaneimi	66.57	25.83	4.8
Oulu	65.10	25.98	4.3
Jyvaskylä	62.40	25.67	3.7
Nurmijärvi	60.52	24.65	3.3

Table 3 : Derived and model values of λ_o, σ and Q_o

Range of $\bar{A}_p$	Derived values λ_o^0	σ^0	Q_o%
0-10	68.1	3.8	5.7
10-15	67.8	3.9	9.3
15-20	66.9	3.6	13.3
20-	65.6	3.6	17.4

For the day sector, which tends to dominate the results, the Foppiano and Bradley model predicts as follows:

Sunspot number (R)	λ_o	σ
0 (min.)	68.0	3.0
100 (max.)	65.3	3.4

Table 4 : Comparison of Q(1) values between Fagurólsmýri, Abisko and Ivalo

	Fag.	Ab.	Iv.
Mean Q(1)	4.8%	5.1%	7.5%
Correlation coefficient with Ivalo	0.8	0.8	

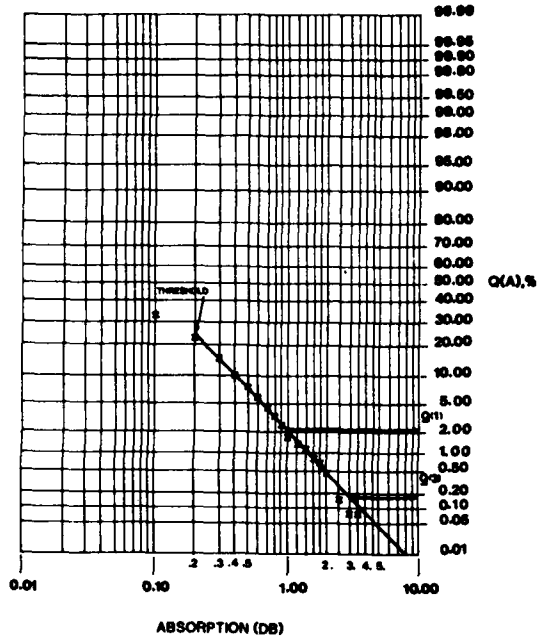


Fig. 1. Log-normal probability distribution of 30 MHz auroral absorption at Abisko, Sweden, for the period 1800-2300 UT during the winters of 1976-78. The probabilities of 1 dB and 3 dB being exceeded are about 2% and 0.15% respectively. Absorption values below 0.2 dB are not considered accurate.

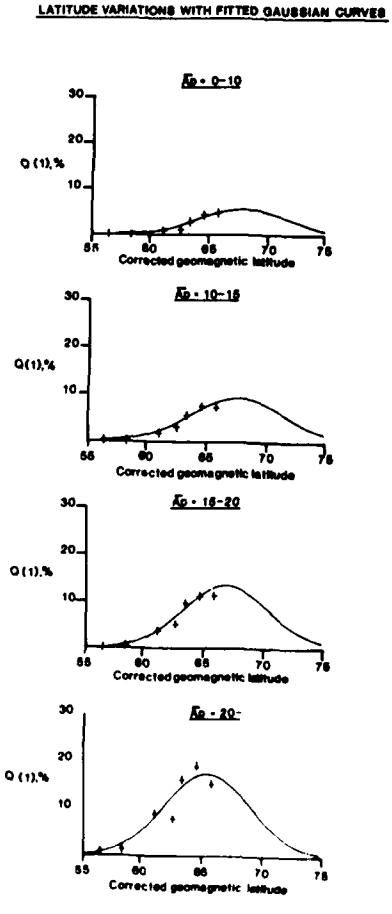


Fig. 2. Latitude variation of Q(1) in Finland for different levels of the monthly mean magnetic activity index, $\bar{A}p$, with fitted Gaussian curves.

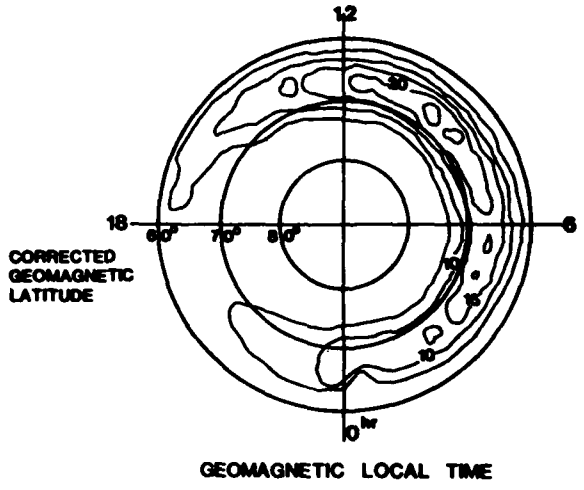


Fig. 3. Contour map showing Q(1) against magnetic latitude and local time for $\bar{A}p$ = 15 to 20.

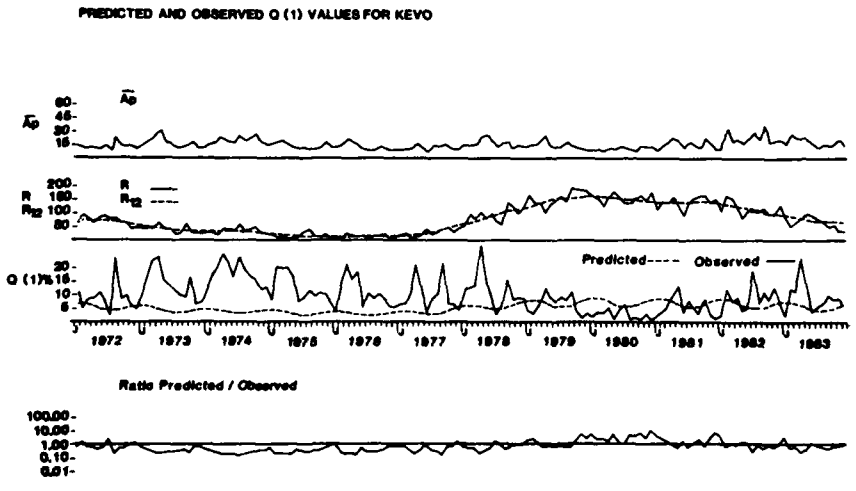


Fig. 4. Observed and predicted Q(1) values for Kevo over a sunspot cycle. $\bar{A}p$ is the monthly mean value of the magnetic activity index Ap. R and R_{12} are respectively the monthly and 12-month running mean sunspot numbers. The ratio of predicted to observed Q(1) value is plotted on a log scale and shows the predictions to be much too low in quiet-sun years.

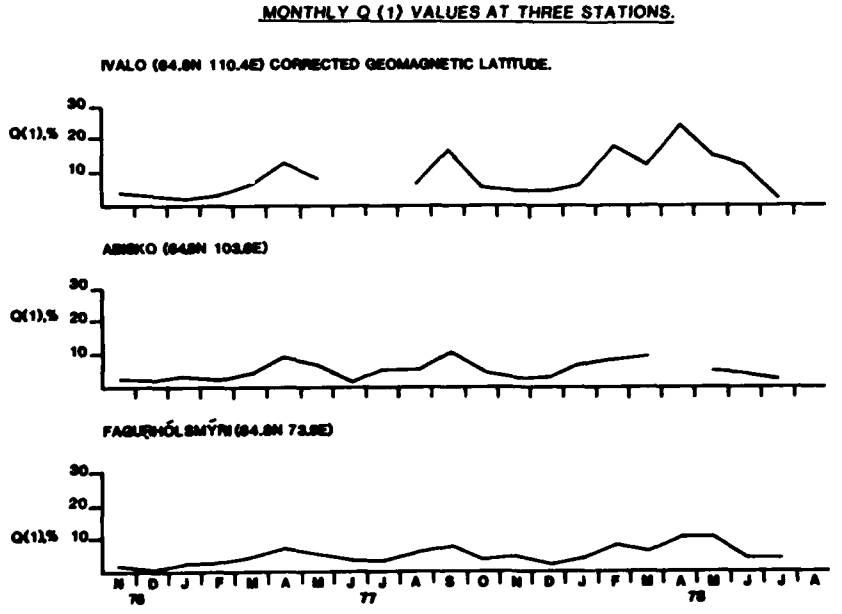


Fig. 5. Comparison of Q(1) values for three stations at the same geomagnetic latitude, November 1976-August 1978.

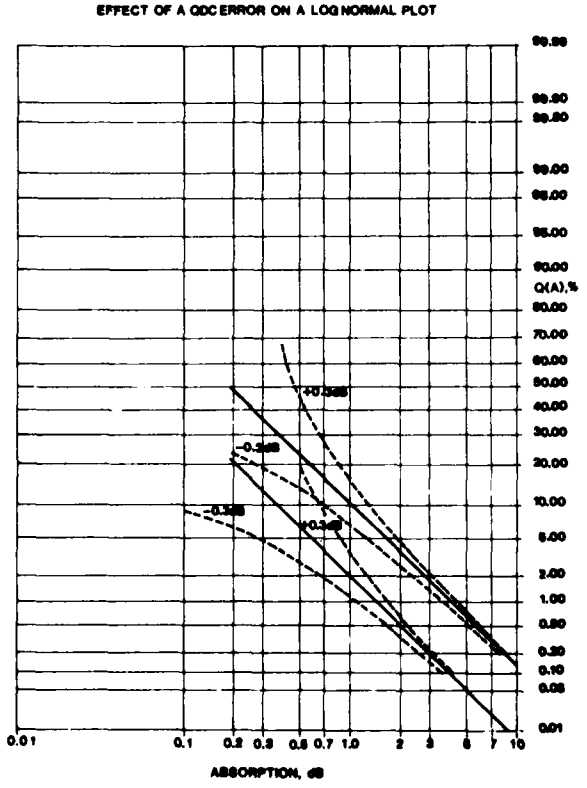


Fig. 6. Construction to illustrate how an error in placing the quiet-day curve affects the derived absorption distribution and Q(1) values.

DISCUSSION

A.Rodger, UK

(1) Your data from Kevo (figure 4 in your paper) shows a very clear semi-annual variation, although, surprisingly, the Ap index does not show this semi-annual variation very clearly as described by (Green, 1984, Planetary and Space Science). Do you consider it worthwhile to include a semi-annual term in your model? COMMENT: From studies of riometer absorption at Siple and Halley in Antarctic, there appears to be about 50% more absorption seen at Halley compared with Siple. These results are considered to be evidence of a very significant longitudinal variation in absorption.

Author's Reply

(1) I think that Ap does contain a semi-annual variation, but whether Q(1) follows that exactly is something we have not looked at. It may be that the established Ap influence already takes this into account, and whether a separate semi-annual term is needed would have to be the subject of a future investigation. (2) I am aware of the Siple-Halley result. A small difference at latitude may show such an effect, but I do not deny the possibility of a longitude effect as well. My point is, that such effects are not always easy to establish reliably from the riometer data.

J.Taagholt, DE

Concerning the uncertainty related to the quiet-day curve I can mention that most of the Danish riometer data are recorded both in analog and digital form, and the digital data can today easily be communicated via geostationary satellites such as METEOSAT or GOES to forecast centers. Today, data are transferred via GOES from Narssarssuaq to Fairbanks via Boulder. Having all the data at a central forecast facility and conducting the data analysis there, might eleminate the effect of individual interpretation and definition of the quiet-day curve.

P.A.Bradley, UK

Does the poor correlation of auroral absorption with sunspot number mean that models of the sort you are discussing should not be used for long term radio circuit and service planning?

Author's Reply

I am not suggesting that there is anything wrong with the concept of the Foppiano and Bradley model, but its accuracy would be improved if the term representing sunspot number dependence were replaced by one depending on geomagnetic activity.

E.Thrane, NO

There exist some work by Oxman & Ranta showing a relation between auroral (riometer) absorption and the direction of the interplanetary magnetic field. Have you considered including such effects in your model?

Author's Reply

I have found such effects myself, too, in conjugate-point studies in the late 1960's. I believe they are more pronounced at the high latitudes, and I agree that they should be included in absorption models.

FORMATION AND DETECTION OF HIGH LATITUDE IONOSPHERIC IRREGULARITIES

M. C. Lee
Research Laboratory of Electronics and
Department of Electrical Engineering and Computer Science
Massachusetts Institute of Technology
Cambridge, Massachusetts 02139, U.S.A.

J. Buchau, H. C. Carlson, Jr., J. A. Klobuchar, E. J. Weber
Ionospheric Physics Division
Air Force Geophysics Laboratory
Hanscom Air Force Base, Massachusetts 01731, U.S.A.

ABSTRACT

Measurements of Total Electron Content(TEC) and airglow variations show that large scale plasma patches appearing in the high-latitude ionosphere have irregular structures evidenced by the satellite phase and amplitude scintillations. Whistler waves, intense quasi-DC electric field, and atmospheric gravity waves can become potential sources of various plasma instabilities. The role of thermal effects in generating ionospheric irregularities by these sources is discussed in this paper. Meter-scale irregularities in the ionospheric E and F regions can be excited parametrically with lower hybrid waves by intense whistler waves. Ohmic dissipation of Pedersen current in the electron gas is able to create ionospheric F region irregularities in plasma blobs or plasma patches (i.e., high ambient plasma density environment) with broad scale lengths ranging from tens of meters to a few kilometers. Through the neutral-charged particle collisions, gravity waves can excite large-scale (> tens of kilometers) ionospheric irregularities simultaneously with forced ion acoustic modes in the E region. The large-scale ionospheric density fluctuations produced in the E region can extend subsequently along the earth's magnetic field to the F region and the topside ionospheric regions. These mechanisms characterized by various thermal effects can contribute additively with other processes to the formation of ionospheric irregularities in the high latitude region.

1. INTRODUCTION

Coordinated experiments using optical and radio waves (digital ionosonde, satellite phase and amplitude scintillation, total electron content, incoherent scatter radar) and in situ measurements have been conducted over the past five years to investigate the large scale structures and dynamics of the high latitude ionosphere and the relation of these to ionospheric irregularities (see, e.g., the 1983 November-December issue of Radio Science: the John Hopkins Applied Physics Laboratory APL Technical Digest(vol. 5, No. 2, 1984): the HILAT satellite; Buchau et at., 1983; Carlson et al., 1984; Klobuchar et al., 1984; Weber and Buchau, 1985). Active research also has been carried out theoretically on the causes of high latitude ionospheric irregularities (e.g., Fejer and Kelley, 1980; Keskinen and Ossakow, 1983). There are various sources that can potentially perturb the high latitude ionosphere, such as particle precipitation, intense quasi-DC electric field probably of magnetospheric origin, plasma instabilities, and atmospheric gravity waves.

The purpose of this paper is to discuss several processes causing plasma temperature perturbations (δT) and the subsequent coupling to plasma density fluctuations (δn) that are, at least in part, responsible for the occurrence of irregularities in the high latitude ionosphere. The thermal pressure force that results from the plasma temperature perturbations provides the nonlinearity of plasma instabilities for exciting ionospheric irregularites as exactly or nearly zero frequency modes. Since the plasma instabilities under consideration are characterized by thermal effects, we term them "thermal plasma instabilities" to distinguish them from those discussed widely in the literature like the Farley-Buneman instability, the $E \times B$ (or gradient drift) instability, the current convective instability, etc.

Among many potential sources of plasma instabilities at high latitudes, we single out for discussion the whistler waves, the atmospheric gravity waves, and the quasi-DC electric field. These whistler waves and gravity waves may originate in natural processes, such as particle precipitation and lightning strokes. The whistler waves may even be man-made, because the injected VLF waves from ground stations change from linear to circular polarization (i.e., whistler mode) on their paths through the neutral atmosphere and into the ionosphere (Kintner et al., 1981). Significant ionospheric and magnetospheric disturbances can be introduced by this man-made source (Lee and Kuo, 1984 (a) & (b)). It has been found that some particle precipitation events were linked to the VLF wave-injection from Russian stations (Koons et al., 1981). Therefore, some events of artificial particle precipitation were probably mis-identified to be cases of natural processes in the past.

Ionospheric irregularities, that are produced by the Whistler waves, the quasi-DC electric field, and the atmospheric gravity waves, have different scale lengths. They range, in order, from a few meters to a few tens of meters, from tens of meters to a few kilometers, and from probably tens of kilometers to a few hundreds of kilometers. Although generated by different sources, these ionospheric irregularities have some characteristics in common: (1) they are field-aligned zero frequency modes, and (2) they are nonlinearly driven by thermal pressure force resulting from different thermal effects. Presented in the following three sections (i.e., Section 2-4) are the generation mechanisms of ionospheric irregualrities due to the thermal effects caused by the whistler wave-plasma interaction, the Ohmic dissipation of Pedersen current driven by cross-field electric field in the electron gas, and the gravity wave-plasma interaction, respectively. The presentation centers on the description of the physics and observations rather than the detailed mathematical formulation. Main results of the theories are summarized for a quantitative analysis. Finally drawn in Section 5 are the conclusions.

2. SHORT-SCALE IONOSPHERIC IRREGULARITIES

Particle precipitation, lightning strokes, and the injected VLF waves can produce whistler waves that, if intense enough,

excite short-lived short-scale (i.e., meters and tens of meters) plasma density irregularities with zero frequency in the high latitude ionosphere. Lower hybrid wave turbulene with the same perpendicular scale lengths can be concomitantly generated. These locally excited lower hybrid waves are able to propagate along but not across the earth's magnetic field, because a standing wave pattern is maintained in the transverse direction.

This generation mechanism of ionospheric irregularities involves a four-wave interaction process that can be represented by the following wave frequency (ω) and wave vector ($\bar{k}$) matching relactions:

$$\omega_+ - \omega_s = \omega_w = \omega_- + \omega_s^*$$

$$\bar{k}_+ - \bar{k}_s = \bar{k}_w = \bar{k}_- + \bar{k}_s$$

where the subscripts w, $-$ ($+$) and s denote the whistler wave, the Stokes (the anti-Stokes) component of the excited lower hybrid waves, and the excited low frequency mode, respectively; $*$ means the complex conjugate. The low frequency mode is assumed to have a space-time dependence of the $exp[i(\bar{k}_s \cdot \bar{r} - \omega_s t)]$ form. For simplicity, the whistler wave is considered as a ducted mode propagating along the geomagnetic field ($\bar{B}_o$), that is, $\bar{k}_w // \bar{B}_o$. The low frequency mode is magnetic field aligned because the simultaneously excited lower hybrid waves have the field-aligned nature, namely, $\bar{k}_s \perp \bar{B}_o$, and $\lambda_s (= 2\pi/k_s) << \lambda_w (= 2\pi/k_w)$. Therefore, the perpendicular and the parallel wavelenghts of the lower hybrid waves are identical to the scale length (λ_s) of the low frequency mode and the wavelength (λ_w) of the ducted whistler wave, respectively. Both the Stokes and the anti-Stokes components of the lower hybrid waves are involved because the low frequency mode (associated with the excited ionospheric irregularities) is a purely growing (i.e., zero frequency) mode, viz., $\omega_s = i\gamma$ and hence $R_e(\omega_\pm) = \omega_w$, where γ is the growth rate of the plasma instability excited by the whistler wave.

When the whistler wave interacts with the ionospheric plasmas, three types of nonlinear effect result and determine the excitation of ionospheric irregularities. They are the non-oscillatory beating current, the ponderomotive force, and the thermal pressure force, that appear in the linearized electron or ion continuity equation, momentum equation, and energy equation, respectively.

The relative importance of these three nonlinear effects depends upon the scale lengths (λ_s) of the instability and the whistler wave frequency (ω_w). In the excitation of field-aligned modes in the ionosphere, the ponderomotive force has been found to be generally small than the thermal pressure force by a factor of $k_s^{-2} r_e^{-2}$ if the scale lengths ($\lambda_s = 2\pi/k_s$) is less than $\pi r_e (2M/m)^{1/2} \sim 15$ meters or by a factor of $(M/2m)$ otherwise (Kuo et al., 1983; Lee and Kuo, 1983) where r_e is the electron gyroradius. The proposed instability can be excited by whistler waves in a broad frequency domain. This frequency domain has a narrow portion: $\omega_{LH}[1 + (M/m)(V_{te}^2/C^2)(\omega_{pe}^2/\Omega_e^2)]^{1/2} < \omega_w < \omega_{pi}$ and a wide portion: $\omega_{pi} < \omega_w << \Omega_e$, wherein the non-oscillatory beating current and the thermal pressure force are the larger nonlinear effect, respectively. The parameters, ω_{pe} (ω_{pi}), V_{te}, Ω_e, C, and ω_{LH} have their conventional meanings of the electron (ion) plasma frequency, the electron thermal velocity, the electron gyrofrequency, the speed of light in vacuum, and the lower hybrid resonance frequency defined by $\omega_{pi}/[1 + (\omega_{pe}^2/\Omega_e^2)]^{1/2}$.

Although the lower hybrid waves involve both electron and ion dynamics, nonlinear effects in the ion gas are less than those in the electron gas by, at least, a factor of $(M/m)^{1/2} \sim 200$ in the whistler wave frequency range of interest, i.e., $\Omega_i << \omega_w << \Omega_e$, where Ω_i is the ion gyrofrequency. Even ions acquire energy from electrons through collisions, this energy gain and the differential Ohmic heating of ions by the whistler wave and the lower hybrid waves do not cause significant ion temperature perturbations because of the relatively large ion cross-field diffusion loss. It is, therefore, reasonable to neglect ion nonlinearities in the analysis of the instability. The detailed formulation of the instability is given in Lee and Kuo (1984b). Here we just elucidate the physical process with the aid of block diagrams and summarize the main results to examine the operation of this instability in the high latitude ionosphere.

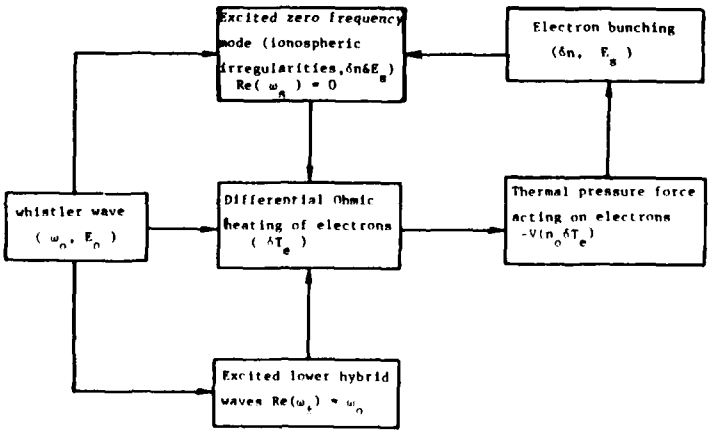


Figure 1 A positive feedback loop of the thermal instability excited by whistler waves

As illustrated in Figure 1, the whistler wave $(\omega_w, \bar{E}_w)$ acts as a pump to excite the lower hybrid waves $(R_r(\omega_\pm) = \omega_w)$ and a zero frequency mode $(R_r(\omega_r) = 0)$ via a thermal instability. The lower hybrid waves are quasi-eigenmodes of the ionosphere, experiencing collisional damping. Whereas, the zero frequency mode is not an eigenmode but a non-linearly driven mode in the ionosphere. The lower hybrid waves and the zero frequency mode can be parametrically excited at the expense of the whistler wave. The specific physical picture is as follows. The differential Ohmic heating of charged particles by the whistler wave and the lower hybrid waves causes significant temperature perturbations (δT_e) in the electron gas rather than the ion gas. A thermal pressure force $(-\nabla n_e \delta T_e)$ thus formed acts on electrons only and results in charge separation $(e\delta n)$. A self-consistent electric field $(\bar{E}_s)$ induced by the electron bunching (δn) causes the ambipolar diffusion of electrons and ions and maintains the quasi-neutrality plasma condition. The plasma density perturbation (δn), thus caused leads to the non-uniform Ohmic dissipation of the whistler wave and the lower hybrid waves, that yields the electron temperature perturbations in turn. These processes represent a positive feedback loop for the thermal instability.

The excitation of this instability requires a threshold. It originates in the fact that the zero frequency mode is a nonlinearly driven mode rather than an eigenmode of the ionosphere. This off-resonance detuning effect turns out to be much more important than the collisional damping of lower hybrid waves. It should be pointed out that electron-ion collisions do not damp the zero frequency mode because electrons and ions move together in the wave vector direction. On one hand, electron-ion collisions cause the Ohmic loss of lower hybrid waves, but on the other hand they bring in a nonlinear heating force (i.e., the thermal pressure force) for exciting the zero frequency mode (i.e., ionospheric irregularities). The optimum excitation of the instability occurs when the whistler wave (ω_w) is slightly off-resonance with the lower hybrid waves (ω_r), viz.,

$$\omega_w^2 = \omega_r^2 + (\nu_r^2 \omega_{LH}^2 / \Omega_e \Omega_i) \left[-R + (R^2 + \omega_r^2/\nu_r^2)^{1/2} \right] \tag{1}$$

where $\omega_r = \omega_{LH}[1 + (M/m)(k_w/k_s)^2]$ is the dispersion relation of lower hybrid waves; $R = 1 + |k_s^2 V_{te}^2 \omega_r / 2\Omega_e \nu_r^2 \eta|/|1 - 1.75 k_s^2 V_{te}^2/\Omega_e \omega_r|$ where $\eta = |1 + (M/m)(k_w/k_s)^2|/|1 - (M/m)(k_w/k_s)^2(\Omega_e/\omega_{pe})^2|$. The minimum threshold field of the whistler wave is found to be

$$E_m = (1.5\nu_r/\Omega_e)^{1/2}(m/e)k_s V_{te}^2 \frac{\left\{ \left[1 + (\nu_r R/\omega_r)^2 \right] - \nu_r R/\omega_r \right\}^{1/2}}{|1 - 1.75 k_s^2 V_{te}^2/\Omega_e \omega_r|^{1/2}} \tag{2}$$

In terms of E_m, the optimum growth rates of the instability has the following expressions:

$$\gamma \sim 0.5 (\nu_r k_s^2 V_{te}^2/\Omega_e^2) [E_R^2 - \quad] \quad for\ E_R^2 << 10 \tag{3a}$$

$$\gamma \sim 1.4 (\nu_r k_s^2 V_{te}^2/\Omega_e^2) E_R \qquad for\ E_R^2 >> 10 \tag{3b}$$

where E_R is the ratio of the whistler wave field intensity (E_w) to the minimum threshold field (E_m).

The generation of ionospheric irregularities by whistler waves is first examined with the following E region parameters: $m/M(NO^+) = 1.8 \times 10^{-5}$, $\Omega_e/2\pi = 1.4\ MHz$, $\omega_{pe}/2\pi = 3\ MHz$ (or $\omega_{pe}/2\pi = 12.8\ KHz$, i.e., $n_e = 1.1 \times 10^{11}\ m^{-3}$), $V_{te} = 6.6 \times 10^4\ m/sec$ (i.e., $T_e = 300^oK$), $\omega_{LH}/2\pi = 5.4\ KHz$, and $\nu_r \simeq \nu_{en} \simeq 1.0\ KHz$. Plotted in Figure (2a) are the threshold fields (curve A) of whistler waves and the scale lengths (curve B) of ionospheric irregularities as a function of whistler wave frequencies. It is seen that irregularities with scale lenghts ranging, for instance, from 2- to 35- meters can be produced by whistler waves in the frequency range from 5.7- to 140 - KHz. The threshold fields are less than 1 mV/m and are generally higher for exciting shorter-scale irregularities. However, the growth rates of irregularities as shown in Figure 2(b) decrease monotonically with the scale lengths because they are proportional inversely to the squared scale lengths (see 3(a) and 3 (b)). Meter-scale irregularities can be generated in a few tenths of a second in the ionospheric E region even if the whistler wave field intensities are a few mV/m.

Displayed in Figure 3(a) and 3(b) are the characteristics of the whistler wave-induced irregularities in the F region, whose parameters are taken to be: $m/M(O^+) = 3.4 \times 10^{-5}$, $\Omega_e/2\pi = 1.4\ MHz$, $\omega_{pe}/2\pi = 10\ MHz$ (or $\omega_{pe}/2\pi = 58.3\ KHz$, i.e., $n_e = 1.25 \times 10^{12}\ m^{-3}$), $V_{te} = 1.2 \times 10^5\ m/sec$, $\omega_{LH}/2\pi = 8.1\ KHz$, and $\nu_r \sim \nu_{in} \sim 1.0\ KHz$. The F region irregularities, that are excited by whistler waves in the same frequency range $(\sim 9 - 140\ KHz)$ have shorter scale lenghts $(\sim 1 - 10$ meters) compared with the E region irregularities. Although higher thresholds $(\sim 3\ mV/m)$ are required, the F region irregularities have larger growth rates. For example, meter-scale irregularities can be excited within tens of milli-seconds by whistler waves with intensities greater than $\sim 10\ mV/m$.

The range of irregularity scale lengths depends upon the frequencies and intensities of whistler waves as well as the life time of whistler wave sources. Most lightning-induced whistler wave energy was found in the 1.6 - to 10 - KHz range with a peak at 5 KHz (Helliwell, 1965; Siefring and Kelley, 1983). Whistler waves were seen to stay in a given range of frequencies for a few tenths of a second. The field intensities of lightning-induced whistlers can be much greater than 1 mV/m (R.A. Helliwell, private communication, 1984). Presumably, the whistler waves of particle precipitation origin have a broad range of frequencies and also have field strengths significantly larger than 1 mV/m. Then, meter-scale irregularities can be favorably excited by whistler waves in both the E and the F ionospheric regions in less than a second. Tens of meter-scale irregularities can also be produced especially in the E region. While field-aligned short-scale irregularities will die out within seconds after the source(s) of whistler waves disappear, tens of meter-scale irregularities can probably survive for a few minutes. These short-lived, short-scale irregularities should be easily sensed by the radar backscatter technique.

Some experimental evidence, that indicates the excitation of proposed instability, namely, the whistler wave-produced

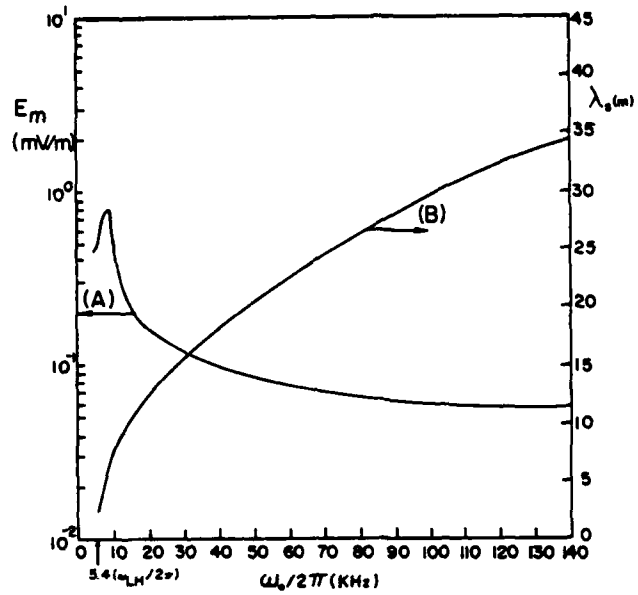


Figure (2a). Threshold fields, E_m (curve A) of whistler waves and scale lengths, λ_s (curve B) of ionospheric irregularities as a function of wshitler wave frequencites ($\omega_s/2\pi$) in the ionospheric E region.

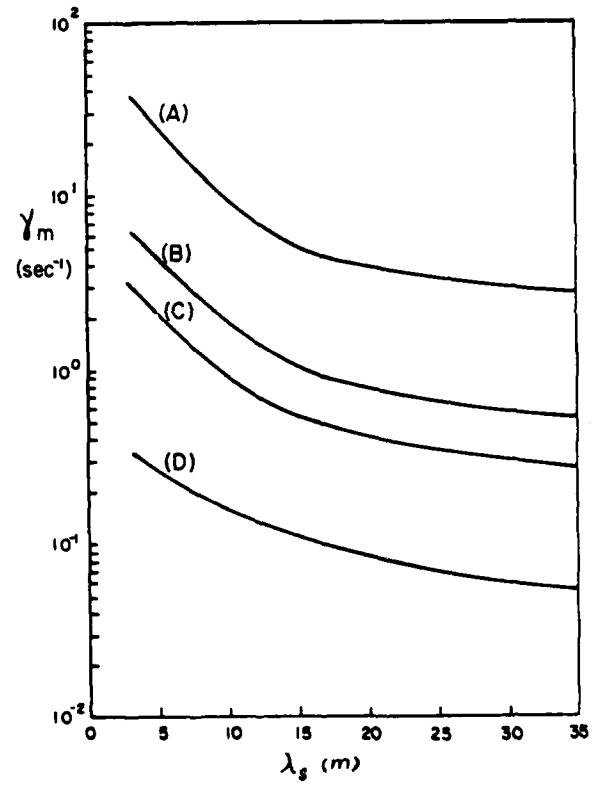


Figure (2b). Growth rates (γ_m) of irregularities in the E region as a function of scale lengths (γ_s) for the whistler wave field intensities (E_s) of (A) 50 mV/m (B) 10 mV/m (C) 5 mV/m and (D) 1 mV/m.

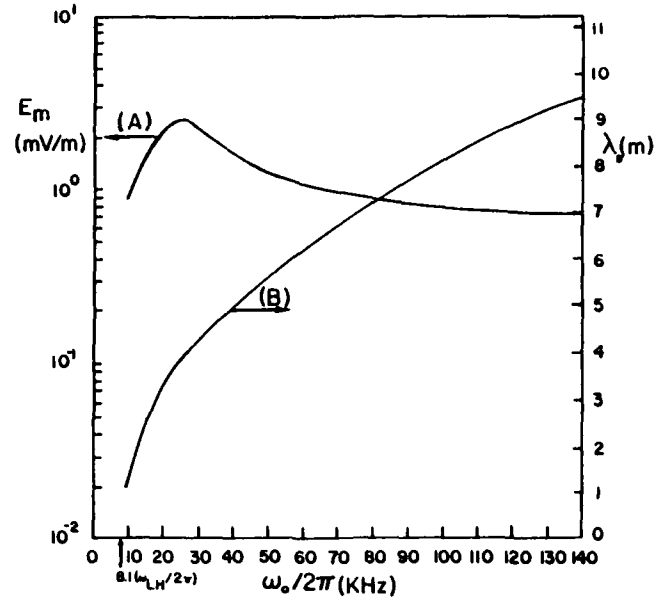


Figure (3a). Threshold fields, E_m (curve A) of Whistler waves and scale lengths, λ_s (curve B) of ionospheric irregularities as a function of whistler wave frequencies ($\omega_o/2\pi$) in the ionospheric F region.

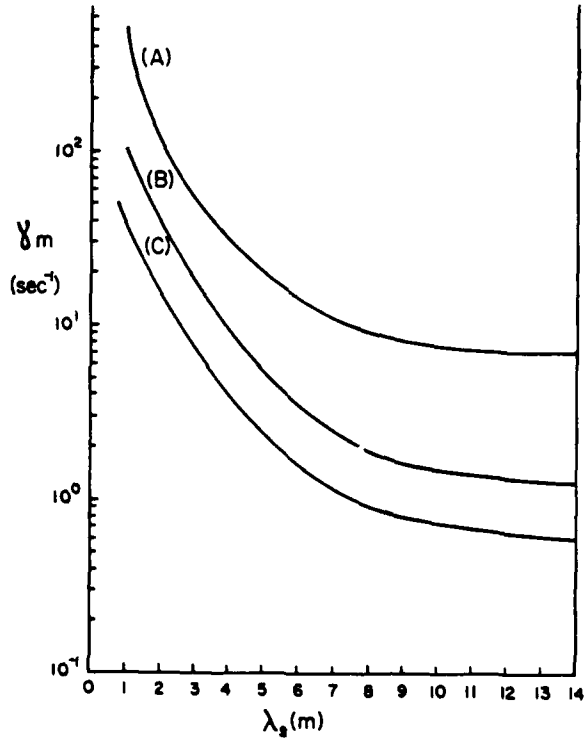


Figure (3b). Growth rates (γ_m) of irregularities in the F region as a function of scale lengths (λ_s) for the whistler wave field intensities (E_o) of (A) 50 mV/m (B) 10 mV/m (C) 5 mV/m.

lower hybrid waves and meter-scale ionospheric irregularities, has been found. For instance, "explosive type" of 3-meter scale irregularities was detected by the Jicamarca VHF (50 MHz) radar in the nightime F region during lightning storms (Woodman, 1984; LaHoz and Haerendel, 1984). The radar signals had rapid rise time and decayed fast. Strong signals near the lower hybrid resonance frequency were recorded during thunderstorms by a rocket in the nighttime E region (Siefring and Kelley, 1983). In experiments on the Franco-Soviet ARCAD 3 satellite, signals around the lower hybrid frequency were also detected at times when the satellite passed over a powerful VLF (15.0 KHz) transmitter located at L = 4.0 in the USSR (Berthelier et al., 1982). The airglow effects connected with the VLF transmitter cycle (Chmyrev et al., 1976) were possibly related to electron acceleration by the VLF wave-excited lower hybrid wave turbulence.

3. MEDIUM-SCALE IONOSPHERIC IRREGULARITIES

The presence of intense quasi-DC electric field (typically, tens of mV/m) at high latitudes is evidenced by large plasma drift velocities (e.g., Weber et al., 1984). Combined with the northward (southward) plasma density gradient (∇n_o), the eastward (westward) DC electric field ($\bar{E}_o$) provides the source of free energy for exciting the $E \times B$ instability in the high latitude ionosphere (see e.g., Vickrey et al., 1980; Kelley et al., 1982). By contrast, a thermal instability discussed in this section can be favorably excited in the high ionospheric density environment (i.e., plasma blobs or plasma patches) in the presence of large quasi-DC electric field (Lee, 1984; Lee and Klobuchar, 1984). While the $E \times B$ instability operates only near the edge of plasma blobs (i.e., ionization enhancement) or plasma patches, the thermal instability can structure ionospheric irregularities throughout the region of plasma enhancement. The AFGL coordinated measurements of TEC and airglow variations performed in Thule, Greenland clearly show the appearance of large-scale (typically, a few hundreds of kilometers) plasma patches in the polar region. Shown in Figure 4 are the TEC data recorded for two successive days,

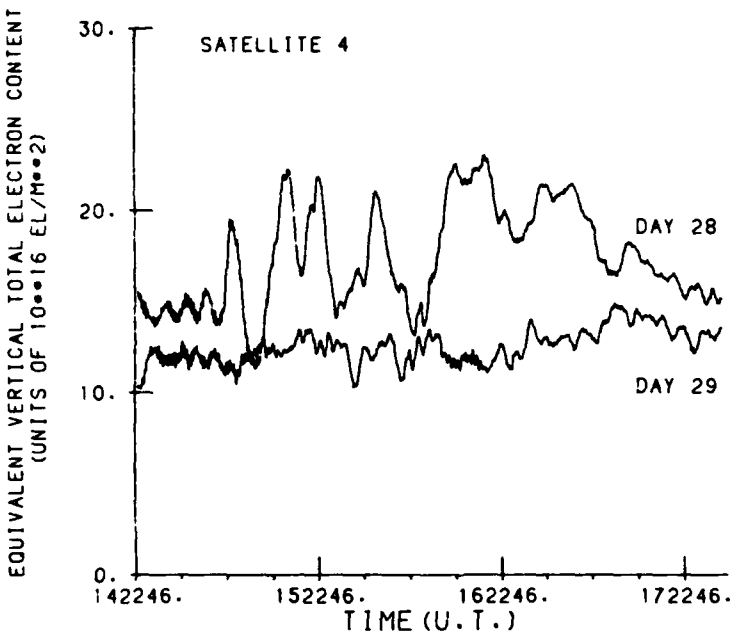


Figure 4. TEC measurements in Thule, Greenland for two successive days (January 28 and 29, 1984), contrasting the large TEC variation in the presence of plasma patches with that in the absence of plasma patches.

contrasting the large TEC variation in the presence of plasma patches (ionization enhancement with horizontal demension of, typically, hundreds of kilometers) with that in the absence of plasma patches. The all-sky photometer images in Figure 5 show a group of sun-aligned arcs and a large plasma patch. The arcs are sun-aligned and extend across the whole field of view, with widths varying between 50 and 150 kilometers; patch diameters range typically from 100 km up to 1000 km. Both of these features, observed close to solar maximum, produced severe (> 25 dB) scintillations on 250 MHz signals. These large-scale plasma patches were not locally generated but were most likely convected from the mid-latitude ionosphere.

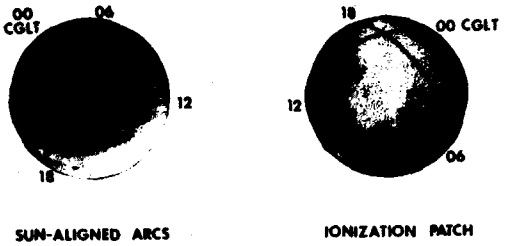


Figure 5. Typical 6300-Å(O I) images of several polar cap F layer aurosal arcs (left) and a large, 1000-km-diameter ionization patch (right), obtained with an all-sky imaging photometer. Corrected geomagnetic (CG) noon/midnight and dawn/dusk meridians are projected into the images at a height of 250 km. The intersection of the meridians is the CG pole. The left image shows clearly the sun-aligned nature of the F layer arcs.

The thermal instability of present interest is caused by the Ohmic dissipation of Pedersen current in the electron gas, driven by the cross-field quasi-DC electric field. This Ohmic process (Q_e), as a consequence of electron-ion collisions, includes the heat generation and the heat loss represented by $\bar{E}_\perp \cdot \bar{J}_P (= J_P^2/\sigma_P)$ and $-3N_e(m/M)\nu_{ei}(T_e - T_i)$, respectively, viz.,

$$Q_e = J_P^2/\sigma_P - 3N_e(m/M)\nu_{ei}(T_e - T_i) \tag{4}$$

where $J_P (= \sigma_P E_\perp)$ and $\sigma_P (= N_e e^2 \nu_{ei}/m\Omega_i^2)$ are the Pedersen current density and the electron cross-field conductivity due to electron-ion collisions. The heat loss arises from the ion-neutral collisions, through which the energy acquired by ions via electron-ion collisions is transferred to neutrals subsequently. The neutrals act as a sink to remove energy directly (indirectly) from ions (electrons). This energy loss process weakens the heat source and inhibits ion temperature perturbations (i.e., $\delta T_i \sim 0$) though electron temperature perturbations (δT_e) are significant. Our detailed analysis (Lee, 1984; Lee and Klobuchar, 1984) shows that the threshold condition of the instability is determined by the balance between the heat *generation rate and the heat loss rate.*

A physical picture is presented in Figure 6, that explains how the electron temperature perturbations (δT_e) caused by the Ohmic dissipation of the DC electric field driven current can couple the plasma density fluctuations (δn). As explained before, the Ohmic dissipation of Pedersen current in the electron gas only introduces electron temperature perturbations (δT_e). The resultant thermal pressure force ($-\nabla(n_e \delta T_e)$) acts on electrons and renders electron bunching (δn). The induced plasma density fluctuations (i.e., ionospheric irregularities) causes perturbations in the Ohmic dissipation rate (Q_e) and, consequnetly, gives rise to electron temperature perturbations (δT_e). This positive feedback loop ensures the excitation of the thermal instability.

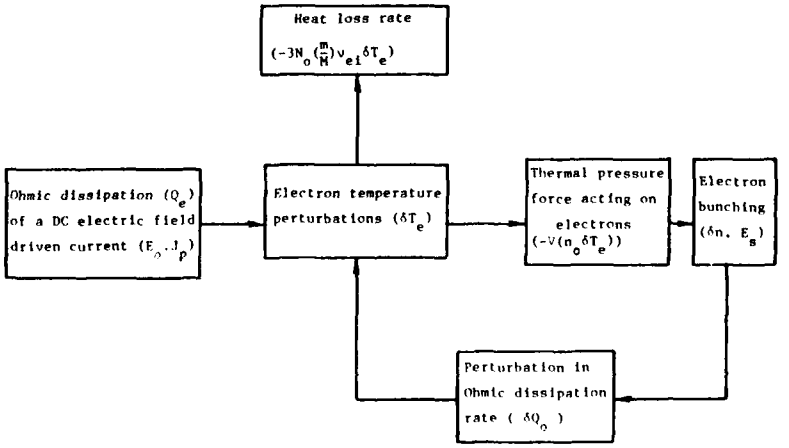


Figure 6 Ohmic dissipation of a cross-field DC electric field driven current leading to the excitation of a thermal instability.

Electron-ion collisions play a key role in generating ionospheric irregularities via the present thermal instability. Their important function has three aspects. (1) Electron-ion collisions cause the Ohmic dissipation of Pedersen current in the electron gas as the source of the thermal instability. (2) The threshold of the instability is determinded by electron-ion collisions. through which, as an intermediate step, energy is transferred from electrons to neutrals as energy sinks. (3) The scale lengths of the excited ionospheric irregularities are also determined by the electron-ion collision frequency. Two scale-length regimes have been found: one is from tens of meters up to hundreds of meters (Regime I), and the other one is from hundreds of meters up to a few kilometers (Regime II). They are discussed separately as follows.

Regime I:

$$\frac{D_{\parallel}^{i}}{D_{\perp}^{i}} << 1 \qquad or \qquad \frac{\lambda_{\perp}^{2}}{\lambda_{\parallel}^{2}} << \frac{\nu_{in}\nu_{en}}{\Omega_{e}\Omega_{i}} \tag{5}$$

and

$$\frac{e\delta\phi}{T_{e0}} + \frac{\delta N}{N_{e0}}\frac{T_{e0}}{T_{i0}} \simeq 0 \tag{6}$$

where $D_{\parallel}^{i}(= T_{i0}k_{\parallel}^{2}/m\nu_{en})$ and $D_{\perp}^{i}(= T_{i0}\nu_{in}k_{\perp}^{2}/M\Omega_{i}^{2})$ are electron and ion diffusion coefficients along and across the earth's magnetic field, multiplied by $k_{\parallel}^{2}$ and $k_{\perp}^{2}$, respectively; $\lambda_{\perp}(= 2\pi/k_{\perp})$, $\lambda_{\parallel}(= 2\pi/k_{\parallel})$, $\delta\phi$, and δN are the perpendicular scale length, the parallel scale length, the electric field potential perturbation, and the plasma density perturbation due to the excited ionospheric irregularities; ν_{in}, $\Omega_{e}(\Omega_{i})$, N_{e0}, and $T_{e0}(T_{i0})$ are the ion-neutral collision frequency, the electron (ion) gyrofrequency, the unperturbed plasma density, and the unperturbed electron (ion) temperature, respectively.

As $\zeta(= D_{\parallel}^{i}/D_{\perp}^{i}) \simeq 0.57\,q^{1/2}$, the minimum threshold of the instability is found to be

$$\frac{\sigma_{p}E_{th}^{2}}{N_{e0}T_{e0}} \simeq 0.93\frac{m}{M}\nu_{en} \tag{7a}$$

or

$$E_{th} \simeq 0.96\,V_{ti}B_{e0} \sim 25\ mV/m \tag{7b}$$

with the substitution of V_{ti} (ion thermal velocity) $= 7.5 \times 10^{2}\ m/sec$ and B_{e0} (the earth's magnetic field strength) $= 3.5 \times 10^{-5}\ Wb/m^{2}$ where q, defined as $(m/M)\nu_{en}/D_{\perp}^{i}(= (m/M)/k_{\perp}^{2}r_{e}^{2})$, is the ratio of the "cooling rate" (that is, the rate of electron energy loss to neutrals) to the cross-field diffusion rate due to electron-ion collisions, where r_{e} is the electron gyroradius ($\sim 2\ cm$ in the ionospheric F region). If O^{+} is assumed to be the dominant ion species (i.e., $m/M(O^{+}) \sim 3.4 \times 10^{-5}$), q is greater than untiy when the perpendicular scale length ($\lambda_{\perp} = 2\pi/k_{\perp}$) exceeds 20 meters. In other words, the "cooling effect" of electron-ion collisions dominates over the electron cross-field diffusion in the excitation of ionospheric irregularities with perpendicular scale lengths greater than 20 meters.

The scale length range of ionospheric irregularities can be found from (5). $D_{\parallel}^{i}/D_{\perp}^{i} << 1$ implies that $\zeta = D_{\parallel}^{i}/D_{\perp}^{i} << D_{\perp}^{i}/D_{\perp}^{i} = M\nu_{in}/m\nu_{en} \sim 20$ where $M(O^{+})/m = 2.94 \times 10^{4}$, $\nu_{in} = 0.5\ Hz$, and $\nu_{en} = 754\ Hz$ (i.e., $N_{e0} = 5 \times 10^{11}\ m^{-3}$ and $T_{e} = 1000^{\circ}K$ assumed). Then, $\zeta \simeq 0.57\,q^{1/2}$ as required for the minimum threshold ranges from 0.57 to 5.7 for $\lambda_{\perp} = 20 - 200$ meters. Therefore, ionospheric irregularities with scale lengths ranging from tens of meters up to a few hundreds of meters can be excited when the quasi-DC electric field exceeds $25\ mV/m$. These ionospheric irregularities are highly field-aligned according to the inequality shown in (5), namely, $\lambda_{\perp}^{2}/\lambda_{\parallel}^{2} << \nu_{in}\nu_{en}/\Omega_{e}\Omega_{i} \sim 2.8 \times 10^{-7}$. It can be seen from (4) and (7a) that the threshold condition is determined by the balance between the heat generation rate and the energy loss rate due to electron-ion collisions. This threshold field refers to the total field intensity rather than to an (east-west or north-south) component of the quasi-DC electric field. A quasi-DC electric field greater than $25\ mV/m$ is not uncommon at high latitudes.

The optimum growth rate is given by

$$\gamma_{m} = 0.47\left(\frac{m}{M}\right)\nu_{en}\left[-\alpha_{I} + \left(\alpha_{I}^{2} + 20.7q^{-1/2}\beta_{I}\right)^{1/2}\right] \tag{8}$$

where $\alpha_{I} = 2.15 - (E_{e0}/E_{th})$ and $\beta_{I} = (E_{e0}/E_{th})^{2} - 1$. The parameter $q\,(= (m/M)/k_{\perp}^{2}r_{e}^{2})$, which is proportional to $\lambda_{\perp}^{2}$, equals unity when $\lambda_{\perp}$ is about 20 meters. It is noted that α_{I} changes from being positive to negative, as E_{e0} is greater than $36.6\ mV/m$. The optimum growth rates (γ_{m}) as a function of perpendicular scale lengths ($\lambda_{\perp}$) are plotted in Figure 7 for $E_{e0} = 30$ and $40\ mV/m$. The growth rates show strong dependence on scale lengths when $E_{e0} < 36.6\ mV/m$ but are almost independent of scale lengths when $E_{e0} > 36.6\ mV/m$. The growth time, defined by γ^{-1}, are generally less than 2 minutes when $E_{e0} = 30\ mV/m$, tens of seconds when $E_{e0} = 40\ mV/m$, and a few seconds when $E_{e0} = 50\ mV/m$.

Regime II

$$\frac{D_{\perp}^{e}}{D_{\perp}^{i}} << 1 \qquad or \qquad \frac{\lambda_{\perp}^{2}}{\lambda_{\parallel}^{2}} << \frac{\nu_{in}\nu_{en}}{\Omega_{e}\Omega_{i}} \tag{9}$$

and

$$1.71\frac{\delta T_{e}}{T_{e0}} + \frac{\delta N}{N_{e0}} - \frac{e\delta\phi}{T_{e0}} \sim 0 \tag{10}$$

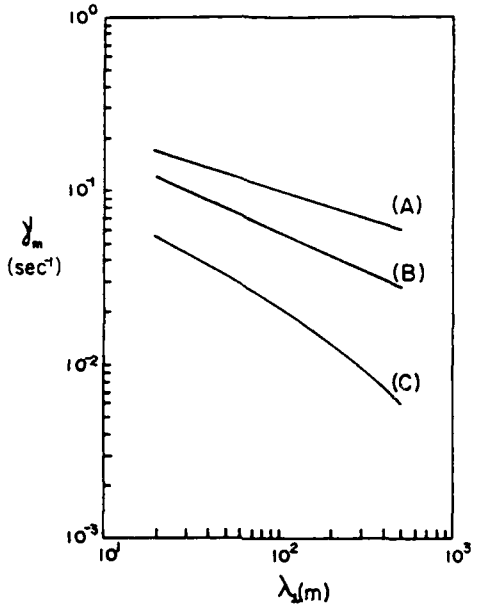


Figure 7. Optimum growth rates (γ_m) as a function of perpendicular scale lengths ($\lambda_\perp$) for intense quasi-DC electric field ($E_\perp$) of (A) 50 mV/m (B) 40 mV/m and (C) 30 mV/m.

The threshold field of the instability in this scale length regime has the form of

$$\frac{\sigma_P E_{th}^2}{N_e T_{e_\perp}} \simeq 1.2\left(\frac{m}{M}\right)\nu_{e_1}\left[1+1.1\left(\frac{2\pi M V_{th}}{\lambda_\parallel M\nu_{e_1}}\right)\right] \tag{11}$$

where $(2\pi MV_{th}/\lambda_\parallel m\nu_{e_1})$ is the ratio of electron parallel diffusion rate $(D_\parallel)$ to the "cooling rate" $(m\nu_{e_1}/M)$ (i.e., the rate of the electron energy loss to neutrals) due to electron-ion collisions. This ratio is negligibly small when $\lambda_\parallel >> 2\pi MV_{th}/m\nu_{e_1} \sim 1.93 \times 10^5$ meters with the substitution of $M(O^+)/m = 2.94 \times 10^4$, $V_{th} = 7.5 \times 10^2$ m/sec, and $\nu_{e_1} = 754$ Hz. The threshold field under this conditions is determined by

$$\frac{\sigma_P E_{th}^2}{N_e T_{e_\perp}} \simeq 1.2\frac{m}{M}\nu_{e_1} \tag{12a}$$

or

$$E_{th} \sim 1.14\, V_{th} B_\perp \sim 2.8\ mV/m. \tag{12b}$$

It is found again that the threshold condition given by (12a) is determined by the "cooling effect" of electron-ion collisions.

Combining the condition $\lambda_\perp >> 2\pi MV_{th}/m\nu_{e_1}$ with that given by (9) determines the range of perpendicular scale lengths of the excited ionospheric irregularities in Regime II, namely, $\lambda_\perp >> 2\pi(M/m)(V_{th}/\Omega_i)(\nu_{in}/\nu_{e_1})^{1/2} \sim 100$ meters. These results show that when the quasi-DC electric field exceeds .28 mV/m, ionospheric irregularities with scale lengths greater than hundreds of meters can be generated. The growth rates of the instability are given by

$$\gamma \simeq 0.6(m/M)\nu_{e_1}\left[-\alpha_{II}+(\alpha_{II}^2+1.1P\beta_{II})^{1/2}\right] \tag{13}$$

where $\alpha_{II} = 1.67(E-E_{th})^2$, $\beta_{II} = (m\nu_{e_1}/M\nu_{in})(E-E_{th})^2 - 1$, and $P = (2\pi MV_{th}/\lambda_\perp m\nu_{e_1})$. As $E_\perp < (>)\ 36.2\ mV/m$, α_{II} is positive (negative). Unless $E_\perp \sim 36.2\ mV/m$ (then $\alpha_{II} \sim 0$), $1.1P\beta_{II} >> \alpha_{II}^2$. Therefore,

$$\gamma \sim 0.33\left(\frac{m}{M}\right)\nu_{e_1}\frac{P\beta_{II}}{\alpha_{II}} \quad for\ E_{th} = 28\frac{mV}{m} < E_\perp < 36.2\frac{mV}{m} \tag{14a}$$

$$\gamma \sim 1.2\left(\frac{m}{M}\right)\nu_{e_1}\alpha_{II} \quad for\ E_\perp < 36.2\frac{mV}{m} \tag{14b}$$

The growth rates, that have rather small values given by (14a) for $E_{th} < E_o < 36.2\ mV/m$ increase to large values given by (14b) for $E_o > 36.2\ mV/m$. For instance, $\gamma = 1.14 \times 10^{-3}$ (4.7×10^{-2}) Hz for $E_o = 40$ (50) mV/m. It thus takes about 1.5 minutes (20 seconds) for kilometer and larger-scale ionospheric irregularities to be developed. These growth rates (or growth times) are comparable to those of ionospheric irregularities with scale lengths in Regime I. Hence, when E_o is sufficiently large (say, greater than $37\ mV/m$), the thermal instability can produce within a couple of minutes field-aligned ionospheric irregularities with broad scale lengths ranging from tens of meters to, say, a few kilometers (allowable for a uniform-medium approximation in the ionosphere).

It is interesting to note that the threshold conditions (see (7b) and (12b)) of the instability turn out to be independent of the electron-ion collision frequency, that plays a crucial role in the excitation of the thermal instability. The reason is that, first of all, electron-ion collisions do not damp the excited zero-frequency modes (i.e., ionospheric irregularities) since electrons and ions move together in the wave vector direction. But the "cooling effect" of electron-ion collisions, through which as an intermediate step, energy is transferred from electrons to neutrals as sinks, weakens the heat source of the instabilty. The threshold conditions are determined by the balance between the generation rate of the heat source and the cooling rate. Since both rates are proportional to the electron-ion collision frequency, it explains why the threshold conditions finally do not depend upon the electron-ion collision frequency. By contrast, the growth rates (see (8) and (13)) are proportional to the electron-ion collision frequency. This is because the cross-field mobility of charged particles is facilitated by electron-ion collisions. The establishment of the collective oscillations (i.e., the field-aligned zero frequency modes) relies on the cross-field mobility. Therefore, electron-ion collisions enhance the growth rates of the thermal instability.

The proposed thermal instability can be favorably excited in environments with high ambient plasma density, such as plasma blobs and plasma patches in general agreement with observations. This fact can be clearly seen from the expressions for the growth rates ((8) and (13)), namely,

$$\gamma \propto \nu_{in} \propto N_o \tag{15}$$

because ν_{in} is approximately proportional to the ambient plasma density (N_o). While the ambient density gradient (∇N_o) combined with a DC electric field (a field-aligned current) provides the source of free energy for the $E \times B$ (the current convective) instability, the ambient density gradient (∇N_o) is expected to impose a convective damping on the thermal instability. This convective damping may become significant for the excitation of ionospherice irregularities whose scale lengths are comparable to the scale size ($\sim 50\ Km$) of the ambient density gradient in plasma blobs or plasma patches. It probalby does not affect the excitation of kilometer and shorter-scale irregularities. These ionospheric irregularities are most interesting to the radio science community because they are responsible for the scintillations of beacon satellite signals from VHF to SHF bands. It should be mentioned that this thermal instability can operate in regions where the $E \times B$ instability cannot. This instability has been analyzed as an F region instability because plasma blobs or plasma patches appear in the F region (Vickrey et al., 1980; Weber et al., 1984). This instability can effectively structure plasma blobs or plasma patches with density irregularities with medium scale lengths ranging from tens of meters to a few kilometers.

4. LARGE-SCALE IONOSPHERIC IRREGULARITIES

Atmospheric gravity waves may interact with the ionosphere and cause large-scale ionospheric disturbances. TIDs (travelling ionospheric disturbances) have been considered to be the manifestation (see Hines, 1974). It has also been believed that gravity waves can seed or trigger the spread F irregularities. Observations made at high latitudes (e.g., Hunsuckar, 1984) and at the equator (e.g., Kelley et al., 1981; Tsunoda and White, 1981) seem to support this general view. Spatial resonance mechanism is the widely discussed process of gravity wave-ionosphere interaction, especially, at the equator (Whitehead, 1971). However, there exist some cases wherein the conditions for spread F do not agree with those for spatial resonance mechanism (Tsunoda et al., 1984). We describe as follows a parametric instability whereby large scale irregularities and forced ion acoustic modes can be excited in the lower ionosphere at the expense of gravity waves. It represents a channel for the neutral atmosphere-ionosphere coupling.

The suggested scenario is outlined in Figure 8. To start with, the solar terminator (Beer, 1973) or a neutral wind shear possibly formed in the E region can become the potential sources of the atmospheric gravity waves. The neutral-plasma interaction primarily through the neutral-ion collisions (ν_{in}) results in a plasma instability that generates forced ion acoustic modes and large-scale field-aligned ionospheric irregularities at the expense of gravity pump waves. These ionospheric irregularities are nearly zero frequency modes whose scale lengths are of the order of the gravity wavelengths. They are caused by the collisional dissipation of both the gravity pump wave and the excited ion acoustic mode in the ion gas rather than the electron gas, because the neutrals and the ions have comparable masses for efficient interactions. The temperature perturbations in the ion gas give rise to a pressure force acting on ions that leads to charge separation, viz., the plasma density perturbations. The self-consistent field thus induced is associated with the excitation of ionospheric irregularities provided the threshold condition can be satisfied. The threshold measured in terms of neutral velocity perturbations is determined by the ion cross-field diffusion damping. In fact, ions can be considered to be unmagnitized in the E region since $\nu_{in} \gg \Omega_i$.

Our analysis has shown that ionospheric irregularities, whose scale lengths are comparable to those ($\sim$ tens of kilometers) of gravity waves, can only be excited by gravity waves with short scale lengths ($\sim$ a few hundreds of kilometers) and short period ($\sim$ one hour). The gravity waves do not produce the large-scale irregularities directly in the upper ionosphere, the electric field perturbations associated with the large-scale irregularities excited in the lower ionosphere can extend along the geomagnetic field and map onto the upper ionosphere (Farley, 1960). This process has been used to explain the following phenomenon. The nighttime ionosphere spatially modulated with scale lengths of the order of 25 km prior to the occurrence of equatorial spread F(ESF) was sensed by the amplitude scintillations of geostationary satellite signals at 136 MHz in our recent experiments in Brazil (Klobuchar and Lee, 1984). However, no TEC variation was found. Displayed in Figure 9 are the individual amplitude fluctuations recorded at five stations (Campo Redondo, Sao Pedra, Ceara-Mirim, Jundiai, and Natal) with an east-west spacing up to 120 kilometers. Spatially periodic structures well correlated at all five locations can be clearly seen. They appeared about 30 minutes before the onset of ESF evidenced by the drastic amplitude fluctuations

that have been truncated at the right end of each panel. We have considered several possibilities of causing these large-scale ionospheric structures and concluded that they were very likely produced by gravity waves via the process described here. These gravity wave-induced ionospheric irregularities can be further amplified by the Rayleigh-Taylor instability that leads

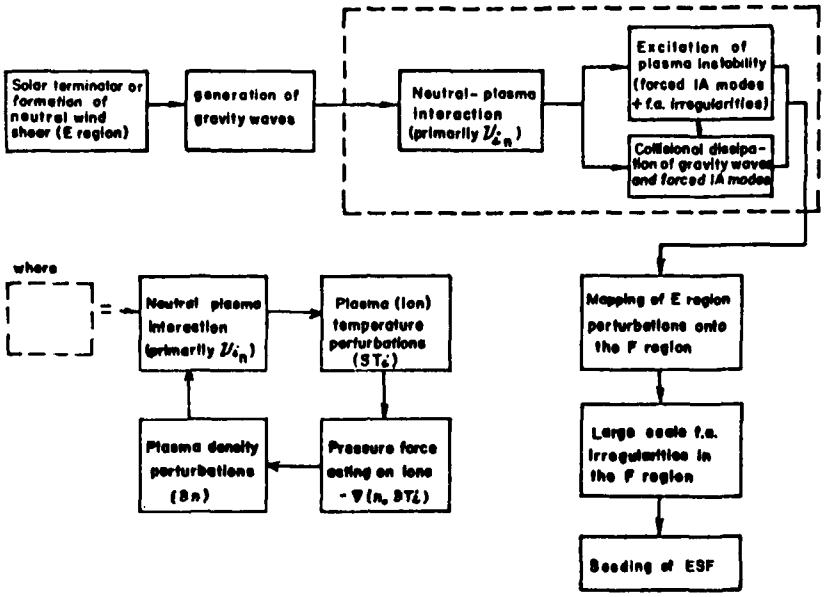


Figure 8. Physical process of gravity wave-produced large-scale irregularities in the ionospheric E and F regions.

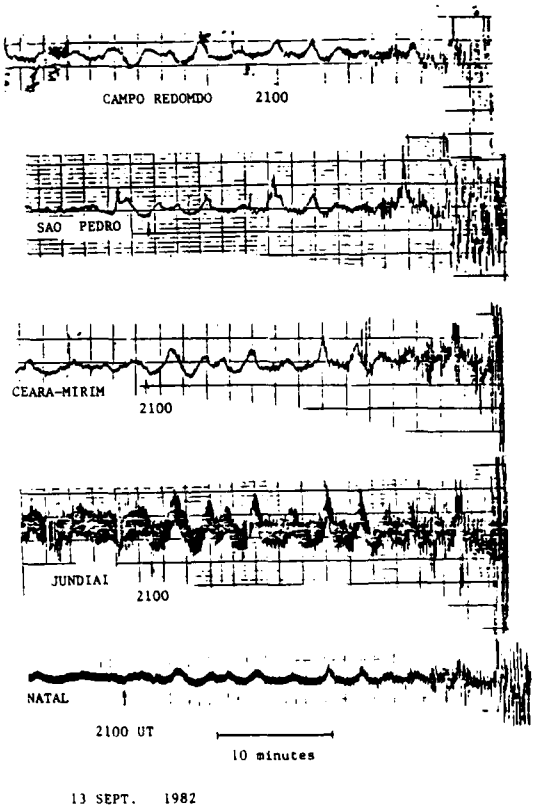


Figure 9. Well correlated individual amplitude scintillations of beacon satellite signals at 136 MHz recorded at all five stations with an east-west spacing up to 120 kilometers.

to the equatorial spread F irregularities causing the drastic amplitude scintillations of our beacon satellite signals.

We are working along the same line on the generation of gravity wave-produced ionospheric irregularities at high latitudes. On the observational basis, the gravity waves at high latitudes typically have periods of a few hours and scale lengths of several thousands of kilometers (see, e.g., Hunsuckar, 1982 and references therein) though shorter period (20 minutes to 1 hour) medium scale (100 – 20 kilometers) gravity waves were also observed. The potential sources of producing short-scale, short-period gravity waves occur frequently at low latitudes, for instance, the solar terminator (Beer, 1973) and the formation of neutral wind shear (Hines, 1968 and 1971) in the nighttime E region. However, neutral wind shear can be created at high latitudes by, for example, the large-scale gravity waves (Rüster et al., 1984) and then becomes the source of gravity waves with short scale lengths and short periods. ESF has some well-known characteristics or symptoms, for instance, a nighttime phenomenon, occurring frequently as the rising ionosphere began to descend. Whereas, the spread F at high latitudes occurs in a relatively sporadic manner. The role of gravity waves or TIDs in contributing to spread F irregularities at high latitudes were discussed by Hunsuckar (1984) on the basis of TEC measurements and ionosonde recordings. We believe that if scintillation measurements similar to those shown in Figure 9 are performed at high latitudes, more clues to the correlation between gravity waves and high latitude spread F may be found.

It should be pointed out that the ambient density gradient has not been included in our theoretical analysis of the problem. It is adequate only for the description of irregularities excited on the horizontal planes where the uniform-medium approximation can be reasonably made for a horizontally stratified ionosphere. In a general theory, the effect of ambient density gradient has to be considered. The results will be reported in our future work.

5. SUMMARY AND CONCLUSIONS

Some sources and causes of high latitude ionospheric irregularities have been discussed in this paper with emphasis on the resultant thermal effects that excite "thermal plasma instabilities". The basic processes are the generation of plasma temperature perturbations (δT) and the subsequent coupling with plasma density fluctuations (δn). More specifically, significant temperature perturbations in the electron (or ion) gas give rise to a thermal pressure force, $-\nabla(n_o \delta T)$, acting on electrons (or ions) only. The charge separation (δn) consequently formed establishes a self-consistent field, $\overline{E}_s$, that is associated with the excitation of ionospheric density irregularities (δn). A threshold condition is required for these thermal instabilities because the excited ionospheric irregularities are not normal modes of the ionosphere but nonlinearly driven modes by a thermal pressure force. These ionospheric irregularities are electrostatic disturbances in nature connected with exactly or nearly zero frequency (i.e., purely growing) modes. Because of their standing wave pattern, these ionospheric irregularities do not propagate. Hence, the radar echoes from these irregularities do not have Doppler shifts.

Whistler waves can produce ionospheric irregularities in both the E and F regions with scale lengths ranging from a few meters to a few tens of meters. Plasma blobs (or patches) appearing in the high latitude ionospheric F region provide a favorable environment for the instability related to the thermal effect caused by the quasi-DC electric field. This thermal instability is effective in structuring plasma blobs (or patches) with medium-scale density irregularities ranging from tens of meters to a few kilometers. Large-scale irregularities can be excited by gravity waves with short periods (< 1 hour) and short scale lengths (~ tens of kilometers to a few hundreds of kilometers) directly in the E rather than the F region. However, the gravity wave-induced electric field (associated with ionospheric irregularities) in the E region is able to map up to the F region along the geomagnetic field and then structure the F region. Short-scale irregularities generally have larger growth rates, for instance, meter-scale irregularities can be excited within fractions of a second or at most several seconds. but the hundreds of meter- and larger-scale irregularities need a few minutes to be developed. After the sources of thermal instabilities disappear, irregularities are weakened by the cross-field deffusion damping that depends upon the irregularity scale lengths. While kilometer- and larger-scale irregularities can survive for hours, the meter-scale irregularities decay within seconds.

In conclusion, whistler waves create short-lived, short-scale ionospheric irregularities in the E and F regions. Medium-scale irregularities are generated throughout the plasma blobs (or patches) by the thermal instability connected with intense quasi-DC electric field. Gravity wave-induced large-scale irregularities extend from the lower to the upper ionospheres. These three mechanisms, characterized by various thermal effects, can contribute additively with other processes to the occurrence of irregularities in the high latitude ionosphere.

ACKNOWLEDGEMENTS

The work at the Massachusetts Institute of Technology was supported by the NASA grant NAG 5-270 and in part by the previous AFGL contract F19628-83-K-0024.

REFERENCES

Beer, T., Supersonic generation of atmospheric waves, **Nature**, 242, 34, 1973.

Berthelier, J. J., F. Lefeuvre, M. M. Mogilevsky, O. A. Molchanov, Yu. I. Galperin, J. F. Karczewski, R. Ney, G. Gogly, C. Guerin, M. Leveque, J. -M. Moreau, and F. X. Sene, Measurements of the VLF electric and magnetic components of waves and DC electric field on board the AUREOL-3 spacecraft: the TBF-ONCH experiment, **Ann. Geophys.**, 38, 643, 1982.

Buchau, J., B. W. Reinisch, E. J. Weber, and J. G. Moore, Structure and dynamics of the winter polar cap F region, **Radio Sci.**, 18, 995, 1983.

Carlson, H .C., V. B. Wickwar, E. J. Weber, J. Buchau, J. G. Moore, and W. Whiting, Plasma characteristics of polar cap F layer arcs, **Geophys. Res. Lett.**, 11, 895, 1984.

Chmyrev, V. M., V. K. Roldugin, I. A. Zhulin, M. M. Mogilevskii, V. I. Di, V. K. Koshelevskii, V. A. Bushmarin, and O. M. Raspopov, Artificial injection of very low frequency waves into the ionosphere and the magnetosphere of the earth, **JETP Lett.**, 23, 409, 1976.

Farley, D. T., A theory of electrostatic fields in the ionosphere at nonpolar geomagnetic latitudes, **J. Geophys. Res.**, 65, 869, 1960.

Fejer, B. G. and M. C. Kelley, Ionospheric irregularities, **Rev. Geophys. Space Phys.**, 18, 401, 1980.

Helliwell, R. A., Whistlers and related ionospheric phenomena, Stanford University Press, Stanford, California, 1965.

Hines, C. O., Tidal oscillations, shorter period gravity waves and shear waves, **Meterological Monographs**, 9, 114, 1968.

Hines, C. O., Generalizations of the Richardson criterion for the onset of atmospheric turbulence, **Quart. Journ. of thef Royal Meterological Soc.**, 97, 429, 1971.

Hines, C. O., The upper atmosphere in motion, **Geophysical Monograph**, 18, American Geophysical Union, 1974.

Hunsucker, R. D., Atmospheric gravity waves generated in the high-latitude ionosphere: a review, **Rev. Geophys. Space Phys.**, 20, 293, 1982.

Hunsucker, R. D., Possible relationships between gravity waves and irregularities in the high latitude ionosphere presented at the **Workshop on "Irregularities in the high latitude ionosphere"** held at the Max-Planck Institut fur Aeronomie, 10-12 September, 1984.

Kelley, M. C., M. F. Larsen, C. La Hoz, and J. P. McClure, Gravity wave initiation of equatorial spread F: a case study, **J. Geophys. Res.**, 86, 9087, 1981.

Kelley, M. C., J. F. Vickrey, C. W. Carlson, and R. Torbet, On the origin and spatial extent of high-latitude F region irregularities, **J. Geophys. Res.**, 87, 4469, 1982.

Keskinen, M. J., and S. L. Ossakow, Theories of high-lattitude ionospheric irregularities: a review, **Radio Sci.**, 18, 1077, 1984.

Kintner, P. M., R. Brittain, M. C. Kelley, D. C. Carpenter, and M. J. Rycroft, In situ measurements of transionospheric VLF wave injection, **J. Geophys. Res.**, 88, 7065, 1983.

Klobuchar, J. A., and M. C. Lee, Periodic amplitude variations as precursors of plumes of irregularities in the equatorial region, paper presented at **AGU Fall Meeting**, San Francisco, California, 3-7 December, 1984.

Klobuchar, J. A., G. J. Bishop, and P. H. Doherty, Total electron content and phase scintillation measurements of the polar cap ionosphere, paper presented at the **Workshop on "Irregularities in the high latitude ionosphere"** held at Max-Planck Institut fur Aeronomie, 10-12 September, 1984.

Koons, H. C., B. C. Edgar, and A. L. Vampola, Precipitation of inner zone electrons by whistler mode waves from the VLF transmitters UMS and NWC, **J. Geophys. Res.**, 86, 640, 1981.

Kuo, S. P., B. R. Cheo, and M. C. Lee, The role of parametric decay instabilities in generating ionospheric irregularities, **J. Geophys. Res.**, 88, 417, 1983.

La Hoz, C., and G. Haerendel, Short-lived ionospheric irregularities observed in Jicamarca, paper presented at the **Workshop on "Irregularities in the high latitude ionosphere"** held at Max-Planck Institut fur Aeronomie, 10-12 September, 1984.

Lee, M. C., Ohmic dissipation of Pederson current as the cause of high-latitude F region ionospheric irregularities, **J. Geophys. Res.**, 89, 7482, 1984.

Lee, M. C., and S. P. Kuo, Excitation of upper-hybrid waves by a thermal parametric instability, **J. Plamsa Phys.**, 30, 463, 1983.

Lee, M. C., and S. P. Kuo, Excitation of magnetostatic fluctuations by filamentation of whistlers, **J. Geophys. Res.**, 89, 2289, 1984(a).

Lee, M. C., and S. P. Kuo, Production of lower hybrid waves and field-aligned plasma density striations by whistlers, **J. Geophys. Res.**, 89, 10873, 1984(b).

Lee, M. C., and J. A. Klobuchar, Irregular polar ionospheric structures associated with large-scale plasma enhancement, paper presented at the **AGU Chapman Confernece on "Magnetospheric polar cap"** held at the University of Alaska, Fairbanks, 6-9 August, 1984.

Rüster, R., P. Czechowsky, J. Klostermeyer, and G. Schmidt, VHF-radar observations of waves and turbulence in the mesosphere, paper presented at the **Workshop on "Irregularities in the high lattitude ionosphere"** held at Max-Planck Institut fur Aeronomie, 10-12 September, 1984.

Siefring, C. L., and M. C. Kelley, The transient electrical response of the ionosphere to lightning strokes, **EOS Trans. AGU**, 64, 778, 1983.

Tsunoda, R. T., D. P. Sipler, and M. A. Biodi, Effects of natural wind, waves and velocity shear on the generation and growth of plasma bubbles, paper presented at the XXIst General Assembly of **International Union of Radio Science**, Florence, Italy, August 28 - September 5, 1984.

Tsunoda, R. T., and B. R. White, On the generation and growth of equatorial backscatter plumes, 1. Wave structure in the bottomside F layer, **J. Geophys. Res.**, 86, 3610, 1981.

Vickrey, J. F., C. L. Rino, and T. A. Potemra, Chatanika/Triad observations of unstable ionization enhancements in the auroral F region, **Geophys. Res. Lett.**, 7, 789, 1980.

Weber, E. J., and J. Buchau, Observations of plasma structure and transport at high latitudes, in Proceedings from the **NATO Advanced Research Workshop on "The Morphology and Dynamics of the Polar Cusp,"** May 6-12, 1984, Lillehammer, Norway, D. Reidel, Hingham, Mass., in press, 1985

Weber, E. J., J. Buchau, J. G. Moore, J. R. Sharber, R. C. Livingston, J. D. Winningham, and R. W. Reinisch, F layer ionization patches in the polar cap, **J. Geophys. Res.**, 89, 1683, 1984.

Whitehead, J. D., Ionization disturbances caused by gravity waves in the presence of an electrostatic field and background wind, **J. Geophys. Res.**, 76, 238, 1971.

Woodman, R. F., A causal relationship between lightning and explosive spread F, paper presented at the 7th **International Symposium on Equatorial Aeronomy,** held in Hong Kong, 22-29 March, 1984.

DISCUSSION

E.Thrane, NO

For your medium scale irregularity regimes, are you able to predict the spectral characteristics, such as spectral slopes?

Author's Reply

No, we work on a linear instability as many people did before. Unless we know how the instability evolves nonlinearly (i.e. saturates), we would not be able to predict the spectral shapes of the induced ionospheric irregularities.

T.A.Croft, US

Since TIDs cause TEC variations, how can scintillations be attributed to TIDs when you detect no TEC variations?

Author's Reply

The spatially periodic ionspheric structure recorded in Brazil is *not* attributed to TECs because no TEC variations are associated with it. We suggest that it be excited by atmospheric gravity waves via a plasma instability as described in Section 4 of our paper. The atmospheric gravity waves can be produced by either the solar terminator or a wind shear in the ionospheric E region. The proposed instability operates in the region where large neutral plasma collisions facilitate the neutral-ionosphere coupling. Large scale ionospheric irregularities induced in the E region can map onto the F region along the earth's magnetic field. Large scale ionization ducts are then formed along the geomagnetic field lines from one hemisphere to the other one.

Direct, in-situ measurements of irregularities in the mesosphere (85 - 50 km) at 69°N (Andenes, Norway)

Hans-Ulrich Widdel
Max-Planck-Institut für Aeronomie, D-3411 Katlenburg-Lindau, FRG

1. INTRODUCTION

One of the problems of the physics of the mesosphere which is apparently not yet completely solved is which hydrodynamic mechanisms can cause transient vertical and horizontal gradients of electron density and neutral air density. Such gradients give rise to scattered signals of radio waves at different frequencies. Well-known are the "partial echoes" observed on short wave frequencies below about 100 km down to about 60 km. They seem to occur at certain "preferred" heights which seem to change with season and latitude.

Because the distribution of ionization at such low altitudes, once produced, is primarily controlled by the neutral atmosphere. Investigations of the dynamics of the neutral atmosphere combined with simultaneous radio wave measurements promise some advance of knowledge.

For probing the neutral atmosphere, the simplest method is to release a target at a certain height and to track its descent either optically or by radar from the ground. Such a target should have a low velocity of descent for a good response to changes of horizontal and vertical winds. The physical quantity which determines primarily the velocity of descent of a target is the mass to area ratio, (m/A). A is the projected area of the target into the direction of descent. If measurements are to be made at greater altitudes (Z > 85 km) it turns out that a solid target cannot be realised technically because the required mass to area ratio cannot be achieved. The solid target has therefore to be replaced by a "soft" target, for example, by a cloud of metallized plastic strips or bands. Their length should be cut to resonance to the tracking radar's frequency ("chaff"or "window"). To the knowledge of the author, chaff was used for the first time for higher altitude research (at heights above 60 km) by L.B. Smith (Smith, 1960) and by Pachomov (Pachomov, 1969). Smith's results were critizised by Rapp (Rapp, 1960). Rapp pointed out several weaknesses of this method, as are: Limited coverage of height (because the chaff cloud dissolves quickly at certain heights), limited accuracy of measurement, because chaff, especially "hair-like" chaff of small diameter, has a strong tendency to become "birds-nested" during deployment: It forms lumps which, because their mass-to-area ratio is larger than the chaff which becomes separated, fall out of the cloud, enlarge it and by this spoil the measurement. Further, no satisfying theoretical description of the flight behaviour of "chaff" existed for greater heights.

In 1967, Widdel developed a "foil cloud" experiment. The chaff elements were 9 mm wide metallized Mylar foils which had an area load of $3.4.10^{-3}$ kg/m^2. The foils were ejected rearwards at apogee of the rocket's trajectory. Proper means of deployment assured that at least 98% of the foils became separated. The results of the first test flights already revealed the existence of rather strong vertical movements at 75 km (Rose and Widdel, 1969). This experiment was used since then extensively during several campaigns, predominantly at lower latitudes (37°N).

During the MAP/WINE campaign (winter 1983/84 at Andenes, 69°N) 18 foil cloud experiments were launched on stretched Super-Loki Dart vehicles. Because a sensitive precision tracking radar was available for this campaign, a physically small chaff cloud could be used (Widdel, 1985). On two experiments, a "heavy" chaff (mass-to-area ratio $13.6.10^{-3}$ kg/m^2) was used as an attempt to penetrate certain levels of turbulence. In these levels clouds of light chaff are dissolved because their velocity of descent becomes of the order of the vertical motions there. Previous experiments have shown that end of tracking of large foil (chaff) clouds occurs mostly of levels at which strong horizontal shears of wind are observed (Fig. 1).

Because foil chaff has a low velocity of descent and a small moment of inertia, it reacts almost instantly on all kind of changes of movements in the atmosphere. On the other hand, the chaff cloud is not a rigid target. The echo return scintillates in range, azimuth and elevation because it is a composition of many individual targets. Under calm conditions, the scintillation in range, azimuth and elevation averages out and one obtains good tracking data. But when an orientated motion, for example, an upcoming wave, affects the cloud, a technical effect known as "range gate-stealing" (c.f. Skolnik, 1973) might come into play which causes the radar to "hunt" over the cloud. If radar tracking data are then the only source of information, it is almost impossible to decide with certainty, if an irregularity seen in the tracking data was caused by a genuine atmospheric effect or was just caused by the radar itself. Continuous recording of the echo seen at the radar range gate remedies this situation. During the MAP/WINE campaign the range gate echo was recorded on every flight in real time on video tape using a home TV camera and a home TV recorder. These records helped tremendously in the interpretation of some effects seen in the radar tracking data which otherwise could have been dismissed as being caused by the radar (Widdel, 1985).

Quantitative description of the flight behaviour of chaff

In the past, results of chaff measurements were often questioned because no satisfying theory existed which described the aerodynamic response of chaff to the atmospheric conditions found at greater altitudes. While horizontal wind speeds cannot be used for a check because they are too variable with time and height, the velocity of descent can because its diving force (gravity) is known. Empirical relations derived from the experimental results or semi-empirical formulas were used in the past (c.f. Smith, 1960, Rose et al, 1972). They allowed an estimate of chaff response to changes of horizontal winds. Nowadays, a fairly detailed atmospheric model is available (Cole and Kantor, 1978) which has turned out to match quite well to reality in the context of other investigations (c.f. Friedrich et al, 1977). Because a model represents mean conditions composed from actual measurements, best agreement should be expected between theory and experiment when means of a greater number of experimental results obtained under same conditions are compared with the model. Such a data bank was available from earlier campaigns (see list of references).

Approach

In order to obtain a fast response of chaff to changes of horizontal wind speed, its velocity of descent should be smaller than the horizontal wind velocity. This condition already determines the flow regime for chaff at high latitudes and sets too a limit to the height up to which chaff can sensibly used for wind measurements (approximately 92-95 km). Considering the Reynolds number $R_e = \frac{\rho \cdot v \cdot d}{\eta_0}$ (ρ: air density, v: velocity, d: characteristic length of the chaff, η_0: viscosity of the environment) one notes that R_e becomes very small for the altitudes under consideration (90 - 60 km). The choice of the diameter as the characteristic length instead of the length of the chaff element follows from the interpretation of the Reynolds number as the ratio between inertial forces and friction forces. For such small Reynolds number, the drag coefficient C_D in Prandtl's expression for the drag force, $F_D = C_D.A.(\rho/2)v^2$ (A: area of the object) becomes simply

$$c_D = \frac{C}{R_e} = \frac{\eta_0}{C \rho v \cdot d}$$

(c.F. Hoerner, 1965 and other textbooks)

Inserting the relevant expressions for η_0(viscosity) and density ρ which relate them to molecular gaskinetic properties one obtains a formula which describes the velocity of descent of "chaff" in a dense atmosphere (mean free path of the molecules << diameter of the chaff). (First part of the formula to follow).

$$v = 6g \sqrt{\pi/8} \frac{C}{\sqrt{MR}} (m/A) d \frac{1}{\sqrt{T}}$$

For greater altitudes however, we have to take into account that the diameter of the chaff becomes smaller than the mean free path of the molecules at those heights. The flow regime there is not defined by the Reynolds number alone but also by the Knudsen number, Kn, which is the ratio between characteristic length d and mean free path length. A proven approach to take into account Knudsen flow conditions is to introduce the Cunningham correction of viscosity

$$\eta = \frac{\eta_0}{1 + 1/d}$$

which has to be modified to $\eta = \frac{\eta_0}{1 + c\lambda/d}$ because the original Cunningham correction does not take into account the "lift" caused by the wake behind a moving body. The numerical value of constant C is obtained through a separate consideration (Energy transfer to a moving body). The final result is then:

$$v = 6g \sqrt{\pi/8} \frac{C}{\sqrt{MR}} (m/A) d \cdot \frac{1}{\sqrt{T}} + \frac{3}{2} g \sqrt{\pi/8} \sqrt{M/R} (m/A) d \cdot \frac{1}{\rho \sqrt{T}}$$

(g: gravity acceleration, σ: molecular collisional cross section, M: Mean mass of air molecules, k: Boltzmann's Constant, (m/A: the mass-to-area ratio of the chaff, T: absolute temperature, ρ: air density.

With mean molecular mass of air (29.3) and $\sigma = 5.10^{-19} m^2$ (Banks and Kockarts, 1973) one obtains a convenient engineering formula for the velocity of descent in m/s: $[224735(m/A).d + 0.54842.(m/A)/\rho]/\sqrt{T}$ (m/A) has to be inserted in kg/m^2, d in m, ρ in kg/m^3). This relation reveals why density and temperature cannot be derived from the vertical velocity of descent of single kind of chaff, but opens (on paper) a possibility to determine air density and air temperature in a calm atmosphere from the descent velocities of two kinds of chaff flown simultaneously. The two kinds of chaff used for such an experiment should at least differ in diameter.

The velocity of descent for chaff 1, v_1, is given by: $v_1 = \frac{1}{\sqrt{T}} \cdot (D + E/\rho)$

that of chaff 2 by: $v_2 = \frac{1}{\sqrt{T}} (F + G/\rho)$

from which immediately follows :
for density

$$\rho = \frac{v_2 \cdot E - v_1 G}{v_1 \cdot F - v_2 \cdot D}$$

and for temperature

$$T = \frac{1}{v_1^2} \left[D + E \left(\frac{v_1 F - v_2 D}{v_2 E - v_1 G} \right) \right]^2$$

provided that the atmosphere is free from vertical movements (waves) or that the waves can be removed from the raw data by some reasoning. However, one should consider that this theoretical approach given here might be incomplete because it yields a velocity of descent which depends, besides on mass-to-area ratio, (m/A), on the diameter of the chaff, d, only. This might not be true. For a complete check of validity results of experiments done with different lengths of chaff but of same mass-to-aera load should be investigated and compared with the results of the theory presented above. Such work has started but was not completed at time of writing.

Check of validity

The bulk of chaff data used for verification was obtained with 9mm wide S-band chaff (48 mm long). This chaff had a mass-to-area ratio of 3.4 g/m^2. Temperature and density data given by the USAF Standard Atmospheres (Cole and Kantor, 1978) for the relevant months and latitudes were converted into velocities of descent. These velocities were compared with the means of measurements as was mentioned already.

Fig. 2, 3, 4 and 5 shows the result which can be considered as satisfactorily.

A further test on validity was possible because the results of another experiment were available. In this experiment, two chaff clouds were released simultaneously. Each cloud was tracked by a separate radar of same type and performance (both radars were MPS 19). The two types of chaff differed by weight-to area ratio and diameter: Chaff 1: "Standard" chaff, 9 mm wide, weight to a area ratio (m/A) = 3.4 g/m^2. Chaff 2:3mm wide, (m/A) = 13.6 g/m^2. The relevant velocities of descent were calculated from the USAF Standard atmosphere and both, theoretical values and measured data were entered into the plot of Fig. 6. The "kinks" seen in the plot were caused by vertical wave motions which affected the descent of the clouds at different height at different times. The amplitude of this vertical motion was 3.1-3.7 m/s.

Consequences and results

The result suggests that a properly designed chaff cloud can be considered as a droplet of a heavy fluid moving under gravity in an incompressible flow. From this it follows that diffusion, often cited as the cause for a premature ending of radar tracking, should be small during descent and that the cloud should not change much its dimensions unless external forces act upon it. This was proven by the records of the radar range gate echo. Two examples are shown in Fig. 7. The legend of Fig. 8 explains how the TV records were evaluated. These two examples were chosen because they display some interesting peculiarities. After deployment, a "triangular shaped" pattern is seen in the range gate echo evaluation record. This triangular-shaped pattern disappears about six minutes later. After this event, the echo width remains, in essence, constant. This indicates that the conclusions drawn about the flight behaviour of an undisturbed cloud are valid. One is tempted to assign this triangular-shaped structure to "a drop-out" of lumps of chaff which fall faster than the main cloud comprising separated foils ("rain-out") and that these lumps get out of sight of the radar later on. The corresponding height vs time of flight plots which show the radar raw data plotted at 1/10 sec interval of time seem to confirm this: (Fig. 8, and 9): Initially, the radar follows one target, then a separation occurs and the radar tries to follow two targets simultaneously up to a certain point where the faster-descending chaff gets out of sight of the radar beam. Only an analysis of the velocity of descent reveals what really has happened: The initial velocity of descent of the cloud after deployment and that of the faster descending target corresponds fairly closely to the velocity expected at that height from theory, while the velocity of descent of the main cloud is far too low: It would correspond to a height 10-12 km lower than the level in which it was measured. Further, the height vs time-plot does not show a monotonous decrease of velocity of descent with height but a wavy structure. This means that the descending cloud was intercepted by an upcoming wave drifting in the wind. Vertical motions were more the rule than the exception at heights below 80 km. "Holds" and "flare-outs" in the height vs time plot of the chaff descent were observed rather frequently. A typical example is shown in Fig. 10. This wavy structure is linked to the horizontal wind speed and wind direction. Fig. 11 shows two examples. The wind vector is entered by magnitude and direction at the relevant heights. Occasionally a "hold" in the z(t) plot (which sometimes shows positive, vertical motions directly) degenerates into what can be best described as a "hopping motion". On one flight, an extreme case was observed in that this "hopping" repeated four times until the cloud dissolved in turbulence. (Fig. 12, Flight-M-C7). The radar ground track (projection of the foil cloud trajectory onto the Earth's surface) showed that each time a "hop" occurred, "the cloud stepped to the side". Without further information one would dismiss such a case as being caused "somehow by the radar". The range gate echo record however, shows that the cloud was affected as a whole and remained together until it was dissolved. This at first sight perplexing motion can be explained as the result of a (laminar) separation of flow of the kind recently described by Hornung and Perry (1984), and Perry and Hornung (1984). Because hydrodynamic flow and magnetic fields both follow the Poisson equation, interactions between vortexes and steady flow can be simulated and studied by appropriate magnetic fields (Fig. 13). Using a plate covered with iron filings as a detector, one obtains "footprints" which can be interpreted as "flowlines" or "skeleton lines" (c.f. Hornung and Perry, l.c). A footprint of an interaction between an upcoming vortex and a steady flow explains what was observed during flight M-C7 (Fig. 14). The results of this flight and those of some others are discussed in more detail in a separate paper (Widdel, 1985). Separation of flow, as it turned out, was by no means a rare event, but it was observed on many flights in the range gate echo records only. One example is seen in Fig. 7, another in Fig. 15. Nothing peculiar is seen in the radar ground track when the flow separation occurred. In this peculiar case (Fig. 15) the split-up echo became stronger than the echo the radar was tracking. This indicates a vertical motion by which the density of foils (number of foils per m^3) becomes larger as a consequence of incompressible flow. When the descent of the cloud is decelerated, the cloud should widen up. This causes a dilution of the foil density and split-up of echos. This, in turn can lead to what is known as "range-gate-stealing" (c.f. Skolnik, 1973): The range gate moves to the stronger part of the echo within the range gate, and the radar starts to "hunt over the cloud". Such effects were observed preferably at lower altitudes (~75-78 km) where vertical movements are more the rule than an exception. They were seen in southern Spain (37.6^{0}N), White Sands (32.4^0) and over Wallops Island too. An effect which might be more frequent at northern latitudes (but this cannot be proven yet due to lack of data) is an "explosive" destruction of a foil cloud in what is believed to be turbulence (Schmidlin et al, 1985), (Fig. 16, Fig. 17): Such an event was observed when aurora activity was strong: The descent of a relatively small cloud (remainder of a larger cloud which disintegrated at a greater altitude) ceased. The cloud was lifted and broke up, spreading upwards. The interesting thing is, that, judged from the data, part of the cloud seemed to descent "normal" - it was occasionally tracked by the radar while the other part was spread upwards. The radar ground track (Fig. 17) suggests that the spread caused by turbulence was larger in the vertical than into horizontal direction.

Turbulence itself is seen in the chaff data at certain heights but difficult to evaluate quantitatively. An attempt is made now to obtain quantitative data from the radar return signal strength of the chaff (AGC voltage of the radar). This analysis is not yet completed.

The high resolution of the radar together with the physically small size of the foil cloud revealed that strong shears of wind (both in speed and direction) seem to occur in very shallow intervals of height sometimes less than 150 m thick leading to "wind corners" (von Zahn and Widdel, 1985). An example for such a "wind corner" (change of direction of wind by 90 degrees) is shown in Fig. 18.

The mechanism which produces such "wind corners" (wind corners are by no means a rare effect or confined to northern latitudes) has still to be investigated.

Concluding remarks

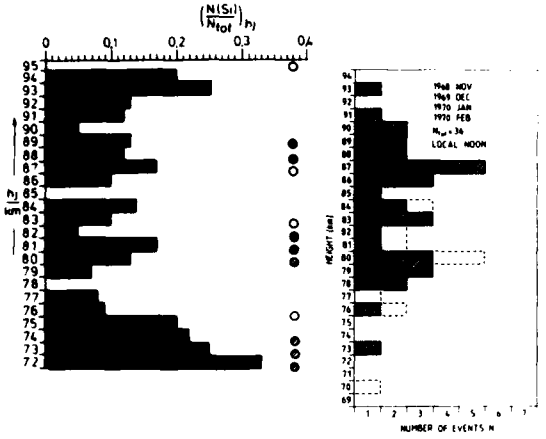
It was shown that small foil clouds, together with proper techniques of observation can be used to study in detail a number of dynamic effects in the neutral atmosphere with high spatial resolution. This high spatial resolution revealed that some atmospheric structures seem to be very local. Further, the radar range gate echo records showed that the radar tracking data do not always tell the full story what had happened. To obtain a better picture, more than one chaff target, separated in space, should be tracked simultaneously. This calls for a 3D-multiaquisition-multitarget radar for tracking.

Acknowledgement

The work was sponsored by Bundesminister für Forschung und Technologie, Grant WRK 90 (results obtained at lower latitudes), WRK 275/2 and 01OE0610.
Thanks go to Professor U. von Zahn and W. Meyer, University of Bonn, for providing wind, density and temperature data obtained during the MAP/WINE campaign winter 1983/84.

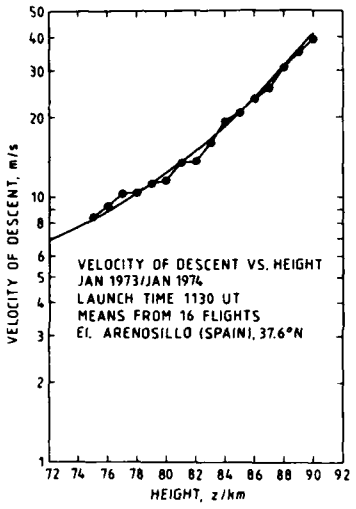
References

Banks, P.M., and G. Kockarts (1973) Aeronomy Part A, Academic press, New York
Cole, A.E., and A.J. Kantor (1978) Air Force Reference Atmospheres. Report AFGL-TR-78-0051 Air Force Surveys in Geophysics, No. 383, Air Force Geophysics Laboratory, Hanscom, AFB, Massachusetts 01731.
Friedrich, M., K. Torkar, S. Ulrich (1977) A rocket borne experiment to measure plasma densities in the D-region, J. Geophys. 44, p. 91.
Hoerner, S.F. (1965) Fluid-dynamic drag, published by the author, 148 Busteed Drive, Midland Park, New Jersey 07432. Library on Congress card no. 64-19666.
Hornung, H., and E.A. Perry (1984) Some aspects of three-dimensional separation, Part I: Stream surface bifurcations, 7. Flugwiss. Weltraumforschung 8, p. 77.
Pachomov, S.V. (1969) Technique of obtaining data about winds in the mesosphere by small meteorological rockets. In: Small rocket instrumentation techniques K.I. Maeda ed. Amsterdam North Holland Publ. Company.
Rapp, R.R. (1960) The accuracy of wind derived by the tracking of chaff at high altitudes. J. Meteorol. 17, p. 507.
Rose, G., H.U. Widdel, A. Azcarraga, L. Sanchez (1977) Results of an experimental investigation of correlation between D-region neutral gas winds, density changes and short-wave radio wave absorption, Phil. Trans. R. Soc. London A 271, p. 529.
Skolnik, M.E. (1970) Radar Handbook McGraw Hill Book Comp. New York.
Skolnik, M.E. (1980) Introduction to radar systems, McGraw Hill Book Comp. New York.
Schmidlin, F.J., M. Carlson, D. Rees, D. Offermann, C.R. Philbrick, and H.U. Widdel (1985) Wind structure and variability in the middle atmosphere during the November 1980 Energy Budget Campaign, J. Atm. Terr. Phys. 47, p. 183.
Smith, L.G. (1960) The measurements of winds between 100000 and 300000 ft by use of chaff rockets, J. Meteorol. 17, p. 296.
von Zahn, U., W. Meyer, and H.U. Widdel (1985) Wind corners and wind strata in the mesosphere, Proceedings on the 7th ESA Symposium on European Rocket and Balloon programmes and related Research, Loen, Norway, 5-11. May 1985 (in press).
von Zahn, U., and H.U. Widdel (1985) Wind corners in the winter mesosphere, Geophys. Res. Lett., (accepted, July 1, 1985).
Widdel, H.-U. (1985) Foil clouds as a tool for measuring wind structure and irregularities in the lower thermosphere (92-50 km), Radio Sci. 20, p. 803.

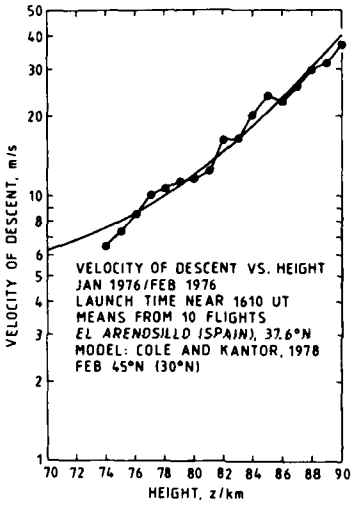


1

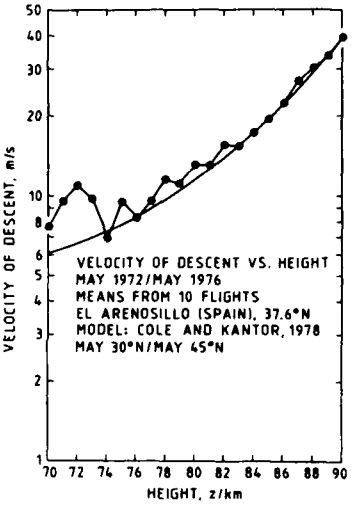
Fig. 1: Indication that foil (chaff) clouds break up in horizontal windshears. Left: Frequency of occurrence of windshears larger than 40 m/s/km N(Si) = Number of observations of shear > 40 m/s/km (N_{tot}) = Number of total observations (flights) at height j. Dots indicate significant correlations between change of horizontal wind and change of (winter-anomalous) radio wave absorption. Right: Number of break-up events observed at height Z. Lower frequency of occurrence at lower height has a trival cause: The cloud broke up at greater heights already. Heights in which strong shears occur most often coincides with heights or are slightly above heights in which break-up of cloud was observed most frequently. Large foil clouds (100.000 foils), 37.6°N, winter. Chaff: 9 mm wide foils, mass-to-area ratio (m/A) = 3.4 g/m^2.



2

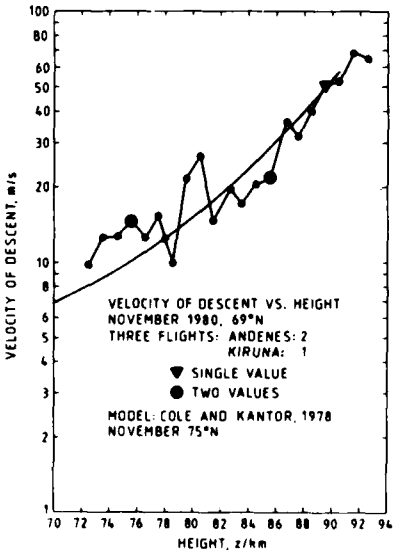


3



4

Fig. 2-5: Results of a comparison between calculated velocities of descent using temperature and density data from the Cole and Kantor model with means of measurements. Deviation from expectation seen at lower altitudes in the data for May can possibly be explained by the fact that these data do not represent averages but are results from a single flight.



5

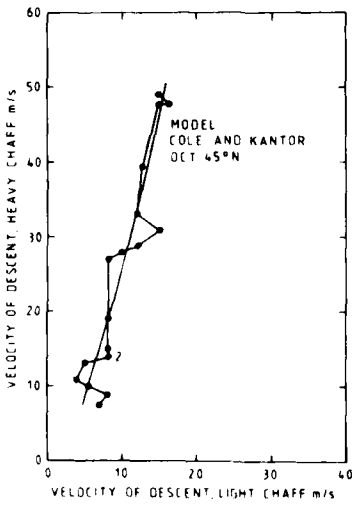
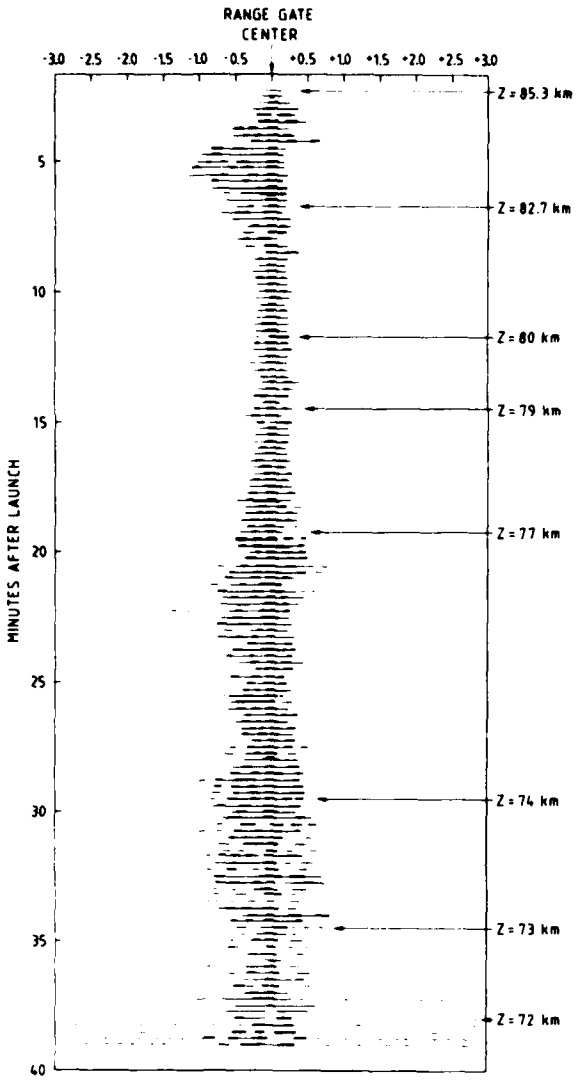
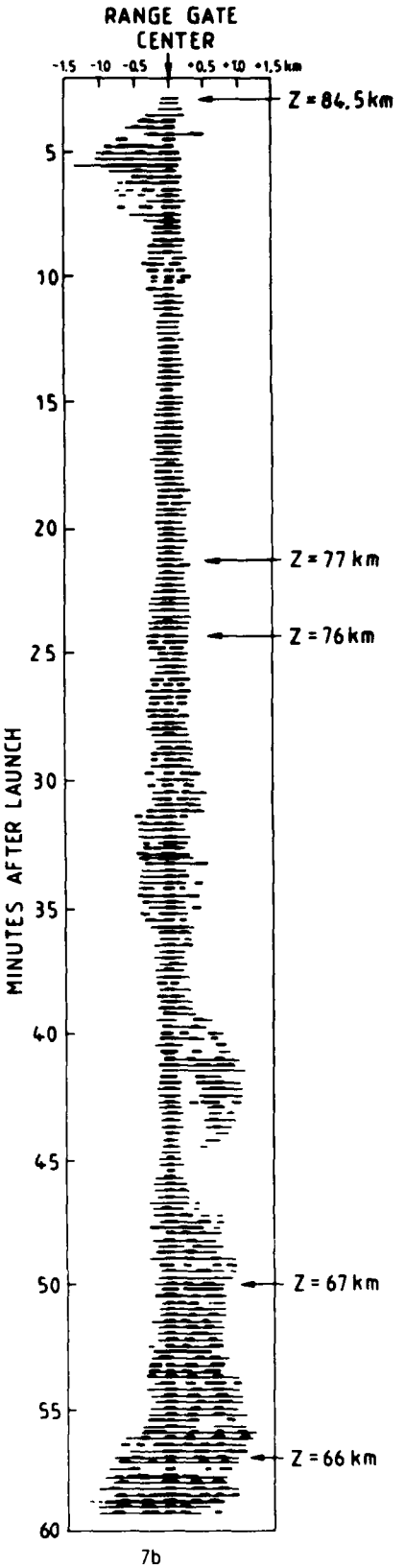


Fig. 6: Comparison between results obtained with "light" chaff (area load (m/A) = 3.4 g/m^2, width = 9 mm) and "heavy" chaff (area load: (m/A) = 13.6 g/m^2, width d = 3 mm). Both clouds were released at the same height at the same time. Quasi-straight line: Expected velocities calculated from model atmosphere October 45°N/30°N (no significant difference in model). "Kinks" caused by vertical upward motion (3.5 m/s): The heavy chaff was hit first, the light chaff later at greater height. Good agreement between "direct" measurements (derived from the individual chaff-measurement) and height/time difference. 3.75 m/s (direct) 3.11 m/s (height-time difference).

6

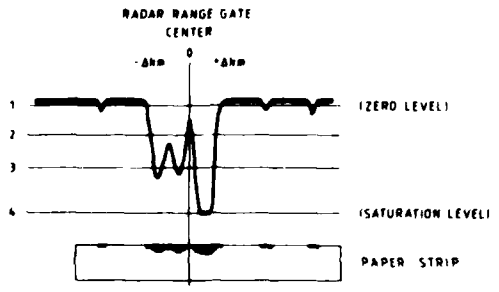


7a



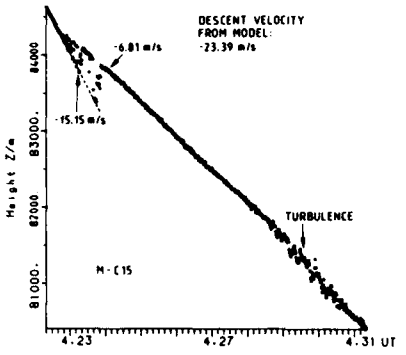
7b

Fig. 7: Two examples of a range gate echo record evaluation
Small foil clouds (23000 foils), C-band foils, 24 mm long, 9 mm wide. Mass-to-area-ratio 3.4 g/m^2. Method of evaluation explained in legend of Fig. 8. Width of radar echo remains about constant for a long time unless external forces act upon the cloud (vertical winds, turbulence). Widening of echo short after deployment (arrows) seen on both flights looks like a drop-out of lumps of chaff from the cloud but is in fact caused by an interaction with an evanescent wave. (See also Fig. 9). Evaluation at 15 sec interval of time.

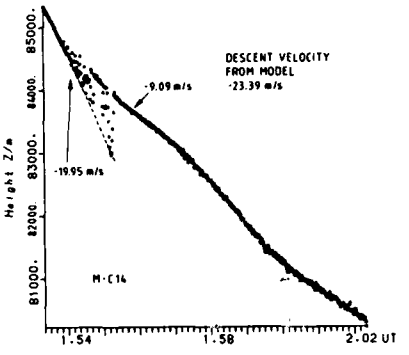


8

Fig. 8: Method of evaluation of TV records of the radar range gate echo on the TV-screen: The echo output from the MPS-36 saturates at a certain level (level 4). Four levels were marked on the screen, a strip of paper was laid on them and the width of the echo which exceeded the level was marked on the paper. Start was at level 1, and at level 4. The result was transferred into an echo width vs time plot.

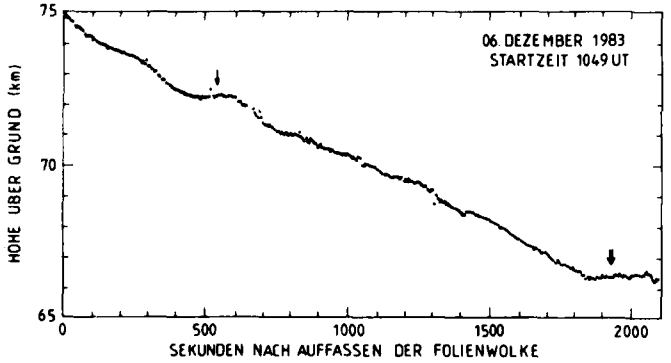


9a



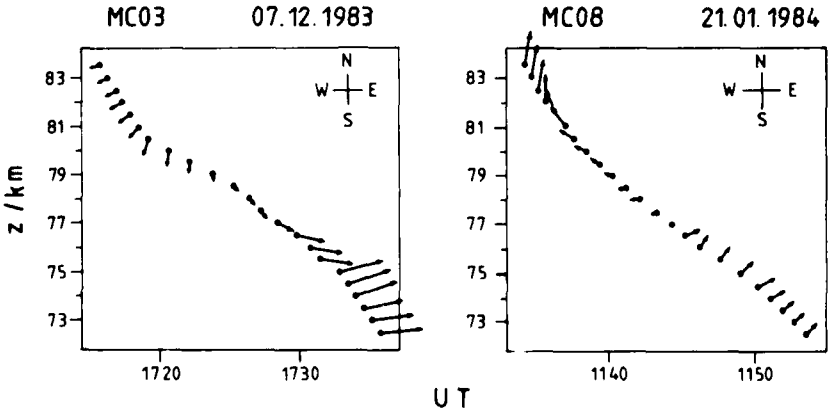
9b

Fig. 9: Height-vs-time plot for the first minutes of the two flights shown by Fig. 7. Short after deployment, the velocity of descent corresponds closely to what should be expected from model calculation, but is then decelerated. The target which falls faster is tracked intermittently by the radar, becomes lost later but is still seen in the radar range gate record. (Fig. 7)
An upwards moving wave (vertical velocity of order 7-9 m/s) was observed in both cases which carried most of the chaff away. The radar ground track (projection of the foil cloud trajectory onto the Earth's surface) shows just a small "kink" which one would assign to a "tracking error of the radar".
Data: unprocessed radar raw data, output at 1/10 sec interval of time.



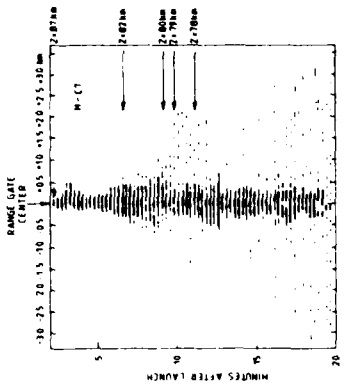
10

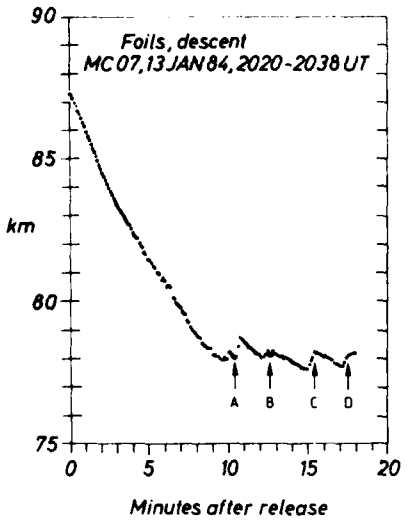
Fig. 10: Typical heights vs time plot obtained during the MAP/WINE campaign, Andenes, 69°N. Unsmoothed radar raw data (*radar plotter output*). Rate: *1 point per* 6 sec. "Hold": descent of cloud stops for a certain while. Velocity of descent v = o or even positive . Flare-out: cloud remains at a certain height for a longer time. End of tracking caused either by dissolution of the cloud in turbulence or caused by lack of time.



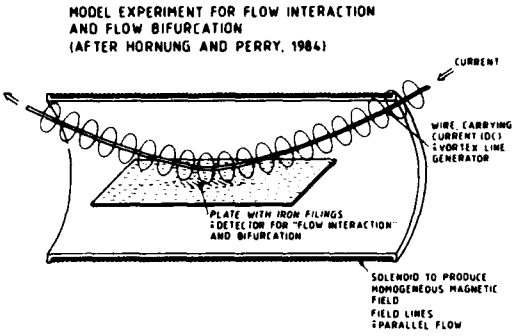
11

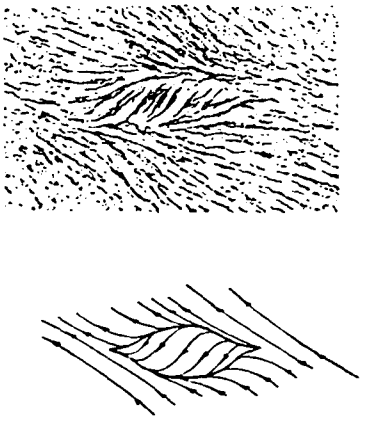
Fig. 11: Linkage between horizontal wind structure and deceleration resp. acceleration of descent. Length of wind arrow (meteorological convention) proportional to wind speed. Wind direction: angle in compass card. Wind obtained by smoothing (polynomial fit through raw data. Winds provided by W. Meyer, University Bonn).





12





13

Fig. 12: Degeneration of a "hold" into a hopping motion of the chaff. Radar raw data plotted at a rate of 1 per six seconds. Each time the chaff cloud is pushed upwards (A, B, C, D) the cloud is moved to the east ("stepping sideways"). Upper part of the figure (range gate echo evaluation) shows that, in essence, the whole cloud was affected by this movement.

Fig. 13: Flow simulation experiment of Hornung and Perry (1984): A steady, parallel flow is simulated by a homogeneous magnetic field realized at the interior of a long solenoid (hydrodynamic flow and magnetic fields obey both the Poisson equation). A vortex is simulated by the magnetic field of a DC current in a wire. Approach and leave of the vortex is simulated by the bend of the wire. Interaction between the two fields is detected by a plate covered with iron-filings. The interaction causes a "footprint" on the plate. Top: Experimental setup, middle: experimental result, bottom: result of calculation (all after Perry and Hornung, Zeitschrift für Flugwissenschaften und Weltraumforschung, 8 p. 155-160, 1984).

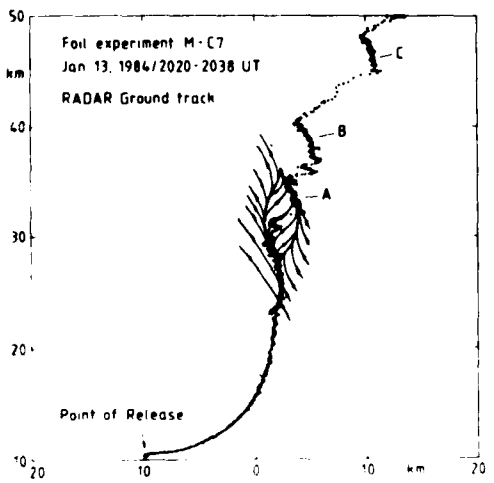
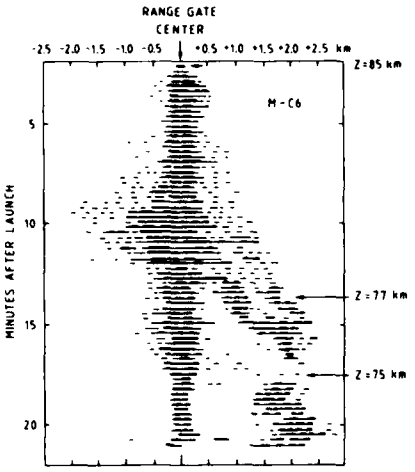
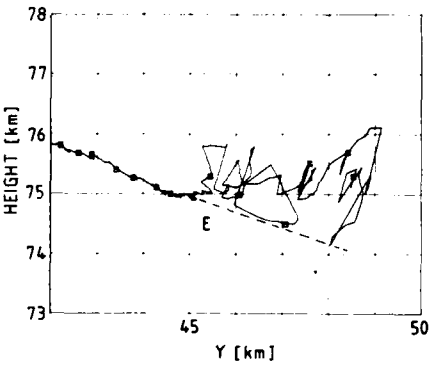


Fig. 14: Application of Hornung and Perry's "footprint" experiment onto radar ground track of flight M-C7.



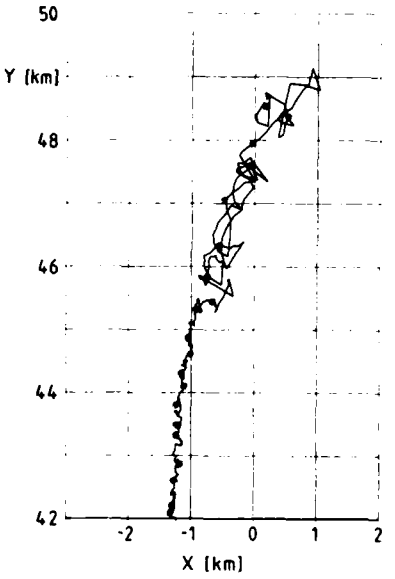
15



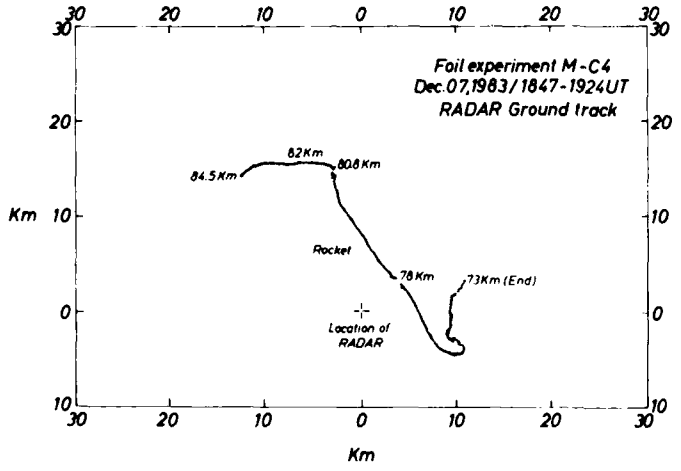
16

Fig. 15: An example of separation of flow which is seen only in the radar range gate echo record. Nothing peculiar is noticed on the radar ground track. The intensity of the split-off echo became occasionally larger than the main echo on which the radar looked on.

Fig. 16, 17: Example for an "explosive" destruction of a foil cloud in turbulence. Fig. 16: Look from the east onto the radar trajectory in the height vs south-north plane. Fig. 17: Radar ground track. Radar raw data, plotted at a rate of 1/sec.



17



18

Fig. 18: Example for a "wind corner" seen in the radar ground track at Z = 80.8 km (wind veers off by 90 degrees within a height interval of less than 300 m). (von Zahn and Widdel, 1985).

DISCUSSION

F.Christophe, FR

Do you think a Doppler measurement could improve the knowledge of the phenomena?

Author's Reply

Yes, I wished the MPS 36 would have had true Doppler capacity which it hasn't. I see an improvement in a monopause pulse-compression radar with 3D — capability. At present I try to analyse the AGC recorded at 1/10 sec intervals, but this work has not yet been completed, so I don't know if this approach yields reasonable results or not.

E.Thrane, NO

Have the flow bifurcations you refer to been observed in the upper atmosphere?

Author's Reply

Yes.

SUMMARY OF SESSION VIII

Low Frequency Propagation

by

Mr J.Taagholt
Session Chairman

The subject of the session was conditions of important for low frequency propagation in the ionosphere's lower D-region and at the Earth's surface.

Field presented lower ionosphere conductivity profiles which were derived from oblique VLF soundings in North Greenland during a large solar proton event. The results obtained were compared with conductivity data derived from satellite measurements of the proton flux, at various energies. Although the results obtained from the two data sources differ, both methods show a conductivity during a solar proton event, which exceeds the conductivity during undisturbed conditions, by two or more orders of magnitude.

Prolss presented a study which comprises theoretical calculations and measurements of lightning discharges. The maximum spectral energy of the pulses are typically in the 5—9 KHz frequency range. The lightning discharges seem to be the predominant natural source of electromagnetic energy in this frequency range, and the analysis has shown, that it is possible to determine the propagation characteristics of the Earth—Ionosphere waveguide at VLF frequencies, by receiving the signals from this source at a distant location. In addition it is possible to determine the location of thunderstorm areas. Absence of signals can be caused both by lack of thunderstorms or by propagation-related factors.

In a second paper, Field presented a study which concerns unexpected attenuation of ELF signals in the Gulf of Alaska during PCA events. Calculations show that the attenuation might be caused by refraction of the ELF field into the Polar Cap during PCA events.

Stokke discussed ground conductivities with particular emphasis on the high latitude region. The earth's conductivity is a determining factor for low frequency propagation. Typical values of arctic ground conductivity, which can vary by six orders of magnitude for different types of terrain was presented. The importance of including information on the seasonal variation of the earth conductivity in the Arctic areas in the first edition of the CCIR conductivity atlas was discussed. An atlas is planned for publication during the fall 1985.

CONDUCTIVITY PROFILES OF THE DISTURBED POLAR IONOSPHERE FROM VLF REFLECTION DATA

P. A. Kossey and J. E. Rasmussen
Rome Air Development Center
Hanscom AFB, Massachusetts 01731

E. C. Field and C. R. Warber
Pacific-Sierra Research Corp.
Los Angeles, California 90025

SUMMARY

Two independent techniques are used to determine conductivity profiles of the lower polar ionosphere during a strong solar proton event (SPE). The first method inverts reflection coefficients measured with a ground-based VLF sounder; the second uses proton fluxes measured on board satellites to calculate ion-pair production rates, which, in turn, are input to lumped-parameter de-ionization equations. Conductivities determined by the two methods exceed ambient by two or more orders of magnitude, but disagree by up to an order of magnitude at altitudes between fifty and sixty kilometers. Full-wave calculations are used to predict the effect of the SPE-disturbed profiles on long range VLF propagation in the earth-ionosphere waveguide. The SPE is found to suppress the geomagnetically converted transverse electric field radiated by a ground-based vertical electric dipole.

1. INTRODUCTION

The lower ionosphere controls the propagation of long radio waves in the earth-ionosphere waveguide. Depending on the season, time of day, location, and solar activity, the most important altitudes lie between, say, 40 to 100 kilometers. Use of rocket-borne instruments to make direct measurements of the ionosphere's conductivity throughout that altitude range is difficult, so indirect methods are often used. The present paper compares profiles determined from two such indirect methods: (1) inversion of long-wave ionosounding data, and (2) chemical calculation using particle flux data. It obtains conductivity profiles for a strong solar proton event (SPE), and calculates the effect of those profiles on very low frequency (VLF) communication signals.

2. 23 SEPTEMBER 1978 SPE REFLECTIVITY DATA

Figure 1 diagrams the VLF/LF pulse ionosounder, developed by the Rome Air Development Center (USAF). The pulses radiated by the vertical antenna are so short that the ground waves arrive and are recorded before the arrival of the ionospherically reflected sky waves. The data are therefore free from groundwave and multi-hop-skywave interference. Although the transmitted pulses are vertically polarized, geomagnetic conversion causes the received skywaves to be elliptically polarized. Crossed-loop antennas receive and separate the "normal" and "converted" components of the skywaves. More detailed descriptions of the facility and its use are given by Lewis et al., [1973] and Rasmussen et al., [1980].

The data used in the present report were measured with the pulse transmitter located at Thule Air Base in Greenland. The receivers were 106 km to the north in Qanaq, Greenland, and were operated by the Danish Meteorological Institute. Those locations are ideal for studying the lower polar ionosphere, especially during disturbances such as energetic particle events.

After Fourier analysis of the received pulses, plane-wave reflection coefficients and effective heights of reflection are derived over most of the VLF spectrum. Fig. 2 shows examples of the reflection coefficients at local noon on 21, 23, and 18 September 1978. A strong (10 dB riometer absorption) SPE began at 1100 UT on 23 September. Also measured, but not shown, are the group reflection heights and the phase of the reflection coefficients. The group heights averaged around 82 km before the SPE (21 September), dropped to between 50 and 55 km on its first day (23 September), and recovered to between 60 and 70 km on its fifth day (28 September).

3. INVERSION OF REFLECTIVITY DATA FOR 23 SEPTEMBER 1978 EVENT

Fig. 2 shows that the normal reflection coefficient increased during the event, whereas the converted coefficient decreased. That decrease in conversion is caused by the pulse being reflected from reduced altitudes, where numerous collisions between electrons and neutral particles disrupt the electrons' rotation in the geomagnetic field. Because the normal coefficients substantially exceed the converted ones during the event, isotropic inversion theory, which uses only the normal reflection coefficient, will provide accurate conductivity profiles [Field, Warren, and Warber, 1983]. To illustrate that fact, we will also give results from the more complex anisotropic theory, which uses both the normal and converted coefficients [Warber and Field, 1984].

Since the theory is discussed in the above references, we summarize the isotropic inversion method only briefly. The anisotropic method uses the same logic as the isotropic one, but matrix operations must be used in place of scalar ones. Fig. 3 diagrams the method, which calculates successive approximations to an initial guess, σ^0, for the conductivity profile. We have found the final profile to be insensitive to the initial guess, as it should be, although a good initial guess does cause the iteration to converge

more quickly. In Fig. 3, the index i denotes the set of frequencies used and R denotes the normal reflection coefficient, R, which is calculated from the well-known equation

$$\frac{2i}{k}\frac{dR}{dz} = Cn^2(1 - R)^2 - \frac{q^2}{n^2C}(1 + R)^2 \qquad (1)$$

where

$$n^2(z) \simeq 1 - i\,\sigma(z)/\omega\varepsilon_0 \qquad (2)$$

$$\sigma(z) \simeq e^2 \sum_\gamma \frac{N_\gamma}{m_\gamma \nu_\gamma} \qquad (3)$$

C = cosine of incidence angle

and

$$q^2 = n^2 - (1 - C^2) \quad .$$

Equations (1-3) are valid at heights below about 70 km where the collision frequency ν_γ exceeds the gyrofrequency. Note that the inversion can determine only the total conductivity; auxiliary data on collision frequency and ion masses m_γ are needed to extract number densities from Eq. (3).

Ionosounding characterizes the conductivity only within the height-range where the ionosphere affects the ground-level reflection coefficients. Consequently, the inversion of VLF/LF reflectivity data can define the ionosphere within a height-range about 10 km in extent, but not at greater or lower heights. Fig. 4 illustrates that behavior and serves as an example of a validity criterion that we apply. It shows the height dependence of the upgoing wave's magnetic intensity H, normalized to unity at the ground and calculated for a profile representative of those that occur during a strong SPE. At low altitudes where $H \cong 1$, the ionosphere is too rarefied to reflect or absorb the wave, whereas at high altitudes where $H < 0.5$, the signal is weak and the return small. The hatched region most strongly affects the reflection coefficients and, therefore, indicates where the inversion can be trusted.

We have inverted the reflection coefficients shown in Fig. 2, using both the isotropic and anisotropic calculations. Fig. 5 shows the results, which we have expressed as equivalent electron density by assuming a nominal collision frequency profile and applying Eq. (3). Both profiles are plotted only within their region of validity, as determined from criteria like the one illustrated in Fig. 4. As expected, the two profiles are nearly identical. We emphasize, however, that neglecting the converted signal and applying the isotropic method is valid only for strong disturbances that suppress the reflection height to well below 70 km.

4. PROTON FLUXES DURING THE 23 SEPTEMBER 1978 SPE

During the 23 September 1978 SPE the GOES-2 geostationary satellite measured differential, omnidirectional proton fluxes in four energy bands defined by 4 to 8, 8 to 16, 36 to 80, and 80 to 215 MeV. Although the satellite was not on the same geomagnetic field line as the ionosounder, experience has shown the proton flux to be fairly uniform across the polar cap once the onset phase of an SPE has passed. The fluxes measured on board GOES-2 should therefore represent conditions on the field lines that intersect the ionosphere above Thule.

Calculation of ion-pair production rates in the ionosphere requires knowledge of the proton flux in a large number of narrow energy bands between about 1 and 300 MeV. Because GOES-2 used only four coarse energy bands, we must use an analytic fit to the spectrum in our calculations. The following empirical formula often gives an excellent fit to the integral flux:

$$J = J_0\, e^{-R/R_0} \quad \text{protons/cm}^2\text{-sec-sr} \qquad (4)$$

where

$$R = \sqrt{E^2 + 2EE_0} \quad \text{MeV}$$

E_0 is the proton rest energy, and J_0 and R_0 define the strength and energy rolloff of the integral flux.

The National Oceanic and Atmospheric Administration (NOAA) has fitted J_0 and R_0 to GOES-2 data throughout the 23 September SPE [Sauer, 1983]; Fig. 6 shows those fits for the first 16 hours. The strength, indicated by J_0, increased with time. The effect of that strength increase is partially cancelled by the decrease in R_0 which indicates a softening of the spectrum and, therefore, a reduction in the fraction of protons that can penetrate to altitudes that govern long-wave reflectivity.

5. PRODUCTION RATES AND DE-IONIZATION EQUATIONS

The first step in computing the ion-pair production rate q is to divide the integral flux, defined by Eq. (5) and Fig. 6, into energy bands so narrow each one can be assumed mono-energetic. Then we use curves of ion-pair production by monoenergetic protons, such as given by Reid [1978], to synthesize the total production rate profile. Fig. 7 shows production rates calculated for local noon and local midnight at Thule during the first day of the 23 September SPE. Although substantial, the production rates shown in Fig. 7 are much smaller than some given by Reagan et al., [1981] for earlier, stronger SPEs.

The production rates are inserted into the three-species, lumped parameter deionization model, which gives the following for the electron density N_e, and the positive ion density N_+ at height h.

$$N_e(h) = \frac{(q + D)}{[A + D + \alpha_d N_+(h)]} \quad , \tag{6}$$

$$N_+(h) = \frac{q}{\alpha} \quad , \tag{7}$$

where

$$\alpha = \frac{A\alpha_i + D\alpha_d + \alpha_i\alpha_d \left[\frac{q(A + D)}{A\alpha_i + D\alpha_d}\right]^{1/2}}{A + D + \alpha_i \left[\frac{q(A + D)}{A\alpha_i + D\alpha_d}\right]^{1/2}} \quad , \tag{8}$$

In the above equations, A is the attachment rate, D the solar detachment rate, and α_i and α_d are the ion-ion and electron-ion recombination rates. Air chemistry models exist which are more detailed than the one used here and which account for many more ionic species. However, uncertainties in the reaction rate coefficients limits the accuracy of even those very complicated models.

We put reaction rate values suggested by Knapp and Schwartz [1978] into Eqs. (6), (7), and (8) to determine the electron and ion densities. We then apply Eq. (3) to convert those densities to conductivities. The curve labeled "air chemistry" in Fig. 8 shows the resulting conductivity profile for local noon on 23 September. For comparison, Fig. 8 also shows (1) a nominal ambient mid-latitude daytime profile, calculated from the model of Pappert and Moler [1974], and (2) the profile obtained by inverting the ionosounder data. The latter profile corresponds to the equivalent electron density plotted in Fig. 5, and is extrapolated to heights above and below the range where the inversion is valid.

6. COMPARISON BETWEEN PROFILES CALCULATED FROM INVERSION AND AIR CHEMISTRY

Figure 8 shows that the conductivity profile obtained from inverting reflectivity data and the one obtained by solving de-ionization equations substantially exceed the nominal ambient conductivity, as expected. However, despite pertaining to the same time and location, they disagree by up to an order of magnitude in the 40-to-60 kilometer height range. That disagreement could be caused by inaccuracies in either the air-chemistry model or the inversion process.

Reaction rates are imprecise, with the recombination coefficients known no better than to within a factor of three. As a check on the chemical calculation, we re-computed the conductivity, using the production rates shown in Fig. 7, but varying the reaction rate coefficients throughout their generally accepted range of uncertainty. Although deviations from the conductivity profile shown in Fig. 8 did occur, in no case did the agreement between the "air-chemistry" and the "inversion" profiles improve substantially.

As a test on the inversion's self-consistency, we generated artificial reflectivity data by integrating Eq. (1), using the "air chemistry" profile from Fig. 8 as an input. We then applied the isotropic version to those calculated reflection coefficients. Fig. 9 shows that the calculated and input profiles agree closely in the 50-to-60 kilometer height range. As expected from the validity criterion plotted in Fig. 4, agreement outside of that range is poor.

We conclude that the disagreement shown in Fig. 8 is not caused by mathematical inaccuracies in the inversion.

7. EFFECT ON TRANSPOLAR VLF/ELF PROPAGATION

Several studies have shown that strong ionospheric disturbances--natural or manmade--can increase attenuation in the earth-ionosphere waveguide and thus degrade long-range VLF/LF signals (e.g., Field [1970]; Westerlund et al., [1969]). Moreover, that degradation is worse for signals that pass over poorly conducting ground, such as occurs in Greenland and parts of Canada, than for signals that propagate over, say, seawater [Field, 1981; Westerlund and Reder, 1973]. Not all strong SPEs cause severe VLF/LF degradation, however. Calculations show that, despite causing high riometer absorption, the 23 September SPE would affect the amplitude of a TM signal only modestly. We therefore examine its effect on the geomagnetically converted signal component.

Long-range VLF/LF signals consist of modes that propagate in the earth-ionosphere waveguide. When the geomagnetic field is ignored, a vertical electric dipole (VED) excites only transverse-magnetic (TM) modes, whose electric vectors are in the plane of propagation and mainly vertical. When the geomagnetic field is accounted for, however, a VED also excites an electric vector normal to the plane of propagation, because: (1) the TM mode--now a quasi TM mode--contains a transverse electric field, and (2) the TM modes are coupled to quasi transverse-electric (TE) modes, whose electric vectors are mainly horizontal and normal to the propagation plane. For discussion purposes we will not distinguish between those two generation mechanisms and refer to the transverse electric field simply as the "TE" field. Similarly, we will call the vertical electric field radiated by a VED the "TM" field.

Although usually unimportant near the earth where the impedence is low, TE fields generated by ground-based VEDs can be received by elevated antennas. For certain orientations, an elevated antenna can more easily receive a TE signal than a TM signal. In addition, geomagnetic conversion of energy radiated by cloud-to-ground lightning strokes can be an important source of atmospheric noise a few kilometers above the ground.

Figure 10 plots calculated TM and TE fields for a height of 30,000 feet. The transmitter is a 100 kilowatt ground based VED; the frequency is 20 kHz. Graphs are plotted for signals propagating in waveguides bounded on top by the three conductivity profiles shown in Fig. 8. We used a full-wave numerical calculation that accounts for the vertical inhomogeneity of the ionosphere and the curvature of the earth, and retained up to 14 waveguide modes, as needed (see Budden [1961]; Pappert [1970]; Field [1970]). Because the calculation includes the geomagnetic field, the charged particle densities and collision frequencies must be input separately, instead of lumped together in the scalar conductivity. We used Eq. (3) with a nominal collision profile to obtain the necessary particle densities. Finally, to highlight SPE-induced effects, we avoided the complicated Canadian/Greenland conductivity transitions by assuming seawater paths.

The three calculated TM signals are nearly the same. The differences between the "inversion" and "air chemistry" profiles therefore do not produce corresponding differences in the TM component--at least for 20 kHz propagation over seawater. Fig. 10 appears to imply the SPE would change the TM signal only slightly from its ambient value. That conclusion is not necessarily valid, however, because our model ambient ionosphere corresponds to mid-latitudes. Its application to high latitudes is open to question.

The most pronounced effect of the SPE is to suppress the TE component 10-to-20 dB. Moreover, we see that the "inversion" profile suppresses the TE component more severely than does the less dense "chemistry" profile. That suppression arises, of course, because the disturbed ionosphere reflects long waves from altitudes below those where geomagnetic conversion is substantial.

8. SUMMARY

We have used two independent techniques to determine ionospheric conductivity profiles during an SPE. The first method inverts reflection coefficients measured with a ground-based VLF sounder; the second uses proton fluxes measured on board satellites to calculate ion-pair production rates, which, in turn, are input to lumped-parameter de-ionization equations. Conductivities determined by the two methods exceed ambient by two or more orders of magnitude, but disagree by up to an order of magnitude at altitudes between fifty and sixty kilometers. Calculations show the SPE will suppress the geomagnetically converted TE component of the long-range signal radiated by a ground-based vertical electric dipole.

REFERENCES

BUDDEN, K. G., 1961, *The Waveguide Mode Theory of Wave Propagation*, Logos Press, London.

FIELD, E. C., 1970, "The Effects of Ions on Very Low Frequency Propagation during Polar Cap Absorption Events," *Radio Sci.*, Vol. 5, No. 2, pp. 591-600.

FIELD, E. C., 1981, "VLF Propagation in Disturbed Environments," presented at AGARD 29th Symposium on Medium, Long, and Very Long Wave Propagation (at frequencies less than 3000 kHz), Brussels, Belgium, 21-25 September 1981, Paper 17.

FIELD, E. C., R. E. WARREN, and C. R. WARBER, 1983, "Calculation of Ionopsheric Conductivity Profiles by Inverting VLF/LF Reflection Data," *Radio Sci.*, Vol. 18, No. 3, pp. 452-460.

KNAPP, W. S., and K. SCHWARTZ, 1975, *Aids for the Study of Electromagnetic Blackout*, Defense Nuclear Agency, Washington, D.C., DNA 3449.

LEWIS, E. A., J. E. RASMUSSEN, and P. A. KOSSEY, 1973, "Measurements of Ionospheric Reflectivity from 6 to 35 kHz," *J. Geophys. Res.*, Vol. 78, pp. 3903-3912.

PAPPERT, R. A., 1970, "Effects of Elevation and Ground Conductivity on Horizontal Dipole Excitation of the Earth-Ionosphere Waveguide," *Radio Sci.*, Vol. 5, No. 3, pp. 579-590.

PAPPERT, R. A., and W. F. MOLER, April 1974, "Propagation Theory and Calculations at Lower Extremely Low Frequencies (ELF)," *IEEE Trans. Comm.*, Vol. COM-22, pp. 438-451.

RASMUSSEN, J. E., P. A. KOSSEY, and E. A. LEWIS, 1983, "Evidence of an Ionospheric Reflecting Layer below the Classical D- Region," *J. Geophys. Res.*, Vol. 85, pp. 3037-3044.

REAGAN, J. B. et al., 1981, "Modeling of the Ambient and Disturbed Ionospheric Media Pertinent to ELF/VLF Propagation," presented at AGARD 29th Symposium on Medium, Long, and Very Long Wave Propagation (at frequencies less than 3000 kHz), Brussels, Belgium, 21-25 September 1981, Paper 33.

REID, G. C., 1978, "Polar Cap Absorption--Observations and Theory," in C. Gordon, V. Canuto, and I. Axford (eds.), *The Earth: 1. The Upper Atmosphere, Ionosphere, and Magnetosphere*, Gordon and Breach, New York City, pp. 269-302.

SAUER, H., 1983, private communication, National Oceanic and Atmospheric Administration, Boulder, Colorado.

WARBER, C. R., and E. C. FIELD, JR., 1984, *Calculation of Ionopsheric Profiles by Inverting VLF/LF Reflection Data: II. Anisotropic Propagation*, Rome Air Development Center, RADC-TR-242, December.

WESTERLUND, S., and F. H. REDER, 1973, "VLF Radio Signals Propagating over the Greenland Ice-Sheet," *J. Atmos. Terr. Phys.*, Vol. 35, pp. 1479-1491.

WESTERLUND, S. et al., 1969, "Effects of Polar Cap Absorption Events on VLF Transmissions," *Planet, Space Sci.*, Vol. 17, pp. 1329-1374.

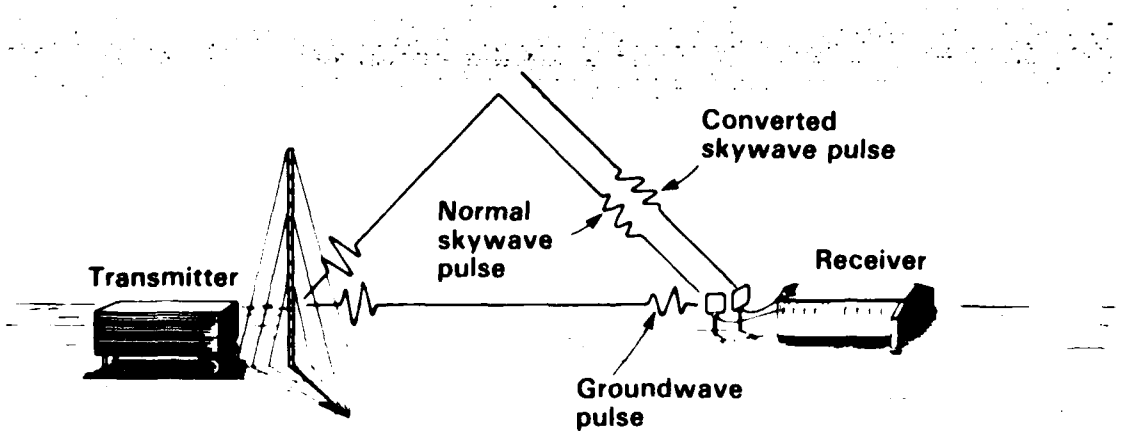


Figure 1. VLF/LF pulse ionosounder

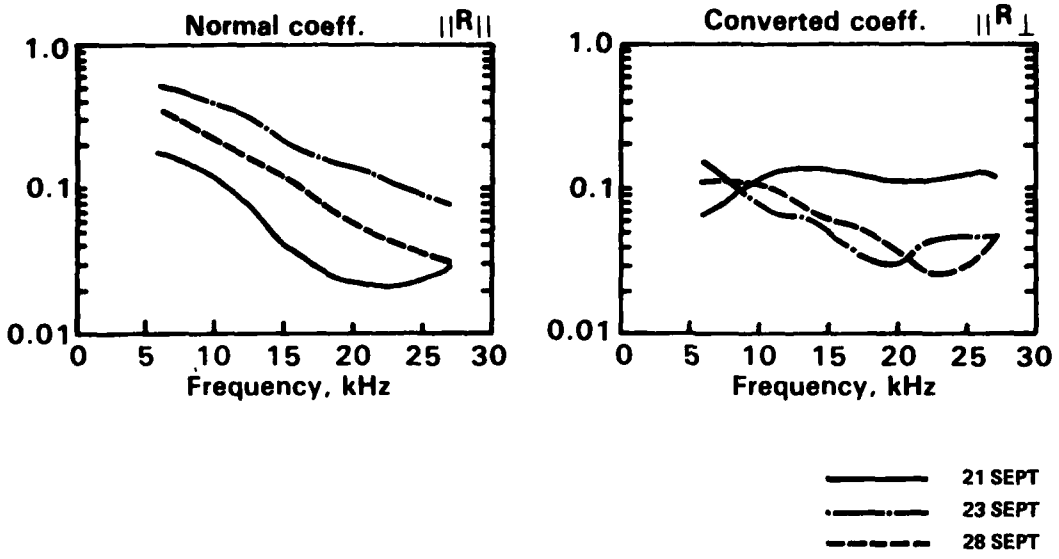


Figure 2. September 1978 PCA reflectivity data (local noon)

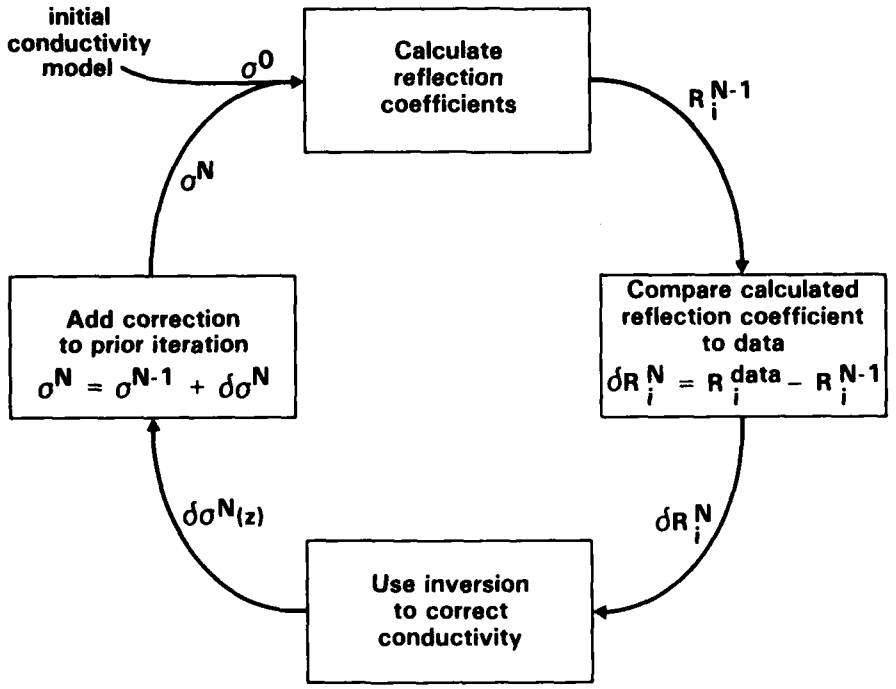


Figure 3. Schematic of isotropic inversion

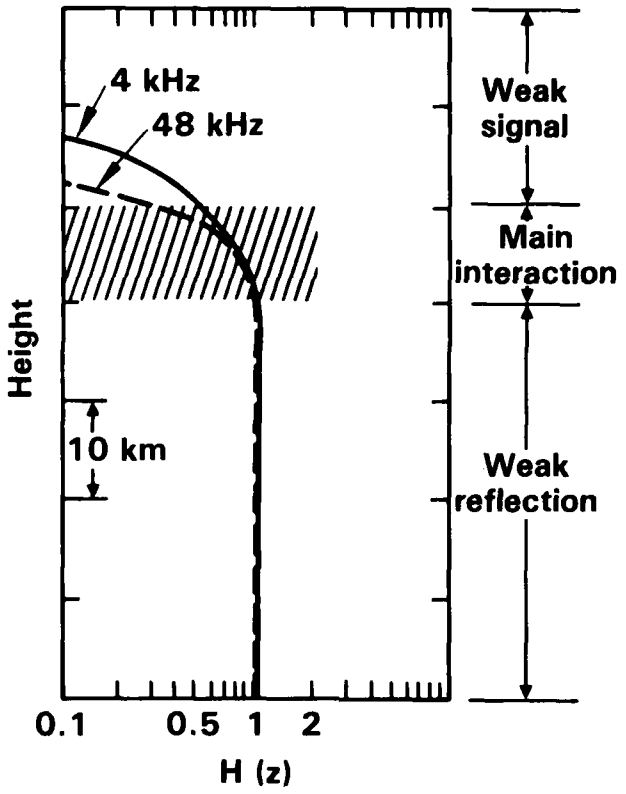


Figure 4. Validity test for calculated profiles

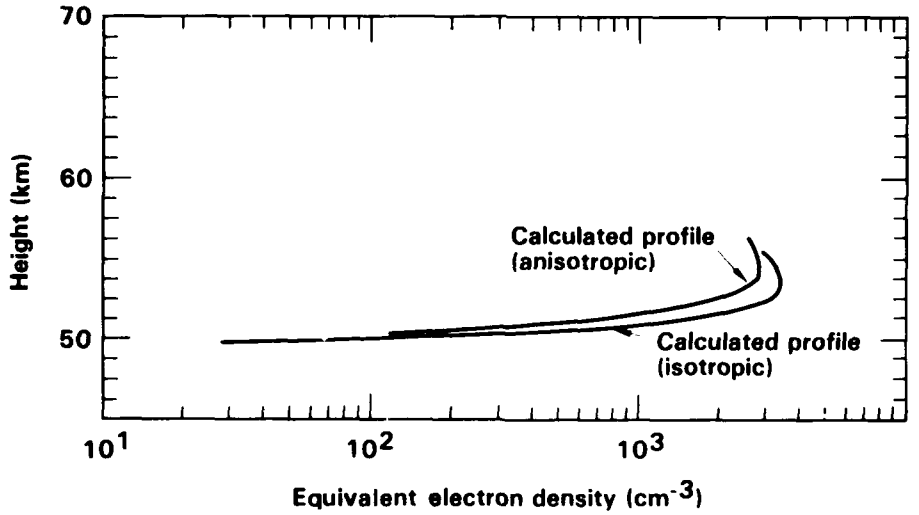


Figure 5. Inversion results for September 23, 1978: Isotropic and anisotropic calculations

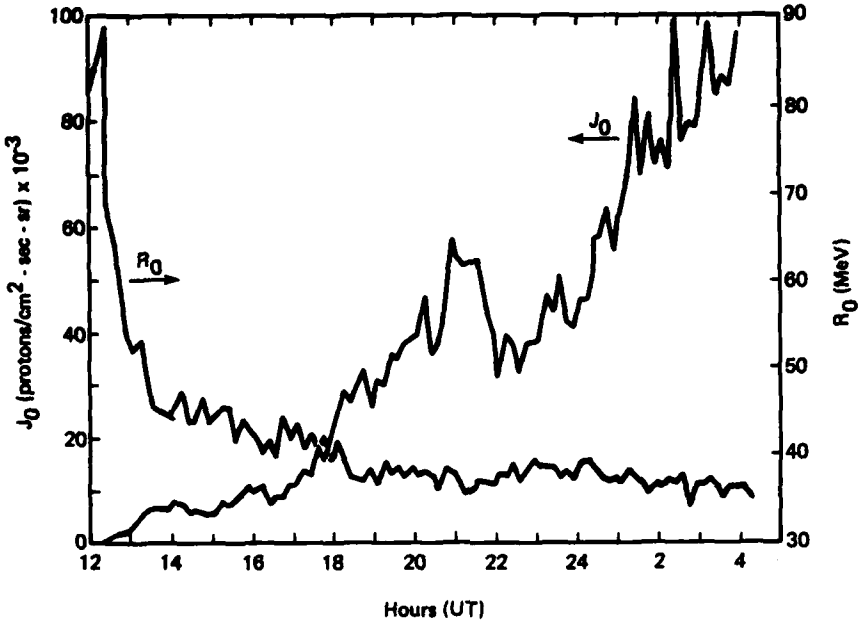


Figure 6. Strength and rigidity: 23 September 1978

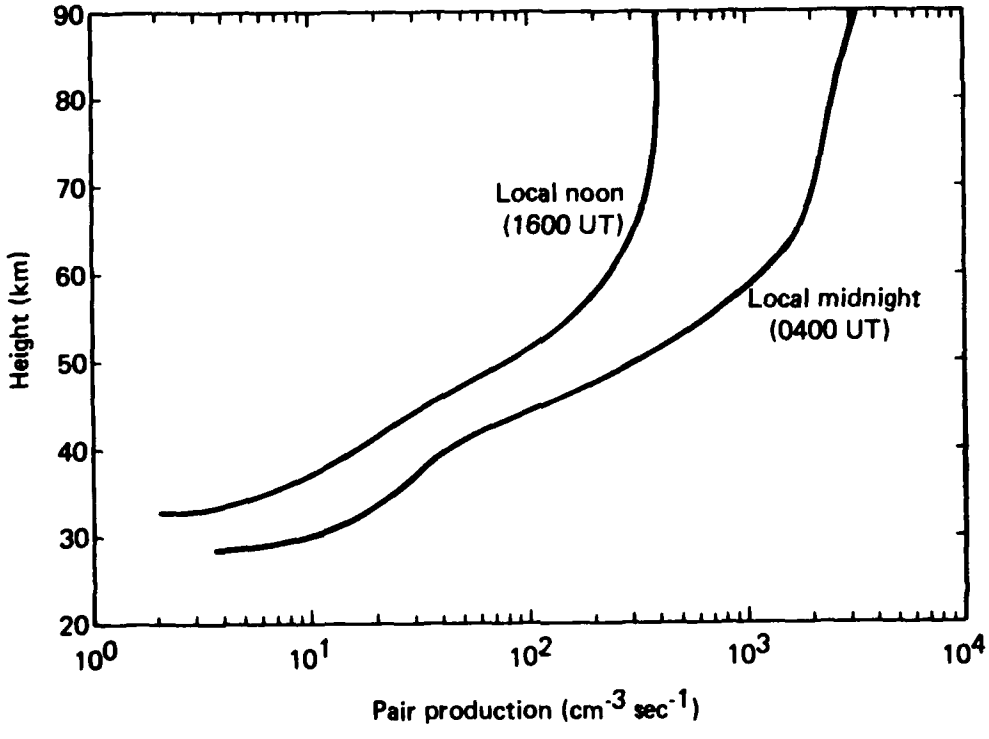


Figure 7. Pair production rates: 23 September 1978

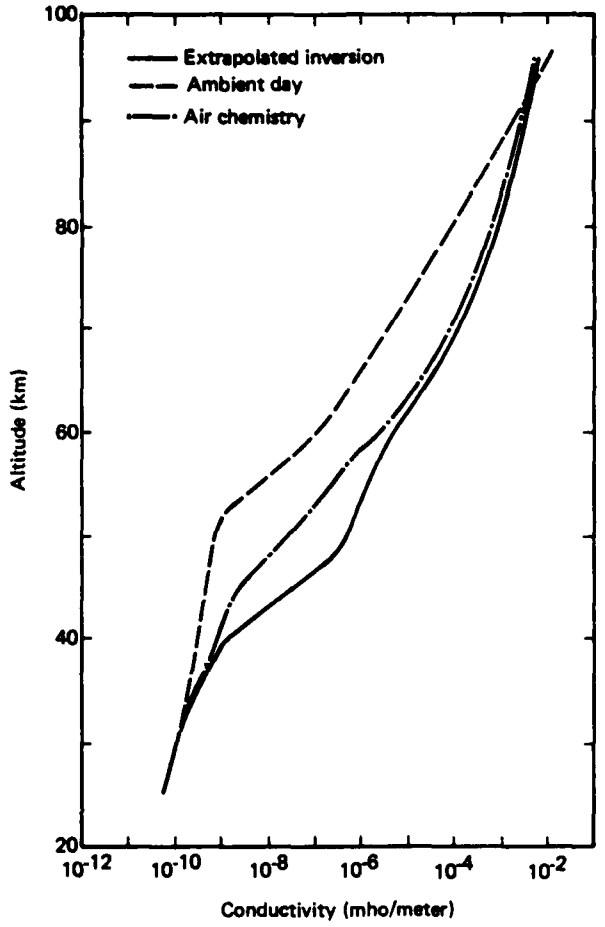


Figure 8. Conductivity profiles: 23 September 1978

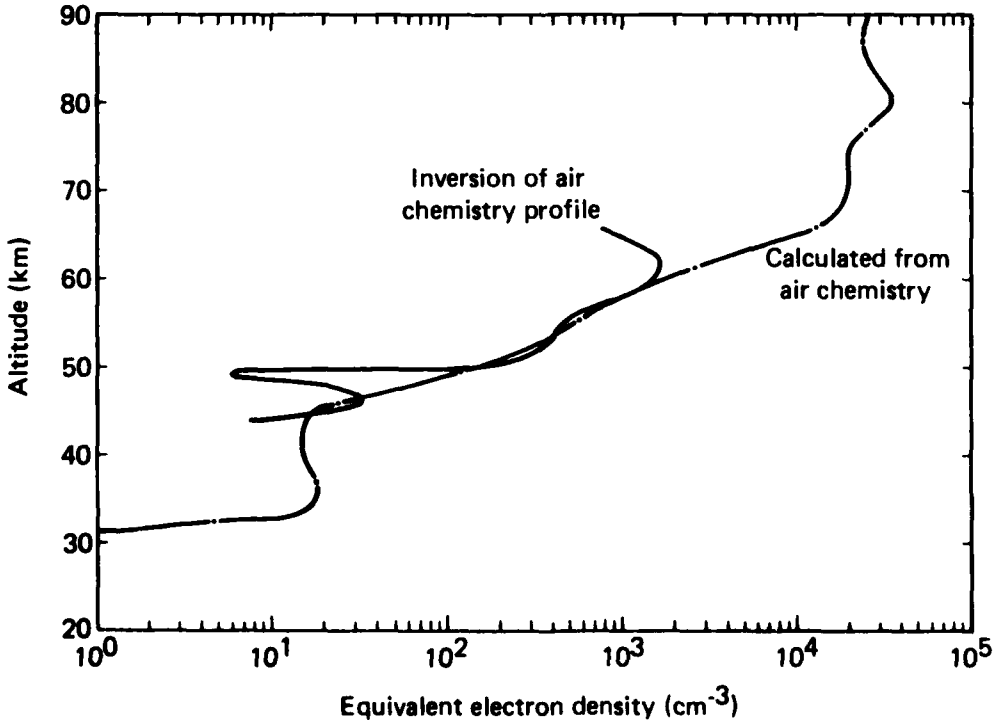


Figure 9. Conductivity profile from air chemistry

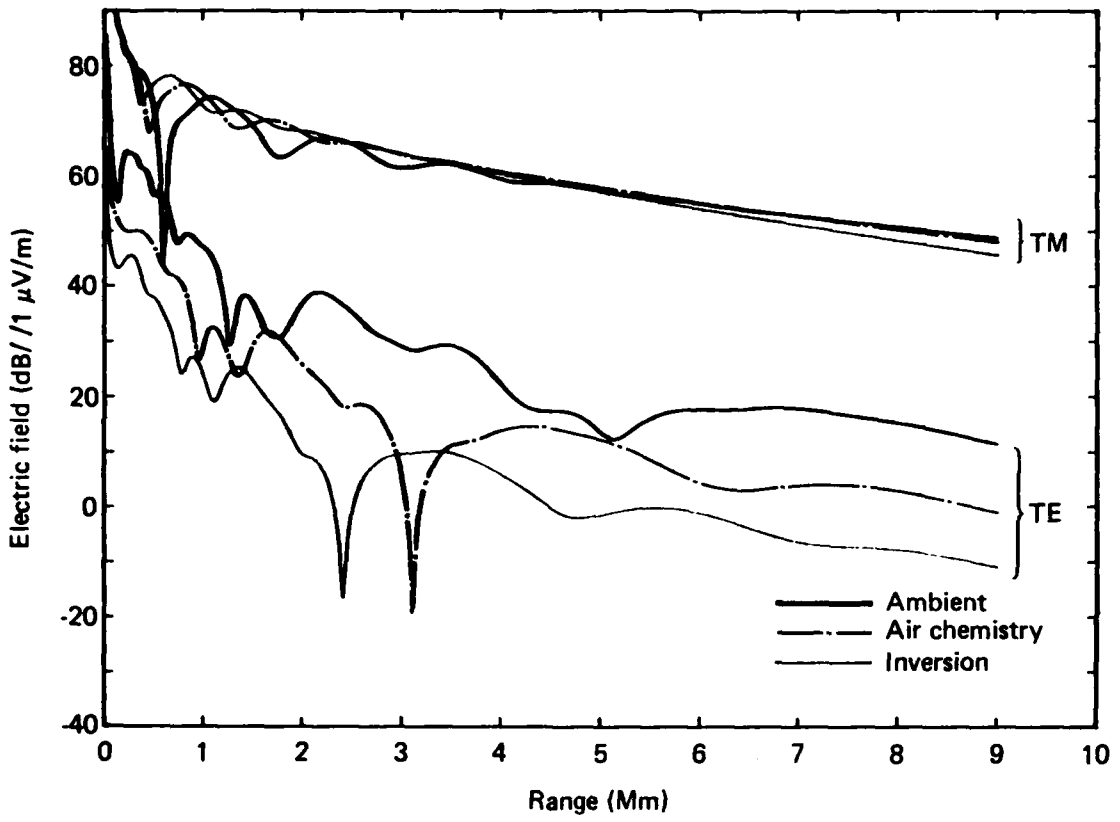


Figure 10. Electric field versus distance at H = 30,000 ft, 100 kw, 20 kHz, ground based VED XMTR sea water path

DISCUSSION

J.S.Belrose, CA

This subject, as you know, was well discussed at an earlier AGARD Symposium (in Brussels in September 1981). I wonder what is new in the results you have presented? For your reply I pose three questions: (1) How do your inversion techniques compare with those of the NOSC Group (Morfitt, Shellman et al)? (2) How does your atmospheric modelling compare with that of the Lockheed Group (Regan et al)? (3) Have you compared your deduced profiles with measured profiles, e.g. Sedden, et al and Ulwick et al measured profiles for a 3 dB absorption event (see my overview lecture in AGARD meeting)? Of course not all 3 dB events will give the same N(h) profile. I might draw your attention to my early COSPAR paper that shows that inversion techniques work very well given sufficient VLF—LF propagation data, preferably steep-incidence data of the type that you have been studying. However the reliability of the profile depends very strongly on the reliability of the propagation data.

Author's Reply

(1) The inversion technique differs mathematically in several respects and it runs more efficiently under disturbed conditions where geomagnetic effects are small.

(2) It compares closely.

(3) No.

E.Thrane, NO

In your model for the recombination did you take into account the height variation of the effective recombination coefficient, and was this variation representative of disturbed conditions?

Author's Reply

Yes.

T.B.Jones, UK

The inversion technique works better when the profile contains only little structure. In the case of a PCA profile the methods should therefore work well. It is perhaps worth noting that in the inversion method there will be a tradeoff between accuracy in the electron density and the resolution in height of the derived N(h) profile.

Author's Reply

I agree. Thank you.

G.Sales, US

(1) Is it possible that the part of the lower ionosphere determined by the inversion process is not the same as that involved in the long range 20 kHz propagation. (2) Could the agreement be improved by calculating the long range VLF at other frequencies, where the altitude agreement might be better?

Author's Reply

Yes. The steep incidence sounder signal penetrates to slightly greater altitudes than the obliquely incident long-range signals. However, because the sounder used frequencies both higher and lower than the 20 kHz long range signal, we feel that the relevant height range is covered adequately.

A STUDY OF VLF PROPAGATION AT HIGH SOUTHERN LATITUDES USING SFERICS

H. Volland[1)], M. Schmolders[1 *)], G. Proelss[2)], and H. Kröninger[3)]

1) Radioastronomical Institute, University of Bonn, 53 Bonn, W.Germany
2) Institute of Astrophysics, University of Bonn, 53 Bonn, W.-Germany
3) National Electrical Engineering Research Institute, Pretoria, South Africa

*) now at Rechenzentrum, Universität Dortmund

SUMMARY

Sferics are electromagnetic pulses generated by lightning events. Their maximum spectral energy is in the frequency range below 15 kHz. These powerful natural VLF transmitters can be used to determine the propagation characteristics of the atmospheric wave guide between earth and ionospheric D layer along virtually every propagation path. A VLF-sferics-analyzer was operating at the German antarctic von-Neumayer station from January to July 1983. This analyzer records sferics from distant lightning events in the frequency range between 5 and 9 kHz. The method of measurement is described. The data of June 1983 are evaluated, and the distances of the sources are determined by a comparison with rainfall records during the same month and, in addition, with sferics recordings from a station in Pretoria, South Africa. The data evaluation of the propagation conditions is compared with theoretical calculations. The main result is that the virtual reflection height of the ionospheric D layer is between about 78 km at noon and about 84 km during midnight in reasonable agreement with the theory. The difference between west-to-east and east-to-west propagation is smaller than the theory predicts indicating that the ionospheric D layer at high southern latitudes behaves more isotropic with respect to VLF propagation than at mid-latitudes.

1. INTRODUCTION

No commercial transmitter is continuously operating in the frequency range below 10 kHz. Studies of the propagation characteristics of these waves can be made using sferics, i. e., electromagnetic pulses generated by lightning strokes. The very low frequency (VLF) component (3 - 30 kHz) of the sferics signal propagates in the atmospheric wave guide between the earth and the ionospheric D layer. The virtual ionospheric reflection height of VLF waves at mid-latitudes is about 70 km during the day and about 80 km during nighttime conditions.

Lightning strokes are powerful transmitters of VLF pulses. These signals become only weakly attenuated in the atmospheric wave guide and can therefore reach large distances (several 1000 km) before they decay below the noise level of the receiver The atmospheric wave guide is dispersive and modulates the wave form of a sferic during its propagation. A measurement of the wave form and the direction of arrival of an individual sferic is therefore, in principle, sufficient to determine the location of the source- the lightning stroke. Several methods exist for locating thunderstorm areas via measurements in the VLF range. For a review, see Volland [1982].

The goal of VLF sferics measurements is directed either to the source properties- the characteristics of the lightning stroke and the distribution of the sources-, or to the properties of the atmospheric wave guide- the changing propagation conditions of the wave guide as function of local time, season, and propagation path. Both subjects are intimately related to each other. In order to study the source properties, one has

to know the wave guide properties, and vice versa. A third goal of sferics observations is the determination of the natural radio noise level which limits long range radio wave communication [Spaulding, 1982].

In this paper, we emphazise the second goal and determine the propagation characteristics of the atmospheric wave guide from VLF sferics measurements using observation at the antarctic von-Neumayer station and at a station in Pretoria, South Africa,during June 1983. The frequency range is between 5 and 9 kHz.

2. METHOD OF MEASUREMENT

We give in this section a brief description of the method of measurement. Additional details about the instrument and the method may be found elsewhere [Volland et al., 1983].

Sferics from sources more than several hundreds of km away from the receiver are mainly the electromagnetic pulses from the vertically oriented section of lightning channels of return strokes. These pulses behave to a first approximation like the radiation component of a vertical electric dipole located on the well-conducting ground. The electromagnetic component of such pulses consists of a (nearly) vertical electric field E_z and a horizontal magnetic field H_ϕ directed (nearly) orthogonal to the direction of arrival. The horizontal magnetic field is used to determine the angle of arrival ϕ by applying the well-known direction finding method with two crossed loop antennas and a whip antenna.

The vertical electric field component of each sferic is Fourier analyzed by means of three narrow band receivers at 5, 7, and 9 kHz. The resultant spectral function is the product of the spectral source function G(f) and the transmission function W(f,p) of the atmospheric wave guide:

$$E_z(f,p) = G(f)\, W(f,p) = |G|\, |W| \exp[i(\varphi+\Psi)] \qquad (1)$$

The transmission function W depends mainly on the frequency f and the distance p between source and receiver. In addition, it depends on the direction of arrival ϕ as well as on local time and season [e.g., Harth, 1982]. The spectral function G depends on frequency, the electric moment of the lightning stroke, and its channel parameters such as channel length and diameter.

The parameters which we measure are the spectral amplitude (SA) of each sferic exceeding the threshold of the receiver:

$$SA = 20 \log |G(f_1)\, W(f_1,p)| \qquad (2)$$

the spectral amplitude ratio (SAR):

$$SAR = 20 \log \frac{|G(f_2)\, W(f_2,p)|}{|G(f_1)\, W(f_1,p)|} \qquad (3)$$

the group time delay difference (GDD):

$$GDD = \frac{\theta(f_1) + \theta(f_2) - 2\theta(f_0)}{2\pi(f_0 - f_1)} \qquad (4)$$

and, in addition, the angle of arrival, or azimuth, ϕ. The frequencies are denoted as f_1 = 5 kHz, f_2 = 9 kHz, and f_0 = 7 kHz. The spectral phase of the signal is $\theta = \Psi + \Psi$. The group time delay difference is in a first approximation the second derivative with respect to the frequency of the spectral phase θ. The first derivative of the spectral phase Ψ of the transmission function is proportional to the reciprocal group velocity. Its second derivative is, therefore, a measurement of the dispersion properties of the atmospheric wave guide.

Each data set (SAR, GDD, SA, ϕ) of a sferic is stored in a desk top computer HP 9825 during a measurement cycle of 20 minutes. Figure 1 shows the observed GDD-values versus azimuth ϕ for a time interval of 18 minutes from 19:40 to 19:58 GMT on 20 August 1984 in Bonn. One clearly notes five clusters of points which can be attributed to five thunderstorm areas. Figure 2 shows the corresponding SAR-data versus azimuth during the same time interval. The same thunderstorms can again be identified. Using a histogram of the number of GDD (or SAR) events at each azimuth, shown in Figure 3 (lower panel), one can determine the azimuth $\overline{\phi}$ of the centers of the thunderstorm areas with an accuracy of about one degree.

Histograms of the GDD, SAR, and SA data may be calculated for each source. The example in Figure 3 (upper panel) belongs to the most intensive source at an azimuth of 104° (which is east-south-east of Bonn). The distance to this source is about 1900 km from Bonn. A Gaussian fit to such histograms yields mean values $\overline{GDD}$, $\overline{SAR}$, and $\overline{SA}$ which are then used in the subsequent data processing for a determination of the distance to the source. This will be discussed in the next section.

The data evaluation is completed in two minutes. The result, consisting of the four numbers $\overline{GDD}$, $\overline{SAR}$, $\overline{SA}$, and $\overline{\phi}$ of each source observed in the measurement cycle, their calculated distances, and code numbers identifying the sources and their strengths, are stored on magnetic tape. The support information represented by Figures 1, 2, and 3 is destroyed prior to the start of the next 20 minute measurement cycle. The locations of the actual thunderstorm centers can be plotted on a map in real time so that an observer can monitor the thunderstorm activity in the far field of the station. One magnetic tape cassette can store data covering about three to four weeks.

3. DATA EVALUATION

In this section, we discuss the evaluation of the distance of each source from the mean values $\overline{GDD}$ and $\overline{SAR}$. The theory of VLF propagation within the atmospheric wave guide predicts a transmission function W at larger distances ($p > 1000$ km) of the form

$$W(f,p) = C\ (p/f)^{1/2}\ \exp[-(A+iB)p] \qquad (5)$$

The attenuation factor A and the propagation factor B depend on frequency f, angle of arrival ϕ, local time, and season [e.g., Harth, 1982]. C is a constant factor.

The spectral function G can be approximated by the spectral function of a vertical electric dipole. If the electric current of such a dipole has a temporal structure proportional to

$$\exp(-\alpha t) - \exp(-\beta t) \qquad (6)$$

then the spectral function becomes

$$G = - \frac{i\omega\alpha\beta\mu M}{4\pi\rho(\alpha - i\omega)(\beta - i\omega)} \qquad (7)$$

with $\mu = 4 \times 10^{-7}$ H/m the permeability of free space, $\omega = 2\pi f$ the angular frequency, M the electric moment of the stroke, and α and β two wave form parameters related to the channel length and channel diameter of the stroke [Volland, 1982].

The averaging process for GDD and SAR assures that the stroke parameters M, α, and β are already mean values within a thunderstorm area, which are assumed not to change very much in different thunderstorms. From eqs. (3) and (7) thus follows a relationship between ρ and $\overline{GDD}$ and $\overline{SAR}$, respectively:

$$\overline{SAR} \propto a_1 + b_1 \rho \quad ; \quad \overline{GDD} \propto a_2 + b_2 \rho \qquad (8)$$

The parameters a_1 and a_2 are sensitive mainly to the average source properties via the mean parameters α and β in eq.(7). Note that the electric moment M of each sferic is eliminated in $\overline{SAR}$ and $\overline{GDD}$. At the output of the receiver, the receiver constants must be added to a_1 and a_2 so that the measured constants a_1 and a_2 do not describe the true source terms.

The parameters b_1 and b_2 reflect the wave guide characteristics via the terms A and B in eq.(5). They depend on azimuth and time. Upon elimination of ρ in eq.(8), one obtains a relationship between $\overline{SAR}$ and $\overline{GDD}$:

$$\overline{SAR} = C_1 + C_2 \overline{GDD} \qquad (9)$$

with

$$a_1 = C_1(\phi) + C_2(\phi)\, a_2 \quad ; \quad C_2 = b_1/b_2 \qquad (10)$$

Figure 4 shows an example of the distribution $\overline{GDD}$ vs $\overline{SAR}$ taken from data of the Pretoria station during the month January 1984, between 12:00 and 16:00 GMT, and for the azimuthal sectors 345^0 - 15^0 and 285^0 - 315^0. The numbers at each point in Figure 4 indicate the number of events at this point during the time interval of one month at daytime hours. This plot verifies the relationship of eq.(9). The dash-dotted lines in Figure 4 are the regression lines. The regression lines of all twelve azimuthal sectors should meet in one point, which is the point (a_1, a_2). In this specific case, we find $a_1 \propto -12$ db; $a_2 \propto -35$ µs, and

$$b_1/b_2 \propto 0.18 + 0.03 \sin(\phi + 12^0) \qquad (11)$$

The phase shift of -12^0 is the geomagnetic declination at Pretoria and indicates the dependence of the propagation conditions on geomagnetic coordinates. One must repeat this evaluation for other times of day and seasons at every station.

The scattering about the regression lines in Figure 4 is due to

(a) man-made noise; these are the singular events far from the regression lines. They can be eliminated by allowing only a maximum deviation from the regression line.

(b) Day-to-day variations of the ionospheric D layer; the effect of such variations is relatively small during sunlit hours along the propagation path but can be substantial during nighttime conditions.

(c) Changes in the average behavior of lightning strokes in different thunderstorms due to changing meteorological conditions; a 20 % variation in the average channel length of the strokes, for instance, would cause the scatter of $\overline{SAR}$ and $\overline{GDD}$ in Figure 4.

It is not possible to eliminate the scatter from effects (b) and (c). This scatter gives rise to errors in the calculated distance. A long living stationary source appears therefore as a cluster of points elongated in the direction of arrival

4. DETERMINATION OF THE DISTANCE OF THE SOURCES

There remains the determination of the coefficients b_1 and/or b_2 from which one can derive the distance of the sources. We determined these parameters from simultaneous observations of strong source areas at Pretoria and at the von-Neumayer station. We compared these with rainfall records prepared by the German Oceanographic Weather Agency (Deutsches Seewetteramt) in Hamburg. Figure 5 shows, as an example, the locations of thunderstorms observed at the von-Neumayer station. Each point in this plot gives the location of one or more thunderstorms measured during every 20 minute cycle in June 1983. The bold points in this plot indicate locations where precipitation of 100 to 300 mm was measured during June 1983. The open circles are places where a rainfall of 300 to 600 mm during June 1983 was recorded. Although rainfall records are only loosely related to thunderstorm activity, they give a fair estimate of thunderstorm rates, at least on a statistical basis. Figure 6 shows the locations of thunderstorms observed from the Pretoria station during nighttime hours (23:00 to 5:00 GMT) in June 1983.

Two strong source areas can be identified from these two records: one broad area of thunderstorms near the east coast of South America between about 20^0 and 35^0 southern latitude, and a second source area in the Indian ocean southeast of South Africa in the general vicinity of Prince Eduard Island. Both source areas can also be seen on the map of thunderstorm days during June to August prepared by the WMO [WMO, 1956].

Determining the distance of these sources from the triangulation as well as from the precipitation map, we derived the coefficients b_1 and b_2 from the data of the von-Neumayer station as function of local time and azimuth. Only small daily variations are visible in the data of the von-Neumayer station. The coefficient b_1 increases and the coefficient b_2 decreases with azimuth. It is

$$b_1 \approx 4.6 \pm 0.8 + 0.7 \sin(\phi+22^0) \quad ; \quad b_2 \approx 36.5 \pm 2.0 - 3.8 \sin(\phi+22^0) \qquad (12)$$

where the phase shift of -22^0 is the geomagnetic declination at the von-Neumayer station. The upper signs in eq.(12) are valid during noon, the lower signs are valid during midnight. b_1 has the dimension (db/Mm); b_2 has the dimension (μs/Mm) with 1 Mm = 1000 km. In the case of the source near the east coast of South America, which is nearly geomagnetically north-west-north from the von-Neumayer station, the numbers in eq.(12) agree reasonably well with theoretical calculations of the propagation conditions in the atmospheric wave guide [Volland et al., 1983]. The virtual

reflection height of the ionospheric D layer for VLF waves below 10 kHz is in this case $z_0 \approx 78$ km at noon and $z_0 \approx 84$ km at midnight, and the electron density profile is

$$N \approx N_0 \exp[\lambda(z-z_0)] \qquad (14)$$

with $N_0 \approx 3 \times 10^8\ m^{-3}$, $\lambda \approx 0.4\ km^{-1}$

The reflection height is similar to nighttime conditions at mid-latitude stations because the propagation path is on the winter hemisphere at high southern latitudes. However, the propagation path from South Africa to the von-Neumayer station, which is nearly geomagnetically east-to-west, exhibits the tendency to more isotropic conditions, compared with the theory. The theory, which is based on mid-latitude conditions, predicts in this case a larger value of b_1 and a much smaller value of b_2 compared with the numbers given in eq.(12).

5. CONCLUSION

VLF sferics data from the German antarctic von-Neumayer station are available from 18 January to 9 July 1983. We have evaluated in this paper the data of June 1983 in order to determine the propagation characteristics of the atmospheric wave guide between earth and ionospheric D layer during this time of year. The propagation conditions along the propagation path from the east coast of South America to the von-Neumayer station are similar to nighttime conditions at mid-latitude stations and agree reasonably well with theoretical calculations. The propagation path from South Africa to the von-Neumayer station exhibits, however, more isotropic conditions than the theory predicts.

6. REFERENCES

Harth,W. (1982): Theory of low frequency wave propagation. in Volland, H. (ed): Handbook of Atmospherics II, p. 133-202.

Spaulding, A.D. (1982): Atmospheric noise and its effect on telecommunication systems performance. in Volland ,H. (ed): Handbook of Atmospherics I, p. 289-328.

Volland, H. (1982): Low frequency radio noise. in Volland, H. (ed): Handbook of Atmospherics I, p. 179-250.

Volland, H., et al. (1983): Registration of thunderstorm centers by automatic atmospherics stations. J. Geophys. Res. 88, 1503-1518.

WMO (1956): World distribution of thunderstorm days. WMO/OMM-No 21, Geneva.

ACKNOWLEDGEMENT

We are very grateful to all people of the G.-von-Neumayer station and at the A.-Wegener Institut für Polarforschung who contributed to the successful operation of the VLFAA station in the Antarctic. Our special thanks are due to Klaus Wallner and Arno Brodscholl who were in charge of the experiment at the von-Neumayer station. The tragic death of Klaus Wallner at the end of this mission is deeply regretted.

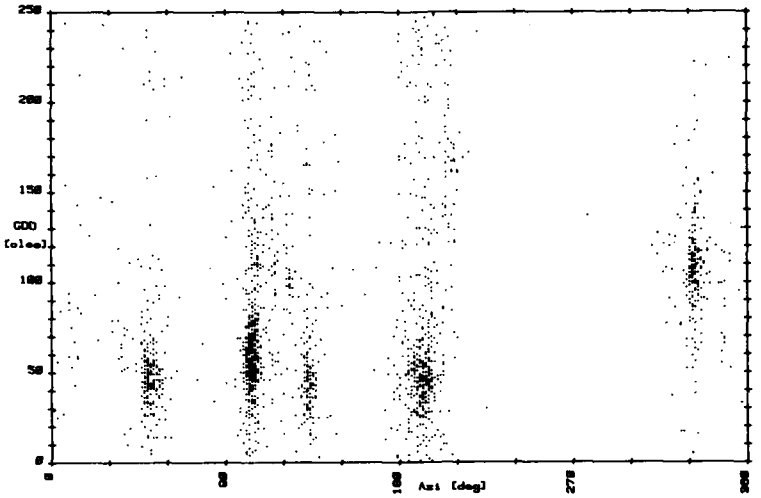


FIGURE 1. GDD-values vs azimuth observed during the time interval from 19:40 to 19:58 GMT on 20 August 1984 in Bonn. Each point represents one or more sferics signals. The azimuth (or direction of arrival) is counted in clockwise direction with $\phi = 0^{o}$ directed to the north, $\phi = 90^{o}$ directed to the east, etc. The units of GDD are arbitrary.

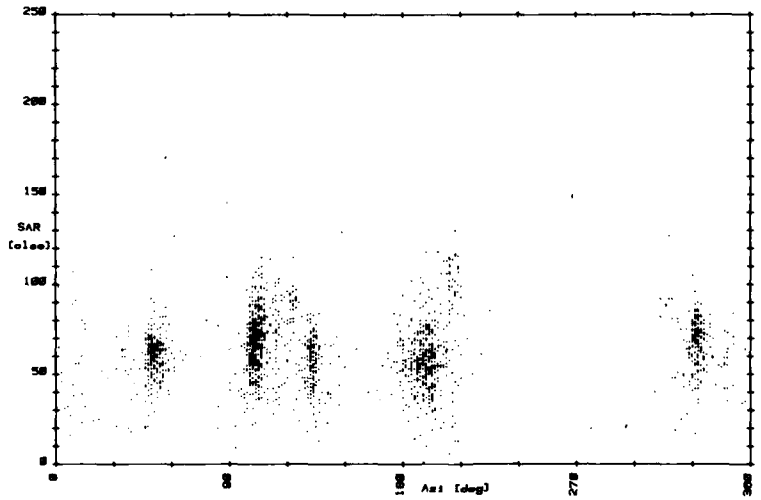


FIGURE 2. SAR-values vs azimuth. Otherwise as in Figure 1.

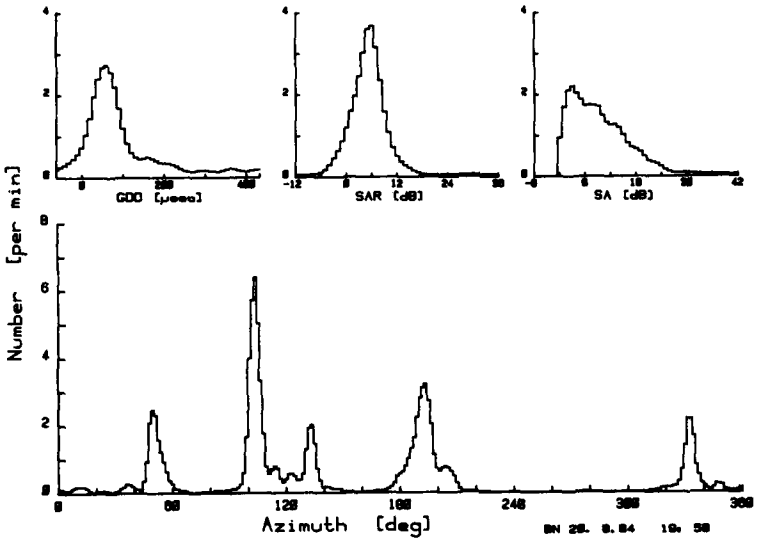


FIGURE 3. Histogram of all recorded GDD-values in Figure 1 as function of azimuth (lower panel); and histograms of the spectral parameters GDD, SAR, and SA of the strongest source at 104° azimuth (upper panel).

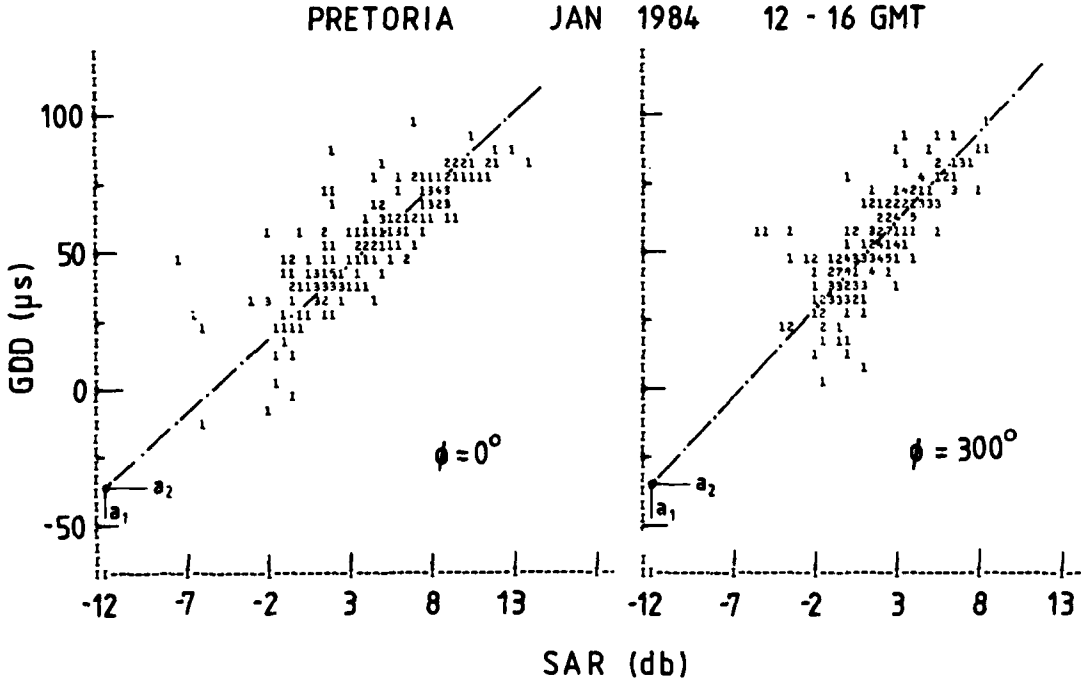


FIGURE 4. Plots of measured GDD-values vs SAR-values during sunlit hours (12:00 to 16:00 GMT) in January 1984 at the Pretoria station. The left diagram is for the azimuthal sector 345° - 15°; the right diagram is for the azimuthal sector 285° - 315°. The dash-dotted lines are the regression lines. The point (a_1, a_2) is the intersection of both regression lines.

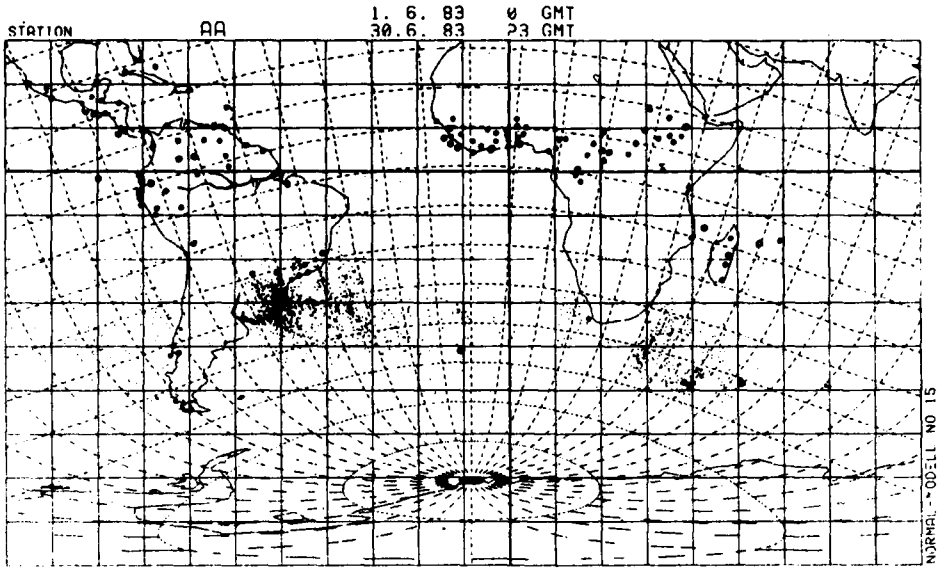


FIGURE 5. Plots of locations of thunderstorms during June 1983, registed at the von-Neumayer station. Each point represents the location of one or more thunderstorm centers observed during the measurement interval of 20 minutes. Dashed curves are isolines of distance (unit: 1000 km) and azimuth (unit: 10°). Bold solid points indicate stations with rainfall records between 100 and 300 mm during June 1983; bold open circles indicate stations with rainfall records between 300 and 600 mm during the same month (prepared by the German Oceanographic Weather Agency [Deutsches Seewetteramt] in Hamburg).

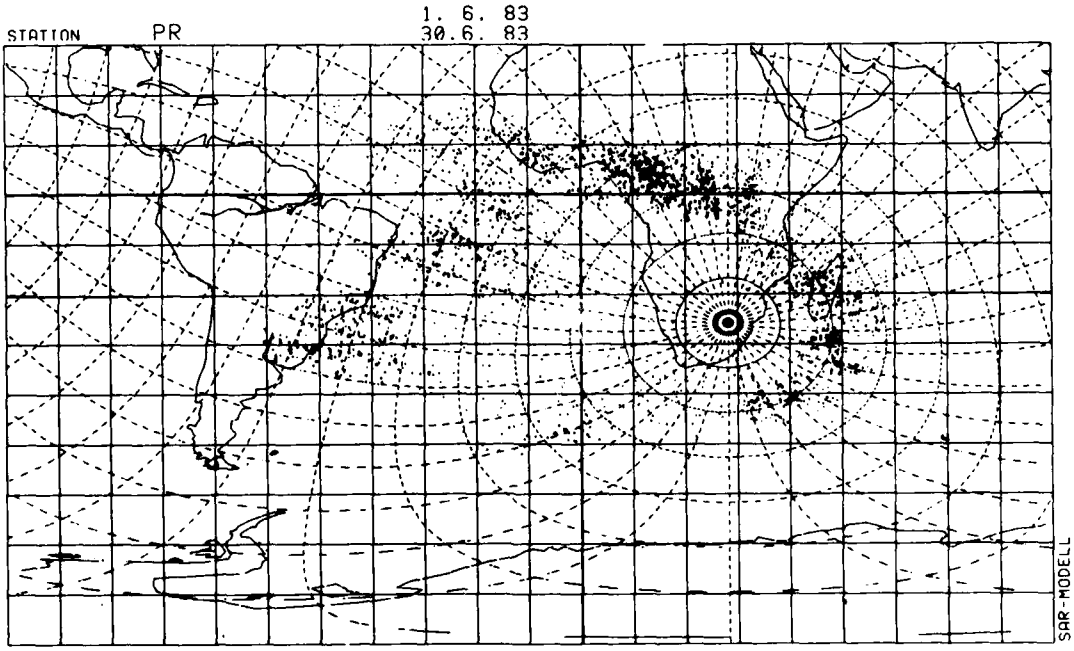


FIGURE 6. Plots of locations of thunderstorms during June 1983, 23:00 to 5:00 GMT recorded at Pretoria. Each point represents one or more thunderstorm centers observed during the measurement interval of 20 minutes.

DISCUSSION

B.Reinisch, US

You used in your analysis the measured spectral amplitude ratio (SAR). This ratio is determined by both the source function and the propagation conditions. How do you separate these effects? What is the resolution of your incidence angle measurements? If you use an interferometer, you must consider the possibility of non-planar wavefronts.

Author's Reply

It is the effective amplitude which is measured at the receiving station. One uses the spectral ratio to eliminate some of the not well known source properties which cancel out if the ratio of the two amplitudes is taken. The measurements are taken in the far field after wave has propagated long distances over ocean. One, therefore, may assume that the waveforms are, more or less, planar.

EFFECTS OF THE IONOSPHERE ON ELF SIGNALS DURING POLAR CAP ABSORPTION EVENTS: COMPARISON OF THEORY AND EXPERIMENTS

E. C. Field and C. R. Warber
Pacific-Sierra Research Corp.
Los Angeles, California 90025

R. G. Joiner
Office of Naval Research
Arlington, Virginia 22217

SUMMARY

In order to calculate ELF propagation when the earth-ionosphere waveguide is not stratified, this paper develops a hybrid method that uses full-wave theory to determine local parameters of the TEM mode, but uses ray theory to describe the field's horizontal variations. The method is applied to several model solar proton events (SPEs), including one based on the weak 23 November 1982 event. Calculations predict diminished fields near the Gulf of Alaska, where a submarine-borne receiver measured an unusually severe signal reduction. That behavior is caused by lateral refraction, which bends the signal away from the polar cap boundary and into the central cap where, during an SPE, the phase velocity of the TEM mode is slowest. The theory also predicts an enhanced field just inside the polar cap boundary, but no data are available to test that result.

1. INTRODUCTION

Extremely low-frequency (ELF) signals radiated from the Wisconsin Test Facility (WTF) occasionally exhibit anomalies too strong and localized to be caused by global changes in the attenuation rate. Nor could such anomalies be caused by mode interference, because, at ELF, only the TEM mode can propagate. A satisfactory explanation must account for lateral gradients in the earth-ionosphere waveguide.

Bannister [1982, 1984] summarizes nocturnal ELF anomalies measured simultaneously in the northeastern U.S. and on board submarines. The northeastern U.S. signals faded by many decibels in a few hours although the propagation paths were only about 1.6 Mm long. In the North Atlantic, three submarines separated by less than 2 Mm measured signals that differed from one another by up to 7 dB. Some of those anomalies had forms similar to ones measured in the northeastern U.S. a few hours earlier.

Pappert [1980, 1984] used an integral equation, similar to one developed by Field and Joiner [1979, 1982], and a scattering model developed by Greifinger and Greifinger [1977], to analyze the effects of sporadic-E patches on ELF propagation. He showed that such patches could cause nocturnal fades consistent with the measurements. The mechanism is resonant attenuation that depends on the vertical wavelength of the ELF wave and the optical thickness of the sporadic-E layer.

The present report develops a hybrid full-wave/ray theory to describe ELF signals whose great-circle path passes near the edge of the disturbed polar cap. It applies the theory to deep fades measured in the Gulf of Alaska during the weak solar proton events (SPEs) of 22 to 26 November 1982 [Katan and Bannister, 1985]. Those fades cannot be explained by theories that attribute ELF propagation phenomena solely to the state of the ionosphere along the great-circle path. Moreover, because the fades were observed in the daytime as well as at night, they could not have been caused by sporadic-E.

2. ELF ANOMALIES MEASURED DURING SOLAR PROTON EVENTS

The Naval Underwater Sound Center (NUSC) measured ELF amplitude and phase during several SPEs between the years 1976 and 1982 [see Katan and Bannister, 1985]. Some of the measurements were made in Connecticut, and others on board submarines. The strengths of those SPEs varied widely--the strongest on 13 February 1978 caused 8 dB of riometer absorption and the weakest on 23 November 1982 caused only 0.8 dB riometer absorption. ELF propagation and riometer absorption are governed by different regions of the ionosphere; ELF effects therefore can be greater during a weak SPE than during a strong one.

A weak SPE commenced at about 1600 UT on 22 November 1982. During that event the WTF signal was monitored on board a submarine in the Gulf of Alaska. Fig. 1 shows, approximately, the geometry of the great-circle propagation path, the disturbed polar cap, and the first Fresnel zone at a frequency of 76 Hz. Although the receiver location can not be specified precisely, we see the path is nearly tangent to the polar cap, which covers about one-half the Fresnel zone.

Fig. 2 plots the signal received in the Gulf of Alaska on 23 November 1982, along with the average ambient signal for that location. The disturbed signal was 3 to 4 dB below ambient during the night, and about 2 dB below ambient during the day. The relative phase remained close to its ambient value throughout the event.

Katan and Bannister [1985] show that the effective attenuation rate on 23 November 1982 exceeded 2.5 dB/Mm at night and 2.7 dB/Mm in the daytime. Such large attenuation rates would be expected only on paths totally exposed to very strong events. The size of the signal loss shown in Fig. 1 is therefore surprising, given; (1) the weakness of the SPE, (2) the shortness of the propagation path (3.5 Mm), and (3) the great-circle path having missed the main portion of the disturbed polar cap. As shown below, the explanation lies

in the propagation geometry, which causes lateral refraction of the TEM mode and, thus, shadow zones.

Katan and Bannister also report the following effective ambient attenuation rates on the Gulf of Alaska path: 1.4 dB/Mm (night) and 1.7 dB/Mm (day). Those rates exceed the ones usually measured in other geographic regions.

3. THE POLAR CAP ON 23 NOVEMBER 1982

The NOAA6 low-altitude polar-orbiting satellite measured integral proton fluxes in four channels defined by E > 2.5, 16, 36, and 80 Mev, where E is the proton energy. Fig. 3 shows those data for the end of 1982 November [Sauer, 1983]. One event began at approximately 1600 UT on 22 November and lasted at least until the middle of 24 November. A second and larger SPE commenced on 26 November. The fluxes plotted in Fig. 3 are averaged over magnetic latitudes higher than 70 deg. As shown by Fig. 4, once an event has developed, the flux is nearly uniform at latitudes above 60 deg. Therefore, the fluxes given in Fig. 3 represent those throughout the main portion of the cap.

As described in the companion paper [Kossey et al., 1985], we use the fluxes to compute, first, the ion-pair production rates and, second, ionospheric electron and ion densities. Fig. 5 shows ionization profiles calculated for 0800 UT on 23 November, as well as the assumed ambient profiles [Pappert and Moler, 1974]. Profiles calculated between 0200 and 1100 UT differed only slightly from the one shown, whereas profiles calculated for several daylight hours differed moderately. Although the densities shown in Fig. 5 substantially exceed ambient, they are at least an order of magnitude below the levels that occur during strong SPEs [Reagan et al., 1981].

In addition to the particle densities, the collision frequencies, mean ionic mass, and geomagnetic field strength must be specified in order to define the electromagnetic properties of the ionosphere. We use nominal electron and ion collision frequency profiles [Pappert and Moler, 1974], a nominal ion mass of 32 amu and a geomagnetic field strength of 0.5 G. We assume an east-west propagation path and a magnetic dip angle of -80 deg.

4. PROPAGATION PARAMETERS FOR 23 NOVEMBER 1982 SPE

In order to define the notation and illustrate the key dependences, we recapitulate the equation for the horizontal magnetic intensity H in a stratified waveguide [e.g., Galejs, 1972]:

$$H_\phi = A(\Lambda_T\Lambda_R)^{1/2}\left(\frac{c}{v}\,d\right)^{-1/2}\exp\left(-\frac{2\pi i}{\lambda}\frac{c}{v}\,d\right)e^{-\beta d/8.7}\cos\phi\ \text{A/m}, \qquad (1)$$

where A depends on the antenna moment, frequency, and ground conductivity, but not on the ionosphere; λ is the wave length in megameters; and ϕ is the angle between the propagation path and the end-fire direction. The excitation factors are Λ_T and Λ_R at the transmitter and receiver locations, c/v is the relative phase velocity, β is the attenuation rate in decibels per megameter of propagation, and d is the distance from the source in megameters.

The amplitude of a long-range ELF signal is most sensitive to changes--first in the attenuation rate β, and second, in the excitation factor Λ. The phase depends mainly on c/v.

In the idealized limit of a perfectly reflecting, sharply bounded ionosphere at a height H_0 above the ground, the excitation factor Λ is equal to $1/2H_0$. Even for diffuse ionospheric boundaries, as treated in this paper, the magnitude of Λ is of the same order as the reciprocal of the nominal ionosphere reflection heights. Thus, an ionospheric disturbance that lowers the effective height will increase Λ.

The literature supplies full-wave methods for calculating β, c/v, and Λ for virtually any ionospheric height profile, as well as numerical results for many models of ambient and disturbed ionospheres [Budden, 1961b; Field, 1970; Wait, 1970; Galejs, 1972; Pappert and Moler, 1974; Greifinger and Greifinger, 1978]. Table 1 lists propagation parameters calculated with such a code using profiles like those in Fig. 5 as inputs.

Table 1

Calculated propagation parameters at 76 Hz

Date	Time (UT)	β(dB/Mm)	c/v	H_0(km)
Ambient	Night	0.87	1.14	67
23 November 1982	0800 (night)	1.62	1.24	54
Ambient	Daylight	0.94	1.19	54
23 November 1982	1600 (daylight)	1.28	1.24	50

The calculated attenuation rates are smaller than the effective rates of 2.5 dB/Mm or more measured by Katan and Bannister on the Gulf of Alaska path for 23 November 1982. Moreover, even the modest attenuation rates shown in Table 1 would not have been fully realized on that path, because: (1) the entire path was not exposed to the main polar cap and, (2) the terminals were near the cap boundary, so some increase in excitation factor would be expected. If account is taken of that geometry, insertion of the numbers given in Table 1 into Eq. (1) predicts little, if any, signal loss during the event in question.

We conclude that the measurements cannot be explained solely by an increase in the waveguide's attenuation rate.

5. POLAR CAP BOUNDARY MODEL

To proceed with the analysis, we need a model of the TEM mode parameters in the polar cap boundary. Fig. 4 shows that the fluxes are approximately constant for magnetic latitudes above 60 deg and roll off between about 60 and 50 deg. Therefore, we assume the disturbed polar cap to be uniform above 60 deg latitude, which is about 3.0 Mm from the pole. The diffuse boundary extends to 50 or 55 deg and is 0.5 to 1 Mm wide. We assume a flat earth, an isotropic ionosphere, symmetry about the north geomagnetic pole, and model the propagation constant as:

$$S(x, y) = S_{SPE} + (S_{AMB} - S_{SPE})/\{1 + \exp[-7.3(r - r_0)/\Delta r]\}, \qquad (2)$$

where S is related to the phase velocity and attenuation rate by the formulas $c/v = \mathrm{Re}S$, and $\beta = -8.6K\ \mathrm{Im}S$. In addition, S_{AMB} and S_{SPE} denote S under ambient and disturbed conditions, respectively, r is the distance from the pole, Δr is the distance over which S makes 95 percent of its transition from disturbed to ambient, $r_2 = r_1 + \Delta r$, and $r_0 = (r_1 + r_2)/2$. Fig. 6 diagrams this model.

The receiver location cannot be specified precisely, so we represent the Gulf of Alaska as a 1 Mm square, centered 3.5 Mm from both the pole and the WTF, which also lies about 3.5 Mm (55 deg mag lat) from the pole. We use a nominal value of 3.0 Mm for r_1. Fig. 7 shows the resulting propagation geometry.

6. TWO-DIMENSIONAL RAY TRACE: LATERAL REFRACTION OF TEM MODE

Depending on geomagnetic activity and SPE strength, both the WTF and Gulf of Alaska sometimes lie in the boundary region, where strong transverse gradients in S could refract the field. More simply, the propagation constant S behaves as a refractive index and bends energy toward the inner cap, where the phase velocity is slowest. Under certain conditions, that effect causes shadow zones that are inaccessible to rays emanating from the WTF.

We test that hypothesis by using a simple ray trace. The results are semiquantitative, because the validity criterion for ray tracing is only marginally satisfied for some of the assumed boundaries and violated for certain abrupt ones.

Field and Joiner [1979] write the field as

$$E \approx A\, \Lambda(x, y)\, \psi(x, y)\, F(z)\ , \qquad (3)$$

where A is a constant involving dipole moment, wave frequency, and ground conductivity; Λ is the excitation factor and is a function of position; F contains the vertical dependence; and ψ contains the main lateral dependence, which can be found by solving

$$\left[\frac{\partial^2}{\partial x^2} + \frac{\partial^2}{\partial y^2} + \frac{\omega^2}{c^2} S^2(x, y)\right] \psi = 0 \qquad (4)$$

The WTF consists of two nearly perpendicular horizontal dipoles. Katan and Bannister [1985] report that the phase difference between the two antenna elements was 290 deg during the 23 November tests. That phase angle gives a radiation pattern that can be assumed symmetric.

We assume a propagation constant S given by Eq. (2). Because the propagation constant is analogous to a refractive index, the problem is mathematically identical to tracing rays obliquely incident on an isotropic ionosphere that varies in two dimensions, but is uniform in the direction perpendicular to the plane of propagation [Budden, 1961a). To isolate refractive effects, we ignore the imaginary part of S and, hence, absorption. Signal anomalies calculated in this fashion are caused solely by lateral focusing or defocusing of the TEM mode.

Figure 8 shows the dependence of ray trajectories on SPE strength. Rays are traced for $r_1 = 3.0$ Mm and three levels of disturbance: (1) weak, equivalent to the 23 November 1982 SPE, characterized by $\mathrm{re}S_{SPE} = 1.25$, (2) moderate, a bit stronger than the 8 December 1982

SPE, characterized by $reS_{SPE} = 1.35$, and (3) very strong, characterized by $reS_{SPE} = 1.50$. In each case we characterize ambient conditions by $reS_{AMB} = 1.15$, which corresponds to nighttime propagation.

In all cases the rays bend away from the Gulf of Alaska, indicated by the shaded square, and toward the polar cap. As expected, the refraction increases as the SPE becomes stronger. For all but the weakest events, a caustic is formed near the inner edge of the boundary region.

Figure 9 shows the dependence of the ray trajectories on boundary thickness. Those results were calculated for the weak SPE (S = 1.25) and values of Δr ranging from 0.5 to 1.0 Mm. As before, r_1 is assumed to be 3.0 Mm. We see that the signal depends strongly on boundary thickness as well as on the strength of the disturbance.

Although the ray trace is a convenient means of locating signal concentrations and rarefactions, Figs. 8 and 9 cannot be used for detailed comparisons between ambient fields and those measured during an SPE. That calculation would require each ray to be weighted by a number that accounts for the waveguide excitation factor. Nonetheless, Figs. 8 and 9 show that lateral refraction can be substantial.

Since the poynting vector is inversely proportional to ray density, we can estimate that, for a 1-Mm thick boundary, refraction reduces the Gulf of Alaska signal as much as 8 dB for the strong SPE; 3.5 dB for the moderate SPE; and 1.4 dB for the weak SPE. That defocussing becomes more pronounced as the boundary becomes more abrupt. For the weak SPE, which corresponds to the 23 November event, the ray trace predicts as much as 6 dB defocussing for the narrowest boundary (0.5 Mm) and 2 dB for the 0.7 Mm boundary. Such reductions in field strength are over and above losses attributable to attenuation. For the weak SPE, that defocussing could cause up to 1.5 dB/Mm increase in apparent attenuation rate on the Gulf of Alaska path.

The field depends on the juxtaposition of the receiver and the boundary. For all cases shown, a region of intensification (focusing) occurs just a few hundred kilometers north of the region of minimum field. Since the exact location of the submarine-borne receiver cannot be specified, a detailed comparison cannot be made between experiment and theory. However, the concept of energy refracting away from the Gulf of Alaska and into the polar cap appears consistent with the measured SPE-induced signal loss.

7. CONCLUSIONS

A two-dimensional ray trace is applied to several model SPEs, including one based on the 23 November 1982 event, for which simultaneous measurements of ELF signal anomalies and proton fluxes are available. Calculations indicate a diminished field in the Gulf of Alaska, where a submarine-borne receiver measured an unusually severe signal loss. That behavior is caused by lateral refraction, which bends energy away from the gulf and into the disturbed polar cap, where the phase velocity of the TEM mode is lowest. The theory also predicts signal intensification just inside the cap boundary, but no data are available to test that result. Because the boundary location depends on a number of geophysical parameters and, hence, time, we would expect signals near the boundary to be variable.

REFERENCES

BANNISTER, P. R., "ELF Propagation Update," *IEEE Journal of Oceanic Engineering*, Vol. OE-9, No. 3, July 1984, pp. 179-188.

BANNISTER, P. R., "Localized ELF Nocturnal Propagation Anomalies," *Radio Sci.*, Vol. 17, No. 3, May-June 1982, pp. 627-634.

BUDDEN, K. G., *Radio Waves in the Ionosphere*, Cambridge University Press, New York City, 1961a.

-----, *The Waveguide Mode Theory of Wave Propagation*, Logos, London, 1961b.

FIELD, E. C., "The Effects of Ions on Very Low Frequency Propagation during Polar Cap Absorption Events," *Radio Sci.*, Vol. 5, No. 2, 1970, pp. 591-600.

FIELD, E, C, and R. G. Joiner, "Effects of Lateral Ionospheric Gradients on ELF Propagation," *Radio Sci.*, Vol. 17, May-June 1982, pp. 693-700.

-----, "An Integral-Equation Approach to Long-Wave Propagation in a Nonstratified Earth-Ionosphere Waveguide," *Radio Sci.*, Vol. 14, November-December 1979, pp. 1057-1068.

GALEJS, J., *Terrestrial Propagation of Long Electromagnetic Waves*, Pergamen Press, New York City, 1972.

GREIFINGER, C., and P. GREIFINGER, "Approximate Method for Determining ELF Eigenvalues in the Earth-Ionosphere Waveguide," *Radio Sci.*, Vol. 13, No. 5, 1978, pp. 831-837.

KATAN, J. R., and P. R. BANNISTER, *Observation of ELF Propagation Variations at Mid and High Latitudes during the November/December 1982 Solar Proton Events*, Naval Underwater Systems Center, New London, Connecticut, Technical Report, 1985 [forthcoming].

KOSSEY, P. A., J. E. Rasmussen, E. C. Field, and C. R. Warber, *Conductivity Profiles of the Disturbed Polar Ionosphere from VLF Reflection Data*, presented at AGARD 36th Symposium of the Electromagnetic Panel, Propagation Effects on Military Systems in the High Latitude Region, Fairbanks, Alaska, USA, 3-7 June 1985.

PAPPERT, R. A., "Calculated Effects of Traveling Sporadic E on Nocturnal ELF Propagation: Comparison with Measurement," *Radio Sci.*, Vol. 20, No. 2, March-April 1985, pp. 229-246.

PAPPERT, R. A., "Effects of a Large Patch of Sporadic-E on Night-Time Propagation at lower ELF," *J. Atmos. Terr. Phys.*, Vol. 42, 1980, pp. 417-425.

PAPPERT, R. A., and W. F. Moler, "Propagation Theory and Calculations at Lower Extremely Low Frequencies (ELF)," *IEEE Trans. Commun.*, Vol. COM-22, No. 4, 1974, pp. 438-451.

REAGAN, J. B. et al., "Modeling of the Ambient and Disturbed Ionospheric Media Pertinent to ELF/VLF Propagation," NATO, *AGARD Conference Proceedings, No. 305*, February 1982, Neuilly sur Seine, France.

SAUER, H., private communication, National Oceanic and Atmospheric Administration, Boulder, Colorado, April 1983.

WAIT, J. R., *Electromagnetic Waves in Stratified Media*, Pergamon Press, New York City, 1970.

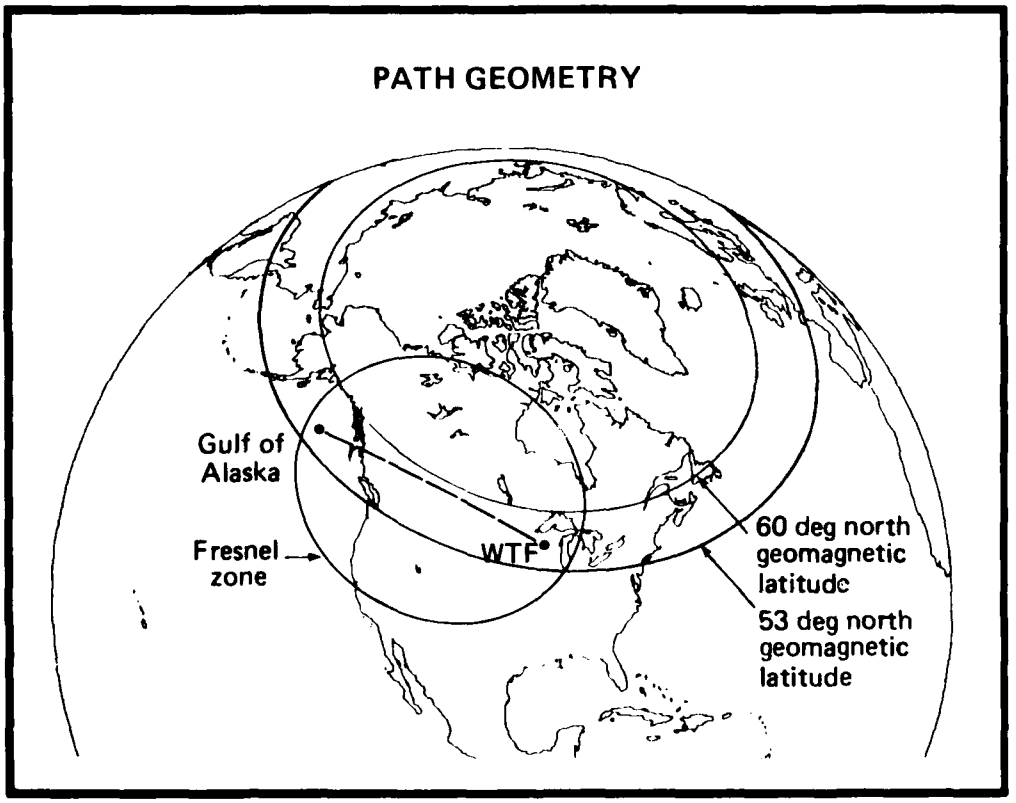


Figure 1. Geometry of propagation path from WTF to Gulf of Alaska

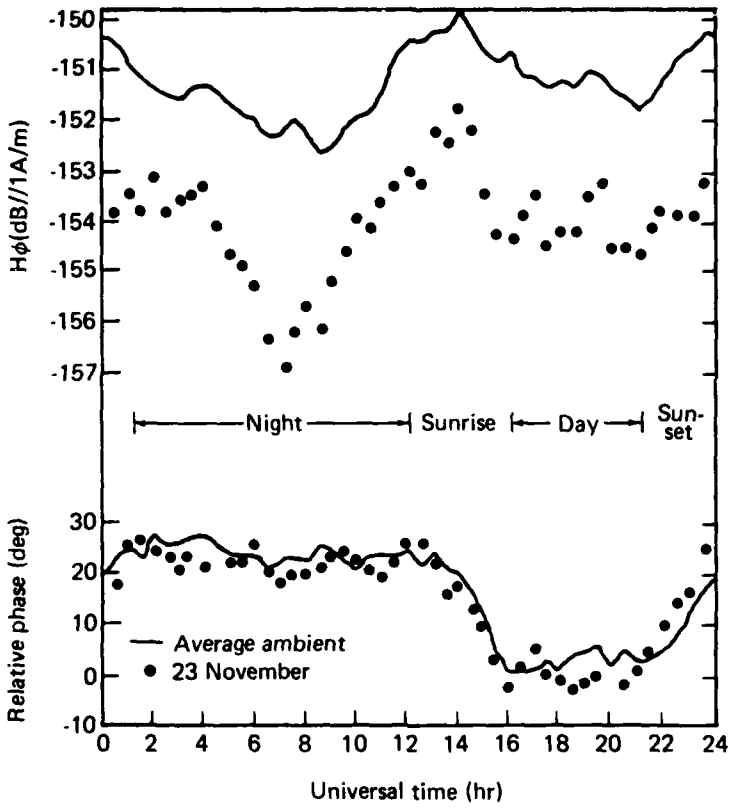


Figure 2. 76 Hz Signal received in Gulf of Alaska: 23 November 1982

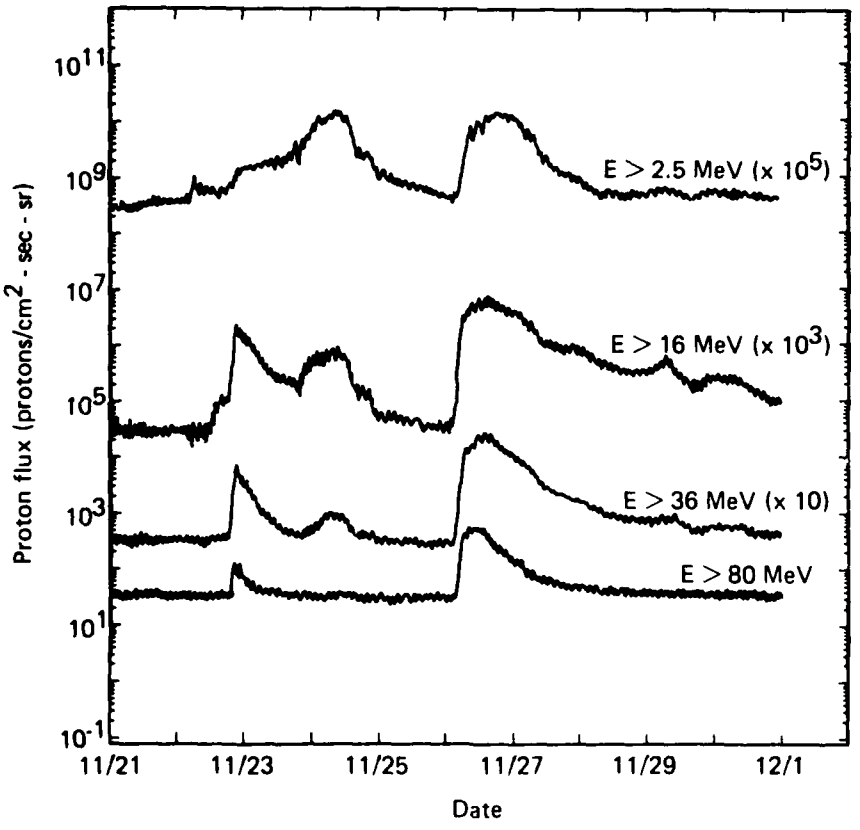


Figure 3. Proton fluxes: Spatial average; $\lambda > 70$ deg.

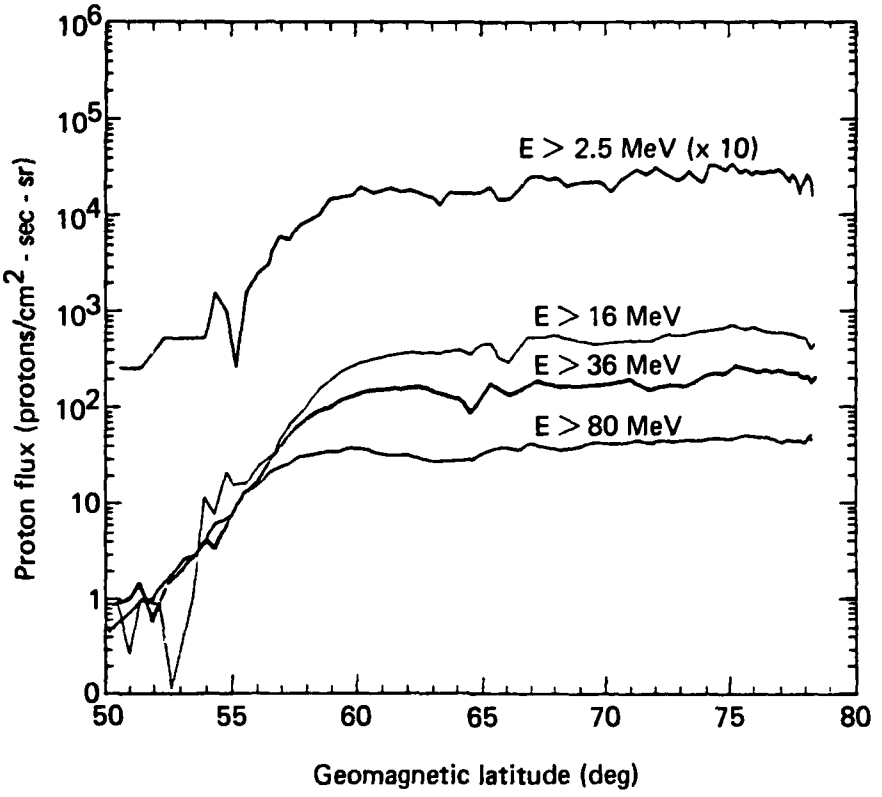


Figure 4. Proton fluxes versus magnetic latitude

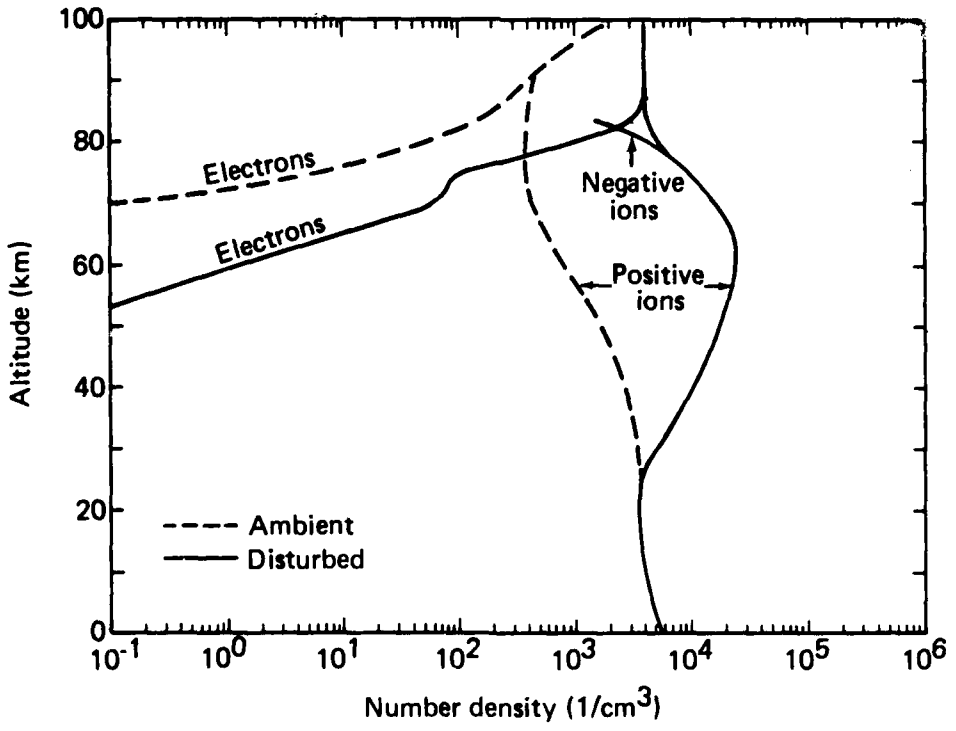


Figure 5. Electron and ion densities at 0800 UT: 23 November 1982

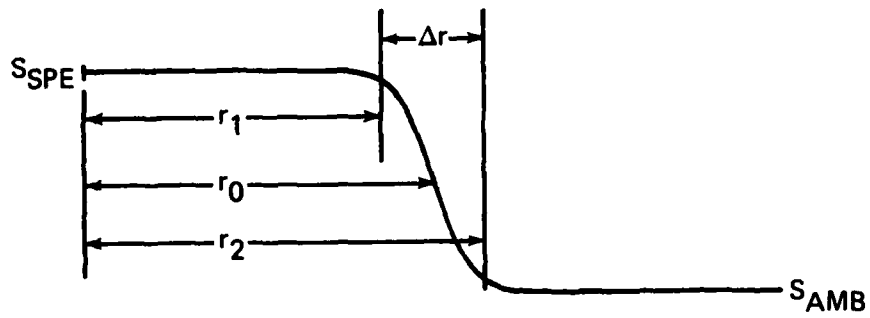


Figure 6. Model of polar cap propagation constant

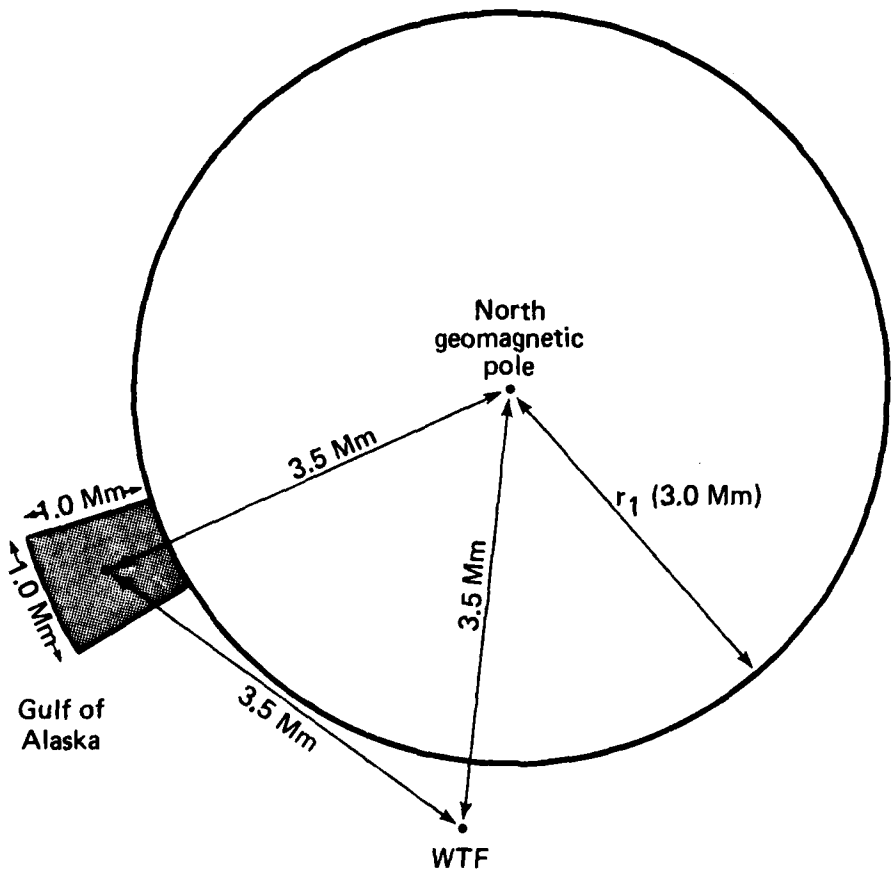


Figure 7. Propagation Model

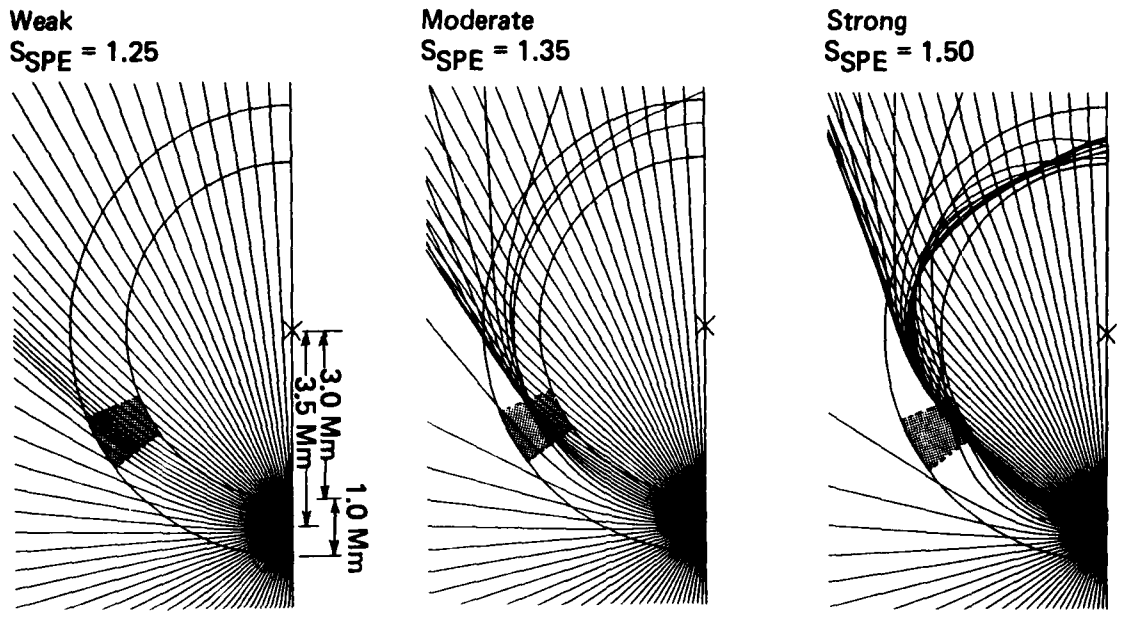


Figure 8. Ray trajectories for three SPE strengths: Δr = 1 Mm

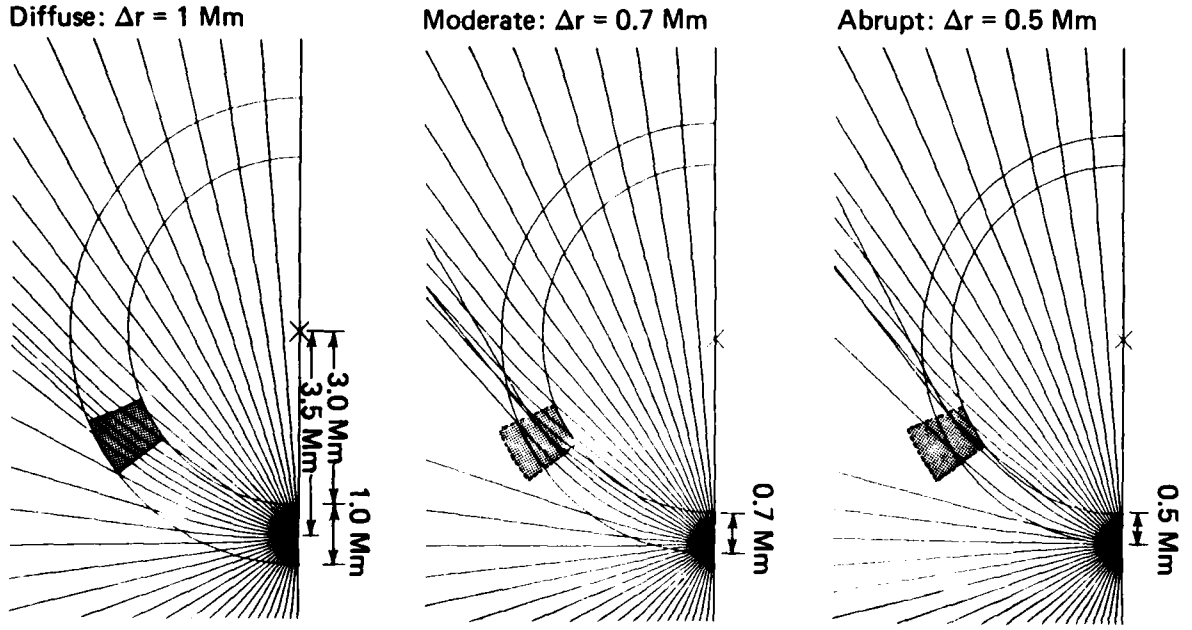


Figure 9. Ray trajectories for three boundary widths; weak SPE

DISCUSSION

E.Thrane, NO

I should like to know how high into the ionosphere it is necessary to know the model characteristics. Your graphs stopped at 100 km, but I would expect the ELF waves to penetrate deeper than this.

Author's Reply

We modelled as high as necessary — in some cases up to 200 km.

WORLD ATLAS OF GROUND CONDUCTIVITIES WITH PARTICULAR EMPHASIS ON THE HIGH LATITUDE REGION

by
Knut N. Stokke
Norwegian Telecommunications Administration
Oslo, Norway

Summary

In 1970 a CCIR Interim Working Party, CCIR IWP 5/1, was established to develop improved methods of predicting the phase and amplitude of ground waves.

An important feature concerning transmission of ground waves, is the ground conductivity. Information about the ground conductivity has been, and is, important for the planning work in the International Telecommunication Union (ITU). Therefore very early in the work of IWP 5/1 the necessity of a ground conductivity atlas was recognized, and in 1978 the IWP 5/1 was formally given the task to produce a world atlas (CCIR Decision 3).

Information about the ground conductivity has been received from about 50 countries, but there are some problems concerning the way in which the informations are presented. However, measuring campaigns will give better data, and will also give better informations from other areas.

The first edition of the Atlas is planned before the CCIR Final Studygroup Meetings September - November 1985.

Introduction

In the International Telecommunication Union (ITU) the CCIR (Comité Consultatif International des Radiocommunications = International Radio Consultative Committee) is responsible for questions concerning radiocommunications.

In the CCIR, several study groups are concerned with special problems in radiocommunications. The CCIR Study Group 5, "Propagation in Non-ionized Media", is, inter alia, dealing with problems concerning ground wave propagation.

Normally the study groups have meetings every second year. There are some problems which must be worked out also in the periods between the study group meetings, and Interim Working Parties (IWP's) have therefore been established.

In 1970 a CCIR Interim Working Party, CCIR IWP 5/1, was established to develop improved methods of predicting phase and amplitude of ground waves. This IWP is composed of members from Algeria, Argentina, Brazil, Canada, the United States of America, Finland, France, India, Iran, Norway, New Zealand, the United Kingdom, Sweden, Yugoslavia, and the EBU (European Broadcasting Union). Sweden has the chairman of IWP 5/1.

An important feature concerning transmission of ground waves is the ground conductivity. Information about the ground conductivity has been, and is, important for the planning work in the ITU. Therefore very early in the work of IWP 5/1 the necessity of a ground conductivity atlas was recognized, and in 1978 the IWP 5/1 was formally given the task of producing a world atlas (CCIR Decision 3-2, 1978). The publication of such an atlas should be at the earliest possible date and in any case before the XVIth Plenary Assembly of the CCIR (1986).

The first information about ground conductivity maps was collected in CCIR Report 717. This information is out of date, and work concerning collection of recent conductivity maps started already before 1978. The first edition of the atlas is supposed to contain primarily maps standardized to 1 MHz.

The attenuation method

One of the major problems when producing conductivity maps is to decide which measuring method to use. In areas where there are few and small changes in ground conductivity, several methods may be used. But in areas where there are many and abrupt changes in terrain and geology, and therefore also in conductivity, some of the methods will give unreliable results. Under such circumstances the use of the attenuation method has proved to be the most appropriate.

The attenuation method is based on Millington's method for calculating field strength over inhomogeneous earth (References 1, 2, and 4). This method takes account of the influence of the changes in conductivity, and gives results which are in good agreement with practical results.

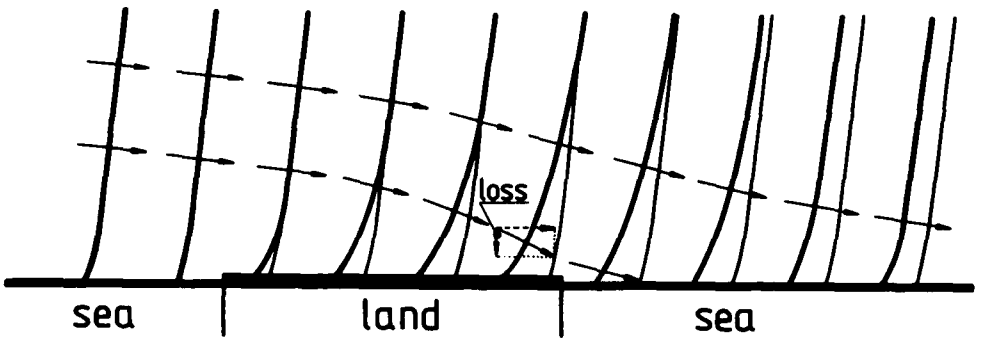


Figure 1. Ground wave tilt along a path

To explain the problems, we will look at what happens when a ground wave travels along a sea path and crosses and island. This is shown in Figure 1. Because of the losses in the ground the wavefront near the ground will get a forward tilt. This tilt will change as the conductivity changes. When the conductivity decreases, the forward tilt will increase. And when the conductivity increases, the tilt will decrease, that is, we get what we call a recovery effect.

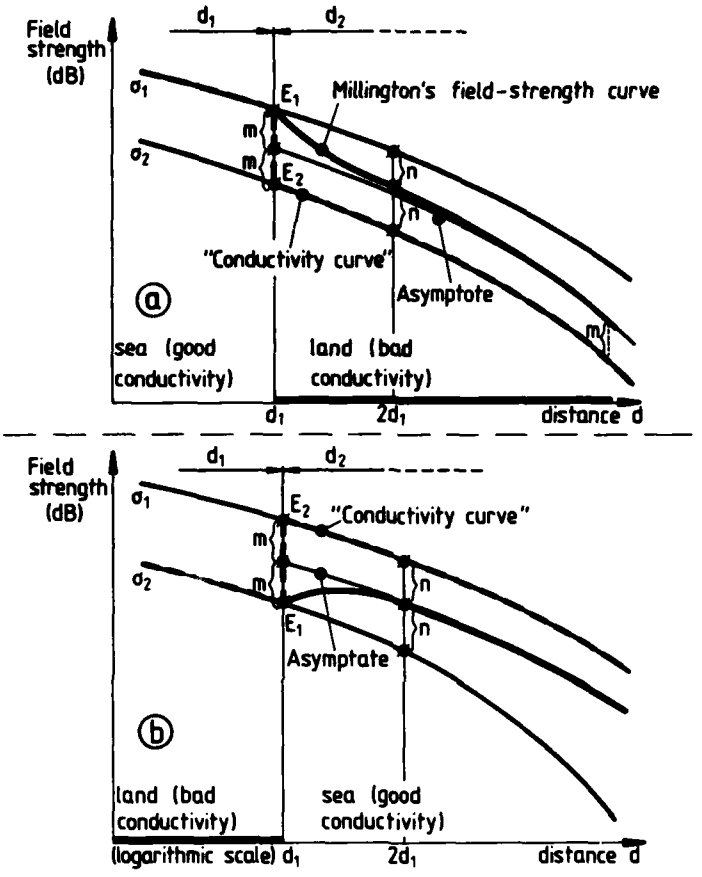


Figure 2. Millington's method for two changes in conductivity

In Figure 2 we can see the same variations explained by using Millington's method. Figure 2a shows that when the wave travels from sea to land, the field strength will decrease to an asymptote higher than the field strength curve for pure land path. This means that a good start will follow a ground wave all the way.

In Figure 2b we can see that when the wave travels from land to sea, that is, from bad to good conductivity, we get the recovery effect. However, the field strength will never reach the values we would have if the whole path were sea. This also indicates that a bad start will follow the ground wave all the way.

If we look at the curves in Figure 2, we see that the "conductivity curve" is not the same as the field strength curve. Therefore we cannot see what conductivity we have only by using the field strength curve. In order to find the "conductivity curve", that is the curve where we directly can read off the conductivity values, the measured field strength curve has to be analysed by using Millington's method (References 5 and 6). This method of finding the conductivity along a path is called the attenuation method.

(CCIR Rec. 368 - 4)

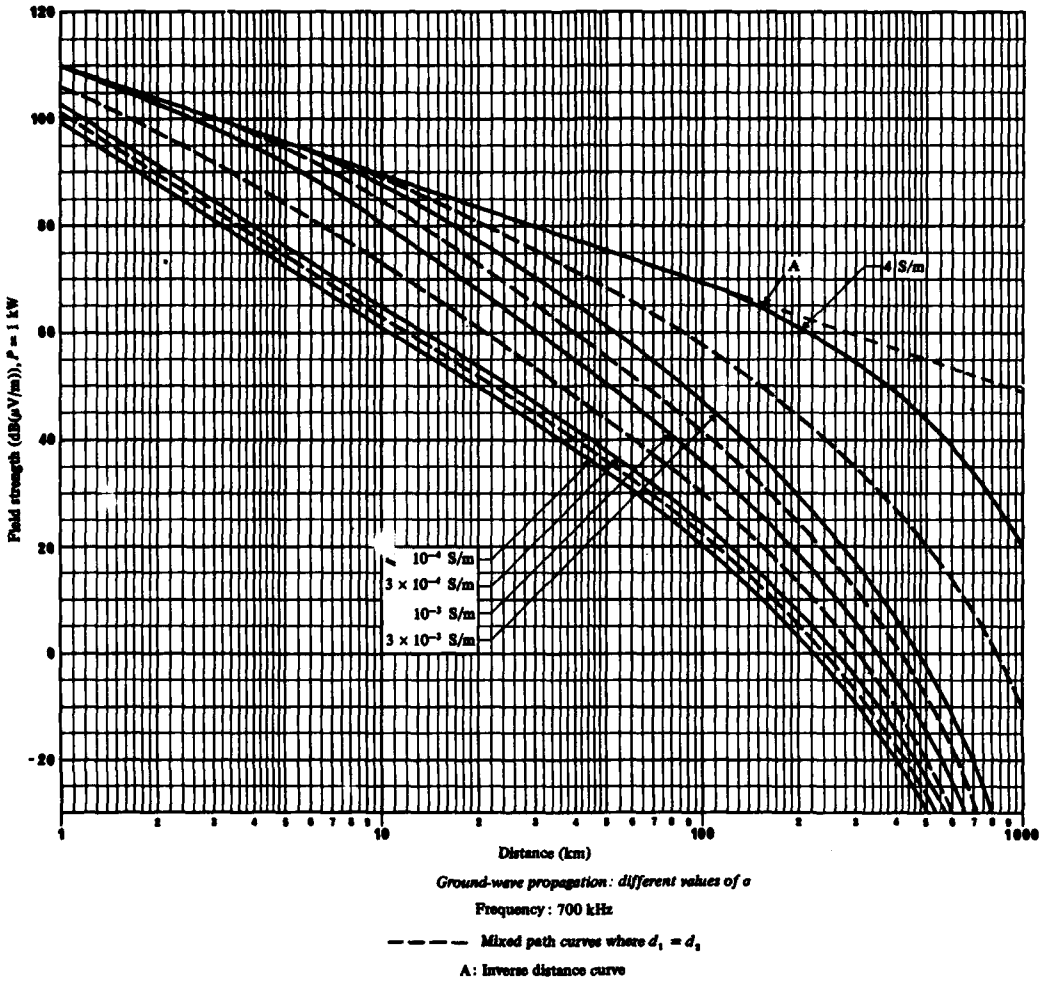


Figure 3. Ground wave field strength curves for different conductivities at 700 kHz

In order to use the attenuation method, we need ground wave curves for different conductivities at definite frequencies or for definite frequency bands. Figure 3 gives an example for 700 kHz. In the ground conductivity atlas such curves will appear. These curves may also be used together with the conductivity maps in order to calculate the ground wave field strength.

The wave tilt method

Another method which may be used to measure the ground conductivity, is the wave tilt method. This method is based on the fact that the wave tilt depends on the ground contants, that is the conductivity σ and the permittivity ε. As shown in

Figure 4, the tilt of the vertically polarized ground wave may be measured by using a short dipole adapted to an RF voltage measuring equipment. However, this method gives misleading results near changes in ground constants. Therefore the wave tilt method should not be used in areas where there are many and abrupt changes in ground constants.

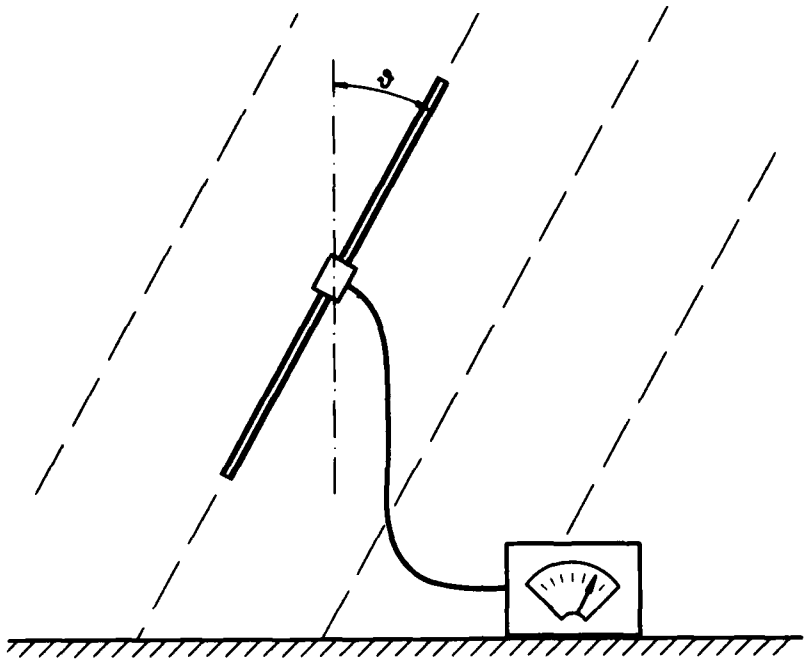
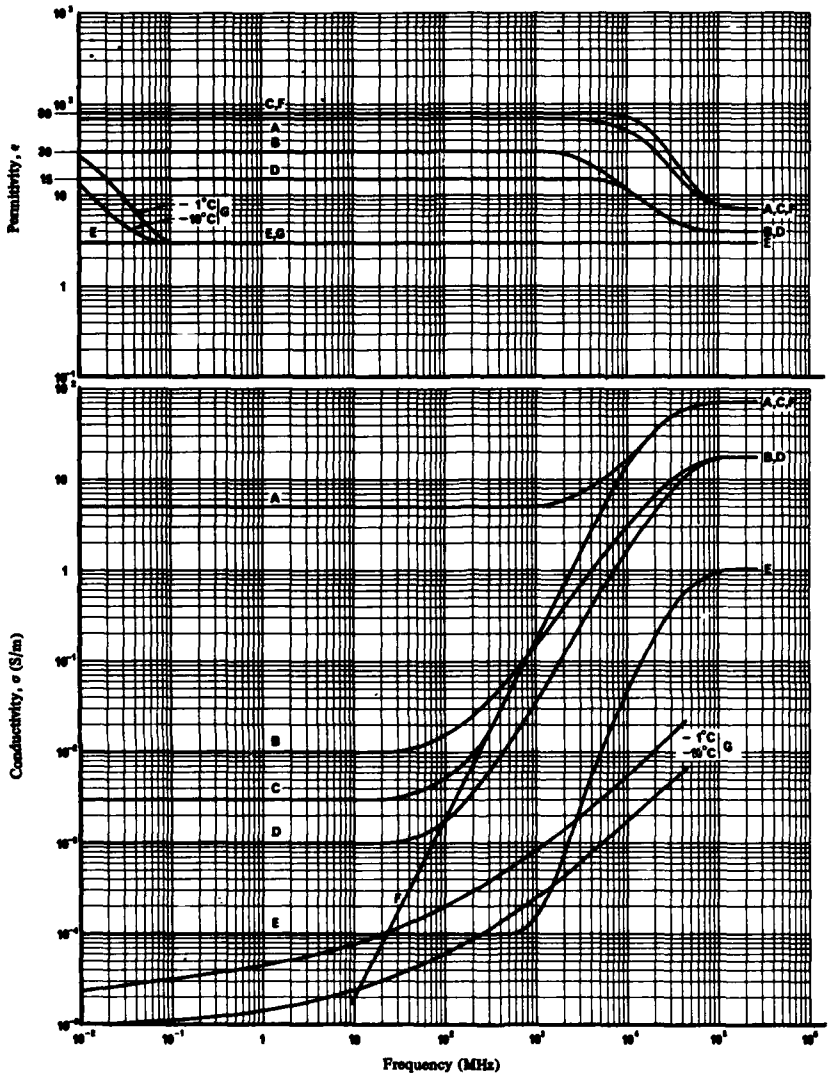


Figure 4. Equipment to use when measuring the wave tilt

Conductivity maps

Up to now the IWP 5/1 has received conductivity maps from about 50 countries, but we hope to get more information as the measuring campaign continues. However, old measurements may also be used, even if the accuracy of the measuring equipment is not well known. In reference 6 is given a method where, by the use of cymomotive force, only the relative values are important.

(CCIR Rec. 527 - 1)



Permittivity, ε, and conductivity, σ, as a function of frequency

A: Sea water (average salinity), 20°C
B: Wet ground
C: Fresh water, 20°C
D: Medium dry ground
E: Very dry ground
F: Pure water, 20°C
G: Ice (Fresh water)

Figure 5. Variation in conductivity and permittivity with frequency for different materials

The conductivity maps should be normalized to 1 MHz, that is, to about the mean of the MF band. If we look at Figure 5, we see that the conductivity σ for most materials is constant between 0,1 MHz and 10 MHz. Therefore the value at 1 MHz normally applies to that frequency band. However, we see that the conductivity for fresh water ice varies, and it is expected that sea ice has a similar variation. When ice and snow are involved

in the results, we may therefore expect a more marked variation with frequency, especially when we have a layer of ice at sea.

Unfortunately there is very little information about the conductivity in polar areas. The IWP 5/1 hopes to get some information also from those areas. Results of measurements during summer and winter, with frozen ground and with different snow depths, would be much appreciated.

TABLE I - *Expected ground conductivities*

(CCIR Rep. 879)

Ground conductivity (S/m)	Type of ground
5	Sea water
10^{-2}	Very moist soil, cultivated soil, fresh water
10^{-3}	Dry soil, clay, forest soil, desert soil, soil in mountainous areas, fresh sea ice
10^{-4}	Granite, dry gravel and sand, mountainous areas in cold regions, old sea ice
10^{-5}	Dry glacier in mountainous areas, permafrost in northern polar areas

Note. **- For areas in the interior of Antarctica, where the absolute humidity is very low, the conductivity may be of the order of 10^{-6} S/m.**

Figure 6. Table of conductivities for some types of ground

The table in Figure 6 gives the expected values of ground conductivities for some characteristic types of ground. However, these values may vary with humidity, and the values given may be taken as mean values. In cold areas, where the absolute humidity is low, some of the values may be even lower, and in warmer areas some of the values may be higher. The influence of frost and permafrost may also change the values, but this effect has to be further investigated. It is therefore important to have measurement results from polar areas, and especially where snow, ice and glaciers are involved. The results from such measurements may be sent to:

IWP 5/1, CCIR Secretariat,
2 Rue de Varembé,
1211 Genève 20,
Switzerland.

The conductivity values should also be normalized to the values used for the curves in CCIR Recommendation 368, that is to: 5 Siemens/meter, $3 \cdot 10^{-2}$ S/m, 10^{-2} S/m, $3 \cdot 10^{-3}$ S/m, 10^{-3} S/m, $3 \cdot 10^{-4}$ S/m, 10^{-4} S/m, $3 \cdot 10^{-5}$ S/m, and 10^{-5} S/m. For lower values the same steps should be used. Measurements from polar areas will indicate whether it is necessary to have curves for values of σ lower than 10^{-5} S/m.

Measurements from the interior of Antarctica, where the absolute humidity is very low, indicate that values of 10^{-6} S/m may be obtained. It should be borne in mind that the influence of the underlaying layers, etc., is included in the measured results. If we measure for only one specific material, the results may be quite different from these effective values.

In the work of A.W. Biggs (Reference 3) is given a table of conductivities for ice and snow. This table is reproduced in Figure 7. From this table we see that soft new snow may have as low conductivity as 10^{-9} to $3 \cdot 10^{-11}$ S/m, that is, a rather good insulator. This means that a LF-, MF- and even an HF-antenna may be laid directly on soft new snow with good results. In polar glacier areas this method may be convenient because of extreme climatic conditions. However, the antennas have to be renewed when they are buried in deep snow, and the buried antennas may even be used as a (capacitive) earthing system or a counterpoise system.

Material	Temperature °C	Conductivity S/m	Relative permittivity
Pure ice	-10	10^{-7}	95
	-40	3×10^{-9}	105
Soft new snow	-10	10^{-9}	4
0.13 g/cm^3	-40	3×10^{-11}	4
Granular snow	-10	10^{-7}	15
0.4 g/cm^3	-40	10^{-9}	15
Glacial snow	0	5×10^{-7}	120
Sea ice	-7	10^{-3}	4
0.5% salinity	-24	10^{-4}	4

Figure 7. Table of conductivities and permittivities for ice and snow

The influence of sea ice is an interesting feature. Measurements of mean or effective conductivity over sea ice of different thicknesses are of great interest, and then the conductivity will rather strongly depend on frequency.

The penetration depth, δ, is often used when characterizing the ability of radio waves to penetrate into a medium. δ is the depth where the field strength has fallen to 1/e of the field strength value at the surface. However, we have to remember that the real course of the field strength into a medium is an exponential curve, as shown in Figure 8.

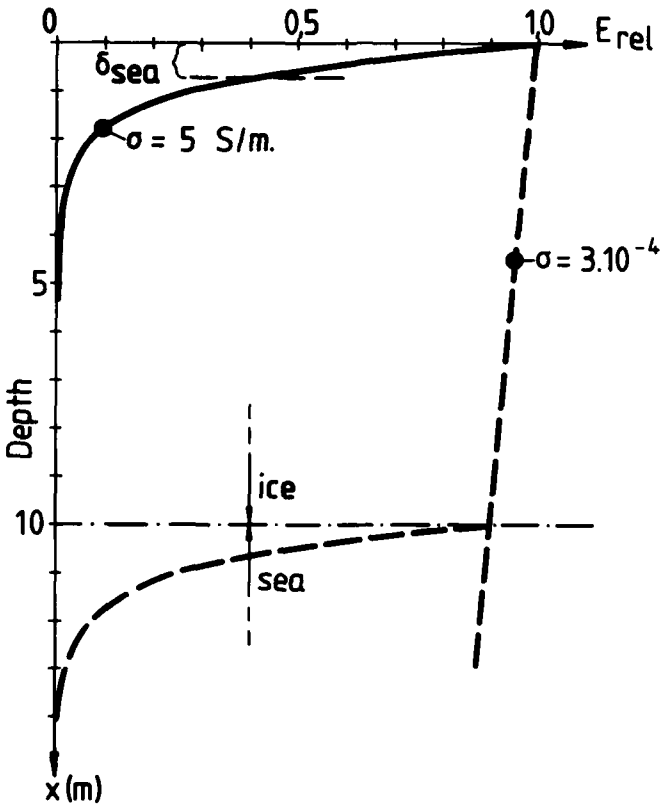


Figure 8. Relative field strength near the surface of the sea and under 10 m of sea ice at 100 kHz

In Figure 8 is shown the relative field strength curve for sea (5 S/m) at 100 kHz. The penetration depth is then about 0.7 m. However, when there is a layer of 10 m of sea ice ($\sigma = 3 \cdot 10^{-4}$ S/m) we have that the surface value has been reduced only by about 10%. Then almost the same communication conditions exist for a submarine under a layer of 9 - 10 m of sea ice as just under the sea surface. This also means that when there are ice, sea ice or glaciers on land, the underlaying layers are very important, and this effect will increase as the frequency decreases.

The density of sea ice is 0.92, and therefore 8% of the ice should be above the sea level, but this does not have any significiant influence on this example.

Example of a conductivity map

In Figure 9 is shown an example of a conductivity map in the atlas. Such maps will be given for each country as information is received. Later on, when the information for an area is complete, a key map of the area will be given.

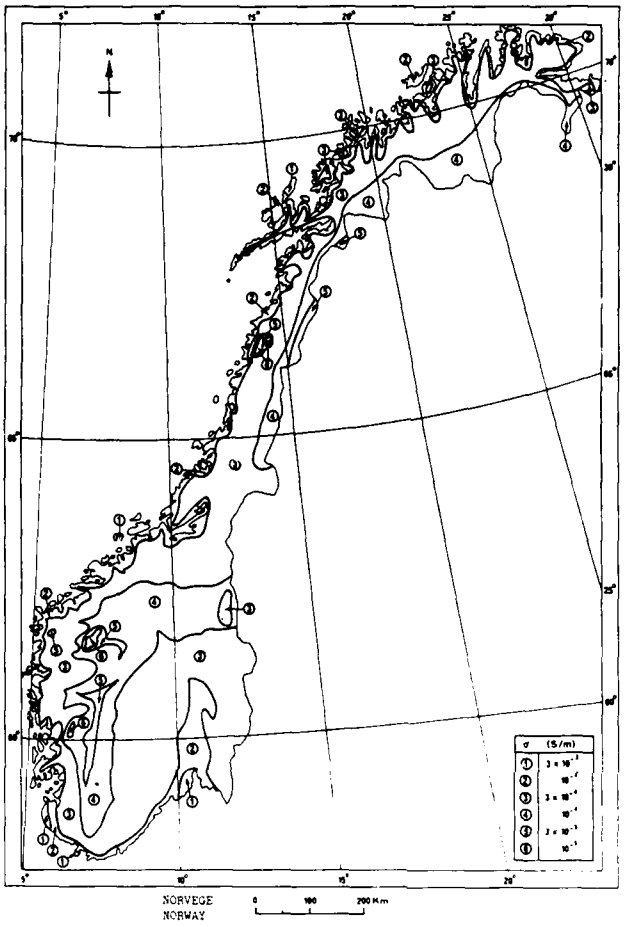
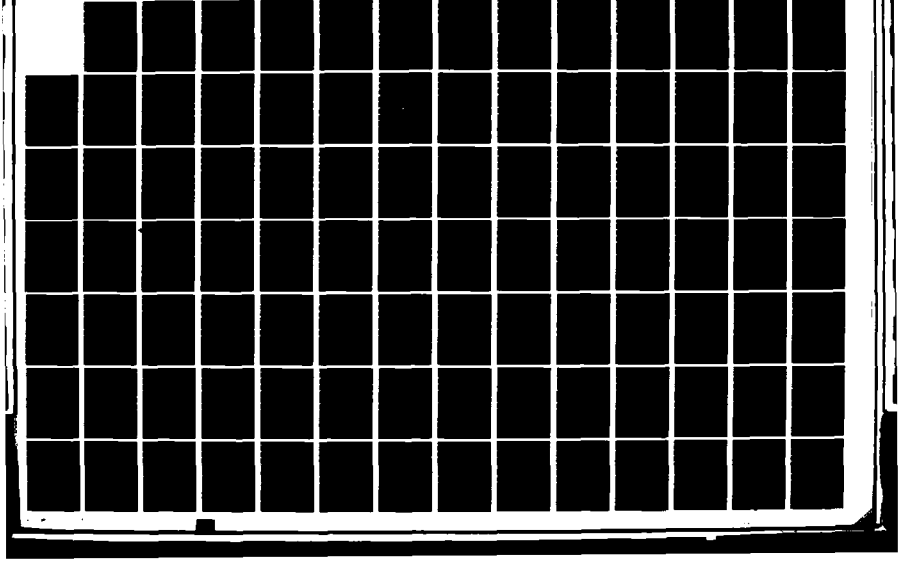


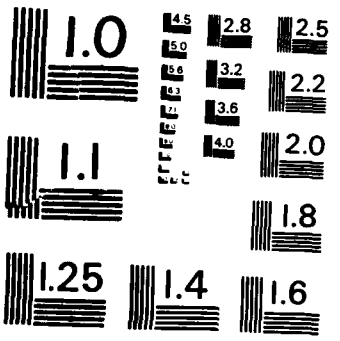
Figure 9. Conductivity map of Norway

The details in the maps will depend on the scales of the maps, and also on what the maps are intended for. Therefore there is also a certain degree of valuation included in a conductivity map. The map shown in Figure 9 is primarily intended for LF and MF planning.

AD-A166 585 CONFERENCE PROCEEDINGS ON PROPAGATION EFFECTS ON MILITARY SYSTEMS IN THE..(U) ADVISORY GROUP FOR AEROSPACE RESEARCH AND DEVELOPMENT NEUILLY.. H SOICER

UNCLASSIFIED NOV 85 AGARD-CP-382 F/G 4/1 NL





MICROCOPY RESOLUTION TEST CHART
NATIONAL BUREAU OF STANDARDS - 1963 - A

References:

1. CCIR: Ground-wave propagation curves for frequencies between 10 kHz and 30 kHz. Recommendation 368-4, Volume V, Geneva, 1982.

2. Millington, G. and Isted, G. A.: Ground-wave propagation over an inhomogeneous smooth earth. Proceedings of the I.E.E., No. 97, July 1950, Part II.

3. A.W. Biggs: Wave propagation over snow and ice. SCAR Symposium on Antarctic Telecommunications, Sandefjord, Norway, 10 to 16 May 1972. Published by Scientific Committee on Antarctic Research, Cambridge, 1972. (pp. 160 - 194).

4. Stokke, K. N.: Some graphical considerations on Millington's method for calculating field strength over inhomogeneous earth. I.T.U. Telecommunication Journal, No. III, March 1975. (pp. 157 - 163).

5. Stokke, K. N.: Problems concerning the measurements of ground conductivity. EBU Review - Technical, June 1978, No. 169.

6. Stokke, K. N.: Ground conductivity measurements. I.T.U. Telecommunication Journal, Vol. 51 - XI/1984. (pp. 611 - 613).

7. Stokke, K. N.: Radiotransmisjon (in Norwegian). Universitetsforlaget, Oslo. (pp. 281 - 289, pp. 301 - 304).

DISCUSSION

H.J.Albrecht, GE

I wish to refer to the variability of ground conductivity as a function of time, e.g. for summer and winter conditions. You mentioned the need for such data with regard to polar areas. In addition, a knowledge of the variations of ground conductivity, at least data for summer and winter, seem to be very important in other latitudes as well, particularly if a better geographical resolution is aimed at, as, for instance, in the case of the atlas of conductivity maps for each country. Variations may be significant and are mainly due to climatic effects; the annual variation of the ground water level is an example. I would like to ask if conductivity maps such as the one shown for Norway represent annual average values of conductivity; if so, I wish to suggest that values for summer and winter should be requested and used for the atlas data, if at all possible.

Author's Reply

Yes, there are seasonal variations in the conductivity, and the map I showed is a map for mean conductivity throughout a year. When there is frozen ground with a layer of dry snow, the conductivity is normally lower. We tried once to measure the influence of a 40-50 cm snow layer, and we got the indication that this lowered the conductivity by about half a decade. However, when we tried to repeat the measurements, the humidity had changed, and we got somewhat confusing results. It is difficult to give an exact answer concerning the influence of snow and frost, but we hope that more measurements may give a better indication of the influence of such parameters.

The conductivity maps should be given as expected mean values throughout a year. However, if the variability, etc, could be given, these results would be of great value for the IWP 5/1. But for the time being I think it is too much to ask, because such measurements are rather complicated and require a lot of work. For the time being we would be happy if we get a mean conductivity map for each country. Later on we hope to get more detailed information.

P.A.Bradley, UK

What is the current status of the program GRNDWAVE used by CCIR Interim Working Party 5/1 to generate the propagation curves given in Report 368 and which, I understand, is intended to be used in the case of elevated antennas?

Author's Reply

The ground-wave curve program, GRWAVE, has caused some problem. The program runs quite well when both the transmitting and the receiving antennas are on the ground. The difficulties arise when one or both of the terminals are elevated. However, it seems that this may be mostly a computer problem, and the IWP 5/1 is trying to find computer facilities where the program may be run properly.

J.S.Belrose, CA

There is very little evidence in the literature for seasonal changes in groundwave field strengths at MF. At least one paper has reported that MF-AM groundwave field strengths are larger in winter than in summer in North America. This is perhaps opposite to what I would have expected, at least for those regions where winters are characterized by frozen ground and snow. I have wondered whether the effect might be due, at least partly, to an antenna system interface problem: perhaps in winter when the radial ground system is buried in frozen ground, it acts more like a counterpoise providing better capacitive coupling to ground strata of high conductivity beneath. There is some evidence that buried insulated wire ground systems provide better seasonal stabilities.

Author's Reply

Concerning higher or lower conductivity during winter, this may be a question of where the measurements are made. In areas where the summer is dry and the winter is wet (wet snow and rain) it may well happen that the conductivity is better during the winter. You may also have relatively large variations in short periods due to climatic conditions.

Concerning earthing wire systems, Mr Lacharway (TDF France) has done much work on both antenna and earthing systems. He has found that capacitive and ohmic coupling to the ground are of about the same efficiency for radio waves. It may even be so that conductivity coupling is better, especially when the ground conductivity is low. This means that a capacitive earthing network (insulated or hung up just over the ground) is quite as good as a blank wire network dug into the ground. In addition, an insulated earthing network is very convenient in areas where there is an active corrosive ground, as for instance in coastal areas, and especially in warm coastal areas. The insulated wires may be laid in loops, and may easily be controlled from the centre by using an ohmmeter.

However, a capacitive network will get problems because of electrostatic charging, but this may be overcome by using non-corrosive sheet-metal (steel, bronze, etc.) dug into the ground.

It is very important to have an efficient earthing system (for frequencies from HF and downwards), especially because near the antenna we have to take account also of the near field. And in order to get efficient earthing systems, the wires should not be buried very deep into the ground. This is, of course, dependent on frequency, but even for low frequencies the wires should not be buried too many cm's below the surface of the ground. This is because, as I mentioned in my paper, the real course of a radio wave field strength into a medium is an exponential curve, and therefore the upper layer is the most important. Especially in winter, when the ground conditions may vary very much, it is important that the earthing system is as near the surface as possible for mechanical reasons.

SUMMARY OF SESSION IX

Meteor Burst/Scatter

by

J.H.Blythe

Session IX, Meteor Burst/Scatter comprised just two papers. However, in combination they give a rather complete account of the current state of the art. Meteor Burst Communication (MBC) systems were actively studied in the 50's and have been under review ever since, but have never been used significantly in military systems. Recent advances in receiver systems and integrated circuit technology have led to renewed interest, reflected in the two papers, which concentrate on aspects relevant to high latitudes.

Paper 9.1 gives a brief historical and physical description of the MBC technique together with a discussion of the advantages of very high frequency MBC, with respect to high frequency communication, when used at high latitude. A recently deployed high latitude MBC experiment between Bodø in Norway and Wick in Scotland (UK) is described and some of the early data gathered at frequencies close to 40 MHz and 70 MHz is presented. A theoretical description of polarisation rotation in a linearly polarised MBC system is developed and used to show that at 40 MHz excess D-region ionisation may cause system performance to differ from its ambient level. Corroborative experimental results over a temperate latitude path are presented. Based upon the early high latitude experimental results and on the theoretical calculations the paper suggests that frequencies close to 40 MHz, in common use in temperate latitude linearly polarised MBC systems, are too low for high latitude operation.

Paper 9.2 also gives a brief historical and physical description of the MBC techniques, and describes effects of Sporadic-E, Auroral Scatter and Polar Cap Absorption. It indicates that the effects of Sporadic-E and of absorption in a polar cap absorption (PCA) event can be mitigated by an increase of frequency. A description is given of an experimental link in Northern Greenland, established to obtain data on the potential performance of MBC systems in the polar region. It is being used to investigate: the availability of useful meteor trails at very high latitudes; the potential communication capacity associated with these trails; the recurrence, persistence and effects of Sporadic-E layers; and the effects of PCA events on the capacity of 45-104 MHz MBC systems, for a variety of chosen signalling techniques. Some initial experimental results are given. These confirm the expected higher information capacity at 45 MHz c.f. 65 MHz under normal conditions, and show the benefit of the use of adaptive signalling rates.

The two papers form a valuable complementary pair, showing that data is being gained which would enable system design to be undertaken with confidence in the event of a decision to deploy. This data covers many new aspects which were not addressed in earlier studies, such as the integrity of security in various propagation events, the effect of polarisation rotation, and the overall influence of frequency.

METEOR SCATTER RADIO COMMUNICATION AT HIGH LATITUDES

by

P.S. Cannon, A.H. Dickson and M.H. Armstrong
Royal Aircraft Establishment,
Farnborough
Hampshire
UK

SUMMARY

A brief historical and physical description of the Meteor Burst Communications (MBC) technique is given together with a discussion of the advantages of very high frequency MBC, with respect to conventional high frequency communication, when used at high latitudes. A recently deployed high latitude MBC propagation experiment, between Bodø in Norway and Wick in Scotland (UK) is described and some of the early data gathered at frequencies close to 40 MHz and 70 MHz is presented. A theoretical description of the effects of Polarisation Rotation in a linearly polarised MBC system is developed and it is shown that at 40 MHz Polarisation Rotation, due to excess D-region ionization may cause the system performance to differ from its ambient level. Corroborative experimental results, over a temperatue latitude path, are presented. Based upon the early high latitude experimental results and on the theoretical calculations the paper suggests that frequencies close to 40 MHz, in common use in temperate latitude linearly polarised MBC systems, are too low for high latitude operation.

1 INTRODUCTION

Meteor burst communication (MBC) is currently experiencing a revival as a means for beyond line of sight (BLOS) communication. The technique utilises the ionization trains created by meteors, between altitudes of 90 and 100 km, to scatter HF (high frequency) and VHF (very high frequency) radio signals over distances between ~200 km and ~2000 km.

It has been known for many years that electromagnetic waves can be propagated by forward scattering from meteor trails. In 1954 Eshleman and Manning[1] suggested that meteor trials might provide a viable means of communication and in 1957 Forsyth *et al*[2] described the first operational MBC system. Several relatively successful point-to-point links were implemented during the late 1950s and early 1970s culminating in the COMET system described by Bartholomé and Vogt[3]. In 1960 it was suggested by Hannum *et al*[4] that the use of MBC for air ground communication should be possible without the need for directional antennas on the aircraft. This view is currently being studied by the Royal Aircraft Establishment in the UK stimulated, to a great extent, by recent developments in microelectronics which promise more compact data handling systems than ever dreamed of in the 1950s and 60s.

For the military user MBC is extremely attractive. The burst nature of digital transmissions, resulting from the short usable trail durations of typically 20 ms to 1.5 s, provides some security. More importantly, however, a MBC system has an inherently low intercept probability due to the small receive footprint associated with each trail (Ince[5]).

After an initial theoretical introduction the paper divides into two parts. In the first we describe a propagation experiment set up to investigate MBC at high latitudes and in the second we examine some theoretical predictions on the subject of Polarisation Rotation in MBC. Corroborative experimental verification of the latter is presented.

2 THEORY OF METEOR SCATTER

The scattering properties of straight meteor ionization trails are highly aspect sensitive. For effective scattering a specular condition must be satisfied and this requires that the trail be tangential to a prolate spheroid whose foci are at the transmitting and receiving terminals. This condition means that the scattering can take place from a large area of the sky.

Theoretically the propagation loss due to scattering from an underdense trail is given by the following expression (Sugar[6]):

$$\frac{P_R}{P_T} = \frac{1}{32\pi^4}\left(\frac{\mu_0 e^2}{4m}\right)^2 \frac{2\lambda^3}{R_1 R_2 (R_1 + R_2)} \frac{G_T G_R q^2 \sin^2\alpha}{1 - \cos^2\beta \sin^2\phi} \exp\left(\frac{-8\pi^2 r_0^2}{\lambda^2 \sec^2\phi}\right) \exp\left(\frac{-32\pi^2 Dt}{\lambda^2 \sec^2\phi}\right) \qquad (1)$$

where P_R = received power (W)

P_T = transmitted power (W)

μ_0 = permeability of free space 4×10^{-17}) (H m^{-1})

e = charge on electron (1.6×10^{-19}) (C)

m = mass of electron (9.1×10^{-31}) (kg)

λ = wavelength of transmission (m)

R_1 = path length from transmitter to meteor trail (m)

R_2 = path length from receiver to meteor trail (m)

G_T = power gain of transmitting antenna relative to isotropic

G_R = power gain of receiving antenna relative to isotropic

q = line density of electrons in trail (electrons/m)

α = angle between E-vector arriving at trail and the direction from the trail to the receiver (degrees)

β = angle between trail and plane of propagation (degrees)

ϕ = semi angle of reflection (degrees)

r_0 = initial radius of trail (m)

D = diffusion coefficient ($m^2\ s^{-1}$)

t = time (s).

Using this expression we can calculate the information flow rate I which is proportional to the bandwidth, b, the duty cycle, D_c, and some function $f(S/N_0)$ of the signal to noise ratio. Thus:

$$I \propto bD_c f\left(\frac{S}{N_0}\right) . \tag{2}$$

It can be shown (eg Sites (7)) that:

$$D_c \propto N_q(q > q_0)\tau = \frac{\lambda^2}{q_0} \tag{3}$$

where N_q is the number of trails with q greater than some threshold value q_0 and τ is the time constant for signal amplitude decay which from equation (1) is given by:

$$\tau = \frac{\lambda^2 \sec^2\phi}{16\pi^2 D} .$$

Rewriting P_R in equation (1) as S, the threshold received power, and expressing the background noise power as $b\lambda^n$ where n describes the noise power spectrum, we have:

$$\frac{S}{N_0} \propto \frac{P_T G_T G_R \lambda^{3-n} q_0^2}{b} . \tag{4}$$

For b and S/N_0 constant it follows from (3) and (4) that:

$$I \propto D_c \propto \left(P_T G_T G_R\right)^{0.5} \lambda^{(7-n)/2} . \tag{5}$$

For ground-to-ground links the background noise level is generally assumed to be determined by cosmic noise and as such $n = 2.3$ (Cottony and Johler[8]). Thus we can write:

$$I \propto \lambda^{2.35} . \tag{6}$$

It follows that when consideration is only given to the scattering process the frequency choice should be as low as possible.

An attractive aspect of VHF MBC relative to HF communications (which still forms the majority of BLOS communication systems) is, however, its immunity to ionospheric disturbances at auroral and polar cap latitudes. For non-deviative absorption the absorption coefficient is given by the well known quasi-longitudinal expression:

$$\kappa = \frac{e^2}{2\varepsilon_0 mc} \frac{N\nu}{(\omega + \omega_H)^2 + \nu^2} \quad \text{neper } m^{-1} \qquad (1 \text{ neper} = 8.7\text{dB}) \tag{7}$$

where c is the velocity of light in vacuo, N is the electron number density (m^{-3}) ν is the electron-neutral collision frequency, ω is the angular frequency and ω_H is the electron gyro frequency. As a consequence of this inverse square relationship with operating frequency a VHF MBC system is more robust to precipitation events than an HF system. The fade margin will, however vary considerably within the, generally adopted, operating frequency range (35 MHz to 100 MHz). Therefore, although, as previously described, the information throughput will under conditions of no absorption vary as $f^{-2.35}$, requiring the frequency choice to be as low as possible, the inclusion of the effects of absorption may indicate that a

higher frequency choice would be better at high latitudes. To investigate this, and other effects, further a sub-auroral meteor burst propagation experiment has been set up. In addition, a theoretical study has been conducted regarding other potentially detrimental effects, with special reference to their frequency dependence.

3 A HIGH LATITUDE METEOR BURST PROPAGATION EXPERIMENT

3.1 Experimental equipment

In order to investigate the possibility of using MBC at high latitudes an experimental propagation link has been set up between Bodø in Northern Norway (67.27N, 14.39E) and Wick in Northern Scotland (58.56N, 3.28W). The location of these stations is shown in Fig 1. The transmitting station (Fig 2), located in Norway, simply consists of a signal generator feeding a 200 watt linear power amplifier which in turn drives a four element Yagi antenna operating at 70 MHz or a dipole operating at 40 MHz. Unfortunately, the feeder cable loss to both antennas is high and the input power to both antennas is only 50 watts. As a consequence of the site flatness and proximity to the sea (200 m) the expected antenna radiation patterns are multi-lobed in the vertical plane, due to the negative ground image. Fig 3 depicts the theoretical pattern for both antennas given a perfectly conducting plane earth. The 70 MHz antenna has a main lobe directed at the path mid-point. The 40 MHz antenna unfortunately fires its main lobe at a higher angle and, therefore, short of the mid-point. Details of the antennas are provided in Table 1.

At the receiving station the antennas, directed towards Norway, include 4-element Yagi antennas at both 70 MHz and 40 MHz. Given a good ground image both have been adjusted for mid-point illumination since 2 April 1985. Prior to this date, however, the 40 MHz antenna was mounted at a height giving higher angle illumination. Experimental calibration of the 70 MHz receive antennas has been carried out and the gain obtained is ~4 dB less than the theoretical maximum given a perfect plane earth. This is not unexpected since this site is rougher than the Norwegian site. In addition to these two antennas others are available but directed towards Farnborough (Hampshire) (51.27N, 359.37E) in southern England. These antenna have been used for temperate latitude experiments of a similar nature.

Signals from the receive antenna are processed by the system shown in the simplified block diagram, Fig 4. Signals at one of two operating frequencies are down-converted and fed into an HF communications receiver. The digitised AGC voltage, which after calibration provides a measure of the signal level, is processed by the desktop computer which searches for meteor and other signals. To be accepted as a signal, rather than noise, the receiver output level must remain >10 dB above the noise for >60 ms. By using a criterion, based upon the rise time of the signal, underdense meteor returns are filtered from overdense and other signals. Data is collected in 3 hour blocks for a 2 or 3 day period, at each frequency, each week, and stored on disc. The stored data consists of signal start and end times and the time that the trail amplitude reaches its maximum value, together with trail durations and maximum signal amplitude. At the end of two or three days the data files are transferred from the remote receiving station in Wick to our laboratory VAX11/730 at Farnborough via a telephone modem data link, for further processing. The data link also allows us to interrogate the system operational characteristics and to upload new operating programs, running schedules etc.

It is appropriate to point out that colocated with the Wick meteor scatter receiving equipment is the British contribution to the Scandinavian and British Radar experiment (SABRE). The SABRE viewing area is shown in Fig 1 and just covers the mid-point of the Bodø to Wick path.

3.2 Experimental results

Figs 5 and 6 show typical diurnal variations obtained for this link at 40 MHz and 70 MHz. Each point represents the total number of trails which occurred during the previous 1 hour period. The expected diurnal variation, (see also section 4.1) due to sporadic meteors, with a peak near dawn and a minimum near dusk is evident. Superimposed on this we see, at ~1300 UT the effect of a meteor shower.

Fig 7 shows 3 days of atypical 40 MHz data. These data were collected on 23, 24 and 25 March 1985. Over most of this period the number of received signals followed the expected distribution but on several occasions the signal count increased considerably. These events can be seen at 24 UT on 23 March at 16, 17 and 23 UT on 24 March and at 06 UT on 25 March. As previously described the amplitude time envelope of each detected signal is not stored but the time and amplitude of the signal maximum is. Fig 8 shows an amplitude time plot for one of these periods on a 3 hour time scale. Each point represents an occasion when the received signal strength exceeded the background noise plus 10 dB for greater than 60 ms. Since these data were collected in 2 minute blocks every 5 minutes, gaps in the plot of less than 3 minutes should not be construed as being physically significant. The vertical amplitude distribution of received signals, between 144 and 180 minutes makes clear the reason for the high signal counts shown in Fig 7. Such high amplitude and frequently occurring signals are not characteristic of those from meteor trails which, are typically described by the widely separated dots previous to this time. By further expansion, Fig 9, we can examine the amplitude time distribution more carefully. We see that the maximum amplitude is mildly oscillatory with an occurrence frequency of ~2 Hz.

At present it is difficult to interpret these results with any physical certainty. On one of the occasions cited SABRE detected a discrete band of radar irregularities which moved ~800 km south in ~10 minutes but in general there exists no one to one correlation between SABRE returns and these bursts of signals. On occasion the received signal has been identified as our own but on other occasions the signals have been logged during periods when the Bodø transmitter was switched off. One likely and not surprising, explanation is propagation of our own and cochannel distant transmissions via an auroral-E_s path. If this is so the use of frequencies as low as 40 MHz, for MBC at high latitudes, must be reconsidered since one of meteor bursts attractions, the secure nature of the transmission mode, will be lost. At no time have such signals been detected at 70 MHz.

4 POLARISATION ROTATION IN HIGH LATITUDE MBC SYSTEMS

4.1 Introduction

In designing an MBC system for operation at any latitude the system designer must address the statistical variation of signals. Both yearly and diurnal variations can be described but only the latter are of interest here. These are variations in meteor arrival rate, variations in meteor velocity, and variations in effective radiant. The sporadic meteor arrival rate has a roughly sinusoidal variation throughout the day with a maximum near 0600 LT and a minimum near 1800 LT. The ratio of maximum to minimum is about 4. The meteor velocity variations follow the same pattern and lead to a diurnal variation in trail height which is strongly coupled to the diffusion time constant, and which in turn leads to a variation in the duration of meteor bursts. Thirdly, due to the orbital motion of the earth, most meteors appear to have radiants concentrated ahead of the earth and very few radiants appear behind the earth. As the earth rotates the position of this concentration moves relative to the transmission path and as a consequence the geometric factors in equation (1) will vary giving rise to a diurnal variation in signal. Meeks and James[9] quantified this complex diurnal variation but the simple (albeit unrealistic) assumption of an isotropic distribution of meteor radiants over the sky can often provide sufficient physical insight. Such a model was first introduced by Eshleman and Manning[1]. We show here that, at frequencies in common usage in MBC systems (~40 MHz), Faraday Rotation is also an important factor effecting the diurnal variation of signals at high latitudes. Cannon[10] has investigated this effect at temperate latitudes.

4.2 Theory

The number of effective trails per unit area varies within the area illuminated by the antenna and is an important system parameter. Following Eshleman and Manning[1] a probability duration factor, P_d, can be defined for a uniform distribution of meteor radiants. Three quantities; echo amplitude, duration and number of echoes are important parameters controlling the efficacy of scattering. P_d expresses the fraction of those trails that pierce a differential area in the horizontal plane at height h_r and which are orientated to produce a signal of a certain amplitude and with a certain duration. P_d is referenced to a standard echo unit the amplitude and duration of which is taken to be the value obtained from a trail if viewed from a backscatter range of D. P_d is shown in Fig 11 (middle panel) for a receiver to transmitter range (2D) of 800 km, applicable to a link Bodø to Oslo (60.0N, 11.1E) which we will examine further later on. It can be seen that the highest percentage of effective trails lie off the great circle path. The dotted lines show azimuthal 3 dB contours for a 4-element Yagi, an antenna in common usage in MBC systems.

At VHF and above the effects of collisions in the Appleton-Hartree equation can often be neglected and, given that the quasi-longitudinal approximation holds (eg Davies[11]), the total Faraday rotation Ω in radians, for a one way passage through the ionosphere is given by Rishbeth and Garriott[12] as:

$$\Omega = \frac{2.36 \times 10^4}{f^2} \int_0^\infty \underline{B} \cos \chi \, N(h) \sec \Phi \, dh \quad , \tag{8}$$

where f = the wave frequency, Hz,
$\underline{B}$ = the local magnetic field, Wb m^{-1},
χ = the angle between the radio wave normal and the magnetic field direction,
Φ = the angle between the wave normal and the vertical
and h = the height, m .

In a MBC system the integration is only applicable over the height range 0 to h_r the mean reflection height, which was determined from the equation given by Brown and Williams[13].

$$h_r = \left(- 17 \log_{10} (f \times 10^{-6}) + 124\right) \times 10^3 \quad m \quad . \tag{9}$$

Typically h_r <100 km and it is, therefore, reasonable to assume that $\underline{B}$ χ and Φ are constant over the path. Writing:

$$\int_0^{h_r} N(h) \sec \Phi \, dh = \Sigma N \sec \Phi \quad , \tag{10}$$

where ΣN is the vertical electron column density (m^{-2}) we have

$$\Omega = \frac{2.36 \times 10^4 \underline{B}}{f^2} \cos \chi \, \Sigma N \sec \Phi \quad . \tag{11}$$

Using (11) the Faraday rotation losses can be calculated for underdense scattering.

Consider a horizontally polarised wave transmitted from a ground station which due to its passage up to the trail, through the ionosphere, is rotated by an angle Ω_u due to Faraday Rotation. At the scattering height the incident wave, $\underline{E}_i$, can be resolved into vertical and horizontal components $E_{i(h,v)}$. For underdense scattering from the train the scattered horizontally and vertically polarised component signals $E_{r(h,v)}$ are dependent upon the angle $\delta_{(h,v)}$, between the incident component signals, $E_{i(h,v)}$ and the reflected wave normal such that:

$$E_{r(h,v)} = a\, E_{i(h,v)} \sin \delta_{(h,v)} \quad , \tag{12}$$

where a is a factor dependent upon the trail electron density and certain geometrical characteristics of the trail and $\delta_{(h,v)}$ accounts for the amplitude pattern of the scattering electrons in the horizontal and vertical planes. For propagation on the great circle path simple geometrical considerations show that $\delta_h = 90$ deg for the horizontally polarised component however $\delta_v \neq 90$ deg for the vertically polarised component. As a result of the differing values of $\delta_{(h,v)}$ one or other component is preferentially scattered and consequently the plane of polarisation is further rotated. On the downleg Faraday Rotation, of magnitude, Ω_d will occur which may be in the same sense, or in the opposite sense, to the upleg rotation. If η is the angle of polarisation after reflection it can be shown that:

$$|E_r| = a\,|E_i| \left[(\cos \Omega_u \sin \delta_h)^2 + (\sin \Omega_u \sin \delta_v)^2 \right]^{\frac{1}{2}} , \tag{13}$$

at

$$\eta = \tan^{-1} \left[\frac{\sin \Omega_u \sin \delta_v}{\cos \Omega_u \sin \delta_h} \right] , \tag{14}$$

where at the mid-part of the great circle path

$$\delta_v = -\cos 2\Phi \quad . \tag{15}$$

and

$$\delta_h = 90° \quad . \tag{16}$$

At other points both on and off the great circle path between the transmitter and the receiver $\delta_{(h,v)}$ take other values. In general if Φ_u and Φ_d are the upleg and downleg values of Φ and α_u and α_d are the azimuthal bearings of the wave normals on the upleg and downleg respectively, (both measured at the trail) then:

$$\delta_v = -\cos(\Phi_u + \Phi_d) \quad , \tag{17}$$

$$\delta_h = -\cos(\alpha_d - \alpha_u) \quad . \tag{18}$$

It follows that for a linearly polarised receive antenna the fraction of incident field available, relative to that available if no polarisation rotation had occurred is:

$$\Delta E_p = \frac{|E_r|}{a\,|E_i|\,|\cos(\eta \pm \Omega_d)|} \quad . \tag{19}$$

4.3 Model calculations

Equation (19) has been evaluated for an auroral radio link Bodø to Oslo using electron density models applicable to two levels of precipitation. Fig 10 shows auroral electron density profiles given by Jesperson *et al*[15] for riometer absorption events of 0 dB and 1.5 dB, both measured at 27 MHz. It is assumed that the precipitation is homogeneous over the entire ionospheric portion of the propagation path. Calculations show that the maximum predicted loss associated with the 0 dB event is only 0.2 dB over an area ±300 km either side of the great circle path and the user will be unaware of its effects. Fig 11 (left panel), however, shows the predicted polarisation rotation losses for the 1.5 dB event. In this case considerable loss occurs over a wide area exhibiting a high value of P_d (middle panel). This loss is controlled by two factors. Firstly the polarisation mismatch at the receive antenna, which is a function of both the up and downleg Faraday rotation and secondly, by the preferential transmission of the horizontal component (at least on the great circle path) which is a function of the upleg Faraday rotation only.

By superposing the Polarisation loss contours and P_d the effect of the losses can be seen. Defining a throughput factor T_f as:

$$T_f = P_d 10^{\Delta E_p/10} \tag{20}$$

we arrive at Fig 11 (right panel) for the 1.5 dB absorption event. Comparison of Fig 11 middle and right panels shows that the contours have been distorted and the areas within each contour reduced. By scaling the areas within the antenna common areas and within each contour for both P_d and T_f the fractional reduction in throughput, (R_f), due to the polarisation mismatch, can be obtained. The results of such an exercise reveals that the system throughput, over the link is only 75% of that which might have been expected had Faraday rotation not occurred. In interpreting the effects of the losses some care must be exercised since the model assumes an isotropic distribution of radiants which is not true in practice. In addition some redemption of the link will probably occur due to the varying ionisation heights for the trails which are all assumed to be at 97 km. It is evident however that the Faraday rotation losses, at 40 MHz, during a moderate 1.5 dB absorption event are sufficient to cause problems on a high latitude MBC link. The Faraday rotation will result in a reduction in the number of trails detected, that is a distortion of the diurnal variation. Equivalently, the data throughput will be reduced. At higher frequencies the effects will, of course, be less and system designers might, therefore be advised to use higher frequencies than previously thought appropriate.

4.4 Experimental validation

As yet the only validation of this theory is over a temperate latitude link (Cannon[10]). Fig 12 shows theoretical predictions, at noon, for a link Wick (Scotland) to Farnborough (Hampshire) (51.3N, 359.3E). This path is again 800 km long and the electron density model used, see Fig 10, is that proposed by Metchtly et al[14] for low and high sunspot number (SSN) periods. Fig 12 shows that the maximum Polarisation rotation losses are only about 4 dB at high SSN, with lower values expected at low SSN.

Since shower meteors would complicate the diurnal variation and data reduction the experiment was conducted during April 1984 when there were few shower meteors. The transmitter power was ~200 W into a horizontally polarised dipole and the receiving antennas were two 4-element Yagi's, one horizontally polarised and one vertically polarised. The experiment consists of a cross polarised approach. Firstly, horizontally polarised signals were transmitted and received and secondly, horizontally polarised signals were transmitted but the vertically polarised signal components were received. The data acquisition program was as previously described and only underdense trails were analysed. The SSN at this time was ~60; relatively low. Fig 13 shows the diurnal variation of signals detected on the horizontally polarised receiving antenna on 17 April 1984. The variation peaks at 0700 LT and reaches a minimum at 1800 LT in accordance with the earlier description of diurnal variations. Due to the relatively small amount of predicted polarisation mismatch on this path, even at high SSN, no statistically significant departure from the normal 4:1 daily variation was expected.

The vertical antenna diurnal variation (Fig 14) for 10 April 1984, however, shows a marked peak towards midday, as might be expected if the amount of rotation and, therefore, the number of detected trails were solar zenith angle controlled via the electron density term in equation (11) for Faraday rotation. By evaluating N_v/N_h, the ratio of the smoothed number of trails received respectively on the vertical and on the horizontal antennas, N_v can be normalised, approximately, to a constant meteor incidence rate. This ratio is shown in Fig 15, which exhibits the expected distribution with few detected trails during the night and a maximum shortly after midday. The discrepancy between the expected maximum at midday and the measured maximum at 1330 LT is not clear. The phase delay might be due to the sluggishness of the bottom part of the ionosphere. Alternatively, it may be due to a difference in the diurnal variation of incident meteors between the vertically polarised measurements on 10 April and the horizontally polarised measurements on 17 April. The results are, however consistent with the suggestion that polarisation rotation can influence the performance of a MBC link to its detriment at temperate latitudes.

5 CONCLUSIONS

In the short time since deployed on a high latitude path, the propagation experiment has already produced some interesting results. The theoretical predictions regarding Faraday rotation losses have been validated over a temperate latitude link and it is hoped that this can be extended to a high latitude path in the near future.

Acknowledgments

The authors wish to acknowledge the considerable help given by Messrs H.L. Spong, I.H. Bowker and J.N Tyler in the deployment of this experiment. In addition we would also like to thank Capt W. Johansen, and Capt Wenseth of the Norwegian Armed Forces for running the Bodø transmitter with such care and Dr I. Thrane at NDRE (Norway) for his interest and help. Prof T.B. Jones and E.C. Thomas are due thanks both for permission to use the Wick field site, alongside SABRE, and also for SABRE range time intensity data. In Wick we would like to thank I. Morrison for monitoring the operation of the equipment.

REFERENCES

1 Eshleman Von R. and Manning L.A., Radio communication by scattering from Meteoric ionization, Proc. IRE, 42, 530-536, 1954

2 Forsyth P.E., Vogan E.L., Hansen D.R., Hines C.O., The principles of JANET - a meteor burst communications sytems, Proc. IRE, 45, 1642-1657, 1957

3 Bartholomé P.J. and Vogt I.M., COMET - A new meteor burst system incorporating ARQ and diversity reception, IEEE Trans., COM-16, 268-278, 1968

4 Hannum A.J., Evans G.L., Chambers J.T. and Otter K., Air to ground meteor scatter communications systems, IRE Trans. Comm. Syst., 8, 113-133, 1960

5 Ince A.N., Interception of signals transmitted via meteor trails, AGARD Symposium "Aspects of Electomagnetic Wave Scattering in Radio Communications, Paper 19, 244, 1977

6 Sugar G.R., Radio propagation by reflection from meteor trails, Proc. IEEE, 52, 2, 116-136, 1964

7 Sites F.J., Communications via meteor trails, AGARD Symposium "Aspects of Electromagnetic Wave Scattering in Radio Communications", Paper 25, 244, 1977

8 Cottony H.V. and Johler J.R., Cosmic radio noise intensities in the VHF band, Proc. IRE, 40, 1053-1060 1952

9 Meeks M.L. and James J.C., On the influence of meteor radiant distributions in Meteor Scatter Communication, Proc. IRE, 45, 1724-1733, December, 1957

10 Cannon P.S., Polarisation rotation in meteor burst communication systems, submitted to Radio Science 1985

11 Davies K., Ionospheric Radio Propagation, National Bureau of Standards Monograph 80, US Government Printing Office, Washington, 1965

12 Rishbeth H. and Garriott O.K., Introduction to Ionospheric Physics, Academic Press, London, 1969

13 Brown D.W. and Williams H.P., The performance of meteor burst communications at different frequencies, AGARD Symposium "Aspects of Electromagnetic Wave Scattering in Radio Communications", Paper 24, 244, 1977

14 Metchtly E.A., Bowhill, S.A. and Smith L.G., Changes of lower electron concentrations with solar activity, J. Atmos. Terr. Phys., 34, 1899-1907, 1972

15 Jesperson M., Haug, A. and Landmark B., Electron density and collision frequency observations in the arctic D-region, "Electron Density Profiles in the Ionosphere and Exosphere", NDRE, 1965

Table 1

ANTENNA CHARACTERISTICS

Location	Antenna type	Operating frequency (MHz)	Theoretical Antenna gain (dBi)	Bearing (true degrees)
Bodø	dipole	40	8	230
Bodø	Yagi	70	15	230
Wick	Yagi	40	15	35
Wick	Yagi	70	15	35
Wick	Yagi	70	15	168
Wick	dipole	40	8	168
Wick	dipole	70	8	168

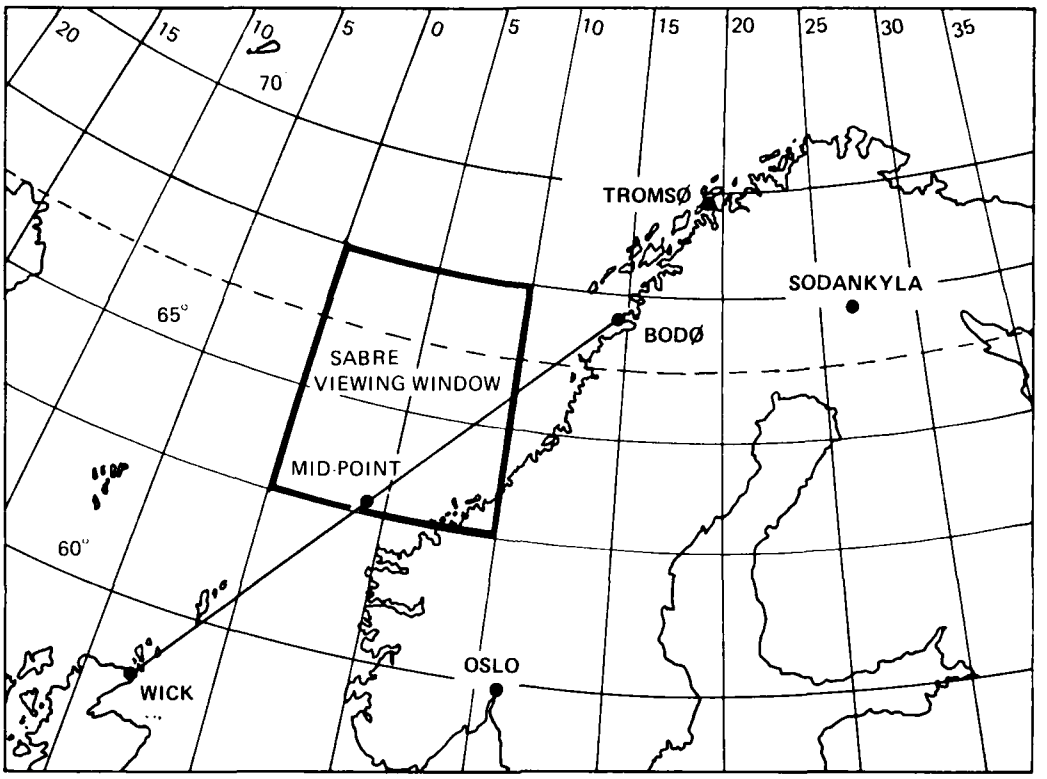


Fig 1 Geographical details

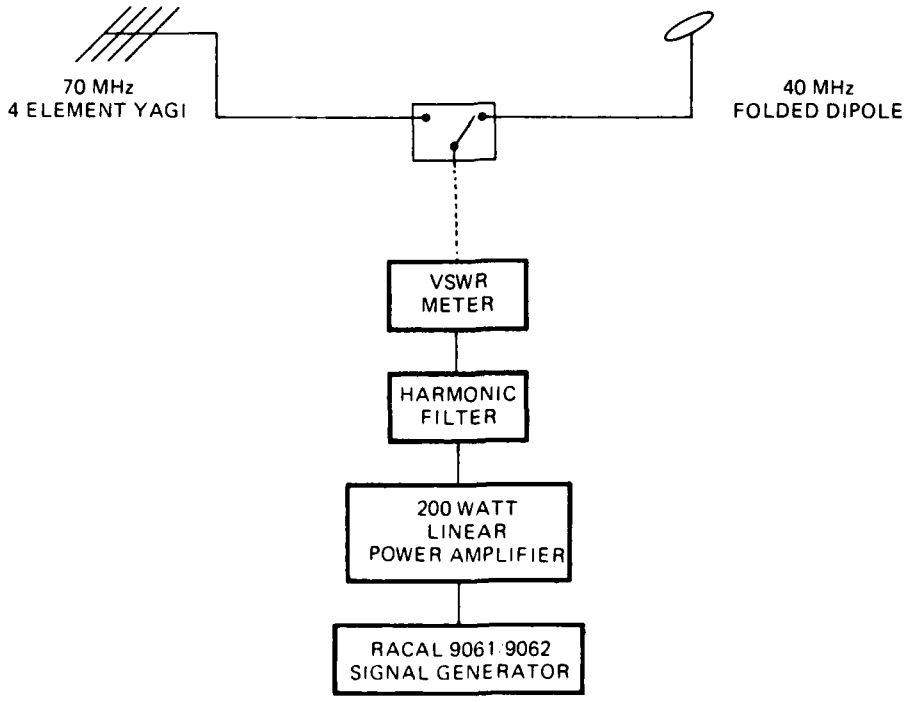


Fig 2 Transmitting station block diagram

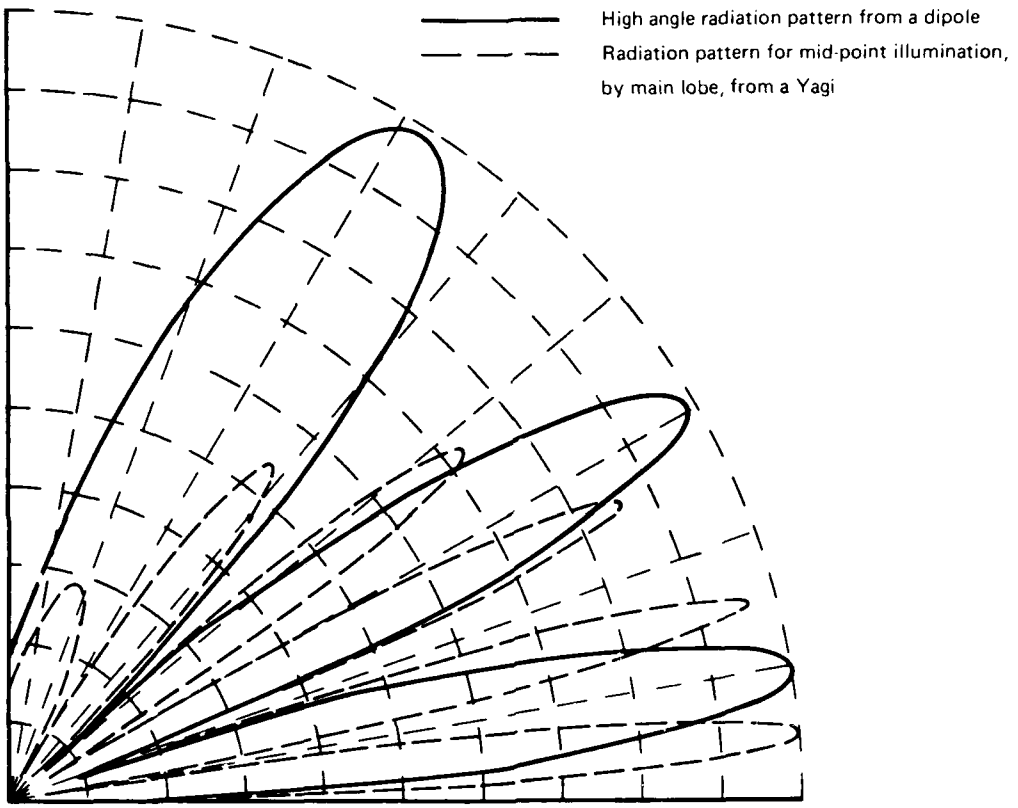


Fig 3 Theoretical polar diagrams (normalised field strength)

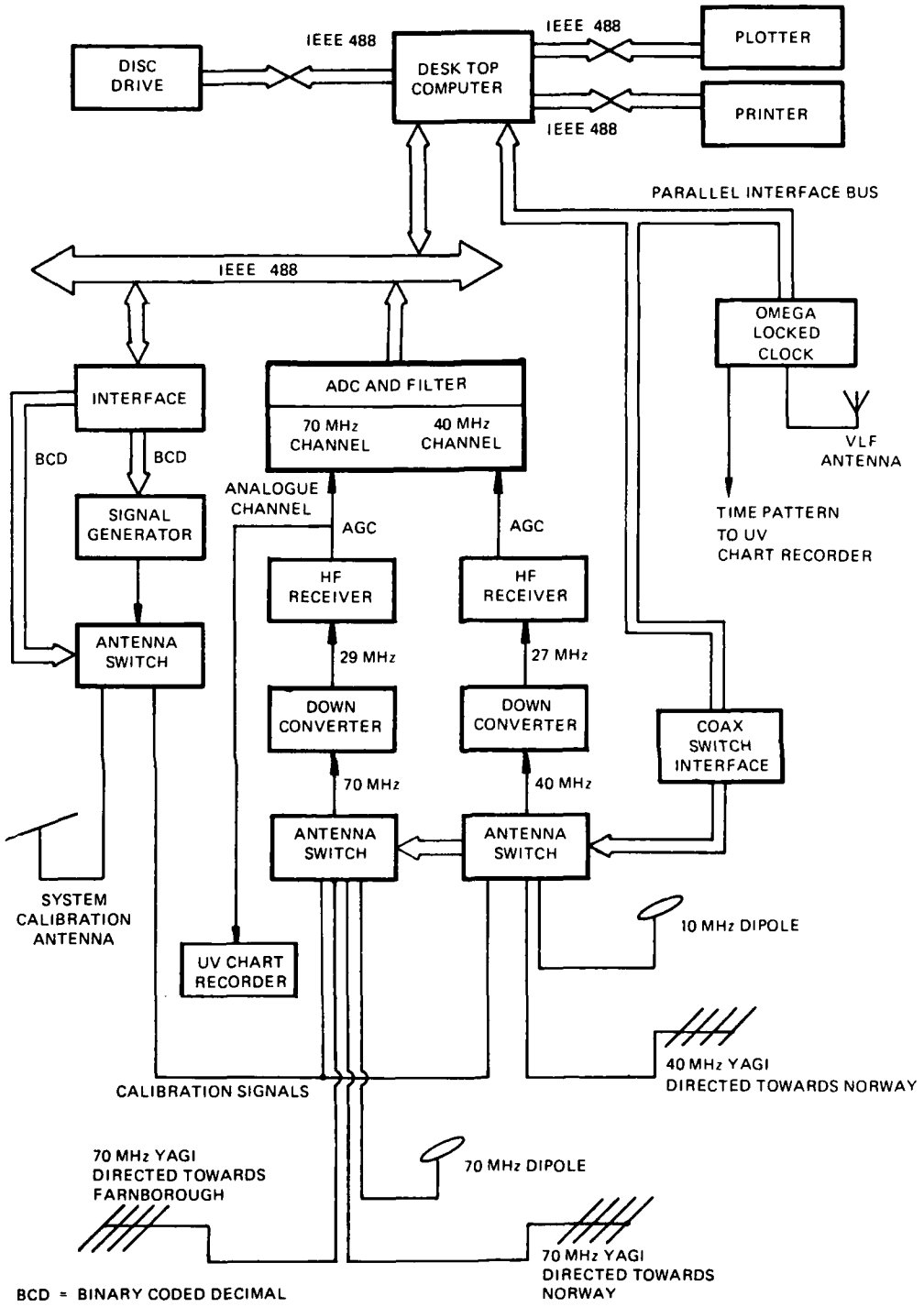


Fig 4 Meteor scatter data logging and control system

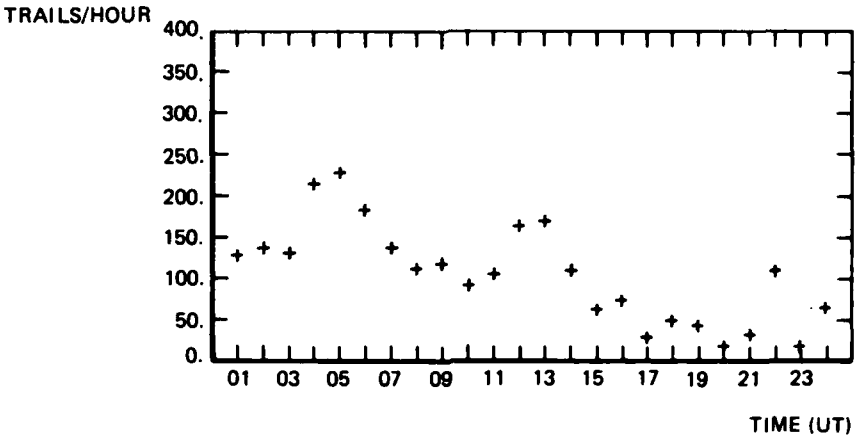


Fig 5 High latitude 40 MHz diurnal variation for 7 April 1985 (day 097)

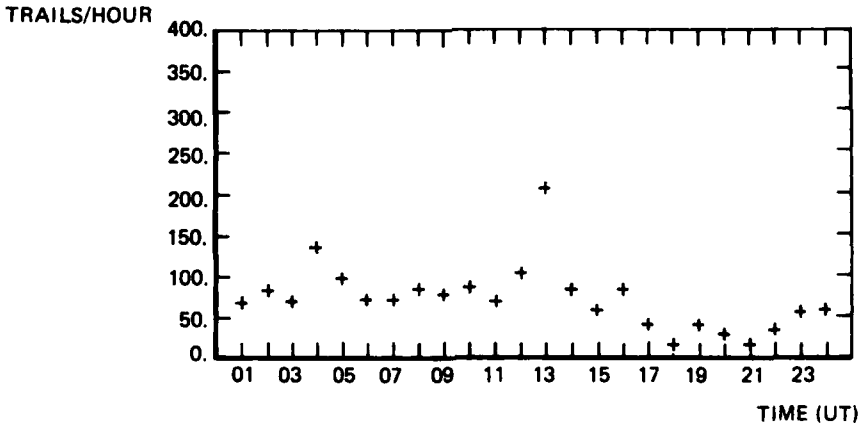


Fig 6 High latitude 70 MHz diurnal variation for 4 April 1985 (day 094)

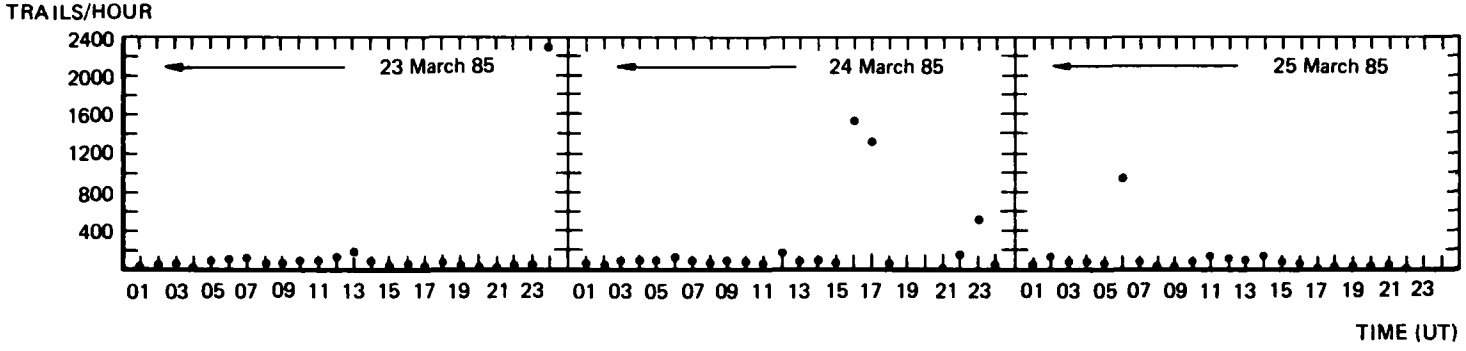


Fig 7 40 MHz diurnal variations for 23, 24 and 25 March 1985 (days 082-084)

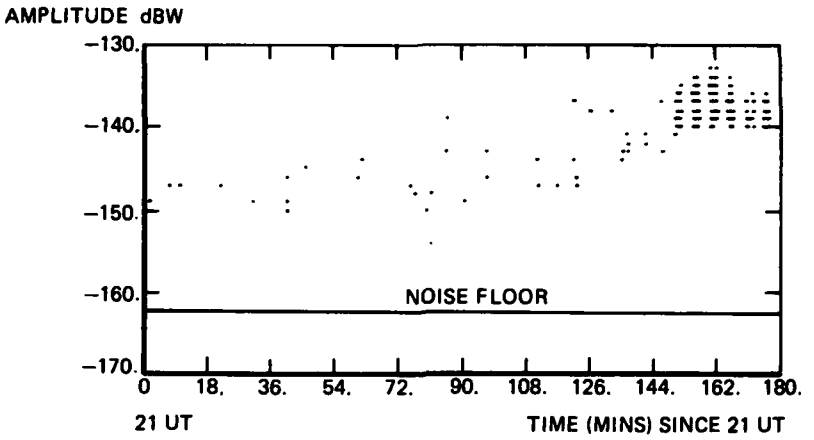


Fig 8 Three hour amplitude – time plot for 23 March 1985 from 2100-2400

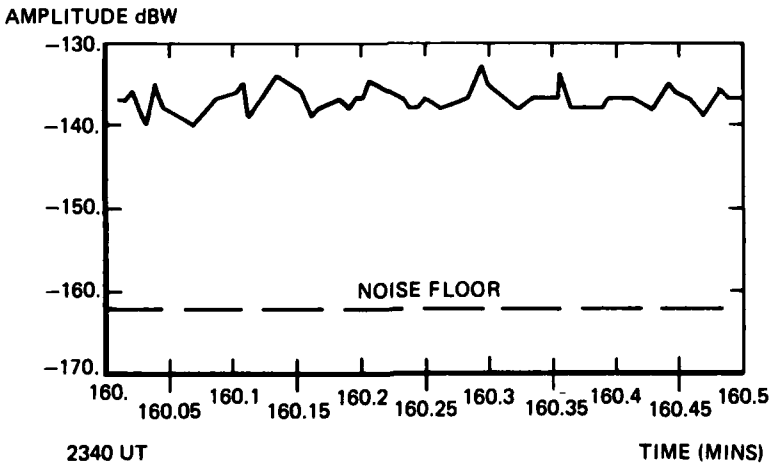


Fig 9 High resolution amplitude – time plot for 23 March 1985 from 2340-2340.5

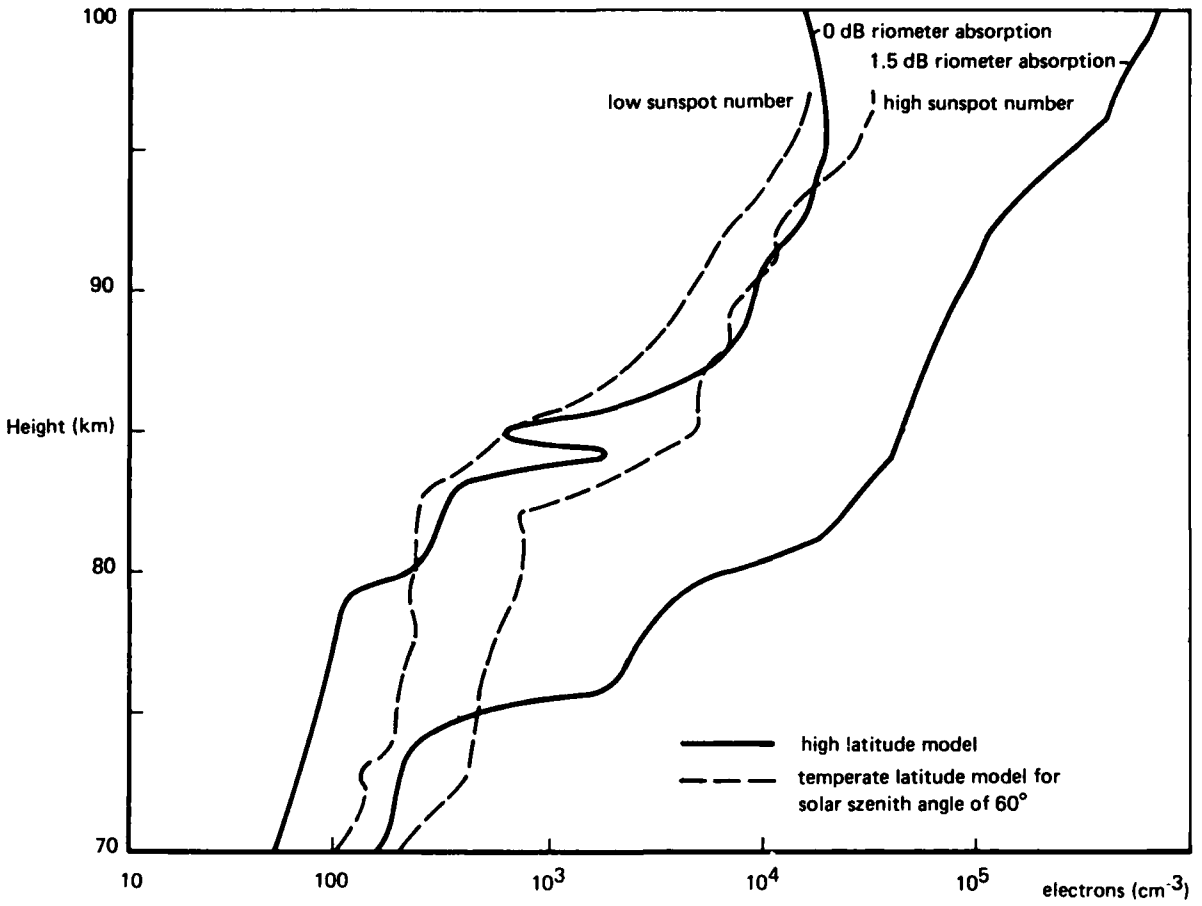


Fig 10 Electron density profiles

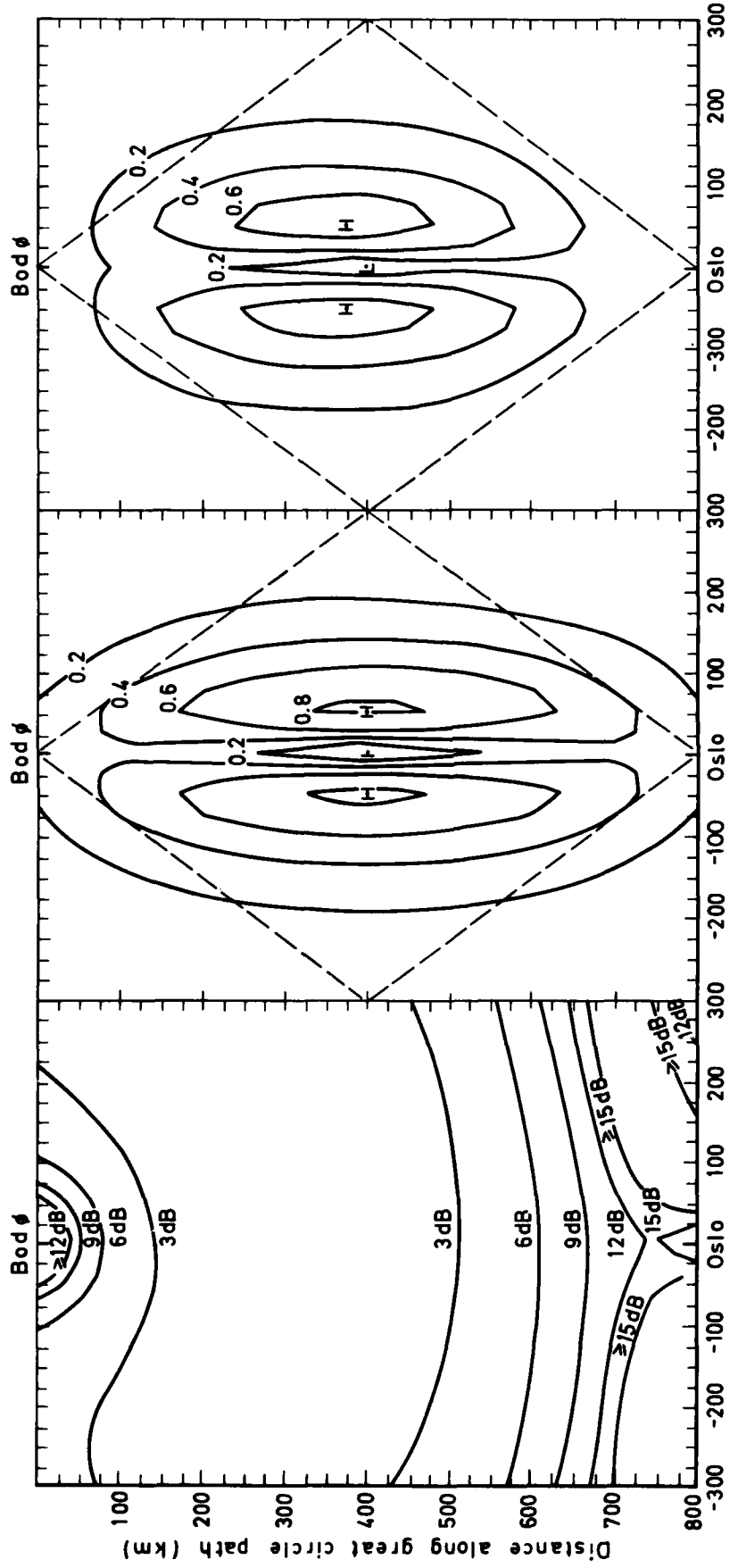


Fig 11 Faraday rotation loss contours, P_d contours and T_f contours for a 1.5 dB riometer absorption event, H and L show local high and low points

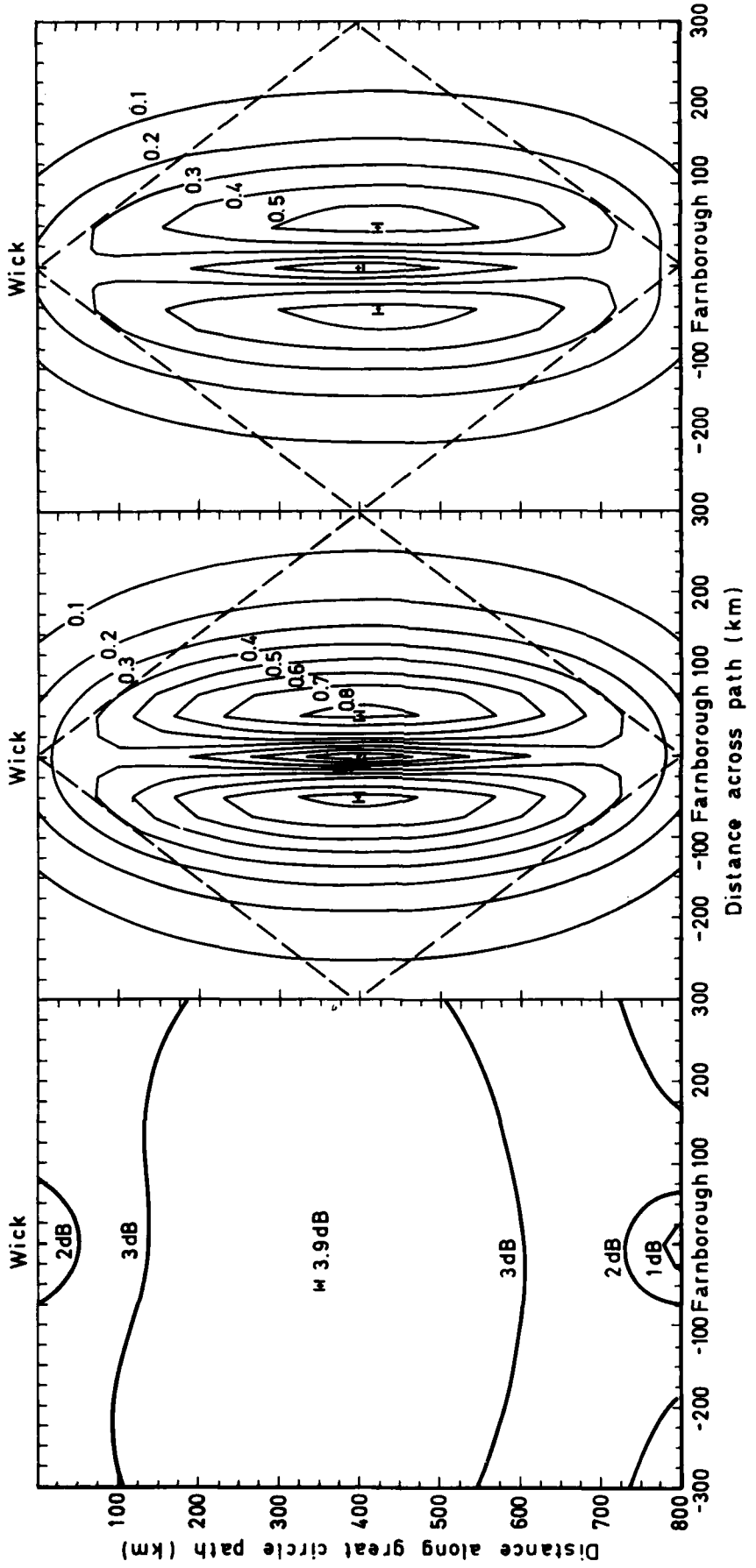


Fig 12 Loss contours, P_d contours and T_f contours respectively for the MBC link Wick to Farnborough at high SSN

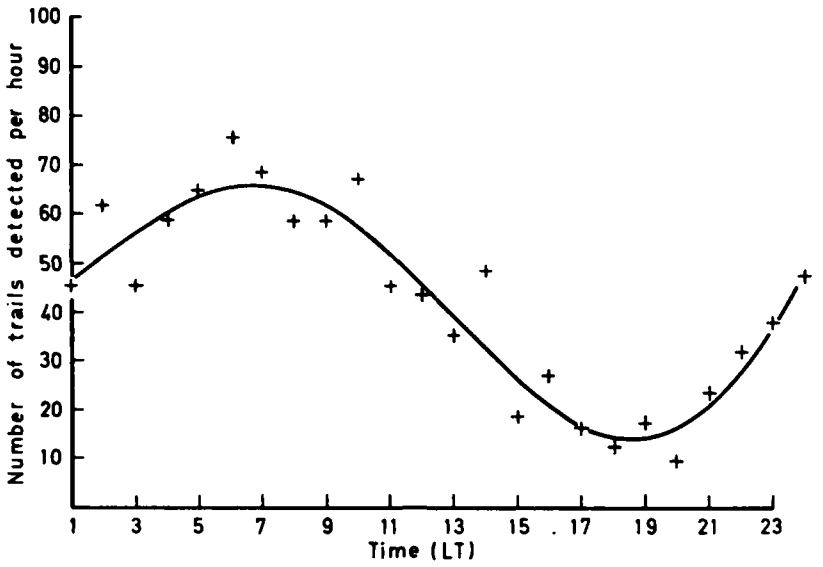


Fig 13 Number of trails received per hour on a horizontally polarised antenna during 17 April 1984

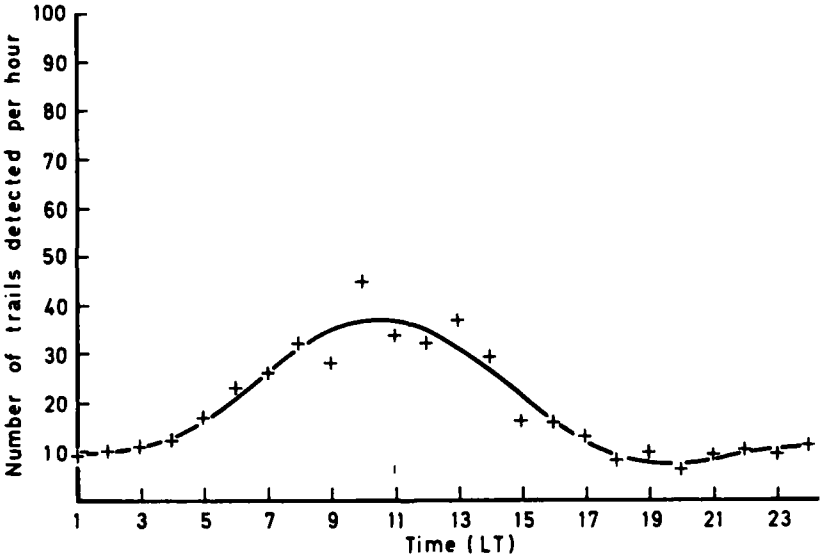


Fig 14 Number of trails received per hour on a vertically polarised antenna during 10 April 1984

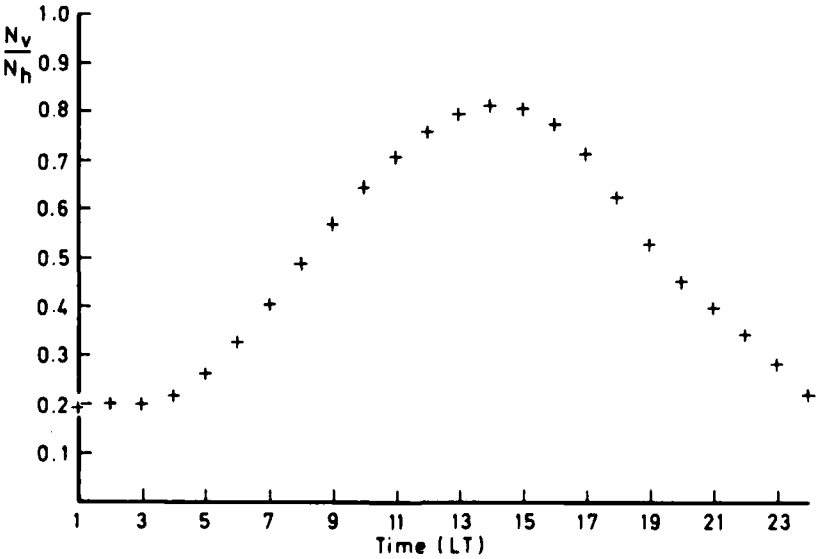


Fig 15 The quotiant N_v/N_h determined from the smoothed curves shown in Figs 13 and 14

DISCUSSION

N.C.Gerson, US

Can you comment on the bandwidth frequency relationship.

Author's Reply

I do not expect a significant variation in operational bandwidth with frequency at least for data rates applicable to our own system (<50 KHz).

E.V.Thrane, NO

You have looked at the meteor scatter circuit as a system in its own right and searched for the optimum frequency. If a meteor scatter system is planned as a backup system for HF communication, that is, as a system that will work during a black-out, the optimum frequency will probably be higher. Have you considered this aspect of meteor scatter communications?

Author's Reply

No we have not, although this is a good point. At present we are trying to configure a system which will operate in its own right and which will provide certain advantages (e.g. good A/J and LPI performance) not found in HF systems. It may also be possible to configure the system for operation at various frequencies, in which case, the operating frequency can be chosen to optimize data throughput during various levels of absorption.

T.Damboldt, GE

Have you considered using M.B.C. as an engineering link on an HF channel which is no longer operating via normal ionospheric mode? Particularly, this might be applicable after the MUF has fallen below the operating frequency.

Author's Reply

No we have not; however, we have conducted temperate latitude meteor scatter propagation experiments at frequencies close to 29 MHz, and, as expected, we find that the potential data throughput is higher in the HF band than for channels operating in the VHF band.

J.S.Belrose, CA

I agree with the conclusions of the author that 40 MHz is too low for high latitude paths. Early Canadian work in the mid-to-late fifties by Forsyth et al (the JANET system) showed that SPEs could disrupt 40 MHz burst communication. Later work in the mid-sixties by Maynard et al employing two frequencies near 40 and 108 MHz, over an Ottawa to Goose Bay path, showed that the high frequency meteor signal was less likely to be "black out", but there were fewer meteor trails having sufficient density to reflect the high frequency signal and these were of shorter duration. However, higher data rates could be employed and useful throughput data rates were feasible.

H.Sepp, STC

COMMENTS: Cost comparison SATCOM/Meteor scatter is unfair (1) achievable data rates differ by a factor of 100,000 (2) vulnerability to airborne jamming. QUESTIONS: (1) What applications do you have in mind? (2) Have you carried out any experiments with mobile receivers (e.g. in aircraft)?

Author's Reply

(1) Our application is the transmission of data, rather than voice, however, we are considering the use of a speech recognizer in conjunction with MBC. (2) Not yet.

CHARACTERISTICS OF HIGH LATITUDE METEOR SCATTER PROPAGATION PARAMETERS OVER THE 45 - 104 MHz BAND

J.C. Ostergaard
ElektronikCentralen
Horsholm, Denmark

J.E. Rasmussen, M.J. Sowa,
J.M. Quinn and P.A. Kossey
Rome Air Development Center
Hanscom AFB, MA 01731

ABSTRACT

Data being acquired on a high latitude test-bed, to assess the performance of meteor scatter propagation over the 45-104 MHz band, are described. Emphasis is on data obtained over a 1200 km path in northern Greenland, which includes initial estimates of: the availability of usable meteor trails, the potential performance of meteor scatter systems, and the application of adaptive data rates to improve system performance. The use of the data to validate and expand propagation prediction techniques for the polar region is also discussed.

1. INTRODUCTION

The first truly operational meteor scatter communication system, JANET (Forsyth et al, 1957), was operated in Canada in the mid 1950's at approximately 40 MHz. The system, however, was severely impaired by a polar cap absorption event during testing between Yellowknife and Edmonton (Crysdale, 1960), and experimental research in meteor scatter propagation essentially vanished. This was partially due to the failure of operation under disturbed conditions and partially because the technology needed to handle the handshaking procedures and intermittent data storage requirements was not available in the 1950's.

SHAPE Technical Center developed and tested a new meteor scatter communication system, COMET (Brown and Williams, 1977), in the mid 1960's in Central Europe and in Norway. This system worked well, but had a fairly low capacity (1-4 telegraph channels). The advent of satellite communication in the late 1960's, with its large available bandwidth and inherently stable propagation, diverted interest away from meteor scatter propagation for obvious reasons of capacity, reliability and economy. Since then, the U.S. Dept. of Agriculture and a number of private corporations have constructed meteor communication systems in the Western U.S. (SNOTEL) and Alaska (MBCS). These systems are currently in operation using fixed data rate signaling and a half duplex handshake configuration.

Recently interest in meteor scatter communication has been revitalized as a result of rapid advances in microprocessor technology. Some suggested uses for modern meteor scatter communication systems have included automatic data collection from unmanned sites and thin-line digital links where privacy and exclusive ownership of the communication terminals are desirable. These could be either point-to-point service, or mobile service, possibly incorporating some form of vehicle tracking. Meteor scatter could also be a candidate for a communication system to be used in the polar regions where geostationary satellites are below the horizon, and where HF systems are regularly blacked out by polar cap absorption (PCA) events. It is expected that meteor scatter systems operating in the 60 to 100 MHz frequency range will be less affected by ionospheric absorption than HF or lower VHF scatter systems and thus might provide a way to communicate during a PCA event.

This paper describes a unique, diagnostic, link installed in northern Greenland by the Rome Air Development Center (RADC/USAF) to obtain data required to assess the potential performance of 45-104 MHz meteor scatter systems operating in the polar region. After a brief section discussing some of the characteristics of meteor scatter propagation, the experimental approach and instrumentation being used in the RADC testbed are described. The current measurement program and some preliminary results are also presented.

2. BACKGROUND

Normally the ionosphere is not sufficiently dense, nor are the ionization gradients large enough to efficiently reflect or scatter VHF signals back to earth. However, from time to time electron densities produced by meteorites entering the earth's atmosphere provide a suitable scattering mechanism. Such meteor trails are typically only about a meter wide, but can have lengths of 25 km, and more. The ionization that scatters the VHF signals is in the 85-125 km altitude range, and it can be used to establish communication links over a range from about 300-2000 kilometers.

Physical considerations show that for a meteor trail to be useful in linking two points on earth it must be tangent to some ellipse having those points as foci, as illustrated in Figure 1. Furthermore, the scatter from such trails illuminates only a relatively small area in the vicinity of the receiver, thus providing the link with a degree of protection against outside interference or detection.

There are regions of the sky which are more important than others, in terms of their contributions to the overall performance of a meteor scatter link. The locations of these regions can be estimated by consideration of propagation loss factors, such as path length and scattering efficiency, and how they vary with the angle of incidence between the propagating wave and the axis of the meteor trail. Figure 2 illustrates an idealized result of such considerations; the relative contributions of the various scattering regions shown there are given with respect to 'hot spots', labeled as '100' in the Figure. The more important scattering regions are to the side of the great circle path between the trans-

mitter and the receiver, in the vicinity of the mid-point of the path. As discussed later, this has important implications with regard to the siting of antennas for a meteor scatter system.

Figure 3 illustrates two basic mid latitude relationships associated with the occurrence of meteor trails, and the radiowave returns (bursts) originating from them, as derived from the COMET experiments in Europe. Figure 3a shows that only half of the returns last for more than 0.4 seconds, and that there is very little diurnal variation in the lengths of the returns. The intervals between returns, however, have a large diurnal variation, as shown in Figure 3b. For example, in the early morning, the average interval between returns is 3-4 seconds, while in the early evening it is 12-13 seconds. Also, there is a significant seasonal variation with the maximum in the summer and the minimum in the winter, as shown in Figure 4. As the result of these diurnal and seasonal variations, the performance of a meteor scatter link varies greatly (a factor of 15 or more) over the course of a year.

Galactic and man-made noise are limiting factors in meteor scatter systems, however, man-made noise can often be avoided through siting considerations. The galactic noise is gaussian distributed and a function of frequency to the -2.3 power. If galactic noise is assumed to be the only channel distortion on a meteor scatter link, then the instantaneous capacity of the link is a function of the instantaneous signal-to-noise ratio in the receiver bandwidth.

One of the goals of the RADC experiments is to obtain data to better quantify the potential performance of a wide variety of candidate meteor scatter systems at high latitudes. In addition to obtaining data describing diurnal and seasonal factors, emphasis is also being placed on obtaining data to quantify the effects of scatter from sporadic E-layers, aurora, and other scattering mechanisms. Also of interest are the observation and quantification of the effects of anomalous absorption, such as that produced during solar particle events within the polar cap.

Effects of Sporadic E.

Sporadic E-layers occur at altitudes comparable to those associated with usable meteor trails. They are known to occur frequently at high latitudes and to cover relatively large areas, often lasting for many minutes, or even hours. Sporadic E-layers can have sufficiently high critical frequencies to reflect VHF radiowaves, so that this mode of propagation can provide greatly enhanced capacity for a meteor scatter system. However, it does not provide the directional properties of meteor scatter. The effects of sporadic E can be mitigated, if desired, by operating at higher VHF frequencies, since the strengths of the reflections from such layers decrease as the wave frequency increases. It is expected that the communication capacity of sporadic E modes of propagation will not be limited by signal-to-noise ratios alone, but by the multipath properties of the channel, as well.

Effects of Auroral Scatter.

VHF signals can be scattered from field-aligned irregularities in the E-region within the auroral oval. This mode of propagation is well known from tests of the Alaskan MBCS system, which have shown that, at times, field aligned scattering accounted for as much as 11% of its total connectivity (Santeford). Signals scattered from aurora can last for tens of minutes and can have severe multipath structures and rapid fading, properties which are not compatible with the coherent signaling techniques commonly used in meteor scatter communication systems. The time and frequency dispersion characteristics of this mode of propagation, and its potential effect on VHF meteor scatter systems, depend on a number of factors including the communication system geometry, the directional properties of the scatter from the field-aligned structures and the morphology of the radio aurora itself.

Effects of Absorption.

Two types of anomalous absorption can be encountered at high latitudes: auroral absorption, which is confined mainly to paths penetrating the upper D- and lower E-regions of the ionosphere within the auroral oval; and polar cap absorption, which affects paths penetrating the D-region inside of the polar cap. Of the two, the PCAs are generally much more severe and longer lasting. They occur following certain solar flares which dump energetic particles (protons) into the lower ionosphere within the polar cap. The effects of such disturbances can include lowering of the ionosphere by tens of kilometers and significant enhancement of D-region electron densities by orders of magnitudes. PCAs are known to seriously degrade HF communications in the polar regions for many days.

Knowledge of the morphology of high latitude absorption events has increased greatly in recent years as the result of a wide variety of experiments, conducted both on the ground and in space (Kossey et al, 1983; Reagan et al, 1982). The possible mitigation of PCA absorption effects by increasing the frequency of operation of a meteor scatter system is illustrated in Figure 5. For simplicity the figure construction assumes that the wave frequency is much greater than the collision frequency in the absorbing region of the ionosphere. Theoretical results shown are for a 1000 km link, a variety of ionospheric conditions ranging from ambient (0 dB 30 MHz riometer absorption) to highly disturbed (greater than 10 dB riometer absorption) and for simplicity, the absorption is assumed to be inversely proportional to the square of the frequency. The results indicate clearly how even modest PCAs can strongly affect a meteor scatter system operating in the lower VHF

band, and how the absorption effects can be reduced significantly by operating at higher frequencies.

The advantage of using higher frequencies to mitigate absorption is offset, however, by a decrease in the capacity of the system, since the received power from meteor scatter is reduced significantly with increased frequency (predicted to be inversely proportional to frequency to the third power). Thus, there is some optimum frequency of operation for any given amount of anomalous absorption.

Galactic noise also suffers absorption during a PCA, but that loss is much less severe as the noise traverses the absorbing region only once, whereas the signal must go through the region twice to reach the receiver.

3. RADC METEOR SCATTER TEST-BED IN NORTHERN GREENLAND

The RADC experimental link in northern Greenland was established to address a number of questions concerning the potential performance of meteor scatter communication systems in the polar region: the availability of useful meteor trails at very high latitudes; the potential communication capacity associated with those trails; the occurrence, persistence and effects of sporadic E-layers; and, the effects of polar cap absorption events on the capacity of 45-104 MHz meteor scatter communication systems, for a variety of signaling techniques.

Conventionally the assessment of the communication capacity and bit-error-rate for meteor scatter systems is obtained by deploying a full duplex message handling system. This method has the advantage of providing some precise (but limited) communication information; however, the information is relevant only to that particular system and provides little data on the specific propagation characteristics of the meteor scatter channel. In contrast the RADC experimental approach exploits the concept that the meteor scatter channel can be considered as a transfer function. One aim of the RADC experiment is to characterize the properties of the transfer function in as much detail as possible. To do this both macroscopic and microscopic time variations are being investigated, including time and frequency dispersion factors caused by multipath propagation.

The link is located entirely within the polar cap, in northern Greenland between Sondrestrom Air Base and Thule Air Base; a distance of 1210 kilometers. As shown in Figure 6, the transmitter (at Sondrestrom) and receiver (at Thule) are not conventional communication system components. Rather, they were developed to investigate features of meteor scatter from a propagation point of view, as well as from a communication viewpoint. The efforts under this initial measurement program have concentrated on characterizing the time and frequency variations of the transfer function including the variation in the instantaneous signal-to-noise ratios of each return from a meteor trail.

Figure 6a shows a block diagram of the transmitter, which is computer controlled and provides periodic transmissions at 45, 65, and 104 MHz. The frequencies are changed every half-hour. In each 30 minute time block, the first 5 minutes are devoid of transmissions so that background noise measurements can be made at the receiver. The output power at all three frequencies can be varied, but is nominally 1 kilowatt. The transmitting antennas are Yagis, mounted so as to radiate horizontally polarized signals. The antenna gains are about 11 dBi and the beamwidths are approximately 55 degrees. A 400 Hz FM modulation is imposed on the transmissions as a signature to identify the signals at the receiver.

Figure 6b shows a block diagram of the receiving system. A feature of the system is a waveform analyzer which captures the time history of each return. This data is recorded in digital form for later reduction and analysis. The receiving antennas are similar to those at the transmitting site. Because of the desire to quantify the effects of polar cap absorption events on the meteor scatter signals and the background noise, a special low noise receiver was built, having a noise temperature of 110 degrees, or a noise figure of 1.3 dB. The receiving system is controlled by a small computer, which cycles the receivers each half hour in accordance with the frequency selected at the transmitter. In addition, it controls the noise measurements that are made during the first five minutes of each half-hour time block, and a system calibration, which is performed once a day.

Early experience with the link showed the importance of locating the transmitting and receiving antennas at heights to produce as uniform illumination of the common scattering volume as possible. Initially, the antennas were mounted between 10 and 12.5 meters above the ground. Calculations, and some limited measurements at Thule, showed that the resultant antenna patterns had an excessive number of nulls for elevation angles between 1-20 degrees, the range that illuminates the regions of the sky which are most important to a meteor scatter system. Further calculations showed that if the antennas were located at heights corresponding to 1.5 wavelengths above the ground, only one lobe would be present in this interval and an additional gain enhancement of about 5 dB would be achieved at an elevation angle of 8 degrees.

Figure 7 shows the result of a calculation of path losses associated with the position of scatterers within the common volume illuminated by the transmitting and receiving antennas of the RADC link. The calculations are for 104 MHz. In Figure 7a the antennas are assumed to be located 1.5 λ or 4.5 m above the ground, while in Figure 7b the antennas are located 3.3 λ or 10 m above the ground. The most important features, when the antennas are located 1.5 λ above the ground (Figure 7a), are the small variations in the losses with respect to the position of the scatterers and the less than 8 dB variation over the most important portion of the common scattering volume. When the antennas are 3.3 λ above the ground

(Figure 7b), the variation in losses is considerably greater, about 20 dB, and includes a 16 dB valley in the middle of the primary scattering area.

The importance of proper positioning of antennas was demonstrated experimentally on the RADC link as an increase in the number of returns resulted when the antennas were moved to the 1.5 λ height.

4. EXAMPLES OF SIGNALS RECORDED AT THULE

This section describes a selection of meteor scatter returns received at Thule AB. To characterize the returns a classification system has been adopted which includes five categories: those from underdense, overdense, and tiny meteor trails, and those from sporadic E-layers and other (unidentified) ionospheric scatter modes. Some of these classes contain waveforms which agree closely with the classical theory of meteor scattering as presented by Eshleman (1955) and McKinley (1961) (those from underdense and overdense trails). At present other classes, such as the returns from "tiny" meteor trails and the other unidentified scatterers, cannot be associated unambiguously with a specific physical mechanism of propagation. However, they occur often enough to warrant separate classifications.

In the data presentations that follow, the received powers are scaled in dB relative to a milliwatt into a 50 ohm load (dBm). This means that the amplitude scales are compressed and that an exponential change in amplitude is presented as a straight line.

4.1 Returns from Underdense Meteor Trails

The returns from underdense trails are characterized by a fast rising leading edge and a slower exponential decay. Underdense trails account for approximately 80-90 percent of signals observed. Figure 8 shows a number of returns from underdense trails. The maximum amplitudes of the waveforms vary over a range of 25 dB and the durations vary from less than 0.1 seconds to several seconds.

Some underdense returns exhibit fading during their exponential decay. This phenomenon usually is observed with long lasting trails, and may be attributed to wind moving portions of the trail to different positions and attitudes such that they fulfill the geometric conditions for scattering between terminals of the link. These fades can be deep, occasionally reaching down to the receiver noise level; i.e., a complete cancellation of the total received power by destructive interference between components of the received signal originating from different parts of the trail (Figure 9). The fading attributed to wind distortion of the trail differs from the amplitude oscillations seen on most of the waveforms near the point of maximum amplitude. These oscillations occur during the formation of the meteor trail, as the meteorite moves through the Fresnel zones of the scattering geometry (e.g., see Manning, 1959).

4.2 Returns from Overdense Meteor Trails

The returns from overdense trails are also characterized by a fast rising leading edge; however, the amplitude continues to increase after the trail is fully formed, and reaches a maximum before decaying exponentially. Examples of returns from overdense trails, which constitute approximately 5% of the returns observed, are shown in Figure 10. The maximum amplitudes are generally larger than those from underdense trails. The returns from overdense trails can have very long durations exceeding the receiver's present observation window of four seconds. The majority of the waveforms which last longer than one second can be classified as returns from overdense trails. There are, however, a number of returns from overdense trails for which the maximum amplitude is comparable to the average maximum amplitude for returns from underdense trails, and which last less than a second.

As the overdense trails generally tend to last longer, they are especially prone to wind distortion, as described previously. Some of the atypical returns from overdense trails are shown in Figure 11.

4.3 Returns from Tiny Meteor Trails

This classification has been established to account for the multitude of very small returns from meteor trails which have a duration of less than 0.1 sec and maximum signal to noise ratios of 10 to 12 dB (30 KHz receiver IF bandwidth). These returns do not exhibit the exponential decay associated with returns from underdense trails. Returns from tiny meteor trails account for 10-15 percent of the total population. Examples are shown in Figure 12.

Two possible physical processes are suggested to explain the shape of these waveforms. One explanation is that the returns are caused by meteor trails diffusing so rapidly that only the part of the trail closest to the burning head of the meteorite scatters the radio waves. This is described by McKinley (1961) and Eshlemann (1955) and termed "head echoes". According to this theory, the head echoes are observed predominantly at the higher frequencies. The shape of the return from a head echo is "bell like", which fits a large number of the waveforms in this category. Many of the tiny returns consist of more than one bell-like shape in succession. This leads to the second suggested explanation; that these waveforms originate from underdense trails whose maximum electron line densities are just large enough to produce a signal which exceeds the receiver's noise floor and a signal is only received for a short while immediately after the passage of the meteor through the principal Fresnel zone. Whichever explanation is valid cannot be determined by the present experiment. A verification would call for the use of simultaneous observations at different frequencies.

the use of different power levels, and the measurement of the Doppler shift produced by the trail.

4.4 Returns from Sporadic E Layers

This classsification is used to account for the occurrence of very strong signals (up to -75 dBm), which can last from a few minutes to more than 25 minutes. Examples of such signals, which are observed occasionally at Thule AB at 45 MHz and 65 MHz, are shown in Figure 13.

These signals do not originate from meteor trails, nor can they originate from the ionosphere's F-layer, as this does not reflect obliquely at VHF frequencies on a path as short as the Sondrestrom AB - Thule AB path. Sporadic E-layers are known to have electron densities large enough to permit oblique reflections at frequencies in the lower VHF spectrum. The main characteristics of the signals, apart from their long duration, are the large amplitudes, and the slow, deep, fades.

Considering the signal to noise ratio alone, which for sporadic E-layers can exceed 40 dB (in a 30 KHz bandwidth), a high signaling speed could be allowed as supported by the signal-to-noise ratio in the required bandwidth. In reality, however, the usable signaling speed is most likely limited by other propagation factors such as time decorrelation. This is presently being investigated under the RADC program.

4.5 Unidentified Scatter Returns

Occasionally, relatively weak but long lasting signals are received that are characterized by rapid fading as illustrated in Figure 14. These returns fit, superficially, the description of scattering from field aligned irregularities as described by Dyce (1955). However, such scattering as a mode of propagation is not plausible for irregularities at F-layer heights. Neither is it very likely for irregularities at E-layer heights, owing to the near vertical geomagnetic field and the positioning of the Sondrestrom AB - Thule AB path north of the auroral oval. Since the signals often precede sporadic E events, they may be reclassified as returns from weak sporadic E-layers after more detailed analysis.

5. DATA REDUCTION PROCEDURES

Data reduction procedures have been developed to calculate capacities and waiting times as a function of bit-error-rates for a number of hypothetical meteor scatter systems. The computations are based on the instantaneous signal-to-noise ratios in the bandwidth of the receiver. This has the advantage that the recorded waveforms can be used to evaluate numerous potential meteor scatter communication techniques, and the results are not limited to any specific modulation or signaling scheme. The use of a conventional message handling system would have given very precise information on the bit-error-rate and capacity for that particular system, but the limitations imposed by the propagation mechanism would not be separable from those imposed by the hardware of the system itself.

The procedure chosen for the data reduction uses the previously mentioned concept of a transfer function for the meteor scatter channel. The usefulness of the approach depends upon the accuracy and the detail with which the function can be measured. Presently, only the instantaneous signal-to-noise ratio in the channel is measured, and the noise is presumed to be of galactic origin with a Gaussian distribution. The only channel distortion accounted for is the antenna and receiver noise. This does not constitute a fully valid channel transfer function, but it has been reported by earlier workers (Grossi and Jahved, 1977; Sites, 1977; Weitzen et al, 1984), that the meteor scatter channel does not exhibit significant channel distortion due to time and frequency dispersion. This leads to the conclusion that, to a first approximation, the properties of the meteor scatter channel can be analyzed on the basis of measurements of the signal-to-noise ratio. It is important that this approximation be validated or modified, if necessary, with the results of actual measurements of differential Doppler spreads and multipath properties of the channel.

5.1 Calculation of Signaling Speed and Message Content

The performance of a digital modulation system, in terms of bit-error-rate (BER), can be expressed as a function of the ratio between signal power and noise power in the channel. Various measures can be used, but the most common is the carrier-to-noise ratio (C/N), expressed as the ratio of the unmodulated carrier power to the noise power in a bandwidth equal to the bit rate. Alternatively, the baseband equivalent (E_b/N_0), defined as the ratio between the average signal energy per bit and the noise power spectral density, can be used.

Using key numbers which link BER and signaling-speed performance specifications to the equivalent C/N or E_b/N_0 requirements (Oetting, 1979), every recorded return is analyzed to determine the maximum signaling speed it could have supported. Distributions of this quantity are calculated to evaluate the range of possible signaling speeds which could be supported by the meteor scatter mechanism. These distributions are important in that the signaling speed is a prime factor in choosing a communication processsor, especially if adaptive signaling schemes are contemplated. It should be kept in mind that the analysis approach described here determines maximum theoretical values, which may not be realized in practice due to synchronization requirements, allowable spectrum allocation and equipment limitations.

The capacity in bits for each individual return can be calculated from the instantaneous carrier-to-noise ratio, for the chosen modulation and signaling schemes. A set of

five commonly used digital modulations has been selected for evaluation: BPSK, QPSK, DPSK, MSK and FSK. Coherent detection is assumed for all the chosen modulations except for FSK. Non-coherent detection of FSK is a simple demodulation technique and is especially attractive for meteor scatter systems because of the relative ease of signal-acquisition. However, its performance relative to the C/N for the channel is not as good as the performance of other coherently detected phase modulation techniques.

The signaling schemes used in the analysis include adaptive signaling, for which the instantaneous signaling speed is chosen to match the instantaneous C/N in the channel; and fixed signaling speeds of 5, 10, and 15 kbits/s. A BER performance of 10^{-4} is assumed in all cases. The use of a fixed signaling rate is not a very efficient mode of communication, as the inherent capacity of a meteor return will not be fully utilized during the periods when the received C/N exceeds that minimumly required for the specified modulation technique and signaling speed. Nevertheless, a fixed signaling speed system might be preferred for many applications, based simply on hardware and cost considerations. Thus, a goal of the data analysis is to investigate the capacity of potential meteor scatter systems for a number of assumed fixed signaling speeds, and to determine an optimum signaling rate, if one exists.

5.2 Data Presentation

A package of computer programs has been developed to perform the calculations of the capacity, the signaling speeds, and the waiting times for fixed length messages from the returns received at Thule AB. The programs generate distributions of the calculated quantities and present them in a series of graphs and tables. Some of these are described below.

6. SAMPLE OF RESULTS FOR FEBRUARY 1985

In this section examples are given to illustrate some of the propagation and communication parameters that can be derived from analysis of the returns received at Thule AB. The results are confined to February 1985, a period with no significant ionospheric disturbances.

Figure 15 presents cumulative distributions of results for the time block between 1000-1200 UT, as obtained from the 45, 65, and 104 MHz returns. Included are return durations, intervals between returns, maximum antenna voltages across 50 ohms, the maximum signaling speeds and the capacities in bits for the returns when using BPSK modulation with adaptive and fixed signaling rates. The figure indicates that for this particular period the return durations and the maximum antenna voltages decreased slightly with increasing frequency while the intervals between returns increased sharply as the frequency increased. It was particularly surprising to find that, for this limited sample, the maximum signaling speed increased with frequency. This was due to an increase in the signal-to-noise ratio with frequency which resulted when the galactic noise power decreased with frequency to the -2.3 power, as expected, while the maximum signal power decreased with frequency to only the -1.7 power, rather than the -3 power expected from simple scattering theory.

Figure 15 also shows that very few returns will support signaling rates exceeding 1 Mbit/s. It is known from earlier experiments (Grossi and Jahved, op. cit.; Sites, op. cit.; Weitzen, et al, op. cit.) that the available bandwidth for the meteor scatter channels exceeds 1-2 MHz, and thus this observation to a certain extent validates the use of a gaussian noise limited channel model for the present computations. Measurements of the time dispersion of the returns are still needed for an absolute validation of this channel model.

The communication capacity of the individual returns decreased as the frequency increased due primarily to the reduced return duration. However, the decrease does not exceed a factor of 1:2 over the 45 MHz to 104 MHz frequency range. It must be concluded, therefore, that the single most important cause of the decrease in the overall communication capacity with increasing frequency is the increase in the interval between returns.

Figure 16 shows the mean diurnal variations for February 1985 of the following basic parameters: return duration, maximum antenna voltage and interval between returns. The diurnal variation in the interval between returns is seen to be approximately 1:2, which is less than that observed at lower latitudes (1:4-5 at northern mid latitudes).

The diurnal variation in the means of the maximum signaling rate and the return capacity for BPSK modulation is presented in Figure 17 for the three operating frequencies of 45, 65 and 104 MHz. The return capacity is shown as a function of the four basic signaling schemes: adaptive signaling, and fixed speed signaling at 5, 10 and 15 kbits/s. This figure shows that the trend indicated in Figure 15 continued throughout the day with the maximum signaling rates at 104 MHz consistently exceeding that at 45 and 65 MHz.

Distributions of the waiting times for the transfer of fixed length messages have been calculated for BPSK modulation. Again the four basic signaling schemes are assumed. The message lengths chosen are 50, 100, 200 and 400 8 bit characters. Message piecing has been used for the calculations. Thus if a message is too long to be transferred on a single meteor burst, the waiting time is calculated as the time elapsed from the start of the message transfer until the whole message has been received after having been transferred in pieces in a number of succeeding bursts.

Figure 18 presents the distribution of waiting times at 45 MHz for the time block 1000-

1200 UT. The curves coincide for short messages, indicating that the four basic signaling schemes perform equally well. For the longer messages of 200 to 400 characters a difference in performance is noted. Adaptive signaling produces the shortest waiting times, while no significant variation is seen for the different fixed speeds. This trend is also observed at 65 and 104 MHz.

The diurnal variations in the mean of the waiting times at 45, 65 and 104 MHz for BPSK modulation and adaptive and 5 Kbits/s fixed signaling rates are given in Figure 19. This figure shows that the advantage of adaptive signaling for longer messages becomes even more significant when the operating frequency is increased from 45 MHz to 104 MHz.

Table 1 provides a statistical summary of some of the 45 MHz results. Of special note are the data indicating the relative contributions of the overdense trails to the overall performance of the link. Even though only about 5% of the returns were from overdense trails, those returns provided 60% of the computed capacity when ideal adaptive signaling was assumed. The contributions of the overdense trails were less, but still very significant, when fixed signaling rates were assumed. The average throughput ranges from 1200 bits/s for adaptive BPSK signaling to 51 bits/s for FSK fixed signaling at 5 kbits/s.

The relative performance of each modulation and signaling technique is given with respect to the FSK, 5 kbit/s mean capacity per return.

	ADAPTIVE SIGNALING		FIXED SIGNALING RATES (kbits/s) BPSK			FSK		
	BPSK	FSK	5	10	15	5	10	15
CAPACITY (kbits)								
ALL RETURNS	2910000	1800000	230000	219000	241000	124000	146000	168000
OVERDENSE RETURNS	1720000	1110000	72400	92800	110000	50300	68500	84820
%-OVERDENSE RETURNS	59.0	61.3	31.5	42.2	45.7	40.5	46.7	50.3
MEAN CAPACITY/RETURN (kbits)	50	45	3.9	3.8	4.2	2.1	2.5	2.9
REL. PERFORMANCE	23.4	14.5	1.8	1.7	1.9	1.0	1.1	1.3
MEAN THROUGHPUT (bits/s)	1200	746	95	91	100	51	61	70

Table 1. Summary of statistics for 45 MHz during February 1985 assuming BPSK and FSK modulation and adaptive and fixed signaling schemes.

Table 2 shows the corresponding results at 65 MHz. Comparison with Table 1 indicates that the calculated capacity of the meteor scatter link at 65 MHz was considerably less than at 45 MHz, as expected. In this case the overdense trails accounted for less than 3% of the returns, yet they contributed over 70% of the capacity calculated for adaptive data rate signaling. At 65 MHz the average throughput ranges from 374 bits/s for adaptive BPSK signaling to 14 bits/s for FSK fixed rate signaling at 5 kbits/s.

	ADAPTIVE SIGNALING		FIXED SIGNALING RATES (kbits/s) BPSK			FSK		
	BPSK	FSK	5	10	15	5	10	15
CAPACITY (kbits)								
ALL RETURNS	905000	594000	51900	60900	65100	33800	39500	46400
OVERDENSE RETURNS	648000	447000	18300	26700	32800	14100	20500	25700
%-OVERDENSE RETURN	71.6	75.1	35.3	43.7	50.4	41.7	51.8	55.3
MEAN CAPACITY/RETURN (kbits)	49	32	2.8	3.3	3.6	1.8	2.2	2.5
REL. PERFORMANCE	26.7	17.5	1.5	1.8	1.9	1.0	1.1	1.3
MEAN THROUGHPUT (bits/s)	374	224	22	25	27	14	16	19

Table 2. Summary of statistics at 65 MHz during February 1985 assuming BPSK and FSK modulation and adaptive and fixed signaling schemes.

Table 3 shows results at 104 MHz. Again the calculated capacity of the meteor scatter link at 104 MHz was considerably less than at 45 and 65 MHz. In this case the overdense trails accounted for less than 3% of the returns yet they contributed nearly 70% of the capacity calculated for adaptive data rate signaling. At 104 MHz the average throughput ranges from 118 bits/s for adaptive BPSK signaling to 3.4 bits/s for FSK fixed rate signaling at 5 kbits/s.

	ADAPTIVE SIGNALING		FIXED SIGNALING RATES (kbits/s) BPSK			FSK		
CAPACITY (kbits/s)	BPSK	FSK	5	10	15	5	10	15
ALL RETURNS	286000	187000	13300	15300	18000	8320	10800	12400
OVERDENSE RETURNS	192000	133000	3590	5390	7090	2840	4480	5860
%-OVERDENSE RETURN	67.0	70.9	26.9	35.2	39.4	34.1	41.4	47.4
MEAN CAPACITY/RETURN (kbits)	46	30	2.1	2.4	2.9	1.3	1.7	2.0
REL. PERFORMANCE	34.3	22.4	1.5	1.8	2.1	1.0	1.2	1.4
MEAN THROUGHPUT (bits/s)	118	77	5.5	6.3	7.4	3.4	4.5	5.1

Table 3. Summary of statistics at 104 MHz during February 1985 for BPSK and FSK modulation and adaptive and fixed signaling schemes.

7. SUMMARY

The RADC meteor scatter link in northern Greenland has been established to investigate the potential performance of meteor scatter communications in the polar region, under a

variety of normal and disturbed ionospheric conditions. The link is designed to obtain the data required to characterize a number of important propagation factors, including: the diurnal and seasonal variations in the availability of usable meteor trails at high latitudes, the effects of sporadic E and other (non-meteor) scatter mechanisms, and the absorption associated with solar energetic particle events (PCAs). A primary goal of the research is to investigate and quantify how these factors vary with frequency over the 45-104 MHz band. In addition, emphasis is given to providing data that can be used to project the performance of potential meteor scatter systems, which may employ both adaptive and fixed signaling rates as well as a number of different modulations.

To a first approximation, the experimental technique and data reduction provide information to describe the meteor scatter channel as a transfer function, in both time and frequency. This requires that the time history of every return be recorded in detail. In doing this, each return also is classified in terms of its origin; i.e., whether it is from a meteor trail (underdense, overdense, or tiny), from a sporadic E-layer, or from some other source of VHF scatter. Such classification is important for the assessment of the relative contributions of each of these scattering mechanisms to the overall performance of potential VHF scatter systems.

An extensive software package has been developed to reduce the large volume of propagation data being acquired on the link. The data reduction and analysis provide statistical distributions of a number of important communication parameters, including the duration of the returns, the time interval between returns, the communication capacity for each return, the waiting times required to pass messages with fixed lengths and the average throughput. These are determined for fixed and adaptive signaling rates, and for commonly used digital modulations; coherent BPSK, QPSK, DPSK and MSK and non-coherent FSK.

Practical experience with the meteor scatter link has confirmed that it is very important (and often difficult) to suppress man-made noise, to insure that the receiving system is limited only by the background galactic noise. Also, theoretical calculations (and some specific measurements at Thule AB) showed that the patterns of the transmitting and receiving antennas depend greatly on the local terrains and the mounting heights. It was found that the throughput over the link was increased when the antennas were remounted at heights which produced patterns providing a uniform illumination of the common scattering volume.

A preliminary investigation of the returns observed during February 1985 revealed that the mean interval between returns was proportional to the frequency squared and varied by a factor of about two throughout the day regardless of frequency. The data also showed that the diurnal variations in the mean duration and maximum amplitude of the returns were about 2:1.

Preliminary calculations, using only a small portion of the data, already provide indications of the potential performance of candidate meteor scatter systems using fixed or adaptive signaling rates and a number of modulation formats. For example, when the fixed signaling rate was increased by a factor of three, from 5 kbits/s to 15 kbits/s, the increase in the throughput of the link was always less than 30% at 45 and 65 MHz regardless of the chosen modulation scheme. In contrast, when ideal adaptive signaling techniques were used, the throughputs increased by about a factor of 12 for the same modulation.

Using the peak amplitude of each return, calculations were made to determine the maximum signaling speed that could be supported. Although it had been expected that the maximum signaling rate would decrease as the frequency increased, the data indicated the opposite with 104 MHz supporting the highest peak rate throughout the day. At 45 MHz it was found that the means of the maximum signaling speed varied between 25 and 35 kbits/s for BPSK modulation while 104 MHz supported speeds between 50 and 120 kbits/s. Based on the received signal-to-noise ratio, about 15% of the returns had peak amplitudes that could support (theoretically) signaling speeds in excess of 100 kbits/s.

The February data show that although only about 5% of the returns were from overdense trails, those returns provided at least 60% of the computed throughput when adaptive signaling was assumed. This result was independent of the chosen modulation technique or frequency of operation. These results indicate that theoretical models that are to be used to predict the performance of meteor scatter systems should include the contributions from overdense trails.

Some statistics for the waiting times to transfer messages of 50, 100, 200, and 400 8 bit characters were also computed. In doing this, message piecing was assumed. For 50 and 100 character messages it was found that the waiting times were almost independent of the signaling rates and modulation scheme that were chosen. Rather, the waiting times were dictated by the time intervals between the meteor scatter returns. For the 200 and 400 character message lengths, however, it was found that the waiting times were decreased significantly when adaptive signaling was assumed, particularly at the higher operating frequencies. This is in accordance with the increase in throughput from each return that is achieved when adaptive signaling rates are used.

Average throughput values for the month of February were calculated as a function of signaling technique (adaptive or fixed data rates), modulation and frequency. These values covered a wide range from 1200 bits/s for adaptive BPSK signaling at 45 MHz to 3.4 bits/s for fixed FSK signaling at 104 MHz.

At present the data provide estimates on the potential performance of VHF meteor scatter systems that are somewhat idealized, in that the results are derived only from signal-tonoise measurements, and do not include limitations that may be due to time and frequency dispersion in the channel. It is expected that this distortion is small. Experiments are currently underway at RADC to validate this assumption.

The primary purpose of this paper has been to describe the RADC meteor scatter link and to illustrate some of the propagation and communication parameters that it can provide. As such, only a very small sample of the data that are being obtained has been included here. Future papers will emphasize that data, its analysis and interpretation, and its use in assessing the potential performance of candidate meteor scatter systems.

REFERENCES

1. Brown, D.W., and H.P. Williams, The Performance of Meteor Burst Communications at Different Frequencies, AGARD Symposium of Aspects of EM Wave Scattering in Radio Communications, AGARD CP-244, 3-7 October 1977.

2. Crysdale, J.H., Analysis of the performance of the Edmonton-Yellowknife JANET circuit, IRE Trans., Com., March 1960.

3. Dyce, R., VHF auroral and sporadic E propagation from Cedar Rapids, Iowa, to Ithaca, New York, IRE Trans., PGAP, April 1955.

4. Eshleman, V.R., Meteors and Radio Propagation, Part A. Meteor Ionization Trails: Their Formation and Radio Echoing Properties, Stanford Univ., RPL Technical Report No. 44, February 1955.

5. Forsyth, P.A., E.L. Vogan, D.R. Hansen, and C.O. Hines, The principles of JANET, a meteor burst communication system, Proc. IRE., December 1957.

6. Grossi, M.D. and A. Jahved, Time and Frequency Spread in Meteor Burst Propagation Paths, AGARD 23rd. EWPP Symposium, 3-7 Oct. 1977.

7. Kossey, P.A., J.P. Turtle, R.P. Pagliarulo, W.I. Klemetti, and J.E. Rasmussen, VLF reflection properties of the normal and disturbed polar ionosphere in northern Greenland, Radio Sci. Vol. 18, No. 6, p. 907-916, Nov-Dec 1983.

8. Manning, L.A., and V.R. Eshleman, Meteors in the ionosphere, Proc. IRE, February 1959.

9. McKinley, D.W.R., Meteor Science and Engineering, McGraw-Hill, 1961.

10. Oetting, J.D., A comparison of modulation techniques for digital radio. IEEE Trans., Com-27., No. 12, December 1979.

11. Reagan, J.B., R.E. Meyerott and R.C. Gunton, Modeling of the Ambient and Disturbed Ionospheric Media Pertinent to ELF/VLF Propagation, Proceedings of the AGARD Symposium on Medium, Long, and Very Long Wave Propagation, AGARD-CP-305, Feb. 1982.

12. Santeford, H.S., Meteor Burst Telemetry Winter Test Program - Test Report, Boeing erospace Company Document No. D182-10423-1.

13. Sites, F.J., Communication Via Meteor Trails, AGARD, 23rd. EWPP Symposium, 3-7 Oct. 1977.

14. Weitzen, J.A., W.P. Birkemeier, and M.D. Grossi, An Estimate of the Capacity of the Meteor Burst Channel, IEEE Trans. on Communications, Vol. Com-32, No. 8, August 1984.

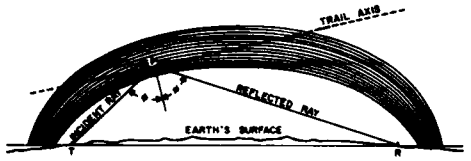


Fig. 1. Geometry of specular scattering from a meteor trail (Oetting, 1980).

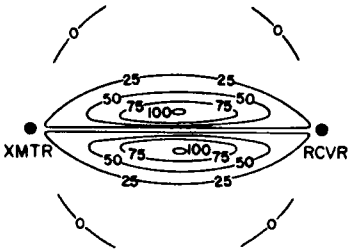
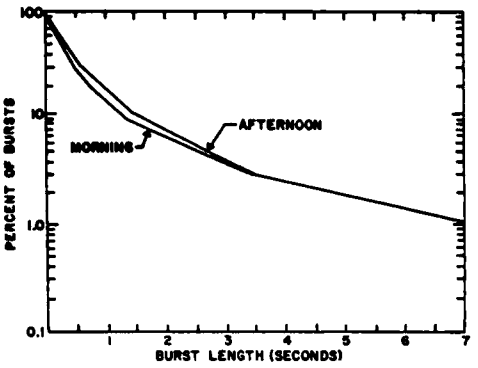
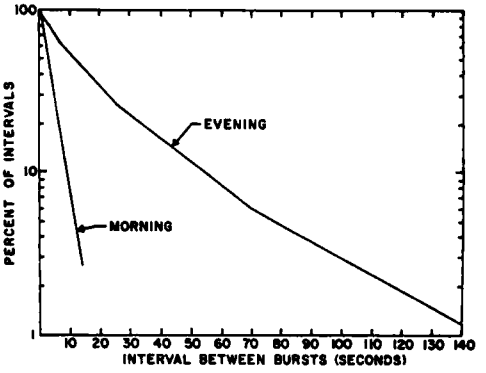


Fig. 2. Relative signal contributions from various parts of the meteor region computed for a 1000 km path (Ince, 1980)



(a)



(b)

Fig. 3. Mid latitude statistics for 40 MHz meteor trail returns. (a) Probability distribution of return length. (b) Probability distribution of return intervals. (Brown and Williams, 1977)

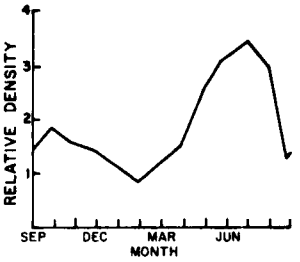


Fig. 4. Variation in the space density of meteors along the earth's orbit (Oetting, 1980).

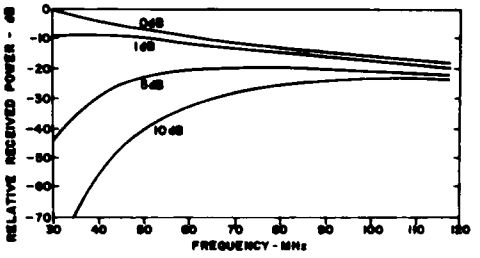
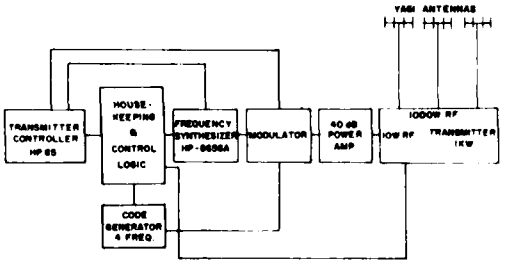
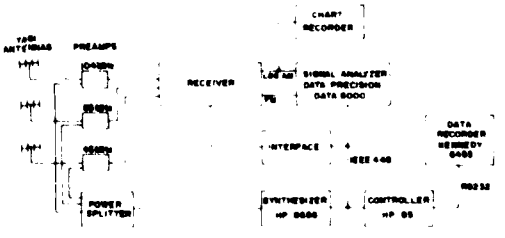


Fig. 5. Predicted relative peak power versus frequency for a 1000 km meteor scatter link in the presence of absorption. Four conditions of the ionosphere are illustrated in terms of 30 MHz vertical incidence riometer absorption (Crysdale, 1960)

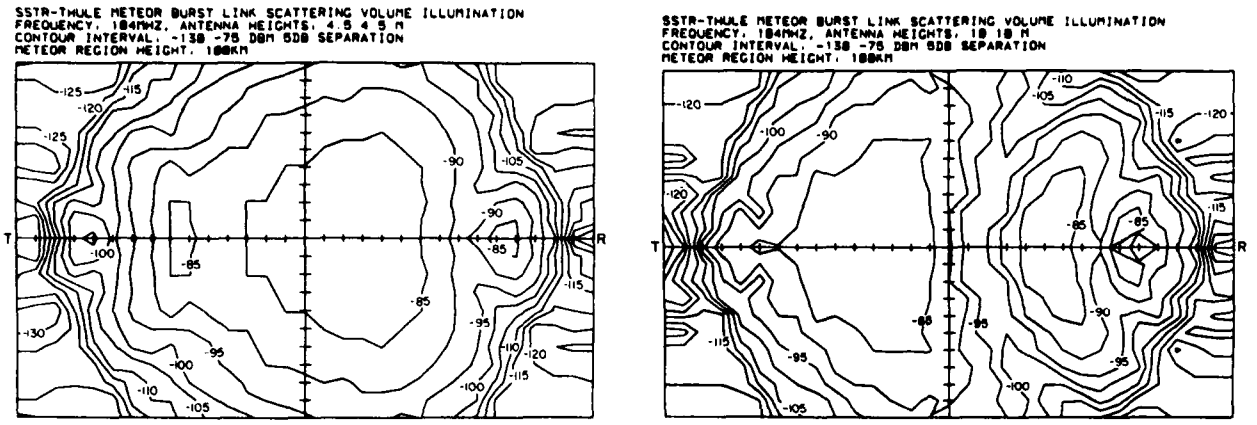


(a)



(b)

Fig. 6. Block diagrams of high latitude test-bed instrumentation. (a) Transmitter at Sondrestrom Air Base and (b) Receiver at Thule Air Base.



(a) (b)

Fig. 7. Calculated illumination of the common scattering volume at 100 km for 104 MHz on the Sondrestom AB - Thule AB path. (a) The antennas are mounted 1.5 λ or 4.5 m above the ground. (b) The antennas are mounted 3.3 λ or 10 m above the ground.

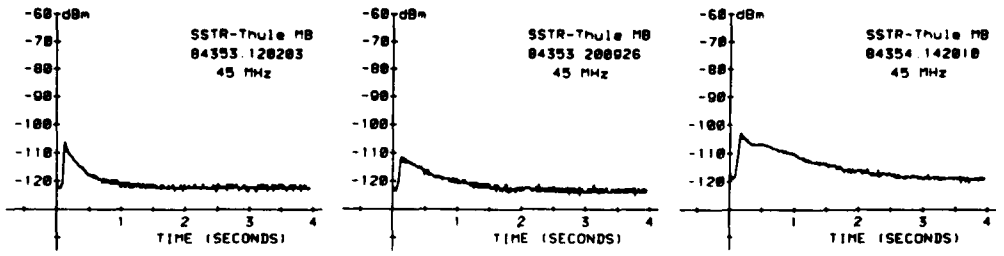


Fig. 8. Examples of returns from underdense meteor trails

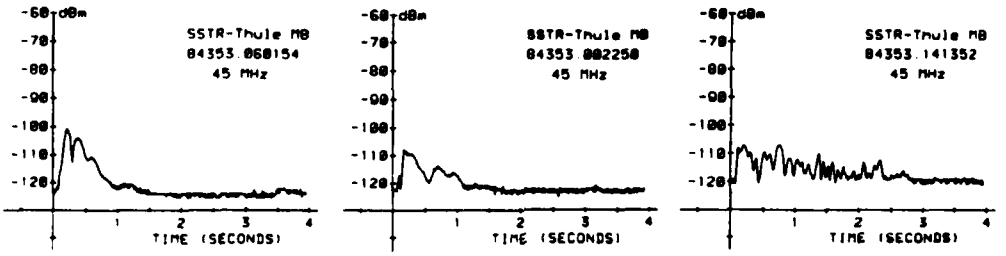


Fig. 9. Examples of returns from underdense trails with severe "wind distortion".

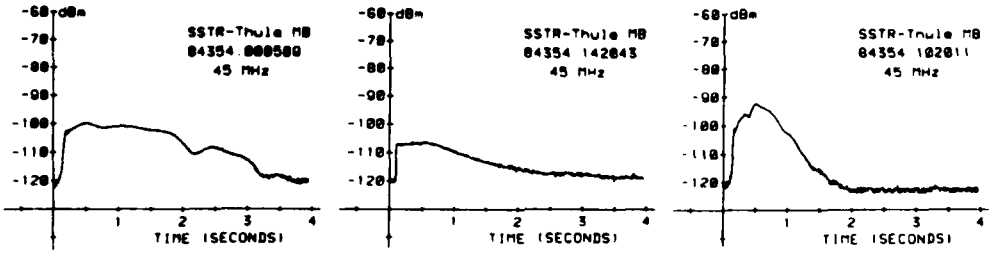


Fig. 10. Examples of returns from overdense meteor trails.

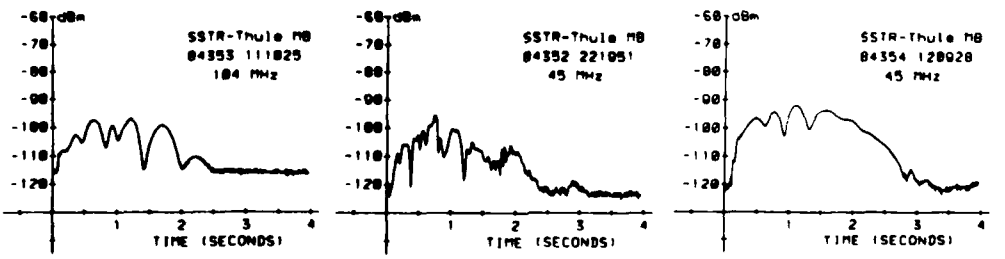


Fig. 11. Examples of returns from atypical overdense meteor trails.

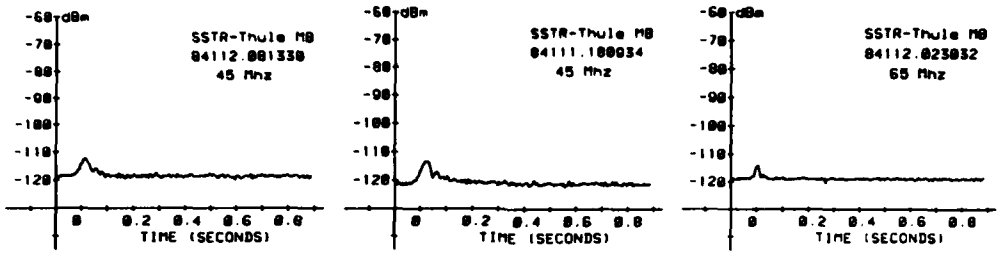


Fig. 12. Examples of returns from "Tiny" meteor trails.

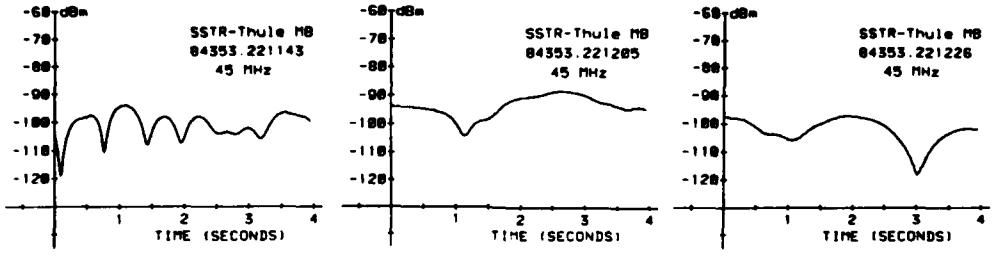


Fig. 13. Examples of signals reflected from sporadic E-layers.

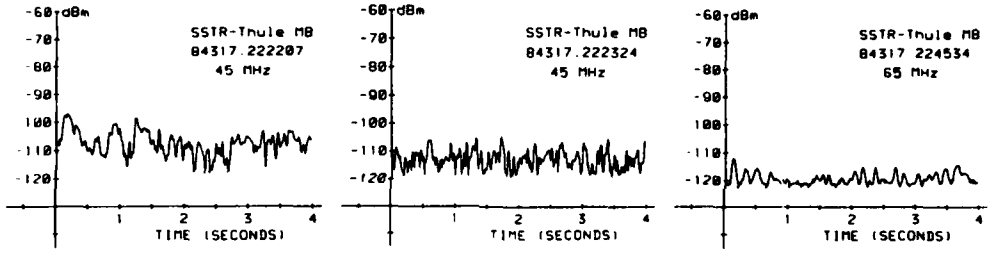


Fig. 14. Examples of a series of waveforms classified as unidentified scatter.

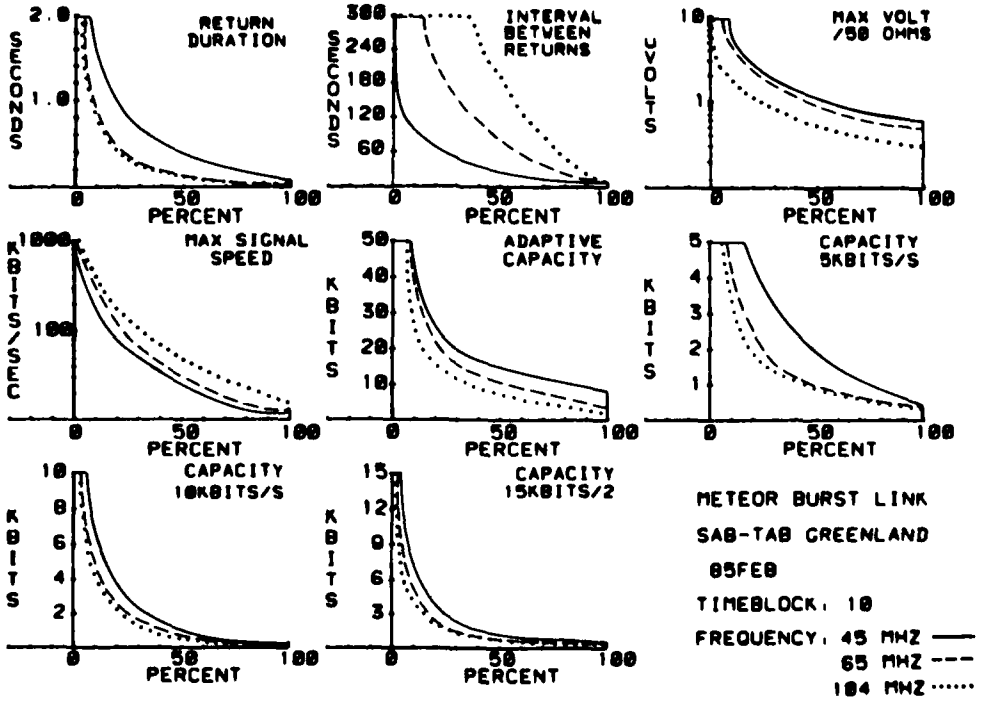


Fig. 15. Cumulative distributions of return duration, interval between returns, maximum antenna voltage across 50 ohms, maximum signaling speed and the capacity in bits for adaptive and fixed signaling rates. The distributions are for the time block from 1000-1200 UT in February 1985 and the capacity calculations are for BPSK modulation.

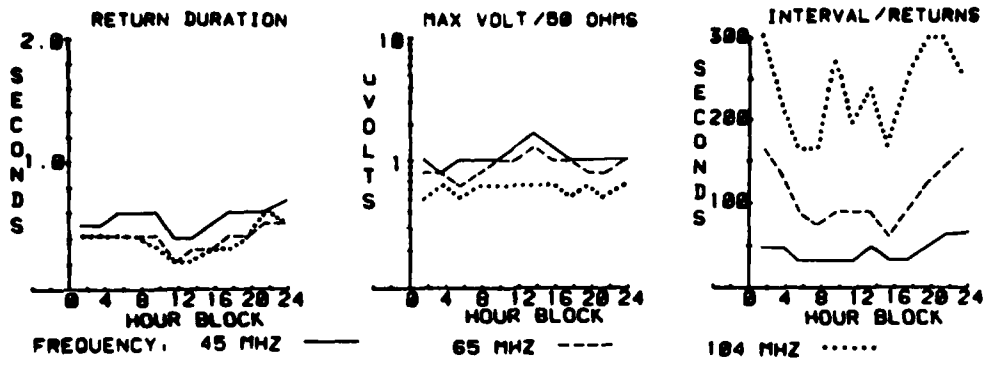


Fig. 16. Mean diurnal variation of return duration, maximum antenna voltage and interval between returns for February 1985.

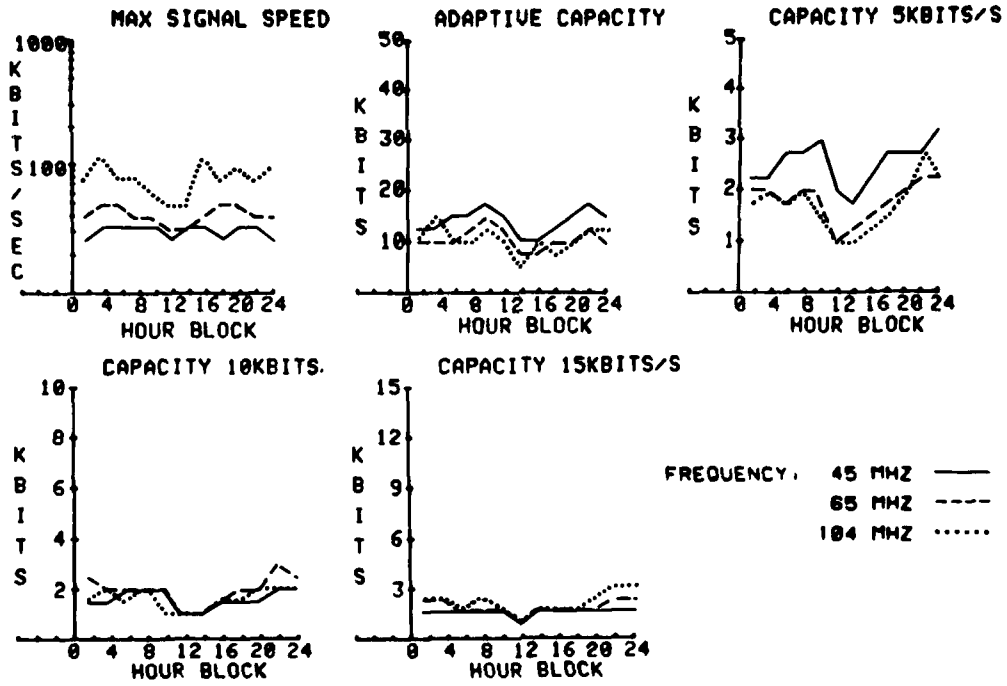


Fig. 17. Diurnal variation in the mean of the maximum signaling rates and return capacities at 45, 65 and 104 MHz during February 1985. BPSK modulation is assumed. The capacities are calculated for adaptive and fixed (5, 10 and 15 kbits/s) signaling schemes.

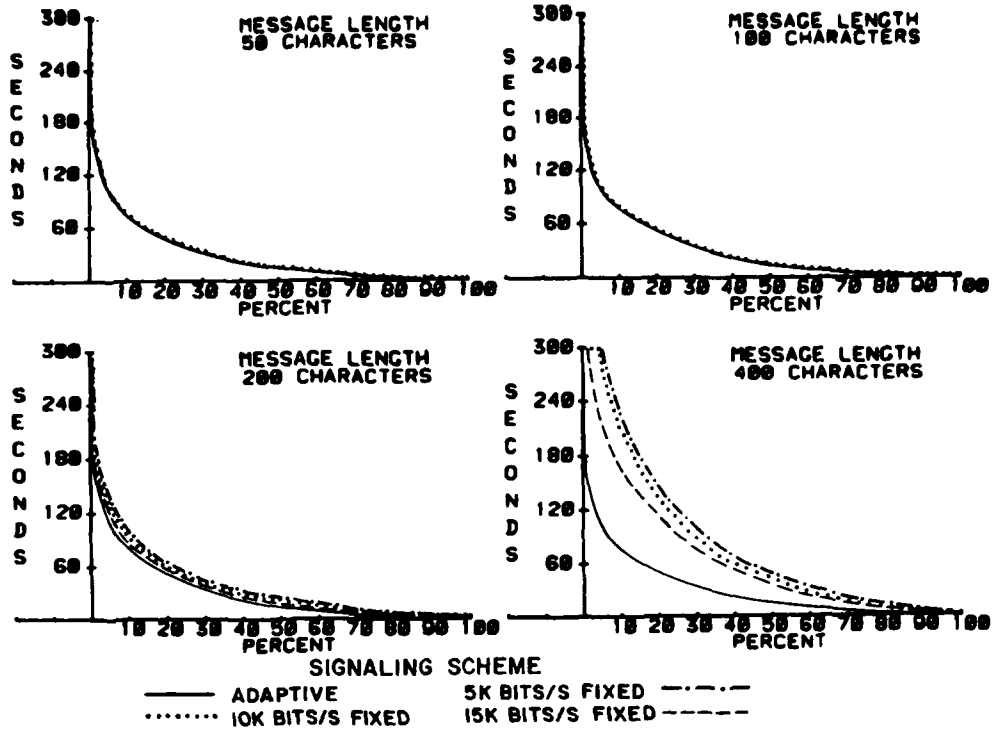


Fig. 18. Cumulative distributions of waiting times at 45 MHz for the 1000-1200 UT time block in February 1985. The calculations are for message lengths of 50, 100, 200 and 400 8 bit characters. The distributions are calculated for BPSK modulation and adaptive and fixed (5, 10, and 15 kbits/s) signaling schemes.

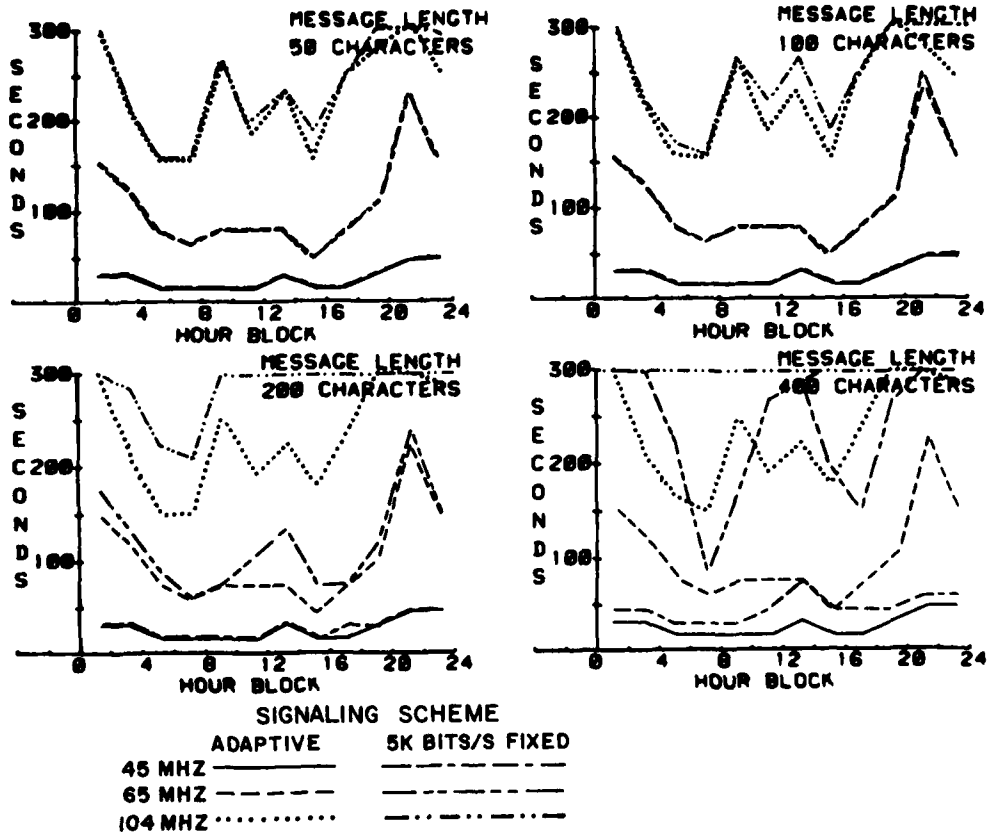


Fig. 19. Diurnal variation in the mean of the waiting times at 45, 65, and 104 MHz for February 1985. The values for adaptive and 5 kbits/s fixed rate signaling with BPSK modulation are presented.

DISCUSSION

N.C.Gerson, US

Would you agree on the basis of your present studies, that the old characterization of meteor scatter still holds; i.e., a meteor scatter system provides a highly reliable low data rate system?

Author's Reply

Due to recent advances in microprocessor technology, meteor scatter communication is being reevaluated. This evaluation is still in its initial stages, and final conclusions on the applicability cannot yet be drawn. However, the results so far obtained with the RADC high latitude testbed indicate that meteor scatter communication does indeed have an unexplored potential which, when utilized, could considerably enhance the capacity of meteor scatter communication systems relative to the systems in use today or the systems investigated in the past.

P.S.Cannon, UK

Does your calculated adaptive data rate and improvement take into account the practical implementation of such a system which must necessarily reduce any such advantage over a fixed rate system?

Author's Reply

The calculated adaptive capacities represent theoretical maxima for the selected frequencies. They do not include overload, as needed for synchronization of coherent detectors, or degradations due to a finite number of signalling rates in an actual system. These overload factors need to be included if the performance of a proposed hardware scheme is to be assessed using the data collected with the RADC meteor scatter tested. They have not been included in the present data analysis, as they will be very dependent on the proposed hardware configuration, and it has been our aim to isolate the propagation induced limitations on high latitude meteor scatter systems.

J.S.Belrose, CA

Just a small comment on one of your slides. The frequency dependence of SPE associated absorption probably depends on the degree of absorption, since the more intense the event the greater will be the absorption at low heights where collision frequency is high. Recall that absorption becomes independent of frequency when absorption occurs in a region where the collision frequency exceeds the wave frequency.

Author's Reply

The computation only includes the f^2 relationship. It is true that collision freqencies in the order of 10^8 collisions/sec., which can occur at app. 50 km altitude will tend to make the absorption frequency independent during PCA'S. However this will not change the fact that a 30-40 MHz meteor scatter system will suffer excessive absorption during such an event, be it 60 or 100 dB extra attenuation induced by the PCA.

ROUND TABLE DISCUSSION

Panel Members

R.D.Hunsucker, Chairman
P.Bauer
R.A.Greenwald
A.S.Rodger
G.Rose
E.Thrane

On the morning of the final day of the AGARD Conference on "Propagation Effects on Military Systems in the High Latitude Region" a panel discussion was held. Each of the panel members gave a short presentation, followed by comments from the floor. A questionnaire consisting of the following four questions was circulated by the Chairman of the Round Table Discussion the previous afternoon and conference participants were asked to consider the questions before attending the discussion.

ROUND TABLE DISCUSSION TOPICS

(1) In the context of the subject of this symposium (Propagation Effects on Military Systems in the High Latitude Region), what is the state of our understanding at this time?

(2) What answers has this symposium provided?

(3) What directions for future research?

(4) What operational needs require this understanding?

The Chairman was responsible for the selection and editing of the statements and bears the sole responsibility for the omission of points which the speaker may have considered to be important.

ROUND TABLE PANEL MEMBERS' COMMENTS

R.A.Greenwald

I'll present this a bit more generally than just referring to the sessions. This is my view of the situation as it exists. The users have their "feet on the ground" — they are concerned about systems and how they work, whereas the ionospheric physicist tends to be "up in the clouds" and we are interested in things like "how beautiful the aurora is". The question is whether the ionospheric physicists can help the users. Some of the users probably wonder after being here for a week. My opinion is that they *can* — I feel that they can in the following areas: first of all, most high latitude systems are ultimately based on engineering models of the ionosphere. The engineers who design these systems, I think — by and large — do not really understand and aren't particularly interested in the physics of the ionosphere. Now at high latitudes, in particular, ionospheric disturbance models have to be included. I think, in general, to this data these models tend to be more statistical in nature in terms of reliability and very often they are based on experience. We have heard many times in the past 20 or 30 years at these meetings how bad the ionosphere can be. This experience has been incorporated into the models in an 'ad hoc' fashion. Often these models contain no physics — just a statistical result — there is no detailed concern about physical processes in terms of *why* the disturbances occur. Even today there is little understanding of the physical processes that cause the disturbances. You must have understanding to get the physics and then you can improve the model. I'm going to go back to ionospheric physics now, and one thing that may not be appreciated is that advancements in science proceed slowly — it's *not* something you can do overnight — you can't give a six month engineering contract to a scientist and say "come up with an answer on the system"; it just doesn't go that way. It takes *time* to do research, it takes even *more* time to do good research. In the last twenty years there have been many advances in the understanding of the disturbed ionosphere.

I think that the situation today in terms of the processes involved — even propagation to some extent, has improved in the past twenty years, and I think that in that whole time it must be recognized that the effort and funds put into it have been at a modest level. There is not a lot of money that goes into research, in comparison to the amount of money that goes into military systems. Now, the question is, "can the users hasten the development of knowledge, if they want to get new systems on line quicker and be sure of their reliability"? I think they can. How? The first point is to communicate the problems, and I don't think there is enough communication of problems that systems have to the ionospheric physicists. If you do have a problem with a system you are not going to be talking about it at an unclassified meeting like

this. A physicist often has to know about things in detail rather than things in generality. Another thing that the users can do is to encourage the support for research, particularly for long-term research. The justification for supporting this research is to get improved engineering models. Finally, one has to have a better understanding of the failure mode of systems. You don't want to know on a *statistical* basis, you want to know the *physics* of why it is failing. One way to do this is to actually encourage the development of research instrumentation. There is a very important difference between research instrumentation and user instrumentation. User instrumentation typically is developed and engineered for the eventual goal for which it is going to be used. It may have problems which nature is throwing at it and the way in which it is built may cause it not to be able to attack these problems. *Research* instrumentation which is directed toward understanding what nature is throwing at you is designed to attack the problems, and so it can at times provide the answer to a problem that a military radar has. One case in point is high latitude OTH systems. This work has been done for probably more than twenty years and all of the measurements made at high latitudes by test systems have shown that there are problems with "clutter". We still don't understand the spectral bandwidth of the clutter. In fact, often the backscattered signals tend to be so broad they cause the overall system noise level to increase. I think that we still have problems with propagation modes on radar systems. We saw some examples of that during the week. What is our current engineering model for high latitude OTH systems? Very simple — "don't look north"! As a research instrument we have the Goose Bay radar that I talked about earlier in the week. It could provide answers on the spectral character of the clutter, and answers on the propagation modes perhaps better than some of the high latitude systems that have been used in the past. It may provide information on the vertical extent of the clutter.The vertical extent of the clutter which affects the OTH radar may be relatively small, and this is important to know. It could eventually be incorporated into improving engineering models.

The summary of my point is that people who are users should give a bit more attention to what is being done in the non-user (research) community and see how the results and equipment that are used there might be supported and might lead to improved understanding of their problems.

P.Bauer

I was asked to say a few words about incoherent scatter in this picture, but before I do I would like to raise a question which was one of the comments of Ray Greenwald which was that there was "too much geophysics". Maybe we can turn the question around — "is there too much statistics"? I think we could agree that the problem is that we need good physical characterization of the propagation channel. We can think of an example — look how complex the magnetospheric processes are.

The other day we saw the aurora and it looked desperate to try to describe this phenomenon and when you think about it you realize that people like Dr Akasofu with very simple inputs (magnetic field measurements and solar wind intensity) are able to give a fairly good description of the whole magnetosphere. Therefore, it depends from where you take the problem, and if you can recall something which happened in the past — for a long time statistics people were arguing about whether the auroral oval was a circle or whether it was closed or open, and the right answer came when we had the right view of it — the DMSP satellite. We need statistics to get some ground but we need also the physical approach, and the two are not opposed but are complementary. So in such a picture, what can an incoherent scatter system do?

If you consider incoherent scatter radars, they are such expensive devices that we can only have a few of them, but are we really far from having a network? I think the answer is much more optimistic, particularly if you consider that in addition to this system, you have other huge systems like HF radars. The present location of the HF radars and incoherent scatter radars give very good coverage of the polar and auroral regions. You have to add to that systems like SABRE, STARE, and the Goose Bay HF radar — so that you have excellent coverage of irregularities and motion in this part of the world. I think that incoherent scatter radars included in the network of other instruments can certainly provide the basic parameters which are needed. However this is the good side. The weaknesses of incoherent scatter are that the systems can only operate for part of the time, they cannot be operated continuously. Right now they operate roughly one-third of the time. They need huge amounts of money and huge amounts of data processing so that is one drawback for incoherent scatter. The other point is that we need to motivate the incoherent scatter community to the problems of interest for you today. Some of the people in this community are already much motivated, but the connection is, generally speaking, very small. Certainly on both sides effort has to be made. This brings up another point, I think the incoherent scatter radar community is doing something good in this direction. In order to be useful to the user community the data has to be available in an easy way. There is a considerable effort under the leadership of Dr Richmond in Boulder to put all the incoherent scatter data in a common data base.

G.Rose

I would like to draw your attention again to the ionospheric modification experiment which is performed by transmitting very intense high frequency waves upwards into the ionosphere. It is a powerful tool to explore the ionospheric plasma and its reactions on the wave energy input. Depending on the transmitting frequency relative to the ionospheric plasma density profile and on the transmitted wave polarization, part of the wave energy can be deposited at any height from the D- up to the maximum of the F-region. In the D-region, ohmic heating is the ionospheric reaction to the intense radio wave input. As a consequence, electron temperatures and electron collision frequencies rise. As a result absorption increases for radio waves passing through the heated D-region. In the D and E region if overhead intense electrojet current is flowing, periodic heating with frequencies up to about 10 KHz will modulate the electrojet current then radiate these low frequency radio emissions like a huge VLF antenna to great distances. At larger, especially at F-layer height O-mode heating is effective. In the vicinity of the reflection level of the high powered heating wave it is the parametric decay instability which causes the decay of part of the electromagnetic heating wave into highly absorbing electrostatic electron plasma waves and ion-acoustic waves. At the same time, field-aligned plasma striations

of scale sizes between a metre and several kilometres are created after some time. Whereas the heating wave and waves of neighbouring frequencies transmitted vertically upwards suffer from anomalous absorption under these conditions, striations can, on the other hand, open new propagation paths. Because the striations generally have irregular spatial structure the radio wave can be scattered from the heated volume, provided that the criterion that the scatterers have a spacing equal to half the radio wavelength is satisfied. For maximum scatter intensity, the incident ray must be orthogonal to the field direction. The intensity decreases by some 6 dB per degree of off-orthogonality. Scatter from the heater-induced-striations have been reported from a wide range of frequencies ranging from ~3 to several hundred megahertz. As may be seen, suitable ionospheric modification experiments can rather straightforwardly be applied to practical applications if wanted.

E.Thrane

I happen to be in charge of the frequency prediction service in Norway and it is in this capacity that I will say a few words now. We are currently using the IONCAP prediction program for our standard frequency predictions. We have a fairly wide range of customers. The operators up north, (civilian and military), the broadcasting corporation for planning of their broadcasts to distant areas and to the north, and occasionally we have system planners who ask for our advice. Now, it is quite obvious that what we are giving these people, as far as the high latitude is concerned, is not very good. We know that! It is somewhat surprising that they really use these predictions. Why do I know they use it? If we are delayed for any reason, they immediately want their predictions. So I conclude from this that these predictions are, after all, useful and certainly needed — although we know they are poor. So how do we go about improving the situation? There are two ways of dealing with this problem. We could say that the propagation medium is so complex in this region that "why don't we forget about predictions"? Why don't we design systems that are capable of adapting to the medium? But I think we must face the fact that very few people can afford to have such systems either in the military and civilian areas. It is cost effective to try and improve these prediction schemes? I would say it probably is, because in high latitudes we haven't really incorporated any of the new and not even some of the old knowledge into the schemes. Take IONCAP as an example (the same goes for any of the other prediction codes), they do not contain such statistics as have been presented by Dr Hargreaves on auroral absorption and its variation with latitude, time and geomagnetic activity, and they certainly contain very little physics of the high latitude region. It will, perhaps, take some time before these physical models are sufficiently developed to be incorporated into prediction schemes. I think there is a chance it could be and I think think that we put so little of what we know into these prediction schemes, that an improvement could be made by fairly simple means. The other point is, what about the short time predictions (in terms of days or maybe even hours)? In this area we also have sufficient knowledge to be able to do something to improve the situation. There are very few places where real-time monitoring and short term prediction is being implemented. So I think that basically there is room for improvement with fairly simple means in these prediction schemes. For example, the people at ITS in Boulder are working on putting some physics into the IONCAP and the F-region predictions to cover the areas where you have very few observations.

A.Rodger

I too, shall express my particular bias on a number of matters. First of all, while I appreciate the advantages of incoherent scatter, we saw during the week a really nice use of simple ionosonde data to supplement incoherent scatter radar. That means that we could instrument the northern high latitudes with relatively simple machines as long as we can understand the patterns (whether they are magnetometers, riometers or ionosondes) from them. Incoherent scatter is certainly one facility that can be used towards this — also some of the more sophisticated ionosondes with direction-finding capabilities.

One of the problems looking at the ionosphere in the Arctic is that there are very few places that we can actually deploy experiments. So I would also advocate the use of coherent backscatter radar for this region of the ionosphere. Going on to modelling, there are a couple of points to be made. Yes, I agree with Ray that the model must be based on physics, if one can do it. The other thing that I would stress, coming from the Antarctic, is that I think that it is absolutely essential to validate these models in the Antarctic. The reason for this is the combination of solar and geophysical coordinate systems down there is fundamentally different. The separation of the geographic and geomagnetic pole in the northern hemisphere is some eleven degrees, whilst in the southern hemisphere the separation is ~2.3°. We will need to test any models developed in the northern hemisphere to make sure we have the physics right.

I'd like to make a comment on the requirement for data also. I fully accept Prof. Akasofu's approach in trying to understand the disturbances that propagate from the sun through the interplanetary medium and the magnetosphere down to the ionosphere to affect radio propagation. I think he would be the first to admit, however, that it is going to be several years before these reach the user community. One of the key features that affects radio propagation at high latitudes is the interplanetary magnetic field control, and recently we have lost interplanetary field data. So one of the real weaknesses, as far as short term predictions, is the fact that we don't have really good indication of what is going to happen to the medium. Another satellite in "halo" orbit would give us an hour or so warning about particles likely to impinge upon the earth, and thus predictions for the future.

I have a particular bias I would like to express toward the midlatitude trough. I think that as physicists we now understand the physics of the production mechanism and some of the variability and have reasonable empirical models to work from. So I think that is an area where the user community and physicists should get together. The trough is a feature that extends over a good part of the NATO area — it extends from north America to Norway.

AUDIENCE RESPONSE

H.Soicher

All the panelists mentioned that the eventual product that users want is models for prediction purposes. I think this is a valid point. Some five years ago this particular panel of AGARD sponsored a symposium on "Modelling and Prediction", and as I recall as Chairman, the final conclusion that came from that symposium was that we have probably reached the state of the art in empirical modelling and the only improvement that will come to modelling and predictions is through *physical* understanding of the processes. For that reason I was particularly pleased to see a lot of physics in this symposium, because that fills a need that was expressed at the Modelling Symposium.

J.Borgholthaus

This is more of an observation — since I'm one of the users who is "stuck firmly to the ground" and I'm trying to grab on to ionospheric physicists who can help me understand what is going on. One of the things that really surprised me is that there are two approaches to gathering data — you use the "vacuum cleaner" approach and you gather all the data that occurs all year long, or you go out when it's convenient for a week and you take a "whole pile of data" then come back and go out four months later for a week. It would seem that particularly in America where scientific research money is going to become much, much tighter than it has been for the last three or four years that some random statistical sampling would be a much better way. And if you were trying to tell me how the circuit really was modelled and you only had a week in February, April and July, December, etc., I'd be really reluctant to say that your data were any good, because "what happens in August"? It seems that a lot of the things that are looked at from a systems engineering point of view are "five-cent problems" that take a lot of money to solve and yet you don't tell me how often the thing occurs. Do I worry about something that will happen two hours out of the year, or is it something that occurs three times a day? I haven't seen these type of problems addressed in this kind of conference.

R.Greenwald

I'd like to respond to that because I think that is a perfect demonstration of what we were trying to say. It is *not* a question of taking a random sample to obtain a uniform distribution so you get better probability curves, but ultimately what you are concerned about is that you *understand* the processes, then you'll know when they'll occur. Once you *understand* the problem then you can model what the *extremes* of the situation are going to be. I would say that the detailed campaign approach is probably the best because that is the only way you can afford to get a large variety of instrumentation in a certain area at a specific time.

N.Gerson

I wonder if I can disagree somewhat with Ray and the others, not completely, only 97%! I think I could fill up all the empty spaces on this campus with papers on the ionosphere written since the 1920s and with unanalyzed data. The point is, that there is a time when you want a fluid dynamicist and there's a time when you want a plumber. This is the case of the practical person. Since the war every communicator who uses the HF ionosphere development of the various scatter circuits some years ago. There are other examples where practical problems have forced practical solutions without understanding the ionosphere.

R.Greenwald

Ionospheric physicists are not in the business of making predictions. I think, however, that the type of work we do would enable people to make better predictions. Results from coherent backscatter studies could improve the reliability and operation of OTH radar systems. Our goal is to try to provide the understanding.

T.Jones

I would just like to respond to Nate' comments. I think that I would tend to agree with him, but I think that one thing you have to be very careful of is that if you dispense with all of your fluid dynamicists and just rely on your "plumbers" there will come a time when you need to "design an aeroplane". Let us keep the basic science and knowledge alive and vigorous. It s only from a good strength in basic science, that you will find new systems. I don't think that the approach of "let's all go and build black boxes" is the way to go at all.

E.Thrane

I think in response to you comment we're facing a very practical situation when you are issuing frequency predictions. Prediction schemes exist, they are being used, and we know that often they are giving the wrong answers. We either have to get rid of them or improve them. I'm not sure which one of the two you would recommend. It seems to me that you have to do *something* about them. Maybe we can't use the new information, but let us at least put in the things we already know.

P.Bauer

Mr Gerson's point is a very good one, because it is not for the ionospheric physicist to determine what is needed. It seems to me that the physicist wants to sell too much and the user does not want to buy enough.

J.Aarons

First of all, I think Nate Gerson is correct in many aspects of what he said, however, he may be concentrating a little too heavily on HF communications. In the military area there are certainly new needs by other systems for ionospheric information.

Chuck Rino described the synthetic aperture radar (SAR) systems which require much more information on phase

fluctuations and amplitude fluctuations within a small area of the ionosphere. We have military communications at 250 MHz which is severely affected by irregularities. In addition, we have errors in the Global Positioning Satellite system in both the military and civilian areas. They are going to have to correct these errors by using years of data on foF2 and TEC. So there are important new needs that the ionosphere commmunity should satisfy. One has to look very seriously at the point that Tudor Jones made, in that the effort in ionospheric research has been decreasing and we are at a minimum level for the users — which in this case are mostly military. We do supply a basic background of information for the user community.

T.Jones

I think that we must treat ionospheric physics as a subject in its own right. Ionospheric research is a valid part of physics, like astronomy. Now if at the same time, that knowledge can be applied and is useful to someone, that's a plus for the subject — not a negative.

R.Greenwald

I think that we *do* provide new knowledge which can be incorporated into the type of system that one builds. I think that very often there is no attempt to incorporate this new knowledge into the systems. It is almost as if there are two communities — the science community and the applied community and they go off into different directions and there is no communication. I was trying to say in my presentation that we *can* make a contribution and I think that you should recognize that and you should support some of the things we want to do if you do use it. There are some tremendous results coming out on the nature of the auroral zone ionosphere from the incoherent scatter radars since 1970.

R.Hunsucker

I guess what we need are interpreters between the two communities.

E.Thrane

Dr Gerson, you said that you consider the high latitude ionosphere to be basically unpredictable and you stressed all the complexities in the physical processes. All the neutral effects are also present at other places on the globe. There remains the fact that in the middle and low latitudes the present HF prediction schemes are really useful and fairly good. My point was that we could bring the high latitude predictions somewhat nearer this state by including in them some of the statistical features that we now have knowledge about. One should be able to do this without great cost: it is a matter of feeding things into the computer in such a way that will reproduce that statistics a little bit better than we do now.

A.Rodger

If you want to improve reliability, you've got to spend money, and that is the stage we've reached in ionospheric physics. In the short time I've been in the field I would say that there has been a fantastic number of developments in modelling techniques. The NCAR and Utah state groups can now reasonably model the ionosphere and that has only been possible with the development of very large and fast computers. We're not yet at the state where we can do realistic ray tracings through the ionosphere to produce what you want — which is a *perfect* communications system. I think that to some extent we are arguing about the last 10% in reliability, and one must pay a lot for that.

J.Belrose

I would like to make a few comments on obtaining resources and support for carrying out, continuing, and maintaining our knowledge base on ionospheric physics. During the past decade resources have significantly decreased for ionospheric work and this is in part because of the problems in total resources available throughout the spectrum. The struggles for resources determine, in part, what one does. Morphological studies are needed as well as detailed studies on a particular geophysical phenomenon. Very often the "highlights" are milked and we don't get down to looking at the morphological studies. We must insure that communication system designers have applied researchers going in the right directions — and there has to be a certain amount of basic research to support this, otherwise they'll invent systems which don't work.

M.Darnell

I think there has been a lot of implied criticism of the physicists that they are not doing responsive research. As an engineer, I think the engineers are also culpable in this respect for not asking the right questions. The EPP has a very important and valuable role to play in fostering this dialogue and mutual education between the two communities.

R.Hunsucker

One closing comment as the chairman — I think in all seriousness that we can say that we really *do* need interpreters between the physicists and the users, and the question I would pose is "who is qualified and willing to be an interpreter".

ADDITIONAL COMMENTS BY THE CHAIRMAN

In addition to the foregoing discussion, some conference participants submitted written responses to the four questions posed at the start. The following points were salient in the written responses:

(1) The EPP should continue to study the arctic ionospheric effects on radio systems.

(2) The arctic regions have a very strong strategic position in the NATO radio communication system.

(3) HF modes may be one of the last means of communication in a conflict.

(4) Future meetings should contain at least one classified session to ensure that specific needs are being met.

LIST OF PARTICIPANTS

AARONS, Dr J.†	Dept of Astronomy, Boston University, 725 Commonwealth Ave., Boston, MA 02215, United States
ADAMS, Dr S.	Harris Corp, P.O. Box 37, Melbourne, FL 32902, United States
AKASOFU, Prof. S.I.†	Geophysical Institute, University of Alaska, Fairbanks, Alaska 99701, United States
ALBRECHT, Dr H.J.*	FGAN/FHP, Neuenahrer Str. 20, 5307 Wachtberg-Werthhoven, Federal Republic of Germany
BAUER, Dr P.†	C.N.R.S., Directeur du Service d'Aéronomie, B.P. N. 3, 91370, Verrières-le-Buisson, France
BELROSE, Dr J.S.*	C.R.C., P.O. Box 11490 Stn H, Ottawa, Ont. K2H 8S2, Canada
BERKEY, Dr F.T.†	Center for Atmospheric and Space Science, Utah State University, UMC-34, Logan, UT 84322, United States
BLYTHE, Dr J.H.* (Panel Chairman)	Communications Research Labs., The Marconi Research Centre, West Hanningfield Road, Chelmsford, Essex CM2 8HN, United Kingdom
BOITHIAS, Mr L.*	C.N.E.T., 38—40, rue du Général Leclerc, 92131 Issy-les-Moulineaux, France
BORGHOLTHAUS, Mr J.	9800 Savage Road (Attn: R334), Department of Defense, Ft. George Meade, MD 20755-6000, United States
BOSSY, Prof. L.*	UCL, 174 Av. W. Churchill, B-1180 Bruxelles, Belgium
BRADLEY, Dr P.A.†	Rutherford Appleton Laboratory, Chilton, Didcot, Oxon, OX11 0QX, United Kingdom
BRANDT, Dr R.G.	Office of Naval Research, 1030 E. Green St., Pasadena, CA 91106-2485, United States
BROWN, Capt. L.W.	Office of Naval Research, Code 400 B, 800 N. Quincy St., Arlington, VA 2217-5000, United States
CANNON, Dr P.†	Royal Aircraft Establishment, Radio & Navigation Dept, Farnborough, Hants GU14 6TD, United Kingdom
CHIOVELLI, Dr O.	Ministero della Difesa, Costarmaereo 6 Divisione, Viale dell'Universita 4, 00100 Roma, Italy
CHRISTOPHE, Mr F.*	ONERA, B.P. 72, 92322 Châtillon Cedex, France
CONKRIGHT, Mr R.O.	NOAA/NGDC, 325 Broadway, Boulder, CO 80303, United States
COYNE, Mr V.J.*	RADC/OCS, Griffiss AFB, N.Y. 13441-5700, United States
CROFT, Dr T.A.	Technology for Communications Int'l, 1625 Stierlin Road, Mountain View, CA 94043, United States
CROWLEY, Dr T.P	Dept of Physics, (UCLA), Los Angeles, CA 90024, United States
DAMBOLDT, Dr T.†	Forschungsinstitut der DBP, Postfach 5000, D-6100 Darmstadt, Federal Republic of Germany
DARNELL, Dr M.†	Dept of Electronics, University of York, Heslington, York YO1 5DD, United Kingdom
FIELD, Mr E.C.†	Pacific Sierra Research Corp., Los Angeles CA 90025, United States
FREMOUW, Dr E.†	Physical Dynamics, Inc., P.O. Box 3027, Bellevue, WA 98009, United States
FUERXER, IPA P.*	Chef du Groupe 2, DRET, 26 Bld Victor, 75996 Paris Armées, France

*Member of Electromagnetic Wave Propagation Panel.
†Author of paper presented at the meeting.

GERSON, Mr N.C.	Laboratory for Physical Sciences, 4928 College Ave., College Park, MD 20740, United States
GOUTELARD, Prof. C.*	Laboratoire d'Etude de Transmissions Ionosphériques, 9, Avenue de la Division Leclerc, 94230 Cachan, France
GREENWALD, Dr R.A.†	Johns Hopkins University, Applied Physics Laboratory, Johns Hopkins Road, Laurel, MD 20707, United States
GREIFINGER, Dr C.C.	R & D Associates, P.O. Box 9695, Marina del Rey, CA 90295, United States
HANBABA, Dr R.	C.N.E.T./SPI, 22301 Lannion Cedex, France
HANUISE, Dr C.†	LSFET CNRS, Université de Toulon, La Giponne, 639 Bld des Armaris, 83100 Toulon, France
HARGREAVES, Dr J.K.†	Department of Environmental Sciences, University of Lancaster, Bailrigg, Lancaster, LA1 4YQ, United Kingdom
HARTH, Prof. Dr W.	Fachhochschule Köln, Reitweg 1, 5000 Köln 21, Federal Republic of Germany
HODARA, Dr H*	President, Tetra Tech Inc., Pasadena, CA 91107-2190, United States
HUNSUCKER, Prof. R.†	Geophysical Institute, University of Alaska, Fairbanks, Alaska 99701, United States
INCE, Prof. Dr A.N.*	Science and Engineering Research Council, Tubitak, Ataturk Bulvari 221, Ankara, Turkey
JOHNSON, MR A.L.†	AFWAL/AAAI, Wright Patterson AFB, OH 45433, United States
JONES, Dr T.B.†	Department of Physics, University of Leicester, University Road, Leicester, LE1 7RH, United Kingdom
KELLY, Dr J.D.†	SRI International, 333 Ravenswood Avenue, Menlo Park, CA 94025, United States
KELLY, Mr T.	KEL Aerospace Pty. Ltd, 1-12 Brennan close, Asquith, NSW, Australia 2708
KERSLEY, Dr L.†	Department of Physics, University College of Wales, Penglais, Aberystwyth, SY23 3BZ, United Kingdom
KHANNA SHYAM, Dr M.	Defence Research Establishment, Ottawa National Defence Hqs, Ottawa, K1A 0Z4, Canada
KLOBUCHAR, Mr J.A.†	LIS, Air Force Geophysics Laboratory, Hanscom AFB, MA 01731, United States
KNOWLES, Dr S.H.	NLR Code 4180, Washington, DC 20375, United States
KOFMAN, Dr W.†	CEPHAG, Domain Universitaire, B.P. 46, 38402 St Martin d'Hérès Cedex, France
LAM, Dr I.†	CRC, P.O. Box 11490, Station H, Ottawa, K2H 8S2, Canada
LEE, Dr M.C.†	Laboratory of Electronics (36-383) MIT, Cambridge, MA 02139, United States
LEFEVER, Dr R.S.	Harris Corp, P.O. Box 37, Melbourne, FL 32902, United States
MAVROKOUKOULAKIS, Dr N.*	Technology Research Center, KETA, Delta Falirou, Palaion Faliron, Athens, Greece
OSTERGAARD, Mr J.†	Elektronikcentralen ATV, Venlighedsvej 4, DK 2970 Horsholm, Denmark
PATRICIO, Ing. J.F.*	CTT-Director dos Servicos de Radiocomunicaçoes, Rua Conde de Redondo, 79—10, 1189 Lisboa Codex, Portugal
PERRY, Mrs J.	1921 Hopefield Rd, Silver Spring, MD 20904, United States
PIEFKE, Prof. Dr G.	Theor. Elektrotechnik TH Darmstadt, Schlossgartenstr. 8, D-6100 Darmstadt, Federal Republic of Germany
PROLSS, Dr G.W.†	Institut für Astrophysik, Auf dem Hugel 71, 5300 Bonn, Federal Republic of Germany

*Member of Electromagnetic Wave Propagation Panel.
†Author of paper presented at the meeting.

QUEGAN, Dr S.†	GEC Research Lab. Marconi Res. Centre, West Hanningfield Rd, Great Baddow, Chelmsford, Essex CM2 8HN, United Kingdom
RASMUSSEN, Mr J.E.†	RADC/EEPS, Hanscom AFB, MA 01731, United States
REED, Dr A.P.C.	Plessey E.S.R.L., Roke Manor, Romsey, Hants, SO5 0ZN, United Kingdom
REINISCH, Dr B.†	University of Lowell, Center for Atmospheric Research, 450 Aiken St, Lowell, MA 01854, United States
RICE, Mr D.	University of Alaska, P.O. Box 80027, Fairbanks, AK 99708, United States
RINO, Dr C.L.†	SRI International, 333 Ravenswood Avenue, Menlo Park, CA 94025, United States
RODGER, Mr A.S.†	British Antarctic Survey, Madingley Road, Cambridge, CB3 0ET, United Kingdom
ROSE, Dr G.†	Max-Planck-Institut für Aeronomie, Postfach 20, D-3411 Katlenburg-Lindau, Federal Republic of Germany
ROTHER, Dr D.*	Standard Elektrik Lorenz AG (SEL), Abt. PC ERM, Ostendstrasse 3, D 7530 Pforzheim, Federal Republic of Germany
SALES, Dr G.†	University of Lowell, Center for Atmospheric Research, 450 Aiken St, Lowell, MA 01854, United States
SEPP, Dr H.*	SHAPE Technical Centre, P.O. Box 174, 2501 CD The Hague, Netherlands
SOICHER, Dr H.*	US Army Communication-Electronic Cmd, Center for Communications Systems, ATTN: AMSEL-COM-RN-1, Fort Monmouth, N.J. 07703-5202, United States
SPRENKELS, Colonel R.C.*	Etat Major de la Force Aérienne, Section Communications et Electronique, (VDM), Quartier Reine Elisabeth, B-1140 Bruxelles, Belgium
STOKKE, Mr K.N.†	Norwegian Telecommunications Administration, Postboks 6701, St Olavs pl. 0130 Oslo 1, Norway
TAAGHOLT, Mr J.*	Danish Scientific Liaison Officer for Greenland, 10 Oster Voldgade, DK 1350 Copenhagen K, Denmark
THRANE, Dr E.†	N.D.R.E., P.O. Box 25, N-2007 Kjeller, Norway
VISSINGA, Mr H.*	F.E.L. T.N.O., Postbox 96864, 2509 JG The Hague, Netherlands
WATKINS, Dr B.J.†	Geophysical Institute, University of Alaska, Fairbanks, Alaska 99701, United States
WIDDEL, Dr H.U.†	Max Planck Institut für Aeronomie, D-3411 Katlenburg-Lindau, Federal Republic of Germany
YEH, Prof. K.C.*	University of Illinois, 1406 W. Green Street, Urbana, IL 61801, United States
ZIMMERMAN, Mr D.†	Mitre Corporation, Box 208, MS J-101, Bedford, MA 01730, United States

*Member of Electromagnetic Wave Propagation Panel.
†Author of paper presented at the meeting.

BIBLIOGRAPHY

This Bibliography with Abstracts has been compiled by Mr G.E.Gleadall B.Sc. of the Defence Research Information Centre, Ministry of Defence, UK, in consultation with the Marconi Research Centre. Preparation of the print master was carried out by the NASA Scientific and Technical Information Facility.

FOREWORD

This bibliography is not a comprehensive review of the existing literature. It is intended as a guide to some of the current literature in the subject area, for the benefit of attendees at the conference. More specific references to individual papers are listed by the authors of the papers.

All references listed here have been obtained from the NASA on-line data base using the ESA-Information Retrieval Service on-line system and cover the period 1980 — February 1985.

The NASA data base contains references to literature on the science and technology of space and aeronautics.

The references are in two broad source categories:

(1) Items prefixed with an accession number containing the letter A, e.g. 85A 11557; these are items listed in the American Institute of Aeronautics and Astronautics publication 'International Aerospace Abstracts' (IAA), which covers world-wide scientific and trade journals, translations of journals and journal articles (usually into English), books and conference papers.

(2) Items prefixed with an accession number containing the letter N, e.g. 85N 13337; items from NASA 'Scientific and Technical Aerospace Reports' (STAR), which provides parallel coverage of current world-wide report literature.

The majority of the items should be available in microfiche form from the NASA Scientific and Technical Information Facility in North America, from the British Library Lending Division, or from the ESA-Information Retrieval Service in Europe.

PRINT 01/2/1-116 TERMINAL=65

85A11557 ISSUE 2 PAGE 79 CATEGORY 46 CNT#: NSF ATM-76-17334 NSF ATM-78-05747 NSF ATM-81-11464 NSF ATM-81-19812 84/10/01 7 PAGES UNCLASSIFIED DOCUMENT

UTTL: Plasma convection in the vicinity of the dayside cleft

AUTH: A/FOSTER, J. C.; B/DOUPNIK, J. R. PAA: A/(Haystack Observatory, Westford, MA); B/(Utah State University of Agriculture and Applied Science, Logan, UT)
Journal of Geophysical Research (ISSN 0148-0227), vol. 89, Oct. 1, 1984, p. 9107-9113.

MAJS: /*CONVECTIVE FLOW/*IONOSPHERIC SOUNDING/*MAGNETOHYDRODYNAMIC FLOW/*SPACE PLASMAS

MINS: / ARCTIC REGIONS/ DAYTIME/ INCOHERENT SCATTER RADAR/ IONOSPHERIC PROPAGATION/ RADIO PROBING

ABA: M.S.K.

ABS: A summary of multiposition observations of the pattern of ionospheric convection equatorward of the noontime cleft made with the Chatanika incoherent scatter radar before 1982 is presented. Data were gathered between 57-73 deg N in both quiescent and disturbed conditions. The undisturbed ionosphere data were taken when the IMF was directed toward the sun and featured a poleward 300 m/sec plasma flow. Vector velocities were not available in perturbed conditions. The cleft moved to a lower latitude during solar maximum and exhibited a convergence region near the noon meridian below 70 deg N, a region of moderate speed poleward flow, and flow divergence from the noon cleft at the highest latitudes. The eastward electric field was 25 mV/m when the geomagnetic index exceeded a value of 4. The radar facility has been moved to Sondre Stromfjord, Greenland, and is now closer to the cleft.

85A11555 ISSUE 2 PAGE 79 CATEGORY 46 84/10/01 5 PAGES UNCLASSIFIED DOCUMENT

UTTL: Observations of sunward propagating waves on the magnetopause

AUTH: A/NIELSEN, E. PAA: A/(Max-Planck-Institut fuer Aeronomie, Katlenburg, West Germany)
Journal of Geophysical Research (ISSN 0148-0227), vol. 89, Oct. 1, 1984, p. 9095-9099.

MAJS: /*AURORAL ZONES/*IONOSPHERIC PROPAGATION/*MAGNETOPAUSE /*RADAR MEASUREMENT

MINS: / DRIFT RATE/ ELECTRIC FIELDS/ EXTREMELY LOW RADIO FREQUENCIES/ LATITUDE/ RADIO PROBING/ WAVE PROPAGATION

ABA: Author

ABS: Observations of ionospheric electric fields during an ULF resonant event are used to infer the presence of waves on or near the magnetopause propagating toward the dayside. Simultaneous satellite measurements at geosynchronous orbit confirm the presence of these surface waves. Immediately following these observations a flux transfer event appears to have occurred (Goertz et al., 1984). It is speculated that the pulsations were associated with that event.

85A11023 ISSUE 1 PAGE 57 CATEGORY 46 84/08/00 8 PAGES UNCLASSIFIED DOCUMENT

UTTL: Day-to-day variability of riometer absorption

AUTH: A/FOPPIANO, A. J.; B/BRADLEY, P. A. PAA: A/(Concepcion, Universidad, Concepcion, Chile); B/(Science and Engineering Research Council, Rutherford, Appleton Laboratory, Didcot, Oxon, England)
Journal of Atmospheric and Terrestrial Physics (ISSN 0021-9169), vol. 46, Aug. 1984, p. 689-696.

MAJS: /*DIURNAL VARIATIONS/*ELECTROMAGNETIC ABSORPTION/*IONOSPHERIC PROPAGATION/*POLAR REGIONS/*PROBABILITY DISTRIBUTION FUNCTIONS/*RIOMETERS

MINS: / AMPLITUDE DISTRIBUTION ANALYSIS/ AURORAL ABSORPTION/ POLAR RADIO BLACKOUT/ RADIO ATTENUATION

ABA: C.D.

ABS: Statistical variations of absorption data measured with a riometer on different days at a given hour are examined. Observational data from a range of different locations are examined and it is shown that they all tend to follow a specific statistical form. Preferred parameters needed to define the distributions are discussed, and numerical values of the different paremeters of the distributions and the approximate interrelationship found to exist between them are considered. The advantages offered by the use of these relationships in defining the morphology of the absorption are highlighted.

85A11020 ISSUE 1 PAGE 56 CATEGORY 46 84/08/00 6 PAGES UNCLASSIFIED DOCUMENT

UTTL: Power spectra of VHF intensity scintillations from F2 and E-region ionospheric irregularities

AUTH: A/KERSLEY, L.; B/CHANDRA, H. PAA: A/(University College of Wales, Aberystwyth, Wales); B/(Physical Research Laboratory, Ahmedabad, India; University College of Wales, Aberystwyth, Wales)
Journal of Atmospheric and Terrestrial Physics (ISSN 0021-9169), vol. 46, Aug. 1984, p. 667-672. Research supported by the Science and Engineering Research Council.

MAJS: /*IONOSPHERIC DISTURBANCES/*IONOSPHERIC PROPAGATION/*IONOSPHERIC SOUNDING/*POLAR REGIONS/*POWER SPECTRA/*SCINTILLATION

MINS: / E REGION/ EISCAT RADAR SYSTEM (EUROPE)/ F 2 REGION/ IONOSPHERIC ELECTRON DENSITY/ SATELLITE TRANSMISSION/ SIGNAL FADING/ VERY HIGH FREQUENCIES

ABA: Author
ABS: An experiment is described for the routine study of scintillations and ionospheric irregularities at high-latitudes using NNSS satellites with additional coordinated observations by means of the EISCAT ionospheric radar facility. Early results, obtained during the development phase of the experiment, are presented of the power spectra of intensity fluctuations at 150 MHz observed at the equatorwards edge of the high-latitude irregularity zone. The spectra of 165 samples of night-time scintillation recorded during October 1982 to May 1983 show a spectral index with a mean value of -3.58 and a steepening of the spectral slope with increasing S4. Some examples of scintillation arising from irregularities at E-layer heights show spectral indices of magnitude generally smaller than for F-region cases. A few spectra have been found with a clear break in spectral slope at around 10 Hz, suggesting two regimes for irregularities of different scale sizes.

84A48960 ISSUE 24 PAGE 3523 CATEGORY 32
83/00/00 7 PAGES In RUSSIAN UNCLASSIFIED DOCUMENT
UTTL: Mean-field modes in a waveguide channel in the presence of vertical disturbances
AUTH: A/ZERNOV, N. N.; B/PROKHOROV, K. V.
IN: VLF propagation in the earth-ionosphere waveguide channel (A84-48951 24-32). Leningrad, Izdatel'stvo Leningradskogo Universiteta, 1983, p. 135-141. In Russian.
MAJS: /*DYSON THEORY/*IONOSPHERIC DISTURBANCES/*IONOSPHERIC PROPAGATION/*PROPAGATION MODES/*WAVEGUIDES
MINS: / ELECTROMAGNETIC SCATTERING/ GEOMAGNETISM/ POLAR REGIONS/ RADIO ATTENUATION/ VERTICAL DISTRIBUTION
ABA: B.J.
ABS: An analysis is made of a situation in which random perturbations cause the natural modes of a regular waveguide channel to interact with one another and to produce only a slight change in the propagation characteristics; this is the case of vertical perturbations extending across the guiding layer. The mean field in the channel with the random perturbations is described by the Dyson equation, and the absorption of the normal modes due to scattering by the perturbations is examined. It is noted that this type of situation can arise in near-polar regions, where inhomogeneities extending along the magnetic field lines are practically vertical.

84A48959 ISSUE 24 PAGE 3523 CATEGORY 32
83/00/00 10 PAGES In RUSSIAN UNCLASSIFIED DOCUMENT
UTTL: Effect of properties of a high-latitude earth-ionosphere waveguide channel on the group and phase delays of LF radio signals singly reflected from the ionosphere
AUTH: A/ZHIVULIN, V. A.; B/TAIBIN, B. Z.; C/FISHKINA, N. P.; D/IANEVICH, IU. M.
IN: VLF propagation in the earth-ionosphere waveguide channel (A84-48951 24-32). Leningrad, Izdatel'stvo Leningradskogo Universiteta, 1983, p. 126-135. In Russian.
MAJS: /*IONOSPHERIC PROPAGATION/*LOW FREQUENCIES/*POLAR RADIO BLACKOUT/*RADIO ECHOES
MINS: / GROUND EFFECT (COMMUNICATIONS)/ GROUP VELOCITY/ IONOSPHERIC ELECTRON DENSITY/ PHASE VELOCITY/ PULSE TIME MODULATION/ RADIO RECEIVERS/ RADIO TRANSMITTERS/ SIGNAL FADING RATE/ TIME LAG
ABA: B.J.
ABS: An analysis is made of the dependence of the group and phase delays of an LF (approximately 100 kHz) radio signal singly reflected from the ionosphere on the distance between the receiver and the transmitter for a number of parameters of the high-latitude earth-ionosphere waveguide. The problem of eliminating the indeterminacy in the assessment of phase delay is examined.

84A48279* ISSUE 24 PAGE 3570 CATEGORY 46
84/09/01 4 PAGES UNCLASSIFIED DOCUMENT
UTTL: O(+) acceleration due to resistive momentum transfer in the auroral field line plasma
AUTH: A/MITCHELL, H. G., JR.; B/PALMADESSO, P. J. PAA: A/(U.S. Navy, Naval Research Laboratory, Washington, DC; Science Applications, Inc., McLean, VA); B/(U.S. Navy, Naval Research Laboratory, Washington, DC)
CORP: Naval Research Lab., Washington, D. C.; Science Applications, Inc., McLean, Va.
Journal of Geophysical Research (ISSN 0148-0227), vol. 89, Sept. 1, 1984, p. 7573-7576. NASA-Navy-supported research.
MAJS: /*AURORAL ZONES/*ION MOTION/*MOMENTUM TRANSFER/* PARTICLE ACCELERATION/*SPACE PLASMAS
MINS: / ELECTRIC FIELDS/ IONOSPHERIC PROPAGATION/ LINES OF FORCE/ OXYGEN IONS/ POSITIVE IONS
ABA: M.S.K.
ABS: An analytical model is defined to demonstrate that parallel acceleration of an O(+) ion beam in the ionosphere can occur naturally due to the presence of a quasi-static parallel electric field. Momentum equations are defined for friction between hydrogen ions and electrons, which produces a quasi-static

electric field. The field can accelerate ions, e.g., the O(+) ions, which do not participate in the frictional momentum exchange. The conditions are shown to be applicable to the auroral field line plasma if a current is present along the magnetic field. A simulation performed with the equations shows that the field line plasma exhibits dynamic behavior after a field-aligned current appears. The resulting momentum gain by O(+) ions can be sufficient for causing a potential drop of several kilovolts along the field line.

84A47522 ISSUE 23 PAGE 3420 CATEGORY 46
84/08/00 8 PAGES In RUSSIAN UNCLASSIFIED DOCUMENT

UTTL: Propagation of MHD waves through the ionospheric plasma and spatial characteristics of geomagnetic variations

AUTH: A/ALPEROVICH, L. S.; B/FEDOROV, E. N. PAA: B/(Akademiia Nauk SSSR, Institut Fiziki Zemli, Moscow, USSR)

Geomagnetizm i Aeronomiia (ISSN 0016-7940), vol. 24, July-Aug. 1984, p. 650-657. In Russian.

MAJS: /*IONOSPHERIC PROPAGATION/*MAGNETIC VARIATIONS/*MAGNETOHYDRODYNAMIC WAVES/*SPACE PLASMAS

MINS: / AMPLITUDES/ ANISOTROPIC MEDIA/ ATMOSPHERIC MODELS/ POLAR REGIONS/ SPATIAL DEPENDENCIES

ABA: B.J.

ABS: The propagation of an MHD-wave beam through the anisotropic polar ionosphere is analyzed theoretically. Spatial relationships of the amplitude and phase of different components of the electromagnetic field are obtained in a wide range of periods for two models of the ionosphere. The role of the earth's conductivity in the formation of the spatial characteristics of the field is shown to be significant. Intrinsic electric-mode waves in the atmospheric waveguide are investigated. The existence of regions with phase velocities of about 100 km/s is shown.

84A47518 ISSUE 23 PAGE 3420 CATEGORY 46
84/08/00 6 PAGES In RUSSIAN UNCLASSIFIED DOCUMENT

UTTL: Absorption of electron-beam energy in a mixture of O I, O2 and N2 gases --- in polar ionosphere

AUTH: A/KIRILLOV, A. S.; B/OSIPOV, N. K.; C/IVANOV, V. E. PAA: C/(Akademiia Nauk SSSR, Poliarnyi Geofizicheskii Institut, Murmansk, USSR)

Geomagnetizm i Aeronomiia (ISSN 0016-7940), vol. 24, July-Aug. 1984, p. 625-630. In Russian.

MAJS: /*ATMOSPHERIC ATTENUATION/*ELECTRON BEAMS/*GAS MIXTURES/*IONOSPHERIC PROPAGATION/*POLAR REGIONS

MINS: / ELECTRON ENERGY/ ENERGY DISSIPATION/ MONTE CARLO METHOD/ NITROGEN/ OXYGEN/ PITCH (INCLINATION)

ABA: B.J.

ABS: The Monte Carlo method is used to investigate the transfer of electrons with initial energies of not less than 0.1 keV and pitch angles ranging from 0 to 70 deg in a mixture of O I, O2, and N2. Dissipation functions are calculated which describe the depthwise distribution of electron-beam energy separated in a gaseous absorber. These functions are compared with available results of experimental measurements. In addition, analytic forms are derived for the dissipation function describing the transfer of electron beams with a pitch angle of 0 deg and with isotropic pitch-angle distribution above the lower hemisphere. The results are pertinent to the study of processes in the polar ionosphere.

84A46315 ISSUE 22 PAGE 3227 CATEGORY 32
84/07/00 11 PAGES UNCLASSIFIED DOCUMENT

UTTL: Non-Maxwellian velocity distribution functions and incoherent scattering of radar waves in the auroral ionosphere

AUTH: A/HUBERT, D. PAA: A/(Meudon, Observatoire, Meudon, Hauts-de-Seine, France)

Journal of Atmospheric and Terrestrial Physics (ISSN 0021-9169), vol. 46, June-July 1984, p. 601-611.

MAJS: /*AURORAL ZONES/*INCOHERENT SCATTER RADAR/*RADAR SCATTERING/*VELOCITY DISTRIBUTION/*WAVE PROPAGATION

MINS: / DISTRIBUTION FUNCTIONS/ MOLECULAR IONS/ NITRIC OXIDE / OXYGEN IONS/ POSITIVE IONS/ PROPAGATION VELOCITY/ SPACE PLASMAS

ABA: Author

ABS: For studies of the high-latitude ionosphere it is important to calculate the effect of convection electric fields on the velocity distribution functions. At an altitude where the plasma is weakly ionized, the appropriate Boltzmann equation is solved in the spatial homogeneous case. The characteristics of the ion nonequilibrium steady state reached for large electric fields are discussed from the macroscopic point of view. From the microscopic point of view, it is shown that the Grad expansion fails to converge rapidly for large electric fields. Generalized polynomial expansions are developed for different models of ion-neutral interactions. The consequences of these non-Maxwellian ion distribution functions on radar waves are presented, and erroneous interpretations of measurements are discussed.

84A46309 ISSUE 22 PAGE 3275 CATEGORY 46
84/07/00 10 PAGES UNCLASSIFIED DOCUMENT

UTTL: Methods of measuring plasma velocity with EISCAT

AUTH: A/WILLIAMS, P. J. S.; B/JONES, G. O. L.; C/JAIN, A. R. PAA: C/(University College of Wales, Aberystwyth, Wales)

Journal of Atmospheric and Terrestrial Physics (ISSN 0021-9169), vol. 46, June-July 1984, p. 521-530.
Research supported by the Science and Engineering Research Council.

MAJS: /*EISCAT RADAR SYSTEM (EUROPE)/*IONOSPHERIC PROPAGATION/*PLASMA DIAGNOSTICS/*RADIO PROBING/*SPACE PLASMAS/*VELOCITY MEASUREMENT

MINS: / ARCTIC REGIONS/ MULTISTATIC RADAR/ PROPAGATION VELOCITY/ RANDOM ERRORS/ TIME RESPONSE

ABA: Author

ABS: Using the EISCAT system it is possible to determine the total vector of plasma velocity - and hence the electric field both in the 'monostatic' and 'tristatic' mode. Results are presented for the evening of 18 May 1982 during the reversal of plasma velocity from westward to eastward. A comparison demonstrates that the random errors in the measured velocity are smallest in the monostatic mode using data taken at Tromso, where the signal-to-noise ratio is highest. There is, however, a systematic error in the monostatic measurements due to horizontal gradients in plasma velocity.

84A43077 ISSUE 21 PAGE 3076 CATEGORY 46
84/08/00 12 PAGES UNCLASSIFIED DOCUMENT

UTTL: ELF and VLF radiation from the 'polar electrojet antenna'

AUTH: A/BARR, R.; B/STUBBE, P. PAA: B/(Max-Planck-Institut fuer Aeronomie, Katlenburg, West Germany)

Radio Science (ISSN 0048-6604), vol. 19, July-Aug. 1984, p. 1111-1122.

MAJS: /*AURORAL ELECTROJETS/*EXTREMELY LOW FREQUENCIES/*IONOSPHERIC SOUNDING/*POLAR REGIONS/*RADIO OBSERVATION /*VLF EMISSION RECORDERS

MINS: / AMPLITUDE MODULATION/ DIPOLE MOMENTS/ ELECTRON DENSITY PROFILES/ HALL EFFECT/ IONOSPHERIC HEATING/ IONOSPHERIC PROPAGATION/ RADIO ANTENNAS/ RECIPROCITY THEOREM/ VERY LOW FREQUENCIES

ABA: Author

ABS: An approximate evaluation is made of the ELF/VLF dipole moment of the polar electrojet antenna established by ionospheric heating via the use of powerful HF waves amplitude modulated with frequencies in the ELF/VLF range. The theory of reciprocity is used to determine the magnitude of the ELF/VLF waveguide excitation produced by such a dipole immersed in the ionosphere. Propagation under a series of ionospheres ranging from quiet auroral nighttime to disturbed auroral daytime is considered.

84A40639 ISSUE 19 PAGE 2729 CATEGORY 19
84/06/00 6 PAGES UNCLASSIFIED DOCUMENT

UTTL: The electron flux J sensor for HILAT

AUTH: A/HARDY, D. A.; B/HUBER, A.; C/PANTAZIS, J. A. PAA: A/(USAF, Geophysics Laboratory, Bedford, MA); C/(AMPTEK, Inc., Bedford, MA)

Johns Hopkins APL Technical Digest (ISSN 0270-5214), vol. 5, Apr.-June 1984, p. 125-130.

MAJS: /*ELECTRON PROBES/*IONOSPHERIC SOUNDING/*POLAR REGIONS /*SATELLITE-BORNE INSTRUMENTS/*SCIENTIFIC SATELLITES

MINS: / BLOCK DIAGRAMS/ E REGION/ ELECTRONIC EQUIPMENT/ F REGION/ FLUX (RATE)/ PARTICLE COLLISIONS/ RADIO TRANSMISSION/ REMOTE SENSORS/ SPECTROGRAMS

ABA: Author

ABS: The J sensor on the HILAT satellite measures the local flux of electrons over the energy range from 20 to 20,000 electronvolts. Such measurements are important to the HILAT mission since it is the collisional interaction of these particles with the upper atmosphere that is thought to play a major role in the production of F and E region ionization. Irregularities in this ionization can then produce phase and amplitude scintillation of radio signals propagating through the ionization regions.

84A40636 ISSUE 19 PAGE 2729 CATEGORY 17
84/06/00 5 PAGES UNCLASSIFIED DOCUMENT

UTTL: The HILAT satellite multifrequency radio beacon

AUTH: A/COUSINS, M. D.; B/LIVINGSTON, R. C.; C/RINO, C. L. ; D/VICKREY, J. F. PAA: D/(SRI International, Menlo Park, CA)

Johns Hopkins APL Technical Digest (ISSN 0270-5214), vol. 5, Apr.-June 1984, p. 109-113.

MAJS: /*IONOSPHERIC SOUNDING/*POLAR REGIONS/*RADIO BEACONS/*SATELLITE TRANSMISSION/*SCIENTIFIC SATELLITES

MINS: / DATA ACQUISITION/ PHASE DETECTORS/ RADIO ANTENNAS/ RADIO TELEMETRY/ SCINTILLATION COUNTERS/ ULTRAHIGH FREQUENCIES/ VERY HIGH FREQUENCIES

ABA: Author

ABS: The HILAT beacon, L-band/UHF antenna, and ground receiver system allow efficient phase scintillation measurements to be made. The L-band signal also accepts bi-phase modulated telemetry data from the other scientific instruments by means of the Science Data Formatter. Thus, the L-band signal serves the dual functions of telemetry channel and phase reference for the scintillation measurements.

84A40635 ISSUE 19 PAGE 2727 CATEGORY 15
84/06/00 5 PAGES UNCLASSIFIED DOCUMENT

UTTL: The HILAT spacecraft

AUTH: A/POTOCKI, K. A. PAA: A/(Johns Hopkins University, Laurel, MD)

Johns Hopkins APL Technical Digest (ISSN 0270-5214), vol. 5, Apr.-June 1984, p. 104-108.

MAJS: /*IONOSPHERIC SOUNDING/*POLAR REGIONS/*SATELLITE DESIGN/*SCIENTIFIC SATELLITES

MINS: / PLASMA DENSITY/ RADIO FREQUENCIES/ RADIO TELEMETRY/ SATELLITE ATTITUDE CONTROL/ SATELLITE CONFIGURATIONS/ SPACECRAFT LAUNCHING/ SPACECRAFT POWER SUPPLIES/ TEMPERATURE CONTROL/ WAVE PROPAGATION

ABA: Author

ABS: The HILAT (high latitude ionosopheric research) satellite was bufit to provide measurements of both ionospheric parameters and their effects on radio frequency wave propagation. This article provides a description of the spacecraft and its early post-launch performance.

84A40634 ISSUE 19 PAGE 2725 CATEGORY 12
84/06/00 6 PAGES UNCLASSIFIED DOCUMENT

UTTL: The HILAT satellite program - Introduction and objectives

AUTH: A/FREMOUW, E. J.; B/WITTWER, L. A. PAA: A/(Physical Dynamics, Inc., Northwest Div., Bellevue, WA); B/(U.S. Defense Nuclear Agency, Washington, DC)

Johns Hopkins APL Technical Digest (ISSN 0270-5214), vol. 5, Apr.-June 1984, p. 98-103.

MAJS: /*ELECTROMAGNETIC WAVE TRANSMISSION/*IONOSPHERE/*PLASMA DENSITY/*SCINTILLATION/*SPACEBORNE EXPERIMENTS

MINS: / AURORAL ZONES/ BEACONS/ MAGNETOMETERS/ MAGNETOSPHERE / PLASMA INTERACTION EXPERIMENT/ POLAR REGIONS/ SATELLITE-BORNE INSTRUMENTS

ABA: D.H.

ABS: The HILAT program - a multiexperiment satellite program investigating the dynamics of irregularities in plasma density in the high-latitude ionosphere - is described. Its five experiments are designed to probe the development, evolution, and decay of irregularities on scales that produce radio wave scintillation (hundreds of kilometers down to tens of meters). High latitudes are defined as those that lie poleward of the plasmapause (where there is a substantial plasma density gradient between the relatively smooth mid-latitude ionosphere and the more varied and structured regions at higher latitudes). The studies are of interest because the performance of both radar and communications systems can be degraded by natural disturbances and by high-altitude nuclear detonations. The five instruments carried are a coherent beacon, a plasma monitor, a vector magnetometer, an electron spectrometer, and an auroral ionospheric mapper. The HILAT ground stations, data distribution network, and data obtained from two passes are dealt with.

84A39089 ISSUE 18 PAGE 2613 CATEGORY 32
84/06/07 3 PAGES UNCLASSIFIED DOCUMENT

UTTL: Effect of a heated patch of auroral ionosphere on VLF-radio wave propagation

AUTH: A/RIETVELD, M. T.; B/KOPKA, H.; C/STUBBE, P.; D/BARR, R. PAA: C/(Max-Planck-Institut fuer Aeronomie, Katlenburg, West Germany)

Nature (ISSN 0028-0836), vol. 309, June 7, 1984, p. 534-536. Research supported by the Deutsche Forschungsgemeinschaft.

MAJS: /*AURORAL ZONES/*IONOSPHERIC HEATING/*IONOSPHERIC PROPAGATION/*RADIO TRANSMISSION/*VERY LOW FREQUENCIES

MINS: / ANOMALIES/ D REGION/ NORWAY/ PHASE DEVIATION/ SIGNAL RECEPTION

ABA: O.C.

ABS: The generation of movable, controlled anomalies in the D-region has become possible through the development of a high frequency heating facility in Tromso, Norway. Attention is given to initial observations on Norwegian territory of the effect of such a movable D-region anomaly on the VLF signals received from the 12.1-kHz Omeg transmitter at Aldra. These observations confirm the validity of earlier theoretical predictions.

84A38909 ISSUE 18 PAGE 2613 CATEGORY 32
84/04/00 6 PAGES UNCLASSIFIED DOCUMENT

UTTL: The 'Polar Electrojet Antenna' as a source of ELF radiation in the earth-ionosphere waveguide

AUTH: A/BARR, R.; B/STUBBE, P. PAA: B/(Max-Planck-Institut fuer Aeronomie, Katlenburg, West Germany)

Journal of Atmospheric and Terrestrial Physics (ISSN 0021-9169), vol. 46, April 1984, p. 315-320.

MAJS: /*AURORAL ELECTROJETS/*EXTREMELY LOW FREQUENCIES/*IONOSPHERIC CURRENTS/*IONOSPHERIC PROPAGATION

MINS: / CURRENT DENSITY/ DIPOLE MOMENTS/ ELECTRIC DIPOLES/ RECIPROCAL THEOREMS/ WAVEGUIDES

ABA: Author

ABS: The ELF currents produced in the auroral ionosphere by a powerful HF wave modulated at ELF are first computed using the method of Stubbe et al. The technique of reciprocity is then used to evaluate the efficiency of excitation of the earth-ionosphere waveguide by this extended ionospheric current source. Computations suggest that radiated powers ranging from a few milliwatts at 100 Hz to a few watts at 2.0 kHz can be

expected for HF effective radiated powers of 150 MW.

84A34631 ISSUE 15 PAGE 2184 CATEGORY 46 CNT#: NSERC-A-2435 84/05/01 8 PAGES UNCLASSIFIED DOCUMENT

UTTL: Propagation of plasma wave energy in the auroral E region

AUTH: A/MOORCROFT, D. R. PAA: A/(Western Ontario, University, London, Canada)

Journal of Geophysical Research (ISSN 0148-0227), vol. 89, May 1, 1984, p. 2963-2970. Sponsorship: Natural Sciences and Engineering Research Council of Canada.

MAJS: /*AURORAL ZONES/*E REGION/*ELECTROSTATIC WAVES/*SPACE PLASMAS/*WAVE PROPAGATION

MINS: / FLOW THEORY/ GROUP VELOCITY/ PROPAGATION VELOCITY/ WAVE PACKETS

ABA: Author

ABS: The propagation of electrostatic plasma wave energy in the auroral E region has been studied using fluid theory. Typically, a wave travels at high speed nearly parallel to the magnetic field, except possibly for a small height interval where it is reflected upward; throughout, the direction of the propagation vector remains virtually unchanged and nearly perpendicular to the magnetic field. If k makes an angle of more than 0.25 deg with the magnetic field, the wave passes through the E region without reflection. Kinks in the magnetic field lines (due to auroral currents) may lead to trapping of waves in layers less than 1 km thick. Secondary irregularities may be limited in both horizontal and vertical extent because of their motion relative to the primary waves on which they depend for growth. The processes determining the amplitude of irregularities have also been considered in the light of this work. Several observed features of radio aurora may have explanations in terms of these properties of energy propagation.

84A34615* ISSUE 15 PAGE 2183 CATEGORY 46 84/05/01 22 PAGES UNCLASSIFIED DOCUMENT

UTTL: Wave normal directions of chorus near the equatorial source region

AUTH: A/GOLDSTEIN, B. E.; B/TSURUTANI, B. T. PAA: B/(California Institute of Technology, Jet Propulsion Laboratory, Pasadena, CA)

CORP: Jet Propulsion Lab., California Inst. of Tech., Pasadena.

Journal of Geophysical Research (ISSN 0148-0227), vol. 89, May 1, 1984, p. 2789-2810. NASA-supported research.

MAJS: /*DAWN CHORUS/*ELECTROMAGNETIC WAVE TRANSMISSION/* EQUATORIAL REGIONS/*WAVE DISPERSION/*WHISTLERS

MINS: / AURORAL ZONES/ MAGNETIC VARIATIONS/ OGO-5/ SATELLITE OBSERVATION/ WAVE PROPAGATION

ABA: C.R.

ABS: OGO 5 triaxial search coil magnetometer data are used to determine the wave propagation directions of postmidnight.chorus in the near-equatorial region at L shells of 6 to 7. The methods used to estimate the wave normal directions involved minimum variance, the imaginary part of the cross-spectral matrix, the eigenvector of the Hermitian cross-spectral matrix, and a fitting of dispersion relations for one-wave and two-wave models to the cross-spectral matrix. Wave propagation at all frequencies within chorus tones is found to occur most frequently along the magnetic field with median and average cone angles of 9.1 deg and 12.2 deg, respectively. It is concluded that for waves propagating parallel to B, wave growth is maximum.

84A34315 ISSUE 15 PAGE 2180 CATEGORY 46 84/05/00 4 PAGES UNCLASSIFIED DOCUMENT

UTTL: First experimental evidence of HF produced electron density irregularities in the polar ionosphere, diagnosed by UHF radio star scintillations

AUTH: A/FREY, A.; B/STUBBE, P.; C/KOPKA, H. PAA: C/(Max-Planck-Institut fuer Aeronomie, Katlenburg, West Germany)

Geophysical Research Letters (ISSN 0094-8276), vol. 11, May 1984, p. 523-526. Research supported by the Deutsche Forschungsgemeinschaft.

MAJS: /*HIGH FREQUENCIES/*IONOSPHERIC DISTURBANCES/* IONOSPHERIC ELECTRON DENSITY/*IONOSPHERIC PROPAGATION /*POLAR REGIONS/*RADIO STARS

MINS: / RADIO TRANSMISSION/ SCINTILLATION/ ULTRAHIGH FREQUENCIES

ABA: C.M.

ABS: Observations made on May 10 and September 9, 1983, during which large scale irregularities in the ionosphere were excited by the HF facility at Tromso, Norway, are discussed. The observations were detected using radio star scintillations at 933 MHz, and the HF-beam was pointed 10-15 deg south. Observations made on September 9 showed the HF-power density threshold to be 22 microW/sq m. It was determined that shorter scale irregularities appear to be preferentially produced during lower HF-power and are not the result of cascading from larger scale irregularities. Consequently, HF-power density thresholds for short scale irregularities do not concur with values proposed by Cragin et al. (1977). Also noted were the irregular growth times (about 10-40 sec) and decay times (1-3 min).

84A34082 ISSUE 15 PAGE 2178 CATEGORY 46
84/04/00 12 PAGES In RUSSIAN UNCLASSIFIED DOCUMENT

UTTL: Plasma convection in the polar ionosphere - Comparison of Cosmos-184-satellite measurements with a model that depends on the IMF vector

AUTH: A/BELOV, B. A.; B/GALPERIN, IU. I.; C/ZININ, L. V.; D/LEVITIN, A. E.; E/AFONINA, R. G.; F/FELDSHTEIN, IA. I.
Kosmicheskie Issledovaniia (ISSN 0023-4206), vol. 22, Mar.-Apr. 1984, p. 201-212. In Russian.

MAJS: /*CONVECTIVE FLOW/*IONOSPHERIC PROPAGATION/*MAGNETOPLASMADYNAMICS/*POLAR REGIONS/*SPACE PLASMAS

MINS: / ATMOSPHERIC MODELS/ COSMOS SATELLITES/ ELECTRIC FIELDS/ FLOW VELOCITY/ MAGNETOHYDRODYNAMIC FLOW/ SATELLITE SOUNDING

ABA: B.J.

ABS: Consideration is given to an IMF-dependent model of the planetary distribution of field-aligned current, large-scale electric field, and plasma convection velocity. Parameters along the trajectories of the Cosmos-184 and Cosmos-484 satellites are calculated using this model, and the calculated results are compared with direct measurements of convection velocity and electric field from these satellites. It is shown that, above the illuminated polar cap, the correlation model of the electric field (calculated assuming uniform ionospheric conductivity) is in satisfactory agreement with experimental data. The scale coefficient, depending on the ionospheric conductivity, the earth's conductivity, and other factors, is determined as a result of the comparison.

84A26527# ISSUE 11 PAGE 1601 CATEGORY 46
84/00/00 13 PAGES In GERMAN UNCLASSIFIED DOCUMENT

UTTL: Aeronomic research in northern Scandinavia from 1940 to 1945

AUTH: A/LANGE-HESSE, G. PAA: A/(Max-Planck-Institut fuer Aeronomie, Katlenburg, West Germany)
(International Union of Radio Science and Nachrichtentechnische Gesellschaft, Gemeinsame Tagung, Kleinheubach, West Germany, Oct. 3-7, 1983)
Kleinheubacher Berichte (ISSN 0343-5725), vol. 27, 1984, p. 505-517. In German.

MAJS: /*AERONOMY/*AURORAL ZONES/*IONOSPHERIC PROPAGATION/*POLAR CAP ABSORPTION/*RADIO FREQUENCY INTERFERENCE/*SHORT WAVE RADIO TRANSMISSION

MINS: / GEOMAGNETISM/ POLAR RADIO BLACKOUT/ RADIO TRANSMISSION/ SCANDINAVIA

84A24577 ISSUE 9 PAGE 1276 CATEGORY 46
84/01/00 5 PAGES UNCLASSIFIED DOCUMENT

UTTL: Interplanetary magnetic field structure and the variations of the ELF and VLF emissions in the topside ionosphere

AUTH: A/LARKINA, V. I.; B/LIKHTER, IA. I. PAA: B/(Akademiia Nauk SSSR, Institut Zemnogo Magnetizma Ionosfery i Rasprostraneniia Radiovoln, Troitsk, USSR)
Journal of Atmospheric and Terrestrial Physics (ISSN 0021-9169), vol. 46, Jan. 1984, p. 5-9.

MAJS: /*EXTREMELY LOW RADIO FREQUENCIES/*INTERPLANETARY MAGNETIC FIELDS/*IONOSPHERIC PROPAGATION/*RADIO EMISSION/*VERY LOW FREQUENCIES

MINS: / AURORAL ZONES/ FIELD STRENGTH/ POLAR CAPS

ABA: Author

ABS: The Intercosmos-13 data obtained when measuring ELF and VLF emission amplitudes during the vernal equinox of 1975 at auroral latitudes and over the polar caps are compared with certain IMF parameters, namely the polarity of the sector structure and the signs and magnitudes of the By and Bz components of the IMF as defined in the Solar Ecliptic coordinate systems (Nishida, 1978). The comparison shows that: (1) the positive polarity of the IMF sector structure (when the IMF vector is directed toward the earth) involves an enhanced probability of the detection of larger emission field intensities (greater than 25-30 dB); (2) the emission median intensity is approximately 20 dB higher at By greater than 0 than at By less than 0; (3) the 0.72 kHz emission median intensity in the polar caps at night-side auroral latitudes is lower when Bz is greater than 0 than when Bz is less than 0; and (4) at vernal equinox there is no north-south asymmetry in the dependence of ELF and VLF emission intensity on the IMF parameters.

84A24132 ISSUE 9 PAGE 1275 CATEGORY 46
83/00/00 6 PAGES In RUSSIAN UNCLASSIFIED DOCUMENT

UTTL: Dynamics of the parameters of the inhomogeneous structure of the auroral ionosphere during substorms

AUTH: A/BLAGOVESHCHENSKII, D. V.; B/BLAGOVESHCHENSKAIA, N. F.; C/PIROG, O. M.
Ionosfernye Issledovaniia, no. 37, 1983, p. 80-85. In Russian.

MAJS: /*AURORAL ZONES/*E REGION/*IONOSPHERIC DISTURBANCES/*POLAR SUBSTORMS

MINS: / INHOMOGENEITY/ NIGHT SKY/ RADIO TRANSMISSION/ RECEPTION DIVERSITY/ SPORADIC E LAYER/ TIME RESPONSE

ABA: C.R.

ABS: Data from frequency-diversity reception along a radio path 1400 km long that passes by the zone of polar auroras are used in investigating the dynamics governing the parameters of the fine structure of the

nighttime auroral E region. Stable patterns are detected in the variations of the fine structure parameters and of the characteristics of the Es formations during substorms. Mechanisms that may explain the origin of small-scale inhomogeneities in the auroral E region of the ionosphere during the various phases of a substorm are considered.

84A24131 ISSUE 9 PAGE 1275 CATEGORY 46
83/00/00 7 PAGES In RUSSIAN UNCLASSIFIED DOCUMENT
UTTL: Scintillations of satellite signals caused by the structure of the high-latitude ionosphere
AUTH: A/SOLODOVNIKOV, G. K.; B/DRUKARENKO, S. P.; C/RUSSKIN, V. M.
Ionosfernye Issledovaniia, no. 37, 1983, p. 73-79. In Russian.
MAJS: /*IONOSPHERIC PROPAGATION/*SATELLITE TRANSMISSION/*SCINTILLATION/*SIGNAL DISTORTION
MINS: / AMPLITUDES/ ATMOSPHERIC TURBULENCE/ MAGNETIC VARIATIONS/ POLAR REGIONS
ABA: C.R.
ABS: Experimental data are presented that validate a Nakagami distribution of the scintillations in the amplitudes of satellite signals in the high-latitude ionosphere given a magnetic activity (K sub p) less than or equal to 5. A relation is obtained linking the s1-s4 scintillation indices to the parameter m (distribution). The increase seen in the fluctuations of satellite signal amplitudes with magnetic activity is explained by the formation of a partially ordered turbulent structure in the ionosphere.

84A22030 ISSUE 8 PAGE 1064 CATEGORY 32
83/11/00 9 PAGES In RUSSIAN UNCLASSIFIED DOCUMENT
UTTL: Approximation of the statistical properties of a communication channel by a generalized power model
AUTH: A/BASALAEV, M. L.
Radiotekhnika i Elektronika (ISSN 0033-8494), vol. 28, Nov. 1983, p. 2129-2137. In Russian.
MAJS: /*CHANNELS (DATA TRANSMISSION)/*COMMUNICATION THEORY/*ELECTROMAGNETIC NOISE/*RADIO TRANSMISSION/*STATISTICAL ANALYSIS
MINS: / APPROXIMATION/ ARCTIC REGIONS/ PROBABILITY DISTRIBUTION FUNCTIONS/ SIGNAL DETECTION/ SIGNAL TO NOISE RATIOS
ABA: B.J.
ABS: A universal model for the probability distribution functions of an additive radio noise envelope in the case of narrow-band reception is presented. The model is applied to signal detection on a background of atmospheric radio noise for the case of VLF and LF radio wave propagation in the eastern Arctic. The results are discussed in relation to the use of optimal and quasi-optimal limiters in radio-navigation receiving systems.

84A21561 ISSUE 8 PAGE 1118 CATEGORY 46
83/00/00 208 PAGES In RUSSIAN UNCLASSIFIED DOCUMENT
UTTL: Additional energy losses in high-latitude radio links --- Russian book
AUTH: A/ZHULINA, E. M.; B/KISHCHA, P. V.; C/LUKASHKIN, V. M.; D/SHIROCHKOV, A. V.
Moscow, Izdatel'stvo Nauka, 1983, 208 p. In Russian.
MAJS: /*AURORAL ABSORPTION/*IONOSPHERIC PROPAGATION/*POLAR RADIO BLACKOUT/*RADIO ATTENUATION/*SHORT WAVE RADIO TRANSMISSION/*TRANSMISSION LOSS
MINS: / AURORAL IONIZATION/ GEOMAGNETISM/ IONOSPHERIC DISTURBANCES/ IONOSPHERIC ELECTRON DENSITY/ MICROWAVE ATTENUATION/ RIOMETERS/ SATELLITE TRANSMISSION/ SIGNAL FADING/ SOLAR TERRESTRIAL INTERACTIONS
ABA: V.L.
ABS: The study is concerned with energy losses in high-latitude short-wave radio links due to auroral absorption. Attention is given to the basic structural characteristics of the high-latitude ionosphere, the morphology of anomalous absorption, and the results of a statistical analysis of empirical data on the absorption of cosmic radio-frequency radiation. An empirical-statistical model of auroral absorption is developed. A method is proposed for estimating the probabilities of energy losses in radio links on the basis of the model proposed here.

84A19512 ISSUE 7 PAGE 954 CATEGORY 46 83/12/00
5 PAGES In RUSSIAN UNCLASSIFIED DOCUMENT
UTTL: The use of data of the oblique sounding of the ionosphere to check trajectory calculations for high-latitude radio paths
AUTH: A/VOVK, V. IA.; B/SHIROCHKOV, A. V. PAA: B/(Gosudarstvennyi Komitet SSSR po Gidrometeorologii i Kontroliu Prirodnoi Sredy, Arkticheskii i Antarkticheskii Nauchno-Issledovatel'skii Institut, Leningrad, USSR)
Geomagnetizm i Aeronomiia (ISSN 0016-7940), vol. 23, Nov.-Dec. 1983, p. 946-950. In Russian.
MAJS: /*IONOSPHERIC SOUNDING/*OBLIQUENESS/*POLAR REGIONS/*SHORT WAVE RADIO TRANSMISSION/*TRAJECTORY ANALYSIS
MINS: / MATHEMATICAL MODELS/ MIDLATITUDE ATMOSPHERE
ABA: B.J.
ABS: The accuracy of model calculations of trajectories of short-wave signals for both the midlatitude and polar ionosphere is assessed on the basis of oblique-sounding data. The limits of existing models

for high-latitude radio paths are indicated, and ways to increase the accuracy of model calculations for such paths are discussed.

84A18049# ISSUE 6 PAGE 790 CATEGORY 46 RPT#: AIAA PAPER 84-0376 84/01/00 9 PAGES UNCLASSIFIED DOCUMENT

UTTL: Remote sensing of the high latitude ionosphere

AUTH: A/MIZERA, P. F.; B/GORNEY, D. J. PAA: B/(Aerospace Corp., Los Angeles, CA)

American Institute of Aeronautics and Astronautics, Aerospace Sciences Meeting, 22nd, Reno, NV, Jan. 9-12, 1984. 9 p.

MAJS: /*IONOSPHERIC PROPAGATION/*IONOSPHERIC SOUNDING/*POLAR REGIONS/*SATELLITE IMAGERY

MINS: / AURORAL ZONES/ E REGION/ IONOSPHERIC CONDUCTIVITY/ IONOSPHERIC ION DENSITY/ SATELLITE SOUNDING

ABA: Author

ABS: Remote sensing of the earth's ionosphere has many applications to radio wave communications. Techniques to monitor perturbations of the quiescent ionosphere at high latitudes from satellites are described, which include observations in the visible, ultra-violet and X-ray wavelengths.

84A15656 ISSUE 4 PAGE 459 CATEGORY 46 82/00/00 4 PAGES UNCLASSIFIED DOCUMENT

UTTL: Ionospheric scintillation monitoring using GPS

AUTH: A/RINO, C. L.; B/COUSINS, M. D.; C/WALKER, N. B.; D/KLOBUCHAR, J. A. PAA: C/(SRI International, Menlo Park, CA); D/(USAF, Geophysics Laboratory, Bedford, MA)

IN: NTC '82; National Telesystems Conference, Galveston, TX, November 7-10, 1982, Conference Record (A84-15623 04-32). New York, Institute of Electrical and Electronics Engineers, Inc., 1982, p. C1.3.1-C1.3.4.

MAJS: /*GLOBAL POSITIONING SYSTEM/*IONOSPHERIC PROPAGATION/*SCINTILLATION/*SIGNAL MEASUREMENT

MINS: / AURORAL ZONES/ IONOSPHERIC DISTURBANCES/ IONOSPHERIC DRIFT/ IONOSPHERIC SOUNDING/ MICROWAVE ATTENUATION/ PHASE DEVIATION/ SATELLITE TRANSMISSION

ABA: Author

ABS: When fully deployed, the GPS system will provide a unique resource for continuous ionospheric monitoring to detect both naturally occurring and man-made disturbances. The use of appropriate data analysis techniques makes it feasible to measure both large-scale (total electron content) and small-scale (scintillation) disturbances. The results of a recent set of observations made at Poker Flat, Alaska-an auroral-zone station where a variety of naturally occurring propagation disturbances occur, are described. Two independent receiver systems were used. By taking advantage of the known transmission times of the signals, standard correlation methods could be applied to determine the irregularity drift component along the receiver baseline. The results are consistent with simultaneous radar data.

84A12170 ISSUE 2 PAGE 193 CATEGORY 46 82/00/00 23 PAGES In RUSSIAN UNCLASSIFIED DOCUMENT

UTTL: Preliminary results obtained from measuring the height characteristics of a radio aurora at a frequency of 90 MHz

AUTH: A/TIMOFEEV, E. E.; B/MIROSHNIKOV, IU. G.

IN: The physics of the polar ionosphere (A84-12161 02-46). Leningrad, Izdatel'stvo Nauka, 1982, p. 120-142. In Russian.

MAJS: /*AURORAL ECHOES/*AURORAL ELECTROJETS/*IONOSPHERIC PROPAGATION/*MICROWAVE SCATTERING/*POLAR SUBSTORMS/*RADIO AURORAS

MINS: / ALTITUDE/ LOWER IONOSPHERE/ MICROWAVE INTERFEROMETERS/ RADAR ECHOES

ABA: C.R.

ABS: On the basis of two substorms, various dependences of the height characteristics are studied in relation to other geophysical data. A definite difference is found between the scattering heights in the eastern and western radar scanning sectors. In addition, a two-layer height structure is detected in the local centers of a diffuse radio aurora, and the spatiotemporal characteristics of this structure forms in the lower ionosphere.

84A12169 ISSUE 2 PAGE 193 CATEGORY 46 82/00/00 10 PAGES In RUSSIAN UNCLASSIFIED DOCUMENT

UTTL: An experimental evaluation of the diurnal variations in the secondary component of a VLF signal on an auroral path

AUTH: A/BELOGLAZOV, M. I.; B/REMENETS, G. F.

IN: The physics of the polar ionosphere (A84-12161 02-46). Leningrad, Izdatel'stvo Nauka, 1982, p. 110-119. In Russian.

MAJS: /*DIURNAL VARIATIONS/*IONOSPHERIC PROPAGATION/*LOWER IONOSPHERE/*RADIO AURORAS/*SIGNAL MEASUREMENT/*VERY LOW FREQUENCIES

MINS: / ANNUAL VARIATIONS/ DEPOLARIZATION/ GEOMAGNETISM/ PHASE CONTRAST/ POLAR REGIONS

ABA: C.R.

ABS: The presence of the secondary component is caused by the ionospheric properties that have to do with magnetic activity. It is shown that on a daytime auroral path, the ratio of the secondary to the

primary component is less than or approximately equal to 3 percent; in winter, however, the value is greater than or approximately equal to 4-7 percent. At nighttime during the summer the value is approximately 2-3 percent in about half the cases; during the winter it is often greater than or approximately equal to 15-30 percent. From statistical processing of the measurements, regular features in the behavior of the secondary component during a change in illumination conditions on the path are determined.

84A12165 ISSUE 2 PAGE 193 CATEGORY 46 82/00/00
13 PAGES In RUSSIAN UNCLASSIFIED DOCUMENT
UTTL: Morphological characteristics of inhomogeneous structures in the upper ionosphere
AUTH: A/SOLODOVNIKOV, G. K.; B/BAKAI, A. S.; C/RUSSKIN, V. M.
IN: The physics of the polar ionosphere (A84-12161 02-46). Leningrad, Izdatel'stvo Nauka, 1982, p. 78-90. In Russian.
MAJS: /*IONOSPHERIC ELECTRON DENSITY/*TRAVELING IONOSPHERIC DISTURBANCES/*UPPER IONOSPHERE
MINS: / GEOMAGNETISM/ IONOSPHERIC SOUNDING/ MIDLATITUDE ATMOSPHERE/ POLAR REGIONS/ STATISTICAL ANALYSIS/ WAVE PROPAGATION
ABA: C.R.
ABS: The statistical and energy characteristics of the fluctuations in electron concentration in inhomogeneous structures in the upper high-latitude and midlatitude ionosphere are analyzed in an investigation of height-latitude relationships. The experimental data were obtained from probes of the ionosphere made from the exterior of the satellite Alouett 1. It is contended that large-scale inhomogeneities in electron concentration have a wavelike structure and occur at heights up to at least 1000 km. These inhomogeneities are excited mainly in the high-latitude ionosphere; their propagation is toward the equator.

84A12161 ISSUE 2 PAGE 192 CATEGORY 46 82/00/00
148 PAGES In RUSSIAN UNCLASSIFIED DOCUMENT
UTTL: The physics of the polar ionosphere
AUTH: A/RASPOPOV, O. M. PAT: A/ED.
Leningrad, Izdatel'stvo Nauka, 1982, 148 p. In Russian.
MAJS: /*ATMOSPHERIC PHYSICS/*IONOSPHERE/*POLAR REGIONS
MINS: / AURORAL ZONES/ GEOMAGNETISM/ IONOSPHERIC DISTURBANCES/ IONOSPHERIC DRIFT/ IONOSPHERIC ELECTRON DENSITY/ IONOSPHERIC HEATING/ IONOSPHERIC ION DENSITY/ IONOSPHERIC PROPAGATION/ IONOSPHERIC SOUNDING/ IONOSPHERIC TEMPERATURE/ PERIODIC VARIATIONS/ RADIO AURORAS/ RECEPTION DIVERSITY/ WIND MEASUREMENT
ABA: C.R.
ABS: Topics discussed include the modeling of physical processes in the polar ionosphere, the dynamics of the polar ionosphere, and ionospheric inhomogeneities. An evaluation is made of the diurnal variations in the secondary component of a VLF signal on an auroral path. The dynamics of the polar ionosphere are investigated using data on drifts and wind obtained by means of diversity reception during vertical sounding. The daily and seasonal changes in the velocities of ion drifts and winds in the auroral zone are also studied. For individual items see A84-12162 to A84-12170

83A49540 ISSUE 24 PAGE 3608 CATEGORY 46
83/00/00 5 PAGES In RUSSIAN UNCLASSIFIED DOCUMENT
UTTL: A possible cause of the winter disturbance of the ionospheric D-region
AUTH: A/RAPOPORT, Z. TS. PAA: A/(Akademiia Nauk SSSR, Institut Zemnogo Magnetizma, Ionosfery i Rasprostraneniia Radiovoln, Troitsk, USSR)
Akademiia Nauk SSSR, Doklady (ISSN 0002-3264), vol. 271, no. 5, 1983, p. 1103-1107. In Russian.
MAJS: /*D REGION/*IONOSPHERIC PROPAGATION/*POLAR CAP ABSORPTION/*POLAR METEOROLOGY/*TRAVELING IONOSPHERIC DISTURBANCES/*WINTER
MINS: / ATMOSPHERIC CIRCULATION/ ATMOSPHERIC DENSITY/ AURORAL ZONES/ MIDLATITUDE ATMOSPHERE/ PARTICLE PRECIPITATION/ RADIO ATTENUATION
ABA: B.J.
ABS: A possible mechanism for the winter anomaly of the D-region, manifested in the elevated absorption of radio waves in winter months, is suggested. It is proposed that both the regular and excess winter absorptions are determined by the location and intensity of the circumpolar vortex together with the varying intensity of particle precipitation in the auroral zone. This mechanism can also explain the poststorm effect (increased ionospheric absorption at midlatitudes, observed during and after the restoration phase of magnetic storms) which is often associated only with the immediate precipitation of particles.

83A46060# ISSUE 22 PAGE 3328 CATEGORY 46
83/09/01 6 PAGES UNCLASSIFIED DOCUMENT
UTTL: Parametric excitation and suppression of convective plasma instabilities in the high-latitude F region ionosphere
AUTH: A/KESKINEN, M. J.; B/OSSAKOW, S. L.; C/CHATURVEDI, P. K. PAA: B/(U.S. Navy, Naval Research Laboratory,

Washington, DC); C/(Science Applications, Inc., McLean, VA)
Journal of Geophysical Research (ISSN 0148-0227), vol. 88, Sept. 1, 1983, p. 7239-7244. Research supported by the U.S. Defense Nuclear Agency and U.S. Navy.
MAJS: /*AURORAL ZONES/*CONVECTION CURRENTS/*F REGION/*IONOSPHERIC DRIFT/*IONOSPHERIC PROPAGATION/*MAGNETOHYDRODYNAMIC STABILITY
MINS: / IONOSPHERIC CURRENTS/ IONOSPHERIC ELECTRON DENSITY/ PLASMA WAVES/ PLASMA-ELECTROMAGNETIC INTERACTION/ POLAR REGIONS
ABA: Author
ABS: Parametric coupling processes of a large-amplitude electromagnetic pump wave with convective plasma fluid instabilities (E cross B gradient drift and current convective) in the high-latitude F region ionosphere have been studied. It is found that a pump wave, with frequency near the upper hybrid frequency and with electric field component perpendicular to the ambient magnetic field, can stabilize or destabilize the E cross B gradient drift and/or current convective instability. For parameters typical of the nighttime high-latitude F region ionosphere, stabilization or destabilization is found with a vertically incident O mode carrying a free space incident power density of the order of 0.0001 W/sq m.

83A41381 ISSUE 19 PAGE 2831 CATEGORY 32
82/00/00 5 PAGES UNCLASSIFIED DOCUMENT
UTTL: Low elevation angle site diversity satellite communications for the Canadian Arctic
AUTH: A/MIMIS, V.; B/SMALLEY, A. PAA: B/(Telesat Canada, Ottawa, Canada)
IN: ICC '82 - The digital revolution; International Conference on Communications, Philadelphia, PA, June 13-17, 1982, Conference Record. Volume 2 (A83-41326 19-32). New York, Institute of Electrical and Electronics Engineers, 1982, p. 4A.4.1-4A.4.5.
MAJS: /*ARCTIC REGIONS/*CANADIAN SPACE PROGRAMS/*DOMESTIC SATELLITE COMMUNICATIONS SYSTEMS/*ELEVATION ANGLE/*RECEPTION DIVERSITY/*RELIABILITY ENGINEERING
MINS: / ATMOSPHERIC REFRACTION/ SIGNAL FADING/ SYNCHRONOUS SATELLITES/ SYSTEMS ENGINEERING/ TEMPERATURE INVERSIONS/ TRANSMISSION EFFICIENCY
ABA: O.C.
ABS: In order to provide reliable satellite communications services for the Canadian Arctic, where geostationary satellite transmissions encounter both low elevation angles and temperature inversion effects during the summer months, a system employing two appropriately separated earth stations is being implemented by Telesat Canada. This space-diverse earth station system, which is the first of its kind for a commercial satellite communications system, is expected to compensate for the atmospheric refractive index irregularities which cause severe 6/4 GHz frequency band signal fluctuations. On the basis of experimental data, the new system's independent signal paths will reduce the required propagation margins from 20 to about 8 dB.

83A40803 ISSUE 18 PAGE 2720 CATEGORY 46
82/00/00 240 PAGES In RUSSIAN UNCLASSIFIED DOCUMENT
UTTL: Propagation of VLF radio waves at high latitudes --- Russian book
AUTH: A/BELOGLAZOV, M. I.; B/REMENETS, G. F.
Leningrad, Izdatel'stvo Nauka, 1982, 240 p. In Russian.
MAJS: /*LONG WAVE RADIATION/*POLAR REGIONS/*RADIO TRANSMISSION/*VERY LOW FREQUENCIES/*VLF EMISSION RECORDERS/*WAVE PROPAGATION
MINS: / AURORAL ZONES/ BALLOON SOUNDING/ CIRCUIT DIAGRAMS/ IONOSPHERIC DISTURBANCES/ IONOSPHERIC ELECTRON DENSITY / IONOSPHERIC PROPAGATION/ ISOTROPIC MEDIA/ SOLAR TERRESTRIAL INTERACTIONS/ TOPOLOGY
ABA: B.J.
ABS: Results of studies of the high-latitude propagation of VLF waves are generalized and systematized. Attention is given to the characteristics of VLF wave propagation in quiet conditions and after solar flares; and to measurements of high-latitude VLF fields arising during periods of the precipitation of high-energy fluxes of solar protons and relativistic electrons. The effect of auroral disturbances on VLF propagation conditions is investigated. Particular attention is given to the relationship between variations of VLF signals and riometer and balloon data; phase fluctuation spectra of VLF signals and their dependence on the auroral disturbance level are evaluated. The possibility of predicting auroral and proton VLF anomalies is considered.

83A38375 ISSUE 17 PAGE 2544 CATEGORY 46
83/04/00 5 PAGES UNCLASSIFIED DOCUMENT
UTTL: Collision frequencies in the high-latitude D-region
AUTH: A/FRIEDRICH, M.; B/TORKAR, K. M. PAA: B/(Graz, Technische Universitaet, Graz, Austria)
Journal of Atmospheric and Terrestrial Physics (ISSN 0021-9169), vol. 45, April 1983, p. 267-271. Research supported by the Fonds zur Foerderung der Wissenschaftlichen Forschung.
MAJS: /*D REGION/*ELECTRON SCATTERING/*PARTICLE COLLISIONS/*POLAR REGIONS
MINS: / ANNUAL VARIATIONS/ ATMOSPHERIC MODELS/ CROSS

SECTIONS/ FREQUENCIES/ IONOSPHERIC PROPAGATION/ RADIO WAVES
ABA: Author
ABS: D-region collision frequencies derived from rocket flights are subjected to a harmonic seasonal analysis. The proportionality between collision frequency and pressure has been derived and found to be in excellent agreement with laboratory data. Some implications of the results are discussed.

83A38369 ISSUE 17 PAGE 2543 CATEGORY 46 CNT#: NSF ATM-80-02423 NSF ATM-80-06496 83/04/00 10 PAGES UNCLASSIFIED DOCUMENT
UTTL: Autumn and winter anomalies in ionospheric absorption as measured by riometers
AUTH: A/ROSENBERG, T. J.; B/DETRICK, D. L.; C/RANTA, H.; D/RANTA, A. PAA: B/(Maryland, University, College Park, MD)
Journal of Atmospheric and Terrestrial Physics (ISSN 0021-9169), vol. 45, April 1983, p. 193-202. Research supported by the Academy of Finland.
MAJS: /*ANNUAL VARIATIONS/*COSMIC NOISE/*IONOSPHERIC PROPAGATION/*RADIO ATTENUATION/*RIOMETERS
MINS: / ANOMALIES/ AURORAL ZONES/ D REGION/ ELECTROMAGNETIC ABSORPTION/ EQUATORIAL ATMOSPHERE/ F REGION/ FINLAND/ TEMPERATE REGIONS
ABA: Author
ABS: Seasonal variation of ionospheric absorption has been studied on the basis of riometer (A2) measurements obtained over a wide latitude range. In agreement with the results of earlier studies of A1 radio wave absorption, equinoctial maxima of approximately equal amplitude are observed in the auroral zone and near the equator. At mid-latitudes riometer absorption maximizes during the fall season, whereas the A1 data show a semi-annual variation with maxima occurring in summer and winter. The autumn maximum, or autumn anomaly, in riometer absorption is observed at much higher geographic latitude in the southern than in the northern hemisphere but at comparable geomagnetic latitudes in both hemispheres. The secondary maximum in riometer absorption at mid-latitudes during the winter months, the winter anomaly, is seen only if absorption is calculated at constant solar zenith angle. The different methods for determining a quiet-day curve are discussed.

83A33034 ISSUE 14 PAGE 2054 CATEGORY 46
83/00/00 9 PAGES In RUSSIAN UNCLASSIFIED DOCUMENT
UTTL: The D region under the conditions of nighttime PCA - The rate of transformation of positive ion clusters and negative ions
AUTH: A/SMIRNOVA, N. V.
Ionosfernye Issledovaniia, no. 35, 1983, p. 67-75. In Russian.
MAJS: /*D REGION/*ION PRODUCTION RATES/*IONOSPHERIC ION DENSITY/*POLAR CAP ABSORPTION
MINS: / IONOSPHERIC PROPAGATION/ NEGATIVE IONS/ NIGHT SKY/ NOCTURNAL VARIATIONS/ POSITIVE IONS

83A33033 ISSUE 14 PAGE 2054 CATEGORY 46
83/00/00 4 PAGES In RUSSIAN UNCLASSIFIED DOCUMENT
UTTL: Transformation of the spectrum of energetic protons during the motion through the atmosphere
AUTH: A/PETROVA, G. A.
Ionosfernye Issledovaniia, no. 35, 1983, p. 63-66. In Russian.
MAJS: /*ENERGY SPECTRA/*IONOSPHERIC ION DENSITY/*PARTICLE MOTION/*PROTON PRECIPITATION
MINS: / ATMOSPHERIC BOUNDARY LAYER/ ATMOSPHERIC IONIZATION/ ION PRODUCTION RATES/ IONOSPHERIC PROPAGATION/ POLAR CAP ABSORPTION
ABA: C.R.
ABS: A formula for the differential spectrum of protons at a particular height is derived on the basis of the spectrum's shape at the boundary of the atmosphere. The method employed in solving the problem of the transformation of the primary spectrum is taken from a study by Maeda (1963), where the flux of ionizing particles entering the atmosphere along the normal is treated. The solution is generalized here for the case of the isotropic incidence of the flux on a hemisphere. In solving the problem of the primary spectrum's transformation, the energy is replaced by the range of the particle path; this is the maximum depth of penetration into the atmosphere of a particle during its motion along the normal. It is shown that the relationship between the range of the particle path and the energy can be obtained from the rate at which the energy of the protons is lost per unit of penetration depth in the atmosphere.

83A30774 ISSUE 13 PAGE 1815 CATEGORY 19
82/00/00 4 PAGES UNCLASSIFIED DOCUMENT
UTTL: Bars - A dual bistatic auroral radar system for the study of electric fields in the Canadian sector of the auroral zone
AUTH: A/MCNAMARA, A. G.; B/MCDIARMID, D. R.; C/SOFKO, G. J.; D/KOEHLER, J. A.; E/FORSYTH, P. A.;

F/MOORCORFT, D. R. PAA: B/(National Research Council, Ottawa, Canada); D/(Saskatchewan, University, Saskatoon, Canada); F/(Western Ontario, University, London, Canada)
(COSPAR and International Union of Radio Science, Workshop on Instruments and Analysis Techniques for Space Physics, Ottawa, Canada, May 16-June 2, 1982)
Advances in Space Research (ISSN 0273-1177), vol. 2, no. 7, 1982, p. 145-148.

MAJS: /*ATMOSPHERIC ELECTRICITY/*AURORAL ZONES/*IONOSPHERIC SOUNDING/*RADAR MEASUREMENT

MINS: / ANTENNA DESIGN/ CANADA/ DATA TRANSMISSION/ DOPPLER RADAR/ ELECTRIC FIELDS/ RADAR RECEIVERS/ RADAR TRANSMITTERS/ SIGNAL PROCESSING

83A30609 ISSUE 13 PAGE 1875 CATEGORY 46
82/00/00 12 PAGES In RUSSIAN UNCLASSIFIED DOCUMENT

UTTL: Investigation of ionospheric irregularities by radio holography

AUTH: A/TERESHCHENKO, E. D.; B/POPOV, A. A.; C/TERESHCHENKO, A. D.; D/KHUDUKON, B. Z.
IN: Investigation of the high-latitude ionosphere and magnetosphere of the earth (A83-30601 13-46). Leningrad, Izdatel'stvo Nauka, 1982, p. 90-101. In Russian.

MAJS: /*IONOSPHERIC DISTURBANCES/*MICROWAVE HOLOGRAPHY/*POLAR REGIONS/*RADIO PROBING/*SATELLITE SOUNDING

MINS: / COHERENT ELECTROMAGNETIC RADIATION/ DELTA FUNCTION/ DIFFRACTION PATTERNS/ DOPPLER EFFECT/ IONOSPHERIC ELECTRON DENSITY/ IONOSPHERIC PROPAGATION/ IONOSPHERIC SOUNDING/ SATELLITE-BORNE INSTRUMENTS/ WAVE DISPERSION

ABA: B.J.

ABS: Methodological aspects of the design of a radio-holography experiment for the investigation of ionospheric irregularities are considered on the basis of a theoretical examination of the formation of a diffraction field by two coherent satellite signals. The equipment needed to implement such an experiment is described, and results of first observations performed at high latitudes (in the Murmansk region) on February 8, 1978 are examined.

83A30608 ISSUE 13 PAGE 1875 CATEGORY 46
82/00/00 8 PAGES In RUSSIAN UNCLASSIFIED DOCUMENT

UTTL: Spectra of irregularities of the high-latitude lower ionosphere according to phase VLF measurements

AUTH: A/BELOGLAZOVA, G. P.; B/BELOGLAZOV, M. I.
IN: Investigation of the high-latitude ionosphere and magnetosphere of the earth (A83-30601 13-46). Leningrad, Izdatel'stvo Nauka, 1982, p. 83-90. In Russian.

MAJS: /*AURORAL ABSORPTION/*IONOSPHERIC ELECTRON DENSITY/*IONOSPHERIC PROPAGATION/*POLAR REGIONS/*SPECTRUM ANALYSIS

MINS: / DIURNAL VARIATIONS/ FLUCTUATION THEORY/ GEOMAGNETISM / LOWER IONOSPHERE/ MAGNETIC DISTURBANCES/ PHASE SHIFT / SIGNAL MEASUREMENT/ VERY LOW FREQUENCIES

ABA: B.J.

ABS: Experimental data on VLF paths at different orientations and frequencies were used to determine spectra of irregularities of the high-latitude lower ionosphere in the range (1.5-100) x 10 to the -5th/m for quiet and disturbed geophysical conditions. It is shown that all the spectra are described well by a power function with an exponent of about 0.9-1.1. On all the auroral paths studied, the intensity of the spectral components is 2-3 times greater in active periods than in quiet conditions. On a transpolar path at sunset, the intensity increases by 1.5-3 times with increasing activity in the low-frequency part of the spectrum. Purely noctural spectra for quiet and disturbed conditions are practically the same.

83A30607 ISSUE 13 PAGE 1875 CATEGORY 46
82/00/00 4 PAGES In RUSSIAN UNCLASSIFIED DOCUMENT

UTTL: Nonlinear limiting mechanism of Buneman-Farley instability --- in auroral ionosphere

AUTH: A/VOLOSEVICH, A. V.; B/LIPEROVSKII, V. A.; C/LIVSHITS, M. A.
IN: Investigation of the high-latitude ionosphere and magnetosphere of the earth (A83-30601 13-46). Leningrad, Izdatel'stvo Nauka, 1982, p. 80-83. In Russian.

MAJS: /*AURORAL ZONES/*IONOSPHERIC DRIFT/*MAGNETOHYDRODYNAMIC STABILITY/*PLASMA WAVES/*RADAR ECHOES

MINS: / ATMOSPHERIC TURBULENCE/ IONOSPHERIC ELECTRON DENSITY / IONOSPHERIC PROPAGATION/ IONOSPHERIC SOUNDING/ PLASMA TURBULENCE/ WAVE INTERACTION

ABA: B.J.

ABS: A theoretical analysis shows that a quasi-steady state can be established in the auroral ionosphere due to the decay interaction of Buneman-Farley waves. Energy estimates show that this mechanism is a sufficiently effective stabilization mechanism. It is noted that, as a result of such a steady state, it is possible to observe radar echoes from regions of wave turbulence in directions that are almost orthogonal to the electron drift velocity.

83A30606 ISSUE 13 PAGE 1875 CATEGORY 46
82/00/00 7 PAGES In RUSSIAN UNCLASSIFIED DOCUMENT

UTTL: N-S radio-aurora forms

AUTH: A/KOZELOVA, T. V.
IN: Investigation of the high-latitude ionosphere and magnetosphere of the earth (A83-30601 13-46). Leningrad, Izdatel'stvo Nauka, 1982, p. 74-80. In Russian.

MAJS: /*AURORAL ECHOES/*AURORAL ELECTROJETS/*GEOMAGNETISM/*IONOSPHERIC SOUNDING/*RADIO AURORAS/*TRAVELING IONOSPHERIC DISTURBANCES

MINS: / DIURNAL VARIATIONS/ GEOMAGNETIC PULSATIONS/ IONOSPHERIC DRIFT/ IONOSPHERIC PROPAGATION/ MAGNETIC DISTURBANCES/ POLAR REGIONS/ POLAR SUBSTORMS/ RADAR ECHOES

ABA: B.J.

ABS: Radar data obtained in the vicinity of Petrozavodsk are used to study the features of N-S radio-aurora forms. It is shown that simultaneously formed reflecting regions, not more than 10 deg in longitude apart, move together like a kind of quasi-rigid system. In addition, it is found that the direction of auroral latitudinal motion depends on local time. The multiple appearance of the N-S forms and their motion along a parallel are connected with Ps6 magnetic variations. It is suggested that N-S radio-aurora forms are due to the curvature of the ionospheric electrojet.

83A30605 ISSUE 13 PAGE 1875 CATEGORY 46
82/00/00 14 PAGES In RUSSIAN UNCLASSIFIED DOCUMENT

UTTL: Features of radio-aurora observations at the high-latitude station Mirnyi

AUTH: A/SERGEEVA, N. G.; B/SVERDLOV, IU. L.
IN: Investigation of the high-latitude ionosphere and magnetosphere of the earth (A83-30601 13-46). Leningrad, Izdatel'stvo Nauka, 1982, p. 61-74. In Russian.

MAJS: /*ANNUAL VARIATIONS/*ANTARCTIC REGIONS/*AURORAL ECHOES/*GEOMAGNETISM/*IONOSPHERIC SOUNDING/*RADIO AURORAS

MINS: / AURORAL ZONES/ IONOSPHERIC PROPAGATION/ RADAR ECHOES/ RADAR SCATTERING

ABA: B.J.

ABS: The observation of auroral radar echoes at the Mirnyi Antarctic station made it possible to define for the first time the configuration of the high-latitude radio-aurora branch, and to determine the dependence of this branch on magnetic activity and season of the year. This paper examines features of the observation of auroral radar echoes at the Mirnyi station, with attention given to the radio-aurora zone at various moments of invariant local time and to the behavior of the radio-aurora zone at various levels of magnetic activity.

83A30604 ISSUE 13 PAGE 1875 CATEGORY 46
82/00/00 7 PAGES In RUSSIAN UNCLASSIFIED DOCUMENT

UTTL: Observation of a radio-aurora storm by a chain of stations

AUTH: A/SVERDLOV, IU. L.; B/SERGEEVA, N. G.; C/VOLOSHINOV, N. N.
IN: Investigation of the high-latitude ionosphere and magnetosphere of the earth (A83-30601 13-46). Leningrad, Izdatel'stvo Nauka, 1982, p. 55-61. In Russian.

MAJS: /*AURORAL ECHOES/*IONOSPHERIC SOUNDING/*POLAR SUBSTORMS/*RADAR NETWORKS/*RADIO AURORAS

MINS: / AURORAL ELECTROJETS/ IONOSPHERIC DISTURBANCES/ IONOSPHERIC PROPAGATION/ RADAR ECHOES/ SIGNAL DISTORTION

ABA: B.J.

ABS: The paper examines the characteristics of the radio-aurora storm of December 11-12, 1977, observed by radar stations at Ustiuzhna, Bolarskaia, Voldozero, and Loparskaia. It is shown that this chain of stations makes it possible to identify a number of characteristics of storm development, while each of the stations alone gives a picture that is strongly distorted by the foreshortening effect.

83A30603 ISSUE 13 PAGE 1875 CATEGORY 46
82/00/00 14 PAGES In RUSSIAN UNCLASSIFIED DOCUMENT

UTTL: The eastward motion of the radio aurora and auroral loops in the morning sector

AUTH: A/USPENSKII, M. V.; B/GRINVALD, R. A.; C/KAILA, K.; D/KUSTOV, A. V.; E/PELLINEN, R. D.; F/PUDOVKINA, E. V.; G/RASPOPOV, O. M.; H/STARKOV, G. V.
IN: Investigation of the high-latitude ionosphere and magnetosphere of the earth (A83-30601 13-46). Leningrad, Izdatel'stvo Nauka, 1982, p. 41-55. In Russian.

MAJS: /*AURORAL ARCS/*AURORAL ECHOES/*IONOSPHERIC CURRENTS/*MAGNETOSPHERIC INSTABILITY/*RADIO AURORAS/*TRAVELING IONOSPHERIC DISTURBANCES

MINS: / AURORAL ELECTROJETS/ IONOSPHERIC DRIFT/ IONOSPHERIC PROPAGATION/ IONOSPHERIC SOUNDING/ MAGNETIC STORMS/ OPTICAL MEASUREMENT/ POLAR REGIONS/ RADAR ECHOES/ SCINTILLATION

ABA: B.J.

ABS: Results of radar and optical observations made by Scandinavian (STARE) and Soviet stations on March 15, 1978 are examined. In the early morning hours, the development of a microsubstorm and an auroral loop was

observed; these structures moved toward the east and intersected the observation zone. Together with the loops, an electric-field 'discontinuity' arose, which also moved toward the east. An analysis is presented of the form of the radar echo filling the loop. It is suggested that the discontinuity in the electric field is an indicator of a magnetospheric disturbance, and that the observed loops and associated phenomena are a consequence of this disturbance.

83A30602 ISSUE 13 PAGE 1875 CATEGORY 46
82/00/00 38 PAGES In RUSSIAN UNCLASSIFIED DOCUMENT

UTTL: The use of the radio aurora to measure electric fields and currents in the auroral ionosphere
AUTH: A/GREENWALD, R.A.
IN: Investigation of the high-latitude ionosphere and magnetosphere of the earth (A83-30601 13-46). Leningrad, Izdatel'stvo Nauka, 1982, p. 3-40. In Russian.
MAJS: /*AURORAL ECHOES/*IONOSPHERIC CURRENTS/*RADIO AURORAS /*TRAVELING IONOSPHERIC DISTURBANCES
MINS: / AURORAL ELECTROJETS/ CURRENT DENSITY/ DOPPLER RADAR/ GEOMAGNETIC MICROPULSATIONS/ IONOSPHERIC DRIFT/ IONOSPHERIC ELECTRON DENSITY/ IONOSPHERIC PROPAGATION/ IONOSPHERIC SOUNDING/ MAGNETIC STORMS/ MAGNETOHYDRODYNAMIC WAVES/ PHASE VELOCITY/ POLAR REGIONS/ RADAR ECHOES
ABA: B.J.
ABS: Studies on the use of radar to investigate electric fields and currents in the auroral ionosphere are surveyed. Particular consideration is given to the theory of E x B current instability, the growth and propagation characteristics of the radio aurora, the phase velocity of auroral irregularities, and the dependence of radio-aurora intensity on current density. Important geophysical applications of the radio aurora are examined. Attention is given to the use of STARE to investigate electric-field models associated with ionospheric and field-aligned currents, magnetospheric convection, the Harang discontinuity, Pc5 micropulsations, and active substorm phases.

83A30601 ISSUE 13 PAGE 1874 CATEGORY 46
82/00/00 152 PAGES In RUSSIAN UNCLASSIFIED DOCUMENT

UTTL: Investigation of the high-latitude ionosphere and magnetosphere of the earth --- Russian book
AUTH: A/LOGINOV, G. A. PAT: A/ED.
Leningrad, Izdatel'stvo Nauka, 1982, 152 p. In Russian.

MAJS: /*AURORAL ZONES/*IONOSPHERE/*IONOSPHERIC PROPAGATION/* MAGNETOSPHERE/*POLAR REGIONS/*RADIO AURORAS
MINS: / AURORAL ECHOES/ GEOMAGNETISM/ INTERPLANETARY MAGNETIC FIELDS/ IONOSPHERIC CURRENTS/ IONOSPHERIC DISTURBANCES/ IONOSPHERIC DRIFT/ IONOSPHERIC SOUNDING/ MAGNETIC DISTURBANCES/ MAGNETIC VARIATIONS/ MAGNETOSPHERIC INSTABILITY/ PARTICLE PRECIPITATION/ POLAR SUBSTORMS/ RADAR ECHOES/ SPORADIC E LAYER/ TRAVELING IONOSPHERIC DISTURBANCES
ABA: B.J.
ABS: Topics discussed include the eastward motion of the radio aurora and auroral loops in the morning sector, features of the observation of the radio aurora at the Mirnyi Antarctic station, N-S radio-aurora forms, and the nonlinear limiting mechanism of Buneman-Farley instability in the auroral ionosphere. Papers are also presented on irregularity spectra of the polar lower ionosphere according to phase VLF measurements, the dynamics of sporadic E layers during magnetic disturbances, and the height distribution of electron density in the polar F2-layer. The dynamics of electron beams injected along the geomagnetic field, the energy spectrum in fast pulsations of precipitating electrons, and the frequency spectrum of variations of the Bz component of the interplanetary magnetic field are also discussed. For individual items see A83-30602 to A83-30615

83A28828 ISSUE 12 PAGE 1750 CATEGORY 46
82/00/00 136 PAGES In RUSSIAN UNCLASSIFIED DOCUMENT

UTTL: The physics of slow MHD waves in the ionospheric plasma --- Russian book
AUTH: A/SOROKIN, V. M.; B/FEDOROVICH, G. V.
Moscow, Energoizdat, 1982, 136 p. In Russian.
MAJS: /*ATMOSPHERIC PHYSICS/*GEOMAGNETISM/*IONOSPHERIC DISTURBANCES/*MAGNETOHYDRODYNAMIC WAVES/*PLASMA PHYSICS/*SPACE PLASMAS
MINS: / DIURNAL VARIATIONS/ GRAVITATIONAL EFFECTS/ MAGNETIC VARIATIONS/ POLAR REGIONS/ TEMPORAL DISTRIBUTION/ VERTICAL DISTRIBUTION/ WAVE AMPLIFICATION/ WAVE EQUATIONS/ WAVE PROPAGATION
ABA: B.J.
ABS: The work examines the basic ideas relating to wave disturbances in the ionosphere and variations of the geomagnetic field characterized by periods from several minutes to several hours. An analysis is presented of space-time dependences of disturbances associated both with natural and artificial sources. The effect of the geomagnetic field on the characteristics of ionospheric wave disturbances is discussed, and theories of the generation and propagation of MHD waves of different types in the

ionospheric plasma are reviewed. Theoretical results are compared with geophysical data.

83A28741 ISSUE 11 PAGE 1620 CATEGORY 46
82/00/00 8 PAGES In RUSSIAN UNCLASSIFIED DOCUMENT
UTTL: The interplanetary magnetic field and the absorption of radio waves in the auroral zone
AUTH: A/RAPOPORT, Z. SH.
Ionosfernye Issledovaniia, no. 36, 1982, p. 50-57. In Russian.
MAJS: /*AURORAL ABSORPTION/*GEOMAGNETISM/*INTERPLANETARY MAGNETIC FIELDS/*IONOSPHERIC PROPAGATION/*POLAR RADIO BLACKOUT/*SOLAR ACTIVITY EFFECTS
MINS: / LINES OF FORCE/ MAGNETIC ANOMALIES/ SOLAR TERRESTRIAL INTERACTIONS
ABA: C.R.
ABS: From an analysis of the relationship between the midday absorption of radio waves in the auroral zone and the interplanetary magnetic field, it is shown that the Bz component of the field has the strongest effect on the absorption. When this component is less than zero, the absorption is found to be greater than when it is greater than zero. The By component also figures in absorption, the latter being on the average greater when this component is greater than zero, that is, when the field is moving 'away from the sun'. The results are explained by referring to the mechanism controlling the reconnection of the lines of force from the interplanetary and geomagnetic fields.

83A25166 ISSUE 9 PAGE 1251 CATEGORY 32
83/02/00 3 PAGES In RUSSIAN UNCLASSIFIED DOCUMENT
UTTL: Approximation of atmospheric radio noise in the Arctic by the Hall model
AUTH: A/BASALAEV, M. L.
Radiotekhnika, Feb. 1983, p. 64-66. In Russian.
MAJS: /*ARCTIC REGIONS/*ATMOSPHERICS/*HALL EFFECT/*IONOSPHERIC PROPAGATION/*MATHEMATICAL MODELS/*POLAR RADIO BLACKOUT/*RADIO FREQUENCY INTERFERENCE
MINS: / APPROXIMATION/ RADIO TRANSMISSION/ STATISTICAL ANALYSIS
ABA: B.J.
ABS: Data acquired over a number of years concerning the statistical characteristics of atmospheric radio noise in the eastern Arctic are examined. It is shown that the Hall model for theta = 4 represents the most adequate approximation for the envelope of atmosphere radio noise in the eastern Arctic.

83A18737 ISSUE 6 PAGE 747 CATEGORY 32 81/00/00
5 PAGES UNCLASSIFIED DOCUMENT
UTTL: High frequency sky-wave prediction methods and observational data for high-latitude communication circuits
AUTH: A/THRANE, E. V.; B/BRADLEY, P. A. PAA: A/(Forsvarets Forskningsinstitutt, Kjeller, Norway); B/(Science Research Council, Rutherford and Appleton Laboratories, Didcot, Oxon, England)
In: International Conference on Antennas and Propagation, 2nd, York, England, April 13-16, 1981, Proceedings. Part 2. (A83-18601 06-32) London, Institution of Electrical Engineers, 1981, p. 258-262.
MAJS: /*IONOSPHERIC PROPAGATION/*PERFORMANCE PREDICTION/*POLAR REGIONS/*SHORT WAVE RADIO TRANSMISSION/*SKY WAVES/*TRANSMISSION EFFICIENCY
MINS: / CIRCUIT RELIABILITY/ HIGH FREQUENCIES/ RADIO COMMUNICATION/ RELIABILITY ANALYSIS/ SYSTEM EFFECTIVENESS
ABA: (Author)
ABS: High-frequency radio-wave propagation via the ionosphere is important for high-latitude communication systems. A number of methods exist for estimating circuit reliabilities for such systems, but accurate predictions are difficult to achieve because of the extreme spatial and temporal ionospheric variations. The present paper studies the advantages of frequency flexibility and signal relaying for two high-latitude circuits, and compares measured reliabilities with those predicted by three methods in current use. The reliabilities for different times of day, season and degree of ionospheric disturbance are discussed.

83A18711 ISSUE 6 PAGE 745 CATEGORY 32 81/00/00
5 PAGES UNCLASSIFIED DOCUMENT
UTTL: Measurements of tropospheric fading and crosspolarisation in the Arctic using orbital test satellite
AUTH: A/GUTTEBERG, O. PAA: A/(Norwegian Telecommunications Administration Research Establishment, Norway)
In: International Conference on Antennas and Propagation, 2nd, York, England, April 13-16, 1981, Proceedings. Part 2. (A83-18601 06-32) London, Institution of Electrical Engineers, 1981, p. 71-75.
MAJS: /*CROSS POLARIZATION/*OTS (ESA)/*POLAR RADIO BLACKOUT /*RADIO COMMUNICATION/*SIGNAL FADING/*TROPOSPHERIC SCATTERING
MINS: / ARCTIC REGIONS/ SATELLITE TRANSMISSION

83A18302* ISSUE 6 PAGE 784 CATEGORY 46 RPT#: AD-A125914 CNT#: NAS5-25690 NGL-16-001-002 NGL-16-001-043 N00014-76-C-0016 83/01/01 12 PAGES UNCLASSIFIED DOCUMENT

UTTL: Auroral hiss, Z mode radiation, and auroral kilometric radiation in the polar magnetosphere - DE 1 observations

AUTH: A/GURNETT, D. A.; B/SHAWHAN, S. D.; C/SHAW, R. R. PAA: C/(Iowa, University, Iowa City, IA)

CORP: Iowa Univ., Iowa City.

Journal of Geophysical Research, vol. 88, Jan. 1, 1983, p. 329-340. Navy-supported research.

MAJS: /*AURORAL ZONES/*HISS/*KILOMETRIC WAVES/*MAGNETOSPHERE /*PLASMA WAVES/*RADIO EMISSION

MINS: / POLAR REGIONS/ WAVE PROPAGATION/ WHISTLERS

ABA: S.C.S.

ABS: The polar-orbiting DE 1 spacecraft has provided the first measurements of high-latitude auroral phenomena. Three types of plasma-wave emissions were observed: auroral hiss, Z-mode radiation, and auroral kilometric radiation. Whistler mode auroral hiss emissions were observed on virtually every pass over the auroral zone. The shape of the auroral hiss frequency-time spectrum is explained by a whistler mode propagation effect if the radiation is emitted from a spatially localized source below the spacecraft. Broadband Z emissions have been observed in the low-density region over the auroral zone and polar cap. The auroral hiss may be distinguished from the Z-mode radiation by the sharp upper cutoff of the whistler mode at the local electron plasma frequency. Auroral kilometric radiation usually occurs at frequencies above electron gyrofrequency, indicating that this radiation is propagating in the free-space R-X mode.

83A13824 ISSUE 3 PAGE 358 CATEGORY 46 82/00/00 160 PAGES In RUSSIAN UNCLASSIFIED DOCUMENT DCAF A438100

UTTL: Natural radio emissions in the earth's magnetosphere --- Russian book

AUTH: A/SAZHIN, S. S.

Moscow, Izdatel'stvo Nauka, 1982. 160 p. In Russian.

MAJS: /*MAGNETOSPHERE/*PLASMA WAVES/*RADIO EMISSION/*WAVE PROPAGATION

MINS: / ANISOTROPIC MEDIA/ AURORAL ZONES/ BIBLIOGRAPHIES/ COLD PLASMAS/ DAWN CHORUS/ ELECTROSTATIC WAVES/ HIGH TEMPERATURE PLASMAS/ HISS/ IONOSPHERE/ RADIO FREQUENCIES/ TROPICAL REGIONS/ WHISTLERS

ABA: C.R.

ABS: The progress that has been made in understanding radio emissions at frequencies ranging from tens of Hz to hundreds of kHz is surveyed, noting theoretical advances and experimental data. The principles underlying the theory of plasma waves and the theory of wave propagation under magnetospheric conditions are set forth. Certain properties of waves whose modes are characteristic of those at which radio emissions propagate are discussed. Particular attention is given to the propagation of electrostatic waves and whistlers in a hot anisotropic plasma whose parameters approximate those under magnetospheric conditions. Possible methods of magnetospheric plasma diagnostics with the aid of natural radio emissions are proposed. The theory and morphology of concrete types of natural radio emissions are considered in detail.

83A12021 ISSUE 2 PAGE 206 CATEGORY 46 CNT#: DNA001-81-C-0076 82/10/00 12 PAGES UNCLASSIFIED DOCUMENT

UTTL: Recent results in auroral-zone scintillation studies

AUTH: A/RINO, C. L.; B/VICKREY, J. F. PAA: B/(SRI International, Radio Physics Laboratory, Menlo Park, CA)

Journal of Atmospheric and Terrestrial Physics, vol. 44, Oct. 1982, p. 875-877, 879-887.

MAJS: /*AURORAL ZONES/*IONOSPHERIC PROPAGATION/*RADIO SIGNALS/*SCINTILLATION

MINS: / E REGION/ F REGION/ IONOSPHERIC CONDUCTIVITY/ NIGHT SKY/ SPACECRAFT COMMUNICATION/ ULTRAHIGH FREQUENCIES/ VERY HIGH FREQUENCIES

ABA: F.G.M.

ABS: Observational data are reviewed that pertain to a prominent nighttime enhancement of auroral-zone scintillation in VHF and UHF satellite signals at the point where the propagation vector lies within the plane of the local L shell. Experimental results that have been used to define the source region are examined, along with theories advanced to explain the occurrence and structure of the F-region irregularity responsible for the enhancement. It is concluded that soft-particle precipitation, convective plasma instabilities, E-layer conductivity, and the high-latitude current-convection pattern play important roles in controlling the detailed morphology of high-latitude F-region irregularities.

83A12016 ISSUE 2 PAGE 205 CATEGORY 46 82/10/00 11 PAGES UNCLASSIFIED DOCUMENT

UTTL: Ionospheric ELF radio signal generation due to LF and/or MF radio transmissions. II - Interpretation

AUTH: A/CANNON, P. S.; B/TURUNEN, T.; C/RYCROFT, M. J. PAA: A/(Southampton, University, Southampton, England); B/(Geophysical Observatory, Sodankyla, Finland); C/(British Antarctic Survey, Cambridge, England)

Journal of Atmospheric and Terrestrial Physics, vol.

44, Oct. 1982, p. 831-841. Research supported by the Science Research Council.
MAJS: /*AURORAL ZONES/*ELECTROJETS/*EXTREMELY LOW RADIO FREQUENCIES/*IONOSPHERIC PROPAGATION/*LOW FREQUENCIES /*RADIO TRANSMISSION
MINS: / D REGION/ E REGION/ ELECTRON DENSITY (CONCENTRATION) / IONOSPHERIC HEATING/ RADIO COMMUNICATION/ RADIO TRANSMITTERS
ABA: F.G.M.
ABS: Four possible mechanisms are considered for the generation of the ELF pips reported by Cannon (1982). The mechanisms involve the heating of the auroral D region or lower E region by AM waves from one or more distant Soviet LF and/or MF radio transmitters, leading to modulation of the large electrojet current, which then radiates at 1 kHz. It is shown that the experimental data favor a mechanism entailing periodic in-phase heating of the ionosphere by two or more synchronized transmitters and that the most likely solutions involve transmissions at 173, 263, 281, and 549 kHz. A 0.6-K peak-to-peak sinusoidal electron-temperature variation superimposed on a 2-K temperature rise is predicted for the combined effect of transmitters in Kaliningrad (173 kHz), Moscow (173 and 263 kHz), and Minsk (281 and 549 kHz). The corresponding 1-kHz magnetic field variations on the ground directly below the source are estimated to be 0.09 pT, in good agreement with the experimental ELF pip field strengths.

83A12015 ISSUE 2 PAGE 205 CATEGORY 46 82/10/00
11 PAGES UNCLASSIFIED DOCUMENT
UTTL: Ionospheric ELF radio signal generation due to LF and/or MF radio transmissions. I - Experimental results
AUTH: A/CANNON, P. S. PAA: A/(Southampton, University, Southampton, England)
Journal of Atmospheric and Terrestrial Physics, vol. 44, Oct. 1982, p. 819-829. Research supported by the Science Research Council.
MAJS: /*AURORAL ZONES/*EXTREMELY LOW RADIO FREQUENCIES/* IONOSPHERIC PROPAGATION/*LOW FREQUENCIES/*RADIO TRANSMISSION
MINS: / DIURNAL VARIATIONS/ ELECTROJETS/ FINLAND/ NORWAY/ RADIO COMMUNICATION/ SWEDEN/ VERY LOW FREQUENCIES
ABA: F.G.M.
ABS: Data obtained in a program of ELF/VLF goniometer recordings in northern Scandinavia are analyzed. The results indicate that six 1-kHz timing signals (pips) received on the hour were produced by a nonlinear demodulation mechanism in the D region of the auroral ionosphere. A positive temporal correlation between ELF pip generation and periods of enhanced local magnetic activity is obtained, demonstrating a close association between the reception of the ELF pips and the auroral electrojet. The pip magnetic field strengths are found to be of the order of 0.1 pT. The originating signals are shown to emanate from one or more Soviet LF and/or MF radio transmitters located at least several hundred km from the favored generation region.

82A47364 ISSUE 24 PAGE 3797 CATEGORY 46
82/09/00 5 PAGES UNCLASSIFIED DOCUMENT
UTTL: On the partial transparency of sporadic E-layers at high latitudes
AUTH: A/JALONEN, L.; B/NYGREN, T.; C/TURUNEN, T. PAA: B/(Oulu, University, Oulu, Finland); C/(Geophysical Observatory, Sodankyla, Finland)
Journal of Atmospheric and Terrestrial Physics, vol. 44, Sept. 1982, p. 731-735.
MAJS: /*COUPLED MODES/*IONOSPHERIC ELECTRON DENSITY/* IONOSPHERIC PROPAGATION/*POLAR REGIONS/*SPORADIC E LAYER/*TRANSPARENCE
MINS: / CRITICAL FREQUENCIES/ IONOSONDES/ PLASMA FREQUENCIES
ABA: (Author)
ABS: Partial transparency of Es-layers caused by coupling between the characteristic modes of the radio wave is studied theoretically assuming various electron density profiles and recording thresholds of the ionosonde. The results show that mode coupling should be important at high latitudes in Es-layers with steep electron density gradients. An investigation is also made to determine whether the coupling mechanism is observable in standard ionosonde data recorded at Sodankyla, Finland. In most cases the partial transparency can be explained in terms of the cloud model, but at moderately high critical frequencies the experimental distribution of the fOEs-fbEs separations shows features most probably indicating the presence of the coupling mechanism.

82A47321 ISSUE 24 PAGE 3796 CATEGORY 46 CNT#: DNA001-82-C-0021 F49620-80-C-0014 82/10/01 10 PAGES UNCLASSIFIED DOCUMENT
UTTL: High-latitude F region irregularities observed simultaneously with ISIS 1 and the Chatanika radar
AUTH: A/MULDREW, D. B.; B/VICKREY, J. F. PAA: A/(Department of Communications, Communications Research Centre, Ottawa, Canada); B/(SRI International, Radio Physics Laboratory, Menlo Park, CA)
Journal of Geophysical Research, vol. 87, Oct. 1, 1982, p. 8263-8272.
MAJS: /*AURORAL ZONES/*F REGION/*IONOSPHERIC DISTURBANCES/*

IONOSPHERIC ELECTRON DENSITY/*IONOSPHERIC F-SCATTER PROPAGATION/*IONOSPHERIC SOUNDING
MINS: / BANDWIDTH/ CROSSED FIELDS/ ELECTRON PRECIPITATION/ HISS/ ISIS SATELLITES/ RADAR TRACKING
ABA: C.R.
ABS: The combination of the ISIS 1 spacecraft and Chatanika radar is seen as ideal for studying ionization irregularities. The radar can obtain electron density profiles with better large-scale resolution than the ISIS 1 sounder in regions of extreme horizontal gradients, and the sounder and ISIS 1 cylindrical electrostatic probes (CEPs) are able to examine small-scale structure that is beyond the resolution of the radar. It is noted that the CEP are Langmuir probes, which measure electron or ion current as the probe voltage is varied. The electron density is in proportion to this current. In the study described here, comparisons of ISIS and radar data give new insight into the east-west extent and spatial coexistence of different size irregularities and into the generation of both large- and small-scale irregularities.

82A42386 ISSUE 21 PAGE 3373 CATEGORY 46
82/08/00 5 PAGES In RUSSIAN UNCLASSIFIED DOCUMENT
UTTL: Characteristics of short-wave propagation on a high-latitude radio path during auroral disturbances
AUTH: A/BLAGOVESHCHENSKII, D. V.; B/SHIROCHKOV, A. V.
PAA: A/(Leningradskii Politekhnicheskii Institut, Leningrad, USSR); B/(Gosudarstvennyi Komitet po Gidrometeorologii i Kontroliu Prirodnoi Sredy, Arkticheskii i Antarkticheskii Nauchno-Issledovatel'skii Institut, Leningrad, USSR)
Geomagnetizm i Aeronomiia, vol. 22, July-Aug. 1982, p. 586-590. In Russian.
MAJS: /*AURORAL ZONES/*IONOSPHERIC DISTURBANCES/*IONOSPHERIC PROPAGATION/*POLAR RADIO BLACKOUT/*SHORT WAVE RADIO TRANSMISSION
MINS: / E REGION/ F 2 REGION/ IONOSPHERIC SOUNDING

82A37394 ISSUE 18 PAGE 2877 CATEGORY 32
82/08/00 10 PAGES UNCLASSIFIED DOCUMENT
UTTL: On the analysis and interpretation of spaced-receiver measurements of transionospheric radio waves
AUTH: A/RINO, C. L.; B/LIVINGSTON, R. C. PAA: B/(SRI International, Menlo Park, CA)
Radio Science, vol. 17, July-Aug. 1982, p. 845-854.
MAJS: /*AURORAL ZONES/*IONOSPHERIC PROPAGATION/*RADIO TRANSMISSION/*SPACECRAFT COMMUNICATION
MINS: / ANISOTROPIC MEDIA/ CORRELATION/ DIFFRACTION PATTERNS / F REGION/ TEMPORAL DISTRIBUTION
ABA: (Author)
ABS: A correlation analysis method developed by Armstrong and Coles (1972) has been applied to spaced-receiver data from the Wideband satellite. The method permits simultaneous estimation of the anisotropy and true drift of the diffraction pattern. The scintillation theory is applied to interpret the measured variations in anisotropy and pattern drift. The results show that in anistropic media, there is a complicated interplay between apparent drifts and the anistropy of the diffraction pattern that must be accommodated in spaced-receiver data analyses. The method has been applied to verify the L-shell aligned, cross-field anisotropy of F region auroral zone irregularities.

82A35953 ISSUE 17 PAGE 2769 CATEGORY 46
82/06/00 2 PAGES In RUSSIAN UNCLASSIFIED DOCUMENT
UTTL: Effective model of the lower ionosphere for VLF signals during auroral disturbances
AUTH: A/BELOGLAZOV, M. I.; B/ZABAVINA, I. N. PAA: B/(Akademiia Nauk SSSR, Poliarnyi Geofizicheskii Institut, Murmansk, USSR)
Geomagnetizm i Aeronomiia, vol. 22, May-June 1982, p. 492, 493. In Russian.
MAJS: /*ATMOSPHERIC MODELS/*AURORAL ZONES/*IONOSPHERIC DISTURBANCES/*IONOSPHERIC PROPAGATION/*LOWER IONOSPHERE/*VERY LOW FREQUENCIES
MINS: / ARCTIC REGIONS/ DAYTIME/ NIGHT SKY/ VERTICAL DISTRIBUTION
ABA: B.J.
ABS: An effective model of the lower ionosphere at high latitudes is developed for investigating the propagation of VLF signals during auroral disturbances. This model agrees well with available experimental data, and, together with a quiet-time model for VLF propagation, describes variations of VLF-signal parameters during transitions from day to night, and quiet to disturbed conditions. The model also agrees with contemporary geophysical conceptions of the ionization of the auroral ionosphere.

82A33445 ISSUE 15 PAGE 2449 CATEGORY 46 CNT#: NSF ATM-80-07039 82/06/00 9 PAGES UNCLASSIFIED DOCUMENT
UTTL: Application of wave field reconstruction of VHF radio waves to investigate single, isolated ionospheric irregularities
AUTH: A/TAURIAINEN, A.
Radio Science, vol. 17, May-June 1982, p. 684-692.
Research supported by the Academy of Finland
MAJS: /*AURORAL ZONES/*IONOSPHERIC PROPAGATION/*VERY HIGH FREQUENCIES/*WAVE DIFFRACTION/*WAVE FRONT RECONSTRUCTION

MINS: / FRESNEL INTEGRALS
ABA: C.D.
ABS: The reconstruction technique of wave fields in complex form is presented, and some examples of reconstructions achieved from auroral zone data are shown. The diffraction of radio waves by a single, isolated ionospheric irregularity, the application of the Fresnel approximation in the space domain, the reconstruction of the wave field in the spatial frequency domain, and the relationships of one-dimensional data to the two-dimensionality of irregularities are considered. The amplitude and phase of the original data and those of the reconstructed wave field are shown. Some reconstructed wave fields at subsequent altitudes corresponding to the ionosphere are presented. Different kinds of structures encountered in the reconstructions are examined. Conclusions on the usefulness of the described method are made, and a future experiment is considered.

82A32066 ISSUE 15 PAGE 2439 CATEGORY 46
82/04/00 11 PAGES UNCLASSIFIED DOCUMENT
UTTL: Variability of D-region electron densities at Tromso
AUTH: A/RASTOGI, P. K.; B/BREKKE, A.; C/HOLT, O.; D/HANSEN, T. PAA: D/(Auroral Observatory, Tromso, Norway)
Journal of Atmospheric and Terrestrial Physics, vol. 44, Apr. 1982, p. 313-323.
MAJS: /*D REGION/*ELECTRON DENSITY PROFILES/*IONOSPHERIC ELECTRON DENSITY/*POLAR CAP ABSORPTION/*RADAR REFLECTORS
MINS: / ATMOSPHERIC IONIZATION/ ATMOSPHERIC STRATIFICATION/ HIGH FREQUENCIES/ IONOSPHERIC PROPAGATION/ NORWAY/ POLAR REGIONS/ RADAR ECHOES/ RIOMETERS/ SOLAR PROTONS
ABA: (Author)
ABS: The 2.75 MHz partial-reflection radar at Ramfjordmoen near Tromso has been used for a study of D-region electron densities by the differential-absorption method on a number of days during 1978-79. Received signals are generally stratified in several layers, typically over 60-80 km. Strong stable echoes are seen down to 55 km during periods of enhanced riometer absorption. Inferred electron densities vary between about 100-1000 per cu cm at about 60-80 km and show well-defined features which persist for about 10-20 min. During periods of high absorption, enhanced electron densities about 600 cm per cu cm are observed below 65 km. During a polar cap absorption event, the inferred electron densities at 60-70 km show a very stable profile. Possible sources of D-region ionization at high latitudes are briefly discussed.

82A31112 ISSUE 14 PAGE 2258 CATEGORY 46
81/00/00 14 PAGES In RUSSIAN UNCLASSIFIED DOCUMENT
UTTL: Experimental statistical model of sporadic-E reflections of the auroral ionosphere
AUTH: A/KATSEVMAN, M. M.; B/KURGANOV, R. A.; C/FEDOTOV, V. G.; D/IAKHINA, G.; E/MIKHAILOVA, N. B.; F/KURGANOVA, I. Z.
Meteornoe Rasprostranenie Radiovoln, no. 17, 1981, p. 53-66. In Russian.
MAJS: /*AURORAL ZONES/*IONOSPHERIC PROPAGATION/*SIGNAL REFLECTION/*SPORADIC E LAYER
MINS: / ATMOSPHERIC MODELS/ PROBABILITY DISTRIBUTION FUNCTIONS/ RADIO AURORAS/ STATISTICAL ANALYSIS/ TEMPORAL DISTRIBUTION
ABA: B.J.
ABS: A statistical model of oblique sporadic-E reflections of the auroral ionosphere has been developed on the basis of continuous round-the-clock measurements made on the Salekhard-Murmansk high-latitude path during 1975-1979. The criterion for the separation of sporadic-E reflections from signals of the regular meteor-ionospheric background (MIB signals) is the duration of the envelope burst above the three-fold median level of a MIB signal which is greater than 20 sec. The criterion for the separation of sporadic-E bursts from radio-aurora bursts is the absence of the high-frequency fading of the signal envelope. Some features of the dynamics and nature of the sporadic-E layer in the auroral ionosphere as determined through this model are discussed.

82A29974 ISSUE 13 PAGE 2128 CATEGORY 46
82/04/00 3 PAGES In RUSSIAN UNCLASSIFIED DOCUMENT
UTTL: Effective model of the undisturbed auroral ionosphere for VLF signals
AUTH: A/BELOGLAZOV, M. I.; B/ZABAVINA, I. N. PAA: B/(Akademiia Nauk SSSR, Poliarnyi Geofizicheskii Institut, Murmansk, USSR)
Geomagnetizm i Aeronomiia, vol. 22, Mar.-Apr. 1982, p. 319-321. In Russian.
MAJS: /*ATMOSPHERIC MODELS/*AURORAL ZONES/*IONOSPHERIC PROPAGATION/*LOWER IONOSPHERE/*VERY LOW FREQUENCIES
MINS: / COMPUTER TECHNIQUES/ SATELLITE OBSERVATION/ VLF EMISSION RECORDERS/ WAVE PROPAGATION

82A29956 ISSUE 13 PAGE 2126 CATEGORY 46
82/04/00 6 PAGES In RUSSIAN UNCLASSIFIED DOCUMENT
UTTL: The dynamics of the lower ionosphere during auroral disturbances studied on the basis of VLF data
AUTH: A/REMENETS, G. F.; B/BELOGLAZOV, M. I. PAA: A/(Leningradskii Gosudarstvennyi Universitet,

Leningrad, USSR); B/(Akademiia Nauk SSSR, Poliarnyi Geofizicheskii Institut, Murmansk, USSR)
Geomagnetizm i Aeronomiia, vol. 22, Mar.-Apr. 1982, p. 205-210. In Russian.

MAJS: /*AURORAL ZONES/*IONOSPHERIC DISTURBANCES/*LOWER IONOSPHERE/*VERY LOW FREQUENCIES/*VLF EMISSION RECORDERS
MINS: / COSMIC NOISE/ IONOSPHERIC PROPAGATION/ REFLECTANCE
ABA: B.J.
ABS: A method for using VLF data to study the dynamics of the lower ionosphere during auroral disturbances is described. Three-frequency relative variations of VLF signals (10-16 kHz), recorded in the central zone of the source, were used to determine the reflection coefficients of the first two ionospheric rays from quiet auroral ionosphere and for several auroral disturbances. The data were obtained at the Apatity station during 1975 and involved five cases of VLF variations and one case of cosmic-noise absorption at 40 MHz.

82A25279 ISSUE 10 PAGE 1635 CATEGORY 46
82/02/00 3 PAGES In RUSSIAN UNCLASSIFIED DOCUMENT
UTTL: Characteristics of the influence of pulsating precipitations on ultrashort-wave radio signals
AUTH: A/KORNILOV, I. A.; B/TAGIROV, V. R. PAA: B/(Akademiia Nauk SSSR, Poliarnyi Geofizicheskii Institut, Murmansk, USSR)
Geomagnetizm i Aeronomiia, vol. 22, Jan.-Feb. 1982, p. 138-140. In Russian.
MAJS: /*IONOSPHERIC PROPAGATION/*NOCTURNAL VARIATIONS/*RADIO SIGNALS/*SHORT WAVE RADIATION
MINS: / AURORAL ZONES/ HISTOGRAMS/ SIGNAL FADING/ TEMPORAL DISTRIBUTION
ABA: B.J.
ABS: A zenith-directed riometer located at the Apatity station observed ultrashort-wave signals, correlated with optical auroral pulsations, on the night of February 28 to March 1, 1981. A qualitative interpretation of the observed phenomenon is presented: irregularities allowing the propagation of ultrashort-wave signals are formed in the E-region due to ion production (whose rate is proportional to the auroral intensity) at some lower threshold value of auroral intensity. The signal is absorbed if there is additional ionization at lower heights; this absorption can determine the upper threshold.

82A25262 ISSUE 10 PAGE 1634 CATEGORY 46
82/02/00 4 PAGES In RUSSIAN UNCLASSIFIED DOCUMENT
UTTL: Concerning one type of phase anomaly of VLF signals on auroral paths
AUTH: A/BELOGLAZOVA, G. P.; B/BELOGLAZOV, M. I. PAA: B/(Akademiia Nauk SSSR, Poliarnyi Geofizicheskii Institut, Murmansk, USSR)
Geomagnetizm i Aeronomiia, vol. 22, Jan.-Feb. 1982, p. 56-59. In Russian.
MAJS: /*AURORAL ZONES/*ELECTRON PRECIPITATION/*IONOSPHERIC ELECTRON DENSITY/*IONOSPHERIC PROPAGATION/*PHASE SHIFT /*VERY LOW FREQUENCIES
MINS: / ANOMALIES
ABA: B.J.
ABS: An analysis is presented of VLF phase anomalies on Norway-Apatity radio paths occurring under quiet geophysical conditions. The duration of the anomalies fluctuates from several minutes to 0.5-1.0 hours, and their characteristic value is 3-6 microsec. It is shown that these anomalies are most probably caused by the precipitation of relativistic electrons.

82A25258 ISSUE 10 PAGE 1634 CATEGORY 46
82/02/00 6 PAGES In RUSSIAN UNCLASSIFIED DOCUMENT
UTTL: Nonstationary processes produced during the disturbance of the nighttime polar ionosphere by radio waves
AUTH: A/BARDEEV, I. N.; B/GUREVICH, A. V.; C/DIMANT, IA. S.; D/KAPUSTIN, I. N.; E/ROIZEN, A. M.; F/ULIANCHENKO, A. A. PAA: F/(Akademiia Nauk SSSR, Institut Zemnogo Magnetizma, Ionosfery i Rasprostranenilia Radiovoln, Akademgorodok; Akademiia Nauk SSSR, Poliarnyi Geofizicheskii Institut, Murmansk, USSR)
Geomagnetizm i Aeronomiia, vol. 22, Jan.-Feb. 1982, p. 33-38. In Russian.
MAJS: /*F REGION/*IONOSPHERIC ELECTRON DENSITY/*NOCTURNAL VARIATIONS/*PLASMA DYNAMICS/*POLAR REGIONS/*RADIO TRANSMISSION
MINS: / DOPPLER EFFECT/ NIGHT SKY/ PLASMA DIFFUSION/ UNSTEADY STATE
ABA: B.J.
ABS: An investigation is presented of plasma motions in the F-layer of the nighttime polar ionosphere produced under the effect of high-power radio waves at a frequency of 3.33 MHz. The frequency of a test radio-signal transmitted through the disturbed region was found to undergo a Doppler shift. Theoretical calculations of this effect are presented, and sufficient agreement with experiment is revealed.

82A24287 ISSUE 10 PAGE 1630 CATEGORY 46
81/00/00 7 PAGES UNCLASSIFIED DOCUMENT

UTTL: The variability and predictability of the main ionospheric trough

AUTH: A/RODGER, A. S.; B/PINNOCK, M. PAA: B/(Natural Environment Research Council, British Antarctic Survey, Cambridge, England)
In: Exploration of the polar upper atmosphere; Proceedings of the Advanced Study Institute, Lillehammer, Norway, May 5-16, 1980. (A82-24251 10-46) Dordrecht, D. Reidel Publishing Co., 1981, p. 463-469.

MAJS: /*GEOMAGNETISM/*IONOSONDES/*IONOSPHERIC ELECTRON DENSITY/*PERIODIC VARIATIONS/*SOLAR CYCLES

MINS: / ANNUAL VARIATIONS/ AURORAL ZONES/ DIURNAL VARIATIONS / MAGNETIC ANOMALIES/ PLASMAPAUSE/ RADIO WAVES/ WAVE PROPAGATION

ABA: O.C.

ABS: Analyses of nighttime ionosonde data from Halley Bay, Antarctica, yield diurnal, seasonal and solar cycle variations in the occurrence and shape of the main ionospheric trough at 70 deg S, and 27 deg W. Varying levels of magnetic activity lead to the identification of five different types of main trough, and it is also shown that the level of magnetic activity is important in determining the local time at which the main trough is seen at Halley Bay. Similarities to known plasmapause movements are noted in the movement of the poleward edge of the main trough. These findings are pertinent to auroral and subauroral region radio wave propagation.

82A24286 ISSUE 10 PAGE 1570 CATEGORY 32
81/00/00 14 PAGES UNCLASSIFIED DOCUMENT

UTTL: Effects of ionospheric disturbances on high latitude radio wave propagation

AUTH: A/LARSEN, T. R. PAA: A/(Forsvarets Forsoks Institutt, Kjeller, Norway)
In: Exploration of the polar upper atmosphere; Proceedings of the Advanced Study Institute, Lillehammer, Norway, May 5-16, 1980. (A82-24251 10-46) Dordrecht, D. Reidel Publishing Co., 1981, p. 449-462.

MAJS: /*ATMOSPHERIC IONIZATION/*IONOSPHERIC DISTURBANCES/* LOWER IONOSPHERE/*POLAR REGIONS/*RADIO TRANSMISSION/* WAVE PROPAGATION

MINS: / AURORAS/ ELECTRON PRECIPITATION/ MAGNETIC STORMS/ POLAR CAPS/ RADIO FREQUENCIES/ RELATIVISTIC ELECTRON BEAMS/ SUDDEN IONOSPHERIC DISTURBANCES

ABA: C.R.

ABS: The effects of anomalous high-latitude ionization on radio wave propagation are described for the main types of disturbances, that is, sudden ionospheric disturbances, relativistic electron events, magnetic storms, auroral disturbances, and polar cap events. Examples of radio wave characteristics for such conditions are given for the frequencies between the very low (3-3000 Hz) and high (3-30 MHz) frequency domains.

82A22404 ISSUE 9 PAGE 1354 CATEGORY 32
81/00/00 180 PAGES In RUSSIAN UNCLASSIFIED DOCUMENT

UTTL: The propagation of decametric radio waves at high latitudes --- Russian book

AUTH: A/BLAGOVESHCHENSKII, D. V.
Moscow, Izdatel'stvo Nauka, 1981. 180 p. In Russian.

MAJS: /*AURORAL ZONES/*DECAMETRIC WAVES/*IONOSPHERIC PROPAGATION/*POLAR REGIONS/*RADIO TRANSMISSION/*WAVE PROPAGATION

MINS: / ARCTIC REGIONS/ D REGION/ GEOMAGNETISM/ INHOMOGENEITY/ IONOSPHERIC SOUNDING/ POLAR SUBSTORMS/ SHORT WAVE RADIO TRANSMISSION/ SIGNAL FADING/ SPORADIC E LAYER

ABA: C.R.

ABS: Wave propagation is considered on the basis of signal representation. Results are presented of comprehensive experiments carried out on wave paths having various orientations with respect to the auroral zone. The polar ionosphere and its fine structure are investigated, as are the properties of signals after being reflected from the ionosphere, here considered as a randomly inhomogeneous medium. It is shown that the relationship between the statistical signal characteristics in radio channels and the parameters of the high-latitude ionosphere depends on such factors as the time of day, the season, the solar activity, and extent of ionospheric disturbance.

82A20596 ISSUE 7 PAGE 992 CATEGORY 17 RPT#: AD-A101028 ESD-TR-81-60 80/00/00 5 PAGES UNCLASSIFIED DOCUMENT

UTTL: MILSATCOM system link availability prediction for polar and inclined orbits

AUTH: A/SCHWAB, L. M. PAA: A/(MIT, Lexington, MA)
In: NTC '80; National Telecommunications Conference, Houston, TX, November 30-December 4, 1980, Conference Record. Volume 1. (A82-20576 07-32) New York, Institute of Electrical and Electronics Engineers, Inc., 1980, p. 17.2.1-17.2.5. Research sponsored by the U.S. Defense Communications Agency and U.S. Air Force.

MAJS: /*ATMOSPHERIC EFFECTS/*AVAILABILITY/*DATA LINKS/* DEFENSE COMMUNICATIONS SATELLITE SYSTEM/*POLAR ORBITS /*PREDICTION ANALYSIS TECHNIQUES

MINS: / ATMOSPHERIC ATTENUATION/ ELECTROMAGNETIC ABSORPTION/ RAINDROPS/ SATELLITE ANTENNAS/ SATELLITE TRANSMISSION/

SYSTEM EFFECTIVENESS

ABA: B.J.

ABS: A numerical link availability prediction model including the combined effects of rain attenuation, atmospheric absorption, slant range differential, and spacecraft antenna pattern effects, has been formulated and programmed using Crane's (1971) rain rate distribution and climate region definitions. The model computes a distribution and resultant contour levels of link availability within a satellite's field of view for a specified value of link margin. The present paper describes the application of this model to MILSATCOM system link architecture for satellites in polar and inclined orbits; computed results for selected 12 and 24 hour period orbits are presented.

82A19983 ISSUE 7 PAGE 1081 CATEGORY 46
81/12/00 5 PAGES UNCLASSIFIED DOCUMENT

UTTL: Storm after-effects observed at Ushuaia and Kerguelen --- D-region disturbances caused by radio signals

AUTH: A/PERES, M. PAA: A/(Laboratorio Ionosferico de la Armada, Buenos Aires, Argentina)
Journal of Atmospheric and Terrestrial Physics, vol. 43, Dec. 1981, p. 1279-1283. Research supported by the Programa Nacional de Radiopropagacion.

MAJS: /*D REGION/*IONOSPHERIC DISTURBANCES/*IONOSPHERIC PROPAGATION/*MAGNETIC STORMS/*MIDLATITUDE ATMOSPHERE/* RADIO TRANSMISSION

MINS: / ARGENTINA/ AURORAL ZONES/ ELECTRON PRECIPITATION/ HIGH ENERGY ELECTRONS/ IONOSPHERIC STORMS/ RIOMETERS

ABA: (Author)

ABS: D-region disturbances have been detected at mid-latitudes after intense magnetic storms by means of a wide range of radiowave signals. Two different mechanisms have been suggested to account for these storm 'after-effects': one implies precipitation of energetic electrons from the radiation belt; the other, transport of neutral constituents from the auroral zones. This paper presents observations of abnormal enhancements of ionospheric absorption arising after two major magnetic storms occurring in March and April 1976. The measurements were made at Ushuaia (54.8 deg S, L equals 1.7) and at Kerguelen (49.4 deg S, L equals 3.7). The former were obtained by means of the pulse reflection method (A1) at MF and the latter by the riometer technique. It is shown that electron precipitation can explain the effects observed at Kerguelen but not those at Ushuaia which also depart significantly from the 'winter anomaly' trend observed at that site. The abnormal ionization at Ushuaia is attributed to transport from the southern auroral zone.

82A18376 ISSUE 6 PAGE 912 CATEGORY 46 81/00/00
7 PAGES In RUSSIAN UNCLASSIFIED DOCUMENT

UTTL: Investigation of decametric radio wave propagation on transpolar paths during auroral substorms

AUTH: A/BLAGOVESHCHENSKAIA, N. F.; B/BUBNOV, V. A.
Radiofizika, vol. 24, no. 11, 1981, p. 1299-1305. In Russian.

MAJS: /*AURORAL ZONES/*DECAMETRIC WAVES/*POLAR SUBSTORMS/* RADIO TRANSMISSION/*WAVE PROPAGATION

MINS: / HIGH FREQUENCIES/ NIGHT SKY/ SIGNAL RECEPTION/ TEMPORAL DISTRIBUTION/ WINTER

ABA: J.F.

ABS: The results from an investigation of the characteristics of the long-range propagation of decametric waves on three transpolar paths are presented. The study was carried out at various phases of the auroral substorms during winter nights in the period 1976-1978. The first radio line covered a distance of 7200 km and had a working frequency of 15 MHz; radio line two had a distance of 8800 km and working frequencies of 13 and 17 MHz; the third path had a distance of 7600 km and a working frequency of about 17 MHz. The distance from the point at which the signal was received to the auroral zone was 600-800 km. Stable regularities in variations of the HF signal intensities were observed during the substorm.

82A18096# ISSUE 6 PAGE 911 CATEGORY 46
81/00/00 11 PAGES UNCLASSIFIED DOCUMENT

UTTL: Anomalous ionospheric refraction associated with the auroral zone

AUTH: A/EVANS, J. V.; B/WAND, R. H. PAA: A/(MIT, Lexington, MA); B/(Haystack Observatory, Westford, MA)
In: Symposium on the Effect of the Ionosphere on Radiowave Systems, Washington, DC, April 14-16, 1981, Preprints. (A82-18051 06-32) Washington, DC, U.S. Naval Research Laboratory, 1981. (4B-6). 11 p. Army-NSF-supported research.

MAJS: /*AURORAL ZONES/*IONOSPHERIC PROPAGATION/*RADAR TRANSMISSION/*RADIO WAVE REFRACTION

MINS: / DAYTIME/ DOPPLER RADAR/ F REGION/ IONOSPHERIC ELECTRON DENSITY/ MAGNETIC DISTURBANCES/ MILITARY TECHNOLOGY

ABA: O.C.

ABS: It is shown that efforts to model the effect of ionospheric refraction on the precision of a VHF or UHF high-latitude defense radar may be inaccurate or misleading when an irregular structure associated with the auroral zone, such as the low electron density region that forms on the nightside, is present. Such low electron density troughs may also be found in the afternoon and evening sectors when the ambient ion

density to the south is high, and appear to give rise to the largest quasi-stationary refraction effects observed during a three-year study. Satellite and incoherent scatter observations suggest that the dayside troughs are caused by a large northwards electric field being impressed on the earth's ionosphere, which increases the charge transfer rate for O(+) ions. The origin of this field may be the partial ring current ions, which penetrate to L-shells lower than those of plasma sheet electrons.

82A18086# ISSUE 6 PAGE 910 CATEGORY 46
81/00/00 6 PAGES UNCLASSIFIED DOCUMENT

UTTL: Occurrence of F layer irregularities in the polar cap

AUTH: A/JOHNSON, A.; B/AARONS, J.; C/BUCHAU, J.; D/MULLEN, J. P.; E/WEBER, E.; F/WHITNEY, H. E.
PAA: A/(USAF, Avionics Laboratory, Wright-Patterson AFB, OH); F/(USAF, Geophysics, Laboratory, Bedford, MA)
In: Symposium on the Effect of the Ionosphere on Radiowave Systems, Washington, DC, April 14-16, 1981, Preprints. (A82-18051 06-32) Washington, DC, U.S. Naval Research Laboratory, 1981. (4A-3). 6 p.
Research supported by the U.S. Defense Nuclear Agency.

MAJS: /*AURORAL ARCS/*F REGION/*IONOSPHERIC DISTURBANCES/*IONOSPHERIC PROPAGATION/*POLAR CAPS/*SATELLITE TRANSMISSION/*SIGNAL FADING

MINS: / ANNUAL VARIATIONS/ DIURNAL VARIATIONS/ IONOSPHERIC DRIFT/ IONOSPHERIC SOUNDING/ RADIO RELAY SYSTEMS/ SCINTILLATION/ TRANSMISSION EFFICIENCY

ABA: O.C.

ABS: Long-term ground and airborne measurements of F layer irregularities and their effect on earth-to-satellite communication links, conducted over the last ten years in the polar cap region, indicate that the occurrence of ionospheric scintillation fading in the polar cap is strongly correlated with solar flux density and season, but poorly correlated with magnetic activity and time-of-day. All-sky imaging photometer data at 6300 A show that intense polar cap scintillations are associated with sun-aligned F layer auroral arcs which drift predominantly in the dawn-to-dusk direction, with occasional reversals. The drift of these structures into the satellite-to-ground ray path results in an increase in scintillation level, implying the existence or more intense ionospheric irregularities within the auroras. Irregularity drift velocities of 40-800 m/sec were recorded, with the drift direction following a complex diurnal pattern with rapid direction reversals, indicating that the irregularities do not follow a simple noon-to-midnight flow pattern within the auroral arcs.

82A18075# ISSUE 6 PAGE 841 CATEGORY 32 CNT#: F19628-79-C-0132 81/00/00 15 PAGES UNCLASSIFIED DOCUMENT

UTTL: Adaptive utilization of HF paths - A way to cope with the ionospheric limitations affecting midlatitude and transauroral short-wave links

AUTH: A/GUPTA, A. K.; B/GROSSI, M. D. PAA: A/(Catholic University of America, Washington, DC); B/(Harvard-Smithsonian Center for Astrophysics, Cambridge, MA)
In: Symposium on the Effect of the Ionosphere on Radiowave Systems, Washington, DC, April 14-16, 1981, Preprints. (A82-18051 06-32) Washington, DC, U.S. Naval Research Laboratory, 1981. (3B-3). 15 p.

MAJS: /*ADAPTIVE CONTROL/*AURORAL ZONES/*DATA LINKS/*IONOSPHERIC PROPAGATION/*MIDLATITUDE ATMOSPHERE/*RADIO RELAY SYSTEMS/*SHORT WAVE RADIO TRANSMISSION

MINS: / CHANNEL CAPACITY/ ERROR ANALYSIS/ FEEDBACK CONTROL/ FREQUENCY SHIFT KEYING/ HIGH FREQUENCIES/ IONOSPHERIC SOUNDING/ TRANSMISSION EFFICIENCY

ABA: D.L.G.

ABS: An adaptive method based on path sounding channel probing, MFSK signaling, and waveform diversity is presented, which makes possible the transmission of data at a rate of 24 kbit/sec with an error rate of 0.0001 in a single hop ionosphere path. The real-time oblique ionospheric sounding and probing functions provide the initial information for the working of the adaptive control loops in a two-way, high data rate, adaptive exchange between the two terminals of the link. An approach applied to midlatitude and transauroral HF links to counteract ionospheric limitations is illustrated, and an application of M-ary transmission to one-way communications and an application of adaptivity to a meteor burst channel are discussed.

82A17809# ISSUE 6 PAGE 907 CATEGORY 46 RPT#: AIAA PAPER 82-0150 CNT#: DNA001-81-C-0092 82/01/00 9 PAGES UNCLASSIFIED DOCUMENT

UTTL: A computer model of high-latitude scintillation

AUTH: A/FREMOUW, E. J. PAA: A/(Physical Dynamics, Inc., Bellevue, WA)
American Institute of Aeronautics and Astronautics, Aerospace Sciences Meeting, 20th, Orlando, FL, Jan. 11-14, 1982, 9 p.

MAJS: /*IONOSPHERIC PROPAGATION/*PLASMA-ELECTROMAGNETIC INTERACTION/*POLAR REGIONS/*RADIO SCATTERING/*SCINTILLATION

MINS: / ATMOSPHERIC MODELS/ CODES/ COMPUTER PROGRAMS/ FLOW CHARTS/ IONOSPHERIC DISTURBANCES/ SATELLITE SOUNDING

ABA: (Author)

ABS: The DNA Wideband satellite experiment provided

extensive data on scintillation produced in high-altitude structured plasmas. A computer program, WBMOD, is being developed to summarize those data in an applications-oriented way. The program contains the phase-screen scattering theory of Rino and a morphological description of ionospheric irregularities (thus far only at auroral latitudes) based on Wideband observations. It permits a user to compute scintillation indices for both phase and intensity as a function of system operating parameters and solar-ionospheric disturbance level. Correction is made for multiple scatter, and the user may choose either one-way (communication) or two-way (radar) propagation.

82A14712 ISSUE 4 PAGE 493 CATEGORY 4 81/00/00
6 PAGES UNCLASSIFIED DOCUMENT

UTTL: Updated station deselection procedures to support automatic Omega receiver operation

AUTH: A/HEALY, R. D.; B/GUPTA, R. R.; C/MORRIS, P. B.
PAA: B/(Analytic Sciences Corp., Reading, MA); C/(U.S. Coast Guard, Washington, DC)
In: NAECON 1981; Proceedings of the National Aerospace and Electronics Conference, Dayton, OH, May 19-21, 1981. Volume 1. (A82-14676 04-01) New York, Institute of Electrical and Electronics Engineers, Inc., 1981, p. 268-273.

MAJS: /*ATMOSPHERIC EFFECTS/*OMEGA NAVIGATION SYSTEM/*POSITION ERRORS/*RADIO TRANSMISSION/*SIGNAL RECEPTION/*WAVE PROPAGATION

MINS: / AUTOMATIC CONTROL/ IONOSPHERIC DISTURBANCES/ MAGNETIC ANOMALIES/ MAGNETIC EQUATOR/ POLAR CAPS

ABA: (Author)

ABS: Many automatic Omega receivers use a station selection criterion which does not employ specific propagation-related tests designed to avoid errors caused by wrong-way paths and westerly signal traverse of the magnetic equator. These errors can introduce navigationally significant errors into the Omega position solution, which can, however, be minimized by using the manual station deselection feature of the receiver. This paper describes these potential error sources and presents an updated Omega station selection chart containing specific recommendations for station deselection in a number of worldwide locations. A simple test for detecting wrong-way path propagation is also included.

82A13638 ISSUE 3 PAGE 406 CATEGORY 46 81/00/00
7 PAGES In RUSSIAN UNCLASSIFIED DOCUMENT

UTTL: Space-time dependences of decameter-wave propagation parameters at high latitudes

AUTH: A/BLAGOVESHCHENSKII, D. V. PAA: A/(Leningradskii Politekhnicheskii Institut, Leningrad, USSR)
Radiofizika, vol. 24, no. 9, 1981, p. 1070-1076. In Russian.

MAJS: /*DECAMETRIC WAVES/*POLAR REGIONS/*RADIO TRANSMISSION

MINS: / AUTOCORRELATION/ CROSS CORRELATION/ SPATIAL DISTRIBUTION/ TIME RESPONSE/ WINTER

ABA: B.J.

ABS: An analysis is presented of the autocorrelation and cross correlation of the parameters of decameter-wave propagation in the high-latitude ionosphere; oblique sounding data from three paths of different length and orientation are analyzed. Recommendations are given on the short-range prediction of the state of the propagation medium under specified geophysical conditions.

81A47927# ISSUE 23 PAGE 4069 CATEGORY 46
81/00/00 8 PAGES UNCLASSIFIED DOCUMENT

UTTL: Ionospheric scintillation in the polar cap

AUTH: A/JOHNSON, A. L. PAA: A/(USAF, Avionics Laboratory, Wright-Patterson AFB, OH)
In: Scientific and engineering uses of satellite radio beacons; Proceedings of the Symposium, Warsaw, Poland, May 19-23, 1980. (A81-47901 23-46) Warsaw, Panstwowe Wydawnictwo Naukowe, 1981, p. 299-306.

MAJS: /*IONOSPHERIC PROPAGATION/*POLAR CAPS/*SCINTILLATION

MINS: / ATMOSPHERIC CIRCULATION/ ATMOSPHERIC MODELS/ FLIGHT TESTS/ SIGNAL FADING

ABA: C.R.

ABS: The state of knowledge of ionospheric scintillation in the polar cap today is compared to the state of knowledge of the equatorial ionosphere a decade ago. Recent airborne measurements made by a team of Avionics Laboratory and Air Force Geophysics Laboratory personnel indicate that the occurrence of scintillation depends on the season and solar flux density. Little dependence of scintillation on magnetic index of day is noted. Nearly simultaneous onsets on scintillation at two aircraft locations 100 km apart indicate a very high ionospheric irregularity velocity in the polar cap. Ionospheric irregularity flow in the polar cap is seen as being away from the noontime auroral oval toward the midnight sector with a two-cell flow back toward the noon sector.

81A43519# ISSUE 20 PAGE 3562 CATEGORY 46
80/00/00 105 PAGES In RUSSIAN UNCLASSIFIED DOCUMENT

UTTL: VLF propagation on transpolar and subpolar paths --- Russian book

AUTH: A/FEDIAKINA, N. I.
Novosibirsk, Izdatel'stvo Nauka, 1980. 105 p. In Russian.

MAJS: /*AURORAL ZONES/*IONOSPHERIC DISTURBANCES/*IONOSPHERIC PROPAGATION/*LONG WAVE RADIATION/*POLAR REGIONS/*VERY LOW FREQUENCIES

MINS: / GEOMAGNETISM/ MIDLATITUDE ATMOSPHERE/ POLAR CAPS/ SIGNAL TO NOISE RATIOS/ SOLAR ACTIVITY EFFECTS

ABA: B.J.

ABS: Experimental data on VLF propagation in the transpolar and subpolar ionosphere are examined. Particular consideration is given to the influence of auroral disturbances on VLF propagation, VLF propagation during polar cap absorption periods, and anomalies in VLF propagation at midlatitudes.

81A42831# ISSUE 20 PAGE 3493 CATEGORY 32
81/06/00 3 PAGES In RUSSIAN UNCLASSIFIED DOCUMENT

UTTL: A possible explanation of weak cyclic variations of the absorption of radio waves at high latitudes

AUTH: A/KOCHENOVA, N. A.; B/FLIGEL, M. D. PAA: B/(Akademiia Nauk SSSR, Institut Zemnogo Magnetizma, Ionosfery i Rasprostraneniia Radiovoln, Akademgorodok, USSR)
Geomagnetizm i Aeronomiia, vol. 21, May-June 1981, p. 556-558. In Russian.

MAJS: /*ATMOSPHERIC ATTENUATION/*LOWER ATMOSPHERE/*MICROWAVE ATTENUATION/*POLAR REGIONS/*RADIO ATTENUATION

MINS: / ATMOSPHERIC IONIZATION/ MIDLATITUDE ATMOSPHERE/ SOLAR ACTIVITY EFFECTS/ SOLAR CYCLES

ABA: C.K.D.

ABS: The contribution of electron streams to the ionization of the lower atmosphere at high latitudes has been estimated to investigate possible reasons for observed differences in the variability of the absorption of radio waves at middle and high latitudes. The electron concentration in the interval from 75 to 85 km varies less over the period of the solar cycle at high latitudes than at middle latitudes. The electron concentration at altitudes of 80 to 88 km is 10-15% higher at high latitudes than at middle latitudes during periods of intense solar activity, and up to 30% higher in quiet periods. Results of the analysis indicate that observed differences in the variability of radio wave absorption may be due to the presence at high latitudes of background electron streams which display little variability with the solar cycle.

81A40635# ISSUE 18 PAGE 3117 CATEGORY 32
80/00/00 97 PAGES In RUSSIAN UNCLASSIFIED DOCUMENT

UTTL: Characteristics of the ionospheric propagation of decametric waves at high latitudes --- Russian book

AUTH: A/GOROKHOV, N. A.
Leningrad, Izdatel'stvo Nauka, 1980. 97 p. In Russian.

MAJS: /*ATMOSPHERIC PHYSICS/*DECAMETRIC WAVES/*IONOSPHERIC DISTURBANCES/*IONOSPHERIC PROPAGATION/*POLAR REGIONS/*RADIO SIGNALS

MINS: / AURORAS/ IONOSPHERIC SOUNDING/ PREDICTION ANALYSIS TECHNIQUES/ RADIO SPECTRA/ STATISTICAL ANALYSIS

ABA: B.J.

ABS: Physical mechanisms responsible for the ionospheric propagation of decametric waves at high latitudes are described. Current ideas on the structure of the high-latitude ionosphere are described, and consideration is given to processes that affect the propagation of decametric waves (these processes include auroral disturbances and large-scale inhomogeneities). Particular attention is given to experimental methods for the study of radio wave propagation in the ionosphere; oblique sounding, trajectory measurements, and investigations of the statistical characteristics of propagating signals are discussed.

81A38966 ISSUE 17 PAGE 2985 CATEGORY 46 CNT#: NSF ATM-75-03986 NSF ATM-78-21768 NSF ATM-79-13748
81/06/01 12 PAGES UNCLASSIFIED DOCUMENT

UTTL: Incoherent scattering of radar waves in the auroral ionosphere

AUTH: A/RAMAN, R. S. V.; B/ST-MAURICE, J. P.; C/ONG, R. S. B. PAA: C/(Michigan, University, Ann Arbor, MI)
Journal of Geophysical Research, vol. 86, June 1, 1981, p. 4751-4762.

MAJS: /*AURORAL ZONES/*INCOHERENT SCATTERING/*IONOSPHERIC PROPAGATION/*RADAR SCATTERING

MINS: / ELECTRON ENERGY/ F REGION/ IONIC MOBILITY/ VELOCITY DISTRIBUTION

ABA: G.R.

ABS: Attention is given to the modification introduced by non-Maxwellian velocity distributions on the ionic part of the spectrum of radar waves scattered incoherently from the ionosphere. The ionospheric region above 150 km at high latitudes is considered. A number of conclusions are discussed with reference to the specific non-Maxwellian ion velocity distributions and the corresponding spectra. It is found that for small values of the perpendicular electric field the ion distribution is better represented by a bi-Maxwellian function. In this case the

characteristic shape of the spectrum does not differ from the characteristic Maxwellian spectral shape. For large values of the perpendicular electric field the shape of the ion distribution in the F region departs from the Maxwellian form quite significantly.

81A36077 ISSUE 16 PAGE 2719 CATEGORY 32
81/00/00 6 PAGES UNCLASSIFIED DOCUMENT

UTTL: ELF radio signals produced in the auroral ionosphere by non-linear demodulation of signals from high-power amplitude-modulated transmitters

AUTH: A/RYCROFT, M. J.; B/CANNON, P. S.; C/TURUNEN, T.
PAA: A/(Natural Environment Research Council, British Antarctic Survey, Cambridge, England); B/(Marconi Space and Defence Systems, Ltd., Portsmouth, England); C/(Geophysical Observatory, Sodankyla, Finland)
(COSPAR, IAGA, and IUPAP, Symposium on Active Experiments in Space Plasmas, Budapest, Hungary, June 2-14, 1980.) Advances in Space Research, vol. 1, no. 2, 1981, p. 449-454. Research supported by the Science Research Council.

MAJS: /*AURORAL ZONES/*DIURNAL VARIATIONS/*EXTREMELY LOW RADIO FREQUENCIES/*IONOSPHERIC PROPAGATION/* PLASMA-ELECTROMAGNETIC INTERACTION

MINS: / AMPLITUDE MODULATION/ DEMODULATION/ ELECTROJETS/ GEOMAGNETISM/ NONLINEARITY/ PULSE DURATION

ABA: C.R.

ABS: ELF and VLF radio signals recorded in the afternoon and early morning (local time) between March 24 and April 4, 1979, in Northern Scandinavia are discussed. In addition to signals of natural origin, timing signals (six pips of equal duration of 105 + or - 8 ms, at 1 kHz + or - 0.5 Hz) were observed on the hour UT. It was found that such signals occur only on days of relatively high geomagnetic activity during enhanced auroral electrojet activity. These signals are thought to be generated by nonlinear demodulation (self-detection) of signals from two or more amplitude modulated transmitters in the USSR, operating at 173, 200, 236, 263, and 657 kHz. The simplest explanation for the observations is thought to be provided by the three transmitters operating at 173 kHz.

81A36038* ISSUE 16 PAGE 2783 CATEGORY 46
81/00/00 6 PAGES UNCLASSIFIED DOCUMENT

UTTL: Very low frequency waves stimulated by an electron accelerator in the auroral ionosphere

AUTH: A/HOLTET, J. A.; B/PRAN, B. K.; C/EGELAND, A.; D/GRANDAL, B.; E/JACOBSEN, T. A.; F/MAEHLUM, B. N.; G/TROIM, J. PAA: C/(Oslo Universitetet, Oslo, Norway); G/(Forsvarets Forskningsinstitutt, Kjeller, Norway)

CORP: Oslo Univ. (Norway).; Norwegian Defence Research Establishment, Kjeller.
(COSPAR, IAGA, and IUPAP, Symposium on Active Experiments in Space Plasmas, Budapest, Hungary, June 2-14, 1980.) Advances in Space Research, vol. 1, no. 2, 1981, p. 117-122. Research sponsored by the Norges Teknisk-Naturvitenskapelige Forskningsrad and NASA.

MAJS: /*AURORAL ZONES/*ELECTRON ACCELERATION/*IONOSPHERIC SOUNDING/*PLASMA WAVES/*ROCKET SOUNDING/*VERY LOW FREQUENCIES

MINS: / ATMOSPHERIC RADIATION/ ELECTROMAGNETIC WAVE TRANSMISSION/ ELECTRON FLUX DENSITY/ ELECTROSTATIC WAVES/ IONOSPHERIC DISTURBANCES/ IONOSPHERIC PROPAGATION/ STIMULATED EMISSION/ THERMAL PLASMAS

ABA: K.S.

ABS: The sounding rocket, Polar 5, carrying a 10 keV electron accelerator in a mother-daughter configuration and other diagnostic instruments, was launched into a slightly disturbed ionosphere with weak auroral activity on February 1, 1976 from Northern Norway to study VLF wave phenomena. The rocket trajectory crossed two auroral regions: one, between 86 and 111 s flight time, and a secondary region between 230 and 330 s. The daughter, carrying the accelerator, was separated axially from the mother in a forward direction at an altitude of 90 km. The VLF experiment, carried by the mother payload, recorded both electromagnetic and electrostatic waves. The receiving antenna was an electric dipole, 0.3 m tip-to-tip, oriented 90 degrees to the rocket spin axis. The onboard particle detector recorded increased electron fluxes in the two auroral regions. A double peaked structure was observed in the fluxes of 4-5 and 12-27 keV electrons within the northern auroral form. The number density of thermal plasma varied during the flight, with maximum density within the main auroral region. To the north of this aurora a slow, steady decrease in the density was observed, with no enhancement in the region of the second aurora.

81A35475 ISSUE 15 PAGE 2513 CATEGORY 32
80/04/00 3 PAGES UNCLASSIFIED DOCUMENT

UTTL: Characteristics of the selective properties of HF radio ducts at high latitudes

AUTH: A/BLAGOVESHCHENSKII, D. V.; B/KURCHENKO, IU. A.; C/KONSTANTINOV, A. A. PAA: C/(Akademiia Nauk SSSR, Institut Zemnogo Magnetizma, Ionosfery i Rasprostraneniia Radiovoln, Irkutsk, USSR)
(Geomagnetizm i Aeronomiia, vol. 19, Sept.-Oct. 1979, p. 840-845.) Geomagnetism and Aeronomy, vol. 19, Apr. 1980, p. 564-566. Translation.

MAJS: /*AURORAL ZONES/*CHANNELS (DATA TRANSMISSION)/*SHORT WAVE RADIO TRANSMISSION/*SIGNAL FADING

MINS: / CROSS CORRELATION/ FREQUENCY RESPONSE/ HIGH FREQUENCIES/ IONOSPHERIC PROPAGATION/ TIME RESPONSE
ABS: (For abstract see issue 01, p. 37, Accession no. A80-10136) See Page 33 for abstract.

81A32344 ISSUE 14 PAGE 2335 CATEGORY 32 RPT#: AD-A097963 ESD-TR-81-12 80/00/00 4 PAGES UNCLASSIFIED DOCUMENT
UTTL: A link availability predictor model for Satcom system architecture
AUTH: A/SCHWAB, L. M.; B/SHERWIN, R. P.; C/WOLFSON, C. R. PAA: A/(MIT, Lexington, Mass.); C/(U.S. Defense Communications Agency, Washington, D.C.)
In: ICC '80; International Conference on Communications, Seattle, Wash., June 8-12, 1980, Conference Record. Volume 3. (A81-32276 14-32) New York, Institute of Electrical and Electronics Engineers, Inc., 1980, p. 40.6.1-40.6.4. Research sponsored by the U.S. Defense Communications Agency and U.S. Air Force.
MAJS: /*DATA LINKS/*MATHEMATICAL MODELS/*PREDICTION ANALYSIS TECHNIQUES/*RAIN/*RCA SATCOM SATELLITES/*SATELLITE TRANSMISSION
MINS: / COMMUNICATION SATELLITES/ METEOROLOGICAL PARAMETERS/ MICROWAVE ATTENUATION/ MILLIMETER WAVES/ POLAR REGIONS / SATELLITE CONTROL
ABA: B.J.
ABS: Neither climatology nor elevation angle alone is an accurate predictor of Satcom link availability. This paper presents a tool for computing and displaying link availability as a composite multivariable function of regional climate effects, system geometry including elevation angle, and spectral effects. The most striking result is the unexpectedly high values of link availability in the polar regions; this is due to the comparatively low values of rain rate coupled with small values of melting layer height.

81A31440# ISSUE 13 PAGE 2188 CATEGORY 46 81/04/00 9 PAGES In RUSSIAN UNCLASSIFIED DOCUMENT
UTTL: The effect of the main ionization trough on the propagation of decametric waves at high latitudes
AUTH: A/BLAGOVESHCHENSKII, D. V.; B/BLAGOVESHCHENSKAIA, N. F. PAA: B/(Akademiia Nauk SSSR, Sibirskii Institut Zemnogo Magnetizma, Ionosfery i Rasprostraneniia Radiovoln, Irkutsk, USSR)
Geomagnetizm i Aeronomiia, vol. 21, Mar.-Apr. 1981, p. 289-297. In Russian.
MAJS: /*DECAMETRIC WAVES/*IONOSPHERIC PROPAGATION/*SHORT WAVE RADIO TRANSMISSION
MINS: / IONOSPHERIC SOUNDING/ NIGHT SKY/ POLAR REGIONS/ SIGNAL REFLECTION
ABA: B.J.
ABS: An analysis is presented of the influence of the main ionization trough and its polar boundary on the transmission of radio signals; the study is based on oblique sounding data and the statistical characteristics of short-wave signals transmitted in the high-latitude ionosphere. Stable patterns are found for variations of signals reflected from the polar boundary of the trough. It is shown that combined measurements on several high-latitude paths can be used to determine the location and motion of the polar 'wall' of the trough.

81A31436# ISSUE 13 PAGE 2187 CATEGORY 46 81/04/00 6 PAGES In RUSSIAN UNCLASSIFIED DOCUMENT
UTTL: Relationship between background corpuscular radiation and solar activity
AUTH: A/RAPOPORT, Z. TS. PAA: A/(Akademiia Nauk SSSR, Institut Zemnogo Magnetizma, Ionosfery i Rasprostraneniia Radiovoln, Akademgorodok, USSR)
Geomagnetizm i Aeronomiia, vol. 21, Mar.-Apr. 1981, p. 266-271. In Russian.
MAJS: /*BACKGROUND RADIATION/*CORPUSCULAR RADIATION/* IONOSPHERIC PROPAGATION/*SOLAR ACTIVITY EFFECTS
MINS: / ATMOSPHERIC ATTENUATION/ AURORAL ZONES/ MIDLATITUDE ATMOSPHERE
ABA: B.J.
ABS: Available data indicate that the influence of solar activity on radio-wave absorption in the midlatitude ionosphere differs from that in the auroral ionosphere. It is shown here that the most probable explanation for the relatively weak solar-activity dependence of absorption in the auroral zone is the weak or inverse variation of background corpuscular fluxes with increasing solar activity.

81A17454 ISSUE 5 PAGE 658 CATEGORY 17 RPT#: AD-A095819 AFOSR-TR-81-0174 CNT#: DNA001-75-C-0111 DNA001-78-C-0042 F49620-78-C-0014 80/10/00 8 PAGES UNCLASSIFIED DOCUMENT
UTTL: Geometrical control of the ratio of intensity and phase scintillation indices --- in satellite-to-earth signal transmission
AUTH: A/FREMOUW, E. J. PAA: A/(Physical Dynamics, Inc., Bellevue, Wash.)
Journal of Atmospheric and Terrestrial Physics, vol. 42, Sept.-Oct. 1980, p. 775-782.
MAJS: /*IONOSPHERIC PROPAGATION/*SCINTILLATION/*SIGNAL TRANSMISSION/*SPACECRAFT COMMUNICATION
MINS: / AURORAL ZONES/ EQUATORIAL ATMOSPHERE/ GROUND STATIONS/ MIDLATITUDE ATMOSPHERE/ PLASMA DENSITY
ABA: A.T.

ABS: The differences in the ratio of the intensity scintillation index S4 to the phase scintillation index sigma sub phi observed by midlatitude, auroral, and equatorial stations from a polar-orbiting satellite are also found in nonsaturated values of S4. Four factors which control the S4/sigma sub phi ratio are determined using the phase-screen theory for the production of scintillation; models are constructed describing the sheetlike and rodlike plasma-density irregularities. The models permit rejection of the effects of static diffraction by field-aligned irregularities; however, the geometrical control of the effective outer scale imposed by detrend filtering in the presence of anisotropic irregularities can explain different behaviors.

81A17201 ISSUE 5 PAGE 673 CATEGORY 32 80/11/00
11 PAGES UNCLASSIFIED DOCUMENT
UTTL: Measurements of VHF/UHF propagation characteristics over arctic paths
AUTH: A/PALMER, F. H. PAA: A/(Department of Communications Research Centre, Ottawa, Canada)
IEEE Transactions on Antennas and Propagation, vol. AP-28, Nov. 1980, p. 733-743.
MAJS: /*ARCTIC REGIONS/*ELECTROMAGNETIC MEASUREMENT/*RADIO TRANSMISSION/*TRANSMISSION LOSS/*ULTRAHIGH FREQUENCIES /*VERY HIGH FREQUENCIES
MINS: / FREQUENCY RESPONSE/ GROUND EFFECT (COMMUNICATIONS)/ ICE ENVIRONMENTS/ OCEAN SURFACE/ POLARIZATION CHARACTERISTICS/ RADIO RECEPTION/ RADIO WAVES/ SEA WATER
ABA: (Author)
ABS: A series of measurements of VHF and UHF radiowave path loss were carried out near Inuvik and Resolute Bay, Northwest Territories, during 1976 and 1977. The transmitter sites were chosen to be representative of those that would be selected for actual communications facilities. Measurements of path loss, for various frequencies, polarizations, and transmitting and receiving antenna heights were made at a number of receiving sites along several radials from each transmitter. The path lengths ranged from 1-100 km and covered land, water, and mixed types of terrain. The measurement program is described, and empirical path loss models derived from the results are presented.

81A17093 ISSUE 5 PAGE 721 CATEGORY 46 80/11/00
4 PAGES UNCLASSIFIED DOCUMENT
UTTL: Excitation of ULF and VLF waves in the ionosphere
AUTH: A/BUJARBARUA, S.; B/SHUKLA, P. K.; C/DAS, A. C. PAA: A/(Bochum, Ruhr-Universitaet, Bochum, West Germany; Dibrugarh University, Dibrugarh, India); B/(Bochum, Ruhr-Universitaet, Bochum, West Germany); C/(Physical Research Laboratory, Ahmedabad, India)
Planetary and Space Science, vol. 28, Nov. 1, 1980, p. 1051-1054.
MAJS: /*EXTREMELY LOW RADIO FREQUENCIES/*IONOSPHERIC NOISE/* VERY LOW FREQUENCIES/*WAVE EXCITATION
MINS: / AURORAL ZONES/ IONOSPHERIC PROPAGATION/ WHISTLERS
ABA: (Author)
ABS: It is shown that a two-dimensional lower-hybrid wave structure can parametrically trigger the growth of VLF and ULF noises in a plasma. Analytical expressions for the increment and threshold of the instability are obtained. Application of our work to the auroral zones of the topside ionosphere is discussed.

81A10970 ISSUE 1 PAGE 24 CATEGORY 32 79/10/00
3 PAGES UNCLASSIFIED DOCUMENT
UTTL: Effect of magnetic activity on the frequency spectra of HF-signal fluctuations in high-latitude radio ducts. II - Spectral characteristics of HF signals during auroral substorms
AUTH: A/BLAGOVESHCHENSKAIA, N. F. PAA: A/(Akademiia Nauk SSSR, Sibirskii Institut Zemnogo Magnetizma, Ionosfery i Rasprostranenila Radiovoln, Irkutsk; Polarnyi Kosmofizicheskii Poligon, USSR)
(Geomagnetizm i Aeronomiia, vol. 19, Mar.-Apr. 1979, p. 274-278.) Geomagnetism and Aeronomy, vol. 19, Oct. 1979, p. 177-179. Translation.
MAJS: /*AURORAL ZONES/*MAGNETOACTIVITY/*POLAR *RADIO* BLACKOUT /*POLAR SUBSTORMS/*SHORT WAVE RADIO TRANSMISSION/* SIGNAL FADING
MINS: / AURORAL SPECTROSCOPY/ FLUCTUATION THEORY/ FREQUENCY DISTRIBUTION/ GEOMAGNETISM/ MAGNETOSPHERE
ABS: (Previously cited in issue 13, p. 2355, Accession no. A79-33289) See Page 33 for abstract.

81A10934 ISSUE 1 PAGE 76 CATEGORY 46 79/08/00
3 PAGES UNCLASSIFIED DOCUMENT
UTTL: Effect of magnetic activity on the frequency spectra of HF signal fluctuations on high-latitude radio paths. I - Dependence of the spectral parameters of HF signal fluctuations on magnetic activity
AUTH: A/BLAGOVESHCHENSKAIA, N. F. PAA: A/(Akademiia Nauk SSSR, Institut Zemnogo Magnetizma, Ionosfery i Rasprostranenila Radiovoln, Irkutsk; Polarnyi Kozmofizicheskii Poligon, USSR)
(Geomagnetizm i Aeronomiia, vol. 19, Jan.-Feb. 1979, p. 63-67.) Geomagnetism and Aeronomy, vol. 19, Aug. 1979, p. 38-40. Translation.
MAJS: /*FREQUENCY RESPONSE/*GEOMAGNETISM/*MAGNETIC EFFECTS/* POLAR REGIONS/*SHORT WAVE RADIO TRANSMISSION/*SIGNAL FADING

MINS: / ANNUAL VARIATIONS/ DIURNAL VARIATIONS/ ENERGY SPECTRA/ FLUCTUATION THEORY/ MAGNETOIONICS/ NIGHT SKY
ABS: (Previously cited in issue 09, p. 1626, Accession no. A79-25034) See Page 33 for abstract.

80A49184# ISSUE 21 PAGE 3946 CATEGORY 46 CNT#: DNA001-77-C-0220 80/08/01 13 PAGES UNCLASSIFIED DOCUMENT
UTTL: On the morphology of auroral zone radio wave scintillation
AUTH: A/RINO, C. L.; B/MATTHEWS, S. J. PAA: B/(SRI International Radio Physics Laboratory, Menlo Park, Calif.)
Journal of Geophysical Research, vol. 85, Aug. 1, 1980, p. 4139-4151.
MAJS: /*AURORAL ZONES/*IONOSPHERIC PROPAGATION/* SCINTILLATION
MINS: / F REGION/ MAGNETIC EFFECTS/ NOCTURNAL VARIATIONS/ PLASMA LAYERS/ POLAR REGIONS/ SATELLITE SOUNDING
ABA: (Author)
ABS: This paper describes the morphology of midnight sector and morning sector auroral zone scintillation observations made over a two-year period using the Wideband satellite, which is in a sun-synchronous, low-altitude orbit. No definitive seasonal variation was found. The nighttime data showed the highest scintillation occurrence levels, but significant amounts of morning scintillation were observed. For the most part the scintillation activity followed the general pattern of local magnetic activity. The most prominent feature in the nighttime data is a localized amplitude and phase scintillation enhancement at the point where the propagation vector lies within an L shell. A geometrical effect due to a dynamic slab of sheetlike structures in the F region is hypothesized as the source of this enhancement. The data have been sorted by magnetic activity, proximity to local midnight, and season. The general features of the data are in agreement with the accepted morphology of auroral zone scintillation.

80A48833# ISSUE 21 PAGE 3944 CATEGORY 46 80/00/00 5 PAGES In RUSSIAN UNCLASSIFIED DOCUMENT DCAF A091080
UTTL: Traveling ionospheric disturbances during a magnetospheric substorm
AUTH: A/KLIMOV, N. N.; B/SHASHUNKINA, V. M.; C/IUDOVICH, L. A.
Ionosfernye Issledovaniia, no. 30, 1980, p. 69-73. In Russian.
MAJS: /*AURORAL ZONES/*GRAVITY WAVES/*MAGNETIC STORMS/* MAGNETOSPHERIC INSTABILITY/*TRAVELING IONOSPHERIC DISTURBANCES
MINS: / ACOUSTIC PROPAGATION/ ATMOSPHERIC HEATING/ INTERNAL WAVES/ WAVE PROPAGATION
ABA: V.P.
ABS: The response of the ionosphere to the isolated substorm of March 2, 1965 is examined. During the substorm, acoustic-gravity waves propagating at 600 m/sec toward the lower latitudes were generated in the auroral zone. Such wave characteristics as their quasi-period and rate of propagation, obtained from an analysis of the distribution of the ion component, are found to correlate well with direct measurements.

80A43098 ISSUE 18 PAGE 3385 CATEGORY 46 79/04/00 2 PAGES UNCLASSIFIED DOCUMENT
UTTL: Auroral inhomogeneities in the lower ionosphere from VLF measurements
AUTH: A/BELOGLAZOVA, G. P.; B/BELOGLAZOV, M. I. PAA: B/(Akademiia Nauk SSSR, Poliarnyi Geofizicheskii Institut, Murmansk, USSR)
(Geomagnetizm i Aeronomiia, vol. 18, Sept.-Oct. 1978, p. 927-929.) Geomagnetism and Aeronomy, vol. 18, Apr. 1979, p. 631, 632. Translation.
MAJS: /*AURORAL ZONES/*IONOSPHERIC DISTURBANCES/*LOWER IONOSPHERE/*RADIO SIGNALS/*VERY LOW FREQUENCIES
MINS: / F REGION/ FREQUENCY DISTRIBUTION/ RADIO HORIZONS/ RADIO TRANSMISSION/ SIGNAL ANALYSIS/ SPECTRUM ANALYSIS
ABS: (Previously cited in issue 04, p. 673, Accession no. A79-16832) See Page 33 for abstract.

80A31541# ISSUE 12 PAGE 2217 CATEGORY 46 80/04/00 4 PAGES In RUSSIAN UNCLASSIFIED DOCUMENT
UTTL: The formation of weak large-scale irregularities in the auroral ionosphere
AUTH: A/GELBERG, M. G. PAA: A/(Akademiia Nauk SSSR, Poliarnyi Geofizicheskii Institut, Murmansk; Akademiia Nauk SSSR, Institut Kosmofizicheskikh Issledovanii i Aeronomii, Yakutsk, USSR)
Geomagnetizm i Aeronomiia, vol. 20, Mar.-Apr. 1980, p. 271-274. In Russian.
MAJS: /*AURORAL ZONES/*F REGION/*IONOSPHERIC DISTURBANCES/* NONUNIFORM PLASMAS/*PLASMA-PARTICLE INTERACTIONS/* RADIO TRANSMISSION
MINS: / ELECTRIC FIELDS/ INFRASONIC FREQUENCIES/ RADIO SIGNALS/ RAREFIED PLASMAS/ WAVE INTERACTION/ WAVE PROPAGATION
ABA: A.T.
ABS: The paper demonstrates that in the presence of external electric fields of specific magnitude, subsonic waves which propagate at small angles to the horizontal can effectively interact with the F-region of the ionosphere by modulating the conductivity of

the ionospheric plasma and the subsequent redistribution of charges because of periodic polarization fields. If the angle between the external electric field and the horizontal component of the wave vector satisfies a condition of spatial resonance derived here, the amplitude of perturbation of electronic density exceeds the amplitude of the subsonic wave.

80A31529# ISSUE 12 PAGE 2217 CATEGORY 46
80/04/00 5 PAGES In RUSSIAN UNCLASSIFIED DOCUMENT
UTTL: Determination of the magnitude of polar cap absorption on the basis of integral parameters of solar microwave radio bursts
AUTH: A/AKINIAN, S. T.; B/CHERTOK, I. M. PAA: B/(Akademiia Nauk SSSR, Institut Zemnogo Magnetizma, Ionosfery i Rasprostraneniia Radiovoln, Akademgorodok, USSR)
Geomagnetizm i Aeronomiia, vol. 20, Mar.-Apr. 1980, p. 192-196. In Russian.
MAJS: /*INTERPLANETARY SPACE/*MICROWAVE ATTENUATION/*POLAR CAP ABSORPTION/*SOLAR RADIO BURSTS
MINS: / ABSORPTION SPECTRA/ ENERGY SPECTRA/ IONOSPHERE/ SOLAR PHYSICS/ SOLAR PROTONS
ABA: A.T.
ABS: The paper determines reference functions of intensity and longitudinal attenuation which connect the magnitude of polar cap absorption with the integral parameters of microwave bursts at frequencies of 3 and 9 GHz. A determination is made of the solar longitude of the burst, conditions of proton discharge into the interplanetary space, and proton energy spectrum.

80A30647# ISSUE 11 PAGE 2048 CATEGORY 46 RPT#: AD-A084299 AFGL-TR-80-0144 80/02/00 13 PAGES UNCLASSIFIED DOCUMENT
UTTL: High-latitude analytical formulas for scintillation levels --- of transionospheric radio signals
AUTH: A/AARONS, J.; B/MACKENZIE, E.; C/BHAVNANI, K. PAA: A/(USAF, Geophysics Laboratory, Bedford, Mass.); B/(Emmanuel College, Boston, Mass.); C/(Logicon, Inc., Bedford, Mass.)
Radio Science, vol. 15, Jan.-Feb. 1980, p. 115-127.
MAJS: /*ATMOSPHERIC MODELS/*AURORAL ZONES/*DATA BASES/*IONOSPHERIC PROPAGATION/*POLAR REGIONS/*SCINTILLATION
MINS: / ANNUAL VARIATIONS/ DIURNAL VARIATIONS/ MAGNETIC VARIATIONS/ RADIO SIGNALS/ SOLAR FLUX
ABA: V.T.
ABS: The paper deals with the seasonal, solar flux, and magnetic dependence at auroral and subauroral latitudes as well as at a mid-latitude station. Analytical formulas are developed from a large data base. The data base used is a series of measurements of the scintillations of one synchronous satellite beacon, ATS 3, transmitting at 137 MHz. The analytical terms provide mean scintillation excursions as a function of time of day, month, solar flux, and magnetic index.

80A30642# ISSUE 11 PAGE 1979 CATEGORY 32 RPT#: AD-A084298 AFGL-TR-80-0145 80/02/00 12 PAGES UNCLASSIFIED DOCUMENT
UTTL: The morphology of high-latitude VHF scintillation near 70 W
AUTH: A/BASU, S.; B/AARONS, J. PAA: A/(Emmanuel College, Boston, Mass.); B/(USAF, Geophysics Laboratory, Bedford, Mass.)
Radio Science, vol. 15, Jan.-Feb. 1980, p. 59-70.
MAJS: /*AURORAL ZONES/*IONOSPHERIC PROPAGATION/*RADIO BEACONS/*SCINTILLATION/*VERY HIGH FREQUENCIES
MINS: / ANNUAL VARIATIONS/ ATS 3/ ELECTRON PRECIPITATION/ GEOMAGNETISM/ PROTON PRECIPITATION/ SATELLITE TRANSMISSION
ABA: (Author)
ABS: The long-term VHF scintillation data from ATS 3 obtained at three stations situated in the North Atlantic sector at auroral and subauroral locations during the period 1968-1974 are used to determine the morphology of high-latitude scintillations near the 70 W longitude sector. The variation of the average level of scintillation at each observatory is studied as a function of time of day, season, and magnetic activity in a manner suitable for incorporation into statistical models of scintillation occurrence. The most prominent feature of the data is a seasonal dependence of scintillations with a 2:1 variation from northern summer to winter under quiet magnetic conditions. This also causes a large variation in the latitudinal gradient of scintillations from 2 dB per degree in summer to 1 dB per degree in winter for latitudes greater than 60 deg invariant. The observed seasonal control of scintillations is related to the variation of the tilt angle of the earth's magnetic dipole and consequent modulation of the particle precipitation in the North Atlantic sector of the auroral oval.

80A24864# ISSUE 9 PAGE 1626 CATEGORY 46
80/02/00 2 PAGES In RUSSIAN UNCLASSIFIED DOCUMENT
UTTL: Vertical component of the electric field in the VLF range from measurements in the subauroral zone
AUTH: A/KLEIMENOVA, N. G.; B/FEDORENKO, IU. V.; C/CHERNYSHEVA, S. P.; D/SHEFTEL, V. M. PAA: D/(Rostovskii Inzhenerno-Stroitel'nyi Institut,

Rostov, USSR)
Geomagnetizm i Aeronomiia, vol. 20, Jan.-Feb. 1980, p. 153, 154. In Russian.
MAJS: /*AURORAL ZONES/*ELECTRIC FIELDS/*ELECTRICAL MEASUREMENT/*IONOSPHERIC CURRENTS/*VERTICAL DISTRIBUTION/*VERY HIGH FREQUENCIES
MINS: / IONOSPHERIC PROPAGATION/ SONOGRAMS/ SPECTRUM ANALYSIS

80A22107# ISSUE 7 PAGE 1244 CATEGORY 46
78/00/00 8 PAGES UNCLASSIFIED DOCUMENT
UTTL: Wideband satellite phase coherent beacon observations at auroral and equatorial latitudes - A review
AUTH: A/RINO, C. L.; B/LIVINGSTON, R. C.; C/COUSINS, M. D.; D/FAIR, B. C. PAA: D/(SRI International, Menlo Park, Calif.)
In: Symposium on Beacon Satellite Measurements of Plasmaspheric and Ionospheric Properties, Florence, Italy, May 22-25, 1978, Proceedings. (A80-22076 07-46) Florence, Italy, Consiglio Nazionale delle Ricerche, 1978, p. 37-1 to 37-8.
MAJS: /*AURORAL ZONES/*IONOSPHERIC PROPAGATION/*PHASE COHERENCE/*RADIO BEACONS/*SATELLITE TRANSMISSION/*WIDEBAND COMMUNICATION
MINS: / ATMOSPHERIC MODELS/ COMMUNICATION SATELLITES/ GROUND STATIONS/ SCINTILLATION/ SUPERHIGH FREQUENCIES/ TRACKING STATIONS/ VERY HIGH FREQUENCIES
ABA: (Author)
ABS: This paper presents a brief review of some of the principal results from the first two years of operation of the Wideband satellite which transmits phase-coherent signals from S-band to VHF. The auroral zone data show narrow regions of enhanced scintillation well equatorward of the discrete aurora. Such enhancements can be explained as a purely geometrical effect if the irregularities within the major precipitation regions have a sheet-like structure. Evidence of a localized irregularity source at the poleward boundary of the plasma trough is also found. Model computations are discussed and applied to the interpretation of equatorial data.

80A18913# ISSUE 5 PAGE 840 CATEGORY 46
79/12/00 4 PAGES In RUSSIAN UNCLASSIFIED DOCUMENT
UTTL: Winter anomaly of radio wave absorption in the auroral ionosphere
AUTH: A/RAPOPORT, Z. TS. PAA: A/(Akademiia Nauk SSSR, Institut Zemnogo Magnetizma, Ionosfery i Rasprostraneniia Radiovoln, Akademgorodok, USSR)
Geomagnetizm i Aeronomiia, vol. 19, Nov.-Dec. 1979, p. 1042-1045. In Russian.
MAJS: /*AURORAL ZONES/*ELECTROMAGNETIC ABSORPTION/*IONOSPHERIC PROPAGATION/*RADIO ATTENUATION/*WINTER
MINS: / GEOPHYSICS

80A18910# ISSUE 5 PAGE 840 CATEGORY 46
79/12/00 7 PAGES In RUSSIAN UNCLASSIFIED DOCUMENT
UTTL: Resonant excitation of oscillations of ionospheric currents
AUTH: A/MOLCHANOV, O. A.; B/LIZUNOV, V. V.; C/SHCHEKOTOV, A. IU. PAA: C/(Akademiia Nauk SSSR, Institut Zemnogo Magnetizma, Ionosfery i Rasprostraneniia Radiovoln, Akademgorodok, USSR)
Geomagnetizm i Aeronomiia, vol. 19, Nov.-Dec. 1979, p. 1026-1032. In Russian.
MAJS: /*IONOSPHERIC CURRENTS/*IONOSPHERIC HEATING/*IONOSPHERIC PROPAGATION/*PLASMA OSCILLATIONS/*POLAR REGIONS/*RADIO FREQUENCY HEATING
MINS: / ELECTROJETS/ RADIO TRANSMISSION/ RADIO TRANSMITTERS/ VERY LOW FREQUENCIES
ABA: B.J.
ABS: The paper examines the mechanism of thermal excitation of oscillations of polar electrojet oscillations and induced VLF wave emission in the ionosphere; allowance is made for the extent of radio-wave heating of the ionosphere. Some results on ionospheric heating by transmission from a ground-based VLF transmitter are discussed; the emission 'aftereffect' is examined.

80A14122 ISSUE 3 PAGE 428 CATEGORY 46 79/02/00
3 PAGES UNCLASSIFIED DOCUMENT
UTTL: Investigation of the frequency-correlated properties of the ionosphere on a high-latitude radio path
AUTH: A/BLAGOVESHCHENSKII, D. V.; B/BLAGOVESHCHENSKAIA, N. F.; C/KURCHENKO, IU. A. PAA: C/(Akademiia Nauk SSSR, Institut Zemnogo Magnetizma, Ionosfery i Rasprostraneniia Radiovoln, Irkutsk, USSR)
(Geomagnetizm i Aeronomiia, vol. 18, July-Aug. 1978, p. 638-641.) Geomagnetism and Aeronomy, vol. 18, Feb. 1979, p. 435-437. Translation.
MAJS: /*IONOSPHERIC SOUNDING/*POLAR REGIONS/*RADIO PROBING/*SHORT WAVE RADIO TRANSMISSION/*SIGNAL RECEPTION
MINS: / CORRELATION COEFFICIENTS/ DRIFT RATE/ INHOMOGENEITY/ POLAR SUBSTORMS/ RECEPTION DIVERSITY/ TURBIDITY
ABS: (For abstract see issue 02, p. 276, Accession no. A79-12916) See Page 33 for abstract.

PRINT 99/2/1-5 TERMINAL=65

80A10136# ISSUE 1 PAGE 37 CATEGORY 32 79/10/00
6 PAGES In RUSSIAN UNCLASSIFIED DOCUMENT

UTTL: Characteristics of the selective properties of short-wave radio channels at high latitudes

AUTH: A/BLAGOVESHCHENSKII, D. V.; B/KURCHENKO, IU. A.; C/KONSTANTINOV, A. A. PAA: C/(Akademiia Nauk SSSR, Institut Zemnogo Magnetizma, Ionosfery i Rasprostraneniia Radiovoln, Irkutsk, USSR)
Geomagnetizm i Aeronomiia, vol. 19, Sept.-Oct. 1979, p. 840-845. In Russian.

MAJS: /*AURORAL ZONES/*CHANNELS (DATA TRANSMISSION)/*SHORT WAVE RADIO TRANSMISSION/*SIGNAL FADING

MINS: / CROSS CORRELATION/ FREQUENCY RESPONSE/ TIME RESPONSE

ABA: V.P.

ABS: In the present paper, selective fadings along a path passing through the auroral zone are analyzed with respect to time and space, to frequency and space, and to time and frequency. The conditions are identified under which the multiparameter cross-correlation function may be expressed in terms of a product of the correlation functions of each of the three arguments.

79A33289# ISSUE 13 PAGE 2355 CATEGORY 32
79/04/00 5 PAGES In RUSSIAN UNCLASSIFIED DOCUMENT

UTTL: Effect of magnetic activity on frequency spectra of short-wave signal fluctuations in high-latitude radio channels. II - Spectral characteristics of short-wave signals during auroral substorms

AUTH: A/BLAGOVESHCHENSKAIA, N. F. PAA: A/(Akademiia Nauk SSSR, Institut Zemnogo Magnetizma, Ionosfery i Rasprostraneniia Radiovoln, Irkutsk; Poliarnyi Kosmofizicheskii Poligon, USSR)
Geomagnetizm i Aeronomiia, vol. 19, Mar.-Apr. 1979, p.274-278. In Russian.

MAJS: /*AURORAL ZONES/*MAGNETOACTIVITY/*POLAR RADIO BLACKOUT/*POLAR SUBSTORMS/*SHORT WAVE RADIO TRANSMISSION/*SIGNAL FADING

MINS: / AURORAL SPECTROSCOPY/ FLUCTUATION THEORY/ FREQUENCY DISTRIBUTION/ GEOMAGNETISM/ MAGNETOSPHERE

79A25034# ISSUE 9 PAGE 1626 CATEGORY 46
79/02/00 5 PAGES In RUSSIAN UNCLASSIFIED DOCUMENT

UTTL: Effect of magnetic activity on the frequency spectra of fluctuations of short-wave signals in high-latitude radio channels. I - Dependence of the parameters of fluctuation spectra of short-wave signals on magnetic activity

AUTH: A/BLAGOVESHCHENSKAIA, N. F. PAA: A/(Akademiia Nauk SSSR, Institut Zemnogo Magnetizma, Ionosfery i Rasprostraneniia Radiovoln, Irkutsk; Poliarnyi Kosmofizicheskii Poligon, USSR)
Geomagnetizm i Aeronomiia, vol. 19, Jan.-Feb. 1979, p. 63-67. In Russian.

MAJS: /*FREQUENCY RESPONSE/*GEOMAGNETISM/*MAGNETIC EFFECTS/*POLAR REGIONS/*SHORT WAVE RADIO TRANSMISSION/*SIGNAL FADING

MINS: / ANNUAL VARIATIONS/ DIURNAL VARIATIONS/ ENERGY SPECTRA/ FLUCTUATION THEORY/ MAGNETOIONICS/ NIGHT SKY

79A16832# ISSUE 4 PAGE 673 CATEGORY 46
78/10/00 3 PAGES In RUSSIAN UNCLASSIFIED DOCUMENT

UTTL: Auroral inhomogeneities in the lower ionosphere from VLF measurements

AUTH: A/BELOGLAZOVA, G. P.; B/BELOGLAZOV, M. I. PAA: B/(Akademiia Nauk SSSR, Poliarnyi Geofizicheskii Institut, Murmansk, USSR)
Geomagnetizm i Aeronomiia, vol. 18, Sept.-Oct. 1978, p. 927-929. In Russian.

MAJS: /*AURORAL ZONES/*IONOSPHERIC DISTURBANCES/*LOWER IONOSPHERE/*RADIO SIGNALS/*VERY LOW FREQUENCIES

MINS: / F REGION/ FREQUENCY DISTRIBUTION/ RADIO HORIZONS/ RADIO TRANSMISSION/ SIGNAL ANALYSIS/ SPECTRUM ANALYSIS

79A12916# ISSUE 2 PAGE 276 CATEGORY 46
78/08/00 4 PAGES In RUSSIAN UNCLASSIFIED DOCUMENT

UTTL: Study of frequency-correlated characteristics of the ionosphere at a high-latitude radio path

AUTH: A/BLAGOVESHCHENSKII, D. V.; B/BLAGOVESHCHENSKAIA, N. F.; C/KURCHENKO, IU. A. PAA: C/(Akademiia Nauk SSSR, Institut Zemnogo Magnetizma, Ionosfery i Rasprostraneniia Radiovoln, Irkutsk, USSR)
Geomagnetizm i Aeronomiia, vol. 18, July-Aug. 1978, p. 638-641. In Russian.

MAJS: /*IONOSPHERIC SOUNDING/*POLAR REGIONS/*RADIO PROBING/*SHORT WAVE RADIO TRANSMISSION/*SIGNAL RECEPTION

MINS: / CORRELATION COEFFICIENTS/ DRIFT RATE/ INHOMOGENEITY/ POLAR SUBSTORMS/ RECEPTION DIVERSITY/ TURBIDITY

ABA: M.L.

ABS: The paper discusses results indicated by the frequency-spaced reception of short-wave signals on a radio path proceeding through the auroral one. The relations of the frequency coefficients o signal correlations in different geophysical environments are analyzed with particular attention to the time of auroral substorms. Values of ionospheric parameters are given for turbidity coefficients, the dimensions of inhomogeneities, and the drift velocity.

PRINT 02/2/1-42 TERMINAL=65

85N13337# ISSUE 4 PAGE 522 CATEGORY 46
83/00/00 16 PAGES UNCLASSIFIED DOCUMENT DCAF E003298

UTTL: Ionospheric scintillation: A brief review
AUTH: A/MULLEN, J. P.; B/AARONS, J.; C/MACKENZIE, E. M.
PAA: C/(Emmanuel Coll., Boston)
CORP: Air Force Geophysics Lab., Hanscom AFB, Mass.
AVAIL.NTIS SAP: HC A23/MF A01
In Observatorio del Ebro Sci. Contrib. in Commemoration of Ebro Observatory's 75th Anniv. p 335-350 (SEE N85-13308 04-42)
MAJS: /*EQUATORIAL ATMOSPHERE/*IONOSPHERIC PROPAGATION/*SCINTILLATION/*WAVE DIFFRACTION
MINS: / ATMOSPHERIC MODELS/ AURORAL ZONES/ GEOMAGNETISM/ GEOPHYSICAL OBSERVATORIES/ SOLAR ACTIVITY EFFECTS
ABA: Author (ESA)
ABS: Irregular diffraction of radio signals by the global ionosphere is studied to predict scintillation using easily measured geophysical parameters. Using a network of equatorial stations it was possible to measure and model the average scintillation characteristics and to relate them to geophysical parameters such as solar flux and geomagnetic indices. Typical models for various stations are shown, including the variations of scintillation as predicted and as measured. The scintillation in auroral regions and the phase distortion caused by the ionosphere are also discussed.

85N11086# ISSUE 2 PAGE 160 CATEGORY 46
84/10/26 1 PAGES UNCLASSIFIED DOCUMENT
Original language doc. was announced as A84-34082

UTTL: Convection of plasma in polar ionosphere, comparison of measurements from Cosmos-184 with model dependent on interplanetary magnetic field vector TLSP: Abstract Only
AUTH: A/BELOV, B. A.; B/GALPERIN, Y. I.; C/ZININ, L. V.; D/LEVITIN, A. Y.; E/AFONINA, R. G.; F/FELDSHTEYN, Y. I.
CORP: Joint Publications Research Service, Arlington, Va.
AVAIL.NTIS SAP: HC A07
In its USSR Rept.: Space (JPRS-USP-84-005) p 63 (SEE N85-11060 02-12) Transl. into ENGLISH from Kosmicheskiye Issled. (Moscow), v. 22, no. 2, Mar.-Apr. 1984 p 201-212
MAJS: /*CONVECTIVE FLOW/*IONOSPHERIC PROPAGATION/*MAGNETOPLASMADYNAMICS/*POLAR REGIONS/*SPACE PLASMAS
MINS: / ATMOSPHERIC MODELS/ COSMOS SATELLITES/ ELECTRIC FIELDS/ FLOW VELOCITY/ MAGNETOHYDRODYNAMIC FLOW/ SATELLITE SOUNDING
ABA: E.A.K.
ABS: A problem arising in the construction of a polar cap plasma model is determination of the average quasisteady picture of the electric field, convection and lingitudinal currents, which are determined by factors external to the magnetosphere such as the interplanetary magnetic field, velocity and pressure of the solar wind, level of solar UV radiation, date and time. Satellite measurements are used to study the variations. A combination of various geophysical measurement methods showed certain characteristic structural elements of the unsteady field and current picture during substorms. The work uses the simplest model which is constructed on a correlation analysis of variations in the geomagnetic field with parameters of the solar wind. It is suggested that elimination of a number of simplifying assumptions would greatly increase the complexity and difficulty of using the model.

84N30573# ISSUE 20 PAGE 3241 CATEGORY 46 RPT#: AD-A142648 AFOSR-84-0510TR CNT#: F49620-83-K-0025
84/05/10 159 PAGES UNCLASSIFIED DOCUMENT

UTTL: High-latitude ionospheric irregularities TLSP: Annual Scientific Report, 1 Mar. 1983 - 29 Feb. 1984
AUTH: A/VICKREY, J. F.; B/LIVINGSTON, R. C.; C/ROBINSON, R. M.; D/WALKER, N. B.
CORP: SRI International Corp., Menlo Park, Calif.
AVAIL.NTIS SAP: HC A08/MF A01
MAJS: /*AURORAL ELECTROJETS/*E REGION/*F REGION/*IONOSPHERIC DISTURBANCES/*IONOSPHERIC PROPAGATION/*STRONGLY COUPLED PLASMAS
MINS: / ATMOSPHERIC MODELS/ ELECTRIC FIELDS/ ELECTRICAL RESISTIVITY/ ELECTRODYNAMICS/ IRREGULARITIES/ MAGNETIC DIFFUSION/ MAGNETOSPHERIC ELECTRON DENSITY/ POLAR REGIONS/ SCINTILLATION/ STRIATION
ABA: GRA
ABS: This document summarizes studies on the morphology of ionospheric structure at high latitudes. The program encompasses both theoretical and experimental investigations into this rapidly developing field. Because of the vast range of scale sizes (hundreds of kilometers to centimeters) that make up the structure, and the need for time-continuous observations, we employ a diverse set of observational techniques. These include in situ observations from rockets and satellites as well as radio propagation and scattering measurements. Topics include: F-Region Cross-Field Diffusion Processes; High-Latitude Conductivity and Field Aligned Current Systems; Low-Altitude Image Striations Associated with Bottomside Equatorial Spread F--Observations and Theory; Irregularity Decay in an Isolated Plasma Bubble; Electrical Coupling Effects on the Temporal Evolution of F-Layer Plasma Structure; Aurora and Electrojet Configuration in the

Early Morning Sector; Auroral Zone Conductivities within the Field-Aligned Current Sheets, and K sub P Dependence of Auroral Zone Field-Aligned Current Intensity.

84N28277*# ISSUE 18 PAGE 2879 CATEGORY 46
RPT#: NASA-TM-86091 NAS 1.15:86091 84/04/00 7 PAGES
UNCLASSIFIED DOCUMENT

UTTL: Field-aligned electron density irregularities near 500 km. Equator to polar cap topside sounder Z mode observations

AUTH: A/BENSON, R. F.

CORP: National Aeronautics and Space Administration. Goddard Space Flight Center, Greenbelt, Md. AVAIL.NTIS SAP: HC A02/MF A01

Presented at the IES Symp. on the Effect of the Ionosphere on C-3I Systems, Alexandria, Va., 1-3 May 1984

MAJS: /*ELECTRON DISTRIBUTION/*IONOSPHERIC ELECTRON DENSITY /*IONOSPHERIC NOISE/*RADIO FREQUENCIES

MINS: / ALOUETTE 2 SATELLITE/ AURORAS/ ECHOES/ ELECTROSTATIC WAVES/ IONOGRAMS/ IONOSPHERE/ IONOSPHERIC F-SCATTER PROPAGATION/ PLASMA WAVES/ POLAR CAPS/ SPACE PLASMAS/ SPACE SHUTTLES/ SPACELAB

ABA: R.S.F.

ABS: In addition to spread F, evidence for field-aligned electron density irregularities is commonly observed on Alouette 2 topside sounder ionograms recorded near perigee (500 km). This evidence is provided by distinctive signal returns from sounder-generated Z mode waves. At low latitudes these waves become guided in wave ducts caused by field-aligned electron density irregularities and give rise to strong long-duration echoes. At high latitudes, extending well into the polar cap, these Z mode waves (and stimulated electrostatic waves at the plasma frequency) produce a series of vertical bars on the ionogram display as the satellite traverses discrete field-aligned density structures. The radio frequency (RF) noise environment to be expected in the 400 to 500 km altitude region from low to high latitudes was examined by analyzing perigee Alouette 2 topside sounder data. All observed noise bands were scaled on nearly 200 topside sounder ionograms recorded near perigee at low, mid, and high latitude telemetry stations. The minimum and maximum frequencies of each noise band were entered into a data base or compuer analysis. The signals of primary interest in the perigee study were found to be sounder-generated.

84N27960# ISSUE 18 PAGE 2829 CATEGORY 32 RPT#: AD-A141237 RADC-TR-83-269 CNT#: AF PROJ. 4600
83/12/00 30 PAGES UNCLASSIFIED DOCUMENT

UTTL: A statistical channel model for adaptive HF communications via a severely disturbed ionosphere

AUTH: A/HAINES, D. M.

CORP: Rome Air Development Center, Griffiss AFB, N.Y. AVAIL.NTIS SAP: HC A03/MF A01

MAJS: /*CHANNELS (DATA TRANSMISSION)/*HIGH FREQUENCIES/* IONOSPHERIC DISTURBANCES/*IONOSPHERIC PROPAGATION

MINS: / ADAPTATION/ ANTENNAS/ ARCTIC REGIONS/ COMMUNICATION EQUIPMENT/ DIGITAL SYSTEMS/ FREQUENCY ASSIGNMENT/ MATCHED FILTERS/ MATHEMATICAL MODELS/ PULSE COMPRESSION/ QUALITY/ SIGNAL PROCESSING/ SPATIAL DISTRIBUTION/ TELECOMMUNICATION/ TIME MEASUREMENT/ WAVEFORMS

ABA: Author (GRA)

ABS: Motivation for the resurgence of interest in improving HF communication is presented. This includes the continued widespread use of the HF band, and the new technology that now makes it feasible to vastly improve the historically poor quality of communications in this band. Non-conventional HF techniques or systems are classified into four general categories according to the technical specialties that spawned them. These categories are Adaptive Frequency Management, Digital Waveform Processing, Networking, and Adaptive Antennas. A 15 parameter channel model is presented which forms the basis for the on-going RADC measurement program. These parameters address the dispersion and dynamics of time, frequency and spatial distortion imposed by the skywave channel. Next, measurement techniques are evaluated for characterization of these parameters, resulting in the selection of a six station Arctic network of wideband pulse compression (matched filter) channel probes. A description of waveform generation, receiver signal processing and the program plans and schedule are presented.

84N27358*# ISSUE 17 PAGE 2727 CATEGORY 46
RPT#: NASA-CR-173641 NAS 1.26:173641 AD-A140586 U-OF-IOWA-84-2 CNT#: NAS5-26363 NAS5-25693 NAG5-310 N000014-76-C-0016 84/02/00 56 PAGES UNCLASSIFIED DOCUMENT

UTTL: Low frequency electric and magnetic noise along the auroral field lines TLSP: Progress Report

AUTH: A/GURNETT, D. A.; B/HUFF, R. L.; C/MENIETTI, J. D.; D/WININGHAM, J. D.; E/BURCH, J. L.

CORP: Iowa Univ., Iowa City.; Southwest Research Inst., San Antonio, Tex. CSS: (Dept. of Physics and Astronomy.) AVAIL.NTIS SAP: HC A04/MF A01

Prepared in cooperation with Southwest Research

Institute, San Antonio, TX
MAJS: /*AURORAL ZONES/*ELECTROMAGNETIC NOISE/*LOW ALTITUDE/* LOW FREQUENCIES/*MAGNETIC VARIATIONS/* MAGNETOHYDRODYNAMIC WAVES/*PLASMA WAVES
MINS: / CONDUCTION ELECTRONS/ ELECTRIC FIELDS/ ELECTRON PRECIPITATION/ IONOSPHERE/ LINES/ MAGNETIC FIELDS/ POLARIZATION/ REFRACTIVITY/ WAVE PROPAGATION
ABA: GRA
ABS: Plasma wave and plasma measurements from the DE-1 spacecraft are used to investigate an intense band of low frequency, < 100 Hz, electric and magnetic noise detected at low altitudes over the auroral zones. This noise is observed by DE-1 on essentially every low altitude pass over the auroral zone and occurs in regions of intense low energy, 100 eV to 10 keV, electron precipitation and field-aligned currents. The electric field polarization in a plane perpendicular to the static magnetic field is random. Correlation measurements between the electric and magnetic fields show that the perpendicular (approx. north-south) electric field fluctuations are closely correlated with the perpendicular (east-west) magnetic field fluctuations, and that the Poynting flux is directed downward, toward the Earth. The total electromagnetic power flow associated with these fluctuations is very large, approx. 10 to the 8th power watts. Two interpretations of the low frequency noise are considered: first, that the noise is produced by quasi-static fields imbedded in the ionosphere, and second, that the noise is due to Alfven waves propagating along the auroral field lines. For the quasi-static interpretation, the ratio of the magnetic to electric field strengths is determined by the Pedersen conductivity at the base of the ionosphere, whereas for the Alfven wave interpretation it is determined by the Alfven index of refraction.

84N24969# ISSUE 15 PAGE 2326 CATEGORY 32
84/02/00 8 PAGES UNCLASSIFIED DOCUMENT
UTTL: VHF and UHF propagation in the Canadian high Arctic
AUTH: A/BUTLER, R. S.; B/STRICKLAND, J. I.; C/BILODEAU, C.
CORP: Communications Research Centre, Ottawa (Ontario). AVAIL.NTIS SAP: HC A14/MF A01
In AGARD Characteristics of the Lower Atmosphere Influencing Radio Wave Propagation 8 p (SEE N84-24943 15-32)
MAJS: /*ACOUSTIC DUCTS/*ARCTIC REGIONS/*VERY HIGH FREQUENCIES/*WAVE PROPAGATION
MINS: / COMMUNICATION NETWORKS/ INTAKE SYSTEMS/ NOISE REDUCTION/ TELECOMMUNICATION
ABA: E.A.K.
ABS: Radio propagation in the Arctic maritime environment was studied. Five UHF radio paths between pairs of elevated points were selected along a 300 km east-west line which parallels a potentially important navigation route through the Arctic Islands. Two VHF paths, each between an elevated site and a point near sea level were also chosen to simulate communications with a ship. Partial results from the summer to winter transition season show that propagation between the elevated points is highly reliable, but that propagation along the slanted paths appears to be strongly affected by radio wave ducting.

84N24948# ISSUE 15 PAGE 2323 CATEGORY 32
84/02/00 12 PAGES UNCLASSIFIED DOCUMENT
UTTL: Measurements of atmospheric effects on satellite links at very low elevation angle
AUTH: A/GUTTEBERG, O.
CORP: Norwegian Telecommunications Administration Research Establishment, Kjeller. AVAIL.NTIS SAP: HC A14/MF A01
In AGARD Characteristics of the Lower Atmosphere Influencing Radio Wave Propagation 12 p (SEE N84-24943 15-32) Sponsored in part by ESA
MAJS: /*ARCTIC REGIONS/*ATMOSPHERIC EFFECTS/*ELEVATION ANGLE /*LINKS/*WAVE PROPAGATION
MINS: / ATMOSPHERIC RADIATION/ CROSS POLARIZATION/ DISCRIMINATION/ RECEPTION DIVERSITY/ SCINTILLATION
ABA: E.A.K.
ABS: Propagation measurements with the Orbital Test Satellite (OTS) at the Arctic islands of Spitzbergen (78 deg) are reported. The elevation angle to the satellite was 3.2 deg and the frequency 11.8 GHz. The experiments included: measurements of atmospheric scintillations, cross polarization discrimination and space diversity improvements. It is shown that the distributions of the received satellite beacon amplitude can be approximated by Rice distributions. Large diversity gain was obtained by using horizontal spacing of 1 km. A wideband (TV) transmission experiment was also performed.

84N20983# ISSUE 11 PAGE 1683 CATEGORY 46 RPT#: AD-A137266 AD-E301301 PD-NW-83-296R DNA-TR-81-276
CNT#: DNA001-81-C-0189 DNA PROJ. I25-AAXH 83/06/13
42 PAGES UNCLASSIFIED DOCUMENT
UTTL: HILAT: A pre-launch overview
AUTH: A/FREMOUW, E. J.
CORP: Physical Dynamics, Inc., Bellvue, Wash. AVAIL.NTIS SAP: HC A03/MF A01
MAJS: /*IONOSPHERIC PROPAGATION/*RADIO WAVES/*SCINTILLATION
MINS: / AURORAL ZONES/ F REGION/ HIGH ALTITUDE/ NUCLEAR WEAPONS/ PLASMA DIAGNOSTICS/ PLASMAS (PHYSICS)
ABA: GRA

ABS: Among the many nuclear-weapons effects that must be accounted for in the design of c3I systems is that of radiowave scintillation produced by scattering in high-altitude structured plasmas. Accordingly, the Defense Nuclear Agency (DNA) conducts a vigorous research program on the nature of such structure and the mechanisms for its production. Past results have indicated significant similarity between that nature and those mechanisms in nuclear-disturbed cases and in the case of the ambient ionosphere disturbed by geophysical process, the variety of which is greatest at high latitudes. To further DoD's knowledge of the three-dimensional spectrum of the scattering structures and its understanding of their production, evolution, and decay, DNA and the Air Force Geophysics Laboratory, along with their respective contractors, have joined together to prepare a multi-experiment satellite mission, called HiLat, to collect definitive data on those processes. In view of applications to any military or civilian system that must transmit radio signals through the disturbed high-latitude ionosphere, including for instance satellite-based search-and-rescue systems, cooperation also is being received from the National Research Council of Canada. The satellite designed to meet these diverse but highly complementary objectives, P83-1, is scheduled for launch from Vanderberg Air Force Base at 1530 Z on 27 June 1983.

84N20748# ISSUE 11 PAGE 1644 CATEGORY 32 RPT#: AD-A137947 SCIENTIFIC-1 AFGL-TR-83-0221 CNT#: F19628-82-K-0045 AF PROJ. 2311 83/11/00 41 PAGES UNCLASSIFIED DOCUMENT

UTTL: Chatanika radar and S3-2 measurements of auroral-zone electrodynamics in the midnight sector TLSP: Scientific Report, 6 Jul. 1982 - 31 Oct. 1983

AUTH: A/ROBINSON, R. M.

CORP: SRI International Corp., Menlo Park, Calif. AVAIL.NTIS SAP: HC A03/MF A01

MAJS: /*AURORAL ZONES/*IONOSPHERIC DISTURBANCES/*MAGNETOSPHERE/*PLASMAS (PHYSICS)/*POLAR REGIONS

MINS: / DISCONTINUITY/ ELECTRIC FIELDS/ GEOMAGNETISM/ INCOHERENT SCATTER RADAR/ IONOSPHERIC PROPAGATION/ MAGNETIC FIELDS/ RADAR ECHOES/ SCIENTIFIC SATELLITES

ABA: Author (GRA)

ABS: Chatanika radar measurements were combined with S3-2 satellite data obtained during passes over the midnight sector auroral zone to study the relationships between conductivities, electric fields, and currents in the Harang discontinuity. Three passes were chosen based on the quality of the radar and satellite data and the availability of supplementary ground-based or satellite measurements. The radar measured electric fields and conductivities as a function of latitude and local time. The satellite measured the latitudinal distribution of electric field and field-aligned current during the three polar passes. The most intenser electric fields were observed in the poleward and equatorward portions of the auroral oval as defined by the region of enhanced ionospheric conductivity. These high electric fields were located at the boundaries between oppositely directed field-aligned-current sheets. The dominant field-aligned-current region in the Harang discontinuity was a broad upward current sheet within which bright auroral arcs were observed. In the three cases examined, there was a net upward current in the discontinuity.

84N18789# ISSUE 9 PAGE 1345 CATEGORY 46 RPT#: AD-A135946 PPG-748 CNT#: N00014-75-C-0476 83/10/00 49 PAGES UNCLASSIFIED DOCUMENT

UTTL: Ohmic heating of the polar f-region by HF (High Frequency) pulse

AUTH: A/SHOUCRI, M. M.; B/MORALES, G. J.; C/MAGGS, J. E.

CORP: California Univ., Los Angeles. CSS: (Center for Plasma Physics and Fusion Engineering.) AVAIL.NTIS SAP: HC A03/MF A01

MAJS: /*F REGION/*HIGH FREQUENCIES/*IONOSPHERIC DISTURBANCES/*PLASMA HEATING/*POLAR REGIONS/*PULSE MODULATION

MINS: / ELECTRIC FIELDS/ ELECTRON DENSITY (CONCENTRATION)/ GEOMAGNETISM/ HEAT TRANSFER/ RADIANT FLUX DENSITY/ RADIO TRANSMISSION/ WEATHER MODIFICATION

ABA: Author (GRA)

ABS: A study of the modifications produced by high power, high frequency (HF) waves in the F-region of a quiet (low solar cycle) polar ionosphere is presented. In the polar geometry, maximum Ohmic heating occurs producing significant changes to the zero order electron temperature and density profiles. The temporal and spatial aspects of these changes are calculated and their effects on relevant ionospheric parameters, such as the d.c. conductivity tensor, are found. An interesting finding is the generation of density cavities at the reflection point of the HF waves. A survey of the dependence of the various effects on HF pump parameters is made.

84N18502# ISSUE 9 PAGE 1300 CATEGORY 32 RPT#: AD-A135890 NOSC/TD-607 CNT#: DNA PROJ. 99-QAXH 83/06/14 197 PAGES UNCLASSIFIED DOCUMENT

UTTL: Propagation of ELF (extremely low frequencies) waves in the spherical Earth-ionosphere waveguide with transverse and longitudinal variation of properties TLSP: Report, 1979 - 1983

AUTH: A/SHELLMAN, C. H.
CORP: Naval Ocean Systems Center, San Diego, Calif. AVAIL.NTIS SAP: HC A09/MF A01
MAJS: /*ELECTROMAGNETIC WAVE TRANSMISSION/*EXTREMELY LOW FREQUENCIES/*IONOSPHERIC PROPAGATION/*WAVE PROPAGATION
MINS: / ATMOSPHERIC EFFECTS/ AURORAL ZONES/ MATHEMATICAL MODELS/ WAVEGUIDES
ABA: Author (GRA)
ABS: A formulation is described for finding the vertical E-field in the spherical Earth-ionosphere waveguide at extremely low frequencies (ELF). A very general model of propagation parameters is allowed since values of the eigenangles and of the excitation factors are specified at elements of a mesh point array that may extend throughout the lateral extent of the spherical-shell guide the solution is based on the condition that the vertical E-field must satisfy the two dimensional wave equation in the vicinity of each mesh point. Eigensolutions are found for ranges from the transmitter for which there is no transverse variation of properties, and these are combined with the more general solution which applies to the region of transverse inhomogeneity. Two examples are given to illustrate both a symmetrical and nonsymmetrical case. It is expected that use of the formulation will make it possible to describe the effects of inhomogeneities such as the auroral zone, land-sea boundaries, the day-night terminator and man-made disturbances to the ionosphere on the amplitude and phase of the vertical E-field.

84N18233# ISSUE 9 PAGE 1261 CATEGORY 12
83/07/00 17 PAGES UNCLASSIFIED DOCUMENT DCAF E003091
UTTL: The ISPM energetic panel particle composition experiment
AUTH: A/KEPPLER, E.; B/BLAKE, B.; C/WANNEBERG, G.; D/KORTH, A.; E/MORFILL, G. E.; F/OLSEN, S.; G/QUENBY, J.; H/RICHTER, A. K.; I/UMLAUFT, G. PAA: B/(Aerospace Corp., Los Angeles); C/(Kiruna Geophysical Inst.); E/(Max-Planck Inst. fuer Extraterrestrische Physik, Garching); F/(Kiruna Geophysical Inst.); G/(Imperial Coll. of Science and Technology)
CORP: Max-Planck-Inst. fuer Aeronomie, Katlenburg-Lindau (West Germany). AVAIL.NTIS SAP: HC A14/MF A01
In ESA The Intern. Solar Polar Mission: Its Sci. Invest. p 105-121 (SEE N84-18227 09-12)
MAJS: /*ENERGETIC PARTICLES/*HELIUM/*INTERPLANETARY MEDIUM/*SOLAR WIND/*ULYSSES MISSION
MINS: / ANALOG CIRCUITS/ CALIBRATING/ CHEMICAL COMPOSITION/ DATA TRANSMISSION/ ION PROBES/ PARTICLE TELESCOPES/ SIGNAL PROCESSING
ABA: Author (ESA)
ABS: The International Solar Polar Mission (ISPM) Energetic Particle Composition Experiment (EPAC) is introduced. It measures the intensities, anisotropies and energy spectra of low-to-medium energetic interplanetary ions and resolves their masses. The EPAC instrument contains 4 particle telescopes, mounted so that the instrument covers 80% of the full sphere during 1 spin rotation. Each telescope consists of two Si-surface barrier detectors (A and B) surrounded by a plastic scintillator anticoincidence cup (S). Background rejection is achieved by multiparameter analysis. The telescopes are self-calibrating, with particle tracks used to obtain conclusive absolute calibrations. Each telescope system can measure the elemental composition of low-energy nuclei from hydrogen to iron. Detector S works in anticoincidence with detectors A and B. Separation of H and He; 3He and 4He, and C, N, and O is possible, but separation of H and D is not. The analog signal processing concept is described.

84N14178# ISSUE 5 PAGE 635 CATEGORY 46
83/07/00 4 PAGES UNCLASSIFIED DOCUMENT DCAF E003091
UTTL: Summary of ionospheric heating experiments at Tromsoe (Norway)
AUTH: A/STUBBE, P.; B/KOPKA, H.
CORP: Max-Planck-Inst. fuer Aeronomie, Katlenburg-Lindau (West Germany). AVAIL.NTIS SAP: HC A17/MF A01
In ESA Active Expts. in Space p 47-50 (SEE N84-14172 05-12)
MAJS: /*AIRGLOW/*ATMOSPHERIC ATTENUATION/*AURORAL ZONES/*BACKSCATTERING/*IONOSPHERIC HEATING/*IONOSPHERIC PROPAGATION/*PHASE MODULATION
MINS: / D REGION/ E REGION/ EXTREMELY LOW FREQUENCIES/ F REGION/ VERY LOW FREQUENCIES
ABA: Author (ESA)
ABS: Experiments with an ionospheric heating facility which generates a CW power of up to 1.5 MW in the frequency range 2.5 to 8 MHz are summarized. Antenna gain is 24 dBi (relative to isotropic antenna), corresponding to a beam width of 14.5 deg or a maximum effective radiated power of 360 MW. Modulation of the polar electrojet at ELF and VLF; D region modification; generation of artificial micropulsations; VHF backscatter from E region irregularities; and HF backscatter from F region striations are described. Anomalous absorption of HF waves; phase changes of a diagnostic HF wave; large scale field aligned irregularities; plasma and ion line irregularities with EISCAT; and stimulated electromagnetic emission of the ionospheric plasma are treated. Airglow modification; F region cross modulation; and in situ

measurements in the modified F region are discussed.

84N10688# ISSUE 1 PAGE 106 CATEGORY 46 RPT#: AD-A131215 DNA-TR 81-87 CNT#: DNA001-81-C-0076 SRI PROJ. 2623 82/03/31 34 PAGES UNCLASSIFIED DOCUMENT

UTTL: The anisotropy of high latitude nighttime F-region irregularities

AUTH: A/LIVINGSTON, R. C.; B/OWEN, J.; C/RINO, C. L.; D/TSUNODA, R. T.

CORP: SRI International Corp., Menlo Park, Calif.
AVAIL.NTIS SAP: HC A03/MF A01

MAJS: /*ANISOTROPY/*AURORAL ZONES/*ELECTRON DENSITY (CONCENTRATION)/*F REGION/*SATELLITE CONTROL/* SCINTILLATION

MINS: / IONOSPHERIC DISTURBANCES/ IONOSPHERIC PROPAGATION/ MAGNETIC FIELDS/ POLAR REGIONS/ RADIO WAVES/ TIME MEASUREMENT

ABA: Author (GRA)

ABS: The anisotropy of intermediate-scale, F-region irregularities in the nighttime auroral zone is described. The study is based upon spaced-receiver phase-scintillation measurements made with the Wideband satellite at Poker Flat, Alaska. A systematic dependence of irregularity anisotropy with local time and magnetic latitude is observed, suggesting convective control. Sheet-like irregularities are confined to the zone of east-west drift near the equatorward boundary of the auroral zone. At the flow reversal, or Harang discontinuity, the cross-field extension of the sheets is reduced. The extension of rod-like irregularities, which are observed poleward of the zonal convection boundary, also shows apparent convection dominance. Mechanisms for convection control of the anisotropy are discussed.

83N29574# ISSUE 18 PAGE 2926 CATEGORY 32 RPT#: AD-A126212 NUSC-TR-6771 83/02/03 63 PAGES UNCLASSIFIED DOCUMENT

UTTL: ELF PVS field strength measurements, April 1977

AUTH: A/BANNISTER, P. R.

CORP: Naval Underwater Systems Center, New London, Conn.
CSS: (Submarine Electromagnetic Systems Dept.)
AVAIL.NTIS SAP: HC A04/MF A01

MAJS: /*FIELD STRENGTH/*GEOMAGNETISM/*IONOSPHERIC PROPAGATION/*RADIO RECEPTION/*SIGNAL TO NOISE RATIOS/* UNDERWATER COMMUNICATION

MINS: / DIURNAL VARIATIONS/ EXTREMELY LOW FREQUENCIES/ ICE/ POLAR CAPS/ SUBMARINES

ABA: Author (GRA)

ABS: From September 1976 to December 1978, extremely low frequency (ELF) field-strength and effective-noise measurements were taken aboard operational submarines. The results of measurements taken in Connecticut and aboard a submarine located under the ice in the Greenland Sea area during April 1977 are discussed. The principal result is that the average daytime and nighttime field strengths measured aboard the submarine are in excellent agreement with previous ELF measurements taken over similar paths. As expected, the presence of the ice cap had no adverse effect on ELF reception.

83N23509# ISSUE 13 PAGE 2023 CATEGORY 32 RPT#: UIO-SR-82-02 ISSN-0349-2699 82/00/00 26 PAGES UNCLASSIFIED DOCUMENT DCAF E003302

UTTL: Observations of HF backscatter associated with the heating experiment at Tromsoe

AUTH: A/HEDBERG, A.; B/DERBLOM, H.; C/THIDE, B.; D/KOPKA, H.; E/STUBBE, P.

CORP: Uppsala Ionospheric Observatory (Sweden).
AVAIL.NTIS SAP: HC A03/MF A01
Presented at URSI Intern. Radio Symp., Fairbanks, Alaska, 9-13 Aug. 1982

MAJS: /*BACKSCATTERING/*DOPPLER EFFECT/*ELECTRON DENSITY PROFILES/*F REGION/*FREQUENCY SHIFT/*MAGNETIC TAPES/* RADIO FREQUENCY HEATING

MINS: / AURORAL ZONES/ IONOSPHERE/ PLASMA FREQUENCIES/ RADIO ECHOES/ RHOMBIC ANTENNAS/ WAVE PROPAGATION/ YAGI ANTENNAS

ABA: Author

ABS: Backscatter echoes from a region modified by radio frequency (RF) heating above Tromso were observed. When the heater output is suddenly varied from ""off'' to ""on'' the backscatter echoes appear and grow to an equilibrium value in some seconds and decay at turn-off in some tens of seconds. Rise and decay time constants are frequency dependent, being longer at lower radar frequencies. The strongest echoes are obtained when the F-layer peak plasma frequency (foF2) is close to the heater pump frequency. Echoes are absent when the heater is operating in ""x''-mode. Variation of heater output from 100% to 12.5% of full power yields a corresponding variation in the received echo amplitude without noticeable threshold effects. Some Doppler shift measurements are also presented indicating that the modified region, as well as the background has a radial motion towards north in the range 0 to 20 m/s.

83N11410# ISSUE 2 PAGE 215 CATEGORY 32 RPT#: AD-A118236 81/00/00 708 PAGES UNCLASSIFIED DOCUMENT

UTTL: Effect of the ionosphere on radiowave systems

AUTH: A/GOODMAN, J. M. PAT: A/ed.

CORP: Naval Research Lab., Washington, D. C. AVAIL.NTIS SAP: HC A99/MF A01

Sponsored in part by AFGL Presented at the Ionospheric Effects Symp., Alexandria, Va., 14-16 Apr. 1981

MAJS: /*COMMUNICATION/*CONFERENCES/*HIGH FREQUENCIES/* IONOSPHERIC PROPAGATION

MINS: / EQUATORIAL REGIONS/ IONOSPHERIC ELECTRON DENSITY/ LATITUDE/ POLAR REGIONS/ REMOTE SENSING/ ROCKET EXHAUST/ SCINTILLATION

ABA: GRA

ABS: IES '81 is the third Ionospheric Effects Symposium to be sponsored by the Naval Research Laboratory. The purpose of this symposium was to improve the information transfer between system architects, managers, and designers on the one hand, and ionospheric physicists and propagation specialists on the other hand. The conference itself covered various topics of current interest to the ionospheric research community. Session topics included the following: Ionospheric Modification, General Reviews and Total Electron Content, Equatorial Scintillation Studies, HF Propagation/Remote Sensing, High-Latitude Scintillation, Sub-HF Propagation and System Effects, Ionospheric and Propagation Models, and Future Plans and Programs.

82N33613# ISSUE 24 PAGE 3426 CATEGORY 32 RPT#: AD-A116838 RADC-TR-82-67 CNT#: N00024-78-C-5384 AF PROJ. 2305 82/06/00 43 PAGES UNCLASSIFIED DOCUMENT

UTTL: Techniques for Doppler spectral estimation of HF radar signals backscattered from high latitude ionosphere irregularities TLSP: Final Technical Report, 1 Oct. 1980 - 30 Sep. 1981

AUTH: A/GREENWALD, R. A.

CORP: Applied Physics Lab., Johns Hopkins Univ., Laurel, Md. AVAIL.NTIS SAP: HC AC /MF A01
Griffiss AFB, N.Y. RADC

MAJS: /*BACKSCATTERING/*IONOSPHERIC F-SCATTER PROPAGATION/* RADAR SCATTERING

MINS: / CONTINUOUS WAVE RADAR/ DOPPLER EFFECT/ POLAR REGIONS / PULSE RADAR/ SIGNAL ANALYSIS/ SPECTRUM ANALYSIS

ABA: GRA

ABS: This report examines various techniques for studying the Doppler spectrum of radar signals backscattered from high latitude ionospheric irregularities. Both pulsed and FM-CW techniques are considered and it is found that most approaches suffer from the need to have sufficiently high pulse or sweep repetition frequencies while at the same time avoiding range aliasing of the backscattered signals.

82N27616# ISSUE 18 PAGE 2545 CATEGORY 32 82/02/00 12 PAGES UNCLASSIFIED DOCUMENT

UTTL: VLF/LF pulse reflection measurements of the polar D-region during quiet and disturbed ionospheric conditions

AUTH: A/TURTLE, J. P.; B/RASMUSSEN, J. E.; C/KLEMETTI, W. I.; D/KOSSEY, P. A.

CORP: Rome Air Development Center, Hanscom AFB, Mass. CSS: (Propagation Branch.) AVAIL.NTIS SAP: HC A12/MF A01
In AGARD Medium, Long and Very Long Wave Propagation 12 p (SEE N82-27613 18-32)

MAJS: /*D REGION/*IONOSPHERIC PROPAGATION/*LOW FREQUENCIES/* POLAR REGIONS/*REFLECTANCE

MINS: / ENERGETIC PARTICLES/ IONOSPHERIC DISTURBANCES/ IONOSPHERIC SOUNDING/ LONG WAVE RADIATION/ SOLAR ACTIVITY

ABA: A.R.H.

ABS: A short pulse VLF/LF ionosounder to determine the characteristics of the polar D-region during quiet and disturbed conditions is described. Data obtained at Thule AB, Greenland, near the center of the polar cap, are presented giving information on the D-region's height and reflectivity as a function of time. Under quiet conditions there are marked variations in the D-region due to the effects of diurnal and seasonal changes in solar illumination. Energetic particle events produce dramatic changes in both the height and reflectivity of the D-region which can exhibit a complex behavior throughout the duration of the event. The severity of the D-region effects is highly dependent on seasonal illumination conditions. Data on ionospheric reflectivity illustrate normal seasonal and diurnal variations, data from disturbed periods show the interaction between propagation parameters and energetic particle ionization, solar ionizing and photodetaching radiations.

82N21479# ISSUE 12 PAGE 1650 CATEGORY 32 RPT#: AD-A110290 PD-BRA-81-244R AFWAL-TR-81-1163 CNT#: DNA001-79-C-0141 AF PROJ. 1227 81/09/00 95 PAGES UNCLASSIFIED DOCUMENT

UTTL: Phase effects of ionospheric irregularities. Results of the Air Force Wright Aeronautical data processing effort TLSP: Final Report, 1 Jan. 1979 - 31 Jul. 1981

AUTH: A/PRETTIE, C. W.

CORP: Berkeley Research Associates, Inc., Calif.
AVAIL.NTIS SAP: HC A05/MF A01
Wright-Patterson AFB, Ohio AFWAL
MAJS: /*IONOSPHERIC PROPAGATION/*PHASE DEVIATION/*SATELLITE TRANSMISSION/*SPACECRAFT COMMUNICATION
MINS: / EQUATORIAL REGIONS/ HISTOGRAMS/ POLAR REGIONS/ POWER SPECTRA/ SCINTILLATION/ STANDARD DEVIATION
ABA: Author (GRA)
ABS: Data processing of Air Force Wright Aeronautical Laboratory flight test satellite signal measurements has been performed to illustrate the phase effects associated with ionospheric irregularities. Measurements are available at 250 MHz satellite signals traversing ionospheric heating induced irregularities, barium ion cloud irregularities, and polar and equatorial irregularities. For each of these environments displays of amplitude, phase difference standard deviation, phase difference histograms and phase power spectral density are given. The results of ionospheric heating measurements imply that underdense heating produces large scale irregularities with fluctuation levels that are conceivably larger than overdense heating fluctuations. The barium measurements from the CASTOR releases by Max Planck Institute in March 1979 near Peru show no barium associated phase effects. Because of the 275 km release altitude it is expected that the associated phase effects should be difficult to resolve. The phase difference histograms from the strong fading observed in the solar and equatorial measurements illustrate the importance of the non-Gaussian nature of the phase to communications. Binary phase-shift keyed (BPSK) irreducible error rates greater then minus ten to the 3rd power are predicted for these environments based upon their similarity with band-limited Gaussian noise.

81N33724# ISSUE 24 PAGE 3374 CATEGORY 46 RPT#: AD-A103957 RADC-TR-81-80 CNT#: AF PROJ. 2305
81/03/00 95 PAGES UNCLASSIFIED DOCUMENT
UTTL: VLF/LF reflectivity of the polar ionosphere TLSP: Interim Report, 4 May - 20 Sep. 1980
AUTH: A/PAGLIARULO, R. P.; B/TURTLE, J. P.; C/RASMUSSEN, J. E.; D/GIFFORD, R. E.; E/KLEMETTI, W. I.
CORP: Rome Air Development Center, Griffiss AFB, N.Y.
AVAIL.NTIS SAP: HC A05/MF A01
MAJS: /*ELECTROMAGNETIC RADIATION/*IONOSPHERIC PROPAGATION/*POLAR REGIONS/*REFLECTANCE
MINS: / IONOSONDES/ MAGNETOMETERS/ POLAR RADIO BLACKOUT/ VERY LOW FREQUENCIES
ABA: Author (GRA)
ABS: This report provides a summary of high-latitude ionospheric reflectivity data, as observed by the USAF high-resolution VLF/LF ionosounder operating in northern Greenland. Ionospheric reflectivity parameters, including reflection heights and coefficients, are presented as a function of time of day. Riometer and magnetometer measurements of the polar propagation environment are presented as supplementary data.

81N33587# ISSUE 24 PAGE 3355 CATEGORY 43 RPT#: BMFT-FB-W-80-029 ISSN-0170-1339 80/12/00 245 PAGES
In GERMAN; ENGLISH summary UNCLASSIFIED DOCUMENT
DCAF E002631
UTTL: Possible applications of communication satellites for research tasks in polar regions TLSP: Final Report
AUTH: A/BOMMAS, G.; B/HANKA, E.; C/HAUSSMANN, J.; D/KLAGES, W.; E/STUERZENHOFAECKER, P.; F/THOMAS, J.
CORP: Dornier-Werke G.m.b.H., Friedrichshafen (West Germany). AVAIL.NTIS SAP: HC A11/MF A01; Fachinformationszentrum, Karlsruhe, West Germany DM 41 Bonn Bundesministerium fuer Forschung und Technologie Sponsored by Bundesministerium fuer Forschung und Technologie
MAJS: /*ANTARCTIC REGIONS/*COMMUNICATION SATELLITES/*POLAR CAP ABSORPTION/*RADIO HORIZONS/*SHORT WAVE RADIO TRANSMISSION
MINS: / AURORAL ZONES/ CLOUD PHOTOGRAPHY/ METEOROLOGICAL PARAMETERS/ POLAR METEOROLOGY/ TIROS SATELLITES/ WEST GERMANY
ABA: Author (ESA)
ABS: The possibilities of using communication satellites to establish beyond-the-horizon communications within Antartica, and between Antartica and the Federal Republic of Germany is examined. Communication is shown to be possible using the following satellites: Marisat for the transmission of speech, telex and data, GOES for the transmission of meteorological data, and TIROS-N for the reception of cloud pictures. The coverage of geostationary satellites is limited to a latitude of approximately 80 deg. Links, south of 80 deg are to be established by means of HF. Line of sight communication up to 50 km is simply established with VHF equipment.

81N26659# ISSUE 17 PAGE 2374 CATEGORY 47
81/02/00 5 PAGES UNCLASSIFIED DOCUMENT DCAF E003091
UTTL: Telecommunication missions --- for meteorological satellites
AUTH: A/EBBESEN, I. K.
CORP: Danish Meteorological Inst., Copenhagen. AVAIL.NTIS SAP: HC A14/MF A01
In ESA Satellite Meteorol. in the Mediterranean p

93-97 (SEE N81-26645 17-47)
MAJS: /*METEOROLOGICAL SATELLITES/*RADIO RELAY SYSTEMS/* TELECOMMUNICATION
MINS: / DATA COLLECTION PLATFORMS/ DATA TRANSMISSION/ POLAR ORBITS/ SATELLITE TRANSMISSION/ SIRIO SATELLITE/ SYNCHRONOUS SATELLITES
ABA: Author (ESA)
ABS: Meteorological satellites are used in solving certain communications problems. For example, collection of data from automatic observation stations is performed both by geostationary satellites and by polar orbiting satellites. Information regarding these missions is given. Different types of data collection platforms are mentioned. The capability of localizing platoforms is discussed. Another use of satellites, namely as substitutes for normal land-line and radio communication (as planned in the SIRIO-2/MDD project) is also considered.

81N26630# ISSUE 17 PAGE 2370 CATEGORY 46 RPT#: AD-A098977 RADC-TR-80-298 CNT#: AF PROJ. 2305 80/10/00 84 PAGES UNCLASSIFIED DOCUMENT
UTTL: VLF/LF reflectivity of the polar ionosphere, 6 Jan. - 3 May 1980
AUTH: A/PAGLIARULO, R. P.; B/TURTLE, J. P.; C/RASMUSSEN, J. E.; D/GIFFORD, R. E.; E/KLEMETTI, W. I.
CORP: Rome Air Development Center, Griffiss AFB, N.Y. AVAIL.NTIS SAP: HC A05/MF A01
Sponsored by AF
MAJS: /*IONOSPHERIC PROPAGATION/*POLAR REGIONS/*VERY LOW FREQUENCIES
MINS: / DIURNAL VARIATIONS/ HIGH RESOLUTION/ IONOSONDES/ RIOMETERS
ABA: Author (GRA)
ABS: This report provides a summary of high latitude ionospheric reflectivity as observed by the USAF high resolution VLF/LF ionosounder operating in northern Greenland. Ionospheric reflectivity parameters, including reflection heights and coefficients, are presented as a function of time of day. Riometer and magnetometer measurements of the polar propagation environment are presented as supplementary data.

81N23132# ISSUE 14 PAGE 1871 CATEGORY 32 80/00/00 9 PAGES UNCLASSIFIED DOCUMENT DCAF E002583
UTTL: Propagation effects in high latitudes --- Intelsat and Symphonie transmissions
AUTH: A/OSEN, O.
CORP: Norwegian Telecommunications Administration Research Establishment, Kjeller. AVAIL.NTIS SAP: HC A99/MF A01
In CNES Symphonie Symp. p 415-423 (SEE N81-23101 14-12)
MAJS: /*ELEVATION ANGLE/*POLAR REGIONS/*RADIO TRANSMISSION/* SATELLITE TRANSMISSION/*SIGNAL FADING
MINS: / ATMOSPHERIC ATTENUATION/ GROUND STATIONS/ INTELSAT SATELLITES/ NOISE TEMPERATURE/ RADIO WAVE REFRACTION/ SIGNAL FADING RATE/ SYMPHONIE SATELLITES
ABA: Author (ESA)
ABS: Transmission properties of communication systems using geostationary satellites are studied for ground station elevation angles 5 deg. Radio experiments were carried out at elevation angles of 1.7 deg and 3.1 deg. Results are compared with signal fading theory. It is argued that the signal can be expressed as specular-plus-Rayleigh fading, or Rice fading. Furthermore, the fading rate is Gaussian distributed. Fading statistics confirm these hypotheses. The fading is probably due to a combination of scattering and reflections in turbulent layers and in internal waves in the atmosphere. Atmospheric attenuation is shown to be due to oxygen absorption, and this gives a significant increase in ground station noise temperature. Reliable (99.9 to 99.99%) satellite communication can be obtained, with a downlink fading margin of 4 to 8 dB in the summer months, and 1 to 3 dB in the winter (at 4 GHz). Uplink fading can effectively be coped with by uplink power control.

81N22645# ISSUE 13 PAGE 1800 CATEGORY 46 RPT#: AD-A096833 AD-E850033 AFGWC/TN-81/001 81/01/00 112 PAGES UNCLASSIFIED DOCUMENT
UTTL: Short term HF forecasting and analysis
AUTH: A/MANLEY, J. A.
CORP: Air Force Global Weather Central, Offutt AFB, Nebr. AVAIL.NTIS SAP: HC A06/MF A01
MAJS: /*ATMOSPHERIC ATTENUATION/*AURORAS/*FORECASTING/*HIGH FREQUENCIES/*MAGNETIC DISTURBANCES/*POLAR CAP ABSORPTION/*UPPER ATMOSPHERE
MINS: / AERONOMY/ GEOMAGNETISM/ PLANETARY MAGNETIC FIELDS/ RADIO TRANSMISSION/ SUDDEN IONOSPHERIC DISTURBANCES
ABA: GRA
ABS: The space forecasting branch of the Air Force Global Weather Central (AFGWC) issues short term HF forecasts and analyses to a wide variety of users. For the forecaster this technical note will illustrate some of the techniques for interpretating the data used in preparing the forecast. For the user of the HF forecast bulletin this technical note will show the limitations of such a forecast.

81N20350# ISSUE 11 PAGE 1478 CATEGORY 32 RPT#: RAE-TM-RAD-NAV-138 BR76254 80/09/00 40 PAGES UNCLASSIFIED DOCUMENT DCAF EO10260

UTTL: An investigation of high frequency propagation over an auroral sub-auroral path --- prediction of usable frequencies

AUTH: A/DAWES, J. B.

CORP: Royal Aircraft Establishment, Farnborough (England). AVAIL.NTIS SAP: HC A03/MF A01 London HMSO

MAJS: /*AURORAL ZONES/*HIGH FREQUENCIES/*MAXIMUM USABLE FREQUENCY/*PREDICTIONS

MINS: / AIRBORNE EQUIPMENT/ COMPUTER PROGRAMS/ FORTRAN/ IONOSONDES/ IONOSPHERIC PROPAGATION/ POLAR REGIONS/ RADIO TRANSMISSION/ SPORADIC E LAYER

ABA: Author (ESA)

ABS: Methods of determining the usable frequencies over a particular auroral sub-auroral path such that digital data may be sent uncorrupted, are described. Tests including flight trials took place between April and July 1980 using transmissions between northern Norway and southern England. Computer programs were used to determine the viability of linearly interpolating the ionospheric propagation parameters from sub-auroral areas to an auroral or polar zone. One of the programs is included. Predicted values of the ionosphere give more reliable results than ionosonde data. Interpolation of the ionospheric parameters over these zones has limited use, however, due to the variablity of the ionosphere with northerly latitude.

81N18595# ISSUE 9 PAGE 1229 CATEGORY 46 RPT#: AD-A094102 RADC-TR-80-189 CNT#: AF PROJ. 4600 80/06/00 81 PAGES UNCLASSIFIED DOCUMENT

UTTL: VLF/LF reflectivity of the polar ionosphere TLSP: Technical Report, 2 Sep. - 22 Dec. 1979

AUTH: A/PAGLIARULO, R. P.; B/TURTLE, J. P.; C/RASMUSSEN, J. E.; D/KLEMETTI, W. I.

CORP: Rome Air Development Center, Griffiss AFB, N.Y. AVAIL.NTIS SAP: HC A05/MF A01

MAJS: /*IONOSPHERIC PROPAGATION/*LOW FREQUENCIES/*POLAR REGIONS/*REFLECTANCE/*VERY LOW FREQUENCIES

MINS: / ABSORPTANCE/ ATTENUATION COEFFICIENTS/ AURORAL ABSORPTION/ MAGNETOMETERS/ RIOMETERS/ SCATTER PROPAGATION

ABA: GRA

ABS: This report provides a summary of high latitude ionospheric reflectivity as observed by the USAF high resolution VLF/LF ionosounder operating in northern Greenland. Ionospheric reflectivity parameters, including reflection heights and coefficients, are presented as a function of time of day. Riometer and magnetometer measurements of the polar propagation environment are presented as supplementary data.

81N13573# ISSUE 4 PAGE 512 CATEGORY 46 RPT#: AD-A091091 RADC-TR-80-12 CNT#: AF PROJ. 4600 80/01/00 86 PAGES UNCLASSIFIED DOCUMENT

UTTL: VLF/LF reflectivity of the polar ionosphere TLSP: Topical Report, 6 May - 1 Sep. 1979

AUTH: A/PAGLIARULO, R. P.; B/TURTLE, J. P.; C/RASMUSSEN, J. E.; D/COOLEY, R. L.; E/KLEMETTI, W. I.

CORP: Rome Air Development Center, Griffiss AFB, N.Y. AVAIL.NTIS SAP: HC A05/MF A01

MAJS: /*GREENLAND/*IONOSPHERIC DISTURBANCES/*IONOSPHERIC PROPAGATION/*POLAR REGIONS/*REFLECTANCE/*VERY LOW FREQUENCIES/*WAVEFORMS

MINS: / MAGNETOMETERS/ RIOMETERS/ SIGNAL TO NOISE RATIOS/ TABLES (DATA)

ABA: GRA

ABS: This report provides a summary of high latitude ionospheric reflectivity as observed by the USAF high resolution VLF/LF ionosounder operating in northern Greenland. Ionospheric reflectivity parameters, including reflection heights and coefficients, are presented as a function of time of day. Measurements of polar propagation environment by a magnetometer and a riometer are presented as supplementary data.

81N11288# ISSUE 2 PAGE 192 CATEGORY 32 RPT#: AD-A090121 PSR-932 DNA-5148T CNT#: DNA001-79-C-0015 79/12/01 52 PAGES UNCLASSIFIED DOCUMENT

UTTL: Measuring and interpreting ELF signals during a PCA aspects of an experimental design TLSP: Topical Report, 1 Dec. 1978 - 1 Dec. 1979

AUTH: A/FIELD, E. C., JR.; B/DEWITT, R. N.

CORP: Pacific-Sierra Research Corp., Santa Monica, Calif. AVAIL.NTIS SAP: HC A04/MF A01

MAJS: /*EXPERIMENT DESIGN/*EXTREMELY LOW FREQUENCIES/* NUCLEAR EXPLOSIONS/*POLAR CAP ABSORPTION/*SIMULATION/* SOLAR FLARES

MINS: / EXTREMELY LOW RADIO FREQUENCIES/ IONOSPHERIC DISTURBANCES/ IONOSPHERIC PROPAGATION/ RADIATION ABSORPTION/ SOLAR CYCLES

ABA: GRA

ABS: Investigates the design of a transpolar extremely-low-frequency (ELF) experiment that would validate Defense Nuclear Agency propagation codes for ELF system performance in nuclear environments. To be conducted during the next solar maximum, when polar cap absorption events (PCAs) might approximate a nuclear environment, the ideal experiment would simultaneously measure both propagation and ionospheric structure. Propagation measurements would be taken at receivers located such that the direct

propagation path did not approach the polar cap boundary; the ELF values would then be compared with computer code outputs. A moderate PCA might cause a 3 to 4 dB reduction in a transpolar ELF signal; a strong event, an 8 or 9 dB reduction. At least 2 hours would be required to resolve amplitude changes in the signal; noise processing to excise large pulses would be essential. Measurements of ionospheric changes would be taken with rocket-borne instruments, entered into computer calculations using the DNA codes, then compared with the propagation measurements. Rocket data should be gathered at 50 km or below; data from previous PCAs obtained only at 60 km or above yield unacceptable uncertainties in calculated field strengths.

81N10290# ISSUE 1 PAGE 44 CATEGORY 32 80/08/00 17 PAGES UNCLASSIFIED DOCUMENT

UTTL: Recent observations of equatorial and high latitude scintillations

AUTH: A/AARONS, J.; B/WHITNEY, H. E.

CORP: Air Force Geophysics Lab., Hanscom AFB, Mass.
AVAIL.NTIS SAP: HC A22/MF A01
In AGARD Propagation Effects in Space/Earth Paths 17 p (SEE N81-10259 01-32)

MAJS: /*ELECTRON DENSITY PROFILES/*IONOSPHERIC PROPAGATION/*MAGNETIC STORMS/*POLAR REGIONS/*SCINTILLATION/*TRANSEQUATORIAL PROPAGATION

MINS: / GLINT/ PHOSPHORESCENCE/ SIGNAL FADING/ SOLAR FLUX/ WAVE DISPERSION/ WAVE PROPAGATION

ABA: L.F.M.

ABS: At equatorial latitudes, combined airborne and ground measurements of radar backscatter, electron density profiles, scintillations, airglow at 6300 A, and total electron content yielded data on the development and decay of the irregularity patches containing the hundred meter irregularities responsible for amplitude and phase scintillation. The use of airglow measurements from aircraft allowed the form of the patch to be deduced. At auroral latitudes, sheets of irregularities were observed at Poker Flat, Alaska and at Goose Bay, Labrador using phase fluctuations of the WIDEBAND signals. WIDEBAND phase and amplitude deviations when correlated with DMSP photographs show intense activity over diffuse and discrete aurora. The increase of intensity of scintillation activity at equatorial and polar latitudes was noted during 1979 and 1980 when very high solar flux levels were recorded. These increases take place even under quiet magnetic conditions when solar flux is high and take place during the increased number of magnetic storms.

80N31691# ISSUE 22 PAGE 2995 CATEGORY 32 RPT#: AD-A087010 REPT-0296-FR-2-PT-2 AFGL-TR-80-0055-PT-2 CNT#: F19628-76-C-0296 AF PROJ. 7663 80/02/00 52 PAGES UNCLASSIFIED DOCUMENT

UTTL: Ground range and bearing error determination and display for an OTH radar system with an Arctic trough ionosphere TLSP: Final Report, Oct. 1976 - Oct. 1979

AUTH: A/BANDES, D.; B/BARRETT, T. B.

CORP: Parke Mathematical Labs., Inc., Carlisle, Mass.
AVAIL.NTIS SAP: HC A04/MF A01
Hanscom AFB, Mass. AFGL

MAJS: /*ACCURACY/*ALGORITHMS/*ARCTIC REGIONS/*COMPUTER PROGRAMS/*IONOSPHERIC PROPAGATION/*OVER-THE-HORIZON RADAR/*RADAR DETECTION/*TROUGHS

MINS: / COMPUTER PROGRAMMING/ ERROR ANALYSIS/ LOW PRESSURE/ NUMERICAL ANALYSIS/ OPTICAL RADAR/ PARAMETERIZATION/ SUBROUTINES

ABA: GRA

ABS: This report describes the algorithms used to determine range and bearing errors which might be incurred in an OTH radar system where the propagating medium includes an arctic trough. Several types of plots for displaying this error information are described along with an example.

80N30619# ISSUE 21 PAGE 2842 CATEGORY 32 RPT#: AD-A087255 LMSC-D681778 CNT#: N00014-79-C-0175 80/01/30 91 PAGES UNCLASSIFIED DOCUMENT

UTTL: Study of elf propagation anomalies as related to improved knowledge of electron density profiles produced by energetic particle precipitation TLSP: Annual Technical Report

AUTH: A/IMHOF, W. L.; B/GUNTON, R. C.; C/LARSEN, T. R.; D/REAGAN, J. B.; E/GAINES, E. E.; F/MEYEROFF, R. E.

CORP: Lockheed Missiles and Space Co., Palo Alto, Calif.
AVAIL.NTIS SAP: HC A05/MF A01

MAJS: /*ANOMALIES/*DENSITY DISTRIBUTION/*ELECTRON DENSITY (CONCENTRATION)/*IONS/*SOLAR ACTIVITY/*WAVE PROPAGATION

MINS: / ATMOSPHERIC PHYSICS/ EXTREMELY LOW FREQUENCIES/ LOW ALTITUDE/ POLAR CAP ABSORPTION

ABA: GRA

ABS: A study has been made of extremely low frequency (ELF) wave propagation anomalies as related to energetic particle precipitation, principally during solar particle events (SPE). Based on calculation of the predicted signal strengths at Tromso for transmissions from the Wisconsin Test Facility (WTF) a criterion has been selected for possible use in a field test operation. If the ion pair production rates at 40 km are equal to or greater than 1 x 1000/cc/sec then it is probable that a 3 dB or larger reduction in signal strength would occur for such an event. Since this

preliminary criterion is based on ELF signal strength computation assuming no local time variations along the propagation path, more detailed calculations of the local time ionospheric effects should be performed. A study was made of the expected effect of local time variations during solar particle events on the ELF propagation over the path from WTF to Tromso. Electron and ion density profiles for the various segments of the test path were calculated with the ion chemistry model, taking into account the local time for each segment. In a comparison of conditions measured and calculated for SPE72 on 4 August 1972 near the peak of the event and conditions measured and calculated for a similar case assuming a season of 21 December, very little difference in signal strength attenuation over the path was found.

80N29557# ISSUE 20 PAGE 2688 CATEGORY 32 RPT#: AD-A085399 NOSC/TR-530 80/02/25 81 PAGES UNCLASSIFIED DOCUMENT

UTTL: Ionospheric profiles for predicting nighttime VLF/LF propagation. Determination of an effective (exponential) model for use in design and deployment of resources for communication and navigation TLSP: Final Report, Jan. 1974 - Sep. 1979

AUTH: A/FERGUSON, J. A.

CORP: Naval Ocean Systems Center, San Diego, Calif.; Defense Communications Agency, Washington, D.C.; Coast Guard, Washington, D.C. AVAIL.NTIS SAP: HC A05/MF A01
Prepared for Defense Communications Agency, Washington, D.C. and Coast Guard, Washington, D.C.

MAJS: /*ATMOSPHERIC MODELS/*IONOSPHERIC PROPAGATION/* REGRESSION ANALYSIS

MINS: / COMMUNICATION NETWORKS/ D REGION/ OMEGA NAVIGATION SYSTEM/ POLAR REGIONS/ VERY LOW FREQUENCIES

ABA: GRA

ABS: The regression analysis of ionospheric profiles from the literature fails to show the high ionospheric variability that is observed in the propagation measurements. Neither does it show the rapid transition in altitude between high and middle latitudes. The measured propagation data are more directly related to the MEECN and Omega system requirements for predicting vlf and lf field strengths. Profiles are suggested on the basis of the analysis of these data.

80N27901# ISSUE 18 PAGE 2450 CATEGORY 46 RPT#: AD-A083240 RADC-TR-79-273 CNT#: AF PROJ. 4600 79/10/00 86 PAGES UNCLASSIFIED DOCUMENT

UTTL: ULF/LF reflectivity of the polar ionosphere TLSP: Technical Report, 31 Dec. - 5 May 1979

AUTH: A/PAGLIARULO, R. P.; B/TUTTLE, J. P.; C/RASMUSSEN, J. E.; D/COLEY, R. L.; E/KLEMETTI, W. I. PAA: E/(Megapulse, Inc.)

CORP: Rome Air Development Center, Griffiss AFB, N.Y. AVAIL.NTIS SAP: HC A05/MF A01

MAJS: /*IONOSPHERIC PROPAGATION/*POLAR REGIONS/*VERY LOW FREQUENCIES/*WAVE REFLECTION

MINS: / DIURNAL VARIATIONS/ GREENLAND/ IONOSPHERIC SOUNDING

ABA: GRA

ABS: This report provides a summary of high latitude ionospheric reflectivity as observed by the USAF high resolution VLF/LF ionosounder operating in northern Greenland. Ionospheric reflectivity parameters, including reflection heights and coefficients, are presented as a function of time of day. VLF long path propagation measurements, along with magnetometer and riometer data, are presented as supplementary data.

80N24717*# ISSUE 15 PAGE 1998 CATEGORY 46 79/12/00 19 PAGES UNCLASSIFIED DOCUMENT

UTTL: Morphology and phenomenology of the high-latitude E and F regions

AUTH: A/HUNSUCKER, R. D.

CORP: Alaska Univ., Fairbanks. CSS: (Geophysical Inst.) AVAIL.NTIS SAP: HC A99/MF A01
In NASA. Marshall Space Flight Center Solar-Terrest. Predictions Proc., Vol. 2 p 543-561 (SEE N80-24678 15-42)

MAJS: /*E REGION/*F REGION/*IONIZATION/*IONOSPHERIC PROPAGATION/*POLAR REGIONS

MINS: / ANNUAL VARIATIONS/ AURORAL ZONES/ DIURNAL VARIATIONS / MAGNETIC VARIATIONS/ SOLAR TERRESTRIAL INTERACTIONS/ SUNSPOT CYCLE

ABA: J.M.S.

ABS: Results obtained at high latitude observatories on the behavior of E and F region ionization are presented including a bibliography. Behavior of E and F region ionization during day and night for quiet and disturbed conditions in the auroral and polar regions is described. Daily, seasonal and sunspot variations are also outlined.

80N19389# ISSUE 10 PAGE 1282 CATEGORY 32
79/11/00 12 PAGES UNCLASSIFIED DOCUMENT
UTTL: Characteristics of the high latitude ionosphere produced by auroral particle precipitation
AUTH: A/WHALEN, J. A.
CORP: Air Force Geophysics Lab., Hanscom AFB, Mass.
AVAIL.NTIS SAP: HC A25/MF A01
In AGARD Spec. Topics in HF Propagation 12 p (SEE N80-19372 10-32)
MAJS: /*AURORAS/*HIGH FREQUENCIES/*IONOSPHERIC PROPAGATION/*POLAR REGIONS
MINS: / MAGNETOSPHERE/ MORPHOLOGY/ SOLAR WIND/ SPATIAL DISTRIBUTION/ TIME
ABA: R.E.S.
ABS: The general domains of the high latitude ionosphere are described. How these domains relate in space and time to general magnetospheric domains and how these relations aid the understanding of high frequency propagation in the high latitudes is discussed.

80N15318# ISSUE 6 PAGE 727 CATEGORY 32 RPT#: AD-A074762 RADC-TR-79-100 CNT#: AF PROJ. 4600
79/03/00 90 PAGES UNCLASSIFIED DOCUMENT
UTTL: VLF/LF reflectivity of the polar ionosphere, 23 April - 2 September 1978
AUTH: A/PAGLIARULO, R. P.; B/TURTLE, J. P.; C/RASMUSSEN, J. E.; D/KLEMETTI, W. I.; E/COOLEY, R. L.
CORP: Rome Air Development Center, Griffiss AFB, N.Y.
AVAIL.NTIS SAP: HC A05/MF A01
MAJS: /*GREENLAND/*IONOSPHERIC PROPAGATION/*POLAR REGIONS/*REFLECTANCE/*VERY LOW FREQUENCIES
MINS: / GRAPHS (CHARTS)/ HIGH RESOLUTION/ IONOSONDES/ MAGNETOMETERS/ RIOMETERS
ABA: GRA
ABS: This report provides a summary of high latitude ionospheric reflectivity as observed by the USAF high resolution VLF/LF ionosounder operating in northern Greenland. Ionospheric reflectivity parameters, including reflection heights and coefficients, are presented as a function of time of day. VLF long path propagation measurements, along with magnetometer and riometer data, are presented as supplementary information.

80N14611# ISSUE 5 PAGE 632 CATEGORY 46
77/00/00 23 PAGES In GERMAN UNCLASSIFIED DOCUMENT
DCAF E019277
UTTL: Polar ionosphere
AUTH: A/OKSMAN, J.
CORP: Oulu Univ. (Finland). CSS: (Abt. fuer Elektrotechnik.) AVAIL.NTIS SAP: HC A06/MF A01
In Max-Planck Inst. fuer Aeronomie Speeches and Lectures delivered on the Occasion of Prof. Dieminger's Retirement p 67-89 (SEE N80-14609 05-46)
MAJS: /*ENERGY TRANSFER/*IONOSPHERIC SOUNDING/*MAGNETOSPHERE /*POLAR REGIONS/*SOLAR WIND
MINS: / AURORAL IONIZATION/ F 1 REGION/ F 2 REGION/ IONOSPHERIC F-SCATTER PROPAGATION/ MAGNETOPAUSE/ PLASMAPAUSE/ SATELLITE OBSERVATION
ABA: Author (ESA)
ABS: A brief definition of the polar ionosphere is offered, then the results of joint German-Finnish ionospheric observations and soundings are reviewed. Radio frequency absorption and reflection at the polar caps are considered. Satellite observations of electron flux density are cited along wtih data obtained during balloon-borne measurements. A model of the ionosphere-magnetosphere configuration around the Earth is suggested, taking into consideration solar wind effects, magnetopause currents, and plasmasphere orientation. Variations in the polar ionospheric characteristics are discussed and possible coupling mechanisms between the solar wind and the magnetosphere hypothesized. The need for further data is emphasized.

80N14317# ISSUE 5 PAGE 594 CATEGORY 32 RPT#: AD-A074475 RADC-TR-79-178 CNT#: AF PROJ. 4600
79/05/00 83 PAGES UNCLASSIFIED DOCUMENT
UTTL: VLF/LF reflectivity of the polar ionosphere, 3 September - 30 December 1978
AUTH: A/PAGLIARULO, R. P.; B/TURTLE, J. P.; C/RASMUSSEN, J. E.; D/COOLEY, R. L.; E/KLEMETTI, W. L. PAA: E/(Megapulse, Inc., Bedford, Maine)
CORP: Rome Air Development Center, Griffiss AFB, N.Y.
AVAIL.NTIS SAP: HC A05/MF A01
MAJS: /*ELECTROMAGNETIC RADIATION/*IONOSONDES/*IONOSPHERIC PROPAGATION/*POLAR REGIONS/*VERY LOW FREQUENCIES
MINS: / DIURNAL VARIATIONS/ GREENLAND/ LOOP ANTENNAS/ MAGNETOMETERS/ RIOMETERS
ABA: GRA
ABS: This report provides a summary of high latitude ionospheric reflectivity as observed by the USAF high resolution VLF/LF ionosounder operating in northern Greenland. Ionospheric reflectivity parameters, including reflection heights and coefficients, are presented as a function of time of day. VLF long path propagation measurements, along with magnetometer and riometer data, are presented as supplementary data.

80N11690# ISSUE 2 PAGE 232 CATEGORY 46 RPT#:
AD-A073113 LMSC-D626959 CNT#: N00014-77-C-0600
78/08/00 33 PAGES UNCLASSIFIED DOCUMENT

UTTL: Coordinated data analysis of ONR-118 data --- ionospheric scintillation and disturbance phenomena
TLSP: Final Report

AUTH: A/JOHNSON, R. G.; B/SHARP, R. D.; C/SHELLEY, E. G.
CORP: Lockheed Missiles and Space Co., Palo Alto, Calif.

CSS: (Research Lab.) AVAIL.NTIS SAP: HC A03/MF A01

MAJS: /*AURORAS/*IONOSPHERIC DISTURBANCES/*IONOSPHERIC ELECTRON DENSITY/*MAGNETOSPHERE/*SCINTILLATION

MINS: / ALASKA/ ENERGETIC PARTICLES/ EXPLORER 12 SATELLITE/ HIGH TEMPERATURE PLASMAS/ IONOSPHERIC PROPAGATION/ POLAR ORBITS

ABA: GRA

ABS: This is the final report of a program to study the physical causes of ionospheric scintillation and disturbance phenomena by performing coordinated observations of the energetic particle inputs to the disturbance region and the resulting disturbance phenomena as observed in the ionosphere.

REPORT DOCUMENTATION PAGE

1. Recipient's Reference	2. Originator's Reference	3. Further Reference	4. Security Classification of Document
	AGARD-CP-382	ISBN 92-835-0383-X	UNCLASSIFIED

5. Originator Advisory Group for Aerospace Research and Development
North Atlantic Treaty Organization
7 rue Ancelle, 92200 Neuilly sur Seine, France

6. Title
PROPAGATION EFFECTS ON MILITARY SYSTEMS IN THE HIGH LATITUDE REGION

7. Presented at
the 36th Symposium of the Electromagnetic Wave Propagation Panel held in Fairbanks, Alaska, USA, 3—7 June, 1985.

8. Author(s)/Editor(s)
Edited by H.Soicher

9. Date
November 1985

10. Author's/Editor's Address
US Army Communications-Electronics Command
Center for Communications Systems
Fort Monmouth, New Jersey 07703, USA

11. Pages
598

12. Distribution Statement
This document is distributed in accordance with AGARD policies and regulations, which are outlined on the Outside Back Covers of all AGARD publications.

13. Keywords/Descriptors

High latitude
Incoherent scatter studies
Irregularity structure
Magnetosphere
Electromagnetic wave propagation
Radiowave propagation
RF spectrum
Geomagnetic field
Geophysical

14. Abstract

With the advent of new systems operating at high latitudes in the field of detection, navigation and communications and with the new experiments at high latitudes ranging from incoherent scatter studies to satellites for studying high latitude irregularity structure, it is of considerable importance to relate the advances in high latitude studies to military systems. The concept of this proposal for a meeting on propagation effects on military systems in the high latitude region was to bring together these two areas.

The behaviour of the propagation environment at high latitudes differs from that at lower latitudes, affecting radiowave propagation across the RF spectrum. The differences are ascribed to rugged terrain, severe climatic conditions, and influences of the interplanetary and magnetospheric geophysical events which are guided earthward by the geomagnetic field.

With the NATO northern flank nations (in both the European and North-American sectors) situated in the high-latitude region, with NATO air routes across the Atlantic traversing that region, and with surveillance and early-warning systems looking in the direction of the region, the propagation characteristics of the high-latitude region are of critical importance to the mission of the alliance in the areas of communications, navigation and surveillance.

AGARD Conference Proceedings No.382
Advisory Group for Aerospace Research and Development, NATO
PROPGATION EFFECTS ON MILITARY SYSTEMS IN THE HIGH LATITUDE REGION
Edited by H.Soicher
Published November 1985
598 pages

With the advent of new systems operating at high latitudes in the field of detection, navigation and communications and with the new experiments at high latitudes ranging from incoherent scatter studies to satellites for studying high latitude irregularity structure, it is of considerable importance to relate the advances in high latitude studies to military systems. The concept of this proposal for a meeting

P.T.O

AGARD-CP-382

High latitude
Incoherent scatter studies
Irregularity structure
Magnetosphere
Electromagnetic wave propagation
Radiowave propagation
RF spectrum
Geomagnetic field
Geophysical

AGARD Conference Proceedings No.382
Advisory Group for Aerospace Research and Development, NATO
PROPGATION EFFECTS ON MILITARY SYSTEMS IN THE HIGH LATITUDE REGION
Edited by H.Soicher
Published November 1985
598 pages

With the advent of new systems operating at high latitudes in the field of detection, navigation and communications and with the new experiments at high latitudes ranging from incoherent scatter studies to satellites for studying high latitude irregularity structure, it is of considerable importance to relate the advances in high latitude studies to military systems. The concept of this proposal for a meeting

P.T.O

AGARD-CP-382

High latitude
Incoherent scatter studies
Irregularity structure
Magnetosphere
Electromagnetic wave propagation
Radiowave propagation
RF spectrum
Geomagnetic field
Geophysical

AGARD Conference Proceedings No.382
Advisory Group for Aerospace Research and Development, NATO
PROPGATION EFFECTS ON MILITARY SYSTEMS IN THE HIGH LATITUDE REGION
Edited by H.Soicher
Published November 1985
598 pages

With the advent of new systems operating at high latitudes in the field of detection, navigation and communications and with the new experiments at high latitudes ranging from incoherent scatter studies to satellites for studying high latitude irregularity structure, it is of considerable importance to relate the advances in high latitude studies to military systems. The concept of this proposal for a meeting

P.T.O

AGARD-CP-382

High latitude
Incoherent scatter studies
Irregularity structure
Magnetosphere
Electromagnetic wave propagation
Radiowave propagation
RF spectrum
Geomagnetic field
Geophysical

AGARD Conference Proceedings No.382
Advisory Group for Aerospace Research and Development, NATO
PROPGATION EFFECTS ON MILITARY SYSTEMS IN THE HIGH LATITUDE REGION
Edited by H.Soicher
Published November 1985
598 pages

With the advent of new systems operating at high latitudes in the field of detection, navigation and communications and with the new experiments at high latitudes ranging from incoherent scatter studies to satellites for studying high latitude irregularity structure, it is of considerable importance to relate the advances in high latitude studies to military systems. The concept of this proposal for a meeting

P.T.O

AGARD-CP-382

High latitude
Incoherent scatter studies
Irregularity structure
Magnetosphere
Electromagnetic wave propagation
Radiowave propagation
RF spectrum
Geomagnetic field
Geophysical

on propagation effects on military systems in the high latitude region was to bring together these two areas.

The behaviour of the propagation environment at high latitudes differs from that at lower latitudes, affecting radiowave propagation across the RF spectrum. The differences are ascribed to rugged terrain, severe climatic conditions, and influences of the interplanetary and magnetospheric geophysical events which are guided earthward by the geomagnetic field.

With the NATO northern flank nations (in both the European and North-American sectors) situated in the high-latitude region, with NATO air routes across the Atlantic traversing that region, and with surveillance and early-warning systems looking in the direction of the region, the propagation characteristics of the high-latitude region are of critical importance to the mission of the alliance in the areas of communications, navigation and surveillance.

Papers presented at the 36th Symposium of the Electromagnetic Wave Propagation Panel held in Fairbanks, Alaska, USA, 3—7 June, 1985.

ISBN 92-835-0383-X

on propagation effects on military systems in the high latitude region was to bring together these two areas.

The behaviour of the propagation environment at high latitudes differs from that at lower latitudes, affecting radiowave propagation across the RF spectrum. The differences are ascribed to rugged terrain, severe climatic conditions, and influences of the interplanetary and magnetospheric geophysical events which are guided earthward by the geomagnetic field.

With the NATO northern flank nations (in both the European and North-American sectors) situated in the high-latitude region, with NATO air routes across the Atlantic traversing that region, and with surveillance and early-warning systems looking in the direction of the region, the propagation characteristics of the high-latitude region are of critical importance to the mission of the alliance in the areas of communications, navigation and surveillance.

Papers presented at the 36th Symposium of the Electromagnetic Wave Propagation Panel held in Fairbanks, Alaska, USA, 3—7 June, 1985.

ISBN 92-835-0383-X

on propagation effects on military systems in the high latitude region was to bring together these two areas.

The behaviour of the propagation environment at high latitudes differs from that at lower latitudes, affecting radiowave propagation across the RF spectrum. The differences are ascribed to rugged terrain, severe climatic conditions, and influences of the interplanetary and magnetospheric geophysical events which are guided earthward by the geomagnetic field.

With the NATO northern flank nations (in both the European and North-American sectors) situated in the high-latitude region, with NATO air routes across the Atlantic traversing that region, and with surveillance and early-warning systems looking in the direction of the region, the propagation characteristics of the high-latitude region are of critical importance to the mission of the alliance in the areas of communications, navigation and surveillance.

Papers presented at the 36th Symposium of the Electromagnetic Wave Propagation Panel held in Fairbanks, Alaska, USA, 3—7 June, 1985.

ISBN 92-835-0383-X

on propagation effects on military systems in the high latitude region was to bring together these two areas.

The behaviour of the propagation environment at high latitudes differs from that at lower latitudes, affecting radiowave propagation across the RF spectrum. The differences are ascribed to rugged terrain, severe climatic conditions, and influences of the interplanetary and magnetospheric geophysical events which are guided earthward by the geomagnetic field.

With the NATO northern flank nations (in both the European and North-American sectors) situated in the high-latitude region, with NATO air routes across the Atlantic traversing that region, and with surveillance and early-warning systems looking in the direction of the region, the propagation characteristics of the high-latitude region are of critical importance to the mission of the alliance in the areas of communications, navigation and surveillance.

Papers presented at the 36th Symposium of the Electromagnetic Wave Propagation Panel held in Fairbanks, Alaska, USA, 3—7 June, 1985.

ISBN 92-835-0383-X

END